

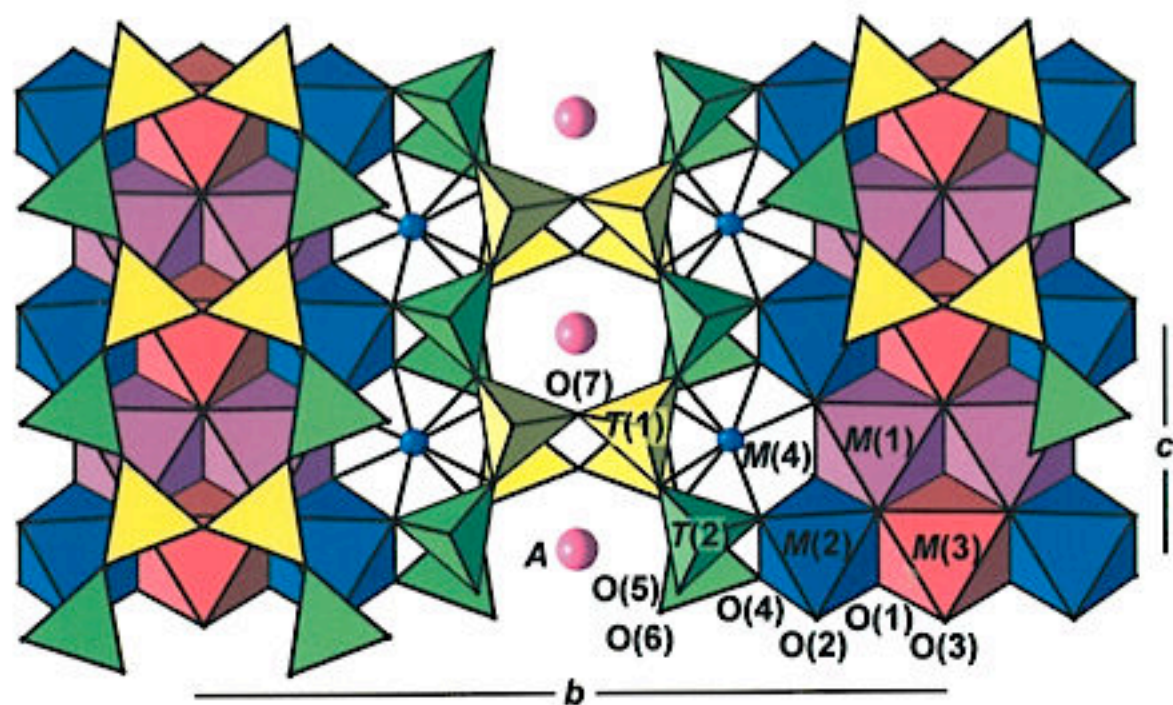


REVIEWS in
MINERALOGY &
GEOCHEMISTRY
Volume 67



AMPHIBOLES:
*Crystal Chemistry, Occurrence,
and Health Issues*

EDITORS: Frank C. Hawthorne, Roberta Oberti,
Giancarlo Della Ventura, Annibale Mottana



*Published in partnership with
Accademia Nazionale dei Lincei*



MINERALOGICAL SOCIETY OF AMERICA
GEOCHEMICAL SOCIETY

Series Editor: Jodi J. Rosso

AMPHIBOLES:

Crystal Chemistry, Occurrence, and Health Issues

67 *Reviews in Mineralogy and Geochemistry* 67

FROM THE EDITORS

This volume was jointly published by the Mineralogical Society of America (MSA) and the Accademia Nazionale dei Lincei (ANL). The chapters represent an extensive review of the material presented by the invited speakers at a three-day short course on *Amphiboles* held at the Accademia Nazionale dei Lincei in Rome, Italy (October 29-31, 2007). Additionally, interested readers could look for a forth-coming special issue of the European Journal of Mineralogy containing original papers on amphiboles from the short course.

Any supplemental material and errata (if any) can be found at the MSA website www.minsocam.org.

Jodi J. Rosso, Series Editor
West Richland, Washington
August 2007

Over 25 years ago, Volume 9 of **Reviews in Mineralogy: Amphiboles and Other Hydrous Pyriboles** seemed to contain all that was possible to know about this group of fascinating minerals. The subsequent twenty-five years have shown that this assessment was wrong: Nature was keeping a lot in reserve, and has since revealed considerable new complexity in the constitution and behavior of amphiboles. Some of the advances in knowledge have been due to the use of new experimental techniques, some have been due to the investigation of hitherto neglected rock-types, and some have been due to the development of new ideas.

- [1] The identification and systematic investigation of variable LLE (Light Lithophile Elements), particularly Li and H, led to the identification of several new amphibole species and the recognition that variable Li and H play an important role in chemical variations in amphiboles from both igneous and metamorphic parageneses. In turn, this work drove the development of microbeam SIMS to analyze LLE in amphiboles.
- [2] Detailed mineralogical work on metasyenites showed hitherto unexpected solid-solution between Na and Li at the $M(4)$ site in monoclinic amphiboles, a discovery that has upset the current scheme of amphibole classification and nomenclature and initiated new efforts in this direction.
- [3] Systematic and well-planned synthesis of amphiboles, combined with careful spectroscopy, has greatly furthered our understanding of cation and anion order in amphiboles.
- [4] The use of bond-valence theory to predict patterns of SRO (Short-Range Order) in amphiboles, and use of these predictions to understand the infrared spectra of

well-characterized synthetic-amphibole solid-solutions, has shown that SRO is a major feature of the amphibole structure, and has resulted in major advances in our understanding of SRO in minerals.

- [5] There has been significant progress relating changes in amphibole composition and cation ordering to petrogenetic conditions and trace-element behavior.
- [6] Work on the nature of fibrous amphiboles and their toxicity and persistence in living organisms has emphasized the importance of accurate mineralogical characterization in environmental and health-related problems.

The current volume has taken a different approach from previous volumes concerned with major groups of rock-forming minerals. Some of the contents have previously been organized by the investigative technique or groups of similar techniques: crystal-structure refinement, spectroscopy, TEM etc. Here, we have taken an approach that focuses on aspects of amphiboles rather than experimental techniques: crystal chemistry, new compositions, long-range order, short-range order etc., and all experimental results germane to these topics are discussed in each chapter. The intent of this approach is to focus on amphiboles, and to emphasize that many techniques are necessary to fully understand each aspect of the amphiboles and their behavior in both natural and industrial processes.

We thank Jodi Rosso for all her work in producing the volume, and Donna Danyluk for all her help to the editors. We also thank all the contributors to this volume for sharing their knowledge and expertise with the scientific community in such a timely fashion. Inspiration for the Short Course and financial assistance for the RiMG volume came from the Mineralogical Society of America and the Accademia Nazionale dei Lincei. Sponsoring by a number of scientific organizations helped produce the meeting where new data on amphiboles will be communicated.

Frank C. Hawthorne, Winnipeg, Canada
Roberta Oberti, Pavia, Italy
Giancarlo Della Ventura, Roma, Italy
Annibale Mottana, Roma, Italy

July 31, 2007

Amphiboles: Crystal Chemistry

Frank C. Hawthorne

*Department of Geological Sciences
University of Manitoba, Winnipeg, Manitoba R3T 2N2, Canada
frank_hawthorne@umanitoba.ca*

Roberta Oberti

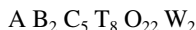
*Istituto di Geoscienze e Georisorse, Consiglio Nazionale delle Ricerche
I-27100 Pavia, Italy
oberti@crystal.unipv.it*

INTRODUCTION

This chapter provides an introduction to the crystal structure, crystal chemistry and chemical composition of the amphiboles. It is not an exhaustive treatment; it is intended as an introduction to the material discussed in the following chapters. More extensive discussion of many points is given in Hawthorne (1981, 1983a), although all later developments are discussed in some detail here. Published crystal-structure refinements are listed in Appendix I.

CHEMICAL FORMULA

The general chemical formula of the amphiboles can be written as



where A = Na, K, □, Ca, Li;
B = Na, Li, Ca, Mn²⁺, Fe²⁺, Mg;
C = Mg, Fe²⁺, Mn²⁺, Al, Fe³⁺, Mn³⁺, Ti⁴⁺, Li;
T = Si, Al, Ti⁴⁺;
W = (OH), F, Cl, O²⁻.

Minor elements such as Zn, Ni²⁺, Co²⁺, V³⁺, Sc, Cr³⁺ and Zr are also observed as C cations. In a mineral group as chemically complicated as the amphiboles, there are many problems connected with (1) the measurement of chemical composition, and (2) calculation of the chemical formula.

SOME ASPECTS OF CHEMICAL ANALYSIS

Chemical composition

The chemical composition of an amphibole is most commonly produced by electron microprobe analysis (EMPA). Instrumentation is very reliable and data reduction (including matrix corrections) are accurate. The main source of error is almost certainly errors in standards, a problem that can be dealt with in a simple but tedious fashion by cross-analyzing all standards. A more serious problem involves the components that cannot be analyzed (or analyzed accurately) by EMPA. Of particular relevance with regard to amphiboles are FeO vs. Fe₂O₃, Li₂O and H₂O, all of which occur commonly as highly variable constituents in amphiboles. We

will focus on microbeam methods of analysis where possible as these avoid heterogeneity and contamination problems.

Li₂O and H₂O. Li can be analyzed by Secondary-Ion Mass Spectrometry (SIMS) and Laser-Ablation Inductively Coupled Mass Spectrometry (LA-ICP-MS). Both these techniques are generally used for trace- and minor-element analysis, but procedures are now available which allow reasonably accurate ($\leq \pm 10\%$) quantification of Li at the major-element level. The presence of significant matrix effects (i.e., the various factors distorting the direct proportionality of secondary-ion intensity to element concentration) in SIMS analysis has been overcome using the voltage-offset technique (Ottolini et al. 1993) and by the construction of reliable matrix-matched calibration curves (Ottolini et al. 1993; Ottolini and Oberti 2000). LA-ICP-MS does not suffer from matrix effects, and thus allows more straightforward quantification of Li (also Be, B) with almost the same precision and accuracy as SIMS (Tiepolo et al. 2005). However, LA-ICP-MS analysis is more destructive than SIMS analysis, and the beam diameter used (20-40 μm) is not ideal for the determination of compositional zoning. Extensive work in the last 15 years has shown that Li is a much more common constituent in amphiboles that had hitherto been realized (e.g., Hawthorne et al. 1992, 1993, 1994, 1996b,c; Caballero et al. 1998, 2002; Oberti et al. 2000, 2003a,b, 2004). In particular, the results of structure refinement offer a rather straightforward way to detect the presence of both ^6Li and ^7Li . In the first case, the occurrence of Li lowers the refined site-scattering at the $M(4)$ site below 22 electrons per formula unit (epfu) (^6Li always being in solid solution with Na). In the second case, the refined site-scattering values at the $M(1)$ and $M(3)$ sites can be used in a diagnostic plot (Fig. 1), where samples falling in the area below the solid line contain ^7Li . If these tests are positive, and in the absence of the oxo component [namely, $^{\text{W}}\text{O}^{2-}$], more quantitative evaluations can be obtained

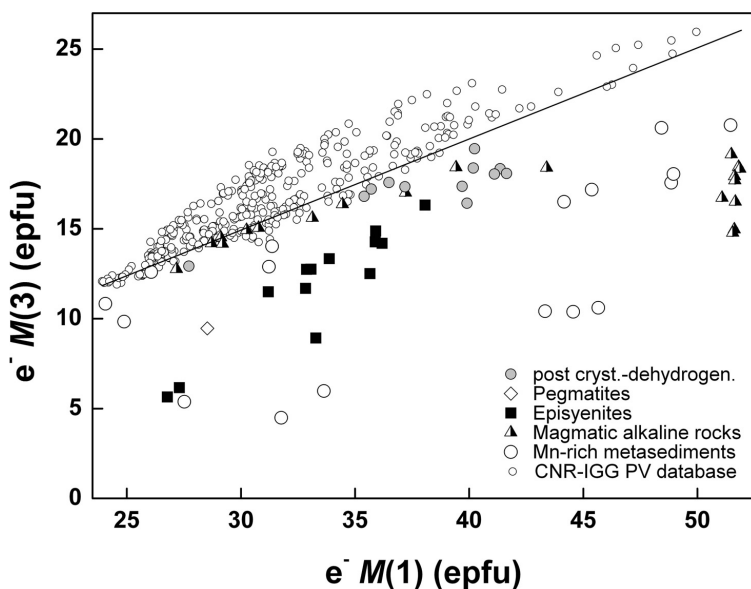


Figure 1. Diagnostic plot for the presence of ^7Li based on the results of structure refinement. Amphiboles fall in the upper left part of the plot, and their distance from the line represents Fe^{2+} -Mg order between the $M(1)$ and $M(3)$ sites. All ^7Li -bearing amphiboles fall well below the line by an amount proportional to the ^7Li content. Oxo-amphiboles, where the loss of H occurred after crystallization via oxidation of Fe^{2+} to Fe^{3+} at the $M(1)$ site, also plot slightly below the line (anti-order). This is an updated version of the plot first proposed by Hawthorne et al. (1994).

by a procedure of formula recalculation which takes into account chemical constraints based on present knowledge of Li crystal-chemistry in amphiboles (no Al at the *T* sites, highly charged cations ≤ 2.0 atoms per formula unit (apfu), and ${}^{\text{C}}\text{Li} \leq A$ -site occupancy; Oberti et al. 2003b).

H can be analyzed by SIMS (e.g., Ottolini et al. 1995; Ottolini and Hawthorne 2001), although matrix effects are quite large and the standard and sample matrices must match very closely, and by hydrogen-line extraction (e.g., Cosca et al. 1991). Considerable work has been done on microbeam analysis of H in amphiboles (e.g., Zanetti et al. 1996; Hawthorne et al. 1998, 2000, 2001; King et al. 1999, 2000; Oberti et al. 2000, 2003a,b, 2004; Caballero et al. 2002; Tait et al. 2005). Because SIMS analysis for H requires much analytical time (each sample must be degassed overnight) and careful check of matrix-matched standards, there have been attempts to relate H content (determined by SIMS) with changes in the structural parameters obtained by structure refinement of the same crystals. Work done at CNR-IGG-PV has shown that H content is inversely related to the *M*(1)-*M*(2) separation, a structural response to avoid repulsive interactions between the high-charge cations at these sites. However, the *M*(1)-*M*(2) distance is sensitive to the type of amphibole (e.g., it is different in richterite than in pargasite-kaersutite), but the methods works well within a given type of amphibole. More details are given in Oberti et al. (2007a).

FeO vs. Fe_2O_3 . Both FeO and Fe_2O_3 are often major constituents in amphiboles, and the absence of $\text{Fe}^{2+}:\text{Fe}^{3+}$ determination must be considered as a major deficiency in a chemical analysis of an amphibole. It is common to calculate the $\text{Fe}^{2+}:\text{Fe}^{3+}$ ratio in an amphibole using the method introduced by Stout (1972) which relies on the fact that expressing Fe as FeO introduces a different amount of oxygen into the formula calculation than expressing Fe as Fe_2O_3 .

The calculation of the unit-cell content of an amphibole is based on a fixed number of anions [e.g., 24 (O,OH,F), 23 (O)] or a fixed number of cations [e.g., 13 (Si,Al,Ti,Mg, $\text{Fe}^{2+},\text{Fe}^{3+},\text{Mn}^{2+}$), 15 (Si,Al,Ti,Mg, $\text{Fe}^{2+},\text{Fe}^{3+},\text{Mn}^{2+},\text{Ca}$)]. The corresponding number of cations or anions results from the requirement of electroneutrality. Alternatively, we can normalize the anions to a fixed number, normalize the cations to a fixed number, and then adjust the $\text{Fe}^{2+}:\text{Fe}^{3+}$ ratio for electroneutrality. Thus we can calculate the formula for 24 (O, OH, F) anions, and vary the $\text{Fe}^{2+}:\text{Fe}^{3+}$ ratio to get a specific number of cations (1) 13 (Si,Al, Ti,Mg, $\text{Fe}^{2+},\text{Fe}^{3+},\text{Mn}^{2+}$) and (2) 15 (Si,Al,Ti,Mg, $\text{Fe}^{2+},\text{Fe}^{3+},\text{Mn}^{2+},\text{Ca}$). Calculation (1) provides a maximum 'estimate' of the amount of Fe^{3+} and calculation (2) provides a minimum 'estimate' of the amount of Fe^{3+} ; normally, the mean is taken as the optimum value. Hawthorne (1983a) examined the efficacy of this method using the superior analysis of Leake (1968); the results are shown in Figure 2. There is no correlation at all between the observed and calculated values for Fe_2O_3 , indicating that no reliance can be placed on this type of calculation. Is there any point in doing such a calculation? Yes: while recognizing that the values are very inaccurate, inspection of Figure 2 indicates that the calculation does provide a better estimate than the alternative of not doing such a calculation: $\text{Fe}_2\text{O}_3 = 0.00$ wt%. Schumacher (1997, 2007) describes in detail the various methods by which such estimates may be made, and Schumacher (1991) shows the effects of the estimation of Fe^{3+} on various geothermobarometers.

What the above discussion does emphasize is the need to have a method for the determination of the $\text{Fe}^{2+}:\text{Fe}^{3+}$ ratio in an amphibole. This may be done in a variety of ways:

- (1) Crystal-structure refinement of amphiboles can determine the amount of Fe^{3+} in the structure by distinguishing between Fe^{2+} and Fe^{3+} on the basis of their different ionic radii ($r[\text{Fe}^{3+}] = 0.645 \text{ \AA}$, $r[\text{Fe}^{2+}] = 0.78 \text{ \AA}$) and their effect on the mean bondlength of the site(s) at which they occur. Useful constraints are based on electroneutrality, where H is determined analytically (or evaluated from some structural parameters) and the content of the *A* site is quantified based on EMP analysis and site-scattering refinement.

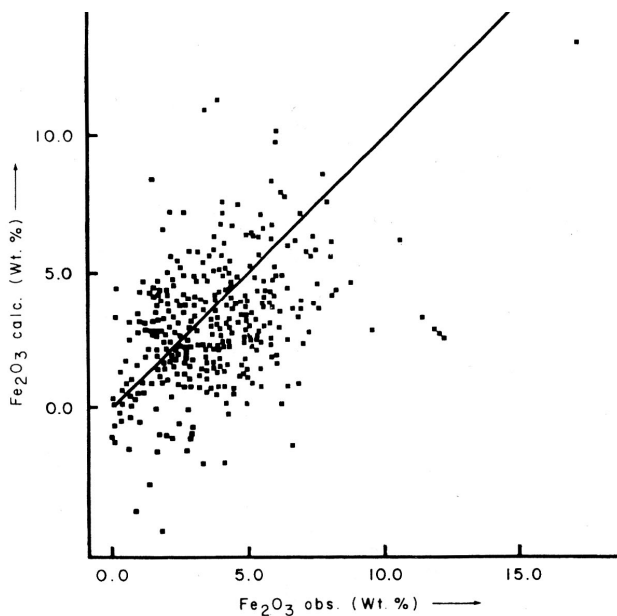


Figure 2. Observed and calculated contents of Fe₂O₃ using the superior analyses of Leake (1968); the diagonal line indicates a 1:1 relation (from Hawthorne 1983a).

- (2) Mössbauer spectroscopy (Bancroft 1973; Hawthorne 1983b, 1988; Murad and Cashion 2004; Dyar et al. 2006) is responsive to the valence state of Fe (Fig. 3) and has been used extensively for determining the Fe²⁺:Fe³⁺ ratio in amphiboles (e.g., Bancroft and Brown 1975; Dyar et al. 1993; Enders et al. 2000; Gunter et al. 2003). Milli-Mössbauer spectroscopy (McCammon 1994) can determine the Fe²⁺:Fe³⁺ ratio of a single grain of a mineral, and this method has been used for amphiboles (Sokolova et al. 2000a,b, 2001; Uvarova et al. 2005). A significant problem with the Mössbauer method is lack of information on the recoil-free fractions of Fe²⁺ and Fe³⁺ in minerals (see discussion by Dyar et al. 2006). Eeckhout and De Grave (2003) report measurements on riebeckite indicating that the recoil-free fraction for Fe³⁺ is significantly larger than that for Fe²⁺. As the recoil-free fractions of the Fe²⁺ and Fe³⁺ are usually assumed to be unity, this assumption introduces errors in the determination of Fe²⁺:Fe³⁺ ratios that may be of the order of 10%. However, determination of the recoil-free fractions in amphiboles will remove this error.
- (3) Milli-XANES (X-ray Absorption Near-Edge Structure) spectroscopy can measure the Fe²⁺:Fe³⁺ ratio (Fig. 4) with a spot size of a few microns, although reasonably good results on amphiboles have been obtained with a beam size of ~ 50 μm (Delaney et al. 1996). Dyar et al. (2002) have shown that orientation effects are a major source of error in determining Fe²⁺:Fe³⁺ ratios in amphiboles, and quote a probable accuracy of ± 20% in randomly oriented crystals. However, by using oriented samples and standards, they suggest that an accuracy of < 2-3% absolute is possible.
- (4) EELS (Electron Energy Loss Spectroscopy) - ELNES (Energy Loss Near-Edge Spectroscopy) can determine Fe²⁺:Fe³⁺ ratios (Fig. 5) at a submicron scale (Garvie and Buseck 1998; van Aken and Liebscher 2002) with quoted accuracies of 0.02. However, electron-beam damage can be a problem, but good values can be obtained at low beam intensity (Garvie et al. 2004).

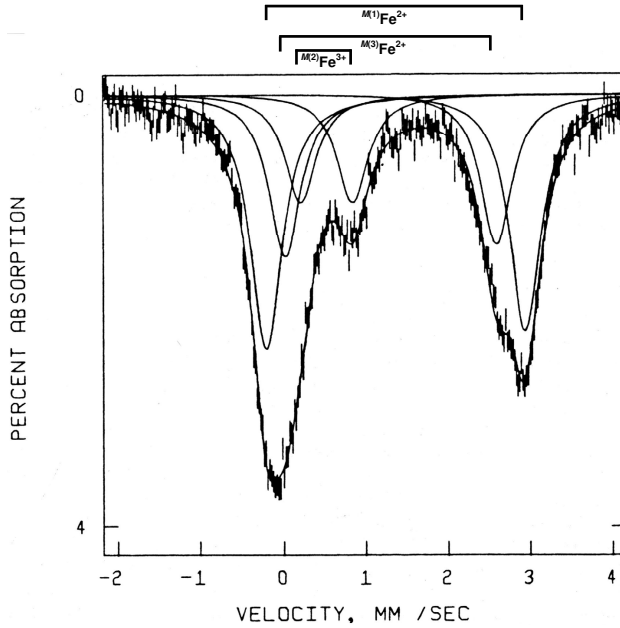


Figure 3. The Mössbauer spectrum of ferrotschermakite, with the absorptions marked (from Hawthorne 1988).

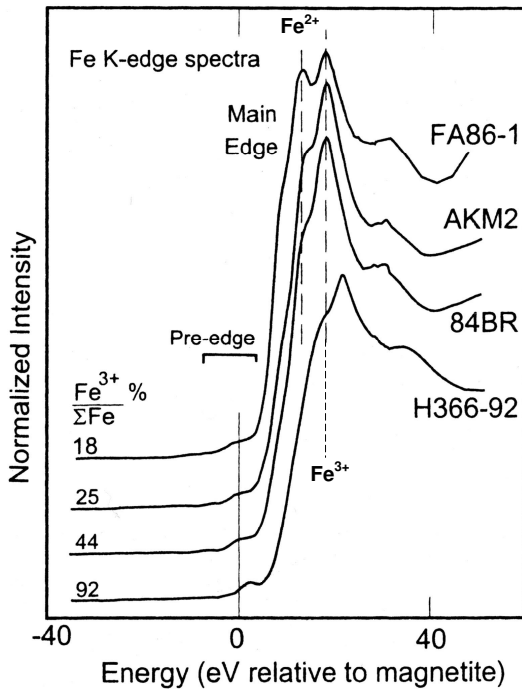


Figure 4. Milli-XANES spectra of several amphiboles, showing the absorptions due to Fe^{3+} and Fe^{2+} and the Fe^{3+}/Fe value for each amphibole. [Used by permission of The Geochemical Society, from Delaney et al. (1996), Special Publication No 5 (Mineral Spectroscopy: A Tribute to Roger G. Burns), Fig. 1, p. 167.]

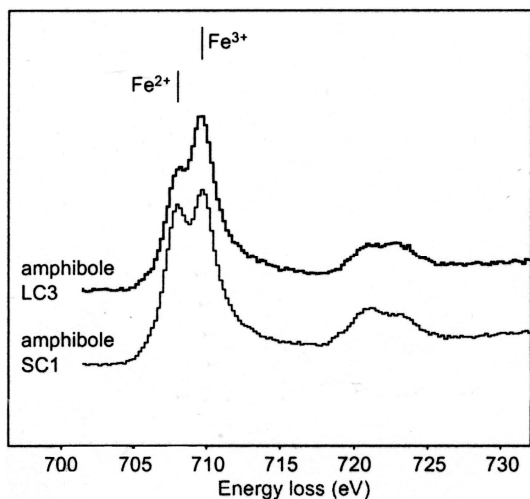


Figure 5. EELS spectra of two amphiboles, showing the absorptions due to Fe^{3+} and Fe^{2+} . [Used by permission of Macmillan Publishers Ltd, from Garvie and Buseck (1998), *Nature*, Vol. 396, Fig. 3, p. 669].

- (5) The Flank method optimizes use of the electron microprobe to use X-ray spectroscopy to determine $\text{Fe}^{2+}:\text{Fe}^{3+}$ ratios via the positions and intensities of the FeL_{α} and FeL_{β} peaks as a function of valence state (Höfer et al. 1994). Enders et al. (2000) have applied/tested the method extensively for sodic amphiboles, and have shown that it can be reasonably accurate down to an $\text{FeO}(\text{total})$ content of 6–8 wt%. However, they also suggest that the calibration procedures are particularly laborious and complicated, suggesting that it will not find use as a routine method for $\text{Fe}^{2+}:\text{Fe}^{3+}$ determination.

None of these methods can be considered as routine in the sense that they are widely available in the community or are simple to use. *Crystal-structure refinement* is the most widely available method, but in view of the fact that one gets a large amount of crystal-chemical information at the same time, it seems wasteful to do this just for one piece of information. Moreover, the method cannot be used for poorly crystalline, microcrystalline or noncrystalline materials, and the instrumentation is relatively expensive. *Milli-Mössbauer spectroscopy* provides a much more economical method, but facilities are very few, particularly in the Earth Science community. *Micro-XPS* currently requires access to synchrotron radiation, and unless conventional laboratory sources increase greatly in intensity, this will not become a standard facility in mineral-analysis laboratories. In our view, the most viable method is milli-Mössbauer spectroscopy. The cost of an electron microprobe is currently approaching US \$1M, and yet they produce amphibole analyses of only limited use. Addition of a milli-Mössbauer facility (approximate cost US \$50,000) to an electron-microprobe lab will result in amphibole (and other mineral) analyses that are far more accurate than anything routinely produced at the present time.

Summary

One thing to stress about the chemical composition and chemical formulae of amphiboles is the importance of complete chemical analyses. We know a lot about the crystal-chemical and chemical characteristics of amphiboles, and partial chemical compositions are no longer very useful in either Mineralogy or Petrology. To be useful, an amphibole *must* be analyzed for Fe^{3+} as well as Fe^{2+} (i.e., FeO). Indeed, in studies of kaersutite, measurement of $\text{Fe}^{3+}/(\text{Fe}^{2+} + \text{Fe}^{3+})$ (e.g., McGuire et al. 1989, 1991; Dyar et al. 1992, 1993; King et al. 1999; Popp et al. 1995, 2006; Nasir and Al-Rawas 2006) has long been considered essential. Furthermore, if it is suspected that Li is present and/or H is not given by $[\text{OH} + \text{F} + \text{Cl}] = 2$ apfu (either from the paragenesis or unusual aspects of the calculated formula), Li and H should be measured

too. Facilities to do this type of analysis are not common; however, this is an indication that we should be pushing for funding for such instrumentation (electron microprobes were rare commodities once upon a time, as for example, SIMS and Mössbauer instruments are today).

CALCULATION OF THE CHEMICAL FORMULA

This is one of the most important issues connected with deriving an accurate chemical formula for an amphibole, and the details of how it is done are often poorly understood. The chemical composition of a mineral is presented as weight % of the oxides of the elements (except for the halogens) present. Classically, the contents of the unit cell were normalized on the density of the mineral; this procedure is not followed now due to the difficulty of measuring accurately the density of most minerals. Present methods are all based on scaling the ratios of the cations and/or anions to some quantity that one believes is constant and known within the unit cell. Current methods are outlined below; Hawthorne (1983a) and Schumacher (1997) give a more detailed discussion of these methods.

24 (O, OH, F, Cl)

This method assumes an anion content of 24 apfu (atoms per formula unit). Presuming that there are no anion vacancies in amphiboles, this method either (1) requires that H (as H₂O) is determined, or (2) assumes that (OH,F,Cl) = 2 apfu. A slightly more complicated variation has been introduced where (OH,F,Cl) < 2 apfu and an amount of O²⁻ occurs at the O(3) site, entering the structure *via* the substitution $M^{(1)}Ti^{4+} + O^{(3)}O^{2-} = M^{(1)}(Mg, Fe^{2+}) + O^{(3)}(OH)^-$. Here, the formula is still normalized on 24 (OH,F,Cl) anions, but (OH,F,Cl) = 2 - 2 × $M^{(1)}Ti^{4+}$ apfu; the issue is whether or not all ⁶³Ti occurs at the M(1) site or not, and this is not currently known (see Oberti et al. 2007a).

The effect of the occurrence of O²⁻ at the O(3) site in the unit formula of an amphibole is illustrated in Table 1 for a strongly dehydrogenated sodic amphibole rich in Ti (which will be soon presented to IMA-CNMMN for approval as “ferri-obertiite”) (Hawthorne et al. 1998) in which the H content was determined by SIMS and the Fe³⁺ content was determined from the crystal structure. Where all components

Table 1. Normalization of a Ti-rich oxygenian sodic amphibole* formula (1) using all components determined and a 24 (O,OH,F) normalization, and (2) using OH + F = 2.0 apfu and Fe³⁺ estimated after the method of Papike et al. (1974).

SiO ₂	52.47	
Al ₂ O ₃	0.09	
TiO ₂	6.51	
Fe ₂ O ₃	4.54	
FeO	18.43	
MnO	0.15	
MgO	5.74	
CaO	0.90	
Na ₂ O	8.70	
K ₂ O	1.51	
Li ₂ O	0.17	
F	0.51	
H ₂ O	0.58	
O=F	<u>-0.21</u>	
Total	100.09	
	(1)	(2)
Si	7.993	7.874
Al	<u>0.007</u>	<u>0.016</u>
ΣT	8.000	7.890
Al	0.009	—
Fe ³⁺	0.520	—
Fe ²⁺	2.348	2.815
Mn	0.019	0.019
Ti	0.746	0.746
Mg	1.303	1.284
Li	<u>0.104</u>	<u>0.103</u>
ΣC	5.049	4.967
Ca	0.147	0.145
Na	<u>1.853</u>	<u>1.855</u>
ΣB	2.000	2.000
Na	0.716	0.702
K	<u>0.293</u>	<u>0.289</u>
ΣA	1.009	0.991
OH	0.589	1.8
F	0.246	0.2
Σ	0.835	2.0
O	1.163	—

* crystal 745 of Hawthorne et al. (1998)

were determined, formula (1), calculated by anion normalization to $24(\text{O,OH,F})$, has A-, C- and T-cation sums that are in accord with the crystal structure (i.e., $\Sigma T = 8$, $\Sigma C \geq 5$, $\Sigma \leq 1$), and the high Ti content is accompanied by a high O^{2-} content at O(3) as occurs in this type of amphibole (Hawthorne et al. 1998). Assuming $\text{OH} + \text{F} = 2.0$ apfu, normalizing to $24(\text{O,OH,F})$ anions and calculating the Fe^{3+} content by the method of Papike et al. (1974) gives formula (2) in Table 1. For formula (2), the T- and C-sums are too low, and no Fe^{3+} was calculated as present. Of course, the example shown in Table 1 is extreme, as it is an oxygenian amphibole; however, the formula still appears reasonable when compared to formulae given in the literature, indicating that major errors can be introduced by inappropriate normalization schemes.

23 (O)

This calculation assumes that $(\text{O,OH,F,Cl}) = 2$ apfu and is similar to the $24(\text{O,OH,F,Cl})$ where it is also assumed that $(\text{OH,F,Cl}) = 2$ apfu. The difference between these two calculations [in which each assumes that $(\text{O,OH,F,Cl}) = 2$ apfu] is that the $24(\text{O,OH,F,Cl})$ calculation also produces the required wt% of H_2O and allows evaluation of the total wt% oxide of the chemical composition.

13 cations

This method assumes that $[\text{Si} + \text{Al} + \text{Ti} + \text{Fe}^{3+} + \text{Fe}^{2+} + \text{Mn}^{2+} + \text{Mg} + (\text{Cr, V } \dots)] = 13$ apfu [i.e., that these cations occupy the $T(1)$, $T(2)$, $M(1)$, $M(2)$ and $M(3)$ sites that contain the T and C cations]. The assumption that Fe^{2+} , Mn^{2+} and/or Mg do not occupy the $M(4)$ site (i.e., are not B cations) is obviously not appropriate for the magnesium-iron-manganese-lithium amphiboles (Hawthorne and Oberti 2007). However, it is also not appropriate for the other groups of amphiboles either, as detailed structural and chemical characterization of many calcic and sodic amphiboles (as well as in clinopyroxenes) has shown the common presence of small divalent cations at $M(4')$ [a site occurring in the $M(4)$ cavity with local [6+2]-coordination similar to that of the $M(4)$ cation(s) in the magnesium-iron-manganese-lithium amphiboles; for more detail, see Rossi et al. (1987) and Oberti and Ghose (1993)]. This method of formula calculation is not recommended.

15 cations

This method assumes that either $[\text{Si} + \text{Al} + \text{Ti} + \text{Fe}^{3+} + \text{Fe}^{2+} + \text{Mn}^{2+} + \text{Mg} + \text{Ca} + \text{Na} + (\text{Cr, V } \dots)] = 15$ apfu or $[\text{Si} + \text{Al} + \text{Ti} + \text{Fe}^{3+} + \text{Fe}^{2+} + \text{Mn}^{2+} + \text{Mg} + \text{Ca} + (\text{Cr, V } \dots)] = 15$ apfu [i.e., that these cations occupy the $T(1)$, $T(2)$, $M(1)$, $M(2)$, $M(3)$ and $M(4)$ sites that contain the T, C and B cations]. The assumption is either that (1) all Na occurs at the $M(4)$ site, or that (2) all Na occurs at the A site. Neither of these assumptions are generally applicable (although they may hold for very specific compositions).

16 cations

This method assumes that all cations fully occupy all sites in the amphibole [i.e., that there are no vacancies at any sites, including the A site]. Although this condition may hold in some amphiboles, it is not a recommended scheme for formula calculation.

Summary

Amphibole formulae should always be calculated based on $24(\text{O,OH,F,Cl})$, unless justification can be given concerning the site occupancies on which any alternate scheme used is based.

AMPHIBOLES: CRYSTAL STRUCTURE

The amphibole structure consists of two principal elements, a double chain of corner-sharing tetrahedra and a strip of edge-sharing octahedra, both of which extend in the *c*-direction

(Fig. 6). Both the tetrahedrally coordinated sites and the tetrahedra themselves are denoted by T , and the octahedrally coordinated sites and the octahedra are denoted by M . There are two topologically distinct types of tetrahedra in the double chain that are designated $T(1)$ and $T(2)$, and three distinct types of octahedra that are designated $M(1)$, $M(2)$ and $M(3)$ (Fig. 6). At the junction of the strip of octahedra and the chain of tetrahedra is the $M(4)$ site, and below the hexagonal ring of tetrahedra is the A site at the center of a large cavity.

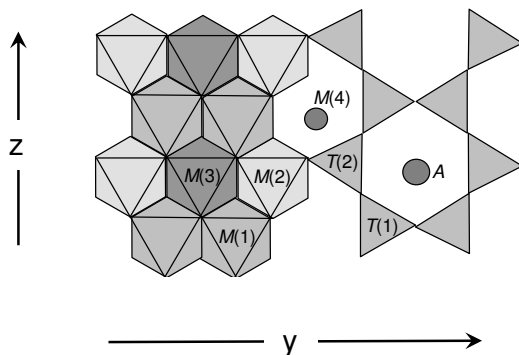


Figure 6. An idealized model of the amphibole structure *sensu lato* showing the chain of tetrahedra, the strip of octahedra, the $M(4)$ site and the A site.

Space groups

There are (currently) six known structural variants of the amphibole arrangement; the space groups and representative amphibole compositions are given in Table 2. We may divide these structures into two types: (1) those that involve different stacking sequences in the a -direction ($C2/m$, $Pnma$ and $Pnmm$), and (2) those that are derivatives of (1) and involve differences in coordination ($P2_1/m$) and/or topochemistry ($P2_1/a$, $C\bar{1}$). All centrosymmetric subgroups of $C2/m$, $Pnma$ and $Pnmm$ are listed in Table 3; these are possible space groups for amphiboles with the same unit cell as the structure with the parent space group. As is apparent from comparison of Tables 2 and 3, there are several structures that are symmetrically possible but have not yet been found. The triclinic $C\bar{1}$ structure has a tripled b cell-dimension relative to all other amphibole structures, and requires the presence of a third (OH) group; thus it occurs only for a very unusual synthetic-amphibole composition.

Cell dimensions

The $C2/m$, $P2_1/m$ and $P2_1/a$ structures have (grossly) similar (monoclinic) cell dimensions. The $P2_1/m$ structure is restricted to Mg- and possibly ^6Li -rich amphiboles of the magnesium-iron-manganese-lithium group and to $B_2 = \text{LiMg}$ and NaMg synthetic amphibole (cf. Oberti et al. 2007b); hence cell dimensions show a restricted range. The $P2_1/a$ structure occurs for just a single (known) composition. In contrast, the $C2/m$ structure shows a wide range of composition and a correspondingly wide range of cell dimensions. The situation is similar for the orthorhombic amphiboles; the $Pnmm$ structure is restricted to Mg-rich amphiboles of the magnesium-iron-manganese-lithium group and the cell dimensions show only a restricted range, whereas the $Pnma$ structure shows a wide range of composition. The $C\bar{1}$ structure is known only for a single (synthetic) composition and is unique among the amphibole structure-types in that it has a b axis that is tripled relative to the b axes in the other structure types. A more detailed discussion of cell dimensions is given later in this chapter.

Site nomenclature

Figure 6 shows the basic cation-site nomenclature of the amphibole arrangement. However, the different space groups of the structures give rise to sites that are crystallographically distinct from one structure to another. To facilitate comparison *between* amphibole structures, it is important to retain this distinction in the site nomenclature while maintaining some sort of congruence for analogous sites in different structures. Hawthorne (1983a) developed such a site nomenclature (Table 4) and Cámara et al. (2004) applied analogous reasoning to formulate a site nomenclature for the $C\bar{1}$ amphibole structure. Here, crystallographic sites are written in

Table 2. Observed amphibole space-groups and representative cell dimensions.

Space group	Amphibole	a (Å)	b (Å)	c (Å)	β (°)	V (Å ³)
<i>C2/m</i>	calcic amphiboles, sodic-calcic amphiboles, alkali amphiboles, monoclinic <i>C</i> -centered (Mg-Fe-Mn-Li) amphiboles	9.35–10.14	17.58–18.40	5.26–5.37	101.8–105.7	846–948
<i>P2₁/m</i>	cummingtonite	9.48–9.51	17.99–18.13	5.28–5.31	102.0–102.1	881–893
<i>P2/a</i>	joesmithite	9.92	17.95	5.24	106.0	897
<i>Pnma</i>	orthorhombic Mg-Fe-Mn amphiboles, holmquistite	18.52–18.62	17.80–18.03	5.26–5.30	–	1738–1777
<i>Pnmm</i>	protoamphibole	9.33–9.43	17.88–18.39	5.29–5.35	–	882–925
<i>C$\bar{1}$</i>	Na Na ₂ Mg ₅ Si ₈ O ₂₁ (OH) ₃	9.88	54.08	5.28	103.07*	2748

For *C $\bar{1}$* : $\alpha = 90.05$, $\gamma = 89.96^\circ$

italics (e.g., *T*(1), *M*(1), *A*, *A*(*m*)), the general formula is written in normal type, e.g., A B₂ C₅ T₈ O₂₂ W₂, and constituent cations are considered as A, B, C or T: thus in end-member tremolite, B₂ = Ca₂, whereas in calcic amphiboles, Ca, Na, Mg, Fe²⁺, Mn²⁺, Li are B cations. This will hopefully remove ambiguity when using letter symbols for the amphiboles.

The *C2/m* amphibole structure

A schematic representation of the *C2/m* structure type is shown in Figure 7. There are two distinct *T* sites that are occupied by the T cations, *T*(1) and *T*(2), that are tetrahedrally coordinated and link to form one distinct type of double-chain of tetrahedra. The *T*(1) site is coordinated by O(1), O(5), O(6) and O(7), and the *T*(2) site is coordinated by O(2), O(4), O(5) and O(6). In the double chain, adjacent *T*(1) and *T*(2) tetrahedra link through O(5) and O(6) oxygen atoms, and adjacent *T*(1) tetrahedra link through O(7) oxygen atoms. The *T*(1) and *T*(2) tetrahedra alternate along the length of the double chain, and the *T*(1) tetrahedra bridge across the double chain.

There are three distinct octahedrally coordinated *M* sites that are occupied by the C cations, and have point symmetries 1, 1 and *2/m*, respectively. The *M*(1) site is coordinated by two O(1) and two O(2) oxygen atoms, and by two O(3) W anions (OH,F,Cl,O) in a *cis* arrangement. The *M*(2) site is coordinated by two O(1), two O(2) and two O(4) oxygen atoms, and the *M*(3) site is coordinated by four O(1) oxygen atoms and two O(3) W anions in a *trans* arrangement. Within the strip of octahedra, there is extensive sharing of edges between the *M*(1), *M*(2) and *M*(3) octahedra. The double chain of tetrahedra links to the strip of octahedra in the *b*-direction through *T*(2)-*M*(2) linkage via common O(4) oxygen atoms, and in the *a*-direction through *T*(1) and *T*(2) linkage to the strip via common O(1) and O(2) oxygen atoms.

The *M*(4) site is situated at the periphery of the strip of octahedra (Figs. 6, 7), has point symmetry 2, and is occupied by B cations. It is surrounded by eight oxygen atoms arranged as a square antiprism: O(2) × 2, O(4) × 2, O(5) × 2, and O(6) × 2, not all of which necessarily bond to the central cation. Note that the cation occupancy of this site (1) is the primary feature on which the major groups of amphiboles are classified, and (2) correlates strongly with the space-group variations in amphiboles.

The *A* site occurs at the center of a large cavity between the back-to-back double-chains of the structure (Fig. 7). The center of the cavity has point symmetry *2/m*, but the *A* cations

Table 3. Subgroups of $C2/m$, $Pnma$ and $Pnmm$ *.

<i>C2/m</i>	<i>Pnma</i>	<i>Pnmm</i>
Monoclinic (Y) [†]	Orthorhombic	Orthorhombic
<i>P2₁/a</i>	<i>Pn2₁a</i>	<i>Pn2n</i>
<i>P2₁/m</i>	<i>Pnm2₁</i>	<i>Pnm2₁</i>
<i>P2/a</i>	<i>P2₁ma</i>	<i>P2₁mn</i>
<i>P2/m</i>	<i>P2₁2₁2₁</i>	<i>P2₁2₁2₁</i>
<i>C2</i>		
<i>Cm</i>	Monoclinic (X)	Monoclinic (X)
<i>P2₁</i>	<i>P2₁/n</i>	<i>P2₁/n</i>
<i>P2</i>	<i>P2₁</i>	<i>P2₁</i>
<i>Pm</i>		
	Monoclinic (Y)	Monoclinic (Y)
Triclinic [‡]	<i>P2₁/m</i>	<i>P2/m</i>
$C\bar{1}$	<i>P2₁</i>	<i>P2</i>
$C\bar{1}$	<i>Pm</i>	<i>Pm</i>
$P\bar{1}$		
$P\bar{1}$	Monoclinic (Z)	Monoclinic (Z)
$P\bar{1}$	<i>P2₁/a</i>	<i>P2₁/n</i>
	<i>P2₁</i>	<i>P2₁</i>
	<i>Pa</i>	<i>Pn</i>
	Triclinic	Triclinic
	$P\bar{1}$	$P\bar{1}$
	<i>P1</i>	<i>P1</i>

* bold = reported as amphibole space-groups

† signifies unique axis

‡ repetition of space-group symbol is indicative of different origins

Table 4. Site-nomenclature scheme for amphibole structure-types (for the $C\bar{1}$ structure, see text).

	<i>C2/m</i>	<i>P2₁/m</i>	<i>P2/a</i>	<i>Pnma</i>	<i>Pnmm</i>
tetrahedrally coordinated sites	<i>T(1)</i> <i>T(2)</i>	<i>T(1A)</i> <i>T(2A)</i>	<i>T(1B)</i> <i>T(2B)</i>	<i>T(1A)</i> <i>T(2A)</i>	<i>T(1B)</i> <i>T(2B)</i>
octahedrally coordinated sites	<i>M(1)</i> <i>M(2)</i> <i>M(3)</i>	<i>M(1)</i> <i>M(2)</i> <i>M(3)</i>	<i>M(1)A)</i> <i>M(2)A)</i> <i>M(3)</i>	<i>M(1)B)</i> <i>M(2)B)</i> <i>M(3)</i>	<i>M1)</i> <i>M2)</i> <i>M3)</i>
cubic antiprismatic sites	<i>M(4)</i>	<i>M(4)</i>	<i>M(4)A)</i> <i>M(4)B)</i>	<i>M4)</i>	<i>M4)</i>
[12] cavity*	<i>A</i>	<i>A</i>	<i>A(2)</i>	<i>A</i>	<i>A</i>
non-bridging anion sites	<i>O(1)</i> <i>O(2)</i> <i>O(3)</i> <i>O(4)</i>	<i>O(1A)</i> <i>O(2A)</i> <i>O(3A)</i> <i>O(4A)</i>	<i>O(1B)</i> <i>O(2B)</i> <i>O(3B)</i> <i>O(4B)</i>	<i>O(1)A)</i> <i>O(2)A)</i> <i>O(3)</i> <i>O(4)A)</i>	<i>O(1)B)</i> <i>O(2)B)</i> <i>O(3A)</i> <i>O(4)A)</i>
bridging anion sites	<i>O(5)</i> <i>O(6)</i> <i>O(7)</i>	<i>O(5A)</i> <i>O(6A)</i> <i>O(7A)</i>	<i>O(5B)</i> <i>O(6B)</i> <i>O(7B)</i>	<i>O(5)A)</i> <i>O(6)A)</i> <i>O(7)</i>	<i>O(5)B)</i> <i>O(6)B)</i> <i>O(7A)</i> <i>O(7B)</i>

* the more complex nomenclature used to describe the positional disorder of cations occupying this site is described in the section on the *A* site.

actually occupy off-centered sites of point symmetry 2 or m , $A(2)$ and $A(m)$, respectively. The cavity is surrounded by twelve oxygen atoms: $O(5) \times 4$, $O(6) \times 4$, and $O(7) \times 4$, but not all of these always bond to the A cations.

The $P2_1/m$ amphibole structure

A schematic representation of the $P2_1/m$ structure type is shown in Figure 8. There are four distinct T -sites that are occupied by the T cations, $T(1A)$, $T(1B)$, $T(2A)$ and $T(2B)$, that are tetrahedrally coordinated and link to form two distinct types of double-chain of tetrahedra, the A-chain and the B-chain. Coordination and linkage of these T sites is analogous to that in the $C2/m$ structure, cations labeled A always bonding to anions labeled A, and likewise for the atoms labeled B: thus $T(1A)$ is coordinated to $O(1A)$, $O(5A)$, $O(6A)$ and $O(7A)$, and the $T(1A)$ and $T(2A)$ tetrahedra link along the length of the A-chain. The A- and B-chains face each other back-to-back across the A cavity, and the B-chain is much more kinked (less extended) than the A-chain (Fig. 8).

There are three distinct M sites that are occupied by the C cations, $M(1)$, $M(2)$ and $M(3)$ with point symmetries 1, 1 and m , respectively. As can be seen in Figure 8, the oxygen atoms on one side of the octahedron strip are A-type oxygen atoms and the oxygen atoms on the other side of the octahedron strip are B-type oxygen atoms, and the $M(1,2,3)$ sites bond to both A- and B-type oxygen atoms. The $M(4)$ site has point symmetry 1 and eight adjacent oxygen atoms, however, the cations occupying this site may not bond to all of these surrounding oxygen atoms, and the existence of this structure type seems to depend on the bonding requirements of the $M(4)$ cation and the surrounding oxygen atoms, especially the aggregate ionic radius of the $M(4)$ cations. All natural amphiboles with this structure type have an unoccupied A cavity (and root composition $\square Mg_2 Mg_5 Si_8 O_{22}(OH)_2$, cummingtonite). However, recent work has shown that synthetic amphiboles of the form $Na B_2 Mg_5 Si_8 O_{22}(OH)_2$ with $B_2 = (Na, Li)Mg$ have $P2_1/m$ symmetry at or below room temperature, and undergo a phase transition to the $C2/m$ structure at higher temperature (cf. Oberti et al. 2007b; Welch et al. 2007). In this case, the A cation occupies a site A with point symmetry 1 which is displaced $\sim 0.25 \text{ \AA}$ from the center of the cavity along a line joining the two farthest O7A and O7B atoms (Cámara et al. 2003).

The $P2/a$ amphibole structure

A schematic representation of the $P2/a$ structure type is shown in Figure 9. There are four distinct T sites that are occupied by the T cations, $T(1A)$, $T(1B)$, $T(2A)$ and $T(2B)$, that are tetrahedrally coordinated and link to form two distinct types of double-chain of tetrahedra, the A-chain and the B-chain. Coordination and linkage of these T sites is analogous to that in the $P2_1/m$ structure, cations labeled A always bonding to anions labeled A, and likewise for the atoms labeled B (Fig. 9).

There are five distinct M sites that are occupied by the C cations, $M(1A)$, $M(1B)$, $M(2A)$, $M(2B)$ and $M(3)$, all of which have point symmetry 2. As can be seen in Figure 9, the oxygen atoms on one side of the octahedron strip are A-type oxygen atoms and the oxygen atoms on the other side of the octahedron strip are B-type oxygen atoms, with the exception of the $O(3)$ and $O(7)$ oxygen atoms, for each of which there is only one symmetrically distinct site. There are two distinct $M(4)$ sites, $M(4A)$ and $M(4B)$, each of which has point symmetry 2 and eight adjacent oxygen atoms to which the constituent cations are bonded. The A cation occupies the $A(2)$ site, an off-centered site within the A cavity that is displaced toward the $T(1B)$ site that is occupied by Be in the only amphibole with this space-group symmetry: joesmithite, $Pb^{2+} Ca_2 Mg_5 (Si_6 Be_2) O_{22} (OH)_2$.

The $Pnma$ amphibole structure

A schematic representation of the $Pnma$ structure type is shown in Figure 10. There are four distinct T sites that are occupied by the T cations, $T1A$, $T1B$, $T2A$ and $T2B$, that are tetrahedrally coordinated and link to form two distinct types of double-chain of tetrahedra, the A-chain

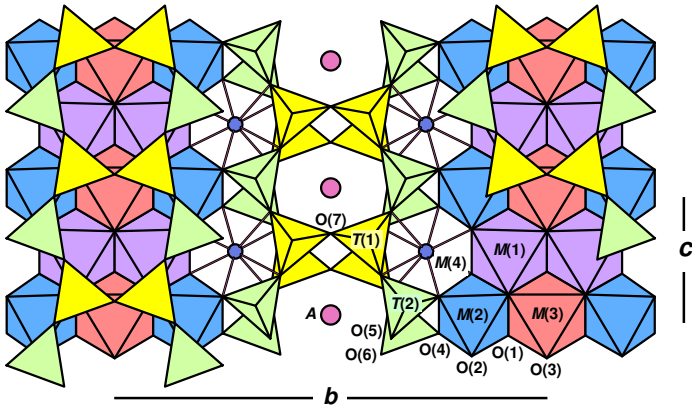


Figure 7. The $C2/m$ amphibole structure projected onto (100); polyhedra: $T(1)$ = yellow, $T(2)$ = pale green, $M(1)$ = mauve, $M(2)$ = blue, $M(3)$ = red; sites: $M(4)$ = blue circle, A = fuchsia circle.

Figure 8. The $P2_1/m$ amphibole structure projected onto (100); polyhedra: $T(1A)$ = bright yellow, $T(2A)$ = bright green, $T(1B)$ = pale yellow, $T(2B)$ = pale green, $M(1)$ = mauve, $M(2)$ = blue, $M(3)$ = red; sites: $M(4)$ = blue circle.

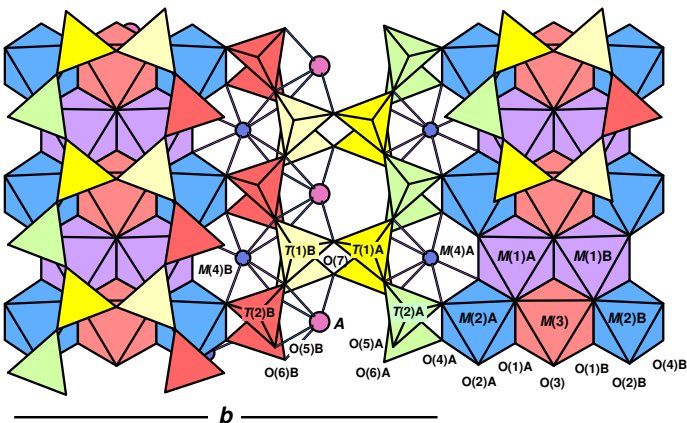
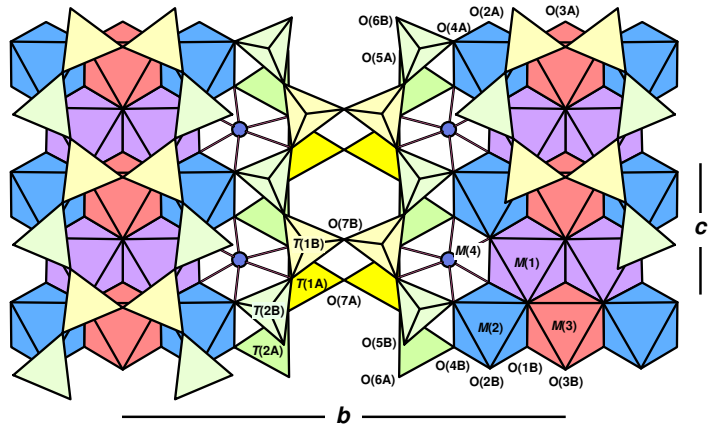


Figure 9. The $P2/a$ amphibole structure projected onto (100); polyhedra: $T(1)A$ = bright yellow, $T(2)A$ = bright green, $T(1)B$ = red, $T(2)B$ = pale green, $M(1)A$ = $M(1)B$ = mauve, $M(2)A$ = $M(2)B$ = dark blue, $M(3)$ = red; sites: $M(4)A$ = $M(4)B$ = blue circle.

and the B-chain. As with the $P2_1/m$ structure, cations labeled A always bond to anions labeled A, and likewise for the atoms labeled B.

There are three distinct M sites that are occupied by the C cations, $M1$, $M2$ and $M3$, with point symmetries 1, 1 and $2/m$, respectively. As with the $P2_1/m$ structure, the A-type cations are on one side and the B-type cations are on the other side of the strip of octahedra. The $M4$ site has point symmetry 2 and is occupied by the B cations. It is surrounded by an antiprism of eight oxygen atoms not all of which necessarily bond to the central cation. The A site occurs at the center of the cavity between the back-to-back double-chains of the structure (Fig. 10). The center of the cavity has point symmetry m , and unlike in the $C2/m$ structure, the A cations actually occupy the special position at the center of the cavity .

The $Pnmm$ amphibole structure

A schematic representation of the $Pnmm$ structure type is shown in Figure 11. There are two distinct T sites that are occupied by the T cations, $T1$ and $T2$, that are tetrahedrally coordinated

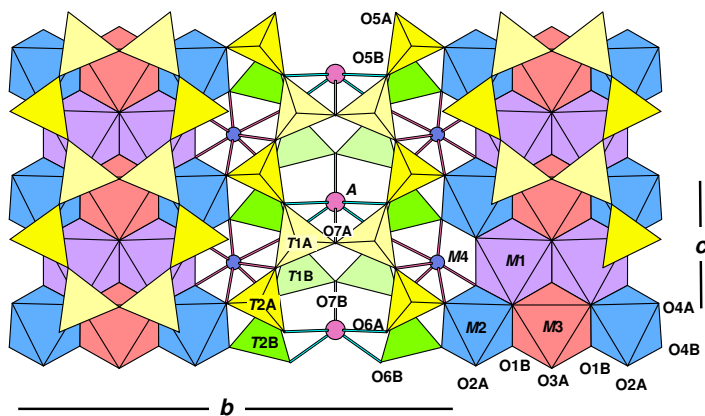


Figure 10. The $Pnma$ amphibole structure projected onto (100); polyhedra: $T1A$ = pale yellow, $T2A$ = bright yellow, $T1B$ = pale green, $T2B$ = bright green, $M1$ = mauve, $M2$ = blue, $M3$ = red; sites: $M4$ = blue circle, A = fuchsia circle.

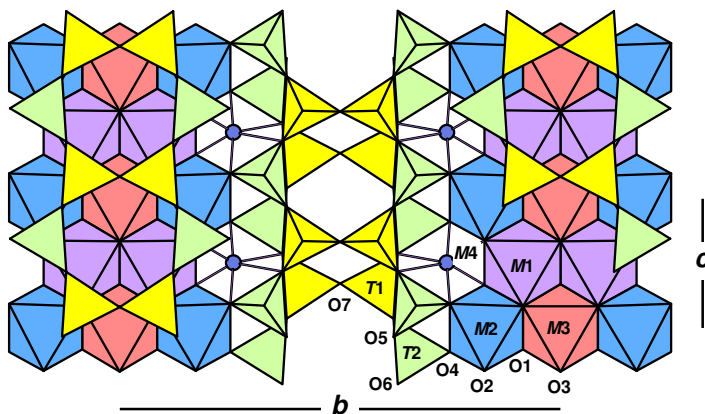


Figure 11. The $Pnmm$ amphibole structure projected onto (100); polyhedra: $T1$ = yellow, $T2$ = green, $M1$ = mauve, $M2$ = blue, $M3$ = red; sites: $M4$ = blue circle.

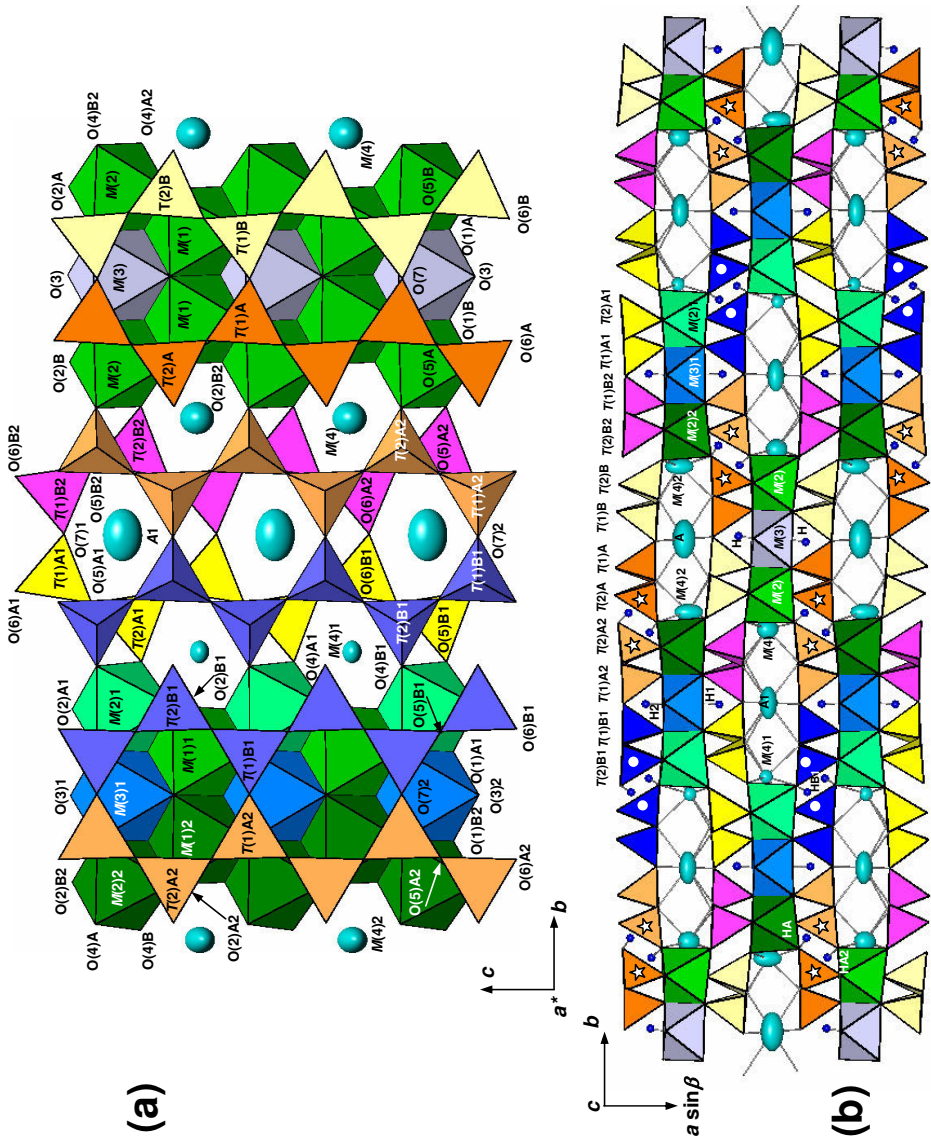
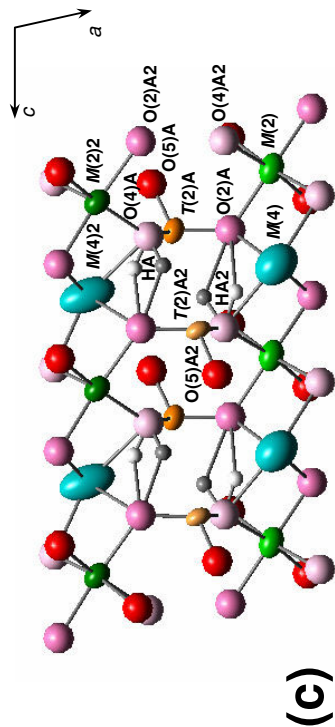
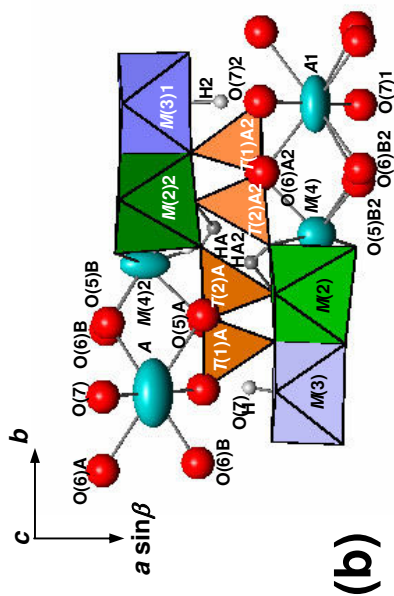
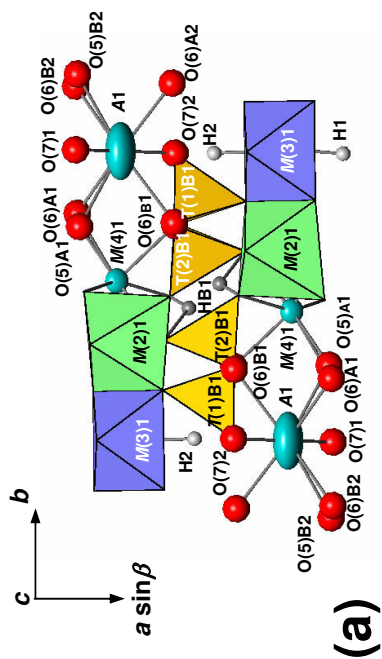


Figure 12. The $C\bar{1}$ amphibole structure ($b = 54.082 \text{ \AA}$) of synthetic $\text{Na Na}_4 \text{Mg}_5 \text{Si}_8 \text{O}_{21}(\text{OH})_3$; (a) projection onto (100); (b) projection onto (001) [note the distinct positions of the $M(4)$ and A sites]. Note the calculated position for the third proton in the unit formula (modified from Cámara et al. 2004).

Figure 13. Possible locations of the excess protons in synthetic $\text{Na Na}_2 \text{Mg}_5 \text{Si}_8 \text{O}_{21} (\text{OH})_3$. Option 1 [H atoms falling outside the $M(4)$ cavity] is shown in gray, option 2 [H atom falling inside the $M(4)$ cavity] is shown in white. (a) HB1-HB1 environment, projection onto (001); (b) HA-HA2 environment, projection onto (001); (c) HA-HA2 environment, projection onto (010). Whatever the solution, excess protons are bonded to the O(4) oxygen atoms farthest from $M(4)$ (modified from Cámara et al. 2004).



and link to form only one distinct type of double-chain of tetrahedra.

There are three distinct M sites that are occupied by the C cations, $M1$, $M2$ and $M3$, with point symmetries 2, 2 and $2/m$, respectively. The coordination of these sites is similar to that of the analogous sites in the $C2/m$ structure. The $M4$ site has point symmetry 2 and is occupied by the B cations. It is surrounded by an antiprism of eight oxygen atoms not all of which bond to the central cation. The A site occurs at the center of the cavity between the back-to-back double-chains of the structure (Fig. 11), it has point symmetry $2/m$.

The $C\bar{1}$ amphibole structure

This structure has only been recorded for one very peculiar composition of a synthetic amphibole: $\text{NaNa}_2\text{Mg}_5\text{Si}_8\text{O}_{21}(\text{OH})_3$ which has one H in excess with respect to the standard amphibole formula (Maresch et al. 1991; Cámara et al. 2004). The site nomenclature was derived by analogy with the monoclinic and orthorhombic structures (Fig. 12a). However, the triclinic nature of the structure, coupled with a b cell-dimension of 54.082 Å (i.e., three times the usual amphibole b edge) increases the complexity of the description. The simplest approach is to take into account the I beams (i.e., the structure module parallel to c which is formed by a strip of octahedra and the two adjacent double-chains of tetrahedra which lay above and below in the $a \sin \beta$ direction). There are two types of I-beams, and their arrangement is shown in Figure 12b.

I-beam I is centrosymmetric. The two sides of the double-chain of tetrahedra in the (100) projection (Fig. 12a) are no longer equivalent, and are named A and B in analogy with the $P2/a$ amphibole structure: $T(1)A$, $T(2)A$, $T(1)B$, and $T(2)B$. These sites repeat themselves (by the $\bar{1}$ operation) in the double chain below the strip of octahedra (cf. the center of Fig. 12b). I-beam I has three [6]-coordinated sites ($M(1)$, $M(2)$ and $M(3)$), and one [7]-coordinated $M(4)$ site. With the exception of O(3) and O(7), all anion sites are duplicated with respect to the $C2/m$ structure, and are named with regard to the T sites to which they are bonded, e.g., O(1)A and O(1)B. There is only one independent H site. The A site is [6]-coordinated and has point symmetry $\bar{1}$.

I-beam II is non-centrosymmetric. Therefore, all the T sites above and below the ribbon of octahedra are no longer equivalent, and a third index must be added to the site name: it is 1 when the tetrahedra are adjacent to I-beam I, e.g., $T(1)A1$, $T(2)A1$, $T(1)B1$ and $T(2)B1$, and 2 when they are adjacent to I-beam II, e.g., $T(1)A2$, $T(2)A2$, $T(1)B2$ and $T(2)B2$. I-beam II has five independent octahedrally coordinated sites: $M(1)1$, $M(1)2$, $M(2)1$, $M(2)2$ and $M(3)1$, and two independent [7]-coordinated $M(4)$ sites: $M(4)1$ and $M(4)2$, where the labels 1 and 2 have the same meaning as for the T sites. I-beam II has twenty-four anion sites. With the exceptions of O(3)1, O(3)2, O(7)1 and O(7)2, for which the index 1 or 2 is arbitrarily chosen, O atoms take their designations from the T site to which they are bonded. Two independent H atoms, H1 and H2, are bonded to O(3)1 and O(3)2, respectively. Above and below I-beam II, there are [8]-coordinated $A(1)$ sites with point symmetry 1 (Fig. 12b).

The $C\bar{1}$ symmetry for the triple- b cell derives from the fact that the two distinct I-beams alternate along b in the sequence $I-II-I-II-I$, the two adjacent I-beams II being related by a center of symmetry coinciding with the A site (Fig. 12b).

The geometries of the double-chains of tetrahedra are significantly different. In I-beam I, the double chain is O-rotated, and both the A- and B-chains have O(5)-O(6)-(O5) angles similar to those found in $C2/m$ amphiboles (O(5)A-O(6)A-O(5)A = 172.8° and O(5)B-O(6)B-O(5)B = 170.4°; cf. Hawthorne 1983a for references). In I-beam II, one double chain is S-rotated (O(5)A2-O(6)A2-O(5)A2 = 183.9° and O(5)B1-O(6)B1-O(5)B1 = 184.0°), whereas the other double-chain is O-rotated (O(5)A1-O(6)A1-O(5)A1 = 162.4° and O(5)B2-O(6)B2-O(5)B2 = 163.5°). The Na atoms at the $M(4)1$ and $M(4)2$ sites have coordination [7] and are displaced significantly along the a and c axes relative to the analogous positions on the diad in the $C2/m$ structure. They have one short and one long $M(4)$ -O(4) distance, and one short and one long $M(4)$ -O(2) distance.

The third proton could not be located from difference-Fourier analysis. Bond-valence calculations [using values from Brown and Altermatt 1985 for Mg-O and Na-O, and from Brese and O'Keeffe (1991) for Si-O] shows that there are two pairs of O(4) anions which are strongly bond-valence deficient: O(4)A, O(4)B1 with 1.50 vu (valence units), and O(4)A2, O(4)B2 with 1.77 vu, and one pair with a nearly ideal value: O(4)B and O(4)A1 with 1.96 vu). Three O(2) sites, O(2)A, O(2)A2 and O(2)B1, are also slightly deficient, suggesting H-bond interactions. Stereochemical analysis shows that in the I-beam II modules, pairs of adjacent $M(4)1$ sites have two different and alternating spatial relations along $a \sin \beta$, one with a shorter $M(4)1-M(4)1$ separation (4.508 Å) and the other with a longer separation (5.599 Å). In the latter case, an excess proton could occur in the pseudo-tetrahedral cavity between two $T(2)B1$ tetrahedra (marked with a white dot in Fig. 12b). A different situation is encountered where B-type sites adjacent to an I-beam I and to an I-beam II (i.e., $M(4)$ and $M(4)2$) alternate along $a \sin \beta$. $M(4)2$ has a very large atomic-displacement, with the major component of the ellipsoid along $a \sin \beta$. It is thus possible to have a proton bonded to the O(4)A site where Na at $M(4)2$ is displaced away from the pseudo-tetrahedral cavity. Thus, the proton could protrude into the pseudo-tetrahedral cavity between two $T(2)A$ and $T(2)A2$ tetrahedra (marked with a white star in Fig. 12b). With only one of the pair of H sites occupied in each cavity, the atom multiplicities for HB1, HA, and H2A are all 2, leading to one excess H pfu ($Z = 6$). Each proton would supply 0.4 vu to the O(4) donor and 0.1 vu to the O(2) acceptor, in good agreement with bond-valence calculations. Possible models for the local stereochemistry of these protons were derived from bond-lengths consideration and are given in Figure 13.

STACKING SEQUENCES AND SPACE GROUPS

Amphiboles may be considered as sheets of octahedra and tetrahedra stacked along the a -direction (Fig. 14). Different ordered

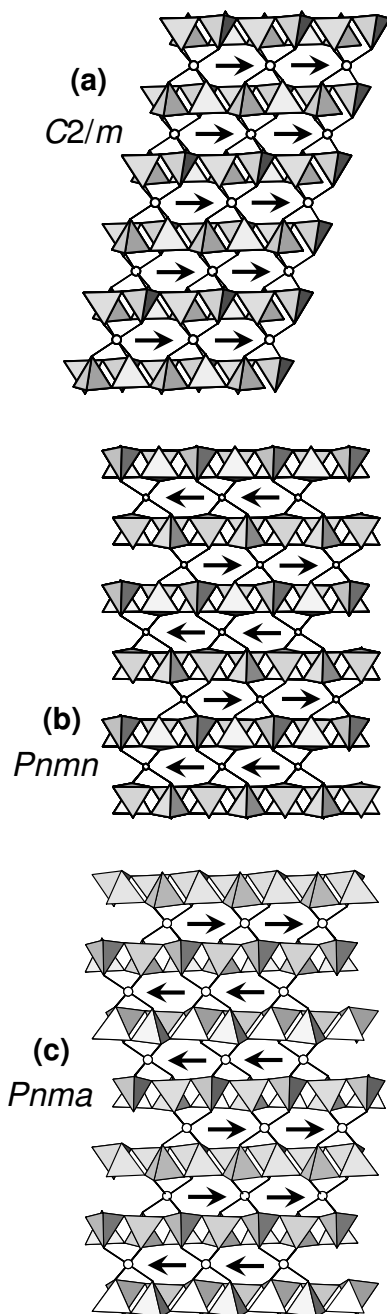


Figure 14. Schematic representation of the stacking of layers projected down the y -axis for the various amphibole structure types: the $P2_1/m$ and $P2_1a$ sequences are the same as for the $C2/m$ structure type and are not shown here.

stacking sequences of these sheets of tetrahedra and octahedra (Gibbs 1966) are associated with the different space-group symmetries of the amphiboles. The space groups $P2_1/a$ and $P2_1/m$ are subgroups of $C2/m$ and involve the same bond topology, and hence we may consider only the space groups $C2/m$, $Pnma$ and $Pnmn$ in this regard. The stacking sequences are shown schematically in Figure 14. The apical O atoms of the tetrahedra provide the anions for the coordination of the octahedra, and hence there is a stagger of $\pm c/3$ between adjacent sheets of tetrahedra. For monoclinic amphiboles, this stagger is always in the same direction (Fig. 14a). For the orthorhombic amphiboles, a regular reversal of this stagger is necessary such that the periodicity in the a -direction is orthogonal to the plane of the sheets. For the $Pnma$ structure, the stagger between adjacent sheets of tetrahedra is $[+c/3, +c/3, -c/3, -c/3]$ (Fig. 14c), whereas for the $Pnmn$ structure type, the stagger between adjacent sheets of tetrahedra is $[+c/3, -c/3, +c/3, -c/3]$ (Fig. 14b).

BOND LENGTHS AND BOND VALENCES IN $^{[4]}\text{Al}$ -FREE AMPHIBOLES

This topic is examined extensively in Hawthorne (1983a) and will be treated only briefly here. Variations in bondlengths can be explained in terms of bond-valence theory (Brown 1981, 2002; Hawthorne 1992, 1994, 1997). Bond-valence tables for selected $^{[4]}\text{Al}$ -free amphiboles are shown in Table 5. The oxygen atoms at O(1), O(2) and O(3) are [4]-coordinated [O(3) is only [3]-coordinated where occupied by F, Cl or O], those at O(4), O(5) and O(6) are [3]-coordinated and O(7) is [4]-, [3]- or [2]-coordinated depending on the nature of the O(3) anion and the occupancy of the A site. The O(1), O(2) and O(4) oxygen atoms are linked to one Si cation. As O(1) and O(2) are [4]-coordinated, their bond-valence requirements are easily satisfied without any major deviations of the incident bondlengths from their mean values. However, O(4) is only [3]-coordinated and hence all bondlengths to O(4) are the shortest of their constituent polyhedra (Table 5). Where O(3) is occupied by (OH), the oxygen atom is bonded to 4 cations: $2 \times M(1) + M(3) + \text{H}$ and the incident bond-valence requirements are easily satisfied. The O(5), O(6) and O(7) oxygen atoms are each linked to two Si cations; in addition, O(5) and O(6) are linked to the $M(4)$ cation via long bonds in accord with their coordination by two Si cations. As a result, the bonds from Si to O(5) and O(6) are usually longer than the $\langle\text{Si-O}\rangle$ bondlengths [and the resulting bond-valences are < 1.00 vu]. The O(7) oxygen atom can be [2]-, [3]- or [4]-coordinated, depending on the type of O(3) anion present and whether the A site is occupied or vacant: [2]-coordinated: O(3) = (F,Cl,O), $A = \square$; [3]-coordinated: O(3) = (F,Cl,O), $A = (\text{Na},\text{K},\text{Ca})$; [3]-coordinated: O(3) = (OH), $A = \square$; [4]-coordinated: O(3) = (OH), $A = (\text{Na},\text{K},\text{Ca})$. The lower the coordination number of O(7), the shorter is the $T(1)$ -O(7) bond and the larger is its corresponding bond-valence (compare fluorotremolite, tremolite, fluororichterite and ferroglaucophane in Table 5). Thus it can be seen that the bond-valence requirements of the anions in the amphibole structure (together with the type of cations at the different cation sites in the structure) dictate the variations in bondlengths in the amphibole structure.

THE DOUBLE-CHAIN OF TETRAHEDRA IN $^{[4]}\text{Al}$ AMPHIBOLES

The substitution of $^{[4]}\text{Al}$ for Si is a major factor in the crystal chemistry of the amphiboles. Reported $^{[4]}\text{Al}$ contents vary between 0.0 and 3.5 apfu, although occurrences in which $^{[4]}\text{Al}$ exceeds 2.00 apfu are relatively uncommon, but not rare (Bunch and Okrusch 1973; Appleyard 1975; Hawthorne and Grundy 1977; Shimazaki et al. 1984; Mogessie et al. 1986; Sawaki 1989; Previde Massara 1990; Oberti et al. 1995a; Banno et al. 2004; Hawthorne and Harlow 2007; Nishio-Hamane pers. comm.). The $^{[4]}\text{Al}$ content of an amphibole is dependent on (1) bulk-rock composition, and (2) the pressure and temperature of crystal/equilibrium of the amphibole (Oberti et al. 1995a).

Table 5. Bond-valence (vu) tables for selected ¹⁴¹Al-free C2/m amphiboles.

	<i>M</i> (1)	<i>M</i> (2)	<i>M</i> (3)	<i>M</i> (4)	<i>A</i>	<i>T</i> (1)	<i>T</i> (2)	Σ	Σ ^p
Cummingtonite: r.m.s. deviations are 3.2% and 9.6%, respectively.									
O(1)	0.375	0.312	0.346 ^{x2} ↓			1.008		2.041	2.000
O(2)	0.325	0.347		0.333			0.992	1.997	2.000
O(3)	0.353 ^{x2} →		0.367					1.073	1.000
O(4)		0.386		0.480			1.035	1.901	1.667
O(5)				(0.045)		1.021	0.956	1.977	2.000
O(6)				0.107		0.984	0.946	2.037	2.333
O(7)						1.024 ^{x2} →		2.048	2.000
Σ	2.103	2.090	2.160	1.840		4.037	3.929		

Tremolite: r.m.s. deviations are 4.4% and 11.3%, respectively.									
O(1)	0.356	0.309	0.351 ^{x2} ↓			1.055		2.071	2.000
O(2)	0.345	0.342		0.287			1.016	1.990	1.917
O(3)	0.342 ^{x2} →		0.361					1.064	1.000
O(4)		0.395		0.341			1.101	1.837	1.583
O(5)				0.133		0.974	0.922	2.029	2.250
O(6)				0.211		0.982	0.878	2.071	2.250
O(7)						1.016 ^{x2} →		2.032	2.000
Σ	2.086	2.092	2.146	1.944		4.027	3.917		

Fluorrichterite (34): r.m.s. deviations are 6.8% and 12.9%, respectively.									
O(1)	0.359	0.278	0.351 ^{x2} ↓			1.113		2.101	2.000
O(2)	0.381	0.359		0.236		0.992	0.992	1.968	1.854
O(3)	0.276 ^{x2} →		0.300			0.951		0.852	1.000
O(4)		0.398		0.273			1.125	1.796	1.521
O(5)				0.103	0.087 ^{x2} ↓		0.910	2.092	2.271
O(6)				0.166	0.061 ^{x2} ↓		0.858	2.036	2.271
O(7)					0.182	0.964 ^{x2} →		2.110	2.200
Σ	2.032	2.070	2.004	1.556	0.956	4.020	3.885		

Ferroglaucophane (69): r.m.s. deviations are 4.1% and 9.2%, respectively.									
O(1)	0.367	0.396	0.339 ^{x2} ↓			0.992		2.094	2.167
O(2)	0.361	0.476		0.193			0.977	1.947	1.958
O(3)	0.341 ^{x2} →		0.382					1.064	1.000
O(4)		0.605		0.220			1.072	1.897	1.625
O(5)				0.094		1.019	0.927	2.040	2.125
O(6)				0.175		0.997	0.917	2.089	2.125
O(7)						1.013 ^{x2} →		2.026	2.000
Σ	2.138	2.954	2.120	1.364		4.021	3.893		

^p Formal (Pauling) bond-strength

Variation in $\langle T-O \rangle$ bondlengths in $C2/m$ amphiboles

There have been numerous treatments of this issue (Papike et al. 1969; Hawthorne and Grundy 1973a,b, 1977; Robinson et al. 1973; Bocchio et al. 1978; Hawthorne 1981, 1983a,c; Oberti et al. 1995a), and although the relations between Al content and mean bondlengths have been improving, the current state of affairs is still far from ideal. Hawthorne (1976) and Ungaretti (1980) suggested that variations in $\langle T-O \rangle$ distances occur as a result of other cation substitutions in the amphibole structure. We may see this in the variation in $\langle T(1)-O \rangle$ and $\langle T(2)-O \rangle$ distances in $^{[4]}Al$ -free amphiboles (Fig. 15). If there is such a relation in $^{[4]}Al$ -free amphiboles, it seems probable that there is a similar relation in $^{[4]}Al$ -bearing amphiboles, particularly at the $T(2)$ site (Ungaretti 1980). Oberti et al. (1995a) incorporated such changes into a relation for the $T(2)$ site, but the relation does not work well for very Al-rich amphiboles. Consequently, it seemed desirable to reconsider this issue here. Data are taken from structure refinements selected from those listed in Appendix I; only about 50% of the structure refinements were used for this purpose as the remainder were identified as containing significant errors, particularly in the assigned site-populations.

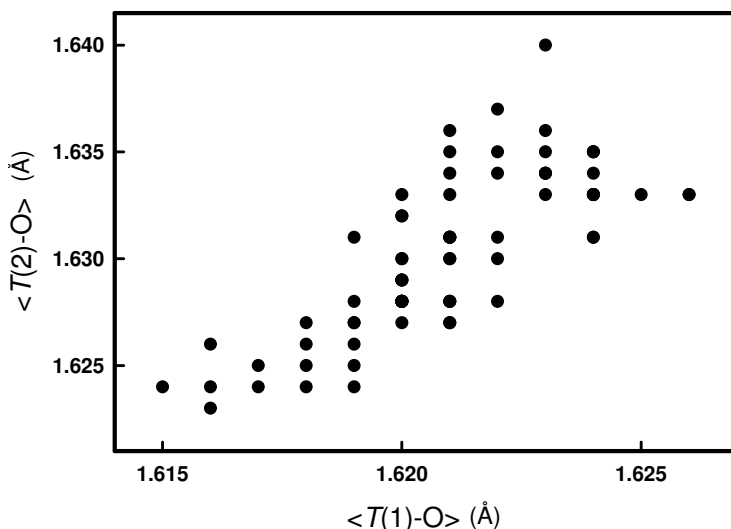


Figure 15. Variation in $\langle T(1)-O \rangle$ and $\langle T(2)-O \rangle$ distances for $C2/m$ amphiboles with $^{[4]}Al < 0.06$ apfu.

$\langle\langle T-O \rangle\rangle$ as a function of $^{[4]}Al$. The variation of $\langle\langle T-O \rangle\rangle$ as a function of $^{[4]}Al$ is shown in Figure 16a. Given that the average standard deviation of the mean bondlengths is of the order of 0.002 \AA , there is a well-developed linear relation above ~ 0.50 $^{[4]}Al$ apfu and much scatter of the data below ~ 0.50 $^{[4]}Al$ apfu. First, this general relation suggests that a single linear model for the variation of $\langle\langle T-O \rangle\rangle$ may not be appropriate. There is more than one way to approach this issue. We may consider just the data with $^{[4]}Al > 0.50$ apfu and fit a straight line to the data. The result of this is shown in Figure 16b and the resulting regression relations is given in Table 6; the standard error of estimate on the mean bondlength is similar to the estimated standard deviation, suggesting that the variation in $\langle\langle T-O \rangle\rangle$ is affected only by the total $^{[4]}Al$ content for $^{[4]}Al > 0.50$ apfu. Developing the inverse relation (Table 6) predicts the amount of $^{[4]}Al$ (greater than 0.50 apfu) with a standard error of the estimate of 0.08 apfu.

Such a simple model is obviously not adequate for small amounts of $^{[4]}Al$, and a more complicated model was investigated by stepwise multiple regression in the region $Al \leq 0.50$

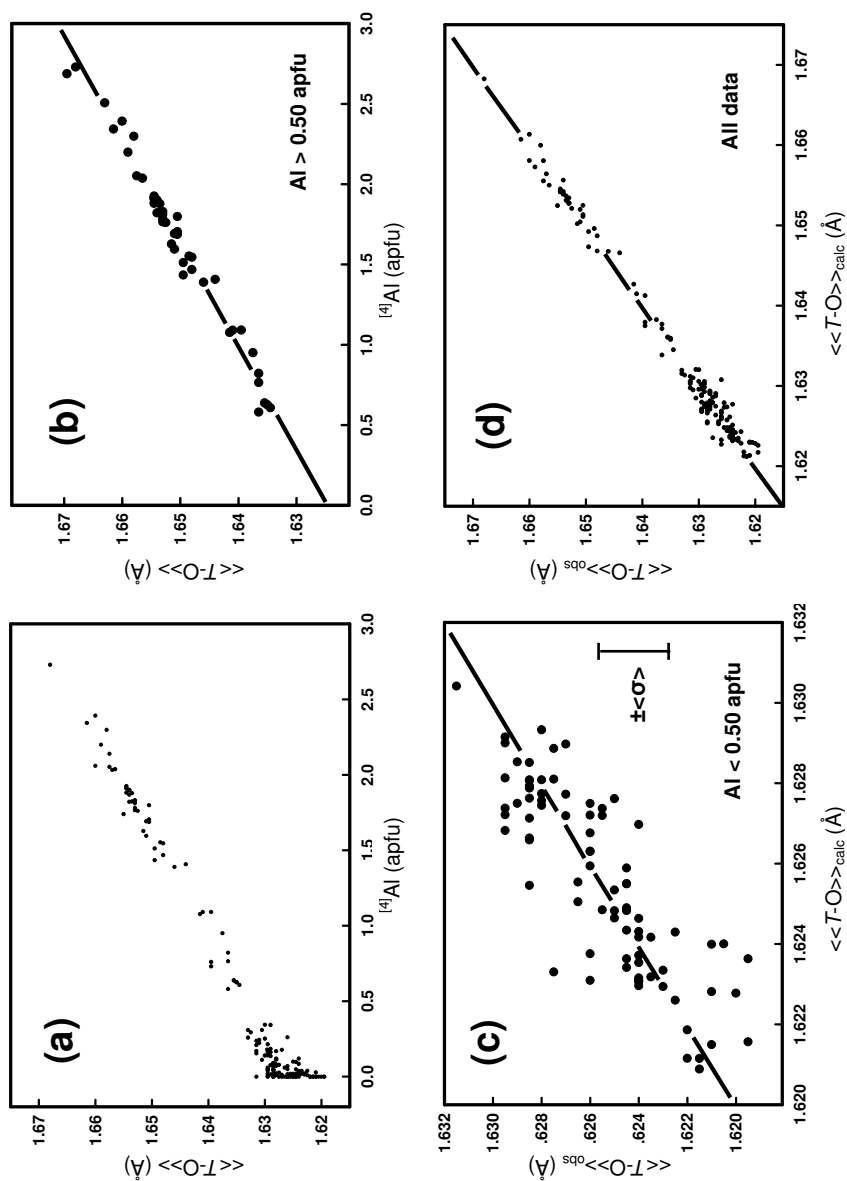


Figure 16. Relations between $\langle\langle T-O \rangle\rangle$ distance and $^{[4]}Al$ content in $C2/m$ amphiboles; (a) $\langle\langle T-O \rangle\rangle$ as a function of $^{[4]}Al$ (all data); (b) $\langle\langle T-O \rangle\rangle$ as a function of $^{[4]}Al$ (where $^{[4]}Al > 0.50$ apfu); (c) observed versus calculated values of $\langle\langle T-O \rangle\rangle$ for amphiboles with $^{[4]}Al < 0.05$ apfu using the stepwise regression results of Table 5, where the 1:1 line is indicated; (d) observed versus calculated values of $\langle\langle T-O \rangle\rangle$ for all amphiboles using the stepwise regression results of Table 5, where the 1:1 line is indicated.

Table 6. Regression results for $\langle T-O \rangle$ (Å) and $^{[4]}Al$ contents (apfu) in $C2/m$ and $Pnma$ amphiboles.

y	x_i	y_0	a_i	R	s^* (Å or apfu)
<u>$C2/m$</u>					
$\langle\langle T-O \rangle\rangle$	$^{[4]}Al$ (>0.50 apfu)	1.6250(6)	0.0153(3)	0.989	0.0012
$^{[4]}Al$ (>0.50 apfu)	$\langle\langle T-O \rangle\rangle$	-102.26(2.26)	62.96(1.37)	0.990	0.08
$\langle\langle T-O \rangle\rangle$	$^{[4]}Al$ (<0.06 apfu)	1.5017	0.014(6)	0.879	0.0014
	$\langle\langle r^{M(1,2,3)} \rangle\rangle$		0.051(9)		
	$\langle r^{O(3)} \rangle$		0.045(14)		
	$\langle r^{M(4)} \rangle$		0.025(2)		
$\langle\langle T-O \rangle\rangle$	$^{[4]}Al$	1.522(11)	0.0156(2)	0.995	0.0013
	$\langle r^{M(1,2,3)} \rangle$		0.0416(6)		
	$\langle r^{O(3)} \rangle$		0.0304(8)		
	$\langle r^{M(4)} \rangle$		0.0246(17)		
	$\langle Z^{M(4)} \rangle$		0.00129(41)		
$^{[4]}Al$	$\langle\langle T-O \rangle\rangle$	-94.4(1.4)	62.6(7)	0.995	0.08
	$\langle r^{M(1,2,3)} \rangle$		-3.69(38)		
	$\langle r^{O(3)} \rangle$		-2.3(5)		
	$\langle r^{M(4)} \rangle$		-1.43(9)		
<u>$C2/m$ for samples with $TAl > 0.50$ apfu</u>					
$\langle T(1)-O \rangle$	$\pi^{(1)}Al$	1.6202(6)	0.0308(4)	0.996	0.0012
$\langle T(2)-O \rangle$	$\pi^{(2)}Al$	1.6293(3)	0.0329(10)	0.981	0.0012
$\pi^{(1)}Al$	$\langle T(1)-O \rangle$	-52.120(699)**	32.177(420)	0.996	0.039
$\pi^{(2)}Al$	$\langle T(2)-O \rangle$	-47.613(1400)	29.228(856)	0.981	0.035
<u>$Pnma$</u>					
$\langle\langle T-O \rangle\rangle$	$^{[4]}Al$	1.6215(9)	0.0173(6)	0.985	0.0015
$^{[4]}Al$	$\langle\langle T-O \rangle\rangle$	-90.98(343)	56.1473(2085)	0.985	0.09

* s = standard error of estimate.

**Values are quoted to several digits in order to avoid significant termination errors.

apfu. The variables that have a significant effect on $\langle\langle T-O \rangle\rangle$ are $^{[4]}Al$, $\langle r^{M(4)} \rangle$ and $\langle r^{M(1,2,3)} \rangle$. The resulting regression equation is given in Table 6 and the observed and calculated $\langle\langle T-O \rangle\rangle$ values are compared in Figure 16c; at first sight, there is a lot of scatter in Figure 16c, but this is not significant in terms of the average standard deviation for the observed data. We also fitted a single model to all the data by stepwise linear regression; the results are given in Table 6 and a comparison of the observed and calculated data is given in Figure 16d. The fit is good, and the regression shows that $\langle\langle T-O \rangle\rangle$ is also affected by $\langle r^{M(1,2,3)} \rangle$, $\langle r^{O(3)} \rangle$ and $\langle r^{M(4)} \rangle$ in that order. We may also use $^{[4]}Al$ as the dependent variable in a stepwise regression to develop a predictive curve for $^{[4]}Al$; the result is given in Table 6.

$\langle T(1)-O \rangle$ and $\langle T(2)-O \rangle$ as a function of $^{[4]}Al$ content. Without independent measurement of the amounts of Al at $T(1)$ and $T(2)$ (e.g., by neutron diffraction or MAS NMR), it is not possible to rigorously assign site populations to $T(1)$ and $T(2)$. However, let us first try and get a sense of the behavior of $\langle T(1)-O \rangle$ and $\langle T(2)-O \rangle$ as a function of $^{[4]}Al$ content; Figure 17 shows this variation. It is immediately apparent from Figure 17 that there are two distinct regimes of behavior of the tetrahedra.

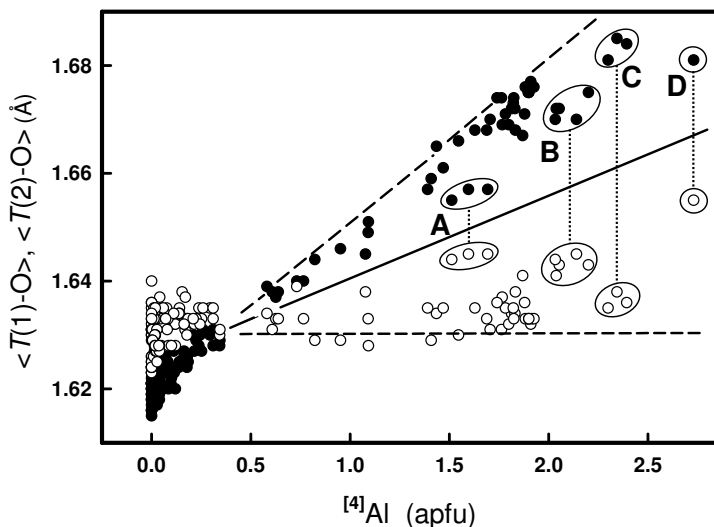


Figure 17. Variation in $\langle T(1)-O \rangle$ (black circles) and $\langle T(2)-O \rangle$ (white circles) as a function of $[{}^{4}\text{Al}]$ in $C2/m$ amphiboles; the full line shows the regression relation from Fig. 16b, the upper dashed line is the limiting envelope for the $T(1)$ data, and the lower dashed line is the reflection of the upper dashed line through the full line parallel to the ordinate. The lines connect values for $T(1)$ (above the full line) and $T(2)$ (below the full line) for specific crystals. See text for the meanings of A, B, C and D.

- (1) below $[{}^{4}\text{Al}] = 0.40$ apfu, the data are densely clustered together; the maximum variation ($1.640 - 1.614 = 0.026$ Å) is at $[{}^{4}\text{Al}] = 0.0$ apfu, and the variation decreases with increasing $[{}^{4}\text{Al}]$ to extrapolate to 0.0 Å at ~ 0.045 $[{}^{4}\text{Al}]$. It is apparent that variation of both $\langle T(1)-O \rangle$ and $\langle T(2)-O \rangle$ are affected by aspects of the structure other than just $[{}^{4}\text{Al}]$ content (note that we already know this in terms of $\langle\langle T-O \rangle\rangle$ (the mean of $\langle T(1)-O \rangle$ and $\langle T(2)-O \rangle$) because of behavior shown in Fig. 16).
- (2) above $[{}^{4}\text{Al}] = 0.50$ apfu, the behavior changes drastically: $\langle T(1)-O \rangle$ increases strongly with increasing $[{}^{4}\text{Al}]$ content (with some scatter), whereas $\langle T(2)-O \rangle$ increases less strongly (but also with considerable scatter).

The solid line in Figure 17 is the regression line from Figure 16b, and Figure 16b also shows that $\langle\langle T-O \rangle\rangle$ values (i.e., $(\langle T(1)-O \rangle + \langle T(2)-O \rangle)/2$) follow this regression line very closely. In Figure 17, the pattern of data scatter about the $\langle\langle T-O \rangle\rangle$ line is extremely informative. Above ~ 0.45 $[{}^{4}\text{Al}]$ apfu, $\langle T(1)-O \rangle$ values fall above the line and $\langle T(2)-O \rangle$ values fall below the line (except for one datum point at $[{}^{4}\text{Al}] \approx 0.7$ apfu). Furthermore, the relative displacements of values on either side of the central line match for each structure. This feature is emphasized in Figure 17 by enclosing data points from specific structures or groups of structures by ellipses and connecting the corresponding $\langle T(1)-O \rangle$ and $\langle T(2)-O \rangle$ ellipses. Several points now become apparent from Figure 17: (1) the coupling of scatter of points about the line implies that their displacements from the central line are due to partial-to-complete order of $[{}^{4}\text{Al}]$ over $T(1)$ and $T(2)$; (2) the pattern of variation of $\langle T(1)-O \rangle$ shows a limiting envelope at higher values, shown by the upper dashed line; (3) the symmetrical equivalent line below the full line is a reasonable limiting envelope for the variation of $\langle T(2)-O \rangle$; (4) the slope of the upper limiting envelope (which was drawn 'by eye') is 0.992 , i.e., not significantly different from 1.0 , the ideal value for a hard-sphere model of $\text{Al} \leftrightarrow \text{Si}$ substitution; this suggests that this envelope provides the limiting line for complete order of $[{}^{4}\text{Al}]$ at $T(1)$; (5) correspondingly, the lower dashed line is the limiting line for zero $[{}^{4}\text{Al}]$ at $T(2)$.

Of course, one expects some scatter of data about a specific relation due to experimental error and inductive effects of the rest of the structure, and hence the two dashed lines might need to be moved slightly closer together (while maintaining the same slopes) to give the true limiting values. The origins of the amphiboles shown in Figure 17 also support this overall interpretation. The amphiboles labeled A are from Punta Falcone, a high-temperature leucogabbro where Oberti et al. (1995a) have identified significant disorder of Al over $T(1)$ and $T(2)$. The amphiboles labeled B are synthetic fluoropargasite (synthesized at 1240 °C for 1 h and cooled to 816 °C over a period of 332 h; Oberti et al. 1995b) and synthetic kaersutites (synthesized at 1270 °C for 1 h, cooled to 1070 °C at 0.5 °C/h, and then held at 1070 °C for 13h; Tiepolo et al. 1999). Synthetic fluoropargasites have a significant cannilloite component (Ca at the A site, a feature which favors incorporation of $^{[4]}Al$ at the $T(1)$ site beyond 2.0 apfu), and amphiboles labeled A and B have unusually high temperatures of synthesis. These features are in intuitive accord with some disorder of $^{[4]}Al$ over $T(1)$ and $T(2)$, and the observed mean bondlengths indicate Al at both $T(1)$ and $T(2)$. The amphiboles labeled C and D are fluorocannilloites and sadanagaite, all with high (> 2.1 apfu $^{[4]}Al$), again in accord with the presence of $^{[4]}Al$ at $T(2)$; in fluorocannillote, the presence of Ca at the A site allows $^{T(1)}Al$ to exceed 2 apfu, whereas in sadanagaite, the lack of significant A-site Ca prevents $^{T(1)}Al$ from significantly exceeding 2 apfu and requires the excess $^{[4]}Al$ beyond 2.0 apfu to occupy $T(2)$.

For amphiboles in which $^{[4]}Al > 0.50$ apfu, Figure 17 also suggests a method for predicting the occupancies of the $T(1)$ and $T(2)$ sites: (1) Consider the data for a single amphibole. The distance between the $T(1)$ datum-point and the upper broken line represents the amount of Al at the $T(1)$ site, and the distance between the $T(2)$ datum-point and the lower broken line represents the amount of Al at the $T(2)$ site. The equation of the upper broken line is $\langle T(1)-O \rangle = 1.620 + 0.0312 \text{ }^{T(1)}Al$ and this can be used to predict an initial estimate of $^{T(1)}Al$ from the observed value of $\langle T(1)-O \rangle$. The relation between the two dashed lines and the central full line in Figure 17 implies that the analogous relation for the $T(2)$ site has the same slope as that for the $T(1)$ site; the intercept of this line can be read from Figure 17: 1.630 Å, and thus the analogous predictive equation for the $T(2)$ site is $\langle T(2)-O \rangle = 1.630 + 0.0312 \text{ }^{T(2)}Al$ and can be used to predict an initial estimate of $^{T(2)}Al$ from the observed value of $\langle T(2)-O \rangle$.

We may then compare the sum of the predicted $^{[4]}Al (= ^{T(1)}Al_{\text{pred}} + ^{T(2)}Al_{\text{pred}})$ with the observed value of $^{[4]}Al$. We may take the difference between these two values and equally distribute the difference between the two values $^{T(1)}Al_{\text{pred}} + ^{T(2)}Al_{\text{pred}}$ and re-examine the relation between $\langle T(1)-O \rangle$ and $\langle T(2)-O \rangle$ and the modified values of $^{T(1)}Al_{\text{pred}} + ^{T(2)}Al_{\text{pred}}$. This is done in Figure 18, and the results of regression analysis are given in Table 6 for both $\langle T(1)-O \rangle$, $\langle T(2)-O \rangle$ in terms of $^{T(1)}Al_{\text{pred}}$, $^{T(2)}Al_{\text{pred}}$. We also did the inverse regressions to give $^{T(1)}Al_{\text{pred}} + ^{T(2)}Al_{\text{pred}}$ as the dependent variables (Table 6). These relations may be used to give the Al contents of the $T(1)$ and $T(2)$ sites with standard errors of estimate of ~ 0.04 Al apfu for amphiboles with $^{T}Al > 0.50$ apfu. It is apparent from Figure 17 that for amphiboles with $^{T}Al < 0.50$ apfu, there are not any simple relations between $\langle T(1)-O \rangle$, $\langle T(2)-O \rangle$ and $^{T(1)}Al$, $^{T(2)}Al$. The regression with $\langle T-O \rangle$ as the dependent variable in Table 6 involves $^{[4]}Al$, $\langle r^{M(1,2,3)} \rangle$, $\langle r^{O(3)} \rangle$, $\langle r^{M(4)} \rangle$ and $\langle Z^{M(4)} \rangle$ as independent variables, and there is no way of evaluating the different effects of $\langle r^{M(1,2,3)} \rangle$, $\langle r^{O(3)} \rangle$, $\langle r^{M(4)} \rangle$ and $\langle Z^{M(4)} \rangle$ on $\langle T(1)-O \rangle$ and $\langle T(2)-O \rangle$ separately. This issue will be addressed in Oberti et al. (2007b) based on regression analysis of the whole CNR-IGG-PV database; in this way, a predictive equation was obtained for $^{T(1)}Al$ (but not for $^{T(2)}Al$) in all the compositional range.

Variation in $\langle T-O \rangle$ bondlengths in *Pnma* amphiboles

Until recently, there has not been much crystal-structure information available on amphiboles of the anthophyllite-gedrite group. Hawthorne (1983a) synthesized the available information, presented a relation between $\langle T-O \rangle$ distance and $^{[4]}Al$ content, and developed predictive curves for the four symmetrically distinct tetrahedrally coordinated sites: $T1A$, $T1B$,

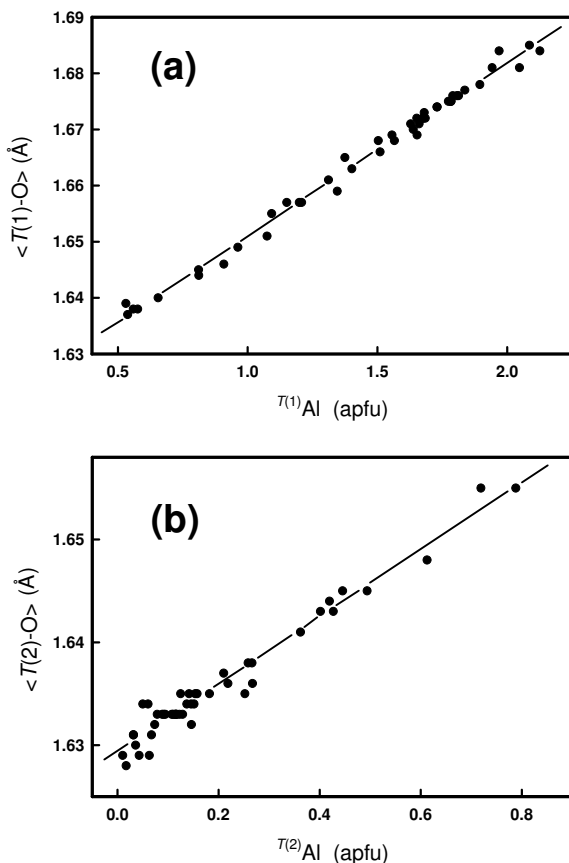


Figure 18. Relations between $\langle T-O \rangle$ distance and $^{[4]}\text{Al}$ content in $C2/m$ amphiboles; (a) $\langle T(1)-O \rangle$ as a function of $T(1)\text{Al}$; (b) $\langle T(2)-O \rangle$ as a function of $T(2)\text{Al}$.

$T2A$, $T2B$. Recently, Schindler et al. (2007) refined the structures of 26 anthophyllite-gedrite amphiboles and examined the stereochemistry of the $Pnma$ amphibole double-chain; these results are given below.

$\langle\langle T-O \rangle\rangle$ as a function of $^{[4]}\text{Al}$. The relation between $^{[4]}\text{Al}$ and the $\langle\langle T-O \rangle\rangle$ distance is shown in Figure 19. The data form a linear trend with a slope that is not significantly different from that characteristic of a hard-sphere model. Two of the data points in the central region fall 0.003–0.004 Å below the general trend. As crystals in this compositional range may be affected by unmixing, these two points were omitted from the linear regression, the results of which are given in Table 6.

$\langle T1A-O \rangle$, $\langle T1B-O \rangle$, $\langle T2A-O \rangle$ and $\langle T2B-O \rangle$ as a function of $^{[4]}\text{Al}$ content. There are four symmetrically distinct cation sites with tetrahedral coordination in the orthorhombic ($Pnma$) amphibole structure: $T1A$, $T2A$, $T1B$ and $T2B$ (Fig. 10). Hawthorne et al. (2007a) developed predictive curves relating the individual $\langle T-O \rangle$ distances to $^{[4]}\text{Al}$ content assuming that the slopes of the curves are the same.

The site occupancies predicted from the equations in Table 6 were adjusted slightly so as to accord exactly with the $^{[4]}\text{Al}$ determined by electron-microprobe analysis, and the $\langle T-O \rangle$

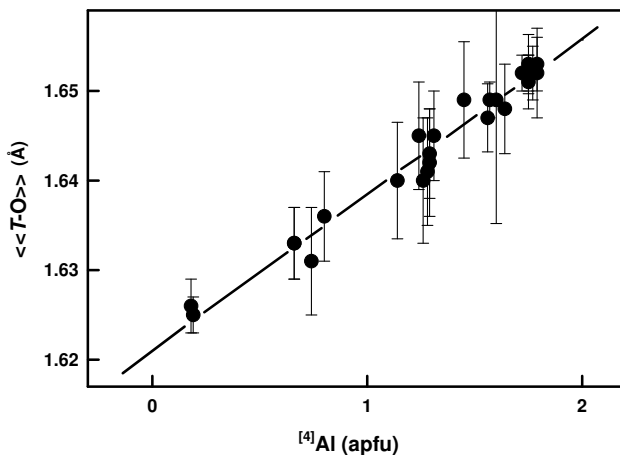


Figure 19. The relation between $\langle\langle T-O \rangle\rangle$ distance and $[4]Al$ in $Pnma$ amphiboles.

distances are shown as a function of constituent Al in Figure 20, where the lines in the figures are the relevant equations of Table 6. As is apparent, $[4]Al$ is ordered over the non-equivalent T sites in the sequence $T1B > T1A > T2B > T2A$.

THE STEREOCHEMISTRY OF THE STRIP OF OCTAHEDRA

The strip of octahedra is the most compliant part of the amphibole structure and shows the greatest variation in size and valence of substituent cations and anions: it accepts cations from 0.535 Å ($[6]Al$) to 0.83 Å ($[6]Mn^{2+}$) and from 1⁺ (Li) to 4⁺ (Ti^{4+}) (and V^{5+} , Nb and Ta in synthetic samples), and the O(3) site can contain (OH), F, Cl and O. There are at least three octahedrally coordinated cation sites in all amphibole structures, and both long-range and short-range cation order can be important factors in their crystal chemistry. There has been an enormous amount of diffraction and spectroscopic work on the cation and anion order in amphiboles (Oberti et al. 2007a; Hawthorne and Della Ventura 2007), and here we examine the stereochemistry of the octahedron strip.

The $C2/m$ amphiboles: variation in mean bondlengths

Variation in $\langle\langle M(1,2,3)-O \rangle\rangle$ distances. The variation in $\langle\langle M(1,2,3)-O \rangle\rangle$ bondlength as a function of the aggregate constituent $M(1,2,3)$ cation radius is shown in Figure 21a, and the results of linear regression are shown in Table 7. There is quite a lot of scatter in Figure 21a and the standard error of estimate from the regression is 0.006 Å. The $\langle\langle M(1,2,3)-O \rangle\rangle$ bondlength will also be affected by the type of anion occupying the O(3) site, as the sizes of the constituent [3]-coordinated anions are significantly different: OH = 1.34, F = 1.30, O = 1.36 Å. In addition, there may be other inductive effects that also affect the $\langle\langle M(1,2,3)-O \rangle\rangle$ bondlength. This issue was examined by stepwise linear regression using the mean constituent ionic radii at the sites in the $C2/m$ amphibole structure, and the results are given in Table 7. $\langle\langle M(1,2,3)-O \rangle\rangle$ is significantly affected by $\langle\langle r^{M(1,2,3)} \rangle\rangle$ and $\langle r^{O(3)} \rangle$ as expected, but also is affected inductively by $\langle r^{M(4)} \rangle$, the mean radius of the cations at the $M(4)$ site. The standard error of estimate is now 0.0028 Å and the correlation coefficient is 0.99; a comparison of the observed and calculated $\langle\langle M(1,2,3)-O \rangle\rangle$ distances is shown in Figure 21b.

Variation in $\langle M(2)-O \rangle$ distances. Figure 22b shows the variation in $\langle M(2)-O \rangle$ as a function of the aggregate size of the constituent cations, $\langle r^{M(2)} \rangle$. There is a well-developed

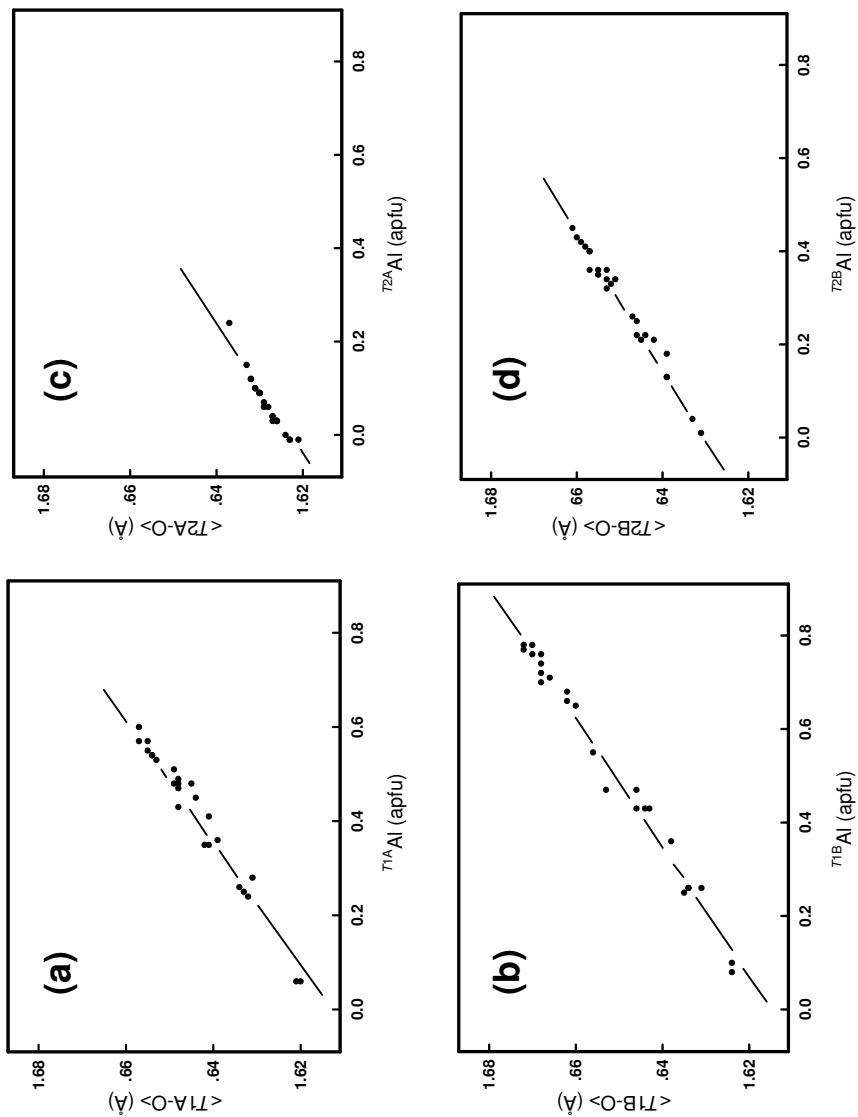


Figure 20. Relations between $\langle T-O \rangle$ distance and Al occupancy in *Pnnia* amphiboles; (a) T1A; (b) T1B; (c) T2A; (d) T2B.

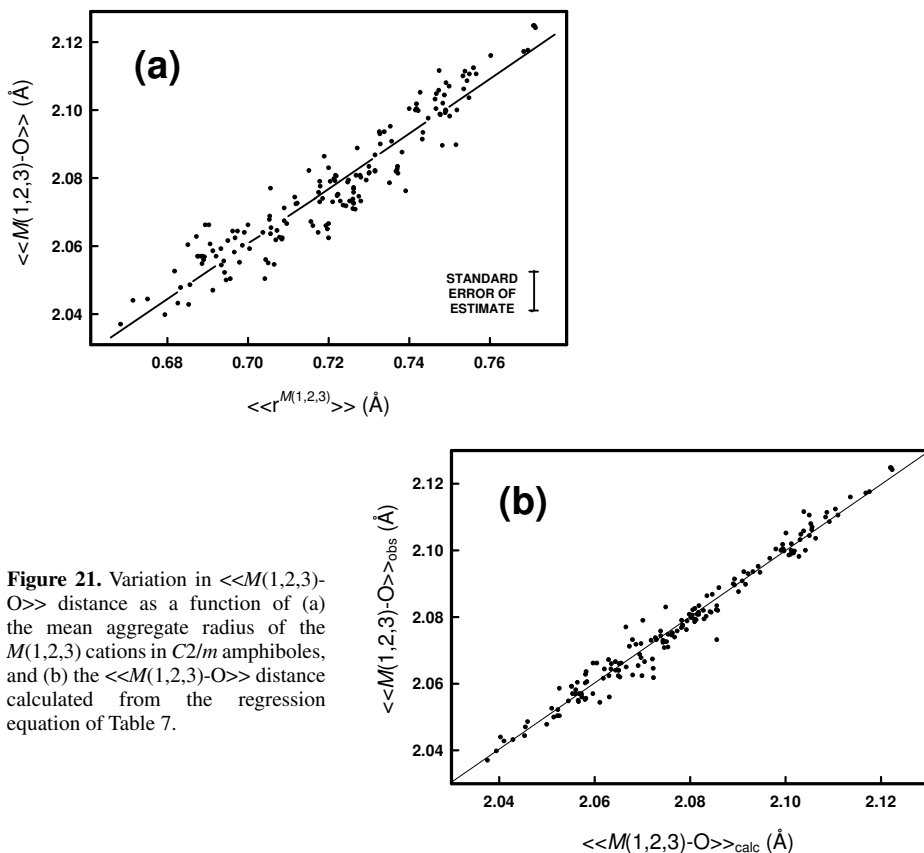


Figure 21. Variation in $\langle M(1,2,3)-O \rangle$ distance as a function of (a) the mean aggregate radius of the $M(1,2,3)$ cations in $C2/m$ amphiboles, and (b) the $\langle M(1,2,3)-O \rangle$ distance calculated from the regression equation of Table 7.

linear correlation, and the results of linear-regression analysis are given in Table 7. Possible inductive effects were investigated by stepwise linear regression using the ${}^T\text{Al}$ content, the mean radii at $M(1,3)$, $M(4)$ and $O(3)$ and the mean formal charges at the $M(4)$ and A sites, but none of these parameters had a significant effect. The regression equation is given in Table 7, and Figure 22e shows the comparison between the observed and predicted $\langle M(2)-O \rangle$ distances.

Variation in $\langle M(1)-O \rangle$ and $\langle M(3)-O \rangle$ distances. The situation for the $M(1)$ and $M(3)$ sites is somewhat more complicated than for the $M(2)$ site, as $M(1)$ and $M(3)$ are coordinated by the $O(3)$ site that shows variable occupancy of OH, F, Cl and O, all of which have significantly different radii: ${}^{13}\text{OH} = 1.34$, ${}^{13}\text{F} = 1.30$, ${}^{13}\text{O} = 1.36$ Å. Figures 22a and 22c show the variation in $\langle M(1)-O \rangle$ and $\langle M(3)-O \rangle$, respectively, as functions of $\langle r^{M(1)} \rangle$ and $\langle r^{M(3)} \rangle$. There is a lot of scatter in the relations, as expected as the graphs do not include the effects of different anions at the $O(3)$ site. In addition, there may be other inductive effects; this issue was examined by stepwise linear regression, and the results are given in Table 7. $\langle M(1)-O \rangle$ and $\langle M(3)-O \rangle$ are significantly affected by $\langle r^{M(1,2,3)} \rangle$, $\langle r^{O(3)} \rangle$ as expected, but inductively by the size of the $M(4)$ cation and the amount of tetrahedrally coordinated Al. The standard errors of estimate are 0.0027 Å and 0.0065 Å, respectively; comparisons of the observed and calculated $\langle M(1)-O \rangle$ and $\langle M(3)-O \rangle$ distances are shown in Figures 22d and 22f, respectively.

Indeed, Oberti et al. (2007c) compared the refined $\langle M(1)-O \rangle$ and $\langle M(3)-O \rangle$ bondlengths in glaucophane, nyböite, fluoronyböite, aluminotaramite, alumino-magnesirotaramite and fluoro-

Table 7. Regression results for $^{[6]}M$ -sites and aggregate radii of cations at M -sites for $C2/m$ and $Pnma$ amphiboles.

y	x_i	y_o	a_i	R	s^* (Å or apfu)
<u>$C2/m$</u>					
$\langle\langle M(1,2,3)-O \rangle\rangle$	$\langle\langle r^{M(1,2,3)} \rangle\rangle$	1.497(15)	0.805(21)	0.950	0.0063
$\langle\langle M(1,2,3)-O \rangle\rangle$	$\langle\langle r^{M(1,2,3)} \rangle\rangle$	1.0709(25)	0.784(14)	0.990	0.0028
	$\langle r^{O(3)} \rangle$		0.347(17)		
	$\langle r^{M(4)} \rangle$		-0.020(3)		
$\langle M(1)-O \rangle$	$\langle r^{M(1)} \rangle$	0.932(24)	0.799(12)	0.990	0.0027
	$\langle r^{O(3)} \rangle$		0.467(16)		
	$\langle r^{M(4)} \rangle$		-0.0532(28)		
	$^{[4]}Al$		0.00358(30)		
$\langle M(2)-O \rangle$	$\langle r^{M(2)} \rangle$	1.476(7)	0.845(9)	0.991	0.0053
$\langle M(3)-O \rangle$	$\langle r^{M(3)} \rangle$	0.627(61)	0.775(19)	0.970	0.0058
	$\langle r^{O(3)} \rangle$		0.728(40)		
	$\langle r^{M(2)} \rangle$		-0.080(12)		
	$\langle r^{M(4)} \rangle$		-0.029(7)		
	Z^A		0.0064(18)		
<u>$Pnma^B(Mg,Fe,Mn)$</u>					
$\langle\langle M1,2,3-O \rangle\rangle$	$\langle\langle r^{M1,2,3} \rangle\rangle$	1.468(29)	0.855(42)	0.973	0.0024
$\langle M1-O \rangle$	$\langle r^{M1} \rangle$	1.464(59)	0.862(79)	0.916	0.0028
$\langle M2-O \rangle$	$\langle r^{M2} \rangle$	1.447(15)	0.899(24)	0.992	0.0039
$\langle M3-O \rangle$	$\langle r^{M3} \rangle$	1.429(87)	0.87(12)	0.841	0.0044
<u>$Pnma^B(Li)$</u>					
$\langle M1-O \rangle$	$\langle r^{M1} \rangle$	1.388(67)	0.954(91)	0.978	
$\langle M2-O \rangle$	$\langle r^{M2} \rangle$	1.435(55)	0.908(99)	0.972	
$\langle M3-O \rangle$	$\langle r^{M3} \rangle$	1.650(59)	0.597(79)	0.959	

* s = standard error of estimate.

alumino-magnesiotalumite. They concluded that the $M(1)$ and $M(3)$ octahedra are larger than expected based on their site populations, and that the difference in size increases with $^{T(1)}Al$; in contrast, the individual $M(1)-O(1)$ and $M(3)-O(1)$ distances shorten with increasing $^{T(1)}Al$, as expected by bond-strength requirements on the shared $O(1)$ oxygen atom. It is possible that other inductive effects produce variations in mean bondlengths not described by the regression equations of Table 7. These could be investigated through examining structural strain as a function of amphibole composition. If structural strain is an issue here, one would expect deviations from the relations of Table 7 in compositions that approach the chemical limits of stability of the amphibole structure.

The $Pnma$ amphiboles with $^B(Mg,Fe,Mn)$: variation in mean bondlengths

Hawthorne (1983) presented relations between the $\langle M-O \rangle$ distances and the aggregate radii of the constituent cations and anions at the M sites. However, not much data were available at that time. With the work of Evans et al. (2001) and Schindler et al. (2007) and Hawthorne et al. (2007), this situation has now changed, and more accurate relations are now available for anthophyllite-gedrite amphiboles.

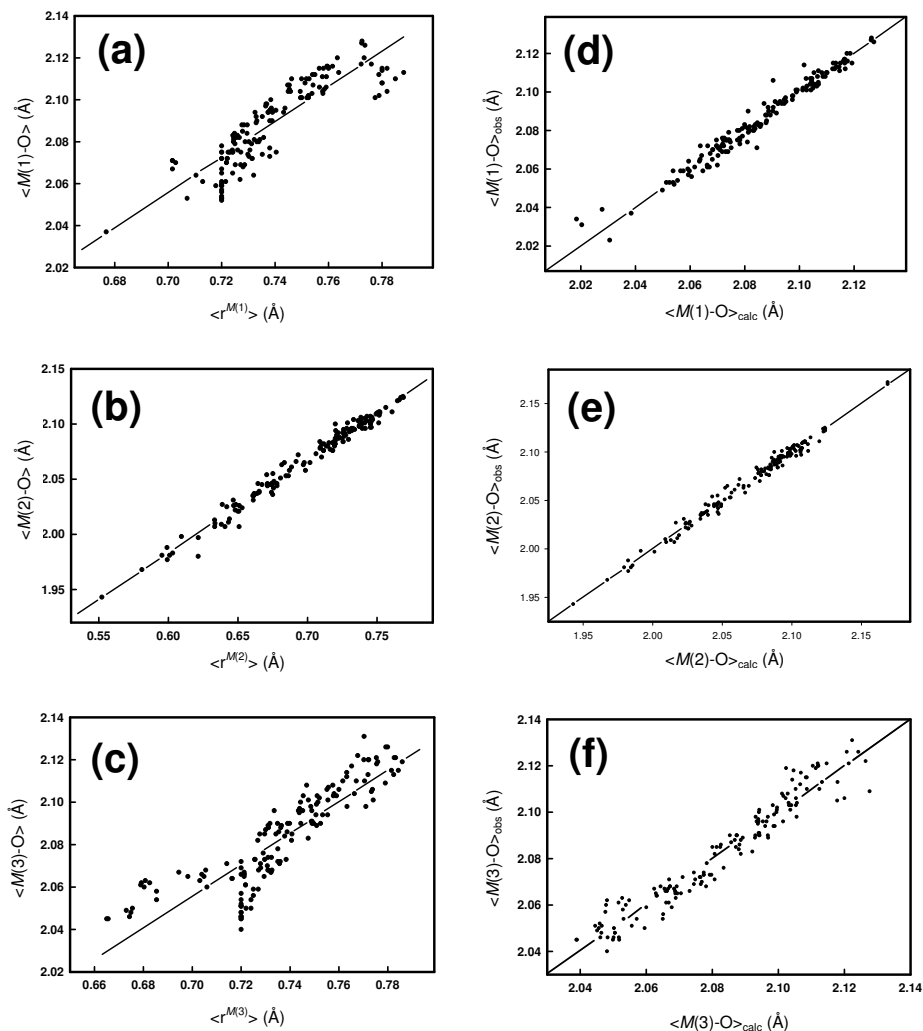


Figure 22. (a,b,c): Variation in $\langle M-O \rangle$ distance as a function of the mean aggregate radius of the M cations in $C2/m$ amphiboles: (a) $M(1)$; (b) $M(2)$; (c) $M(3)$; comparison of observed and calculated (from the regression relations of Table 5) $\langle M-O \rangle$ distances: (d) $M(1)$; (e) $M(2)$; (f) $M(3)$.

Variation in $\langle\langle M1,2,3-O \rangle\rangle$ distances. The variation in $\langle\langle M1,2,3-O \rangle\rangle$ bondlength as a function of the aggregate constituent $M1,2,3$ cation radius for amphiboles of the anthophyllite-gedrite series is shown in Figure 23, and the results of linear regression are shown in Table 7. The data are quite linear, given the large standard deviations in the intermediate range of composition (where the refinements are affected by exsolution), and the values are not materially affected by the small amounts of F occupying the O(3) site in these crystals. In the $C2/m$ amphiboles, the $\langle\langle M(1,2,3)-O \rangle\rangle$ distances were inductively affected by variation in the aggregate size of the cations occupying the $M(4)$ site. There is no sign of such an effect in the $Pnma$ amphiboles, which is not surprising, given the small amount of variation in $\langle r^{M4} \rangle$ relative to the analogous variation in the $C2/m$ amphiboles.

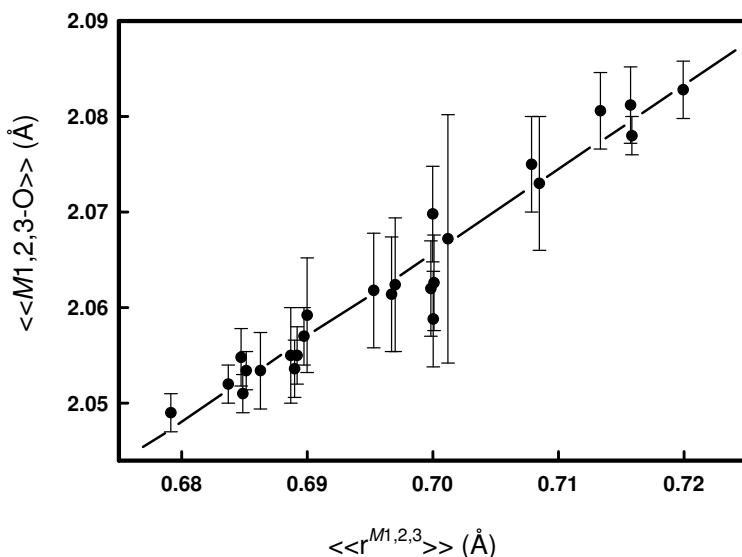


Figure 23. Variation in $\langle M1,2,3-O \rangle$ distance as a function of the mean aggregate radius of the $M1,2,3$ cations in $Pnma$ amphiboles with $^B(Mg,Fe,Mn)$.

The $M1$ and $M3$ sites. The $M1$ and $M3$ sites are occupied predominantly by Mg and Fe^{2+} . In principle, the mean bond-lengths at these sites are dependent not only on the cation site-populations, but also on the anion site-populations at the $O3A$ and $O3B$ sites (cf. monoclinic amphiboles, Table 7). However, the $Pnma$ amphiboles generally contain only minor F , and we may omit consideration of the monovalent-anion content and focus just on the site populations of $M1$ and $M3$. Figures 24a, c show the variation of $\langle M1-O \rangle$ and $\langle M3-O \rangle$ as functions of mean constituent-cation radii for amphiboles of the anthophyllite-gedrite series. The variations are linear for each site, and no data deviate significantly (> 2.7 standard deviations) from the least-squares line. The regression curves are given in Table 7. The correlation coefficients are much lower for the $M1$ and $M3$ sites than that for the $M2$ site, a result of the much smaller spread of the data for the former two sites (where the standard deviation for each data point is proportionately much greater relative to the total range of the data for the $M1$ and $M3$ sites compared to the $M2$ site).

The $M2$ site. The $M2$ site is occupied predominantly by Mg , Al , Fe^{2+} and small amounts of Ti^{4+} and Fe^{3+} . The relation between $\langle M2-O \rangle$ and the mean constituent-cation radius is shown in Figure 24b, and the equation of the linear-regression curve is given in Table 7. The slope and intercept of the curve are reasonably similar to the analogous values for the $M(2)$ site in the $C2/m$ amphiboles.

The $Pnma$ amphiboles with $^B Li$: variation in mean bondlengths

The behavior observed in holmquistites is significantly different from that of the other $Pnma$ amphiboles discussed above. The crucial point in holmquistite crystal-chemistry is the presence of two monovalent cations pfu at the $M4$ site, which implies the presence of two trivalent cations pfu at the $M2$ site. The geometry of the strip of octahedra, does not allow incorporation of Al into the double chain of tetrahedra. Holmquistite, ideally $A^{\square} B Li_2^C (Mg_3 Al_2)^T Si_8 O_{22} (OH)_2$, is actually the amphibole composition composed of the smallest possible structural modules. Crystallization in $Pnma$ symmetry, where the two double-chains of tetrahedra can assume different conformations, is probably required by the need to obtain a more suitable [5 + 1]-

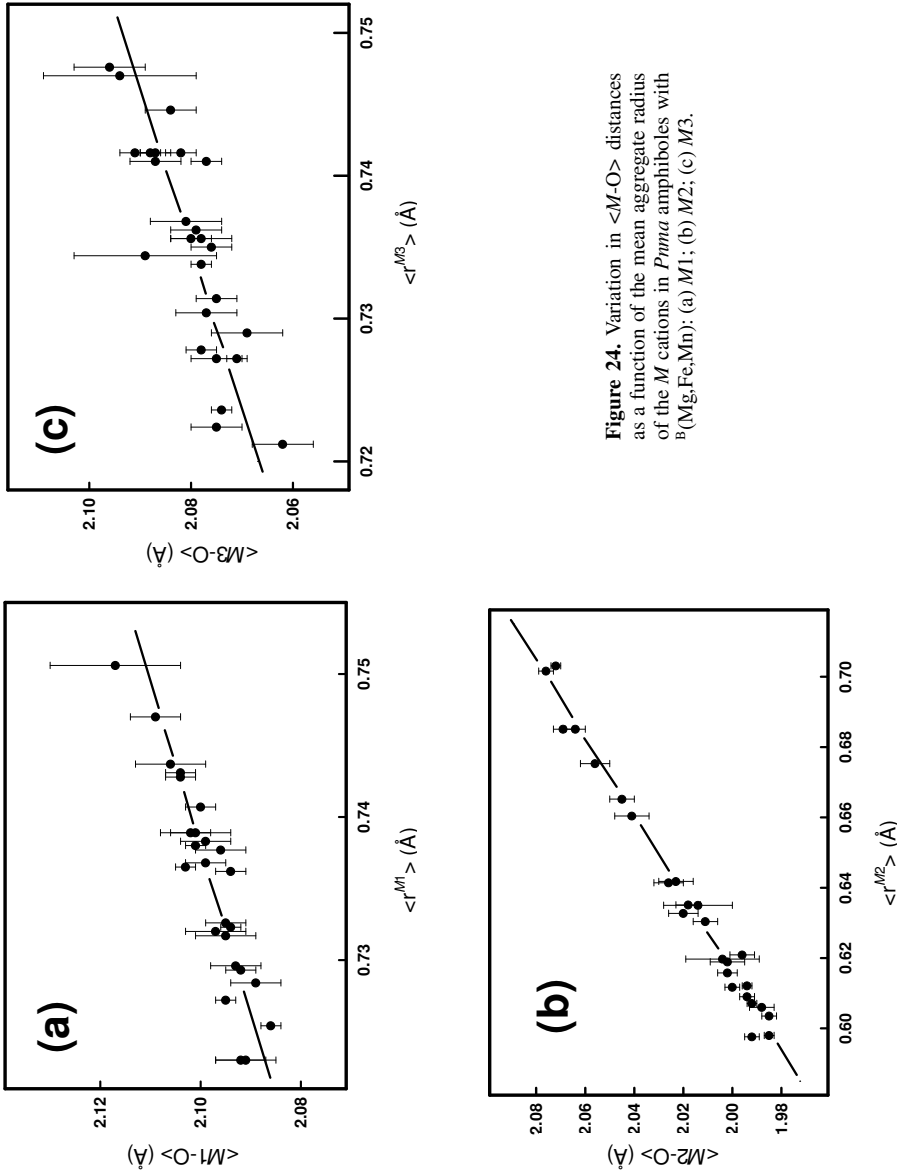


Figure 24. Variation in $\langle M-O \rangle$ distances as a function of the mean aggregate radius of the M cations in *PrIMA* amphiboles with $\text{P}(\text{Mg,Fe,Mn})$: (a) $M1$; (b) $M2$; (c) $M3$.

coordination for ${}^B\text{Li}$, and to shrink the cation-cation distances. This arrangement does not allow extensive incorporation of larger homovalent substituents, which are hosted via mechanisms implying distortion of the octahedra. Actually, only one occurrence of ferroholmquistite has been reported so far (Cámara and Oberti 2005).

Cámara and Oberti (2005) also provided structure refinements and complete chemical analyses of samples from reported occurrences of holmquistite. The observed trends are reported in Figure 25, and the relevant regression equations are given in Table 6. Comparison with those reported for *Pnma* amphiboles with ${}^B(\text{Mg,Fe,Mn})$ confirms the different relations between composition and geometry in the two series.

THE STEREOCHEMISTRY OF THE $M(4)$ SITE

The $M(4)$ site occurs at the junction of the strip of octahedra and the double-chain of tetrahedra in all amphibole structure types, and is occupied by B cations (Na , Li , Ca , Mn^{2+} , Fe^{2+} , Mg). The B cation bonds to oxygen atoms of both the strip of octahedra and the double-chain of tetrahedra, and is the primary link between these two parts of the structure. As a result, this site and its constituent cations are a major influence on the symmetry, crystal chemistry and chemical composition of the amphiboles (Warren 1930; Whittaker 1960; Papike et al. 1969). In monoclinic amphiboles, the nature of the B cation significantly affects the β angle, and thus the periodicity along the stacking direction, a^* ($= a \sin \beta$). Within compositional series with homovalent B cations, there is a reasonable linear correlation (with obvious systematic scatter) between the aggregate ionic radius at $M(4)$ [$\langle r^{M(4)} \rangle$] and the β angle. We may investigate

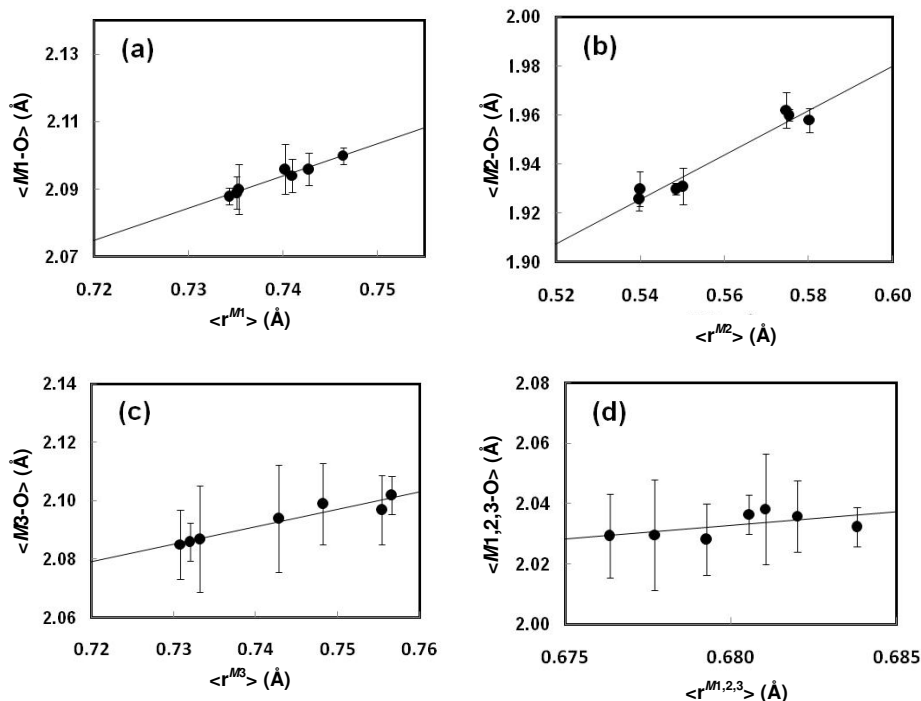


Figure 25. Variation in $\langle M-O \rangle$ distances as a function of the mean aggregate radius of the M cations in *Pnma* amphiboles with ${}^B\text{Li}$: (a) $M1$; (b) $M2$; (c) $M3$; (d) $M1,2,3$.

the origin of the scatter in Figure 26 by stepwise regression analysis, the results of which are given in Table 8. After the aggregate size of the $M(4)$ cations, the following parameters correlate significantly with the β angle: the aggregate formal charge, Z , of the $M(4)$ cations, the aggregate size of the $M(1,2,3)$ cations, and the $^{[4]}Al$ content. This behavior is in accord with the β angle being controlled by the linkage requirements of the double-chain of tetrahedra and the strip of octahedra.

The calcic, sodic-calcic and sodic amphiboles

These amphiboles have space-group symmetry $C2/m$; the $M(4)$ site has point symmetry 2 and is surrounded by eight O atoms. In these groups with large B cations, the $M(4)$ site occupies a position at $0 \sim 0.28 \frac{1}{2}$. In $C2/m$ amphiboles with small B cations, the $M(4')$ site

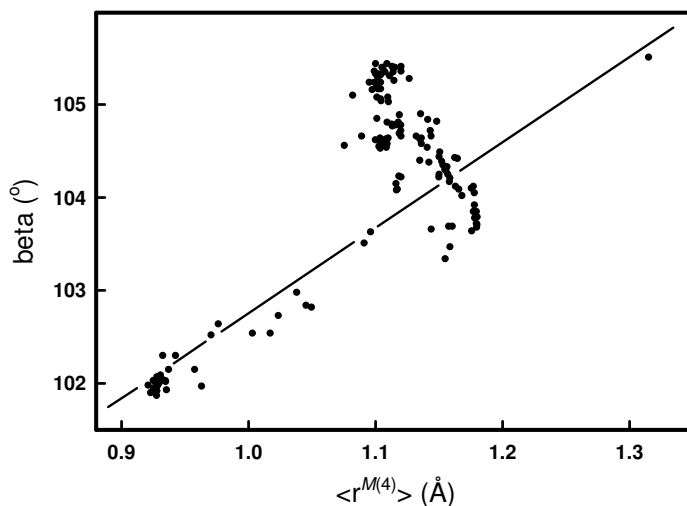


Figure 26. Variation in the β angle in as a function of the aggregate radius of the $M(4)$ cations for selected $C2/m$ amphiboles.

Table 8. Regression results for the $M(4)$ -sites in $C2/m$ amphiboles and $^{[6]}M4$ in $Pnma$ amphiboles.

Y	x_j	y_o	a_i	R	s^* (° or Å)
β	$\langle r^{M(4)} \rangle$	92.8(1.3)	1.86(36)	0.965	0.31
	$Z^{M(4)}$		1.33(9)		
	$\langle r^{M(1,2,3)} \rangle$		-5.7(1.8)		
	$^{[4]}Al$		0.33(6)		
$\langle M(4)-O \rangle$	$^{[4]}Al$	1.306	-0.0262(17)	0.934	0.011
	$\langle r^{M(1,2,3)} \rangle$		0.68(6)		
	$\langle r^{O(3)} \rangle$		0.446(78)		
	$\langle r^{M(4)} \rangle$		0.106(14)		
	Z^A		0.049(4)		
$\langle M4-O \rangle$	$\langle r^{M1,2,3} \rangle$	1.363(74)	1.37(11)	0.938	0.006

* s = standard error of estimate.

occupies a position at $0 \sim 0.26 \frac{1}{2}$, and in calcic, sodic-calcic and sodic amphiboles with a significant component of $^B(\text{Mg}, \text{Fe}, \text{Mn})$, both sites can be identified (Rossi et al. 1987; Oberti and Ghose 1993). A detailed discussion of the coordination at the $M(4)$ site is given by Hawthorne (1983a). The size of the $M(4)$ polyhedron increases from $M(4) = \text{Ca}_2 \rightarrow \text{CaNa} \rightarrow \text{Na}_2$, but is also strongly affected by the size of the $M(2)$ polyhedron (cation), $\langle M(4)\text{-O} \rangle$ increasing with increasing $\langle M(2)\text{-O} \rangle$ for a fixed size of the $M(4)$ cation.

Amphiboles with small B cations (magnesium-iron-manganese-lithium, magnesium-sodium and lithium-sodium)

The orthorhombic amphiboles have space-group symmetries $Pnma$ and $Pnmm$, and the $M4$ sites have point symmetries 1 and 2, respectively. The monoclinic amphiboles have space-group symmetries $C2/m$ and $P2_1/m$, and the $M(4)$ sites have point symmetries 2 and 1, respectively. As in the $C2/m$ amphiboles, with large B cations, the $M(4)$ site occupies a position at $0 \sim 0.28 \frac{1}{2}$, whereas with small B cations, the $M(4')$ site occupies a position at $0 \sim 0.26 \frac{1}{2}$. In $^B\text{Na}\text{-}^B\text{Li}$ solid-solutions, both sites can be identified by crystal-structure refinement (Oberti et al. 2004).

The $C2/m$ amphiboles: variation in $\langle M(4)\text{-O} \rangle$ bondlengths

In the $C2/m$ amphiboles, the $M(4)$ site can be occupied by a wide variety of cations of different charge and size: Li, Mg, Fe^{2+} , Mn^{2+} , Ca, Na (and even K and Sr in various synthetic amphiboles), and the $\langle M(4)\text{-O} \rangle$ distance shows considerable variation in these amphiboles: 2.45–2.62 Å. However, within the calcic, sodic-calcic, sodic, and magnesium-iron-manganese-lithium amphibole groups, there is no significant simple correlation between $\langle M(4)\text{-O} \rangle$ and $\langle r^{M(4)} \rangle$. The amphiboles of the magnesium-iron-manganese-lithium group show a significant correlation of $\langle M(4)\text{-O} \rangle$ and $\langle r^{M(1,2,3)} \rangle$ (Fig. 27a, Table 7). This relation suggests that $\langle M(4)\text{-O} \rangle$ is significantly affected by the articulation requirements of the strip of octahedra and the double-chain of tetrahedra. As the size of the strip of octahedra increases (i.e., increasing $\langle r^{M(1,2,3)} \rangle$), the double-chain straightens to maintain linkage, and the $M(4)\text{-O}$ bonds lengthen accordingly, thereby increasing $\langle M(4)\text{-O} \rangle$.

The factors affecting $\langle M(4)\text{-O} \rangle$ in the $C2/m$ amphiboles as a whole were investigated using stepwise linear regression with $\langle M(4)\text{-O} \rangle$ as the dependent variable and the following sets of independent variables: (1) $^{[4]}\text{Al}$, $\langle r^{M(1)} \rangle$, $\langle r^{M(2)} \rangle$, $\langle r^{M(3)} \rangle$, $\langle r^{M(4)} \rangle$, $\langle r^{O(3)} \rangle$, $Z^{M(4)}$ and Z^A (where $Z^{M(4)}$ and Z^A are the formal charges of the $M(4)$ - and A -site cations, respectively); (2) $^{[4]}\text{Al}$, $\langle r^{M(1,2,3)} \rangle$, $\langle r^{M(4)} \rangle$, $\langle r^{O(3)} \rangle$, $Z^{M(4)}$ and Z^A . The second option gave the more significant fit and the results are given in Table 8. The most important parameters are $^{[4]}\text{Al}$, $\langle r^{M(1,2,3)} \rangle$ and Z^A . These are the principal parameters affecting the relative sizes of the double-chain of tetrahedra ($^{[4]}\text{Al}$) and the strip of octahedra ($\langle r^{M(1,2,3)} \rangle$), and ability of the double chain to vary its $\text{T-O}_{\text{bridging}}\text{-T}$ distances (Z^A , a measure of the occupancy of the A site), and are in accord with the idea that the stereochemistry of the $M(4)$ site has a major influence on the crystal chemistry and bulk composition of the amphiboles.

The $Pnma$ amphiboles: variation in $\langle M4\text{-O} \rangle$ bondlengths

The $M4$ site is occupied predominantly by Fe^{2+} , Mn^{2+} , Mg and Li; however, there is no significant correlation between $\langle M4\text{-O} \rangle$ and $\langle r^{M4} \rangle$, the mean radius of the constituent $M4$ cations. However, as with the monoclinic magnesium-iron-manganese-lithium amphiboles, there is a strong correlation between $\langle M4\text{-O} \rangle$ and the mean constituent-cation radius of the $M(1,2,3)$ sites (Fig. 27b): the equation of the linear-regression relation is given in Table 8. The slope and intercept of the curve are reasonably similar to the analogous values for the $M(4)$ site in the monoclinic magnesium-iron-manganese-lithium amphiboles (Fig. 27a, Table 8), indicating the same cause for this relation.

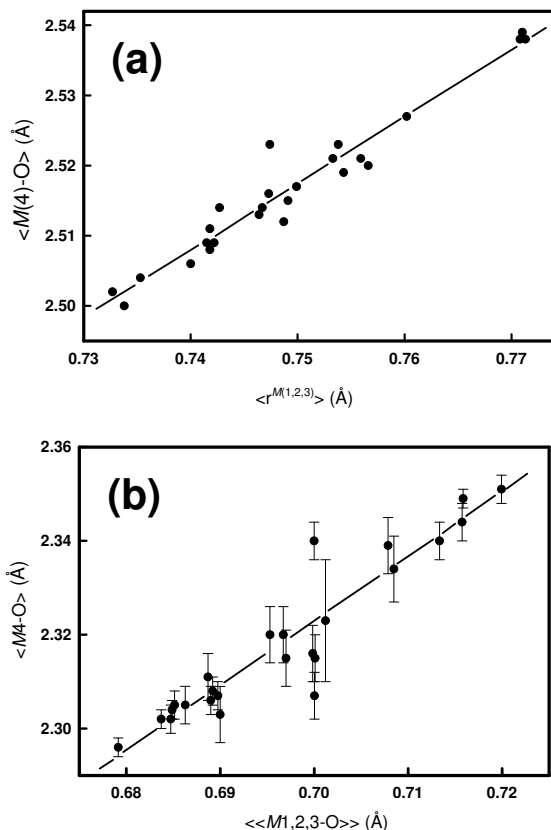


Figure 27. (a) Variation in $\langle M(4)-O \rangle$ distance in $C2/m$ Mg-Fe-Mn-Li amphiboles as a function of the aggregate radius of the $M(1,2,3)$ cations; (b) variation in $\langle M4-O \rangle$ distance in $Pnma$ Mg-Fe-Mn-Li amphiboles as a function of the aggregate radius of the $M1,2,3$ cations.

THE STEREOCHEMISTRY OF THE A SITE

The A site occurs in the large cavity between the back-to-back chains of tetrahedra in the amphibole structure. This site may be occupied or vacant, and like the $M(4)$ site, the details of this occupancy are very dependent on structure type (i.e., space group) as the relative displacement of the back-to-back chains is dependent on space-group symmetry and stacking of the layers (Fig. 14). The A cavity may be occupied by monovalent (Na, K, Li) or divalent (Ca, Pb^{2+}) cations, and the siting of these cations are strongly influenced by short-range bond-valence constraints. It is notable that in the $P2_1/m$ and $Pnmm$ structures, the A site is vacant in natural amphiboles, but may be occupied by $B(NaMg)$ in synthetic $P2_1/m$ amphiboles (Oberti et al. 2007b; Welch et al. 2007).

The $C2/m$ amphiboles

The arrangement of polyhedra around the A site is shown in Figure 28, and typical A-O distances for different amphiboles are shown in Table 9. The pattern of distances is similar in each structure, but the variation is considerable (up to 0.3 Å) for each individual distance. This variation is accompanied by rotation of the chains [variation in the O(5)-O(6)-O(5) angle] that moves the O(5), O(6) and O(7) anions relative to the central A position].

Figure 28. The arrangement of polyhedra around the A cavity and the A sites in the $C2/m$ amphibole structure.

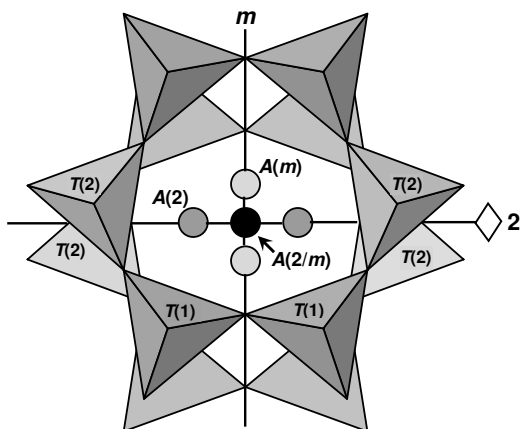


Table 9. A–O distances (Å) in selected $C2/m$ amphiboles.

		Cumm	Trem	Parg	Winch	Taram
A–O(5)	×4	2.824	2.970	3.045	2.77	3.008
A–O(6)	×4	3.278	3.156	3.068	3.13	3.152
A–O(7)	×2	2.295	2.486	2.432	2.539	2.520
<A–O>		2.900	2.948	2.932	2.87	2.968
		Nyb	Kato	Arf	Glauc	Rieb
A–O(5)	×4	2.913	2.970	2.755	2.814	2.832
A–O(6)	×4	3.137	3.108	3.212	3.216	3.252
A–O(7)	×2	2.446	2.419	2.629	2.519	2.550
<A–O>		2.909	3.091	2.913	2.916	2.944

Refs: Cumm: Ghose (1961), Hawthorne (1983a); Trem: Papike et al. (1969); Parg: Bocchio et al. (1978); Winch: Sokolova et al. (2001); Taram: Hawthorne and Grundy (1978); Nyb: Hawthorne et al. (1996a); Kato: Oberti et al. (1998); Arf: Hawthorne (1976); Glauc: Hawthorne (1979); Rieb: Hawthorne (1978).

The A cations do not occupy the central site [$A(2/m)$] at $(0, \frac{1}{2}, 0)$ (notation from Hawthorne and Grundy 1972). Figure 28 shows the sites that are actually occupied in the many hundreds of amphibole structures refined to the present time; a few studies have put cations at a general site [$A(1): x, y, z$], but further work has shown that these assignments are not warranted. Where the A cation is K, the electron density occurs at the $A(m)$ site (Papike et al. 1969; Cameron et al. 1983). The maxima of the electron density are confined to the mirror plane through $(0, \frac{1}{2}, 0)$ and occur on both sides of the $A(2/m)$ site with the density elongated in the general direction of the nearer O(7) anions. The distance between the two maxima is of the order of 0.29 \AA , too short for simultaneous occupancy of both sites in a single A cavity, and hence K may be considered as positionally disordered off the central position with only one (or sometimes neither if $K < 1$ apfu) position occupied in a specific cavity.

The situation where $A = \text{Na}$ is much more complicated as electron density can occur at $A(m)$, $A(2)$ or both. As indicated in Figure 29, where distributed over the $A(m)$ and $A(2)$ sites, the electron density is best shown in a difference-Fourier map parallel to (201) and through $(0, \frac{1}{2}, 0)$. Figure 30 shows the distribution of electron density for a series of amphiboles with $^{\text{A}}\text{Na}$ cations ≈ 1 apfu. It is apparent from Figure 30 that Na may occur only at $A(m)$, only at $A(2)$, or disordered over $A(m)$ and $A(2)$. There has been a considerable amount of work trying to

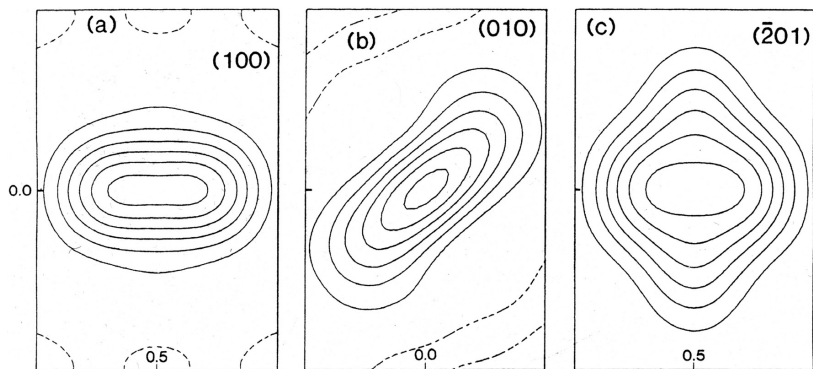


Figure 29. The electron density in the A cavity for nyböite with $A \approx \text{Na}$; (a) section parallel to (100); (b) section parallel to (010); (c) section parallel to (201); the contour interval is $1 e/\text{\AA}^3$ and the broken line is the zero contour (from Hawthorne et al. 1996a).

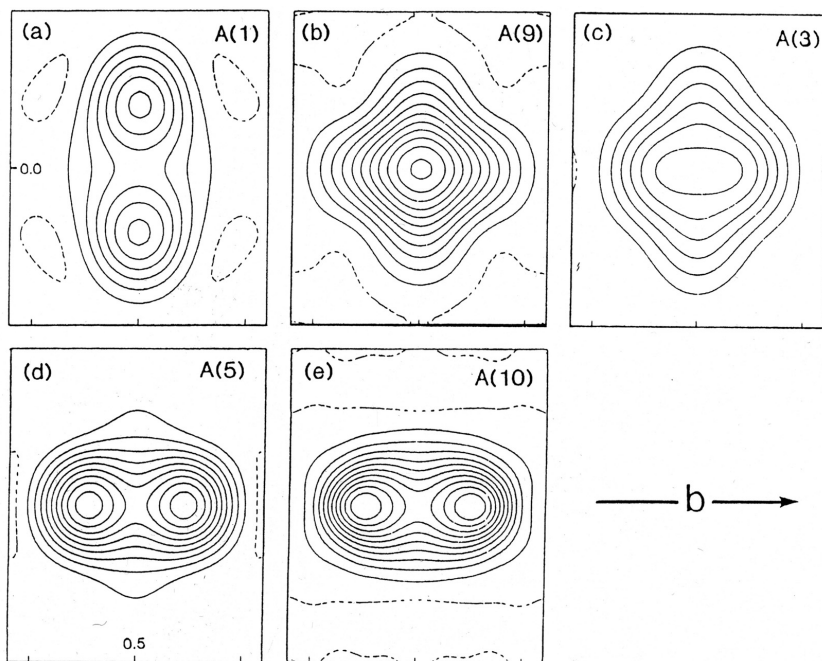


Figure 30. Sections parallel to $\bar{2}01$ showing the electron density in the A cavity for a series of $C2/m$ amphiboles with $A \approx \text{Na}$; legend as in Fig. 28 (from Hawthorne et al. 1996a); (a) fluoronyböite; (b) pargasite; (c) nyböite; (d) taramite; (e) pargasite.

understand the details of this disorder, often focusing on variations in bond valence (and hence bond lengths) (see summary by Hawthorne 1983a). However, Hawthorne et al. (1996a) showed that the order-disorder relations within the A cavity are actually controlled by short-range bond-valence requirements; these will be dealt with by Hawthorne and Della Ventura (2007).

The $P2/a$ amphibole

The polyhedra arrangement around the *A* site is shown in Figure 31, and the A-O distances and analogous bond-valences for joesmithite are shown in Table 10. Moore (1969) suggested that the occurrence of Pb^{2+} may be fortuitous, but Hawthorne (1983a) noted that the off-centered arrangement of Pb^{2+} indicates lone-pair stereoactivity. As discussed by Moore (1969) and Moore et al. (1993), Pb^{2+} is displaced off the central position toward the $T(1)B$ site occupied by Be, suggesting that bond-valence requirements are driving this arrangement (Oberti et al. 2007b).

The $Pnma$ amphiboles

The arrangement of polyhedra around the *A* site is shown in Figure 32. Comparison with the arrangement in the $C2/m$ amphiboles (Fig. 28) shows significant differences. First, the chains in the $Pnma$ structure are more displaced relative to each other than the chains in the $C2/m$ structure (cf. Figs. 28 and 32). Second, the difference in degree of rotation of the A- and B-chains in the $Pnma$ structure significantly affects the A-O distances; thirdly, the *A* site does not occur in the center of the cavity (Fig. 32). The collective result of these factors is that the arrangement of anions around the *A* site in the $Pnma$ structure is more compact than the analogous arrangement in the $C2/m$ structure. As a result of the difference in symmetry, there is no longer a center of symmetry at the centre of the *A* cavity (as there is for the $C2/m$ structure). The only symmetry involving the *A* cavity is the mirror plane parallel to the *b*-axis. In all structures so far refined, the *A* site is confined to this mirror plane with coordinates $(x, -1/4, z)$. Typical A-O distances in $Pnma$ amphiboles with *A* cations are shown in Table 11 (Fe-

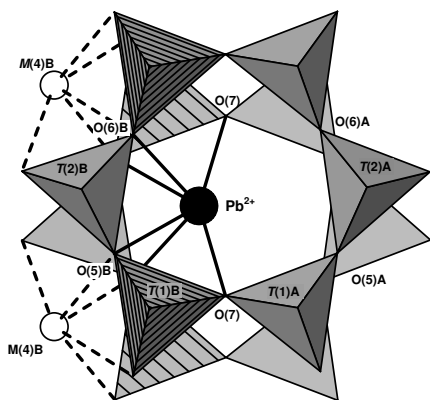


Figure 31. The arrangement of polyhedra around the *A* cavity and the *A* site in the $P2/a$ amphibole structure.

Table 10. A–O distances (Å) in joesmithite*.

A–O(5)A	3.517(5)
A–O(5)B	2.589(5)
A–O(6)A	2.568(4)
A–O(6)B	3.433(5)
A–O(7)	2.580(6)
<A–O>	2.937

* from Moore et al. (1993)

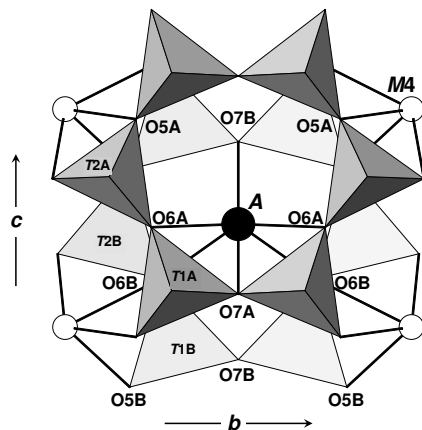


Figure 32. The arrangement of polyhedra around the *A* cavity and the *A* site in the $Pnma$ amphibole structure.

Table 11. A–O distances (Å) in anthophyllite and sodicgedrite.

$^{[4]}Al$ (apfu)	0.17	1.79
A–O6A ×2	2.677	2.654
A–O6B ×2	2.808	2.624
A–O7A	2.287	2.387
A–O7B	2.370	2.378

* from Schindler et al. (2007)

poor anthophyllite and holmquistite have very low A-site occupancies (e.g., Robinson et al. 1971; Cámara and Oberti 2005).

The *Pnmm* amphiboles

In the synthetic protoamphibole reported by Gibbs (1969), the chemical analysis (Gibbs et al. 1960) indicated Li at the A site, but Li could not be located by structure refinement. Sueno et al. (1998) reported the occurrence and structures of proto-ferro-anthophyllite and proto-mangano-ferro-anthophyllite, but in both these structures, the A site is vacant.

THE STEREOCHEMISTRY OF THE O(3) SITE

The O(3) site is located at the center of the strip of *M*(1,2,3) octahedra and can be occupied by monovalent [(OH), F, Cl] and divalent (O) anions that are bonded to two *M*(1) and one *M*(3) cations (Fig. 33a; the siting of the O(3) site in other amphibole structure types is analogous to that in the *C2/m* structure). Where occupied by (OH), the associated H atom is situated ~ 1 Å away from the O(3) site with the O-H bond orthogonal to the plane of the strip of *M*(1,2,3) octahedra.

The *C2/m* amphiboles

O(3) = (OH). The arrangement of atoms around the O(3) site [where O(3) = (OH)] in the *C2/m* amphibole structure is shown in Figure 33b. The position of the H atom in tremolite was located by Hawthorne and Grundy (1976) [O(3)-H = 0.957(6) Å] and Hanisch (1966) showed by polarized infrared spectroscopy that the O-H bond is orthogonal to (100). It is notable that the H atom hydrogen-bonds only to one O(7) atom [H...O(7) = 2.775 Å in tremolite, Hawthorne and Grundy 1976], although this situation may change for short-range arrangements in ^[4]Al-bearing amphiboles.

O(3) = F. Above, we note that there is a hydrogen bond to the O(7) anion. Where O(3) = F, this hydrogen bond is no longer present, and as a consequence, the valence-sum rule (Brown 1981, 2002; Hawthorne 1994, 2006) predicts that the *T*(1)-O(7) distance should be slightly shorter in fluorotremolite than in tremolite. This conclusion is in accord with the *T*(1)-O(7) distances in tremolite (1.622 Å, Evans and Yang 1998, sample 11B, Si = 7.997 apfu) and synthetic fluorotremolite (1.606 Å, Cameron and Gibbs 1973, Si = 8 apfu).

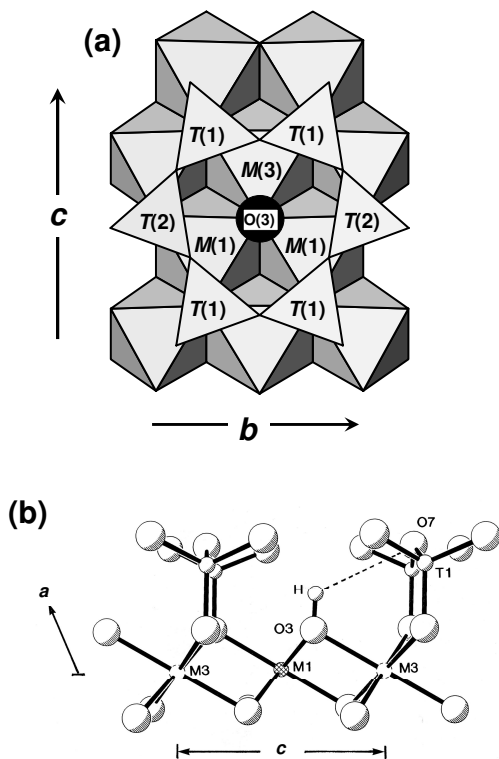


Figure 33. The O(3) site in the *C2/m* amphibole structure; the O(3) site is shown by a black circle; (a) projected onto (100); (b) projected onto (010) with perspective and with the *T*(2) sites omitted for clarity, the H atom is shown by a small circle, and the H...O(7) hydrogen bond is shown by a dashed line. [Used by permission of Schweizerbart'sche Verlagsbuchhandlung, from Della Ventura et al. (1999), *European Journal of Mineralogy*, Vol. 11, Fig. 7, p. 88.]

O(3) = Cl. Where O(3) = Cl, the site is significantly displaced with reference to the strip of $M(1,2,3)$ octahedra relative to where O(3) = (OH),F. Figure 34 shows the electron density through the O(3) site for a series of amphiboles with increasing Cl content. The Cl atom is displaced from the position of the O atom, in accord with the much larger radius of Cl relative to that of O [$r(\text{Cl}) = 1.81$, $r(\text{O}) = 1.36 \text{ \AA}$, Shannon 1976]. Indeed, for the crystal with Cl = 0.98 apfu, the distances from the M cations to Cl are much greater than the corresponding distances to O at O(3): $M(1)\text{-O}(3) = 2.147$, $M(1)\text{-Cl} = 2.462$; $M(3)\text{-O}(3) = 2.105$, $M(3)\text{-Cl} = 2.400 \text{ \AA}$ (Oberti et al. 1993); similar values are reported by Rastsvetaeva et al. (1996).

There are two possible mechanisms whereby Cl can replace (OH) at O(3) in the amphibole structure: (1) the strip of octahedra could expand to incorporate the larger anion (as suggested by Volfingier et al. 1985), and (2) the larger anion could take up a position displaced from the plane of the O anions of the octahedron strip into the A cavity. Oberti et al. (1993) show that both mechanisms are operative, and that mechanism (2) is more important than mechanism (1). Cl-rich amphiboles are generally rich in Fe^{2+} and K (Krutov 1936; Dick and Robinson 1979; Volfingier et al. 1985; Vanko 1986; Suwa et al. 1987; Castelli 1988; Morrison 1991; Enami et al. 1992; Zhu et al. 1994; Kullerud 1996; Leger et al. 1996; Sato et al. 1997; McCormick and McDonald 1999), indicating the effect of increasing Fe^{2+} in increasing the dimensions of the strip of octahedra, and increasing K promoting the bonding between K at the $A(m)$ site and Cl at O(3) (see also Oberti et al. 2007b).

O(3) = O. The occurrence of O at O(3) places considerable restrictions on occupancy of the adjacent $M(1)$ and $M(3)$ sites as the bond-valence requirements of the oxygen atom at O(3) must be satisfied by the three adjacent $M(1)$ and $M(3)$ cations. In turn, this requirement places considerable restrictions on the chemical composition of the amphibole. At least some of the $M(1)$ and $M(3)$ cations must be of high charge in order to provide sufficient bond-valence to O(3). Thus the compositions of oxygenian amphiboles tend to be characterized by Ti^{4+} as a prominent C cation. However, this is not always the case: ungarrettiite is characterized by $M(1) = M(3) = \text{Mn}^{3+}$, where the Jahn-Teller distortion of the constituent polyhedra provides sufficiently short bondlengths to O(3) to satisfy local bond-valence requirements (Hawthorne et al. 1995). These amphiboles are discussed in more detail by Oberti et al. (2007a).

UNIT-CELL PARAMETERS AND COMPOSITION IN $C2/m$ AMPHIBOLES

We have shown above that the geometry (size and distortion) of each module of the amphibole structure is significantly affected by its constituent site-population, and by the composition of the other modules. The unit-cell parameters are a measure of the volume occupied by the complete structure, and thus must be sensitive to (1) the intrinsic geometry of the strip of octahedra and of the double-chain of tetrahedra; (2) the geometry of their connections through the shared oxygen atoms to form what is usually called an I-beam; (3) the geometry of the connections between the I-beams through the $M(4)$ site; (4) the size of the A cation. Therefore, variations in chemical composition and cation ordering are expected to strongly affect unit-cell parameters. It may also be expected that some combinations of site populations will not allow articulation of the structure modules, and thus cannot occur, at least under specific P and T conditions.

An understanding of the relations between the composition and unit-cell parameters in amphiboles would, in principle, help to understand the structural constraints on amphibole stability. Several statistical studies have been made (beginning with Whittaker 1960 and Colville et al. 1966). However, none of these have been truly comprehensive. Four factors have hampered this analysis: (1) lack of reliable site-populations; (2) lack of precise and accurate unit-cell dimensions obtained with a reasonably similar procedure; (3) lack of reliable site-

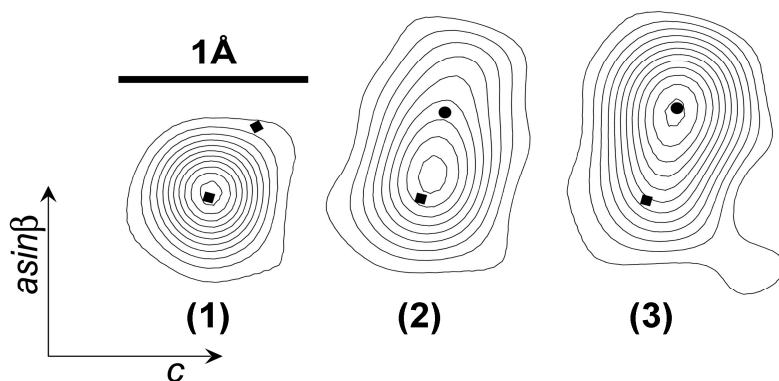


Figure 34. The electron density through the O(3) site in amphiboles with different amounts of Cl at the O(3) site, showing the displacement of the positions of O, H and Cl at this site; (a) Cl = 0.00 apfu; (b) Cl = 0.56 apfu; (c) Cl = 0.98 apfu; Circle: O atom; diamond: H atom; square: Cl atom; contours are drawn at 5, 10, 15, 20 and 25 $e/\text{Å}^3$ (from Oberti et al. 1993).

populations and chemical compositions for synthetic amphiboles; (4) the observation that a fixed cation-O distance (for instance, as calculated from constituent ionic radii) cannot be used for all amphibole compositions. The latter two points make the determination of site populations a difficult task, as it will be further discussed in Oberti et al. (2007a).

The crystal-chemical database for amphiboles at the IGG-CNR-PV satisfies all the above requirements. It contains unit formulae and structural data representative of every known $C2/m$ amphibole composition (but sadanagaite), and were obtained by the same procedure. In particular, site populations were optimized by combining chemical analyses with quantitative models of structural change as a function of composition (a peculiar case of structure modeling) in the COMAMP procedure, as described in more detail by Oberti et al. (2007a). The ranges of variation observed in the data base are: $a = 9.357\text{--}10.143 \text{ Å}$, $b = 17.580\text{--}18.402 \text{ Å}$, $c = 5.262\text{--}5.365 \text{ Å}$, $\beta = 101.84\text{--}105.71^\circ$, $V = 846.21\text{--}948.23 \text{ Å}^3$.

As a first step, the unit-cell parameters were plotted one against the other to understand whether there are forbidden zones for their combination. Figure 35 shows that amphiboles do not occupy all available space, and that discrete populations can be identified which are mainly related to the nature of the B cations. Multiple stepwise linear regression was then done using the unit-cell parameters as dependent variables. Due to the constraint of the full occupancy of the T and M sites, only the following independent chemical constituents were used: ${}^A\text{K}$, ${}^A\text{Na}$, ${}^B\text{Na}$, ${}^B(\text{Fe},\text{Mn})^{2+}$, ${}^B\text{Li}$, ${}^B\text{Mg}$, ${}^C\text{Al}$, ${}^C\text{Ti}$, ${}^C\text{Fe}^{2+}$, ${}^C\text{Fe}^{3+}$, ${}^C\text{Li}$, ${}^T\text{Al}$, ${}^W\text{F}$, ${}^W\text{O}^{2-}$. In this way, the equations predict deviations from ideal tremolite, $\square \text{Ca}_2 \text{Mg}_5 \text{Si}_8 \text{O}_{22} (\text{OH})_2$. Four regression equations were obtained, which allow calculation of the unit-cell parameters starting from the unit-formula (Table 12). For a , b and β , multiple correlation coefficients are higher than 0.99, and the lower value obtained for the c edge (0.930) is justified by its far smaller variance. The y_0 values given in Table 12 represent the unit-cell parameters extrapolated for pure tremolite: $a = 9.873(15)$, $b = 18.057(11)$, $c = 5.268(5) \text{ Å}$, $\beta = 104.94(8)^\circ$, giving $V = 907.4 \text{ Å}^3$. They are consistent with those extrapolated by Gottschalk et al. (1999) based on Rietveld analysis of a series of samples in the much simpler synthetic system tremolite-cummingtonite: $a = 9.8354(18)$, $b = 18.0562(14)$, $c = 5.2768(6) \text{ Å}$, $\beta = 104.74(2)^\circ$, $V = 906.3 \text{ Å}^3$.

It is not easy to interpret the relative importance of the various chemical descriptors on the variation of the dependent variable because the regression coefficient must be weighted for the possible abundance of each cation/anion. For the a edge, the key role is played by ${}^A\text{K}$ and by the incorporation of highly charged cations at the $M(1,2,3)$ sites. However, each

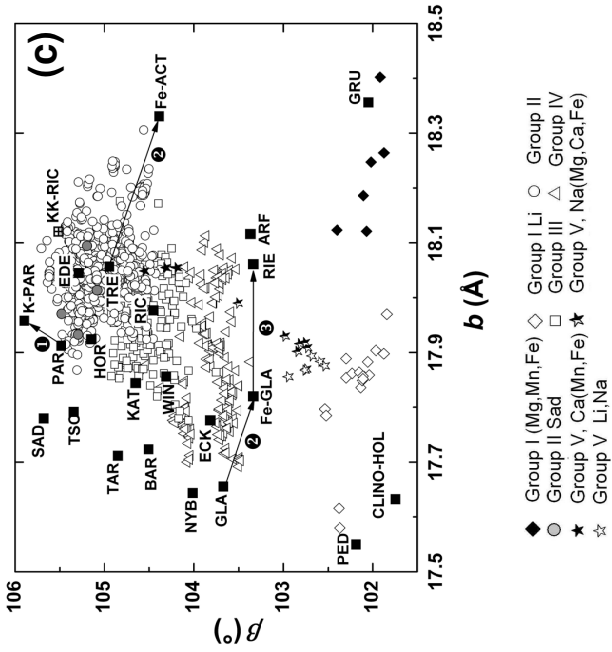


Figure 35. Variation of unit-cell parameters of amphiboles in the CNR-IJG-PV database. The values for end-member compositions (black squares) were calculated using the equations reported in Table 12. Synthetic $M^{VI}K$ -richterite (KK-RIC; Yang et al. 1999), and magnesiosadganite (Banno et al. 2004), potassic-ferrisadganite (Sokolova et al. 2000a), ferri-ferrosadganite (Hawthorne and Grundy 1977) (all as gray dots) are also reported. In figure (c), the following homovalent substitutions are shown: ① ${}^A\text{Na} \rightarrow {}^A\text{K}$, ② $\text{C}M\text{g} \rightarrow \text{C}Fe^{2+}$, ③ $\text{C}Al \rightarrow \text{C}Fe^{3+}$. Mixing among the groups along the abscissa is due to the widespread exchange ④ in natural samples. The prediction for grunerite is somewhat poor for the (anomalous) b edge, but is still in reasonable agreement with the experimental data.

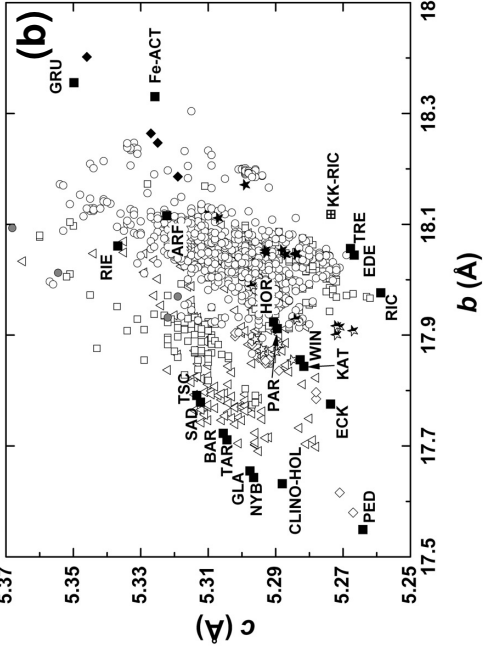
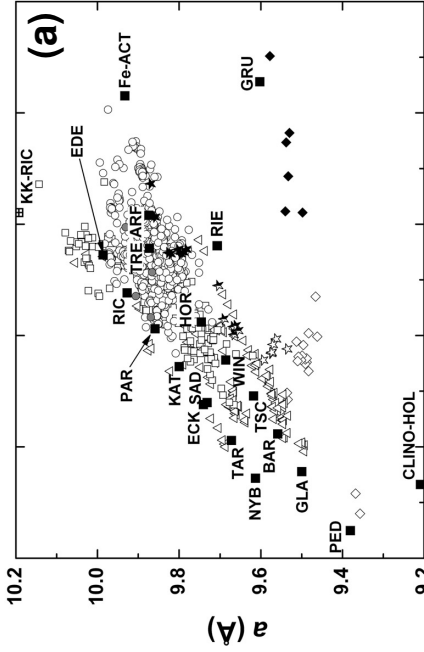


Table 12. Predictive equations for the unit-cell parameters obtained by multiple regression analysis of the CNR-IGG-PV data base.

x_i	a (Å)			b (Å)			c (Å)			β (°)
	a_i	x_i	a_i	x_i	a_i	x_i	a_i	x_i		
^A K	0.2030(58)	^C Al	-0.1207(25)	^C Ti	0.0093(18)	^B Li	-1.5980(245)			
^C Ti	-0.1968(126)	^C Li	-0.0828(75)	^A Na	-0.0239(14)	^B Mg	-1.2021(1082)			
^C Al	-0.1866(25)	^B Li	-0.0915(37)	^T Al	0.0228(8)	^B (Fe,Mn)	-1.1678(166)			
^B (Fe,Mn)	-0.1652(69)	^B Na	-0.0800(22)	^B Na	0.0149(8)	^B Na	-0.6355(116)			
^B Li	-0.1453(41)	^C Fe ²⁺	0.0548(9)	^B (Fe,Mn)	0.0120(22)	^A K	0.5539(235)			
^C Li	0.1174(120)	^A K	0.0456(42)	^C Fe ²⁺	0.0116(4)	^C Li	0.2992(505)			
^B Mg	-0.1083(215)	^W F	-0.0207(17)	^B Li	0.0101(14)	^T Al	0.1979(132)			
^C Fe ³⁺	-0.1010(34)	^W O ²⁻	0.0192(20)	^A K	-0.0062(17)	^A Na	0.1422(247)			
^A Na	0.0543(44)	^B (Fe,Mn)	0.0126(49)	^C Fe ³⁺	0.0022(8)	^C Fe ²⁺	-0.1119(71)			
^T Al	0.0591(17)	^T Al	-0.0119(18)							
^W F	-0.0439(24)									
^W O ²⁻	0.0416(65)									
^C Fe ²⁺	0.0120(14)									
^A K	0.2030(58)									
y_0	9.8728	y_0	18.0569	y_0	5.2678	y_0	104.944			
R	0.991	R	0.994	R	0.930	R	0.992			
s^*	0.015	s	0.011	s	0.0050	s	0.083			

* s = standard error of estimate

of these substitutions (heterovalent with respect to tremolite) implies a coupled heterovalent substitution, which also affects the dependent variable in a different and sometimes inverse way. For the *b* edge, substitutions at the *M*(1,2,3) and the O(3) site are particularly significant. For the β angle, the results confirm the regression done in a previous section based on aggregate ionic radius: the most important factors are the type of B cation and the amount of $^{\text{T}}\text{Al}$.

These equations can provide a rapid tool to (1) verify whether or not the structure predicted for amphibole compositions not found in Nature falls in an allowed region, (2) calculate the molar volume of pure end-members, (3) detect the occurrence or the effects of anomalous site-partitioning. They can also be used as a check for anomalous or incomplete chemical analyses.

SUMMARY

In the last 25 years, there have been major advances in our knowledge of both long-range and short-range order of both cations and anions. Experimental procedures for characterizing order and chemical composition of amphiboles have made major strides, and we now see widespread use of SREF, SIMS and infrared spectroscopy. In the future, we need to focus much more on the difficult-to-measure constituents: H (in particular), $\text{Fe}^{3+}/\text{Fe}^{2+}$ and Li, until their accurate measurement becomes routine in the same way that electron-microprobe analysis and SREF are today. Most of the advances discussed here have been experimental. Bond-valence requirements exert major control on short-range order of heterovalent cations and anions in amphiboles (and therefore on long-range order as well, as long-range order is the average of all short-range-order arrangements in a structure). However, the effects of temperature and pressure on SRO and bond-valence requirements are almost unknown. We still lack much understanding of the mechanistic controls on order-disorder of homovalent cations, particularly Mg and Fe^{2+} ; this is particularly unfortunate, as order-disorder of Mg and Fe^{2+} in many minerals is commonly quite sensitive to differences in temperature of equilibration. Thus there is much theoretical work and structure modeling to be done to understand temperature- and pressure-dependent ordering in amphiboles.

The range of chemical composition occupied by amphibole structures has widened significantly since the last Amphibole Short Course. Then, there was no knowledge either of the richness of the crystal chemistry of Li in amphiboles, or the occurrence of exotic oxygenian amphiboles. In the last 10 years, this state of affairs has changed radically. Monoclinic Li-dominant amphiboles have been discovered, and a new group of amphiboles has been recognized: the (Mg-Fe-Mn-Na-Li) amphiboles, with solid solution of Na and Li at the *M*(4) site in the *C2/m* structure. It is tempting to say that we have drawn bounds around the possible compositions of amphiboles, but we thought that 25 years ago, and it was patently untrue; perhaps the future holds more new and exotic chemistries, maybe in the area of synthetic amphiboles where novel compositions and structures are being discovered. In summary, the last 25 years have produced a lot of new knowledge about amphiboles; undoubtedly the next 25 years will do the same.

ACKNOWLEDGMENTS

FCH was supported by a Canada Research Chair in Crystallography and Mineralogy, and by a Discovery grant, both from NSERC, the Natural Sciences and Engineering Research Council of Canada. In addition, much of the work reviewed here was also supported by NSERC Major Equipment Grants and by grants from the Canada Foundation for Innovation. RO was supported by the Italian Consiglio Nazionale delle Ricerche through the project TAP01.004.002.

REFERENCES

- Appleyard EC (1975) Silica-poor hastingsitic amphiboles from the metasomatic alkaline gneisses at Wolfe, eastern Ontario. *Can Mineral* 13:342-351
- Bancroft GM (1973) Mössbauer Spectroscopy. An Introduction for Inorganic Chemists and Geochemists. McGraw-Hill, New York
- Bancroft GM, Brown JR (1975) A Mössbauer study of coexisting hornblendes and biotites: quantitative Fe³⁺/Fe²⁺ ratios. *Am Mineral* 60:265-272
- Banno Y, Miyawaki R, Matsubara S, Makino K, Bunno M, Yamada S, Kamiya T (2004) Magnesiosadanagaite, a new member of the amphibole group from Kasuga-mura, Gifu Prefecture, central Japan. *Eur J Mineral* 16:177-183
- Bocchio R, Ungaretti L, Rossi G (1978) Crystal chemical study of eclogitic amphiboles from Alpe Arami, Lepontine Alps, Southern Switzerland. *Rend Soc Ital Mineral Petrol* 34:453-470
- Brese NE, O'Keeffe M (1991) Bond-valence parameters for solids. *Acta Crystallogr B* 47:192-197
- Brown ID (1981) The bond valence method. An empirical approach to chemical structure and bonding. *In: Structure and Bonding in Crystals II*. O'Keeffe M, Navrotsky A (eds) Academic Press, New York, p 1-30
- Brown ID (2002) The Chemical Bond in Inorganic Chemistry. The Bond Valence Model. Oxford University Press
- Brown ID, Altermatt D (1985) Bond-valence parameters obtained from a systematic analysis of the inorganic crystal structure database. *Acta Crystallogr B* 41:244-247
- Bunch TE, Okrusch M (1973) Al-rich pargasite. *Am Mineral* 58:721-726
- Caballero JM, Monge A, La Iglesia A, Tornos F (1998) Ferri-clinoholmquistite, Li₂(Fe²⁺,Mg)₃Fe³⁺₂Si₈O₂₂(OH)₂, a new ⁶Li clin amphibole from the Pedriz Massif, Sierra de Guadarrama, Spanish Central System. *Am Mineral* 83:167-171
- Caballero JM, Oberti R, Ottolini L (2002) Ferripedrizite, a new monoclinic ⁶Li amphibole end-member from the Eastern Pedriz Massif, Sierra de Guadarrama, Spain, and a restatement of the nomenclature of Mg-Fe-Mn-Li amphiboles. *Am Mineral* 87:976-982
- Cámara F, Oberti R, Iezzi G, Della Ventura G (2003) The P₂/m ↔ C₂/m phase transition in synthetic amphibole Na NaMg Mg₅ Si₈ O₂₂ (OH)₂: thermodynamic and crystal-chemical evaluation. *Phys Chem Mineral* 30:570-581
- Cámara F, Oberti F, Della Ventura G, Welch MD, Maresch WV (2004) The crystal-structure of synthetic Na Na₂ Mg₅ Si₈ O₂₁ (OH)₃, a triclinic C₁ amphibole with a triple-cell and excess hydrogen. *Am Mineral* 89:1464-1473
- Cámara F, Oberti R (2005) The crystal-chemistry of holmquistites: Ferroholmquistite from Greenbushes (Western Australia) and hints for compositional constraints in ⁶Li amphiboles. *Am Mineral* 90:1167-1176
- Cameron M, Gibbs GV (1973) The crystal structure and bonding of fluor-tremolite: a comparison with hydroxyl tremolite. *Am Mineral* 58:879-888
- Cameron M, Sueno S, Papke JJ, Prewitt CT (1983) High temperature crystal chemistry of K and Na fluor-richterites. *Am Mineral* 68:924-943
- Castelli D (1988) Chlorpotassium ferro-pargasite from Sesia-Lanzo marbles (Western Italian Alps): A record of highly saline fluids. *Rend Soc Ital Mineral Petrol* 43:129-138
- Colville PA, Ernst WG, Gilbert MC (1966) Relationships between cell parameters and chemical compositions of monoclinic amphiboles. *Am Mineral* 51:1727-1754
- Cosca MA, Essene EJ, Bowman JR (1991) Complete chemical analyses of metamorphic hornblendes: implications for normalizations, calculated H₂O activities, and thermobarometry. *Contrib Mineral Petrol* 108:472-484
- Delaney JS, Bajt S, Sutton SR, Dyar MD (1996) In situ microanalysis of Fe³⁺/ΣFe in amphibole by X-ray absorption near edge structure (XANES) spectroscopy. *In: Mineral Spectroscopy: A Tribute to Roger G. Burns*. Dyar MD, McCammon C, Schaefer MW (eds). Geochemical Society Special Publication 5:165-171
- Della Ventura G, Hawthorne FC, Robert J-L, Delbove F, Welch MF, Raudsepp M (1999) Short-range order of cations in synthetic amphiboles along the richterite-pargasite join. *Eur J Mineral* 11:79-94
- Dick LA, Robinson GW (1979) Chlorine-bearing potassian hastingsite from a sphalerite skarn in southern Yukon. *Can Mineral* 17:25-26
- Dyar MD, McGuire AV, Mackwell SJ (1992) Fe³⁺/H⁺ and D/H in kaersutites: Misleading indicators of mantle source fugacities. *Geol* 20:565-568
- Dyar MD, Mackwell SJ, McGuire AV, Cross LR, Robertson JD (1993) Crystal chemistry of Fe³⁺ and H⁺ in mantle kaersutite: Implications for mantle metasomatism. *Am Mineral* 78:968-979
- Dyar MD, Gunter ME, Delaney JS, Lanzarotti A, Sutton SR (2002) Systematics in the structure and XANES spectra of pyroxenes, amphiboles, and micas as derived from oriented single crystals. *Can Mineral* 40:1375-1393

- Dyar MD, Agresti DG, Schaefer MW, Grant CA, Sklute EC (2006) Mössbauer Spectroscopy of Earth and Planetary Materials. *Ann Rev Earth Planet Sci* 34:83-125
- Eeckhout SG, De Grave E (2003) Evaluation of ferrous and ferric Mössbauer fractions. Part II. *Phys Chem Mineral* 30:142-146
- Enami M, Liou JG, Bird DK (1992) Cl-bearing amphibole in the Salton Sea geothermal system, California. *Can Mineral* 30:1077-1092
- Enders M, Speer D, Maresch WV, McCammon CA (2000) Ferric/ferrous iron ratios in sodic amphiboles: Mössbauer analysis, stoichiometry-based model calculations and the high-resolution microanalytical flank method. *Contrib Mineral Petrol* 140:135-147
- Evans BW, Yang H (1998) Fe-Mg order-disorder in tremolite-actinolite-ferro-actinolite at ambient and high temperature. *Am Mineral* 83:458-475
- Evans BW, Ghiorsio MS, Yang H, Medenbach O (2001) Thermodynamics of the amphiboles: Anthophyllite-ferroanthophyllite and the ortho-clino phase loop. *Am Mineral* 86:640-651
- Garvie LAJ, Buseck PR (1998) Ratios of ferrous to ferric iron from nanometer-sized areas in minerals. *Nature* 396:667-670
- Garvie LAJ, Zega TJ, Rez P, Buseck PR (2004) Nanometer-scale measurements of $\text{Fe}^{3+}/\Sigma\text{Fe}$ by electron energy-loss spectroscopy: A cautionary note. *Am Mineral* 89:1610-1616
- Ghose S (1961) The crystal structure of cummingtonite. *Acta Crystallogr* 14:622-627
- Gibbs GV (1966) Untitled article. *In: AGI Short Course Lecture Notes on Chain Silicates*. p 1-23
- Gibbs GV (1969) The crystal structure of protoamphibole. *Mineral Soc Am Spec Pap* 2:101-110
- Gibbs GV, Bloss FD, Shell HR (1960) Protoamphibole, a new polytype. *Am Mineral* 45:974-989
- Gottschalk M, Andrut M, Melzer S (1999) The determination of the cummingtonite content of synthetic tremolite. *Eur J Mineral* 11:967-982
- Gunter ME, Dyar MD, Twamley B, Foit FF Jr, Cornelius S (2003) Composition, $\text{Fe}^{3+}/\Sigma\text{Fe}$, and crystal structure of non-asbestiform and asbestiform amphiboles from Libby, Montana, U.S.A. *Am Mineral* 88:1970-1978
- Hanisch K (1966) Messung des Ultrarot-Pleochroismus von Mineralen. VI. Der Pleochroismus des OH-Streckfrequenz in Riebeckit. *N Jahrb Mineral Monatsh* 109-112
- Hawthorne FC (1976) The crystal chemistry of the amphiboles. V. The structure and chemistry of arfvedsonite. *Can Mineral* 14:346-356
- Hawthorne FC (1978) The crystal chemistry of the amphiboles. VIII. The crystal structure and site-chemistry of fluor-riebeckite. *Can Mineral* 16:187-194
- Hawthorne FC (1979) The crystal chemistry of the amphiboles. X. Refinement of the crystal structure of ferroglaucophane and an ideal polyhedral model for clinoamphiboles. *Can Mineral* 17:1-10
- Hawthorne FC (1981) Crystal chemistry of the amphiboles. *Rev Mineral* 9A:1-102
- Hawthorne FC (1983a) The crystal chemistry of the amphiboles. *Can Mineral* 21:173-480
- Hawthorne FC (1983b) Quantitative characterization of site occupancies in minerals. *Am Mineral* 68:287-306
- Hawthorne FC (1983c) Characterization of the average structure of natural and synthetic amphiboles. *Per Mineral Roma* 52:543-581
- Hawthorne FC (1988) Mössbauer spectroscopy. *Rev Mineral* 18:255-340
- Hawthorne FC (1992) The role of OH and H_2O in oxide and oxysalt minerals. *Z Kristallogr* 201:183-206
- Hawthorne FC (1994) Structural aspects of oxides and oxysalt crystals. *Acta Crystallogr B* 50:481-510
- Hawthorne FC (1997) Short-range order in amphiboles: a bond-valence approach. *Can Mineral* 35:201-216
- Hawthorne FC (2006) Landmark Papers: Structure Topology. Mineralogical Society of Great Britain and Ireland, London
- Hawthorne FC, Della Ventura G (2007) Short-range order in amphiboles. *Rev Mineral* 67:xxx-yyy
- Hawthorne FC, Grundy HD (1972) Positional disorder in the A-site of clino-amphiboles. *Nature* 235:72
- Hawthorne FC, Grundy HD (1973a) The crystal chemistry of the amphiboles. I. Refinement of the crystal structure of ferrotschermakite. *Mineral Mag* 39:36-48
- Hawthorne FC, Grundy HD (1973b) The crystal chemistry of the amphiboles. II. Refinement of the crystal structure of oxykaersutite. *Mineral Mag* 39:390-400
- Hawthorne FC, Grundy HD (1976) The crystal chemistry of the amphiboles. IV. X-ray and neutron refinements of the crystal structure of tremolite. *Can Mineral* 14:334-345
- Hawthorne FC, Grundy HD (1977) The crystal chemistry of the amphiboles. III. Refinement of the crystal structure of a sub-silicic hastingsite. *Mineral Mag* 41:43-50
- Hawthorne FC, Grundy HD (1978) The crystal chemistry of the amphiboles. VII. The crystal structure and site chemistry of potassian ferri-taramite. *Can Mineral* 16:53-62
- Hawthorne FC, Harlow GE (2007) The crystal chemistry of Al-rich amphiboles: sadanagaite and potassic-ferrisadanagaite. *Can Mineral* (submitted)
- Hawthorne FC, Oberti R (2007) The crystal chemistry of the amphiboles. *Rev Mineral* 67:xxx-yyy
- Hawthorne FC, Oberti R, Ungaretti L, Grice JD (1992) Leakeite, $\text{Na Na}_2(\text{Mg}_2\text{Fe}^{3+}_2)\text{Si}_8\text{O}_{22}(\text{OH})_2$, a new alkali amphibole from the Kajlidongri manganese mine, Jhabua district, Madhya Pradesh, India. *Am Mineral* 77:1112-1115

- Hawthorne FC, Ungaretti L, Oberti R, Bottazzi P, Czamanske GK (1993) Li: An important component in igneous alkali amphiboles. *Am Mineral* 78:733-745
- Hawthorne FC, Ungaretti L, Oberti R, Cannillo E, Smelik EA (1994) The mechanism of ^{6}Li incorporation in amphiboles. *Am Mineral* 79:443-451
- Hawthorne FC, Oberti R, Cannillo E, Sardone N, Zanetti A, Grice JD, Ashley PM (1995) A new anhydrous amphibole from the Hoskins mine, Grenfell, New South Wales, Australia: Description and crystal structure of ungarettiite, $\text{Na Na}_2(\text{Mn}^{2+}_2\text{Mn}^{3+}_3)\text{Si}_8\text{O}_{22}\text{O}_2$. *Am Mineral* 80:165-172
- Hawthorne FC, Oberti R, Sardone N (1996a) Sodium at the A site in clin amphiboles: the effects of composition on patterns of order. *Can Mineral* 34:577-593
- Hawthorne FC, Oberti R, Ottolini L, Foord EE (1996b) Lithium-bearing fluor-arfvedsonite from Hurricane Mountain, New Hampshire: a crystal-chemical study. *Can Mineral* 34:1015-1019
- Hawthorne FC, Oberti R, Ungaretti L, Ottolini L, Grice JD, Czamanske GK (1996c) Fluor-ferro-leakeite, $\text{Na Na}_2(\text{Fe}^{2+}_2\text{Fe}^{3+}_2\text{Li})\text{Si}_8\text{O}_{22}\text{F}_2$, a new alkali amphibole from the Cañada Pinabete pluton, Questa, New Mexico, U.S.A. *Am Mineral* 81:226-228
- Hawthorne FC, Oberti R, Zanetti A, Czamanske GK (1998) The role of Ti in hydrogen-deficient amphiboles: Sodic-calcic and sodic amphiboles from Coyote Peak, California. *Can Mineral* 36:1253-1265
- Hawthorne FC, Cooper MA, Grice JD, Ottolini L (2000) A new anhydrous amphibole from the Eifel region, Germany: Description and crystal structure of obertiite, $\text{Na Na}_2(\text{Mg}_3\text{Fe}^{3+}_2\text{Ti}^{4+})\text{Si}_8\text{O}_{22}\text{O}_2$. *Am Mineral* 85:236-241
- Hawthorne FC, Oberti R, Cannillo E, Ottolini L, Roelofsen J, Martin RM (2001) Li-bearing arfvedsonitic amphiboles from the Strange Lake peralkaline granite, Quebec. *Can Mineral* 39:1161-1170
- Hawthorne FC, Schindler M, Sokolova E, Abdu J, Evans BW, Ishida K (2007) The crystal chemistry of the gedrite-group amphiboles: II: Stereochemistry and chemical relations. *Can Mineral* (submitted)
- Höfer HE, Brey GP, Schulz-Dobrick B, Oberhänsli R (1994) The determination of the iron oxidation state by the electron microprobe. *Eur J Mineral* 6:407-418
- King PL, Hervig RL, Holloway JR, Vennemann TW, Righter K (1999) Oxy-substitution and dehydrogenation in mantle-derived amphibole megacrysts. *Geochim Cosmochim Acta* 62:3635-3651
- King PL, Hervig RL, Holloway JR, Delaney JS, Dyar MD (2000) Partitioning of $\text{Fe}^{3+}/\text{Fe}^{\text{total}}$ between amphibole and basanitic melt as a function of oxygen fugacity. *Earth Planet Sci Lett* 178:97-112
- Krutov GA (1936) Dashkesanite, a new chlorine-bearing amphibole of the hastingsite group. *Izv Akad Nauk Ser Geol* 341-373 (in Russian)
- Kullerud K (1996) Chlorine-rich amphiboles: interplay between amphibole compositions and an evolving fluid. *Eur J Mineral* 8:355-370
- Leake BE (1968) A catalog of analyzed calciferous and subcalciferous amphiboles together with their nomenclature and associated minerals. *Geol Soc Am Spec Pap* 98
- Léger A, Rebbert C, Webster J (1996) Cl-rich biotite and amphibole from Black Rock Forest, Cornwall, New York. *Am Mineral* 81:495-504
- Maresch WV, Mieke G, Czank M, Fuess H, Schreyer W (1991) Triclinic amphibole. *Eur J Mineral* 3:899-903
- McCammon CA (1994) A Mössbauer milliprobe: Practical considerations. *Hyperfine Interactions* 92:1235-1239
- McCormick KA, McDonald AM (1999) Chlorine-bearing amphiboles from the Fraser mine, Sudbury, Ontario, Canada: Description and crystal chemistry. *Can Mineral* 37:1385-1403
- McGuire AV, Dyar MD, Ward KW (1989) Neglected $\text{Fe}^{3+}/\text{Fe}^{2+}$ ratios: A study of Fe^{3+} content of megacrysts from alkali basalts. *Geol* 17:687-690
- McGuire AV, Dyar MD, Nielson JE (1991) Metasomatic oxidation of upper mantle peridotite. *Contrib Mineral Petrol* 107:252-264
- Mogessie A, Purtscheller F, Tessadri R (1986) High alumina calcic amphiboles (alumino pargasite-magnesio sadanagaite) from metabasites and metacarbonates of Central Oetztal, Eastern Alps (Northern Tyrol, Austria). *N Jahrb Mineral Abh* 154:21-39
- Moore PB (1969) Joesmithite: a novel amphibole crystal chemistry. *Mineral Soc Am Spec Pap* 2:111-115
- Moore PB, Davis AM, Van Derveer DG, Sen Gupta PK (1993) Joesmithite, a plumbous amphibole revisited and comments on bond valences. *Mineral Petrol* 48:97-113
- Morrison J (1991) Compositional constraints on the incorporation of Cl into amphiboles. *Am Mineral* 76:1920-1930
- Murad E, Cashion J (2004) *Mössbauer Spectroscopy of Environmental Materials and Their Industrial Utilization*. Kluwer, Dordrecht
- Nasir S, Al-Rawas AD (2006) Mössbauer characterization of upper mantle ferrikaersutite. *Am Mineral* 91:1163-1169
- Oberti R, Ghose S (1993) Crystal-chemistry of a complex Mn-bearing alkali amphibole ("tiroidite") on the verge of exsolution. *Eur J Mineral* 5:1153-1160
- Oberti R, Ungaretti L, Cannillo E, Hawthorne FC (1993) The mechanism of Cl incorporation in amphibole. *Am Mineral* 78:746-752

- Oberti R, Ungaretti L, Cannillo E, Hawthorne FC, Memmi I (1995a) Temperature-dependent Al order-disorder in the tetrahedral double-chain of *C2/m* amphiboles. *Eur J Mineral* 7:1049-1063
- Oberti R, Sardone N, Hawthorne FC, Raudsepp M, Turnock AC (1995b) Synthesis and crystal-structure refinement of synthetic fluor-pargasite. *Can Mineral* 33:25-31
- Oberti R, Hawthorne FC, Cámara F, Raudsepp M (1998) Synthetic fluoro-amphiboles: site preferences of Al, Ga, Sc and inductive effects on mean bond-lengths of octahedra. *Can Mineral* 36:1245-1252
- Oberti R, Caballero JM, Ottolini L, López-Andrés S, Herreros V (2000) Sodic-ferripedrizite, a new monoclinic amphibole bridging the magnesium-manganese-lithium and the sodium-calcium groups. *Am Mineral* 85:578-585
- Oberti R, Cámara F, Caballero JM, Ottolini L (2003a) Sodic-ferri-ferropedrizite and ferri-clinoferroholmquistite: Mineral data and degree of order of the A-site cations in Li-rich amphiboles. *Can Mineral* 41:1345-1354
- Oberti R, Cámara F, Ottolini L, Caballero JM (2003b) Lithium in amphiboles: detection, quantification and incorporation mechanisms in the compositional space bridging sodic and ⁶Li amphiboles. *Eur J Mineral* 15:309-319
- Oberti R, Cámara F, Caballero JM (2004) Ferri-ottoliniite and ferriwhittakerite, two new end-members of the new Group 5 for monoclinic amphiboles. *Am Mineral* 89:888-893
- Oberti R, Hawthorne FC, Cannillo E, Cámara F (2007a) Long-range order in amphiboles. *Rev Mineral* 67:xxx-yyy
- Oberti R, Della Ventura G, Cámara F (2007b) New amphibole compositions. *Rev Mineral* 67:xxx-yyy
- Oberti R, Boiocchi M, Smith DC, Medenbach O (2007c) Aluminotaramite, aluminomagnesirotaramite, and fluoro-alumino-magnesirotaramite: mineral data and crystal chemistry. *Am Mineral* 92:1428-1435
- Ottolini L, Hawthorne FC (2001) SIMS ionization of hydrogen in silicates: A case study of kornepupine. *J Anal Atomic Spectrom* 16:1266-1270
- Ottolini L, Oberti R (2000) Accurate quantification of H, Li, Be, B, F, Ba, REE, Y, Th and U in complex matrices: a combined approach based on SIMS and single-crystal structure refinement. *Anal Chem* 72(16):3731-3738
- Ottolini L, Bottazzi P, Vannucci R (1993) Quantification of Li, Be and B in silicates by secondary ion mass spectrometry using conventional energy filtering. *Anal Chem* 65:1960-1968
- Ottolini L, Bottazzi P, Zanetti A, Vannucci R (1995) Determination of hydrogen in silicates by secondary ion mass spectrometry. *Analyst* 120:1309-1313
- Papike JJ, Ross M, Clarke JR (1969) Crystal chemical characterization of clinoamphiboles based on five new structure refinements. *Mineral Soc Am Spec Pap* 2:117-136
- Papike JJ, Cameron KL, Baldwin K (1974) Amphiboles and pyroxenes: characterization of OTHER than quadrilateral components and estimates of ferric iron from microprobe data. *Geol Soc Am Abstr Prog* 6:1053-1054
- Popp RK, Virgo D, Yoder HS Jr, Hoering TC, Phillips MW (1995) An experimental study of phase equilibria and Fe oxy-component in kaersutitic amphibole: implications for the f_{H_2} and $a_{\text{H}_2\text{O}}$ in the upper mantle. *Am Mineral* 80:534-548
- Popp RK, Hibbert HA, Lamb WM (2006) Oxy-amphibole equilibria in Ti-bearing calcic amphiboles: Experimental investigation and petrologic implications for mantle-derived amphiboles. *Am Mineral* 91:54-66
- Previde Massara E (1990) Studio cristallografico delle principali fasi mineralogiche delle eclogiti di Liset (Western Gneiss Region, Norvegia). PhD Dissertation, Università di Pavia, Italy
- Rastsvetaeva RK, Puscharovskii DY, Vinogradova RA, Pekov IV (1996) Crystal structure of dashkesanite. *Crystallogr Rep* 41(1):58-62
- Robinson K, Gibbs GV, Ribbe PH, Hall MR (1973) Cation distributions in three hornblendes. *Am J Sci* 273A:522-535
- Robinson P, Ross M, Jaffe HW (1971) Composition of the anthophyllite-gedrite series, comparisons of gedrite-hornblende, and the anthophyllite-gedrite solvus. *Am Mineral* 56:1004-1041
- Rossi G, Oberti R, Dal Negro A, Molin GM, Mellini M (1987) Residual electron density at the M2 site in *C2/c* clinopyroxenes: relationships with bulk chemistry and sub-solidus evolution. *Phys Chem Mineral* 14:514-520
- Sato H, Yamaguchi Y, Makino K (1997) Cl incorporation into successively zoned amphiboles from the Ramnes cauldron, Norway. *Am Mineral* 82:316-324
- Sawaki T (1989) Sadanagaite and subsilicic ferroan pargasite from thermally metamorphosed rocks in the Nogo-Hakusan area, central Japan. *Mineral Mag* 53:99-106
- Schindler M, Sokolova E, Abdu J, Hawthorne FC, Evans BW, Ishida K (2007) The crystal chemistry of the gedrite-group amphiboles: I: Crystal structure and site populations. *Can Mineral* (submitted)
- Schumacher JC (1991) Empirical ferric iron corrections: necessity, assumptions, and effects on selected geothermobarometers. *Mineral Mag* 55:3-18

- Schumacher JC (1997) Appendix 2. The estimation of the proportion of ferric iron in the electron-microprobe analysis of amphiboles. *Can Mineral* 35:238-246
- Schumacher JC (2007) Metamorphic amphiboles: compositions and coexistence. *Rev Mineral* 67: xxx-yyy
- Shannon RD (1976) Revised effective ionic radii and systematic studies of interatomic distances in halides and chalcogenides. *Acta Crystallogr A* 32:751-767
- Shimazaki H, Bunno M, Ozawa T (1984) Sadanagaite and magnesio-sadanagaite, new silica-poor members of calcic amphibole from Japan. *Am Mineral* 69:465-471
- Sokolova EV, Hawthorne FC, Kabalov Y, Schneider J, McCammon C (2000a) The crystal chemistry of potassic-ferrisadanagaite. *Can Mineral* 38:669-674
- Sokolova EV, Kabalov YuK, McCammon C, Schneider J, Konev, AA (2000b) Cation partitioning in an unusual stromtrian potassicrichterite from Siberia: Rietveld structure refinement and Mössbauer spectroscopy. *Mineral Mag* 64:19-24
- Sokolova EV, Hawthorne FC, Gorbatova V, McCammon C, Schneider J (2001) Ferrian winchite from the Ilmen Mountains, Southern Urals, Russia, and some problems with the current scheme for amphibole nomenclature. *Can Mineral* 39:171-177
- Stout JH (1972) Phase petrology and mineral chemistry of coexisting amphiboles from Telemark, Norway. *J Petrol* 13:99-145
- Sueno S, Matsubara S, Gibbs GV, Boisen MB Jr (1998) A crystal chemical study of protoanthophyllite: orthoamphiboles with the protoamphibole structure. *Phys Chem Mineral* 25:366-377
- Suwa K, Enami M, Horiuchi T (1987) Chlorine-rich potassium hastingsite from West Ongul Island, Lützow-Holm Bay, East Antarctica. *Mineral Mag* 51:709-714
- Tait KT, Hawthorne FC, Grice JD, Ottolini L, Nayak VK (2005) Dellaventuraite, Na₂(MgMn³⁺₂Ti⁴⁺Li)Si₈O₂₂O₂, a new anhydrous amphibole from the Kajlidongri Manganese Mine, Jhabua District, Madhya Pradesh, India. *Am Mineral* 90:304-309
- Tiepolo M, Zanetti A, Oberti R (1999) Detection, crystal-chemical mechanisms and petrological implications of ¹⁶Ti⁴⁺ partitioning in pargasite and kaersutite. *Eur J Mineral* 11:345-354
- Tiepolo M, Zanetti A, Vannucci R (2005) Determination of lithium, beryllium and boron at trace levels by laser ablation-inductively couple plasma-sector field mass spectrometry. *Geostandards Geoanalytical Res* 29:211-224
- Ungaretti L (1980) Recent developments in X-ray single crystal diffractometry applied to the crystal-chemical study of amphiboles. *God Jugosl Cent Krist* 15:29-65
- Uvarova Y, McCammon C, Sokolova E, Hawthorne FC, Lobanov KV, Kazansky VI (2005) Fe³⁺ content and Ti⁴⁺ ordering in amphiboles from the Kola Superdeep Borehole: Correlation of crystal-chemical and Mössbauer measurements. GAC-MAC-CSPG-CSSS Joint Meeting, Halifax, Abstracts 30:197
- van Aken PA, Liebscher B (2002) Quantification of ferrous/ferric ratios in minerals: new evaluation schemes of Fe L_{2,3} electron energy-loss near-edge spectra. *Phys Chem Mineral* 29:188-200
- Vanko DA (1986) High-chlorine amphiboles from oceanic rocks: product of highly saline hydrothermal fluids? *Am Mineral* 71:51-59
- Volfinger M, Robert JL, Vielzeuf D, Neiva AMR (1985) Structural control of the chlorine content of OH-bearing silicates (micas and amphiboles). *Geochim Cosmochim Acta* 49:37-48
- Warren BE (1930) The crystal structure and chemical composition of the monoclinic amphiboles. *Z Kristallogr* 72:493-517
- Welch MD, Cámara F, Della Ventura G, Iezzi G (2007) Non-ambient *in situ* studies of amphiboles. *Rev Mineral* 67: xxx-yyy
- Whittaker EJW (1960) The crystal chemistry of the amphiboles. *Acta Crystallogr* 13:291-298
- Zanetti A, Vannucci R, Bottazzi P, Oberti R, Ottolini L (1996) Infiltration metasomatism at Lherz as monitored by systematic ion-microprobe investigations close to a hornblende vein. *Chem Geol* 134:113-133
- Zhu C, Xu H, Ilton ES, Veblen DR, Henry DJ, Tivey MK, Thompson G (1994) TEM-AEM observations of Cl-rich amphibole and biotite and possible petrologic implications. *Am Mineral* 79:909-920

APPENDIX 1: CRYSTAL-STRUCTURE REFINEMENTS OF AMPHIBOLE

- Bocchio R, Ungaretti L, Rossi G (1978) Crystal chemical study of eclogitic amphiboles from Alpe Arami, Lepontine Alps, Southern Switzerland. *Rend Soc Ital Mineral Petrol* 34:453-470
- Bojar H-P, Walitzi F (2006) Fluor-magnesiohastingsite from Dealul Uroi (Hunedoara county, Romania): Mineral data and crystal structure of a new amphibole end-member. *Eur J Mineral* 18:503-508
- Boschmann K, Burns PC, Hawthorne FC, Raudsepp M, Turnock AC (1994) A-site disorder in synthetic fluor-edenite, a crystal structure study. *Can Mineral* 32:21-30
- Caballero JM, Monge A, La Iglesia A, Tornos F (1998) Ferri-clinoholmquistite, Li₂(Fe²⁺,Mg)₃Fe³⁺₂Si₈O₂₂(OH)₂, a new ^BLi clinioamphibole from the Pedriz Massif, Sierra de Guadarrama, Spanish Central System. *Am Mineral* 83:167-171

- Caballero JM, Oberti R, Ottolini L (2002) Ferripedrizite, a new monoclinic ${}^{\text{B}}\text{Li}$ amphibole end-member from the Eastern Pedriza Massif, Sierra de Guadarrama, Spain, and a restatement of the nomenclature of Mg-Fe-Mn-Li amphiboles. *Am Mineral* 87:976-982
- Cámara F, Oberti R (2005) The crystal-chemistry of holmquistites: Ferroholmquistite from Greenbushes (Western Australia) and hints for compositional constraints in ${}^{\text{B}}\text{Li}$ amphiboles. *Am Mineral* 90:1167-1176
- Cámara F, Oberti R, Iezzi G, Della Ventura G (2003) The $P2_1/m \leftrightarrow C2/m$ phase transition in synthetic amphibole $\text{Na NaMg Mg}_5 \text{Si}_8 \text{O}_{22} (\text{OH})_2$: thermodynamic and crystal-chemical evaluation. *Phys Chem Mineral* 30:570-581
- Cámara, F, Oberti F, Della Ventura G, Welch MD, Mareschi WV (2004) The crystal-structure of synthetic $\text{NaNa}_2\text{Mg}_5\text{Si}_8\text{O}_{21}(\text{OH})_3$, a triclinic $\text{C}\bar{1}$ amphibole with a triple-cell and excess hydrogen. *Am Mineral* 89:1464-1473
- Cameron M, Gibbs GV (1971) Refinement of the crystal structure of two synthetic fluor-richferites. *Carnegie Inst Wash Year Book* 70:150-153
- Cameron M, Gibbs GV (1973) The crystal structure and bonding of fluor-tremolite: a comparison with hydroxyl tremolite. *Am Mineral* 58:879-888
- Cameron M, Sueno S, Papike JJ, Prewitt CT (1983) High temperature crystal chemistry of K and Na fluor-richferites. *Am Mineral* 68:924-943
- Evans BW, Yang H (1998) Fe-Mg order-disorder in tremolite-actinolite-ferro-actinolite at ambient and high temperature. *Am Mineral* 83:458-475
- Evans BW, Ghiorso MS, Yang H, Medenbach O (2001) Thermodynamics of the amphiboles: Anthophyllite-ferroanthophyllite and the ortho-clino phase loop. *Am Mineral* 86:640-651
- Ghose S (1961) The crystal structure of cummingtonite. *Acta Crystallogr* 14:622-627
- Gibbs GV (1969) The crystal structure of protoamphibole. *Mineral Soc Am Spec Pap* 2:101-110
- Gunter ME, Dyar MD, Twamley B, Foit FF Jr, Cornelius S (2003) Composition, $\text{Fe}^{3+}/\Sigma\text{Fe}$, and crystal structure of non-asbestiform and asbestiform amphiboles from Libby, Montana, U.S.A. *Am Mineral* 88:1970-1978
- Hawthorne FC (1976) The crystal chemistry of the amphiboles. V. The structure and chemistry of arfvedsonite. *Can Mineral* 14:346-356
- Hawthorne FC (1978) The crystal chemistry of the amphiboles. VIII. The crystal structure and site-chemistry of fluor-riebeckite. *Can Mineral* 16:187-194
- Hawthorne FC (1979) The crystal chemistry of the amphiboles. X. Refinement of the crystal structure of ferroglaucophane and an ideal polyhedral model for clinoamphiboles. *Can Mineral* 17:1-10
- Hawthorne FC (1983) The crystal chemistry of the amphiboles. *Can Mineral* 21:173-480
- Hawthorne FC, Grundy HD (1973a) The crystal chemistry of the amphiboles. I. Refinement of the crystal structure of ferrotschermakite. *Mineral Mag* 39:36-48
- Hawthorne FC, Grundy HD (1973b) The crystal chemistry of the amphiboles. II. Refinement of the crystal structure of oxykaersutite. *Mineral Mag* 39:390-400
- Hawthorne FC, Grundy HD (1976) The crystal chemistry of the amphiboles. IV. X-ray and neutron refinements of the crystal structure of tremolite. *Can Mineral* 14:334-345
- Hawthorne FC, Grundy, HD (1977) The crystal chemistry of the amphiboles. III. Refinement of the crystal structure of a sub-silicic hastingsite. *Mineral Mag* 41:43-50
- Hawthorne FC, Grundy HD (1978) The crystal chemistry of the amphiboles. VII. The crystal structure and site chemistry of potassian ferri-taramite. *Can Mineral* 16:53-62
- Hawthorne FC, Harlow GE (2007) The crystal chemistry of Al-rich amphiboles: sadanagaite and potassic-ferri-sadanagaite. *Can Mineral* (submitted)
- Hawthorne FC, Griep JL, Curtis L (1980) A three amphibole assemblage from the Tallan Lake sill, Peterborough County, Ontario. *Can Mineral* 18:275-284
- Hawthorne FC, Oberti R, Ungaretti L, Grice JD (1992) Leakeite, $\text{NaNa}_2(\text{Mg}_2\text{Fe}^{3+}_2)\text{Si}_8\text{O}_{22}(\text{OH})_2$, a new alkali amphibole from the Kajlidongri manganese mine, Jhabua district, Madhya Pradesh, India. *Am Mineral* 77:1112-1115
- Hawthorne FC, Ungaretti L, Oberti R, Bottazzi P, Czamanske GK (1993) Li: An important component in igneous alkali amphiboles. *Am Mineral* 78:733-745
- Hawthorne FC, Ungaretti L, Oberti R, Cannillo E, Smelik EA (1994) The mechanism of ${}^{6}\text{Li}$ incorporation in amphiboles. *Am Mineral* 79:443-451
- Hawthorne FC, Oberti R, Cannillo E, Sardone N, Zanetti A, Grice JD, Ashley PM (1995) A new anhydrous amphibole from the Hoskins mine, Grenfell, New South Wales, Australia: Description and crystal structure of ungarettiite, $\text{NaNa}_2(\text{Mn}^{2+}_2\text{Mn}^{3+}_3)\text{Si}_8\text{O}_{22}\text{O}_2$. *Am Mineral* 80:165-172
- Hawthorne FC, Oberti R, Sardone N (1996a) Sodium at the A site in clinoamphiboles: the effects of composition on patterns of order. *Can Mineral* 34:577-593
- Hawthorne FC, Oberti R, Ottolini L, Foord EE (1996b) Lithium-bearing fluor-arfvedsonite from Hurricane Mountain, New Hampshire: a crystal-chemical study. *Can Mineral* 34:1015-1019

- Hawthorne FC, Oberti R, Ungaretti L, Ottolini L, Grice JD, Czamanske GK (1996c) Fluor-ferro-leakeite, $\text{NaNa}_2(\text{Fe}_2^{2+}\text{Fe}_3^{2+}\text{Li})\text{Si}_8\text{O}_{22}\text{F}_2$, a new alkali amphibole from the Cañada Pinabete pluton, Questa, New Mexico, U.S.A. *Am Mineral* 81:226-228
- Hawthorne FC, Oberti R, Ungaretti L, Grice JD (1996d) A new hyper-calcic amphibole with Ca at the A site: Fluor-cannilloite from Pargas, Finland. *Am Mineral* 81:995-1002
- Hawthorne FC, Oberti R, Zanetti A, Czamanske GK (1998) The role of Ti in hydrogen-deficient amphiboles: Sodic-calcic and sodic amphiboles from Coyote Peak, California. *Can Mineral* 36:1253-1265
- Hawthorne FC, Cooper MA, Grice JD, Ottolini L (2000) A new anhydrous amphibole from the Eifel region, Germany: Description and crystal structure of obertiite, $\text{NaNa}_2(\text{Mg}_3\text{Fe}^{3+}\text{Ti}^{4+})\text{Si}_8\text{O}_{22}\text{O}_2$. *Am Mineral* 85:236-241
- Hawthorne FC, Oberti R, Cannillo E, Ottolini L, Roelofsen J, Martin RM (2001) Li-bearing arfvedsonitic amphiboles from the Strange Lake peralkaline granite, Quebec. *Can Mineral* 39:1161-1170
- Hawthorne FC, Oberti R, Martin RF (2006) Short-range order in amphiboles from the Bear Lake diggings, Ontario. *Can Mineral* 44:1171-1179
- Hawthorne FC, Schindler M, Sokolova E, Abdu J, Evans BW, Ishida K (2007) The crystal chemistry of the gedrite-group amphiboles: II: Stereochemistry and chemical relations. *Can Mineral* (submitted)
- Karanovic LJ, Krstanovic I, Ungaretti L (1990) Crystal structure and cation distribution in hornblendes. *Bulletin, Academie Serbe des Sciences et des Arts, Classe des Sciences Mathematiques et Naturelles, Sciences Naturelles* 32:21-28
- Makino K, Tomita K (1989) Cation distribution in the octahedral sites of hornblendes. *Am Mineral* 74:1097-1105
- Mancini F, Sillanpää R, Marshall B, Papunen H (1996) Magnesian hornblende from a metamorphosed ultramafic body in Southwestern Finland: crystal chemistry and petrological implications. *Can Mineral* 34:835-844
- Matsubara S, Miyawaki R, Kurosawa M, Suzuki Y (2002) Potassicleakeite, a new amphibole from the Tanohata mine, Iwate prefecture, Japan. *J Mineral Petrol Sci* 97:177-184
- Mitchell JT, Bloss FD, Gibbs GV (1971) Examination of the actinolite structure and four other $C2/m$ amphiboles in terms of double bonding. *Z Kristallogr* 133:273-300
- Moore PB (1969) Joesmithite: a novel amphibole crystal chemistry. *Mineral Soc Am Spec Pap* 2:111-115
- Moore PB, Davis AM, Van Derveer DG, Sen Gupta PK (1993) Joesmithite, a plumbous amphibole revisited and comments on bond valences. *Mineral Petrol* 48:97-113
- Oberti R, Ghose S (1993) Crystal-chemistry of a complex Mn-bearing alkali amphibole ("tiroditite") on the verge of exsolution. *Eur J Mineral* 5:1153-1160
- Oberti R, Ungaretti L, Cannillo E, Hawthorne FC (1992) The behaviour of Ti in amphiboles. I. Four- and six-coordinate Ti in richterite. *Eur J Mineral* 3:425-439
- Oberti R, Ungaretti L, Cannillo E, Hawthorne FC (1993a) The mechanism of Cl incorporation in amphibole. *Am Mineral* 78:746-752
- Oberti R, Hawthorne FC, Ungaretti L, Cannillo E (1993b) The behaviour of Mn in amphiboles: Mn in richterite. *Eur J Mineral* 5:43-52
- Oberti R, Hawthorne FC, Ungaretti L, Cannillo E (1995a) $^{6\text{Al}}$ disorder in amphiboles from mantle peridotites. *Can Mineral* 33:867-878
- Oberti R, Ungaretti L, Cannillo E, Hawthorne FC, Memmi I (1995b) Temperature-dependent Al order-disorder in the tetrahedral double-chain of $C2/m$ amphiboles. *Eur J Mineral* 7:1049-1063
- Oberti R, Sardone N, Hawthorne FC, Raudsepp M, Turnock AC (1995c) Synthesis and crystal-structure refinement of synthetic fluor-pargasite. *Can Mineral* 33:25-31
- Oberti R, Hawthorne FC, Raudsepp M (1997) The behaviour of Mn in amphiboles: Mn in synthetic fluor-edenite and synthetic fluor-pargasite. *Eur J Mineral* 9:115-122
- Oberti R, Hawthorne FC, Cámara F, Raudsepp M (1998) Synthetic fluoro-amphiboles: site preferences of Al, Ga, Sc and inductive effects on mean bond-lengths of octahedra. *Can Mineral* 36:1245-1252
- Oberti R, Hawthorne FC, Cámara F, Raudsepp M (1999) Unusual $^{\text{C}}\text{M}^{3+}$ cations in synthetic amphiboles with nominal fluoro-eckermannite composition: Deviations from stoichiometry and structural effects of the cummingtonite component. *Am Mineral* 84:102-111
- Oberti R, Caballero JM, Ottolini L, López-Andrés S, Herreros V (2000) Sodic-ferripedrizite, a new monoclinic amphibole bridging the magnesium-manganese-lithium and the sodium-calcium groups. *Am Mineral* 85:578-585
- Oberti R, Cámara F, Caballero JM, Ottolini L (2003a) Sodic-ferri-ferropedrizite and ferri-clinoferroholmquistite: Mineral data and degree of order of the A-site cations in Li-rich amphiboles. *Can Mineral* 41:1345-1354
- Oberti R, Cámara F, Ottolini L, Caballero JM (2003b) Lithium in amphiboles: detection, quantification and incorporation mechanisms in the compositional space bridging sodic and $^{\text{B}}\text{Li}$ amphiboles. *Eur J Mineral* 15:309-319
- Oberti R, Boiocchi M, Smith DC (2003c) Fluoronyböite from Jianchang (Su-Lu, China) and nyböite from Nybø (Nordfjord, Norway): description and comparison of two high-pressure amphibole end-members. *Mineral Mag* 67:769-782

- Oberti R, Cámara F, Caballero JM (2004) Ferri-ottoliniite and ferriwhittakerite, two new end-members of the new Group 5 for monoclinic amphiboles. *Am Mineral* 89:888-893
- Oberti R, Boiocchi M, Smith DC, Medenbach O (2007) Aluminotaramite, alumino-magnesiostaramite, and fluoro-alumino-magnesiostaramite: Mineral data and crystal chemistry. *Am Mineral* 92:1428-1435
- Papike JJ, Ross M, Clarke JR (1969) Crystal chemical characterization of clinoamphiboles based on five new structure refinements. *Mineral Soc Am Spec Pap* 2:117-136
- Pechar F, Fuess H, Joswig W (1989) Refinement of the crystal structure of kaersutite (Vlci Hora Bohemia) from neutron diffraction. *N Jahrb Mineral Mh* 1989:137-143
- Phillips MW, Popp RK, Clowe CA (1988) Structural adjustments accompanying oxidation-dehydrogenation in amphiboles. *Am Mineral* 73:500-506
- Phillips MW, Draheim JE, Popp RK, Clowe CA, Pinkerton AA (1989) Effects of oxidation-dehydrogenation in tschermakitic hornblende. *Am Mineral* 74:764-773
- Pushcharovskii DYu, Lebedeva YuS, Pekov IV, Ferraris G, Novakova AA, Ivaldi G (2003) Crystal structure of magnesiokatophorite. *Crystallogr Rep* 48:16-23
- Rastsvetaeva RK, Puscharovskii DY, Vinogradova RA, Pekov IV (1996) Crystal structure of dashkesanite. *Crystallogr Rep* 41:58-62
- Redhammer GJ, Roth G (2002) Crystal structure and Mössbauer spectroscopy of the synthetic amphibole potassic-ferri-ferrorichterite at 298 K and low temperatures (80–110 K). *Eur J Mineral* 14:105-114
- Robinson GW, Grice JD, Gault RA, Lalonde AE (1997) Potassicpargasite, a new member of the amphibole group from Pargas, Turku-Pori, Finland. *Can Mineral* 35:1535-1540
- Robinson K, Gibbs GV, Ribbe PH, Hall MR (1973) Cation distributions in three hornblendes. *Am J Sci* 273A:522-535
- Schindler M, Sokolova E, Abdu J, Hawthorne FC, Evans BW, Ishida K (2007) The crystal chemistry of the gedrite-group amphiboles: I: Crystal structure and site populations. *Can Mineral* (submitted)
- Sokolova EV, Hawthorne FC, Kabalov Y, Schneider J, McCammon C (2000a) The crystal chemistry of potassic-ferrisadanagaite. *Can Mineral* 38:669-674
- Sokolova EV, Kabalov YuK, McCammon C, Schneider J, Konev, AA (2000b) Cation partitioning in an unusual strontian potassicrichterite from Siberia: Rietveld structure refinement and Mössbauer spectroscopy. *Mineral Mag* 64:19-24
- Sokolova EV, Hawthorne FC, Gorbatova V, McCammon C, Schneider J (2001) Ferrian winchite from the Ilmen Mountains, Southern Urals, Russia, and some problems with the current scheme for amphibole nomenclature. *Can Mineral* 39:171-177
- Sueno S, Matsubara S, Gibbs GV, Boisen MB Jr (1998) A crystal chemical study of protoanthophyllite: orthoamphiboles with the protoamphibole structure. *Phys Chem Mineral* 25:366-377
- Tait T, Hawthorne FC, Grice JD, Ottolini L, Nayak VK (2005) Dellaventuraite, $\text{NaNa}_2(\text{MgMn}^{3+}_2\text{Ti}^{4+}\text{Li})\text{Si}_8\text{O}_{22}\text{O}_2$, a new anhydrous amphibole from the Kajlidongri Manganese Mine, Jhabua District, Madhya Pradesh, India. *Am Mineral* 90:304-309
- Tartarotti P, Caucia F (1993) Coexisting cummingtonite - sodic amphibole pair in metaquartzites from the ophiolite's sedimentary cover (St. Marcel Valley, Italian Western Alps): A X-ray structure refinement and petrology study. *N Jahrb Mineral Abh* 165:223-243
- Tiepolo M, Zanetti A, Oberti R (1999) Detection, crystal-chemical mechanisms and petrological implications of $^{69}\text{Ti}^{4+}$ partitioning in pargasite and kaersutite. *Eur J Mineral* 11:345-354
- Ungaretti L (1980) Recent developments in X-ray single crystal diffractometry applied to the crystal-chemical study of amphiboles. *God Jugosl Cent Krist* 15:29-65
- Walitzi EM, Walter F (1981) Verfeinerung der Kristallstruktur eines basaltischen Magnesio-Hastingsites. *Z Kristallogr* 156:197-208
- Walitzi EM, Eitinger K (1986) Verfeinerung der Kristallstruktur eines Tremolites vom Ochsenkogel (Gleinalpe/Steiermark), Oesterreich. *N Jahrb Mineral Mh* 1986:360-366
- Warren BE (1930) The crystal structure and chemical composition of the monoclinic amphiboles. *Z Kristallogr* 72:493-517
- Yang H, Evans BW (1996) X-ray structure refinements of tremolite at 140 and 295K: Crystal chemistry and petrologic implications. *Am Mineral* 81:1117-1125
- Yang H, Konzett J, Prewitt CT, Fei Y (1999) Single-crystal structure refinement of synthetic ^{84}K -substituted potassic richterite, $\text{K}(\text{KCa})\text{Mg}_5\text{Si}_8\text{O}_{22}(\text{OH})_2$. *Am Mineral* 84:681-684

Classification of the Amphiboles

Frank C. Hawthorne

*Department of Geological Sciences
University of Manitoba, Winnipeg, Manitoba R3T 2N2, Canada
clhawth@ms.umanitoba.ca*

Roberta Oberti

*Istituto di Geoscienze e Georisorse, Consiglio Nazionale delle Ricerche
I-27100 Pavia, Italy
oberti@crystal.unipv.it*

INTRODUCTION

Classification is always a highly contentious issue, particular when dealing with a group of minerals as structurally and chemically complicated as the amphiboles, and when trying to satisfy the needs and different scientific philosophies of crystallographers, mineralogists, petrologists and geochemists. As a result, the classification of the amphiboles has long been a *work in progress*. Leake (1968) provided a classification for calcic amphiboles, and this was expanded into the IMA (International Mineralogical Association) classification of Leake (1978). An IMA Subcommittee on Amphibole Classification was formed, and eleven years and approximately 1200 pages of memos later, Leake et al. (1997) reported on the current classification, as modified by Leake et al. (2003) to incorporate new discoveries in amphibole compositions in the intervening years. Here, we will (1) describe the current IMA-approved classification scheme, (2) discuss some shortcomings of the current scheme, and (3) discuss some of the features that may be considered as desirable in any new scheme of amphibole classification that may emerge in the future. We make no apology for dealing with these issues here; if the community who deals with amphiboles is to get the classification that it wants, that community has to be prepared to involve itself in the process of developing such a classification.

THE CURRENT CLASSIFICATION SCHEMES

The first thing to note is that the above title refers to classification schemes. There are two distinct classification schemes:

- (1) Hand-specimen and thin-section classification;
- (2) Classification by chemical formula.

Virtually all attention has focused on classification (2) and classification (1) seems to have escaped the attention of most critics of amphibole classification. Here, we will describe both schemes which are given by Leake et al. (1997, 2003).

HAND-SPECIMEN (FIELD) CLASSIFICATION OF AMPHIBOLES

To quote from Leake et al. (1997), “for amphiboles of which the general nature only is known, for instance from optical properties without a chemical analysis, it is not generally possible to assign a precise name. The nearest assigned amphibole name should then be made

into an adjective followed by the word *amphibole*. Thus, anthophyllitic amphibole, tremolitic amphibole, etc. The familiar word *hornblende* can still be used where appropriate for calcic amphiboles in both hand specimen and thin section, because hornblende is never used without an adjective in the (chemical) classification....”.

Although the need for a hand-specimen (field) and thin-section classification is recognized, the scheme that is provided cannot be considered as adequate. First, identification of amphiboles in hand specimen and in thin section are two very different processes; polarized-light microscopy is capable of being far more discerning than recognition by the naked eye alone, and two classification schemes are more appropriate than one to deal with these two situations. Secondly, each classification will be precise, and the accuracy of the process depends on the expertise of the practitioner. Thus it is to be hoped that any new generation of amphibole classification will provide suitable classification schemes for amphiboles identified in hand specimen and thin section.

Asbestiform amphiboles should be named such that their asbestiform character is conveyed by their name. Where the type of amphibole is unknown, *asbestos* or *amphibole asbestos* is appropriate. Where the approximate nature of the amphibole is known, the name of the amphibole is turned into an adjective and used as a prefix to the word asbestos: *anthophyllitic asbestos*, *tremolitic asbestos*. Where the chemical composition of the amphibole is known, the exact name of the amphibole is used, followed by the suffix -asbestos: *anthophyllite-asbestos*, *tremolite-asbestos*.

AMPHIBOLE CLASSIFICATION BY CHEMICAL FORMULA

The production of a satisfactory classification of the amphiboles seems to be a process with a long gestation period. The first IMA classification scheme was published almost thirty years ago (Leake 1978). A new approach was initiated in 1986, and culminated in the scheme of Leake et al. (1997), but subsequent discoveries of novel compositions of amphiboles (e.g., Oberti et al. 2000, 2003, 2004; Caballero et al. 2002) forced revision of this scheme (Leake et al. 2003). Hawthorne and Oberti (2006) considered the classification of amphiboles in general, and discussed many aspects of classification that impact on the establishment of a new classification scheme. Here, we will describe the current classification scheme (Leake et al. 1997, as modified by Leake et al. 2003), and then will discuss aspects of amphibole classification that will/should be considered in any new classification scheme that will be developed in the future.

Prefixes

The topic of prefixes and adjectival modifiers has generated much discussion since Leake et al. (1978) formalized their use for amphiboles. First, it must be noted that *the use of prefixes has nothing to do with the number of species*; the number of species is dictated (1) by the details of the classification criteria, and (2) by Nature herself; the issue here is what kind of names are preferable. There are two types of names that we may use: (1) each distinct species is a trivial name; (2) we may identify root names corresponding to distinct charge arrangements, and indicate homovalent variants by prefixes. The amphibole classifications of Leake (1978) and Leake et al. (1997) chose the second option and discarded 220 trivial names for amphiboles, and few would wish to return to a situation where there are several hundred trivial names for amphiboles. Thus we use root names plus indicators of homovalent variants. We prefer word prefixes to element suffixes, although recent classification schemes for other mineral groups have adopted multiple element suffixes. However, the complexity of the amphibole formula, combined with the variations in space group, may require an unwieldy concatenation of suffixes (see below for additional discussion). Prefixes defined by Leake et al. (1997, 2003) are listed in Table 1. Burke and Leake (2004) specified in which order prefixes (when more than one is used) must be attached to the root-name. Their sequence is proto-parvo (magno)-fluoro (chloro)-potassic (sodic)-

Table 1. Prefixes (from Leake et al. 1997, 2003).

Prefix	Meaning (apfu)	Applicable to
Alumino	$^{[6]}Al > 1.00$	Calcic and sodic-calcic groups only
Chloro	$Cl > 1.00$	All groups
Chromio	$Cr > 1.00$	All groups
Ferri	$Fe^{3+} > 1.00$	All groups except sodic
Ferric	$Fe^{3+} > 1.00$	Sodic amphiboles only
Fluoro	$F > 1.00$	All groups
Mangano	$1.00 < Mn^{2+} < 4.99$	All groups, except for kozulite and ungarrettiite
Permangano	$3.00 < Mn^{2+} < 4.99$	All groups, except for kozulite
Mangani	$Mn^{3+} > 1.00$	All groups, except for kornite and ungarrettiite
Magno	$^B Li \leq 0.50$ $^B (Mg+Fe^{2+}+Mn+Li) > 1.00$	Na-Ca-Mg-Fe-Mn-Li group only
Parvo	$^B Li \leq 0.50$ $^B (Ca+Na) > 1.00$	Na-Ca-Mg-Fe-Mn-Li group only
Potassic	$K > 0.50$	All groups
Sodic	$Na > 0.50$	Mg-Fe-Mn-Li group only
Titano	$Ti > 0.50$	All groups, except for kaersutite
Zinco	$Zn > 1.00$	All groups

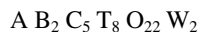
ferri (alumino, mangani)-ferro(mangano, magnesio). In addition, the first prefix attached to the root name does not involve a hyphen (e.g., ferropargasite, ferritaramite) *unless* the conjunction of the two words involves two adjacent vowels (e.g., ferro-edenite instead of ferroedenite) or an inelegant combination of consonants (e.g., potassic-richterite instead of potassicrichterite).

Adjectival modifiers

Although their suggested ranges are specified, adjectival modifiers are *not* part of previous classifications of amphiboles (Leake 1978; Leake et al. 1997, 2003); their use is optional, and they are used to provide more information about an amphibole composition than is present in its formal name. For example, the presence of 0.89 Cl apfu in an amphibole is obviously of considerable crystal-chemical and petrological interest, but is not represented in the name of the amphibole; in the interest of propagating this information (particularly in this age of databases and keywords), the use of the adjectival modifier is a useful option both for an author and for a reader interested in Cl in amphiboles. However, a recent IMA-CNMMN (International Mineralogical Association Commission on New Minerals and Mineral Names) decision (voting proposal 03A; Bayliss et al. 2005) discredits the use of Schaller modifiers. Hence we suggest using expressions of the type *Cl-rich* or *Cl-bearing* preceding the root-name.

THE CURRENT CLASSIFICATION SCHEME (LEAKE ET AL. 1997, 2003)

The general chemical formula of the amphiboles can be written as



where A = Na, K, □, Ca, Li
 B = Na, Li, Ca, Mn^{2+} , Al, Fe^{3+} , Mn^{3+} , Ti^{4+} , Li;
 T = Si, Al, Ti^{4+} ;
 W = (OH), F, Cl, O^{2-} .

Minor elements such as Zn, Ni^{2+} , Co^{2+} , V^{3+} , Sc, Cr^{3+} and Zr are also observed as C cations.

The primary classification of the amphiboles is on the basis of the identity and amounts of the B cations:

- Group 1: ${}^B(\text{Mg,Fe,Mn,Li}) \geq 1.5$ apfu defines the *magnesium-iron-manganese-lithium group*.
- Group 2: ${}^B(\text{Mg,Fe,Mn,Li}) \leq 0.5$, ${}^B(\text{Ca,Na}) \geq 1.5$ and ${}^B\text{Na} < 0.5$ apfu defines the *calcic group*.
- Group 3: ${}^B(\text{Mg,Fe,Mn,Li}) \leq 0.5$, ${}^B(\text{Ca,Na}) \geq 1.5$ and $0.50 < {}^B\text{Na} < 1.5$ apfu defines the *sodic-calcic group*.
- Group 4: ${}^B(\text{Mg,Fe,Mn,Li}) \leq 0.5$ and ${}^B\text{Na} \geq 1.5$ apfu defines the *sodic group*.
- Group 5: $0.5 < {}^B(\text{Mg,Fe,Mn,Li}) < 1.5$ and $0.5 \leq {}^B(\text{Ca,Na}) < 1.5$ apfu defines the *sodium-calcium-magnesium-iron-manganese-lithium group*.

The magnesium-iron-manganese-lithium amphiboles

These amphiboles may be orthorhombic (*Pnma* or *Pnmm*) or monoclinic (*C2/m*, *P2₁/m*). The classification is shown graphically in Figure 1 and end-member compositions are listed in Table 2.

Orthorhombic amphiboles. The space group *Pnma* is assumed, the space group *Pnmm* is indicated by the prefix *proto*.

- (1) The anthophyllite series has the general formula $\text{Na}_x \text{Li}_z (\text{Mg,Fe}^{2+}, \text{Mn}^{2+})_{7-y-z} \text{Al}_y (\text{Si}_{8-x-y+z} \text{Al}_{x+y-z}) \text{O}_{22} (\text{OH,F,Cl})_2$ where $\text{Si} > 7.00$ apfu and $\text{Li} < 1.00$ apfu. This definition is not satisfactory as the end-member composition for sodicanthophyllite lies on the edge of the anthophyllite field (according to the above definition, it is actually excluded from the anthophyllite series). Note that the composition $\text{Na Mg}_7 (\text{Si}_7\text{Al}) \text{O}_{22} (\text{OH})_2$ corresponds to that of end-member sodicanthophyllite, whereas the composition $\text{Na} (\text{Mg}_{6,9}\text{Al}_{0,1}) (\text{Si}_{6,9}\text{Al}_{1,1}) \text{O}_{22} (\text{OH})_2$ lies in the compositional field of gedrite.
- (2) The gedrite series has the general formula $\text{Na}_x \text{Li}_z (\text{Mg,Fe}^{2+}, \text{Mn}^{2+})_{7-y-z} \text{Al}_y (\text{Si}_{8-x-y+z} \text{Al}_{x+y-z}) \text{O}_{22} (\text{OH,F,Cl})_2$ where $(x + y - z) \geq 1.00$ apfu (and hence $\text{Si} < 7.00$ apfu) and $\text{Li} < 1.00$ apfu.
- (3) The holmquistite series has the general formula $\square \text{Li}_2 (\text{Mg,Fe}^{2+})_3 (\text{Al,Fe}^{3+})_2 \text{Si}_8 \text{O}_{22} (\text{OH,F,Cl})_2$ with $\text{Li} \geq 1.00$ apfu.

Monoclinic amphiboles. Most members of the cummingtonite-grunerite series have the space group *C2/m*; those with the space group *P2₁/m* may optionally have this symbol added as a suffix at the end of the name.

- (1) The cummingtonite-grunerite series has the general formula $\square (\text{Mg,Fe}^{2+}, \text{Mn}^{2+}, \text{Li})_7 \text{Si}_8 \text{O}_{22} (\text{OH,F,Cl})_2$ where $\text{Li} < 1.00$ apfu.
- (2) The clinoholmquistite series has the general formula $\square \text{Li}_2 (\text{Mg,Fe}^{2+})_3 (\text{Al,Fe}^{3+})_2 \text{Si}_8 \text{O}_{22} (\text{OH,F,Cl})_2$ with $\text{Li} \geq 1.00$ apfu.

The calcic amphiboles

The classification is shown graphically in Figure 2 and end-member compositions are listed in Table 3.

The sodic-calcic amphiboles

The classification is shown graphically in Figure 3 and end-member compositions are listed in Table 4.

Mg-Fe-Mn-Li amphiboles

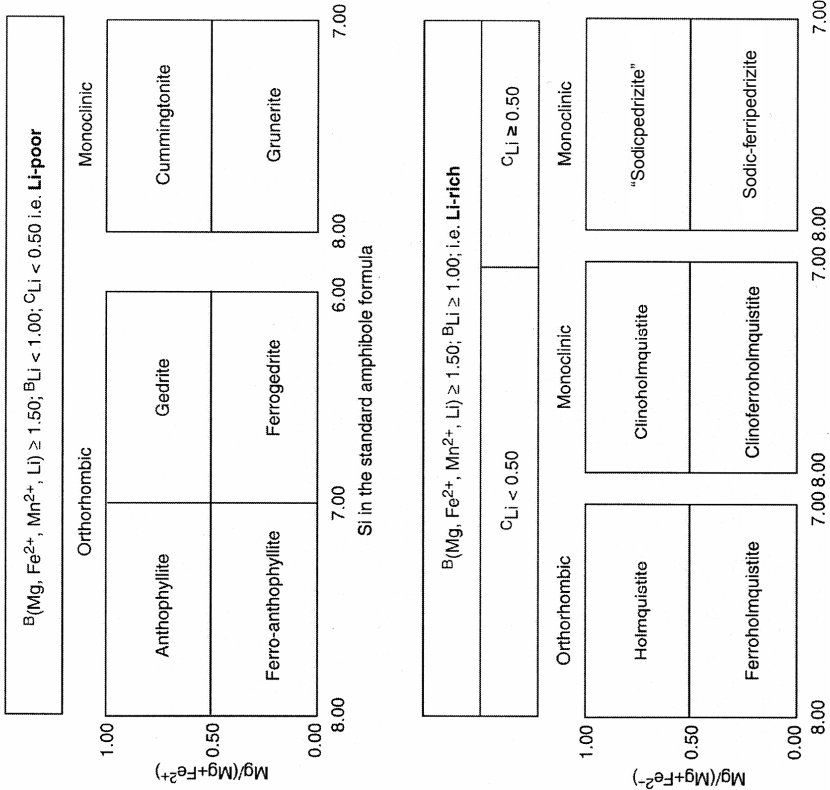


Figure 1. Classification of the magnesium-iron-manganese-lithium amphiboles; amounts of atoms are expressed in apfu (modified from Leake et al. 2003).

Table 2. End-member compositions for Mg-Fe-Mn-Li amphiboles (Leake et al. 1997, 2003).

Orthorhombic	
Anthophyllite	□ Mg ₇ Si ₈ O ₂₂ (OH) ₂
Ferro-anthophyllite	□ Fe ²⁺ ₇ Si ₈ O ₂₂ (OH) ₂
Sodic-anthophyllite	□ NaMg ₇ Si ₇ AlO ₂₂ (OH) ₂
Sodic-ferro-anthophyllite	□ NaFe ²⁺ ₇ Si ₇ AlO ₂₂ (OH) ₂
Gedrite	□ Mg ₅ Al ₂ Si ₆ Al ₂ O ₂₂ (OH) ₂
Ferrogedrite	□ Fe ²⁺ ₅ Al ₂ Si ₆ Al ₂ O ₂₂ (OH) ₂
Sodicgedrite	□ NaMg ₆ AlSi ₆ Al ₂ O ₂₂ (OH) ₂
Sodic-ferrogedrite	□ NaFe ²⁺ ₆ AlSi ₆ Al ₂ O ₂₂ (OH) ₂
Holmquistite	□ (Li ₂ Mg ₅ Al ₂)Si ₈ O ₂₂ (OH) ₂
Ferroholmquistite	□ (Li ₂ Fe ²⁺ ₅ Al ₂)Si ₈ O ₂₂ (OH) ₂
Monoclinic	
Cummingtonite	□ Mg ₇ Si ₈ O ₂₂ (OH) ₂
Grunerite	□ Fe ²⁺ ₇ Si ₈ O ₂₂ (OH) ₂
Manganocummingtonite	□ Mn ₂ Mg ₅ Si ₈ O ₂₂ (OH) ₂
Manganogrunerite	□ Mn ₂ Fe ²⁺ ₅ Si ₈ O ₂₂ (OH) ₂
Permanganogrunerite	□ Mn ₄ Fe ²⁺ ₃ Si ₈ O ₂₂ (OH) ₂
Manganogrunerite	□ Mn ₂ Fe ²⁺ ₅ Si ₈ O ₂₂ (OH) ₂
Clinoholmquistite	□ (Li ₂ Mg ₅ Al ₂)Si ₈ O ₂₂ (OH) ₂
Clinoferroholmquistite	□ (Li ₂ Fe ²⁺ ₅ Al ₂)Si ₈ O ₂₂ (OH) ₂
Cli-no-ferriholmquistite	□ (Li ₂ Mg ₃ Fe ³⁺ ₂)Si ₈ O ₂₂ (OH) ₂
Cli-no-ferri-ferroholmquistite	□ (Li ₂ Fe ²⁺ ₃ Fe ³⁺ ₂)Si ₈ O ₂₂ (OH) ₂
"Sodicpedrizite"	□ NaLi ₂ (Mg ₇ Al ₂)Si ₈ O ₂₂ (OH) ₂
Sodic-ferripedrizite	□ NaLi ₂ (Mg ₇ Fe ³⁺ ₂ Li)Si ₈ O ₂₂ (OH) ₂
Sodic-ferri-ferropedrizite	□ NaLi ₂ (Fe ²⁺ ₇ Fe ³⁺ ₂ Li)Si ₈ O ₂₂ (OH) ₂

calcic amphiboles

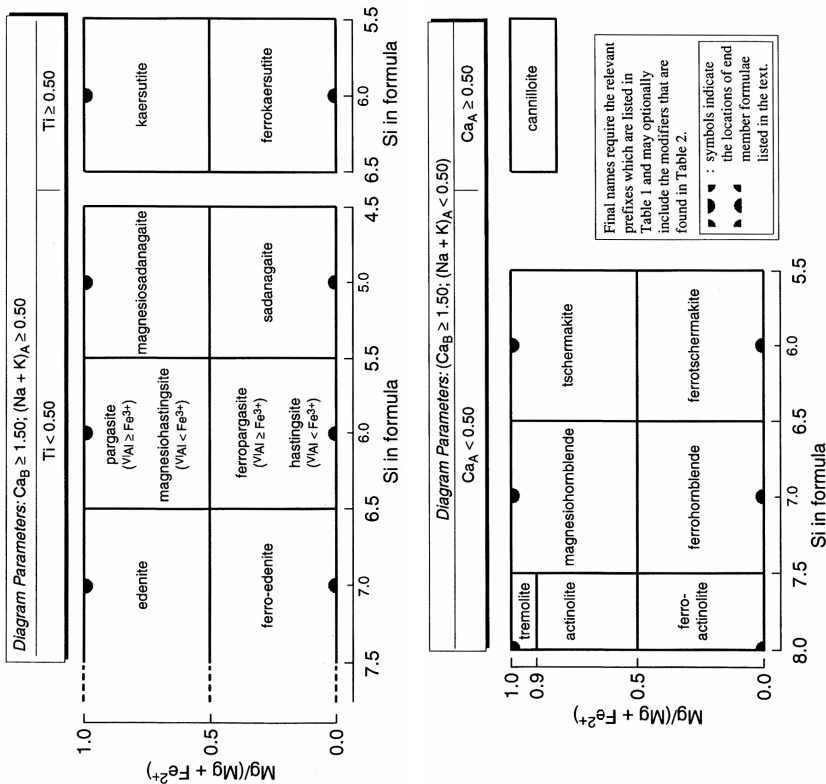


Figure 2. Classification of the calcic amphiboles; amounts of atoms are expressed in apfu (from Leake et al. 1997).

Table 3. End-member compositions for Ca amphiboles (Leake et al. 1997, 2003).

Tremolite	□ $Ca_2 Mg_5 Si_8 O_{22} (OH)_2$
Ferro-actinolite	□ $Ca_2 Fe^{2+}_5 Si_8 O_{22} (OH)_2$
Magnesiophornblende	□ $Ca_2 [Mg_4 (Al, Fe^{3+}) Si_7 Al O_{22} (OH)_2]$
Ferrohornblende	□ $Ca_2 [Fe^{2+}_4 (Al, Fe^{3+}) Si_7 Al O_{22} (OH)_2]$
Tschermakite	□ $Ca_2 (Mg_3 Al Fe^{3+}) Si_6 Al_2 O_{22} (OH)_2$
Ferrotschermakite	□ $Ca_2 (Fe^{2+}_3 Al Fe^{3+}) Si_6 Al_2 O_{22} (OH)_2$
Aluminotschermakite	□ $Ca_2 (Mg_3 Al_2) Si_6 Al_2 O_{22} (OH)_2$
Alumino-ferrotschermakite	□ $Ca_2 (Fe^{2+}_3 Al_2) Si_6 Al_2 O_{22} (OH)_2$
Ferritschermakite	□ $Ca_2 (Mg_3 Fe^{3+}_2) Si_6 Al_2 O_{22} (OH)_2$
Ferri-ferrotschermakite	□ $Ca_2 (Fe^{2+}_3 Fe^{3+}_2) Si_6 Al_2 O_{22} (OH)_2$
Edenite	Na $Ca_2 Mg_5 Si_7 Al O_{22} (OH)_2$
Ferro-edenite	Na $Ca_2 Fe^{2+}_5 Si_7 Al O_{22} (OH)_2$
Pargasite	Na $Ca_2 (Mg_4 Al) Si_6 Al_2 O_{22} (OH)_2$
Ferropargasite	Na $Ca_2 (Fe^{2+}_4 Al) Si_6 Al_2 O_{22} (OH)_2$
Magnesiosthenohastingsite	Na $Ca_2 (Mg_4 Fe^{3+}) Si_6 Al_2 O_{22} (OH)_2$
Hastingsite	Na $Ca_2 (Fe^{2+}_4 Fe^{3+}) Si_6 Al_2 O_{22} (OH)_2$
Magnesiosthenohastingsite	Na $Ca_2 [Mg_3 (Fe^{3+}_2 Al)_2] Si_5 Al_3 O_{22} (OH)_2$
Sadanagaite	Na $Ca_2 [Fe^{2+}_3 (Fe^{3+}_2 Al)_2] Si_5 Al_3 O_{22} (OH)_2$
Kaersutite	Na $Ca_2 (Mg_4 Ti) Si_6 Al_2 O_{23} (OH)$
Ferrotschermakite	Na $Ca_2 (Fe^{2+}_4 Ti) Si_6 Al_2 O_{23} (OH)$
Cannilloite	Ca $Ca_2 (Mg_4 Al) Si_5 Al_2 O_{22} (OH)_2$

Table 4. End-member compositions for Ca-Na amphiboles (Leake et al. 1997, 2003).

Richterite	Na (Ca Na) Mg ₅ Si ₈ O ₂₂ (OH) ₂
Ferrorichterite	Na (Ca Na) Fe ²⁺ ₅ Si ₈ O ₂₂ (OH) ₂
Winchite	□ (Ca Na) Mg ₄ (Al, Fe ³⁺) Si ₈ O ₂₂ (OH) ₂
Ferrowinchite	□ (Ca Na) Fe ²⁺ ₄ (Al, Fe ³⁺) Si ₈ O ₂₂ (OH) ₂
Barroisite	□ (Ca Na) Mg ₃ Al Fe ³⁺ Si ₇ Al O ₂₂ (OH) ₂
Ferrobarroisite	□ (Ca Na) Fe ²⁺ ₃ Al Fe ³⁺ Si ₇ Al O ₂₂ (OH) ₂
Aluminobarroisite	□ (Ca Na) Mg ₃ Al ₂ Si ₇ Al O ₂₂ (OH) ₂
Alumino-ferrobarroisite	□ (Ca Na) Fe ²⁺ ₃ Al ₂ Si ₇ Al O ₂₂ (OH) ₂
Ferribarroisite	□ (Ca Na) Mg ₃ Fe ³⁺ ₂ Si ₇ Al O ₂₂ (OH) ₂
Ferri-ferrobarroisite	□ (Ca Na) Fe ²⁺ ₃ Fe ³⁺ ₂ Si ₇ Al O ₂₂ (OH) ₂
Magnesiokatophorite	Na (Ca Na) Mg ₄ (Al, Fe ³⁺) Si ₇ Al O ₂₂ (OH) ₂
Katophorite	Na (Ca Na) Fe ²⁺ ₄ (Al, Fe ³⁺) Si ₇ Al O ₂₂ (OH) ₂
Magnesiotaramite	Na (Ca Na) Mg ₃ Al Fe ³⁺ Si ₆ Al ₂ O ₂₂ (OH)
Taramite	Na (Ca Na) Fe ²⁺ ₃ Al Fe ³⁺ Si ₆ Al ₂ O ₂₂ (OH)
Alumino-magnesiotaramite	Na (Ca Na) Mg ₃ Al ₂ Si ₆ Al ₂ O ₂₂ (OH) ₂
Aluminotaramite	Na (Ca Na) Fe ²⁺ ₃ Al ₂ Si ₆ Al ₂ O ₂₂ (OH) ₂
Ferri-magnesiotaramite	Na (Ca Na) Mg ₃ Fe ³⁺ ₂ Si ₆ Al ₂ O ₂₂ (OH) ₂
Ferritaramite	Na (Ca Na) Fe ²⁺ ₃ Fe ³⁺ ₂ Si ₆ Al ₂ O ₂₂ (OH) ₂

sodic-calcic amphiboles

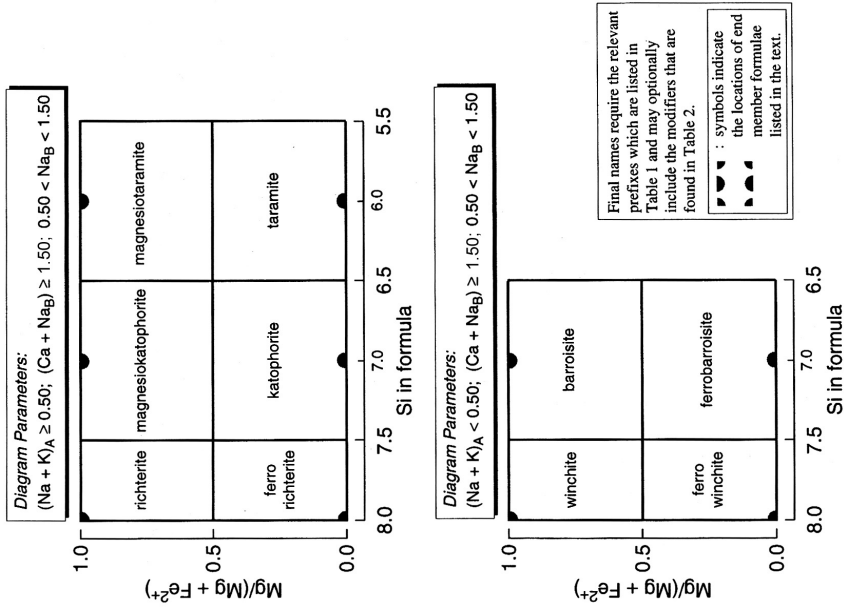


Figure 3. Classification of the sodic-calcic amphiboles; amounts of atoms are expressed in apfu (modified from Leake et al. 1997).

The sodic amphiboles

The classification is shown graphically in Figure 4 and end-member compositions are listed in Table 5.

Table 5. End-member compositions for Na amphiboles (Leake et al. 1997).

Glaucofanane	$\square \text{Na}_2(\text{Mg}_3\text{Al}_2)\text{Si}_8\text{O}_{22}(\text{OH})_2$
Ferroglaucophane	$\square \text{Na}_2(\text{Fe}^{2+}_3\text{Al}_2)\text{Si}_8\text{O}_{22}(\text{OH})_2$
Magnesioriebeckite	$\square \text{Na}_2(\text{Mg}_3\text{Fe}^{3+}_2)\text{Si}_8\text{O}_{22}(\text{OH})_2$
Riebeckite	$\square \text{Na}_2(\text{Fe}^{2+}_3\text{Fe}^{3+}_2)\text{Si}_8\text{O}_{22}(\text{OH})_2$
Eckermannite	$\text{NaNa}_2(\text{Mg}_4\text{Al})\text{Si}_8\text{O}_{22}(\text{OH})_2$
Ferro-eckermannite	$\text{NaNa}_2(\text{Fe}^{2+}_4\text{Al})\text{Si}_8\text{O}_{22}(\text{OH})_2$
Magnesio-arfvedsonite	$\text{NaNa}_2(\text{Mg}_4\text{Fe}^{3+})\text{Si}_8\text{O}_{22}(\text{OH})_2$
Arfvedsonite	$\text{NaNa}_2(\text{Fe}^{2+}_4\text{Fe}^{3+})\text{Si}_8\text{O}_{22}(\text{OH})_2$
Kozulite	$\text{NaNa}_2\text{Mn}^{2+}_4(\text{Fe}^{3+},\text{Al})\text{Si}_8\text{O}_{22}(\text{OH})_2$
Nyböite	$\text{NaNa}_2(\text{Mg}_3\text{Al}_2)\text{Si}_7\text{AlO}_{22}(\text{OH})_2$
Ferroyböite	$\text{NaNa}_2(\text{Fe}^{2+}_3\text{Al}_2)\text{Si}_7\text{AlO}_{22}(\text{OH})_2$
Ferric-nyböite	$\text{NaNa}_2(\text{Mg}_3\text{Fe}^{3+}_2)\text{Si}_7\text{AlO}_{22}(\text{OH})_2$
Ferric-ferroyböite	$\text{NaNa}_2(\text{Fe}^{2+}_3\text{Fe}^{3+}_2)\text{Si}_7\text{AlO}_{22}(\text{OH})_2$
Leakeite	$\text{NaNa}_2(\text{Mg}_2\text{Fe}^{3+}_2\text{Li})\text{Si}_8\text{O}_{22}(\text{OH})_2$
Ferroleakeite	$\text{NaNa}_2(\text{Fe}^{2+}_2\text{Fe}^{3+}_2\text{Li})\text{Si}_8\text{O}_{22}(\text{OH})_2$
Kornite*	$\text{KNa}_2(\text{Mg}_2\text{Mn}^{3+}_2\text{Li})\text{Si}_8\text{O}_{22}(\text{OH})_2$
Ungarettiite	$\text{NaNa}_2(\text{Mn}^{2+}_2\text{Mn}^{3+}_2)\text{Si}_8\text{O}_{22}\text{O}_2$

*Although Leake et al. (1997) write the formula of kornite as $(\text{Na}, \text{K})\text{Na}_2(\text{Mg}_2\text{Mn}^{3+}_2\text{Li})\text{Si}_8\text{O}_{22}(\text{OH})_2$, the original chemical composition reported by Armbruster et al. (1993) gives K as the dominant A cation.

The sodium-calcium-magnesium-iron-manganese-lithium amphiboles

The classification is shown graphically in Figure 5 and end-member compositions are listed in Table 6. As a general criterion, a root name is attributed where $^{\text{B}}\text{Li} > 0.50$ apfu; where $^{\text{B}}\text{Li} \leq 0.50$ apfu, the root name for the dominant B cations (large: Ca, Na; or small: Mg, Fe, Mn) is adopted, and the prefix “parvo-” or “magno-” is used to indicate the presence of a smaller or larger constituent, respectively.

Named amphiboles

The IMA-CNMMN introduced a new category of amphibole: *named amphiboles* (Burke and Leake 2004). These are names that are in accord with the current IMA-approved nomenclature scheme but have not been formally approved as accredited mineral species by the IMA-CNMMN. The use of these names is thus allowed, but a formal description for official recognition is still requested.

SIGNIFICANT ISSUES INVOLVED IN THE CLASSIFICATION OF AMPHIBOLES

The above classification has generated a lot of critical discussion in the community. Having been involved in the development of the current classification, we (the authors) are (hopefully) aware of all the issues, the most difficult of which is the balancing of diametrically opposed opinions by different sectors of the community involved in work on amphiboles. In addition,

Sodic Amphiboles

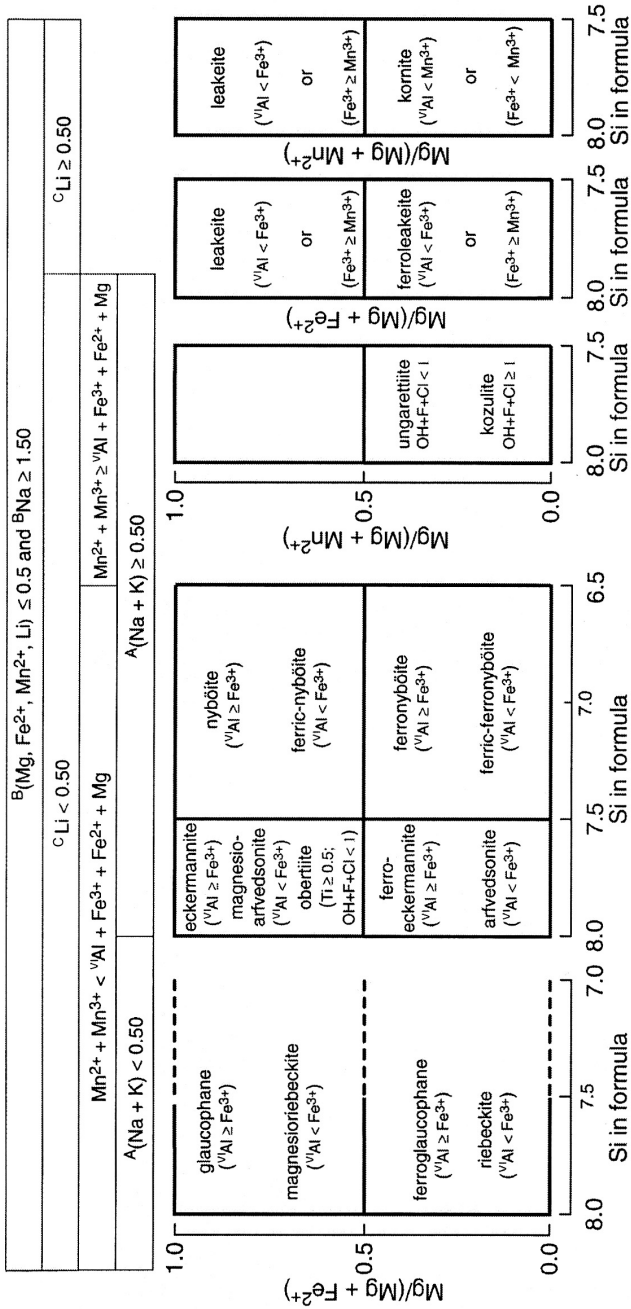


Figure 4. Classification of the sodic amphiboles; amounts of atoms are expressed in apfu (modified from Leake et al. 2003).

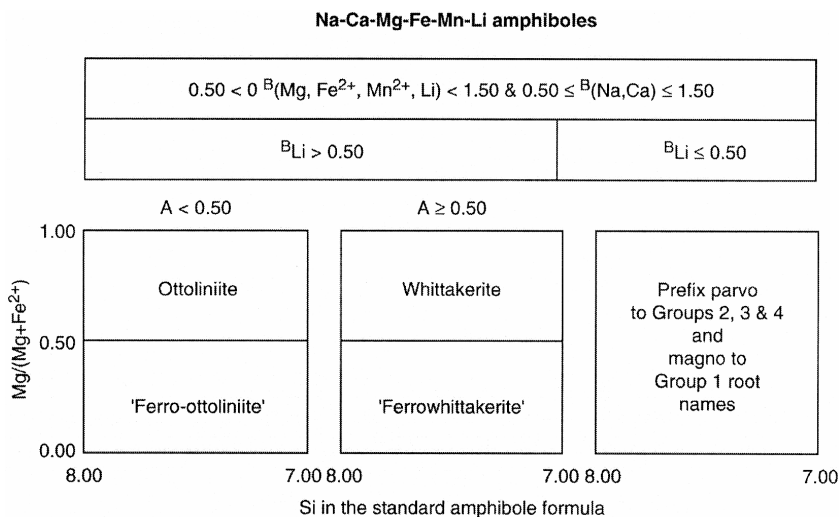


Figure 5. Classification of the sodic-calcic-magnesium-iron-manganese-lithium amphiboles; amounts of atoms are expressed in apfu (from Leake et al. 2003).

Table 6. End-member compositions for Na-Ca-Mg-Fe-Mn-Li amphiboles (Leake et al. 2003).

Ottoliniite	$\square (\text{NaLi}) (\text{Mg}_3 \text{Fe}^{3+} \text{Al}) \text{Si}_8 \text{O}_{22} (\text{OH})_2$
Ferro-ottoliniite	$\square (\text{NaLi}) (\text{Fe}^{2+}_3 \text{Fe}^{3+} \text{Al}) \text{Si}_8 \text{O}_{22} (\text{OH})_2$
Ferri-ottoliniite	$\square (\text{NaLi}) (\text{Fe}^{2+}_3 \text{Fe}^{3+}_2) \text{Si}_8 \text{O}_{22} (\text{OH})_2$
Whittakerite	$\text{Na} (\text{NaLi}) (\text{Li} \text{Mg}_2 \text{Fe}^{3+} \text{Al}) \text{Si}_8 \text{O}_{22} (\text{OH})_2$
Ferrowhittakerite	$\text{Na} (\text{NaLi}) (\text{Li} \text{Fe}^{2+}_2 \text{Fe}^{3+} \text{Al}) \text{Si}_8 \text{O}_{22} (\text{OH})_2$
Ferriwhittakerite	$\text{Na} (\text{NaLi}) (\text{Li} \text{Fe}^{2+}_2 \text{Fe}^{3+}_2) \text{Si}_8 \text{O}_{22} (\text{OH})_2$

new analytical techniques have become available and/or more widely available, allowing better chemical characterization of amphiboles than was possible 20 years ago, when the development of the current classification scheme began. Also, the IMA-CNMMN has adopted new principles involving the definition of new mineral species, and the current amphibole classification is not compatible with these principles. As a result of this, Hawthorne and Oberti (2006) considered the general problem of amphibole classification, taking into account (1) new analytical techniques, (2) the discovery of extensive $0^B(\text{Na}, \text{Li})$ solid-solution, (3) the recently clarified major complexity of the crystal-chemistry and ordering of the C cations, and (4) the principle that minerals are defined by *the dominant cation or anion at a site*, rather than the specific amount of a cation or anion in the formula of the mineral. They presented two distinct classification schemes *in order to illustrate the problems associated with amphibole classification*. These issues will now be considered here in the hope that the problems inherent in amphibole classification will be better understood. In particular, it must be realized that all communities (crystallographers, mineralogists, petrologists, geochemists) must relax their requirements in order for a consensus to emerge with regard to amphibole classification.

The role of Fe, (OH) and Li

Prior to the development of the electron microprobe, all major and minor constituents in amphiboles were analyzed as a matter of course, and compilations such as that of Leake (1968)

are invaluable sources of complete results of chemical analysis. The advent of the electron microprobe completely changed the situation with regard to mineral analysis. It became relatively easy to make numerous chemical analyses at a very fine scale, making available chemical data on finely zoned materials. However, this step forward came at a cost: the concentration of some elements (e.g., H, Li) cannot be so established, and valence state is not accessible. For many minerals, these limitations are not relevant; for amphiboles, they are major disadvantages. Recent work has shown that (1) Li is a much more common constituent in amphiboles than had hitherto been realized (Hawthorne et al. 1994; Oberti et al. 2003), and (2) H, as (OH), can be a variable component in amphiboles unassociated with the process of oxidation-dehydrogenation (Hawthorne et al. 1998). Moreover, the role of Fe in amphiboles is very strongly a function of its valence state. Lack of knowledge of these constituents results in formulae that generally must be regarded as only semiquantitative. Of course, if Li and Fe^{3+} are not present and $(\text{OH} + \text{F}) = 2$ apfu, the resulting formula can be accurate. However, such a situation is uncommon [few amphiboles have $\text{Li} = \text{Fe}^{3+} = 0$ and $(\text{OH} + \text{F}) = 2$ apfu], resulting in formulae with significant systematic error.

All previous amphibole classifications have obscured this issue by not incorporating Cations into the classification procedure, and thus the problem is not visually apparent in the classification diagrams. However, the problem is still present in that the formulae are still inaccurate, and the lack of H, Li and Fe^{3+} seriously distorts the amounts of other constituents, particularly those that are distributed over two different groups (e.g., ${}^{\text{T}}\text{Al}$ and ${}^{\text{C}}\text{Al}$, ${}^{\text{B}}\text{Na}$ and ${}^{\text{A}}\text{Na}$). There are methods available for the analysis of these components, and amphibole analysts should be acquiring or using these on a routine basis. For “small-laboratory” instrumentation, SIMS (Secondary-Ion Mass Spectrometry) can microbeam-analyze amphiboles for H and Li (using the appropriate methodology and standards), LA-ICP-MS (Laser-Ablation Inductively Coupled Plasma Mass Spectrometry) can microbeam-analyze materials for Li, single-crystal structure refinement can characterize the levels of Li, Fe^{2+} and Fe^{3+} at a scale of ≥ 30 μm , and with structure-based equations, one can estimate the amount of H; EELS (Electron Energy-Loss Spectroscopy) can measure $\text{Fe}^{3+}/(\text{Fe}^{2+}+\text{Fe}^{3+})$ at a scale of ≥ 1 μm , and milli-Mössbauer spectroscopy can measure $\text{Fe}^{3+}/(\text{Fe}^{2+}+\text{Fe}^{3+})$ at a scale of ≥ 50 μm . For “big-laboratory” instrumentation, usually involving a synchrotron light-source, single-crystal refinement of the structure can characterize Li, Fe^{2+} and Fe^{3+} at a scale of ≥ 2 μm , and milli-XPS (X-ray Photoelectron Spectroscopy) can measure $\text{Fe}^{3+}/(\text{Fe}^{2+}+\text{Fe}^{3+})$ at a scale of ≥ 40 μm . Where only small amounts of separate are available (a few milligrams), hydrogen-line extraction and Karl-Fischer titration can give accurate values for H (as H_2O) content. Values for $\text{Fe}^{3+}/(\text{Fe}^{2+}+\text{Fe}^{3+})$ can also be calculated using assumed site-occupancy limitations and the electroneutrality principle, and although the values obtained are not very accurate (Hawthorne 1983), they are in general better than assuming $\text{Fe}^{3+}/(\text{Fe}^{2+}+\text{Fe}^{3+}) = 0.0$ (unless additional evidence indicates otherwise).

Below, we make a case for basing amphibole classification on the contents of the A, B and C cations (see general formula above). This being the case, the Fe^{3+} content of an amphibole will play a major role in the classification scheme. Hopefully, this forced recognition of the present deficiencies in amphibole analysis will encourage us to use some of the techniques outlined above, in addition to electron-microprobe analysis, to characterize the amphiboles in which we are interested, and to characterize their chemical formulae accurately. To make an analogy with 40 years ago, wet-chemical analysis was in widespread use and the electron microprobe was a novel instrument. However, the ability of the electron microprobe to deal with heterogeneous material and obviate problems of sample contamination led to its current extensive use. We are in a similar situation today. The electron microprobe is in widespread use, and the techniques outlined above are far less widespread. However, these techniques considerably increase our ability to analyze minerals accurately. To increase our knowledge of the chemistry of minerals in general (and amphiboles in particular), as a community we need to acquire this instrumentation so that in the near future, it becomes as routine as electron microprobe analysis.

Root names

Compositional variation may involve cations of the same valence [homovalent variation] or cations of different valence [heterovalent variation]. Previous classifications have recognized that distinct arrangements of formal charges at the sites (or groups of sites) in the amphibole structure warrant distinct *root names*, and are, by implication, distinct species; for a specific root name, different homovalent cations (e.g., Mg vs. Fe²⁺) or anions (e.g., OH vs. F) are indicated by prefixes. The expression “a distinct arrangement of formal charges” was not defined in previous classifications. Moreover, the 1978 and 1997 classifications actually do not adhere to the definition that only distinct arrangements of formal charges warrant distinct root names. If they did, they would not differentiate, for instance, between the magnesium-iron-manganese group and the calcic group, as $B_2 = M^{2+}_2$ in both these groups. The definition that only distinct arrangements of formal charges for each amphibole group warrant distinct root names applies only to the A, B and T cations in the 1978 and 1997 classifications, and it applies only to the A, B and C cations in the present discussions. Furthermore, this issue of what constitutes a “distinct arrangement of formal charges” needs to be clarified, as it is at the core of any classification that takes this approach; it is examined in the next paragraph.

Authors of the 1978 and 1997 classifications tacitly assumed that a distinct arrangement of formal charges in the amphibole structure is one in which the numbers and types of integer charge in each group is unique. Thus, in calcic amphiboles, the arrangement $\{^A O_1 \ ^B B_2 \ ^C C_2 \ ^T T_4 \ O_{22} \ ^W W_1 \ ^-_2\}$ (where numbers associated with cation sites are assigned a positive charge) is different from the arrangement $\{^A O_1 \ ^B B_2 \ ^C (2_4 \ 3_1) \ ^T (4_7 \ 3_1) \ O_{22} \ ^W W_1 \ ^-_2\}$; for convenience, we may denote the former as the *tremolite* arrangement, and the latter as the *hornblende* arrangement (the italics serving to indicate that the names do not refer to specific chemical species at the sites or groups of sites). However, consider the arrangement $\{^A O_1 \ ^B B_2 \ ^C (2_3 \ 3_2) \ ^T (4_6 \ 3_2) \ O_{22} \ ^W W_1 \ ^-_2\}$, which we may denote as the *tschermakite* arrangement. The *hornblende* arrangement can be factored into 50% *tremolite* arrangement and 50% *tschermakite* arrangement, and it is not clear that we should necessarily recognize the *hornblende* arrangement as distinct because it is not irreducible. This issue is at the heart of the classification problem, and we see no clear solution to it. Here, we present two possible classification schemes. In SCHEME 1 [which includes the sodic-calcic group], we identify all different arrangements of integer charges (corresponding to the cations and anions found in amphiboles), and in SCHEME 2 [which does not include the sodic-calcic group], we recognize only irreducible arrangements of integer charges that are crystal-chemically compatible with the amphibole structure [note: richterite and Na (NaMg) Mg₅ Si₈ O₂₂ (OH)₂ are irreducible, but are not present in SCHEME 2].

More on root names

It would be good to have consistent use of prefixes in amphibole names. Most root names apply to the Mg-Al-dominant species, e.g., tremolite, pargasite, glaucophane. However, (1) some amphiboles were originally described as the ferro- and/or ferri- equivalent of the Mg-Al-containing species, and (2) some amphiboles are defined without specifying the dominant trivalent cation [e.g., winchite = □ (CaNa) Mg₄ (AlFe³⁺) Si₈ O₂₂ (OH)₂]. We may define all root names as referring to the Mg-Al-dominant compositions; thus, for example, leakeite, currently Na Na₂ (Mg₂Fe³⁺Li) Si₈ O₂₂ (OH)₂, becomes Na Na₂ (Mg₂Al₂Li) Si₈ O₂₂ (OH)₂, and winchite becomes □ (CaNa) (Mg₄Al) Si₈ O₂₂ (OH)₂. If this is done, we may dispense with the prefixes *magnesio* and *alumno*. Can we do this? Yes, but only at a price; for example, riebeckite will become “ferro-ferri-glaucophane” and arfvedsonite will become “ferro-ferri-eckermannite”, and a riebeckite-arfvedsonite granite will become.... On the other hand, uncommon amphiboles may possibly be redefined without hardship. Again, we offer two extreme schemes: in SCHEME 1, we retain all current root names, whereas in SCHEME 2, we define all root names as the equivalent Mg-Al-dominant species.

Criteria for the recognition of distinct species

The IMA CNMMN uses the criterion of the *dominant species at a site* to recognize the existence of a distinct mineral species. This is not necessarily a satisfactory criterion for rock-forming minerals, and has not been strictly adhered to in previous classifications. There are several problems involved in the strict application of this criterion: (1) this criterion requires recognition only of irreducible charge arrangements as distinct species; this would result in discreditation of such minerals as *argasite* and *hornblende*, names (and amphibole compositions) that are embedded not only in Mineralogy but also in Petrology and Geochemistry, and are used in the nomenclature of rocks. (2) With this criterion, one cannot recognize amphiboles such as richterite, $\text{Na}(\text{NaCa})\text{Mg}_5\text{Si}_8\text{O}_{22}(\text{OH})_2$, which is a formal end-member in amphibole composition space, despite the fact that it does not have a dominant B cation.

In order to expose the problems inherent in the often conflicting goals of simplicity and conservatism, we will develop two different classifications, one adhering to current convention and the other striving for simplicity of naming. A pragmatic combination of these two schemes may be the best solution.

Prefixes

The use of prefixes greatly decreases the number of trivial names, and although it has generated a lot of complaint in the community, we cannot believe that the community would prefer several hundred new trivial amphibole names instead of the use of prefixes. One possibility that has been advanced is the use of element suffixes [e.g., ferro-actinolite = actinolite-(Fe²⁺)]. We prefer word prefixes to element suffixes on two counts: (1) ease of use of multiple prefixes; at least for us, the meaning of fluoro-potassic-ferri-ferrohornblende is much more transparent than “hornblende-(F)-(K)-(Fe³⁺)-(Fe²⁺)”, and much easier to use in speech; (2) some space groups are indicated by suffixes (e.g., cummingtonite-P2₁/m; having to combine space-group symbols with element or cation and anion suffixes further complicates this approach.

Current usage. The current use of prefixes cannot be considered as satisfactory for several reasons. Burke and Leake (2004) define three types of prefixes for amphiboles: (i) primary prefixes that “are an essential part of the root name,” e.g. *ferro*, *magnesio*; (ii) secondary prefixes such as *proto*, *clino*, *magno*, *parvo*; (iii) prefixes such as *potassic*, *titano*, *chloro*, *ferri* “which indicate richness in particular elements.” First, there is no definition given of a root-name prefix. Second, we emphasize that there is no difference between prefix types (i) and (iii). *Ferro* (type i) indicates dominance of Fe²⁺ and *ferri* (type iii) indicates dominance of Fe³⁺; there is no crystal-chemical difference between these two prefixes, as they do not change the charge distribution over the sites in the amphibole structure which, in turn, defines a root composition that is associated with a root name. The claimed appearance “in the IMA-CNMMN classification diagrams” is not a good argument to identify primary prefixes. Burke and Leake (2004) state that “root-name prefixes should never be split apart from their root names.” However, many type (iii) prefixes must be considered as root-name prefixes, e.g. *ferri*, and hence should not be split from the root name according to Burke and Leake (2004): thus “ferriferrohornblende.”

Leake et al. (1997) state that a prefix should be used with a hyphen where “an unhyphenated name is awkward, and a hyphen assists in deciphering the name.” It seems to be left to the user when to use a hyphen; thus some users will insert a hyphen and some will not *for the same amphibole*. Where there is juxtaposition of two vowels, a hyphen should be used according to current amphibole nomenclature. Where a consonant and a vowel are in juxtaposition, normal pronunciation emphasizes combination of consonant and vowel. Thus sodicanthophyllite will tend to be pronounced “*sodi-canthophyllite*.” A hyphen is obviously desirable to indicate correct pronunciation. Where there is juxtaposition of two consonants, the situation is much more complicated and also undefined. Three distinct situations can be identified:

- (1) Adjacent consonants that retain their individual sounds: in such cases, there is no linguistic ambiguity as to pronunciation, e.g., potassicpargasite, and a hyphen need not be used.
- (2) A *consonant blend*: here, adjacent consonants from the prefix and root name blend smoothly to form a single sound. As an example, the consonants *c* and *l* blend to form *cl*, as in the work *click*; in terms of amphiboles, potassiccleakeite will contain the *cl* sound and be pronounced as *potassi-cleakeite*. Obviously, this is not satisfactory; such examples warrant use of a hyphen.
- (3) A *consonant digraph*: here, adjacent consonants from the prefix and root name combine to form a single different sound (as distinct from a blend of two sounds). As an example, the consonants *c* and *h* blend to form *ch*, as in the work *chocolate*; in terms of amphiboles, potassichastingsite will contain the *ch* sound and be pronounced as *potassi-chastingsite*. Such examples warrant use of a hyphen.

It should be noted that the above suggestions are within the general IMA amphibole-nomenclature guideline that a prefix should be used with a hyphen where “an unhyphenated name is awkward, and a hyphen assists in deciphering the name.”

Recommendations for the future. We recommend retaining the use of a set of redefined prefixes, each of which is always followed by a hyphen so that root names are easily identified in the complete name. This latter feature is particularly desirable in this age of databases. In addition, it is preferable to use prefixes in a specific order as comparison of names is made simpler in this case. Burke and Leake (2004) specified in which order prefixes (when more than one is used) must be attached to the root-name. Their sequence is proto (clino)-parvo (magno)-fluoro (chloro)-potassic (sodic)-ferri (alumino, mangani)-ferro(mangano, magnesio). We recommend a different sequence, which follows the order of the amphibole formula itself: $A B_2 C_5 T_8 O_{22} W_2$; hence, *proto-potassic-ferro-ferri-fluoro-* followed by the root name.

Synthetic amphiboles

There are many recent studies focusing on the synthesis and characterization of amphibole compositions which are important in understanding such issues as (1) stability, (2) symmetry, (3) thermodynamics, and (4) short-range order. Some of these studies have produced compositions that have not (yet) been observed in Nature, either because the chemical systems in which they occur are enriched in geochemically rare elements or because the synthetic system is chemically simpler than is usual in geological systems. As a result, there is a need to find a logical and practical system to handle synthetic amphiboles. Bayliss et al. (2005) recently stated that any synthetic species that is still unknown in Nature should be named with the mineral name followed by a suffix indicating the exotic substitution, and that the whole name must be quoted within commas, e.g., “topaz-(OH).”

In the case of the amphiboles, the situation is more complicated, as new root compositions may occur in synthesis experiments. Obviously it is inappropriate to designate a new name for such compositions (until or unless they are discovered as minerals). It seems natural to designate them by their chemical formula, possibly preceded by the word *synthetic* in order to distinguish it from hypothetical compositions (such as end members) or suggested formulae. Where the natural analogue of the root composition of a synthetic amphibole does exist, the directive of Bayliss et al. (2005) seems appropriate.

THE PRINCIPAL VARIABLES USED IN THE CLASSIFICATION PROCEDURE

The total variation in amphibole composition can be described in the quinary system A-B-C-T-W; however, this variation is constrained by the electroneutrality principle and hence only

four of these five variables are needed to formally represent this variation. The 1978 and 1997 schemes used variations in the A, B, T cations and W anions as their primary classification parameters. However, are these the best parameters to use in this context? We will examine this issue next.

The T cations

Consider the following points:

- (1) In most scientific problems, one focuses on the variables that show the greatest degree of relative variation, as these are the most informative;
- (2) IMA procedures concerning the definition of distinct minerals focus on the dominant species (cation or anion) at a site.

Of the A, B, C, T cations and W anions, all except T show a variety of dominant cations or anions in the set of all amphibole compositions; T is always dominated by Si (i.e., ${}^T\text{Al} < 4.0$ apfu: atoms per formula unit). These issues indicate that the T cations should *not* be used as a primary parameter in an amphibole classification.

The W anions

Although there is continuous variation in (OH,F) and O contents in amphiboles, the great majority of amphiboles have $W_2 \approx (\text{OH,F,Cl})_2$ [and have high-charge cations ordered at the $M(2)$ site]. Amphiboles with $1 < (\text{OH,F,Cl}) < 2$ apfu are very uncommon, and amphiboles with $(\text{OH,F,Cl}) < 1$ apfu are very rare [and all contain high-charge cations at the $M(1)$ and $M(3)$ sites].

In general, amphiboles show wide chemical variation in terms of their A, B and C constituents. These considerations suggest that the W constituents be used to divide amphiboles into two broad classes: (1) hydroxy-fluoro-chloro-amphiboles with $(\text{OH,F,Cl}) \geq 1.00$ apfu, and (2) oxo-amphiboles with $(\text{OH,F,Cl}) < 1.00$ apfu (we do not use the term *oxy* as this has too many associations with the *process* of oxidation-dehydroxylation). Within these two classes, the A, B and C constituents are used to classify the amphiboles further.

The B cations

Previous classifications have been based on the type of B cations as the primary (first) classification parameter, which gives five main groups (see above). The compositional fields of these groups are shown in Figure 6; this Figure is obviously not in accord with the dominance criterion. Moreover, there are many problems with this stage of the current amphibole classification; some of these issues are discussed next.

The role of ${}^B\text{Li}$. There is no good crystal-chemical or chemical reason for including Li in the *magnesium-iron-manganese-lithium* group. Lithium is an alkali metal, is formally monovalent, and shows complete solid-solution with Na at the $M(4)$ site in monoclinic amphiboles, e.g., leakeite–pedrizite: $\text{Na Na}_2 (\text{Fe}^{3+}_2\text{Mg}_2\text{Li}) \text{Si}_8 \text{O}_{22} (\text{OH})_2 - \text{Na Li}_2 (\text{Fe}^{3+}_2\text{Mg}_2\text{Li}) \text{Si}_8 \text{O}_{22} (\text{OH})_2$, Oberti et al. (2003); magnesianriebeckite–clino-ferriholmquistite: $\square \text{Na}_2 (\text{Fe}^{3+}_2\text{Mg}_3) \text{Si}_8 \text{O}_{22} (\text{OH})_2 - \square \text{Li}_2 (\text{Fe}^{3+}_2\text{Mg}_3) \text{Si}_8 \text{O}_{22} (\text{OH})_2$, Oberti et al. (2004).

These points indicate that amphiboles with Li dominant at $M(4)$ should *not* be included as part of the magnesium-iron-manganese group. There are two possible ways in which to treat such amphiboles: (1) recognize a separate group of amphiboles with Li as the dominant B cation (analogous to the *sodic* group), or (2) include ${}^B\text{Li}$ with ${}^B\text{Na}$ as a principal constituent of an alkali amphibole group. However, ${}^B\text{Li}$ amphiboles have some features that are not shared with ${}^B\text{Na}$ amphiboles; for instance, ${}^B\text{Li}$ amphiboles may occur with orthorhombic $Pnma$ symmetry (holmquistite) and are also expected to occur with monoclinic $P2_1/m$ symmetry (clinoholmquistite). Hence, the simpler solution is to define a distinct group for ${}^B\text{Li}$ amphiboles.

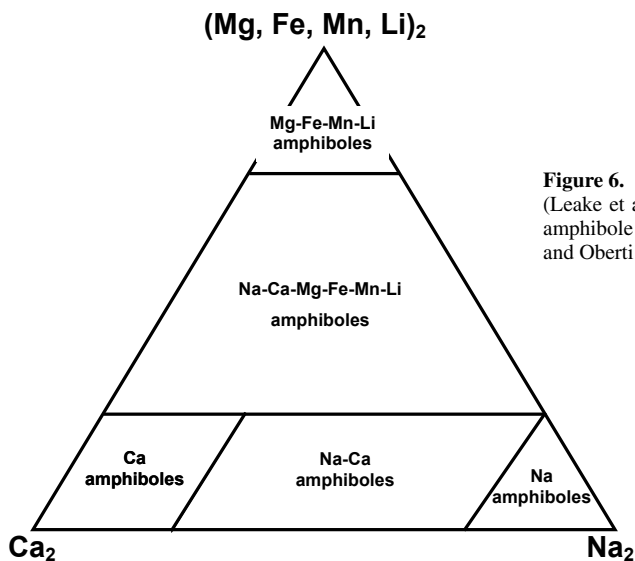


Figure 6. The present classification (Leake et al. 2003) for the five main amphibole groups (from Hawthorne and Oberti 2006).

The names of the principal groups. If we recognize a separate group with Li as the dominant B cation, it is obvious that the term “lithic”, in accord with “calcic” and “sodic”, is not suitable. Moreover, the names of the current five groups (Leake et al. 2003) are rather inhomogeneous, using both nouns (e.g., magnesium), element symbols (e.g., Mg) and adjectives (e.g., calcic, sodic). Here, we will use nouns to name these groups. The other inhomogeneity with regard to the names of these groups is the use of element symbols: the magnesium-iron-manganese group is frequently referred to as the Mg-Fe-Mn group (indeed, this is done in Leake et al. 1997), whereas the calcium group is not referred to as the Ca group. Some sort of consistency is required here; the most democratic solution is to allow either element names or symbols to be used, as long as they are used consistently.

The role of the sodium-calcium group. One of the principal origins of the complexity in the classification of amphiboles is the recognition of the sodium-calcium group. This group was defined by Leake (1978) and redefined by Leake et al. (1997), but its use was not justified from a nomenclature perspective. As noted above, IMA procedures involving the definition of distinct minerals focus on the dominant species at a site. Using this criterion, the sodium-calcium group of amphiboles would not be recognized: amphiboles with $2.00 > Ca > 1.00$ apfu would belong to the calcium group, and amphiboles with $2.00 > Na > 1.00$ apfu would belong to the sodium group. Using this criterion to reduce the number of primary groups would certainly reduce both the complexity of the nomenclature and the number of distinct amphiboles. However, inspection of Figure 7 shows that use of this criterion will have a problem with richterite.

This issue is investigated in Figure 7, which shows A-B-C compositional space for amphiboles with only Ca and Na as B cations (note that this excludes magnesium-iron-manganese and lithium amphiboles). Compositions of previous ‘end-members’ are shown as black squares and white circles. Note that the compositions represented by white circles can always be represented as a 50:50 mixture of other ‘end-member’ compositions. Thus hornblende can be represented as 0.50 tremolite and 0.50 tschermakite, and barroisite can be represented as 0.50 tschermakite and 0.50 glaucophane. However, richterite cannot be represented by a combination of two end-members, as is apparent graphically from Figure 7; richterite is thus a true end-member according to the criteria of Hawthorne (2002). However, IMA criteria for the recognition of a valid mineral species do not involve its status as a valid end-member. The

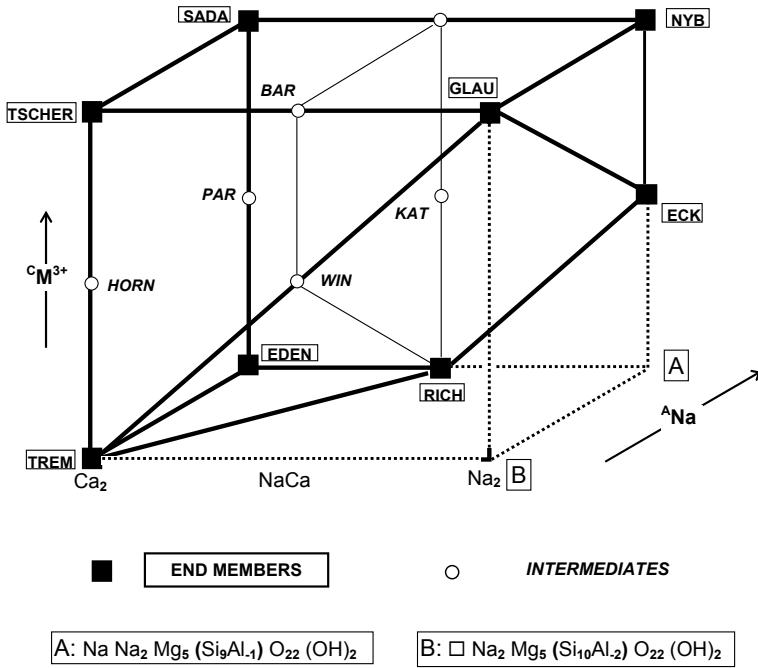


Figure 7. A-B-C amphibole space; the plane TREM-RICH-ECK-GLAU-WIN-TREM outlined by heavy black lines shows the limit of amphibole compositions (to the right of this plane, electroneutrality is not satisfied for positive numbers of cations in the amphibole structure). Formal end-member compositions are shown as black squares, and their names are shown in boxes; intermediate compositions corresponding to distinct charge-arrangements are shown as white circles, and their names are shown in boxes; the boxes marked A and B denote compositions that are algebraically in accord with the general amphibole formula, but that contain negative coefficients and hence are physically impossible (modified from Hawthorne and Oberti 2006).

criteria include the dominance of a specific cation at a site or group of sites. This approach would definitely dispose of pargasite and hornblende as distinct amphibole species. There are (at least) two opinions on this issue: (1) names that are extremely common, not just in Mineralogy but also in Petrology and Geochemistry, and carry other scientific implications along with their name (e.g., conditions of formation) or are involved in definitions or names of rock types, should be retained as a matter of scientific convenience; (2) a better classification is paramount, and such inconveniences as mentioned in (1) should be endured until the old names are supplanted in the minds of working scientists by the new names.

These are not easy issues with which to deal, and are made more difficult by the fact that few people appreciate the points of view of the ‘opposing’ group of opinions. What we will do here, in part to illustrate the problems, is examine two approaches to classification, one that retains the familiar compositions of ‘intermediate’ amphiboles [SCHEME 1] and one that strives to minimize the number of root names [SCHEME 2].

Calcium-lithium, magnesium-lithium and magnesium-sodium compositions. The above discussion concerning the sodium-calcium amphibole group can be applied to all mixed-valence B-cation-pairings. Thus $B_2 = (\text{LiCa}), (\text{LiMg}), (\text{NaMg})$ and their ${}^B\text{Fe}^{2+}$ and ${}^B\text{Mn}^{2+}$ analogues will all result in end-member compositions of the type $\text{Na } B_2 \text{Mg}_5 \text{Si}_8 \text{O}_{22} \text{W}_2$ that cannot be decomposed into calcium-, lithium-, magnesium-iron-manganese- or sodium-group compositions. In this regard, consider the composition ${}^A(\text{Na}_{0.33}\text{K}_{0.03})_{\Sigma 0.36} {}^B(\text{Na}_{0.82}\text{Ca}_{0.39}\text{Mn}_{0.57}$

$Mg_{0.22}\Sigma_{2.00}{}^C(Mg_{3.83}Mn^{2+}_{0.37}Fe^{3+}_{0.73}Li_{0.07})\Sigma_{5.00}{}^T(Si_{7.86}Al_{0.11})\Sigma_{7.97}O_{22}(OH_{1.60}F_{0.40})$, reported from Tirodi, India, by Oberti and Ghose (1993). This amphibole is close to the root composition $A\Box^B(NaMn)^C(Mg_4Fe^{3+})^T Si_8 O_{22} (OH)_2$ and is presently named fluorian manganooan parvowinchite (IMA-CNMMN 2003-066; Leake et al. 2003). This composition gives rise to a new root name, and hence to a new group of $B(Na(Mg,Fe,Mn))$ amphiboles in SCHEME 1, but not in SCHEME 2.

The $B(NaMg)$ and $B(LiMg)$ joins have been investigated by synthesis; intermediate compositions with a “richterite-like” charge-arrangement are stable and have $P2_1/m$ symmetry at room temperature (Cámara et al. 2003; Iezzi et al. 2004, 2005a,b; see Oberti et al. (2007) for more details). We will take the pragmatic course of not considering the existence of synthetic lithium-calcium or lithium-magnesium amphiboles in SCHEME 1 and SCHEME 2, as these schemes refer to minerals (i.e., natural compositions). We take the boundary between the lithium and calcium, and lithium and magnesium-iron-manganese amphiboles at $Li : Ca$ and $Li : (Mg + Fe + Mn)$ ratios of 0.50 (i.e., use the criterion of the dominant cation or, in the case of the magnesium-iron-manganese amphiboles, the dominant group of cations) in both SCHEME 1 and SCHEME 2.

The A and C cations

Having divided amphiboles into five groups based on the B cations, we have the A and C cations to classify within these groups and to assign specific names to specific compositional ranges and root compositions. For the A cations, the variation observed in Nature spans the complete range possible from a structural perspective: \Box , Na, K and Ca can vary in the range 0-1 apfu. The situation for the C cations is more complicated, as these cations occur at three distinct sites in amphibole structures: $M(1)$, $M(2)$ and $M(3)$ in all common amphibole structure-types (but not in the $P2/a$ and $C\bar{1}$ structures, where there are five and eight M sites, respectively). Most heterovalent variations occur at the $M(2)$ site, where there is complete solid-solution among Mg, Fe^{2+} , Al, Fe^{3+} and Ti^{4+} . Some Al can disorder over $M(2)$ and $M(3)$ in Mg-rich calcium amphiboles (Oberti et al. 1995), and some Fe^{3+} can occur at $M(1)$ owing to post-crystallization oxidation-dehydroxylation, but trivalent cations are never dominant at $M(1)$ or $M(3)$ in amphiboles with $(OH,F,Cl) \geq 1.00$ apfu. Lithium can become dominant at the $M(3)$ site, normally being accompanied by Fe^{3+} at the $M(2)$ site.

Representation of C cations. We need to be able to represent the variation in C cations by a single variable, which therefore must be their aggregate formal charge. The most common variation in C involves divalent and trivalent cations. If we consider C cations of formal charge greater than 2^+ , i.e., Al, Fe^{3+} , Cr^{3+} , V^{3+} , Ti^{4+} , Sc and Zr, we can express their aggregate formal charge as M^{3+} where $M^{3+} = Al + Fe^{3+} + Cr^{3+} + V^{3+} + Sc + 2 \times Ti^{4+} + 2 \times Zr^{*}$. If we are dealing with amphiboles in which $W = (OH,F,Cl)_2$, all of these cations will occur at the $M(2)$ site [except for some Al-Mg disorder over $M(2)$ and $M(3)$ in Mg-rich calcium amphiboles], and thus the high-charge cations cannot exceed 2 apfu, although the aggregate charge, M^{3+} , can exceed 2. However, real amphiboles have two compositional characteristics that can modify this situation: (1) the presence of Li as a C cation, and (2) the presence of O^{2-} as a non-dominant component of the W anions.

${}^C Li$ enters the amphibole structure *via* the substitution $M^{(3)}Li + M^{(2)}Fe^{3+} \rightarrow M^{(2,3)}Fe^{2+}_2$. As ${}^C Li$ is not incorporated into the A-B-C classification procedure as represented in Figure 7 but is considered separately, it is necessary to adjust the value of M^{3+} for the effect of the substitution $M^{(3)}Li + M^{(2)}Fe^{3+} \rightarrow M^{(2,3)}Fe^{2+}_2$. This is done by subtracting an amount of trivalent cations equal to the amount of ${}^C Li$.

* Replacement of M^{2+}_n by M^{3+}_n increases the aggregate charge by n^+ ; replacement of M^{2+}_n by M^{4+}_n increases the aggregate charge by $2n^+$.

The behavior of ${}^C\text{Ti}^{4+}$ also affects M^{3+} because of the different roles that ${}^C\text{Ti}^{4+}$ plays in amphiboles: (1) ${}^C\text{Ti}^{4+}$ may occur at the $M(2)$ site where it contributes $2 \times {}^C\text{Ti}^{4+}$ to M^{3+} ; (2) ${}^C\text{Ti}^{4+}$ may occur at the $M(1)$ site where it is coupled to the occurrence of O^{2-} at the $\text{O}(3)$ site [i.e., as a W anion]; in this role, it will not contribute to M^{3+} . The same is true for Fe^{3+} occurring at the $M(1)$ and $M(3)$ sites in calcic oxo-amphiboles from volcanic environments, where dehydrogenation is related to post-crystallization oxidation processes (more detail in Oberti et al. 2007b). However, without detailed structural and analytical work (SIMS and Mössbauer), correct assignment of Ti^{4+} and Fe^{3+} to the $M(1,2,3)$ sites is not possible. The oxo component must be accounted for by subtracting a proper amount of Fe^{3+} or Ti^{4+} trivalent cations from M^{3+} before classification.

NEW SCHEMES FOR THE CLASSIFICATION OF AMPHIBOLES

First, amphiboles are divided into two classes according to the dominant W species:

- (1) ${}^W(\text{OH},\text{F},\text{Cl})$ -dominant amphiboles;
- (2) ${}^W\text{O}$ -dominant amphiboles.

AMPHIBOLES WITH (OH,F,Cl) DOMINANT AT W

These are divided into a number of groups according to the dominant B cation or group of B cations. In order to make the notation simpler, let us write the sum of the small divalent cations as $\sum\text{Mg} = {}^B\text{Mg} + {}^B\text{Fe}^{2+} + {}^B\text{Mn}^{2+}$, and the sum of the B cations as $\sum\text{B} = {}^B\text{Li} + {}^B\text{Na} + \sum\text{Mg} + {}^B\text{Ca}$ (which generally is equal to 2.00 apfu). Thus the dominant B constituents may be represented as follows.

	<u>SCHEME 1</u>	<u>SCHEME 2</u>
Magnesium-iron-manganese	$\sum\text{Mg}$	$\sum\text{Mg}$
Calcium	${}^B(\text{Ca} + \text{Na})$	${}^B\text{Ca}$
Sodium-calcium	${}^B(\text{Ca} + \text{Na})$	—
Sodium	${}^B(\text{Ca} + \text{Na})$	${}^B\text{Na}$
Lithium	${}^B\text{Li}$	${}^B\text{Li}$
Sodium-(magnesium-iron-manganese)	$\sum\text{Mg} + {}^B\text{Na}$	—

The dominant constituent or group of constituents defines the group. In SCHEME 1, ${}^B(\text{Ca} + \text{Na})$ defines only the dominance of the calcium, sodium-calcium and sodium groups collectively. Once the dominance of a collective group is established, which group occurs is defined by the ratio ${}^B\text{Ca} / {}^B(\text{Ca} + \text{Na})$ as indicated below.

	<u>SCHEME 1</u>	<u>SCHEME 2</u>
Calcium	${}^B\text{Ca} / {}^B(\text{Ca} + \text{Na}) \geq 0.75$	${}^B\text{Ca} / \sum\text{B} \geq \sum\text{Mg} / \sum\text{B}, {}^B\text{Na} / \sum\text{B}, {}^B\text{Li} / \sum\text{B}$
Sodium-calcium	$0.75 > {}^B\text{Ca} / {}^B(\text{Ca} + \text{Na}) > 0.25$	—
Sodium	$0.25 \geq {}^B\text{Ca} / {}^B(\text{Ca} + \text{Na})$	${}^B\text{Na} / \sum\text{B} > \sum\text{Mg} / \sum\text{B}, {}^B\text{Ca} / \sum\text{B}, {}^B\text{Li} / \sum\text{B}$

The magnesium-iron-manganese amphiboles

Defined by $\sum\text{Mg} / \sum\text{B} > {}^B(\text{Ca} + \text{Na}) / \sum\text{B}$ and $> {}^B\text{Li} / \sum\text{B}$.

Amphiboles of this group may be orthorhombic (space groups $Pnma$ or $Pnmm$) or monoclinic (space groups $C2/m$ or $P2_1/m$). Although we distinguish between the B and C cations in amphiboles in general, we cannot identify accurately the partitioning of Mg and Fe^{2+} between the B and C cations in the magnesium-iron-manganese-group amphiboles without crystal-structure refinement or Mössbauer spectroscopy. Hence for this group, we treat the divisions between Mg- Fe^{2+} homovalent analogues in terms of the sum of the B and C

cations. However, Mn^{2+} has a significant site preference for $M(4)$, and hence distinct species are recognized with Mn^{2+} as the dominant B cation.

Orthorhombic magnesium-iron-manganese amphiboles. The space group $Pnma$ is assumed, the space group $Pnmm$ is indicated by the prefix *proto*. There are four root compositions with Mg dominant at C (Table 7). The composition $\text{Na Mg}_2 \text{Mg}_5 (\text{Si}_7\text{Al}) \text{O}_{22} (\text{OH})_2$ is named sodicanthophyllite in the current IMA classification. However, this composition has a different charge arrangement from other root compositions for orthorhombic amphiboles and hence warrants a new root name. For example, the relation between anthophyllite and rootname1 is the same as that between tremolite and edenite; thus use of the name sodicanthophyllite (1) violates the association of a distinct root-name with a distinct charge arrangement in A-B-C or A-B-T space, and (2) would, by analogy, require the name “sodictremolite” for the composition $\text{Na Ca}_2 \text{Mg}_5 (\text{Si}_7\text{Al}) \text{O}_{22} (\text{OH})_2$ that is currently named edenite. The composition $\text{Na Mg}_2 (\text{Mg}_3\text{Al}_2) (\text{Si}_5\text{Al}_3) \text{O}_{22} (\text{OH})_2$ is introduced as a new root composition, replacing sodicgedrite, $\text{Na Mg}_2 (\text{Mg}_4\text{Al}) (\text{Si}_6\text{Al}_2) \text{O}_{22} (\text{OH})_2$, in the current IMA classification. There are four homovalent analogues involving Fe^{2+} instead of Mg dominant at (B + C) with the following compositions. The compositional ranges of the orthorhombic magnesium-iron-manganese amphiboles are shown in Figure 8.

Monoclinic magnesium-iron-manganese amphiboles. The space group $C2/m$ is assumed, the space group $P2_1/m$ is indicated by the hyphenated suffix $P2_1/m$. There is one root composition with Mg dominant at (B + C), one analogue involving Fe^{2+} instead of Mg dominant at (B + C), and two additional analogues with Mn^{2+} dominant at (B + C) and at B only. Leake et al. (1997) designated the Mn^{2+} analogues by the prefix *mangano*. However, it is not consistent to apply the prefix *mangano* to the composition $\square \text{Mn}^{2+}_2 \text{Mg}_5 \text{Si}_8 \text{O}_{22} (\text{OH})_2$ as all other prefixes are used to indicate compositions at the A and C sites. Thus the composition $\square \text{Mn}^{2+}_2 \text{Mg}_5 \text{Si}_8 \text{O}_{22} (\text{OH})_2$ warrants a new root name: rootname3, $\square \text{Mn}^{2+}_2 \text{Fe}^{2+}_5 \text{Si}_8 \text{O}_{22} (\text{OH})_2$ is ferro-rootname3, and $\square \text{Mn}^{2+}_2 \text{Mn}^{2+}_5 \text{Si}_8 \text{O}_{22} (\text{OH})_2$ is mangano-rootname3; note that the prefix *mangano* is used only for ${}^c\text{Mn}^{2+}$.

The compositional ranges of the monoclinic Mg-Fe-Mn amphiboles are shown in Figure 9 and end-member compositions are given in Table 7.

The calcium amphiboles

Defined as follows:

SCHEME 1

$${}^B(\text{Ca}+\text{Na})/\sum\text{B} \geq \sum\text{Mg}/\sum\text{B}, \text{Na}/\sum\text{B}, \text{Li}/\sum\text{B}$$

$${}^B\text{Ca}/{}^B(\text{Ca}+\text{Na}) \geq 0.75$$

SCHEME 2

$${}^B\text{Ca}/\sum\text{B} \geq \sum\text{Mg}/\sum\text{B}, \text{Na}/\sum\text{B}, \text{Li}/\sum\text{B}$$

The root compositions are given in Figure 10 and Table 8. SCHEME 1 accepts current root names and their compositions. SCHEME 2 has all root compositions with Mg and Al dominant at C. Thus in SCHEME 1, one uses the prefixes *magnesio-* and *alumno-* where the root names are defined as the ferrous or ferric analogues (or both), whereas in SCHEME 2, one never uses the prefixes *magnesio-* and *alumno-*. Note that in SCHEME 1, the name *hornblende* is never used without a prefix, as was the case in the previous classification of Leake et al. (1997), in order to allow the name to be available for field or optical-microscopy classification schemes. Also, kaersutite is no longer considered as an ${}^W(\text{OH},\text{F},\text{Cl})$ -dominant calcium amphibole; it is classified as an ${}^W\text{O}^{2-}$ -dominant amphibole. Ferrous-iron and ferric-iron analogues are generally named by the prefix *ferro-* and *ferri-* (Table 8). However, in SCHEME 1, some compositions retain their traditional name (e.g., hastingsite, magnesio-hastingsite) because of the petrological importance of these names. Ferrous- and ferric-iron analogues are generally named by the prefixes *ferro-ferri-* (Table 8).

Table 7. End-member compositions in the magnesium-iron-manganese amphiboles in SCHEME 1 and SCHEME 2.

End-member formula	SCHEME 1	SCHEME 2
$\square \text{Mg}_2 \text{Mg}_5 \text{Si}_8 \text{O}_{22} (\text{OH})_2$	Anthophyllite	Anthophyllite
$\text{Na} \text{Mg}_2 \text{Mg}_5 (\text{Si}_7 \text{Al}) \text{O}_{22} (\text{OH})_2$	Rootname1	Rootname1
$\square \text{Mg}_2 (\text{Mg}_3 \text{Al}_2) (\text{Si}_6 \text{Al}_2) \text{O}_{22} (\text{OH})_2$	Gedrite	Gedrite
$\text{Na} \text{Mg}_2 (\text{Mg}_3 \text{Al}_2) (\text{Si}_5 \text{Al}_3) \text{O}_{22} (\text{OH})_2$	Rootname2	Rootname2
$\square \text{Fe}^{2+}_2 \text{Fe}^{2+}_5 \text{Si}_8 \text{O}_{22} (\text{OH})_2$	Ferro-anthophyllite	Ferro-anthophyllite
$\text{Na} \text{Fe}^{2+}_2 \text{Fe}^{2+}_5 (\text{Si}_7 \text{Al}) \text{O}_{22} (\text{OH})_2$	Ferro-rootname1	Ferro-rootname1
$\square \text{Fe}^{2+}_2 (\text{Fe}^{2+}_3 \text{Al}_2) (\text{Si}_6 \text{Al}_2) \text{O}_{22} (\text{OH})_2$	Ferro-gedrite	Ferro-gedrite
$\text{Na} \text{Fe}^{2+}_2 (\text{Fe}^{2+}_3 \text{Al}_2) (\text{Si}_5 \text{Al}_3) \text{O}_{22} (\text{OH})_2$	Ferro-rootname2	Ferro-rootname2
$\square \text{Mg}_2 \text{Mg}_5 \text{Si}_8 \text{O}_{22} (\text{OH})_2$	Cummingtonite	Cummingtonite
$\square \text{Fe}^{2+}_2 \text{Fe}^{2+}_5 \text{Si}_8 \text{O}_{22} (\text{OH})_2$	Grunerite	Ferro-cummingtonite
$\square \text{Mn}^{2+}_2 \text{Mg}_5 \text{Si}_8 \text{O}_{22} (\text{OH})_2$	Rootname3	Rootname3
$\square \text{Mn}^{2+}_2 \text{Fe}^{2+}_5 \text{Si}_8 \text{O}_{22} (\text{OH})_2$	Ferro-rootname3	Ferro-rootname3

Figure 8. Root compositions for the orthorhombic magnesium-iron-manganese amphiboles; note that compositions with Na dominant at A require new root names in SCHEMES 1 and 2 (modified from Hawthorne and Oberti 2006).

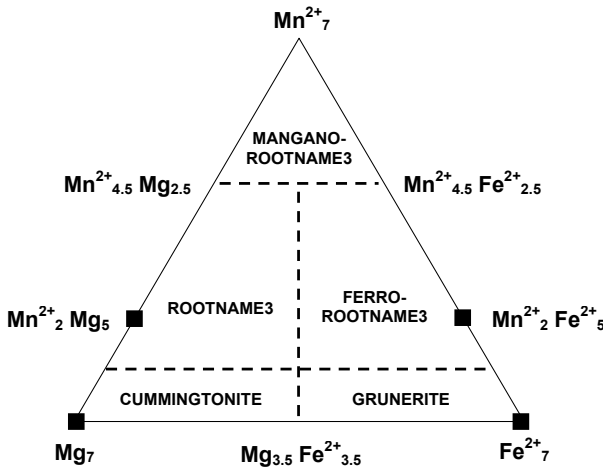
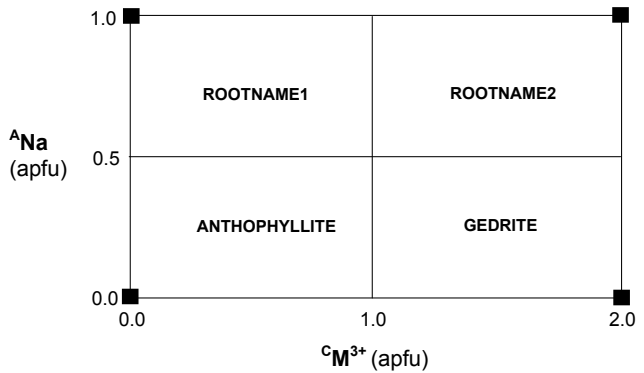
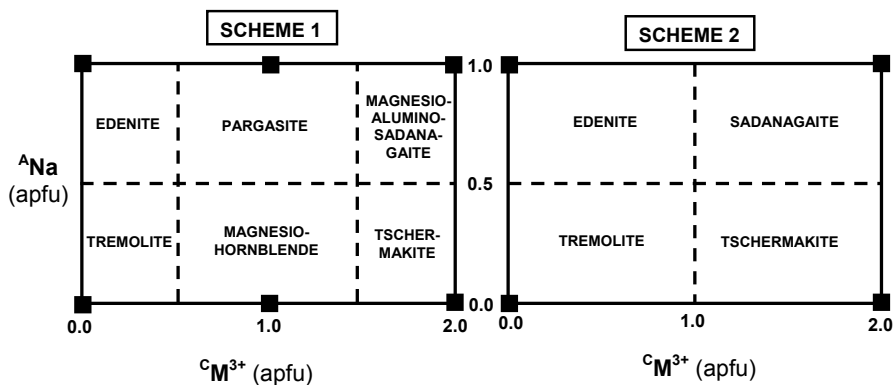


Figure 9. Root compositions and compositional variations for the monoclinic magnesium-iron-manganese amphiboles; note that compositions with Mn^{2+} dominant at C require a new root name in SCHEMES 1 and 2 (modified from Hawthorne and Oberti 2006).

Table 8. End-member compositions in the calcium amphiboles in SCHEME 1 and SCHEME 2.

End-member formula	SCHEME 1	SCHEME 2
$\square \text{Ca}_2\text{Mg}_5\text{Si}_8\text{O}_{22}(\text{OH})_2$	Tremolite	Tremolite
$\square \text{Ca}_2(\text{Mg}_4\text{Al})(\text{Si}_7\text{Al})\text{O}_{22}(\text{OH})_2$	Magnesio-hornblende	—
$\square \text{Ca}_2(\text{Mg}_3\text{Al}_2)(\text{Si}_6\text{Al}_2)\text{O}_{22}(\text{OH})_2$	Tschemmakite	Tschemmakite
$\text{NaCa}_2\text{Mg}_5(\text{Si}_7\text{Al})\text{O}_{22}(\text{OH})_2$	Edenite	Edenite
$\text{NaCa}_2(\text{Mg}_4\text{Al})(\text{Si}_6\text{Al}_2)\text{O}_{22}(\text{OH})_2$	Pargasite	—
$\text{NaCa}_2(\text{Mg}_3\text{Al}_2)(\text{Si}_5\text{Al}_3)\text{O}_{22}(\text{OH})_2$	Magnesio-alumino-sadanagaite	Sadanagaite
$\text{CaCa}_2(\text{Mg}_4\text{Al})(\text{Si}_5\text{Al}_3)\text{O}_{22}(\text{OH})_2$	Cannilloite	Cannilloite
$\square \text{Ca}_2\text{Fe}^{2+}_5\text{Si}_8\text{O}_{22}(\text{OH})_2$	Actinolite	Ferro-tremolite
$\square \text{Ca}_2(\text{Fe}^{2+}_4\text{Al})(\text{Si}_7\text{Al})\text{O}_{22}(\text{OH})_2$	Ferro-hornblende	—
$\square \text{Ca}_2(\text{Fe}^{2+}_3\text{Al}_2)(\text{Si}_6\text{Al}_2)\text{O}_{22}(\text{OH})_2$	Ferro-tschemmakite	Ferro-tschemmakite
$\text{NaCa}_2\text{Fe}^{2+}_5(\text{Si}_7\text{Al})\text{O}_{22}(\text{OH})_2$	Ferro-edenite	Ferro-edenite
$\text{NaCa}_2(\text{Fe}^{2+}_4\text{Al})(\text{Si}_6\text{Al}_2)\text{O}_{22}(\text{OH})_2$	Ferro-pargasite	—
$\text{NaCa}_2(\text{Fe}^{2+}_3\text{Al}_2)(\text{Si}_5\text{Al}_3)\text{O}_{22}(\text{OH})_2$	Alumino-sadanagaite	Ferro-sadanagaite
$\text{CaCa}_2(\text{Fe}^{2+}_4\text{Al})(\text{Si}_5\text{Al}_3)\text{O}_{22}(\text{OH})_2$	Ferro-cannilloite	Ferro-cannilloite
$\square \text{Ca}_2(\text{Mg}_4\text{Fe}^{3+})(\text{Si}_7\text{Al})\text{O}_{22}(\text{OH})_2$	Ferri-hornblende	—
$\square \text{Ca}_2(\text{Mg}_3\text{Fe}^{3+}_2)(\text{Si}_6\text{Al}_2)\text{O}_{22}(\text{OH})_2$	Ferri-tschemmakite	Ferri-tschemmakite
$\text{NaCa}_2(\text{Mg}_4\text{Fe}^{3+})(\text{Si}_6\text{Al}_2)\text{O}_{22}(\text{OH})_2$	Magnesio-hastingsite	—
$\text{NaCa}_2(\text{Mg}_3\text{Fe}^{3+}_2)(\text{Si}_5\text{Al}_3)\text{O}_{22}(\text{OH})_2$	Magnesio-sadanagaite	Ferri-sadanagaite
$\square \text{Ca}_2(\text{Fe}^{2+}_4\text{Fe}^{3+})(\text{Si}_7\text{Al})\text{O}_{22}(\text{OH})_2$	Ferro-ferri-hornblende	—
$\square \text{Ca}_2(\text{Fe}^{2+}_3\text{Fe}^{3+}_2)(\text{Si}_6\text{Al}_2)\text{O}_{22}(\text{OH})_2$	Ferro-ferri-tschemmakite	Ferro-ferri-tschemmakite
$\text{NaCa}_2(\text{Fe}^{2+}_4\text{Fe}^{3+})(\text{Si}_6\text{Al}_2)\text{O}_{22}(\text{OH})_2$	Hastingsite	—
$\text{NaCa}_2(\text{Fe}^{2+}_3\text{Fe}^{3+}_2)(\text{Si}_5\text{Al}_3)\text{O}_{22}(\text{OH})_2$	Sadanagaite	Ferro-ferri-sadanagaite

**Figure 10.** Root compositions and compositional variations for the calcium amphiboles; Na = Na + K (modified from Hawthorne and Oberti 2006).

The sodium-calcium amphiboles

Defined as follows:

SCHEME 1

$${}^B(\text{Ca} + \text{Na}) / \sum B \geq \sum \text{Mg} / \sum B, \text{Na} / \sum B, \text{Li} / \sum B$$

$$0.75 > {}^B\text{Ca} / {}^B(\text{Ca} + \text{Na}) > 0.25$$

SCHEME 2

DOES NOT OCCUR

There are five root compositions with Mg and Al dominant at C, together with their ferrous-iron, ferric-iron and ferrous-ferric-iron analogues (Table 9). However, some compositions retain their traditional name (e.g., katophorite) because of the petrological importance of this name. The compositional ranges of the root sodium-calcium amphiboles are shown in Figure 11.

Table 9. End-member compositions in the sodium-calcium amphiboles in SCHEME 1 and SCHEME 2.

End-member formula	SCHEME 1	SCHEME 2
□ Ca Na (Mg ₄ Al) Si ₈ O ₂₂ (OH) ₂	Winchite	—
□ Ca Na (Mg ₃ Al ₂) (Si ₇ Al) O ₂₂ (OH) ₂	Barroisite	—
Na Ca Na Mg ₅ Si ₈ O ₂₂ (OH) ₂	Richterite	—
Na Ca Na (Mg ₄ Al) (Si ₇ Al) O ₂₂ (OH) ₂	Magnesio-katophorite	—
Na Ca Na (Mg ₃ Al ₂) (Si ₆ Al ₂) O ₂₂ (OH) ₂	Magnesio-taramite	—
□ Ca Na Fe ²⁺ ₅ Si ₈ O ₂₂ (OH) ₂	Ferro-richterite	—
□ Ca Na (Fe ²⁺ ₄ Al) Si ₈ O ₂₂ (OH) ₂	Ferro-winchite	—
□ Ca Na (Fe ²⁺ ₃ Al ₂) (Si ₇ Al) O ₂₂ (OH) ₂	Ferro-barroisite	—
Na Ca Na (Fe ²⁺ ₄ Al) (Si ₇ Al) O ₂₂ (OH) ₂	Katophorite	—
Na Ca Na (Fe ²⁺ ₃ Al ₂) (Si ₆ Al ₂) O ₂₂ (OH) ₂	Taramite	—
□ Ca Na (Mg ₄ Fe ³⁺) Si ₈ O ₂₂ (OH) ₂	Ferri-winchite	—
□ Ca Na (Mg ₃ Fe ³⁺ ₂) (Si ₇ Al) O ₂₂ (OH) ₂	Ferri-barroisite	—
Na Ca Na (Mg ₄ Fe ³⁺) (Si ₇ Al) O ₂₂ (OH) ₂	Magnesio-ferri-katophorite	—
Na Ca Na (Mg ₃ Fe ³⁺ ₂) (Si ₆ Al ₂) O ₂₂ (OH) ₂	Magnesio-ferri-taramite	—
□ Ca Na (Fe ²⁺ ₄ Fe ³⁺) Si ₈ O ₂₂ (OH) ₂	Ferro-ferri-winchite	—
□ Ca Na (Fe ²⁺ ₃ Fe ³⁺ ₂) (Si ₇ Al) O ₂₂ (OH) ₂	Ferro-ferri-barroisite	—
Na Ca Na (Fe ²⁺ ₄ Fe ³⁺) (Si ₇ Al) O ₂₂ (OH) ₂	Ferri-katophorite	—
Na Ca Na (Fe ²⁺ ₃ Fe ³⁺ ₂) (Si ₆ Al ₂) O ₂₂ (OH) ₂	Ferri-taramite	—

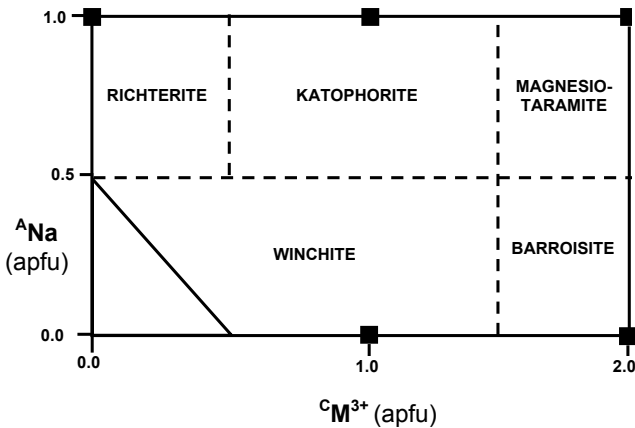


Figure 11. Root compositions and compositional variations for the sodium-calcium amphiboles; note that the amphiboles of this group only exist in scheme 1 (modified from Hawthorne and Oberti 2006).

The sodium amphiboles

Defined as follows:

SCHEME 1

$${}^B(\text{Ca} + \text{Na}) / \Sigma B \geq \Sigma \text{Mg} / \Sigma B, {}^B\text{Na} / \Sigma B, \text{Li} / \Sigma B$$

$${}^B\text{Ca} / ({}^B\Sigma\text{Ca} + \text{Na}) \leq 0.25$$

SCHEME 2

$${}^B\text{Na} / \Sigma B \geq \Sigma \text{Mg} / \Sigma B, {}^B\text{Ca} / \Sigma B, \text{Li} / \Sigma B$$

The root compositions are shown in Figure 12 and all end-member compositions are listed in Table 10. For the sodium amphiboles, there are also Mn^{2+} analogues that are denoted by root (trivial) names (Table 10). Kozulite is the mangano- analogue of arfvedsonite, and kornite is the mangani- analogue of leakeite. We strongly suggest that in SCHEME 1, they be named mangano-arfvedsonite and mangani-leakeite, respectively.

Table 10. End-member compositions in the sodium amphiboles in SCHEME 1 and SCHEME 2.

End-member formula	SCHEME 1	SCHEME 2
$\square \text{Na}_2(\text{Mg}_3\text{Al}_2)\text{Si}_8\text{O}_{22}(\text{OH})_2$	Glaucofane	Glaucofane
$\text{NaNa}_2(\text{Mg}_4\text{Al})\text{Si}_8\text{O}_{22}(\text{OH})_2$	Eckermannite	Eckermannite
$\text{NaNa}_2(\text{Mg}_3\text{Al}_2)(\text{Si}_7\text{Al})\text{O}_{22}(\text{OH})_2$	Nyböite	Nyböite
$\text{NaNa}_2(\text{Mg}_2\text{Al}_2\text{Li})\text{Si}_8\text{O}_{22}(\text{OH})_2$	Alumino-leakeite	Leakeite
$\square \text{Na}_2(\text{Fe}^{2+}_3\text{Al}_2)\text{Si}_8\text{O}_{22}(\text{OH})_2$	Ferro-glaucofane	Ferro-glaucofane
$\text{NaNa}_2(\text{Fe}^{2+}_4\text{Al})\text{Si}_8\text{O}_{22}(\text{OH})_2$	Ferro-eckermannite	Ferro-eckermannite
$\text{NaNa}_2(\text{Fe}^{2+}_3\text{Al}_2)(\text{Si}_7\text{Al})\text{O}_{22}(\text{OH})_2$	Ferro-nyböite	Ferro-nyböite
$\text{NaNa}_2(\text{Fe}^{2+}_2\text{Al}_2\text{Li})\text{Si}_8\text{O}_{22}(\text{OH})_2$	Ferro-alumino-leakeite	Ferro-leakeite
$\square \text{Na}_2(\text{Mg}_3\text{Fe}^{3+}_2)\text{Si}_8\text{O}_{22}(\text{OH})_2$	Magnesio-riebeckite	Ferri-glaucofane
$\text{NaNa}_2(\text{Mg}_4\text{Fe}^{3+})\text{Si}_8\text{O}_{22}(\text{OH})_2$	Magnesio-arfvedsonite	Ferri-eckermannite
$\text{NaNa}_2(\text{Mg}_3\text{Fe}^{3+}_2)(\text{Si}_7\text{Al})\text{O}_{22}(\text{OH})_2$	Ferri-nyböite	Ferri-nyböite
$\text{NaNa}_2(\text{Mg}_2\text{Fe}^{3+}_2\text{Li})\text{Si}_8\text{O}_{22}(\text{OH})_2$	Leakeite	Ferri-leakeite
$\square \text{Na}_2(\text{Fe}^{2+}_3\text{Fe}^{3+}_2)\text{Si}_8\text{O}_{22}(\text{OH})_2$	Riebeckite	Ferro-ferri-glaucofane
$\text{NaNa}_2(\text{Fe}^{2+}_4\text{Fe}^{3+})\text{Si}_8\text{O}_{22}(\text{OH})_2$	Arfvedsonite	Ferro-ferri-eckermannite
$\text{NaNa}_2(\text{Fe}^{2+}_3\text{Fe}^{3+}_2)(\text{Si}_7\text{Al})\text{O}_{22}(\text{OH})_2$	Ferro-ferri-nyböite	Ferro-ferri-nyböite
$\text{NaNa}_2(\text{Fe}^{2+}_2\text{Fe}^{3+}_2\text{Li})\text{Si}_8\text{O}_{22}(\text{OH})_2$	Ferro-leakeite	Ferro-ferri-leakeite
$\text{NaNa}_2(\text{Mn}^{2+}_4\text{Fe}^{3+})\text{Si}_8\text{O}_{22}(\text{OH})_2$	Kozulite	Mangano-ferri-glaucofane
$\text{NaNa}_2(\text{Mg}_2\text{Mn}^{3+}_2\text{Li})\text{Si}_8\text{O}_{22}(\text{OH})_2$	Kornite	Mangani-leakeite

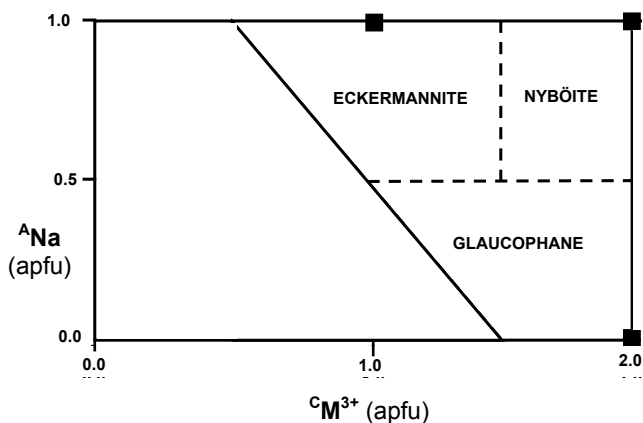


Figure 12. Root compositions and compositional variations for the sodium amphiboles (modified from Hawthorne and Oberti 2006).

The lithium amphiboles

Defined by ${}^B\text{Li}/\Sigma\text{B} > {}^B\text{Mg}/\Sigma\text{B}$ and ${}^B(\text{Ca} + \text{Na})/\Sigma\text{B}$.

Amphiboles of this group may be orthorhombic (space group *Pnma*) or monoclinic (space group *C2/m*).

Orthorhombic lithium amphiboles. There is one root composition plus its ferro-, ferri- and ferro-ferri- analogues (Table 11).

Monoclinic lithium amphiboles. There are two root compositions plus their ferro-, ferri- and ferro-ferri- analogues (Table 11). Note that “clino-holmquistite” has recently been discredited (Oberti et al. 2005); also, current knowledge and comparison with cummingtonite suggests that compositions close to that of end-member “clino-holmquistite” (if stable) should have the space group *P2₁/m*.

Table 11. End-member compositions in the lithium amphiboles in SCHEME 1 and SCHEME 2.

End-member formula	SCHEME 1	SCHEME 2
$\square \text{Li}_2(\text{Mg}_3\text{Al}_2)\text{Si}_8\text{O}_{22}(\text{OH})_2$	Holmquistite	Holmquistite
$\square \text{Li}_2(\text{Fe}^{2+}_3\text{Al}_2)\text{Si}_8\text{O}_{22}(\text{OH})_2$	Ferro-holmquistite	Ferro-holmquistite
$\square \text{Li}_2(\text{Mg}_3\text{Fe}^{3+}_2)\text{Si}_8\text{O}_{22}(\text{OH})_2$	Ferri-holmquistite	Ferri-holmquistite
$\square \text{Li}_2(\text{Fe}^{2+}_3\text{Fe}^{3+}_2)\text{Si}_8\text{O}_{22}(\text{OH})_2$	Ferro-ferri-holmquistite	Ferro-ferri-holmquistite
$\square \text{Li}_2(\text{Mg}_3\text{Al}_2)\text{Si}_8\text{O}_{22}(\text{OH})_2$	“Clino-holmquistite”	“Clino-holmquistite”
$\text{NaLi}_2(\text{Mg}_2\text{Al}_2\text{Li})\text{Si}_8\text{O}_{22}(\text{OH})$	Pedrizite	Pedrizite
$\square \text{Li}_2(\text{Fe}^{2+}_3\text{Al}_2)\text{Si}_8\text{O}_{22}(\text{OH})_2$	Clino-ferro-holmquistite	Clino-ferro-holmquistite
$\text{NaLi}_2(\text{Fe}^{2+}_2\text{Al}_2\text{Li})\text{Si}_8\text{O}_{22}(\text{OH})_2$	Ferro-pedrizite	Ferro-pedrizite
$\square \text{Li}_2(\text{Mg}_3\text{Fe}^{3+}_2)\text{Si}_8\text{O}_{22}(\text{OH})_2$	Clino-ferri-holmquistite	Clino-ferri-holmquistite
$\text{NaLi}_2(\text{Mg}_2\text{Fe}^{3+}_2\text{Li})\text{Si}_8\text{O}_{22}(\text{OH})_2$	Ferri-pedrizite	Ferri-pedrizite
$\square \text{Li}_2(\text{Fe}^{2+}_3\text{Fe}^{3+}_2)\text{Si}_8\text{O}_{22}(\text{OH})_2$	Clino-ferro-ferri-holmquistite	Clino-ferro-ferri-holmquistite
$\text{NaLi}_2(\text{Fe}^{2+}_2\text{Fe}^{3+}_2\text{Li})\text{Si}_8\text{O}_{22}(\text{OH})_2$	Ferro-ferri-pedrizite	Ferro-ferri-pedrizite

The sodium-magnesium-iron-manganese amphiboles

Defined as follows:

<u>SCHEME 1</u>	<u>SCHEME 2</u>
${}^B(\text{Mg} + \text{Fe}^{2+} + \text{Mn}^{2+} + \text{Na})/\Sigma\text{B} > {}^B\text{Ca}/\Sigma\text{B}$ and $> {}^B\text{Li}/\Sigma\text{B}$	DOES NOT OCCUR
$0.75 > {}^B\text{Na}/{}^B(\text{Mg} + \text{Fe}^{2+} + \text{Mn}^{2+} + \text{Na}) > 0.25$	

At the moment, there is only one root composition, $\square (\text{Mn}^{2+}\text{Na})(\text{Mg}_4\text{Fe}^{3+})\text{Si}_8\text{O}_{22}(\text{OH})_2$, found in Nature (Oberti and Ghose 1993). A new name must be assigned in SCHEME 1. The analogues with ferrous iron at C are generally named by the prefix *ferro-*, and the analogues with ferric iron at C are generally named by the prefix *ferri-*. By analogy with the magnesium-iron-manganese group [e.g., $\square \text{Mn}^{2+}_2\text{Mg}_5\text{Si}_8\text{O}_{22}(\text{OH})_2$ = rootname3], we propose to recognize the dominant B cation (where known). Thus Mg, e.g., B = NaMg, is recognized by a *root name*; B = Na(Mg,Fe²⁺) cannot be distinguished from B = NaMg by chemical analysis and does not receive a separate name, whereas B = NaMn²⁺ can be distinguished by chemical analysis and should receive a new rootname. The compositional ranges of the sodium-(magnesium-iron-manganese) amphiboles are shown in Figure 13.

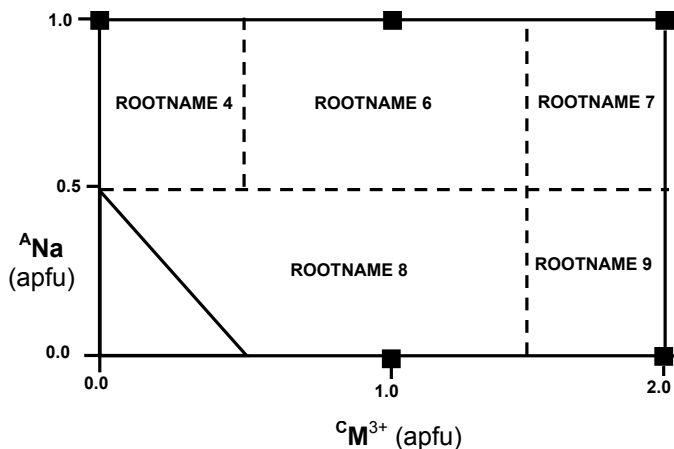


Figure 13. Root compositions and compositional variations for the sodium-(magnesium-iron-manganese) amphiboles (modified from Hawthorne and Oberti 2006).

AMPHIBOLES WITH O^{2-} DOMINANT AT W

Dominance of W by O^{2-} is accompanied by the occurrence of additional high-charge ($\geq 3^+$) C cations ordered at the $M(1)$ and/or $M(3)$ sites; this means the aggregate charge at C may exceed 12^+ . There are four distinct root-compositions (Table 12) and ferrous-iron analogues can be indicated by the prefix *ferro*- (or any other as appropriate).

Three of these amphiboles (obertiite, ungarettiite and dellaventuraitite) are rare, and analysis for H to characterize these species may not be regarded as unduly onerous by the mineralogical community. However, this is not the case for kaersutite, which is a reasonably common and petrologically important amphibole. Thus a different criterion would be convenient for the classification of kaersutite; this can be done on the basis of the Ti content, as indicated in Figure 14. In principle, the inclusion of “Ti-rich pargasite” in Figure 14 is not formally correct as the term “Ti-rich” is functioning as an adjectival modifier (and adjectival modifiers are not part of a classification scheme). However, we suggest that the term “Ti-rich pargasite” be used as it fulfills a very useful function from a petrological perspective.

MAJOR DIFFERENCES BETWEEN THE CURRENT CLASSIFICATION AND SCHEMES 1 AND 2

It is useful to summarize the principal differences between the classification schemes presented here and those of Leake et al. (1997, 2003).

- (1) We have changed the criterion to identify the different groups, bringing it more into accord with the *dominant-cation* criterion of current IMA-CNMMN nomenclature. Leake et al. (1997, 2003) referred to specific atom contents in the formula unit to define the boundary between groups. Thus an amphibole is presently assigned to the calcic group where ${}^B(\text{Mg, Fe}^{2+}, \text{Mn}^{2+}, \text{Li}) \leq 0.50$, ${}^B(\text{Ca, Na}) \geq 1.50$ and ${}^B\text{Na} \leq 0.50$ apfu. In the two schemes described here, amphiboles are assigned to various groups based on the *dominant cation* (or group of cations) at a site (or group of sites). Thus an amphibole is assigned to the calcium group where ${}^B\text{Ca}$ is dominant over ΣMg , ${}^B\text{Na}$ and ${}^B\text{Li}$.
- (2) Leake et al. (1997, 2003) considered ${}^B\text{Li}$ together with ${}^B(\text{Mg, Fe}^{2+}, \text{Mn}^{2+})$, ${}^B\text{Ca}$ and ${}^B\text{Na}$ to define a sodium-calcium-magnesium-iron-manganese-lithium group, in which

Table 12. End-member compositions in the oxo amphiboles in SCHEMES 1 and 2.

End-member formula	SCHEME 1	SCHEME 2
$\text{NaNa}_2(\text{Mg}_3\text{Fe}^{3+}\text{Ti}^{4+})\text{Si}_8\text{O}_{22}\text{O}_2$	Obertiite	Ferri-obertiite
$\text{NaNa}_2(\text{MgMn}^{3+}_2\text{Ti}^{4+}\text{Li})\text{Si}_8\text{O}_{22}\text{O}_2$	Dellaventuraite	Mangani-dellaventuraite
$\text{NaNa}_2(\text{Mn}^{2+}_2\text{Mn}^{3+}_3)\text{Si}_8\text{O}_{22}\text{O}_2$	Ungarettiite	Mangano-mangani-ungarettiite
$\text{NaCa}_2(\text{Mg}_3\text{Ti}^{4+}\text{Al})(\text{Si}_6\text{Al}_2)\text{O}_{22}\text{O}_2$	Kaersutite	Kaersutite
$\text{NaCa}_2(\text{Fe}^{2+}_3\text{Ti}^{4+}\text{Al})(\text{Si}_6\text{Al}_2)\text{O}_{22}\text{O}_2$	Ferro-kaersutite	Ferro-kaersutite

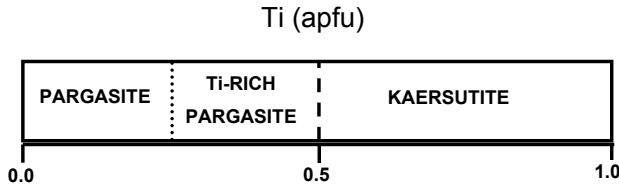


Figure 14. Compositional variation and classification for kaersutite (modified from Hawthorne and Oberti 2006).

intermediate compositions require (1) new root name if ${}^B\text{Li} > 0.50$ apfu, or (2) the prefixes *parvo* and *magno* if ${}^B\text{Li} \leq 0.50$ apfu.

The crystal-chemical behavior of Li is very different from that of $(\text{Mg}, \text{Fe}^{2+}, \text{Mn}^{2+})$ and Ca, and is more similar to that of Na. Moreover, extensive recent work (Caballero et al. 1998, 2002; Oberti et al. 2003, 2004) has shown complete solid-solution between ${}^B\text{Li}$ and ${}^B\text{Na}$, behavior that is different from that of the ${}^B(\text{Mg}, \text{Fe}^{2+}, \text{Mn}^{2+})$ amphiboles. Moreover, the existence of ${}^B\text{Li}$ amphibole with orthorhombic and monoclinic primitive symmetries indicates that ${}^B\text{Li}$ -dominant amphiboles should be a distinct group.

- (3) Leake et al. (1997, 2003) used both nouns and adjectives to define the five main groups of amphiboles (e.g., magnesium-iron-manganese-lithium, calcic, sodic). We propose to use nouns (e.g., magnesium-iron-manganese, calcium, sodium) or element or cation symbols in all cases.
- (4) Leake et al. (1997, 2003) used the A, B and T cations for classification purposes. However, the dominant T cation does not change: it is invariably Si, and hence compositional variation at T is not an appropriate variable to use for classification. All other groups show two or more cations as dominant, and hence the A, B, and C cations are more appropriate for classification purposes and accord with the dominant-cation principle currently used in IMA nomenclature. This point is the major difference between the two schemes. The use of C cations for classification may be implemented by considering the variation in ${}^C\text{M}^{3+}$, the amount of highly charged C cations not involved in the processes related to the oxo component, as a classification variable.

Two major crystal-chemical issues have been explored in detail since publication of the current scheme of classification (Leake et al. 1997): (a) the behavior of ${}^C\text{Li}$, and (b) the occurrence of dominant O^{2-} at W. In both these cases, electroneutrality is maintained by incorporation of “unusual” cations at sites containing “normal” C cations: (a) ${}^{M(3)}\text{Li}$ is accompanied by ${}^{M(2)}\text{Fe}^{3+}$; (b) ${}^W\text{O}^{2-}$ is accompanied by ${}^{M(1)}\text{Ti}^{4+}$ or ${}^{M(1,3)}(\text{Fe}^{3+}, \text{Mn}^{3+})$. For classification purposes, these components can be dealt with by subtracting the relevant amounts of Fe^{3+} and Ti^{4+} from ${}^C\text{M}^{3+}$ before using the standard compositional diagrams.

- (5) The schemes introduced here recognize a distinct group of amphiboles with O^{2-} as the dominant W anion (oxo-amphiboles). These amphiboles contain high-charge C cations, and have distinct root-names.
- (6) With the schemes suggested, we propose a different (and hopefully more rational) use of prefixes. Moreover, if some root compositions are redefined as their magnesio-alumino- analogues, then the prefixes *sodic*, *magnesio* and *alumino* can be eliminated. Appendix I lists the root names that are redefined here.

THE TWO SCHEMES: FOR AND AGAINST

Before we consider the two schemes described here, we should state that various features of each of these schemes are not restricted to one or the other scheme. For example, all redefinitions and removal of root names from IMA97 have been done within SCHEME 2, and yet some of the redefinitions can also be incorporated into SCHEME 1 (e.g., for kornite and kozulite or to avoid the use of the prefixes magnesio- and alumino-).

Recognition of the sodium-calcium and lithium-(magnesium-iron-manganese) groups

On the basis of the dominant-cation principle, these two groups should not be recognized. The root compositions do not have a dominant B cation, having $B_2 = NaCa$ and $B_2 = Li(Mg,Fe,Mn)_2$, and compositions in these fields can be identified as (1) calcium amphiboles (Ca dominant at B) or sodium amphiboles (Na dominant at B), and (2) lithium amphiboles (Li dominant at B) or magnesium-iron-manganese amphiboles [(Mg,Fe,Mn) dominant at B]. SCHEME 2 thus has the advantage of (1) adherence to the dominant-cation principle, and (2) simplicity.

On the other hand, richterite, root composition $Na (CaNa) Mg_5 Si_8 O_{22} (OH)_2$, is an end-member amphibole in composition space (see Fig. 7). From a geochemical perspective, this needs to be recognized, as richterite will have specific thermodynamic properties that are necessary to quantitatively describe the behavior of amphibole compositions as a function of pressure and temperature. Furthermore, sodium-calcium amphiboles can occur in very specific parageneses (e.g., richterite in lamproite) and substituting the name of a sodium-calcium amphibole by a calcium amphibole and a sodium amphibole (where compositions span the composition $B = Na_{1.0}Ca_{1.0}$) may be regarded as undesirable by the petrological community.

Retention versus removal of intermediate amphibole compositions

SCHEME 2 seeks to minimize the number of root names, and does so by following the dominant-cation principle. Thus the composition $\square Ca_2 (Mg_4Al) (Si_7Al) O_{22} (OH)_2$, corresponding to magnesio-hornblende in SCHEME 1, is the boundary composition between tremolite, $\square Ca_2 Mg_5 Si_8 O_{22} (OH)_2$, and tschermakite, $\square Ca_2 (Mg_3Al_2) (Si_6Al_2) O_{22} (OH)_2$ in SCHEME 2. Similarly, the composition $Na Ca_2 (Mg_4Al) (Si_6Al_2) O_{22} (OH)_2$, corresponding to pargasite in SCHEME 1, is the boundary composition between tremolite, $\square Ca_2 Mg_5 Si_8 O_{22} (OH)_2$, and sadanagaite, $Na Ca_2 (Mg_3Al_2) (Si_5Al_3) O_{22} (OH)_2$, in SCHEME 2. Elimination of these two end members would produce a major simplification in terms of the number of root compositions and names. Conversely, some of these names are in common use in both Mineralogy and Petrology, and their removal may be regarded by many as detrimental to issues of amphibole paragenesis in Petrology.

SUMMARY

We have discussed many issues pertaining to the classification of amphiboles, and we have developed two new schemes of classification. We emphasize that we are not proposing

that either of these two schemes be adopted at the moment, or used without due IMA process. Our intentions are as follows:

- (1) to outline the problems associated with any classification of the amphiboles;
- (2) to suggest a different approach to amphibole classification based on the *dominant cation* (or *group of cations*) rather than on a specific number of cation(s) as was done in previous classifications;
- (3) to propose that any future classification be based on chemical variations of the A, B and C cations of the amphibole general formula, rather than the A, B and T cations as was done in previous classifications;
- (4) to examine issues of simplification versus the *status quo* in terms of root compositions and root names.

We emphasize that any classification scheme, particularly one involving a group of minerals as complicated as the amphiboles, is of necessity a compromise: simplicity will often conflict with convenience of use. Moreover, crystallographers, mineralogists and petrologists will generally have different expectations of a classification. Crystallographers will want a classification that encompasses all aspects of the crystal chemistry of the amphiboles in as concise a way as possible, whereas petrologists will be more concerned with the utility and convenience of use from a petrological perspective. The most satisfactory classification will emerge only when all constituents of the community interested in amphiboles recognize the concerns of each other and are sympathetic to their incorporation into a final classification scheme.

ACKNOWLEDGMENTS

This work was supported by the Natural Sciences and Engineering Research Council of Canada through a Canada Research Chair in Crystallography and Mineralogy and a Discovery Grant to FCH and by the Italian Consiglio Nazionale delle Ricerche through project TA01.004.002 to RO.

REFERENCES

- Armbruster T, Oberhänsli R, Bermanec V, Dixon R (1993) Hennomartinite and kornite: two new Mn^{3+} rich silicates from the Wessels Mine, Kalahari, South Africa. *Schweiz Mineral Petrogr Mitt* 73:349-355
- Bayliss P, Kaesz HD, Nickel EH (2005) The use of chemical-element adjectival modifiers in mineral nomenclature. *Can Mineral* 43:1429-1433
- Burke EAJ, Leake BE (2004) "Named amphiboles": a new category of amphiboles recognized by the International Mineralogical Association (IMA), and the proper order of prefixes to be used in amphibole names. *Can Mineral* 42:1881-1883
- Caballero JM, Monge A, La Iglesia A, Tornos F (1998) Ferri-clinoholmquistite, $Li_2(Fe^{2+},Mg)_3Fe^{3+}_2Si_8O_{22}(OH)_2$, a new ${}^B Li$ clinoamphibole from the Pedriza Massif, Sierra de Guadarrama, Spanish Central System. *Am Mineral* 83:167-171
- Caballero JM, Oberti R, Ottolini L (2002) Ferripedrizite, a new monoclinic ${}^B Li$ amphibole end-member from the Eastern Pedriza Massif, Sierra de Guadarrama, Spain, and improvements in the nomenclature of Mg-Fe-Mn-Li amphiboles. *Am Mineral* 87:976-982
- Cámara F, Oberti R, Iezzi G, Della Ventura G (2003) The $P2_1/m \rightarrow C2/m$ phase transition in the synthetic amphibole $Na NaMg Mg_5 Si_8 O_{22} (OH)_2$: Thermodynamic and crystal-chemical evaluation. *Phys Chem Minerals* 30:570-581
- Hawthorne FC (1983) The crystal chemistry of the amphiboles. *Can Mineral* 21:173-480
- Hawthorne FC (2002) The use of end-member charge arrangements in defining new mineral species and heterovalent substitutions in complex minerals. *Can Mineral* 40:699-710
- Hawthorne FC, Oberti R (2006) On the classification of amphiboles. *Can Mineral* 44:1-21
- Hawthorne FC, Ungaretti L, Oberti R, Cannillo E, Smelik EA (1994) The mechanism of ${}^{16}Li$ incorporation in amphibole. *Am Mineral* 79:443-451

- Hawthorne FC, Oberti R, Zanetti A, Czamanske GK (1998) The role of Ti in hydrogen-deficient amphiboles: sodic-calcic and sodic amphiboles from Coyote Peak, California. *Can Mineral* 36:1253-1265
- Iezzi G, Della Ventura G, Oberti R, Cámara F, Holtz F (2004) Synthesis and crystal-chemistry of $\text{Na}(\text{NaMg})\text{Mg}_5\text{Si}_8\text{O}_{22}(\text{OH})_2$, a $P2_1/m$ amphibole. *Am Mineral* 89:640-646
- Iezzi G, Gatta GD, Kockelmann W, Della Ventura G, Rinaldi R, Schäfer W, Piccinini M, Gaillard F (2005a) Low- T neutron powder-diffraction and synchrotron-radiation IR study of synthetic amphibole $\text{Na}(\text{NaMg})\text{Mg}_5\text{Si}_8\text{O}_{22}(\text{OH})_2$. *Am Mineral* 90:695-700
- Iezzi G, Tribaudino M, Della Ventura G, Nestola F, Bellatreccia F (2005b) High- T phase transition of synthetic $^{\text{A}}\text{Na}^{\text{B}}(\text{LiMg})^{\text{C}}\text{Mg}_5\text{Si}_8\text{O}_{22}(\text{OH})_2$ amphibole: an X-ray synchrotron powder diffraction and FTIR spectroscopic study. *Phys Chem Mineral* 32:515-523
- Leake BE (1968) A catalog of analyzed calciferous and sub-calciferous amphiboles together with their nomenclature and associated minerals. *Geol Soc Am Spec Paper* 98
- Leake BE (1978) Nomenclature of amphiboles. *Can Mineral* 16:501-520
- Leake BE, Woolley AR, Arps CES, Birch WD, Gilbert MC, Grice JD, Hawthorne FC, Kato A, Kisch HJ, Krivovichev VG, Linthout K, Laird J, Mandarino JA, Maresch WV, Nickel EH, Rock NMS, Schumacher JC, Smith DC, Stephenson NCN, Ungaretti L, Whittaker EJW, Guo Y (1997) Nomenclature of amphiboles: Report of the subcommittee on amphiboles of the International Mineralogical Association, Commission on New Minerals and Mineral Names. *Can Mineral* 35:219-246
- Leake BE, Woolley AR, Birch WD, Burke EAJ, Ferraris G, Grice JD, Hawthorne FC, Kisch HJ, Krivovichev VG, Schumacher JC, Stephenson NCN, Whittaker EJW (2003) Nomenclature of amphiboles: additions and revisions to the International Mineralogical Association's amphibole nomenclature. *Can Mineral* 41:1355-1370
- Oberti R, Ghose S (1993) Crystal-chemistry of a complex Mn-bearing alkali amphibole on the verge of exsolution. *Eur J Mineral* 5:1153-1160
- Oberti R, Hawthorne FC, Ungaretti L, Cannillo E (1995) ^{61}Al disorder in amphiboles from mantle peridotite. *Can Mineral* 33:867-878
- Oberti R, Caballero JM, Ottolini L, Lopez-Andres S, Herreros V (2000) Sodic-ferripedrizite, a new monoclinic amphibole bridging the magnesium-iron-manganese-lithium and the sodium-calcium group. *Am Mineral* 85:578-585
- Oberti R, Cámara F, Ottolini L, Caballero JM (2003) Lithium in amphiboles: detection, quantification, and incorporation mechanisms in the compositional space bridging sodic and $^{\text{B}}\text{Li}$ amphiboles. *Eur J Mineral* 15:309-319
- Oberti R, Cámara F, Caballero JM (2004) Ferri-ottoliniite and ferriwhittakerite, two new end-members of the new Group 5 for monoclinic amphiboles. *Am Mineral* 88:888-893
- Oberti R, Cámara F, Ottolini L (2005) Clinoholmquistite discredited: the new amphibole end-member fluorosodic-pedrizite. *Am Mineral* 90:732-736
- Oberti R, Della Ventura G, Cámara F (2007) New amphibole compositions: natural and synthetic. *Rev Mineral Geochem* 67:89-123

APPENDIX I: REJECTED, REDEFINED AND RENAMED END-MEMBERS*

End-member formula**	Leake et al. (1997, 2003)	SCHEME 1	SCHEME 2
NaMg ₂ Mg ₅ (Si ₇ Al)O ₂₂ (OH) ₂	Sodicanthophyllite	Rootname1	Rootname1
NaFe ²⁺ ₂ Fe ²⁺ ₅ (Si ₇ Al)O ₂₂ (OH) ₂	Sodic-ferro-anthophyllite	Ferro-rootname1	Ferro-rootname1
NaMg ₂ (Mg ₄ Al)(Si ₆ Al ₃)O ₂₂ (OH) ₂	Sodicgedrite	Rootname2	Rootname2
NaMg ₂ (Mg ₅ Al ₂)(Si ₅ Al ₃)O ₂₂ (OH) ₂	-----	Sodic-ferro-gedrite	Sodic-ferro-gedrite
NaFe ²⁺ ₂ (Fe ²⁺ ₃ Al ₂)(Si ₅ Al ₃)O ₂₂ (OH) ₂	Grunerite	Grunerite	Ferro-cummingtonite
□Fe ²⁺ ₂ Fe ²⁺ ₅ Si ₈ O ₂₂ (OH) ₂	Manganocummingtonite	Rootname3	Rootname3
□Mn ²⁺ ₂ Mg ₅ Si ₈ O ₂₂ (OH) ₂	Manganogrunerite	Ferro-rootname3	Ferro-rootname3
□Mn ²⁺ ₂ Fe ²⁺ ₅ Si ₈ O ₂₂ (OH) ₂	Permanganocummingtonite	-----	-----
□Mn ²⁺ ₂ (Mn ²⁺ ₂ Mg ₃ Si ₈ O ₂₂ (OH) ₂	Permanganogrunerite	-----	-----
□Mn ²⁺ ₂ (Mn ²⁺ ₂ Fe ²⁺ ₂)Si ₈ O ₂₂ (OH) ₂	-----	Manganogrunerite	Manganogrunerite
□Mn ²⁺ ₂ Mn ²⁺ ₅ Si ₈ O ₂₂ (OH) ₂	-----	-----	-----
□Ca ₂ Fe ²⁺ ₅ Si ₈ O ₂₂ (OH) ₂	Ferro-actinolite	Actinolite	Ferro-tremolite
□Ca ₂ [Mg ₄ (Al,Fe ³⁺)](Si ₇ Al)O ₂₂ (OH) ₂	Magnesiophorblende	-----	-----
□Ca ₂ (Mg ₄ Al)(Si ₇ Al)O ₂₂ (OH) ₂	-----	Magnesiophorblende	-----
□Ca ₂ [Fe ²⁺ ₄ (Al,Fe ³⁺)](Si ₇ Al)O ₂₂ (OH) ₂	Ferrohornblende	-----	-----
□Ca ₂ (Mg ₄ Fe ³⁺)(Si ₇ Al)O ₂₂ (OH) ₂	-----	Ferro-hornblende	-----
□Ca ₂ (Fe ²⁺ ,Al)(Si ₇ Al)O ₂₂ (OH) ₂	-----	Ferro-hornblende	-----
□Ca ₂ (Fe ²⁺ ₄ Fe ³⁺)(Si ₇ Al)O ₂₂ (OH) ₂	-----	Ferro-ferri-hornblende	-----
□Ca ₂ [Mg ₃ AlFe ³⁺](Si ₆ Al ₂)O ₂₂ (OH) ₂	Tschermakite	-----	-----
□Ca ₂ (Mg ₃ Al ₂)(Si ₆ Al ₂)O ₂₂ (OH) ₂	Aluminotschermakite	Tschermakite	Tschermakite
□Ca ₂ [Mg ₃ Fe ³⁺](Si ₆ Al ₂)O ₂₂ (OH) ₂	Ferrotschermakite	Ferri-tschermakite	Ferri-tschermakite
□Ca ₂ [Fe ²⁺ ,AlFe ³⁺](Si ₆ Al ₂)O ₂₂ (OH) ₂	Ferrotschermakite	-----	-----
□Ca ₂ (Fe ²⁺ ₃ Al ₂)(Si ₆ Al ₂)O ₂₂ (OH) ₂	Alumino-ferrotschermakite	Ferro-tschermakite	Ferro-tschermakite
□Ca ₂ (Fe ²⁺ ₃ Fe ³⁺)(Si ₆ Al ₂)O ₂₂ (OH) ₂	Ferri-ferrotschermakite	Ferro-ferri-tschermakite	Ferro-ferri-tschermakite
NaCa ₂ (Mg ₃ Al)(Si ₆ Al ₂)O ₂₂ (OH) ₂	Pargasite	Pargasite	-----
NaCa ₂ (Fe ²⁺ ,Al)(Si ₆ Al ₂)O ₂₂ (OH) ₂	Ferropargasite	Ferro-pargasite	-----
NaCa ₂ (Mg ₃ Fe ³⁺)(Si ₆ Al ₂)O ₂₂ (OH) ₂	Magnesiosthastingsite	Magnesiosthastingsite	-----
NaCa ₂ (Fe ²⁺ ₄ Fe ³⁺)(Si ₆ Al ₂)O ₂₂ (OH) ₂	Hastingsite	Hastingsite	-----

End-member formula**	Leake et al. (1997, 2003)	SCHEME 1	SCHEME 2
$\text{NaCa}_2[\text{Mg}_3(\text{Fe}^{2+}, \text{Al})_2](\text{Si}_5\text{Al}_3)\text{O}_{22}(\text{OH})_2$	Magnesiumsadanagaite	-----	-----
$\text{NaCa}_2[\text{Fe}^{2+}_3(\text{Fe}^{3+}, \text{Al})_2](\text{Si}_5\text{Al}_3)\text{O}_{22}(\text{OH})_2$	Ferrosadanagaite	-----	-----
$\text{NaCa}_2(\text{Mg}_3\text{Al}_2)(\text{Si}_5\text{Al}_3)\text{O}_{22}(\text{OH})_2$	-----	Magneso-alumino-sadanagaite	Sadanagaite
$\text{NaCa}_2(\text{Fe}^{2+}_2\text{Al})_2(\text{Si}_5\text{Al}_3)\text{O}_{22}(\text{OH})_2$	-----	Alumino-sadanagaite	Ferro-sadanagaite
$\text{NaCa}_2(\text{Mg}_3\text{Fe}^{2+}_2)(\text{Si}_5\text{Al}_3)\text{O}_{22}(\text{OH})_2$	-----	Magneso-sadanagaite	Ferro-sadanagaite
$\text{NaCa}_2(\text{Fe}^{2+}_3\text{Fe}^{3+}_2)(\text{Si}_5\text{Al}_3)\text{O}_{22}(\text{OH})_2$	-----	Sadanagaite	Ferro-ferri-sadanagaite
$\square \text{CaNa}[\text{Mg}_4(\text{Al}, \text{Fe}^{3+})\text{Si}_8\text{O}_{22}(\text{OH})_2]$	Winchite	-----	-----
$\square \text{CaNa}[\text{Fe}^{2+}_4(\text{Al}, \text{Fe}^{3+})\text{Si}_8\text{O}_{22}(\text{OH})_2]$	Ferrowinchite	-----	-----
$\square \text{CaNa}(\text{Mg}_4\text{Al})\text{Si}_8\text{O}_{22}(\text{OH})_2$	-----	Winchite	-----
$\square \text{CaNa}(\text{Mg}_4\text{Fe}^{3+})\text{Si}_8\text{O}_{22}(\text{OH})_2$	-----	Ferri-winchite	-----
$\square \text{CaNa}(\text{Fe}^{2+}_4\text{Al})\text{Si}_8\text{O}_{22}(\text{OH})_2$	-----	Ferro-winchite	-----
$\square \text{CaNa}(\text{Fe}^{2+}_4\text{Fe}^{3+})\text{Si}_8\text{O}_{22}(\text{OH})_2$	-----	Ferro-ferri-winchite	-----
$\square \text{CaNa}(\text{Mg}_5\text{AlFe}^{3+})(\text{Si}_7\text{Al})\text{O}_{22}(\text{OH})_2$	Barroisite	-----	-----
$\square \text{CaNa}(\text{Fe}^{2+}_3\text{AlFe}^{3+})(\text{Si}_7\text{Al})\text{O}_{22}(\text{OH})_2$	Ferrobarrisite	-----	-----
$\square \text{CaNa}(\text{Mg}_5\text{Al}_2)(\text{Si}_7\text{Al})\text{O}_{22}(\text{OH})_2$	Aluminobarrisite	Barroisite	-----
$\square \text{CaNa}(\text{Mg}_5\text{Fe}^{3+}_2)(\text{Si}_7\text{Al})\text{O}_{22}(\text{OH})_2$	Ferribarrisite	Ferri-barrisite	-----
$\square \text{CaNa}(\text{Fe}^{2+}_3\text{Al}_2)(\text{Si}_7\text{Al})\text{O}_{22}(\text{OH})_2$	Alumino-ferrobarrisite	Ferro-barrisite	-----
$\square \text{CaNa}(\text{Fe}^{2+}_3\text{Fe}^{3+}_2)(\text{Si}_7\text{Al})\text{O}_{22}(\text{OH})_2$	Ferri-ferrobarrisite	Ferro-ferri-barrisite	-----
$\text{NaCaNaMg}_5\text{Si}_8\text{O}_{22}(\text{OH})_2$	Richterite	Richterite	-----
$\square \text{CaNaFe}^{2+}_5\text{Si}_8\text{O}_{22}(\text{OH})_2$	Ferri-richterite	Ferro-richterite	-----
$\text{NaCaNa}[\text{Mg}_4(\text{Al}, \text{Fe}^{3+})\text{Si}_7\text{Al}]\text{O}_{22}(\text{OH})_2$	Magnesiokatophorite	-----	-----
$\text{NaCaNa}[\text{Fe}^{2+}_4(\text{Al}, \text{Fe}^{3+})\text{Si}_7\text{Al}]\text{O}_{22}(\text{OH})_2$	Katophorite	-----	-----
$\text{NaCaNa}(\text{Mg}_4\text{Al})(\text{Si}_7\text{Al})\text{O}_{22}(\text{OH})_2$	-----	Magneso-katophorite	-----
$\text{NaCaNa}(\text{Mg}_4\text{Fe}^{3+})(\text{Si}_7\text{Al})\text{O}_{22}(\text{OH})_2$	-----	Magneso-ferri-katophorite	-----
$\text{NaCaNa}(\text{Fe}^{2+}_4\text{Al})(\text{Si}_7\text{Al})\text{O}_{22}(\text{OH})_2$	-----	Katophorite	-----
$\text{NaCaNa}(\text{Fe}^{2+}_4\text{Fe}^{3+})(\text{Si}_7\text{Al})\text{O}_{22}(\text{OH})_2$	-----	Ferri-katophorite	-----

End-member formula**	Leake et al. (1997, 2003)	SCHEME 1	SCHEME 2
NaCaNa(Mg ₃ AlFe ³⁺)(Si ₆ Al ₂)O ₂₂ (OH) ₂	Magnesiotaramite	-----	-----
NaCaNa(Fe ²⁺ ₃ AlFe ³⁺)(Si ₆ Al ₂)O ₂₂ (OH) ₂	Taramite	-----	-----
NaCaNa(Mg ₃ Al ₂)(Si ₆ Al ₂)O ₂₂ (OH) ₂	Alumino-magnesiotaramite	Magneso-taramite	-----
NaCaNa(Mg ₃ Fe ³⁺ ₂)(Si ₆ Al ₂)O ₂₂ (OH) ₂	Ferri-magnesiotaramite	Magneso-ferri-taramite	-----
NaCaNa(Fe ²⁺ ₃ Al ₂)(Si ₆ Al ₂)O ₂₂ (OH) ₂	Aluminotaramite	Alumino-taramite	-----
NaCaNa(Fe ²⁺ ₃ Fe ³⁺ ₂)(Si ₆ Al ₂)O ₂₂ (OH) ₂	Ferritaramite	Ferri-taramite	-----
All other sodium-calcium amphiboles are the same as in Leake et al. (1997) and SCHEME 1.			
NaNa ₂ (Mg ₂ Al ₂ Li)Si ₈ O ₂₂ (OH) ₂	-----	Alumino-leakeite	Leakeite
NaNa ₂ (Fe ²⁺ ₂ Al ₂ Li)Si ₈ O ₂₂ (OH) ₂	-----	Ferro-alumino-leakeite	Ferro-leakeite
NaNa ₂ (Mg ₂ Fe ³⁺ ₂ Li)Si ₈ O ₂₂ (OH) ₂	Leakeite	Leakeite	Ferri-leakeite
NaNa ₂ (Fe ²⁺ ₂ Fe ³⁺ ₂ Li)Si ₈ O ₂₂ (OH) ₂	Ferroleakeite	Ferro-leakeite	Ferro-ferri-leakeite
NaNa ₂ (Mg ₂ Mn ³⁺ ₂ Li)Si ₈ O ₂₂ (OH) ₂	Sodic-kornite	Kornite	Mangani-leakeite
KNa ₂ (Mg ₂ Mn ³⁺ ₂ Li)Si ₈ O ₂₂ (OH) ₂	Kornite	Potassic-kornite	Potassic-kornite
NaNa ₂ (Mg ₃ Fe ³⁺ ₂)Si ₇ AlO ₂₂ (OH) ₂	Ferric-nyböite	Ferri-nyböite	Ferri-nyböite
NaNa ₂ (Fe ²⁺ ₃ Fe ³⁺ ₂)Si ₇ AlO ₂₂ (OH) ₂	Ferri-ferronyböite	Ferro-ferri-nyböite	Ferro-ferri-nyböite
□Na ₂ (Mg ₃ Fe ³⁺ ₂)Si ₈ O ₂₂ (OH) ₂	Magnesianiebeckite	Magneso-niebeckite	Ferri-glaucophane
NaNa ₂ (Mg ₄ Fe ³⁺)Si ₈ O ₂₂ (OH) ₂	Magneso-arfvedsonite	Magneso-arfvedsonite	Ferri-eckermannite
□Na ₂ (Fe ²⁺ ₃ Fe ³⁺ ₂)Si ₈ O ₂₂ (OH) ₂	Riebeckite	Riebeckite	Ferro-ferri-glaucophane
NaNa ₂ (Fe ²⁺ ₄ Fe ³⁺ ₂)Si ₈ O ₂₂ (OH) ₂	Arfvedsonite	Arfvedsonite	Ferro-ferri-eckermannite
NaNa ₂ Mn ²⁺ ₄ (Al,Fe ³⁺)Si ₈ O ₂₂ (OH) ₂	Kozulite	-----	-----
NaNa ₂ (Mn ²⁺ ₄ Fe ³⁺)Si ₈ O ₂₂ (OH) ₂	-----	Kozulite	Mangano-ferri-eckermannite
□Li ₂ (Fe ²⁺ ₃ Al ₂)Si ₈ O ₂₂ (OH) ₂	Ferroholmquistite	Ferro-holmquistite	Ferro-holmquistite
□Li ₂ (Mg ₃ Fe ³⁺ ₂)Si ₈ O ₂₂ (OH) ₂	Ferriholmquistite	Ferri-holmquistite	Ferri-holmquistite
□Li ₂ (Fe ²⁺ ₃ Fe ³⁺ ₂)Si ₈ O ₂₂ (OH) ₂	Ferri-ferroholmquistite	Ferro-ferri-holmquistite	Ferro-ferri-holmquistite
□Li ₂ (Mg ₃ Al ₂)Si ₈ O ₂₂ (OH) ₂	Clinoholmquistite	Clino-holmquistite	Clino-holmquistite
□Li ₂ (Fe ²⁺ ₃ Al ₂)Si ₈ O ₂₂ (OH) ₂	Clino-ferroholmquistite	Clino-ferro-holmquistite	Clino-ferro-holmquistite
□Li ₂ (Mg ₃ Fe ³⁺ ₂)Si ₈ O ₂₂ (OH) ₂	Clino-ferriholmquistite	Clino-ferri-holmquistite	Clino-ferri-holmquistite
□Li ₂ (Fe ²⁺ ₃ Fe ³⁺ ₂)Si ₈ O ₂₂ (OH) ₂	Clino-ferri-ferroholmquistite	Clino-ferri-ferri-holmquistite	Clino-ferri-ferri-holmquistite
NaLi ₂ (Mg ₂ Al ₂ Li)Si ₈ O ₂₂ (OH) ₂	Sodicpedrizite	Pedrizite	Pedrizite

End-member formula**	Leake et al. (1997, 2003)	SCHEME 1	SCHEME 2
$\text{NaLi}_2(\text{Fe}^{2+}_2\text{Al}_2\text{Li})\text{Si}_8\text{O}_{22}(\text{OH})_2$	Sodic-ferropedrizite	Ferro-pedrizite	Ferro-pedrizite
$\text{NaLi}_2(\text{Mg}_2\text{Fe}^{3+}_2\text{Li})\text{Si}_8\text{O}_{22}(\text{OH})_2$	Sodic-ferripedrizite	Ferri-pedrizite	Ferri-pedrizite
$\text{NaLi}_2(\text{Fe}^{2+}_2\text{Fe}^{3+}_2\text{Li})\text{Si}_8\text{O}_{22}(\text{OH})_2$	Sodic-ferri-ferropedrizite	Ferro-ferri-pedrizite	Ferro-ferri-pedrizite
$\square(\text{NaLi})(\text{Mg}_3\text{Al}_2)\text{Si}_8\text{O}_{22}(\text{OH})_2$	Otolimite	-----	-----
$\text{Na}(\text{NaLi})(\text{Mg}_2\text{Al}_2\text{Li})\text{Si}_8\text{O}_{22}(\text{OH})_2$	Whittakerite	-----	-----
$\square(\text{NaLi})(\text{Mg}_3\text{Fe}^{3+}_2)\text{Si}_8\text{O}_{22}(\text{OH})_2$	Ferri-otolimite	-----	-----
$\text{Na}(\text{NaLi})(\text{Mg}_2\text{Fe}^{3+}_2\text{Li})\text{Si}_8\text{O}_{22}(\text{OH})_2$	Ferri-whittakerite	-----	-----
$\text{Na}(\text{NaMg})\text{Mg}_5\text{Si}_8\text{O}_{22}(\text{OH})_2$	-----	Rootname 4	-----
$\text{Na}(\text{NaMn}^{2+})\text{Mg}_5\text{Si}_8\text{O}_{22}(\text{OH})_2$	-----	Rootname 5	-----
$\text{Na}(\text{NaMg})(\text{Mg}_4\text{Al})(\text{Si}_7\text{Al})\text{O}_{22}(\text{OH})$	-----	Rootname 6	-----
$\text{Na}(\text{NaMg})(\text{Mg}_3\text{Al}_2)(\text{Si}_6\text{Al}_2)\text{O}_{22}(\text{OH})$	-----	Rootname 7	-----
$\square(\text{NaMg})(\text{Mg}_4\text{Al})\text{Si}_8\text{O}_{22}(\text{OH})$	-----	Rootname 8	-----
$\square(\text{NaMg})(\text{Mg}_3\text{Al}_2)(\text{Si}_7\text{Al})\text{O}_{22}(\text{OH})$	-----	Rootname 9	-----
$\square(\text{NaMn}^{2+})(\text{Mg}_4\text{Al})\text{Si}_8\text{O}_{22}(\text{OH})$	-----	Rootname 10	-----
$\square(\text{NaMn}^{2+})(\text{Mg}_4\text{Fe}^{3+})\text{Si}_8\text{O}_{22}(\text{OH})$	Parvowinchite	Ferri-rootname 10	-----
$\text{NaCa}_2(\text{Mg},\text{Ti}^{4+})(\text{Si}_6\text{Al}_2)\text{O}_{22}(\text{OH})\text{O}$	Kaersutite	-----	-----
$\text{NaCa}_2(\text{Mg},\text{Ti}^{4+}\text{Al})(\text{Si}_6\text{Al}_2)\text{O}_{22}\text{O}_2$	-----	Kaersutite	Kaersutite
$\text{NaNa}_2(\text{Mg}_3\text{Fe}^{3+}\text{Ti}^{4+})\text{Si}_8\text{O}_{22}\text{O}_2$	Obertiite	Obertiite	Ferri-obertiite
$\text{NaNa}_2(\text{Mg},\text{Mn}^{3+}\text{Ti}^{4+}\text{Li})\text{Si}_8\text{O}_{22}\text{O}_2$	Dellaventurite	Dellaventurite	Mangano-dellaventurite
$\text{NaNa}_2(\text{Mn}^{2+}\text{Mn}^{3+}\text{Li})\text{Si}_8\text{O}_{22}\text{O}_2$	Ungarettiite	Ungarettiite	Mangano-mangani-ungarettiite

* This list specifically addresses end-member compositions; the ranges of composition of each species often differs from one scheme to another.

** All compositions listed below have names; however, these are not given unless the composition is defined as an end member in that particular nomenclature scheme.

New Amphibole Compositions: Natural and Synthetic

Roberta Oberti¹, Giancarlo Della Ventura^{2,1} and Fernando Cámara¹

¹*Istituto di Geoscienze e Georisorse, Consiglio Nazionale delle Ricerche
I-27100 Pavia, Italy*

oberti@crystal.unipv.it, camara@crystal.unipv.it

²*Dipartimento di Scienze Geologiche
Università di Roma Tre, I-00146 Roma, Italy*

dellaven@uniroma3.it

INTRODUCTION

The crystal-chemical formula and the major-element composition of amphiboles have been discussed in Hawthorne and Oberti (2007a), and the amphibole compositional space has been defined in terms of root-names and allowed charge arrangements in Hawthorne and Oberti (2007b). Although the number of possible homovalent substitutions occurring at the various structural sites is very high, geochemically exotic cations generally do not reach the limits required to assign a distinct prefix to the root-name. Thus prefixes are so far confined to the presence of Na, K, Mg, Al, Ti, Mn, Fe, F and Cl.

In this chapter, we examine the new amphibole compositions which have been found and characterized since 1981, i.e. since the publication of volume 9A of the MSA Reviews in Mineralogy. We divide the chapter in two sections. The first section describes new charge arrangements found in Nature, and the second section describes the extensive studies of synthetic amphiboles of novel composition done to clarify the crystal chemistry of exotic cations which are normally found as minor components. This chapter deals exclusively with monoclinic amphiboles, as the compositional space of orthorhombic amphiboles has not expanded since the former review. Although natural occurrences of protoamphibole (with space group *Pnmm*) have been described only in the last twenty years (Sueno et al. 1998; Konishi et al. 2003), their composition is within the compositional range previously defined for *Pnma* amphiboles.

NEW NATURAL-AMPHIBOLES COMPOSITIONS

The main extensions of the traditional amphibole compositional space recognized in between the 1978 and the 1997 classification schemes (Leake 1978; Leake et al. 1997) are due to the discovery of: (1) sadanagaite, calcic amphiboles of ideal compositions ${}^A\text{R}^+ {}^B\text{Ca}_2 {}^C(\text{R}^{2+}_3\text{R}^{3+}_2) {}^T(\text{Si}_5\text{Al}_3)\text{O}_{22} {}^W(\text{OH})_2$ (Shimazaki et al. 1984; Sokolova et al. 2000; Banno et al. 2004; Nishio-Hamane et al. in prep.); (2) fluorocannilloite, a calcic amphibole of ideal composition ${}^A\text{Ca} {}^B\text{Ca}_2 {}^C(\text{Mg}_4\text{Al}) {}^T(\text{Si}_5\text{Al}_3)\text{O}_{22} {}^W\text{F}_2$ (Hawthorne et al. 1996a); (3) leakeite and kornite, sodic amphiboles of ideal composition ${}^A\text{R}^+ {}^B\text{Na}_2 {}^C(\text{R}^{2+}_2\text{R}^{3+}_2\text{Li}) {}^T\text{Si}_8 \text{O}_{22} {}^W(\text{OH})_2$ (Hawthorne et al. 1992, 1996b; Armbruster et al. 1993; Matsubara et al. 2002); (4) ungarrettiite, the first anhydrous sodic amphibole, of ideal composition ${}^A\text{Na} {}^B\text{Na}_2 {}^C(\text{Mn}^{2+}_2\text{Mn}^{3+}_3) {}^T\text{Si}_8 \text{O}_{22} {}^W\text{O}_2$ (Hawthorne et al. 1995; Kawachi et al. 2002).

In the last ten years, the availability of *in situ* ion-microprobe analysis of Li has allowed complete characterization of the crystal-chemistry of Li in amphiboles, resulting in the discovery of sodic-pedrizites, ${}^B(\text{Mg,Fe,Mn,Li})$ amphiboles of ideal composition ${}^A\text{Na} {}^B\text{Li}_2 {}^C(\text{R}^{2+}_2\text{R}^{3+}_2\text{Li})$

${}^T\text{Si}_8 \text{O}_{22} {}^W(\text{OH})_2$, which are the ${}^B\text{Li}$ counterparts of leakeites, but also the only ${}^B(\text{Mg,Fe,Mn,Li})$ monoclinic amphiboles with a full A site (Caballero et al. 2002; Oberti et al. 2003a,b).

Even more important, a series of Li-bearing amphiboles was found which destroyed the previous assumption of substantial immiscibility between amphiboles with small (Li,Mg,Fe) and large (Na,Ca) cations at the $M(4)$ site, an assumption which was the basis for the recognition of four main amphibole groups. In particular, complete solid-solution was observed between the root compositions magnesio-riebeckite and clinoferrholmquistite, as well as between leakeite and sodic-ferripedrizite (according to the substitution ${}^B\text{Na}_{-1}{}^B\text{Li}_1$; Oberti et al. 2003a; 2004). Sporadic samples fall between the root-compositions tremolite and manganocummingtonite, and between edenite and its hypothetical counterpart in the ${}^B(\text{Mg,Fe,Mn,Li})$ group (Oberti et al. 2006). These findings forced the introduction of a fifth amphibole group, with B-site compositions intermediate between ${}^B(\text{Na, Ca})$ and ${}^B(\text{Mg,Fe,Mn,Li})$ amphiboles (see Leake et al. 2003 and Hawthorne and Oberti 2007b for more detail on the classification procedure to be used for these compositions).

Other significant findings in the latest few years are the recognition of other anhydrous sodic amphiboles, such as obertiite (Hawthorne et al. 2000) and dellaventuraite (Tait et al. 2005), with ideal compositions ${}^A\text{Na} {}^B\text{Na}_2 {}^C(\text{Mg}_3\text{Fe}^{3+}\text{Ti}^{4+}) {}^T\text{Si}_8 \text{O}_{22} {}^W\text{O}_2$ and ${}^A\text{Na} {}^B\text{Na}_2 {}^C(\text{MgMn}^{3+}_2\text{Ti}^{4+}\text{Li}) {}^T\text{Si}_8 \text{O}_{22} {}^W\text{O}_2$, respectively.

The following sections will provide comments on the crystal-chemical peculiarities of the above mentioned amphibole compositions which enlarge the number of compositional species, and Table 1 lists the empirical formulae of their holotypes. Ideal formulae of all the new amphibole species recognized after 1981, including those based solely on homovalent substitutions, are listed in Table 2.

Sadanagaites: how much ${}^T\text{Al}$ can occur in the amphibole structure?

Modern analysis of amphiboles with ${}^T\text{Al}$ contents higher than 2.5 atoms per formula unit (apfu) were first reported by Appleyard (1975) from alkaline rocks at Wolfe, Ontario, Canada, and a structure refinement of a sample with ${}^T\text{Al} = 2.73$ was provided by Hawthorne and Grundy (1977). At that time, these amphiboles were classified as subsilicic hastingsites; at present, they should be named *sadanagaites*.

Shimazaki et al. (1984) characterized a series of low-Si amphiboles from Al-, Ti- and Fe-rich skarns in marbles in the Yuge and Myojin islands, Seto Inland Sea, Southwestern Japan. The authors noted that ${}^A\text{K}$ was predominant over ${}^A\text{Na}$, but considered that this feature and the significant Fe^{3+} content are essential to allow incorporation of large amounts of a large T cation such as Al^{3+} . They proposed the name *sadanagaite* for the composition 1 in Table 1, ideally ${}^A\text{K} {}^B\text{Ca}_2 {}^C(\text{Fe}^{2+}_3\text{Al}_2) {}^T(\text{Si}_5\text{Al}_3) \text{O}_{22} {}^W(\text{OH})_2$, and *magnesiosadanagaite* for composition 2, ideally ${}^A\text{K} {}^B\text{Ca}_2 {}^C(\text{Mg}^{2+}_3\text{Al}_2) {}^T(\text{Si}_5\text{Al}_3) \text{O}_{22} {}^W(\text{OH})_2$. Sadanagaites were later found in skarns in Cornwall, England (van Marcke de Lumen and Verkaeren 1985), in thermally metamorphosed rocks in the Nogo-Hakusan area, Japan (Sawaki 1989) and in Caledonian metamorphic rocks in the Western Baikal region, Russia (Savel'eva and Korikovskii 1998). Magnesiosadanagaite was also reported in metabasites and metacarbonates in the Eastern Alps (Mogessie et al. 1986) and in a ruby deposit in China (Wang et al. 1997). These latter samples have low K content. Reconsideration of amphibole nomenclature (Leake et al. 1997) therefore used the prefix *potassic* for the two holotypes described by Shimazaki et al. (1984) and restricted the root-name *sadanagaite* to the sodic varieties.

Potassic-ferrisadanagaite was described by Bazhenov et al. (1999) from an alkaline complex in the Ilmen Mountains, Russia. The structure refinement was reported by Sokolova et al. (2000), who also found the presence of the oxo component $[\text{O}^{(3)}\text{O}^{2-} = 0.38 \text{ apfu}]$, which is balanced by 0.19 Ti pfu ordered at the $M(1)$ site. The empirical formula is given in Table 1 under the code 3.

Table 1. Empirical formulae of the new species which extension of amphibole compositional space.

1. potassic-sadanagaite	$A(N_{40,29}K_{0,71})$	$B(C_{32,01})$	$C(Mg_{1,50}Mn_{0,02}Fe^{2+}_{1,55}Al_{1,07}Fe^{3+}_{0,40}Ti_{0,46})$	$T(Si_{4,61}Al_{1,39})$	$W(OH)_{2,00}$
2. potassic-magnestiosadanagaite	$A(N_{40,22}K_{0,75})$	$B(C_{32,07})$	$C(Mg_{1,84}Mn_{0,01}Fe^{2+}_{1,37}Al_{0,94}Fe^{3+}_{0,39}Ti_{0,38})$	$T(Si_{4,95}Al_{1,05})$	$W(OH)_{2,00}$
3. potassic-ferri-sadanagaite	$A(N_{40,32}K_{0,66})$	$B(C_{31,73}Mn_{0,04}Na_{0,23})$	$C(Mg_{0,55}Mn_{0,25}Fe^{2+}_{2,16}Al_{0,78}Fe^{3+}_{1,11}Ti_{0,19})$	$T(Si_{3,33}Al_{2,67})$	$W(OH)_{1,21}F_{0,41}O_{3,38}$
4. magnestiosadanagaite	$A(N_{40,91}K_{0,09})$	$B(C_{31,95}Mn_{0,02}Na_{0,03})$	$C(Mg_{2,91}Fe^{2+}_{0,76}Al_{0,97}Fe^{3+}_{0,07}Ti_{0,29})$	$T(Si_{3,39}Al_{2,61})$	$W(OH)_{1,86}F_{0,13}Cl_{0,01}$
5. fluorocannilloite	$A(N_{40,35}K_{0,12}Ca_{0,52})$	$B(C_{31,92}Mn^{2+}_{0,05}Fe^{2+}_{0,03})$	$C(Mg_{5,73}Fe^{2+}_{0,45}Al_{0,92}Ti_{0,02})$	$T(Si_{5,65}Al_{2,37})$	$W(OH)_{0,46}F_{1,54}$
6. joesmithite	$A(Pb_{0,98}Ba_{0,02}K_{0,01})$	$B(C_{31,36}Na_{0,16})$	$C(Mg_{2,52}Fe^{2+}_{0,38}Mn^{2+}_{0,34}Al_{0,10}Fe^{3+}_{1,65})$	$T(Si_{6,22}Be_{1,78})$	$W(OH)_{1,81}F_{0,19}$
7. leakeite	$A(N_{40,75}K_{0,20})$	$B(Na_{1,92}Ca_{0,08})$	$C(Mg_{2,32}Mn^{2+}_{0,42}Al_{1,14}Fe^{3+}_{1,31}Li_{0,81})$	$T(Si_{7,93}Al_{0,07})$	$W(OH)_{1,49}F_{0,51}$
8. fluoro-ferroleakeite	$A(N_{40,76}K_{0,23})$	$B(Na_{1,97}Ca_{0,03})$	$C(Mg_{0,46}Mn^{2+}_{0,59}Fe^{2+}_{1,14}Zn_{0,02}Al_{0,02}Fe^{3+}_{1,93}Ti_{0,08}Li_{0,66})_{\Sigma=4,90}$	$T(Si_{7,81}Al_{0,19})$	$W(OH)_{0,61}F_{1,39}$
9. kornite	$A(N_{40,31}K_{0,65})$	$B(Na_{1,79}Li_{0,21})$	$C(Mg_{2,12}Mn^{2+}_{1,43}Fe^{2+}_{0,52}Li_{0,91})$	$T(Si_{8,00})$	$W(OH)_{2,00}$
10. potassic-leakeite	$A(N_{40,46}K_{0,57})$	$B(Na_{1,98}Ca_{0,02})$	$C(Mg_{1,35}Mn^{2+}_{0,95}Al_{0,05}Fe^{2+}_{1,02}V_{0,64}Ti_{0,03}Li_{0,70})$	$T(Si_{7,98}Al_{0,02})$	$W(OH)_{2,00}$
11. clinio-sodic-ferri-ferroholmquistite	$A(N_{40,43}K_{0,05})$	$B(Li_{1,66}Na_{0,30}Ca_{0,04})$	$C(Mg_{1,21}Mn^{2+}_{0,07}Fe^{2+}_{1,35}Zn_{0,02}Al_{0,20}Fe^{3+}_{1,54}Ti^{4+}_{0,12}Li_{0,49})$	$T(Si_{8,00})$	$W(OH)_{1,58}F_{0,42}$
12. clinio-ferri-ferroholmquistite	$A(N_{40,22}K_{0,00})$	$B(Li_{1,90}Na_{0,08}Ca_{0,02})$	$C(Mg_{1,06}Mn_{0,14}Fe^{2+}_{1,55}Zn_{0,02}Al_{0,26}Fe^{3+}_{1,68}Ti_{0,11}Li_{0,28})$	$T(Si_{8,00})$	$W(OH)_{1,76}F_{0,24}$
13. sodic-ferripedrizite	$A(N_{40,95}K_{0,05})$	$B(Li_{1,60}Na_{0,35}Ca_{0,05})$	$C(Mg_{1,77}Mn_{0,07}Fe^{2+}_{0,61}Zn_{0,01}Al_{0,21}Fe^{3+}_{1,38}Ti_{0,11}Li_{0,84})$	$T(Si_{8,00})$	$W(OH)_{1,07}F_{0,93}$
14. sodic-ferri-ferropedrizite	$A(N_{40,53}K_{0,05})$	$B(Li_{1,82}Na_{0,15}Ca_{0,03})$	$C(Mg_{0,95}Mn^{2+}_{0,07}Fe^{2+}_{1,49}Zn_{0,01}Al_{0,21}Fe^{3+}_{1,55}Ti_{0,13}Li_{0,58})$	$T(Si_{8,00})$	$W(OH)_{1,48}F_{0,52}$
15. ferriwhitakerite	$A(N_{40,64}K_{0,13})$	$B(Li_{0,62}Na_{1,27}Ca_{0,11})$	$C(Mg_{1,47}Fe^{2+}_{0,58}Mn^{2+}_{0,12}Zn_{0,40}Al_{0,10}Fe^{3+}_{1,48}Ti_{0,12}Li_{0,73})$	$T(Si_{8,00})$	$W(OH)_{1,28}F_{0,72}$
16. ferri-otolimitite	$A(N_{40,38}K_{0,07})$	$B(Li_{1,24}Na_{0,70}Ca_{0,06})$	$C(Mg_{1,35}Mn^{2+}_{0,13}Fe^{2+}_{0,92}Zn_{0,31}Al_{0,10}Fe^{3+}_{1,71}Ti_{0,06}Li_{0,42})$	$T(Si_{8,00})$	$W(OH)_{1,53}F_{0,47}$
17. fluoro-sodic-pedrizite	$A(N_{40,64}K_{0,01})$	$B(Li_{1,93}Na_{0,05}Ca_{0,04})$	$C(Mg_{1,82}Mn_{0,02}Fe^{2+}_{0,52}Zn_{0,01}Al_{1,98}Cr_{0,01}Li_{0,64})$	$T(Si_{7,96}Al_{0,04})$	$W(OH)_{0,99}F_{1,10}$
18. parvowinchite	$A(N_{40,30}K_{0,05})$	$B(Na_{0,97}Ca_{0,39}Mg_{0,17}Mn_{0,57})$	$C(Mg_{5,84}Mn_{0,38}Fe^{2+}_{0,72}Li_{0,06})$	$T(Si_{7,88}Al_{0,12})$	$W(OH)_{1,69}F_{0,40}$
19. parvo-mangano-edenite	$A(N_{40,74}K_{0,02})$	$B(Ca_{1,27}Mn_{0,73})$	$C(Mg_{4,51}Mn^{2+}_{0,28}Fe^{2+}_{0,05}Al_{0,12}Fe^{3+}_{0,03}Ti_{0,01})$	$T(Si_{7,07}Al_{0,93})$	$W(OH)_{2,00}$
20. parvo-mangano-tremolite	$A(N_{40,44}K_{0,01})$	$B(Na_{0,04}Ca_{1,13}Mn_{0,83})$	$C(Mg_{4,69}Mn^{2+}_{0,21}Fe^{2+}_{0,03}Al_{0,06}Fe^{3+}_{0,01})$	$T(Si_{7,52}Al_{0,48})$	$W(OH)_{2,00}$
21. ungariteite	$A(N_{40,82}K_{0,19})$	$B(Na_{1,97}Ca_{0,03})$	$C(Mg_{0,34}Mn^{2+}_{1,66}Mn^{3+}_{2,96}Fe^{2+}_{0,06}Zn_{0,01})$	$T(Si_{7,99}Al_{0,01})$	$W_{2,00}$
22. oberiteite	$A(N_{40,84}K_{0,18})$	$B(Na_{1,36}Ca_{0,08}Fe^{2+}_{0,06})$	$C(Mg_{5,09}Fe^{2+}_{0,41}Zn_{0,01}Al_{0,03}Mn^{3+}_{0,37}Fe^{3+}_{0,29}Ti^{4+}_{0,86}Li_{0,03})$	$T(Si_{8,00})$	$W(OH)_{0,20}F_{0,26}O_{1,54}$
23. ferro-oberiteite	$A(N_{40,72}K_{0,29})$	$B(Na_{1,30}Ca_{0,15})$	$C(Mg_{1,30}Mn^{2+}_{0,02}Fe^{2+}_{2,35}Al_{0,01}Fe^{3+}_{0,52}Ti^{4+}_{0,75}Li_{1,10})$	$T(Si_{7,99}Al_{0,01})$	$W(OH)_{0,59}F_{0,25}O_{1,16}$
24. dellaventranteite	$A(N_{40,61}K_{0,40})$	$B(Na_{1,71}Ca_{0,29})$	$C(Mg_{1,81}Ni_{0,02}Zn_{0,01}Al_{0,10}Mn^{3+}_{0,85}Fe^{3+}_{0,71}Ti^{4+}_{0,60}Li_{0,90})$	$T(Si_{7,96}Al_{0,04})$	$W(OH)_{0,80}O_{1,20}$

1, 2; Shimazaki et al. (1984); 3; Bazhenov et al. (1999); 4; Banno et al. (2004); 5; Hawthorne et al. (1996a); 6; Moore (1969), revised by Moore et al. (1992); 7; Hawthorne et al. (1992); 8; Hawthorne et al. (1993, 1996b); 9; Armbruster et al. (1993); 10; Matsubara et al. (2002); 11; Caballero et al. (1998); 12; Oberti et al. (2003a,b); 13; Oberti et al. (2000a); 14; Oberti et al. (2003a,b); 15, 16; Oberti et al. (2004); 17; Oberti et al. (2005); 18; Oberti and Ghose (1993); 19, 20; Oberti et al. (2006); 21; Hawthorne et al. (1995); 22; Hawthorne et al. (2000); 23; Hawthorne et al. (1998); 24; Tait et al. (2005).

Table 2. New amphibole species recognized by IMA-CNMMN since 1981; names have been re-arranged according to the rules given by Burke and Leake (2004).

	Ideal Formula	Space Group	IMA refs.	Ref.
Group 1				
proto-ferro-anthophyllite	$A^{\square} B^{\square} (Fe^{2+})_2 C (Fe^{2+})_5 T Si_8 O_{22}^w (OH)_2$	<i>Pmmn</i>	1986-006	1,2*
proto-mangano-ferro-anthophyllite	$A^{\square} B^{\square} (Mn^{2+})_2 C (Fe^{2+})_5 T Si_8 O_{22}^w (OH)_2$	<i>Pmmn</i>	1986-007	1,2*
clino-sodic-ferri-ferroholmquistite	$A^{\square} B^{\square} Li_2 C (Fe^{2+}_3 Fe^{3+}_2) T Si_8 O_{22}^w (OH)_2$	<i>C2/m</i>	1995-045b	3
sodic-ferripedrizite	$ANa^B Li_2 C (Mg_2 Fe^{3+}_2 Li) T Si_8 O_{22}^w (OH)_2$	<i>C2/m</i>	1998-061	4
proto-anthophyllite	$A^{\square} B^{\square} (Mg)_2 C (Mg)_5 T Si_8 O_{22}^w (OH)_2$	<i>Pmmn</i>	2001-065	5
clino-ferri-ferroholmquistite	$A^{\square} B^{\square} Li_2 C (Fe^{2+}_3 Fe^{3+}_2) T Si_8 O_{22}^w (OH)_2$	<i>C2/m</i>	2001-066	6
sodic-ferri-ferropedrizite	$ANa^B Li_2 C (Fe^{2+}_2 Fe^{3+}_2 Li) T Si_8 O_{22}^w (OH)_2$	<i>C2/m</i>	2001-068	6
fluoro-sodicpedrizite	$ANa^B Li_2 C (Mg_2 Al_2 Li) T Si_8 O_{22}^w F_2$	<i>C2/m</i>	2004-002	7
ferroholmquistite	$A^{\square} B^{\square} Li_2 C (Fe^{2+}_3 Al_2) T Si_8 O_{22}^w (OH)_2$	<i>Pmma</i>	2004-030	8
Group 2				
potassicsadanagaite	$A^{\square} K^B Ca_2 C (Fe^{2+}_3 Al_2) T (Si_5 Al_3) O_{22}^w (OH)_2$	<i>C2/m</i>	1980-027	9
potassic-magnesiumsadanagaite	$A^{\square} K^B Ca_2 C (Mg_3 Al_2) T (Si_5 Al_3) O_{22}^w (OH)_2$	<i>C2/m</i>	1982-102	9
fluoro-cannilloite	$A^{\square} Ca^B Ca_2 C (Mg_4 Al) T (Si_5 Al_3) O_{22}^w F_2$	<i>C2/m</i>	1993-033	10
potassicpargasite	$A^{\square} K^B Ca_2 C (Mg_4 Al) T (Si_6 Al_2) O_{22}^w (OH)_2$	<i>C2/m</i>	1994-046	11
potassic-ferrisadanagaite	$A^{\square} K^B Ca_2 C (Fe^{2+}_3 Fe^{3+}_2) (Si_5 Al_3) O_{22}^w (OH)_2$	<i>C2/m</i>	1997-035	12,13*
fluoro-edenite	$ANa^B Ca_2 C Mg_5 T (Si_7 Al) O_{22}^w F_2$	<i>C2/m</i>	2000-049	14
chloro-potassicpargasite	$A^{\square} K^B Ca_2 C (Mg_4 Al) T (Si_6 Al_2) O_{22}^w Cl_2$	<i>C2/m</i>	2001-036	15
magnesiumsadanagaite	$ANa^B Ca_2 C (Mg_3 Al_2) T (Si_5 Al_3) O_{22}^w (OH)_2$	<i>C2/m</i>	2002-051	16
fluoropargasite	$ANa^B Ca_2 C (Mg_4 Al) T (Si_6 Al_2) O_{22}^w F_2$	<i>C2/m</i>	2003-050	17
potassic-magnesiumsthasingsite	$A^{\square} K^B Ca_2 C (Mg_4 Fe^{3+}) T (Si_6 Al_2) O_{22}^w (OH)_2$	<i>C2/m</i>	2004-027b	18
fluoro-magnesiumsthasingsite	$ANa^B Ca_2 C (Mg_4 Fe^{3+}) T (Si_6 Al_2) O_{22}^w F_2$	<i>C2/m</i>	2005-002	19
fluoro-potassiumsthasingsite	$A^{\square} K^B Ca_2 C (Fe^{2+}_4 Fe^{3+}) T (Si_6 Al_2) O_{22}^w F_2$	<i>C2/m</i>	2005-006	20
chloro-potassiumsthasingsite	$A^{\square} K^B Ca_2 C (Fe^{2+}_4 Fe^{3+}) T (Si_6 Al_2) O_{22}^w Cl_2$	<i>C2/m</i>	2005-007	21
Group 3				
fluoro-potassicrichterite	$A^{\square} K^B (CaNa) C Mg_5 T Si_8 O_{22}^w F_2$	<i>C2/m</i>	1986-046	22
fluorrichterite	$ANa^B (CaNa) C Mg_5 T Si_8 O_{22}^w F_2$	<i>C2/m</i>	1992-020	23

ferriwinchite	$A^{\square} B^{\square} (CaNa) C (Mg_4Fe^{3+}) TSi_8O_{22} W(OH)_2$	C2/m	2004-034	24,25*
aluminotaramite	$A^{\square} Na^B (CaNa) C (Fe^{3+}Al_2) T(Si_6Al_2) O_{22} W(OH)_2$	C2/m	2006-023	26
alumno-magnesiotaramite	$A^{\square} Na^B (CaNa) C (Mg_3Al_2) T(Si_6Al_2) O_{22} W(OH)_2$	C2/m	2006-024	26
fluoro-alumino-magnesiotaramite	$A^{\square} Na^B (CaNa) C (Mg_3Al_2) T(Si_6Al_2) O_{22} W(OH)_2$	C2/m	2006-025	26
potassic-aluminotaramite	$A^{\square} K^B (CaNa) C (Fe^{3+}Al_2) T(Si_6Al_2) O_{22} W(OH)_2$	C2/m	2007-015	27

Group 4

nyböite	$A^{\square} Na^B Na_2 C (Mg_3Al_2) T(Si_7Al) O_{22} W(OH)_2$	C2/m	1980-047	28
leakeite	$A^{\square} Na^B Na_2 C (Mg_2Fe^{3+}Li) TSi_8 O_{22} W(OH)_2$	C2/m	1991-028	29
kornite	$A^{\square} K^B Na_2 C (Mg_2Mn^{3+}Li) TSi_8 O_{22} W(OH)_2$	C2/m	1992-032	30
fluoro-ferroleakeite	$A^{\square} Na^B Na_2 C (Fe^{3+}Fe^{3+}Li) TSi_8 O_{22} W(OH)_2$	C2/m	1993-026	31
ungarettite	$A^{\square} Na^B Na_2 C (Mn^{2+}Mn^{3+}) TSi_8 O_{22} W(OH)_2$	C2/m	1994-004	32
obertite	$A^{\square} Na^B Na_2 C (Mg_3Fe^{3+}Ti^{4+}) TSi_8 O_{22} W(OH)_2$	C2/m	1998-046	33
fluoro-magnesio-arfvedsonite	$A^{\square} Na^B Na_2 C (Mg_4Fe^{3+}) TSi_8 O_{22} W(OH)_2$	C2/m	1998-056	34
potassicleakeite	$A^{\square} K^B Na_2 C (Mg_2Fe^{3+}Li) TSi_8 O_{22} W(OH)_2$	C2/m	2001-049	35
fluoronyböite	$A^{\square} Na^B Na_2 C (Mg_3Al_2) T(Si_7Al) O_{22} W(OH)_2$	C2/m	2002-010	28
potassicarfvedsonite	$A^{\square} K^B Na_2 C (Fe^{3+}Fe^{3+}) TSi_8 O_{22} W(OH)_2$	C2/m	2003-043	36
dellaventurite	$A^{\square} Na^B Na_2 C (MgMn^{3+}LiTi^{4+}) TSi_8 O_{22} W(OH)_2$	C2/m	2003-061	37
ferro-obertite	$A^{\square} Na^B Na_2 C (Fe_3Fe^{3+}Ti^{4+}) TSi_8 O_{22} W(OH)_2$	C2/m	in prep.	38

Group 5

ferri-ottolimitite	$A^{\square} B^{\square} (Na_{1,0-1,3}Li_{0,5-1,0})_2 C (Mg_4Fe^{3+}_2) TSi_8 O_{22} W(OH)_2$	C2/m	2001-067a	39
ferriwhitakerite	$A^{\square} Na^B (Na_{1,0-1,5}Li_{0,5-1,0})_2 C (Mg_2Fe^{3+}_2Li) TSi_8 O_{22} W(OH)_2$	C2/m	2001-069	39
parvo-mangano-edenite	$A^{\square} Na^B (CaMn) C Mg_5 T(Si_7Al) O_{22} W(OH)_2$	C2/m	2003-062	40
parowinchite	$A^{\square} B^{\square} (NaMn) C (Mg_4Fe^{3+}) TSi_8 O_{22} W(OH)_2$	C2/m	2003-066	41
parvo-manganotremolite	$A^{\square} B^{\square} (CaMn) C Mg_5 TSi_8 O_{22} W(OH)_2$	C2/m	2004-045	40

Notes: * description of crystal structure.

References: 1: Sueno and Matsubara (1986); 2: Sueno et al. (1998); 3: Caballero et al. (1998); 4: Oberti et al. (2000a); 5: Komishi et al. (2003); 6: Oberti et al. (2003b); 7: Oberti et al. (2005); 8: Cámara and Oberti (2005); 9: Shimazaki et al. (1984); 10: Hawthorne et al. (1996a); 11: Robinson et al. (1997); 12: Bazhenov et al. (1999); 13: Sokolova et al. (2000); 14: Gianfagna and Oberti (2001); 15: Chukanov et al. (2002); 16: Banno et al. (2004); 17: Lupulescu et al. (2005); 18: Korinevsky and Korinevsky (2006); 19: Bojar and Wälter (2006); 20: Lupulescu et al. (2007); 21: Pekov et al. (2005); 22: Della Ventura et al. (1992); 23: Bazhenov et al. (1993); 24: Bazhenov et al. (2005); 25: Sokolova et al. (2001); 26: Oberti et al. (2007b); 27: Oberti et al. (in prep); 28: Oberti et al. (2003c); 29: Hawthorne et al. (1992); 30: Armbruster et al. (1993); 31: Hawthorne et al. (1996b); 32: Hawthorne et al. (1995); 33: Hawthorne et al. (2000); 34: Bazhenov et al. (2000); 35: Matsubara et al. (2002); 36: Pekov et al. (2004); 37: Tait et al. (2005); 38: Hawthorne et al. (in prep); 39: Oberti et al. (2004); 40: Oberti et al. (2006); 41: Oberti and Ghose (1993).

Magnesiosadanagaite was described by Banno et al. (2004) in rocks from a contact aureole in Kasuga-mura, central Japan; the crystal are strongly zoned, the core being pargasite and the rim magnesiosadanagaite. A series of compositions was reported, and the unit formula of the most Al-rich K-poor crystal (sample GSJM35151-1, rim) is given in Table 1 with the code 4. More recently, sadanagaite amphiboles with ^TAl up to 3.55 apfu and Ti up to 0.66 apfu have been reported in metamorphosed laterites from Yuge Island (the type locality for potassic-sadanagaite); the extreme composition is $^A(\text{Na}_{0.20} \text{K}_{0.79}) ^B\text{Ca}_{2.05} ^C(\text{Mg}_{1.68} \text{Mn}_{0.03} \text{Fe}^{2+}_{1.39} \text{Al}_{0.76} \text{Fe}^{3+}_{0.45} \text{Ti}_{0.66}) ^T(\text{Si}_{4.45} \text{Al}_{3.55}) \text{O}_{22} ^W[(\text{OH})_{1.80} \text{F}_{0.20}]$ (Nishio-Hamane, personal communication; Fig. 1). The measured unit-cell parameters [$a = 9.964(4)$, $b = 18.024(8)$, $c = 5.369(3)$ Å, $\beta = 105.46(4)^\circ$ and $V = 929.4$ Å³], when compared to those reported for potassic-sadanagaite [$a = 9.922(10)$, $b = 18.03(2)$, $c = 5.352(9)$ Å, $\beta = 105.30(10)^\circ$ and $V = 923.5$ Å³; Shimazaki et al. 1984], indicate higher ^TAl and ^CTi contents. Chemical correlations suggest that the coupled heterovalent substitution of relevance is $^{M(2)}\text{Fe}^{3+} - ^T\text{Si}_{-1} ^{M(2)}\text{Ti}_1 ^T\text{Al}_1$. If significant dehydrogenation did not occur in sadanagaite, this substitution suggests a possible new end-member: $^A\text{K} ^B\text{Ca}_2 ^C(\text{Mg}^{2+}_3\text{Fe}^{3+}\text{Ti}) ^T(\text{Si}_4\text{Al}_4) \text{O}_{22} ^W(\text{OH})_2$ (Nishio-Hamane et al., work in progress), which represents a new charge arrangement for amphiboles and would extend the maximum amount of ^TAl to 4.0 apfu (more or less equally partitioned between the $T(1)$ and $T(2)$ sites).

Amphibole formulae which should be referred to potassian “*chloro-ferrosadanagaite*” (we chose to use “” for species not yet approved, although their names are already fixed by present rules, i.e. for the “named amphiboles” of Burke and Leake 2004) have been reported by Kullerud and Erambert (1999). These amphiboles formed during ductile shear deformation associated with infiltration of an externally derived Cl-bearing fluid in a gabbroanorthosite at Nufsjord (Lofoten, Norway).

The main crystal-chemical peculiarity of sadanagaite resides in their large amounts of ^TAl . The few available structure refinements (Hawthorne and Grundy 1977; Sokolova et al. 2000; Banno et al. 2004) suggest that around 2.0 apfu are incorporated at the $T(1)$ site, and that most

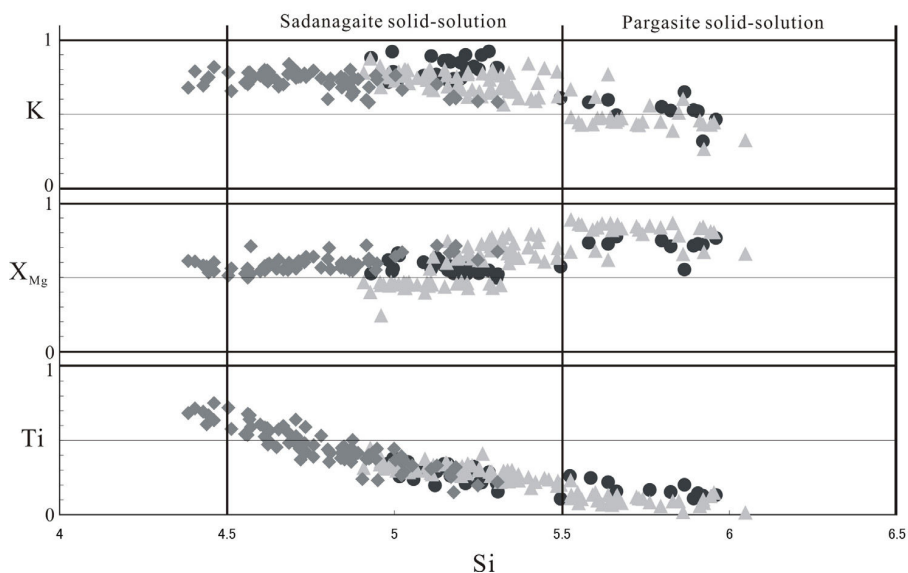


Figure 1. Chemical variation in amphiboles from Yuge, Myojin and Mutsuki Island. Thick gray diamonds are from Yuge Island, black circles are from Myojin Island and light gray triangles are from Mutsuki Island (D. Nishio Hamane, pers. com.)

of if not all excess ${}^T\text{Al}$ is incorporated at the $T(2)$ site. This conclusion may however not be completely correct, as it is based on a correlation between the ${}^{T(2)}\text{Al}$ content and the mean $\langle T(2)\text{-O} \rangle$ distance which was developed using amphiboles with lower Al and Fe contents by Oberti et al. (1995a). The issue of Al ordering at the T sites is discussed in more detail in Hawthorne and Oberti (2007a) and Oberti et al. (2007a). The occurrence of ${}^T\text{Al}$ linearly increases the size of the tetrahedra, and hence the repeat distance of the double-chain of tetrahedra. If incorporation of ${}^T\text{Al}$ is related to that of ${}^C\text{Ti}^{4+}$, the strip of octahedra cannot expand in the same way, especially along the c direction, and linkage between the two structural units is maintained by kinking of the double-chain, measured by the O(5)-O(6)-O(5) angle between the basal oxygen atoms of the tetrahedra. The values of the O(5)-O(6)-O(5) angle are very low in sadanagaites, and that in magnesiosadanagaite (160.4° ; Banno et al. 2004) is the lowest ever recorded.

Fluorocannilloite and joesmithite: constraints for divalent cations at the A site

Fluorocannilloite was found and characterized by Hawthorne et al. (1996a) in a marble from Pargas (Finland), rather ironically the type locality of pargasite. Attention was drawn on this sample by its anomalously high Ca content (always higher than 2.40 apfu in the studied amphiboles). The empirical formula of the holotype is given in Table 1 with the code 5. Before this finding, Ca and other large divalent cations were thought to be confined to the $M(4)$ site [but for joesmithite, ${}^A\text{Pb} {}^B\text{Ca}_2 {}^C(\text{Mg}_3\text{Fe}^{3+}_2) {}^T(\text{Si}_6\text{Be}_2) \text{O}_{22} {}^W(\text{OH})_2$, which is a very anomalous amphibole crystallizing in the $P2/a$ space group; Moore 1969; Moore et al. 1993]. Refinement of the crystal structure confirmed that Ca is an A cation in fluorocannilloite, and analysis of the electron density maps showed that it tends to order at the $A(2)$ site. Figure 2 shows the local coordination at the A site in fluorocannilloite, and identifies strong bond-valence interactions between $A(2)$ and the basal oxygen atoms of the $T(1)$ tetrahedron. Accordingly, all samples of fluorocannilloite examined have ${}^T\text{Al}$ higher than 2.0 apfu and strongly ordered at the $T(1)$ site, a behavior which is rarely observed in other amphiboles. This feature must be related to bond-valence requirements, and implies short-range order. In fact, the bond-valence requirements of the O(7) anion do not allow Al-O(7)-Al linkages where Na is the A cation, but require Al-O(7)-Al linkages when Ca is the A cation.

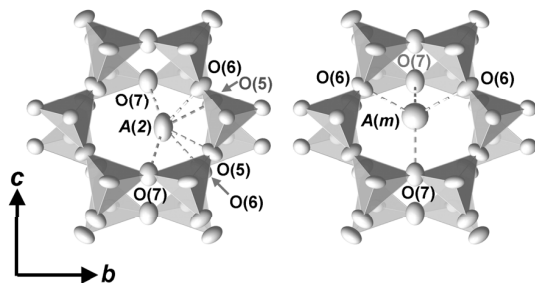


Figure 2. A projection onto (100) showing the coordination around the $A(2)$ and $A(m)$ sites in fluorocannilloite. Only the bonds shorter than 3.0 \AA have been drawn.

Other fluoropargasite samples with Ca in excess of 2.0 apfu were found in the literature or were synthesized, and structure refinement showed the same crystal-chemical behavior (Oberti et al. 1995b). Examination of the analyses reported by Leake (1968) for amphiboles in marbles from Pargas, Finland, shows coupling between high ${}^T\text{Al}$ content and high Ca content. We can thus conclude that the occurrence of Ca as an A cation may be more common than previously thought, at least in this paragenesis. In contrast, at least in the authors' experience, many (generally green) "cannilloites" circulating among mineral collectors are actually pargasite or chromian pargasite.

In fluorocannilloite, off-centering of the A cations is very strong, leading to short $A(2)$ and $A(m)$ distances to O(7) ($\sim 2.47 \text{ \AA}$). The H atom in amphiboles protrudes into the A cavity, restricting off-centering of the A cation. Thus Ca as an A cation is probably confined to F-rich compositions.

The only other amphibole composition with a divalent A cation is *joesmithite*, ideally ${}^A\text{Pb} {}^B\text{Ca}_2 {}^C(\text{Mg}_3\text{Fe}^{3+}_2) {}^T(\text{Si}_6\text{Be}_2) \text{O}_{22} {}^W(\text{OH})_2$, which was found so far only at Långban, Sweden, as very inhomogeneous crystals. Its crystal chemistry was revised by Moore et al. (1993), and the empirical formula of the holotype is given in Table 1 with the code 6. Similar to but with more drastic bond-valence requirements than Al^{3+} , Be^{2+} can be incorporated at one of the $T(1)$ sites, namely $T(1)\text{B}$. In order to satisfy the bond-valence requirements of the $\text{O}(5)\text{B}$, $\text{O}(6)\text{B}$, and $\text{O}(7)$ anions, Pb^{2+} is strongly displaced parallel to the b -axis (in a position analogous to the $A(2)$ site in $C2/m$ amphiboles) and can assume an almost one-sided [6]-coordination that is compatible with its stereoactive lone-pair behavior (Fig. 3). In fact, the $6s^2$ lone pair can project into the large space provided by the one-sided coordination, whereas such coordination is very unfavorable for “spherical” cations. Thus there is a strong short-range order between one Pb^{2+} and two Be^{2+} pfu occurring at the $T(1)\text{B}$ tetrahedron (cf. Hawthorne and Della Ventura 2007). This strongly asymmetric environment implies a different space-group symmetry ($P2/a$) but does not imply steric hindrance and repulsion with the protons. However, this combination of local bond-valence requirements and stereochemistry accounts for the very high selectivity of the A cavity for Pb^{2+} in *joesmithite* and for its fixed stoichiometry.

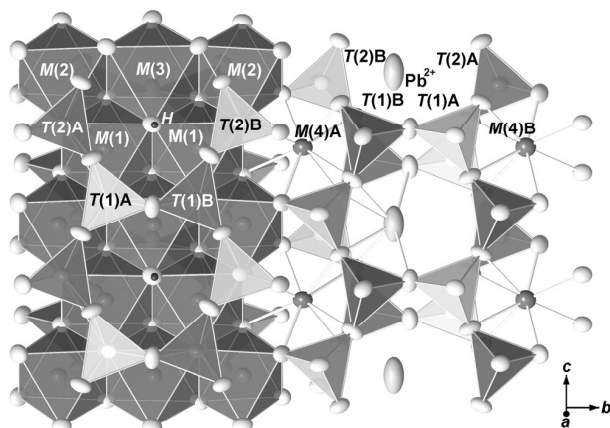


Figure 3. The one-sided coordination of Pb^{2+} in *joesmithite*. This arrangement allows appropriate bond-valence sums at the basal oxygen atoms of the $T(1)\text{B}$ tetrahedron occupied by Be^{2+} [$\text{O}(5)\text{B}, \text{O}(6)\text{B}, \text{O}(7)$], and leaves room for the $6s^2$ lone pair.

Li in amphiboles: clinoholmquistites, leakeites and sodic-pedrizites

Before 1990, Li was considered to be a major constituent of amphiboles only as a B cation, giving rise to the holmquistite series, ${}^A\Box {}^B\text{Li}_2 {}^C(\text{R}^{2+}_3\text{R}^{3+}_2) {}^T\text{Si}_8 \text{O}_{22} {}^W(\text{OH})_2$, which can occur either with monoclinic $C2/m$ symmetry (clinoholmquistite) or with orthorhombic $Pnma$ symmetry (holmquistite). However, Hawthorne (1978) reported 0.34 ${}^C\text{Li}$ pfu in a fluororiebeckite sample, and Ghose et al. (1986) reported lithian winchites and juddites (${}^C\text{Li} = 0.13\text{--}0.18$ apfu) from Indian manganese mines.

In 1990, samples from manganeseiferous metasediments in the Kajlidongri area, Jhabua district, Madhya Pradesh, India, showed low total oxides in EMP analysis (97–98 wt%) and anomalously low refined site-scattering values at the $M(3)$ site (down to 4.5 electrons per formula unit, epfu; see also Fig. 1 in Hawthorne and Oberti 2007a). The presence of vacancies at the C sites (in analogy with micas) was discarded because the significant Mg content did not allow the valence-sum rules to be satisfied. Li analysis was done first by atomic absorption and then by ion microprobe with the procedure described in Ottolini et al. (1993).

Leakeite was the first new amphibole species found at Kajlidongri, and the end-member composition was defined as ${}^A\text{Na} {}^B\text{Na}_2 {}^C(\text{Mg}_2\text{Fe}^{3+}_2\text{Li}) {}^T\text{Si}_8 \text{O}_{22} {}^W(\text{OH})_2$ (Hawthorne et al. 1992).

The prefix ferri- was not adopted because Fe^{3+} was considered as an essential constituent of $^{\text{C}}\text{Li}$ amphiboles. The empirical formula of the holotype is given in Table 1 with the code 7. On a crystal-chemical basis, leakeite can be derived either from magnesio-arfvedsonite via the exchange $^{\text{M}(2,3)}\text{Mg}^{2+}_{-2} \text{ } ^{\text{M}(2)}\text{Fe}^{3+}_1 \text{ } ^{\text{M}(3)}\text{Li}_1$ or from magnesioriebeckite via the exchange $^{\text{A}}\square_{-1} \text{ } ^{\text{M}(3)}\text{Mg}^{2+}_{-1} \text{ } ^{\text{A}}\text{Na}_1 \text{ } ^{\text{M}(3)}\text{Li}_1$. Systematic investigation at Kajlidongri showed that the first is the most likely crystal-chemical mechanism, and bond-valence calculations showed that the occurrence of $^{\text{C}}\text{Li}$, ordered at the $\text{M}(3)$ site, is confined to sodic amphiboles with a filled A site and Si close to 8.0 apfu (Hawthorne et al. 1994). This work also showed that the amphibole compositions are indicative of strongly oxidizing conditions, and that a significant oxo component is present in some samples. Later, a fully anhydrous Li-bearing amphibole composition, *dellaventurait*, ideally $^{\text{A}}\text{Na} \text{ } ^{\text{B}}\text{Na}_2 \text{ } ^{\text{C}}(\text{MgMn}^{3+}_2\text{Ti}^{4+}\text{Li}) \text{ } ^{\text{T}}\text{Si}_8 \text{ } \text{O}_{22} \text{ } ^{\text{W}}\text{O}_2$, was found at Kajlidongri (Tait et al. 2005). It is described in more detail in the section dealing with dehydrogenated amphiboles, but should be mentioned here to show that $^{\text{C}}\text{Li}$ is not incompatible with the occurrence of the oxo component at the $\text{O}(3)$ site.

These conclusions were confirmed in the study of alkali amphiboles from a series of silica oversaturated peralkaline rocks from the Questa caldera, New Mexico (Hawthorne et al. 1993). This work showed that: (1) stoichiometric problems previously encountered in arfvedsonitic amphiboles were largely due to the omission of Li and Zn from the analysis, and to inappropriate renormalization procedures, e.g. the assumption that $\text{OH} + \text{F} = 2$ apfu; (2) previous graphical representations of magmatic subsolidus and oxidation trends in alkali amphiboles from silica-saturated peralkaline igneous rocks do not take into consideration the substitution $\text{Fe}^{2+}_{-2} \text{ } \text{Fe}^{3+}_1 \text{ } \text{Li}_1$, and thus can give totally misleading results (Fig. 4). The Li-bearing amphiboles found at Questa can be referred as fluoro-ferri-ferrokatophorite, fluoro-ferri-magnesioikatophorite, arfvedsonite and fluoro-arfvedsonite. The new species *fluoro-ferroleakeite*, ideally $^{\text{A}}\text{Na} \text{ } ^{\text{B}}\text{Na}_2 \text{ } ^{\text{C}}(\text{Fe}^{2+}_2\text{Fe}^{3+}_2\text{Li}) \text{ } ^{\text{T}}\text{Si}_8 \text{ } \text{O}_{22} \text{ } ^{\text{W}}\text{F}_2$, was also found. The unit formula of the holotype specimen is given

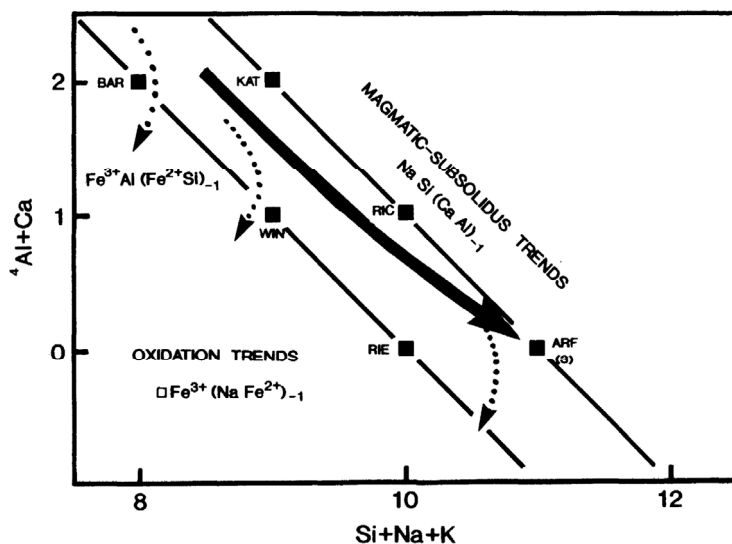


Figure 4. Magmatic subsolidus ($\text{Fe}^{3+}/\text{Fe}_{\text{tot}} = 0.20$; right) and oxidation trends ($\text{Fe}^{3+}/\text{Fe}_{\text{tot}} = 0.40$; left) in alkali amphiboles from silica-saturated peralkaline granites as defined by Strong and Taylor (1984). The presence of the $\text{Li}_1 \text{ } \text{Fe}^{3+}_1 \text{ } \text{Fe}^{2+}_{-2}$ substitution implies far more oxidizing conditions ($\text{Fe}^{3+}/\text{Fe}_{\text{tot}} = 0.50$; pointed arrows) than inferred from this diagram. Note that in this plot arfvedsonite ($\text{Fe}^{3+}/\text{Fe}_{\text{tot}} = 0.20$) coincides with fluoro-ferroleakeite ($\text{Fe}^{3+}/\text{Fe}_{\text{tot}} = 0.50$) [from Hawthorne et al. (1993), *American Mineralogist*, 78, Fig. 8, p. 743].

in Table 1 with the code 8. Note that the low sum of C cations suggests either underestimation of Li or a small but significant $^{O(3)}O^{2-}$ component (Hawthorne et al. 1993, 1996b).

Li-rich fluoro-arfvedsonites (${}^C\text{Li} = 0.48$ apfu) were also found into miarolitic cavities in a pegmatite phase of a riebeckite granite at Hurricane Mountain, Carroll County, New Hampshire (Hawthorne et al. 1996c). Holotype potassic arfvedsonite from Ilímaussaq, South Greenland, with unit formula ${}^A(\text{Na}_{0.22}\text{K}_{0.67}){}^B\text{Na}_{2.0}{}^C(\text{Mn}_{0.20}\text{Fe}^{2+}_{3.19}\text{Fe}^{3+}_{1.27}\text{Ti}_{0.06}\text{Li}_{0.28}){}^T\text{Si}_8\text{O}_{22}{}^W[(\text{OH})_{1.80}\text{F}_{0.20}]$ has significant Li at the $M(3)$ site, and even larger ${}^C\text{Li}$ contents were found in the co-type sample from the Lovozero Massif (Kola Peninsula, Russia): ${}^A(\text{K}_{0.73}\text{Na}_{0.28}){}^B(\text{Na}_{1.99}\text{Ca}_{0.01}){}^C(\text{Fe}^{2+}_{1.77}\text{Mg}_{1.10}\text{Fe}^{3+}_{0.98}\text{Li}_{0.45}\text{Mn}_{0.42}\text{Ti}_{0.09}\text{Zn}_{0.01}){}^T(\text{Si}_{8.09})\text{O}_{22}{}^W[(\text{OH})_{1.41}\text{F}_{0.59}]$ (Pekov et al. 2004).

Armbruster et al. (1993) described *kornite*, actually the ${}^A\text{K}$ - and ${}^{M(2)}\text{Mn}^{3+}$ - equivalent of leakeite, from the Wessels Mine, Kalahari Manganese field, South Africa, where it occurs as a hydrothermal reaction product of primary ore. Its empirical formula is listed in Table 1 with the code 9. Interestingly, Li occurs both as a B and C cation, a feature that will be discussed in more detail when dealing with sodic-pedrizite. Kornite is a rare amphibole which has so far been found only as fine [001] fibers, and for which a structural determination is still lacking. Interestingly, Armbruster et al. (1993) suggested that kornite has a primitive lattice (space group $P2_1/m$ or $P2/a$) based on long-exposure precession and Weissenberg photographs, a feature which should be verified because all leakeites have $C2/m$ symmetry.

The latest member of the leakeite family is *potassic-leakeite* (Matsubara et al. 2002), which occurs in pegmatite-like veinlets that cut a Mn ore-body in the Tanohata mine, Iwate Prefecture, Japan. It was considered to have crystallized during later stages of hydrothermal activity of contact metamorphism. The empirical formula reported for the holotype specimen is listed in Table 1 with the code 10. It is unusually enriched in V, which was assigned to the $M(2)$ site.

The above findings prompted a systematic re-examination of alkali amphiboles for which electron-microprobe analysis did not yield satisfactory results. In the Strange lake peralkaline granite pluton (Lac Brisson, Quebec, Canada), there are Li-bearing arfvedsonitic amphiboles from the least evolved to the most evolved intrusive units, near the core of the pluton. These samples are relatively enriched in Zn, Zr, Mn and K, and depleted in Mg, Ca and Al; some have significant oxo component (up to $0.37 O^{2-}$ apfu). ${}^C\text{Li}$ is ≤ 0.40 apfu, and thus compositions do not reach “ferroleakeite.” A number of interesting direct (Mn vs. Zn) and inverse (Li vs. Ca; K vs. Al) chemical correlations were found, but were ascribed to the petrogenetic process, i.e. to progressive fractionation and increase in f_{O_2} (Hawthorne et al. 2001, and references therein).

In contrast, a series of sodic and sodic-calcic amphiboles from lithic-wacke inclusions in the alkali ultramafic diatreme at Coyote Peak, Humboldt Co. (California) have low ${}^{M(3)}\text{Li}$ contents which are inversely correlated with Ca content (Hawthorne et al. 1998). Some of these amphiboles have very high Ti and $^{O(3)}O^{2-}$ contents, pointing toward the new end-member “ferro-obertiite” (characterization still in progress; cf. the section below).

Based on the above evidence, Li occurs as a major B cation in holmquistite and Fe-rich clinoholmquistites from Li-rich pegmatites, and as a major $M(3)$ cation in sodic amphibole from either peralkaline granites or manganeseiferous metasediments. A further step toward clarification of the crystal-chemistry of Li in amphiboles was taken during systematic investigation of a series of episyenites from the East sector of the Pedriza Massif (Sierra de Guadarrama, Spanish Central System). This unusual occurrence provided samples which span the compositional space magnesioriebeckite, clino-ferroholmquistite, leakeite and sodic-pedrizite (and their ferro- or ferri- counterparts) (Fig. 5). All amphiboles formed during episyenitic alteration (silicification and albitisation) of a cordierite-bearing porphyritic monzogranite by aqueous non-magmatic fluids of low salinity, at temperatures around 500°C and fluid pressures ranging from 60 to 160 MPa. Relatively higher Mg/Fe ratios suggest crystallization at the highest T experienced, which occurred at the beginning of the alteration process.

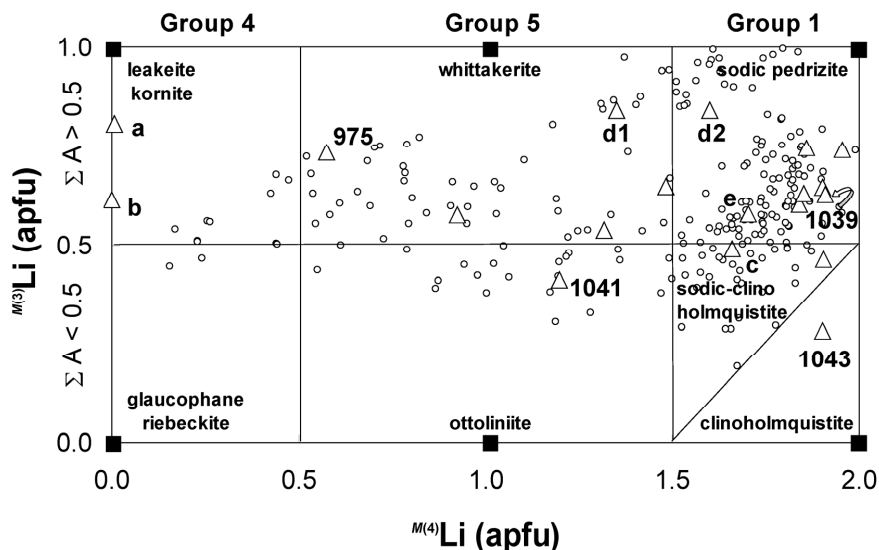


Figure 5. The compositional diagram relevant to the ${}^B(\text{Li,Na})$ solid solution in amphiboles. Because ${}^C\text{Li}$ is always $\leq {}^A(\text{Na,K})$ the ordinate implicitly corresponds to the A-site occupancy. a = leakeite (Hawthorne et al. 1992); b = fluoro-ferrileakeite (Hawthorne et al. 1998); c = clino-sodic-ferri-ferroholmquistite (Caballero et al. 1998); d1 = ferriwhittakerite, d2 = sodic-ferripedrizite (Oberti et al. 2000); e = sodic-ferripedrizite (Caballero et al. 2002); open triangles and open circles are the refined crystals and the analyses reported by Oberti et al. (2003a), respectively; 975 = ferriwhittakerite and 1041 = ferri-ottoliniite (Oberti et al. 2004); 1039 = sodic-ferri-ferropedrizite and 1043 = clino-ferri-ferroholmquistite (Oberti et al. 2003b) [from Oberti et al. (2004), *American Mineralogist*, 89, Fig. 1, p. 892].

Six new end-members were found at Pedriza (Oberti et al. 2003a,b, 2004, and references therein), confirming the extensive inter- and intracrystalline chemical variability. Some of their names were later modified because the decisions of the IMA-CNMMN and of its Subcommittee on Amphiboles evolved with the new findings, which caused two subsequent re-definitions of the use of the prefix sodic in ${}^B(\text{Mg,Fe,Mn,Li})$ amphiboles and eventually the definition of Group 5 amphiboles. Here, we refer to the classification in force after Leake et al. (2003) and Burke and Leake (2004).

Clino-sodic-ferri-ferroholmquistite, ideally ${}^A\Box{}^B\text{Li}_2{}^C(\text{Fe}^{2+}_3\text{Fe}^{3+}_2){}^T\text{Si}_8\text{O}_{22}{}^W(\text{OH})_2$ but with $\text{Na}_{\text{tot}} > 0.50$ apfu [although partitioned between the A and the M(4) site] is the name presently used for the sample reported by Caballero et al. (1998), the empirical formula of which is given in Table 1 with the code 11.

Clino-ferri-ferroholmquistite, ideally ${}^A\Box{}^B\text{Li}_2{}^C(\text{Fe}^{2+}_3\text{Fe}^{3+}_2){}^T\text{Si}_8\text{O}_{22}{}^W(\text{OH})_2$, was first reported by Oberti et al. (2003a) as sample 1043; its mineral data are given in Oberti et al. (2003b). The empirical formula of the holotype is listed in Table 1 with the code 12.

Sodic-ferripedrizite, ideally ${}^A\text{Na}{}^B\text{Li}_2{}^C(\text{Mg}_2\text{Fe}^{3+}_2\text{Li}){}^T\text{Si}_8\text{O}_{22}{}^W(\text{OH})_2$, is the correct name for sample P2 in Oberti et al. (2000a), whereas sample P1 became ferriwhittakerite after the introduction of Group 5 amphiboles. The empirical formula of the holotype is listed in Table 1 with the code 13.

Sodic-ferri-ferropedrizite, ideally ${}^A\text{Na}{}^B\text{Li}_2{}^C(\text{Fe}^{2+}_2\text{Fe}^{3+}_2\text{Li}){}^T\text{Si}_8\text{O}_{22}{}^W(\text{OH})_2$, was first reported by Oberti et al. (2003a) as sample 1039, and its mineral data are given in Oberti et al. (2003b). The empirical formula of the holotype is listed in Table 1 with the code 14.

Ferriwhittakerite, ideally ${}^A\text{Na}{}^B(\text{NaLi}){}^C(\text{Mg}_2\text{Fe}^{3+}_2\text{Li}){}^T\text{Si}_8\text{O}_{22}{}^W(\text{OH})_2$ was described by

Oberti et al. (2004) with the empirical formula listed in Table 1 with the code 15.

Ferri-ottoliniite, ideally $A^{\square} B(NaLi) C(Mg_3Fe^{3+}_2) TSi_8 O_{22} W(OH)_2$, was described by Oberti et al. (2004) with the empirical formula listed in Table 1 with the code 16.

An additional species of the sodic-pedrizite series was identified in a rock samples from the Tastyg spodumene deposit, Tuva, Siberia, Russia, where holotype clinoholmquistite had been described (Ginzburg 1965; Litvin et al. 1975). It was shown that the amphibole composition obtained by wet-chemical analysis by Ginzburg (1965) actually refers to a mixture of two distinct amphiboles, *fluoro-sodic-pedrizite* and tremolite (Oberti et al. 2005). Holotype fluoro-sodic-pedrizite, ideally $A^{\square} Na^B Li_2 C(Mg_2 Al_2 Li) TSi_8 O_{22} W F_2$, has the empirical formula 17 in Table 1, and is the first amphibole species with Li dominant at *M*(3) found in Fe-poor geologic environments. The coexisting tremolite contains only 0.002 wt% Li_2O and 0.06 wt% B_2O_3 , the latter probably ordered at the *T*(1) site. The interesting issue is that recognition of these two amphiboles by *in situ* EMP and SIMS analysis resulted in discreditation of clinoholmquistite, which has been described only from this locality (IMA-CNMMN 2004-002). Further support for discreditation is the close similarity of the unit-cell parameters of clinoholmquistite refined by Litvin et al. (1975) with those of fluoro-sodic-pedrizite refined by Oberti et al. (2005).

Despite the different geological environment of crystallization, all $^C Li$ -rich amphiboles (but fluoro-sodic-pedrizite) so far reported contain either dominant Fe^{3+} (cf. the above list plus Li-bearing fluoro-arfvedsonites from the granitic pegmatite at Hurricane Mountains, New Hampshire, Hawthorne et al. 1996c) or dominant Mn^{3+} (kornite, dellaventurite, and some Mn-bearing leakeites coexisting with ungarettiite; Oberti, still unpublished).

The occurrence of fluoro-sodic-pedrizite in the Tastyg spodumene deposit is thus an oddity in this scenario. It might be due to a very unusual geochemical environment and to unusual *P-T* conditions of crystallization; the presence of large amounts of F should also be important in stabilizing the structure. The unit-cell volume of fluoro-sodic-pedrizite is among the smallest observed for monoclinic amphiboles, as is to be expected based on the occurrence of small cations at all the structural sites, namely Mg at *M*(1,3), Al at *M*(2), Li at *M*(4), and Si at *T*(1,2). The presence of F both reduces the size of the *M*(1) and *M*(3) octahedra and eliminates steric hindrance between the proton and Na at the *A*(*m*) site. There is no information on the compositional and genetic relations between monoclinic and orthorhombic $^B Li$ amphiboles. However, systematic investigation of the known occurrences of holmquistite (Cámara and Oberti 2005) has not identified any Li-bearing monoclinic amphibole.

The instability of the clinoholmquistite structure is also supported by recent experimental studies in the system $Li_2O-Na_2O-FeO-MgO-Al_2O_3-Fe_2O_3-Si_2O-H_2O$, done at $450 < T < 900$ °C, $0.1 < P < 1.5$ GPa, and $\log(f_{O_2})$ 0.5 below and 3 above that of the Ni-NiO buffer (Iezzi 2001; Iezzi et al. 2004a). In the system $Li_2O-MgO-Al_2O_3-Si_2O-H_2O$, clinoholmquistite was never obtained, whereas introduction of Fe^{3+} to the system resulted in crystallization of clinoferriholmquistite. Only a limited amount of Al (around 10%) was incorporated at lower *T* (500-600 °C) and *P* (0.1 GPa), whereas solid solution between Mg and Fe^{2+} is complete in clinoferriholmquistite (Iezzi et al. 2005a), Mg-rich compositions being more stable (up to 800 °C) than Fe^{2+} -rich compositions (up to 500-600 °C). In contrast, there are many reported occurrences of holmquistite, and only one known occurrence of ferrohalmquistite (Cámara and Oberti 2005). The reason for this must be sought by additional crystal-chemical studies and structure modeling of holmquistite.

Thus Li-bearing amphiboles span a large compositional range: the *A* site may be either empty (if Li occurs only as a B cation) or filled by Na or K (if Li occurs both as a B and C cation); the *M*(1,2,3) sites may be dominantly occupied either by Mg or Fe^{2+} and by Al or Fe^{3+} , the *O*(3) site may be significantly occupied by O^{2-} (cf. below the description of the Li-bearing anhydrous amphibole dellaventurite). The only general rule we have found is that Li occurs in amphiboles with monovalent B-cations (with no restraints to the $^B Na_{-1} ^B Li_1$ solid solution) and

nearly complete Si occupancy at the T sites, and that $^{\text{C}}\text{Li}$ is always coupled with at least an equal amount of A-site occupancy.

All the Li-bearing amphiboles so far examined have a high degree of cation ordering. When Li is a B cation, Li occupies a position closer to the strip of octahedra than that occupied by Na, and assumes [5+1]- or [6]-coordination in orthorhombic and monoclinic amphiboles, respectively. When Li is a C cation, it invariably orders at the $M(3)$ site. Chemical correlations and bond-valence calculations show that $^{\text{C}}\text{Li}$ always couples with a trivalent cation at the $M(2)$ site, with Si at the $T(1)$ site and with an occupied A site, where the A cation is ordered at a strongly off-centered $A(m)$ site. All this evidence confirms the critical role of bond-valence requirements of the basal oxygen atoms of the tetrahedra.

The sodic-pedrizite series thus represents the amphibole composition with the highest Li content, namely 3.0 apfu. In the episyenites from Pedriza, the total Li content in amphiboles depends primarily on the composition of the coexisting fluid during crystallization. However, the $^{\text{C}}\text{Li}$ content is directly related to the Mg number, and thus to the T of crystallization, whereas the $^{\text{B}}\text{Li}$ content is inversely related to the Mg number. Accordingly, the $^{\text{B}}\text{Li}$ -free, $^{\text{C}}\text{Li}$ -rich amphiboles from peralkaline granites formed under much higher T condition than those estimated for Pedriza (around 500 °C). Some of the rocks studied in Pedriza provided further constraints (Oberti et al. 2003a). Samples C3 and C5 define a trend from leakeite toward the boundary between sodic-ferri-ferropedrizite and clino-sodic-ferri-ferroholmquistite; this feature can be interpreted in terms of an open metasomatic system, where a progressive increase in Li/Na ratio is coupled with a decrease in T . Other samples (namely, C2, C20-24, and C4) define a transition from sodic-pedrizite to clinoholmquistite, in which $^{\text{B}}\text{Li}$ is nearly constant or decreases slightly with Mg number, whereas $^{\text{C}}\text{Li}$ increases with Mg number.

Other amphiboles with nearly equal amounts of large (Na, Ca) and small (Li, Mg, Mn, Fe) B cations: composition and symmetry

There are two other amphiboles reported in the literature that occur in the former compositional gap between $^{\text{B}}(\text{Na,Ca})$ and $^{\text{B}}(\text{Mg,Fe,Mn,Li})$ amphiboles.

Oberti and Ghose (1993) reported a very unusual amphibole from the metamorphosed manganese deposit at Tirodi, Maharashtra, India, which was characterized by electron- and ion-microprobe, Mössbauer analysis and single-crystal structure refinement, giving the empirical formula given in Table 1 with the code 18. It is a member of the $^{\text{B}}(\text{Na,Mn})$ solid-solution series. Several samples of similar composition had extensive $(\bar{1}01)$ and (100) exsolution lamellae, and rare inclusions of two chemically different amphiboles (magnesio-arfvedsonite with a magnesioriebeckite component, and manganocummintonite with a richterite component), indicating a miscibility gap (Ghose 1981; Shau et al. 1993). The sample examined by Oberti and Ghose (1993), however, showed no evidence of exsolution as determined by single-crystal precession photographs, and was thus considered to be on the verge of exsolution either in terms of allowed composition or in terms of high- T crystallization and rapid quenching.

This sample shows normal cation ordering for amphibole, with $^{\text{C}}\text{Li}$ ordered at $M(3)$, Fe^{3+} at $M(2)$ and Mn partitioned according to $M(4) \gg M(1) = M(2) = M(3)$. The solid solution at the $M(4)$ sites is confirmed by the oblong shape of the electron density, which could be modeled with two separate maxima, $M(4)$ and $M(4')$, each with different coordination geometry. Geometrical analysis of the long-range-averaged $M(4)$ site clearly indicates behavior intermediate between $^{\text{B}}(\text{Na,Ca})$ and $^{\text{B}}(\text{Mg,Fe,Mn,Li})$ amphiboles. After Leake et al. (2003), this sample is named parvowinchite because the sodic-calcic component is dominant among the B cations.

“Manganoan silicic edenite” was reported by Benimoff et al. (1991) from the Grenville marble of the Arnold Mine, Fowler, St. Lawrence Co., New York. According to Leake (2003), it is a member of Group 5, belonging to the $^{\text{B}}(\text{Ca,Mn})$ solid-solution. Re-examination of the original rock specimen (Oberti et al. 2006) showed significant inter- and intra-crystalline compositional variations which can be expressed by the $^{\text{A}}\text{Na}_{-1}^{\text{T}}\text{Al}_{-1}^{\text{A}}\square_{-1}^{\text{T}}\text{Si}_1$ and $^{\text{B}}\text{Ca}_{-2}^{\text{B}}\text{Mn}_2$

exchange vectors. The first vector relates parvo-mangano-edenite, ideally ${}^A\text{Na} {}^B(\text{Ca},\text{Mn})_2 {}^C\text{Mg}_5 {}^T(\text{Si}_7\text{Al}) \text{O}_{22} {}^W(\text{OH})_2$ with $\text{Ca} > 1$, to parvo-manganotremolite, ideally ${}^A\text{Ca} {}^B(\text{Ca},\text{Mn})_2 {}^C\text{Mg}_5 {}^T\text{Si}_8 \text{O}_{22} {}^W(\text{OH})_2$ with $\text{Ca} > 1$. The second mechanism was never found to reach Mn dominance; however, crystal-chemical analysis does not provide any evidence of structural limits, and the magno- counterparts of the Group 5 amphiboles of this work (“magno-manganocummingtonite”) may occur in similar but Mn-richer environments. The composition closest to parvo-mangano-edenite is listed in Table 1 with the code 19. It has $a = 9.8260(5)$, $b = 18.0487(9)$, $c = 5.2840(4)$ Å, $\beta = 104.55(1)^\circ$, $V = 907.1$ Å³. Holotype parvo-manganotremolite has composition 20 in Table 1, with $a = 9.7807(5)$, $b = 18.0548(9)$, $c = 5.2928(4)$ Å, $\beta = 104.19(1)^\circ$, $V = 906.1$ Å³ ($Z = 2$). Core-to-rim compositional zoning is common.

All natural Group 5 amphiboles which belong to the ${}^B(\text{Na},\text{Li})$, ${}^B(\text{Na},\text{Mn})$ and ${}^B(\text{Ca},\text{Mn})$ solid-solutions, whether their A site is filled or empty, have monoclinic $C2/m$ symmetry. In contrast, the A-site filled synthetic samples belonging to the ${}^B(\text{Na},\text{Mg})$ and ${}^B(\text{Li},\text{Mg})$ solid-solutions (discussed later in this Chapter), have $P2_1/m$ symmetry at room T , and undergo phase transitions at variable T_c , depending on their chemical composition (see Welch et al. 2007 for more details). The $P2_1/m$ symmetry is stabilized either by the presence of small B-cations (e.g., in cummingtonite) or by a B composition where a large monovalent cation (Na) and a small divalent cation (Mg) occur in a ratio close to 1:1. However, the size of the C cations also plays a significant role in determining the transition behavior (cf. Welch et al. 2007 for more discussion). We can thus provisionally conclude that the $C2/m$ symmetry observed for the ${}^B(\text{Na},\text{Mn})$ solid-solution is due either to the larger ionic radius of Mn (compared to Mg) or to the presence of large cations (such as Mn and Fe) at the $M(1,2,3)$ sites.

Anhydrous sodic amphiboles: ungarettiite, obertiite, dellaventuraite

Before 1995, the replacement of a monovalent species (OH^- , F^- , Cl^-) with O^{2-} at the O(3) site was considered to be a major issue only for calcic amphiboles crystallized in high- T environments (pargasites and kaersutites). However, the occurrence of minor oxo component had also been reported for Li-bearing sodic amphibole from peralkaline granites (Hawthorne et al. 1993) and for Ti-bearing richterite from lamproites (Oberti et al. 1992), and synthetic “oxopotassic richterite” has been recently obtained at upper-mantle conditions ($P = 1.4$ GPa and $T = 850$ - 1020 °C) from a lamproite starting material (Tiepolo et al. 2003).

The O(3) site is coordinated by two $M(1)$ and one $M(3)$ sites; hence, the mechanisms involving satisfaction of the valence-sum rule in dehydrogenated amphiboles must involve the presence of highly charged cations at these sites. The crystal-chemical mechanisms related to the occurrence of the oxo component are

- (1) the occurrence of one Ti atom at one of the $M(1)$ sites, which locally allows complete loss of hydrogen [${}^{M(1)}\text{R}^{2+} {}_{-1} \text{O}^{(3)}(\text{OH}^-) {}_{-2} {}^{M(1)}\text{Ti}^{4+} {}_{+1} \text{O}^{(3)}\text{O}^{2-} {}_{-2}$, kaersutitic substitution];
- (2) the occurrence of 1 or 2 R^{3+} cations at the two $M(1)$ sites (or at one $M(1)$ and one $M(3)$ site), according to ${}^{M(1)}\text{R}^{2+} {}_{-n} \text{O}^{(3)}(\text{OH}^-) {}_{-n} {}^{M(1)}\text{R}^{3+} {}_{+n} \text{O}^{(3)}\text{O}^{2-} {}_{-n}$.

Mechanism (1) implies primary crystallization with the oxo component, whereas mechanism (2) may also imply post-crystallization oxidation and dehydrogenation. More details on this issue are given in Oberti et al. (2007a) and Hawthorne and Della Ventura (2007).

The discovery of *ungarettiite*, ideally ${}^A\text{Na} {}^B\text{Na}_2 {}^C(\text{Mn}^{2+} {}_2\text{Mn}^{3+}) {}^T\text{Si}_8 \text{O}_{22} {}^W\text{O}_2$, in the manganese silicate and oxide rocks of the Hoskins mine, New South Wales, Australia, allowed a more detailed crystal-chemical picture of the role of the oxo component in amphiboles (Hawthorne et al. 1995); it was later confirmed by electron- and ion-probe characterization of a second occurrence in the nearby Woods mine (Kawachi et al. 2002). In both occurrences, ungarettiite occurs in both reduced and oxidized assemblages. Although it coexists with Li-bearing amphiboles of low H content, it does not contain either Li (but for at a few ppm level) or H. In both occur-

rences, the sample composition is very close to the ideal stoichiometry (empirical formula 21 in Table 1); the only significant deviations involve small amounts of K substituting for Na at the A site (0.02-0.15 apfu) and Mg substituting for Mn²⁺ at the M(2) site (0.01-0.34 apfu).

The main peculiarity of ungarrettiite is the inverse ordering of C cations [R²⁺ at M(2) and R³⁺ at M(1) and M(3)], which indicates that its occurrence must be confined to Mn-rich environments. Mn³⁺ has a high-spin *d⁴* configuration, and would have a small stabilization energy relative to its electronically degenerate state in a fairly regular octahedral environment. The symmetry arguments associated with the Jahn-Teller effect predict a tetragonal distortion, and the structure refinement shows that all three octahedra are strongly distorted: M(1) has four short bonds (1.955 Å) and two long bonds (2.184 Å) in a *trans* configuration, whereas M(3) has four long bonds (2.047 Å) to the equatorial O(1) oxygen atoms and two short bonds (1.933 Å) to the apical O(3) oxygen atoms (according to the local bond-valence requirements of the oxo component). The matching of the small M(1) and M(3) octahedra with the large M(2) octahedron occupied by Mn²⁺ produces a very unusual pattern of distortion of the O-O edges (more detail in Hawthorne et al. 1995). The occurrence of a Fe³⁺ analogue of ungarrettiite is to be discarded, because Fe³⁺ cannot assume the same type of distorted coordination as Mn³⁺ without the benefit of the Jahn-Teller effect. Formally, ungarrettiite can be derived from the (Mn²⁺, Mn³⁺) analogue of eckermannite via the exchange vector $^{M(1)}R^{2+}_{-2} \text{ }^{O(3)}OH_{-2} \text{ }^{M(1)}R^{3+}_{+2} \text{ }^{O(3)}O^{2-}_{-2}$ and inversion of the ordering pattern for C cations [$^{M(2)}R^{3+}_{-1} \text{ }^{M(3)}R^{2+}_{-1} \text{ }^{M(2)}R^{2+}_{+1} \text{ }^{M(3)}R^{3+}_{+1}$].

Obertiite, ideally ^ANa ^BNa₂ ^C(Mg₃Fe³⁺Ti⁴⁺) ^TSi₈ O₂₂ ^WO₂, occurs in vugs of volcanic rocks at the Bellerberg quarry, Eifel region, Germany (Hawthorne et al. 2000). The deviations from ideal stoichiometry are due to the occurrence of K at the A site and of Mn substituting for Fe; the empirical formula of the holotype is listed in Table 1 with the code 22. The ^CR²⁺ content is always higher than expected by stoichiometry due to the occurrence of some Ca and (Mn, Fe)²⁺ at the M(4) site. Obertiite can be derived from magnesio-arfvedsonite by the exchange vector $^{M(1)}R^{2+}_{-1} \text{ }^{O(3)}(OH)^{-}_{-2} \text{ }^{M(1)}Ti^{4+}_{+1} \text{ }^{O(3)}O^{2-}_{-2}$. Its Li-bearing ferro- analogue had been previously reported (without realizing it) in an alkali ultramafic diatreme at Coyote Peak, Humboldt County, California by Hawthorne et al. (1998). The empirical formula is given in Table 1 with the code 23, and the formal description is currently in preparation.

Dellaventuraite, ideally ^ANa ^BNa₂ ^C(MgMn³⁺₂Ti⁴⁺Li) ^TSi₈ O₂₂ ^WO₂, was characterized by Tait et al. (2005) during a systematic investigation of Li-bearing amphiboles from the Kajlidongri manganese mine (where leakeite had also been discovered). Deviations from stoichiometry include substantial K at the A site (0.40-0.44 apfu), Ca at the M(4) site (0.29-0.33 apfu), and Fe³⁺ substituting for Mn³⁺. The empirical formula of the holotype specimen is given in Table 1 with the code 24.

In contrast to ungarrettiite, the normal ordering pattern expected for C cations is followed in dellaventuraite: Ti is completely ordered at M(1) (together with 0.63 Mn³⁺ pfu) and balances the dehydrogenation measured by ion-microprobe analysis, Li is ordered at M(3) and the other trivalent cations pfu (Mn³⁺ and Fe³⁺) are ordered at M(2). Hence, dellaventuraite can be derived from kornite by the exchange vector $^{M(1)}R^{2+}_{-1} \text{ }^{O(3)}(OH)^{-}_{-2} \text{ }^{M(1)}Ti^{4+}_{+1} \text{ }^{O(3)}O^{2-}_{-2}$.

From the above discussion, we can conclude that the charge arrangements of the newly discovered dehydrogenated sodic amphiboles can all be derived from that of eckermannite, ^ANa ^BNa₂ ^C(Mg₄Al) ^TSi₈ O₂₂ ^W(OH)₂ and/or of its ^CLi-bearing analogue leakeite, ^ANa ^BNa₂ ^C(Mg₂Fe³⁺₂Li) ^TSi₈ O₂₂ ^W(OH)₂ via the exchange vectors related to the oxo component [$^{M(1)}R^{2+}_{-1} \text{ }^{O(3)}(OH)^{-}_{-2} \text{ }^{M(1)}Ti^{4+}_{+1} \text{ }^{O(3)}O^{2-}_{-2}$ and $^{M(1)}R^{2+}_{-2} \text{ }^{O(3)}(OH)^{-}_{-2} \text{ }^{M(1)}R^{3+}_{+2} \text{ }^{O(3)}O^{2-}_{-2}$] and the appropriate homovalent substitutions. Ungarrettiite is the only amphibole found so far which violates the standard ordering pattern of C cations, a situation which is due to the requirements of the electronic configuration of Mn³⁺. Although it contains significant amounts of Mn³⁺, dellaventuraite obeys the standard ordering pattern, most likely because the presence of Ti and substantial Fe does not allow the required distortion of the octahedron.

NEW COMPOSITIONS FOR SYNTHETIC AMPHIBOLES

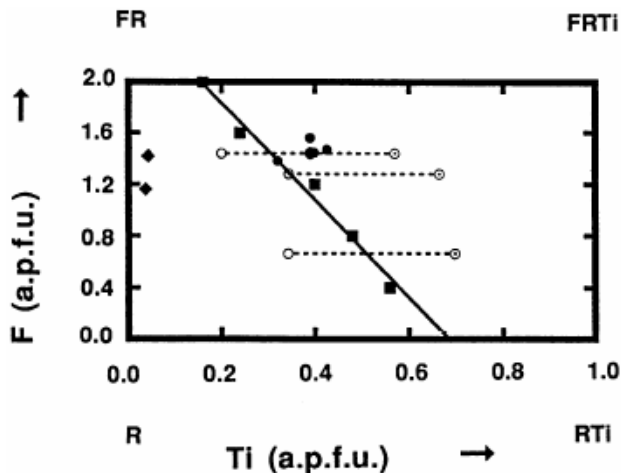
In this second section, we review the literature on amphibole synthesis published during the last 25 years. Particular attention will be paid to syntheses focused on the incorporation in the amphibole structure of elements uncommon in Nature, and focused on understanding the physico-chemical constraints of solid-solutions rarely found in Nature (e.g., ${}^{T(2)}\text{Si}_{-1}{}^{T(2)}\text{Ti}_1$ and ${}^{\text{B}}\text{Na}_{-2}{}^{\text{B}}\text{Li}_2$). For the earlier literature on synthetic amphiboles, Ernst (1968) and Gilbert et al. (1982) summarize work done in 1950-1980. In Tables 3 and 4, respectively, detail is given on the experimental conditions used and the unit-cell data for the compositions discussed here. The experimental studies on the incorporation of trace elements are treated in a separate chapter (Tiepolo et al. 2007). This section is organized by groups of sites, while separately we review data on the extensive experimental work done in the system $\text{Na}_2\text{O}-\text{Li}_2\text{O}-\text{MgO}-\text{SiO}_2-\text{H}_2\text{O}-\text{HF}$ (LNMSH).

Experimental work on amphiboles during the last decades has been aimed at two main goals: (1) characterization of the stability and phase-relations of geologically relevant compositions as a function of variable P , T , X , f_{O_2} conditions in order to define tools for thermodynamic modeling and the interpretation of observed metamorphic or igneous paragenesis; (2) synthesis of homovalent or heterovalent solid-solutions, irrespective of their geological relevance, targeted at testing available crystal-chemical/structural models on amphiboles, or at calibrating their spectroscopic features for analytical purposes (at both the long-range and short-range scale). The results obtained following this second experimental philosophy are reviewed here, whereas a reasoned review of the results of the first approach is given in Evans (2007); additional work is discussed in Hawthorne and Della Ventura (2007) and Oberti et al. (2007a).

Synthetic amphiboles with cations other than Si and Al at the T sites

The ${}^{\text{T}}\text{Si}_{-1}{}^{\text{T}}\text{Ti}_1$ solid-solution in potassic-richterite. Following the work of Wagner and Velde (1986) who suggested the possible presence of ${}^{\text{T}}\text{Ti}$ in potassic-richterite from lamproites, Oberti et al. (1992) studied a suite of samples from different occurrences and showed that Ti^{4+} is a T cation in these amphiboles and is ordered at the more distorted $T(2)$ tetrahedron. To elucidate the incorporation mechanism of Ti^{4+} in the amphibole structure, Della Ventura et al. (1991, 1996a) investigated the synthetic join $[\text{K}^{\text{B}}(\text{NaCa})^{\text{C}}\text{Mg}_5^{\text{T}}\text{Si}_8\text{O}_{22}^{\text{W}}(\text{OH})_2]_x - [\text{K}^{\text{B}}(\text{NaCa})^{\text{C}}\text{Mg}_5^{\text{T}}(\text{Si}_7\text{Ti})\text{O}_{22}^{\text{W}}(\text{OH})_2]$, and showed that the amount of ${}^{\text{T}}\text{Ti}$ in potassic-richterite increases with T up to ~ 0.7 apfu at $T = 800$ °C, and that no significant increase in ${}^{\text{T}}\text{Ti}$ is observed at higher T . This finding is in agreement with the work of Oberti et al. (1992), who showed that in potassic-richterite, the dimension of the strip of octahedra is the largest in amphiboles, and couples with an A site filled with the largest monovalent cation available. In this amphibole composition, incorporation of T cations larger than Si^{4+} is thus favored. This is particularly true in high- T environments, when considering the larger thermal expansion of the octahedra with respect to the tetrahedra. The location of Ti^{4+} in these synthetic amphiboles was inferred by Della Ventura et al. (1991) by means of FTIR and Raman spectra, and later confirmed by synchrotron-radiation XAS (X-ray absorption spectroscopy: Mottana et al. 1990; Paris et al. 1993) and powder X-ray Rietveld refinement (Della Ventura et al. 1993a). The short-range distribution of Ti between the T sites was later clarified by Della Ventura et al. (1996a), using FTIR spectroscopy (see Hawthorne and Della Ventura 2007). Della Ventura et al. (1993a) studied OH-F substitution at the O(3) site in Ti-rich potassic-richterites along the nominal join $[\text{K}^{\text{B}}(\text{NaCa})^{\text{C}}\text{Mg}_5^{\text{T}}(\text{Si}_{7.4}\text{Ti}_{0.6})\text{O}_{22}^{\text{W}}(\text{OH}_{1.8}\text{F}_{0.2-x})]$, with $0 < x < 2$. Rietveld refinement of the $T(2)$ site occupancies showed that the amount of ${}^{\text{T}}\text{Ti}$ decreases rapidly from 0.60 to 0.16 apfu with increasing F in the solid-solution series (Fig. 6), again in agreement with the crystal-chemical model of Oberti et al. (1992). The incorporation of F linearly decreases the size of the $M(1)$ and $M(3)$ octahedra, and hence of the whole strip of octahedra; therefore, substitutions enlarging the tetrahedra make matching between the structure units more difficult. The geometrical control on the incorporation of ${}^{\text{T}}\text{Ti}$ in the structure of potassic-richterite predicts a favorable effect of Fe^{2+}

Figure 6. Schematic representation of Ti-rich potassic-richterite as a function of increasing F contents. R = potassic-richterite, FR = fluoro-potassic-richterite, RTi = Ti-rich potassic-richterite, FRTi = Ti-rich fluoro-potassic-richterite. Solid squares: synthetic compositions; all other symbols: natural samples from Oberti et al. (1992). [from Della Ventura et al. (1993a), *American Mineralogist*, 78, Fig. 8, p. 986].



substituting for Mg at the octahedra; to investigate this point, Sergent et al. (1996) studied the ${}^T\text{Si}_{-1}{}^T\text{Ti}_1$ exchange in synthetic potassic-ferrichterite [${}^A\text{K}{}^B(\text{NaCa}){}^C\text{Fe}^{2+}_5{}^T\text{Si}_8\text{O}_{22}{}^W(\text{OH})_2$] under variable f_{O_2} conditions. The incorporation of ${}^T\text{Ti}$ is significantly affected by the oxygen fugacity: under reducing conditions (MW buffer), the ${}^T\text{Ti}$ content reaches 0.6 apfu at 700 °C, to be compared with $\text{Ti} < 0.4$ apfu at 600 °C in potassic-richterite (Della Ventura et al. 1991), thus confirming the role of the size of the strip of octahedra.

The ${}^T\text{Si}_{-1}{}^T\text{Ge}_1$ solid-solution in richterite. The ${}^T\text{Si}_{-1}{}^T\text{Ge}_1$ substitution in richterite was studied by Senda et al. (2005). EMP data gave Si/Ge values in the crystals very close to the nominal ones, and refinement of the site occupancies showed that Ge has a strong preference for the $T(2)$ site (Fig. 7a). Notably, with increasing ${}^T\text{Si}_{-1}{}^T\text{Ge}_1$ substitution (and hence of the aggregate radius at the T sites) there is significant increase in kinking of the double chain (measured by a decrease of the O(5)-O(6)-O(5) angle, Fig. 7b). The OH-stretching spectra show one-mode behavior, which had never been observed in this spectral region for any type of substitution in monoclinic amphiboles: for increasing Ge in the sample, there is a linear downward shift ($\sim 40\text{ cm}^{-1}$) of both the main band assigned to the $\text{MgMgMg}^A\text{NaOH}(\text{Si,Ge})$ configuration and the minor band ($\sim 30\text{ cm}^{-1}$) assigned to the $\text{MgMgMg}^A\text{OH}(\text{Si,Ge})$ configuration. Such a behavior is consistent with the absence of short-range (Si,Ge) ordering at the T sites.

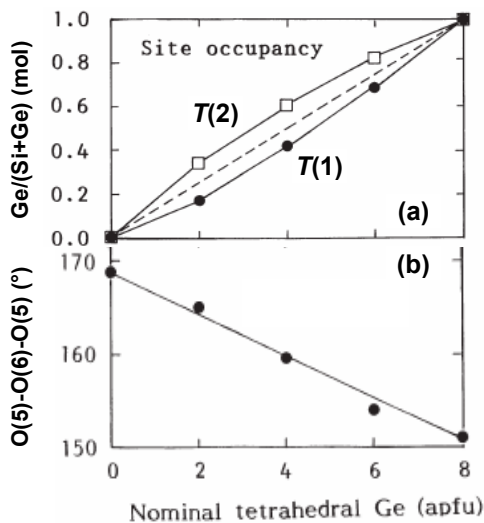


Figure 7. (a) Molar ratio of $\text{Ge}/(\text{Ge}+\text{Si})$ at the $T(1)$ and $T(2)$ sites as a function of nominal Ge (apfu); (b) variation of the O(5)-O(6)-O(5) kinking angle along the richterite-“Ge-richterite” join. Used by permission of the Mineralogical Society of America, from Senda et al. (2005), *American Mineralogist*, 90, Fig. 4, p. 1066 and Fig. 5, p. 1069.

Table 3. Experimental and analytical conditions for the amphiboles series reviewed in this chapter (in order of appearance); PXRD = powder X-ray diffraction, RREF = Rietveld refinement (X-ray), SREF = single-crystal refinement (X-ray), WCA = wet-chemical analysis, PNREF = Rietveld refinement of powder neutron diffraction data, DSC = differential scanning calorimetry, ED = electron diffraction.

Reference	R	T (°C)	P (kbar)	fO_2	Analytical techniques used to characterize the synthesis products
Della Ventura et al. (1991, 1996a)	1,2	900	1.0	—	SEM, PXRD, FTIR
Della Ventura et al. (1993a)	3	900	1.0	—	SEM, PXRD, RREF, FTIR, Raman
Senda et al. (2005)	4	795-905	7.20-7.56	—	SEM, HRTEM, AN-TEM, EMPA, RREF, FTIR
Sergent et al. (1996)	5	700	1.0	MW, NNO, HM	PXRD, FTIR, Mössbauer
Kohn and Komeforo (1955)	6	cooling from melt	0.001	—	WCA, PXRD, optical microscopy
Della Ventura et al. (1993b, 1996b)	7,8	750	1.0	—	SEM, RREF, FTIR
Della Ventura et al. (1997)	9	750	1.0	—	SEM, HRTEM, RREF, FTIR
Della Ventura et al. (1998)	10	700	2.0	—	SEM, HRTEM, EMPA, RREF, FTIR
Raudsepp et al. (1987a)	11	1273-799*	0.001*	—	SEM, RREF, MAS-NMR, FTIR
		800-930**	1.0-3.0**	—	
Raudsepp et al. (1991)	12	1273-816*	0.001*	—	SEM, PXRD, EMPA, FTIR
		718-903**	1.0-3.0**	—	
Raudsepp et al. (1987b)	13	1000	0.001	—	SEM, RREF
Oberti et al. (1998)	14	1200-770	0.001	—	EMPA, SREF
Oberti et al. (1999)	15	1270-800	0.001	—	EMPA, SREF
Fialips-Guédón et al. (2000)	16	900	3.0, 20.0	—	PXRD, EMPA, FTIR, AAS
Jenkins and Hawthorne (1995)	17	975-1000	2.92-3.20	—	SEM, RREF, EMPA,
Jenkins et al. (2002)	18	750-850**	10.0-17.5**	—	EMPA, RREF, FTIR
		986-1001*	7.11-6.93*	—	

Pavlovich Jr. and Jenkins (2003)	19	900	14.7-15.2	—	RREF, EMPA,
Della Ventura and Robert (1990), Robert et al. (1993)	20,21	750-800	1.0	—	PXRD, RREF, SEM, FTIR
Gottschalk et al. (1998)	22	750	2.0	—	SEM, RREF, EMPA, HRTEM, FTIR
Yang et al. (1999)	23	1400	150	—	EMPA, SREF
Iezzi et al. (2003a)	24	500	2.0-7.0	NNO to NNO+3	SEM, PXRD, Mössbauer, FTIR
Iezzi et al. (2004b)	25	700-800	4.0-5.5	NNO to NNO+3	SEM, PXRD, SREF, EMPA, Mössbauer, FTIR
Iezzi et al. (2005a)	26	500-600	1.0	NNO	SEM, PXRD, Mössbauer, FTIR
Iezzi et al. (2003b)	27	500	4.0	NNO	SEM, PXRD, Mössbauer, FTIR
Della Ventura et al. (2005a)	28	700	4.0	NNO+1	SEM, PXRD, Mössbauer, FTIR
Della Ventura et al. (2005b)	29	700-800	4.0	NNO to NNO+2,3	SEM, PXRD, EMPA, Mössbauer, FTIR
Maresch and Langer (1976)	30	750-875	1.0	—	PXRD, WCA, FTIR
Della Ventura (1992)	31	800	1.0	—	PXRD, FTIR
Melzer et al. (1998)	32	800	2.0	—	SEM, PXRD, HRTEM, EMPA, ICP-AES,
Gibbs et al. (1962)	33	Melt and solid- state reaction	0.001	—	WCA, PXRD, optical microscopy
Gier et al. (1964)	34	575-700	2-3	—	PXRD, WCA
Maresch et al. (1991), Liu et al. (1996), Cámara et al. (2004)	35,36,37	600	1.0	—	HRTEM, RREF, PNREF, DSC, ED, SREF, HT-FTIR, MAS-NMR
Iezzi et al. (2004c)	38	750-900	4.0-5.0	—	SEM, PXRD, EMPA, SREF, FTIR
Iezzi et al. (2006)	39	800	4.0	—	SEM, PXRD, TEM, ED, FTIR

* = F—series, ** = OH—series; R = reference code for Table 4.

Table 4. Selected unit-cell data for the amphiboles discussed in the text. The grouping refers to the nomenclature of Leake et al. (2003) and is based on charge arrangements.

Nominal composition	<i>a</i> (Å)	<i>b</i> (Å)	<i>c</i> (Å)	β (°)	<i>V</i> (Å ³)	Reference code*
Group 1						
A□ ^B Li ₂ C(Fe ²⁺ , Fe ³⁺) ^T Si ₈ O ₂₂ ^W (OH) ₂	9.489(2)	18.036(7)	5.313(3)	101.59(3)	890.80	24
A□ ^B Li ₂ C(Mg ₃ Fe ³⁺) ^T Si ₈ O ₂₂ ^W (OH) ₂	9.428(1)	17.878(3)	5.282(1)	102.06(2)	870.8(3)	25
A ^B Na ^B (LiMg) C ^M Mg ₅ ^T Si ₈ O ₂₂ ^W (OH) ₂	9.640(1)	17.907(3)	5.261(2)	101.98(2)	888.4(3)	39
Group 2						
A ^B Na ^B Ca ₂ C ^M Mg ₅ ^T (Si ₇ B) O ₂₂ ^W F ₂	9.807(5)	17.957(4)	5.266(6)	104.67**	897.13**	6
A ^B Na ^B Ca ₂ C(Mg ₄ Al) ^T (Si ₆ Al ₂) O ₂₂ ^W (OH) ₂	9.897(3)	17.940(5)	5.279(2)	105.54(4)	903.0(4)	10
A ^B Na ^B Ca ₂ C(Co ₄ Al) ^T (Si ₆ Al ₂) O ₂₂ ^W (OH) ₂	9.930(1)	17.869(2)	5.2980(7)	105.39(1)	911.46(1)	10
A ^B Na ^B Ca ₂ C(Mg ₄ Al) ^T (Si ₆ Al ₂) O ₂₂ ^W (OH) ₂	9.904(3)	17.941(5)	5.281(2)	105.54(3)	904.0(4)	12
A ^B Na ^B Ca ₂ C(Mg ₄ Cr) ^T (Si ₆ Al ₂) O ₂₂ ^W (OH) ₂	9.917(3)	17.998(6)	5.287(2)	105.41(2)	909.8(3)	12
A ^B Na ^B Ca ₂ C(Mg ₄ Ga) ^T (Si ₆ Al ₂) O ₂₂ ^W (OH) ₂	9.910(4)	17.976(7)	5.289(2)	105.54(3)	907.9(2)	12
A ^B Na ^B Ca ₂ C(Mg ₄ Al) ^T (Si ₆ Al ₂) O ₂₂ ^W F ₂	9.820(4)	17.896(6)	5.294(2)	105.30(3)	897.4(2)	12 ^S
A ^B Na ^B Ca ₂ C(Mg ₄ Ga) ^T (Si ₆ Al ₂) O ₂₂ ^W F ₂	9.850(4)	17.934(8)	5.301(2)	105.32(4)	903.1	14
A ^B Na ^B Ca ₂ C(Mg ₄ Se) ^T (Si ₆ Al ₂) O ₂₂ ^W F ₂	9.8852(4)	18.1574(7)	5.3186(2)	105.213(2)	921.18	11
A□ ^B Ca ₂ C(Mg ₃ Ga ₂) ^T (Si ₆ Ga ₂) O ₂₂ ^W (OH) ₂	9.8146(4)	18.052(1)	5.2807(3)	104.653(3)	905.2(1)	18
A□ ^B Ca ₂ C(Mg ₃ Ga ₂) ^T (Si ₆ Ga ₂) O ₂₂ ^W F ₂	9.8168(6)	18.020(1)	5.2820(4)	104.737(5)	903.7(1)	18
A□ ^B Ca ₂ C ^M Mg ₅ ^T Si ₈ O ₂₂ ^W (OH) ₂	9.8266(6)	18.0506(6)	5.2761(2)	104.684(3)	905.29(10)	22
A□ ^B Si ₂ C ^M Mg ₅ ^T Si ₈ O ₂₂ ^W (OH) ₂	10.1012(5)	18.2648(6)	5.2807(2)	105.704(3)	937.90(7)	22
A□ ^B Ca ₂ C ^M Mg ₅ ^T Si ₈ O ₂₂ ^W F ₂	9.8043(3)	18.021(1)	5.2657(2)	104.649(3)	900.1(1)	18
Group 3						
A ^B K ^B (CaNa) C ^M Mg ₅ ^T (Si _{7,2} Ti _{0,8}) O ₂₂ ^W (OH) ₂	10.086(2)	18.042(4)	5.300(2)	104.89(2)	932.1(4)	1
A ^B Na ^B (CaNa) C ^M Mg ₅ ^T Ge ₈ O ₂₂ ^W (OH) ₂	10.3244(8)	18.282(1)	5.3994(4)	106.015(4)	979.6(1)	4
A ^B Na ^B (CaNa) C ^M Mg ₅ ^T Si ₈ O ₂₂ ^W (OH) ₂	9.9076(6)	17.988(1)	5.2706(4)	104.252(4)	910.41	9

$^A\text{Na}^B(\text{CaNa})\text{C}\text{Ni}_5\text{T}_{18}\text{O}_{22}^{\text{w}}(\text{OH})_2$	9.890(1)	17.925(2)	5.2527(6)	104.501(8)	901.52	9
$^A\text{Na}^B(\text{CaNa})\text{C}\text{Co}_5\text{T}_{18}\text{O}_{22}^{\text{w}}(\text{OH})_2$	9.9724(7)	18.069(1)	5.2775(3)	104.261(5)	921.65	9
$^A\text{K}^B(\text{CaNa})\text{C}\text{Mg}_5\text{T}_{18}\text{O}_{22}^{\text{w}}(\text{OH})_2$	10.0547(8)	17.997(1)	5.2746(4)	104.832(5)	922.66	7
$^A\text{K}^B(\text{CaNa})\text{C}\text{Ni}_5\text{T}_{18}\text{O}_{22}^{\text{w}}(\text{OH})_2$	10.0297(7)	17.942(1)	5.2576(3)	104.982(5)	913.96	7
$^A\text{K}^B(\text{CaNa})\text{C}\text{Co}_5\text{T}_{18}\text{O}_{22}^{\text{w}}(\text{OH})_2$	10.1166(9)	18.066(1)	5.2752(4)	104.846(6)	931.94	7
$^A\text{Na}^B(\text{CaNa})\text{C}(\text{Mg}_5\text{Sc})\text{T}_{18}\text{Al}\text{O}_{22}^{\text{w}}\text{F}_2$	9.853(3)	18.061(8)	5.295(2)	104.49(3)	912.3	14
$^A\text{Na}^B(\text{NaSr})\text{C}\text{Mg}_5\text{T}_{18}\text{O}_{22}^{\text{w}}(\text{OH})_2$	10.024(2)	18.111(9)	5.2643(3)	104.96(1)	923.3(7)	20
$^A\text{K}^B(\text{NaSr})\text{C}\text{Mg}_5\text{T}_{18}\text{O}_{22}^{\text{w}}(\text{OH})_2$	10.1534(5)	18.115(1)	5.2723(4)	105.421(3)	934.82	21
$^A\text{Rb}^B(\text{NaCa})\text{C}\text{Mg}_5\text{T}_{18}\text{O}_{22}^{\text{w}}(\text{OH})_2$	10.1219(8)	18.006(1)	5.2752(4)	105.008(5)	928.6(1)	31
$^A\text{Na}^B(\text{NaCa})\text{C}\text{Mg}_5\text{T}_{18}\text{O}_{22}^{\text{w}}\text{F}_2$	9.840(6)	17.984(5)	5.260(6)	104.34(8)	901.8(14)	#
$^A\text{K}^B(\text{NaCa})\text{C}\text{Mg}_5\text{T}_{18}\text{O}_{22}^{\text{w}}\text{F}_2$	9.985(1)	17.984(4)	5.267(1)	104.85(1)	914.3(4)	#
Group 4						
$^A\text{Na}^B\text{Na}_2\text{C}(\text{Mg}_4\text{Al})\text{T}_{18}\text{Si}_8\text{O}_{22}^{\text{w}}(\text{OH})_2$	9.710(2)	17.927(3)	5.270(1)	102.67(1)	897.7(2)	12
$^A\text{Na}^B\text{Na}_2\text{C}(\text{Mg}_4\text{Cr})\text{T}_{18}\text{Si}_8\text{O}_{22}^{\text{w}}(\text{OH})_2$	9.787(5)	17.851(6)	5.277(3)	103.53(3)	896.3(6)	12
$^A\text{Na}^B\text{Na}_2\text{C}(\text{Mg}_4\text{In})\text{T}_{18}\text{Si}_8\text{O}_{22}^{\text{w}}\text{F}_2$	9.8527(3)	18.0966(7)	5.2928(2)	103.521(2)	917.55	13
$^A\text{Na}^B\text{Na}_2\text{C}(\text{Mg}_4\text{Sc}_2)\text{T}_{18}\text{Al}\text{O}_{22}^{\text{w}}\text{F}_2$	9.8425(5)	18.157(1)	5.3381(3)	103.979(4)	925.72	13
$^A\text{Na}^B\text{Na}_2\text{C}(\text{Mg}_4\text{Sc})\text{T}_{18}\text{Si}_8\text{O}_{22}^{\text{w}}\text{F}_2$	9.820(4)	18.036(6)	5.290(2)	103.64(2)	910.5	15
$^A\text{Na}^B\text{Na}_2\text{C}(\text{Mg}_4\text{Sc})\text{T}_{18}\text{Si}_8\text{O}_{22}^{\text{w}}\text{F}_2$	9.722(4)	17.813(6)	5.282(2)	103.69(2)	888.7	15
$^A\text{K}^B(\text{NaK})\text{C}\text{Mg}_5\text{T}_{18}\text{O}_{22}^{\text{w}}(\text{OH})_2$	10.1926(5)	18.1209(3)	5.2736(2)	105.514(5)	938.53(6)	23
$\square^A\text{B}\text{Na}_2\text{C}(\text{Fe}^{2+}_3\text{Fe}^{3+}_2)\text{T}_{18}\text{Si}_8\text{O}_{22}^{\text{w}}(\text{OH})_2$	9.773(1)	18.078(2)	5.3319(7)	103.40(1)	916.51	27
$\square^A\text{B}\text{Na}_2\text{C}(\text{Mg}_3\text{Fe}^{3+}_2)\text{T}_{18}\text{Si}_8\text{O}_{22}^{\text{w}}(\text{OH})_2$	9.7667(2)	17.9722(7)	5.3100(3)	103.501(3)	906.42(5)	29
$^A\text{Na}^B\text{Na}_2\text{C}(\text{Mg}_4\text{Fe}^{3+})\text{T}_{18}\text{Si}_8\text{O}_{22}^{\text{w}}(\text{OH})_2$	9.8144(2)	18.0236(6)	5.3062(2)	103.236(3)	913.70(5)	29
Group 5						
$^A\text{Na}^B(\text{NaMg})\text{C}\text{Mg}_5\text{T}_{18}\text{O}_{22}^{\text{w}}(\text{OH})_2$	9.738(1)	17.937(1)	5.272(1)	102.57(1)	898.95(16)	38
$^A\text{Na}^B(\text{NaMg})\text{C}\text{Mg}_5\text{T}_{18}\text{O}_{22}^{\text{w}}\text{F}_2$	9.648(3)	17.914(5)	5.264(3)	102.68(5)	887.6(5)	12

* see Table 3 for reference code. ** Recalculated from Kohn and Comפור (1955). § Data from Oberti et al. (1995b).

Data from Robert et al. (1989)

The ${}^T\text{Al}_{-1}{}^T\text{B}_1$ solid-solution in fluoro-edenite. Boron is an uncommon constituent in rock-forming silicates; however, it forms numerous silicoborates in which it occurs both in [3]- and in [4]-coordination (Anovitz and Grew 1996; Fleet and Muthupari 2000). Attempts to substitute ${}^T\text{Al}$ with ${}^T\text{B}$ in the amphibole structure date back to the sixties. However, to the best of our knowledge, only Kohn and Comeforo (1955) gave convincing proof of the synthesis of the boron analogue of fluoro-edenite with proposed composition: ${}^A\text{Na}_{0.93}{}^B(\text{Ca}_{1.87}\text{Na}_{0.13}){}^C\text{Mg}_{4.92}{}^T(\text{Si}_{7.16}\text{B}_{0.92})\text{O}_{22}{}^W\text{F}_{2.12}$. In fact, the reported unit-cell dimensions (Table 2) are in agreement with the presence of a smaller cation at the *T* sites (i.r. ${}^{14}\text{B} = 0.11 \text{ \AA}$) and with a lower *A*-site occupancy than in fluoro-edenite.

The ${}^T\text{Si}_{-1}{}^T\text{Ga}_1$ solid-solution in calcic amphiboles. The incorporation of ${}^T\text{Ga}$ in the amphibole structure has been investigated along the joins tremolite–Ga–pargasite (Jenkins and Hawthorne 1995), and tremolite–Ga–tschermakite (Jenkins et al. 2002). However, because the incorporation of ${}^T\text{Ga}$ is somewhat related with that of ${}^C\text{Ga}$, these experiments will be described in the following paragraph dealing with *C* cations.

Synthetic amphiboles with uncommon *C* cations

Divalent cations. Solid solution of ${}^C\text{Ni}$ and ${}^C\text{Co}$ has received much attention during the last few decades. Although these elements are not common constituents of natural amphiboles, they provide an excellent opportunity to characterize the control of the amphibole structure on substitutions involving divalent *C* cations without the complexity of manipulating (and analyzing) elements of variable oxidation state such as iron and manganese (synthesis of iron and manganese amphiboles has also been extensive, but will not be treated here; for these, the reader can refer to Ernst 1968; Charles 1974, 1975, 1980; Popp et al. 1976; Maresch and Czank 1983, 1988; Raudsepp et al. 1991; Holtstam 1992; Oberti et al. 1997).

Della Ventura (1992) and Della Ventura et al. (1993b, 1996b, 1997) investigated both richterite and potassic-richterite with variable amounts of ${}^C\text{Ni}$, ${}^C\text{Mg}$, and ${}^C\text{Co}$. HRTEM showed homogeneous defect-free structure, and no chain-arrangement faults in all the samples examined. The change in the measured unit-cell parameters as a function of composition revealed a strong effect of the electronic configuration of the *C* cation on site partitioning (more detail in Oberti et al. 2007a). Rietveld refinement gave compositions very close to the nominal ones, and showed that both Ni and Co are preferentially incorporated at the *M*(1,3) sites, with a slight preference for the *M*(3) octahedron; no Co or Ni was ever detected at the *M*(4) site. XANES (X-ray absorption near-edge structure) spectra recorded at the Ni *K*-edge on intermediate (Ni,Mg) potassic-richterite samples showed variations related to increasing ${}^C\text{Mg}_{-1}{}^C\text{Ni}_1$ substitution (Giuli et al. 2000). Calculation of XANES spectra (using the multiple-scattering theory) from the results of Della Ventura et al. (1993b) reproduced very well the experimental spectra, and suggested little or no Ni clustering in the samples, in agreement with the FTIR results of Della Ventura et al. (1996b).

The Co analogue of pargasite, ${}^A\text{Na}{}^B\text{Ca}_2{}^C(\text{Co}_4\text{Al}){}^T(\text{Si}_6\text{Al}_2)\text{O}_{22}{}^W(\text{OH})_2$, was synthesized by Della Ventura et al. (1998). Rietveld structure-refinement of powder X-ray diffraction data showed that Al is strongly ordered at the *M*(2) site in this composition, in agreement with the suggestion made by Oberti et al. (1995c) that the disorder of ${}^C\text{Al}$ over the *M*(3) and *M*(2) sites in pargasite is related to the fact that the size of the *M*(3) octahedron in this composition is smaller than expected on the basis of the aggregate ionic radius (more detail in Oberti et al. 2007a; Fig. 6). In line with this conclusion, the OH-stretching FTIR spectrum of the Co analogue of pargasite shows a single absorption band in the OH-stretching region, which indicates the occurrence of Co only at the *M*(1,3) sites (see also Oberti et al. 2007a).

Trivalent cations. Pargasitic amphiboles containing uncommon trivalent *C* cations [${}^A\text{Na}{}^B\text{Ca}_2{}^C(\text{Mg}_4\text{R}^{3+}){}^T(\text{Si}_6\text{Al}_2)\text{O}_{22}{}^W\text{W}_2$, with $\text{R}^{3+} = \text{Al, Ga, Cr, Sc and In}$ and $\text{W} = \text{OH or F}$] were synthesized and characterized by Raudsepp et al. (1987a, 1991). In the OH series, only for R^{3+}

= Al and Ga the product was close to the nominal composition (${}^C\text{Al} = 1.0$ apfu, ${}^C\text{Ga} = 0.91$ apfu, respectively), while for $\text{R}^{3+} = \text{Cr}, \text{Sc}$ and In , significant departure from the nominal composition was observed ($\text{Cr} = 0.56$, $\text{Sc} = 0.41$, $\text{In} = 0.17$ apfu, respectively; Raudsepp et al. 1991). Rietveld refinement of site occupancies and infrared spectroscopy showed the R^{3+} cations to be disordered over the $M(2)$ and $M(3)$ sites (Raudsepp et al. 1987a). In the F series, systematic deviations from the nominal compositions were observed for all cations: EMP analysis gave ${}^C\text{Al} = 0.81$ apfu, $\text{Cr} = 0.42$ apfu and $\text{Sc} = 0.92$ apfu, respectively (Raudsepp et al. 1991). Refinement of site occupancies showed all R^{3+} cations to be almost completely ordered at $M(2)$, in contrast with their OH- analogues. Ga-bearing fluoro-pargasite was later characterized by single-crystal structure refinement by Oberti et al. (1998), who found Ga almost equally partitioned between the octahedra and the tetrahedra (${}^C\text{Ga} = 0.45$ apfu, ${}^T\text{Ga} = 0.56$ apfu), with ${}^C\text{Ga}$ strongly ordered at the $M(2)$ site and ${}^T\text{Ga}$ disordered between the $T(1)$ and $T(2)$ sites.

The incorporation of Cr^{3+} in pargasite was also investigated by Fialips-Guédon et al. (2000). The crystal chemical formula of the most Cr-rich composition was: ${}^A\text{Na}_{0.93}{}^B(\text{Ca}_{1.83}\text{Na}_{0.17}){}^C(\text{Mg}_{3.88}\text{Al}_{0.63}\text{Cr}_{0.42}){}^T(\text{Si}_{6.31}\text{Al}_{1.69})\text{O}_{22}{}^W(\text{OH})_2$, very close (considering an intrinsic error of ± 10 -15% for the EMP analysis of fine-grained materials) to that reported by Raudsepp et al. (1991, sample 4). Analysis of the OH-stretching FTIR spectra suggested that Cr has a significant preference for $M(3)$ over $M(2)$, in agreement with the fact that this transition element systematically favors irregular coordination with different anions (in this case, four O and two ${}^W\text{OH}$; Robert and Gaspérin 1985; Della Ventura et al. 1993b, 1998).

Sodic-calcic amphiboles of nominal composition related to fluoro-magnesiokatophorite [${}^A\text{Na}{}^B(\text{NaCa}){}^C(\text{Mg}_4\text{R}^{3+}){}^T(\text{Si}_7\text{Al})\text{O}_{22}{}^W\text{F}_2$ with $\text{R}^{3+} = \text{Al}, \text{Ga}, \text{Sc}$] were studied by Oberti et al. (1998). Almost no Al was incorporated at the $M(2)$ site (0.03 apfu), actually yielding fluoro-edenite. Gallium was preferentially incorporated at the two independent $T(1,2)$ sites (0.47 apfu) rather than at the $M(2)$ site (0.20 apfu), yielding a Ga-rich fluoro-edenite. In contrast, a nearly stoichiometric fluoro-Sc-katophorite was obtained.

Raudsepp et al. (1987b, 1991) and Oberti et al. (1999) reported the synthesis and crystal chemistry of a series of eckermannitic amphiboles of nominal stoichiometry ${}^A\text{Na}{}^B\text{Na}_2{}^C(\text{Mg}_4\text{R}^{3+}){}^T\text{Si}_8\text{O}_{22}\text{W}_2$, with $\text{R}^{3+} = \text{Al}, \text{Ga}, \text{Cr}, \text{Ti}^{3+}, \text{V}^{3+}, \text{Sc}$ and In , and either OH or F as the W anion. In the OH series, all trivalent cations (but Cr) yielded significant deviation of the run product toward a composition intermediate between ${}^A\text{Na}{}^B(\text{NaMg}){}^C\text{Mg}_5{}^T\text{Si}_8\text{O}_{22}{}^W(\text{OH})_2$ and substituted glaucophane; the maximum Cr content was only 0.52 apfu (Raudsepp et al. 1991). A combination of chemical, structural and spectroscopic investigation of the crystals synthesized for the F series (Raudsepp et al. 1987b; Oberti et al. 1999) showed that compositions substituted with Sc, In and Cr^{3+} are closer to the nominal fluoro-eckermannite stoichiometry, whereas compositions substituted with Al, Ti^{3+} , V^{3+} and Ga contain almost negligible amounts of the nominal trivalent cation, and a strong excess of ${}^B\text{Mg}$, i.e. they deviate systematically from the nominal stoichiometry toward ${}^A\text{Na}{}^B(\text{NaMg}){}^C\text{Mg}_5{}^T\text{Si}_8\text{O}_{22}{}^W\text{F}_2$. Refinement of site occupancies showed that the highly charged cations are ordered at the $M(2)$ site, in agreement with a well-defined linear relation between $\langle M(2)\text{-O} \rangle$ and the aggregate cation radius at $M(2)$ (Fig. 8). Such strong deviations in samples synthesized under the same experimental conditions led Oberti et al. (1999) to conclude that ionic radius is not the only relevant factor, and that the electronic properties of the trivalent C cation have a significant effect on the stability of fluoro-eckermannite, at least under the experimental conditions used. In other words, for spherically symmetric trivalent cations, the increase in the ionic radius plays a significant role in the incorporation of a chemical species in the structure. Non-spherically symmetric cations behave differently, and their crystal-chemical role depends on their electronic configuration: Cr^{3+} ($3d^3$) stabilizes the fluoro-eckermannite structure, whereas V^{3+} ($3d^2$) does not. Recent studies with more powerful X-ray sources and area detectors (Cámara et al. 2007) show that at least some of these amphiboles are actually $P2_1/m$, with T_c close to room- T , but this feature does not modify the

conclusions about cation incorporation and partitioning discussed above. Therefore, the above results imply that end-member fluoro-eckermannite and eckermannite are unlikely to be stable phases, a conclusion with significant consequences for modeling of amphibole solid-solutions.

Raudsepp et al. (1987b, 1991) also reported the synthesis of the Sc analogue of fluoronyböite, with a composition very close to nominal ${}^A\text{Na} {}^B\text{Na}_2 {}^C(\text{Mg}_3\text{Sc}_2) {}^T(\text{Si}_7\text{Al}) \text{O}_{22} {}^W\text{F}_2$, and Sc strongly ordered at the $M(2)$ site. Nyböite and fluoronyböite are high- P amphiboles stable at T around 800 °C, and are replaced by taramite at lower P (Ungaretti et al. 1981; Oberti et al. 2003c); synthesis of the Sc analogue of nyböite at 1 atm suggests that the presence of ${}^C\text{Al}$ is critical to crystallization at high P , but that the charge arrangement of nyböite may be stable at lower P conditions when larger C cations occur.

Extensive experiments on the incorporation of Ga in amphiboles were done during the last two decades by D. Jenkins and co-workers with the intent of using Ga to decipher the Al behavior in amphiboles (incorporation and partitioning) for quantitative geothermobarometry. Jenkins and Hawthorne (1995) studied the join fluorotremolite–Ga–fluoropargasite [${}^A\Box {}^B\text{Ca}_2 {}^C\text{Mg}_5 {}^T\text{Si}_8 \text{O}_{22} {}^W\text{F}_2$ – ${}^A\text{Na} {}^B\text{Ca}_2 {}^C(\text{Mg}_4\text{Ga}) {}^T(\text{Si}_6\text{Ga}_2) \text{O}_{22} {}^W\text{F}_2$], where the composition of the amphibole can be expressed *via* the “Ga-pargasite” exchange ${}^A\Box_{-1} {}^C\text{Mg}_{-1} {}^T\text{Si}_{-2} {}^A\text{Na}_1 {}^C\text{Ga}_1 {}^T\text{Ga}_2$, which is a 1:1 combination of the “Ga-tschermak” ${}^C\text{Mg}_{-1} {}^T\text{Si}_{-1} [{}^6\text{Ga}] {}^T\text{Ga}_1$ and “Ga-edenite” ${}^A\Box_{-1} {}^T\text{Si}_{-1} {}^A\text{Na}_1 {}^T\text{Ga}_1$ exchanges. EMP analysis showed saturation in Ga in the amphibole at ~ 2.4 Ga apfu; Rietveld-refinement of site occupancies showed that ${}^C\text{Ga}$ is completely ordered at the $M(2)$ site and ${}^T\text{Ga}$ preferentially orders at the $T(1)$ site. The ratio ${}^T\text{Ga} : {}^C\text{Ga}$ along the join was systematically higher than expected. The authors suggested that F may favor the incorporation of Ga as a T cation. Jenkins et al. (2002) investigated the cation distribution in amphiboles along the join tremolite–Ga–tschermakite [${}^A\Box {}^B\text{Ca}_2 {}^C(\text{Mg}_3\text{Ga}_2) {}^T(\text{Si}_6\text{Ga}_2) \text{O}_{22} {}^W(\text{OH})_2$] and its F counterpart. In the OH series, the incorporation of Ga into the amphibole according to tschermak-type exchange is very limited (~ 0.3 apfu). In the F series, the incorporation of Ga in the amphibole is higher (~ 0.6 apfu) and follow the ${}^C\text{Ga} : {}^T\text{Ga}$ 1:2 ratio typical of the pargasite exchange. More recently, Pavlovich and Jenkins (2003) studied the join fluorotremolite–Ga–“fluoroglaucophane” [${}^A\Box {}^B\text{Na}_2 {}^C(\text{Mg}_3\text{Ga}_2) {}^T\text{Si}_8 \text{O}_{22} {}^W\text{F}_2$], and showed that the run products are complex solid-solutions in the fluoro-edenite–fluoronyböite–“fluoroglaucophane”–fluoro-magnesiokatophorite–“fluorocummingtonite” system, in close agreement with previous studies of Al-bearing systems (e.g. Pawley 1992; Welch and Graham 1992; Tropper et al. 2000). Syntheses with low Ga contents were primarily influenced by the edenite exchange, while those with high Ga contents were dominated by the glaucophane ${}^B\text{Ca}_{-1} {}^C\text{Mg}_{-1} {}^B\text{Na}_1 {}^C\text{Ga}_1$ exchange. Rietveld refinement showed that ${}^C\text{Ga}$ is ordered at the $M(2)$ site and ${}^T\text{Ga}$ is ordered at the $T(1)$ site (Pavlovich and Jenkins 2003).

Synthetic amphiboles with uncommon B cations

Cations larger than Na. The Sr-bearing analogues of richterite and potassic-richterite [${}^A\text{R}^+ {}^B(\text{NaSr}) {}^C\text{Mg}_5 {}^T\text{Si}_8 \text{O}_{22} {}^W(\text{OH})_2$, with $\text{R}^+ = \text{Na}$ or K] were synthesized by Della Ventura

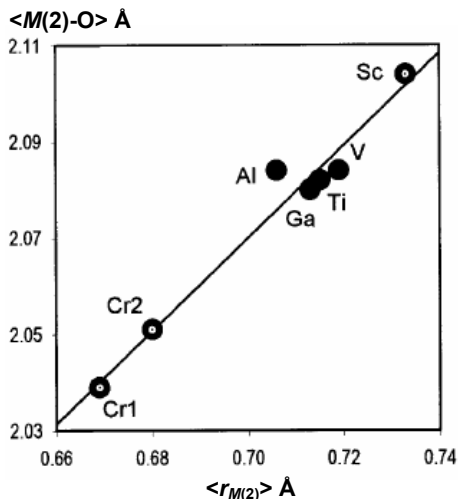


Figure 8. Correlation between the refined $\langle M(2)\text{-O} \rangle$ distance and the aggregate cation radius at the $M(2)$ site. Dotted circles: fluoro-eckermannite; filled circles: fluorrichterite [modified from Oberti et al. (1999), *American Mineralogist*, 84, Fig. 3, p.108].

and Robert (1990). Rietveld refinement of powder X-ray patterns (Robert et al. 1993) yielded site-occupancies consistent with Sr ordering at the $M(4)$ site; accordingly, a linear trend was observed for the $\langle M(4)\text{-O} \rangle$ distance, whereas the grand $\langle\langle M\text{-O} \rangle\rangle$ distance did not show any systematic variation. No violation of the $C2/m$ symmetry was detected.

Gottschalk et al. (1998) examined ${}^B\text{Ca}_{-1}{}^B\text{Sr}_1$ solid-solution in tremolite. HRTEM showed that the Sr analogue of tremolite is virtually free from structural defects, and that an increasing concentration of chain-multiplicity faults is observed with increasing Ca in the structure. The OH-stretching FTIR spectra show significant hyperfine modifications for increasing Sr in the amphibole, and bands at $3676\text{-}3679\text{ cm}^{-1}$ were assigned to configurations involving ${}^B\text{Sr}$ (Gottschalk et al. 1998). The FTIR lattice vibrational modes ($1400\text{-}600\text{ cm}^{-1}$) of these synthetic ${}^B(\text{Ca}, \text{Sr})$ -tremolites were analyzed by Andrut et al. (2000), who observed one-mode behavior for all the Si-O, Si-O-Si and O-Si-O modes, consistent with the absence of short-range order for Na/Ca and Ca/Sr at the $M(4)$ site.

Yang et al. (1999) synthesized at high- P conditions (15 GPa) the ${}^B\text{K}$ analogue of potassic-richterite, with composition close to ${}^A\text{K}{}^B(\text{KCa}){}^C\text{Mg}_5{}^T\text{Si}_8\text{O}_{22}{}^W(\text{OH})_2$. Single-crystal X-ray structure refinement showed that the substitution of K for Na at the $M(4)$ site significantly reduces the difference among the individual $M(4)\text{-O}$ bond lengths. The major structural adjustments were: (1) a shift of the B cation along the b -axis further away from the strip of octahedra; (2) an increase in the kinking and bowing of the double-chain of tetrahedra; (3) a decrease in the relative displacement of two adjacent double chains, which in this sample is the smallest found in amphiboles, in agreement with the extremely large value of the β angle (105.51°); (4) a simultaneous increase of the separation between two back-to-back double-chains of tetrahedra.

The incorporation of ${}^B\text{Li}$. Most of the experimental work on uncommon solid-solutions at the $M(4)$ site done during the last few years involves the study of the incorporation of ${}^B\text{Li}$ and ${}^B\text{Mg}$ in amphiboles. The crystal-chemistry of ${}^B\text{Mg}$ will be discussed in other chapters (Hawthorne and Oberti 2007b; Welch et al. 2007), because major ${}^B\text{Mg}$ in the amphibole structure (in cummingtonites, gedrites and anthophyllites) involves structural rearrangements leading to $P2_1/m$ or $Pnma$ space-group symmetry, respectively; here we will describe the results obtained with ${}^B\text{Li}$ as a major constituent, in essentially ${}^B\text{Mg}$ -free compositions.

Clinoholmquistite and its analogues. Recent studies have shown that there is no evidence for the occurrence of clinoholmquistite, the holotype being a mixture of tremolite and fluorosodic-pedrizite (Oberti et al. 2005). On the other hand, clinoholmquistites with dominant ${}^C\text{Fe}^{2+}$ and/or ${}^C\text{Fe}^{3+}$ are quite common although there is little evidence of their relative stability as a function of P and T (cf. the first part of this Chapter for more detail). End-member clinoferriferroholmquistite [${}^A\Box{}^B\text{Li}_2{}^C(\text{Fe}^{2+}_3\text{Fe}^{3+}_2){}^T\text{Si}_8\text{O}_{22}{}^W(\text{OH})_2$] was synthesized by Iezzi et al. (2003a), who showed that this composition is stable in a very limited T range ($500\text{-}600^\circ\text{C}$) for a wide range of pressures. Mössbauer and OH-stretching FTIR data show a strongly ordered cation distribution, in agreement with the prediction of Hawthorne (1997) on bond-valence grounds, and with single-crystal structure refinements of Li-rich amphiboles (Oberti et al. 2003a). The synthesis of clino-ferriferroholmquistite, ideally ${}^A\Box{}^B\text{Li}_2{}^C(\text{Mg}_3\text{Fe}^{3+}_2){}^T\text{Si}_8\text{O}_{22}{}^W(\text{OH})_2$, at varying f_{O_2} conditions was reported by Iezzi et al. (2004b). Based on single-crystal structure refinement of one sample, all X-ray powder patterns could be indexed in the space group $C2/m$. At low redox conditions, the amphibole departs strongly from the nominal composition according to the coupled exchange ${}^C\text{Fe}^{3+}{}_{-1}{}^B\text{Li}_1{}^C(\text{Mg}, \text{Fe}^{2+})_1{}^B(\text{Mg}, \text{Fe}^{2+})_1$ (never observed in natural amphiboles), leading to a charge arrangement close to ferriwinchite but with a totally new composition [$(\text{Mg}, \text{Fe}^{2+})_1\text{Li}_1$] at the $M(4)$ site. From a petrological point of view, an important conclusion of the work of Iezzi et al. (2004b) is the observation that under very oxidizing conditions, the amphibole composition is close to that of the starting bulk system, whereas the reverse is true for reducing conditions. In the system investigated, oxidizing conditions favor crystal-

lization of ferri-spodumene (Cámara et al. 2003); however, at these conditions, the ${}^{\text{C}}\text{Fe}^{3+} {}^{\text{B}}\text{Li}_{-1}$ ${}^{\text{C}}(\text{Mg}, \text{Fe}^{2+})_1 {}^{\text{B}}(\text{Mg}, \text{Fe}^{2+})_1$ exchange vector is almost non-active, and the composition of the amphibole is close to nominal. Reducing conditions favor crystallization of the amphibole relative to pyroxene, but they promote the ${}^{\text{C}}\text{Fe}^{3+} {}^{\text{B}}\text{Li}_{-1}$ ${}^{\text{C}}(\text{Mg}, \text{Fe}^{2+})_1 {}^{\text{B}}(\text{Mg}, \text{Fe}^{2+})_1$ exchange, and the amphibole composition diverges from the expected stoichiometry. In other words, the amphibole composition is ultimately controlled by local electroneutrality. Complete Mg-Fe²⁺ solid-solution (Fig. 9) in clino-ferriholmquistite, ideally ${}^{\text{A}}\square {}^{\text{B}}\text{Li}_2 {}^{\text{C}}[(\text{Mg}, \text{Fe}^{2+})_3\text{Fe}^{3+}_2] {}^{\text{T}}\text{Si}_8 \text{O}_{22} {}^{\text{W}}(\text{OH})_2$ was obtained by Iezzi et al. (2005a). Mössbauer spectra showed Fe³⁺ to be strongly ordered at the *M*(2) site, and Fe²⁺ disordered over the *M*(4) and *M*(1,2,3) sites; the infrared OH-stretching spectra of intermediate compositions showed an almost complete Mg-Fe²⁺ substitution at the *M*(1,3) sites, which occurs without significant short-range order.

The ${}^{\text{B}}\text{Li}_{-1} {}^{\text{B}}\text{Na}_1$ substitution has been studied experimentally in the Mg-free system along the clino-ferri-ferroholmquistite–riebeckite join $[{}^{\text{A}}\square {}^{\text{B}}\text{Li}_2 {}^{\text{C}}(\text{Fe}^{2+}_3\text{Fe}^{3+}_2) {}^{\text{T}}\text{Si}_8 \text{O}_{22} {}^{\text{W}}(\text{OH})_2 - {}^{\text{A}}\square {}^{\text{B}}\text{Na}_2 {}^{\text{C}}(\text{Fe}^{2+}_3\text{Fe}^{3+}_2) {}^{\text{T}}\text{Si}_8 \text{O}_{22} {}^{\text{W}}(\text{OH})_2]$ by Iezzi et al. (2003b), and in the Mg-bearing system along the clino-ferriholmquistite–magnesioriebeckite join $[{}^{\text{A}}\square {}^{\text{B}}\text{Li}_2 {}^{\text{C}}(\text{Mg}_3\text{Fe}^{3+}_2) {}^{\text{T}}\text{Si}_8 \text{O}_{22} {}^{\text{W}}(\text{OH})_2 - {}^{\text{A}}\square {}^{\text{B}}\text{Na}_2 {}^{\text{C}}(\text{Mg}_3\text{Fe}^{3+}_2) {}^{\text{T}}\text{Si}_8 \text{O}_{22} {}^{\text{W}}(\text{OH})_2]$ by Della Ventura et al. (2005a). These data allow us to conclude that in the Mg-free system, ${}^{\text{B}}\text{Li}_{-1} {}^{\text{B}}\text{Na}_1$ solid-solution is almost complete. In Mg-bearing system, solid solution is more complicated, and the variation in composition of the amphiboles synthesized can be described by the coupled exchange ${}^{\text{A}}\square_{-1} {}^{\text{B}}\text{Na}_{-1} {}^{\text{C}}\text{Fe}^{3+}_{-2} {}^{\text{A}}\text{Na}_1 {}^{\text{B}}\text{R}^{2+}_1 {}^{\text{C}}(\text{Mg}, \text{Fe}^{2+})_2$, where $\text{R}^{2+} = \text{Mg}, \text{Fe}^{2+}$ (Della Ventura et al. 2005a, 2005b). Li occurs at the *A* and *M*(4) site in (nominal) end-member clino-ferriholmquistite, and is ordered at the *M*(4) site in their solid solutions (Della Ventura et al. 2005a). The above exchange is coherent with the chemical variation observed for most natural alkali amphiboles (where, however, R²⁺ is predominantly Ca) in the magnesio-arfvedsonite–magnesioriebeckite join, as published in the literature from a wide range of occurrences (Fig. 10). Such a well-defined relation suggests that amphibole composition may be used to monitor f_{O_2} during crystallization (Della Ventura et al. 2005b).

As a last example of uncommon elements occurring at the *M*(4) site in amphiboles, Oberti et al. (2000b) showed that some synthetic amphiboles obtained by Maresch and Langer (1976) in the system Li₂O-Na₂O-MgO-SiO₂-H₂O (LNMSH) have *P*₂/*m* symmetry and composition ${}^{\text{A}}\text{Na}_{1.00} {}^{\text{B}}(\text{Mg}_{1.00} \text{Li}_{0.27} \text{H}_{0.12} \text{Na}_{0.61}) {}^{\text{C}}\text{Mg}_5 {}^{\text{T}}\text{Si}_8 \text{O}_{22} {}^{\text{W}}(\text{OH})_2$. This amphibole has the same charge arrangement as richterite, with only Mg at the *M*(1,2,3) sites and a very peculiar *M*(4) composition, which includes Mg, Li and minor but significant H. More detail on the issue of excess H in amphiboles is given in Oberti et al. (2007a).

Synthetic amphiboles with uncommon A cations

Iezzi et al. (2004b) produced a series of clino-ferri-ferroholmquistites with significant (up to ~0.2 apfu) Li at the *A* site, where the amount of ^ALi is inversely correlated with the f_{O_2} conditions of the synthesis. The reason for the incorporation of Li at the *A* site in clino-ferri-ferroholmquistite is not clear. It is worth noting here that the possible presence of Li at the *A* site in amphiboles was previously supported by Maresch and Langer (1976) in an orthorhombic amphibole with excess OH, synthesized in the system LiO₂-MgO-SiO₂-H₂O. In that case, the structural formula of the run product, obtained by combining wet chemical analysis of the bulk product with deductions from the FTIR OH-stretching spectra was ${}^{\text{A}}(\text{Li}_{0.27}\square_{0.73}) {}^{\text{B}}(\text{Mg}_{0.89}\text{Li}_{1.11}) {}^{\text{C}}\text{Mg}_{5.00} {}^{\text{T}}\text{Si}_{8.01} [\text{O}_{21.20} (\text{OH})_{0.80}] {}^{\text{W}}(\text{OH})_{2.00}$.

Della Ventura (1992) reported preliminary results on the synthesis of the Rb-analogue of richterite with variable amounts of ^W(OH,F). FTIR OH-spectroscopy indicated an *A* site virtually filled with Rb, i.e. a composition very close to nominal for the OH end-member. Melzer et al. (1998) studied the partition of Rb between richterite and aqueous alkali-rich chloride solutions, allowing the amphibole to grow in the presence of excess fluid containing Na, K and Rb. The resulting crystals were analyzed by EMP, and the coexisting fluids were analyzed by ICP-AES. HRTEM observations showed that the amphiboles are structurally well-ordered. The Rb-

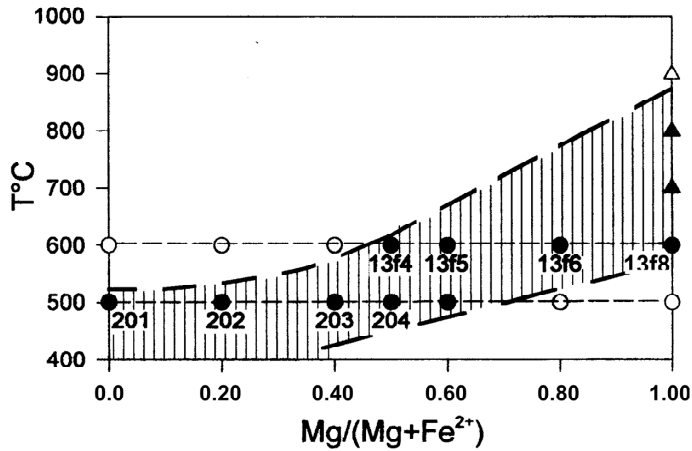


Figure 9. Schematic thermal stability field (stippled) of clino-ferrinolmquistite as a function of $\text{Mg}/(\text{Mg} + \text{Fe}^{2+})$ at 500 °C and 600 °C. Filled symbol: amphibole dominant, hollow symbol: pyroxene dominant. Filled triangles: data from Iezzi (2001) [from Iezzi et al. (2005a), *European Journal of Mineralogy*, 17, Fig. 2, p.735].

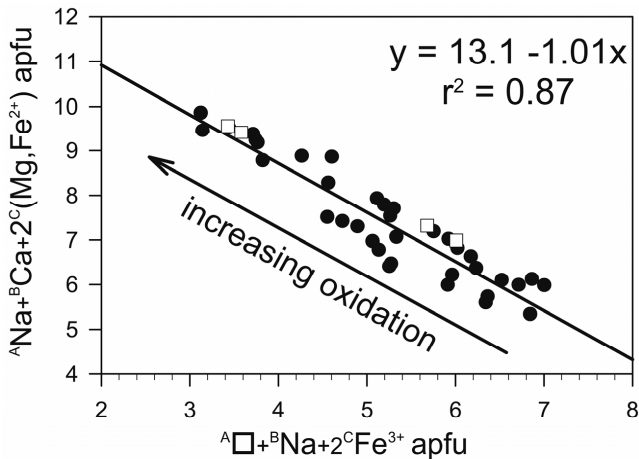


Figure 10. The ${}^{\text{C}}\text{Fe}^{3+} - {}^{\text{B}}\text{Na} - {}^{\text{C}}(\text{Mg}, \text{Fe}^{2+})_1$ vs. the ${}^{\text{A}}\square - {}^{\text{C}}\text{Fe}^{3+} - {}^{\text{A}}\text{Na} - {}^{\text{C}}(\text{Mg}, \text{Fe}^{2+})_1$ exchange for alkali amphiboles in the mineralogical literature (filled circle) and synthetic amphiboles in the magnesio-arfvedsonite–magnesioriebeckite join [from Della Ventura et al. (2005b), *American Mineralogist*, 90, Fig. 8, p.1381].

rich richterite synthesized in the presence of a Na-rich fluid has significant A-site vacancy, the most Rb-rich sample having an average composition ${}^{\text{A}}(\text{Rb}_{0.56}\text{Na}_{0.20}\square_{0.24})$. Experiments done in the presence of Na-K-Rb fluids showed even higher amounts of vacancy and A-site populations involving Na, K and Rb. In this series, the most Rb-rich sample has an average composition ${}^{\text{A}}(\text{Rb}_{0.43}\text{K}_{0.11}\text{Na}_{0.11}\square_{0.35})$. Strong enrichment of Rb in the fluid phase coexisting with the solid (Fig. 11) was observed, suggesting that K-Rb fractionation between alkali amphibole and fluid might have important consequences on the genesis of MARID-type rocks.

A final A cation, which should be mentioned in this context, is Ca in nominally synthetic fluoropargasite (with compositional deviation toward fluorocannilloite, Oberti et al. 1995b).

Detailed inspection of difference Fourier maps of these crystals suggested Ca to be mainly ordered at the A(2) site.

Common and uncommon W anions

The W anions common in Nature are OH^- , F^- , Cl^- and O^{2-} , and they occur at the O(3) site (Hawthorne and Oberti 2007a). Extensive experimental studies concerned the OH-F solid-solution at the O(3) site; however, because this is a common feature in Nature, it will not be treated here. Issues related to long-range order will be treated in Oberti et al. (2007a), and those related to OH-F short-range order will be discussed in Hawthorne and Della Ventura (2007).

A further uncommon W anion is the OD group; the substitution of D for H has been experimentally attempted only to use the D-enriched samples for spectroscopic or neutron diffraction studies; hence, this topic will be not treated here. For some detail, the reader can refer, among the others, to Iezzi et al. (2005b) and Ishida and Hawthorne (2006).

Synthesis of amphiboles in the system $\text{Na}_2\text{O-Li}_2\text{O-MgO-SiO}_2\text{-H}_2\text{O-HF}$ (LNMSH)

The first synthesis of a compound with composition close to $^A\text{Na}^B(\text{NaMg})^C\text{Mg}_5^T\text{Si}_8\text{O}_{22}^W\text{F}_2$ was reported by Gibbs et al. (1962). Two years later Gier et al. (1964) synthesized the OH-analogue of this compound.

Amphiboles have been synthesized extensively in the system $\text{Na}_2\text{O-MgO-SiO}_2\text{-H}_2\text{O} \pm \text{LiO}_2$ [(L)NMSH] by W. Maresch and co-workers during the 70's and 80s. Preliminary results in the Li-free system were published by Witte et al. (1969), who also reported the synthesis of an amphibole with nominal stoichiometry $^A\text{Na}^B\text{Na}_2^C\text{Mg}_5^T\text{Si}_8\text{O}_{21}(\text{OH})^W(\text{OH})_2$. Two new batches of this composition were synthesized by Maresch et al. (1991). HRTEM observations indicated less than 10% of triple-chain silicate in the crystallites, and minor amounts of SiO_2 -rich quench material, suggesting a composition of the amphibole close to nominal. Rietveld refinement of neutron-diffraction data on powders and electron diffraction indicate triclinic ($C1$ or $C\bar{1}$) symmetry. Electron diffraction also indicated a superstructure with a tripling of the b edge (Maresch et al. 1991). Heating experiments showed a phase transition to monoclinic C symmetry in the T range 100-160 °C, which was later investigated in details by Liu et al. (1996) (see Welch et al. 2007 for more details). These features were

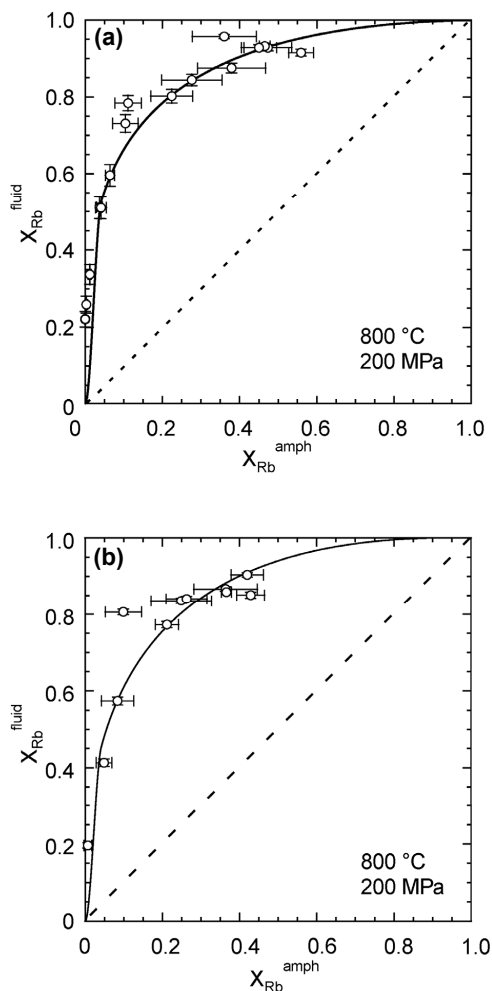


Figure 11. The amphibole/liquid partition coefficient for Rb in (a) K-free system, and (b) K-bearing system. $X_{\text{Rb}}^{\text{amph}} = {}^A\text{Rb}/A$ occupancy; $X_{\text{Rb}}^{\text{fluid}} = \text{Rb}/(\text{Rb}+\text{Na}\pm\text{K})$. [Used by permission of Springer/Berlin, from Melzer et al. (1998), *Contributions to Mineralogy and Petrology*, 133, Fig. 6, p.325.]

confirmed by single-crystal X-ray structure refinement by Cámara et al. (2004), and details on the structure and phase transition are given in Hawthorne and Oberti (2007a) and Welch et al. (2007), respectively.

Iezzi et al. (2004c) synthesized the nominal composition ${}^A\text{Na} {}^B(\text{NaMg}) {}^C\text{Mg}_5 {}^T\text{Si}_8 \text{O}_{22} \text{W}_2$ ($\text{W} = \text{OH}$ or F) at different conditions. EMP analysis showed that F is not incorporated into the amphibole structure under the hydrous experimental conditions used, whereas Raudsepp et al. (1991) obtained the F end-member [${}^A\text{Na} {}^B(\text{NaMg}) {}^C\text{Mg}_5 {}^T\text{Si}_8 \text{O}_{22} {}^W\text{F}_2$] in anhydrous conditions at $T = 816\text{--}1239$ °C and $P = 1$ atm. EMP analysis showed progressive departure from the nominal composition with increasing T , in accord with the exchange ${}^A\text{Na}_{-1} {}^B\text{Na}_{-1} {}^A\Box_1 {}^B\text{Mg}_1$. This feature suggests entropic stabilization of excess ${}^B\text{Mg}$ (Iezzi et al. 2004c), as also is the case for tremolite (Jenkins 1987; Hawthorne 1995). Single-crystal structure refinement shows that these amphiboles are $P2_1/m$ at room- T , allowing for a local environment more suitable for Na and Mg alternating at the $M(4)$ site. The infrared spectra of all samples show two well-defined absorption bands at 3742 and 3715 cm^{-1} , which can be assigned to O-H bands associated with the two independent anion sites [$\text{O}(3\text{A})$ and $\text{O}(3\text{B})$] in $P2_1/m$ symmetry.

Complete replacement of Na by Li along the ${}^A\text{Na} {}^B(\text{Na}_x\text{Li}_{1-x}\text{Mg}) {}^C\text{Mg}_5 {}^T\text{Si}_8 \text{O}_{22} {}^W(\text{OH})_2$ join was obtained by Iezzi et al. (2006). TEM analysis showed the presence of $h + k$ odd reflections in all samples, indicative of a P -type lattice for all compositions.

CONCLUDING REMARKS

All the work done in the last twenty five years on naturally occurring and synthetic amphiboles has greatly improved our knowledge of amphibole crystal-chemistry. It is now clear that the amphibole structure is rather unique, among silicate minerals, in its capability to incorporate at the major-element level most of the geologically relevant elements. However, some theoretically conceivable compositions (e.g., clinoholmquistite and eckermannite) cannot be attained, showing that the compliance of the amphibole structure is not enough to cover all the nominal compositional space. This evidence can be explained at least in two ways: (1) some amphibole compositions are less stable than other mineral assemblages under peculiar P , T , X conditions; (2) some amphibole compositions do not allow a proper matching of the different structural units.

Present crystal-chemical knowledge on amphiboles clearly shows that amphibole composition and cation ordering are ruled by several factors, among which the most important are: (1) electroneutrality and satisfaction of bond-valence requirements; (2) the geometric and electronic requirements of the various constituents; (3) the P and T conditions of crystallization. All these issues will be addressed in the following Chapters, and all the independent information collected in the last decades will be used to provide a detailed picture of the compliance of the amphibole structure and of its response to changes in the P , T , X conditions.

ACKNOWLEDGMENTS

Daisuke Nishio-Hamane is warmly thanked for providing unpublished data related to “potassic-titano-magnesianadanagaite”. Funding from the CNR project TAP01.004.002 is acknowledged.

REFERENCES

- Andrut M, Gottschalk M, Melzer S, Najorka J (2000) Lattice vibrational modes in synthetic tremolite–Srtremolite and tremolite-richterite solid-solutions. *Phys Chem Mineral* 27:301-309

- Anovitz LM, Grew ES (1996) Mineralogy, petrology and geochemistry of boron: an introduction. *Rev Mineral* 33:1-40
- Appleyard EC (1975) Silica-poor hastingsitic amphiboles from metasomatic alkaline gneisses at Wolfe, eastern Ontario. *Can Mineral* 13:342-351
- Armbruster T, Oberhänsli R, Bermanec V, Dixon R (1993) Hennomartinite and kornite, two new Mn³⁺ rich silicates from the Wessels mine, Kalahari, South Africa. *Schweiz Mineral Petrograph Mitt* 73:349-355
- Banno Y, Miyawaki R, Matsubara S, Makino K, Bunno M, Yamada S, Kamiya T (2004) Magnesiosadanagaite, a new member of the amphibole group from Kasuga-mura, Gifu Prefecture, central Japan. *Eur J Mineral* 16:177-183
- Bazhenov AG, Nedosekova IL, Petersen EU (1993) Fluorrichterite Na₂Ca(Mg,Fe)₅[Si₈O₂₂](F,OH)₂: A new mineral species in the amphibole group. *Zapiski VMO* 122(3):98-102 (in Russian)
- Bazhenov AG, Bazhenova LF, Krinova TV, Khvorov PV (1999) Potassicferrisadanagaite (K,Na) Ca₂(Fe²⁺,Mg)₃(Fe³⁺,Al)₂[Si₅Al₃O₂₂](OH)₂, a new mineral of the amphibole group (the Ilmen Mountains, the Southern Urals). *Zap Vser Mineral Obshchest* 128(4):50-55 (in Russian)
- Bazhenov AG, Nedosekova IL, Krinova TV, Mironov AB, Kvorov PV (2000) Fluormagnesioarfvedsonite Na Na₂(Mg,Fe²⁺)₄Fe³⁺[Si₈O₂₂](F,OH)₂ — A new mineral species of the amphibole group (Ilmen-Vishnevye Mountains alkaline massif, south Urals). *Zapiski VMO* 129(6):28-35 (in Russian, English abs.)
- Bazhenov AG, Mironov AB, Muftakhov VA, Kvorov PV (2005) Ferriwinchite NaCaMgFe³⁺[Si₈O₂₂](OH,F)₂ — a new amphibole-group mineral (Ilmenogorsky alkaline complex, Southern Urals) *Zapiski VMO* 134(3):74-77
- Benimoff AI, Benoit PH, Moore PB, Sclar CB (1991) A unique manganese-rich silicic edenite in the Grenville marble, Fowler, New York. *Am Mineral* 76:1431-1433
- Bojar H-P, Walter F (2006) Fluoro-magnesiohastingsite from Dealul Uroi (Hunedoara county, Romania): Mineral data and crystal structure of a new amphibole end-member. *Eur J Mineral* 18:503-508
- Burke EAJ, Leake BE (2004) "Named amphiboles": a new category of amphiboles recognized by the International Mineralogical association (IMA) and a defined sequence order for the use of the prefixes in amphibole names. *Am Mineral* 90:516-517
- Caballero JM, Monge A, La Iglesia A, Tornos F (1998) Ferri-clinoholmquistite, Li₂(Fe²⁺,Mg)₃Fe³⁺Si₈O₂₂(OH)₂, a new ⁶Li clin amphibole from the Pedriza Massif, Sierra de Guadarrama, Spanish Central System. *Am Mineral* 83:167-171
- Caballero JM, Oberti R, Ottolini L (2002) Ferripedrizite, a new monoclinic ⁶Li amphibole end-member from the Eastern Pedriza Massif, Sierra de Guadarrama, Spain, and a restatement of the nomenclature of Mg-Fe-Mn-Li amphiboles. *Am Mineral* 87:976-982.
- Cámara F, Iezzi G, Oberti R (2003) HT-XRD study of synthetic ferrian magnesium spodumene: the effect of site dimension on the P2₁/c ↔ C2/c phase transition. *Phys Chem Mineral* 30:20-30
- Cámara F, Oberti R, Della Ventura G, Maresch WV, Welch MD (2004) The crystal-structure of synthetic Na Na₂Mg₅Si₈O₂₁(OH)₃, a triclinic C¹ amphibole with a triple-cell and H excess. *Am Mineral* 89:1464-1473
- Cámara F, Oberti R (2005) The crystal-chemistry of holmquistites: Ferroholmquistite from Greenbushes (Western Australia) and hints for compositional constraints in ⁶Li amphiboles. *Am Mineral* 90:1167-1176
- Cámara F, Oberti R, Casati N (2007) The P2₁/m ↔ C2/m phase transition in amphiboles: new data on synthetic Na(NaMg)Mg₅Si₈O₂₂F₂ and the role of differential polyhedral expansion. *Zeit Kristallogr* (in press)
- Charles RW (1974) The physical properties of the Mg-Fe richterites. *Am Mineral* 59:518-528
- Charles RW (1975) The phase equilibria of richterite and ferrichterite. *Am Mineral* 60:367-374
- Charles RW (1980) Amphiboles on the join pargasite-ferropargasite. *Am Mineral* 65:996-1001
- Chukanov NV, Konilov AN, Zadov AE, Belakovsky DI, Pekov IV (2002) The new amphibole potassic chloropargasite (K,Na) Ca₂(Mg,Fe²⁺)₄Al(Si₆Al₂O₂₂)(Cl,OH)₂ and conditions of its formation in the granulite complex of Sal'nye Tundry Massif (Kola Peninsula). *Zapiski VMO* 131(2):58-62
- Della Ventura G (1992) Recent developments in the synthesis and characterization of amphiboles. *Synthesis and crystal-chemistry of richterites*. *Trends Mineral* 1:153-192
- Della Ventura G, Robert JL (1990) Synthesis, XRD and FT-IR studies of strontium richterites. *Eur J Mineral* 2:171-175
- Della Ventura G, Robert JL, Bény JM (1991) Tetrahedrally coordinated Ti⁴⁺ in synthetic Ti-rich potassic richterite: Evidence from XRD, FTIR and Raman studies. *Am Mineral* 76:1134-1140
- Della Ventura G, Parodi GC, Maras A (1992) Potassium-fluor-richterite, a new amphibole from San Vito, Monte Somma, Campania, Italy. *Rendiconti Acc Lincei, Serie 9*, 3:239-245
- Della Ventura G, Robert JL, Bény JM, Raudsepp M, Hawthorne FC (1993a) The OH-F substitution in Ti-rich potassic-richterites: Rietveld structure refinement and FTIR and microRaman spectroscopic studies of synthetic amphiboles in the system K₂O-Na₂O-CaO-MgO-SiO₂-TiO₂-H₂O-HF. *Am Mineral* 78:980-987
- Della Ventura G, Robert JL, Raudsepp M, Hawthorne FC (1993b) Site occupancies in monoclinic amphiboles: Rietveld structure refinement of synthetic nickel magnesium cobalt potassium richterite. *Am Mineral* 78:633-640
- Della Ventura G, Robert JL, Hawthorne FC, Prost R (1996a) Short-range disorder of Si and Ti in the tetrahedral double-chain unit of synthetic Ti-bearing potassium-richterite. *Am Mineral* 81:56-60

- Della Ventura G, Robert JL, Hawthorne FC (1996b) Infrared spectroscopy of synthetic (Ni,Mg,Co)-potassium-richterite. *Geochim Cosmochim Acta*, spec. vol. 5:55-63
- Della Ventura G, Robert JL, Raudsepp M, Hawthorne FC, Welch M (1997) Site occupancies in synthetic monoclinic amphiboles: Rietveld structure-refinement and infrared spectroscopy of (nickel, magnesium, cobalt)-richterite. *Am Mineral* 82:291-301
- Della Ventura G, Robert JL, Hawthorne FC, Raudsepp M, Welch MD (1998) Contrasting ^{69}Al ordering in synthetic Mg- and Co-pargasite. *Can Mineral* 36:1237-1244
- Della Ventura G, Redhammer GJ, Iezzi G, Hawthorne FC, Papin A, Robert JL (2005a) A Mössbauer and FTIR study of synthetic amphiboles along the magnesioriebeckite-ferri-clinoholmquistite join. *Phys Chem Mineral* 32:103-113
- Della Ventura G, Iezzi G, Redhammer GJ, Hawthorne FC, Scaillet B, Novembre D (2005b) Synthesis and crystal-chemistry of alkali amphiboles in the system $\text{Na}_2\text{O-MgO-FeO-Fe}_2\text{O}_3\text{-SiO}_2\text{-H}_2\text{O}$ as a function of f_{O_2} . *Am Mineral* 90:1375-1383
- Ernst WG (1968) *Amphiboles*. Springer-Verlag, Berlin.
- Evans BW (2007) The synthesis and stability of some end-member amphiboles. *Rev Mineral Geochem* 67:261-286
- Fleet ME, Muthupari S (2000) Boron K-edge XANES of borate and borosilicate minerals. *Am Mineral* 85:1009-1021
- Fialips-Guédon CI, Robert JL, Delbove F (2000) Experimental study of Cr incorporation in pargasite. *Am Mineral* 85:687-693
- Ghose S (1981) Subsolidus reaction and microstructures in amphiboles. *Rev Mineral* 9A:325-372
- Ghose S, Kersten M, Langer K, Rossi G, Ungaretti L (1986) Crystal field spectra and Jahn Teller effect of Mn^{3+} in clinopyroxene and clin amphiboles from India. *Phys Chem Mineral* 13:291-305
- Gianfagna A, Oberti R (2001) Fluoro-edenite from Biancavilla (Catania, Sicily, Italy): Crystal chemistry of a new amphibole end-member. *Am Mineral* 86:1489-1493
- Gibbs GV, Miller JL, Shell HR (1962) Synthetic fluor-magnesio-richterite. *Am Mineral* 47:75-82
- Gier TE, Cox NL, Young HS (1964) The hydrothermal synthesis of sodium amphiboles. *Inorg Chem* 3:1001-1004
- Gilbert MC, Helz RT, Popp RK, Spear FS (1982) Experimental studies of amphibole stability. *Rev Mineral* 9B:229-353
- Ginzburg IV (1965) Holmquistite and its structural variety clinoholmquistite. *Trudy Mineralogicheskogo Muzeya Akademii Nauk SSSR* 16:73-89
- Giuli G, Paris E, Ziyu W, Berrettoni M, Della Ventura G, Mottana A (2000) Nickel site distribution and clustering in synthetic double-chain silicates by experimental and theoretical XANES spectroscopy. *Phys Review B* 62:5473-5477
- Gottschalk M, Najorka J, Andrut M (1998) Structural and compositional characterization of synthetic (Ca,Sr)-tremolite and (Ca,Sr)-diopside solid solutions. *Phys Chem Mineral* 25:415-428
- Hawthorne FC (1978) The crystal chemistry of the amphiboles. VIII. The crystal structure and site chemistry of fluor-riebeckite. *Can Mineral* 16:187-194
- Hawthorne FC (1995) Entropy driven disorder in end-member amphiboles. *Can Mineral* 33:1189-1204
- Hawthorne FC (1997) Short-range order in amphiboles: a bond-valence approach. *Can Mineral* 35:201-216
- Hawthorne FC, Della Ventura G (2007) Short-range order in amphiboles. *Rev Mineral Geochem* 67:173-222
- Hawthorne FC, Grundy HD (1977) The crystal chemistry of the amphiboles. III. Refinement of the crystal structure of a sub-silicic hastingsite. *Mineral Mag* 41:43-50
- Hawthorne FC, Oberti R (2007a) Amphiboles: crystal chemistry. *Rev Mineral Geochem* 67:1-54
- Hawthorne FC, Oberti R (2007b) Classification of the amphiboles. *Rev Mineral Geochem* 67:55-88
- Hawthorne FC, Oberti R, Ungaretti L, Grice JD (1992) Leakeite, $\text{Na Na}_2 (\text{Mg}_2\text{Fe}^{3+}\text{Li}) \text{Si}_8 \text{O}_{22} (\text{OH})_2$, a new alkali amphibole from the Kajlidongri manganese mine, Jhabua district, Madhya Pradesh, India. *Am Mineral* 77:1112-1115
- Hawthorne FC, Ungaretti L, Oberti R, Bottazzi P (1993) Li: an important component in igneous alkali amphiboles. *Am Mineral* 78:733-745
- Hawthorne FC, Ungaretti L, Oberti R, Cannillo E, Smelik EA (1994) The mechanism of ^{69}Li incorporation in amphibole. *Am Mineral* 79:443-451
- Hawthorne FC, Oberti R, Cannillo E, Sardone N, Zanetti A, Grice JD, Ashley PM (1995) A new anhydrous amphibole from the Hoskins mine, Grenfell, New South Wales, Australia: description and crystal structure of ungarrettite, $\text{Na Na}_2 (\text{Mn}^{3+}_3 \text{Mn}^{2+}_2) \text{Si}_8 \text{O}_{22} \text{O}_2$. *Am Mineral* 80:165-172
- Hawthorne FC, Oberti R, Ungaretti L, Grice JD (1996a) A new hyper-calcic amphibole with Ca at the A site: Fluor-cannilloite from Pargas, Finland. *Am Mineral* 81:95-1002
- Hawthorne FC, Oberti R, Ungaretti L, Ottolini L, Grice JD, Czamanske GK (1996b) Fluor-ferro-leakeite, $\text{Na Na}_2 (\text{Fe}_2^{2+}\text{Fe}_3^{3+}\text{Li}) \text{Si}_8 \text{O}_{22} \text{F}_2$, a new alkali amphibole from the Canada Pinabete Pluton, Questa, New Mexico, U.S.A. *Am Mineral* 81:226-228

- Hawthorne FC, Oberti R, Ottolini L, Foord EE (1996c) Lithium-bearing fluor-arfvedsonite from Hurricane Mountain, New Hampshire: a crystal-chemical study. *Can Mineral* 34:1015-1019
- Hawthorne FC, Oberti R, Zanetti A, Czamanske GK (1998) The role of Ti in hydrogen-deficient amphiboles: sodic-calcic and sodic amphiboles from Coyote Peak, California. *Can Mineral* 36:1253-1265
- Hawthorne FC, Cooper MA, Grice JD, Ottolini L (2000) A new anhydrous amphibole from the Eifel region, Germany: Description and crystal structure of obertiite, $\text{Na Na}_2 (\text{Mg}_3\text{Fe}^{3+}\text{Ti}^{4+}) \text{Si}_8 \text{O}_{22} \text{O}_2$. *Am Mineral* 85:236-241
- Hawthorne FC, Oberti R, Cannillo E, Ottolini L, Roelofsen JN, Martin RM (2001) Li-bearing arfvedsonitic amphiboles from the Strange Lake peralkaline granite, Quebec. *Can Mineral* 39:1161-1170
- Holtstam D (1992) Hydrothermal synthesis of manganese-richterite and the Mg/Mn-substitution in richteritic amphiboles. *Neues J Miner Mh* 1992:241-250
- Iezzi G (2001) Cristalochimie des amphiboles à lithium, approche expérimentale. Unpublished PhD Thesis, University of Orléans (France).
- Iezzi G, Della Ventura G, Pedrazzi G, Robert JL, Oberti R (2003a) Synthesis and characterisation of ferri-clinoferroholmquistite, $\square \text{Li}_2 (\text{Fe}^{2+}_3\text{Fe}^{3+}_2) \text{Si}_8 \text{O}_{22} (\text{OH})_2$. *Eur J Mineral* 15:321-327
- Iezzi G, Della Ventura G, Cámara F, Pedrazzi G, Robert JL (2003b) The $^{\text{B}}\text{Na}$ - $^{\text{B}}\text{Li}$ exchange in A-site vacant amphiboles: synthesis and cation ordering along the ferri-clinoferroholmquistite-riebeckite join. *Am Mineral* 88:955-961
- Iezzi G, Della Ventura G, Cámara F, Oberti R, Robert J-L (2004a) Li-bearing amphiboles: synthesis, stability and composition of clinoholmquistites. 32nd International Geological Congress, Abstracts:231.7
- Iezzi G, Cámara F, Della Ventura G, Oberti R, Pedrazzi G, Robert JL (2004b) Synthesis, crystal structure and crystal-chemistry of ferri-clinoholmquistite, $\square \text{Li}_2 (\text{Mg}_3\text{Fe}^{3+}_2) \text{Si}_8 \text{O}_{22} (\text{OH})_2$. *Phys Chem Mineral* 31:375-385
- Iezzi G, Della Ventura G, Oberti R, Cámara F, Holtz F (2004c) Synthesis and crystal-chemistry of Na (NaMg) $\text{Mg}_5 \text{Si}_8 \text{O}_{22} (\text{OH})_2$, a $P2_1/m$ amphibole. *Am Mineral* 89:640-646
- Iezzi G, Della Ventura G, Hawthorne FC, Pedrazzi G, Robert JL, Novembre D (2005a) The (Mg,Fe²⁺) substitution in ferri-clinoholmquistite, $\square \text{Li}_2 (\text{Mg},\text{Fe}^{2+})_3 \text{Fe}^{3+}_2 \text{Si}_8 \text{O}_{22} (\text{OH})_2$. *Eur J Mineral* 17:733-740
- Iezzi G, Gatta GD, Kockelmann W, Della Ventura G, Rinaldi R, Schäfer W, Piccinini, M, Gaillard F (2005b) Low-T neutron powder diffraction and synchrotron-radiation IR study of synthetic amphibole Na NaMg $\text{Mg}_5 \text{Si}_8 \text{O}_{22} (\text{OH})_2$. *Am Mineral* 90:695-700
- Iezzi G, Della Ventura G, Tribaudino M (2006) Synthetic $P2_1/m$ amphiboles in the system Li_2O - Na_2O - MgO - SiO_2 - H_2O (LNMSH). *Am Mineral* 91:425-429
- Ishida K, Hawthorne FC (2006) Assignment of the OH-stretching bands in calcic amphiboles through deuteration and heat treatment. *Am Mineral* 91:871-879
- Jenkins DM (1987) Synthesis and characterization of tremolite in the system H_2O - CaO - MgO - SiO_2 . *Am Mineral* 72:707-715
- Jenkins DM, Hawthorne FC (1995) Synthesis and Rietveld refinement of amphibole along the join $\text{Ca}_2\text{Mg}_5\text{Si}_8\text{O}_{22}\text{F}_2$ - $\text{NaCa}_2\text{Mg}_4\text{Ga}_3\text{Si}_6\text{F}_2$. *Can Mineral* 33:13-24.
- Jenkins DM, Ishida K, Liogys V, Ghosh D (2002) Cation distribution in amphiboles synthesized along the Ga analogue of the tremolite-aluminotschermakite join. *Phys Chem Mineral* 29:87-97
- Kawachi Y, Coombs DS, Leake BE, Hinton RW (2002) The anhydrous amphibole ungarrettiite from the Woods mine, New South Wales, Australia. *Eur J Mineral* 14:75-377
- Kohn JA, Comeforo JE (1955) Synthetic asbestos investigations, II: X-ray and other data on synthetic fluor-richterite, -edenite, and -boron edenite. *Am Mineral* 40:410-421
- Konishi H, Groy TL, Dódony I, Miyawaki R, Matsubara S, Buseck PR (2003) Crystal structure of protoanthophyllite: A new mineral from the Takase ultramafic complex, Japan. *Am Mineral* 88:1718-1723
- Korinevsky VG, Korinevsky EV (2006) Potassic-magnesiosthastingsite (K,Na) $\text{Ca}_2 (\text{Mg},\text{Fe}^{2+})_4 (\text{Fe}^{3+},\text{Al},\text{Ti}) [\text{Si}_6\text{Al}_2\text{O}_{22}] (\text{OH},\text{Cl})_2$ – the new mineral species of amphiboles. *Zapiski VMO* 135(2):49-57
- Kullerød K, Erambert M (1999) Cl-scapolite, Cl-amphibole, and plagioclase equilibria in ductile shear zones at Nusfjord, Lofoten, Norway; implications for fluid compositional evolution during fluid-mineral interaction in the deep crust. *Geochim Cosmochim Acta* 63:3829-3844
- Leake BE (1968) A catalog of analyzed calciferous and subcalciferous amphiboles together with their nomenclature and associated minerals. Geological Society of America Special Paper 98
- Leake BE (1978) Nomenclature of amphiboles. *Can Mineral* 16:501-520
- Leake BE, Woolley AR, Arps CES, Birch WD, Gilbert MC, Grice JD, Hawthorne FC, Kato A, Kisch HJ, Krivovichev VG, Linthout K, Laird J, Mandarino JA, Maresch WV, Nickel EH, Rock NMS, Schumacher JC, Smith DC, Stephenson NCN, Ungaretti L, Whittaker EJW, Guo Y (1997) Nomenclature of amphiboles: Report of the subcommittee on amphiboles of the International Mineralogical Association, Commission on New Minerals and Mineral Names. *Am Mineral* 82:1019-1037

- Leake BE, Woolley AR, Birch WD, Burke EAJ, Ferraris G, Grice JD, Hawthorne FC, Kisch HJ, Krivovichev VG, Schumacher JC, Stephenson NCN, Whittaker EJW (2003) Nomenclature of amphiboles: additions and revisions to the International Mineralogical Association's amphibole nomenclature. *Can Mineral* 41:1355-1370
- Litvin AL, Ginzburg IV, Egorova LN, Petrunina AA (1975) On the crystal structure of clinoholmquistite. *Konstitutsiya i Svoystva Mineralov* 9:3-6
- Liu S, Welch MD, Klinowski J, Maresch WV (1996) A MAS NMR study of a monoclinic/triclinic phase transition in an amphibole with excess OH: $\text{Na}_3\text{Mg}_5\text{Si}_8\text{O}_{21}(\text{OH})_3$. *Eur J Mineral* 8:223-229
- Lupulescu MV, Rakovan J, Robinson GW, Hughes JM (2005) Fluoropargasite, a new member of the Group 2, calcic amphiboles, from Edenville, Orange County, New York. *Can Mineral* 43:1423-1428
- Lupulescu MV, Rakovan J, Dyar MD, Robinson GW, Hughes JM (2007): Fluoro-potassichastingsite from Greenwood mine (Orange County, New York, USA): a new end member of the calcic amphiboles. *Can Mineral* 44 (n press)
- Maresch WV, Langer K (1976) Synthesis, lattice constants and OH-valence vibrations of an orthorhombic amphibole with excess OH in the system $\text{Li}_2\text{O}-\text{MgO}-\text{SiO}_2-\text{H}_2\text{O}$. *Contrib Mineral Petrol* 56:27-34
- Maresch WV, Czank M (1983) Phase characterization of synthetic amphiboles on the join $\text{Mn}_{2-x}\text{Mg}_{7-x}[\text{Si}_8\text{O}_{22}](\text{OH})_2$. *Am Mineral* 68:744-753
- Maresch WV, Czank M (1988) Crystal chemistry, growth kinetics and phase relationships of structurally disordered ($\text{Mn}^{2+}, \text{Mg}$)-amphiboles. *Fortsch Mineral* 66:69-121
- Maresch WV, Miehe G, Czank M, Fuess H, Schreyer W (1991) Triclinic amphibole. *Eur J Mineral* 3:899-903
- Matsubara S, Miyawaki R, Kurosawa M, Suzuki Y (2002) Potassicleakeite, a new amphibole from the Tanohata mine, Iwate Prefecture, Japan. *J Mineral Petrol Sci* 97:177-184
- Melzer S, Gottschalk M, Heinrich W (1998) Experimentally determined partitioning of Rb between richterites and aqueous (Na,K)-chloride solutions. *Contrib Mineral Petrol* 133:315-328
- Mogessie A, Purtscheller F, Tessadri R (1986) High alumina calcic amphiboles (alumino pargasite-magnesio sadanagaite) from metabasites and metacarbonates of central Oetztal, Eastern Alps (Northern Tyrol, Austria). *N Jb Mineral Abh* 154:21-39
- Moore PB (1969) Joesmithite: a novel amphibole crystal chemistry. *In: Pyroxenes and amphiboles: crystal chemistry and phase petrology*. Papike JJ (ed) Mineralogical Society of America Special Paper 2:111-115
- Moore PB, Davis AM, Van Derveer DG, Sen Gupta, PK (1993) Joesmithite, a plumbous amphibole revisited and comments on bond valences. *Mineral Petrol* 48:97-113
- Mottana A, Paris E, Della Ventura G, Robert JL (1990) Spectroscopic evidence for tetrahedrally coordinated titanium in richteritic amphiboles. *Rendiconti Accademia dei Lincei* 9:387-392
- Oberti R, Ghose S (1993) Crystal-chemistry of a complex Mn-bearing alkali amphibole on the verge of exsolution. *Eur J Mineral* 5:1153-1160
- Oberti R, Ungaretti L, Cannillo E, Hawthorne FC (1992) The behaviour of Ti in amphiboles: I. four- and six-coordinated Ti in richterites. *Eur J Mineral* 4:425-439
- Oberti R, Ungaretti L, Cannillo E, Hawthorne FC, Memmi I (1995a) Temperature-dependent Al order-disorder in the tetrahedral double chain of $C2/m$ amphiboles. *Eur J Mineral* 7:1049-1063
- Oberti R, Sardone N, Hawthorne FC, Raudsepp M, Turnock AC (1995b) Synthesis and crystal-structure refinement of synthetic fluor-pargasite. *Can Mineral* 33:25-31
- Oberti R, Hawthorne FC, Ungaretti L, Cannillo E (1995c) $^{6\text{Al}}$ disorder in amphiboles from mantle peridotites. *Can Mineral* 33:867-878
- Oberti R, Hawthorne FC, Raudsepp M (1997) The behaviour of Mn in amphiboles: Mn in synthetic fluor-edenite and synthetic fluor-pargasite. *Eur J Mineral* 9:115-122
- Oberti R, Hawthorne FC, Cámara F, Raudsepp M (1998) Synthetic fluoro-amphiboles: site preferences of Al, Ga, Sc and inductive effects on mean bond-lengths of octahedra. *Can Mineral* 36:1245-1252
- Oberti R, Hawthorne FC, Cámara F, Raudsepp M (1999) Unusual M^{3+} cations in synthetic amphiboles with nominal fluoro-eckermannite composition: Deviations from stoichiometry and structural effects of the cummingtonite component. *Am Mineral* 84:102-111
- Oberti R, Caballero JM, Ottolini L, López-Andrés S, Herreros V (2000a) Sodic-ferripedrizite, a new monoclinic amphibole bridging the magnesium-iron-manganese-lithium and the sodium-calcium groups. *Am Mineral* 85:578-585
- Oberti R, Della Ventura G, Ottolini L, Prella D (2000b) An anomalous space group for a synthetic amphibole with anomalous composition. 30^o AIC Meeting, Abstracts:51
- Oberti R, Cámara F, Ottolini L, Caballero JM (2003a) Lithium in amphiboles: detection, quantification and incorporation mechanisms in the compositional space bridging sodic and $^{\text{6}}\text{Li}$ amphibole. *Eur J Mineral* 15:309-319
- Oberti R, Cámara F, Caballero JM, Ottolini L (2003b) Sodic-ferriferropedrizite and ferri-clinoferroholmquistite, mineral data and degree of order of A-site cations in Li-rich amphiboles. *Can Mineral* 91:1345-1356

- Oberti R, Boiocchi M, Smith DC (2003c) Fluoronyboite from Jianchang (Su-Lu, China) and nyboite from Nybo (Nordfjord, Norway): a petrological and crystal-chemical comparison of these two high-pressure amphiboles. *Mineral Mag* 67:769-782
- Oberti R, Cámara F, Caballero JM (2004) Ferri-ottoliniite and ferriwhittakerite, two new end-members of the new Group 5 for monoclinic amphiboles. *Am Mineral* 89:888-893
- Oberti R, Cámara F, Ottolini L (2005) Clinoholmquistite discredited: the new amphibole end-member fluorosodic-pedrizite. *Am Mineral* 90:732-736
- Oberti R, Cámara F, Della Ventura G, Iezzi G, Benimoff AI (2006) Parvo-mangano-edenite and parvo-manganotremolite, two new Group 5 monoclinic amphiboles from Fowler, New York, and comments on the solid solution between Ca and Mn²⁺ at the M4 site. *Am Mineral* 91:526-532
- Oberti R, Hawthorne FC, Cannillo E, Cámara F (2007) Long-range order in amphiboles. *Rev Mineral Geochem* 67:124-171
- Oberti R, Boiocchi M, Smith DC, Medenbach O (2007b) Aluminotaramite, alumino-magnesiostaramite, and fluoro-alumino-magnesiostaramite: mineral data and crystal chemistry. *Am Mineral* 92:1428-1435
- Ottolini L, Bottazzi P, Vannucci R (1993) Quantification of Li, Be and B in silicates by secondary ion mass spectrometry using conventional energy filtering. *Anal Chem* 65:1960-1968
- Paris E, Mottana A, Della Ventura G, Robert JL (1993) Titanium valence and coordination in synthetic richterite-Ti-richterite amphiboles: A synchrotron-radiation XAS study. *Eur J Mineral* 5:455-464
- Pavlovich MS Jr, Jenkins DM (2003) Assessment of cation substitutions along the gallium and fluorine analogue of the tremolite-glaucophane join. *Am Mineral* 88:1486-1495
- Pawley AR (1992) Experimental study of the compositions and stabilities of synthetic nyböite and nyböite-glaucophane amphiboles. *Eur J Mineral* 4:171-192
- Pekov IV, Chukanov NV, Lebedeva YuS, Pushcharovsky DYu, Ferraris G, Gula A, Zadov AE, Nováková AA, Petersen OV (2004) Potassicarfvedsonite, K Na₂ Fe²⁺₄Fe³⁺ Si₃ O₂₂(OH)₂, a K-dominant amphibole of the arfvedsonite series from the apaitic pegmatites: mineral description and refinement of the crystal structure. *N Jb Miner Mh* 2004:555-574
- Pekov IV, Chukanov NV, Nefedova ME, Pushcharovsky DYu, Rastsvetaeva RK (2005) Chloro-potassichastingsite (K,Na) Ca₂ (Fe²⁺,Mg)₄Fe³⁺ [Si₆Al₂O₂₂] (Cl,OH)₂: revalidation and the new name of dashkesanite. *Zapiski VMO* 134(6):31-36. (Russian with English abstract).
- Popp RK, Gilbert CG, Craig JR (1976) Synthesis and X-ray properties of Fe-Mg orthoamphiboles. *Am Mineral* 61:1267-1279
- Raudsepp M, Turnock A, Hawthorne FC, Sheriff B, Hartman JS (1987a) Characterization of synthetic pargasitic amphiboles Na Ca₂ Mg₄M³⁺ Si₆Al₂ O₂₂ (OH,F)₂; M³⁺ = Al, Cr, Ga, Sc, In) by infrared spectroscopy, Rietveld structure refinement and ²⁷Al, ²⁹Si, and ¹⁹F MAS-NMR spectroscopy. *Am Mineral* 72:580-593
- Raudsepp M, Turnock A, Hawthorne FC (1987b) Characterization of cation ordering in synthetic scandium-fluor-eckermannite, indium-fluor-eckermannite, and scandium-fluor-nyböite by Rietveld structure refinement. *Am Mineral* 72:959-964
- Raudsepp M, Turnock A, Hawthorne FC (1991) Amphiboles at low pressure: what grows and what doesn't. *Eur J Mineral* 3:983-1004
- Robert JL, Gaspérin M (1985) Crystal structure refinement of hendricksite, a Zn- and Mn-rich trioctahedral potassium mica: contribution to the crystal chemistry of zinc-bearing minerals. *Tschermak Mineral Petrol Mitt* 34:1-14
- Robert JL, Della Ventura G, Thauvin JL (1989) The infrared OH-stretching region of synthetic richterites in the system Na₂O-K₂O-CaO-MgO-SiO₂-H₂O-HF. *Eur J Mineral* 1:203-211
- Robert JL, Della Ventura G, Raudsepp M, Hawthorne FC (1993) Rietveld structure refinement of synthetic strontium-rich potassium-richterites. *Eur J Mineral* 5: 199-206
- Robinson GW, Grice JD, Gault RA, Lalonde AE (1997) Potassicpargasite, a new member of the amphibole group from Pargas, Turku-pori, Finland. *Can Mineral* 35:1535-1540
- Savel'eva VB, Korikovskii RSP (1998) Sadanagaite from biotite-corundum-margarite-spinel-anorthite schists of the Western Baikal region. *Doklady Earth Sciences* 360:477-479
- Sawaki T (1989) Sadanagaite and subsilicic ferroan pargasite from thermally metamorphosed rocks in the Nogo-Hakusan area, central Japan. *Mineral Mag* 53:99-106
- Senda K, Ishida K, Jenkins DM (2005) X-ray Rietveld refinement and FTIR spectra of synthetic (Si,Ge)-richterites. *Am Mineral* 90:1062-1071
- Sergent J, Robert JL, Boukili B, Della Ventura G (1996) Effect of X_{Fe} and f_{O₂} on the FTIR and Mössbauer spectra of richterites in system the K₂O-Na₂O-CaO-FeO-Fe₂O₃-TiO₂-SiO₂-H₂O. *Phys Chem Mineral* 23:308
- Shau Y-H, Peacor DR, Ghose S, Phakey PP (1993) Submicroscopic exsolution in Mn-bearing alkali amphiboles from Tirodi, Maharashtra, India. *Am Mineral* 78:96-106
- Shimazaki H, Bunno M, Ozawa T (1984) Sadanagaite and magnesio-sadanagaite, new silica-poor members of calcic amphibole from Japan. *Am Mineral* 69:465-471

- Sokolova EV, Hawthorne FC, Kabalov YK, Schneider J, McCammon C (2000) The crystal chemistry of potassic-ferrisadanagaite. *Can Mineral* 38:669-674
- Sokolova EV, Hawthorne FC, Gorbatova V, McCammon C, Schneider J (2001) Ferrian winchite from the Ilmen Mountains, Southern Urals, Russia, and some problems with the current scheme for amphibole nomenclature. *Can Mineral* 39:171-177
- Strong DF, Taylor RP (1984) Magmatic-subsolidus and oxidation trends in composition of amphiboles from silica-saturated peralkaline igneous rocks. *Tschermaks Mineral Petrol Mitt* 32:211-222
- Sueno S, Matsubara S (1986) A mineralogical study of the two natural protoamphiboles. 14th International Mineralogical Association Meeting Abstract 14:241
- Sueno S, Matsubara S, Gibbs GV, Boisen MBJr (1998) A crystal chemical study of protoanthophyllite: orthoamphiboles with the protoamphibole structure. *Phys Chem Mineral* 25:366-377
- Tait KT, Hawthorne FC, Grice JD, Ottolini L, Nayak VK (2005) Dellaventuraita, $\text{Na Na}_2 (\text{MgMn}^{3+}_2\text{Ti}^{4+}\text{Li}) \text{Si}_8 \text{O}_{22} \text{O}_2$, a new anhydrous amphibole from the Kajlidongri Manganese Mine, Jhabua District, Madhya Pradesh, India. *Am Mineral* 90:304-309
- Tiepolo M, Zanetti A, Oberti R, Brumm R, Foley S, Vannucci R (2003) Trace-element partitioning between synthetic potassic-richterites and silicate melts, and contrasts with the partitioning behaviour of pargasites and kaersutites. *Eur J Mineral* 15:329-340
- Tiepolo M, Oberti R, Zanetti A, Vannucci R, Foley SF (2007) Trace-element partitioning between amphibole and silicate melt. *Rev Mineral Geochem* 67:417-451
- Tropper P, Manning CE, Essene EJ, Kao LS (2000) The compositional variation of synthetic sodic amphiboles at high and ultra-high pressures. *Contrib Mineral Petrol* 139:146-162
- Ungaretti L, Smith DC, Rossi G (1981) Crystal chemistry by X-ray structure refinement and electron microprobe analysis of a series of sodic-calcic to alkali-amphiboles from the Nybø eclogite pod, Norway. *Bull Minéral* 104:400-412
- van Marcke de Lumen G, Verkaeren J (1985) Mineralogical observations and genetic considerations relating to skarn formation at Botallack, Cornwall, England. Proc. High Heat Production (HHP) Granites, Hydrothermal Circulation and Ore Genesis Conference, The Institution of Mining and Metallurgy, London, 535-547
- Yang H, Konzett J, Prewitt CT, Fei Y (1999) Single-crystal structure refinement of synthetic ^{84}K -substituted potassic richterite. *Am Mineral* 84:681-684
- Wagner C, Velde D (1986) The mineralogy of K-richterite-bearing lamproites. *Am Mineral* 71:17-37
- Wang L, Wang P, Zhang J, Bai J (1997) Discovery of magnesio-sadanagaite in a ruby deposit of Yunnan and its significance. *Dizhi Lunping (Geological Review)* 43:409-414 (in Chinese with English abstract)
- Welch MD, Graham CM (1992) An experimental investigation of glaucophanic amphiboles in the system $\text{Na}_2\text{O}-\text{MgO}-\text{Al}_2\text{O}_3-\text{SiO}_2-\text{SiF}_2$ (NMAF): some implications for glaucophane stability in natural and synthetic systems at high temperatures and pressures. *Contrib Mineral Petrol* 111:248-259.
- Welch MD, Camara F, Della Ventura G, Iezzi G (2007) Non-ambient *in situ* studies of amphiboles. *Rev Mineral Geochem* 67:223-260
- Witte P, Langer K, Seifert F, Schreyer W (1969) Synthetische Amphibole mit OH-Uberschuss im System $\text{Na}_2\text{O}-\text{MgO}-\text{SiO}_2-\text{H}_2\text{O}$. *Die Naturwissenschaften* 8:414-415

Long-Range Order in Amphiboles

Roberta Oberti¹, Frank C. Hawthorne²,
Elio Cannillo¹ and Fernando Cámara¹

¹*Istituto di Geoscienze e Georisorse, Consiglio Nazionale delle Ricerche
I-27100 Pavia, Italy*

oberti@crystal.unipv.it, cannillo@crystal.unipv.it, camara@crystal.unipv.it

²*Department of Geological Sciences
University of Manitoba, Winnipeg, Manitoba R3T 2N2, Canada
frank_hawthorne@umanitoba.ca*

INTRODUCTION

Comprehensive knowledge of the order-disorder relations in amphiboles is essential to (1) complete understanding of the crystal chemistry of these minerals, and to (2) the use of amphiboles in thermodynamic calculations (e.g., of temperature and pressure of equilibration) where accurate activity models are critical to the accuracy of such treatments. Moreover, such information is essential to our understanding of phase relations, optical and electrical properties and dehydrogenation mechanisms. As a result, more effort has been expended on characterizing site occupancies in amphiboles than in any other group of minerals. Hawthorne (1983a,b) reviewed in detail all work prior to 1983. Here, we will briefly summarize this work, and focus more on what has been learned since then.

METHODS OF DERIVING SITE POPULATIONS

We will briefly review the common methods of deriving site populations. It is important that everyone who uses site populations has an appreciation of the methods used to derive this information, as a significant fraction of the data in the literature is wrong, and the user has to be in a position to assess the accuracy and precision of the data that they will use. The most comprehensive method of deriving site populations is crystal-Structure REFinement (SREF), as this method senses every atom (in significant amounts) in a crystal. However, this universality has a negative side. Some atomic species cannot be distinguished as they scatter radiation in a very similar way. Different types of radiation (e.g., X-rays, neutrons) can compensate for this drawback: for example, X-ray scattering cannot easily distinguish between Fe and Mn or Fe and Ti (differences in size of these species can be used for this purpose, but this becomes inaccurate to ineffective in more complicated compositions), whereas neutron scattering can distinguish these species. However, there are many instances where such differentiation is not possible. It is here that spectroscopy can be useful, as many spectroscopic techniques are species sensitive and are not complicated by the presence of other elements in a mineral. Thus Mössbauer spectroscopy can “see” only Fe in a very complicated amphibole, and can easily sense valence-state differences that are not easy to characterize by SREF. Frequently, a much better characterization of site populations can be attained by a combination of techniques that can compensate for each other’s inadequacies.

Single-crystal Structure REFinement

SREF is the method most commonly used to address calculation of site populations and

thus of cation and anion partitioning in minerals. It can be actually regarded as a method of chemical analysis. X-ray SREF is an electron-counting technique with spatial resolution (Hawthorne and Grice 1990), and neutron scattering yields an aggregate site-scattering length which can be further interpreted with the incorporation of additional chemical information. SREF allows accurate and precise determination of:

- (1) the relative positions, point symmetry and numbers of sites, from which derive the stoichiometric requirements of the formula unit; in addition, the relative positions give accurate interatomic distances and angles which are used extensively for crystal-chemical analysis.
- (2) the relative scattering power at each site; note that some sites are assumed to have fixed scattering power (usually the anion sites), and these serve to scale the relative scattering at those sites considered to have variable scattering in the refinement process.

For X-rays, the refined scattering corresponds to the mean atomic number of *all* constituents at that site (i.e., averaged over the diffraction volume). When properly scaled, the refined site-scattering values give the total number of electrons per formula unit (epfu) (Hawthorne et al. 1995a) with a precision (depending on how well the scattering curves used in the refinement procedure approach the real site-populations) of $\sim 0.1 e^-$ in high-quality structure refinements (i.e., $R_{\text{obs}} \approx 1\text{-}2\%$). For neutrons, the refined scattering corresponds to the mean scattering length of *all* constituents at that site. If there is sufficient difference in scattering power of constituents occupying a site, binary site-occupancies can be determined. Where a site is occupied by more than two species (e.g., Mg, Fe, Mn), a single SREF experiment cannot determine site occupancies. One may deal with this issue in two ways: (1) in some circumstances, one may do two SREF experiments with different radiations if there are significant differences in scattering values for different pairs of species with the two radiations. In the example given above, X-ray scattering can distinguish between Mg and (Fe + Mn) but not between Fe and Mn, whereas neutrons can distinguish between Fe and Mn; thus structure refinement on the same material with X-rays and with neutrons will give unique site-occupancies for Mg, Fe and Mn. The problem here is that not all combinations of scattering species have such differences in scattering by X-rays and neutrons. (2) Alternatively, one may *assume* a site occupancy for one species and leave it as fixed in the refinement process; the other two occupancies can then be refined in the usual way. To do this, one needs (i) an accurate chemical analysis of the crystal, and (ii) knowledge that the species considered as fixed only occupies one site (i.e., it is completely ordered at a specific site). For example, this will work for the refinement of Mg, Fe and Cr over the $M(1,2,3)$ sites where Cr is assumed to occur only at the $M(2)$ site whereas Mg and Fe are partly disordered over the $M(1)$, $M(2)$ and $M(3)$ sites, and here the Cr content is known from microchemical analysis of the crystal. Note that this procedure cannot work where all three constituents are partly disordered (e.g., for Mg, Fe and Mn over the $M(1,2,3)$ sites) as knowing the composition of the crystal does not determine the site occupancies of any of the three constituents.

A major advance in our knowledge of the chemical composition of amphiboles since the last amphibole Short Course (1981) is the common occurrence of *variable* light lithophile elements, specifically H and Li, in amphiboles. The presence of these variable constituents was detected by SREF and subsequent crystal-chemical analysis. A number of convincing examples are now available (Hawthorne et al. 1993; Hawthorne and Oberti 2007), and diagrams suitable to detect and quantify Li and H based on SREF results are reported elsewhere in this volume by Hawthorne and Oberti (2007, Fig. 1) and in a following section. Interestingly, this has promoted the development of SIMS for the analysis of LLE (Light Lithophile Elements) in amphiboles (Ottolini et al. 1993, 1995; Ottolini and Oberti 2000).

Crystal-chemical constraints. A lot of work has been focused on improving and validating refinement procedures, and on developing crystal-chemical relations that can be used to confirm or assign site-populations. Some procedures for structure refinement of amphiboles and other rock-forming minerals are described in detail by Ungaretti (1981), and the relevance of particular reflections on the estimation of crystal-chemical parameters has been discussed by Merli et al. (2000, 2001).

The refined model generally has two or three scattering curves assigned to each site, whose relative occupancy is refined under the constraint that the total occupancy is 1.0. The core of the problem is to convert these (possibly) fictive site occupancies into real site-populations which sum directly to give the structural formula. The site population proposed for a particular site *must* be consistent with the refined site-scattering values and mean bond-lengths, as well as with local bond-valence requirements. Furthermore, the sum of all the site populations must sum to a value close to the chemical composition of the crystal as determined by an independent technique (usually electron- and ion-microprobe analysis), and the unit-cell content must be electroneutral.

Derivation of site populations: general features. SREF gives the scattering at each site in the crystal, and the issue then is to derive site populations from these values. As noted above, SREF does not directly provide a unique solution to this problem, and other information has to be incorporated into the derivation of site populations, particularly in the case of amphiboles where a site is often occupied by several constituents. Primary scattering information is as follows:

- (1) the sum of the site occupancies is 1.0; note that a site constituent may be a vacancy, and assumptions or external knowledge is required as to whether a vacancy can occur at a specific site.
- (2) the site-scattering values from the SREF procedure.

Additional information is as follows:

- (3) the sum of the unit-cell contents must be electroneutral; note that this is a rigid constraint, as we know that the rule of electroneutrality must be obeyed exactly.
- (4) the observed mean bondlengths and assigned site-populations must be in accord with previously established relations between these quantities.
- (5) the chemical composition of the crystal. This may be (a) observations (i.e., the unit formula derived from a chemical analysis, usually an electron and ion-microprobe analysis possibly supplemented with spectroscopic information giving valence states of some cations), (b) a guesstimate of the composition (e.g., Si, Al, Mg, Fe, Mn, Ca, Na, K, O, F and H only are assumed to be present), or (c) the presence or amount of a constituent (e.g., ${}^{\text{B,C}}\text{Li}$, ${}^{\text{B}}\text{Mg}$, ${}^{\text{M(1)Ti}}$) as indicated by diagnostic signals from the structure refinement such as anomalous site-scattering values and/or atom-displacement parameters.

Site populations may be derived either by manual solution of a series of simultaneous equations involving equal distribution of error among experimental parameters, or by least-squares minimization of a system of suitable equations relating the full occupancy, the refined site-scattering value, the refined mean bondlength and the overall electroneutrality to the content of the four main cations. Both of these approaches have been used extensively for the assignment of amphibole site-populations.

Derivation of site populations: a least-squares procedure. For calcic, sodic-calcic and sodic-amphiboles with $(\text{OH})_2$ at the O(3) site, a least-squares procedure was applied by Cannillo et al. (1981) to 130 structure refinements of amphiboles, and later optimized by

Cannillo et al. (1986) on a more representative database of around 500 structure refinements. Here, we report for the first time the results of a recent re-examination of the problem with a database of more than 1100 structure refinements comprehensively covering the composition space of monoclinic amphiboles. The resulting program (COMAMPH) will be described in detail in a manuscript in preparation, and is available on request from R. Oberti.

Multiple regression analysis of 440 selected crystals with complete chemical analyses and superior agreement with SREF results gave predictive equations relating the main chemical variables in the crystal-chemical formula [^AK , ^BLi , ^BNa , ^BCa , ^BMg , $^B(\text{Fe}^{2+}, \text{Mn}^{2+})$, ^CLi , ^CMg , $^C(\text{Fe}^{2+} \text{Mn}^{2+})$, ^CAl , $^C(\text{Fe}^{3+}, \text{Mn}^{3+})$, ^CTi , ^TAl , $^{O(3)}\text{F}$, $^{O(3)}\text{O}^{2-}$] and the net positive charges at the A, M(4) and M(1,2,3) sites with all the geometric and atomic-displacement parameters of the structure. The equations and their regression parameters are given in Table 1. ^TSi , and $^{O(3)}\text{OH}$ are calculated by difference to the complete group-site occupancy. For the A site, which has variable occupancy, ^ANa is calculated based on the predicted positive charge. $^{T(1)}\text{Al}$ is calculated based on the revised equation

$$^{T(1)}\text{Al} (\text{apfu}) = [\langle T(1)\text{-O} \rangle - 1.6193] \times 34.2199 \quad R = 0.997 \quad \sigma = 0.048$$

which has been newly derived based on the whole CNR-IGG database, and which is slightly different from that given by Oberti et al. (1995a) based on a smaller dataset, $[\langle T(1)\text{-O} \rangle - 1.6187] \times 33.2055$. As discussed in Hawthorne and Oberti (2007), there is some spreading in $\langle T(1)\text{-O} \rangle$ distances of amphiboles with ^TAl (from EMP analyses) < 0.30 apfu (cf. for instance their Fig. 17 and Fig. 10 in this Chapter). This feature mostly derives from errors in the analysis and in the calculation of the unit formula; however, amphiboles with significant amount of small B cations (namely, Li, Mg, Fe) and Si = 8.0 apfu have $\langle T(1)\text{-O} \rangle$ distances significantly shorter than 1.619 Å. Therefore, caution must be used when dealing with very low ^TAl contents.

The total amounts of the B and C cations are subsequently normalized to the stoichiometric values (2.0 and 5.0 apfu, respectively). At this point, the site populations are optimized by minimizing the differences between the calculated and refined site-scattering values. Lastly, the resulting crystal-chemical formula is optimized to achieve overall electroneutrality using an iterative procedure which changes the cumulative charges of the A, B, C, T and W species

Table 1. The relation between the chemical composition and the amphibole structure. Predictive equations have been obtained by stepwise multiple regression analysis of the CNR-IGG-PV data base. They are now used in the COMAMPH program.

Dependent variable	Number of parameters	R	see	Dependent variable	Number of parameters	R	see
^AK	65	0.996	0.021	$^C(\text{Fe}, \text{Mn})^{2+}$	60	0.993	0.096
^BNa	47	0.998	0.040	$^C\text{Fe}^{3+}$	76	0.984	0.095
^BCa	55	0.999	0.039	^CLi	50	0.995	0.016
^BLi	52	0.998	0.021	^TAl	39	0.998	0.043
^BMg	56	0.937	0.029	$^{O(3)}\text{F}$	74	0.988	0.073
$^B(\text{Fe}, \text{Mn})^{2+}$	40	0.990	0.028	$^{O(3)}\text{O}^{2-}$	70	0.985	0.076
^CAl	57	0.996	0.045	A charge	47	0.996	0.028
^CMg	63	0.999	0.055	B charge	52	0.991	0.086
^CTi	68	0.989	0.031	C charge	61	0.991	0.086

R is the multiple correlation coefficient; see is the standard error of the estimate.

while keeping the corresponding site-scattering values fixed. Starting from the formula obtained with the above procedure, which provides a good estimate of the OH content and of the $\text{Fe}^{3+}/\text{Fe}^{2+}$ ratio, $M(1)$, $M(2)$ and $M(3)$ site populations can be derived by assigning the cations according to the site preferences discussed in a following section, and checked against the refined site-scattering values.

The accuracy of this method was first tested on a group of ~100 samples for which some chemical information is available, and then used on the whole database. The results show that this method generally produces accurate crystal-chemical formulae. Discrepancies with the available chemical information could be always explained by (1) analytical problems [e.g., (Na+K) or (Si+Al) contents inconsistent with amphibole stoichiometry], (2) erroneous formula recalculation (e.g., underestimation of the oxo component), or (3) incorrect structure refinement (e.g., too high atom-displacement parameters at the A sites, which wrongly increases the refined site-scattering value).

Notably, with this procedure, we can obtain reliable estimates of those chemical variables which escape routine EMP analysis, i.e., Li, F, $\text{O}^{(3)}\text{O}^{2-}$ (and thus H), $\text{Fe}^{3+}/\text{Fe}^{2+}$ ratio, and of cation partitioning between the group sites [e.g., Li, Mg and (Fe + Mn) between B and C sites]. This information is crucial to the correct classification of the sample, and possibly to draw attention to the need of further chemical or spectroscopic analysis.

As shown by multiple regression (Cannillo and Ungaretti 1982) and leverage analysis (Merli et al. 2000, 2001), some reflections from the complete set of diffraction data are particularly sensitive to the variation of structural parameters. Based on this relation, another program has been developed which predicts the crystal-chemical formula based solely on unit-cell parameters and measured structure factors. Because it takes into account all data for common and uncommon $C2/m$ amphibole compositions, this approach is particularly useful in producing an appropriate structure model to begin normal least-squares refinement of the structure. The program is called PREDICT, and is available on request from R. Oberti. In this case, stepwise multiple regression analysis gave a series of equations which estimate the scattering values and the mean bondlengths at each site, together with other geometrical parameters which provide information on the Li, F and O^{2-} contents (see Hawthorne and Oberti 2007 for more details). In particular, the site-scattering values at the A, $A(m)$, $A(2)$, $M(4)$ and $M(4')$ sites are treated separately. At the end of an optimization procedure similar to that for COMAMPH, the program provides a highly reliable formula (simplified to major elements, e.g., $\text{Fe}^{2+} = \text{Fe}^{2+} + \text{Mn}^{2+}$, $\text{Fe}^{3+} = \text{Fe}^{3+} + \text{Cr}^{3+}$, ...) and thus a consistent set of scattering factors to be used in the proper proportions in a straightforward structure refinement.

Mössbauer spectroscopy

The Mössbauer effect involves the recoil-free emission and absorption of γ -rays by a specific atomic nucleus. The emission of a γ -ray during a nuclear transition normally causes a recoil of the emitting atom; this recoil energy dissipates by transfer to the phonon spectrum of the structure. As the phonon spectrum is quantized, this transfer must occur in integral multiples of the phonon energy and the probability exists that no energy is transferred. The effective line-width of the zero-phonon (recoil-free) process is that of the γ -ray; this is extremely small (Wertheim 1964, Chap. 4, Fig. 1) in relation to the characteristic energies of interaction between the nucleus and its surrounding electrons. If the zero-phonon γ -ray encounters another nucleus, its energy may be absorbed by raising that nucleus to an excited state, provided the transition energies of the emission and absorption events are equal to within the line-width of the γ -ray. As the linewidth of the γ -ray is much smaller than the characteristic interaction energies between nuclei and electrons, a change in structural environment is generally sufficient to bring the two nuclei out of resonance. However, the energy of the γ -ray may be modulated by applying a Doppler shift to bring the system into resonance. In this way, nuclear transition energies may be compared in different environments.

A change in the s -electron density at the nucleus of an atom will result in a shift in the nuclear energy levels. Where such a variation occurs between emitter and absorber, the processes are separated in the energy spectrum by an amount known as the *Isomer Shift* (IS) or *Chemical Shift* (CS). This quantity is thus a measure of the relative s -electron density at the nucleus. Two factors are principally responsible for variations in isomer shift. Screening of s -electrons from the nucleus by valence electrons is strongly affected by valence state and degree of covalent bonding. Thus isomer shift may be used to characterize valence state and coordination number. If the nucleus does not have a uniform charge density, a quadrupole moment arises which can interact with the electric field gradient (EFG) at the nucleus to lift the degeneracy of the nuclear states. The splitting of the nuclear energy levels gives rise to a series of possible transitions between the ground and excited states of the nucleus, the number of which depends on the nuclear spin quantum number. For ^{57}Fe ($I = 1/2$) in paramagnetic materials, the ground state is not split and the first excited state ($I = 3/2$) is split into two levels; the two allowable transitions give rise to a doublet in the energy spectrum; the separation of the two components is known as the *Quadrupole Splitting* (QS) and is thus a measure of the EFG at the nucleus. Principal factors affecting the EFG at the nucleus are the non-spherical electron distribution in the atom itself, a function of valence state, and the nonspherical component of the crystal field. Thus quadrupole splitting may be used to characterize valence state and variations in structural environment. More detailed discussions of the Mössbauer effect in Mineralogy are given by Bancroft (1973), Hawthorne (1988), Murad and Cashion (2004) and Dyar et al. (2006), and Hawthorne (1983c) considers issues associated with the derivation of site occupancies and their attendant standard deviations in detail.

Site-occupancy derivation. There are thirty or so isotopes that are sensitive to the Mössbauer effect, but only ^{57}Fe is of interest to amphibole crystal chemistry. An experimental Mössbauer spectrum is shown in Figure 1. The counts at the margins of the spectrum represent the background counts and are approximately constant. Toward the center of the spectrum, the counts decrease due to the resonant absorption of γ -rays of this specific energy by the sample,

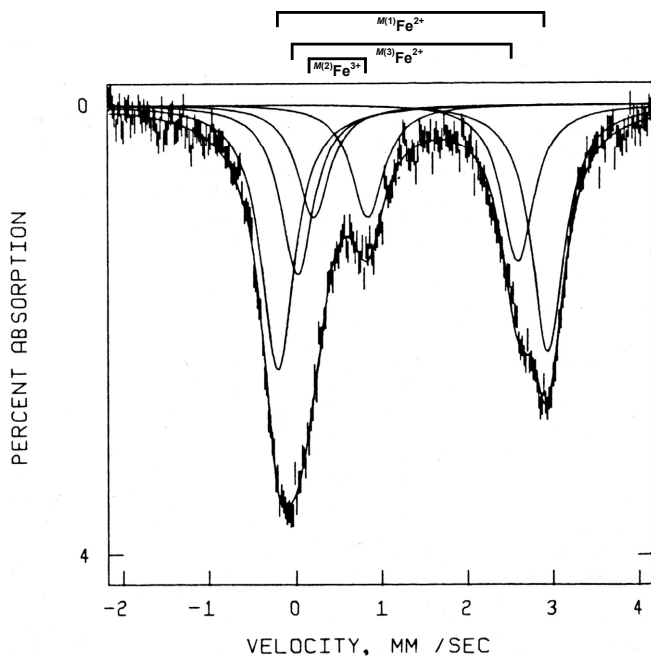


Figure 1. The Mössbauer spectrum of ferrotschermakite, showing the absorption of γ -rays as a function of energy (velocity). Each data point is shown by a broken line, the length of which is 2 standard deviations (based on counting statistics). The spectrum is fitted to component pairs of bands (doublets) that correspond to Fe of a particular valence state and at a particular site (marked above the spectrum). (Modified from Hawthorne 1983a).

and the observed spectrum consists of a series of peaks, the number and characteristics of which are a function of the valence(s) of Fe in the sample, the number of sites occupied by Fe, and the occupancies of those sites. Unfolding the observed envelope into its component peaks is done by least-squares refinement.

Inspection of Figure 1 shows that peaks in the spectrum can overlap strongly, causing problems in the least-squares process. These problems may be alleviated somewhat by incorporating into the model additional information that is external to the spectral data itself. There are two types of constraints that are widely used: (1) *Width constraints*: Mössbauer spectral examination of many end-member compounds suggests that the peak widths corresponding to Fe²⁺ in various sites are equal in a specified sample. Thus in the spectrum refinement procedure, the width of all the peaks can be constrained to be equal, with a considerable improvement in both the convergence rate and standard deviations. (2) *Area constraints*: Experimental evidence suggests that the individual peaks of a quadrupole-split doublet should have approximately equal intensity. This is another very powerful constraint that is frequently used in spectral refinement. This constraint may not be strictly correct as preferred orientation in a sample can give rise to intensity asymmetry in quadrupole-split doublets. In complex, poorly-resolved spectra, the final solution is only as good as the constraints which were used in the fitting procedure. If the constraints are true, then the fitted parameters are valid; however, if the constraints are wrong (or inappropriate) then the solution will be wrong.

Precision. Least-squares refinement is a widely used method in Science. The reason for this is that once convergence has been attained, some kind of precision (a standard deviation) can easily be assigned to the variable parameters of the model. However, many Mössbauer studies in the literature do not report standard deviations for their assigned site-population. These values are of little use without some estimation (a minimum estimation in the case of least-squares modeling) of their precision. For an extensive discussion on precision in spectral fitting, see Hawthorne (1988) and Hawthorne and Waychunas (1988).

Infrared spectroscopy

Vibrational spectroscopy involves the interaction between electro-magnetic radiation and the vibrational modes of a crystal. A vibrational mode in a crystal will absorb electromagnetic radiation if the frequencies of the vibration and the radiation are coincident and if the excited vibration results in a change in the dipole moment of the crystal; this gives rise to *infrared absorption spectroscopy*. Infrared spectroscopy in the principal (OH)-stretching region (3800-3600 cm⁻¹ in amphiboles) is a powerful method for characterizing order in amphiboles.

A fragment in many common hydroxyl-bearing minerals is the trimer of edge-sharing octahedra [M₃φ₁₂(OH)] (φ = unspecified anion) (see Hawthorne and Della Ventura 2007, Figure 3a); this trimer is embedded for instance in the structures of the humites, the amphiboles, the micas, talcs and chlorites. The exact position (energy) of the fundamental band of the corresponding OH stretching vibration is a function of the nature of the next-nearest and next-next-nearest neighbor cations [at 2 M(1), M(3), M(4) and A] and of the strength of hydrogen bonding [involving O(7) in amphiboles, Hawthorne and Della Ventura 2007, Fig. 3b]; stronger hydrogen bonds are associated with lower wavenumbers (values in cm⁻¹). Amphiboles with a completely ordered arrangement of cations in this cluster [i.e., M(1)M(1)M(3) = MgMgMg] show a single sharp band in this region. However, this band in minerals of intermediate composition shows considerable fine structure. Strens (1966) and Burns and Strens (1966) interpreted the fine-structure bands in amphiboles in terms of cation disorder over the octahedrally coordinated sites in the structure, and used the relative intensity of the various bands to derive the frequency of occurrence of the different possible combinations of cations and the cation ordering over the non-equivalent sites in the structure (e.g., Burns and Greaves 1971). This issue is discussed in some detail by Hawthorne (1983a), Hawthorne et al. (2005) and Hawthorne and Della Ventura (2007).

Other considerations. The derivation of site-occupancies from band intensities assumes that the band intensity for a specific configuration is related to the frequency of occurrence of that configuration in the same way that all other bands are related to their corresponding configurations. Thus the transition moment of the OH vibration should be independent of the type of configuration. However, weak hydrogen bonding may significantly affect the transition moment of the OH band, whether or not the strength of the hydrogen bonding is related to the cation configuration at the coordinating M sites. In older work on the derivation of site populations (see surveys by Strens 1974 and Hawthorne 1981, 1983c), it was implicitly assumed that the molar absorptivity of all fundamental OH-stretching bands is the same. However, Skogby and Rossman (1991) showed that this is not the case for polarized single-crystal absorption spectra of amphiboles, where the molar absorptivity (ϵ) of OH-stretching bands can increase strongly with decreasing absorption frequency (Fig. 2).

Della Ventura et al. (1997) measured the powder infrared spectra of (magnesium, nickel)- and (magnesium, cobalt)-potassic-richterite solid-solutions (Fig. 3) and showed that the molar absorptivities of the four OH-stretching bands are the same in a single powder sample (Fig. 4), and hence the method can be used to derive long-range site-populations when dealing just with disorder of divalent cations over the $M(1)$, $M(2)$ and $M(3)$ sites, and where there are no changes in the formal charges of the next-nearest and next-next-nearest neighbor cations. Thus the situation regarding variation in molar absorptivity as a function of band frequency in amphiboles is currently unclear. However, it is clear that we must consider possible variations in molar absorptivity in relating band intensities to structural and chemical features.

Another problem that can arise in natural amphiboles involves the effects of anion variations. In many amphiboles, the O(3) site may be occupied by F, Cl (and O^{2-}) in addition to the OH group. In order to apply infrared spectroscopy to calculate site populations, it is necessary to assume that there is random mixing of OH groups and F, Cl anions with no segregation at specific cation configurations. Unfortunately, this does not appear to be the case, as Fe^{2+} tends to avoid F-coordinated sites (Rosenberg and Foit 1977). In addition, stretching frequencies are sensitive to coupling of OH-OH or OH-F(Cl) through the A site (Robert et al. 2000 and references therein). Despite these problems, infrared spectroscopy can be a very useful method where used in the appropriate circumstances and on well characterized samples.

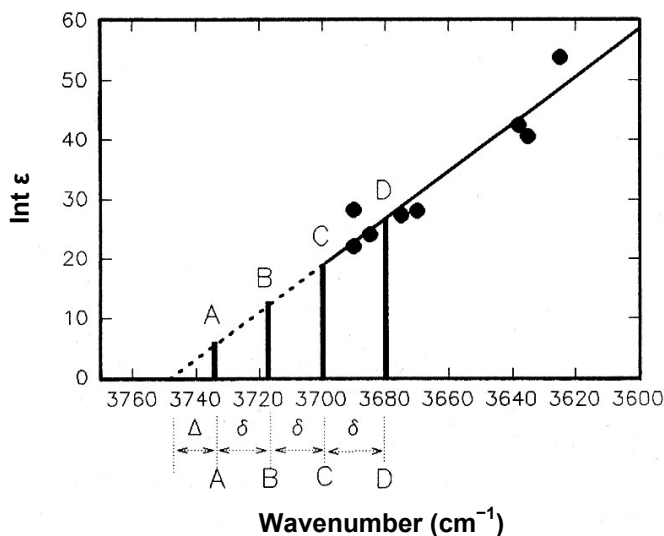


Figure 2. The variation in integrated molar absorptivity as a function of absorption frequency (data from Skogby and Rossman 1991). Band frequencies for synthetic (Ni,Mg,Co)-richterite solid-solutions are shown by the letters A, B, C, D corresponding the local arrangements $M(1)M(1)M(3) = MgMgMg$, $MgMgM^{2+}$, $MgM^{2+}M^{2+}$, $M^{2+}M^{2+}M^{2+}$; the lengths of the vertical lines are relative measures of the integrated molar absorptivities at the corresponding absorption frequencies. (Modified from Della Ventura et al. 1996).

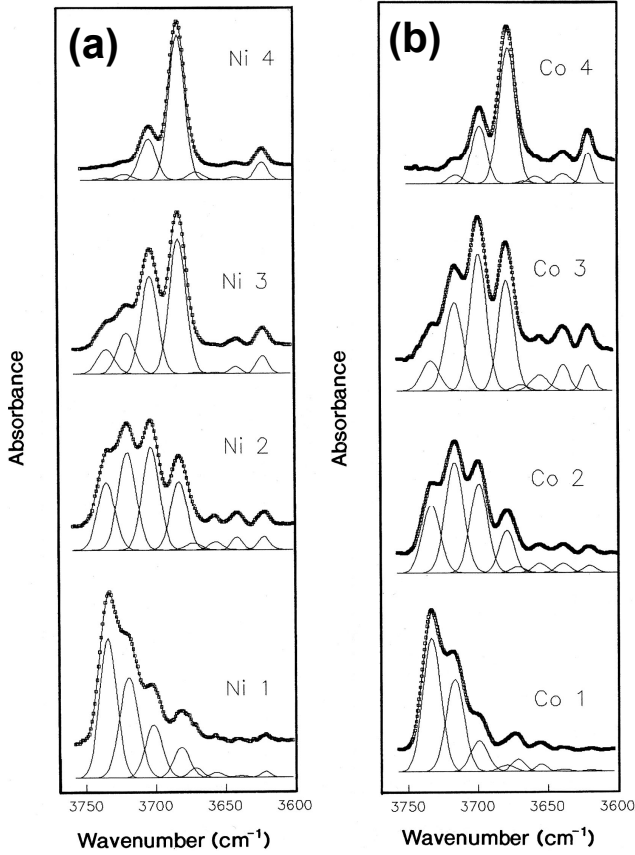
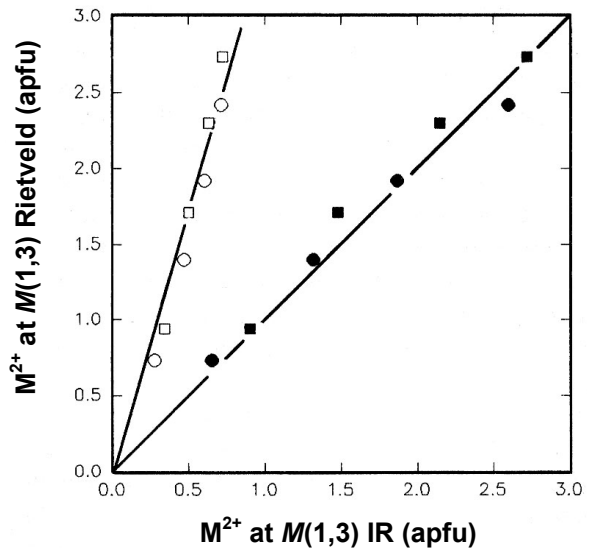


Figure 3. Infrared spectra in the principal (OH)-stretching region for (a) synthetic (Ni,Mg)- and (b) synthetic (Co,Mg)-richterite solid-solutions (from Della Ventura et al. 1996).

Figure 4. Variation in Ni (squares) and Co (circles) content of the $M(1)$ and $M(3)$ sites in synthetic (Ni,Mg)- and synthetic (Co,Mg)-richterite solid-solutions calculated from the band intensities of the infrared spectra (Fig. 3) versus the corresponding values measured by Rietveld refinement. The hollow symbols were calculated using the integrated molar absorptivities indicated by Fig. 2, and the filled symbols were calculated using an integrated molar absorptivity of 1.0 for all bands (from Della Ventura et al. 1996).



Other spectroscopic methods

Other methods have not been used extensively to derive quantitative site-occupancies in amphiboles. Of course, there are important examples of site-occupancy information being derived for amphiboles where the standard methods of SREF or Mössbauer spectroscopy are not effective. However, they are sufficiently infrequent that descriptions of these methods are not warranted here. Of interest in this regard are Magic-Angle-Spinning Nuclear Magnetic Resonance (MAS NMR), electron paramagnetic (spin) resonance (EPR, ESR), electronic absorption spectroscopy and X-ray absorption spectroscopy (XAS). The reader is referred to other sources for an introduction to these techniques.

SITE PREFERENCES OF THE MOST COMMON CATIONS

A detailed discussion of cation distribution in amphiboles was given by Hawthorne (1983a). In the last twenty five years, much work has been done on both natural and synthetic amphiboles to understand cation site preference and partitioning. As a result, our understanding has improved substantially. The principal advances generally involve

- (1) unusual site preferences under peculiar chemical or pressure/temperature conditions;
- (2) patterns of order for the A cations as a function of bulk composition and short-range order;
- (3) patterns of orders for Al and Ti between and within the $T(1,2)$ and $M(2,3)$ sites as a function of composition and P, T, f_{H_2O} conditions of crystallization;
- (4) crystal-chemical mechanisms affecting the incorporation of Li at the $M(3)$ site and its partitioning between the $M(3)$ and $M(4)$ sites;
- (5) detection of the oxo component and our understanding of the crystal-chemical mechanisms controlling primary incorporation of $O^{(3)}O^{2-}$ and secondary dehydrogenation [$O^{2-}_1(OH)_{-1}$] at $O(3)$.

The present knowledge on site-preference is discussed below for the major cations arranged in alphabetic order. Details are given only for monoclinic amphiboles, because recent work on the ordering of C and T cations in $Pnma$ amphiboles has been discussed in Hawthorne and Oberti (2007). The oxo-component is discussed in a separate section. Information on long-range order of trace elements is given in Tiepolo et al. (2007).

Aluminum

Aluminum is a T and a C cation (Warren 1930). There is presently a general consensus that CAl is preferred in high- P environments and TAl is preferred in high- T environments.

CAl . Semet (1973) provided incontrovertible IR evidence [Fig. 5, spectrum (c)] that CAl (and Fe^{3+}) occur at more than one of the $M(1,2,3)$ sites in synthetic magnesiohastingsite. Despite this evidence, early structure work continued to assign CAl to $M(2)$. Raudsepp et al. (1987a,b, 1991) confirmed this behavior for CAl and showed that this disorder of trivalent cations also occurs for Cr^{3+} , V^{3+} and Ga in synthetic pargasites.

Oberti et al. (1995b) first documented by SREF that CAl is partly disordered over the $M(2)$ and $M(3)$ sites in pargasites from the peridotites at Finero (Ivrea Verbano, Italy); they also showed that ${}^{M(3)}Al$ is higher in samples with high Mg content (which also crystallized at the higher T). Figure 6 shows the $\langle M(1)-O \rangle$ and $\langle M(3)-O \rangle$ distances in calcic amphiboles (without significant oxo component) in the CNR-IGG-PV database. The samples mentioned above have anomalously small $\langle M(3)-O \rangle$ distances, and the departure from the general trend is maximal for the highest-Mg compositions (with the smallest $\langle M(1,3)-O \rangle$ distances for the group identified by black triangles). Similar behavior has since been found in mantle pargasites and kaersutites

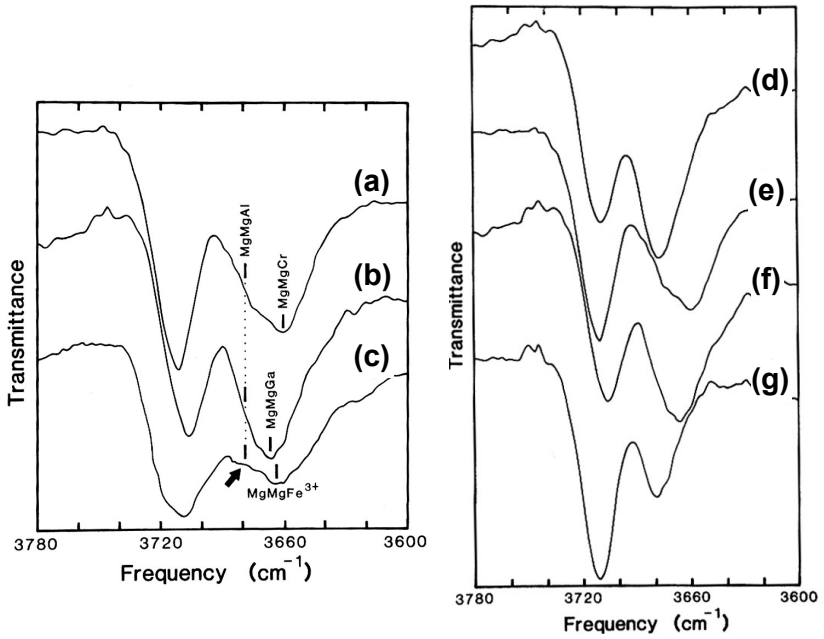


Figure 5. Infrared spectra in the principal (OH)-stretching region for synthetic (a,e) Cr-pargasite (b,f) Ga-pargasite, (c) magnesiohastingsite (Semet 1973), (d) pargasite, (g) Sc-pargasite (from Raudsepp et al. 1987a, Fig 3 and 4).

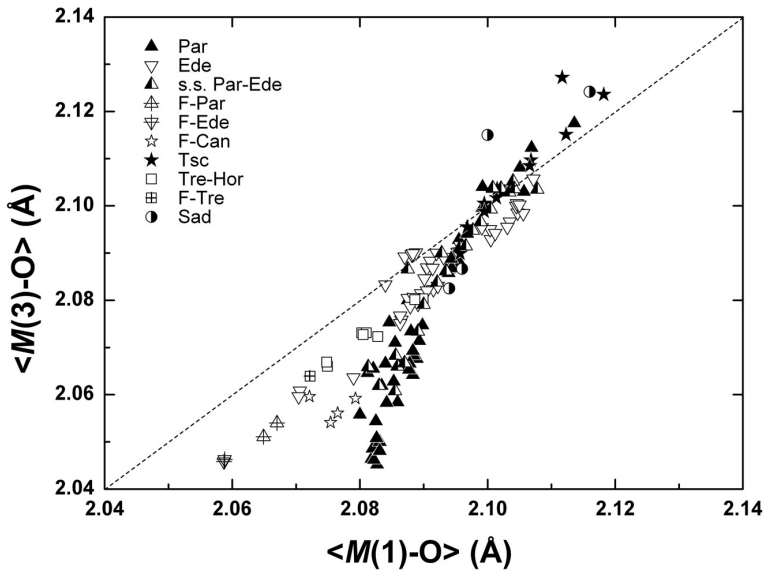


Figure 6. The variation in $\langle M(3)-O \rangle$ versus $\langle M(1)-O \rangle$ in calcic amphiboles with 2 (OH,F,Cl) pfu. Note that $\langle M(3)-O \rangle$ is always shorter than $\langle M(1)-O \rangle$ when $Mg \gg Fe^{2+}$. Even shorter $\langle M(3)-O \rangle$ distances indicate Al occupancy of the $M(3)$ site, which occurs in Mg-rich pargasite and solid-solutions between pargasite and edenite.

from world-wide occurrences, e.g., in hornblende veins and peridotites at Lherz, Eastern Pyrenees, France (Zanetti et al. 1996), in megacrysts in basalt and in composite mantle xenoliths from the Carpatho-Pannonian Region (Zanetti et al. 1995), in peridotites and pyroxenites at Zabargad Island, Red Sea (Zanetti et al. 2000), and also in pargasite from metamorphic rocks, e.g., marbles along the Soper river, Baffin Island (Tait et al. 2001).

The effect of divalent cations on the ordering of Al over $M(2)$ and $M(3)$ was further elucidated by Della Ventura et al. (1998) who showed that while ${}^c\text{Al}$ is almost completely disordered over $M(2)$ and $M(3)$ in synthetic pargasite, ${}^c\text{Al}$ is completely ordered at $M(2)$ in the Co^{2+} analogue of pargasite, ${}^{\text{A}}\text{Na} {}^{\text{B}}\text{Ca}_2 {}^{\text{C}}(\text{Co}^{2+}_4\text{Al}) {}^{\text{T}}(\text{Si}_6\text{Al}_2) \text{O}_{22} {}^{\text{W}}(\text{OH})_2$ (Fig. 7). The spectrum of synthetic pargasite shows two prominent components at ~ 3710 and 3678 cm^{-1} , assigned to $\text{MgMgMg}-(\text{OH})$ and $\text{MgMgAl}-(\text{OH})$, indicating that Al is almost completely disordered over $M(2)$ and $M(1,3)$ [note that the spectroscopic evidence indicates only that Al occurs at $M(2)$ and $M(1,3)$; it cannot tell us whether Al occurs at $M(1)$ or $M(3)$ or both]. In contrast, the OH-stretching spectrum of Co-substituted pargasite consists of a single band at 3656 cm^{-1} . This band is assigned to a local ${}^{M(1)}\text{Co}{}^{M(1)}\text{Co}{}^{M(3)}\text{Co}$ configuration (Della Ventura et al. 1998), and indicates complete order of Al at the $M(2)$ site in this sample, which is also supported by Rietveld structure refinement of site occupancies (Della Ventura et al. 1998). Figure 7 also shows the OH-stretching spectrum of a Mg-rich pargasite from Finero (sample 229-18 in Oberti et al. 1995b); note the similarity to the spectrum of synthetic pargasite: both show two prominent bands in the OH-stretching spectrum, which are assigned to OH-groups bonded to ${}^{M(1)}\text{Mg}{}^{M(1)}\text{Mg}{}^{M(3)}\text{Mg}$ and ${}^{M(1)}\text{Mg}{}^{M(1)}\text{Mg}{}^{M(3)}\text{Al}$, respectively.

Further work on synthetic (Della Ventura et al. 1999, 2003; Welch et al. 1994; Welch and Knight 1999; Najorka and Gottschalk 2003; Jenkins et al. 2003) and natural amphiboles (Bellatreccia et al. in prep.) confirm that disorder of ${}^c\text{Al}$ is a common feature of Mg-rich calcic amphiboles. Welch et al. (1994) and Hawthorne et al. (2000) further confirmed by MAS NMR that ${}^c\text{Al}$ occurs at both the $M(2)$ and $M(1,3)$ sites. Figure 8 shows the triple-quantum MAS NMR ${}^{27}\text{Al}$ spectrum of synthetic pargasite. There are three distinct signals, one due to ${}^{\text{T}}\text{Al}$ and two due to ${}^c\text{Al}$; Hawthorne et al. (2000) argue that if Al occurred at the $M(1)$, $M(2)$ and $M(3)$ sites, three signals should be observed. If this is the case, the results are in accord with those of Oberti et al. (1995b), although they do not indicate which of the $M(1)$ or $M(3)$ sites are occupied by Al. Welch and Knight (1999) studied a synthetic end-member pargasite crystallized at 932°C by Rietveld refinement of data collected by neutron diffraction on powders, FTIR and ${}^1\text{H}$ MAS NMR spectroscopy. They concluded that ${}^c\text{Al}$ disorder is higher [50% at $M(3)$ and 50% at $M(2)$] than in natural samples, where the maximum disorder detected is statistical [34% at $M(3)$ and 66% at the two $M(2)$ sites pfu (Oberti et al. 1995b)]. Actually, the refined natural samples contain significant amounts of larger cations (down to $1.25 {}^c\text{Fe}^{2+}$ apfu), thus confirming their effect on ordering.

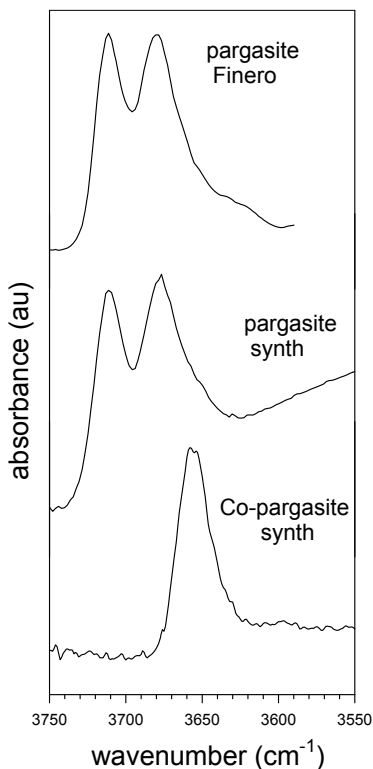


Figure 7. OH-stretching FTIR spectra of pargasite from Finero (top), synthetic pargasite (from Della Ventura et al. 1999, middle) and synthetic Co-substituted pargasite (from Della Ventura et al. 1998, bottom).

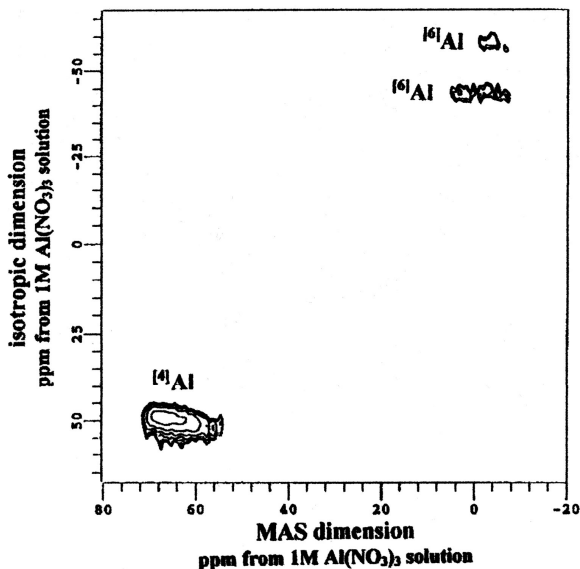


Figure 8. Triple-quantum (3Q) MAS NMR spectrum of a synthetic amphibole approximately on the tremolite–aluminohornblende join. Three distinct signals are observed, and their assignments are indicated on the figure; see text for discussion (from Hawthorne et al. 2000).

Palin et al. (2003, 2005) did Monte Carlo simulations of Al-Mg and Al-Si non-convergent ordering in glaucophane and along the tremolite–tschermakite solid-solution at different T . The goal was to check for their potential use in geothermobarometry under X,T conditions where other minerals are not stable. Indeed, the ordering process of homovalent cations is relatively fast, and their high- T distribution can thus be easily reset. In contrast, ordering of heterovalent cations is much slower and can register accurately crystallization temperatures. Palin et al. (2003) predicted complete Al ordering at the $M(2)$ site in glaucophane even at T above 1000 K, a result confirmed by OH-stretching IR spectroscopy on the synthetic samples synthesized by Pawley (1992). A very different situation was obtained in calcic amphiboles, where simulations considered both Al/Si and Al/Mg ordering and obtained only a marked preference of Al for the $T(1)$ and the $M(2)$ sites, respectively (Palin et al. 2005). In magnesian hornblende, Al at $T(2)$ was found to reach 20% but Al at $M(2)$ was higher than 55% at T around 1500 K. Admittedly, Monte Carlo simulation give high Al occupancy at $M(1)$, even higher than at $M(3)$, a result conflicting with experimental evidence on natural and synthetic amphiboles.

Both structure refinement and FTIR show that high F contents hinder Al disorder over the $M(1,2,3)$ sites. In fluoro-amphiboles, ^{27}Al behaves exactly as the other highly charged C cations, and is always ordered at the $M(2)$ site (Oberti et al. 1998). Accordingly, calcic fluoro-amphiboles plot closer to the dotted line in Figure 6.

^{27}Al . Ordering of Al over the $T(1)$ and the $T(2)$ sites is a bit more complicated. Aluminum is commonly strongly ordered at the $T(1)$ site in $C2/m$ amphiboles, where the local bond-valence requirements can be satisfied by incorporation of (1) highly charged cations at the $M(2)$ site, (2) A cations, (3) divalent cations at the $M(4)$ site (in sodic amphiboles).

The occurrence of ^{27}Al beyond 2.0 apfu was first reported by Adams and Harrington (1896) in a sample from the Hasting County, Ontario. Admittedly, these authors reported Si = 5.75 apfu, but with a total cation excess of 0.7 apfu. Appleyard (1975) provided modern analyses of “sub-silicic hastingsite” (to be presently named ferri-ferrosadanagaite) from metasomatic alkaline gneisses at Wolfe, Ontario; he recorded Al up to 2.73 apfu, but did not propose any scheme for Al ordering over the $T(1)$ and $T(2)$ sites. The latter was provided based on structure refinement by Hawthorne and Grundy (1977a), who concluded that all the Al in excess of

2.0 apfu is incorporated at the $T(2)$ site. Hawthorne et al. (1996a) reported the discovery and characterization of fluorocannilloite with 2.40 TAl apfu ordered at the $T(1)$ site and the A sites slightly over half-filled by Ca. Oberti et al. (1995c) refined the structure of synthetic fluoropargasite with 0.30 Ca apfu at the A sites and 2.20 Al at the $T(1)$ site. Sadanagaite was reported by Sawaki (1989), and Sokolova et al. (2000) and Banno et al. (2004) reported structure refinements of sadanagaite in which nearly all TAl beyond 2.0 apfu is incorporated at the $T(2)$ site. From this work, it became apparent that the order-disorder of Al over $T(1)$ and $T(2)$ is significantly affected by amphibole composition.

Oberti et al. (1995a) reported crystal-structure refinements for a suite of magnesiohornblendes and pargasites from a leucogabbro from Punta Falcone (Sardinia, Italy), in which the TAl contents range from 1.0 to 1.7 apfu. They showed that TAl is partly disordered over the $T(1)$ and the $T(2)$ sites in the amphiboles from Punta Falcone, and found different degrees of Al disorder in amphiboles equilibrated under different temperatures (Fig. 9), indicating that increasing disorder of TAl is related to higher- T (magmatic) equilibration conditions. The maximum degree of disorder observed is 25% in pargasites with 1.60-1.69 TAl apfu, for which the estimated crystallization temperature was around 1000 °C. In agreement with these results, Welch and Knight (1999) reported 15% long-range disorder of TAl in a synthetic pargasite crystallized at 932 °C at 1 kbar with 1.71 TAl apfu.

Bond-valence calculations show that Al-O(7)-Al linkages between adjacent $T(1)$ sites are unfavorable in amphiboles with vacancy or monovalent cations at the A site (Hawthorne 1978b, 1997), whereas they can occur where divalent cations are (locally) present at the A site. Thus a general scheme of ordering for TAl implies incorporation of Al at the $T(1)$ site up to 2.0 apfu, followed by incorporation of Al at the $T(2)$ site. Aluminum contents at $T(1)$ beyond 2.0 apfu should be allowed solely in the presence of a cannilloite component, whereas TAl disorder between the $T(1)$ and $T(2)$ sites below 2.0 apfu is a signal of high- T crystallization.

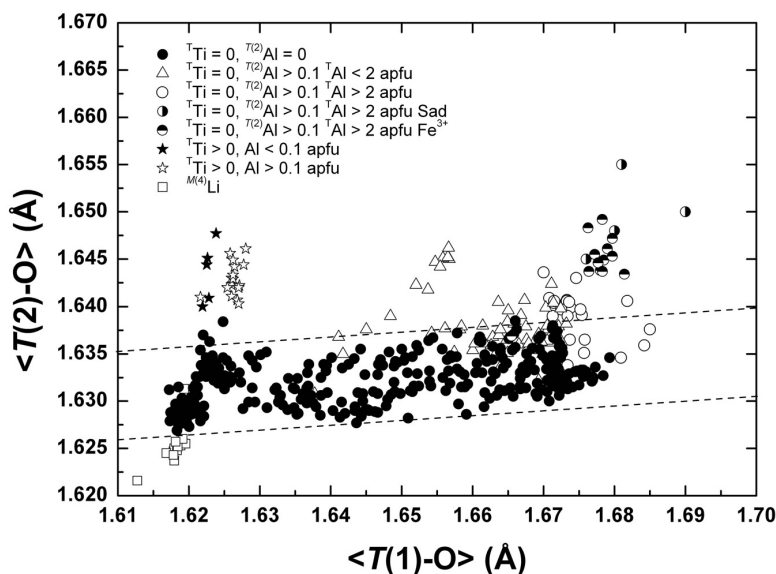


Figure 9. The variation of $\langle T(1)-O \rangle$ is strongly correlated only with the Al content at $T(1)$, whereas $\langle T(2)-O \rangle$ is sensitive to a number of substitutions at different sites. Deviations above the band limited by the broken lines implies substitution at the $T(2)$ site: Ti (black stars), Ti and Al (stars), Al beyond 2.0 apfu TAl (circles), Al below 2.0 apfu TAl (triangles, disorder). The half black dots identify sadanagaite (vertical cut) and volcanic amphiboles with high Fe^{3+} content (horizontal cut).

Figure 9 shows the relative variation of $\langle T(1)\text{-O} \rangle$ and $\langle T(2)\text{-O} \rangle$ in the CNR-IGG-PV amphibole database. Consideration of their crystal-chemical formulae suggests that nearly all the samples within the broken lines have $T(2)$ occupied only by Si. The data above the upper broken line have Ti and/or Al at the $T(2)$ site; those below the lower broken line have significant amounts of Li at the $M(4)$ site. Figure 10 shows the relation between $\langle T(1)\text{-O} \rangle$ and the ${}^T\text{Al}$ content; the line represents the (updated) equation relating ${}^{T(1)}\text{Al}$ and $\langle T(1)\text{-O} \rangle$ obtained by regression analysis and discussed in a previous section, namely ${}^{T(1)}\text{Al}$ (apfu) = $[\langle T(1)\text{-O} \rangle - 1.6193] \times 34.2199$ ($R = 0.997$, $\sigma = 0.048$). It is clear that the majority of amphiboles have ${}^T\text{Al}$ ordered at the $T(1)$ site, and that $\langle T(1)\text{-O} \rangle$ has a limit around 1.680 Å (which should correspond to ${}^{T(1)}\text{Al} = 2.08 \pm 0.05$ apfu). The only amphiboles with $\langle T(1)\text{-O} \rangle$ clearly beyond that limit, besides the ferri-ferrosadanagaite of Hawthorne and Grundy (1977a) with 1.681 Å, are the fluorocannilloites of Hawthorne et al. (1996a), and the synthetic fluoropargasites of Oberti et al. (1995c), for which the bond-valence requirements of the Al-O(7)-Al linkages are fulfilled by the occurrence of Ca at the $A(2)$ site. Notably, the $\langle T(1)\text{-O} \rangle$ value of 1.69(1) Å given by Sokolova et al. (2000) derives from Rietveld refinement, and is most probably overestimated. If we take into account the reported standard deviation, it is compatible with 2.08 Al apfu at $T(1)$ and 0.59 Al apfu at $T(2)$, which would bring this sample closer to the trend in Figure 11.

Figure 11 shows the relation between the refined $\langle T(2)\text{-O} \rangle$ distance and ${}^{T(2)}\text{Al}$ obtained by subtracting ${}^{T(1)}\text{Al}$ from ${}^T\text{Al}$ (estimated by COMAMPH). Negative ${}^{T(2)}\text{Al}$ values are an artifact due to the esd of the method, and are limited to 0.10 Al apfu (i.e., 0.025 Al per site). There is a clear positive trend, which is compared to that modeled for the $T(1)$ site (broken line). However, the variance is large, and no simple linear equation can be used to evaluate ${}^{T(2)}\text{Al}$ from the refined $\langle T(2)\text{-O} \rangle$ value.

A stepwise multiple regression analysis was done on the 413 samples with no ${}^T\text{Ti}$ to relate the $\langle T(2)\text{-O} \rangle$ distance with the chemical composition of the groups of sites. The resulting

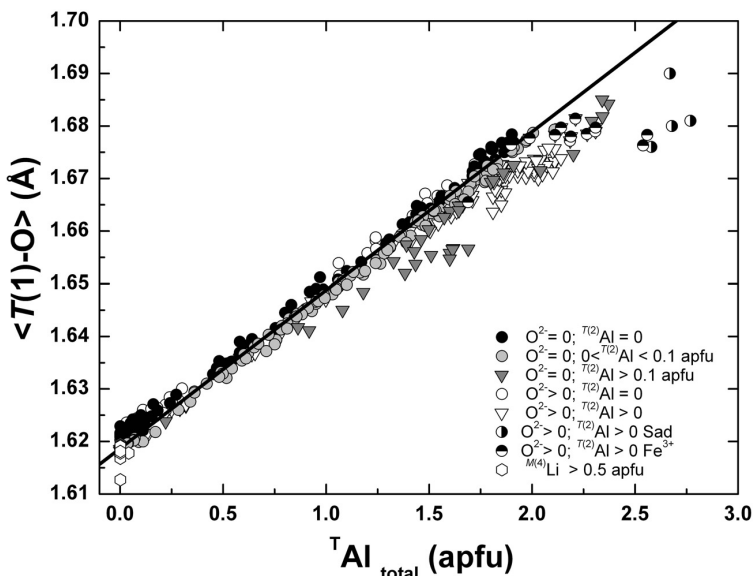


Figure 10. Total ${}^T\text{Al}$ as a function of $\langle T(1)\text{-O} \rangle$. The solid line represents the regression equation ${}^{T(1)}\text{Al}$ (apfu) = $[\langle T(1)\text{-O} \rangle - 1.6193] \times 34.2199$, which was calculated for amphiboles with no Al at the $T(2)$ site in the CNR-IGG-PV database. $\langle T(1)\text{-O} \rangle$ values longer than 1.678 Å correspond to Al at the $T(1)$ site beyond 2.0 apfu.

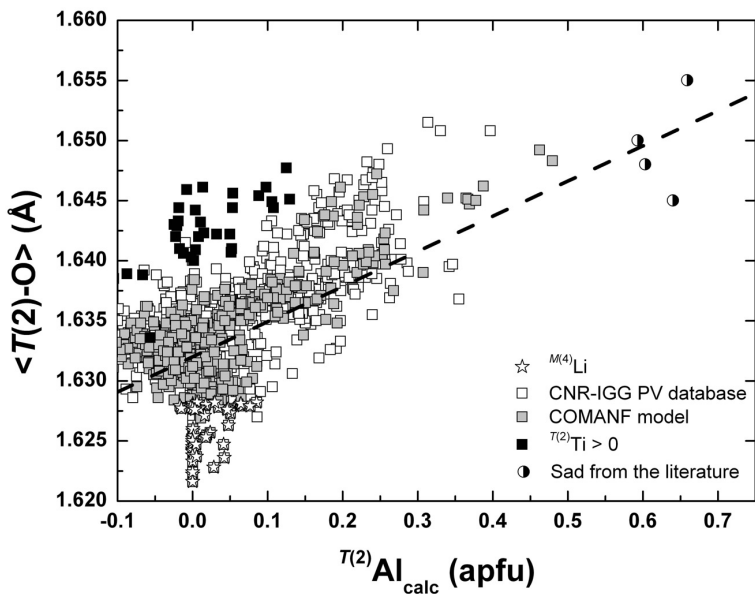


Figure 11. Relation between the Al content at $T(2)$ (expressed as the difference between $T(2)Al$ calculated by COMAMP and $T(1)Al$ calculated by the regression equation of Fig. 10) and the refined $\langle T(2)-O \rangle$ bond length. For the potassic-ferrisadanagaites reported by Sokolova et al. (2000), $T(1)Al$ is calculated based on $\langle T(1)-O \rangle = 1.680 \text{ \AA}$ (see text for discussion).

polynomial equation has 14 terms, the most critical of which is $T(2)Al$ (calculated as $T(2)Al - T(1)Al$); R is 0.956 and the standard error of the estimate (see) is 0.001. Similar results were obtained using the compositions obtained by COMAMP for all the database (1092 samples; $R = 0.927$ and $see = 0.002$). Hence, the $\langle T(2)-O \rangle$ distance is strongly dependent on all the compositional changes in the various sites, the least important being those of the A cations. The same approach was used for the 316 samples with complete Si occupancy at the $T(2)$ site (those falling below the upper broken line in Fig. 9); the resulting polynomial equation has 13 terms, $R = 0.899$ and $see = 0.001$.

Oberti et al. (1995a) provided an equation which relates the $T(2)Al$ content with the difference between the refined $\langle T(2)-O \rangle$ value and that calculated based on the composition of the A, $M(4)$, $M(1,2,3)$ and $T(1)$ sites by means of an equation similar to that described in the previous paragraph. The proposed equation [$T(2)Al = \Delta \langle T(2)-O \rangle \times 35.2592$, $R = 0.985$] worked well for magnesiohornblends and pargasites crystallized under high- T conditions at Punta Falcone, Sardinia. Since then, the equation gave reasonable results for pargasites, but failed for Mg-rich pargasites and sadanagaites (Sokolova et al. 2000). We have seen above that the calculated value of the $\langle T(2)-O \rangle$ distance in the absence of $T(2)Al$ is not well constrained. This is probably the reason why a further attempt to relate $\Delta \langle T(2)-O \rangle$ with $T(2)Al$ within the database could not provide a relation of general use. Therefore, we cannot presently provide a simple procedure to evaluate $T(2)Al$ based on structure refinement.

Beryllium

The only occurrence of Be in amphiboles is in the $P2/a$ amphibole joesmithite, ${}^A\text{Pb}{}^B\text{Ca}_2\text{C}(\text{Mg}_3\text{Fe}^{3+}_2)\text{T}(\text{Si}_6\text{Be}_2)\text{O}_{22}\text{W}(\text{OH})_2$, where Be orders at the $T(1)B$ site, and both electroneutrality and local bond-valence requirements are satisfied by the occurrence of Pb^{2+} at the A site in a strongly asymmetric coordination (Moore 1969; Moore et al. 1993).

Boron

Boron has been reported so far only as a very minor constituent in amphiboles (maximum value = 0.06 apfu in the IGG-CNR-PV database). However, synthesis of a B-rich fluoroedenite (Kohn and Comeforo 1955) with 0.92 B apfu, shows that B can be a major element in amphiboles. No information is available on the site preference, but analogy with Al and Be suggests that it should order at the $T(1)$ site.

Calcium

Calcium is generally a B cation in amphiboles. However, Ca is the dominant A cation in fluorocannilloite (Hawthorne et al. 1996a), and is significant in natural and synthetic fluoropargasites (Oberti et al. 1995c), where it orders at the $A(2)$ site. In all these samples, ^ACa is presumed to locally couple with Al at the two adjacent $T(1)$ sites.

Cobalt and nickel

Della Ventura et al. (1993a, 1996, 1997) showed that both Ni and Co preferentially enter the $M(1,3)$ sites in synthetic richterite and potassic-richterite, with a slight preference for the $M(3)$ site. The partition coefficients calculated on the basis of the Rietveld-derived site-populations [defined as $K_d^{M^{2+}} = (M^{2+}/\text{Mg})_{M(1,3)}/(M^{2+}/\text{Mg})_{M(2)}$, with $M^{2+} = \text{Ni}^{2+}$ or Co^{2+}] are $K_d^{\text{Ni}} = 2.98 \pm 0.37$ and $K_d^{\text{Co}} = 1.34 \pm 0.31$, and $K_d^{\text{Ni}} = 4.26 \pm 0.56$ and $K_d^{\text{Co}} = 1.92 \pm 0.29$ for the K and Na series, respectively (Fig. 12). This evidence confirms that electronic structure has a significant effect on long-range ordering of cations in the amphibole structure. Ni^{2+} is smaller than Mg, whereas Co^{2+} is larger than Mg; if long-range ordering of cations were controlled solely by their size, then the K_d value for Ni^{2+} -Mg ordering should be > 1.0 , whereas that for Co^{2+} -Mg ordering should be < 1.0 , which is not the case for these amphiboles (Fig. 12). Both Rietveld site-occupancy refinement and FTIR spectroscopy shows that Co and Ni are not incorporated at the $M(4)$ site in these synthetic amphiboles (Della Ventura et al. 1993b, 1996, 1997). Stoichiometric Co-pargasite was synthesized by Della Ventura et al. (1998), who showed that Co is ordered at the $M(1)$ and $M(3)$ sites (see Oberti et al. 2007 and Hawthorne and Della Ventura 2007 for more details).

Chromium, vanadium, scandium and indium

All these lithophile transition-elements are known to occur in limited amounts in monoclinic amphiboles. Chromium rarely exceeds 0.15 apfu; 0.38 Cr apfu was reported for glaucophane in jadeitite from Burma (Mével and Kienast 1986), and 0.35 Cr apfu for pargasite in a lherzolite xenolith from Nunivak, Alaska (Francis 1976). The highest reported V content in amphibole is 0.64 apfu in potassic-leakeite from pegmatite-like veinlets that cut a Mn ore-body in the Tanohata mine, Iwate Prefecture, Japan (Matsubara et al. 2002).

Systematic work on synthetic analogues has shown that Sc, In and Cr^{3+} can be major components in calcic (pargasite: Raudsepp et al. 1987a, 1991; Oberti et al. 1998), sodic-calcic (katophorite: Oberti et al. 1998) and sodic amphiboles (eckermannite, nyböite: Raudsepp et al.

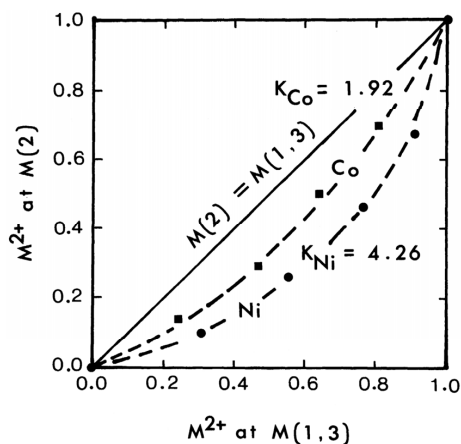


Figure 12. Relation between the refined Ni-Mg and Co-Mg occupancies at the $M(1,3)$ and $M(2)$ sites. Circles: the Ni,Mg series; squares; the Co-Mg series (from Della Ventura et al. 1993a).

1987b, 1991; Oberti et al. 1999). Therefore, Cr^{3+} incorporation is probably controlled solely by its geochemical availability. Structure refinement shows that in OH-amphiboles, these elements are disordered between the $M(2)$ and $M(3)$ sites; accordingly, OH-stretching FTIR spectroscopy shows absorption bands which can be ascribed to transition elements at the $M(1)$ and $M(3)$ sites (Raudsepp et al. 1987a; Fialips-Guédon et al. 2000) (Fig. 5; see Hawthorne and Della Ventura 2007 for more details). In the F analogues, the transition metals are ordered at the $M(2)$ site (Raudsepp et al. 1987a,b; Oberti et al. 1998, 1999). Oberti et al. (1999) first noted that the electronic properties of the transition element have a major control on their incorporation into the amphibole structure, and that the nature of the O(3) anion (OH^- , F^-) has a strong control on cation ordering within the $M(1,2,3)$ sites.

Gallium

The behavior of Ga is analogous to that of Al. Gallium is both a C and a T cation in synthetic pargasites and magnesiokatophorites, with a significant preference for [4]-coordination. $^{\text{C}}\text{Ga}$ can partition between $M(2)$ and $M(3)$ in pargasite (e.g., Raudsepp et al. 1987a), but is ordered at the $M(2)$ site in fluoropargasite (Oberti et al. 1998; Jenkins and Hawthorne 1995). $^{\text{T}}\text{Ga}$ generally orders at the $T(1)$ sites, but incorporation at the $T(2)$ site has been detected in Ga-bearing fluoropargasite (Jenkins and Hawthorne 1995; Oberti et al. 1998). Similar to Al, Ga partitioning between the $M(2,3)$ and $T(1,2)$ sites depends on the conditions of crystallization; however, Pavlovich and Jenkins (2003) reported a correlation between Ga at the $M(2)$ site and Na at the $M(4)$ site in synthetic magnesiokatophorites crystallized at fixed T and P conditions of 900 °C and 1.5 GPa. Incorporation of $^{\text{T}}\text{Ga}$ can be easily detected by a strong progressive increase in the refined site-scattering values coupled with a decrease in the O(5)-O(6)-O(5) angle, a measure of the kinking of the double-chain of tetrahedra. Figure 13 shows the effects of incorporating larger trivalent (Al and Ga, with ionic radii 0.39 and 0.47 Å, respectively) and tetravalent cations (Ti and Ge, with ionic radii 0.42 and 0.39 Å, respectively) on the kinking

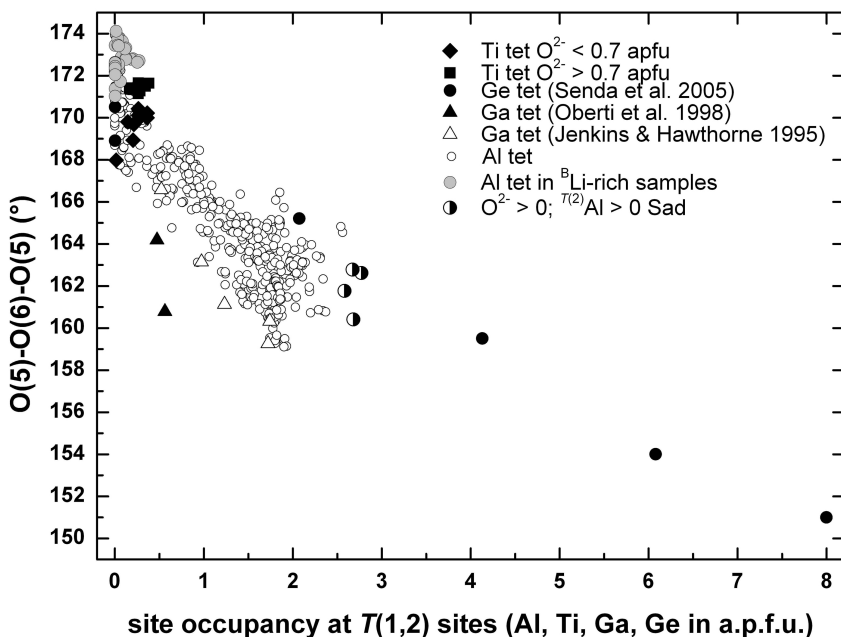


Figure 13. Variation in the O(5)-O(6)-O(5) angle as a function of the amount of Al (i.r. = 0.39 Å), Ti^{4+} (0.42 Å), Ga (0.47 Å) or Ge (0.39 Å) substituting for Si (0.26 Å) at the $T(1,2)$ sites.

of the double chain of tetrahedra. Papers relevant to this issue are Raudsepp et al. (1987a,b), Oberti et al. (1998), Jenkins and Hawthorne (1995), Jenkins et al. (2002), Pavlovich and Jenkins (2003), Hawthorne and Della Ventura (2007).

In geochemical modeling of the partition coefficients for transition elements, only the fraction of Ga occurring at the $M(2,3)$ sites should be compared with amounts of the other trivalent C cations.

Germanium

Synthesis of Ge-bearing amphiboles was reported by Wiecek et al. (1992), but no information on site occupancy is provided. Senda et al. (2005) showed that Ge can substitute completely for Si in synthetic richterite. Rietveld refinement of X-ray powder data shows that along the ${}^A\text{Na} {}^B(\text{NaCa}) {}^C\text{Mg}_5 {}^T\text{Si}_8 \text{O}_{22} {}^W(\text{OH})_2 - {}^A\text{Na} {}^B(\text{NaCa}) {}^C\text{Mg}_5 {}^T\text{Ge}_8 \text{O}_{22} {}^W(\text{OH})_2$ join, Ge has a marked preference for $T(2)$ over $T(1)$. Increasing Ge correlates linearly with an increase in both $\langle T(1)\text{-O} \rangle$ and $\langle T(2)\text{-O} \rangle$, and in the kinking of the double chain of tetrahedra (measured by the $\text{O}(5)\text{-O}(6)\text{-O}(5)$ angle, Fig. 13).

Ferrous iron

Similar to Mg and Mn^{2+} , Fe^{2+} can be both a B and a C cation. The C site-preference is usually $M(3) > M(1) \gg M(2)$; random partitioning between the $M(1)$ and $M(3)$ sites is however observed at high- T conditions of crystallization or during annealing. In cummingtonites, the presence of Fe^{2+} at the $M(4)$ site lowers the transition temperature to the $C2/m$ structure (see Welch et al. 2007).

There have been numerous measurements of site populations of Fe^{2+} in amphiboles by SREF, Mössbauer and infrared spectroscopies. SREF can have problems with amphiboles of particularly complicated compositions due to the large number of scattering species and possible variations in valence state of Fe. Mössbauer spectroscopy has the advantage of “seeing” only Fe (in amphiboles), but spectra are often poorly resolved (allowing only partial interpretation, as in the spectra of the Mg-Fe-Mn-Li amphiboles), and do not address the other components of the structure. The same issues affect infrared spectroscopy, with the added complication that it “sees” all components of the structure and can have such poor resolution that spectra cannot be interpreted at all. This being said, all methods have produced useful information on ordering of Fe^{2+} .

Figure 14 shows the distribution of Fe^{2+} over the $M(1)$ and $M(3)$ sites in amphiboles of the glaucophane–ferroglaucophane–magnesianriebeckite–riebeckite series (●) and nyboite (■) (data from Ungaretti et al. 1978). There is strong site-preference for $M(3)$ and very regular behavior as a function of bulk composition. Note the posi-

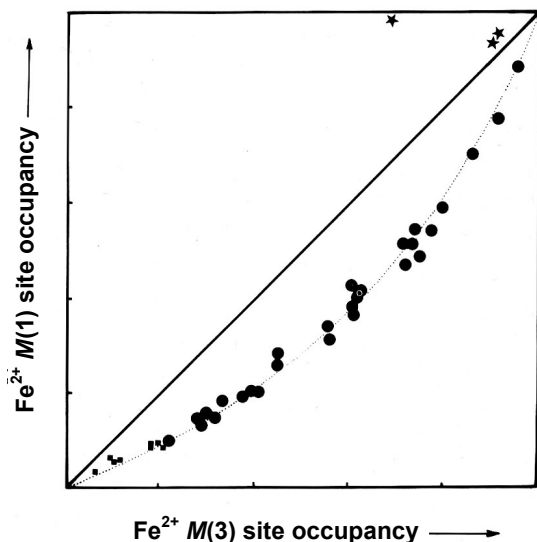


Figure 14. The distribution of Fe^{2+} over the $M(1)$ and $M(3)$ sites in amphiboles of the glaucophane–ferroglaucophane–magnesianriebeckite–riebeckite series (●) and nyboite (■), data from Ungaretti et al. (1978). The star indicates riebeckite containing ${}^C\text{Li}$ (from Hawthorne 1983a).

tion of the Li-bearing riebeckites indicated by the stars in Figure 14; the deviation from the general trend for these amphiboles is caused by the presence of Li at the $M(3)$ site. Figure 15 shows the distribution of Fe^{2+} over the $M(1)$, $M(2)$ and $M(3)$ sites in amphiboles of the tremolite–ferro-actinolite series (Yang and Evans 1996; Evans and Yang 1998). Here we see very different behavior: the distribution of Fe^{2+} over the $M(1)$ and $M(3)$ sites is now very similar (Fig. 15b); there is no longer any strong site-preference of Fe^{2+} for the $M(3)$ site. Almost the same behavior is seen in the amphiboles of the cummingtonite–grunerite series (Fig. 16; Hirschman et al. 1994); Figure 16b shows the slightest suggestion of a preference of Fe^{2+} for the $M(1)$ site. Amphiboles of the tremolite–ferro-actinolite and cummingtonite–grunerite series are significantly different from the amphiboles of the glaucophane–ferroglaucophane–magnesioriebeckite–riebeckite series in that they have divalent cations (primarily Mg and Fe^{2+}) dominant at the $M(2)$ site. In tremolite–ferro-actinolite, Fe^{2+} is equally distributed over $M(1)$ and $M(2)$ (Fig. 15a) and $M(2)$ and $M(3)$ (Fig. 15c), whereas in cummingtonite–grunerite, Fe^{2+} shows a distinct preference for $M(1)$ relative to $M(2)$ (Fig. 16c). The strong preference of Fe^{2+} for $M(3)$ relative to $M(1)$ in glaucophane–ferroglaucophane–magnesioriebeckite–riebeckite amphiboles and the lack of such preference in tremolite–ferro-actinolite and cummingtonite–grunerite amphiboles is in accord with the observation of Hawthorne (1983a) that the degree of ordering of Fe^{2+} at $M(3)$ relative to $M(1)$ is strongly an inverse function of the aggregate size of the $M(2)$ cations.

In Mg-Fe-Mn amphiboles, the $M(4)$ site is occupied by Mg, Fe^{2+} and Mn^{2+} . Extensive Mössbauer spectroscopy showed that Fe^{2+} is strongly ordered at $M(4)$ relative to $M(1)$, $M(2)$ and $M(3)$ (e.g., Bancroft 1967; Hafner and Ghose 1971; Ghose and Weidner 1972). Figure 17 shows the spectra of cummingtonite and grunerite; the inner doublet is due to Fe^{2+} at $M(4)$ and the outer doublet is due to Fe^{2+} at $M(1,2,3)$ combined. In cummingtonite close to nominal composition (Fig. 17a), the amount of Fe^{2+} is very small and most of it occurs at the $M(4)$ site; in grunerite (Fig. 17b), the amount of Fe^{2+} is large, and although the site occupancy is higher at $M(4)$ and lower at $M(1,2,3)$, the fact that there are two $M(4)$ sites and five $M(1,2,3)$ sites in the structural formula means that the total amount of Fe^{2+} is higher at $M(1,2,3)$ than at $M(4)$, and hence the outer doublet is more intense than the inner doublet (compare Figs. 17b and 17a). Hirschmann et al. (1994) showed that (1) this site-preference of Fe^{2+} for $M(4)$ extends across the complete cummingtonite–grunerite series, and (2) it is much stronger than any other site preference of Fe^{2+} in this series (Fig. 16). Also apparent from Figure 16a is the fact that the degree of order of Fe^{2+} at $M(4)$ relative to $M(1)$ [or $M(2)$ or $M(3)$] is strongly sensitive to the temperature of equilibration. Similar results have been obtained for the orthorhombic Mg-Fe-Mn amphiboles (e.g., Bancroft et al. 1966; Law 1981; Seifert 1977, 1978).

In calcic amphiboles, it is common to have C cations in excess of 5.0 apfu, implying that some of the C cations occur at the $M(4)$ site. The first direct evidence of this is shown in Figure 18 (Goldman and Rossman 1977; Goldman 1979). The Mössbauer spectrum of tremolite containing 1.9 wt% FeO (Fig. 18a) is very similar to the Mössbauer spectrum of grunerite containing 37.0 wt% FeO (Fig. 18b); in both cases, the inner doublet was assigned to Fe^{2+} at the $M(4)$ site and the outer doublet was assigned to Fe^{2+} at the (overlapped) $M(1,2,3)$ sites. Can we be sure of this assignment? Figures 18c and 18d show the electronic absorption spectra of the same two amphiboles. Both spectra show an intense band at 1030 nm in the β polarization, a band that is absent in the spectrum of a pargasite (Goldman and Rossman 1977) that contains no “excess” (Mg, Fe^{2+} , Mn^{2+}) to assign to $M(4)$. The intensity of an absorption is a function of the probability of that transition. The transition probability is governed by the Laporte selection rule (King 1964) which forbids transitions between $3d$ orbitals. When a transition metal occupies a site without a center of symmetry, mixing between the $3d$ and $4p$ orbitals allows a transition, the intensity of which is a function of the degree of mixing which, in turn, is related to the deviation of the cation environment from centrosymmetry. Thus when a transition-metal cation occurs at more than one site in a crystal, the intensities of the $d-d$ bands are a function of both the cation site-populations and the deviation of the cation environment from centrosymmetry. For Fe^{2+} in the amphibole structure, the $M(4)$ site occupies a far less centrosymmetric environment than the

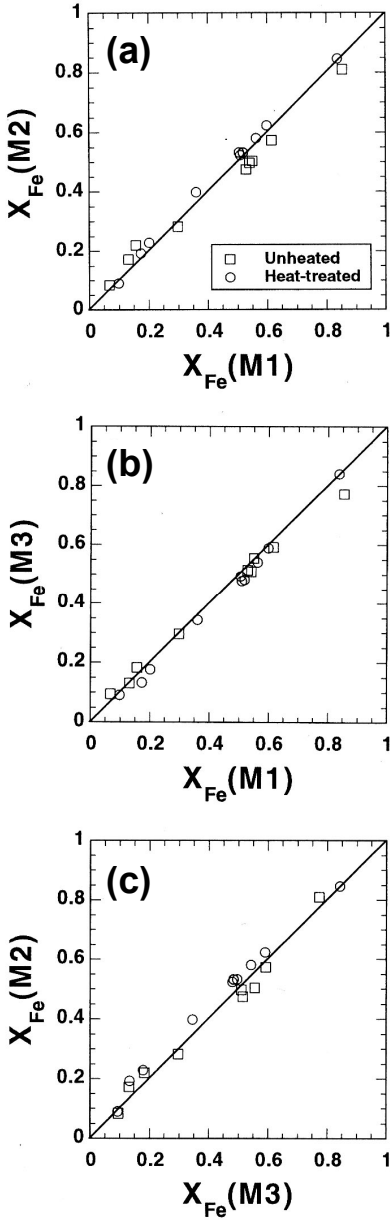


Figure 15. The distribution of Fe^{2+} over the $M(1)$, $M(2)$ and $M(3)$ sites in amphiboles of the tremolite-ferro-actinolite series; (a) $M(2)$ vs. $M(1)$; (b) $M(3)$ vs. $M(1)$; (c) $M(2)$ vs. $M(3)$ (from Evans and Yang 1998).

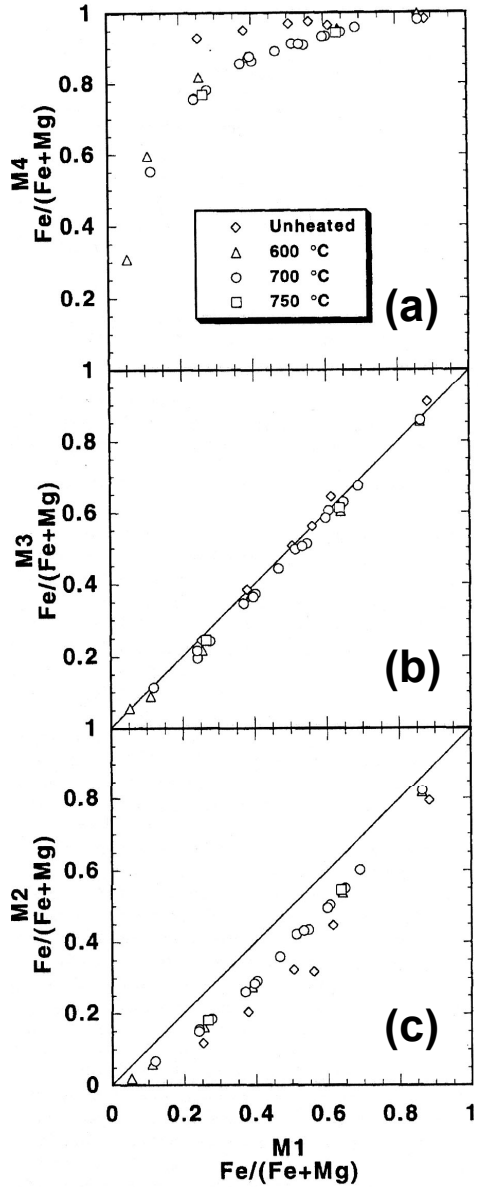


Figure 16. The distribution of Fe^{2+} over the $M(1)$, $M(2)$, $M(3)$ and $M(4)$ sites in amphiboles of the cummingtonite-grunerite series; (a) $M(4)$ vs. $M(1)$; (b) $M(3)$ vs. $M(1)$; (c) $M(2)$ vs. $M(1)$ (from Hirschmann et al. 1994).

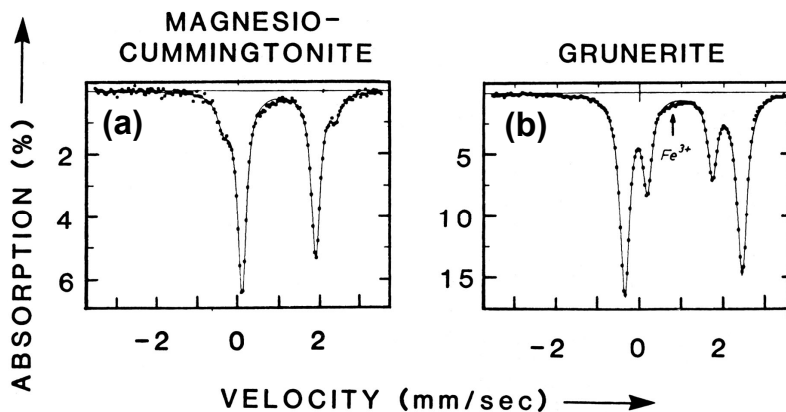


Figure 17. Mössbauer spectra of (a) magnesiocummingtonite, and (b) grunerite (modified from Hafner and Ghose 1971).

$M(1,2,3)$ sites, and hence any Fe^{2+} at $M(4)$ will absorb far more strongly than Fe^{2+} at $M(1,2,3)$, accounting for the relative intensity of the 1030 nm band in the spectrum of grunerite (Fig. 18d). However, this band is also observed in the spectrum of tremolite containing 1.9 wt% FeO (Fig. 18c), indicating that this band may be assigned to Fe^{2+} at the $M(4)$ site.

As with the amphiboles of the cummingtonite–grunerite series, the distribution of Fe^{2+} between $M(4)$ and $M(1,2,3)$ shows a strong temperature dependence in amphiboles of the tremolite–actinolite series (Skogby and Annersten 1985; Skogby 1987; Evans and Yang 1998; Skogby and Ferrow 1989; Driscall et al. 2005). Figure 19 (from Driscall et al. 2005) is a composite plot of data from several sources showing the distribution of Fe^{2+} over $M(4)$ and $M(1,2,3)$ together with the temperatures of equilibration and the isotherms calculated for ΔG° (1073 K) = 20 kJ (broken lines), and ΔG° (298 K) = 62 kJ and ΔS° (298 K) = 54 kJ/K (broken lines).

When considering equilibration of cations over different sites in a structure, it is important to know the kinetics of the process such that one can estimate (1) whether equilibrium has been achieved in laboratory experiments, and (2) whether it is possible to quench cation distributions in natural processes. Skogby and Annersten (1985) and Skogby (1987) examined this issue in Fe-bearing tremolite; Figure 20 shows that equilibrium is achieved after about 5 hours at 650 and 750 °C.

An important factor in the occurrence of ($\text{Mg}, \text{Fe}^{2+}, \text{Mn}^{2+}$) at the $M(4)$ site is whether the ($\text{Mg}, \text{Fe}^{2+}, \text{Mn}^{2+}$) at $M(4)$ resides in exsolved Mg-Fe-Mn amphibole in a calcic host (i.e., shows extreme short-range order) or is truly a component of the calcic amphibole. Skogby and Ferrow (1989) and Driscall et al. (2005) examined their samples in the tremolite–actinolite join [in which they characterized Fe^{2+} at $M(4)$] and did not report any exsolution structures (just a small % of chain-multiplicity faults), indicating that $^B(\text{Mg}, \text{Fe}^{2+}, \text{Mn}^{2+})$ is a true component of the calcic amphibole, at least at concentrations significant but usually < 0.50 apfu. However, these cations order at a position [namely, $M(4')$] closer to the strip of octahedra, and assume a coordination more similar to [6]-fold.

Ferric iron

Trivalent iron is always ordered at the $M(2)$ site in amphiboles with $W = (\text{OH}, \text{F}, \text{Cl})_2$, but can occur at all the $M(1,2,3)$ sites in the presence of the oxo component. The oxidation of iron at the $M(1)$ and $M(3)$ sites is the principal mechanism to achieve local bond-valence satisfaction during post-crystallization dehydrogenation processes (and experimental annealing). More details on the dehydrogenation process are given in a following section of this chapter.

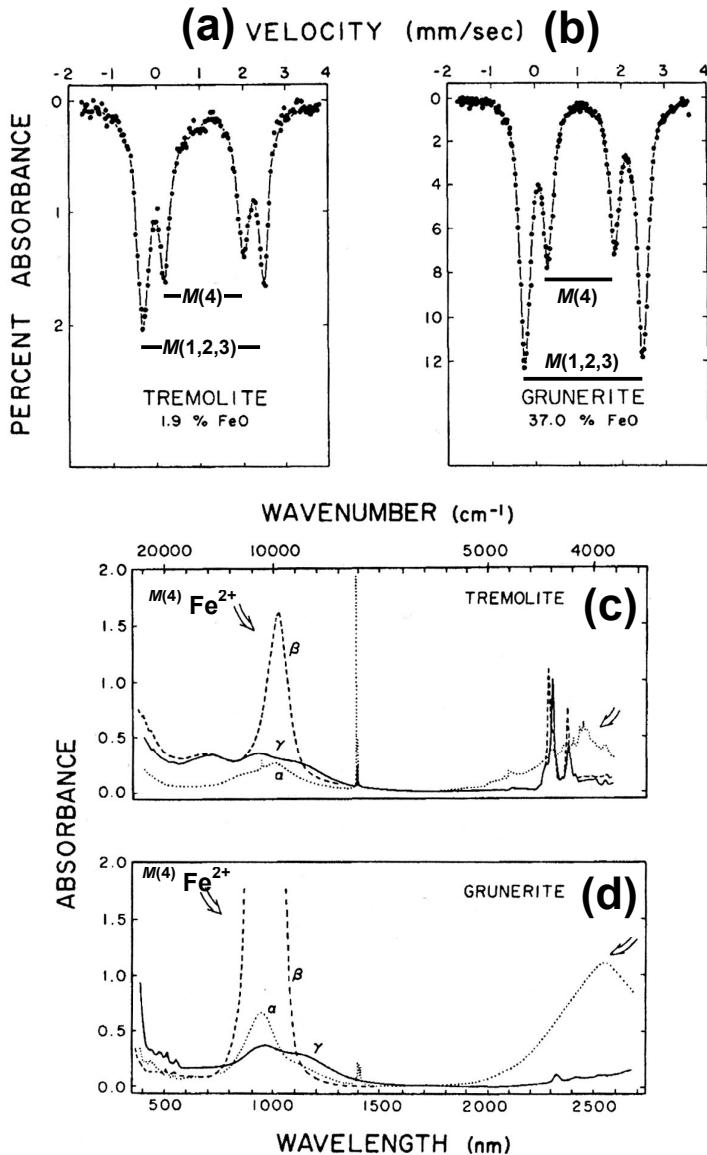


Figure 18. Mössbauer spectra of (a) low-Fe tremolite, and (b) Fe-rich grunerite; electronic absorption spectra of (c) low-Fe tremolite, and (d) Fe-rich grunerite [modified from Goldman and Rossman (1978) and Goldman (1979)].

One significant issue is the lack of Fe³⁺ as a T cation. There are chemical analyses in the literature in which Si + Al + Ti < 8.0 apfu. However, we have investigated several of these amphiboles over the past 30 years, and all showed the same result: either Mössbauer spectroscopy or SREF showed no evidence of ^[4]Fe³⁺, and re-analysis of the amphibole resulted in formulae with Si + Al + Ti > 8.0 apfu. Hawthorne and Grundy (1977b) reported 0.04 ^[4]Fe³⁺ apfu based on Mössbauer spectroscopy, but inspection of the spectrum shows that the relevant doublet is a result of overfitting the spectrum (i.e., fitting an additional doublet

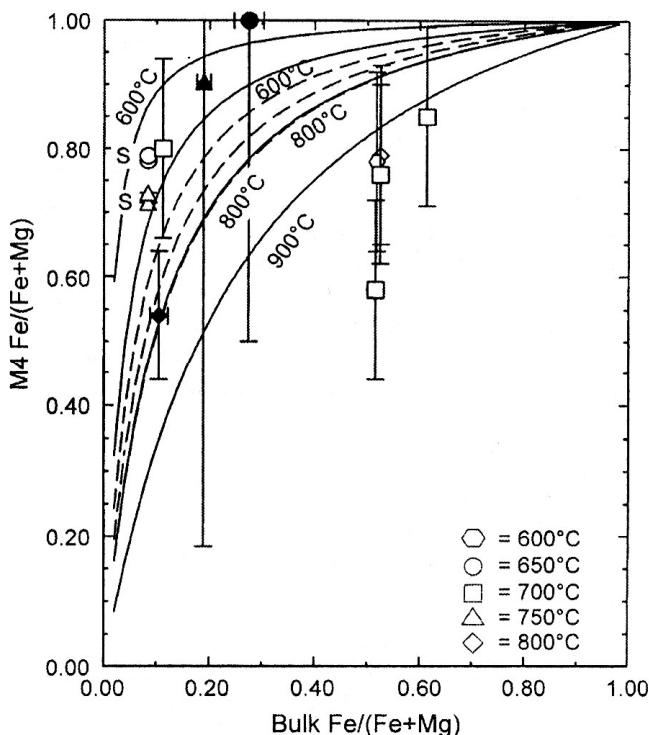


Figure 19. The distribution of Fe²⁺ over M(4) and M(1,2,3), together with the temperatures of equilibration and the isotherms calculated for ΔG° (1073 K) = 20 kJ (broken lines), and ΔG° (298 K) = 62 kJ and ΔS° (298 K) = 54 kJ/K (broken lines) (from Driscall et al. 2005).

to compensate for orientational asymmetry in the spectrum). The reason why ⁴Fe³⁺ is not present in amphiboles is not clear. ⁴Fe³⁺ is present in pyroxene (e.g., Mössbauer: Huckenholz et al. 1969; Hafner and Huckenholz 1971; Virgo 1972; SREF: Cellai et al. 1994) and in mica (e.g., Mössbauer: Rancourt et al. 1992; SREF: Brigatti et al. 1996), and the similarity between these structures would seem to suggest that ⁴Fe³⁺ should occur in amphiboles. However, (1) this does not seem to be the case, and (2) the reason why ⁴Fe³⁺ does not occur in amphiboles is not understood. The behavior of Fe³⁺ in amphibole will be described more extensively in the section on the oxo component below.

Lithium

Until 1992, Li was considered exclusively a B cation in amphiboles, and thus confined to Mg-Fe-Mn-Li amphiboles (e.g., Ginzburg 1965; Litvin et al. 1975). The occurrence of ^cLi in minor amounts in sodic amphiboles was indicated by chemical analyses (e.g., Borley 1963; Hawthorne 1978a) and by anomalously low scattering at the M(3) site (Hawthorne 1978a; Ungaretti et al. 1978). However, the discovery of leakeite, ^ANa ^BNa₂ ^C(Mg₂Fe³⁺₂Li) ^TSi₈ O₂₂ ^W(OH)₂ (Hawthorne et al. 1992), kornite, ^AK ^BNa₂ ^C(Mg₂Mn³⁺₂Li) ^TSi₈ O₂₂ ^W(OH)₂ (Armbruster et al. 1993) and, more recently, fluoro-ferroleakeite, ^ANa ^BNa₂ ^C(Fe²⁺₂Fe³⁺₂Li) ^TSi₈ O₂₂ ^W(OH)₂ (Hawthorne et al. 1996c), potassic-leakeite, ^AK ^BNa₂ ^C(Mg₃Fe³⁺₂Li) ^TSi₈ O₂₂ ^W(OH)₂ (Matsubara et al. 2002), and dellaventurite, ^ANa ^BNa₂ ^C(MgMn³⁺₂Ti⁴⁺Li) ^TSi₈ O₂₂ ^WO₂ (Tait et al. 2005), showed that ^cLi can be a major constituent in amphiboles in manganeseiferous metasediments, and Hawthorne et al. (1993, 1994, 1996c, 2001) went on to show that ^cLi is a not-uncommon major constituent in sodic amphiboles from Si-saturated peralkaline granites.

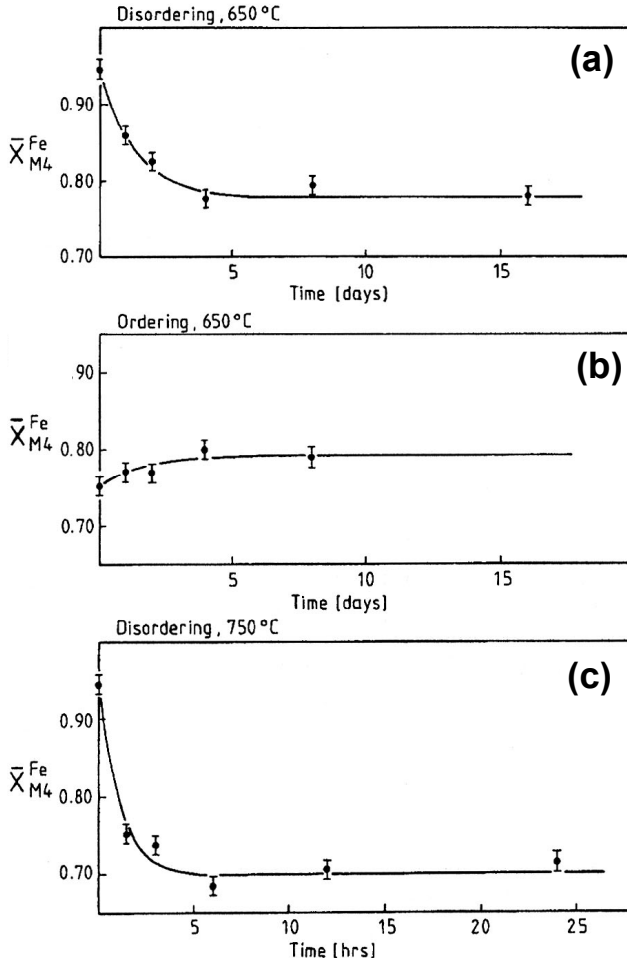
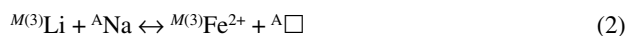
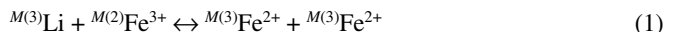


Figure 20. Kinetic experiments on Fe-bearing tremolite in the presence of H₂O: (a) disordering at 650 °C; (b) ordering at 650 °C; (c) disordering at 750 °C (modified from Skogby 1987).

Crystal-structure refinement has shown that ^cLi is restricted to the *M*(3) site (Hawthorne et al. 1993, 1994), and is easily apparent from the anomalously low site-scattering observed at the *M*(3) site (Hawthorne and Oberti 2007, Fig. 1). The introduction of Li at the *M*(3) site must be accompanied by additional substitutions at adjacent sites to satisfy the bond-valence requirements at the anions bonded to ^M(3)Li. Hawthorne et al. (1994) showed that this involves incorporation of trivalent cations (usually Fe³⁺) at the *M*(2) site. In all the ^cLi amphiboles studied, ^ANa ≥ ^cLi and is usually ordered at a particularly off-centred *A*(*m*) site, showing that ^ANa helps to satisfy bond-strength requirements; the proposed mechanism involves changes in individual *T*(1)-O distances, *T*(1)-O(1) being always very short in ^cLi-bearing amphiboles (Oberti et al. 2003a). This conceptual mechanism may be written as



where (2) might occur in amphiboles with vacant *A* sites (e.g., riebeckite).

Li has long been known as a B cation in amphiboles, specifically in the *Pnma* amphibole holmquistite, ideally $A^{\square} B Li_2 C(Mg_3Al)_2 T Si_8 O_{22} W(OH)_2$. However, the discovery of several monoclinic amphiboles with essential $B Li$ has greatly expanded the compositional and structural range of $B Li$ -bearing amphiboles: clino-ferriholmquistite, $A^{\square} B Li_2 C(Fe^{2+}_3Fe^{3+}_2) T Si_8 O_{22} W(OH)_2$ (Caballero et al. 1998), sodic-ferripedrizite, $A Na B Li_2 C(Mg_2Fe^{3+}_2Li) T Si_8 O_{22} W(OH)_2$ (Oberti et al. 2000a; note that sodic-ferripedrizite was originally defined by Oberti et al. 2000a with $B = (NaLi)$, but was redefined by Leake et al. 2003 with $B = Li_2$), ferripedrizite, $A Na B Li_2 C(Mg_2Fe^{3+}_2Li) T Si_8 O_{22} W(OH)_2$ (Caballero et al. 2002), sodic-ferri-ferropedrizite, $A Na B Li_2 C(Fe^{2+}_2Fe^{3+}_2Li) T Si_8 O_{22} W(OH)_2$ (Oberti et al. 2003b), clino-ferri-ferroholmquistite, $A^{\square} B Li_2 C(Fe^{2+}_3Fe^{3+}_2) T Si_8 O_{22} W(OH)_2$ (Oberti et al. 2003b), ferri-ottoliniite, $A^{\square} B(LiNa) C(Mg_3Fe^{3+}_2) T Si_8 O_{22} W(OH)_2$ (Oberti et al. 2004), and ferriwhittakerite, $A Na B(LiNa) C(Mg_2Fe^{3+}_2Li) T Si_8 O_{22} W(OH)_2$ (Oberti et al. 2004). Of great importance was the observation that there is $Li \leftrightarrow Na$ solid-solution at the $M(4)$ site, and Oberti et al. (2004) showed that this solid solution is complete (Fig. 21) (more details are given in Oberti et al. 2007). Full occupancy of Li at the $M(4)$ site in naturally occurring amphiboles has been reported only in *Pnma* holmquistite (with no Li at $M(3)$, see Cámara and Oberti 2005), in clino-ferri-ferroholmquistite, and in *C2/m* sodic-pedrizite with up to 0.90 Li apfu at the $M(3)$ site. In the compositional space of clinoholmquistite, only Fe-rich varieties have been characterized so far (Oberti et al. 2005). Note that amphiboles with mixed $B(Na,Li)$ occupancy always have significant Li at $M(3)$.

The parageneses of relevance are metamorphosed episyenites and alkali ultramafic diatremes (cf. Oberti et al. 2003a and Cámara and Oberti 2005 for comprehensive reviews). The incorporation of Li into the amphibole structure is strongly related to the geochemistry of the coexisting fluid. In addition, analysis of Mg-Fe-Mn-Li and Na-Ca-Mg-Fe-Mn-Li amphiboles in episyenites from the Pedriza Massif, Sierra de Guadarrama, Spain (Oberti et al. 2003a) shows that high- T of crystallization favors incorporation of Li at the $M(3)$ site, which is consistent with the occurrence of only $C Li$ in peralkaline granites and the absence of $B Li$ in amphiboles from low- T Mn-rich metasediments.

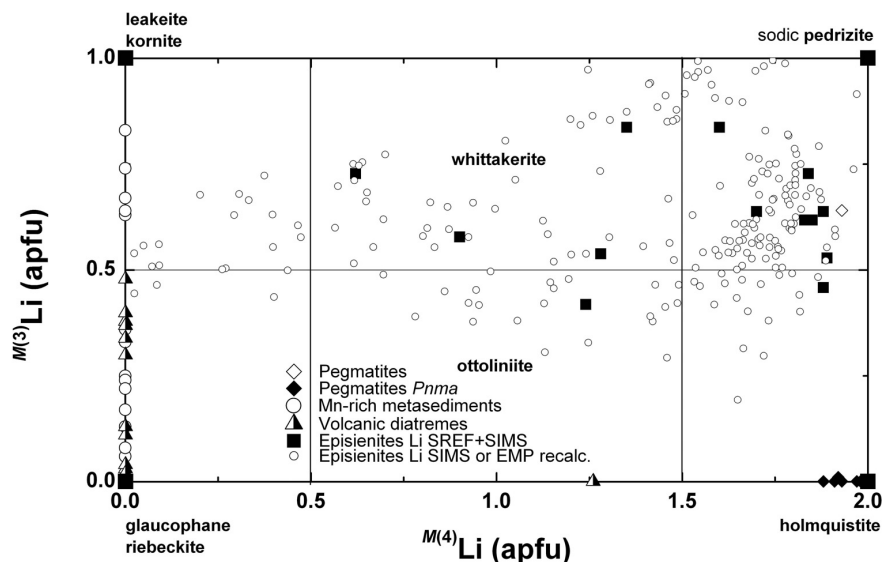


Figure 21. Li partitioning between the $M(3)$ and $M(4)$ sites in amphiboles from various geochemical and petrogenic environments. The data available in the literature have been combined with the CNR-IGG-PV database. This plot does not show homovalent substitutions such as $Mg_{-1}Fe^{2+}_1$ or $Al_{-1}(Fe^{3+}, Mn^{3+})_1$.

There is spectroscopic evidence of ~ 0.20 Li apfu at the A site in a synthetic clinoferritoholmquistite (Iezzi et al. 2004). Therefore, Li must be considered a frequent and important element in amphibole crystal-chemistry, as is apparent by the rapid evolution of amphibole classification at this time (Leake et al. 1997, 2003).

Magnesium

Magnesium is one of the major constituents of amphiboles. The composition $A^{\square} B^{\text{Mg}}_2 C^{\text{Mg}_5} T^{\text{Si}_8} O_{22} W^{\text{(OH)}_2}$ (cummingtonite) is used as the starting point for classification of Mg-Fe-Mn-Li amphiboles, and $A^{\square} B^{\text{Ca}_2} C^{\text{Mg}_5} T^{\text{Si}_8} O_{22} W^{\text{(OH)}_2}$ (tremolite) as the starting point for the classification of calcic, sodic-calcic and sodic amphiboles.

The only significant recent improvement in our understanding of Mg crystal-chemistry in amphiboles concerns the detection and characterization of mixed Na, Ca and Mg occupancy at the $M(4)$ site. Due to their different ionic radii and preferred coordination, the occurrence of large and small cations at the $M(4)$ site is represented in the long-range perspective by a non-spherical distribution of electron density, indicative of two distinct sub-sites [$M(4)$ and $M(4')$] in the structure (Fig. 22). Smaller cations order closer to the wall of octahedra [at the $M(4')$ site], and tend to assume [6]-coordination.

The presence of a significant $B^{\text{(Mg,Fe)}^{2+}}$ component (up to 0.35 apfu) is common in amphiboles crystallized under high- T , P conditions, such as mantle environments. It is also common in synthetic amphiboles (Oberti et al. 1999). Amphiboles with high $B^{\text{(Mg,Fe)}^{2+}}$ components have anomalously low values of the β angle, smaller unit-cell volumes, and slightly more kinked chains of tetrahedra [as measured by the $O(5)$ - $O(6)$ - $O(5)$ angle]. A peculiar series of synthetic amphiboles with $B = (\text{NaMg})$ (i.e., with the charge arrangement of richterite) was studied in detail because of its relevance to phase-transitions in amphiboles. In fact, this particular composition at the $M(4)$ site implies crystallization in the space group $P2_1/m$ (Oberti et al. 2007; Welch et al. 2007).

Manganese

Similar to Mg, Mn^{2+} can be incorporated at the $M(4')$ and at the $M(1,2,3)$ sites. Mn^{2+} is preferentially ordered at the $M(4')$ site (e.g., Oberti et al. 1993b, 2006), suggesting that its site preference is controlled by ionic radius, and at the $M(1)$ or $M(3)$ site, depending on the overall amphibole composition. In synthetic manganean fluoro-edenite and fluoropargasite, where the presence of F strongly decreases the size of the $M(1)$ and $M(3)$ sites (cf. the paragraph on fluorine) and the $M(3)$ is particularly small (cf. the paragraph on Al), the site preference is $M(4) \gg M(2) \gg M(1) \gg M(3)$ (Oberti et al. 1997). Mn disorder during annealing has been studied

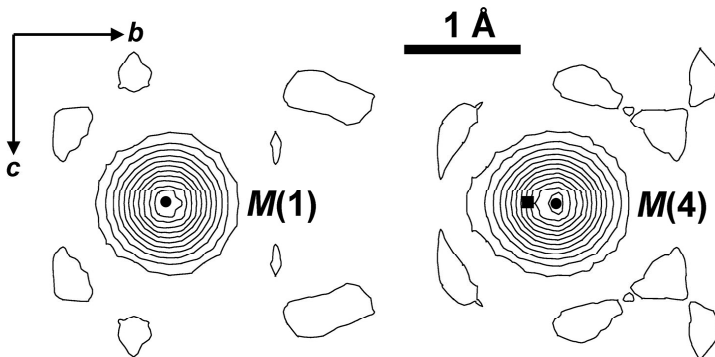


Figure 22. The electron density at the $M(4)$ site in parvowinchite with $M(4) = \text{Na}_{0.87}\text{Ca}_{0.39}\text{Mn}_{0.57}\text{Mg}_{0.17}$ (Oberti and Ghose 1993); the black square marks the $M(4')$ site. Contours show steps of $5 e^{-}/\text{\AA}$ from 0.0.

in detail with reference to the phase-transition behavior (Reece et al. 2000, 2002; as reported in Welch et al. 2007).

Mn^{3+} is normally ordered at the $M(2)$ site (Ghose et al. 1986; Oberti et al. 1993b). However, in ungarrettiite, $^A\text{Na}^B\text{Na}_2^C(\text{Mn}^{2+}_2\text{Mn}^{3+}_3)^T\text{Si}_8\text{O}_{22}^W\text{O}$ (Hawthorne et al. 1995b; Kawachi et al. 2002), Mn^{3+} orders at $M(1)$ and $M(3)$ and Mn^{2+} orders at $M(2)$, i.e., inverse to that expected in the amphibole structure. This unusual order results from cooperative interaction of three factors: (1) the typical Jahn-Teller distortion of $(\text{Mn}^{3+}\text{O}_6)$ octahedra, (2) the occurrence of O^{2-} at the O(3) site, and (3) the bond-valence requirements of O^{2-} at O(3). The result is extremely short Mn^{3+} -O(3) distances, very strong Mn^{3+} -O(3) bonds, and satisfaction of bond-valence requirements at O(3) (Hawthorne et al. 1995b).

Potassium

Potassium can be a major A cation in calcic, sodic-calcic and sodic amphiboles, and is generally ordered at the $A(m)$ site. In contrast, K is generally very low (< 0.05 apfu) in Mg-Fe-Mn-Li amphiboles. Coupling of K and Fe is expected for both geochemical and structural reasons. However, K can be dominant at the A site also in Mg-rich compositions, and even in Fe-rich Mg-rich compositions (e.g., potassic-fluorrichterite), showing that there is no structural constraint to complete solid-solution with Na. For a recent review on the occurrence and paragenesis of K-dominant amphiboles, see Mazdab (2003).

A series of high- P experiments produced richterites with K up to 1.95 apfu, and showed a correlation between excess K and pressure (Sudo and Tatsumi 1990; Luth 1997; Inoue et al. 1998; Konzett et al. 1997). Yang et al. (1999) provided a single-crystal structure refinement of a sample with $B = (\text{KCa})$. The main structural variations due to the incorporation of K at $M(4)$ are discussed by Oberti et al. (2007). Here we note the high values measured for the a and b edges and the β angle (10.193 and 18.121 Å and 105.51°, respectively; cf. Hawthorne and Oberti 2007, Fig. 35).

Sodium

Sodium can be an A and B cation in amphiboles in all compositional groups. The only significant advance since Hawthorne (1983a) is the understanding of the reasons for Na ordering within the A cavity. Analysis of the experimental Fourier maps (Hawthorne and Oberti 2007, Fig. 30) and bond-strength considerations confirmed that Na orders at the $A(m)$ site in fluoro-amphiboles, and distributes between the $A(m)$ and $A(2)$ sites in OH-dominant amphiboles. The preferred local arrangements are $^{M(4)}\text{Ca}-^{\text{O}(3)}\text{OH}-^{\text{A}(2)}\text{Na}$ and $^{M(4)}\text{Na}-^{\text{O}(3)}\text{OH}-^{\text{A}(m)}\text{Na}$ (Hawthorne et al. 1996b; Hawthorne and Oberti 2007; Hawthorne and Della Ventura 2007). Other studies showed that the presence of Li at the $M(3)$ site implies a further shift of the $A(m)$ site toward the chain of tetrahedra (Oberti et al. 2003a).

Strontium

Strontium is incorporated at the $M(4)$ site, replacing Ca in synthetic richterite (Della Ventura and Robert 1990), potassic-richterite (Robert et al. 1993) and tremolite (Gottschalk et al. 1998). In potassic-richterite with increasing Sr content, Rietveld refinement shows a linear increase in $\langle M(4)\text{-O} \rangle$ with increasing aggregate ionic radius at the $M(4)$ site ($^{81}\text{Sr}^{2+} = 1.26$ Å). Careful analysis of the X-ray diffraction patterns indicated no evidence of violation of $C2/m$ symmetry, excluding the possibility of long-range Na-Sr order at $M(4)$ in these amphiboles (Robert et al. 1993). Analysis of the FTIR Si-O, Si-O-Si and O-Si-O lattice modes (1400-600 cm^{-1}) of synthetic tremolites with increasing Sr content shows no evidence of short-range order of Ca-Sr at $M(4)$ (Andrut et al. 2000).

Titanium

The ordering of Ti over the various sites of the amphibole structure has been the subject of much work in the last twenty years, and is briefly summarized here. There is no evidence of Ti^{3+}

in amphiboles, and all Ti is assumed to be tetravalent. Ti^{4+} is a C cation except in richterite and its homovalent analogues where it can occur both as a C and a T cation.

Partitioning of Ti over the $M(1,2,3)$ and $T(1,2)$ sites in potassic-richterites was originally suggested by numerous chemical analyses of amphiboles from lamproites (e.g., Wagner and Velde 1986) and confirmed structurally by Oberti et al. (1992) for natural amphiboles and by Della Ventura et al. (1991, 1993a, 1994, 1996) and Tiepolo et al. (2003) for synthetic amphiboles. $^{\text{T}}\text{Ti}$ is completely ordered at the $T(2)$ site (Oberti et al. 1992) and is easily detected by the high values of the refined site-scattering at $T(2)$ and the high angular variance of the $T(2)$ tetrahedron. This latter feature suggests a reason for the ordering of $^{\text{T}}\text{Ti}^{4+}$ at the $T(2)$ site; in fact, the $T(2)$ tetrahedron is generally more distorted than the $T(1)$ tetrahedron in amphiboles, which fits better with the electronic configuration of Ti^{4+} . The occurrence of $^{\text{T}}\text{Ti}$ significantly lengthens both $\langle T(2)\text{-O} \rangle$ and the c unit-cell edge. The occurrence of $^{\text{T}}\text{Ti}$ only in richteritic compositions can be explained by the matching requirements of the various structural units in potassic-richterite, which has only divalent C cations and nearly stoichiometric amounts of the largest A cation. Experimental work shows that the solubility of $^{\text{T}}\text{Ti}$ in richterite increases with T up to ~ 0.7 apfu at $T = 800$ °C but decreases rapidly from 0.60 to 0.16 apfu with increasing F in the system (Della Ventura et al. 1993a). The inverse correlation between F and $^{\text{T}}\text{Ti}$ confirms the critical role of the relative dimensions of the octahedra. Because it crystallizes in Al-free environments, richterite generally has low amounts of highly charged cations, and $M(2)$ is even the largest of the M octahedra. Ti can be an exception to this rule in ultrapotassic magmatic rocks (silica-rich lamproites) and in rare types of mantle xenoliths [metasomatically altered peridotites, MARID (Mica-Amphibole-Rutile-Ilmenite-Diopside; Dawson and Smith, 1977) and cumulate xenoliths; Tiepolo et al. 2003 and references therein]. Kushiro and Erlank (1970) synthesized potassic-richterites at 3 GPa from a starting material similar in composition to the samples investigated by Oberti et al. (1992), and found very limited TiO_2 contents ($\sim 0.5\%$, to be compared with 3.6-4%), showing that the incorporation of $^{\text{T}}\text{Ti}$ is unfavorable at high P . Konzett (1997) characterized the stability and composition of Ti-bearing potassic-richterite in MARID-type rocks (in the range $0.5 < P < 8$ GPa, $900 < T < 1400$ °C, and concluded that amphibole is stable up to 1300 °C at 8 GPa, that Ti is almost completely incorporated at the T sites, and that its amount significantly increases with T (e.g., from 0.8 apfu at 900 °C to 0.28 apfu at 1200 °C at 4 GPa) and decreases with P (e.g., from 0.23 apfu at 3 GPa to 0.05 apfu at 8 GPa at 1100 °C).

The distribution of Ti over the $M(1,2,3)$ sites is controlled by two different mechanisms. Titanium at $M(1)$ provides local electroneutrality to the oxo component at the O(3) site *via* local ordering $^{M(1)}\text{Ti}^{4+} \text{O}^{(3)}\text{O}^{2-}_2$. In contrast, Ti at the $M(2)$ and $M(3)$ sites is involved in the exchange $^{M(2),M(3)}\text{Ti}^{4+} \text{Al}_2^{3+} \text{Al}_2^{3+} \text{Mg,Fe}^{2+}_{-1} \text{Si}^{4+}_{-2}$ (for a detailed discussion, see Tiepolo et al. 1999). The occurrence of Ti at the $M(3)$ site was first inferred by neutron diffraction by Kitamura et al. (1975). However, analysis of the CNR-IGG-PV database showed that it is rather rare (8 out of the 250 Ti-bearing amphiboles), and is restricted to compositions with low amounts of $^{\text{C}}\text{Al}$. The most striking case is a sample from a gabbro from the type locality of kaersutite (Kaersut, Greenland). This samples couples one of the highest Ti contents ever reported in nature for amphiboles (0.72 apfu) with a relatively low oxo-component (0.96 $\text{O}^{(3)}\text{O}$ apfu); the residual, 0.24 Ti apfu are nearly equally partitioned between the $M(2)$ and $M(3)$ sites, because SREF provides evidence of ≈ 0.10 Ti apfu at the $M(3)$ site. In this sample, $^{\text{C}}\text{Al}$ is 0.17 apfu; therefore, $^{\text{C}}\text{Ti}$ seems to play the same role as $^{M(3)}\text{Al}$ whenever the composition of the system is depleted in Al or when the high T of crystallization increases Al preference for tetrahedral coordination.

A decrease in the $^{\text{Amph/L}}\text{D}_{\text{Ti}}$ with increasing P was observed in sodic-calcic (richterites) and calcic amphiboles (titanian pargasites) synthesized by Sweeney et al. (1992) and Adam and Green (1994, 2003) in carbonatitic and basaltic systems, respectively. The data by Sweeney et al. (1992) show a clear negative correlation between $^{\text{Amph/L}}\text{D}_{\text{Ti}}$ and H_2O content, suggesting that the role of Ti in mantle amphiboles is related mainly to the oxo component.

Titanium at $M(1)$ occupies a position different from that of Mg, Fe^{2+} and Fe^{3+} . From a long-range perspective, static disorder implies first an increase in the $M(1)$ atom-displacement factor, and (at higher Ti contents) non-spherical electron density within the $M(1)$ octahedron, which must be modeled by two sites [$M(1)$ and $M(1')$] during structure refinement (Fig. 23a). Shortening of the $M(1)$ -O(3) distance couples with a shortening of the O(3)-O(3) edge, which reaches 2.62 Å (the sum of the ionic radii) in the most dehydrogenated amphiboles. At the $M(3)$ site, where the two O(3) oxygen atoms are in a *trans* configuration, the occurrence of Ti increases the atom-displacement parameter in the O(3)-O(3) direction (Fig. 23b), and shortens all the $M(3)$ -O(1,3) distances. Therefore, SREF allows straightforward detection of the Ti distribution over the $M(1,2,3)$ sites *via* analysis of the atom-displacement parameters and individual M-O distances (Tiepolo et al. 1999). In particular, Ti at $M(3)$ implies shorter $M(3)$ -O(1) and longer $M(3)$ -O(3) distances than expected in the presence of $^{M(3)}\text{Fe}^{3+}$ balancing dehydrogenation.

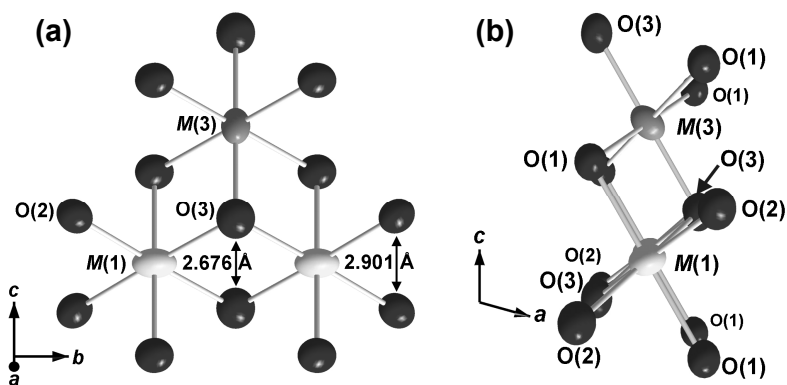


Figure 23. Long-range effects of the incorporation of Ti at the $M(1)$ and $M(3)$ sites. Two projections of the local environment of Ti, showing positional disorder (a) along b at the $M(1)$ site, and (b) approximately along the line joining the two O(3) sites at the $M(3)$ site. The O(3)-O(3) edge shortens significantly in amphiboles with Ti ordered at the $M(1)$ site. Ellipsoids drawn at 98% probability.

Zinc

Zinc is a rare constituent in amphiboles. Zinc contents up to 1.22 apfu have been reported in Mg-Fe-Mn-Li amphiboles from Franklin, New Jersey (Klein and Ito 1968), and structure refinement of samples with 0.76 Zn apfu showed the following site preference: $M(1) > M(3) \gg M(2)$ (Hawthorne and Grundy 1977b). More recently, low Zn contents (up to 0.10 apfu) in Li-bearing fluoro-arfvedsonites were assigned to the $M(2)$ site based on refined bondlengths and site-scattering values (Hawthorne et al. 1993, 1996c). Higher Zn contents (up to 0.48 apfu) have also been found in amphiboles from episyenites at the Pedriza Massif (Sierra de Guadarrama, Spain). The site-preference proposed for these amphiboles is $M(2) \gg M(1)$.

Zirconium

Chemical analysis shows that amphiboles from nepheline syenites and peralkaline granites (e.g., Jones and Peckett 1980; Pearce 1989; Preston et al. 2000) can contain up to several wt% ZrO_2 . Hawthorne et al. (2001) assigned Zr to the $M(2)$ site in a series of arfvedsonitic amphiboles from Strange Lake, Quebec, Canada. The absence of Mg from these amphiboles allowed assignment of Zr via the refined site-scattering values, showing that Zr occurs at the $M(2)$ site. On the basis of EXAFS data, Farges et al. (1994) showed that Zr is [6]-coordinated in arfvedsonite from a phonolite from the Rumoi Hill, Cameroon, and further showed that

Zr occurs at the $M(2)$ site. At the trace-element level, Oberti et al. (2000b) compared refined mean bondlengths and lattice-strain models and concluded that Zr is ordered at the $M(2)$ site in synthetic pargasite and kaersutite from alkali basalts and basanites, and at the $M(1)$ site in strongly dehydrogenated synthetic richterite from lamproites. Hence, the behavior of Zr strongly resembles that of Ti, despite the significant difference in their size.

ANION INCORPORATION IN AMPHIBOLES

O(3) is the only anion site in the amphibole structure where chemical substitution is possible. This site can host either the homovalent constituents OH^- , F and Cl, or O^{2-} . In the latter case, extra positive charge is provided by high-charge C cations, and the occurrence of the oxo component may eventually lead to oxo amphiboles.

Chlorine

Only two amphibole compositions with Cl dominant at the O(3) site have been formally recognized so far: chloro-potassicpargasite (Chukanov et al. 2002) and chloro-potassic-hastingsite (formerly “dashkesanite”; Pekov et al. 2005). These amphiboles may contain nearly stoichiometric amounts of Cl (Deer et al. 1997), and occur in the granulite complex of Sal’nye Tundry Massif (Kola Peninsula) and in magnetite orebodies at Dashkesan (Transcaucasia, Azerbaijan), respectively. Other reported but not formally recognized compositions are: “chloro-potassic-ferro-edenite” with Cl = 1.38 apfu in a calc silicate rock from Willroy Mine (Ontario, Canada; Pan and Fleet 1992); “chloro-potassic-ferropargasite” with Cl up to 1.16 apfu from marbles in the Sesia Lanzo Zone (Italian Western Alps; Castelli 1998); potassic “chloro-ferrosadanagaite” with Cl up to 1.5 apfu from Nusfjord (Lofoten, Norway; Kullerud and Erambert 1999); chloro-potassic-hastingsite with Cl = 1.15 apfu from a granodioritic charnockite (Airport Hill, Visakhapatnam, India; Kamineni et al. 1982). In general, Cl-rich amphiboles are rich in Fe^{2+} and K (e.g., Dick and Robinson 1979; Morrison 1991; McCormick and McDonald 1999), indicating the effect of increasing Fe^{2+} in increasing the dimensions of the strip of octahedra, and increasing K in promoting the bonding between K at the $A(m)$ site and Cl at the O(3) site. For a detailed review on the occurrence of Cl in amphiboles, refer to Deer et al. (1997), pages 280-284, and for the association of Cl with K in alkali-chloride metasomatism, refer to Mazdab (2003).

There is general consensus on (1) the dependence of the Cl content on the composition of the mineral-forming fluid; (2) the positive correlation between Cl, Fe^{2+} and $^{\text{T}}\text{Al}$, which has been explained by the need to enlarge both the strip of octahedra and the double-chain of tetrahedra in order to allow incorporation of Cl at the O(3) site. However, the incorporation of Fe^{2+} does not by itself produce more room for a larger anion.

Oberti et al. (1993a) examined chlorian amphiboles from the Sesia-Lanzo marbles (Castelli 1998), and compared these results with the structure refinement of a similar Cl-free composition. The results they obtained have been later confirmed by many structure refinements of Cl-bearing amphiboles done at CNR-IGG-PV and one by Rastsvetaeva et al. (1996) on chloro-potassic-hastingsite with 1.31 Cl apfu.

Even very low Cl contents significantly increase the atom-displacement parameters of the O(3) site, particularly the component along [100]. At higher Cl content, the shape of the electron density changes significantly, and the best-fit model has two distinct positions for the oxygen atom and the chlorine atom, the second becoming dominant at Cl > 0.60 apfu (Fig. 24a). The distance between the two sites is around 0.5 Å in samples with 0.98 Cl apfu (as measured with a data set collected within $\theta_{\text{max}} = 40^\circ$). Rastsvetaeva et al. (1996) gave an O(3)-O(3') distance of 0.76 Å when working on 485 independent reflections collected up to $\theta_{\text{max}} = 30^\circ$; however, inspection of their model shows that the position of the weaker O(3) site is

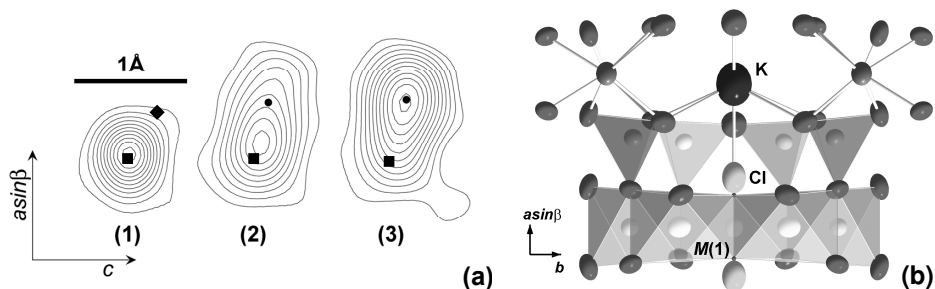


Figure 24. Long-range effects of the incorporation of Cl at the O(3') site: (a) The electron density at the normal O(3) site occupied by O (square) and at the split site O(3) occupied by Cl (dot) in (1) an OH-dominant amphibole, and in chlorian potassic-ferropargasites, with 0.56 (2) and 0.98 (3) Cl apfu, respectively. The diamond indicates the position occupied by the proton (contours at steps of $5 e/\text{\AA}$ starting from 0.0) (modified from Oberti et al. 1993a). (b) The local environment of Cl, which protrudes from the strip of octahedra toward K at the $A(m)$ site. Also visible is the static disorder at the adjacent $M(1)$ sites, which confirms the local relaxation resulting from the incorporation of Cl. Ellipsoids drawn at 98% probability.

poorly determined and too close to the $M(3)$ site. With increasing amounts of Cl at the O(3) site, the $M(1)$ and $M(3)$ sites become enriched in Fe^{2+} . The distances between the $M(1,3)$ cations and the O(1,2) oxygen atoms do not change much (and thus these bonds become relatively stronger than in Cl-free amphiboles). We thus conclude that Cl protrudes out of the strip of octahedra in the direction of the A cavity (Fig. 24b), and that the presence of large $M(1,3)$ cations allows bonding with Cl. However, Cl receives less than 1 vu from the $M(1,2,3)$ cations (see above), and thus interaction with the A cation is important; in fact, the refined $A(m)$ -Cl distance is particularly short (2.93 Å in Oberti et al. 1993a, 2.96 Å in Rastsvetaeva et al. 1996), even shorter than the K-Cl distances in sylvite and other inorganic compounds (> 3.15 Å). In contrast, the OH bond is somewhat bent away from the a direction, to avoid interaction of the proton with the A cation. In Cl-bearing amphiboles, however, the proton is masked by the electron density of Cl, and cannot be detected.

The incorporation of Cl in amphiboles also implies an expansion of the strip of octahedra in the (011) plane, which can be monitored with the $M(1)$ - $M(1)$ distance, always larger than expected based on the $M(1)$ site population. Analysis of the atom-displacement parameters at the $M(1)$ site also confirms significant relaxation close to Cl (Fig. 24b). The increase in the unit-cell edges is $b \sim c > a$, confirming that Cl protrudes significantly into the A cavity, avoiding lengthening of the a edge.

Fluorine

The incorporation of F in amphiboles is a very widespread phenomenon in all except the Mg-Fe-Mn-Li amphiboles. The F content seems to depend primarily on its geochemical availability and not on structural constraints. The only observed inverse correlation is with the Fe^{2+} content, which is in agreement with the well-known criterion of Fe^{2+} -F avoidance in silicates (Rosenberg and Foit 1977), a result of the smaller crystal-field stabilization energy provided by F.

The fact that the local environment of F implies Mg at the adjacent $M(1)$ and $M(3)$ sites has been confirmed by FTIR analysis. Detailed spectroscopic work has shown that the substitution of F for OH in the amphibole structure is strongly controlled by the bond-valence sum at the O(3) site. In local configurations involving $M^{(3)}\text{Al}$ in pargasite (Robert et al. 2000) or in the pargasite-richterite solid solution (Della Ventura et al. 2001), the bond-valence contribution from the C cations incident to O(3) is > 1.0 vu. Hence, the hydroxyl proton contributes less

than 1.0 vu, and can be involved in significant hydrogen bonding with the surrounding oxygen atoms, especially O(7). This feature is confirmed by the lower stretching frequency observed in the FTIR spectrum. In such a case, the hydroxyl group is less easily replaced by F (Della Ventura et al. 2001).

The occurrence of F at the O(3) site causes significant shortening of the $M(1)$ -O(3) and $M(3)$ -O(3) distances, which reduces $\langle M(1)\text{-O,OH,F} \rangle$ and $\langle M(1)\text{-O,OH,F} \rangle$ (Hawthorne 1983a). An attempt to quantitatively evaluate this effect was done by Oberti et al. (1993b) in a series of richterites with variable F content. The resulting regression equations [$\langle M(1)\text{Mg-O} \rangle = 2.0769 - 0.0130 F$ apfu and $\langle M(3)\text{Mg-O} \rangle = 2.0696 - 0.0128 F$ apfu, with $R = 0.994$ and 0.978 , respectively] confirm that incorporation of F affects the two sites almost equally [the *cis* and *trans* arrangements of the O(3) site being thus irrelevant], and that the shortening is roughly proportional to the difference in the ionic radii of $^{13}\text{OH}^-$ and $^{13}\text{F}^-$ (1.34 and 1.30 Å, respectively). However, the fictive $\langle \text{Mg-O} \rangle$ values vary considerably among the various (Mg,Al) amphibole end-members, and thus only the shortening coefficient can be transferred to other amphibole compositions.

As discussed above, the incorporation of F also has a strong ordering effect on the distribution of Al and all transition metals over the $M(2)$ and $M(3)$ site. These cations disorder over the $M(2)$ and $M(3)$ sites in Mg-rich compositions (see above discussions for Al, Fe^{3+} , V^{3+} and Cr^{3+}), whereas they are always fully ordered at $M(2)$ in fluoro-amphiboles.

Hydrogen (as OH^-)

The observed OH^- content in amphibole can vary from 0 to 3 pfu. In monoclinic and orthorhombic amphiboles, only the O(3) site is commonly available for OH^- , which results in 2.0 (OH) pfu. Values lower than 2.0 (OH) pfu are related either to substitution of (OH) by F or Cl (the effects of which have been discussed above), or by O^{2-} (the oxo component), which implies either crystallization under low $f_{\text{H}_2\text{O}}$ conditions and/or high- T , or loss of H during post-crystallization oxidation processes. Values higher than 2.0 (OH) pfu are still a matter of debate, and has been incontrovertibly proven only in a triclinic sample with a tripling of the b edge (Witte et al. 1969; Liu et al. 1996; Cámara et al. 2004). The issues of the oxo component and of excess (OH) will be discussed separately in the next two sections.

The O-H bond points in the direction of the A cavity, and thus repulsive interactions are possible between the proton and the A cations, especially when ordered at the closest $A(m)$ site. In contrast, incorporation of F and Cl allows cation-anion interactions, and thus favor the ordering of K and Na at the $A(m)$ site. More details on the local environment of the proton are given in Hawthorne and Oberti (2007) and Hawthorne and Della Ventura (2007).

THE OXO COMPONENT: A DETAILED DISCUSSION

Rather ironically, amphiboles were long considered as anhydrous minerals, similar to pyroxenes (for a survey, see Cipriani 2007). Notwithstanding the generally low total of the oxide wt%, Schaller (1916) was the first to consider H_2O as an essential constituent of amphiboles, and the definitive confirmation came from the structure refinement of tremolite done by Warren (1930). However, the first attempt to investigate dehydrogenation in amphiboles by heating experiments was done by Posnjak and Bowen (1931).

Oxburgh (1964) first noted the role that amphibole could have in mantle processes. Saxena and Ekström (1970) discussed the statistical relevance of the oxo component [$^{\text{O}(3)}\text{O}^{2-}$] in calcic amphiboles, stressed its positive correlation with the Ti content, and did not find any significant correlation with the Fe^{3+} content. From the 70s, many experimental studies were done to determine amphibole stability as a function of pressure, temperature, composition and volatile content under mantle conditions and in meteorites (for comprehensive references, see

Popp et al. 1995a,b and King et al. 1999), but they could not *in situ* measure the H content. Incidentally, evaluation of the H₂O content by difference to 100% oxides is not reliable for mantle amphiboles if independent estimates of the Fe³⁺ contents are not available. However, the volatile content of amphiboles was used to estimate water activity ($a_{\text{H}_2\text{O}}$) of the melt from which the amphibole crystallized, as well as the hydrogen fugacity (f_{H_2}) of the melt.

The first modern and comprehensive study of dehydrogenation in calcic amphiboles was published by King et al. (1999, 2000) who examined major elements and H analyses (by SIMS) for 38 natural and synthetic Ti-rich calcic amphiboles crystallized at mantle conditions. They concluded that the high Ti contents derive from crystallization from mafic-ultramafic melts at low to moderate pressure (≤ 1.0 GPa), high temperature (> 950 °C) and low to moderate oxygen fugacity (f_{O_2}), and that iron oxidation state in amphiboles is affected by f_{O_2} and f_{H_2} in the melt. The oxo component and the Fe³⁺/Fe_{tot} ratios are a function of both initial crystallization conditions and dehydrogenation, with variations occurring due to different pressure-temperature- f_{H_2} -time paths. Amphibole dehydrogenation likely occurs at the surface or en route to the surface where f_{H_2} is low, cooling is slow, or grain attributes tend to favor rapid H diffusion. A schematic representation of the stability of calcic amphibole in hydrous volcanic systems and of the factors affecting the oxo component is shown in Figure 25.

As discussed in Oberti et al. (2007), much evidence has been found in the last 15 years that all amphibole compositions can crystallize with low (OH,F,Cl) (i.e., volatile element) contents under different P , T , X , $f_{\text{H}_2\text{O}}$ conditions. In the CNR-IGG-PV amphibole database, around 25% of the 1150 entries have volatile contents significantly less than 2.0 pfu. For almost 90% of them, petrologic analysis suggests that this deficiency in volatile components is a feature of primary crystallization. Commonly, low volatile contents occur in magmatic amphiboles (from both intrusive and extrusive rocks), and are very frequent in high-grade metamorphic environments. Most calcic amphiboles with volatile-element contents between 0 and 0.8 pfu are volcanic in

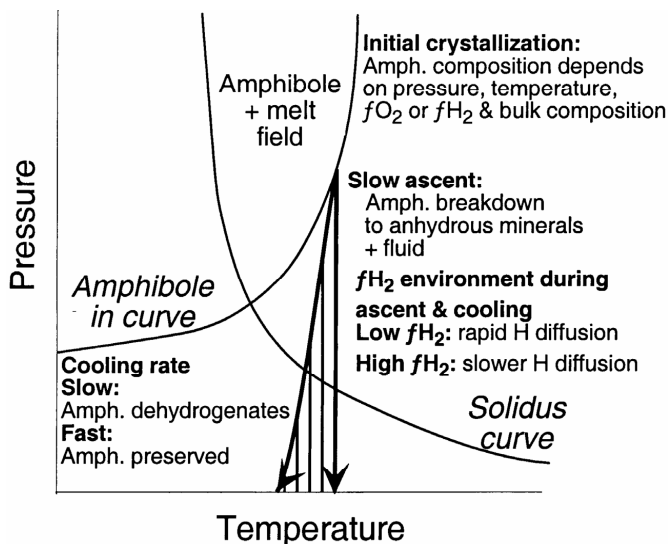


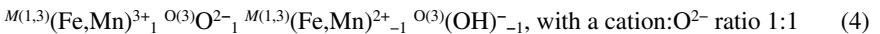
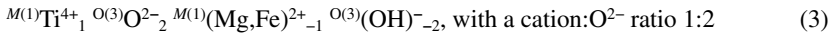
Figure 25. Schematic pressure vs. temperature diagram showing amphibole stability and some factors possibly affecting the oxo component in calcic amphiboles from hydrous volcanic systems. Initial crystallization conditions control both the oxo component and the incorporation of C cations. The final amount of the oxo component depends on the ascent rate and f_{H_2} gradient. [Used by permission of Elsevier, from King et al. (1999), *Geochimica et Cosmochimica Acta*, 63, Fig. 8, p. 3647.]

origin, and for many of them, the low volatile content is related to post-crystallization oxidation processes (dehydrogenation). Thus detection of the oxo component, and understanding the mechanisms that satisfy local bond-valence requirements are of major and general interest to amphibole crystal-chemistry. Notably, investigation of amphiboles in mantle and volcanic-arc environments is presently considered by some as an issue of great relevance in petrogenetic and geochemical studies. In this regard, the detection and quantification of the oxo component is critical for the correct calculation of the unit formulae to be used either for thermodynamic modeling or for the interpretation of trace-element behavior (Tiepolo et al. 2007).

Electron-microprobe analysis of F in minerals is still difficult to do accurately because of second-order peak interferences from Mg and Al, and first-order *L*-lines from Fe and other transition elements, and because peak shape is strongly affected by matrix effects (including orientation effects in the standards; Stormer et al. 1993; Ottolini et al. 2000).

SIMS analysis is the only method available to detect and quantify the H content *in situ* (on μm -scale areas), a requirement that is extremely important for (1) small and rare crystals, and (2) compositionally zoned crystals. Although reasonable accuracy can now be achieved ($\pm 10\%$ rel., although the precision and accuracy still need to be improved significantly), the use of proper calibration curves is still crucial, because matrix effects (non-linear ion yields of hydrogen due to changes in bulk chemistry) severely affect hydrogen quantification (Ottolini et al. 1995). The ability to detect and quantify the oxo component directly from the results of structure refinement will complement SIMS analysis, and agreement will further validate each method and allow a rigorous evaluation of accuracy.

The oxo component at the O(3) site can be locally balanced by two different crystal-chemical mechanisms:



Mechanism (3) has been discussed in detail in the section dealing with Ti. Mechanism (4) has been examined in a series of experimental studies after the pioneering works on hornblende (Barnes 1930) and crocidolite (Addison et al. 1962a,b). Ernst and Wai (1970) annealed iron-bearing sodic amphiboles in air at ~ 700 °C, and found that hydrogen loss couples with oxidation of Fe^{2+} at the *M*(1) and *M*(3) sites. In fact, complete dehydrogenation was reached within one h in riebeckite, whereas in magnesioriebeckite and in glaucophane, the bands of the IR spectrum assigned to local configurations involving at least one Fe^{2+} cation disappear after one hour but those assigned to $[\text{MgMgMg}]\text{-OH}$ persist after 95 hours of annealing.

A more quantitative model for mechanism (4) was provided by the work of Popp et al. (1995a,b; 2006a,b) who did heating experiments under controlled *P*, *T* and f_{H_2} conditions on three titanian pargasites and kaersutites, and monitored the dehydrogenation-protonation process *via* variation in the $\text{Fe}^{3+}/\text{Fe}_{\text{tot}}$ content measured by Mössbauer spectroscopy. They concluded that high $\text{Fe}^{3+}/\text{Fe}_{\text{tot}}$ ratios observed in most natural kaersutitic amphiboles can result from *P-T-f_{H2}* conditions characteristic of the upper mantle, rather than from oxidation during ascent or eruption, and that closed-system cooling favors reduction, not oxidation, of amphibole. With the intent of estimating f_{H_2} of the system from amphibole composition, Popp et al. (2006a,b) expressed the equilibrium constant (*K*) of the dehydrogenation-protonation reaction as $K = K_x \Phi$, where K_x is the thermodynamic mole fraction (which includes f_{H_2}), and Φ is the activity coefficient. Variations in K_x were quantified experimentally as a function of *P*, *T*, f_{H_2} and composition, and allow evaluation of the equilibrium $\log f_{\text{H}_2}$ within 0.3 log units. The main problem with this work is the lack of crystal-chemical control of the assumptions. While monitoring only mechanism (4), Popp et al. (2006a,b) estimated the oxo component as $2.0 - \text{Fe}^{3+} - \text{TiO}^{2-} - \text{F} - \text{Cl}$ (apfu), where TiO^{2-} is the Ti content accommodated by the Ti oxo substitution expressed as $\text{Ti}^{4+}_1 \text{O}^{2-}_1 (\text{R}^{n+})_{-1} (\text{OH})^{-}_1$. As shown above (and even better

shown below), this mechanism is incorrect, because Ti^{4+} at the $M(1)$ site is not related to post-crystallization dehydrogenation, but solely to the primary oxo component with a cation: O^{2-} ratio 1:2. Also, Popp et al. (2006a,b) considered the overall Ti content of the amphibole, not just the fraction related to the oxo component, and the overall Fe^{3+} content and not just the fraction occurring at the $M(1)$ and $M(3)$ sites. This issue is particularly relevant because one of the three samples is the kaersutite from Kaersut, Greenland, whose unusual Ti distribution is described in the paragraph on Ti site-partitioning. Moreover, the equations were derived based on a random mixing model for the C cations, which is certainly inappropriate, given the strong site preferences discussed above.

The statistical analysis of King et al. (1999, 2000) showed that the overall (OH) content correlates well with the $^{\text{C}}(\text{Al,Ti,Fe}^{3+})$ content, and provides a way to calculate the $\text{Fe}^{3+}/\text{Fe}^{2+}$ ratio for the samples where SIMS quantification of H is available and better evaluate the oxo-substitution mechanisms. Again, their model is biased by an incorrect evaluation of the role played by the different highly charged species, and the equation fails for some compositions.

Systematic work combining structure refinement and complete (EMP+SIMS) microanalysis of 75 natural and synthetic calcic amphiboles (some of which are in common with the database of King et al. 1999) has been recently done at CNR-IGG-PV. The amphiboles either belong to ultramafic mantle associations or occur as megacrysts in basaltic lavas, and are representative of the P - T - $f_{\text{H}_2\text{O}}$ conditions of crystallization observed for the upper-mantle/deep-crust in the subcontinental region. The constraints of the structure refinement (in particular the site-scattering values refined at the A , $A(m)$, $A(2)$, $M(4)$, $M(1)$, $M(2)$ and $M(3)$ sites and the accurate determination of $^{\text{T}}\text{Al}$ based on the refined bondlength) allowed calculation of reliable crystal-chemical formulae. Mechanism (3) is definitely dominant at least for $^{\text{O}(3)}\text{O}^{2-}$ contents up to 1.0 apfu. Beyond that limit (and solely in volcanic environments), the oxidation of Fe^{2+} (rarely of Mn) becomes the prevailing mechanism for incorporation of $^{\text{O}(3)}\text{O}^{2-}$. Figure 26 shows the chemical correlations observed for calcic amphiboles from different petrologic environments, and confirms the stoichiometry and relative importance of mechanisms (3) and (4). Figure 27 shows the concomitant variations observed for the $M(1)$ -O(3) and $M(3)$ -O(3) distances normalized over the aggregate mean bondlength in order to cancel the effect of changes in composition, and confirms that the substitutions occurring at $M(1)$ are more important, the $M(3)$ site becoming active only at $^{\text{O}(3)}\text{O}^{2-}$ contents higher than 1.2 apfu. Figure 28 provides a simple way to detect the nature of the highly charged cation that is incorporated at the $M(1)$ site to balance the oxo component. In fact, the occurrence of Ti does not significantly affect the parameter $\Delta (\sum_{i=1,6} [(M-O)_i - <M-O>] / <M-O>)^2 / 6 \times 10^4$; Brown and Shannon 1973), which is on the contrary very sensitive to the occurrence of Fe^{3+} . Based on these observations and on Mössbauer analysis of a subset of selected samples, site populations were derived and related to the observed geometrical changes. A good linear correlation was obtained between $^{\text{O}(3)}\text{O}^{2-}$ (in apfu) and the $M(1)$ - $M(2)$ distance. The $M(2)$ site is not directly involved in the charge balance of the oxo component. However, its geometry is strongly affected by the oxo component, because the O-O edges shared with $M(1)$ and $M(3)$ [O(1)-O(2) and O(1)-O(1), respectively] shorten, whereas the M - M distances lengthen. Therefore, the correlation between the oxo component and the $M(1)$ - $M(2)$ distance must be interpreted as a mechanism of structural relaxation *via* octahedron distortion, which minimizes repulsion between highly charged cations. Obviously, the $M(1)$ - $M(2)$ distance also depends on the bulk chemistry (see above for a discussion on the variation in $<Mg-O>$ in amphiboles) and thus different regression equations must be used for different subsets of amphiboles.

Statistical analysis of the amphibole database provided two different regression equations that can be reliably used to quantify the oxo component in terms of solid-solution between pargasite-hastingsite and kaersutite, and in Ti-bearing richterites from mantle environments. The trends and the equations are shown in Figure 29. Further work is in progress in order to obtain more general relations which take into account the overall chemistry, as discussed above

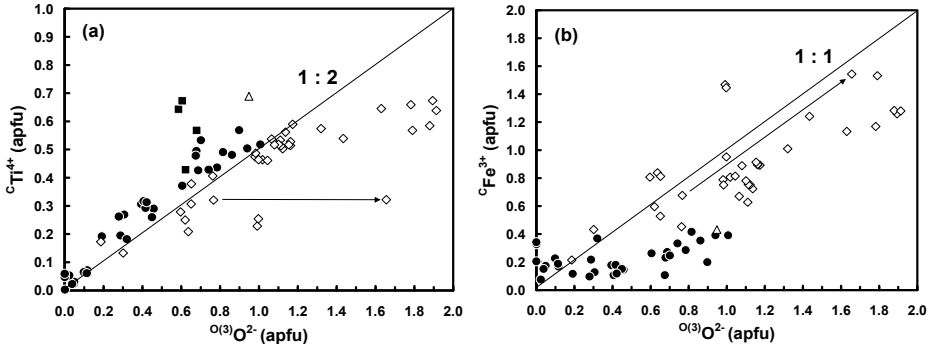


Figure 26. The relation between the oxo component [$O(3)O^{2-}$] and Ti^{4+} (a) and Fe^{3+} (b) contents in the 75 calcic amphiboles in the CNR-IGG-PV database for which SIMS analyses for H are available. Dots: amphiboles from upper-mantle metamorphic lithologies; diamonds: amphiboles from magmatic lithologies; triangle: the sample from a gabbro at Kaersut discussed in the paragraph on titanium; squares: synthetic Fe-free samples with Ti at $M(2)$ and $M(3)$ (Tiepolo et al. 1999). The arrow joins two phenocrysts found in a pyroclastic deposit at Stromboli (Sicily), which share the same major-element composition but have different oxo components (post-crystallization oxidation).

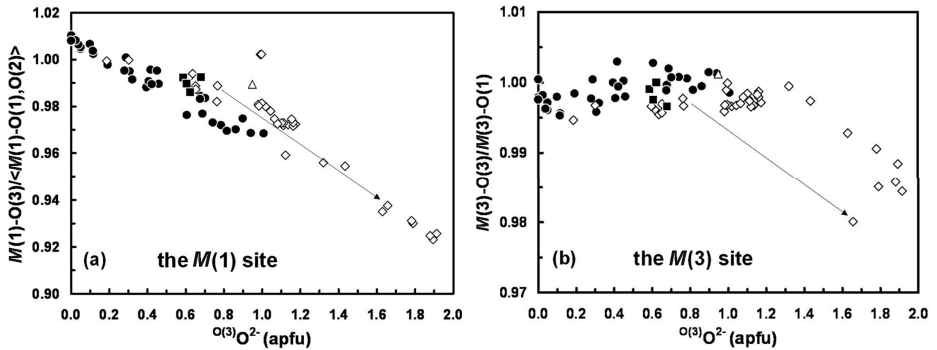


Figure 27. The variation in $M-O(3)$ distances in the calcic amphiboles of Figure 26. In order to remove the effects of compositional variation, the measured distances have been normalized to the average of the other distances. Legend as in Figure 26.

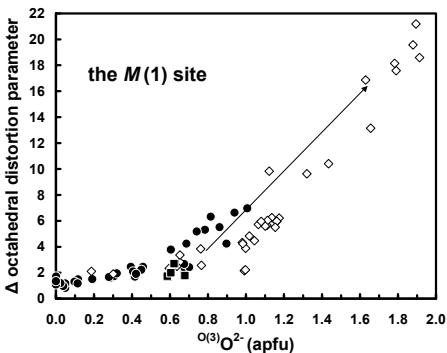


Figure 28. Octahedron distortion $\Delta^{M(1)}$ as a function of oxo component in amphiboles.

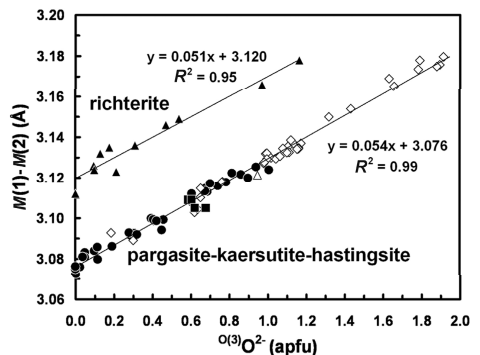


Figure 29. The relation between the $M(1)-M(2)$ distance and the oxo component in amphiboles.

when dealing with the program COMAMPH. In order to test the reliability of this method, the oxo component was calculated for all the calcic and sodic-calcic amphiboles with possible (OH) deficiency for which SIMS analyses were not available. Fixing the oxo component allowed calculation of crystal-chemical formulae which obey all the constraints of amphibole stoichiometry and are in excellent agreement with the results of the structure refinement. A detailed discussion of these results, of the amphibole compositions considered, and of the trends discussed in Figures 26-29 will be given in a manuscript in preparation.

HYDROGEN IN EXCESS OF 2.0 APFU

The possible occurrence of (OH) in amphiboles beyond the stoichiometric limit of 2.0 pfu has been debated for many years. In his review of the available amphibole analysis, Leake (1968) reported some "superior" analyses with (OH,F,Cl) values up to 2.99 pfu. Kemp and Leake (1975) reported analyses of two aluminotschermakites enriched in (OH) (2.60 pfu), and concluded that the (OH) excess was related to the large amounts of Al substituting for Si. However, the samples reported by Kemp and Leake (1975) were re-investigated at CNR-IGG-PV (courtesy of Bernard Leake), and no evidence was found of excess H.

Using Mössbauer and IR spectroscopy, Semet (1973) characterized a series of magnesiohastingsites synthesized at different f_{O_2} conditions, and suggested that: (1) excess H may balance reduction from Fe^{3+} to Fe^{2+} ; (2) the reaction is reversible; (3) the most likely anion site candidate for protonation is O(4). The main evidence for excess (OH) in the specimen synthesized or reduced to low f_{O_2} conditions was the growth of a broad absorption band between 3640 and 3540 cm^{-1} in the infrared spectra. However, Mössbauer analysis showed Fe^{3+} to be ordered primarily at the $M(2)$ site, but occurring also at the $M(1)$ and $M(3)$ sites, which is in favor of the occurrence of an oxo component.

Kuroda et al. (1975) reported increasing H_2O contents (up to 3 wt%, as determined by hydrogen extraction) in richterite₅₀tremolite₅₀ solid-solutions synthesized at increasing f_{H_2O} at P from 5 to 20 kbar, but did not speculate on the crystal-chemical significance of their results.

Witte et al. (1969) synthesized in the system Na_2O - MgO - SiO_2 - H_2O (NMSH) amphiboles tending to the unusual formula $^A Na$ $^B Na_2$ $^C Mg_5$ $^T Si_8$ O_{21} (OH)₃. Further syntheses and characterization (Maresch et al. 1991; Liu et al. 1996) suggested triclinic symmetry, which converts to monoclinic symmetry by annealing as shown by infrared and MAS NMR spectroscopy. A broad band peaking at 3430 cm^{-1} was also observed in all the run products, which could recently be ascribed to the excess proton based on structure refinement (Cámara et al. 2004).

Several hypotheses have been made on the possible location of the excess proton in the amphibole structure, among them H_2O occupancy at the A site or the presence of an (OH) group (tentatively proposed at the O(4) site) in the double-chain of tetrahedra (Zussman 1955). Recently, Cámara et al. (2004) refined the crystal structure of triclinic $^A Na$ $^B Na_2$ $^C Mg_5$ $^T Si_8$ O_{21} (OH)₃, and found that it has a $C\bar{1}$ symmetry and a unit cell with a tripled b edge. Interpretation of previous FTIR and MAS NMR results based on structure refinement showed that excess protons are bonded to the O(4) oxygen atoms [O(4)A, O(4)A2, O(4)B1] farthest from the $M(4)$ cation, and weakly interact with the adjacent O(2) oxygen atoms [O(2)A, O(2)A2, O(2)B1]. Consideration of site multiplicities gives a maximum excess H content of 1 apfu. Notably, in this very peculiar sample the presence of excess H is sterically allowed by the shift of the $^B Na$ atoms away from the diad, a feature which is possible only in the triclinic symmetry (more detail in Hawthorne and Oberti 2007). The broad band at around 3430 cm^{-1} in the FTIR spectrum of this sample could be unambiguously assigned to the excess proton. The question now is whether excess hydrogen can occur also in monoclinic amphiboles, and what is its possible location.

Acicular amphiboles with significant excess H (measured by vacuum extraction followed by manometric measurements and coulometric titration) were synthesized in the seventies in Bochum (Germany) during a thorough study of the system $\text{Na}_2\text{O-Li}_2\text{O-MgO-SiO}_2\text{-H}_2\text{O}$ (LNMSH) (W. Maresch, pers. com.). This sample has been re-examined recently in Pavia and Rome by structure refinement, EMP and SIMS analysis, and FTIR spectroscopy. Combination of chemical analyses and refined site-scattering values gives the formula $^{\text{A}}\text{Na}_{1.00} \text{ } ^{\text{B}}(\text{Mg}_{1.00} \text{ Li}_{0.27} \text{ H}_{0.12} \text{ Na}_{0.61}) \text{ } ^{\text{C}}\text{Mg}_5 \text{ } ^{\text{T}}\text{Si}_8 \text{ O}_{22} \text{ } ^{\text{W}}(\text{OH})_2$; the space group is $P2_1/m$, and the crystal undergoes a $P2_1/m \rightarrow C2/m$ transition at around 260 °C. Again, FTIR analysis shows a broad band around 3400 cm^{-1} . Albeit the excess H is within the analytical error, there is independent evidence suggesting excess protons ordered at $M(4)$. The shape of the electron density at $M(4)$ is very irregular (as expected from the complex site-population), and studies at low temperature will hopefully give some information on the H coordination. All evidence discussed above seems to indicate that there is no room for an excess proton in the $C2/m$ amphibole structure, and that this anomalous component is sterically tolerated only when (1) the lowering of symmetry allows an anomalous distribution of the B cations which are strongly off-centered and displaced off the diad; (2) the bulk chemistry is very peculiar (and would not otherwise allow for electroneutrality, as is the case of the triclinic sample) or is deficient in B cations.

FACTORS AFFECTING ORDERING OF CATIONS IN THE AMPHIBOLE STRUCTURE

Although much effort has been expended on characterizing the state of order of cations in the amphibole structure, not much work has been done on the reasons why such order occurs. This is obviously an area for future work.

Whittaker (1949) explained the preferential occupancy of the $M(2)$ site by trivalent cations in “crocidolite” as a result of the “lower electrostatic potential” at $M(2)$ that results from occupancy of the adjacent $M(4)$ site by a monovalent cation. Ghose (1965) also suggested local charge-balance as one of the factors controlling cation order at both the M and T sites in the amphibole structure. Whittaker (1971) did the first quantitative work on this issue. He calculated the Madelung energies and electrostatic site-potentials in a variety of cation arrangements and showed that the results are compatible with the cation arrangements in glaucophane, riebeckite and pargasite. However, the patterns of order predicted for tschermakite and aluminohornblende do not agree with those subsequently observed in crystal-structure refinements. Hawthorne (1978b) calculated the RMS (Root Mean Square) deviation from exact agreement with Pauling’s second rule (Pauling 1929) for all possible charge arrangements of the twelve most common amphibole stoichiometries, and showed that the observed patterns of order are those with the lowest RMS deviation from Pauling’s second rule for each stoichiometry. Thus Pauling’s second rule seemed to be the principal factor controlling the ordering of polyvalent cations in the amphibole structure.

Hawthorne (1997) proposed that bond-valence theory (Brown 1981, 2002) is applicable also at the local (short-range) scale, and showed that certain short-range arrangements of cations are much more stable according to the valence-sum rule than other arrangements also consonant with the overall stoichiometry of the amphibole under consideration. This approach has been very successful in understanding short-range effects in amphiboles and aiding assignment of fine-structure bands in the infrared spectra in the principal (OH)-stretching region (Hawthorne and Della Ventura 2007). As the long-range order is the sum of all of the short-range-order configurations in the structure, it is apparent that the local (short-range) constraint of the valence-sum rule affects the long-range order in the structure. Similar results have been obtained for glaucophane (Palin et al. 2003) and compositions along the tremolite–magnesianhornblende join (Palin et al. 2005) by Monte Carlo simulation as a function of temperature.

Thus the valence-sum rule (Brown 1981, 2002; Hawthorne 1994, 1997) provides a fairly comprehensive explanation for the observed order of heterovalent cations in amphiboles. It is apparent from both observed ordering patterns that some (e.g., Al completely ordered at $M(2)$ in glaucophane) are independent of temperature or pressure, whereas others (e.g., order of Al over $T(1)$ and $T(2)$ in pargasite) are dependent on temperature and/or pressure. The next step is to investigate these effects of temperature and pressure on the ordering of heterovalent cations.

Little quantitative work has been done on the factors that affect ordering of homovalent cations in the amphibole structure(s). This is an area waiting for work to be done.

ACKNOWLEDGMENTS

A huge amount of work on amphibole crystal-chemistry has been done in the last 25 years in Pavia, providing the crystal-chemical database which is the basis of many of the results reported here. The authors wish to acknowledge the seminal contributions of the late Giuseppe Rossi and Luciano Ungaretti, who started this project in the productive environment of the CNR-Centro di Studi per la Cristallografia e la Cristallografia. In particular, Luciano Ungaretti was the enthusiastic mover of the developments of the procedures for structure refinement and comparative analysis until his untimely end. Alberto Zanetti is warmly thanked for providing still unpublished data on oxo amphiboles. Giancarlo Della Ventura helped with constructive comments and useful information. FCH was supported by a Canada Research Chair in Crystallography and Mineralogy, and by a Discovery grant from the Natural Sciences and Engineering Research Council of Canada. RO and FC were supported by CNR funding to the project TAP01.004.002.

REFERENCES

- Adam J, Green TH (1994) The effects of pressure and temperature on the partitioning of Ti, Sr and REE between amphibole, clinopyroxene and basaltic melts. *Chem Geol* 117:219-233
- Adam J, Green TH (2003) The influence of pressure, mineral composition and water on trace element partitioning between clinopyroxene, amphibole and basaltic melts. *Eur J Mineral* 15:831-841
- Adams FD, Harrington BJ (1896) On a new alkali hornblende and a titaniferous andradite from the nepheline syenite of Dungannon, Hasting County, Ontario. *Am J Sci* 1:210-218
- Addison CC, Addison WE, Neal GH, Sharp JH (1962a) Amphiboles. Part I. The oxidation of crocidolite. *J Chem Soc* 1468-1471
- Addison WE, Neal GH, Sharp JH (1962b) Amphiboles. Part II. The kinetics of oxidation of crocidolite. *J Chem Soc* 1472-1475
- Andrut M, Gottschalk M, Melzer S, Najorka J (2000) Lattice vibrational modes in synthetic tremolite-Sr-tremolite and tremolite-richterite solid-solutions. *Phys Chem Mineral* 27:301-309
- Appleyard EC (1975) Silica-poor hastingsitic amphiboles from metasomatic alkaline gneisses at Wolfe, eastern Ontario. *Can Mineral* 13:342-351
- Armbruster T, Oberhänsli R, Bermanec V, Dixon R (1993) Hennomartinite and kornite, two new Mn^{3+} rich silicates from the Wessels mine, Kalahari, South Africa. *Schweiz Mineral Petrogr Mitt* 73:349-355
- Bancroft GM (1967) Quantitative estimates of site populations in an amphibole by the Mössbauer effect. *Phys Lett* 26A:17-18
- Bancroft GM (1973) *Mössbauer Spectroscopy. An Introduction for Inorganic Chemists and Geochemists.* McGraw Hill, New York
- Bancroft GM, Maddock AG, Burns RG, Strens RGJ (1966) Cation distribution in anthophyllite from Mössbauer and infrared spectroscopy. *Nature* 212:913-915
- Banno Y, Miyawaki R, Matsubara S, Makino K, Bunno M, Yamada S, Kamiya T (2004) Magnesiosadanagaite, a new member of the amphibole group from Kasuga-mura, Gifu Prefecture, central Japan. *Eur J Mineral* 16:177-183
- Barnes VE (1930) Changes in hornblende at about 800 °C. *Am Mineral* 15:393-417
- Borley GD (1963) Amphiboles from the younger granites of Nigeria. I. Chemical classification. *Mineral Mag* 33:358-376

- Brigatti MF, Medici L, Poppi L (1996) Refinement of the structure of natural ferriphlogopite. *Clays Clay Miner* 44:540-545
- Brown ID (1981) The bond valence method. An empirical approach to chemical structure and bonding. *In: Structure and Bonding in Crystals II*. O'Keeffe M, Navrotsky A (eds) Academic Press, New York, p 1-30
- Brown ID (2002) The Chemical Bond in Inorganic Chemistry. The Bond Valence Model. Oxford University Press
- Brown ID, Shannon RD (1973) Empirical bond strength–bond lengths curves for oxides. *Acta Crystallogr A* 29:266-282.
- Burns RG, Strens RGJ (1966) Infrared study of the hydroxyl bands in clinoamphiboles. *Science* 153:890-892
- Burns RG, Greaves CJ (1971) Correlations of infrared and Mössbauer site population measurements of actinolites. *Am Mineral* 56:2010-2033
- Caballero JM, Monge A, La Iglesia A, Tornos F (1998) Ferri-clinoholmquistite, $\text{Li}_2(\text{Fe}^{2+}, \text{Mg})_3\text{Fe}^{3+}_2\text{Si}_8\text{O}_{22}(\text{OH})_2$, a new ^6Li clinoamphibole from the Pedriza Massif, Sierra de Guadarrama, Spanish Central System. *Am Mineral* 83:167-171
- Caballero JM, Oberti R, Ottolini L (2002) Ferripedrizite, a new monoclinic ^6Li amphibole end-member from the Eastern Pedriza Massif, Sierra de Guadarrama, Spain, and a restatement of the nomenclature of Mg-Fe-Mn-Li amphiboles. *Am Mineral* 87:976-982
- Cámara F, Oberti R (2005) The crystal-chemistry of holmquistites: Ferroholmquistite from Greenbushes (Western Australia) and hints for compositional constraints in ^6Li amphiboles. *Am Mineral* 90:1167-1176
- Cámara F, Oberti R, Della Ventura G, Welch MD, Maresch WV (2004) The crystal-structure of synthetic $\text{NaNa}_2\text{Mg}_5\text{Si}_8\text{O}_{21}(\text{OH})_3$, a triclinic $C\bar{1}$ amphibole with a triple-cell and excess hydrogen. *Am Mineral* 89:1464-1473
- Cannillo E, Ungaretti L (1982) Prediction of the crystal-chemical composition of clinoamphiboles from X-ray intensity measurements of selected reflections (PREVEDI computer program). *Rend SIMP* 38:643-647
- Cannillo E, Oberti R, Ungaretti L (1981) "CORANF", un programma per il calcolo e la elaborazione di parametri chimici e geometrici degli anfibioli. *Rendiconti SIMP* 37:613-621
- Cannillo E, Ungaretti L, Oberti R, Smith DC (1986) An updated version of computer program CORANF for determining the site populations and the bulk-mineral composition of $C2/m$ amphiboles by single crystal X-ray diffractometry and refinement, XIV General Meeting IMA, Stanford (USA) Abstracts:70
- Castelli D (1998) Chlorpotassium ferro-pargasite from Sesia-Lanzo Marbles (Western Italian Alps): a record of highly saline fluids. *Rend SIMP* 43:129-38
- Cellai D, Conticelli S, Menchetti S. (1994) Crystal-chemistry of clinopyroxenes from potassic and ultrapotassic rocks in central Italy: implications on their genesis. *Contrib Mineral Petrol* 116:301-315
- Chukanov NV, Konilov AN, Zadov AE, Belakovsky DI, Pekov IV (2002) The new amphibole potassic chloropargasite $(\text{K}, \text{Na})\text{Ca}_2(\text{Mg}, \text{Fe}^{2+})_4\text{Al}(\text{Si}_6\text{Al}_2\text{O}_{22})(\text{Cl}, \text{OH})_2$ and conditions of its formation in the granulite complex of Sal'nye Tundry Massif (Kola Peninsula). *Zapiski VMO* 131(2):58-62
- Cipriani C (2007) Amphiboles: historical perspective. *Rev Mineral Geochem* 67:517-546
- Dawson JB, Smith JV (1977) The MARID (mica-amphibole-rutile-ilmenite-diopside) suite of xenoliths in kimberlite. *Geochim Cosmochim Acta* 41:309-323
- Deer WA, Howie RA, Zussman J (1997) *Rock Forming Minerals*, Volume 2B, Second Edition, Double-chain Silicates. The Geological Society, London
- Della Ventura G, Robert JL (1990) Synthesis, XRD and FT IR studies of strontium richterites. *Eur J Mineral* 2:171-175
- Della Ventura G, Robert JL, Bény JM (1991) Tetrahedrally coordinated Ti^{4+} in synthetic Ti rich potassic richterite: Evidence from XRD, FTIR and Raman studies. *Am Mineral* 76:1134-1140
- Della Ventura G, Robert JL, Bény JM, Raudsepp M, Hawthorne FC (1993a) The OH-F substitution in Ti-rich potassic-richterites: Rietveld structure refinement and FTIR and microRaman spectroscopic studies of synthetic amphiboles in the system $\text{K}_2\text{O}-\text{Na}_2\text{O}-\text{CaO}-\text{MgO}-\text{SiO}_2-\text{TiO}_2-\text{H}_2\text{O}-\text{HF}$. *Am Mineral* 78:980-987
- Della Ventura G, Robert J-L, Raudsepp M, Hawthorne FC (1993b) Site occupancies in monoclinic amphiboles: Rietveld structure refinement of synthetic nickel magnesium cobalt potassium richterite. *Am Mineral* 78:633-640
- Della Ventura G, Robert JL, Hawthorne FC (1994) The influence of the A-cation on the solubility of Ti in richteritic amphiboles: an FTIR spectroscopic study. *Terra Abstracts* 6:14
- Della Ventura G, Robert J-L, Hawthorne FC (1996) Infrared spectroscopy of synthetic (Ni, Mg, Co)-potassium-richterite. *In: Mineral Spectroscopy: A Tribute to Roger G. Burns*. The Geochemical Society, Special Publication Number 5:55-63
- Della Ventura G, Robert J-L, Raudsepp M, Hawthorne FC, Welch M (1997) Site occupancies in synthetic monoclinic amphiboles: Rietveld structure-refinement and infrared spectroscopy of (nickel, magnesium, cobalt)-richterite. *Am Mineral* 82:291-301
- Della Ventura G, Robert J-L, Hawthorne FC, Raudsepp M, Welch MD (1998) Contrasting patterns of ^{60}Al order in synthetic pargasite and Co-substituted pargasite. *Can Mineral* 36:1237-1244

- Della Ventura G, Hawthorne FC, Robert J-L, Delbove F, Welch MD, Raudsepp M (1999) Short-range order of cations in synthetic amphiboles along the richterite–pargasite join. *Eur J Mineral* 11:79-94
- Della Ventura G, Robert JL, Sergeant J, Hawthorne FC, Delbove F (2001) Constraints on F vs. OH incorporation in synthetic ⁶Al-bearing monoclinic amphiboles. *Eur J Mineral* 13:841-847
- Della Ventura G, Hawthorne FC, Robert JL, Iezzi G (2003) Synthesis and infrared spectroscopy of amphiboles along the tremolite–pargasite join. *Eur J Mineral* 15:341-347
- Dick LA, Robinson GW (1979) Chlorine-bearing potassian hastingsite from a sphalerite skarn in the southern Yukon. *Can Mineral* 17:25-26
- Driscall J, Jenkins DM, Dyar MD, Bozhilov KN (2005) Cation ordering in synthetic low-calcium actinolite. *Am Mineral* 90:900-911
- Dyar MD, Agresti DG, Schaefer MW, Grant CA, Sklute EC (2006) Mossbauer spectroscopy of Earth and planetary materials. *Ann Rev Earth Planet Sci* 34:83-125
- Ernst WG, Wai CM (1970) Mössbauer, infrared, X-ray and optical study of cation ordering and dehydrogenation in natural and heat treated sodic amphiboles. *Am Mineral* 55:1226-1258
- Evans BW, Yang H (1998) Fe-Mg order-disorder in tremolite-actinolite-ferro-actinolite at ambient and high temperatures. *Am Mineral* 83:458-475
- Farges F, Brown GE Jr, Velde D (1994) Structural environment of Zr in two inosilicates from Cameron: mineralogical and geochemical implications. *Am Mineral* 79:838-847
- Fialips-Guédon CI, Robert JL, Delbove F (2000) Experimental study of Cr incorporation in pargasite. *Am Mineral* 85:687-693
- Francis DM (1976) The origin of amphiboles in lherzolite xenoliths from Nunivak Island, Alaska. *J Petrol* 17:357-378
- Ghose S (1965) A scheme of cation distribution in the amphiboles. *Mineral Mag* 35:46-54
- Ghose S, Weidner JR (1972) Mg²⁺-Fe²⁺ order-disorder in cummingtonite, (Mg,Fe)₇Si₈O₂₂(OH)₂: a new geothermometer. *Earth Plan Sci Lett* 16:346-354
- Ghose S, Kersten M, Langer K, Rossi G, Ungaretti L (1986) Crystal field spectra and Jahn Teller effect of Mn³⁺ in clinopyroxene and clin amphiboles from India. *Phys Chem Mineral* 13:291-305
- Ginzburg IV (1965) Holmquistite and its structural variety clinholmquistite. *Trudy Mineralogicheskogo Muzeya Akademii Nauk SSSR* 16:73-89
- Goldman DR (1979) A reevaluation of the Mössbauer spectroscopy of calcic amphiboles. *Am Mineral* 64:109-118
- Goldman DR, Rossman GR (1977) The identification of Fe²⁺ in the M(4) site of calcic amphibole. *Am Mineral* 62:205-216
- Gottschalk M, Najorka J, Andrut M (1998) Structural and compositional characterization of synthetic (Ca,Sr)-tremolite and (Ca,Sr)-diopside solid solutions. *Phys Chem Mineral* 25:415-428
- Hafner SS, Ghose S (1971) Iron and magnesium distribution in cummingtonites, (Fe,Mg)₇Si₈O₂₂(OH)₂. *Z Krist* 133:301-326
- Hafner SS, Huckenholz HG (1971) Mössbauer spectrum of synthetic ferri-diopside. *Nature (Phys Sci)* 233:9-11
- Hawthorne FC (1978a) The crystal chemistry of the amphiboles. VIII. The crystal structure and site chemistry of fluor-riebeckite. *Can Mineral* 16:187-194
- Hawthorne FC (1978b) The crystal chemistry of the amphiboles. IX. Polyvalent cation ordering in clin amphiboles. *Can Mineral* 16:521-525
- Hawthorne FC (1981) Crystal chemistry of the amphiboles. *Rev Mineral* 9A:1-102
- Hawthorne FC (1983a) The crystal-chemistry of the amphiboles. *Can Mineral* 21:173-480
- Hawthorne FC (1983b) Characterization of the average structure of natural and synthetic amphiboles. *Per Mineral Roma* 52:543-581
- Hawthorne FC (1983c) Quantitative derivation of site occupancies in minerals. *Am Mineral* 68:287-306
- Hawthorne FC (1981) Crystal chemistry of the amphiboles. *Rev Mineral* 9A:1-102
- Hawthorne FC (1988) Mössbauer spectroscopy. *Rev Mineral* 18:255-340
- Hawthorne FC (1994) Structural aspects of oxides and oxysalt crystals. *Acta Crystallogr B* 50:481-510
- Hawthorne FC (1997) Short-range order in amphiboles: a bond-valence approach. *Can Mineral* 35:201-216
- Hawthorne FC, Della Ventura G (2007) Short-range order in amphiboles. *Rev Mineral Geochem* 67:173-222
- Hawthorne FC, Grice JD (1990) Crystal-structure analysis as a chemical analytical method: application to light elements. *Can Mineral* 28:693-702
- Hawthorne FC, Grundy HD (1977a) The crystal chemistry of the amphiboles. III. Refinement of the crystal structure of a sub-silicic hastingsite. *Mineral Mag* 41:43-50
- Hawthorne FC, Grundy HD (1977b) The crystal structure and site chemistry of a zincian tirodite by least-squares refinement of X-ray and Mössbauer data. *Can Mineral* 15:309-320
- Hawthorne FC, Oberti R (2007) Amphiboles: crystal chemistry. *Rev Mineral Geochem* 67:1-54
- Hawthorne FC, Waychunas GA (1988) Spectrum fitting methods. *Rev Mineral* 18:63-98

- Hawthorne FC, Oberti R, Ungaretti L, Grice JD (1992) Leakeite, $\text{Na Na}_2 (\text{Mg}_2\text{Fe}^{3+}\text{Li}) \text{Si}_8 \text{O}_{22} (\text{OH})_2$, a new alkali amphibole from the Kajlidongri manganese mine, Jhabua district, Madhya Pradesh, India. *Am Mineral* 77:1112-1115
- Hawthorne FC, Ungaretti L, Oberti R, Bottazzi P, Czamanske GK (1993) Li: an important component in igneous alkali amphiboles. *Am Mineral* 78:733-745
- Hawthorne FC, Ungaretti L, Oberti R, Cannillo E, Smelik EA (1994) The mechanism of ^6Li incorporation in amphibole. *Am Mineral* 79:443-451
- Hawthorne FC, Ungaretti L, Oberti R (1995a) Site populations in minerals: terminology and presentation of results. *Can Mineral* 33:907-911
- Hawthorne FC, Oberti R, Cannillo E, Sardone N, Zanetti A, Grice JD, Ashley PM (1995b) A new anhydrous amphibole from the Hoskins mine, Grenfell, New South Wales, Australia: description and crystal structure of ungarrettiite, $\text{Na Na}_2 (\text{Mn}^{3+}_3\text{Mn}^{2+}_2) \text{Si}_8 \text{O}_{22} \text{O}_2$. *Am Mineral* 80:165-172
- Hawthorne FC, Oberti R, Ungaretti L, Grice JD (1996a) A new hyper-calcic amphibole with Ca at the A site: fluor-cannilloite from Pargas, Finland. *Am Mineral* 81:995-1002
- Hawthorne FC, Oberti R, Sardone N (1996b) Sodium at the A site in clin amphiboles: the effects of composition on patterns of order. *Can Mineral* 34:577-593
- Hawthorne FC, Oberti R, Ottolini L, Foord EE (1996c) Lithium-bearing fluor-arfvedsonite from Hurricane Mountain, New Hampshire: a crystal-chemical study. *Can Mineral* 34:1015-1019
- Hawthorne FC, Welch MD, Della Ventura G, Liu S, Robert J-L, Jenkins DM (2000) Short-range order in synthetic aluminous tremolites: An infrared and triple-quantum MAS NMR study. *Am Mineral* 85:1716-1724
- Hawthorne FC, Oberti R, Cannillo E, Ottolini L, Roelofsen JN, Martin RM (2001) Li-bearing arfvedsonitic amphiboles from the Strange Lake peralkaline granite, Quebec. *Can Mineral* 39:1161-1170
- Hawthorne FC, Della Ventura G, Oberti R, Robert J-L, Iezzi G (2005) Short-range order in minerals: amphiboles. *Can Mineral* 43:1895-1920
- Hirschmann M, Evans BW, Yang, H (1994) Composition and temperature dependence of Fe-Mg ordering in cummingtonite-grunerite as determined by X-ray diffraction. *Am Mineral* 79:862-877
- Huckenholtz HG, Schairer JF, Yoder HS (1969) Synthesis and stability of ferri-diopside. *Mineral Soc Am Spec Pap* 2:163-177
- Iezzi G, Cámara F, Della Ventura G, Pedrazzi G, Oberti R, Robert J-L (2004) Synthesis, crystal structure and crystal-chemistry of ferri-clinoholmquistite, $\text{Li}_2 \text{Mg}_3 \text{Fe}^{3+}_2 \text{Si}_8 \text{O}_{22} (\text{OH})_2$. *Phys Chem Mineral* 31:375-385
- Inoue T, Irifune T, Yurimoto H, Miyagi I (1998) Decomposition of K-amphibole at high pressure and implications for subduction zone volcanism. *Phys Earth Planet Interiors* 107:221-231
- Jenkins DM, Hawthorne FC (1995) Synthesis and Rietveld refinement of amphibole along the join $\text{Ca}_2 \text{Mg}_5 \text{Si}_8 \text{O}_{22} \text{F}_2$ - $\text{Na Ca}_2 \text{Mg}_4 \text{Ga}_3 \text{Si}_6 \text{F}_2$. *Can Mineral* 33:13-24
- Jenkins DM, Ishida K, Liogys V, Ghosh D (2002) Cation distribution in amphiboles synthesized along the Ga analogue of the tremolite-aluminotschermakite join. *Phys Chem Mineral* 29:87-97
- Jenkins DM, Bozhilov KN, Ishida K (2003) Infrared and TEM characterization of amphiboles synthesized near the tremolite-pargasite join in the ternary system tremolite-pargasite-cummingtonite. *Am Mineral* 88:1104-1114
- Jones AP, Peckett A (1980) Zirconium bearing aegirine from Motzfeld, South Greenland. *Contr Mineral Petrol* 75:251-255
- Kamini DC, Bonardi M, Rao AJ (1982) Halogen-bearing minerals from Airport Hill, Visakhapanam, India. *Am Mineral* 67:1001-1004
- Kawachi Y, Coombs DS, Leake BE, Hinton RW (2002) The anhydrous amphibole ungarrettiite from the Woods mine, New South Wales, Australia. *Eur J Mineral* 14:375-377
- Kemp AJ, Leake BE (1975) Two hydrous-rich aluminous hornblendes. *Mineral Mag* 40:308-311
- King GW (1964) Spectroscopy and Molecular Structure. Holt, Reinhart and Winston Inc, New York
- King PL, Hervig RL, Holloway JR, Vennemann TW, Righter K (1999) Oxy-substitution and dehydrogenation in mantle-derived amphiboles megacrysts. *Geochim Cosmochim Acta* 62:3635-3651
- King PL, Hervig RL, Holloway JR, Delaney JS, Dyar MD (2000) Partitioning of $\text{Fe}^{3+}/\text{Fe}_{\text{total}}$ between amphibole and basanitic melt as a function of oxygen fugacity. *Earth Planet Sci Letters* 178:97-112
- Kitamura M, Tokonami M, Morimoto N (1975) Distribution of titanium atoms in oxy-kaersutite. *Contrib Mineral Petrol* 51:167-172
- Klein CJr, Ito J (1968) Zincian and manganoan amphiboles from Franklin, New Jersey. *Am Mineral* 53:1264-1275
- Kohn JA, Comeforo JE (1955) Synthetic asbestos investigations, II: X-ray and other data on synthetic fluor-richterite, -edenite, and -boron edenite. *Am Mineral* 40:410-421
- Konzett J (1997) Phase relations and chemistry of Ti-rich K-richterite-bearing mantle assemblages: an experimental study to 8 GPa in a Ti-KNCMASH system. *Contrib Mineral Petrol* 128:385-404
- Konzett J, Sweeney RJ, Thompson AB, Ulmer P (1997) Potassium amphibole stability in the upper mantle: an experimental study in a peralkaline KNCMASH system to 8.5 GPa. *J Petrol* 38:537-568

- Kullerud K, Erambert M (1999) Cl-scapolite, Cl-amphibole, and plagioclase equilibria in ductile shear zones at Nusfjord, Lofoten, Norway; implications for fluid compositional evolution during fluid–mineral interaction in the deep crust. *Geochim Cosmochim Acta* 63:3829-3844
- Kuroda Y, Hariya Y, Suzuki T, Matsuo S (1975) Pressure effect on water content of amphiboles. *Geophys Res Lett* 2:529-531
- Kushiro I, Erlank AJ (1970) Stability of potassic richterite. *Carnegie Inst Wash Yearbook* 68:231-233
- Law AD (1981) Studies of orthoamphiboles. II. Hydroxyl spectra of anthophyllites. *Soc franç Minéral Cristallogr Bull* 104:423-430
- Leake BE (1968) A catalog of analyzed calciferous and subcalciferous amphiboles together with their nomenclature and associated minerals. *Geol Soc Am Spec Paper* 98, 210 pp, Boulder, Colorado
- Leake BE, Woolley AR, Arps CES, Birch WD, Gilbert MC, Grice JD, Hawthorne FC, Kato A, Kisch HJ, Krivovichev VG, Linthout K, Laird J, Mandarino JA, Maresch WV, Nickel EH, Rock NMS, Schumacher JC, Smith DC, Stephenson NCN, Ungaretti L, Whittaker EJW, Guo Y (1997) Nomenclature of amphiboles: Report of the subcommittee on amphiboles of the International Mineralogical Association, Commission on New Minerals and Mineral Names. *Am Mineral* 82:1019-1037
- Leake BE, Woolley AR, Birch WD, Burke EAJ, Ferraris G, Grice JD, Hawthorne FC, Kisch HJ, Krivovichev VG, Schumacher JC, Stephenson NCN, Whittaker EJW (2003) Nomenclature of amphiboles: additions and revisions to the International Mineralogical Association's 1997 recommendations. *Can Mineral* 41:1355-1370
- Litvin AL, Ginzburg IV, Egorova LN, Petrunina AA (1975) On the crystal structure of clinoholmquistite. *Konstitutsiya i Svoystva Mineralov* 9:3-6
- Liu S, Welch MD, Klinowski J, Maresch WV (1996) A MAS NMR study of a monoclinic/triclinic phase transition in an amphibole with excess OH: $\text{Na}_3\text{Mg}_5\text{Si}_8\text{O}_{21}(\text{OH})_3$. *Eur J Mineral* 8:223-229
- Luth RW (1997) Experimental study of the system phlogopite-diopside from 3.5 to 17 GPa. *Am Mineral* 82:1198-1209
- Maresch WV, Miede G, Czank M, Fuess H, Schreyer W (1991) Triclinic amphibole. *Eur J Mineral* 3:899-903
- Matsubara S, Miyawaki R, Kurosawa M, Suzuki Y (2002) Potassic leakeite, a new amphibole from the Tanohata mine, Iwate Prefecture, Japan. *J Mineral Petrol Sci* 97:177-184
- Mazdab FK (2003) The diversity and occurrence of potassium-dominant amphiboles. *Can Mineral* 41:1329-1344
- McCormick KA, McDonald AM (1999) Chlorine-bearing amphiboles from the Fraser mine, Sudbury, Ontario, Canada: Description and crystal chemistry. *Can Mineral* 37:1383-1403
- Merli M, Ungaretti L, Oberti R (2000) Leverage analysis and structure refinement of minerals. *Am Mineral* 85:532-542
- Merli M, Oberti R, Caucia F, Ungaretti L (2001) Determination of site population in olivine: warnings on X-ray data treatment and refinement. *Am Mineral* 86:55-65
- Mével C, Kienast JR (1986) Jadeite-kosmochlor solid solution and chromian sodic amphiboles in jadeites and associated rock from Tawmaw (Burma). *Bull Mineral* 109:617-633
- Moore PB (1969) Joesmithite: a novel amphibole crystal chemistry. *In: Pyroxenes and amphiboles: crystal chemistry and phase petrology*. Papike JJ (ed) *Mineral Soc Am Spec Pap* 2:111-115
- Moore PB, Davis AM, Van Derveer DG, Sen Gupta, P.K. (1993) Joesmithite, a plumbous amphibole revisited and comments on bond valences. *Mineral Petrol* 48:97-113
- Morrison J (1991) Compositional constraints on the incorporation of Cl into amphiboles. *Am Mineral* 76:1920-1930
- Murad E, Cashion J (2004) *Mössbauer Spectroscopy of Environmental Materials and Their Industrial Utilization*. Kluwer, Dordrecht
- Najorka J, Gottschalk M (2003) Crystal chemistry of tremolite-tschermakite solid solutions. *Phys Chem Mineral* 30:108-124
- Oberti R, Ghose S (1993) Crystal-chemistry of a complex Mn-bearing alkali amphibole on the verge of exsolution. *Eur J Mineral* 5:1153-1160
- Oberti R, Ungaretti L, Cannillo E, Hawthorne FC (1992) The behaviour of Ti in amphiboles: I. four- and six-coordinated Ti in richterites. *Eur J Mineral* 4:425-439
- Oberti R, Ungaretti L, Cannillo E, Hawthorne FC (1993a) The mechanism of Cl incorporation in amphibole. *Am Mineral* 78:746-752
- Oberti R, Hawthorne FC, Ungaretti L, Cannillo E (1993b) The behaviour of Mn in amphiboles: Mn in richterite. *Eur J Mineral* 5:43-51
- Oberti R, Ungaretti L, Cannillo E, Hawthorne FC, Memmi I (1995a) Temperature-dependent Al order-disorder in the tetrahedral double chain of *C2/m* amphiboles. *Eur J Mineral* 7:1049-1063
- Oberti R, Hawthorne FC, Ungaretti L, Cannillo E (1995b) ⁶¹Al disorder in amphiboles from mantle peridotites. *Can Mineral* 33:867-878
- Oberti R, Sardone N, Hawthorne FC, Raudsepp M, Turnock AC (1995c) Synthesis and crystal-structure refinement of synthetic fluor-pargasite. *Can Mineral* 33:25-31

- Oberti R, Hawthorne FC, Raudsepp M (1997) The behaviour of Mn in amphiboles: Mn in synthetic fluor-edenite and synthetic fluor-pargasite. *Eur J Mineral* 9:115-122
- Oberti R, Hawthorne FC, Cámara F, Raudsepp M (1998) Synthetic fluoro-amphiboles: site preferences of Al, Ga, Sc and inductive effects on mean bond-lengths of octahedra. *Can Mineral* 36:1245-1252
- Oberti R, Hawthorne FC, Cámara F, Raudsepp M (1999) Unusual Ca^{2+} cations in synthetic amphiboles with nominal F-eckermannitic composition: Deviations from stoichiometry and structural effects of the cummingtonite component. *Am Mineral* 84:102-111
- Oberti R, Caballero JM, Ottolini L, López-Andrés S, Herreros V (2000a) Sodic-ferripedrizite, a new monoclinic amphibole bridging the magnesium-iron-manganese-lithium and the sodium-calcium groups. *Am Mineral* 85:578-585
- Oberti R, Vannucci R, Zanetti A, Tiepolo M, Brumm R (2000b) A crystal-chemical re-evaluation of amphibole/melt and amphibole/clinopyroxene D_{Ti} values in petrogenetic studies. *Am Mineral* 85:407-409
- Oberti R, Cámara F, Ottolini L, Caballero JM (2003a) Lithium in amphiboles: detection, quantification and incorporation mechanisms in the compositional space bridging sodic and $^{\text{B}}\text{Li}$ amphibole. *Eur J Mineral* 15:309-319
- Oberti R, Cámara F, Caballero JM, Ottolini L (2003b) Sodic-ferri-ferropedrizite and ferri-clinoferroholmquistite, mineral data and degree of order of A-site cations in Li-rich amphiboles. *Can Mineral* 91:1345-1356
- Oberti R, Cámara F, Caballero JM (2004) Ferri-ottoliniite and ferriwhittakerite, two new end-members of the new Group 5 for monoclinic amphiboles. *Am Mineral* 89:888-893
- Oberti R, Cámara F, Ottolini L (2005) Clinoholmquistite discredited: the new amphibole end-member fluoro-sodic-pedrizite. *Am Mineral* 90:732-736
- Oberti R, Cámara F, Della Ventura G, Iezzi G, Benimoff AI (2006) Parvo-mangano-edenite and parvo-manganotremolite, two new Group 5 monoclinic amphiboles from Fowler, New York, and comments on the solid solution between Ca and Mn^{2+} at the M4 site. *Am Mineral* 91:526-532
- Oberti R, Della Ventura G, Cámara F (2007) New amphibole compositions: natural and synthetic. *Rev Mineral Geochem* 67:89-123
- Ottolini L, Oberti R (2000) Accurate quantification of H, Li, Be, B, F, Ba, REE, Y, Th, and U in complex matrices: a combined approach based on SIMS and single-crystal structure-refinement. *Anal Chem* 72:3731-3738
- Ottolini L, Bottazzi P, Vannucci R (1993) Quantification of Li, Be and B in silicates by secondary ion mass spectrometry using conventional energy filtering. *Anal Chem* 65:1960-1968
- Ottolini L, Bottazzi P, Zanetti A, Vannucci R (1995) Determination of hydrogen in silicates by secondary ion mass spectrometry. *Analyst* 120:1309-1313
- Ottolini L, Cámara F, Bigi S (2000) An investigation of matrix effects in the analysis of fluorine in humite-group minerals by EMPA, SIMS, and SREF. *Am Mineral* 85:89-102
- Oxburgh ER (1964) Petrological evidence for the presence of amphibole in the upper mantle and its petrogenetic and geophysical implications. *Geol Mag* 101:1-19
- Palin EJ, Guiton BS, Graig MS, Welch MD, Dove MT, Redfern SAT (2003) Computer simulation of Al-Mg ordering in glaucophane and a comparison with infrared spectroscopy. *Eur J Mineral* 15:893-901
- Palin EJ, Dove MT, Welch MD, Redfern SAT (2005) Computer investigation of Al/Si and Al/Mg ordering in aluminous amphiboles. *Mineral Mag* 69:1-20
- Pan Y, Fleet ME (1992) Mineralogy and genesis of calc-silicates associated with Archean volcanogenic massive sulphide deposits at the manitouwadge mining camp, Ontario. *Can J Earth Sci* 29:1375-1388
- Pauling L (1929) The principles determining the structures of complex ionic crystals. *J Am Chem Soc* 51:1010-1026
- Pavlovich MS Jr, Jenkins DM (2003) Assessment of cation substitutions along the gallium and fluorine analogue of the tremolite-glaucophane join. *Am Mineral* 88:1486-1495
- Pawley AR (1992) Experimental study of the compositions and stabilities of synthetic nyböite and nyböite-glaucophane amphiboles. *Eur J Mineral* 4:171-192
- Pearce NJG (1989) Zirconium-bearing amphiboles from the Igaliko dyke swarm, South Greenland. *Mineral Mag* 53:107-110
- Pekov IV, Chukanov NV, Nefedova ME, Pushcharovsky DYu, Rastsvetaeva RK (2005) Chloro-potassichastingsite $(\text{K},\text{Na})\text{Ca}_2(\text{Fe}^{2+},\text{Mg})_4\text{Fe}^{3+}[\text{Si}_6\text{Al}_1\text{O}_{22}](\text{Cl},\text{OH})_2$: revalidation and the new name of dashkesanite. *Zapiski VMO* 134:31-36 (Russian with English abstract)
- Popp RK, Virgo D, Phillips MW (1995a) H deficiency in kaersutitic amphiboles: experimental verification. *Am Mineral* 80:1347-1350
- Popp RK, Virgo D, Yoder HS Jr, Hoering TC, Phillips MW (1995b) An experimental study of phase equilibria and Fe oxy-component in kaersutitic amphibole: Implications for the f_{H_2} and $a_{\text{H}_2\text{O}}$ in the upper mantle. *Am Mineral* 80:534-548
- Popp RK, Hibbert HA, Lamb WM (2006a) Oxy-amphibole equilibria in Ti-bearing calcic amphiboles: Experimental investigation and petrologic implications for mantle-derived amphiboles *Am Mineral* 91:54-66

- Popp RK, Hibbert HA, Lamb WM (2006b) Erratum: oxy-amphibole equilibria in Ti-bearing calcic amphiboles: Experimental investigation and petrologic implications for mantle-derived amphiboles. *Am Mineral* 91:716
- Posnjak E, Bowen NL (1931) The role of water in tremolite. *Am J Sci* 22:202-214
- Preston RJ, Hole MJ, Still J (1980) The occurrence of Zr-bearing amphiboles and their relationships with the pyroxenes and biotites in the teschenite and nepheline syenites of a differentiated dolerite boss, Islay, NW Scotland. *Mineral Mag* 64:459-468
- Rancourt DG, Dang MZ, Lalonde AE (1992) Mössbauer spectroscopy of tetrahedral Fe³⁺ in trioctahedral micas. *Am Mineral* 77:34-43
- Rastsvetaeva RK, Pushcharovskii DYu, Vinogradova RA, Pekov IV (1996) Crystal structure of Dashkenasite. *Crystallogr Rep* 41:65-69
- Raudsepp M, Turnock AC, Hawthorne FC, Sheriff BL, Hartman JS (1987a) Characterization of synthetic pargasitic amphiboles (Na Ca₂ Mg₄M³⁺ Si₆ Al₂ O₂₂ (OH,F)₂; M³⁺ = Al, Gr, Ga, Sc, In) by infrared spectroscopy, Rietveld structure refinement and ²⁷Al, ²⁹Si, and ¹⁹F MAS NMR spectroscopy. *Am Mineral* 72:580-593
- Raudsepp M, Turnock A, Hawthorne FC (1987b) Characterization of cation ordering in synthetic scandium-fluor-eckermannite, indium-fluor-eckermannite, and scandium-fluor-nyböite by Rietveld structure refinement. *Am Mineral* 72:959-964
- Raudsepp M, Turnock A, Hawthorne FC (1991) Amphiboles at low pressure: what grows and what doesn't. *Eur J Mineral* 3:983-1004
- Reece JJ, Redfern SAT, Welch MD, Henderson CMB (2000) Mn-Mg disordering in cummingtonite: a high-temperature neutron powder diffraction study. *Mineral Mag* 64:255-266
- Reece JJ, Redfern SAT, Welch MD, Henderson CMB, McCammon CA (2002) Temperature-dependent Fe²⁺-Mn²⁺ order-disorder behaviour in amphiboles. *Phys Chem Mineral* 29:562-570
- Robert JL, Della Ventura G, Raudsepp M, Hawthorne FC (1993) Rietveld structure refinement of synthetic strontium-rich potassium-richterites. *Eur J Mineral* 5:199-206
- Robert JL, Della Ventura G, Welch MD, Hawthorne FC (2000) OH-F substitution in synthetic pargasite at 1.5 kbar, 850 °C. *Am Mineral* 85:926-931
- Rosenberg PE, Foit FFJr (1977) Fe²⁺-F avoidance in silicates. *Geochim Cosmochim Acta* 41:345-346
- Sawaki T (1989): Sadanagaite and subsilicic ferroan pargasite from thermally metamorphosed rocks in the Nogo-Hakusan area, central Japan. *Mineral Mag* 53:99-106
- Saxena SK, Ekström TK (1970) Statistical chemistry of calcic amphiboles. *Contrib Mineral Petrol* 26:276-284
- Seifert F (1977) Compositional dependence of the hyperfine interaction of ⁵⁷Fe in anthophyllite. *Phys Chem Mineral* 1:43-52
- Seifert F (1978) Equilibrium Mg-Fe²⁺ cation distribution in anthophyllite. *Am J Sci* 278:1323-1333
- Semet MP (1973) A crystal-chemical study of synthetic magnesiohastingsite. *Am Mineral* 58:480-494
- Senda K, Ishida K, Jenkins DM (2005) X-ray Rietveld refinement and FTIR spectra of synthetic (Si, Ge)-richterites. *Am Mineral* 90:1062-1071
- Schaller WT (1916) Mineralogical notes, series 3. The chemical composition of tremolite. *Bull US Geol Survey* 610:136
- Skogby H (1987) Kinetics of intracrystalline order-disorder reactions in tremolite. *Phys Chem Mineral* 14:521-526
- Skogby H, Annersten H (1985) Temperature dependent Mg-Fe-cation distribution in actinolite-tremolite. *Neues J Mineral Mh* 1985:193-203
- Skogby H, Ferrow E (1989) Iron distribution and structural order in synthetic calcic amphiboles studied by Mössbauer spectroscopy and HRTEM. *Am Mineral* 74:360-366
- Skogby H, Rossman GR (1991) The intensity of amphibole OH bands in the infrared absorption spectrum. *Phys Chem Mineral* 18:64-68
- Sokolova EV, Hawthorne FC, Kabalov YK, Schneider J, McCammon C (2000) The crystal chemistry of potassic-ferrisadanagaite. *Can Mineral* 38:669-674
- Stormer FC Jr, Pierson ML, Tacker RC (1993) Variation of F and Cl X-ray intensity due to anisotropic diffusion in apatite during electron microprobe analysis. *Am Mineral* 78:641-648
- Strens RGJ (1966) Infrared study of cation ordering and clustering in some (Fe, Mg) amphibole solid solutions. *Chem Comm* 15:519-520
- Strens RGJ (1974) The common chain, ribbon, and ring silicates. *In: The Infrared Spectra of Minerals*. Farmer VC (ed) Mineral Soc, London
- Sudo A, Tatsumi Y (1990) Phlogopite and K-amphibole in the upper mantle: Implication for magma genesis in subduction zones. *Geophys Res Lett* 17:29-32
- Sweeney RJ, Green DH, Sie SH (1992) Trace and minor element partitioning between garnet and amphibole and carbonatitic melt. *Earth Planet Sci Lett* 113:1-14
- Tait KT, Hawthorne FC, Della Ventura G (2001) Al-Mg disorder in a gem-quality pargasite from Baffin Island, Nanavut, Canada. *Can Mineral* 39:1725-1732

- Tait KT, Hawthorne FC, Grice JD, Ottolini L, Nayak VK (2005) Dellaventuraite, Na Na₂ (MgMn³⁺₂Ti⁴⁺Li) Si₈O₂₂O₂, a new anhydrous amphibole from the Kajlidongri Manganese Mine, Jhabua District, Madhya Pradesh, India. *Am Mineral* 90:304-309
- Tiepolo M, Zanetti A, Oberti R. (1999) Detection, crystal-chemical mechanisms and petrological implications of ⁶⁰Ti⁴⁺ partitioning in pargasite and kaersutite. *Eur J Mineral* 11:345-354
- Tiepolo M, Zanetti A, Oberti R, Brumm R, Foley S, Vannucci R (2003) Trace-element partitioning between synthetic potassic-richterites and silicate melts, and contrasts with the partitioning behaviour of pargasites and kaersutites. *Eur J Mineral* 15:329-340
- Tiepolo M, Oberti R, Zanetti A, Vannucci R, Foley SF (2007) Trace-element partitioning between amphibole and silicate melt. *Rev Mineral Geochem* 67:417-451
- Ungaretti L (1981) Recent developments in X-ray single crystal diffractometry applied to the crystal-chemical study of amphiboles. *God Jugosl Centr Kristalogr* 15:29-65
- Ungaretti L, Mazzi F, Rossi G, Dal Negro A (1978) Crystal-chemical characterization of blue amphiboles. *Proc XI Gen Meet IMA, Rock-Forming Minerals*, 82-110
- Virgo D (1972) ⁵⁷Fe Mössbauer analyses of Fe³⁺ clinopyroxenes. *Carnegie Inst Wash Year Book* 71:534-538
- Wagner C, Velde D (1986) The mineralogy of K-richterite bearing lamproites. *Am Mineral* 71:17-37
- Warren BE (1930) The crystal structure and chemical composition of the monoclinic amphiboles. *Z Kristallogr* 72:493-517
- Welch MD, Knight KS (1999) A neutron diffraction study of cation ordering in high-temperature synthetic amphiboles. *Eur J Mineral* 11:321-331
- Welch MD, Kolodziejcki W, Klinowski J (1994) A multinuclear NMR study of synthetic pargasite. *Am Mineral* 79:261-268
- Welch MD, Camara F, Della Ventura G, Iezzi G (2007) Non-ambient *in situ* studies of amphiboles. *Rev Mineral Geochem* 67:223-260
- Wertheim GK (1964) The Mössbauer Effect. Principles and Applications. Academic Press, New York
- Whittaker EJW (1949) The structure of Bolivian crocidolite. *Acta Cryst* 2:312-317
- Whittaker EJW (1971) Madelung energies and site-preferences in amphiboles. I. *Am Mineral* 56:980-996
- Wiecek E, Szczepaniak M, Bielichowska-Cybula G, Woźniak H (1992) Asbestos substitutes and their biological effects. 2. Synthetic amphiboles--their physico-chemical characteristics. *Medycyna Pracy* 43:251-256
- Witte P, Langer K, Seifert F, Schreyer W (1969) Synthetische Amphibole mit OH- Überschuß im System Na₂O-MgO-SiO₂-H₂O. *Naturwissenschaften* 56:414-415
- Yang H, Evans BW (1996) X-ray structural refinements of tremolite at 140 and 295 K: Crystal chemistry and petrologic implications. *Am Mineral* 81:1117-1125
- Yang H, Konzett J, Prewitt CT, Fei Y (1999) Single-crystal structure refinement of synthetic ⁴⁰K-substituted potassic richterite, K(KCa)Mg₅Si₈O₂₂(OH)₂. *Am Mineral* 84:681-684
- Zanetti A, Vannucci R, Oberti R, Dobosi G (1995) Trace-element composition and crystal-chemistry of mantle amphiboles from the Carpatho-Pannonian Region. *Acta Vulcanologica* 7:265-276
- Zanetti A, Vannucci R, Bottazzi P, Oberti R, Ottolini L (1996) Infiltration metasomatism at Lherz as monitored by systematic ion-microprobe investigations close to a hornblendite vein. *Chem Geol* 134:113-133
- Zanetti A, Oberti R, Piccardo GB, Vannucci R (2000) Light lithophile elements (Li, Be and B), volatile (H, F and Cl) and trace element composition of mantle amphiboles from Zabargad peridotite: Insights into the multistage subsolidus evolution of subcontinental mantle during Red Sea rifting. *J Conf Abstr* 5:1120
- Zussman J (1955) The crystal structure of an actinolite. *Acta Crystallogr* 8:301-308

Short-Range Order in Amphiboles

Frank C. Hawthorne

*Department of Geological Sciences, University of Manitoba
Winnipeg, Manitoba, R3T 2N2, Canada
clhawth@ms.umanitoba.ca*

Giancarlo Della Ventura

*Dipartimento di Scienze Geologiche, Terza Università di Roma
via Ostiense 169, I-00154 Roma, Italy
dellaven@uniroma3.it*

INTRODUCTION

Extensive spectroscopic, diffraction and theoretical work in the last ten years has shown that short-range order (SRO) of both cations and anions is a common feature of amphiboles (Hawthorne et al. 2005). From an experimental perspective, the problem is that SRO does not obey the translational symmetry of the structure in which it occurs, and hence SRO is difficult to detect and decipher directly by standard diffraction methods. There is information on SRO resident in diffuse scattering from a crystal, but this information is quite difficult to extract, particularly when the SRO is complicated, and this approach has only been used for simpler materials. SRO can be detected by several spectroscopic techniques [e.g., infrared spectroscopy, magic-angle-spinning nuclear magnetic resonance (MAS NMR) spectroscopy], but the problem is that only part of the local arrangement is derived, and the complete picture of SRO is often not clear. Here, we examine SRO of cations and anions in monoclinic amphiboles, and show that detailed information on SRO can be derived by a combination of infrared spectroscopy and *local* bond-valence theory, augmented by results from Rietveld and single-crystal diffraction.

LONG-RANGE ORDER

Let us first examine the issue of LRO for a simple (two-dimensional) crystal of general composition $M_2\text{SiO}_4$ where $M = \text{Mg}, \text{Fe}^{2+}$, and consider the composition $\text{Mg}_{0.8}\text{Fe}^{2+}_{1.2}\text{SiO}_4$ for the case where there are two distinct sites, $M(1)$ and $M(2)$, in the unit cell (Fig. 1). Maximum order involves complete occupancy of one site by Fe^{2+} and occupancy of the other site by a mixture of Mg and Fe^{2+} . Either $M(1)$ or $M(2)$ can be fully occupied by Fe^{2+} , leading to the two long-range ordered arrangements indicated in Figure 1. Long-range disorder occurs when Mg and Fe^{2+} occur in equal amounts at the $M(1)$ and $M(2)$ sites, indicated in Figure 1. As indicated above, the states of order shown in Figure 1, and any states intermediate between them, can be easily determined by various diffraction and spectroscopic techniques. Why are we interested in such states of LRO? We are interested because the state of LRO affects the stability of the crystal through the associated configurational entropy and enthalpy of order-disorder.

SHORT-RANGE ORDER

Let us now examine the issue of SRO for the same (two-dimensional) crystal shown in Figure 1. LRO involves the occupancies of the sites *averaged over the complete crystal*,

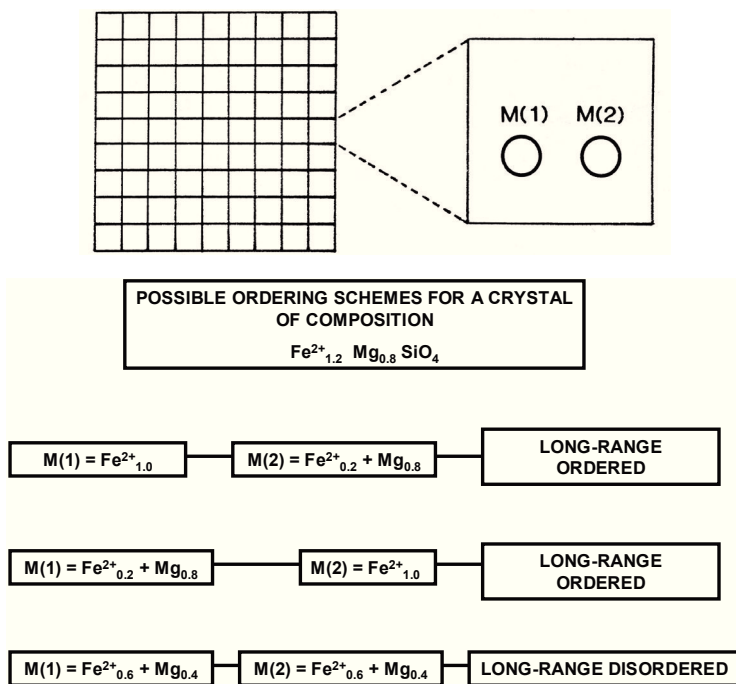


Figure 1. Sketch of a symbolic (two-dimensional) crystal structure showing a series of unit cells containing two cation sites, $M(1)$ and $M(2)$, together with long-range ordered and long-range disordered site populations for a bulk composition $Mg_{0.8}Fe^{2+}_{1.2}SiO_4$ (from Hawthorne et al. 2005).

whereas SRO involves the occupation of individual (i.e., non-averaged) sites over a scale of a few Å. This situation is illustrated in Figure 2 by a few unit cells of the crystal. The $M(1)$ site in the central unit cell is surrounded by four other sites, two $M(1)$ sites and two $M(2)$ sites. SRO involves the formation of *local* clusters of atoms that occur either more or less than predicted by a random distribution. The four nearest-neighbor M sites surrounding the central $M(1)$ site (Fig. 2) may be occupied by Fe^{2+}_4 , Fe^{2+}_3Mg , $Fe^{2+}_2Mg_2$, $Fe^{2+}Mg_3$, or Mg_4 . For a crystal of composition $Mg_{0.8}Fe^{2+}_{1.2}SiO_4$, a random distribution of nearest-neighbor cations will give the frequencies of occurrence of the possible clusters indicated in Figure 2. On the other hand, the local distribution may not be random (i.e., disordered); it may be ordered whereby some clusters occur more often than a random distribution indicates and other clusters may occur less often than a random distribution indicates. This situation is shown in Figure 2 where the cluster Mg_4 occurs much more often and the cluster $Fe^{2+}_2Mg_2$ occurs much less often than for a random distribution (i.e., short-range ordered). What is complete short-range disorder? It is where the frequency of occurrence of each local arrangement conforms to that calculated as the product of the fraction of each component, weighted according to the number of times it occurs in the local arrangement; the resultant values are then normalized to sum to unity. Thus for the example in Figure 2, the calculated relative frequencies for complete short-range disorder are 0.6^4 , $0.6^3 \times 0.4$, $0.6^2 \times 0.4^2$, 0.6×0.4^3 and 0.4^4 , which normalize to the values given in Figure 2 for the short-range disordered arrangement. The frequencies of occurrence for partial SRO given in Figure 2 are examples (that are compatible with the bulk composition of the crystal).

The above discussion involves SRO of homovalent cations. Of more interest from a crystal-chemical and mineralogical perspective is SRO involving heterovalent cations (or anions), as these states of order involve much greater changes in local bond-valence distribution than do

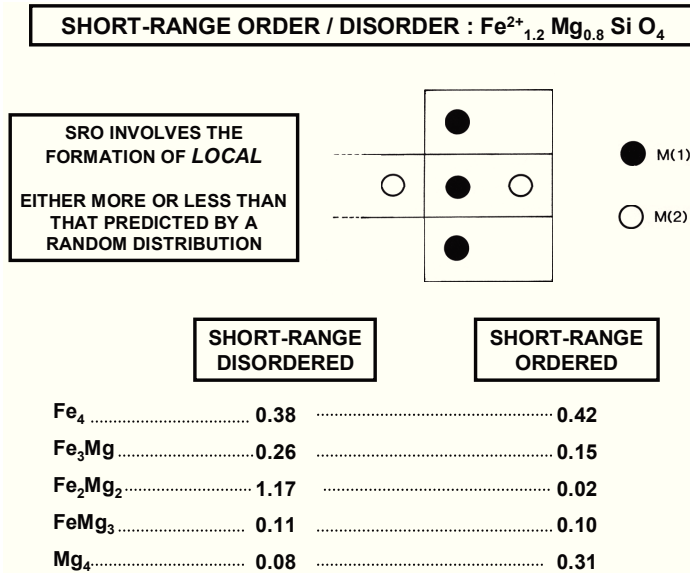


Figure 2. Sketch of a four unit-cell fragment of the symbolic structure of Figure 1, showing the *local* (next-nearest neighbor) environment around one $M(1)$ site, together with short-range ordered and short-range disordered arrangements for a bulk composition $\text{Mg}_{0.8} \text{Fe}^{2+}_{1.2} \text{SiO}_4$ (from Hawthorne et al. 2005).

changes in states of SRO involving homovalent cations (Hawthorne 1997). In turn, the resultant bond-valence constraints on local arrangements may have significant effects on the variation in chemical composition and stability of minerals. Given that short-range order-disorder is quite difficult to characterize experimentally, why should we be interested in SRO? We should be interested in SRO because it will affect the stability of a mineral in the same way as LRO: through its associated configurational entropy and enthalpy of order-disorder, and it will also affect the exchange of elements between coexisting minerals.

BOND-VALENCE ASPECTS OF SRO

Brown (1981, 2002) has developed a simple but powerful approach to chemical bonding in inorganic structures. A crystal is considered as an array of atoms connected by a network of chemical bonds. Any path through this network consists of alternating cations and anions, and the total array is subject to the constraint of electroneutrality. Bond valence is a measure of the strength of a chemical bond, and can be calculated from the curves of Brown and Altermatt (1985) if the bond lengths are known. The *valence-sum rule* states that the sum of the bond valences incident at each atom is equal to the magnitude of the formal valence of that atom. If the interatomic distances are not known, the bond valences can be approximated by the formal Pauling bond-strengths (Pauling 1929). Bond-valence arguments are normally applied to the long-range aspects of a structure, and Preiser et al. (1999) have shown how bond-valence theory can be derived from an ionic model. However, Burdett and Hawthorne (1993) showed how aspects of the theory can be derived from a localized molecular-orbital description of a solid in which there is a significant energy gap between interacting orbitals on adjacent atoms. This suggests that bond-valence theory can also be applied to local arrangements within a structure, and Hawthorne (1997) applied such arguments to derive the most probable arrangements of SRO in a wide variety of monoclinic amphiboles. A key feature of this approach is the application of the short-range valence-sum rule to all possible short-range arrangements: *those arrangements*

that most closely conform to the valence-sum rule are the short-range arrangements that are most likely to occur.

Of course, except in completely ordered amphiboles (in which the patterns of LRO are also the patterns of SRO), we do not know the local bondlengths. There are two ways in which we can approach this problem: (1) we can use the formal Pauling bond-strengths; (2) we can take the observed bond-valences in an amphibole in which the LRO is similar to that in the structure of interest (usually the structure of the amphibole of interest itself) and modify them by the ratio of the formal aggregate charge of the ions at a site to the formal charge of the ions at that site in the SRO arrangement under consideration.

SRO of heterovalent versus homovalent cations and anions

The valence-sum rule indicates that SRO will be far more common where mixed occupancies at specific sites involve cations or anions of different formal charge than where mixed occupancies involve cations or anions of the same formal charge. Indeed, we predict that SRO will be uncommon where homovalent ions are involved, and common where heterovalent ions are involved.

(OH) AS A PROBE OF LOCAL ORDER IN AMPHIBOLE

The O(3) site and its local environment are illustrated in Figure 3a for the $C2/m$ amphibole structure. When O(3) = (OH), the O-H distance is $\sim 0.96 \text{ \AA}$ (Hawthorne and Grundy 1976) and the associated O-H bond is approximately orthogonal to (100) (Hanisch 1966). The O(3) anion bonds to two M(1) and one M(3) cations. The point symmetry of the O(3) site is m in the $C2/m$ amphibole structure, but inspection of Figure 3a shows that there is pseudo-trigonal symme-

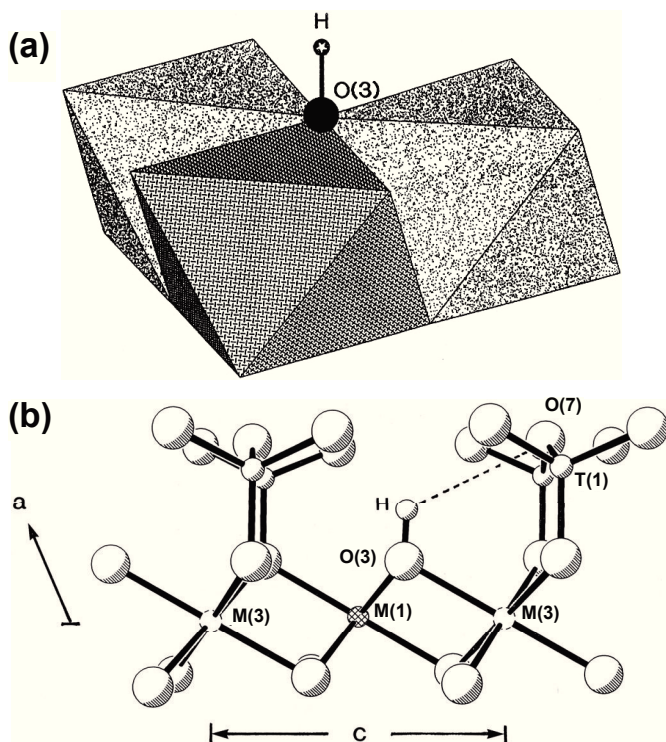


Figure 3. The (OH) group in the amphibole structure, associated with the M(1) (dark) and M(3) (stippled) polyhedra. The O atom at the O(3) site is shown as a large black circle, and its associated H atom is shown as a small black starred circle; (a) projected onto (100); (b) projected onto (010) with perspective, the T(2) sites have been omitted for clarity. [Used by permission of Schweizerbart'sche Verlagsbuchhandlung, from Della Ventura et al. (1999), *European Journal of Mineralogy*, Vol. 11, Fig. 7, p. 88].

try along the O-H bond, a very important factor that affects the resolution of the infrared spectra (Strens 1966). It is notable that the H atom hydrogen-bonds only to one O(7) atom (Fig. 3b).

The exact position (energy) of the principal OH-stretching band in the infrared spectrum of an hydroxyl-bearing mineral is a function of the relative strength of the O-H bond (Huggins and Pimental 1956). As this strength depends on the degree of hydrogen bonding between the H atom and the surrounding O atoms, the relative strength of the O-H bond is sensitive to the local arrangement of atoms around the OH group, i.e., by the cation distribution in the immediate vicinity of the H atom. These arrangements involve the *M*(1) and *M*(3) sites, and we will begin by considering the effect on the infrared spectrum of Mg-Fe²⁺ order over the *M*(1) and *M*(3) sites.

Mg-Fe²⁺ order-disorder over *M*(1) and *M*(3) and its effect on the infrared spectrum

Consider two cation species (e.g., Mg and Fe²⁺) at the *M*(1) and *M*(3) sites. As O(3) bonds to these *M* sites, there are $2 \times 2 \times 2 = 8$ different possible short-range arrangements around an (OH) anion at O(3); these are listed in Table 1. The spectrum that results from this situation (Fig. 4) shows only four absorption bands. This difference in number of bands arises from the pseudo-trigonal nature of the local arrangement: the two *M*(1) and one *M*(3) cations are pseudo-symmetrically related, introducing an accidental degeneracy into the spectrum (Table 1). The bands in the spectrum of Figure 4 are labeled A, B, C and D, and their assignments are shown in Table 1. The relations between site populations and band intensities for this simple case of Mg-Fe²⁺ are given in Appendix I.

M²⁺-M³⁺ order-disorder over *M*(1) and *M*(3) and its effect on the infrared spectrum

Early crystal-structure studies on calcic amphiboles assumed that C-group

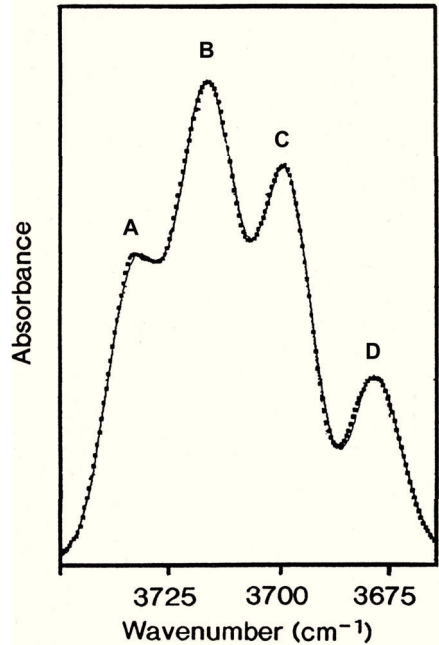


Figure 4. The infrared spectrum in the principal (OH)-stretching region of a synthetic (Mg,Co)-potassic-rich richterite of composition $K(\text{CaNa})(\text{Mg}_3\text{Co}_2)\text{Si}_6\text{O}_{22}(\text{OH})_2$; modified from Hawthorne et al. 1996c.

Table 1. Possible local arrangements around the O(3) site in amphiboles with (Mg,M²⁺) at *M*(1) and *M*(3).

	<i>M</i> (1)	<i>M</i> (1)	<i>M</i> (3)	Band*	Band ⁺
(1)	Mg	Mg	Mg	A	A
(2)	Mg	Mg	M ²⁺	B'	
(3)	M ²⁺	Mg	Mg	B''	B
(4)	Mg	M ²⁺	Mg		
(5)	M ²⁺	M ²⁺	Mg	C'	
(6)	M ²⁺	Mg	M ²⁺	C''	C
(7)	Mg	M ²⁺	M ²⁺		
(8)	M ²⁺	M ²⁺	M ²⁺	D	D

* ideal band-structure; (3) and (4) are symmetry equivalent and give rise to only one band: B''; similarly, (5) and (6) are symmetry equivalent and give rise to only one band: C''.

⁺ band structure usually observed; (2) and [(3)+(4)] are pseudo-symmetrically degenerate, and only one band (B) is observed experimentally; similarly, (5) and [(6)+(7)] are pseudo-symmetrically degenerate and only one band (C) is observed experimentally.

trivalent cations are completely ordered at the $M(2)$ site. However, Semet (1973) and Raudsepp et al. (1987a, 1991) showed that this is not the case. Semet (1973) noted the presence of two broad bands centered on 3711 and 3678 cm^{-1} in synthetic pargasite (Fig. 5a) and magnesiohastingsite, and suggested that these are due to Al-Mg and Fe^{3+} -Mg disorder over the $M(1)$ and $M(3)$ sites. Raudsepp et al. (1987a, 1991) presented similar spectra for pargasite and M^{3+} -substituted pargasite ($\text{M}^{3+} = \text{Cr}, \text{Sc}, \text{In}$), and found that the lower-frequency band is shifted to lower wavenumber in the substituted pargasites, in accord with the replacement of Al by a heavier trivalent cation at the $M(1,3)$ sites. This disorder of heavier trivalent cations over the $M(1,3)$ sites was confirmed by Rietveld structure-refinement (Raudsepp et al. 1987a, 1991). Welch et al. (1994) showed an analogous two-peak ^1H MAS NMR spectrum for pargasite (Fig. 5c), indicating disorder of Al over the $M(2)$ and one or both of the $M(1,3)$ sites. Detailed crystal-structure work by Oberti et al. (1995a) showed that ^{61}Al is partly disordered over the $M(2)$ and $M(3)$ sites in Mg-rich pargasite, the degree of disorder increasing with increase in the amount of Mg in the structure. Della Ventura et al. (1998a) showed that ^{61}Al is disordered in synthetic pargasite but completely ordered at $M(2)$ in the Co analogue $\text{Na Ca}_2 (\text{Co}^{2+}_4 \text{Al}) (\text{Si}_6 \text{Al}_2) \text{O}_{22} (\text{OH})_2$, i.e., $M(1) = M(3) = \text{Co}^{2+}$. However, comparison with the infrared spectrum of tremolite (Fig. 5b) shows the peaks in the pargasite spectrum to be very broad, suggesting the presence of more than two bands (components) in the spectrum. However, inspection of the spectrum of pargasite (Fig. 5a) shows that there is not a lot of information in the envelope on additional components.

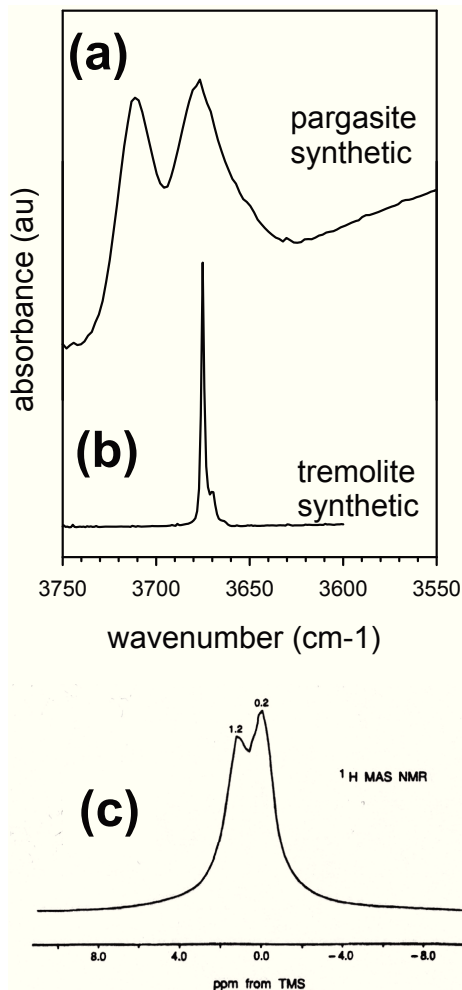


Figure 5. The spectra of selected $C2/m$ amphiboles in the principal (OH)-stretching region; (a) the infrared spectrum of synthetic pargasite; (b) the infrared spectrum of synthetic tremolite; (c) the ^1H MAS NMR spectrum of synthetic pargasite [(a) and (b) from Hawthorne et al. 2005, (c) from Welch et al. 1994].

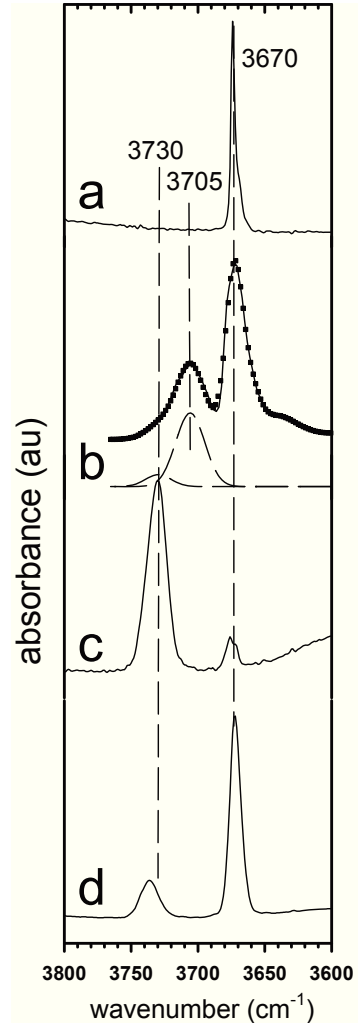
NEXT-NEAREST NEIGHBOR EFFECTS: SRO OF HETEROVALENT-CATIONS IN TREMOLITE

Hawthorne et al. (1996b) first showed that strong SRO of heterovalent cations does occur in monoclinic amphiboles. Figure 6a shows the infrared spectrum of synthetic tremolite of composition close to $\square (\text{Ca}_{1.8} \text{Mg}_{0.2}) \text{Mg}_5 \text{Si}_8 \text{O}_{22} (\text{OH})_2$ and Figure 6b shows the spectrum of tremolite(56) (Hawthorne 1983), the composition of which is given in Table 2. The spectrum

Figure 6. Infrared absorption spectra in the principal (OH)-stretching region for (a) synthetic tremolite, (b) tremolite (56) of Hawthorne and Grundy (1976), (c) synthetic richterite with a minor tremolite component, (d) synthetic tremolite-potassic-richterite of composition $TR_{80}KR_{20}$. The dashed peaks in (b) represent two component bands of the higher-energy peak (from Hawthorne et al. 1996b).

Table 2. Chemical composition (wt%) and unit formula (apfu) for tremolite(56).

SiO ₂	56.57	Si	7.767
Al ₂ O ₃	1.41	Al	0.228
TiO ₂	0.01	ΣT	7.995
Fe ₂ O ₃	0.01		
FeO	0.08	Ti	0.001
MnO	0.03	Fe ³⁺	0.001
MgO	24.41	Fe ²⁺	0.009
CaO	12.25	Mn	0.003
Na ₂ O	1.44	Mg	4.995
K ₂ O	0.68	ΣC	5.009
H ₂ O	1.46		
F	1.52	Ca	1.802
O≡F	-0.64	Na	0.198
Sum	99.23	ΣB	2.000
		Na	0.184
		K	0.119
		ΣA	0.303
		(OH)	1.330
		F	0.658



of synthetic tremolite consists of an intense narrow band at 3674 cm^{-1} due to the configuration $MgMgMg\text{-(OH)}$ [$M(1) = M(3) = Mg$], together with a narrow shoulder at $\sim 3670\text{ cm}^{-1}$ due to the configuration $MgMgMg\text{-(OH)}$ with a neighboring $M(4)$ site(s) occupied by Mg rather than by Ca . The spectrum of tremolite in Figure 6b also has an intense band at 3674 cm^{-1} , in accord with the composition of its C-group cations. However, there is also an intense band at 3705 cm^{-1} in the spectrum of Figure 6b, and the composition of this amphibole indicates that this band must be related to occupancy of the A , $M(4)$ and $T(1)$ sites by cations not present in synthetic tremolite [i.e., ${}^A(\text{Na}, \text{K})$, ${}^{M(4)}\text{Na}$ and ${}^{T(1)}\text{Al}$]. Hence the bands in the principal (OH)-stretching region of the infrared must also be affected by not just the cations that are nearest neighbors to the $O(3)$ anion, but also by cations that are next-nearest-neighbors of $O(3)$.

Infrared absorption in related amphiboles

Inspection of Table 2 shows that the tremolite under consideration has significant (Na, K) at the A site, Na at the $M(4)$ site and Al at the $T(1)$ site. Let us first consider the effect of

(Na, K) at the A site on the MgMgMg-(OH) absorption. This may be assessed by examining the infrared spectra of synthetic richterite (Fig. 6c) of nominal end-member composition Na (CaNa) Mg₅ Si₈ O₂₂ (OH)₂ and synthetic tremolite–potassic-richterite solid-solution of nominal composition TR₈₀KR₂₀ (Fig. 6d). In synthetic richterite, the principal absorption occurs at 3730 cm⁻¹ with a minor peak at 3674 cm⁻¹ (Fig. 6c), whereas in synthetic TR₈₀KR₂₀, the principal absorption occurs at 3674 cm⁻¹ with a minor peak at 3735 cm⁻¹ (Fig. 6d). The bands at 3730 and 3735 cm⁻¹ are assigned to the local arrangement MgMgMg-(OH) with a neighboring A site occupied by Na and K, respectively, which we will refer to as the richterite (or potassic-richterite) arrangement. In the spectrum of synthetic TR₈₀KR₂₀ (Fig. 6d), the band at 3674 cm⁻¹ can be assigned to the local arrangement MgMgMg-(OH) with a neighboring A-site vacant, which we will refer to as the tremolite arrangement. A band due to the tremolite arrangement also occurs in the spectrum of synthetic richterite (Fig. 6c), indicating that it is not of end-member composition, but has significant vacancy at the A site.

The effect of next-nearest-neighbor (NNN) cations

Let us now consider the *possible* local arrangements of next-nearest-neighbor cations (Table 3) in tremolite(56) of composition given in Table 2. Obviously, arrangements of the type MgMgMg-F do not give rise to an (OH)-stretching absorption. However, the O(3) sites occur in pairs along the edge of the M(1) octahedron, and the occurrence of (OH)-F arrangements here may or may not give rise to additional bands. Arrangement (1) (Table 3) is the tremolite configuration and gives a band at 3674 cm⁻¹. Substitution of F in tremolite (Robert et al. 1999) does not give rise to any additional bands (one-mode behavior, see section on SRO of (OH) and F in amphiboles later in this chapter) and hence arrangement (2) will not give rise to an (OH) absorption. Arrangement (3) is the richterite (potassic-richterite) configuration and gives a band at 3730 (3735) cm⁻¹. Arrangement (4) involves F at the neighboring O(3) site. As shown by Della Ventura et al. (1998b) and Robert et al. (1999), this arrangement gives rise to an additional band at 3714 cm⁻¹ in both F-bearing richterite and potassic-richterite (two-mode behavior). Substitution of Al for Si in micas reduces the frequency of the principal absorption band by ~ 25 cm⁻¹. Because the local arrangement around (OH) in richterite and potassic-richterite is similar to that in Si-rich micas, substitution of Al for Si in a local richterite configuration will reduce the frequency of the principal (OH)-absorption band by ~ 25 cm⁻¹: 3730 – 25 = 3705 cm⁻¹. Substitution of Al for Si in a local tremolite configuration [arrangement (5)] would reduce the frequency of the principal (OH) absorption to give a band at 3674 – 25 = 3649 cm⁻¹. Substitution of Al for Si in a local richterite configuration [arrangement (6)] would reduce the frequency of the principal (OH) absorption to give a band at 3730 – 25 = 3705 cm⁻¹. Substitution of Al for Si in a local richterite configuration with F at an adjacent O(3) site [arrangement (7)] would reduce the frequency of the principal (OH) absorption to give a band at 3714 – 25 = 3689 cm⁻¹.

Table 3. Possible local arrangements and predicted band frequencies for tremolite(56).

	A	O(3)	T(1)	M(4)	Frequency (cm ⁻¹)
(1)	□	OH	Si	Ca	3674
(2)	□	F	Si	Ca	3674
(3)	(Na,K)	OH	Si	Na	3730
(4)	(Na,K)	F	Si	Na	3714
(5)	□	(OH,F)	Al	Ca	3649
(6)	(Na,K)	OH	Al	Ca	3705
(7)	(Na,K)	F	Al	Ca	3689

Derivation of patterns of SRO

We may now compare the band positions and local arrangements of Table 3 with the observed bands in Figure 6b. Arrangement (1), with its band at 3574 cm^{-1} is obviously the dominant local arrangement in this amphibole. The weak intensity of the band at 3730 cm^{-1} in Figure 6b is not in accord with all the A cations being involved in arrangement (3). Arrangement (4) would give rise to a band at 3714 cm^{-1} that is significantly displaced from the maximum at 3705 cm^{-1} ; this arrangement may be present in a minor amount, but the spectrum is not compatible with most of the F being involved in this arrangement. Arrangement (5) is obviously not present as there is no trace of a band at 3649 cm^{-1} in the spectrum. Arrangement (6) will give rise to a band at 3705 cm^{-1} ; as the dominant secondary band in the spectrum is at 3705 cm^{-1} (Fig. 6b), we may conclude that this arrangement is the second most-frequent arrangement in this crystal. There is no band at 3689 cm^{-1} corresponding to arrangement (7), and hence this does not occur.

Thus the two most important local arrangements in the tremolite(56) of Table 2 are (1) and (6) (Table 3). However, arrangement (3) involves equal amounts of $^A(\text{Na}, \text{K})$ and $^{T(1)}\text{Al}$, and inspection of the formula of the tremolite (Table 2) shows that $^A(\text{Na}, \text{K})$ exceeds $^{T(1)}\text{Al}$. The excess $^A(\text{Na}, \text{K})$ gives rise to a small amount of arrangement (3) and is in accord with the weak band at 3730 cm^{-1} in the spectrum (Fig. 6b). As none of the arrangements identified so far as being present involve F, there must be a fourth arrangement that does involve this component. Inspection of Table 3 shows that arrangement (2) is the only possibility. Note that we cannot use the relative intensities of the bands to derive accurate estimates of the amounts of these arrangements present in the amphibole as (1) the absorptivity is related to relative concentration in a complex way that is currently not understood (Skogby and Rossman 1991; Hawthorne et al. 1997); (2) arrangements that involve F have no spectral expression. However, despite this limitation, it is apparent that the non-tremolite components in the amphibole of Table 2 are not randomly distributed within the amphibole structure but show extreme SRO.

SRO of heterovalent cations in tremolite(56): application of bond-valence theory

Let us apply the local version of bond-valence theory to the example of tremolite(56) considered in the previous section. As indicated in Table 2, the principal non-tremolite components in this amphibole are $^A(\text{Na}, \text{K})$, $^{M(4)}\text{Na}$ and $^{T(1)}\text{Al}$. The environment of these sites is shown in Figure 7. Of key importance here are the O(5), O(6) and O(7) anions that link to the A(2), M(4) and T(1) sites, as the bond valences incident at these sites will be strongly affected by the local occupancies of the A(2), M(4) and T(1) sites. Table 4 shows the bond-valences of the cation arrangements of Table 3 (exclusive of those involving F).

Arrangement (1) is the ordered tremolite configuration and has incident bond-valence sums in accord with the valence-sum rule. Arrangement (3) is the richterite configuration; it also has reasonable bond-valence sums, and corresponds with both the chemical composition of the crystal and the weak band at 3730 cm^{-1} in the spectrum of Figure 6b. Arrangement (5) has Al at T(1), Ca at M(4) and a vacant A-site; the bond-valence sums are very low, indicating that this local arrangement will not occur, in agreement with the absence of a band at 3649 cm^{-1} . For arrangement (6), the bond-valence sum for O(5) is low and the sums for O(6) and

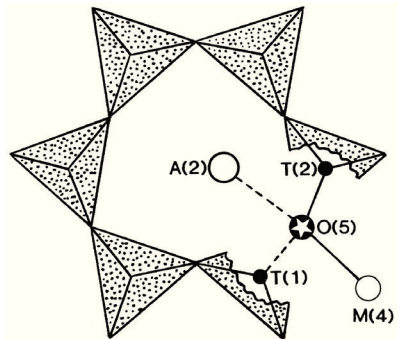


Figure 7. The A(2), M(4) and T(1) sites in tremolite, together with their coordinating anions and neighboring coordination polyhedra.

Table 4. Local bond-valence (vu) patterns for selected local arrangements of Table 3.

Arrangement (1)						Arrangement (3)					
$M^{(4)}Ca$	$A\Box$	$T^{(1)}Si$	$T^{(2)}Si$	Σ		$M^{(4)}Na$	$A\Box$	$T^{(1)}Si$	$T^{(2)}Si$	Σ	
O(5)	0.13	–	0.97	0.92	2.02	O(5)	0.06	0.07	0.99	0.91	2.03
O(6)	0.21	–	0.98	0.88	2.07	O(6)	0.10	0.08	0.95	0.86	1.99
O(7)	–	–	1.02 $\times 2 \rightarrow$	–	2.04	O(7)	–	0.18	0.96 $\times 2 \rightarrow$	–	2.10

Arrangement (5)						Arrangement (6)					
$M^{(4)}Ca$	$A\Box$	$T^{(1)}Al$	$T^{(2)}Si$	Σ		$M^{(4)}Ca$	$A\Box$	$T^{(1)}Al$	$T^{(2)}Si$	Σ	
O(5)	0.13	–	0.73	0.91	1.77	O(5)	0.13	0.07	0.73	0.91	1.84
O(6)	0.21	–	0.74	0.86	1.81	O(6)	0.21	0.08	0.74	0.86	1.89
O(7)	–	–	0.76	–	1.78	O(7)	–	0.18	0.76	–	1.96
			1.02	}				1.02	}		

O(7) are acceptable. As arrangements (5) and (6) are the only arrangements that include Al at $T(1)$, it is a question of which arrangement is to be preferred. From the sums in Table 4, it is clear that (6) is the preferred arrangement, in accord with the band position at 3705 cm^{-1} (Fig. 6b). Other arrangements are also possible, specifically those that just involve the addition or replacement of one component, but these are unfavorable from a bond-valence perspective.

NEAREST- AND NEXT-NEAREST-NEIGHBOR EFFECTS

The simple example given above shows that next-nearest-neighbor (NNN) effects give rise to significant bands in the spectra of amphiboles, which is very fortunate as these NNN “effects” are our short-range arrangements of atoms, and the presence and intensities of the resultant bands contain information on SRO. So before we consider any specific amphiboles, we need to characterize the local arrangements of sites that are involved in these possible patterns of SRO, and we also need to develop a nomenclature to denote these site configurations (note that we use the term “configuration” when we are dealing with sites, and the term “arrangement” when we are dealing with atoms).

Nearest-neighbor sites: configuration symbols and atom arrangements

The O(3) site is bonded to two $M(1)$ and one $M(3)$ sites (Fig. 3a), and the H atom of that O(3) site projects out into the A cavity. The distance between the H atom and any A cation is of the order of 2.8 \AA , and hence one expects a repulsion interaction between the two cations. Comparison of the infrared spectra of amphiboles with $M(1) = M(3) = Mg$, $O(3) = (OH)$ and $A = \Box$ and Na, respectively, should indicate the effect of the A cation on the spectrum. Comparison of the infrared spectra of synthetic tremolite (Fig. 6a) and synthetic richterite (Fig. 6c) shows that the principal (OH)-stretching band is shifted to higher wavenumber (energy) where H is locally associated with Na at the A site. This effect of the A cations is general (e.g., Rowbotham and Farmer 1974; Robert et al. 1989; Hawthorne et al. 1997; Gottschalk and Andrut 2003). Thus we need to incorporate the character of the A -site occupancy into any notation describing the local configuration of sites. We may denote this configuration as $M(1)M(1)M(3)-O(3)-A$, and local arrangements of atoms will be written as follows: MgMgMg-OH- \Box ...end-member tremolite arrangement, MgMgMg-OH-Na...end-member richterite arrangement.

NNN sites: the *T* sites

Consider the local environment of the H atom in the monoclinic amphibole structure (Fig. 3b). The H atom is in such a position as to form a hydrogen bond to the closest O(7) atom (Hawthorne 1983), and it is the strength of this interaction that affects the shift in the frequency of the principal OH-stretching vibration. So what affects the strength of this hydrogen bond? The key issue here is that the valence-sum rule must be satisfied at the O(7) anion, and this is affected only by the atoms occupying the locally associated pair of *T*(1) sites (Fig. 3b). We can incorporate the *T*(1)*T*(1) configuration by appending it to the site configuration symbol: *M*(1)*M*(1)*M*(3)-O(3)-A:*T*(1)*T*(1).

NNN sites: the *M* sites

The NN and NNN *M* sites are shown in Figure 8. The effect of the next-nearest-neighbor *M*(2) and *M*(3) sites is subtle to decipher as it produces new bands which usually are poorly resolved in the spectrum and only contribute to the broadening of the main absorptions. Comparison of Figures 8a and 8b indicates that there are two stereochemically distinct types of next-nearest-neighbor polyhedra: (1) polyhedra which share two edges with polyhedra of the NN cluster [*M*(2)*M*(2)*M*(3)] (Fig. 8a), and (2) polyhedra which share one edge with polyhedra of the NN cluster [*M*(1)*M*(1)*M*(2)*M*(2)] and [*M*(4)*M*(4)] (Fig. 8b). It seems reasonable to expect that cation variation in type-1 polyhedra will produce spectral bands that have better resolution than do those resulting from cation variation in type-2 polyhedra.

Della Ventura et al. (1999) discussed this issue, and considered two models: (1) the three NNN *M* sites *M*(2)*M*(2)*M*(3), and (2) the five NNN *M* sites *M*(2)*M*(2)*M*(3)*M*(2)*M*(2) which were used to interpret the infrared spectra of synthetic richterite-pargasite amphiboles (Della Ventura et al. 1999) and synthetic aluminous-tremolite solid-solutions (Hawthorne et al. 2000a). However, the *M*(4) site (Fig. 8b) also has an effect. This is most clearly indicated by Gottschalk et al. (1998, 1999), who resolved bands due to occupancy of the two NNN *M*(4) sites (Fig. 8b) in synthetic tremolite--Sr-tremolite by Ca, Sr and Mg, and in synthetic tremolite by Ca and Mg. What seems apparent here is that the degree of resolution in amphibole spectra depends on the chemical complexity of the amphibole examined. Hence one needs a flexible site-configuration symbol to cater for these different requirements.

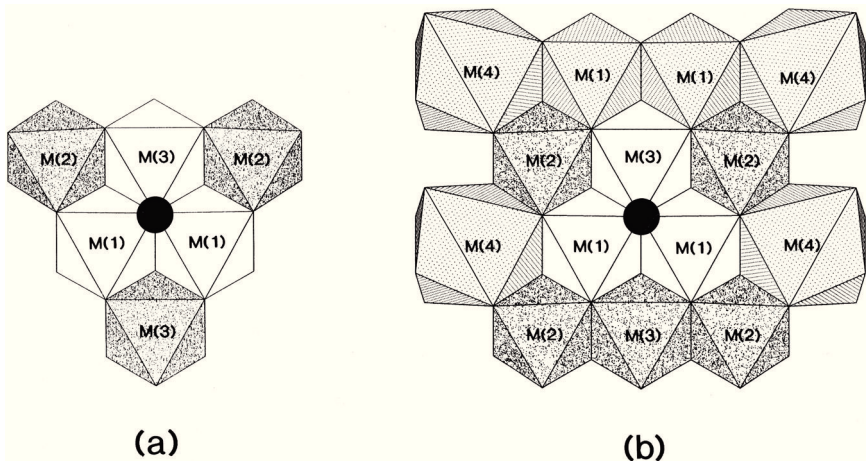


Figure 8. (a) Nearest-neighbor and (b) next-nearest-neighbor octahedra about the O(3) site in the monoclinic amphibole structure; the O(3) site is marked by a large black circle (modified from Della Ventura et al. 1999).

We can incorporate the NNN sites into a site-configuration symbol by appending the NNN sites to the NN symbol as follows:

$M(1)M(1)M(3)-O(3)-A: T(1)T(1)-M(2)M(2)M(3)$ (Fig. 8a)

$M(1)M(1)M(3)-O(3)-A: T(1)T(1)-M(2)M(2)M(3)-M(2)M(2)$

$M(1)M(1)M(3)-O(3)-A: T(1)T(1)-M(2)M(2)M(3)-M(1)M(1)M(2)M(2)-M(4)M(4)M(4)M(4)$ (Fig. 8b)

where we have separated type-1 NNN sites from type-2 NNN sites by a dash.

The number of possible short-range arrangements of cations

Let us examine the site-configuration symbol $M(1)M(1)M(3)-O(3)-A:T(1)T(1)-M(2)M(2)M(3)$ to see how many local arrangements are possible. This problem depends on the number of species that are available for incorporation; we will consider this problem for a relatively straightforward example: Let the $M(1)$ and $M(3)$ sites be occupied by Mg and Al, the $O(3)$ site be occupied only by (OH), the A site be occupied by Na, \square and Ca, and the $T(1)$ site be occupied by Si and Al. Setting pseudosymmetric arrangements as identical, the NN $M(1)$ and $M(3)$ sites give rise to four arrangements: MgMgMg, MgMgAl, MgAlAl and AlAlAl; the A site gives rise to three arrangements: Na, \square and Ca; the NNN $T(1)$ site pair gives rise to three arrangements: SiSi, SiAl and AlAl; the NNN $M(2)$ and $M(3)$ sites give rise to four arrangements: MgMgMg, MgMgAl, MgAlAl and AlAlAl. Thus the total number of algebraically possible arrangements is $4 \times 3 \times 3 \times 4 = 144$; if we extend the NNN arrangement of octahedra to the next two $M(2)$ sites, this number rises to $144 \times 3 = 432$. Of course, many of these arrangements will be unstable on bond-valence grounds (Hawthorne 1997), but a random short-range arrangement of cations would give rise to this many arrangements for this particular composition.

SHORT-RANGE ORDER AND SHORT-RANGE DISORDER

Above, we calculated all combinatorially possible arrangements of cations over a specific cluster in the amphibole structure, and it can be shown that many of these arrangements are not stable on bond-valence grounds. Let us consider a series of situations that will illuminate the issues of SRO. (1) Consider the extreme situation where some fraction, x , of the possible number of short-range arrangements are not favored from a bond-valence perspective, and the remaining $(1 - x)$ arrangements are equally favored. There will be extreme SRO as x arrangements will not occur and $(1 - x)$ arrangements will occur as dictated by the statistical distribution of atoms for a specific bulk composition. (2) Consider the situation where some fraction, x , of the possible number of short-range arrangements are not favored from a bond-valence perspective, and the remaining $(1 - x)$ arrangements are unequally favored. There will be extreme SRO as x arrangements will not occur and $(1 - x)$ arrangements will occur as dictated by the preference of occurrence on bond-valence grounds for a specific bulk composition. (3) Consider the situation where all combinatorially possible short-range arrangements are unequally favored from a bond-valence perspective. There will be extensive SRO as all arrangements may occur as dictated by the preference of occurrence on bond-valence grounds for a specific bulk composition. Of course, other factors, such as structural strain, may affect the fraction of any specific arrangement. However, despite this issue, the three examples outlined above indicate that the situation with regard to SRO is more complicated than it initially appears. For (1), there is extreme SRO from the point of view that many arrangements do not occur, but there is also short-range disorder as the arrangements that do occur will occur as dictated by the statistical distribution of atoms for a specific bulk composition. For (2), there is extensive SRO as for (1), but there is partial SRO of observed arrangements as the fractions of these arrangements do not accord with those dictated by the statistical distribution of atoms for a specific bulk composition. For (3), there is partial SRO as

all arrangements occur, but not in the fractions dictated by the statistical distribution of atoms for a specific bulk composition.

The above discussion indicates a lot of potential complexity in the incorporation of SRO into thermodynamic models of amphiboles, and can also lead to confusion in description, as there may be strong SRO and strong short-range disorder [e.g., example (1) above] involving the same sites in the same crystal.

SPECTRAL VARIATION IN THE INFRARED SPECTRA OF AMPHIBOLES

We are interested in the number and relative intensities of bands in the (OH)-stretching region of the infrared spectra of amphiboles, as they provide us with insight into SRO. The possibility of deriving this information from the spectra depends on the resolution of the bands which, in turn, depends on the positions and widths of the bands. Here, we briefly consider these issues for amphiboles.

Peak width and band width

Here, we will use the word “peak” to designate an envelope in the spectrum with only one maximum, and the word “band” to denote an absorption deriving from a specific single local arrangement in the structure. In optimum circumstances, peak widths of a few wavenumbers can be obtained in amphibole spectra. However, some amphiboles show extremely broad peaks without obvious resolution of any component bands (i.e., without a change in the second derivative of the intensity with respect to energy apart from those required to define the primary peak); this variation in peakwidth is shown in Figures 5a and 5b, and Figures 6a and 6c.

What causes this variation in peakwidth?

- (1) The peak may consist of more than one band, where the bands are not sufficiently resolved to produce subsidiary maxima (or even changes in the second derivative of wavelength with respect to energy); such an example is seen in the spectrum of synthetic pargasite (Fig. 5a) which consists of two very broad peaks, each of which has been shown to contain several bands (Della Ventura et al. 1999).
- (2) Bands that are close in energy and physically close in the structure may couple to produce broadening. This is the case in the spectrum of synthetic richterite (Fig. 6c). The halfwidth of the principal absorption in synthetic richterite is $\sim 25 \text{ cm}^{-1}$, whereas the halfwidth of the principal absorption in synthetic tremolite is $\sim 2 \text{ cm}^{-1}$ (Fig. 6a). The configuration symbol for richterite is as follows: $M(1)M(1)M(3)\text{-O}(3)\text{-A: } T(1)T(1)\text{-}M(2)M(2)M(3)\text{-}M(1)M(1)M(2)M(2)M(4)M(4)$ (Fig. 8b). All sites are ordered except for the two $M(4)$ sites, which results in the possible arrangements: $M(4)M(4)$: CaCa, CaNa, NaNa. Thus the intense peak in the spectrum of synthetic richterite must consist of three bands. As the intrinsic width of the CaCa (i.e., tremolite-type) band is $\sim 2 \text{ cm}^{-1}$, assuming an intrinsic width for the other two arrangements, the three bands will not give rise to a composite peak as wide as $\sim 25 \text{ cm}^{-1}$ just by overlap. It seems reasonable to propose that arrangements across the occupied A site couple to produce broadening of the component bands. It is this coupling that contributes significantly to the broad peak in the richterite spectrum. In this regard, it should be noted that all A -site-occupied amphiboles have spectra with peaks much broader than those in the spectra of A -site-vacant amphiboles.

Band position (energy) as a function of composition

As discussed above, the exact wavelength (energy) of the principal OH-stretching band in the infrared spectrum of a hydroxyl-bearing mineral is a function of the local arrangement of atoms around the OH group. If we designate the arrangement in tremolite as a reference

point, we may list the differences in OH-stretching frequencies for different arrangements, and produce a relation between these differences (often referred to as “shifts”) and the local compositional differences of the amphibole structure (Strens 1966; Della Ventura and Robert 1990; Della Ventura 1992). The current status of these relations is given in Table 5.

Resolution in infrared spectra

There are two issues relating to resolution of infrared spectra: (1) how “well-resolved” is the experimental spectrum, and (2) how do we numerically resolve the experimental spectrum to extract the maximum amount of information? With regard to (1), the resolution of the spectrum depends on the degree of structural and chemical complexity of the amphibole. As a rule of thumb, spectral resolution decreases with increasing complexity of order and composition of the amphibole. Simple ordered amphiboles give simple well-resolved spectra. However, any degree of disorder will normally decrease the spectral resolution, which is

Table 5. The differences in OH-stretching frequency for different arrangements of cations, relative to the OH-stretching frequency and cation arrangements in tremolite.

Substitution	Frequency shift (cm ⁻¹)	Reference
^A □ ↔ ^A A		
^A Na	+55	Robert et al. (1989)
^A K	+60	Robert et al. (1989)
^A Rb	+60	Della Ventura (1992)
^A Li	+50	Iezzi et al. (2004)
^T Si ↔ ^T T		
^{T(2)} Ti	-13 to -23	Della Ventura et al. (1996b)
^{T(1)} Al	-20	Della Ventura et al. (1999)
^{M(1,3)} Mg ↔ ^{M(1,3)} M ²⁺		
^{M(1,3)} Ni	-15 to -18	Della Ventura et al. (1996a, 1997)
^{M(1,3)} Co	-15 to -18	Della Ventura et al. (1996a, 1997)
^{M(1,3)} Fe ²⁺	-15 to -18	Iezzi et al. (2005)
^{M(1,3)} Mn ²⁺	-15	Reece et al. (2002)
^{M(1,3)} Mg ↔ ^{M(1,3)} M ³⁺		
^{M(1,3)} Al ³⁺	-33	Della Ventura et al. (1999)
^{M(1,3)} Sc ³⁺	-40	Raudsepp et al. (1987a,b)
^{M(1,3)} Ga ³⁺	-45	Raudsepp et al. (1987a,b)
^{M(1,3)} Cr ³⁺	-50	Fialips-Guédon et al. (2000)
^{M(1,3)} Fe ³⁺	-50	Raudsepp et al. (1987a)
^{M(4)} Ca ↔ ^{M(4)} M ²⁺		
^{M(4)} Mg	-8	Hawthorne et al. (1997)
^{M(4)} Sr	+2	Gottschalk et al. (1998)
^{M(4)} Na ↔ ^{M(4)} M ⁺		
^{M(4)} Li	-4	Iezzi et al. (2003)
^{O(3)} OH ↔ ^{O(3)} F	-15 to -20	Robert et al. (1999, 2000)
^{O(3)} OH ↔ ^{O(3)} O ²⁻	-23	Della Ventura et al. (2007)

particularly unfortunate as it is for disordered amphiboles that we look to spectroscopy to give us information on their state of order-disorder. So we must take a pragmatic view to the fitting of spectra: we must extract the information that we can; although we may not necessarily be able to extract all the information pertinent to the structure, we need to extract as much as we can, and complement it with information from other experimental methods and theoretical considerations (e.g., local bond-valence theory).

With regard to (2) above, how do we cope with this problem of complexity in the spectra? This issue was discussed by Della Ventura et al. (1999) who synthesized amphiboles along the richterite-pargasite join. The spectrum of synthetic richterite is well understood, and so this gives us a start in spectrum fitting and assignment. The general approach here is *to fit one model to all the spectra of the series*, as in this way we can considerably increase the number of observations without greatly increasing the number of fitting parameters. We can identify the key features of this approach as follows: (1) numerical fitting of the spectra to component bands must be congruent for all spectra; (2) the intensities of the component bands must vary systematically with changes in chemical composition; (3) the variations in ordering derived from the spectral assignments must be in accord with the variation in cell dimensions across the series.

Here, we have covered the general aspects of SRO with respect to amphiboles. Now we will consider the work that has been done on specific minerals and synthetic systems. It is worthwhile pointing out that, due to the work done by all the authors cited here, we know far more about SRO in amphiboles than we do in any other complicated rock-forming mineral group.

SHORT-RANGE DISORDER OF DIVALENT B CATIONS IN TREMOLITE

Chemical analyses of $C2/m$ amphiboles (Leake 1968) show that tremolite-actinolite amphiboles commonly have minor amounts of small divalent cations (Mn^{2+} , Fe^{2+} , Mg) at the $M(4)$ site (i.e., as B cations). Jenkins (1981) noted the presence of small amounts of Mg as a B cation in their synthesis work on tremolite, and this is commonly expressed as a cummingtonite component (i.e., $\square Mg_2 Mg_2 Si_8 O_{22} (OH)_2$ in $\square Ca_2 Mg_2 Si_8 O_{22} (OH)_2$). There have been many subsequent studies of synthetic tremolite (Jenkins 1987, 1988, 1994; Jenkins and Clare 1990; Jenkins et al. 1997; Ahn et al. 1991; Smelik et al. 1994; Chernosky et al. 1998; Gottschalk et al. 1999), and all have confirmed the presence of a cummingtonite component in synthetic tremolite, although the amount of this component has been the subject of some debate until fairly recently, when Gottschalk et al. (1999) showed that the amount of cummingtonite component in synthetic tremolite varies between 0.01 and 0.06. Extensive single-crystal structure refinement of a range of Ca-rich $C2/m$ amphiboles (e.g., Oberti et al. 1995a) has shown the presence of a second $M(4')$ site with a bond geometry very similar to the analogous arrangement in cummingtonite (Table 6)(see Evans 2007 for additional discussion).

Table 6. Comparison of $M(4)$ -O and $M(4')$ -O distances (Å) in synthetic fluoropargasite* and cummingtonite**.

	Synthetic Fluoropargasite	Cummingtonite	Synthetic Fluoropargasite	
$M(4)$ -O(2)	2.413	2.164	2.066	$M(4')$ -O(2)
$M(4)$ -O(4)	2.330	2.023	2.264	$M(4')$ -O(4)
$M(4)$ -O(5)	2.597	3.143	2.878	$M(4')$ -O(5)
$M(4)$ -O(6)	2.561	2.691	2.914	$M(4')$ -O(6)

*Oberti et al. 1995b, 1998; **Hawthorne 1983.

There are three possibilities with regard to incorporation of the cummingtonite component: (1) it occurs as domains or lamellae of cummingtonite in a tremolite host; (2) Ca and Mg are short-range disordered at the $M(4)$ site; (3) Ca and Mg are short-range ordered at the $M(4)$ site. High-Resolution Transmission Electron Microscopy (HRTEM) (Gottschalk et al. 1999) showed no sign of a second (possibly exsolved) phase, and thus possibility (1) can be discounted. Thus we are left with possibilities (2) and (3): are Ca and Mg at $M(4)$ short-range disordered or short-range ordered? Above, we used the valence-sum rule to predict that SRO will be uncommon where homovalent ions are involved, and common where heterovalent ions are involved. Thus we expect Ca and Mg at $M(4)$ and $M(4')$ in tremolite to be short-range disordered.

The infrared spectrum of synthetic tremolite

Gottschalk et al. (1999) presented very detailed spectra for synthetic tremolite synthesized at a variety of experimental conditions. As with previous work, a second peak was observed at $\sim 3669 \text{ cm}^{-1}$. However, it was shown that the intensity of this peak varies with the details of synthesis. Moreover, Gottschalk et al. (1999) considered the possible local arrangements of Ca and Mg at the NNN $M(4)$ sites using the configuration symbol $M(1)M(1)M(3)-O(3)-A: T(1)T(1)-M(2)M(2)M(3)-M(1)M(1)M(2) M(2)M(4)M(4)M(4)M(4)$ (where we have bolded the sites involved in the binary occupancy of Ca and Mg). Table 7 shows the possible local arrangements of cations at the quartet of $M(4)$ sites, together with their probabilities of occurrence assuming a random distribution. Inspection of Figure 8b shows that there are two distinct pairs of $M(4)$ sites, and these are distinguished in Table 7 as “nearer” and “further.” Inspection of Table 7 shows that bands G, H and I should have almost negligible intensity ($\leq 0.02\%$) and bands D and E should be extremely weak (0.23%) due to the small amount of ^{25}Mg present in tremolite. Thus we expect to observe three distinct bands of significant intensity in the tremolite spectrum, and this is indeed the case. Figure 9 shows the spectrum of synthetic tremolite with close to the maximum observed content of ^{25}Mg . There are two discrete peaks (at 3674.7 and 3669.2 cm^{-1}), but fitting of the spectra shows the presence of two additional bands of significant intensity. The highest-energy band (3676.4 cm^{-1}) is assigned to the presence of minor amounts of talc in the run product (a common feature of amphibole synthesis, Raudsepp et al. 1991). The intense band at 3674 cm^{-1} was assigned to the arrangement $M(4)M(4)-M(4)M(4) = \text{CaCa}-\text{CaCa}$, and the bands at 3672.4 and 3669.2 cm^{-1} were assigned to the arrangements $\text{CaCa}-\text{CaMg}$ and $\text{CaMg}-\text{CaCa}$ (some of the very weak bands were also assigned, but the presence of these bands cannot be evaluated without the associated

Table 7. Probabilities for random distribution of $M(4)$ cation arrangements in the $C2/m$ amphibole structure.

	$M(4)$ -sites: distance from H		Probability of cation arrangement	Probabilities calculated for $X^{M(4)}_{\text{Ca}}$	
	nearer	further		0.95	0.90
A	CaCa	CaCa	x^4_{Ca}	81.45	65.61
B	CaMg	CaCa	$2 x_{\text{Mg}} x^3_{\text{Ca}}$	8.57	14.58
C	CaCa	CaMg	$2 x_{\text{Mg}} x^3_{\text{Ca}}$	8.57	14.58
D	MgMg	CaCa	$x^2_{\text{Mg}} x^2_{\text{Ca}}$	0.23	0.81
E	CaCa	MgMg	$x^2_{\text{Mg}} x^2_{\text{Ca}}$	0.23	0.81
F*	CaMg	CaMg	$4 x^2_{\text{Mg}} x^2_{\text{Ca}}$	0.90	3.24
G	CaMg	MgMg	$2 x^3_{\text{Mg}} x_{\text{Ca}}$	0.02	0.18
H	MgMg	CaMg	$2 x^3_{\text{Mg}} x_{\text{Ca}}$	0.02	0.18
I	MgMg	MgMg	x^4_{Mg}	0.00	0.01

*Cis and trans arrangements are not distinguished.

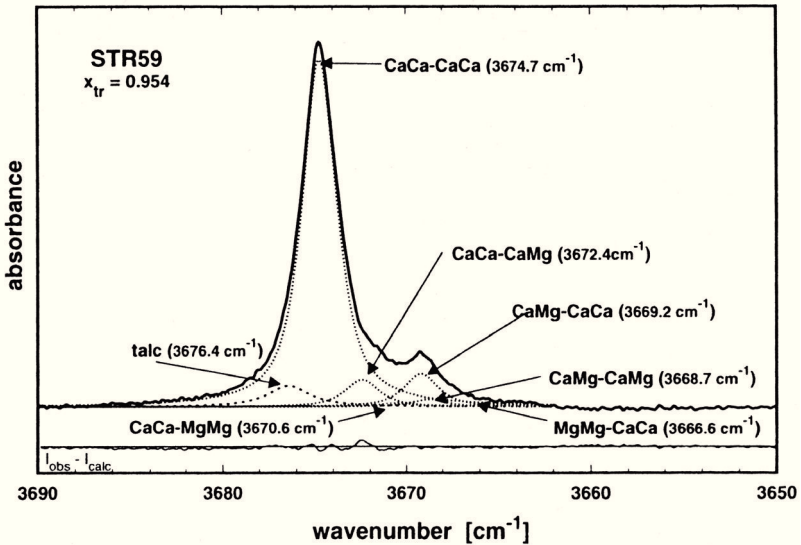


Figure 9. The infrared spectrum of tremolite (synthesized at 700 °C and 500 MPa from a mixture of CaCO_3 , MgO and SiO_2 in a solution of 30 mg of H_2O and 63 mg of $\text{Ag}_2\text{C}_2\text{O}_4$). Note the presence of a talc band (a common product in the synthesis of tremolite) at 3670.6 cm^{-1} . [Used by permission of Schweizerbart'sche Verlagsbuchhandlung, from Gottschalk et al. (1999), *European Journal of Mineralogy*, Vol. 11, Fig. 6, p. 977.]

standard deviations for their relative intensities from the least-squares fitting procedure). The relative band intensities from the fitted spectrum of Figure 9 are in accord with the probabilities of the arrangements calculated from a random distribution (Gottschalk et al. 1999). Hence Ca and Mg are short-range disordered in tremolite, as predicted from the short-range valence-sum rule of bond-valence theory.

The Sr analogue of tremolite can be synthesized and Gottschalk et al. (1998) examined the solid-solution of Ca and Sr at the $M(4)$ site in synthetic tremolite and the synthetic Sr-analogue of tremolite. HRTEM showed well-ordered structures for most run conditions, and complete solid-solution along the Ca-Sr join. Infrared spectra of end-member compositions gave two distinct bands, whereas intermediate compositions gave additional bands. Gottschalk et al. (1998) interpreted these bands in terms of the configuration symbol $M(1)M(1)M(3)-O(3)-A: T(1)T(1)-M(2)M(2)M(3)-M(1)M(1)M(2) M(2)M(4)M(4)$ [with two less $M(4)$ sites than were used to interpret the spectrum in Figure 9]. The spectra of Ca-rich synthetic tremolites were interpreted assuming a random distribution of Ca and Mg over the two nearest $M(4)$ sites, with the probabilities given by $p(\text{CaCa}) = x_{\text{Ca}} x_{\text{Ca}}$, $p(\text{CaMg}) = 2 x_{\text{Ca}} x_{\text{Mg}}$, $p(\text{MgMg}) = x_{\text{Mg}} x_{\text{Mg}}$. The spectra of Sr-rich synthetic analogue-tremolites were interpreted assuming a random distribution of Ca, Sr and Mg over the two nearest $M(4)$ sites with zero occurrence assumed for the arrangement CaMg, with the probabilities given by $p(\text{SrCa}) = 2 x_{\text{Ca}} x_{\text{Ca}}$, $p(\text{SrMg}) = 2 x_{\text{Ca}} x_{\text{Mg}}$, $p(\text{SrSr}) = x_{\text{Sr}} x_{\text{Sr}}$. Across the series, the band intensities calculated for a random distribution (within the constraints of the initial assumptions: CaMg and MgMg do not occur at Sr-dominant compositions) are in close agreement with the observed intensities, indicating that there is no SRO in this series (apart from the anti-order assumed with regard to CaMg and MgMg at Sr-dominant compositions). This result is further supported by Andrut et al. (2000), who examined the lattice-vibrational modes in this solid-solution series. They showed that the stretching frequencies for the $[\text{Si}_4 \text{O}_{11}]$ unit show one-mode behavior (see section on SRO of (OH)-F in amphiboles), indicating that there cannot be any short-range order of Ca and Sr at the $M(4)$ sites.

SRO IN RICHTERITE-PARGASITE SOLID-SOLUTIONS

Early crystal-structure studies on pargasite assumed that ^{61}Al is completely ordered at the $M(2)$ site. However, Semet (1973) showed that the infrared spectrum of pargasite consists of two broad bands centered on 3711 and 3678 cm^{-1} and suggested that these are due to Al-Mg disorder over the $M(1)$ and $M(3)$ sites. This conclusion was supported by later infrared and Rietveld work (Raudsepp et al. 1987a, 1991) and MAS NMR spectroscopy (Welch et al. 1994). Detailed crystal-structure work by Oberti et al. (1995a) showed that ^{61}Al is partly disordered over the $M(2)$ and $M(3)$ sites in Mg-rich pargasite, the degree of disorder increasing with increase in the amount of Mg in the structure. Della Ventura et al. (1998a) showed that ^{61}Al is disordered in synthetic pargasite but completely ordered at $M(2)$ in the Co analogue: $\text{Na Ca}_2 (\text{Co}^{2+}_4 \text{Al}) (\text{Si}_6 \text{Al}_2) \text{O}_{22} (\text{OH})_2$.

The very broad peaks in the spectrum of synthetic pargasite (Fig. 5a) suggest that each is an envelope that consists of more than one band. There is little information in this spectrum to support fitting of more than one component to each peak, even though the width of the peaks suggests that they consist of several component bands. However, this problem was, if not overcome, somewhat alleviated by fitting a single model (i.e., the same set of components with the same positions and widths) to the spectra of a series of samples along the synthetic-amphibole join richterite-pargasite (Della Ventura et al. 1999). The spectra of this series are shown in Figure 10. The fitting process started with the top spectrum of Figure 10, and then proceeded through to the bottom spectrum of Figure 10, fixing the positions of the peaks present in the previous spectra (these constraints were relaxed somewhat once all the spectra were fitted); the results are shown in Figure 11. How do we assign these bands?

The number of stable arrangements

Above, we showed that there are 144 algebraically distinct arrangements for the configuration symbol $M(1)M(1)M(3)\text{-O}(3)\text{-A:T}(1)T(1)\text{-}M(2)M(2)M(3)$, and 432 distinct arrangements for the configuration symbol $M(1)M(1)M(3)\text{-O}(3)\text{-A:T}(1)T(1)\text{-}M(2)M(2)M(3)M(2)M(2)$. Let us consider the case for the simpler configuration. Using the bond-valence arguments of Hawthorne (1997), we can reduce this number somewhat to what is possible with regard to the local valence-matching principle. Any arrangement with two or three Al at $M(1)M(1)M(3)$ will lead to an unacceptable excess in bond valence at O(3) (1.33 and 1.50 vu using Pauling bond-strengths), and hence only MgMgMg and MgMgAl can occur, reducing the number to $144/2 = 72$. Although Ca can occur at the A site in monoclinic amphiboles (Hawthorne et al. 1995), it is unlikely that such an arrangement is possible in the absence of F, as Ca would get too close to the H

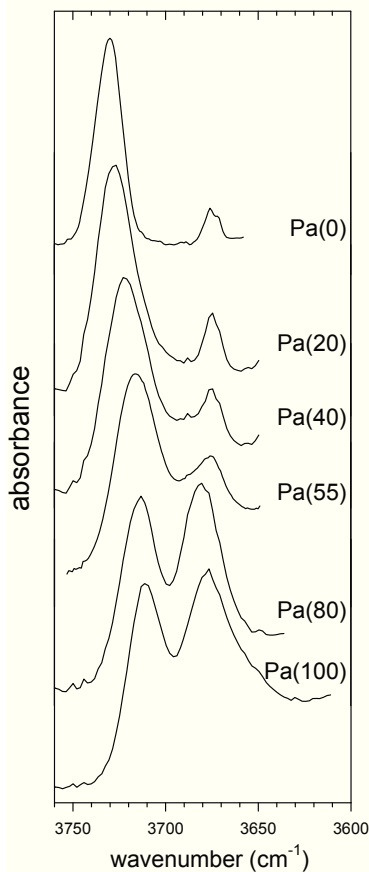


Figure 10. The infrared spectrum of amphiboles, synthesized along the join richterite-pargasite, in the principal (OH)-stretching region; modified after Della Ventura et al. (1999).

atom of the (OH) group at O(3). Examination of pargasitic amphiboles (plus fluorocannilloite, Hawthorne et al. 1996d) shows that F is always in excess of ${}^4\text{Ca} \times 2$. Thus only Na and \square are possible at the A site, reducing the number of arrangements to $72 \times 2/3 = 48$. The local arrangement

$T(1)T(1) = \text{AlAl}$ cannot occur as it requires local association of Ca at the A site (which above we show does not occur in the absence of F) to avoid unacceptably low bond-valence sums at the O(7) site, and hence the number further decreases to $48 \times 2/3 = 32$. The four possible arrangements of NNN cations [at the $M(2)M(2)M(3)$ sites] are MgMgMg, MgMgAl, MgAlAl and AlAlAl; neither AlAlAl nor MgAlAl can occur with the NN arrangement MgMgAl as an excess of bond valence results at the anions linked to two Al cations, reducing the number to $32/2 = 16$.

Band assignment

Note that in end-member pargasite, the arrangement $T(1)T(1) = \text{SiSi}$ cannot occur as the bulk composition of the crystal would also force an equal number of arrangements of the type $T(1)T(1) = \text{AlAl}$, and these cannot occur because of the absence of F (and hence ${}^4\text{Ca}$), resulting in low bond-valence sums incident at the O(7) anion. This argument is in accord with the spectra of Figures 10 and 11: Band A, which we assign to the MgMgMg-(OH)-Na: SiSi-MgMgMg arrangement in richterite, decreases in intensity with increasing pargasite content in the amphibole to disappear at end-member pargasite (and hence the number of possible local arrangements in end-member pargasite reduces to $16/2 = 8$). Bands B and C involve NN arrangements of the form MgMgMg-OH-Na; they also have to incorporate ${}^{44}\text{Al}$ and hence have the NNN arrangement $T(1)T(1) = \text{SiAl}$. Bands D and F involve NN arrangements of the form MgMgAl-OH-Na; they also have to incorporate ${}^{44}\text{Al}$ and hence have the NNN arrangement $T(1)T(1) = \text{SiAl}$. So what distinguishes between bands B and C, and between bands D and F? This is the NNN arrangement involving the $M(2)$ and $M(3)$ sites: MgMgMg and AlMgMg, respectively. The G and H bands occur only in end-member pargasite, and were assigned to NNN M configurations involving two Al atoms (Della Ventura et al. 1999). The alternative is that bands G and H could be due to configurations involving partly vacant A-sites in the structure, as their frequencies correspond closely to that of bands B and B' of synthetic magnesiohornblende (see below). However, it is difficult at the moment to argue convincingly for one assignment versus the other.

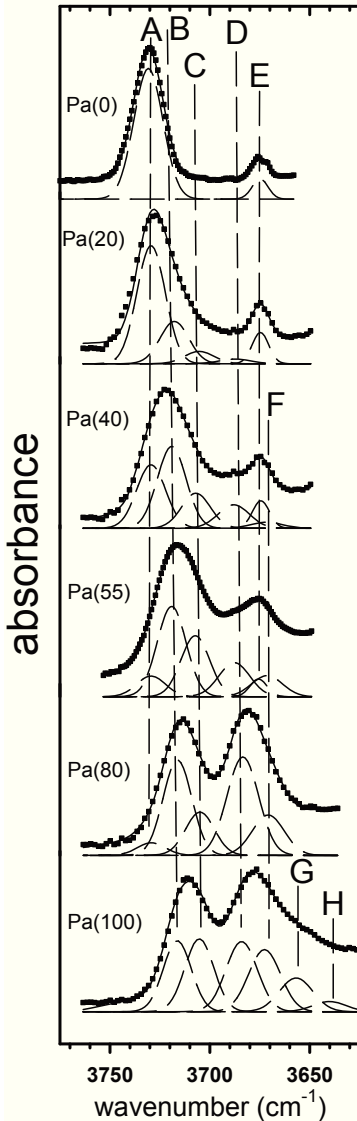


Figure 11. Resolution of the infrared spectra of richterite-pargasite solid solutions into component bands A to H. [Used by permission of Schweizerbart'sche Verlagsbuchhandlung, from Della Ventura et al. (1999), European Journal of Mineralogy, Vol. 11, Fig. 5, p. 85.]

Thus short-range order is extensive in amphiboles of the richterite-pargasite series. The short-range arrangements that occur are those which most closely obey the valence-matching principle applied to local arrangements.

SRO IN TREMOLITE-MAGNESIOHORNBLLENDE SOLID-SOLUTIONS

There has been a considerable amount of work on the synthesis of amphiboles nominally along the join tremolite-tschemmakite (Jasmund and Schäfer 1972; Oba 1978; Cao et al. 1986; Jenkins 1981, 1983, 1988, 1994; Jenkins et al. 1997; Cho and Ernst 1991; Smelik et al. 1994; Hoschek 1995; Quirion and Jenkins 1998; Hawthorne et al. 2000a; Najorka and Gottschalk 2003). Careful characterization of the run products has shown that amphiboles cannot be synthesized in the tschemmakite-dominant part of the system (i.e., more aluminous than aluminohornblende). Furthermore, Mg is incorporated at the $M(4)$ site, leading to Ca contents below the ideal value of 2 apfu. Considerable efforts have been made to characterize the resultant amphiboles (Jenkins et al. 1997; Hawthorne et al. 2000a; Najorka and Gottschalk 2003), but the situation is still not completely clear. However, what is clear is that there is considerable short-range order involving some cation arrangements, and there may also be short-range disorder involving different cation arrangements.

Jenkins et al. (1997) reported infrared spectra and ^{29}Si and ^{27}Al MAS NMR spectra of amphiboles (run products) in the compositional range $\text{Al} = 0$ (0) to 1.84(2.0) apfu. The MAS NMR spectra are shown in Figure 12. The ^{27}Al MAS NMR spectra (Fig. 12a) shows a single peak at 68 ppm, assigned to [4]-coordinated Al, and a doublet at ~ 0 ppm assigned to [6]-coordinated Al. There is no sign of two components in the 68 ppm peak, and hence there is no information about site occupancy for [4]-coordinated Al. The doublet at ~ 0 ppm indicates that [6]-coordinated Al occurs at (at least) two sites, in accord with the infrared spectra, but we cannot distinguish between sole occupancy of $M(1)$, sole occupancy of $M(3)$, or occupancy of both $M(1)$ and $M(3)$ by Al. Jenkins et al. (1997) interpret the ^{29}Si MAS NMR spectra (Fig. 12b) as indicating complete disorder of Al over the $T(1)$ and $T(2)$ sites. However, their calculations take no account of SRO, a situation that the bond-valence arguments of Hawthorne (1997) and the experimental observations of Della Ventura et al. (1999) indicate as most unlikely. Moreover, the neutron structure work of Welch and Knight (1999) shows that ^{141}Al is ordered at $T(1)$ in synthetic pargasite, a compositionally similar amphibole synthesized at similar conditions.

Hawthorne et al. (2000a) reported infrared and triple-quantum MAS NMR spectra of synthetic aluminous amphiboles nominally along the join tremolite-tschemmakite with a small ($\leq 10\%$ content of cummingtonite component) but extending only as far as aluminohornblende. Figure 13 shows the ^{27}Al MAS NMR spectra of an amphibole with $^{141}\text{Al} = ^{161}\text{Al} = 0.4$ apfu. The ^{27}Al MAS NMR spectrum (Fig. 13a) is conformable with those of Jenkins et al. (1997) (see Fig. 12) and is interpreted in the same fashion. The 3Q MAS NMR spectrum has an isotropic component that allows Al bands that overlap in the MAS NMR spectrum to be resolved (this is usually not possible for the single-pulse spectrum because of significant quadrupolar components of the spectrum that lead to considerable peak-overlap). The 3Q spectrum (Fig. 13b) clearly resolves two distinct signals for [6]-coordinated Al, indicating that Al occurs at only two of the $M(1,2,3)$ sites. The single-crystal structure-refinement results of Oberti et al. (1995a) indicates that these two sites are $M(2)$ and $M(3)$.

The infrared spectra of these amphiboles are shown in Figure 14. Based on the argument that it is only statistically justified to fit a component if there is a change in sign of the second derivative of intensity with respect to energy (wavenumber), Hawthorne et al. (2000a) identified 5 distinct bands (A, B, B', C and C', Fig. 14a) and fit all spectra of the series to these bands (Fig. 14b). As only 5 bands were resolved, Hawthorne et al. (2000a) interpreted the spectra in terms of the configuration symbol $M(1)M(1)M(3)-O(3)-A: T(1)T(1)-M(2)M(2)M(3)$. Figure 15a shows the relevant cluster of octahedra, Figure 15b shows a graphical representation of this

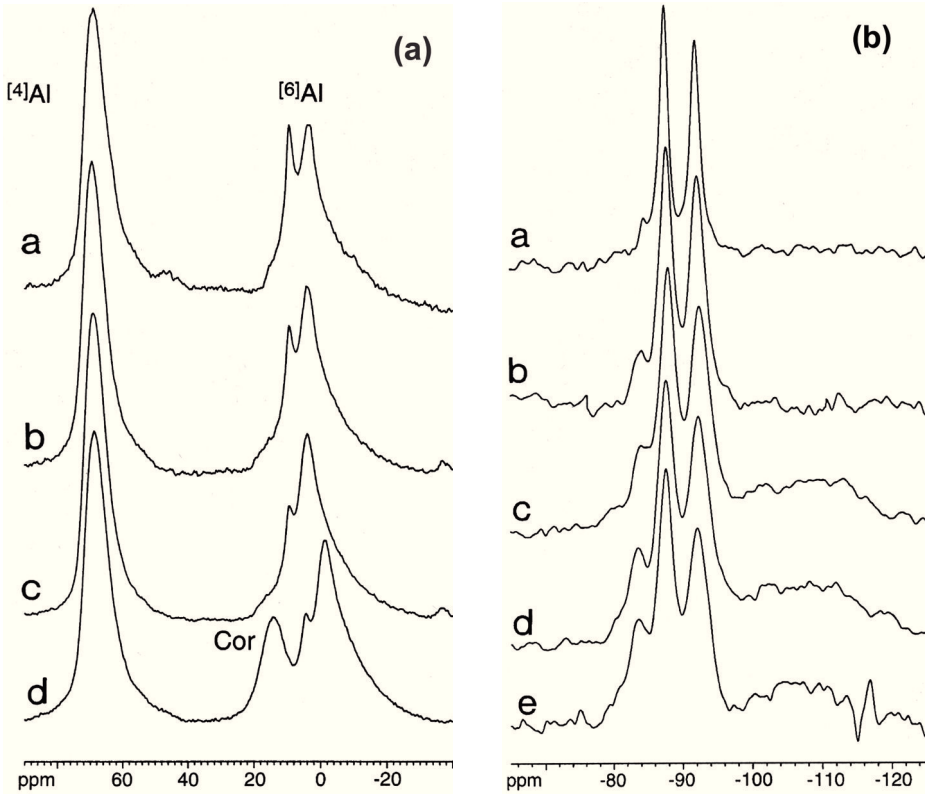


Figure 12. MAS NMR spectra for amphiboles along the nominal join tremolite-aluminohornblende; (a) ^{27}Al ; (b) ^{29}Si (from Jenkins et al. 1997).

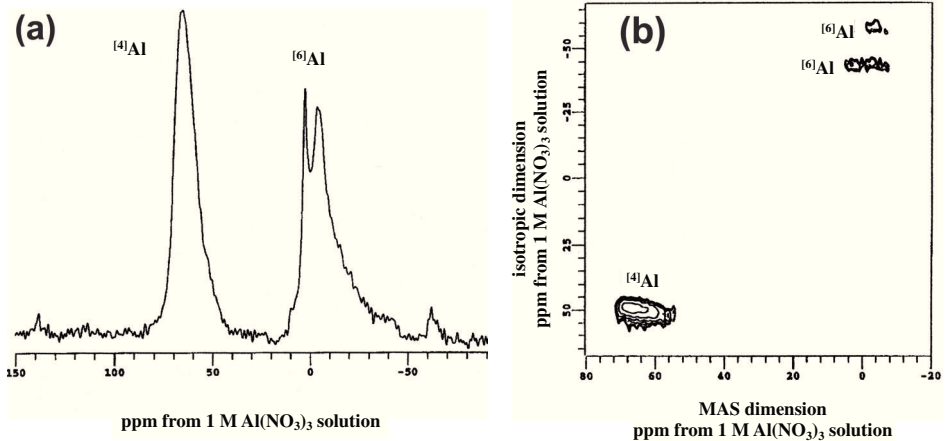


Figure 13. MAS NMR spectra for an amphibole along the nominal join tremolite-aluminohornblende with $^{[4]}\text{Al} = ^{[6]}\text{Al} = 0.4$ apfu; (a) ^{27}Al MAS NMR spectrum; (b) triple-quantum (3Q) ^{27}Al MAS NMR spectrum (from Hawthorne et al. 2000a).

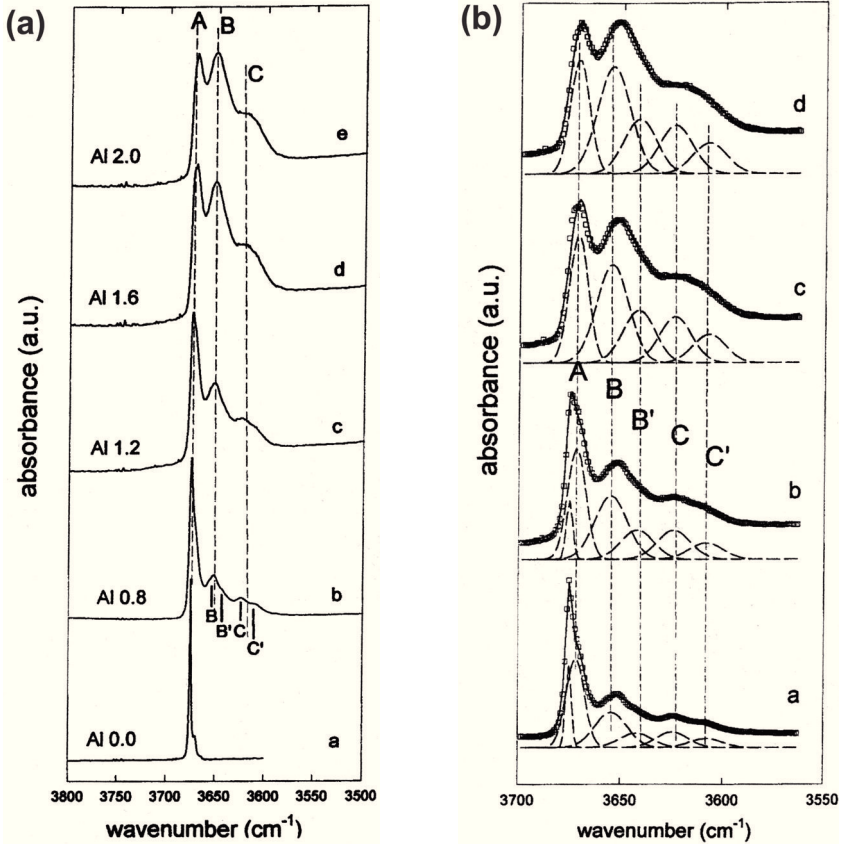


Figure 14. Infrared spectra of synthetic tremolite-aluminohornblende amphiboles in the principal (OH)-stretching region; (a) raw spectra; (b) spectra resolved (from Hawthorne et al. 2000a).

cluster, and Figure 15c shows the possible NN and NNN cation-arrangements for occupancy of these octahedra by Mg and Al [with Al restricted to $M(2)$ and $M(3)$]. Inspection of Figure 15c shows 8 arrangements that are acceptable from a bond-valence perspective (those marked by a central black diamond). However, there is also distinct symmetry and pseudosymmetry among these arrangements (i.e., those arrangements connected by broken and dotted lines). Incorporating these equivalences results in 4 distinct arrangements: (1) $\text{MgMgMg-O}(3)\text{-}\square$: $T(1)T(1)\text{-MgMgMg}$; (2) $\text{MgMgMg-O}(3)\text{-}\square$: $T(1)T(1)\text{-MgMgAl}$; (3) $\text{MgMgAl-O}(3)\text{-}\square$: $T(1)T(1)\text{-MgMgMg}$; (4) $\text{MgMgAl-O}(3)\text{-}\square$: $T(1)T(1)\text{-MgMgAl}$. This leaves the $T(1)T(1)$ part of the configuration to be considered. As discussed by Della Ventura et al. (1999) for synthetic amphiboles of the richterite-pargasite series, the possible cation arrangements for $T(1)T(1)$ are SiSi and SiAl (AlAl can only occur where $A = \text{Ca}$, Hawthorne et al. 1996d). These arguments result in the eight arrangements given in Table 8. There are only five resolved components in the spectra of Figure 14b, and Hawthorne et al. (2000a) assigned the arrangements to the component absorptions using the frequency shifts listed in Table 5. Although Hawthorne et al. (2000a) could not derive band intensities for all eight bands listed in Table 8 (as only five components were resolved), the small number of bands observed (compared with the large number of combinatorially possible bands) indicates strong short-range order arising from local bond-valence requirements.

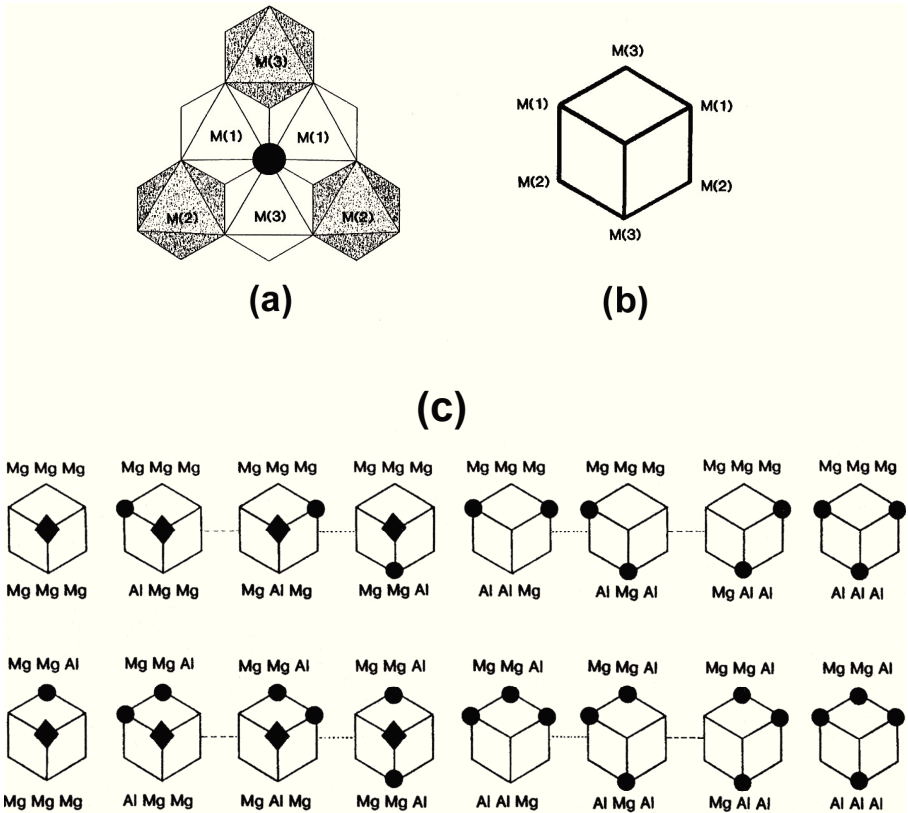


Figure 15. NN and NNN cation arrangements in synthetic amphiboles (approximately) along the join tremolite-aluminohornblende (with a small cummingtonite component); (a) polyhedron representation of the cluster of octahedra; (b) graphical representation of the cluster shown in (a); (c) possible NN and NNN arrangements in the cluster shown in (a), (b) under the constraint that Al does not occur at $M(1)$; undecorated nodes represent Mg, shaded circles represent Al. The NN cations are indicated above each graph [$M(1)M(1)M(3) = \text{MgMgMg}$ or MgMgAl]; the NNN cations are shown below each graph [$M(2)M(2)M(3) = \text{MgMgMg}$, AlMgMg ($=\text{MgAlMg} = \text{MgMgAl}$), AlAlMg ($=\text{AlMgAl} = \text{MgAlAl}$) and AlAlAl]. The most stable arrangements from a bond-valence perspective are shown by occupancy of the central node by a black diamond. Symmetrically equivalent arrangements are connected by broken lines, pseudosymmetrically equivalent arrangements are connected by dotted lines (from Hawthorne et al. 2000a).

Najorka and Gottschalk (2003) also examined synthetic amphiboles nominally along the join tremolite-aluminohornblende; their spectra are very similar to those of Hawthorne et al. (2000a), but the fitting and interpretation are different. The cluster used to interpret the spectra is shown in Figure 16, the usual constraints [^{44}Al at $T(1)$ only, ^{60}Al at $M(2,3)$ only] were used, and thirty-six possible cation arrangements were identified (Fig. 17). A maximum of twelve bands were fitted to the IR spectra (Fig. 18). There do not appear to be a sufficient number of changes in the second derivative of the spectral envelope to justify this number of components (Hawthorne and Waychunas 1988). On the other hand, one can extract more information from a spectrum that is present in the raw information if one can input additional correct information in the fitting model (e.g., the width of the component bands, the relative positions of the component bands, the number of component bands, of which one may have information independent of the spectrum).

Table 8. Possible cation arrangements around the OH group in synthetic amphiboles of the tremolite-magnesiohornblende series, together with the assigned bands and observed band frequencies.

No.	Configuration	Observed	Band frequency (cm ⁻¹)
1	[MgMgMg]-SiSi-MgMgMg	3675	A
2*	[MgMgMg]-SiSi-MgMgAl	3671	A'
3	[MgMgMg]-SiAl-MgMgMg	3655	B
4*	[MgMgMg]-SiAl-MgMgAl	3642	B'
5	[MgMgAl]-SiSi-MgMgMg	3642	B'
6*	[MgMgAl]-SiSi-MgMgAl	3625	C
7	[MgMgAl]-SiAl-MgMgMg	3625	C
8*	[MgMgAl]-SiAl-MgMgAl	3608	C'

*M(2)M(3)M(2) = MgMgAl and MgAlMg are indistinguishable.

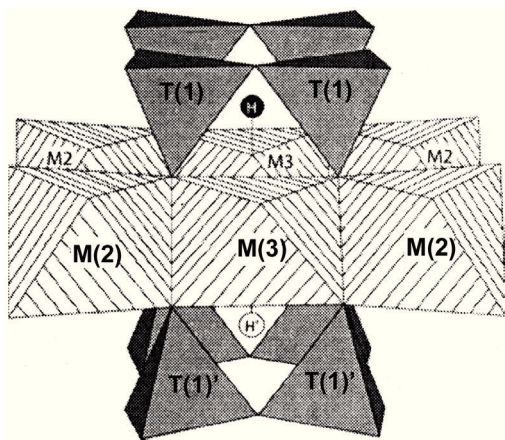


Figure 16. NN and NNN cation arrangements in the amphibole structure at which Al occurs in tremolite-aluminohornblende solid-solutions. [Used with kind permission of Springer Science and Business Media, from Najorka and Gottschalk (2003), *Physics and Chemistry of Minerals*, Vol. 30, Fig. 10, p. 120.]

Najorka and Gottschalk (2003) divide their cation arrangements into groups under the assumption that the spectral shift from the tremolite arrangement is proportional to the distance from the proton at which the Al occurs. This results in three groups (Fig. 17): I: $T^{(1)}\text{Si}$ only, $^{[6]}\text{Al} = 1-2$ at $M(2)$ and/or $M(3)_{\text{far}}$; II: $T^{(1)}\text{Al} = 1$, $^{[6]}\text{Al} = 1-3$ at $M(2)$ and/or $M(3)_{\text{far}}$; III: $^{[6]}\text{Al} = 1-4$ at $M(2)$ and either Al at $M(3)_{\text{near}}$ or $T^{(1)}\text{Al} = 2$. Furthermore, they assume that groups I-III correspond to the three groups of bands with different half-widths (Fig. 18). The variation in relative intensity of these groups of bands is shown in Figure 19, where they are compared with the variation calculated assuming a statistical distribution of cations. The agreement is closer assuming a random distribution of Al over $M(2)$ and $M(3)$ rather than a random distribution of Al and Mg at $M(2)$.

It is apparent that there are different philosophies of spectral fitting operative in this area, and there has not been sufficient work done on complicated amphiboles to evaluate which approach is more profitable (note that we do not use the rather emotive term 'correct'). This issue must await resolution, if indeed it can be resolved. One may be restricted to a more pragmatic approach where one extracts what insight one can from the infrared spectrum, and appeals to other experimental methods for additional information.

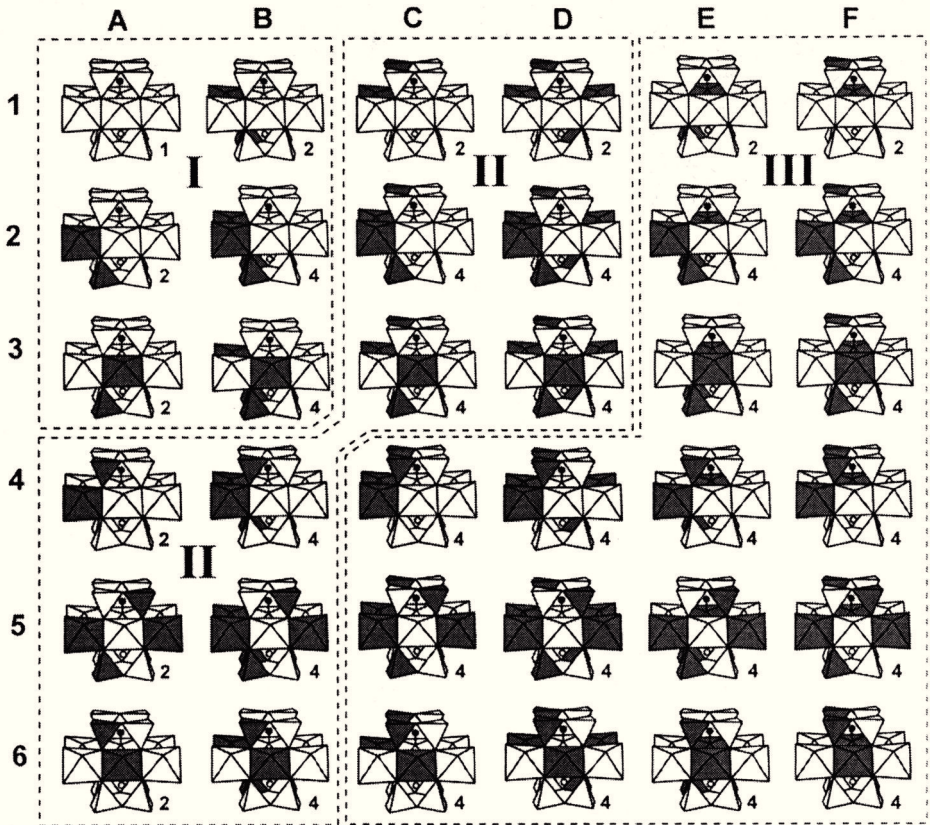


Figure 17. The 36 possible cation arrangements for (Mg,Al) and (Si,Al) occurrence in the cluster of Fig. 16 for the occupancy constraints discussed in the text; unshaded polyhedra are occupied by Mg or Si, shaded polyhedra are occupied by Al; the numbers to the bottom right of each arrangement indicate the multiplicity of that arrangement; the arrangements are divided into four types, indicated by the Roman numbers. [Used with kind permission of Springer Science and Business Media, from Najorka and Gottschalk (2003), *Physics and Chemistry of Minerals*, Vol. 30, Fig. 11, p. 121.]

SRO IN PARVO-MANGANO-EDENITE

Oberti et al. (2006) described recently two new group-5 amphiboles with a *B*-site composition intermediate between that of calcic and Mg-Fe-Mn-Li amphibole (Oberti et al. 2007a). Application of the bond-valence approach (Hawthorne 1997) suggests three possible local arrangements in edenite based on the site-configuration symbol $M(1)M(1)M(3)-O(3)-A$: $T(1)T(1)$: (1) MgMgMg-OH-Na: SiAl, (2) MgMgMg-OH-□: SiSi, (3) MgMgMg-OH-Na: SiSi. The first two arrangements are part of a neutral formula, whereas the third arrangement is charged: it is equivalent to a tremolite-like arrangement with additional Na, and thus implies additional bond-valence incident at the O(5) and O(6) anions that could be accommodated by relaxation of bond lengths. The FTIR spectrum of parvo-mangano-edenite (Fig. 20) was modeled using eight Gaussian components, labeled A to H, the assignment of which is reported in Table 9. The spectrum is in accord with this model; bands B and C (Table 9) are associated with the edenite(1) configuration, and bands D to G are associated with the edenite(2) configuration. The strong intensity of these latter bands accords with the Si excess measured by EMP analysis. The edenite(3) configuration is assigned to band A. The presence

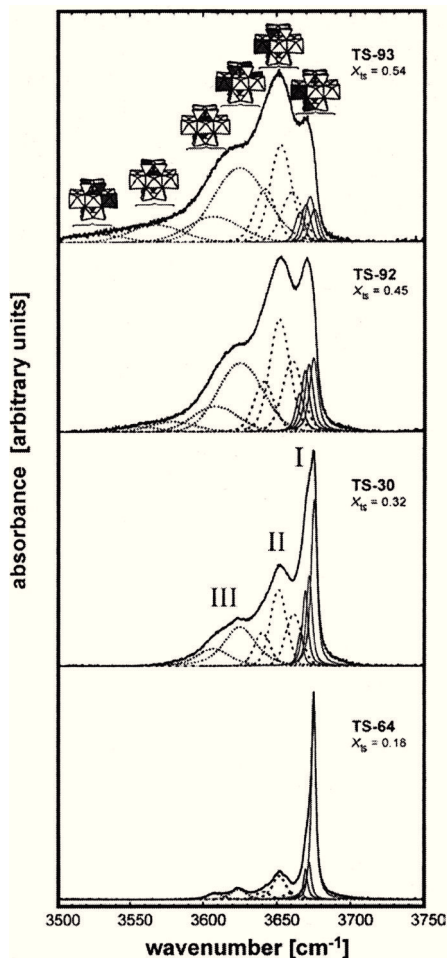


Figure 18. Infrared spectra of selected amphiboles along the join tremolite-aluminohornblende (expressed as the fraction of tschermakite, TS); the cation arrangements associated with each band or group of bands is shown in the top spectrum, and the type of arrangement is indicated by the Roman numbers in the spectrum for TS-30. [Used with kind permission of Springer Science and Business Media, from Najorka and Gottschalk (2003), *Physics and Chemistry of Minerals*, Vol. 30, Fig. 9, p. 120.]

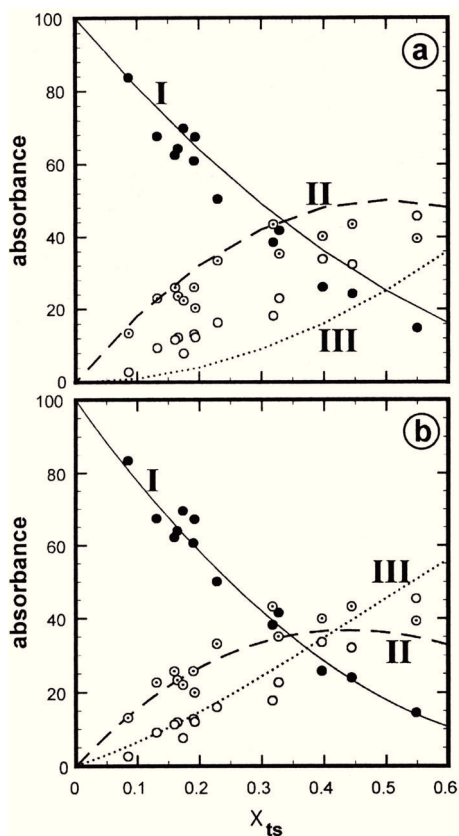


Figure 19. Comparison of observed (points) and calculated (lines) relative absorbances for the groups I-III (Fig. 17) for (a) random distribution of (Mg,Al) at $M(2)$, and (b) random distribution of (Mg,Al) over $M(2)$ and $M(3)$; shaded circles = Group I, dotted circles = Group II, unshaded circles = Group III. [Used with kind permission of Springer Science and Business Media, from Najorka and Gottschalk (2003), *Physics and Chemistry of Minerals*, Vol. 30, Fig. 12, p. 122.]

of all configurations predicted on bond-valence grounds by Hawthorne (1997) is in accord with significant short-range order in this composition.

SHORT-RANGE ORDER-DISORDER OF (OH) AND F IN AMPHIBOLES

Many monoclinic amphiboles show solid solution of (OH) and F, but little has been published on the mechanism of this solid solution: do (OH) and F show complete short-range disorder, or is this substitution associated with SRO? Infrared spectroscopy can provide

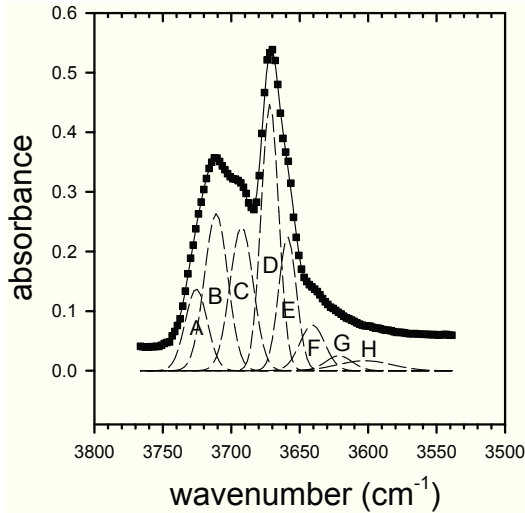


Figure 20. Fitted infrared spectra in the principal (OH)-stretching region for parvo-mangano-edenite (from Oberti et al. 2006).

Table 9. Band labels, position (cm^{-1}), and assignment for the spectrum of parvo-mangano-edenite.

Band	Wavenumber (cm^{-1})	Configuration
A	3725	${}^A\text{Na-MgMgMg-SiSi}$
B	3711	${}^A\text{Na-MgMgMg-AlSi}$
B*	3709	${}^A\text{Na-MgMgMn-SiSi}$
C	3692	${}^A\text{Na-MgMgMn-AlSi}$
C*	3693	${}^A\text{Na-MgMnMn-SiSi}$
D	3672	${}^A\square\text{-MgMgMg-SiSi}$
D*	3677	${}^A\text{Na-MnMnMn-SiSi}$
E	3659	${}^A\square\text{-MgMgMn-SiSi}$
F	3641	${}^A\square\text{-MgMnMn-SiSi}$
G	3621	${}^A\square\text{-MnMnMn-SiSi}$
H	3603	${}^A\square\text{-MgMgM}^{3+}\text{-SiSi}$

*Values calculated with a constant negative shift of 16 cm^{-1} for the different (Mg,Mn) configurations at $M(1,3)$ (e.g., Reece et al. 2002)

us with a window into this type of behavior. Robert et al. (1989, 1999) examined (OH)-F solid-solutions in synthetic tremolite--fluorotremolite, synthetic richterite--fluororichterite and synthetic potassic-richterite--potassic-fluororichterite. The salient feature of all these amphiboles is that the $M(1)$, $M(2)$ and $M(3)$ sites are occupied only by Mg; hence the only NN $M(1)M(1)M(3)$ arrangement that occurs is MgMgMg, and the NNN M -site arrangements involve only Mg. Similarly, the $T(1)$ sites are occupied only by Si. Hence all local arrangements are as follows: MgMgMg-(OH)- \square :SiSi-MgMgMg and MgMgMg-(OH)-Na:SiSi-MgMgMg, and their F-analogues MgMgMg-F- \square :SiSi-MgMgMg and MgMgMg-F-Na:SiSi-MgMgMg that are invisible in the infrared. The only potential for local order involves (OH) and F at O(3) sites adjacent to the (OH) group of the arrangement.

One-mode and two-mode behavior

In amphiboles of the tremolite-fluorotremolite series, there is a single (OH)-stretching band at 3674 cm^{-1} . The position of this band does not change significantly with decreasing F content

of the amphibole, and the band intensity decreases monotonically with decreasing F content. This type of spectrum is called *one-mode behavior*. In the amphiboles of the richterite-fluorrichterite series, the spectra are more complicated (Fig. 21). The richterite spectrum (Fig. 21a) contains a single intense band A at 3730 cm^{-1} due to the arrangement $\text{MgMgMg}(\text{OH})\text{-Na}:\text{SiSi-MgMgMg}$, together with a weak band C at 3674 cm^{-1} due to the arrangement $\text{MgMgMg}(\text{OH})\text{-}\square:\text{SiSi-MgMgMg}$ from the minor tremolite component in the amphibole. The spectrum of fluorrichterite with a nominal F content of 1.2 apfu (Fig. 21b) contains a single intense band A at 3730 cm^{-1} due to the arrangement $\text{MgMgMg}(\text{OH})\text{-Na}:\text{SiSi-MgMgMg}$, together with a weak band C at 3674 cm^{-1} due to the arrangement $\text{MgMgMg}(\text{OH})\text{-}\square:\text{SiSi-MgMgMg}$ from the minor tremolite component, plus an additional band B of intermediate intensity at 3711 cm^{-1} . This appearance of a new band in such circumstances is known as *two-mode behavior* (Chang and Mitra 1968). Moreover, with increasing F content of the amphibole, the intensity of the B band increases at the expense of the A band.

The stereochemistry of local coupling within the amphibole structure

The one-mode behavior of the synthetic tremolite-fluorotremolite solid-solution indicates that local arrangements involving an (OH) group are not significantly affected by adjacent arrangements involving F. Thus we may conclude that in tremolite-fluorotremolite, there is no coupling between adjacent O(3) anions, either through the O(3)-O(3) edge in the octahedral strip or across the vacant A cavity. The two-mode behavior of richterite-fluorrichterite solid-solutions indicates that the local arrangement involving an (OH) group is significantly affected by adjacent arrangements involving F. The only local difference between tremolite and richterite is that the A cavity is vacant in tremolite and is occupied by Na in richterite, indicating that the two-mode behavior in the latter is due to coupling of arrangements across the A cavity through the resident Na atom.

What factors are pertinent to the possibility of coupling across the A cavity? First, comparison of the principal (OH)-stretching frequency in tremolite (3674 cm^{-1}) and richterite (3730 cm^{-1}) indicates that there is a strong repulsive interaction between H and Na at the A site. Second, comparison of the electron-density arrangements in the A cavity when $\text{O}(3) = (\text{OH})$ and when $\text{O}(3) = \text{F}$ (Fig. 22) indicates that Na occupies a more central position in the cavity when $\text{O}(3) = (\text{OH})$ than when $\text{O}(3) = \text{F}$. In turn, this indicates that an (OH) group will interact less strongly with Na when the opposing O(3) site is occupied by F rather than by (OH). Hence Na will move toward F and away from (OH), reducing the repulsive interaction between H and Na and causing the constituent (OH) group to absorb at a lower frequency [as is observed for band B in the spectrum of fluorrichterite (Fig. 21b)]. Thus local coupling of arrangements occurs across an occupied A cavity but not across an unoccupied A cavity. This is an important generalization as it provides constraints on what bands can and cannot occur in amphibole solid-solutions.

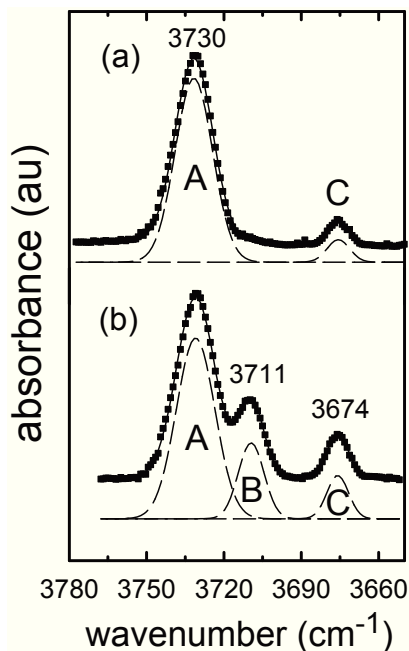


Figure 21. Infrared spectra in the principal (OH)-stretching region for (a) an amphibole of intermediate composition in the tremolite-fluorotremolite solid-solution; (b) an amphibole of intermediate composition in the richterite-fluorrichterite solid-solution (from Robert et al. 1999).

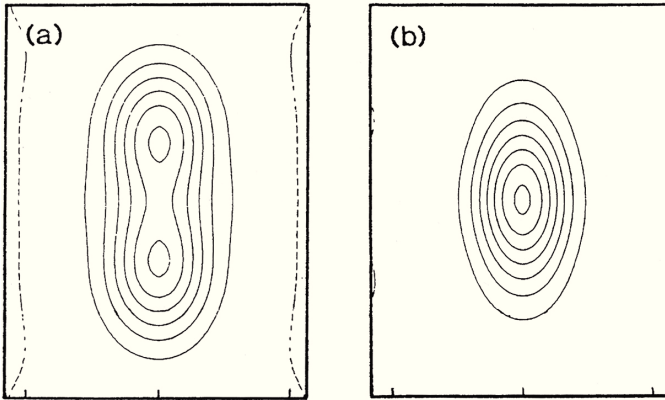


Figure 22. Electron-density distribution in the A cavity projected on to (201) in (a) fluoro-arfvedsonite, and (b) arfvedsonite; contour interval is $1 \text{ e}/\text{\AA}^3$ (from Hawthorne et al. 1996a).

Local arrangements in (OH,F)-bearing amphibole solid-solutions

In order to quantitatively interpret the spectra presented here, we have to understand what is happening around the A site in these amphiboles. This issue is examined in Figure 23 which shows sketches of all possible arrangements around the A cavity in richterite and tremolite. In richterite, where both O(3) sites are occupied either by (OH) [arrangement (1)] or by F [arrangement (3)], Na interacts equally with each (OH) group, whereas when one O(3) site is occupied by (OH) and the other is occupied by F, Na moves toward F [and away from (OH)], giving rise to the second band. In tremolite, the occupancy of one O(3) site does not affect the other O(3) site as there is no A cation to transmit this effect across the cavity.

Testing for SRO of (OH) and F in richterite

Let us now consider the quantitative effect of the arrangements in Figure 23 on the infrared spectra. There are two important points here: (1) arrangements (3) and (6) are invisible to infrared in the principal (OH)-stretching region; (2) arrangements 4 and 5 will give rise to degenerate principal (OH)-stretching bands; (3) the sum of the relative proportions of the six

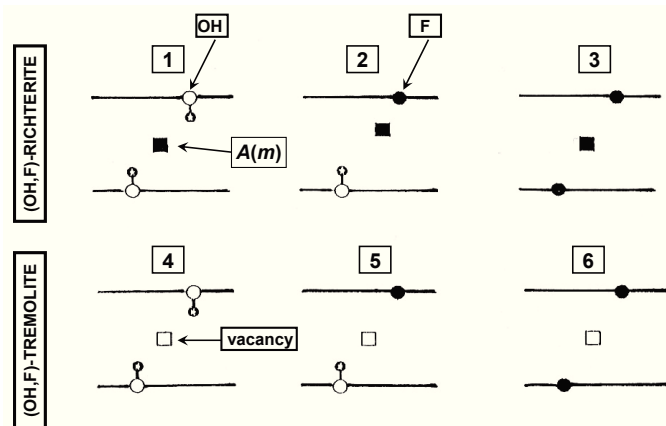


Figure 23. Local arrangements in the A cavity involving (OH) and F: (a) (OH,F)-bearing richterite; (b) (OH,F)-bearing tremolite. White circles: O atoms of (OH) groups; small black starred circles: H atoms; large black circles: F atoms; black square: Na at the $A(m)$ site; white square: vacant $A(m)$ site (modified from Robert et al. 1999).

arrangements is unity. There are six arrangements and only three bands in the spectrum, and we cannot explicitly derive quantitative information on SRO. In addition, the bands due to richterite have different molar absorptivities than the bands due to tremolite (Hawthorne et al. 1997), and hence the intensities of the richterite and tremolite bands do not relate to the frequency of occurrence of local arrangements in the same way. Despite these problems, we can test a model for complete local disorder using the relative intensities of bands A and B, as the arrangements involved couple through the Na at the A site and hence have the same molar absorptivities.

Let X be the proportion of richterite component [arrangement (4)], $(1 - X)$ be the proportion of tremolite component, x be the fraction of F [$x = X_F = F / (OH + F)$], n_i be the probability of occurrence of local arrangement (i) ($i = 1-6$) such that $\sum n_i = 1$. Assuming no SRO, the probabilities of occurrence of these arrangements can be written as follows:

$$\begin{aligned} n_1 &= X(1-x)^2 \\ n_2 &= 2X(1-x)x \\ n_3 &= Xx^2 \\ n_4 &= (1-X)(1-x)^2 \\ n_5 &= 2(1-X)(1-x)x \\ n_6 &= (1-X)x^2 \end{aligned} \quad (1)$$

The individual band intensities should vary as follows:

$$\begin{aligned} I_A &\propto 2n_1 = 2X(1-x)^2 \approx X(1-x) \\ I_B &\propto n_2 = 2X(1-x)x \approx Xx \\ I_C &\propto 2n_4 + n_5 = 2(1-X)(1-x)^2 + 2(1-X)(1-x)x \approx 1 - X \end{aligned} \quad (2)$$

where the approximation assumes that the extinction coefficients of bands A, B and C are equal [i.e., that the total band intensity $I_A + I_B + I_C$ is $2(1-x)$]. The constituent arrangements for bands A and B have the same molar absorptivities, and hence we can test a model of complete local disorder using the intensities of the two bands. We do not know the value of X , but X is not involved in the *relative* intensities of the A and B bands:

$$\begin{aligned} I_A / (I_A + I_B) &= X(1-x) / [X(1-x) + Xx] = 1 - x \\ I_B / (I_A + I_B) &= Xx / [X(1-x) + Xx] = x \end{aligned} \quad (3)$$

Figure 24 compares the calculated and observed intensity ratios for the A and B bands in richterite-fluorichterite solid-solutions; the agreement is in accord with complete short-range disorder of (OH) and F in these amphiboles.

The spectra discussed above indicate that (OH) and F are short-range disordered. However, we must emphasize that this disorder is with regard to each other (i.e., they are randomly disordered with regard to each other). Hawthorne et al. (1996a) showed that local arrangements of atoms at the $M(4)$ and $O(3)$ sites are preferentially associated with Na at the $A(2)$ and $A(m)$ sites. This issue has recently been addressed by Hawthorne et al. (2006) on a series of F-rich amphiboles from Bear Lake, Ontario (Canada), in which there are significant to complete short-range associations of the type $\text{Na-F}^{M(4)}\text{Na}$ and $\square\text{-(OH)}^{M(4)}\text{Ca}$. Thus (OH)

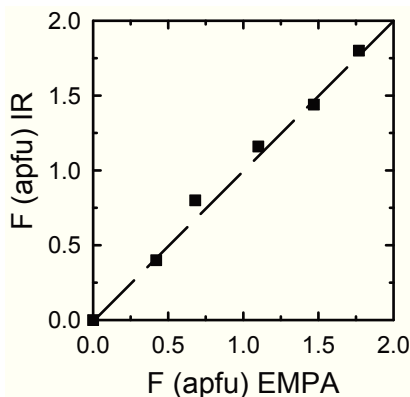


Figure 24. Variation in the observed band intensities and the values calculated for complete short-range disorder of (OH) and F in richterite-fluorichterite solid-solutions (from Robert et al. 1999).

and F may be randomly arranged with respect to each other, but they can also show SRO involving other atoms in the amphibole structure.

Testing for SRO of (OH) and F in pargasite

Richterite, potassic-richterite and tremolite are characterized by the $M(1)M(1)M(3)$ arrangement MgMgMg, and we examined the short-range behavior of (OH) and F with respect to each other. The presence of the $M(1)M(1)M(3)$ arrangements MgMgMg and MgMgAl in pargasite (see above) allows us to test the potential for SRO of both (OH) and F with respect to these to NN arrangements.

Robert et al. (2000) examined the (OH,F) substitution in synthetic pargasite; the infrared spectra of the amphiboles are shown in Figure 25. As shown above, the spectrum of synthetic end-member pargasite consists of six bands, but Robert et al. (2000) fitted only three aggregate bands because the appearance of the spectra in Figure 25 make it apparent that the principal changes relate to the NN arrangements MgMg-Mg and MgMgAl (and not to the NNN arrangements). The spectra of the F-bearing amphiboles were resolved into four bands; bands A and B in F-free pargasite can also be identified in the spectra of the F-bearing pargasite, and it is notable that the intensity of band B decreases strongly with increasing F content of the amphibole (Fig. 25). Moreover, the A' and B' bands increase rapidly in intensity with increasing F, indicating that the associated arrangements involve F, and that these bands are the result of two-mode behavior. The greater decrease in intensity of band B [MgMgAl-OH] relative to that of band A [MgMgMg-OH] indicates a relative decrease in the number of MgMgAl-OH arrangements with increasing F content. There are two possibilities here: (1) F occurs preferentially at the MgMgAl arrangement; (2) Al is displaced to the $M(2)$ site by F occurring at O(3). Single-crystal structure refinement of fluoropargasite (Oberti et al. 1995b) shows all Al ordered at $M(2)$, indicating that mechanism (2) is operative in these amphiboles.

Della Ventura et al. (2001) examined amphiboles of nominal composition [richterite_{0.60}-pargasite_{0.40}] with varying amounts of (OH) and F: Na (Na_{0.6} Ca_{1.4}) (Mg_{4.6} Al_{0.4}) (Si_{7.2} Al_{0.8}) O₂₂ (OH,F)₂. The infrared spectra are shown in Figure 26. Comparison of the spectrum of F-bearing richterite (Fig. 26a) with that of end-member richterite (Fig. 26b) shows the addition of a new band in the former at 3711 cm⁻¹, a result of the new arrangement in which F replaces (OH) at the O(3) site across the A cavity (see above). The spectrum of end-member pargasite (Fig. 26e) has two (composite) bands at 3710 and 3678 cm⁻¹, and addition of F gives rise to two new bands at 3694 and 3658 cm⁻¹ (Fig. 26d, also see above). The spectrum of Ri_{0.40}Pa_{0.60} (Fig. 26c) shows a broad absorption at 3705 cm⁻¹ and a weaker absorption at 3674 cm⁻¹. Comparison with the other spectra of Figure 26 suggests that the 3705 cm⁻¹ band corresponds to overlap

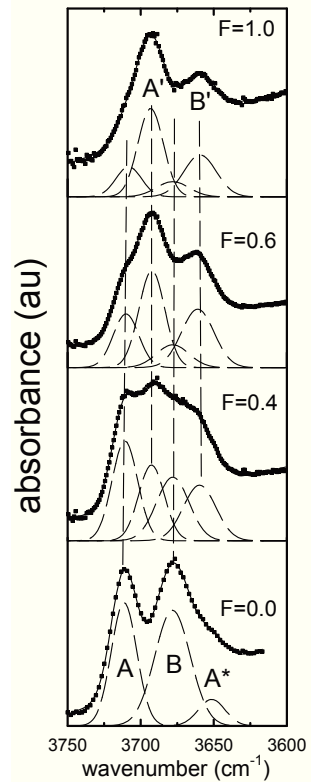


Figure 25. Infrared spectra in the principal (OH)-stretching region for pargasite-fluoropargasite solid-solution (from Robert et al. 2000).

of the 3711 band in richterite [from association of (OH) and F at neighboring sites across the A cavity], the 3710 cm^{-1} band in pargasite [from the arrangement $\text{MgMgMg}-(\text{OH})-(\text{OH})$], and the 3694 cm^{-1} band in pargasite [from the arrangement $\text{MgMgMg}-(\text{OH})-\text{F}$]. The band due to the arrangement $\text{MgMgAl}-(\text{OH})-\text{F}$ (at 3658 cm^{-1}) and the 3730 cm^{-1} band in richterite are not present in the spectrum of (OH,F)-bearing $\text{Ri}_{0.40}\text{Pa}_{0.60}$ (Fig. 26c). These spectra thus show that F completely replaces (OH) in local $\text{MgMgMg}-(\text{OH})-\text{Na}:\text{SiSi}$ (richterite-like) arrangements, and partly replaces (OH) groups in $\text{MgMgMg}-(\text{OH})-\text{Na}:\text{SiAl}$ (one of the pargasite-like) arrangements. Note that in $\text{MgMgAl}-(\text{OH}):\text{SiAl}$ arrangements, F cannot replace (OH). The latter is to be expected on bond-valence grounds: MgMgAl will provide incident bond-valence significantly greater than 1 vu, and the (OH) group can accommodate this because the O-H bond can adjust its length to provide whatever bond valence is needed (i.e., 1.0-0.7 vu). On the other hand, F needs to receive exactly 1 vu from its coordinating cations; there is no problem when these are MgMgMg ($\approx 0.33 \times 3 = 1$ vu), but when they are MgMgAl , the resulting sum ($0.33 + 0.33 + 0.50 = 1.17$ vu) is too large to be accommodated by F.

SHORT-RANGE DISORDER OF Ti^{4+} AND Si

It has long been known that K-bearing richterite from lamproites often shows Si + Al less than 8 apfu, and it was customary to assign Ti to the T-group cations to bring the total to 8 apfu (e.g., Papike et al. 1969; Wagner and Velde 1986). XAS (Mottana et al. 1990; Paris et al. 1993) and infrared spectroscopy (Della Ventura et al. 1991, 1993a) showed that Ti is indeed a tetrahedrally coordinated cation in synthetic Ti-bearing potassic-richterite. Site-scattering refinement of a series of Ti-bearing richterite crystals (Oberti et al. 1992) showed that Ti^{4+} is a T cation and is completely ordered at the T(2) site. However, the question now arises as to whether there is short-range order involving Ti^{4+} and Si at the T(2) site. This issue was examined by Della Ventura et al. (1996b) who synthesized amphiboles along the join potassic-richterite $[\text{K}(\text{Ca Na})\text{Mg}_5\text{Si}_8\text{O}_{22}(\text{OH})_2]$ - Ti^{4+} -bearing potassic-richterite $[\text{K}(\text{Ca Na})\text{Mg}_5(\text{Si}_7\text{Ti}^{4+})\text{O}_{22}(\text{OH})_2]$ and characterized them by infrared spectroscopy. Their spectra are shown in Figure 27. There is prominent multi-mode behavior and the spectra were fitted to four bands, A, B, C and T; bands A, B and C were assigned to A-site-full arrangements and band T was assigned to the tremolite arrangement (see above). There is also a very weak band in the spectrum of Ti-free potassic-richterite (Fig. 27a) at ~ 3720 cm^{-1} ; this is due to slight asymmetry in the band (which was fitted by a symmetrical Gaussian curve),

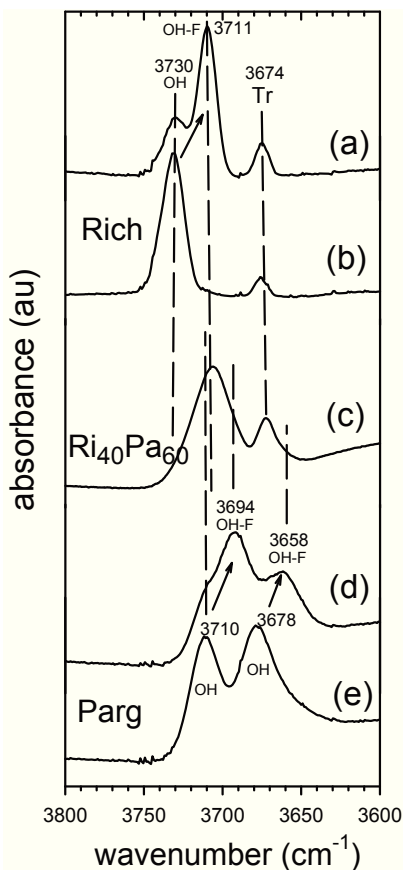


Figure 26. Infrared spectra in the principal (OH)-stretching region for the synthetic solid-solution Richterite_{0.40}Pargasite_{0.60}(OH, F). [Used by permission of Schweizerbart'sche Verlagsbuchhandlung, from Della Ventura et al. (2001), European Journal of Mineralogy, Vol. 13, Fig. 7, p. 846.]

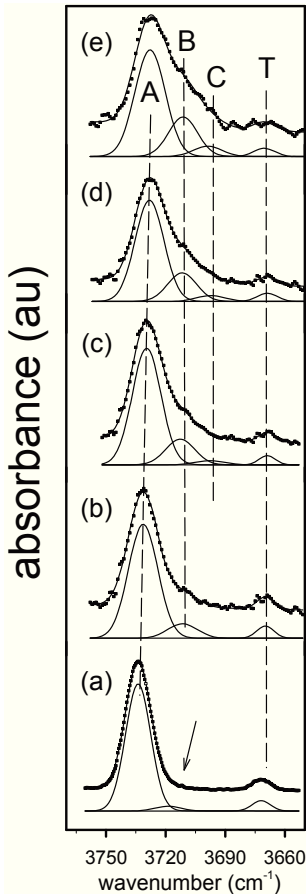


Figure 27. Infrared spectra in the principal (OH)-stretching region for synthetic amphiboles along the join potassic-richertite-K CaNa Mg₅ (Si₇Ti⁴⁺) O₂₂ (OH)₂ (from Della Ventura et al. 1996b).

bands must be caused by the different local distortions of the six-membered rings of tetrahedra resulting from the different *T*(2) arrangements.

and was ignored in the following arguments as it is less than 5% of the total intensity.

Band assignment

The occurrence of multi-mode behavior suggests the existence of distinct local arrangements, and the increase in intensity of bands B and C with increasing Ti (Fig. 28) indicates that these local arrangements must involve Ti⁴⁺. There are two *T*(2) sites in each ring of six tetrahedra (Hawthorne and Oberti 2007, Fig. 3), and each of these may be occupied by Si or Ti⁴⁺. Thus there are only three possible arrangements around each (OH) group: SiSi, SiTi⁴⁺ and Ti⁴⁺Ti⁴⁺. The intensity of an (OH)-stretching band is proportional to the number of (OH) groups in each arrangement. Assuming a random distribution of Si and Ti⁴⁺ over the two sites, the probability of occurrence of each *T*(2)*T*(2) pair as a function of bulk composition is as follows:

$$\begin{array}{ll} \text{SiSi:} & (1 - x / 4)^2 \\ \text{SiTi}^{4+}: & 2(1 - x / 4)(x / 4) \\ \text{Ti}^{4+}\text{Ti}^{4+}: & (x / 4)^2 \end{array} \quad (4)$$

where $x = \text{Ti}^{4+}$ apfu. Figure 29 shows the observed relative intensities of the three resolved bands as a function of the calculated probabilities of occurrence of the three possible arrangements for a random distribution. There is close accord between the observed and calculated values, and this agreement leads us to assign band B to the SiTi⁴⁺ arrangement and band C to the Ti⁴⁺Ti⁴⁺ arrangement. The close agreement between the observed and calculated values indicates that there is complete short-range disorder of Si and Ti⁴⁺ over the *T*(2) sites in the double chain of tetrahedra in the structure of potassic-richertite.

Local stereochemistry

The Ti⁴⁺ → Si substitution does not modify the charge distribution around the locally associated (OH) groups, and hence the appearance of the lower-frequency

SHORT-RANGE ORDER OF Ti⁴⁺ AND O²⁻

The association between Ti⁴⁺ and deficiency in monovalent anions has long been recognized in kaersutitic amphiboles (Leake 1968; Saxena and Ekstrom 1970). However, the situation is complicated by the fact that dehydrogenation in amphiboles can proceed by oxidation of Fe²⁺ to Fe³⁺ (e.g., Barnes 1930; Addison et al. 1962; Ernst and Wai 1970; Dyar et al. 1993; Popp et al. 1995), and hence other factors *can* affect the amount of monovalent anions in the amphibole structure. Site-scattering refinement with neutron-diffraction data (Kitamura and Tokonami 1971; Kitamura et al. 1973, 1975; Jirak et al. 1986; Pechar et al. 1989) has shown that Ti is partly to completely ordered at the *M*(1) site. The same conclusions have been made

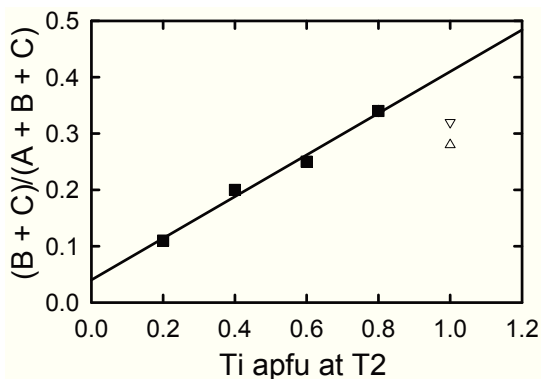
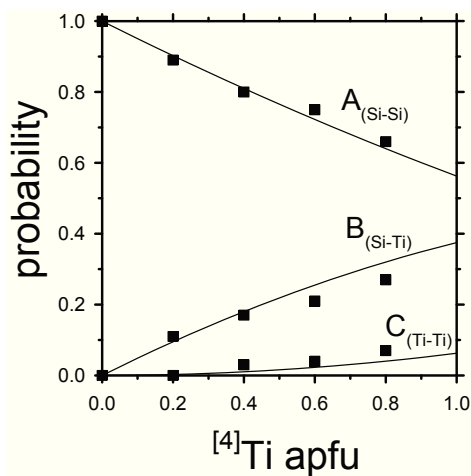
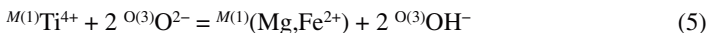


Figure 28. The relative intensity of bands B + C in synthetic amphiboles along the join potassic-richterite-K CaNa Mg₅ (Si₇ Ti⁴⁺) O₂₂ (OH)₂ as a function of Ti content (modified from Della Ventura et al. 1996b).

Figure 29. Relative intensities of bands A, B and C in synthetic amphiboles along the join potassic-richterite-K CaNa Mg₅ (Si₇ Ti⁴⁺) O₂₂ (OH)₂ as a function of Ti content; the lines are calculated for Equation (9) with a random distribution (from Della Ventura et al. 1996b).



from crystal-structure refinement with X-rays, focusing on the stereochemistry of the *M*(1) site. Hawthorne et al. (1998) showed that there is a very strong correlation between the Ti content of a suite of sodic-calcic and sodic amphiboles from Coyote Creek, California (Fig. 30), where the H contents were determined by SIMS. The slope of the line in Figure 30 is in accord with the equation (note that this is **not** a chemical reaction!)



Oberti et al. (1992) proposed that the atoms involved are locally associated in the amphibole structure. This proposal makes sense from a local bond-valence perspective, as the absence of a H atom from the coordination of O(3) necessitates incidence of considerable additional bond valence from the locally coordinating cations. The association of a high-valence cation with the occurrence of a divalent anion at the O(3) site is a notable feature in amphiboles. In addition to kaersutite, there are several other amphiboles with dominant O²⁻ at the O(3) site (Table 10). All of them except ungarrettiite have Ti⁴⁺ as an essential constituent, and in all of them, the local version of bond-valence theory indicates that there local association of Ti⁴⁺ at *M*(1) with O²⁻ at O(3). For ungarrettiite, the situation is somewhat different. Here, Mn³⁺ is dominant at the *M*(1) and *M*(3) sites; moreover, Mn³⁺ is a Jahn-Teller cation when in octahedral coordination, and it forms very short bonds to the O(3) site (Hawthorne et al. 1995), providing the necessary bond valence for O²⁻ at the O(3) site.

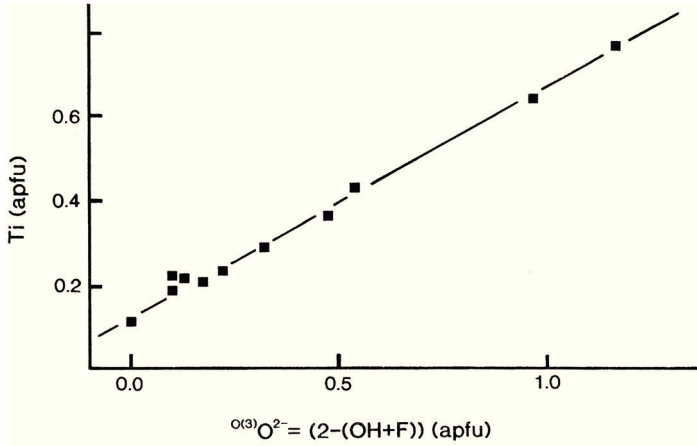


Figure 30. Variation in Ti^{4+} as a function of the O^{2-} content of the O(3) site in amphiboles from Coyote Peak (from Hawthorne et al. 1998).

Table 10. Amphibole end-members with O^{2-} dominant at the O(3) site.

Name	Formula	Ref.
Obertiite	$\text{Na Na}_2 (\text{Mg}_3\text{Fe}^{3+}\text{Ti}^{4+}) \text{Si}_8 \text{O}_{22} \text{O}_2$	(1)
Dellaventurait	$\text{Na Na}_2 (\text{MgMn}^{3+}_2\text{Ti}^{4+}\text{Li}) \text{Si}_8 \text{O}_{22} \text{O}_2$	(2)
Ungarettiite	$\text{Na Na}_2 (\text{Mn}^{2+}_2\text{Mn}^{3+}_3) \text{Si}_8 \text{O}_{22} \text{O}_2$	(3)

References: (1) Hawthorne et al. (2000b); (2) Tait et al. (2005); (3) Hawthorne et al. (1995).

Della Ventura et al. (2007) studied a suite of well-characterized Ti-rich pargasites from the Lherz peridotite, previously characterized by Zanetti et al. (1996). A combination of XREF, EMPA and SIMS data showed all amphiboles to be Ti-rich pargasites of fairly constant *M*-site composition, with $^{61}\text{Al}_{\text{tot}} \sim 0.55$ apfu, $^{61}\text{Ti} \sim 0.45$ apfu and $^{61}\text{Fe}^{3+} \sim 0.40$ apfu, and an anion composition at O(3) = OH \approx O²⁻ \approx 1.0 apfu, with negligible F (max. = 0.06 apfu). The principal variation in these amphiboles involves the different degree of ^CAl disorder between the *M*(2) and *M*(3) sites. The FTIR spectra of these amphiboles (e.g., Fig. 31c) are significantly different from those of both synthetic pargasite (Fig. 31a) and natural pargasite (Fig. 31b), both of which show a characteristic pattern of two peaks. The Lherz spectrum is very similar to spectra of synthetic OH-F exchanged pargasite (Fig. 31d). Della Ventura et al. (2007) assign the component bands in the spectra of the Lherz pargasites to local arrangements involving OH-OH (components A, C and E, Fig. 32) and OH-O²⁻ (components B and D, Fig. 32). This suggests that FTIR spectroscopy is an effective way to detect the presence of O²⁻ at O(3). Moreover, the OH-bearing local arrangements visible in the IR spectra are exclusively of the type MgMgMg or MgMgM³⁺ with M³⁺ predominantly Al, in accord with the complete local association of ^M(1)Ti⁴⁺ and ^M(1)Fe³⁺/^M(3)Fe³⁺ with O²⁻ at O(3).

SHORT-RANGE ORDER OF CATIONS AROUND THE A SITE

C2/m amphiboles

The A site in *C2/m* amphiboles may be occupied by Na, K or □ (vacancy), and rarely by Ca. As discussed in Oberti et al. (2007b), the A cations do not occupy the central A2/*m*

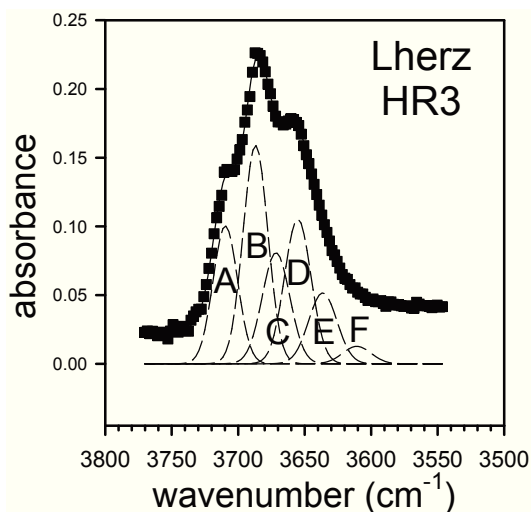
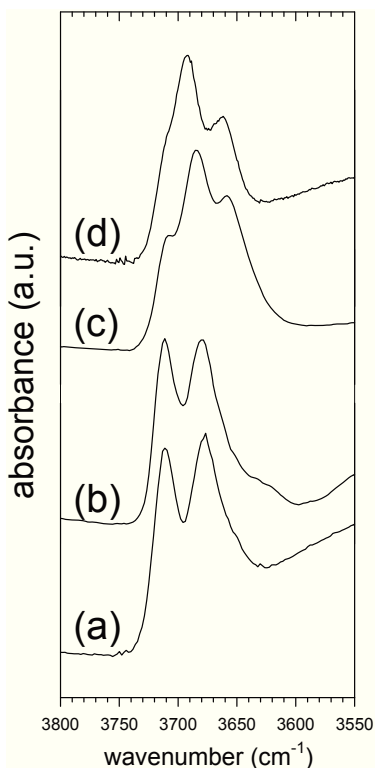


Figure 31 (to the left). Infrared spectra in the principal (OH)-stretching region for (a) synthetic pargasite; (b) pargasite from Finero; (c) Ti-rich pargasite from Lherz (sample HR3); (d) synthetic fluoropargasite with $(\text{OH}_{0.8} \text{F}_{1.2})$ (from Della Ventura et al. 2007).

Figure 32 (above). Infrared spectra in the principal (OH)-stretching region for Ti-rich pargasite from Lherz (sample HR3) (modified from Della Ventura et al. 2007).

site: K always occupies the $A(m)$ site, whereas Na can occupy the $A(m)$ and/or the $A(2)$ sites. Hawthorne et al. (1996a) showed that the various occupancies of the $A(m)$ and $A(2)$ sites by Na are controlled by the short-range bond-valence requirements of the cations involved in the disorder and the anions to which they are bonded. Figure 27 of Hawthorne and Oberti (2007) shows the distribution of electron density in a series of amphiboles, the compositions of which are given in Table 11. In this regard, it is important to recognize that the factors influencing ^ANa order are short range rather than long range, and the presence of significant SRO may significantly affect the long-range data that we derive from crystal-structure refinement. This situation is illustrated schematically in Figure 33, where the O(3) site is occupied by two anions, X^- and Y^- . The $A(2/m)$ site (Fig. 33a) is equidistant from the two closest O(3) sites, whereas the $A(m)$ site (Fig. 33b) is displaced toward one of the two nearer O(3) sites. Consider the situation where (1) occupancy of O(3) by Y^- couples to local occupancy of $A(m)$ by Na, (2) occupancy of O(3) by X^- couples to local occupancy of $A(2)$ by Na, and (3) arrangement (1) is energetically preferable to arrangement (2). Let us sum the local arrangement in Figure 33b over the crystal: $\sum ({}^{A(m)}\text{Na} - {}^{\text{O}(3)}Y + {}^{A(2)}\square - {}^{\text{O}(3)}X) = {}^{A(m)}\text{Na}_{1.0} {}^{A(2)}\square_{1.0} - X_{1.0}Y_{1.0} = {}^{A(m)}\text{Na} - X_1Y_1$. The variation in $A(m)$ and $A(2)$ site-populations as a function of bulk composition of the crystal is shown in Figure 33c. At $X = 2$ apfu, all ^ANa must be associated with X at O(3), and Na occupies the $A(2)$ site. As Y increases, all Y couples to ^ANa and causes ^ANa to occupy $A(m)$. At a composition $\text{O}(3) = X_1Y_1$, all ^ANa is coupled to Y at the O(3) site, and hence all ^ANa occupies $A(m)$, even though O(3) is only half-occupied by Y . This example shows how the pattern of ^ANa order can change in a non-linear fashion as a function of chemical composition of the crystal, an important issue to bear in mind where considering SRO of A cations in amphiboles.

Table 11. Formulae (apfu) of *C2/m* amphiboles of Figures 34 and 35.*

	Fluoro-nyböite	Fluoro-** arfvedsonite	Syn. fluoro-edenite	Syn. fluoro-pargasite	Arfvedsonite [†]	Pargasite	Taramite	Fluoro-taramite	Nyböite
Si	7.178	7.825	7.000	6.000	7.855	6.187	6.238	6.592	6.908
Al	0.822	0.141	1.000	2.000	0.137	1.813	1.762	1.408	1.092
ΣT	8.000	7.966	8.000	8.000	7.992	8.000	8.000	8.000	8.000
Al	1.251	0.000	—	1.000	0.000	0.937	1.120	0.851	1.384
Ti	0.014	0.116	—	—	0.059	0.018	0.040	0.017	0.031
Fe ³⁺	0.262	1.252	—	—	1.334	0.070	0.500	0.836	0.380
Fe ²⁺	0.836	1.887	—	—	3.255	0.756	0.411	0.832	0.502
Mn	0.008	0.923	—	—	0.147	0.001	—	0.019	0.001
Mg	2.612	0.759	5.000	4.000	0.005	3.413	2.929	2.426	2.773
ΣC	4.986	5.187	5.000	5.000	5.002	5.195	5.000	4.988	5.073
Fe ₃ Mn	0.000	0.187	—	—	0.002	0.195	—	0.000	0.073
Ca	0.484	0.066	2.000	2.000	0.065	1.760	1.062	0.793	0.401
Na	1.516	1.747	—	—	1.933	0.045	0.938	1.207	1.526
ΣB	2.000	2.000	2.000	2.000	2.000	2.000	2.000	2.000	2.000
Na	0.787	0.833	1.000	1.000	0.362	0.791	1.000	0.905	0.746
K	0.035	0.183	—	—	0.589	0.018	—	0.004	0.043
ΣA	0.822	1.016	1.000	1.000	0.951	0.809	1.000	0.909	0.789
F ⁻	1.135	1.616	—	—	0.187	—	0.004	1.020	0.228
OH	(0.865)	0.384	2.000	2.000	1.813	(2.000)	(1.996)	(0.980)	(1.772)

*from Hawthorne et al. (1993, 1996a); nominal formulae are given for synthetic amphiboles;

** includes 0.247 Li and 0.003 Zn apfu;

† includes 0.186 Li and 0.016 Zn apfu.

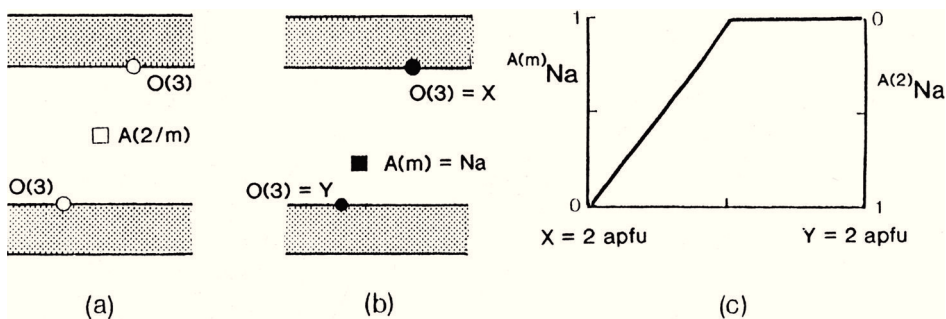


Figure 33. Possible local order at the A site: (a) Sketch of the A(2/m) site sandwiched between two octahedral strips, with the closest O(3) sites indicated; (b) occupancy of O(3) sites by anions X^- and Y^- , with ${}^A\text{Na}$ preferentially occupying the A(m) site where locally associated with Y^- , rather than the A(2) site where locally associated with X^- ; (c) the resulting variation in A(m) and A(2) site-populations as a function of bulk anion composition (from Hawthorne et al. 1996a).

The effects of variation in $T(\text{Al,Si})$ and $C(\text{M}^{2+}, \text{M}^{3+})$

In order to understand the possible effects of variation in $T(\text{Al,Si})$ and $C(\text{M}^{2+}, \text{M}^{3+})$, we need to compare the patterns of A-site electron density in structures with different values of $T(\text{Al,Si})$ and $C(\text{M}^{2+}, \text{M}^{3+})$. In Figure 34a, b, this is done for fluoro-arfvedsonite [$C \approx (\text{M}^{2+}_4 \text{M}^{3+})$, $T \approx (\text{Si}_8)$] and fluoronyböite [$C \approx (\text{M}^{2+}_3 \text{M}^{3+}_2)$, $T \approx (\text{Si}_7\text{Al})$]. Inspection of the formulae of fluoronyböite and fluoro-arfvedsonite (Table 11) indicates significant variation at the O(3) site; however, in the following section, we will see that variation in (OH,F) does not affect ordering of Na over the A(2) and A(m) sites. Inspection of Figures 34a, b shows that Na is ordered at the A(m) site in both crystals, and hence the compositional difference between these two crystals [i.e., $C \approx (\text{M}^{2+}_3 \text{M}^{3+}_2)$, $T \approx (\text{Si}_7\text{Al})$ versus $C \approx (\text{M}^{2+}_4 \text{M}^{3+})$, $T \approx (\text{Si}_8)$] does not result in any difference in ordering of ${}^A\text{Na}$.

Figure 34c, d show the A-site electron density in synthetic fluoro-edenite [$C \approx \text{M}^{2+}_5$, $T \approx (\text{Si}_7\text{Al})$] and synthetic fluoropargasite [$C \approx (\text{M}^{2+}_4 \text{M}^{3+}_1)$, $T \approx (\text{Si}_6\text{Al}_2)$], the nominal compositions of which are given in Table 11. Both crystals have similar patterns of electron density at the A(m) and A(2) sites, and hence we can conclude that the compositional differences between fluoro-edenite and fluoropargasite [i.e., $C \approx \text{M}^{2+}_5$, $T \approx (\text{Si}_7\text{Al})$ versus $C \approx (\text{M}^{2+}_4 \text{M}^{3+})$, $T \approx (\text{Si}_6\text{Al}_2)$] does not result in any difference in ordering of ${}^A\text{Na}$. Note that fluoropargasites from Oberti et al. (1995) have significant Ca at the A site, which modifies the distribution of the electron density (similar to that of cannilloite).

Both these examples show that compositional variations at the M(1,2,3) and T sites do not correlate directly with A-site ordering of Na in amphiboles (this result is also apparent in comparisons of other compositions in C2/m amphiboles). Of course, electroneutrality compels compositional variation at these sites to correlate with compositional variations at other sites that do correlate strongly with the distribution of Na over the A(m) and A(2) sites. However, below we will see that variation in B cations has a much more direct correlation with ordering of ${}^A\text{Na}$ than variation of C or T cations, as one would expect from local bond-topology and the ensuing local bond-valence requirements of the anions: (1) The majority of the anions bonded to A cations are also bonded to B cations, whereas this is not the case for C cations. Hence one does not expect such a direct correlation between bond-valence variations at the M(1,2,3) sites and the A sites as between the M(4) site and the A sites. The situation is not so clearcut at the T sites, as the T cations bond to all the anions coordinating the A sites. However, the examples given above show no change in the A-site electron-density with variation in T-cation composition and constant B-cation composition (fluoronyböite versus

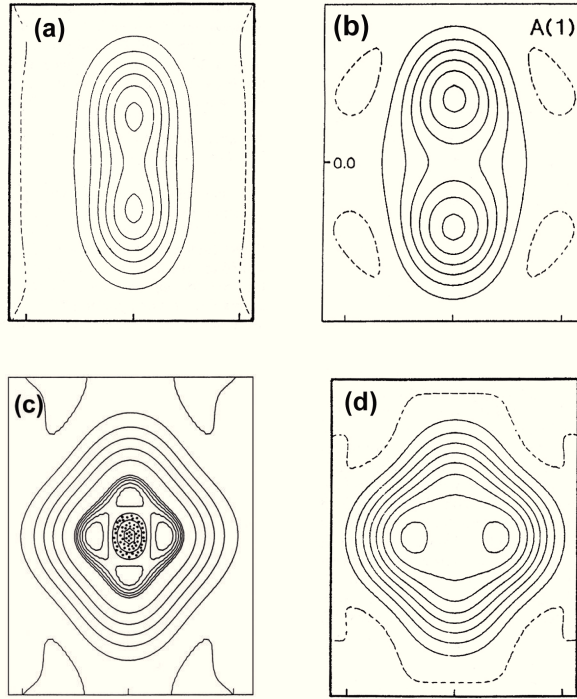


Figure 34. Difference-Fourier sections through the A cavity for (a) fluoro-arfvedsonite, (b) fluoronyböite, (c) synthetic fluoro-edenite, (d) synthetic fluoropargasite [(a), (b), (d) from Hawthorne et al. 1996a, (c) from Boschmann et al. 1994].

fluoro-arfvedsonite and fluoro-edenite versus fluoropargasite), whereas they do show change in the A-site electron-density with variation in B-cation composition and constant T-cation composition (fluoronyböite versus fluoro-edenite).

The effects of variation in $O(3)(OH,F)$

Comparison of the electron-density distribution in arfvedsonite (Fig. 35a, Table 11) and fluoro-arfvedsonite (Fig. 34a) shows that ordering of ${}^A\text{Na}$ at $A(m)$ is not affected by variation in (OH,F) where $M(4) = \text{Na}$. However, the $A(m)$ site is displaced much further from the center of the A cavity where $O(3) = \text{F}$ than where $O(3) = (\text{OH})$, indicating significant repulsion of ${}^A\text{Na}$ and H.

In pargasite (Fig. 35b, Table 11), ${}^A\text{Na}$ is ordered at $A(2)$, whereas arfvedsonite (Fig. 35a) has ${}^A\text{Na}$ ordered at $A(m)$. Both amphiboles have $C \approx (M^{2+}_4 M^{3+})$ and $O(3) \approx (\text{OH})$, and hence the difference in A-site order must be due to either Ca versus Na at $M(4)$ or Al versus Si at T (or both). However, above we saw that variation in (Al,Si) does not correlate strongly with variation in ${}^A\text{Na}$ order. Hence, in hydroxy-amphiboles, Na at $M(4)$ causes ${}^A\text{Na}$ to occupy $A(m)$ and Ca at $M(4)$ causes ${}^A\text{Na}$ to occupy $A(2)$. We may write this in the following way: $M(4)\text{Na}-O(3)(\text{OH})-A(m)\text{Na}$ and $M(4)\text{Ca}-O(3)(\text{OH})-A(2)\text{Na}$ are preferred local arrangements.

As fluoro-arfvedsonite (Fig. 34a) has Na at $A(m)$ and F at $O(3)$, we may also conclude that $M(4)\text{Na}-O(3)\text{F}-A(m)\text{Na}$ is a preferred local arrangement. Next, compare the electron density in fluoronyböite (Fig. 34b) and nyböite (Fig. 35c). In fluoronyböite, $M(4) \approx \text{Na}_{1.5}\text{Ca}_{0.5}$ (Table 11), $O(3) \approx \text{F}$, and only the $A(m)$ site is occupied; hence the possible schemes of local order in fluorony-

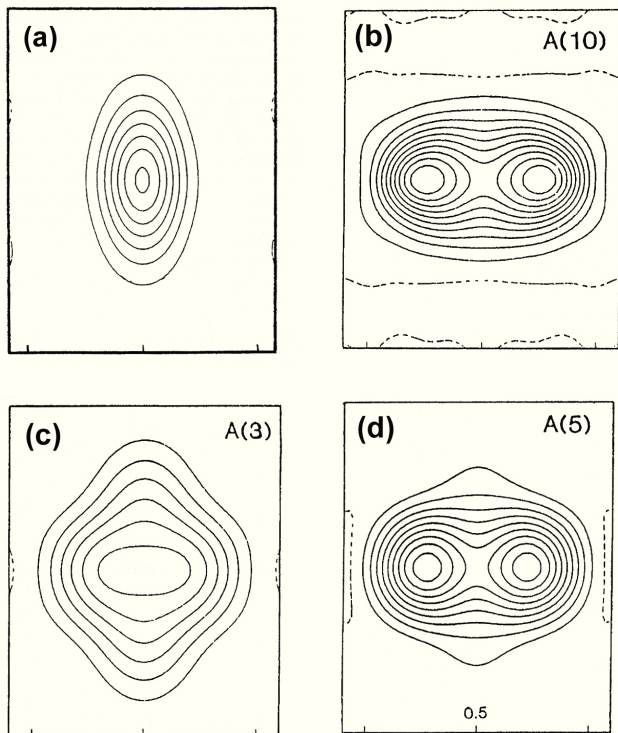


Figure 35. Difference-Fourier sections through the A cavity for (a) arfvedsonite, (b) pargasite, (c) nyböite, (d) taramite (from Hawthorne et al. 1996a).

böite are $M^{(4)}\text{Na-O}^{(3)}\text{F-A}(m)\text{Na}$, $M^{(4)}\text{Na-O}^{(3)}(\text{OH})\text{-A}(m)\text{Na}$ and $M^{(4)}\text{Ca-O}^{(3)}\text{F-A}(m)\text{Na}$ (we know from pargasite, Fig. 35b, that the arrangement $M^{(4)}\text{Ca-O}^{(3)}(\text{OH})\text{-A}(m)\text{Na}$ does not occur). In nyböite (Fig. 35c), $M(4) \approx \text{Na}_{1.6}\text{Ca}_{0.4}$ (Table 11), $\text{O}(3) \approx (\text{OH})$, and the $A(m)$ and $A(2)$ sites are about equally occupied; hence the possible schemes of local order in nyböite are $M^{(4)}\text{Na-O}^{(3)}(\text{OH})\text{-A}(m)\text{Na}$ and $M^{(4)}\text{Ca-O}^{(3)}(\text{OH})\text{-A}(2)\text{Na}$ (above, we showed that $M^{(4)}\text{Na-O}^{(3)}\text{F-A}(2)\text{Na}$ and $M^{(4)}\text{Ca-O}^{(3)}(\text{OH})\text{-A}(m)\text{Na}$ do not occur). In nyböite (Table 11), there is sufficient Ca at $M(4)$ to be locally associated with Na at $A(2)$ where half the $^{\text{A}}\text{Na}$ occurs at $A(m)$. In fluoronyböite, the arrangement $M^{(4)}\text{Ca-O}^{(3)}(\text{OH})\text{-A}(2)\text{Na}$ cannot occur as only $A(m)$ is occupied (Fig. 34b). From these considerations, we may conclude that $M^{(4)}\text{Ca-O}^{(3)}(\text{OH})\text{-A}(2)\text{Na}$ is preferred over $M^{(4)}\text{Na-O}^{(3)}(\text{OH})\text{-A}(m)\text{Na}$.

We may test this prediction with an amphibole that has $M(4) = \text{NaCa}$ and $\text{O}(3) = \text{OH}$; taramite is such an amphibole, and we thus predict that in taramite, $M^{(4)}\text{Ca-O}^{(3)}(\text{OH})\text{-A}(2)\text{Na}$ should occur (being preferred to $M^{(4)}\text{Na-O}^{(3)}(\text{OH})\text{-A}(m)\text{Na}$). In accord with this prediction, the electron density in the A cavity of taramite (Fig. 35d) has $^{\text{A}}\text{Na}$ completely ordered at $A(2)$. Consider next fluorotaramite (which shows the same electron-density distribution as fluoronyböite, Fig. 34b) with $M(4) \approx \text{Na}_{1.2}\text{Ca}_{0.8}$, $\text{O}(3) = \text{F}_1(\text{OH})_1$ and Na ordered at $A(m)$, an arrangement dramatically different from that in taramite (cf. Figs. 34b and 35d). As noted, the local arrangement of $^{\text{A}}\text{Na}$ in fluorotaramite cannot involve Ca or (OH) as the $A(2)$ site is not occupied, and hence the arrangements that occur must be more favorable than $M^{(4)}\text{Ca-O}^{(3)}(\text{OH})\text{-A}(2)\text{Na}$. The possible local arrangements in fluorotaramite are $M^{(4)}\text{Na-O}^{(3)}\text{F-A}(m)\text{Na}$ and $M^{(4)}\text{Ca-O}^{(3)}\text{F-A}(m)\text{Na}$. The ordering of $^{\text{A}}\text{Na}$ in synthetic fluoro-edenite (Fig. 34c) and synthetic fluoropargasite (Fig. 34d) indicates that $M^{(4)}\text{Ca-O}^{(3)}\text{F-A}(m)\text{Na}$ locally couples to $M^{(4)}\text{Ca-O}^{(3)}\text{F-A}(2)\text{Na}$, and does not occur as an isolated arrangement. As the $A(2)$ site is not occupied by Na in fluorotaramite (which has the same pattern of electron density as in fluoronyböite, Fig. 34b) the local arrangement must

be $M(4)\text{Na}-O(3)\text{F}_{A(m)}\text{Na}$. Comparison of the electron density in fluorotaramite with that in taramite (Fig. 35d) thus shows that arrangement $M(4)\text{Na}-O(3)\text{F}_{A(m)}\text{Na}$ is preferred over arrangement $M(4)\text{Ca}-O(3)(\text{OH})_{A(2)}\text{Na}$.

Consider next the electron density in fluoro-edenite (Fig. 34c) and fluoropargasite (Fig. 34d). The $A(m)$ and $A(2)$ sites are equally occupied by Na in both crystals, indicating that the local arrangements $M(4)\text{Ca}-O(3)\text{F}_{A(2)}\text{Na}$ and $M(4)\text{Ca}-O(3)\text{F}_{A(m)}\text{Na}$ occur in equal amounts. Boschmann et al. (1994) suggested that these two arrangements are locally coupled, accounting for their occurrence in equal amounts on crystals with $M(4) = \text{Ca}_2$ and $O(3) = \text{F}_2$. Now consider fluorotaramite with $M(4) = \text{Na}_{1.2}\text{Ca}_{0.8}$ and $O(3) = \text{F}_1(\text{OH})_1$; this crystal has all A Na ordered at $A(m)$ (which shows the same electron-density distribution as fluoronyböite, Fig. 34b), and hence arrangements involving $M(4)\text{Ca}$, $O(3)\text{F}$ and an occupied A site cannot occur (or there would be Na at $A(2)$, which there is not) owing to local coupling to $M(4)\text{Ca}-O(3)\text{F}_{A(m)}\text{Na}$. As this is not the case, we can conclude that the arrangements $M(4)\text{Ca}-O(3)\text{F}_{A(m)}\text{Na}$ and $M(4)\text{Ca}-O(3)\text{F}_{A(2)}\text{Na}$ are less favorable than $M(4)\text{Na}-O(3)\text{F}_{A(m)}\text{Na}$.

It is difficult to evaluate the relative stability of $M(4)\text{Ca}-O(3)\text{F}_{A(m)}\text{Na} + M(4)\text{Ca}-O(3)\text{F}_{A(2)}\text{Na}$ versus $M(4)\text{Ca}-O(3)(\text{OH})_{A(2)}\text{Na}$ and $M(4)\text{Na}-O(3)(\text{OH})_{A(m)}\text{Na}$. For $M(4)\text{Ca}-O(3)\text{F}_{A(m)}\text{Na} + M(4)\text{Ca}-O(3)\text{F}_{A(2)}\text{Na}$ versus $M(4)\text{Ca}-O(3)(\text{OH})_{A(2)}\text{Na}$, Nature has not provided us with the appropriate amphibole compositions. For $M(4)\text{Ca}-O(3)\text{F}_{A(m)}\text{Na} + M(4)\text{Ca}-O(3)\text{F}_{A(2)}\text{Na}$ versus $M(4)\text{Na}-O(3)(\text{OH})_{A(m)}\text{Na}$, $M(4)\text{Na}-O(3)\text{F}_{A(m)}\text{Na}$ and $M(4)\text{Ca}-O(3)(\text{OH})_{A(2)}\text{Na}$ would occur instead, as the resulting composition of the crystal would be similar. However, the fact that natural amphiboles of appropriate composition to resolve this problem do not occur (or are extremely rare and have not yet been found) suggests that the arrangement $M(4)\text{Ca}-O(3)\text{F}_{A(m)}\text{Na} + M(4)\text{Ca}-O(3)\text{F}_{A(2)}\text{Na}$ is less favorable than either $M(4)\text{Ca}-O(3)(\text{OH})_{A(2)}\text{Na}$ or $M(4)\text{Na}-O(3)(\text{OH})_{A(m)}\text{Na}$.

The relative stability of local arrangements

We are now in a position to summarize the relative stability (preference of occurrence) of local arrangements for the configuration symbol $M(4)-O(3)-A$, listed in order of decreasing preference (Table 12): (1) > (2) > (3) >> (4) \approx (5).

Assignment of local arrangements in structures

As the sum of the short-range arrangements has to be equal to the bulk composition of the crystal, we may use the chemical composition and the measured electron-density at the A sites to derive the relative amount of each arrangement. Hawthorne et al. (2006) have done this for fluorotremolite, fluororichterite and two potassian fluoromagnesiokatophorite crystals from Bear Lake, Ontario; the chemical formulae are given in Table 13. All of these crystals have Na ordered at the $A(m)$ site, and they also contain significant amounts of K (Table 13). As the $A(2)$ site is not occupied in these amphiboles, local arrangements (2) and (5) in Table 12 do not occur. Thus arrangement (1) will be preferred, with arrangements (3) and (4) occurring only if there are residual chemical components after assignment to arrangement (1). Inspection of Table 12 shows that arrangements (1) and (3) have Na at both $M(4)$ and A , and that the amount of F at $O(3)$ always exceeds the amount of Na at $M(4)$ and A (Fig. 36a); hence the amount of local arrangement (1) is not restricted by the amount of F in the amphibole. Figure 36b shows the variation of $A(\text{Na} + \text{K})$ as a function of $M(4)\text{Na}$ in the Bear Lake amphiboles. As the amount of Na at $M(4)$ always equals amount of Na at A , local arrangement (1) accounts for all Na at $M(4)$ and Na at A in these crystals. The remaining arrangements can only involve $M(4)\text{Ca}$, $O(3)(\text{OH},\text{F})$ and $A\Box$, and the amounts of these arrangements are dictated by the amount of (OH) and the remaining amounts of $O(3)\text{F}$. The amounts of local arrangements in the Bear Lake amphiboles are given in Table 14.

Table 12. Patterns of SRO involving cation sites adjacent to the A cavity, in order of preference*.

(1)	$M(4)\text{Na} - O(3)\text{F}_{A(m)}\text{Na}$
(2)	$M(4)\text{Ca} - O(3)\text{OH}_{A(2)}\text{Na}$
(3)	$M(4)\text{Na} - O(3)\text{OH}_{A(m)}\text{Na}$
(4)	$M(4)\text{Ca} - O(3)\text{F}_{A(m)}\text{Na}$
(5)	$M(4)\text{Ca} - O(3)\text{F}_{A(2)}\text{Na}$

*from Hawthorne et al. (1996a).

Table 13. Chemical compositions (wt%) and unit formulae (apfu) of the Bear Lake amphiboles.

	757	761	721	762
Si	8.035	7.909	7.374	7.362
Al	0.000	0.091	0.626	0.638
ΣT	8.035	8.000	8.000	8.000
Al	0.016	0.020	0.030	0.053
Ti	0.002	0.004	0.063	0.081
Fe ³⁺	0.000	0.061	0.478	0.486
Fe ²⁺	0.249	0.215	0.908	1.007
Mn	0.022	0.013	0.052	0.049
Mg	4.644	4.700	3.427	3.276
Zn	0.004	0.006	0.006	0.003
Li	0.000	0.000	0.023	0.023
ΣC	4.937	5.019	4.987	4.978
□	0.000	0.019	0.000	0.000
Ca	1.610	1.466	1.232	1.177
Na	0.390	0.515	0.768	0.823
ΣB	2.000	2.000	2.000	2.000
Na	0.176	0.342	0.506	0.507
K	0.177	0.174	0.297	0.315
ΣA	0.353	0.516	0.803	0.822
F	0.584	0.721	1.210	1.277
OH	1.416	1.279	0.790	0.723

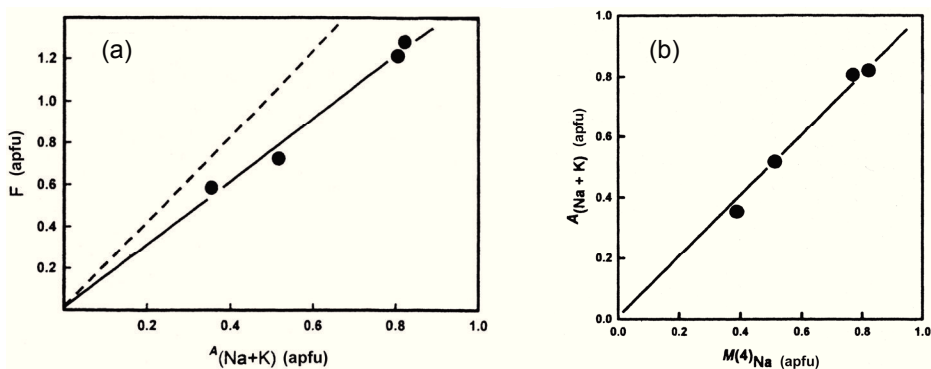


Figure 36. Bear Lake amphiboles: (a) The variation in F as a function of $A(\text{Na} + \text{K})$; the black line is drawn as a guide to the eye, the broken line indicates a 2:1 relation; (b) The variation of $A(\text{Na} + \text{K})$ as a function of $M^{(4)}\text{Na}$ in the Bear Lake amphiboles of Table 6; the line indicates a 1:1 relation (from Hawthorne et al. 2006).

Table 14. Proportion of SRO arrangements in the Bear Lake amphiboles.

	757	761	721	762
Richterite	0.37	0.43	0.16	0.18
Tremolite	0.63	0.48	0.21	0.18
Katophorite	0.00	0.09	0.63	0.64

Hawthorne (1997) examined the issue of SRO in amphiboles from a bond-valence perspective and emphasized the importance of defining an FBB (Fundamental Building Block) for patterns of SRO. The FBB involves all symmetrically distinct sites in the structure, and thus the arrangements of atoms in the configuration symbol $M(4)\text{-O}(3)\text{-A}$ dictate the composition of the rest of the crystal. Arrangement (1) involves patterns resembling richterite and katophorite (Hawthorne 1997), and arrangements $M(4)\text{Ca-O}(3)(\text{OH,F})\text{-A}\square$ can involve patterns resembling those in tremolite, aluminohornblende and tschermakite. We may identify which patterns of order are present from the other (C and T) cations in the crystal. Consider crystal 757 (Tables 12, 13, 14), with $0.37 M(4)\text{Na-O}(3)\text{F-A}(m)\text{Na}$ and $0.63 M(4)\text{Ca-O}(3)(\text{OH,F})\text{-A}\square$. There is no ${}^T\text{Al}$ in this crystal, and hence the local arrangements must be if the richterite type and the tremolite type (with Si = 8 apfu). The amounts of these SRO arrangements are shown for each crystal in Table 14.

Oberti et al. (2003a, b) noted the preferential order of the A-site cation at $A(m)$ in ${}^B,{}^C\text{Li}$ -rich amphiboles. Figure 37 shows electron-density maps through the A site for a series of amphiboles with increasing ${}^A(\text{Na,K}):{}^C\text{Li}$ and ${}^B\text{Li}:{}^C\text{Li}$ ratios, in which the $A(m)\text{-}A(m)$ separation increases strongly. ${}^B\text{Li}$ occurs at the $M(4')$ site and has a weaker interaction with O(5) and O(6) than Na (or Ca) at $M(4)$. The local version of the valence-sum rule at O(5) and O(6) indicates that where Li occurs at $M(4')$, the O(6) anion requires additional bond-valence, and ${}^A\text{Na}$ at $A(m)$ moves away from $A(2m)$, increasing the bond valence received at O(6) from ${}^A\text{Na}$, and Oberti et al. (2003b) show that the bond valences are in accord with this behavior. They also emphasize that the presence of F at O(3) is an important factor in allowing ${}^A\text{Na}$ to shift within the A cavity without the steric hindrance of the presence of H present as (OH) at O(3). Oberti

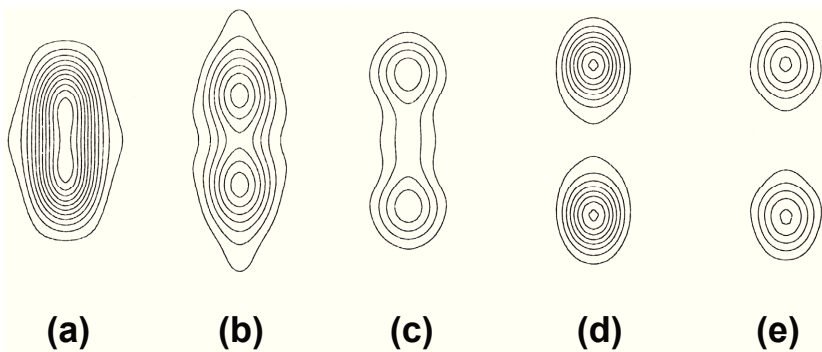


Figure 37. Difference-Fourier sections through the A cavity (parallel to $\bar{2}01$) for (a) leakite (A2 from Hawthorne et al. 1994: ${}^A(\text{Na,K}) = 0.69$, ${}^B\text{Li} = 0.00$, ${}^C\text{Li} = 0.74$, F = 0.49 apfu), (b) ferriwhittakerite and (c) ferri-ottoliniite (Oberti et al. 2004: ${}^A(\text{Na,K}) = 0.77$, ${}^B\text{Li} = 0.62$, ${}^C\text{Li} = 0.73$, F = 0.72 and ${}^A(\text{Na,K}) = 0.45$, ${}^B\text{Li} = 1.24$, ${}^C\text{Li} = 0.42$, F = 0.47 apfu, respectively), (d) sodic ferri-ferropedrizite and (e) ferri-clinoferroholmquistite (Oberti et al. 2003b: ${}^A(\text{Na,K}) = 0.56$, ${}^B\text{Li} = 1.82$, ${}^C\text{Li} = 0.58$, F = 0.52 and ${}^A(\text{Na,K}) = 0.0.28$, ${}^B\text{Li} = 1.90$, ${}^C\text{Li} = 0.28$, F = 0.0.24 apfu, respectively (modified from Oberti et al. 2003b).

et al. (2003b) conclude that the sequence of preferred local arrangements in ${}^B\text{Li}$ is ${}^{M(4)}\text{Li}\text{-}{}^{O(3)}\text{F}\text{-}{}^{A(m)}\text{Na} > {}^{M(4)}\text{Li}\text{-}{}^{O(3)}\text{OH}\text{-}{}^{A(m)}\text{Na}$, similar to the sequence ${}^{M(4)}\text{Na}\text{-}{}^{O(3)}\text{F}\text{-}{}^{A(m)}\text{Na} > {}^{M(4)}\text{Na}\text{-}{}^{O(3)}\text{OH}\text{-}{}^{A(m)}\text{Na}$ observed in ${}^B\text{Na}$ -bearing ${}^T\text{Al}$ -free amphiboles by Hawthorne et al. (1996a).

SUMMARY

Extensive work in the last ten years has shown that short-range order is a common feature of synthetic amphiboles, is present in some natural amphiboles, and is probably an extremely common feature of natural amphiboles. The results described here also suggest that short-range order may be common in other rock-forming minerals such as micas and pyroxenes. To summarize the results on the amphiboles:

- (1) LRO (Long-Range Order) involves the occurrence of atoms at different crystallographic sites in a structure such that the average arrangement over all the unit cells in the crystal does not concur with that predicted by a random distribution;
- (2) SRO (Short-Range Order) involves the formation of local clusters of atoms that occur either more or less frequently than predicted by a random local distribution.
- (3) Infrared spectroscopy in the principal OH-stretching region is particularly effective in characterizing local (short-range) arrangements of atoms in amphiboles.
- (4) Extension of bond-valence theory to local arrangements (Hawthorne 1997) shows that short-range bond-valence requirements exert strong constraints on the local arrangements of atoms that can occur (i.e., that are stable).
- (5) Infrared spectroscopy and bond-valence constraints show that local ordering of cations is very pronounced in a crystal of tremolite with significant Na and Al contents.
- (6) The results mentioned in (5) show that the principal OH-stretching frequency in amphiboles is affected by the cations at both nearest-neighbor and next-nearest-neighbor sites.
- (7) A site-configuration symbol can be used to denote the sites affecting the principal (OH)-stretching frequency in amphiboles: $M(1)M(1)M(3)\text{-}(\text{OH})\text{-}A\text{:}T(1)T(1)\text{-}M(2)M(2)M(3)$; local arrangements of atoms can then be denoted by inserting the atoms at the relevant sites: e.g., $\text{MgMgMg}\text{-}(\text{OH})\text{-}\text{Na}\text{:}\text{SiAl}\text{-}\text{MgMgMg}$ or $\text{MgMgAl}\text{-}(\text{OH})\text{-}\text{Na}\text{:}\text{SiAl}\text{-}\text{MgMgAl}$.
- (8) Synthesis and infrared spectroscopy show that monoclinic calcium-rich amphiboles in the system tremolite-cummingtonite and synthetic amphiboles in the system tremolite--Sr-tremolite show short-range disorder involving divalent cations at the $M(4)$ [and $M(4')$] site.
- (9) Synthesis, infrared spectroscopy and local bond-valence arguments show that monoclinic amphiboles in the systems richterite-pargasite, tremolite-pargasite and tremolite~hornblende show strong SRO involving T, C and A cations.
- (10) Synthesis and infrared spectroscopy for amphiboles with (OH)-F solid-solution show that amphiboles with \square (vacancy) at the A site (e.g., tremolite-fluorotremolite) show one-mode behavior, whereas amphiboles with Na or K at the A site (e.g., richterite-fluororichterite) show two-mode behavior; it is apparent from this observation that nearest-neighbor arrangements of atoms couple through an occupied A site, but do not couple through a vacant A site.
- (11) The relative band intensities in (OH)-F amphibole solid-solutions showing two-mode behavior indicate that (OH) and F are completely short-range disordered *with respect to each other* in the amphibole series examined thus far.

- (12) Synthesis, infrared spectroscopy and local bond-valence arguments show that monoclinic amphiboles in the system pargasite-fluoropargasite show strong SRO of (OH) and F with regard to the cations occupying the associated nearest-neighbor $M(1)M(1)M(3)$ sites: arrangements involving MgMgAl-(OH) are far more common than arrangements involving MgMgAl-F.
- (13) Synthesis and infrared spectroscopy for Ti-bearing richteritic amphiboles show that $^{[4]}Ti^{4+}$ and Si are short-range disordered with regard to each other.
- (14) Crystal-structure refinement, SIMS analysis and local bond-valence requirements suggest that $^{[6]}Ti^{4+}$ and $O^{(3)O^{2-}}$ are locally associated at adjacent $M(1)$ and $O(3)$ sites in nearly all amphiboles with a significant oxo-component related to primary crystallization.
- (15) The variation in occupancy of the $A(m)$ and $A(2)$ sites by Na in $C2/m$ amphibole is caused by the occurrence of a number of preferred arrangements of cations and anions at the adjacent $M(4)$ and $O(3)$ sites. The arrangements and their relevant stabilities are as follows: $^{M(4)}Na-O^{(3)}F-A(m)Na > ^{M(4)}Ca-O^{(3)}(OH)-A(2)Na > ^{M(4)}Na-O^{(3)}(OH)-A(m)Na \gg ^{M(4)}Ca-O^{(3)}F-A(m)Na \approx ^{M(4)}Ca-O^{(3)}F-A(2)Na$, and they can be understood in terms of local bond-valence requirements within the amphibole structure.
- (16) It is apparent from this review of recent results that SRO is very common in monoclinic amphiboles. Although much work remains to be done to fully characterize SRO across the complexities of amphibole composition-space, the general features are already emerging: local bond-valence requirements seem to be the (principal) factor controlling this type of order.
- (17) SRO is of significance in that it will affect the stability of amphiboles (and other minerals in which it occurs) through its entropy (and enthalpy) effects; the way in which these effects can be formulated for such a complicated case is not yet clear, but what is clear is that future thermodynamic models need to consider SRO in amphiboles and probably in other minerals in which heterovalent substitutions are common.

ACKNOWLEDGMENTS

This work was supported by the Natural Sciences and Engineering Research Council of Canada in the form of a Canada Research Chair in Crystallography and Mineralogy, Research Tools and Equipment, and Discovery Grants to FCH, and by the Canada Foundation for Innovation in the form of Innovation grants to FCH.

REFERENCES

- Addison CC, Addison WE, Neal GH, Sharp JH (1962) Amphiboles. I. The oxidation of crocidolite. *J Chem Soc* 1962:1468-1471
- Ahn JH, Cho M, Jenkins DM, Buseck PR (1991) Structural defects in synthetic tremolitic amphiboles. *Am Mineral* 76:1811-1823
- Andrut N, Gottschalk M, Melzer S, Najorka J (2000) Lattice vibrational modes in synthetic tremolite-Sr-tremolite and tremolite-richterite solid solutions. *Phys Chem Mineral* 27:301-309
- Barnes VE (1930) Changes in hornblende at about 800°. *Am Mineral* 15:393-417
- Boschmann K, Burns PC, Hawthorne FC, Raudsepp M, Turnock AC (1994) A-site disorder in synthetic fluor-edenite, a crystal structure study. *Can Mineral* 32:21-30
- Brown ID (1981) The bond valence method. An empirical approach to chemical structure and bonding. *In: Structure and Bonding in Crystals II*. O'Keeffe M, Navrotsky A (eds) Academic Press, New York, p 1-30
- Brown ID (2002) The Chemical Bond in Inorganic Chemistry. The Bond Valence Model. Oxford University Press

- Brown ID, Altermatt D (1985) Bond-valence parameters obtained from a systematic analysis of the inorganic crystal structure database. *Acta Crystallogr B* 41:244-247
- Burdett JK, Hawthorne FC (1993) An orbital approach to the theory of bond valence. *Am Mineral* 78:884-892
- Cao R-L, Ross C, Ernst WG (1986) Experimental studies to 10 kb of the bulk composition tremolite₅₀-tschermakite₅₀ + excess H₂O. *Contrib Mineral Petrol* 93:160-167
- Chang IF, Mitra SS (1968) Application of a modified random-element-isodisplacement model to long-wavelength optic phonons of mixed crystals. *Phys Rev* 172:924-933
- Chernosky JV, Berman RG, Jenkins DM (1998) The stability of tremolite: New experimental data and a thermodynamic assessment. *Am Mineral* 83:726-738
- Cho M, Ernst WG (1991) An experimental determination of calcic amphibole solid solution along the join tremolite-tschermakite. *Am Mineral* 76:985-1001
- Della Ventura G (1992) Recent developments in the synthesis and characterization of amphiboles. *Synthesis and crystal-chemistry of richterites*. *Trends in Mineral* 1:153-192
- Della Ventura G, Robert J-L (1990) Synthesis, XRD and FTIR studies of strontium richterites. *Eur J Mineral* 2:171-175
- Della Ventura G, Robert J-L, Bény J-M (1991) Tetrahedrally coordinated Ti⁴⁺ in synthetic Ti-rich potassic richterite: Evidence from XRD, FTIR, and Raman studies. *Am Mineral* 76:1134-1140
- Della Ventura G, Robert J-L, Bény J-M, Raudsepp M, Hawthorne FC (1993a) The OH-F substitution in Ti-rich potassium-rich richterites: Rietveld structure refinement and FTIR and micro-Raman spectroscopic studies of synthetic amphiboles in the system K₂O-Na₂O-CaO-MgO-SiO₂-TiO₂-H₂O-HF. *Am Mineral* 78:980-987
- Della Ventura G, Robert J-L, Raudsepp M, Hawthorne FC (1993b) Site occupancies in monoclinic amphiboles: Rietveld structure refinement of synthetic nickel magnesium cobalt potassium richterite. *Am Mineral* 78:633-640
- Della Ventura G, Robert J-L, Hawthorne FC (1996a) Infrared spectroscopy of synthetic (Ni,Mg,Co)-potassium richterite. *In: Mineral Spectroscopy: A Tribute to Roger G. Burns*. Dyar MD, McCammon C, Schaefer MW (eds) *Geochem Soc Spec Pub No.* 5:55-63
- Della Ventura G, Robert J-L, Hawthorne FC, Prost R (1996b) Short-range disorder of Si and Ti in the tetrahedral double-chain unit of synthetic Ti-bearing potassium richterite. *Am Mineral* 81:56-60
- Della Ventura G, Robert JL, Raudsepp M, Hawthorne FC, Welch MD (1997) Site occupancies in synthetic monoclinic amphiboles: Rietveld structure refinement and infrared spectroscopy of (nickel, magnesium, cobalt)-richterite. *Am Mineral* 82:291-301
- Della Ventura G, Robert J-L, Hawthorne FC, Raudsepp M, Welch MD (1998a) Contrasting patterns of ⁶Al order in synthetic pargasite and Co-substituted pargasite. *Can Mineral* 36:1237-1244
- Della Ventura G, Robert J-L, Hawthorne FC (1998b) Characterization of OH-F short-range order in potassium-fluor-rich richterite by infrared spectroscopy in the OH-stretching region. *Can Mineral* 36:181-185
- Della Ventura G, Hawthorne FC, Robert J-L, Delbove F, Welch MF, Raudsepp M (1999) Short-range order of cations in synthetic amphiboles along the richterite-pargasite join. *Eur J Mineral* 11:79-94
- Della Ventura G, Robert J-L, Sergent J, Hawthorne FC, Delbove F (2001) Constraints on F vs. OH incorporation in synthetic ⁶Al-bearing in monoclinic amphiboles. *Eur J Mineral* 13:841-847
- Della Ventura G, Oberti R, Hawthorne FC, Bellatreccia F (2007) Single-crystal FTIR study of Ti-rich pargasites from Lherz: Detection and short-range order of ⁰⁽³⁾O²⁻ in amphiboles. *Am Mineral* (accepted)
- Dyar MD, Mackwell SJ, McGuire AV, Cross LR, Robertson JD (1993) Crystal chemistry of Fe³⁺ and H⁺ in mantle kaersutite: Implications for mantle metasomatism. *Am Mineral* 78:968-979
- Ernst WG, Wai CM (1970) Mössbauer, infrared, X-ray and optical study of cation ordering and dehydrogenation in natural and heat-treated sodic amphiboles. *Am Mineral* 55:1226-1258
- Fialips-Guédon CI, Robert J-L, Delbove F (2000) Experimental study of Cr incorporation in pargasite. *Am Mineral* 85:687-693
- Gottschalk M, Andrut M (2003) Crystal chemistry of tremolite-tschermakite solid solutions. *Phys Chem Mineral* 30:108-124
- Gottschalk M, Najorka J, Andrut M (1998) Structural and compositional characterization of synthetic (Ca,Sr)-tremolite and (Ca,Sr)-diopside solid-solutions. *Phys Chem Mineral* 25:415-428
- Gottschalk M, Andrut M, Melzer S (1999) The determination of cummingtonite content of synthetic tremolite. *Eur J Mineral* 11:967-982
- Hanisch K (1966) Messung des Ultrarot-Pleochroismus von Mineralen. VI. Der Pleochroismus des OH-Streckfrequenz in Riebeckit. *Neues Jahrb Mineral Monatsh* 109-112
- Hawthorne FC (1983) The crystal chemistry of the amphiboles. *Can Mineral* 21:173-480
- Hawthorne FC (1997) Short-range order in amphiboles: a bond-valence approach. *Can Mineral* 35:201-216
- Hawthorne FC, Grundy HD (1976) The crystal chemistry of the amphiboles. IV. X-ray and neutron refinements of the crystal structure of tremolite. *Can Mineral* 14:334-345
- Hawthorne FC, Oberti R (2007) Amphiboles: crystal chemistry. *Rev Mineral Geochem* 67:1-54
- Hawthorne FC, Waychunas GA (1988) Spectrum Fitting Methods. *Rev Mineral* 18:63-98

- Hawthorne FC, Ungaretti L, Oberti R, Bottazzi P, Czamanske GK (1993) Li: An important component in igneous alkali amphiboles. *Am Mineral* 78:733-745
- Hawthorne FC, Ungaretti L, Oberti R, Cannillo E, Smelik EA (1994) The mechanism of ^{6}Li incorporation in amphiboles. *Am Mineral* 79:443-451
- Hawthorne FC, Oberti R, Cannillo E, Sardone N, Zanetti A, Grice JD, Ashley PM (1995) A new anhydrous amphibole from the Hoskins mine, Grenfell, New South Wales, Australia: Description and crystal structure of ungarettiite, $\text{NaNa}_2(\text{Mn}^{2+}_2\text{Mn}^{3+}_3)\text{Si}_8\text{O}_{22}\text{O}_2$. *Am Mineral* 80:165-172
- Hawthorne FC, Oberti R, Sardone N (1996a) Sodium at the A site in clin amphiboles: the effects of composition on patterns of order. *Can Mineral* 34:577-593
- Hawthorne FC, Della Ventura G, Robert J-L (1996b) Short-range order of (Na,K) and Al in tremolite: An infrared study. *Am Mineral* 81:782-784
- Hawthorne FC, Della Ventura G, Robert J-L (1996c) Short-range order and long-range order in amphiboles: a model for the interpretation of infrared spectra in the principal OH-stretching region. *In: Mineral Spectroscopy: A Tribute to Roger G. Burns*. Dyar MD, McCammon C, Schaefer MW (eds) *Geochem Soc Special Publication No 5*:49-54
- Hawthorne FC, Oberti R, Ungaretti L, Grice JD (1996d) A new hyper-calcic amphibole with Ca at the A site: fluor-cannilloite from Pargas, Finland. *Am Mineral* 81:995-1002
- Hawthorne FC, Della Ventura G, Robert J-L, Welch MF, Raudsepp M, Jenkins DM (1997) A Rietveld and infrared study of synthetic amphiboles along the potassium-richterite--tremolite join. *Am Mineral* 82:708-716
- Hawthorne FC, Oberti R, Zanetti A, Czamanske GK (1998) The role of Ti in hydrogen-deficient amphiboles: Sodic-calcic and sodic amphiboles from Coyote Peak, California. *Can Mineral* 36:1253-1265
- Hawthorne FC, Welch MD, Della Ventura G, Liu S, Robert J-L, Jenkins DM (2000a) Short-range order in synthetic aluminous tremolites: An infrared and triple-quantum MAS NMR study. *Am Mineral* 85:1716-1724
- Hawthorne FC, Cooper MA, Grice JD, Ottolini L (2000b) A new anhydrous amphibole from the Eifel region, Germany: Description and crystal structure of obertiite, $\text{NaNa}_2(\text{Mg}_3\text{Fe}^{3+}\text{Ti}^{4+})\text{Si}_8\text{O}_{22}\text{O}_2$. *Am Mineral* 85:236-241
- Hawthorne FC, Della Ventura G, Oberti R, Robert J-L, Iezzi G (2005) Short-range order in minerals: amphiboles. *Can Mineral* 43:1895-1920
- Hawthorne FC, Oberti R, Martin R F (2006) Short-range order in amphiboles from the Bear Lake diggings, Ontario. *Can Mineral* 44:1171-1179
- Hoschek G (1995) Stability relations and Al content of tremolite and talc in CMASH assemblages with kyanite + zoisite + quartz + H_2O . *Eur J Mineral* 7:353-362
- Huggins CM, Pimentel GC (1956) Systematics of the infrared spectral properties of hydrogen-bonded systems: frequency-shift, half width and intensity. *J Phys Chem* 60:1615-1619
- Iezzi G, Della Ventura G, Cámara F, Pedrazzi G, Robert J-L (2003) The $^{\text{B}}\text{Na}$ - $^{\text{B}}\text{Li}$ exchange in A-site vacant amphiboles: synthesis and cation ordering along the ferri-clinoferroholmquistite – riebeckite join. *Am Mineral* 88:955-961
- Iezzi G, Cámara F, Della Ventura G, Oberti R, Pedrazzi G, Robert J-L (2004) Synthesis, crystal structure and crystal-chemistry of ferri-clinoholmquistite, $\square\text{Li}_2\text{Mg}_3\text{Fe}^{3+}_2\text{Si}_8\text{O}_{22}(\text{OH})_2$. *Phys Chem Mineral* 31:375-385
- Iezzi G, Della Ventura G, Hawthorne FC, Pedrazzi G, Robert J-L, Novembre D (2005) The $(\text{Mg},\text{Fe}^{2+})$ substitution in ferri-clinoholmquistite, $\square\text{Li}_2(\text{Mg},\text{Fe}^{2+})_3\text{Fe}^{3+}_2\text{Si}_8\text{O}_{22}(\text{OH})_2$. *Eur J Mineral* 17:733-740
- Jasmund K, Schäfer R (1972) Experimentelle Bestimmung der P-T-Stabilitätsbereiche in der Mischkristallreihe Tremolit-Tschermakite. *Contrib Mineral Petrol* 34:101-115
- Jenkins DM (1981) Experimental phase relations of hydrous peridotites modelled in the system H_2O -CaO-MgO-Al $_2\text{O}_3$ -SiO $_2$. *Contrib Mineral Petrol* 77:166-176
- Jenkins DM (1983) Stability and composition relations of calcic amphiboles in ultramafic rocks. *Contrib Mineral Petrol* 83:375-384
- Jenkins DM (1987) Synthesis and characterization of tremolite in the system H_2O -CaO-MgO-SiO $_2$. *Am Mineral* 72:707-715
- Jenkins DM (1988) Experimental study of the join tremolite-tschermakite: A reinvestigation. *Contrib Mineral Petrol* 99:392-400
- Jenkins DM (1994) Experimental reversal of the aluminum content in tremolitic amphiboles in the system H_2O -CaO-MgO-Al $_2\text{O}_3$ -SiO $_2$. *Am J Sci* 294:593-620
- Jenkins DM, Clare AK (1990) Comparison of the high-temperature and high-pressure stability limits of synthetic and natural tremolite. *Am Mineral* 75:358-366
- Jenkins DM, Sherriff BL, Cramer J, Xu Z (1997) Al, Si, and Mg occupancies in tetrahedrally and octahedrally coordinated sites in synthetic aluminous tremolite. *Am Mineral* 82:280-290
- Jirak Z, Pechar F, Vratislav S (1986) Distribution of cations and the proton location in kaersutite. *Cryst Res Technol* 21:1517-1519
- Kitamura M, Tokonami M (1971) The crystal structure of kaersutite. *Sci Rep Tohoku Univ, Ser 3* 11:125-141

- Kitamura M, Tokonami M, Koto K, Horiuchi H, Morimoto N (1973) Cation ordering in kaersutite by neutron diffraction. *Mineral Soc Japan J* 11:49
- Kitamura M, Tokonami M, Morimoto N (1975) Distribution of titanium atoms in oxy-kaersutite. *Contrib Mineral Petrol* 51:167-172
- Law AD (1976) A model for the investigation of hydroxyl spectra of amphiboles. *In: The Physics and Chemistry of Minerals and Rocks*. Strens RGJ (ed) J. Wiley and Sons, London, p 677-686
- Leake BE (1968) A catalog of analyzed calciferous and subcalciferous amphiboles together with their nomenclature and associated minerals. *Geol Soc Am Spec Pap* 98
- Mottana A, Paris E, Della Ventura G, Robert, J-L (1990) Spectroscopic evidence for tetrahedrally-coordinated titanium in richteritic amphiboles. *Rend Fis Accad. Lincei* 1:387-392
- Najorka J, Gottschalk M (2003) Crystal chemistry of tremolite – tschermakite solid solution. *Phys Chem Mineral* 30:108-124
- Oba T (1978) Phase relationship of $\text{Ca}_2\text{Mg}_3\text{Al}_2\text{Si}_6\text{Al}_2\text{O}_{22}(\text{OH})_2$ - $\text{Ca}_2\text{Mg}_3\text{Fe}^{3+}_2\text{Si}_6\text{Al}_2\text{O}_{22}(\text{OH})_2$ join at high temperature and high pressure – the stability of tschermakite. *J Fac Sci, Hokkaido Univ Ser IV* 18:339-350
- Oberti R, Ungaretti L, Cannillo E, Hawthorne FC (1992) The behavior of Ti in amphiboles. I. Four- and six-coordinate Ti in richterite. *Eur J Mineral* 3:425-439
- Oberti R, Hawthorne FC, Ungaretti L, Cannillo E. (1995a) ^{60}Al disorder in amphiboles from mantle peridotites. *Can Mineral* 33:867-878
- Oberti R, Sardone N, Hawthorne FC, Raudsepp M, Turnock AC (1995b) Synthesis and crystal-structure refinement of synthetic fluor-pargasite. *Can Mineral* 33:25-31
- Oberti R, Hawthorne FC, Cámara F, Raudsepp M (1998) Synthetic fluoro-amphiboles: site preferences of Al, Ga, Sc and inductive effects on mean bond-lengths of octahedra. *Can Mineral* 36:1245-1252
- Oberti R, Camara F, Ottolini L, Caballero JM (2003a) Lithium in amphiboles: detection, quantification and incorporation mechanisms in the compositional space bridging sodic and ^6Li amphiboles. *Eur J Mineral* 15:309-319
- Oberti R, Camara F, Caballero JM, Ottolini L (2003b) Sodic-ferri-ferropedrizite and ferri-clinoferroholmquistite: mineral data and degree of order of the A-site cations in Li-rich amphiboles. *Can Mineral* 41:1345-1354
- Oberti R, Cámara F, Caballero JM (2004) Ferri-ottoliniite and ferriwhittakerite, two new end-members of the new Group 5 for monoclinic amphiboles. *Am Mineral* 88:888-893
- Oberti R, Camara F, Della Ventura G, Iezzi G, Benimoff AI (2006) Parvo-mangano edenite, parvo-mangano tremolite, and the solid-solution between Ca and Mn^{2+} at the M4 site in amphiboles. *Am Mineral* 91:526-532
- Oberti R, Della Ventura G, Cámara F (2007a) New amphibole compositions: natural and synthetic. *Rev Mineral Geochem* 67:89-123
- Oberti R, Hawthorne FC, Cannillo E, Cámara F (2007b) Long-range order in amphiboles. *Rev Mineral Geochem* 67:124-171
- Papike JJ, Cameron KL, Baldwin K (1969) Crystal chemical characterization of clin amphiboles based on five new structure refinements. *Mineral Soc Am Spec Pap* 2:117-136
- Paris E, Mottana A, Della Ventura G, Robert J-L (1993) Titanium valence and coordination in synthetic richterite-Ti-richterite amphiboles: A synchrotron-radiation XAS study. *Eur J Mineral* 5:455-464
- Pauling L (1929) The principles determining the structures of complex ionic crystals. *J Am Chem Soc* 51:1010-1026
- Pechar F, Fuess H, Joswig W (1989) Refinement of the crystal structure of kaersutite (Vlčí Hora, Bohemia) from neutron diffraction. *Neues Jahrb Mineral Mh* 1989:137-143
- Popp RK, Virgo D, Phillips M (1995) H deficiency in kaersutitic amphiboles: Experimental verification. *Am Mineral* 80:1347-1350
- Preiser C, Lösel J, Brown ID, Kunz M, Skowron A (1999) Long range Coulomb forces and localized bonds. *Acta Crystallogr B* 55:698-711
- Quirion DM, Jenkins DM (1998) Dehydration and partial melting of tremolitic amphibole coexisting with zoisite, quartz, anorthite, diopside, and water in the system H_2O -CaO-MgO- Al_2O_3 - SiO_2 . *Contrib Mineral Petrol* 130:379-389
- Raudsepp M, Turnock AC, Hawthorne FC, Sherriff BL, Hartman JS (1987a) Characterization of synthetic pargasitic amphiboles ($\text{NaCa}_2\text{Mg}_3\text{M}^{3+}\text{Si}_6\text{Al}_2\text{O}_{22}(\text{OH},\text{F})_2$; $\text{M}^{3+} = \text{Al}, \text{Cr}, \text{Ga}, \text{Sc}, \text{In}$) by infrared spectroscopy, Rietveld structure refinement and ^{27}Al , ^{29}Si , and ^{19}F MAS NMR spectroscopy. *Am Mineral* 72:580-593
- Raudsepp M, Turnock AC, Hawthorne FC (1987b) Characterization of cation ordering in synthetic scandium-fluor-eckermannite, indium-fluor-eckermannite and scandium-fluor-nyböite by Rietveld structure refinement. *Am Mineral* 72:959-964
- Raudsepp M, Turnock AC, Hawthorne FC (1991) Amphiboles synthesis at low-pressure: what grows and what doesn't. *Eur J Mineral* 3:983-1004
- Reece JJ, Redfern SAT, Welch MD, Henderson CMB, McCammon CA (2002) Temperature-dependent Fe^{2+} - Mn^{2+} order-disorder behavior in amphiboles. *Phys Chem Mineral* 29:562-570

- Robert J-L, Della Ventura G, Thauvin J-L (1989) The infrared OH-stretching region of synthetic richterites in the system $\text{Na}_2\text{O}-\text{K}_2\text{O}-\text{CaO}-\text{MgO}-\text{SiO}_2-\text{H}_2\text{O}-\text{HF}$. *Eur J Mineral* 1:203-211
- Robert J-L, Della Ventura G, Hawthorne FC (1999) Near-infrared study of short-range disorder of OH and F in monoclinic amphiboles. *Am Mineral* 84:86-91
- Robert J-L, Della Ventura G, Welch MD, Hawthorne FC (2000) The OH-F substitution in synthetic pargasite at 1.5 kbar, 850°C. *Am Mineral* 85:926-931
- Rowbotham G, Farmer VC (1974) The effect of the "A" site occupancy upon the hydroxyl stretching frequency in clin amphiboles. *Contrib Mineral Petrol* 38:147-149
- Saxena SK, Ekstrom TK (1970) Statistical chemistry of calcic amphiboles. *Contrib Mineral Petrol* 26:276-284
- Semet MP (1973) A crystal-chemical study of synthetic magnesiohastingsite. *Am Mineral* 58:480-494
- Shannon RD (1976) Revised effective ionic radii and systematic studies of interatomic distances in halides and chalcogenides. *Acta Crystallogr A* 32:751-767
- Skogby H, Rossman GR (1991) The intensity of amphibole OH bands in the infrared absorption spectrum. *Phys Chem Mineral* 18:64-68
- Smelik EA, Jenkins DM, Navrotsky A (1994) A calorimetric study of synthetic amphiboles along the tremolite-tschermakite join and the heats of formation of magnesiohornblende and tschermakite. *Am Mineral* 79:1110-1122
- Strens RGJ (1966) Infrared study of cation ordering and clustering in some (Fe,Mg) amphibole solid solutions. *Chem Comm (Chem Soc London)* 15:519-520
- Strens RGJ (1974) The common chain, ribbon and ring silicates. *In: The Infrared Spectra of Minerals*. Farmer VC (ed) Mineralogical Society, London, p 305-330
- Tait KT, Hawthorne FC, Grice JD, Ottolini L, Nayak VK (2005) Dellaventuraite, $\text{NaNa}_2(\text{MgMn}^{3+}_2\text{Tl}^{4+}\text{Li})\text{Si}_8\text{O}_{22}\text{O}_2$, a new anhydrous amphibole from the Kajlidongri Manganese Mine, Jhabua District, Madhya Pradesh, India. *Am Mineral* 90:304-309
- Wagner C, Velde D (1986) The mineralogy of K-richterite bearing lamproites. *Am Mineral* 71:17-37
- Welch MD, Knight KS (1999) A neutron powder diffraction study of cation ordering in high-temperature synthetic amphiboles. *Eur J Mineral* 11:321-331
- Welch MD, Kolodziejewski W, Klinowski J (1994) A multinuclear NMR study of synthetic pargasite. *Am Mineral* 79:261-268
- Zanetti A, Vannucci R, Bottazzi P, Oberti R, Ottolini L (1996) Infiltration metasomatism at Lherz as monitored by systematic ion-microprobe investigations close to a hornblende vein. *Chem Geol* 134:113-133

APPENDIX I: (Mg,Fe²⁺) ORDER-DISORDER AND BAND INTENSITIES IN THE IR SPECTRUM

As the bands A, B, C and D are related to different short-range arrangements of the $M(1)$ and $M(3)$ cations around $O(3)$, then the relative intensities of these bands are related to the relative frequencies of occurrence of these short-range arrangements in the structure; moreover, the sum of all the short-range arrangements must be equal to the bulk composition. Strens (1966, 1974) derived the criteria for identifying both LRO and SRO, but Law (1976) showed that these criteria are not correct. Law (1976) developed a model for LRO assuming no SRO is present, but application to two amphiboles characterized by crystal-structure refinement and Mössbauer spectroscopy showed poor agreement between the various site-occupancies.

Following Strens (1966, 1974) and Law (1976), we may write the site occupancies and C-group-cation composition as follows:

$$\begin{aligned} y_{M(1)} &= M^{2+} \text{ at } M(1) \\ y_{M(3)} &= M^{2+} \text{ at } M(3) \\ x_{M(1)} &= \text{Mg at } M(1) \\ x_{M(3)} &= \text{Mg at } M(3) \end{aligned} \quad (\text{A1})$$

$$\begin{aligned} X &= \text{total Mg at } M(1,3) = 2 x_{M(1)} + x_{M(3)} \\ Y &= \text{total } M^{2+} \text{ at } M(1,3) = 2 y_{M(1)} + y_{M(3)} \end{aligned} \quad (\text{A2})$$

We may express all occupancies in terms of x and y by manipulating Equations (A1) and (A2):

$$\begin{aligned} x_{M(1)} &= 1 - y_{M(1)} = 1 - 1/2 [Y - y_{M(3)}] \\ y_{M(1)} &= 1/2 [Y - y_{M(3)}] \\ x_{M(3)} &= 1 - y_{M(3)} \end{aligned} \quad (\text{A3})$$

For no SRO, the relative intensities of the bands, $I_{A,B,C,D}^C$ are given by

$$\begin{aligned} I_A^C &= x_{M(1)}^2 x_{M(3)} \\ I_B^C &= x_{M(1)}^2 y_{M(3)} + 2 x_{M(1)} y_{M(1)} x_{M(3)} \\ I_C^C &= y_{M(1)}^2 x_{M(3)} + 2 x_{M(1)} y_{M(1)} y_{M(3)} \\ I_D^C &= y_{M(1)}^2 y_{M(3)} \end{aligned} \quad (\text{A4})$$

where the superscript C on the band intensities denotes that they are *calculated* values. Substituting (A2) into (A3) gives the following:

$$\begin{aligned} I_A^C &= 1 - 1/2 [Y - y_{M(3)}]^2 (1 - y_{M(3)}) \\ I_B^C &= (1 - 1/2 [Y - y_{M(3)}])^2 y_{M(3)} + 2 (1 - 1/2 [Y - y_{M(3)}]) 1/2 [Y - y_{M(3)}] (1 - y_{M(3)}) \\ I_C^C &= 1/4 [Y - y_{M(3)}]^2 (1 - y_{M(3)}) + 2 (1 - 1/2 [Y - y_{M(3)}]) 1/2 [Y - y_{M(3)}] y_{M(3)} \\ I_D^C &= 1/4 [Y - y_{M(3)}]^2 y_{M(3)} \end{aligned} \quad (\text{A5})$$

Equation (A5) give the calculated band intensities as a function of cation order (i.e., $y_{M(3)}$) for a specific composition Y where there is no SRO present (i.e., there is short-range disorder). Following Law (1976), we may assume that there is no SRO and use Equation (A5) to derive the state of LRO from the observed values of the band intensities ($I_{A,B,C,D}^O$). Alternatively, we may measure the state of LRO (i.e., $y_{M(3)}$) by some other method (e.g., Rietveld refinement, Raudsepp et al. 1987a,b; Della Ventura et al. 1993a, b) and use the observed ($I_{A,B,C,D}^O$) and calculated ($I_{A,B,C,D}^C$) band intensities to derive information on SRO of divalent cations over the $M(1)$ and $M(3)$ sites (Hawthorne et al. 1996c; Della Ventura et al. 1996a).

Non-Ambient *in situ* Studies of Amphiboles

Mark D. Welch

*Department of Mineralogy The Natural History Museum
Cromwell Road, London SW7 5BD, United Kingdom
mdw@nhm.ac.uk*

Fernando Cámara

*Istituto di Geoscienze e Georisorse, Consiglio Nazionale delle Ricerche
I-27100 Pavia, Italy
camara@crystal.unipv.it*

Giancarlo Della Ventura

*Dipartimento di Scienze Geologiche
Università di Roma Tre, I-00146 Roma, Italy
dellaven@uniroma3.it*

Gianluca Iezzi

*Dipartimento di Scienze della Terra, Università G. D'Annunzio
I-66013 Chieti Scalo, Italy
g.iezzi@unich.it*

INTRODUCTION

This chapter is concerned with *in situ* studies of the structural behavior of amphiboles under non-ambient conditions. Relatively few such studies have been made compared with those on samples studied under ambient conditions (room- P and T), which form the staple of many spectroscopic and diffraction studies of short-range and long-range order.

Collecting data under non-ambient conditions often imposes significant additional complexities in the data-collection and data-handling procedures than are necessary in ambient studies. For example, collecting high-pressure X-ray data for a sample in a diamond-anvil cell (DAC) usually means a much-reduced dataset due to limited access to reciprocal space (about 40%) imposed by the pressure cell. In order to get good coverage of reciprocal space, it is sometimes necessary to run two crystals of the same sample cut and mounted in the DAC in different orientations. The presence of pressure or temperature assemblies (DACs, multi-anvil devices, cryostats, furnaces) also requires the application of high-quality background corrections. Suffice it to say that many non-ambient *in situ* experiments are not trivial to perform and, in some cases, they require access to national facilities (e.g., synchrotron and neutron sources). For these reasons, non-ambient *in situ* studies are much less common than “quench-and-look” approaches (particularly spectroscopy), which tend to focus upon compositional systematics. However, the importance of *in situ* studies of non-ambient behavior cannot be overstated. Many materials undergo non-quenchable displacive phase transitions at high pressure and high temperature, and these transitions can produce microtextures and be associated with anomalous thermodynamic behavior. The determination of compressibilities and expansivities provides fundamental thermodynamic data and allows the behavioral trends to be identified between structurally and compositionally related phases.

It is well-known that monoclinic amphiboles with significant Mg occupancy of $M(4)$ undergo a reversible displacive phase transition involving $P2_1/m$ and $C2/m$ polymorphs. For the studies reported here, which are either variable- T /room- P or variable- P /room- T , the transitions are P -induced $C2/m \rightarrow P2_1/m$ or T -induced $P2_1/m \rightarrow C2/m$. However, recent studies have reported evidence for the existence of a high- P transition from the $P2_1/m$ to a new $C2/m$ structure which has highly-kinked (rotated) double-chains of tetrahedra, unlike the low- P /high- T $C2/m$ structure which has almost straight chains. It will ensure clarity later if we now follow the literature and distinguish the two different C -centered amphiboles as HT- $C2/m$ and HP- $C2/m$. A corresponding transition and HP- $C2/c$ polymorph has been identified in clinopyroxene containing significant Mg at $M(2)$, the pyroxene counterpart of the amphibole $M(4)$ site. We discuss this transition in detail toward the end of the chapter.

This chapter is divided into three parts. The first section deals with T - and P -induced structural phase transitions in amphiboles, and focuses primarily on the $P2_1/m \leftrightarrow$ HT- $C2/m$ transition in natural cummingtonite and synthetic $^A\text{Na}^B(\text{Na}_x\text{Li}_{1-x}\text{Mg})_2^C\text{Mg}_5^D\text{Si}_8\text{O}_{22}^E(\text{OH},\text{F})_2$ amphiboles, comparing their characteristics with those of the analogous $P2_1/c \leftrightarrow$ HT- $C2/c$ transition in pyroxenes. The second section of the chapter is concerned with *in situ* studies of temperature-induced non-convergent cation disorder in cummingtonite and ^BMg -analogues of richterite, with some surprising results. Finally, we finish with a brief discussion of compressibilities and thermal expansivities.

TRANSITIONAL BEHAVIOR

Compared with pyroxene, relatively few studies of amphibole structural behavior as a function of P and T have been made. In part, this is due to the much lower thermal stability of amphibole at room- P in the absence of water-saturated experimental conditions, so that the window for studying interesting high- T behavior is quite limited (usually < 700 °C). Until very recently, studies of pressure-induced transitional behavior have been largely restricted to the cummingtonite-grunerite join.

The nature of the $P2_1/m \leftrightarrow$ HT- $C2/m$ transition in amphiboles

The dependence of the displacive $P2_1/m \leftrightarrow$ HT- $C2/m$ transition in cummingtonite upon T , P and composition has been studied extensively over the past 15 years. Most studies infer that the transition arises from the behavior of the distorted $M(4)$ polyhedron coupled with rotations of the adjacent tetrahedra (e.g., Prewitt et al. 1970; Sueno et al. 1972; Zhang et al. 1992; Yang and Smith 1996; Yang et al. 1998; Boffa Ballaran et al. 2000, 2001, 2004; Reece et al. 2000). The oxygen atoms bonded to the $M(4)$ cation [O(2), O(4), O(5), O(6)] lie on general positions, affording this polyhedron considerable flexibility: this site can accommodate a wide range of monovalent and divalent cations (Na, Li, K, Mg, Ca, Fe, Mn, Sr) of radii ranging from Mg^{2+} ($r_{\text{oct}} = 0.72$ Å) to K^+ ($r_{\text{oct}} = 1.38$ Å). The key pre-requisite for potential P - C transitional behavior in amphibole and pyroxene is the presence of a significant proportion of a small cation at the $M(4)$ site. In all studies of the P - C transition in amphibole, this small cation is Mg^{2+} and sometimes accompanied by Li.

In $C2/m$ cummingtonite and synthetic $^A\text{Na}^B(\text{Na}_{1-x}\text{Li}_x\text{Mg})^C\text{Mg}_5\text{Si}_8\text{O}_{22}^E(\text{OH},\text{F})_2$, there are four short bonds at $2 - 2.2$ Å to O(2) and O(4) and two longer bonds to O(6) at $2.65 - 2.80$ Å; the two $M(4)$ -O(5) distances are > 3.1 Å. Thus, $M(4)$ is effectively in [6]-fold [4 + 2] coordination (Fig. 1). At room conditions, in $P2_1/m$ cummingtonite, the four short bonds involve the O(2A), O(2B), O(4A) and O(4B) atoms; O(6A) is closer to $M(4)$ (< 2.5 Å), whereas O(6B) is further away (> 2.8 Å) and O(5A) and O(5B) remain effectively unbonded to $M(4)$ (> 3.1 Å), as O(5) in $C2/m$. Thus, the coordination in $P2_1/m$ cummingtonite is [4 + 1 + 1] (Fig. 1). At high pressures both $M(4)$ -O(6A) and $M(4)$ -O(5B) become shorter (< 2.30 and 2.55 Å,

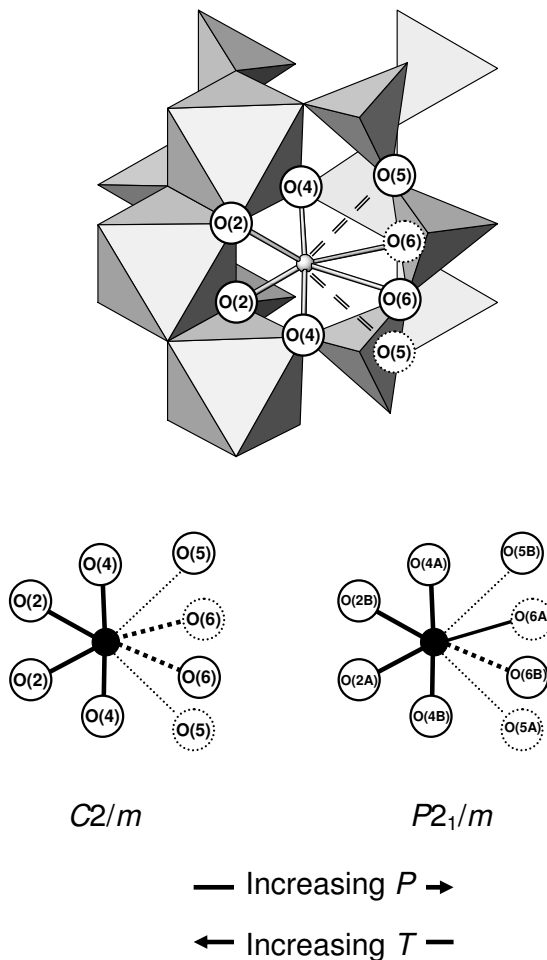


Figure 1. The environment of the $M(4)$ site in clin amphibole. The top figure shows the $M(4)$ site of the $HT-C2/m$ polymorph in which the coordination of the cation can be considered as a distorted octahedron involving O(2), O(4) and O(6) oxygen atoms, or an 8-fold distorted square antiprism which includes the two more distant O(5) oxygen atoms. Beware that both coordinations are calculated and quoted in the literature, so that $\langle r_{M(4)} \rangle$ may refer to either coordination. The $[4 + 2]$ and $[4 + 1 + 1]$ [6]-coordinations of the $M(4)$ cation that are characteristic of $HT-C2/m$ and $P2_1/m$ polymorphs, respectively, are also shown.

respectively) and effective coordination becomes $[5 + 1]$. It is the response of the O(2)-O(4)-O(6)/O(2A,B)-O(4A,B)-O(6A,B) octahedron to P , T and composition that has been the focus of most work on the $P2_1/m \leftrightarrow HT-C2/m$ transition.

The amphibole structure can be regarded as comprising alternating layers of octahedra and tetrahedra parallel to (100). As the sizes of the polyhedra vary, linkage can be maintained by rotation of the tetrahedra of the double chain through an axis orthogonal to the layers. Two types of rotations can be defined: S-rotation (bringing the triangular basal face of a tetrahedron into the parallel orientation with the adjacent octahedron faces at the apex of the tetrahedron) and O-rotation (bringing the basal triangular face of a tetrahedron into the opposite orientation to the adjacent parallel octahedron faces). In the $P2_1/m$ structure there is an S-rotated A-chain and an O-rotated B-chain, whereas the unique double-chain of the $C2/m$ structure is

O-rotated. The degree of chain rotation is characterized by the O(5)-O(6)-O(5) angle (Fig. 1). The distortion of the $M(4)$ polyhedron occurs by coupled rigid rotations of the tetrahedra in the adjacent double chain: expansion causes straightening of the double-chain, whereas shortening causes kinking. Given the nature of the structural changes associated with the phase transition, it can be expected that increasing pressure will stabilize the $P2_1/m$ structure and, conversely, increasing temperature will stabilize the $C2/m$ structure. Hence, in P - T space, compositional isopleths for the transition will have positive $\partial P/\partial T$ and, at fixed pressure, T_c will decrease with increasing substitution of a larger cation at $M(4)$, e.g., Fe for Mg in cummingtonite. Similarly, at fixed temperature, P_c increases with increasing substitution of the larger cation at $M(4)$, as this substitution favors the $C2/m$ structure. Having outlined these trends and their structural basis, we now describe the details of P - C transitional behavior in specific amphiboles and recognize significant compositional trends, including the effects of different degrees of long-range order on P_c and T_c , i.e., ordering involving preferential occupancy of $M(4)$ by larger cations.

Application of the Landau Theory of phase transitions

As in many other cases, much of the insight into the thermodynamics of the $P2_1/m \leftrightarrow HT-C2/m$ transition in amphiboles has come from the application of Landau Theory, a mean-field theory, which uses a macroscopic description of structural change (e.g., variations in the relative intensities of superlattice and sublattice reflections) to quantify key physical variables such as P_c and T_c . Indeed, it provides a consistent method by which to determine values for these variables, rather than by simply fitting arbitrary functions to transition data. An excellent description of the theoretical basis of Landau Theory, including a discussion of its successes and limitations, is given by Dove (1997). Detailed didactic mineralogical examples of the application of Landau Theory are given by Carpenter et al. (1998). A key feature of the theory is that it incorporates the effects of symmetry constraints upon the transition. In as far as a basic understanding of the approach is useful for what follows and will help readers to engage more fully with the literature, we now give a short summary of the basis for using structural data to determine the thermodynamic characteristics of structural phase transitions.

The goal of this approach is to use experimental observations to quantify the excess free-energy, G_{excess} , associated with the transition. To this end, it is necessary to recognize a fully-ordered state and to define an "order-parameter," Q , that varies from unity for the fully-ordered state to zero for the fully-disordered state. In practice this amounts to identifying suitable properties or characteristics of a phase transition. In selecting such a property/parameter, it is essential to identify how that property/parameter relates to Q . Any suitably sensitive physical property that is measured through the transition, (e.g., quadrupole splitting, ΔE_Q , and/or the relative intensities of superlattice and sublattice reflections) can be regarded as a measure of the order-parameter.

For example, in the case of P - C displacive transitions in amphibole and pyroxene, the ratio of the intensities of $h + k = odd$ (type- b , the reflections incompatible with the high-symmetry C -centered lattice) and $h + k = even$ reflections (type- a), abbreviated as " I_{odd}/I_{even} " or " I_b/I_a ," is a very reliable index of the progress of the transition (Fig. 2). In general, the intensity of superlattice reflections is proportional to Q^2 (Bruce and Cowley 1981).

The variation of Q with P or T (or X) is, via the Landau formalism, correlated with the excess free energy, G_{excess} , of the transition and formulated as a Taylor expansion of the excess free energy in Q . The character of this expansion depends upon the order of the transition. A second-order transition has only even coefficients (typically 2-4, 2-6, or 2-4-6), whereas a first-order transition also requires odd terms (see discussion in Dove 1997). For a continuous (second-order or tricritical) transition, the temperature variation of G_{excess} is:

$$G_{excess} = \frac{1}{2}a(T - T_c)Q^2 + \frac{1}{4}bQ^4 + \frac{1}{6}cQ^6 + \dots \quad (1)$$

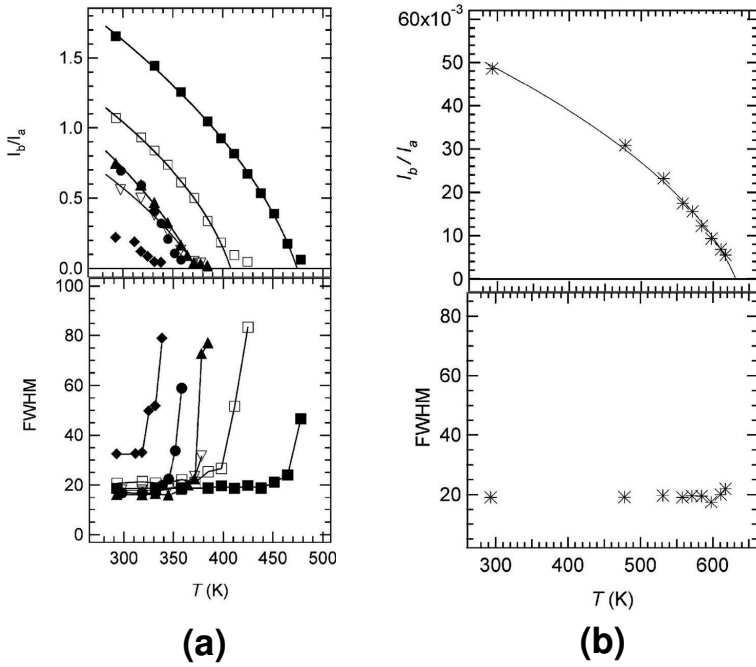


Figure 2. (a) Comparison of I_b/I_a and Γ_b as indices of the $P2/m \rightarrow HT-C2/m$ transition for a series of Mg-Fe²⁺ cummingtonites. The open and filled squares are for unheated and heat-treated samples having $X_{Fe} = 0.22$. The intensity data are fit to a 2-4-6 Landau potential. (b) Fe-free cummingtonite. From Boffa Ballaran et al. (2004).

where T_c is the “critical temperature” of the transition and a, b, c, \dots are called the Landau coefficients. In most cases, six or fewer fractional coefficients are needed to describe the transition adequately. T_c (or P_c) is found by fitting the most appropriate Taylor expansion to the data. The values of the Landau coefficients depend upon the order of transition, and so provide this key information.

Differentiation of G_{excess} with respect to Q gives the equilibrium relation:

$$\frac{\partial G}{\partial Q} = 0 = a(T - T_c)Q + bQ^3 + cQ^5 \tag{2}$$

and recognizing that

$$T = T_c - \frac{b}{a}Q^2 - \frac{c}{a}Q^4 \tag{3}$$

Landau Theory identifies the following relation between Q and T (or P) for displacive transitions:

$$Q = \left[\frac{T_c - T}{T_c} \right]^\beta \tag{4}$$

whence

$$\ln Q = \beta \ln \left[\frac{T_c - T}{T_c} \right] \tag{5}$$

in which the exponent β is called the “critical exponent”; for an ideally second-order transition, $\beta = 1/2$, and for ideally tricritical behavior $\beta = 1/4$. The order of a transition can be found by determining β from a plot of $\ln Q$ against $\ln [(T_c - T)/T_c]$, the critical temperature having been determined from Equation (3). The value of the quadratic term in Equation (3) (i.e., the b/a Landau parameter) indicates the order of the transition: it is negative for first-order and positive for second-order transitions. The temperature dependence of Q can now be used to derive T_c , the critical temperature of the transition (and similarly for P_c). Correct determination of this parameter is essential for comparing transitions in different materials, e.g., the compositional dependence of P_c or T_c for the P - C transition in different amphiboles.

If we now consider that the change in symmetry is induced by changing the pressure, the effect of pressure can be included explicitly in the Landau expansion:

$$G_{\text{excess}} = \frac{1}{2}a(T - T_c)Q^2 + \frac{1}{4}bQ^4 + \frac{1}{6}cQ^6 + \dots + \frac{1}{2}a_v P Q^2 \quad (6)$$

that rearranges to

$$G_{\text{excess}} = \frac{1}{2}a \left[T - \left(T_c - \frac{a_v}{a} P \right) \right] Q^2 + \frac{1}{4}bQ^4 + \frac{1}{6}cQ^6 + \dots \quad (7)$$

for which T_c is the transition temperature at zero pressure and $T_c^* = T_c - (a_v/a)P$ is the transition temperature at non-zero pressure. At constant temperature the transition pressure can be derived from the expression:

$$P_c = \frac{a}{a_v}(T_c - T) \quad (8)$$

Substitution back into Equation (7) gives:

$$G_{\text{excess}} = \frac{1}{2}a_v(P - P_c)Q^2 + \frac{1}{4}bQ^4 + \frac{1}{6}cQ^6 + \dots \quad (9)$$

that at equilibrium ($\partial G/\partial Q = 0$) becomes:

$$Q = \left[\frac{a_v}{b}(P_c - P) \right]^\beta \quad (10)$$

where $\beta = 1/2$ for a second-order transition and $\beta = 1/4$ if it is tricritical.

Equating I_b/I_a with Q^2 in Equation (3) allows determination of the coefficients. Although the $P2_1/m \leftrightarrow HT-C2/m$ transition in amphibole is always continuous or near-continuous (second-order or tricritical, depending on the amphibole), the corresponding $P2_1/c \leftrightarrow C2/c$ transition in pyroxene can be first-order, second-order or tricritical. We shall return to this comparison toward the end of the chapter. Figure 2 shows the variations of I_b/I_a and $\Gamma(I_b)$ (Γ = FWHM, the full-width of a peak at half-maximum height) with T through the $P2_1/m \leftrightarrow HT-C2/m$ transition for a series of cummingtonite crystals with different bulk $\text{Fe}^{2+}/(\text{Mg} + \text{Fe}^{2+})$ ratios [referred to hereafter as X_{Fe}] and the same ratio at the $M(4)$ site [defined hereafter as $X_{\text{Fe}}^{M(4)}$] (Fig. 2a), and an almost Fe-free cummingtonite (Fig. 2b). In both cases, the I_b/I_a data are fit to a 2-4-6 Landau potential. However, the behavior of $\Gamma(I_b)$ is very different: for cummingtonite, Γ increases sharply near T_c , whereas for Fe-free cummingtonite, there is almost no change at T_c . This example illustrates that Γ behaves very differently for the two types of amphibole, unlike I_b/I_a , it is not easily quantified.

One of the most easily determined features of a structural phase transition is the lattice distortion or relaxation that accompanies a displacive phenomenon at the macroscopic scale. This lattice distortion is a consequence of cooperative changes that occur at the microscopic

scale. By analogy with the spontaneous magnetization or spontaneous polarization occurring at a ferromagnetic or ferroelectric transition, the variation of the strain related to the phase transition is called the *spontaneous strain*, ϵ_s (Newnham 1974). Spontaneous strain is governed by the point-group symmetry of the crystal and is a second-rank tensor. Therefore, its tensor components can be defined as a function of the lattice parameters on the basis of the symmetry of the forms involved in the phase transition by the general equations of Schlenker et al. (1978). For the $P2_1/m \leftrightarrow C2/m$ transition, these equations simplify to

$$e_{11} = \frac{a}{a_0} - 1 \quad (11)$$

$$e_{22} = \frac{b}{b_0} - 1 \quad (12)$$

$$e_{33} = \frac{c \sin \beta}{c_0 \sin \beta_0} - 1 \quad (13)$$

$$e_{12} = e_{23} = e_{21} = e_{32} = 0 \quad (14)$$

$$e_{13} = e_{31} = \frac{1}{2} \left(\frac{c \cos \beta}{c_0 \sin \beta_0} - \frac{a \cos \beta_0}{c_0 \sin \beta_0} \right) \quad (15)$$

The volume strain is simply:

$$V_s = \frac{V}{V_0} - 1 \quad (16)$$

The quantities a , b , c , β and V are the lattice parameters of the low-symmetry form ($P2_1/m$) at a specified temperature and pressure, and a_0 , b_0 , c_0 , α_0 , β_0 and V_0 are the values associated with the high-symmetry form ($C2/m$) at that temperature and pressure had the transition not occurred (Carpenter et al. 1998). The latter values must be obtained by extrapolating the fit to the lattice-parameter data for the high-symmetry phase beyond T_c (or P_c). A linear extrapolation is often adequate where the external applied variable is T . However, an equation-of-state is required to extrapolate high-symmetry data where the externally applied variable is P . A helpful review of how to deal with extrapolation from HP data is given by Angel (2000).

The spontaneous strain can also be referred to its principal axes by diagonalization of the strain tensor. The eigenvalues (ϵ_1 , ϵ_2 , and ϵ_3) are the tensile strain along three principal orthogonal axes which can be rotated with respect to the reference axes. For strains of less than a few %, the volume strain can be approximated as $V_s = \epsilon_1 + \epsilon_2 + \epsilon_3$, and this relation provides a test of the reliability of the strain calculations.

The total strain accompanying a phase transition can be defined as the *scalar spontaneous strain*, ϵ_{ss} . Salje (1993) defined it as

$$\epsilon_{ss} = \sqrt{\sum_i e_i^2} \quad (17)$$

The spontaneous strain accompanying a phase transition is a measure of the extent of the transformation and so is an indirect way of obtaining information about the variation of the order-parameter, Q . The interaction between spontaneous strain and Q is described as strain/order-parameter coupling. Fluctuations of the order-parameter are suppressed through this coupling, thus conforming to the mean-field predictions of Landau Theory for large

temperature intervals. The excess energy due to a displacive phase transition described in terms of Equation (1) includes different contributions that are incorporated into the coefficients a , b , c Some of these contributions can be separated and expressed explicitly in the Landau free-energy expansion. In order to investigate how spontaneous strain relates to Q , we can treat the strain energy separately. We now include the Hook's law elastic energy, $\frac{1}{2}\sum_{i,k}C_{ik}^o e_i e_k$, and the "coupling energies" due to interactions between spontaneous strain and Q . Following Carpenter et al. (1998), Equation (1) transforms to:

$$G_{\text{excess}}(Q, e) = \frac{1}{2}a(T - T_c)Q^2 + \frac{1}{4}bQ^4 + \frac{1}{6}cQ^6 + \dots + \sum_{i,m,n} \lambda_{i,m,n} e_i^m Q^n + \frac{1}{2} \sum_{i,k} C_{ik}^o e_i e_k \quad (18)$$

where e_i is the i^{th} component of the strain tensor, λ_i is the coupling coefficient and C_{ik}^o are the bare elastic constants (Carpenter and Salje 1998). Equation (18) can be also expressed in terms of scalar spontaneous strain ε_{ss} as

$$G_{\text{excess}}(Q, \varepsilon) = \frac{1}{2}a(T - T_c)Q^2 + \frac{1}{4}bQ^4 + \frac{1}{6}cQ^6 + \dots + \sum_{i,m,n} \lambda_{i,m,n} \varepsilon_i^m Q^n + f\varepsilon^2 \quad (19)$$

where $\frac{1}{2}f\varepsilon^2$ corresponds to the Hook's law elastic-energy term, for which f is the spring (or force) constant and a function of the elastic constants.

At this point, it is useful to mention that in the $P2_1/m \leftrightarrow C2/m$ phase transition, both high and low-symmetry forms belong to the same crystal system (monoclinic) and so the transition is associated with a special point on the Brillouin zone boundary, and the spontaneous strain is non-symmetry-breaking, transforming as the Γ identity (co-elastic behavior, Salje 1993). This means that linear-quadratic coupling ($\lambda \varepsilon_{\text{ss}} Q^2$) is allowed by symmetry, while other coupling terms are zero (Carpenter et al. 1998).

At equilibrium, the crystal must be stress free ($\delta G/\delta \varepsilon = 0$) and hence

$$0 = \lambda Q^2 + 2f\varepsilon, \quad \text{whence } \varepsilon = -\frac{\lambda}{2f} Q^2 \quad (20)$$

Substituting for ε , Equation (19) becomes:

$$G_{\text{excess}} = \frac{1}{2}a(T - T_c)Q^2 + \frac{1}{4}bQ^4 + \frac{1}{6}cQ^6 + \dots - \frac{1}{4} \frac{\lambda^2}{f} Q^4 \quad (21)$$

and collecting terms gives

$$G_{\text{excess}} = \frac{1}{2}a(T - T_c)Q^2 + \frac{1}{4} \left(b - \frac{\lambda^2}{f} \right) Q^4 + \frac{1}{6}cQ^6 + \dots \quad (22)$$

Therefore, the effect of the strain energy is to lower the value of the fourth-order coefficient. This contribution may be sufficient to change the character of the transition from second-order in a strain-free crystal to first-order in a crystal under significant strain. The term $\lambda \varepsilon_{\text{ss}} Q^2$ also implies that Q^2 can be calculated from the variation of the lattice parameters through the phase transition.

Studies of the $P2_1/m \leftrightarrow C2/m$ transition using different experimental methods reveal some significant differences in the behavior of the order-parameter and the thermodynamic behavior of the transition as registered at the macroscopic level by long-range data from X-ray diffraction (e.g., lattice parameters, I_b/I_a , bond lengths, torsion angles) and Mössbauer spectroscopy (quadrupole splitting), compared with short-range data (e.g., ν_{OH}). The differences in order-parameter variation determined by various methods are sometimes so marked that it becomes necessary to distinguish between a "macroscopic order-parameter" Q and a "local

order-parameter" q (e.g., Boffa Ballaran et al. 2004). In terms of the mathematical treatment, both order-parameters are analogous, but they need to be distinguished in order to discuss and evaluate the different behavior they record. Figure 3 compares the values of I_b/I_a ($\propto Q^2$) with infrared-active vibrational modes ($\propto q^2$) for Mg-Fe cummingtonite with variable X_{Fe} (and $X_{\text{Fe}}^{M(4)}$); the clear non-linearity indicates differences between Q and q . The different correlation lengths of measurements giving Q or q sample different structural aspects of a phase transition, and comparison of their order-parameter behavior allows additional insight into the microscopic behavior associated with the transition.

Different P_c , T_c and transition orders imply different structural mechanisms or variations within a given mechanism. As we discuss later in comparing P - C transitional behavior in amphibole and pyroxene, the absence of first-order behavior in amphibole and its presence in pyroxene can be interpreted in terms of the subtly differing roles of the chains of tetrahedra in the two structures. Such a detailed model of the transition was obtained by the systematic application of Landau Theory to structurally-related minerals.

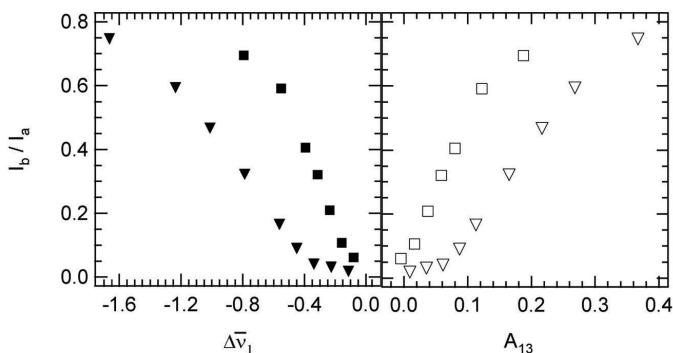


Figure 3. The relation between Q as represented here by the aggregate I_b/I_a ($\propto Q^2$) and the local order-parameter, q , derived from spectroscopic measurements of infrared vibrational modes (and one a mode difference) of cummingtonite. The non-linearity indicates a significant difference between Q and q . From Boffa Ballaran et al. (2004).

Spectroscopy of structural phase transitions in amphibole: introductory comments

Infrared spectroscopy has proven a very effective probe for determining short-range cation and anion order in amphiboles, due to the high sensitivity of the OH-stretching frequency to the occupancies of the adjacent $M(1)$ and $M(3)$ sites, and to more distant interactions (see Hawthorne and Della Ventura 2007, this volume). Infrared spectroscopy can also register different hydrogen-bonded interactions between the hydroxyl proton and bridging oxygen atoms of the neighboring six-membered ring of $(\text{Al,Si})\text{O}_4$ tetrahedra, leading to additional fine structure in OH vibrational spectra (Hawthorne et al. 2000). Moreover, the two non-equivalent OH groups of the $P2_1/m$ structure can be distinguished in OH spectra, and so infrared spectroscopy is a rapid method for identifying the occurrence of the P - C transition in amphibole.

Mössbauer spectroscopy has been used successfully to quantify the ordering of Fe^{2+} between $M(4)$ and the C -sites. The $M(4)$ polyhedron is more distorted than the $M(1,2,3)$ octahedra and is more affected by the phase transition. Figure 4 (Boffa Ballaran et al. 2002) shows the quadrupole splitting, ΔE_Q , of Fe^{2+} at the $M(4)$ and $M(1,2,3)$ sites as a function of T . The transition occurs at 270 K. The $M(1, 2, 3)$ octahedra are too similar geometrically for Mössbauer to resolve the constituent Fe^{2+} individually, whereas Fe^{2+} at the $M(4)$ site is easily distinguished. It is evident from Figure 4 that ΔE_Q for Fe^{2+} at the $M(1,2,3)$ varies smoothly and

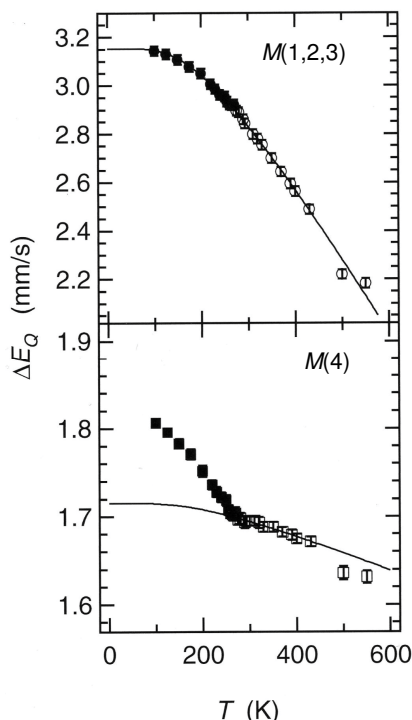


Figure 4. Quadrupole splitting, ΔE_Q , as a function of T for $M(4)$ and unresolved $M(1,2,3)$ doublets. The (aggregate) quadrupole splitting for the $M(1,2,3)$ sites varies continuously through the $P2_1/m \rightarrow HT-C2/m$ transition. In contrast, the quadrupole splitting for $M(4)$ shows a sharp discontinuity at T_c (270 K). This differential behavior reflects the much greater distortion of the $M(4)$ polyhedron at the transition. From Boffa Ballaran et al. (2002).

of Hirschmann et al. (1994), Boffa Ballaran et al. (2004) found that cation disorder in cummingtonite increases T_c by 70–100 °C (Fig. 5), as indicated by the variation of I_b/I_a . Figure 6 shows the variation of the OH-stretching mode (split into two in P -cummingtonite) with T through the transition for an amphibole ($X_{Fe} = 0.36$) unheated and heat-treated at 700 °C (sample codes 118125 and 118125-1c). These two samples had $X_{Fe}^{M(4)} = 0.91$ and $X_{Fe}^{M(4)} = 0.72$, respectively. T_c defined by the behavior of ν_{OH} is close to that determined from I_{odd}/I_{even} .

(Mg,Fe) cummingtonite: high- P studies of the $HT-C2/m \rightarrow P2_1/m$ transition

The symmetry reduction of the $C \rightarrow P$ transition allows independent rotation of the tetrahedra in the two independent double-chains of $P2_1/m$ amphibole, optimizing coordination around the $M(4)$ cation and permitting effective compression of this key polyhedron, thus stabilizing P -cummingtonite to high pressure. The first systematic *in situ* high-pressure (HP) study of cummingtonite done by Yang et al. (1998) determined the compositional dependence (Mg:Fe²⁺) of the critical pressure of the $HT-C2/m \rightarrow P2_1/m$ transition. P_c , as determined approximately using absolute intensities of many I_b reflections has a marked composition dependence (Fig. 7a). The well-defined trend of the square of a single I_b reflection with P is shown in Figure 7b. The

linearly through the transition and as such does not register it. In contrast, the quadrupole splitting of Fe²⁺ at the $M(4)$ site is highly sensitive to the transition and shows a sharp discontinuity at T_c . The excess quadrupole splitting due to the occurrence of a phase transition, $\delta\Delta E_Q$, is proportional to Q^2 .

(Mg,Fe) cummingtonite: high- T studies

There is a strong dependence of the transition temperature T_c on bulk Fe²⁺/(Mg + Fe²⁺), referred to hereafter as X_{Fe} , although different studies have determined different critical compositions. Hirschmann et al. (1994) found that cummingtonite with X_{Fe} as high as 0.38 has $P2_1/m$ symmetry, whereas the data of Boffa Ballaran et al. (2004, their Fig. 10), obtained using three samples studied by Hirschmann et al. (1994), suggest X_{Fe} near 0.45 for the critical composition. In both studies, $P2_1/m$ amphiboles near the critical composition have very high $X_{Fe}^{M(4)}$ values. Yang and Hirschmann (1995) report that cummingtonite with $X_{Fe}^{M(4)} < 0.85$ is primitive, and Boffa Ballaran et al. (2004) found that the near-critical amphibole composition $X_{Fe} = 0.45$ had $X_{Fe}^{M(4)} = 0.91$. Hirschmann et al. (1994) found that cummingtonite heat-treated at 600 °C (1 month) and 700 °C (2 d) had undergone significant disorder [$X_{Fe}^{M(4)}$ decreasing], with the $M(4)$ occupancies changing by up to 20%.

Boffa Ballaran et al. (2004) showed that T_c also depends significantly upon the state of cation order, which involves Mg-Fe exchange between the $M(4)$ and $M(1,2,3)$ sites, principally $M(2) \leftrightarrow M(4)$. Using three heat-treated samples

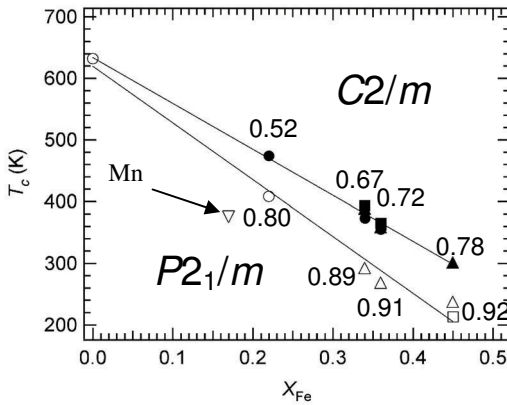
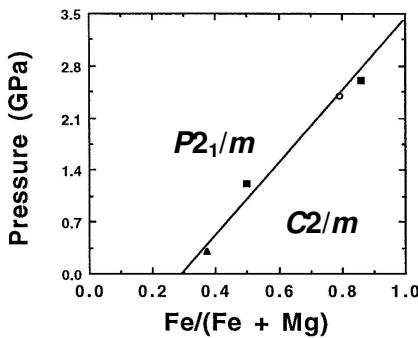
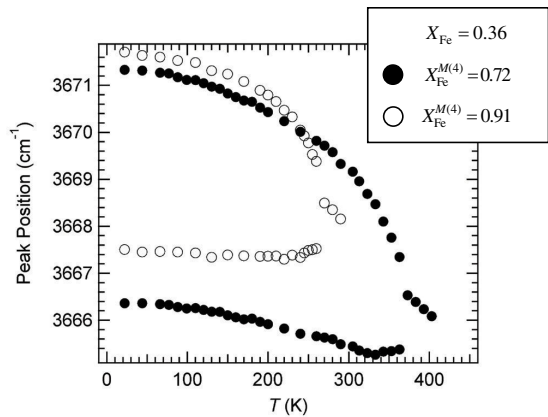
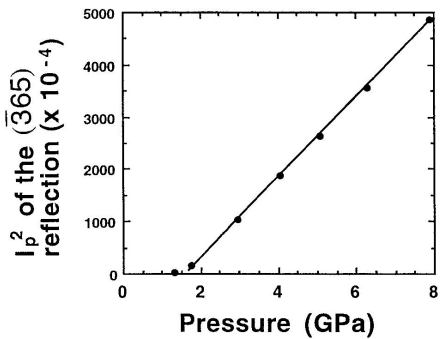


Figure 5. The effect of heat treatment upon T_c in cummingtonite-grunerite. Filled symbols are heat-treated samples, open symbols untreated. The number at each symbol is $X_{Fe}^{M(4)}$ determined by single-crystal XRD. Modified from Boffa Ballaran et al. (2004).

Figure 6. Variations of $\nu_{OH\ max}$ with T for cummingtonite with $X_{Fe}=0.36$. Open and filled symbols refer to untreated and heat-treated samples, respectively. From Boffa Ballaran et al. (2004).



(a)



(b)

Figure 7. (a) Compositional dependence of P_c in cummingtonite-grunerite amphiboles. (b) A well-defined linear correlation between I_{odd}^2 and P . From Yang et al. (1998).

structural characteristics of this high- P phase transition are now known in detail. The key structural changes at the atomic scale reported by Yang et al. (1998) are:

- (i) The A chain becomes S-rotated just above the transition, whereas the B chain remains O-rotated (Fig. 8), with the O(5)-O(6)-O(5) angle decreasing from about 170° to 160° at the transition, and the difference between this angle, $\Delta\theta$, for the A and B chains increases continuously with pressure from 16.8° (1.32 GPa) to 42.5° (7.90 GPa).
- (ii) The oxygen atoms coordinating the $M(4)$ cation change: O(6B) becomes increasingly distant, whereas O(5B) enters the coordination of this cation (Fig. 9).

There are also clear correlations between various structural features. For example, there are well-defined linear correlations between β angle and chain-displacement factor "CDF", the distance between the center of the two opposing six-membered ring of tetrahedra (Fig. 10). There is also a strong linear correlation between the differential A/B chain-kinking, $\Delta\theta$, and I_b (Fig. 11). Clearly, a wealth of diagnostic structural data is available to characterize the $HT-C2/m \rightarrow P2_1/m$ transition in amphibole.

The major polyhedral change with compression is the exchange of O(6B) and O(5B) oxygen atoms in the coordination of the $M(4)$ cation that leads to a new high- P $M(4)$ octahedron O(2A)-O(2B)-O(4A)-O(4B)-O(5B)-O(6A). These changes are shown in Figure 9.

The rotations of tetrahedra reflect a change in the coordination environment of the large and compressible $M(4)$ polyhedron: principally, the O(5B) oxygen atom in the HP -structure moves nearer to the $M(4)$ cation (from 3.2 to 2.95 Å at the transition pressure), whereas O(5A) oxygen atom moves away (Fig. 1). The O(2A,B) and O(4A,B) oxygen atoms remain close to the cation, as in the HT -

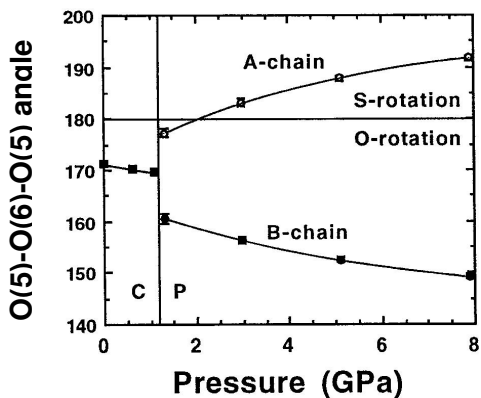


Figure 8. P -induced changes in the sense of rotation of tetrahedra in cummingtonite $X_{Fe} = 0.50$ through the $HT-C2/m \rightarrow P2_1/m$ transition ($P_c = 1.32$ GPa). From Yang et al. (1998).

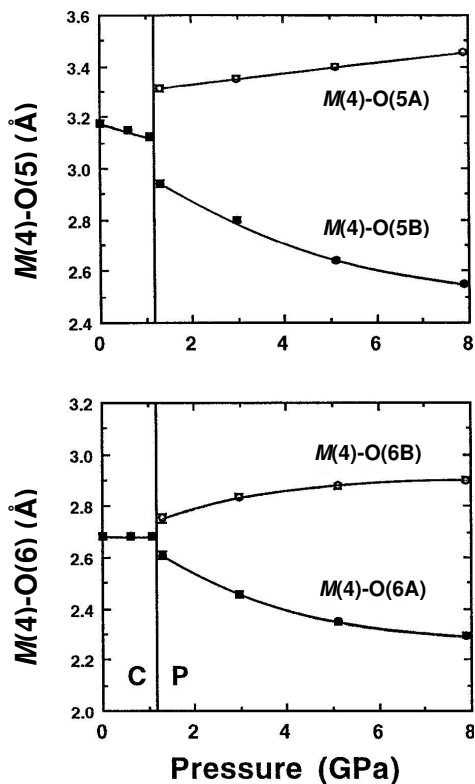


Figure 9. Variations of $M(4)$ -O(5) and $M(4)$ -O(6) bond lengths through the $HT-C2/m \rightarrow P2_1/m$ transition. Note the marked compression of $M(4)$ -O(5B) and $M(4)$ -O(6B) compared with the almost P -invariant behavior of $M(4)$ -O(5A) and $M(4)$ -O(6A) bonds. From Yang et al. (1998).

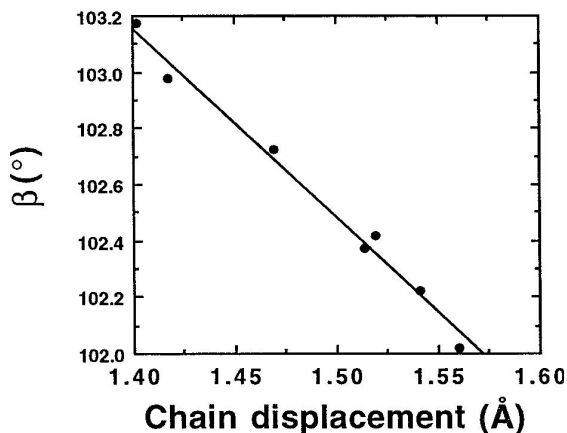
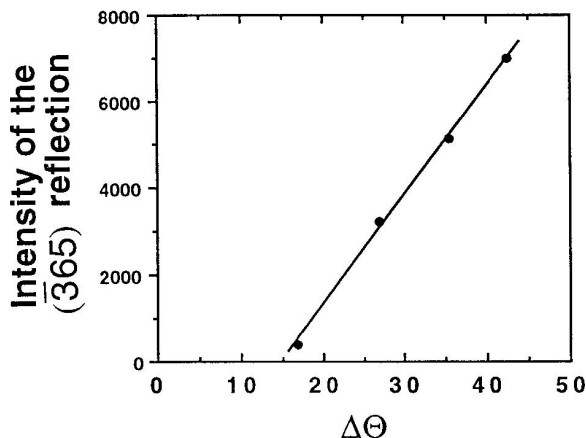


Figure 10. The chain-displacement factor (CDF), the distance between the centers of the two opposed 6-membered rings of tetrahedra shows a well-defined linear correlation with the β angle. From Yang et al. (1998).

Figure 11. Linear correlation between the intensity of a diagnostic primitive-only reflection and the difference between the kinking angles of A and B chains, indicating a strong linear-quadratic coupling between $\Delta\Theta$ and Q . From Yang et al. (1998).



$C2/m$ structure. Pressure has a significant effect upon the $M(4)$ -O(5B) bond, which shortens to 2.55 Å at 7.9 GPa.

Yang et al. (1998) found that the square of the intensity of a “superlattice” reflection (I_{odd} : $h + k = 2n + 1$) is proportional to the square of the order-parameter. This relation means that Q is proportional to $(P_c - P)^\beta$ with $\beta = 1/4$, suggesting that the $HT-C2/m \rightarrow P2_1/m$ transition is probably tricritical. They also reported infra-red OH spectra for their 50:50 cummingtonite (sample DH484) as a function of pressure (Fig. 12). At 1.54 GPa, there is the onset of peak splitting and at 2.62 GPa all four peaks of the ambient spectrum are doublets. Each doublet has components from the A and B chains of the $P2_1/m$ structure. Within each doublet the peak separation (5–7 cm^{-1}) varies little with pressure, although peak-widths increase as pressure increases. Three of the four doublets show small blue shifts with increasing P , the exception being the lower frequency FeFeFe doublet which has a very slight red shift.

In a more detailed high-pressure study of the effects of composition and cation disorder (Mg-Fe^{2+}) upon the $HT-C2/m \rightarrow P2_1/m$ transition in cummingtonite, Boffa Ballaran et al. (2000) found that the transition is close to second-order rather than tricritical. Figure 13 shows the variation of I_b/I_a with pressure for cummingtonite samples with different X_{Fe} . All intensity data fit very well to a 2-4-6 Landau potential and indicate second-order behavior. Only sample

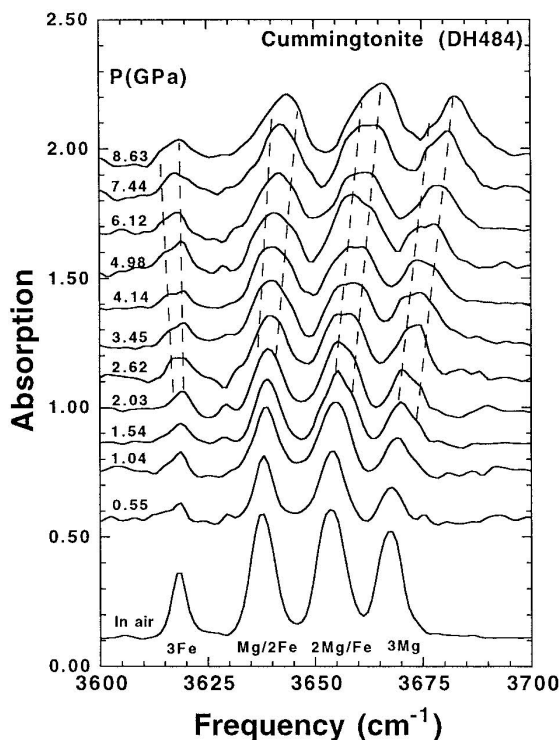


Figure 12. Infrared absorption spectra in the principal OH-stretching region of cummingtonite ($X_{\text{Fe}} = 0.50$) with changing pressure through the $HT-C2/m \rightarrow P2_1/m$ transition. Peaks of the ambient in-air spectrum of the $HT-C2/m$ polymorph are labeled with the composition of the triplet of $M(1,3)$ sites adjacent to the OH group. Transformation to the $P2_1/m$ polymorph is seen as peak broadening at 1.54 GPa and doubling of each peak at higher pressure due to the two non-equivalent OH groups of the $P2_1/m$ structure. From Yang et al. (1998).

Y42XB (Fig. 13a) of Boffa Ballaran et al. (2000) has significantly lower values for the b/a Landau coefficient (Eqn. 3), providing evidence for slight tricritical character. Similar behavior was obtained for the variation of the volume strain, the scalar strain and the strain components (Fig. 14). In addition, volume strain scales with I_b/I_a (Fig. 15a) and thus with Q^2 , as is the case for the scalar strain (Fig. 15b). This behavior confirms linear-quadratic coupling between strain and order-parameter, as expected for a phase transition associated with a point on the Brillouin zone boundary. Note also that there is a marked compositional dependence of P_c . Figure 16 shows the lattice parameters as a function of P for a cummingtonite with $X_{\text{Fe}} = 0.45$ (sample Y42XB). The axial moduli for this amphibole indicate that, at the transition, there is a marked softening along c (K_{c0} : 101 \rightarrow 69 GPa), a slight softening along b (K_{b0} : 85 \rightarrow 79 GPa) and, in contrast, stiffening along a (K_{a0} : 51 \rightarrow 58 GPa). All these features are consistent with a tetrahedron rotation mechanism

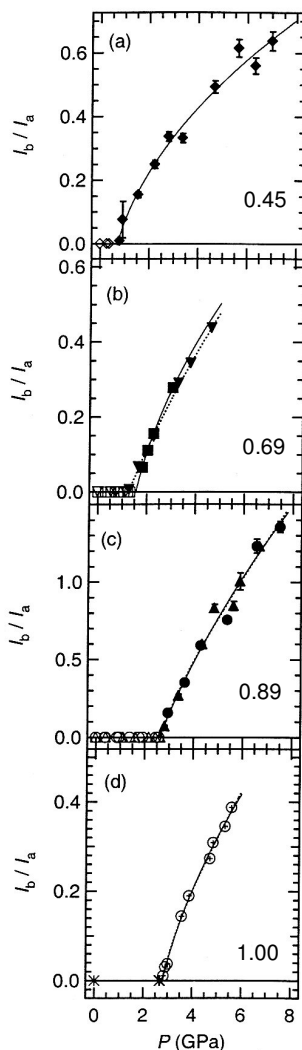


Figure 13. Changes in I_b/I_a of cummingtonite-grunerite with X_{Fe} (indicated on each diagram) and P . [Used by permission of Schweitzerbart'sche Verlagsbuchhandlung OHG, www.schweitzerbart.de. Modified from Boffa Ballaran et al. (2000), *European Journal of Mineralogy*, 12, Fig. 4, p. 1205.]

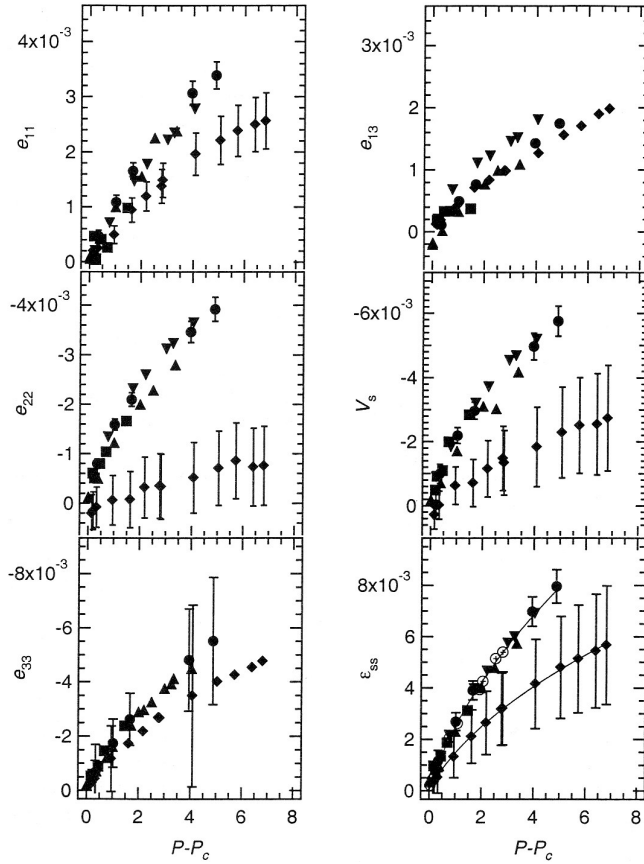


Figure 14. Changes in the principal and scalar spontaneous strains and volume strain with pressure in cummingtonite. [Used by permission of Schweitzerbart'sche Verlagsbuchhandlung OHG, www.schweitzerbart.de. From Boffa Ballaran et al. (2000), *European Journal of Mineralogy*, 12, Fig. 5, p. 1207.]

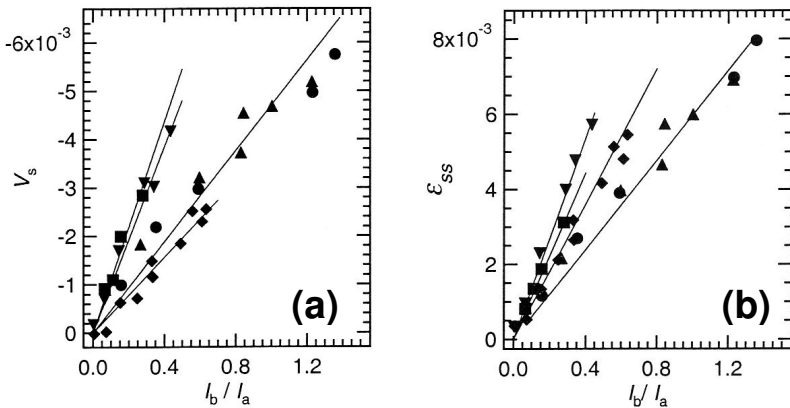


Figure 15. Correlation between I_b/I_a (I_{odd}/I_{even}) and (a) volume strain and (b) scalar spontaneous strain for cummingtonite. [Used by permission of Schweitzerbart'sche Verlagsbuchhandlung OHG, www.schweitzerbart.de. From Boffa Ballaran et al. (2000), *European Journal of Mineralogy*, 12, Figs. 7 and 8, p. 1208.]

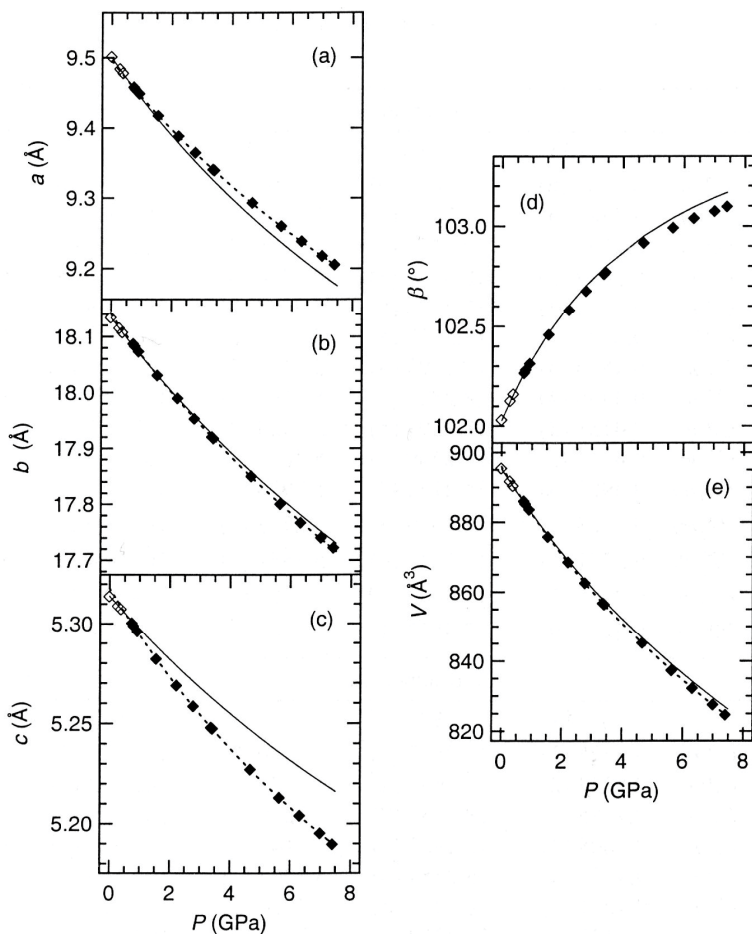


Figure 16. Compression curves for lattice parameters through the HT-C2/m \rightarrow P2₁/m transition of cummingtonite with $X_{\text{Fe}} = 0.45$. Compression data for each polymorphs are fit using a Murnaghan equation of state. [Used by permission of Schweitzerbart'sche Verlagsbuchhandlung OHG, www.schweitzerbart.de. From Boffa Ballaran et al. (2000), *European Journal of Mineralogy*, 12, Fig. 3, p. 1204.]

for the HT-C2/m \rightarrow P2₁/m transition. Boffa Ballaran et al. (2000) found a strong composition dependence for P_c , similar to that reported by Yang et al. (1998) and showed that heat treatment also affects P_c . Figure 17 shows P_c - X_{Fe} data from Boffa Ballaran et al. (2000) for untreated and heated cummingtonites (all annealed at 700 °C for 55 h), from which it is evident that annealing can result in significant changes in P_c , e.g., for the sample with $X_{\text{Fe}} = 0.69$, $P_c = 1.57$ GPa for untreated and 1.26 GPa for annealed samples.

It seems clear that, for a fixed amphibole composition, the extent of non-convergent order can have a detectable effect upon the compression of cummingtonite-grunerite and P_c of the HT-C2/m \rightarrow P2₁/m transition, as well as on thermal expansion and T_c of the P2₁/m \rightarrow HT-C2/m transition.

Mn-Mg cummingtonite

No transitional behavior has been observed at room pressure in (Fe,Mn)-rich amphiboles

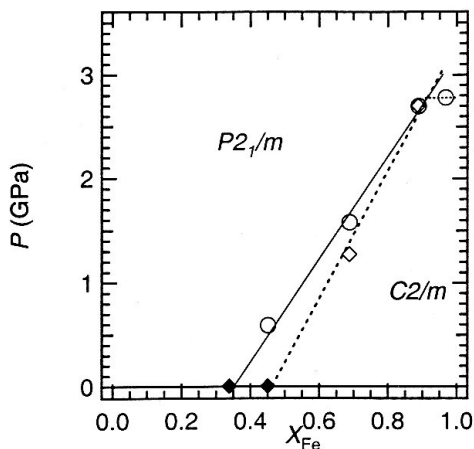


Figure 17. Effect of heat treatment upon P_c for cummingtonite-grunerite. Circles = untreated, diamonds = heat-treated. [Used by permission of Schweitzerbart'sche Verlagsbuchhandlung OHG, www.schweitzerbart.de. From Boffa Ballaran et al. (2000), *European Journal of Mineralogy*, 12, Fig. 11, p. 1211.]

such as mangano-grunerites (Reece et al. 2002). However, Reece et al. (2000) observed the $P2_1/m \leftrightarrow HT-C2/m$ transition at 107 °C/room- P in an Fe-free (Mg,Mn)-cummingtonite of composition $Na_{0.13} Ca_{0.41} Mg_{5.23} Mn_{1.13} Si_8 O_{22} (OH)_2$ from Talcville, New York, USA. The ambient site occupancies of this amphibole are $A^{\square} B(Na_{0.13} Ca_{0.41} Mg_{0.46} Mn_{1.00})^C (Mg_{4.87} Mn_{0.13})^T Si_8 O_{22} W(OH)_2$, and $\langle [^8]r_{M(4)} \rangle = 0.93 \text{ \AA}$. The scalar spontaneous strain for cummingtonite- $P2_1/m$ has a linear temperature dependence, indicating that the transition is essentially second-order, as is the case for the transition in Mg-Fe cummingtonite (Boffa Ballaran et al. 2004).

$P2_1/m \leftrightarrow HT-C2/m$ transition in synthetic amphiboles

Recently, the compositional dependence of this phase transition has been studied in synthetic amphiboles of the $Na_2O-Li_2O-MgO-SiO_2-H_2O-F$ system. The amphiboles studied have always $X_{Mg}^{M(4)} \approx 0.5$ and Li and Na in variable proportions at the $M(4)$ site. Li is slightly larger than Mg ($[^8]Li = 0.92$ and $[^8]Mg = 0.89 \text{ \AA}$, respectively), while Na is much larger ($[^8]Na = 1.18 \text{ \AA}$). Here, 50-100 % of the $M(4)$ site is occupied by small cations (NaMg, LiMg). All compositions have $P2_1/m$ symmetry at room- T . An advantage of studying these synthetic compositions is the absence of Fe^{2+} , thus excluding non-convergent ordering between the B and C sites, that in cummingtonite-grunerite couples with the displacive transition (see above).

$^A Na^B (LiMg)^C Mg_5^T Si_8 O_{22} W(OH)_2$. The synthetic amphibole studied by Iezzi et al. (2005) has an $M(4)$ composition Li:Mg = 1:1 and space group $P2_1/m$ at ambient conditions. The presence of significant Mg and another small cation ($[^8]Li^+$) at the $M(4)$ site suggests that a $P2_1/m \leftrightarrow HT-C2/m$ phase transition is likely to occur in this amphibole: the transition was observed at 320-330 °C. This T_c is to be compared with the value of 359 °C reported by Boffa Ballaran et al. (2004) for specimen J ($X_{Fe} = 0.004$ and $\langle [^8]r_{M(4)} \rangle = 0.89 \text{ \AA}$). If the aggregate ionic radius at the $M(4)$ site is taken into account, this $^{M(4)}(LiMg)$ amphibole with $\langle [^8]r_{M(4)} \rangle = 0.905 \text{ \AA}$ has T_c about 125 °C higher than that of the annealed sample W82-900 studied by Boffa Ballaran et al. (2004) with $\langle [^8]r_{M(4)} \rangle = 0.917 \text{ \AA}$. Iezzi et al. (2005) suggested that the cause of the higher T_c is the presence of a filled A-site. Analysis of the variation of unit-cell parameters with temperature (Fig. 18) indicates tricritical rather than second-order character: fitting of the scalar strain to a tricritical 2-6 Landau potential gives $T_c = 325(10) \text{ °C}$, with a critical exponent $\beta = 0.27$.

Infrared absorption spectra of this amphibole on heating through the transition were also collected by Iezzi et al. (2005) and are instructive. The OH-stretching region is particularly sensitive to the transition (Fig. 19). The A and B absorption bands are assigned to MgMgMg-

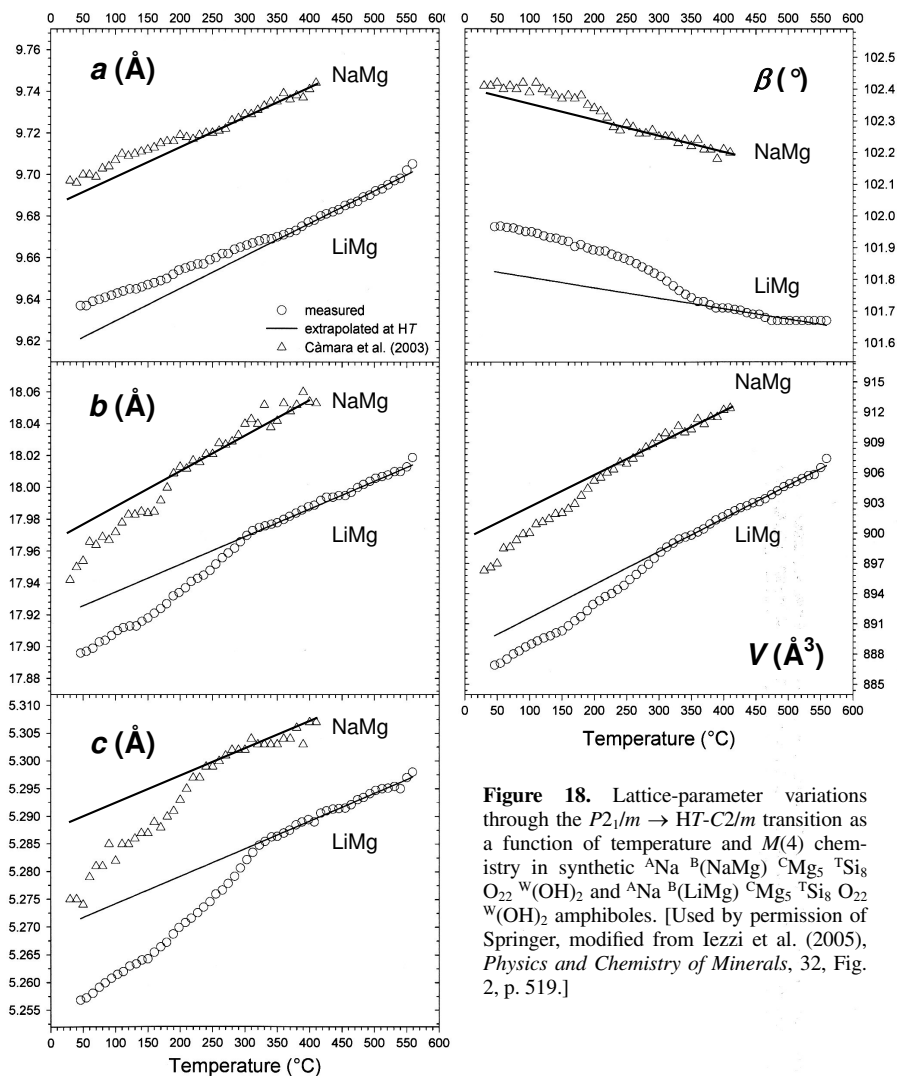


Figure 18. Lattice-parameter variations through the $P2_1/m \rightarrow HT-C2/m$ transition as a function of temperature and $M(4)$ chemistry in synthetic ${}^A\text{Na}{}^B(\text{NaMg}){}^C\text{Mg}_5{}^T\text{Si}_8\text{O}_{22}{}^W(\text{OH})_2$ and ${}^A\text{Na}{}^B(\text{LiMg}){}^C\text{Mg}_5{}^T\text{Si}_8\text{O}_{22}{}^W(\text{OH})_2$ amphiboles. [Used by permission of Springer, modified from Iezzi et al. (2005), *Physics and Chemistry of Minerals*, 32, Fig. 2, p. 519.]

$\text{OH}\dots{}^A\text{Na}$ (A-chain) and $\text{MgMgMg-OH}\dots{}^A\text{Na}$ (B-chain) of the $P2_1/m$ phase, respectively, and at room- T are very well separated ($\Delta\nu_{\text{OH}} \sim 45 \text{ cm}^{-1}$). The weak C and D bands correspond to local A-site-vacant configurations $\text{MgMgMg-OH}\dots{}^A\Box$ (A-chain) and $\text{MgMgMg-OH}\dots{}^A\Box$ (B-chain), respectively, and are also well-separated ($\Delta\nu_{\text{OH}} \sim 20 \text{ cm}^{-1}$). These A-site-vacant bands imply a small departure from ideal (A-site-full) stoichiometry. On heating through the transition, the A and B bands converge until they are indistinguishable at $\sim 320^\circ\text{C}$, and there is a single band assigned to the $\text{MgMgMg-OH}\dots{}^A\text{Na}$ of the unique OH group of the $HT-C2/m$ polymorph. Above T_c , there is no change in $\Delta\nu_{\text{OH}}$.

${}^A\text{Na}{}^B(\text{NaMg}){}^C\text{Mg}_5{}^T\text{Si}_8\text{O}_{22}{}^W(\text{OH})_2$. New insight into the structural controls on the transition was provided by a high- T study of the synthetic amphibole ${}^A\text{Na}_{0.8}{}^B(\text{Na}_{0.8}\text{Mg}_{1.2}){}^C\text{Mg}_5{}^T\text{Si}_8\text{O}_{22}{}^W(\text{OH})_2$ by Cámara et al. (2003). This amphibole was studied by single-crystal X-ray diffraction. Variations of lattice parameters with temperature, determined from single-crystal

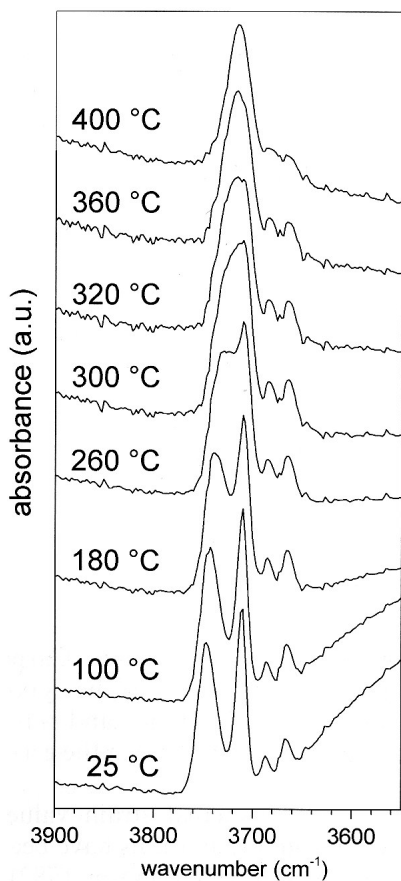


Figure 19. Variable- T infrared absorption spectra in the principal OH-stretching region of synthetic ${}^A(\text{Na}_{0.95}\square_{0.05}){}^B(\text{Li}_{0.95}\text{Mg}_{1.05}){}^C\text{Mg}_5{}^T\text{Si}_8\text{O}_{22}{}^W(\text{OH})_2$. See text for peak assignments. [Used by permission of Springer, from Iezzi et al. (2005), *Physics and Chemistry of Minerals*, 32, Fig. 1, p. 517.]

short A–O(7A,B) distances (2.37 and 2.35 Å, respectively) and two different long A–O(7A,B) distances (3.62 and 3.92 Å, respectively). In $C2/m$ symmetry, Na is ordered at the analogous $A(m)$ site, and is increasingly displaced from the center of the cavity with increasing T (0.50 and 0.62 Å, respectively, at 270 and 370 °C).

${}^A\text{Na}{}^B(\text{Na}_x\text{Li}_{1-x})\text{Mg}{}^C\text{Mg}_5{}^T\text{Si}_8\text{O}_{22}{}^W(\text{OH})_2$ solid solutions. Della Ventura and coworkers (unpublished data) extended the compositional range of the $M(4)$ site to include synthetic ${}^A\text{Na}{}^B(\text{Na}_x\text{Li}_{1-x})\text{Mg}{}^C\text{Mg}_5{}^T\text{Si}_8\text{O}_{22}{}^W(\text{OH})_2$ solid solutions. High- T FTIR spectroscopy on four compositions was used to follow the evolution of two main bands at ~ 3740 and 3715 cm^{-1} in the OH-stretching region and peak shifting and band broadening. For amphiboles of the LNMSH system, the size of the $M(4)$ polyhedron is the only factor controlling T_c . However, it was found that T_c is only slightly dependent upon $\langle r_{M(4)} \rangle$ (Fig. 22). This behavior contrasts with that of cummingtonite-grunerite, for which there is a strong composition dependence

XRD, are shown in Figure 18. At ambient conditions, this amphibole has space group $P2_1/m$. As in cummingtonite, the transition involves a change in the A-chain rotation from S- to O-rotated, but the observed $T_c = 257(3)$ °C is anomalously high for an $M(4)$ composition ($\text{Na}_{0.8}\text{Mg}_{1.2}$), which has a large $\langle {}^{[8]}r_{M(4)} \rangle = 1.006$ Å compared with (Mg,Fe)-cummingtonite (0.89–0.92 Å). The question arises as to why this amphibole, having a significant proportion of large cations at $M(4)$, should have $P2_1/m$ symmetry and such an unexpectedly high T_c . Cámara et al. (2003) argued that T_c depends also on the aggregate size of the $M(1,2,3)$ cations. As mentioned above, rotation of the tetrahedra correlates with changes in b and c lattice parameters. The b parameter is sensitive to the $M(4)$ cation and to the composition of the ribbon of octahedra: widening of the ribbon of octahedra (substitution of larger cations such as Fe^{2+}) will cause straightening of chains. Conversely, narrowing of the ribbon (e.g., by substitution of Mg), causes chain-kinking, i.e., stabilization of the $P2_1/m$ structure relative to $C2/m$ and a corresponding increase in T_c . Thus, it seems that the key relation is between $\langle {}^{[8]}r_{M(4)} \rangle$ and $\langle r_{M(1,2,3)} \rangle$, alternatively represented by $\langle {}^{[8]}M(4)\text{-O} \rangle$ and $\langle {}^{[6]}M(1,2,3)\text{-O} \rangle$, respectively. Calculation of strains from lattice parameters (Fig. 20) indicate that the transition is second-order, not tricritical as in the case of ${}^A\text{Na}{}^B(\text{LiMg}){}^C\text{Mg}_5{}^T\text{Si}_8\text{O}_{22}{}^W(\text{OH})_2$.

The evolution of the structure and of the atomic displacement parameters at the A, B and oxygen sites as a function of increasing T is summarized in Figure 21a,b. There is only one A site in $P2_1/m$ symmetry, which is significantly off-centered (~ 0.25 Å) along the imaginary line joining the two farthest O(7A) and O(7B) oxygen atoms, so that there are two nearly equal

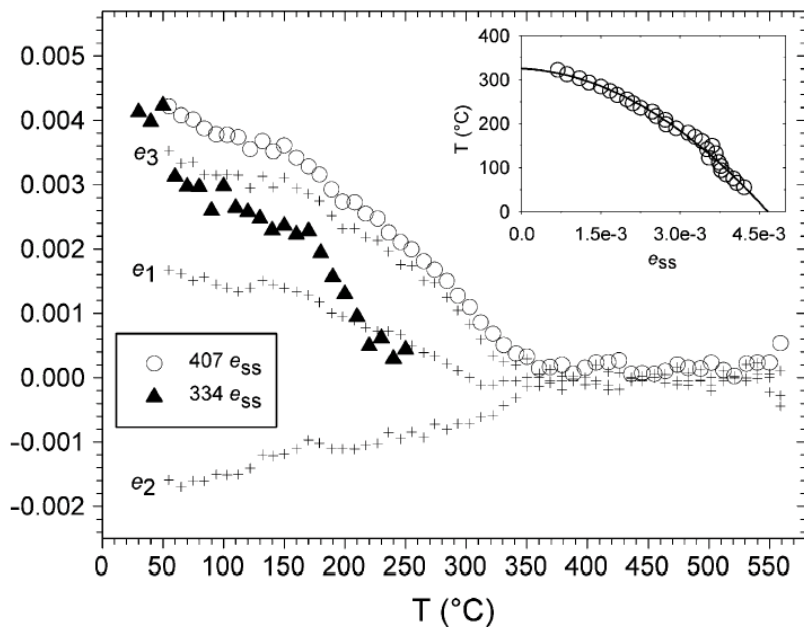


Figure 20. Variations of the principal components of the spontaneous strain in synthetic ${}^A\text{Na}{}^B(\text{LiMg}){}^C\text{Mg}_5{}^T\text{Si}_8\text{O}_{22}{}^W(\text{OH})_2$ (sample 407) and ${}^A\text{Na}{}^B(\text{NaMg}){}^C\text{Mg}_5{}^T\text{Si}_8\text{O}_{22}{}^W(\text{OH})_2$ (sample 334) amphiboles through the $P2_1/m \rightarrow HT-C2/m$ transition. Inset shows a quadratic Landau fit to the scalar spontaneous strain. [Used by permission of Springer, from Iezzi et al. (2005), *Physics and Chemistry of Minerals*, 32, Fig. 3, p. 520.]

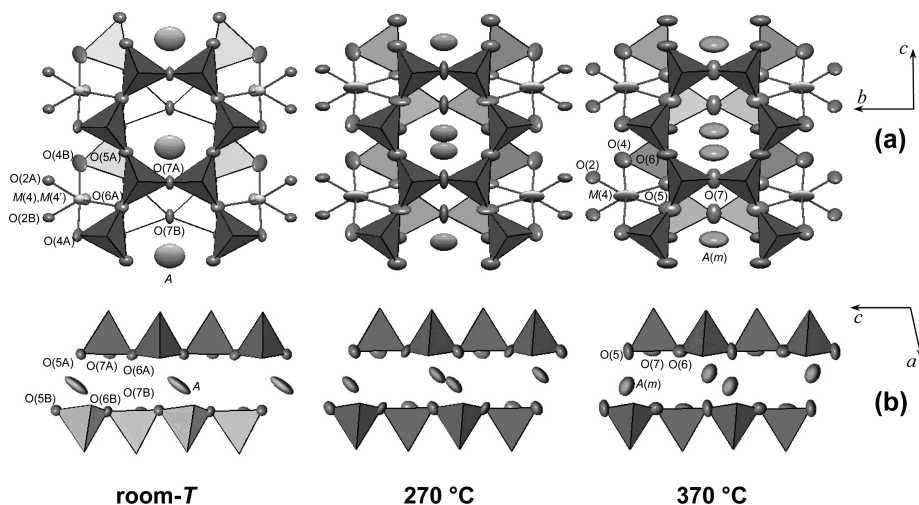


Figure 21. (a) (100) and (b) (010) projections of the partial structure of synthetic ${}^A\text{Na}{}^B(\text{NaMg}){}^C\text{Mg}_5{}^T\text{Si}_8\text{O}_{22}{}^W(\text{OH})_2$ amphibole through the $P2_1/m \rightarrow HT-C2/m$ transition, showing straightening of the B chain, splitting and re-orientation of the A-sites (Na). [Used by permission of Springer, modified from Cámara et al. (2003), *Physics and Chemistry of Minerals*, 30, Fig. 4, p. 579.]

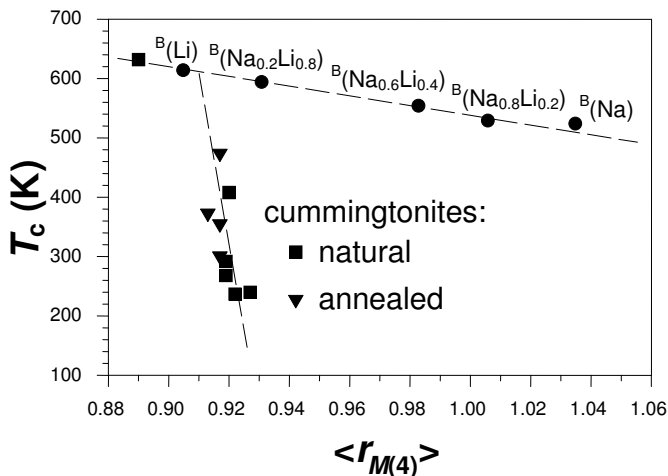


Figure 22. Dependence of T_c for the $P2_1/m \rightarrow HT-C2/m$ transition upon the mean radius of the $M(4)$ cation for cummingtonite-grunerite and a series of synthetic ${}^A\text{Na}^B(\text{Na}_x\text{Li}_{1-x}\text{Mg})^C\text{Mg}_5^T\text{Si}_8\text{O}_{22}^W(\text{OH})_2$ amphiboles (filled circles) for which the $M(4)$ compositions are shown.

and a sharp cut-off at $\langle r_{M(4)} \rangle = 0.93 \text{ \AA}$. As significant changes in $\langle r_{M(1,2,3)} \rangle$ are present in the cummingtonite-grunerite solid solution, this result indicates that $\langle r_{M(4)} \rangle$ cannot be the only parameter affecting T_c in compositional systems where non-convergent ordering is possible.

${}^A\text{Na}^B(\text{Na},\text{Mg})^C\text{Mg}_5^T\text{Si}_8\text{O}_{22}^W\text{F}_2$. Cámara et al. (2007) made a variable-temperature (100–944 K) study of synthetic ${}^A\text{Na}^B(\text{NaMg})^C\text{Mg}_5^T\text{Si}_8\text{O}_{22}^W\text{F}_2$, aimed at testing the proposal of Cámara et al. (2003) concerning the effect of size of the $M(1,2,3)$ cations on T_c . The $\text{OH} \rightarrow \text{F}$ substitution leads to narrowing of the ribbon of $M(1,2,3)$ octahedra, primarily by contraction of the $M(1)$ and $M(3)$ octahedra, and does not affect the size of the $M(4)$ polyhedron. At room-temperature, the difference in the aggregate bond length of the octahedra, $\langle\langle M(1,2,3)\text{-O} \rangle\rangle$, between the F- and OH-endmembers is 0.012 \AA . ${}^W\text{F}$ increases the thermal stability of the structure, so that higher temperatures can be reached, and the evolution of the high- T structure modeled reliably. At ambient conditions this amphibole has space group $P2_1/m$ and $T_c = 125(5)^\circ\text{C}$. Therefore, the $\text{OH} \rightarrow \text{F}$ substitution involves a decrease in T_c of 132°C . This marked difference cannot be ascribed either to non-convergent cation ordering or to the presence of a filled A site and indicates the importance of the relative size of the M polyhedra.

Overall compositional trends and the $P2_1/m \leftrightarrow HT-C2/m$ transition

Key data relating to this transition are summarized in Table 1. There is a strong correlation between the aggregate $M(4)$ cation radius, $\langle {}^8r_{M(4)} \rangle$, and $P_c(T_c)$ of this transition: increasing $\langle {}^8r_{M(4)} \rangle$ causes P_c to increase (at constant T) and T_c to decrease (at constant P), so that compositional isopleths of $\langle {}^8r_{M(4)} \rangle$ have positive slopes in P - T space. The data for synthetic ${}^A\text{Na}^B(\text{Na},\text{Li},\text{Mg})^C\text{Mg}_5^T\text{Si}_8\text{O}_{22}^W(\text{OH})_2$ amphiboles indicate that $P_c(T_c)$ also correlate, although less strongly, with the aggregate size of the $M(1,2,3)$ cations. Our survey of the compositional controls on T_c suggests that for $\langle {}^8r_{M(4)} \rangle$ higher than 0.93 \AA , cummingtonites will have $C2/m$ symmetry and $T_c < 298 \text{ K}$. In principle, the approximate positions of compositional isopleths for the $P2_1/m \leftrightarrow C2/m$ transition in cummingtonite could be obtained by combining high- T (T_c) and high- P (P_c) data for various compositions.

Comparisons with the $P2_1/c \leftrightarrow C2/c$ transitions in pyroxenes

It is now well-established that clinopyroxene undergoes a rapid reversible and non-quenchable displacive phase transition in which the $P2_1/c$ polymorph transforms to a high- T $C2/c$ form (“HT- $C2/c$ ”) at room- P and a high- P $C2/c$ form (“HP- $C2/c$ ”) at or below room- T (Angel et al. 1992, clinoenstatite; Hugh-Jones et al. 1994, clinoferrosilite; Arlt et al. 1998,

Table 1. Transition temperatures (T_C) for the $P_{2,1/m} \leftrightarrow HT-C2/m$ phase transition and transition pressures (P_C) for the $HT-C2/m \leftrightarrow P_{2,1/m}$ and the $P_{2,1/m} \leftrightarrow HP-C2/m$ phase transitions available for amphiboles from literature.

Reference	Composition	$\langle^{87}r_{M(4)}\rangle$ (Å)	$\langle^{67}r_{M(4,2,3)}\rangle$ (Å)	T_C (K)	P_C (GPa)
1	A□ _B (Na _{0.06} Ca _{0.36} Mn _{0.96} Mg _{0.62}) ⁺ CaMg _{5.00} Si ₈ O ₂₂ ^W (OH) ₂	0.974	0.718	373	—
2	A□ _{B,C} (Fe ²⁺ _{5.33} Mg _{1.46} Na _{0.05} Fe ³⁺ _{0.14} Al _{0.01})Si ₈ O ₂₂ ^W [(OH) _{1.92} F _{0.05} Cl _{0.01}] ⁺ *	0.927	0.732	235	2.43
3	A□ _B (Fe ²⁺ _{1.11} Mg _{0.75} Ca _{0.11} Mn _{0.03}) ⁺ C(Mg _{4.35} Fe ²⁺ _{0.65})Si ₈ O ₂₂ ^W (OH) ₂	0.927	0.738	—	2.60
4 DH7-482	A□ _B (Fe ²⁺ _{1.74} Mg _{0.09} Ca _{0.06} Mn _{0.13}) ⁺ C(Mg _{5.38} Fe ²⁺ _{1.52})Si ₈ O ₂₂ ^W (OH) ₂	0.991	0.717	380	—
5 R14473	A□ _B (Na _{0.13} Ca _{0.41} Mg _{0.46} Mn _{1.00}) ⁺ C(Mg _{4.87} Mn _{0.13})Si ₈ O ₂₂ ^W (OH) ₂	0.890	0.720	632	—
6 J	A□ _B (Mg _{1.97} Fe ²⁺ _{0.03}) ⁺ C(Mg _{5.00})Si ₈ O ₂₂ ^W (OH) ₂	0.920	0.721	408	—
6 W82-900 (natural) [§]	A□ _B (Fe ²⁺ _{1.11} Mg _{0.75} Ca _{0.11} Mn _{0.03}) ⁺ C(Mg _{4.52} Fe ²⁺ _{0.43} Mn _{0.01} Al _{0.04})Si ₈ O ₂₂ ^W (OH) ₂	0.917	0.721	474	—
6 W82-900 (annealed) [§]	A□ _B (Fe ²⁺ _{1.04} Mg _{0.84} Ca _{0.09} Mn _{0.03}) ⁺ C(Mg _{4.35} Fe ²⁺ _{0.48} Mn _{0.01} Al _{0.05})Si ₈ O ₂₂ ^W (OH) ₂	0.919	0.728	470	—
6 1997-4 (natural)	A□ _B (Fe ²⁺ _{1.77} Mg _{0.21} Ca _{0.02}) ⁺ C(Mg _{4.66} Fe ²⁺ _{0.34})Si ₈ O ₂₂ ^W (OH) ₂	0.913	0.732	373	—
6 1997-4 (annealed)	A□ _B (Fe ²⁺ _{1.35} Mg _{0.63} Ca _{0.02}) ⁺ C(Mg _{4.26} Fe ²⁺ _{0.74})Si ₈ O ₂₂ ^W (OH) ₂	0.919	0.731	219	—
6 118125 (natural)	A□ _B (Fe ²⁺ _{1.82} Mg _{0.16} Ca _{0.01}) ⁺ C(Mg _{4.40} Fe ²⁺ _{0.60})Si ₈ O ₂₂ ^W (OH) ₂	0.917	0.734	355	—
6 118125 (annealed)	A□ _B (Fe ²⁺ _{1.44} Mg _{0.52} Ca _{0.04}) ⁺ C(Mg _{4.04} Fe ²⁺ _{0.96})Si ₈ O ₂₂ ^W (OH) ₂	0.922	0.731	237	0.7
6 Y42XB (natural)	A□ _B (Fe ²⁺ _{1.84} Mg _{0.12} Ca _{0.04}) ⁺ C(Mg _{5.85} Fe ²⁺ _{1.15})Si ₈ O ₂₂ ^W (OH) ₂	0.917	0.734	301	—
6 Y42XB (annealed)	A□ _B (Fe ²⁺ _{1.36} Mg _{0.41} Ca _{0.03}) ⁺ C(Mg _{5.60} Fe ²⁺ _{1.40})Si ₈ O ₂₂ ^W (OH) ₂	0.921	0.746	—	1.57
7 BM93-400 (natural)	A□ _B (Fe ²⁺ _{1.02} Mg _{0.06} Ca _{0.02}) ⁺ C(Mg _{5.07} Fe ²⁺ _{2.93})Si ₈ O ₂₂ ^W (OH) ₂	0.920	0.748	—	1.26
7 BM93-400 (annealed)	A□ _B (Fe ²⁺ _{1.86} Mg _{0.12} Ca _{0.02}) ⁺ C(Mg _{1.93} Fe ²⁺ _{3.07})Si ₈ O ₂₂ ^W (OH) ₂	0.924	0.758	—	2.7
7 1-K (natural)	A□ _B (Fe ²⁺ _{1.93} Mg _{0.02} Ca _{0.05}) ⁺ C(Mg _{6.70} Fe ²⁺ _{4.30})Si ₈ O ₂₂ ^W (OH) ₂	0.925	0.759	—	2.7
7 1-K (annealed)	A□ _B (Fe ²⁺ _{1.92} Mg _{0.02} Ca _{0.06}) ⁺ C(Mg _{6.60} Fe ²⁺ _{4.31})Si ₈ O ₂₂ ^W (OH) ₂	0.934	0.763	—	2.77
7 153620	A□ _B (Fe ²⁺ _{1.86} Ca _{0.14}) ⁺ C(Mg _{0.23} Fe ²⁺ _{4.77})Si ₈ O ₂₂ ^W (OH) ₂	1.006	0.734	428	—
8	A ^B Na _{0.83} ^B (Na _{0.83} Mg _{1.17}) ⁺ C(Mg _{5.00} Si ₈ O ₂₂ ^W (OH) ₂)	0.904	0.720	598	—
9	A ^B Na _{0.95} ^B (Li _{0.95} Mg _{1.05}) ⁺ C(Mg _{5.00} Si ₈ O ₂₂ ^W (OH) ₂)	1.035	0.720	520	23
10, 12	A ^B Na _{1.00} ^B (Na _{1.00} Mg _{1.00}) ⁺ C(Mg _{5.00} Si ₈ O ₂₂ ^W (OH) ₂)	0.983	0.720	559	18
10, 12	A ^B Na _{1.00} ^B (Na _{0.60} Li _{0.40} Mg _{1.00}) ⁺ C(Mg _{5.00} Si ₈ O ₂₂ ^W (OH) ₂)	0.931	0.720	581	13
10, 12	A ^B Na _{1.00} ^B (Na _{0.20} Li _{0.80} Mg _{1.00}) ⁺ C(Mg _{5.00} Si ₈ O ₂₂ ^W (OH) ₂)	0.905	0.720	590	10
11	A ^B Na _{0.90} ^B (Na _{0.92} Mg _{1.08}) ⁺ C(Mg _{4.98} Y ³⁺ _{0.02})Si ₈ O ₂₂ ^W F ₂	1.035	0.720	398	—

Note: * site assignment not reported, thus average ionic radii have not been calculated based on present knowledge of cation partitioning[§] formulae from Hirschmann et al. (1994); † Sueno et al. (1972); ‡ Zhang et al. (1992); § Yang and Smith (1996); ¶ Yang et al. (1998); †† Reece et al. (2000); ††† Boffa Ballaran et al. (2004); †††† Boffa Ballaran et al. (2001); ††††† Iezzi et al. (2005); †††††† Della Ventura et al. (pers. comm.); ††††††† Cámara et al. (2007); †††††††† Iezzi et al. (2007)

kanoite). The two *C*-centered polymorphs have very different structures: the *HT-C2/c* phase has a fully-extended chain of tetrahedra, whereas the *HP-C2/c* phase has a strongly kinked chain. Analogously to amphiboles, compression of the *HT-C2/c* phase (which can be stable at room-*T*) causes transformation to the *P2₁/c* structure. Further compression transforms the *P2₁/c* to *HP-C2/c* structure. Later, we discuss evidence for the analogous *P2₁/m* → *HP-C2/m* transition in amphibole. First, we make some observations on the *P2₁/c* ↔ *HT-C2/c* transition in clinopyroxene.

***P2₁/c* ↔ *HT-C2/c*.** This transition has been studied either by heating or cooling at room-*P* (*P2₁/c* → *HT-C2/c*, e.g., pigeonite, kanoite, Li Fe³⁺ Si₂ O₆, Li Ga Si₂ O₆) or by compression at room-*T* (*HT-C2/c* → *P2₁/c*, e.g., spodumene, Li Sc Si₂ O₆, Zn₂ Si₂ O₆).

High-*T* studies of this transition in M²⁺₂ Si₂ O₆ and (Na,Li)_{Σ=1} M³⁺ Si₂ O₆ clinopyroxenes indicate a clear inverse dependence of *T_c* on the aggregate cation size at the pyroxene *M*(2) site, <*r_M(2)*> and at the *M*(1) site (<*r_M(1)*>) respectively (Prewitt et al. 1971; Arlt and Armbruster 1997; Arlt et al. 2000; Redhammer and Roth 2002; Tribaudino et al. 2003). The *M*(2) site in pyroxene is the counterpart of the *M*(4) site in amphibole, and the strong inverse correlation between *T_c* and <*r_M(2)*> mirrors that observed for <*r_M(4)*> in cummingtonite and synthetic ^ANa ^B(NaMg) ^CMg₅ ^TSi₈ O₂₂ ^W(OH)₂ – ^ANa ^B(LiMg) ^CMg₅ ^TSi₈ O₂₂ ^W(OH)₂ amphiboles described above. Furthermore, when the *M*(2) site is occupied by Li in clinopyroxene *T_c* depends on <*r_M(1)*> (Redhammer and Roth 2004). Such behavior recalls the roles of both *M*(4) and *M*(1,2,3) in the redational behavior of ^ANa ^B(NaMg) ^CMg₅ ^TSi₈ O₂₂ ^W(OH)₂ and ^ANa ^B(NaMg) ^CMg₅ ^TSi₈ O₂₂ ^WF₂ amphiboles described above. The thermodynamic character of the *P2₁/c* ↔ *HT-C2/c* transition in most M²⁺₂ Si₂ O₆ clinopyroxenes is either first-order (Smyth 1974; Tribaudino et al. 2002) or tricritical (Tribaudino et al. 2003), but can also be second-order (Cámara et al. 2002). In Li M³⁺ Si₂ O₆ clinopyroxenes, the transition is either second-order or tricritical (Redhammer and Roth 2004).

High-pressure studies of M⁺ M³⁺ Si₂ O₆ clinopyroxenes with only Li at the *M*(2) site show that *P_c* depends on the size of the *M*(1) cation: 3.19 GPa in spodumene (<*r_M(1)*> = 0.535 Å, Arlt and Angel 2000); 0.7–1.0 GPa in Li Fe³⁺ Si₂ O₆ (<*r_M(1)*> = 0.645 Å, Pommier et al. 2005); 0.6 GPa in Li Sc³⁺ Si₂ O₆ (<*r_M(1)*> = 0.745 Å, Arlt and Angel 2000). In amphibole, *P_c* depends on <*r_M(4)*> and <*r_M(1,2,3)*>. Compression studies of the *HT-C2/c* → *P2₁/c* transition at room-*T* have been made on spodumene, Li Sc Si₂ O₆ and Zn₂ Si₂ O₆ (Arlt and Angel 2000) for which the *P_c* value is 1.92 GPa, respectively. Spodumene and Zn₂ Si₂ O₆ show marked first-order behavior, whereas the transition is tricritical for Li Sc Si₂ O₆ (as determined from the behavior of superlattice intensities by Arlt and Angel 2000).

As we have seen, the *P2₁/m* ↔ *HT-C2/m* transition in amphibole is characteristically second-order, although Iezzi et al. (2005) found tricritical behavior for ^ANa ^B(LiMg) ^CMg₅ ^TSi₈ O₂₂ ^W(OH)₂. *What seems to be clear is that there is no evidence of first-order (“discontinuous”) behavior for this transition in amphiboles.* A plausible explanation for the distinctly continuous (second-order) high-*T* behavior of cummingtonite is that the linking of the two chains of tetrahedra in amphiboles, at O(7) in *C2/m* and O(7A,B) in *P2₁/m*, acts as a brake on rotation of *T*(1), thereby damping any possible first-order behavior: tetrahedra in amphibole are less easily rotated than are those of pyroxene. This explanation may also apply to the behavior of cummingtonite-grunerite solid solutions at the *HT-C2/m* → *P2₁/m* transition at high pressure, which is usually second-order, but occasionally tricritical.

***P2₁/c* ↔ *HP-C2/c*.** Clinoenstatite, clinoferrrosilite, kanoite, Cr Mg Si₂ O₆ and Mn Si O₃ pyroxenes undergo a *P*-induced transition from the *P2₁/c* structure to a new *C*-centered polymorph, the *HP-C2/c* phase referred to in the Introduction. Kudoh et al. (1989) and Arlt and Angel (2000) found that Zn₂ Si₂ O₆ pyroxene has two phase transitions in isothermal compression: *HT-C2/c* ↔ *P2₁/c* at 1.92 GPa, and *P2₁/c* ↔ *HP-C2/c* at 4.9 GPa. The chain of tetrahedra of the *HP-C2/c* structure is highly kinked, unlike the straight chain of the *HT-*

$C2/c$ phase. This transition is markedly first-order in all five pyroxenes in which it has been recognized, and it involves large volume decreases (2-3 %). The transition has not yet been observed in $M^+ M^{3+} Si_2 O_6$ clinopyroxenes. For example, Gatta et al. (2005) did not observe the transition in their study of synthetic magnesian ferri-spodumene $M^{(2)}(Li_{0.85}Mg_{0.09}Fe^{2+}_{0.06})M^{(1)}(Fe^{3+}_{0.85}Mg_{0.15})Si_2O_6$ up to 7.4 GPa.

Given the structural similarities between pyroxene and amphibole, the possibility arises that amphibole may also undergo an analogous high-pressure $P2_1/m \rightarrow$ “HP- $C2/m$ ” transition. We now consider recent evidence for the occurrence of this transition.

A possible high-pressure $P2_1/m \leftrightarrow$ “HP- $C2/m$ ” transition in amphibole: synthetic ${}^A Na {}^B (NaMg) {}^C Mg_5 {}^T Si_8 O_{22} {}^W (OH)_2$ and ${}^A Na {}^B (LiMg) {}^C Mg_5 {}^T Si_8 O_{22} {}^W (OH)_2$

Iezzi et al. (2006) studied synthetic ${}^A Na {}^B (NaMg) {}^C Mg_5 {}^T Si_8 O_{22} {}^W (OH)_2$ at room-temperature and pressures up to 30 GPa using synchrotron infrared spectroscopy and found evidence (doublets of OH-stretching peaks) for a transition at ~ 23 GPa from the $P2_1/m$ structure to a new high-pressure $C2/m$ polymorph, provisionally designated as “HP- $C2/m$ ” by analogy with high-pressure HP- $C2/c$ pyroxene. In a further study using synchrotron IR spectroscopy, Iezzi et al. (2007) studied the effects of $M(4)$ composition upon the compressional responses of ${}^A Na {}^B (Na_x Li_{1-x} Mg) {}^C Mg_5 {}^T Si_8 O_{22} {}^W (OH)_2$ solid solutions. The same kind of spectroscopic behavior of ν_{OH} as observed for ${}^A Na {}^B (NaMg) {}^C Mg_5 {}^T Si_8 O_{22} {}^W (OH)_2$ was noted and a possible $P2_1/m \rightarrow$ HP- $C2/m$ transition identified. The spectroscopic changes as a function of compression for the amphibole ${}^A Na {}^B (LiMg) {}^C Mg_5 {}^T Si_8 O_{22} {}^W (OH)_2$ are shown in Figure 23. The A and B bands identified in the HT study of the $P2_1/m \leftrightarrow$ HT- $C2/m$ transition by Iezzi et al. (2005) as characteristic of the $P2_1/m$ phase (see above) are initially separated by 45 cm^{-1} ; on compression the B band undergoes a marked blue shift, compared with the A band which is almost unchanged to 6.3 GPa. The B band converges on the A band, and at 9.1 GPa, there is only a single band, assigned to the unique OH of the HP- $C2/m$ structure. The relative behavior of the A and B bands is very different from that observed for the $P2_1/m \leftrightarrow$ HT- $C2/m$ transition in this amphibole (see Fig. 19). Fitting of the OH spectra allowed approximate P_c values to be obtained which show a well-defined linear increase with $\langle {}^{[8]}r_{M(4)} \rangle$ (Fig. 24). The lowest P_c is 10 GPa for ${}^A Na {}^B (LiMg) {}^C Mg_5 {}^T Si_8 O_{22} {}^W (OH)_2$. The proposed

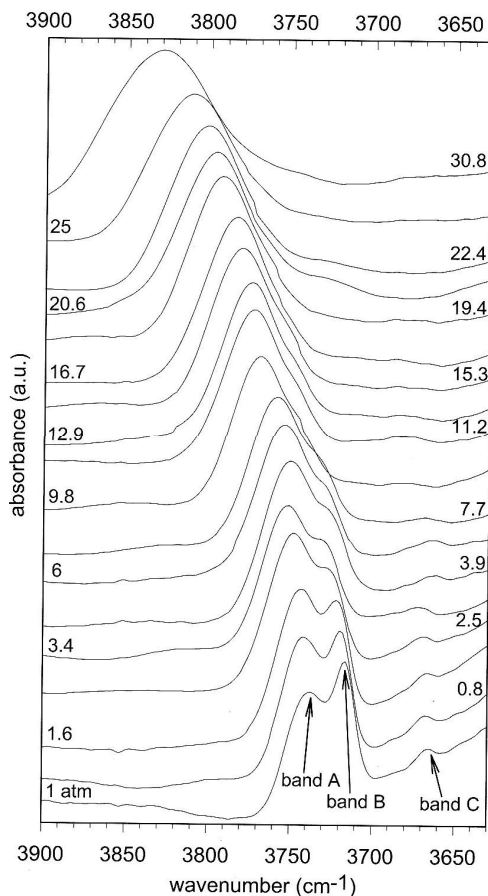
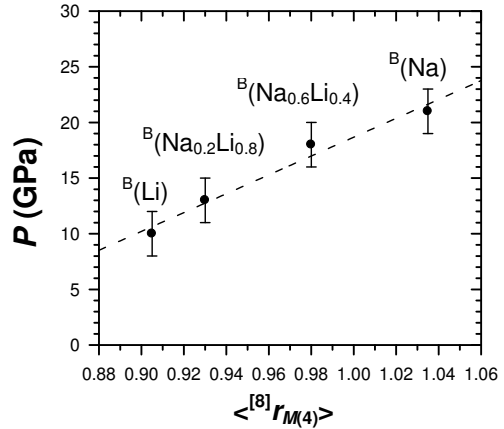


Figure 23. Variable- P , room- T infrared absorption spectra in the principal OH-stretching region of synthetic ${}^A Na {}^B (LiMg) {}^C Mg_5 {}^T Si_8 O_{22} {}^W (OH)_2$ through the HT- $C2/m \rightarrow$ $P2_1/m$ transition. See text for peak assignments. From Iezzi et al. (2006).

Figure 24. Correlation between $\langle [8]r_{M(4)} \rangle$ and P_c for the proposed high-pressure transition $P2_1/m \rightarrow \text{HP-C2}/m$.



$P2_1/m \leftrightarrow$ “HP-C2/ m ” transition occurs at much higher pressures in amphibole than it does in pyroxene. Until structural data or quality high- P powder IR spectra in the 1000-2000 cm^{-1} range are available, the character of the transition in amphibole (first-order as in pyroxene?) remains to be determined.

Other transitional behavior

The $C\bar{1} \leftrightarrow C2/m$ displacive transition in synthetic $^A\text{Na}^B(\text{NaNa})^C\text{Mg}_5^T\text{Si}_8\text{O}_{21}(\text{OH})_3$. Although recognized more than 30 years ago, the occurrence of amphiboles with a large excess of structural OH has, until very recently, eluded structural characterization. The most OH-rich amphibole reported, synthetic $^A\text{Na}^B(\text{NaNa})^C\text{Mg}_5^T\text{Si}_8\text{O}_{21}(\text{OH})_3$, has three OH groups per formula unit. At ambient conditions, this amphibole is triclinic (space group $C\bar{1}$) with a triple- b supercell (Maresch et al. 1991; Cámara et al. 2004). The structure of this complex amphibole is shown in Hawthorne and Oberti (2007, this volume). On heating, X-ray powder diffraction registers a change to monoclinic metric symmetry at 130 °C, with loss of the superlattice reflections (Maresch et al. 1991). Observations by electron diffraction (TEM) on heating through the transition indicate that intermediate incommensurate states are involved, with modulations of less than $3b$ in length.

Liu et al. (1996) studied this transition using ^{29}Si and ^1H MAS NMR spectroscopy from room-temperature to 240 °C. A complex sequence of spectral changes was observed. Figure 25 shows the ^{29}Si MAS NMR spectra of $^A\text{Na}^B(\text{NaNa})^C\text{Mg}_5^T\text{Si}_8\text{O}_{21}(\text{OH})_3$. The room-temperature spectrum comprises at least nine resonances. On heating, these nine peaks resolve into two major groups, corresponding to the $T(1)$ and $T(2)$ sites. The room-temperature spectrum is consistent with the triple- b superstructure determined by Cámara et al. (2004), for which there are twelve non-equivalent T sites. At 100 °C, there are at least five different $T(1)$ and three different $T(2)$ resonances, and at 120-130 °C there are essentially two main $T(1)$ peaks and one main $T(2)$ peak, a situation which is characteristic of the ^{29}Si MAS NMR spectra of richteritic amphiboles (Welch et al. 1998), where the differential (spectroscopic) splitting of the $T(1)$ sites relative to the single $T(2)$ peak seems to be characteristic of m point symmetry of the A -site cation, which is displaced toward one of the double-chains of tetrahedra within the (010) mirror plane. At 180 °C, the $T(1)$ and $T(2)$ sites are each represented by a single peak. These two peaks narrow on further heating to 240 °C. The simple two-peak spectrum is similar to that of tremolite and is only consistent with $C2/m$ symmetry; space groups Cm or $C2$ would both have two $T(1)$ and two $T(2)$ sites. Transient Cm -like or $C2$ -like states are consistent with the 170 °C and 180 °C spectra. The complex changes in the number and proportions of different Si sites registered by

the ^{29}Si MAS NMR spectra are consistent with the occurrence of incommensurate states, as indicated by electron diffraction.

The room-temperature ^1H MAS NMR spectrum of the triclinic polymorph (Fig. 26) has three well-defined resonances corresponding to the “normal” $\text{O}^{(3)}\text{H}$ protons and the $[\text{O}(4)\text{-H}(1)+\text{H}(2)]$ and $\text{O}(4)\text{-H}(3)$ excess H. On close inspection it is seen that the $\text{O}^{(3)}\text{H}$ peak comprises two peaks in ratio 2:1, consistent with the 3-*I*-beam (3*b*) character of the superstructure. On heating (Fig. 26), the two peaks due to excess H merge and at 180 °C are indistinguishable, consistent with *C2/m* symmetry indicated by the ^{29}Si MAS NMR study. The behavior of the excess H in this amphibole is not yet understood. Despite this uncertainty,

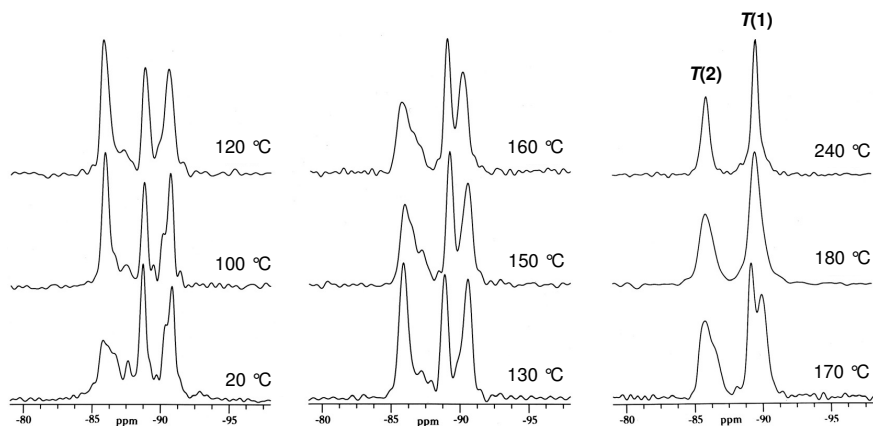


Figure 25. Variable- T ^1H - ^{29}Si cross-polarization (CP) MAS spectra of synthetic $^{\text{A}}\text{Na}^{\text{B}}(\text{NaNa})^{\text{C}}\text{Mg}_5^{\text{T}}\text{Si}_8\text{O}_{21}^{\text{W}}(\text{OH})_3$ having one excess proton per formula unit. A return-to-ambient spectrum (not shown) is almost identical to the initial 20 °C spectrum shown above. [Used by permission of Schweitzerbart'sche Verlagsbuchhandlung OHG, www.schweitzerbart.de. From Liu et al. (1996), *European Journal of Mineralogy*, 8, Fig. 1, p. 225.]

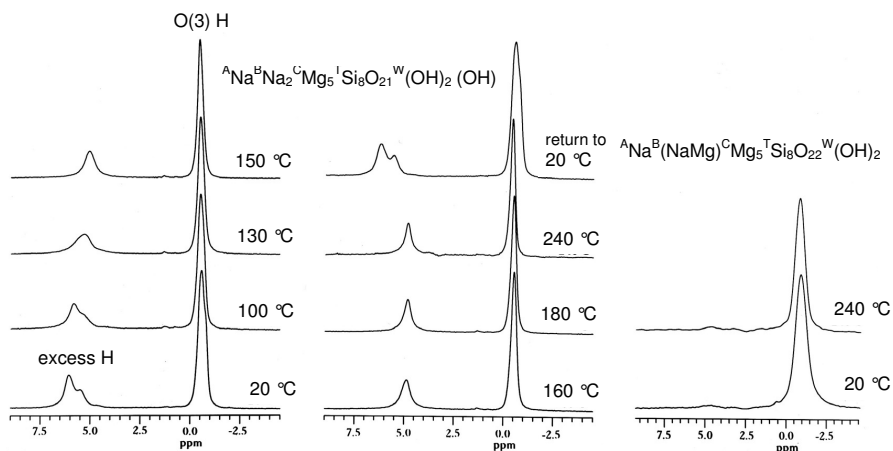


Figure 26. Variable- T ^1H MAS spectra of synthetic $^{\text{A}}\text{Na}^{\text{B}}(\text{NaNa})^{\text{C}}\text{Mg}_5^{\text{T}}\text{Si}_8\text{O}_{21}(\text{OH})_3$ and $^{\text{A}}\text{Na}^{\text{B}}(\text{NaMg})^{\text{C}}\text{Mg}_5^{\text{T}}\text{Si}_8\text{O}_{22}^{\text{W}}(\text{OH})_2$. The resonances from the excess H and normal $^{\text{W}}\text{H}$ are indicated. [Used by permission of Schweitzerbart'sche Verlagsbuchhandlung OHG, www.schweitzerbart.de. From Liu et al. (1996), *European Journal of Mineralogy*, 8, Fig. 2, p. 226.]

there is excellent agreement between the structure determined by X-ray diffraction and the spectroscopic data.

IN SITU HIGH-TEMPERATURE STUDIES OF CATION ORDER-DISORDER

In most cases, the state of long-range order of cations at non-ambient T has been determined by *ex situ* single-crystal X-ray diffraction on quenched samples (Hirschmann et al. 1994; Evans and Yang 1998). Recently, *in situ* determinations of the state of long-range cation ordering in amphiboles have been made using neutron powder diffraction (Reece et al. 2000, 2002; Welch et al. 2007). These neutron-diffraction studies showed that detectable cation disorder occurs within 1-2 h above 400 °C, and that there is some re-ordering on cooling. We now consider the results of these *in situ* neutron diffraction studies of cation order/disorder.

***In situ* high- T neutron diffraction studies of amphiboles**

Neutrons, unlike X-rays, are not significantly attenuated or absorbed by environmental devices surrounding the sample (heaters, cryostats, glassware, metal capsules). In principle, therefore, neutron diffraction provides a very useful means by which high-temperature processes in hydrous minerals can be studied at water-saturated conditions, thus stabilizing such phases to significantly higher temperatures than are allowed by water-undersaturated conditions. For example, in a high- PT study of brucite at 6 GPa and at water-undersaturated conditions (Le Godec et al. 2001) the mineral decomposed 400° below its water-saturated dehydration curve within an hour. Achieving high temperature at water-saturated conditions remains a challenge for *in situ* large-volume diffraction experiments.

There is a further important advantage that neutron scattering has over X-ray scattering: as neutron scattering lengths are not wavevector-dependent, adjacent or nearby elements in the periodic table often have very different scattering powers and can be readily distinguished. This feature allows the refinement of site occupancies of pairs of elements which commonly substitute at the same crystallographic sites in rock-forming minerals. For example, Fe and Mn have coherent neutron scattering lengths of 9.45 fm and -3.73 fm, respectively, corresponding to a contrast of more than 13 fm and thereby allowing their ratio at mixed sites to be refined to high precision (1-2%). Similarly, site occupancies involving iso-electronic species can be determined *directly* (refined from site scattering) by neutron diffraction. A drawback of neutron powder diffraction studies is that samples usually need to be large (> 1 g) in order to get strong enough signals for a sequence of short (e.g., 6 h) variable-temperature runs. We now discuss the results of recent *in situ* high- T studies of cation order/disorder in natural manganogrunerite and synthetic richterite.

Mg-Mn and Fe-Mn ordering in manganocummingtonite and manganogrunerite

Reece et al. (2000) studied the temperature dependence of Mg-Mn ordering between $M(1,2,3)$ and $M(4)$ sites in a natural iron-free manganocummingtonite (Talcville, New York) by time-of-flight neutron powder diffraction. At room-temperature this amphibole has the composition and site occupancies: $A^{\square} B(Na_{0.13}Ca_{0.41}Mg_{0.46}Mn^{2+}_{1.00})^C(Mg_{4.87}Mn_{0.13})^T Si_8 O_{22} W(OH)_2$. The presence of 0.13 Na at $M(4)$ implies that 0.13 ^{161}Mn is trivalent and as such is not expected to exchange with Mg at $M(4)$. A 5 g sample was heated under vacuum to 700 °C in 50-degree increments and then some datasets were collected on cooling to room temperature. As Mn has a negative scattering length (-3.73 fm), the scattering contrast for the Mg-Mn pair is considerable: $5.375 - (-3.73) = 9.105$ fm. Such large scattering contrast allows small changes in site occupancies to be determined. For this amphibole the net scattering at the $M(4)$ site is only 1.12

fm. Consequently, care is needed in refining its U_{iso} . However, the other $M(4)$ cations in this amphibole (Na, Ca) order completely at this site and so have fixed (unrefined) occupancies. Hence, the problem reduces to determining the Mg/Mn ratios at the $M(1,2,3)$ and $M(4)$ sites. Initial refinement of the ambient structure of this amphibole gave the site occupancies shown above. The evolution of the site occupancy of $M(4)$ site as a function of temperature is shown in Figure 27 (standard deviations are only 0.01 atom per formula unit). The data show an initial small increase in Mn at $M(4)$ as the sample tries to achieve a higher degree of order commensurate with 450-500 °C. There is progressive disordering from 600-700 °C, leading to a minimum $X_{\text{Fe}}^{M(4)}$ of 0.49. This state of order is retained upon cooling to 200 °C. Interestingly, the changed state of the more disordered amphibole is registered as clear changes in b , c and β lattice parameters, as shown in Figure 28. The on-heating curves of b , c and β parameters have three distinct linear segments that correspond to the low- T $P2_1/m \leftrightarrow C2/m$ transition ($T_c = 107$ K), linear expansion

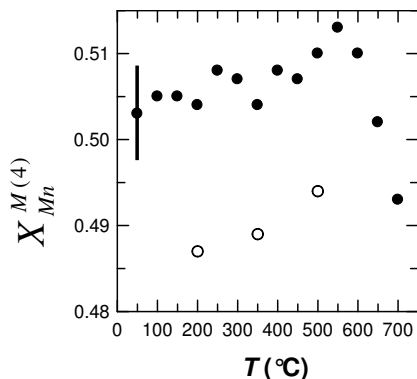


Figure 27. Variation in the Mn content at $M(4)$ with T for a natural Fe-free manganocummingtonite (Talcville) determined by *in situ* neutron powder diffraction. Filled data points were collected on heating, open ones on cooling from 700 °C. A representative standard-error bar is shown. [Used by permission of the Mineralogical Society of Great Britain and Ireland. Modified from Reece et al. (2000), *Mineralogical Magazine*, 64, Fig. 3, p. 261.]

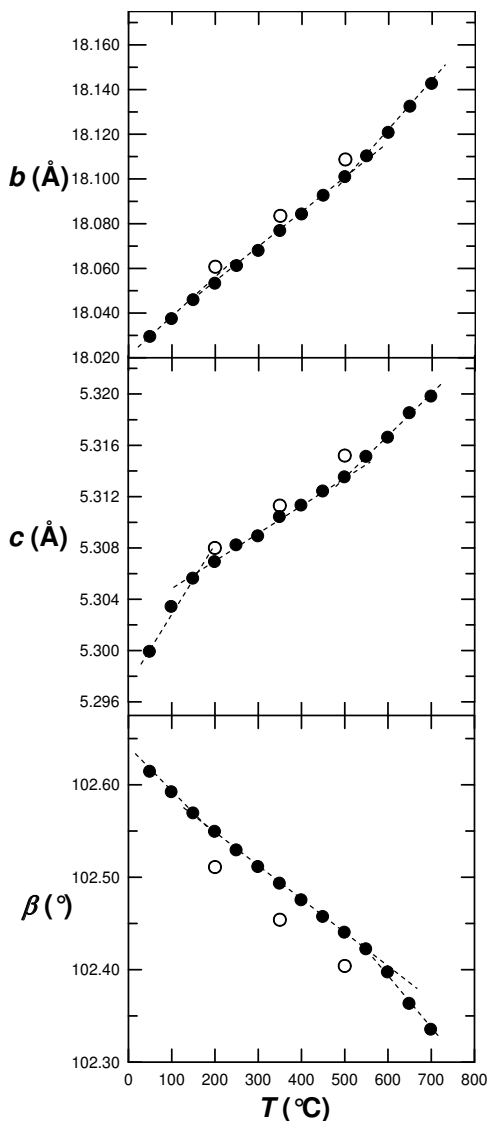
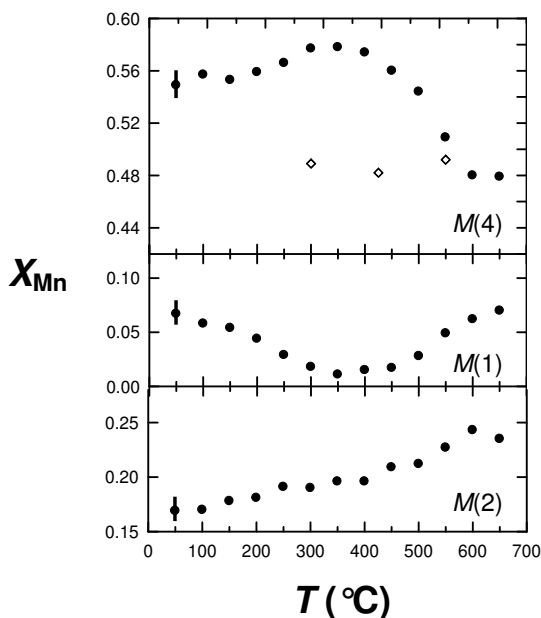


Figure 28. Variations with T of b , c and β lattice parameters for the Talcville manganocummingtonite determined by *in situ* neutron powder diffraction. Filled circles are data points collected on heating, open circles on cooling. Experimental errors are smaller than symbols. The three distinct linear segments of the heating curves are indicated by dashed lines. [Used by permission of the Mineralogical Society of Great Britain and Ireland. Modified from Reece et al. (2000), *Mineralogical Magazine*, 64, Fig. 4, p. 262.]

to ~ 450 °C, and finally a segment from 550-750 °C associated with cation disordering. The data-points collected on cooling (open circles in Fig. 28), for which the 750 °C site occupancy is retained, show a parallel, but clearly displaced trend relative to the on-heating series.

Analogous, but more pronounced, T -induced disordering effects were observed by Reece et al. (2002) in a neutron powder-diffraction study of Mn-Fe²⁺ order/disorder in two natural manganogrunerite. The scattering contrast between Mn and Fe is very large at 13.18 fm and allows very small changes in Mn-Fe site occupancies to be determined for these amphiboles (errors on occupancies are $\leq 2\%$). Refinements of the initial site occupancies of these amphiboles indicate that relative Mn occupancies are $M(4) \gg M(2) > M(1) \gg M(3)$ sites, with Mn occupancies of $M(1,2,3)$ sites being < 0.2 apfu. The variation with temperature of the Mn contents of $M(1)$, $M(2)$ and $M(4)$ sites for sample BM1980,280 are shown in Figure 29. Some clear trends are evident: (a) above 400 °C, the Mn occupancy of $M(4)$ decreases sharply from 0.58 to 0.48 at 600-650 °C, corresponding to $\sim 35\%$ disorder at 650 °C; (b) the variations in $M(1)$ and $M(2)$ site occupancies indicate that the main exchange involves Mn-Fe at $M(4)$ and $M(2)$, as is also found for Mn-Mg exchange in the Talcville amphibole described above. The site-exchange energies of the Mn between $M(4)$ and $M(1,2,3)$ sites for the two amphiboles, calculated from the temperature dependence of the refined site occupancies, is -14.9 ± 0.5 kJ mol⁻¹. This value is significantly lower than the 24.6 ± 1.5 kJ mol⁻¹ calculated for the Fe-free Talcville amphibole (Reece et al. 2000). The partitioning of a smaller cation (Fe²⁺) into $M(4)$ is mitigation of the effect of thermal expansion on $\langle M(4)-O \rangle$ in the case of BM1980,280 (Fig. 30), for which confirmation of the expected thermal response of $\langle M(4)-O \rangle$ at fixed $M(4)$ occupancy (0.48) is shown by the three data-points collected on cooling. Hence, the *in situ* neutron experiments can register changes in site occupancies *via* site scattering and $\langle M(4)-O \rangle$. Furthermore, as with the behavior of the Talcville amphibole, the high- T disordering has clear effects on the b , c and β lattice parameters (Fig. 31). Here, we see again that the T -induced disordered state of the amphibole is retained on cooling, leading to curves for these parameters that are clearly displaced from those of the heating curves.

Figure 29. Mn contents of the $M(1)$, $M(2)$ and $M(4)$ sites of $C2/m$ manganogrunerite (Swedish Bergslagen) determined by *in situ* neutron powder diffraction. A representative standard-error bar is shown. [Used by permission of Springer, modified after Reece et al. (2002), *Physics and Chemistry of Minerals*, 29, Fig. 3, p. 565.]



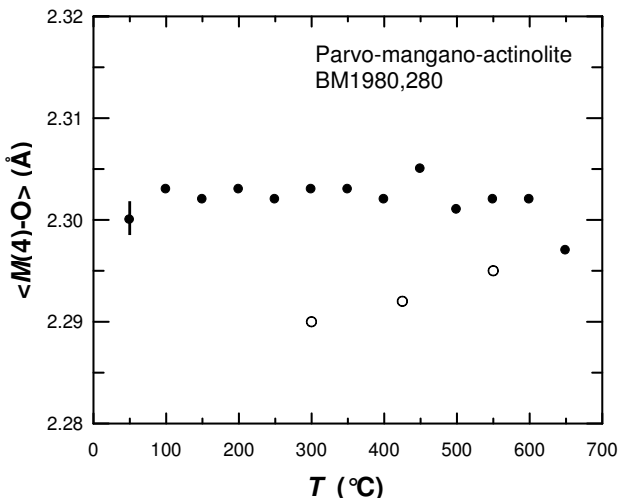


Figure 30. Variation of $\langle M(4)\text{-O} \rangle$ with T for the same sample as Figure 29. A representative standard-error bar is shown. [Used by permission of Springer, modified from Reece et al. (2002), *Physics and Chemistry of Minerals*, 29, Fig. 4, p. 566.]

^c(Ni-Mg) disorder in K-richterite

Welch et al. (2007) studied *in situ* T -induced partitioning of Ni and Mg over $M(1,2,3)$ sites in synthetic potassic-richterite $^A\text{K}^B(\text{NaCa})^C(\text{Mg}_{2.5}\text{Ni}_{2.5})^T\text{Si}_8\text{O}_{22}^W(\text{OH})_2$ by neutron powder diffraction to 700 °C on a 3.5 g sample synthesized at 0.1 GPa, 750 °C, 4 days. Three-hour data collections on the POLARIS time-of-flight diffractometer (ISIS, UK) were made at each temperature. Figure 32 shows a Rietveld refinement of the 50 °C dataset, with the few diagnostic peaks sensitive to the state of Ni-Mg order starred. Figure 33 shows that on heating to 700 °C, there is a progressive exchange of Ni from $M(2)$ to $M(1)$, with the Ni content of $M(3)$ independent of T ($X_{\text{Ni}}^{M(3)} = 0.68$) in this temperature range. The T -dependent ordering involving $M(1)$ and $M(2)$ is also shown in Figure 34 in which it is seen that the initial Ni distribution between $M(1)$ and $M(2)$, corresponding to the distribution in the quenched synthesis product, agrees closely with the 750 °C isotherm defined by the synthesis data of Della Ventura et al. (1993) for synthetic Ni-Mg K-richterites, lending credence to the ordering trend observed here. No subsequent disordering at high T was observed in this study because of the short data collections used.

AMPHIBOLE COMPRESSIBILITIES

Compared with pyroxene, relatively few measurements of amphibole compressibilities have been made. Figure 35a shows the compression data of Comodi et al. (1991) for tremolite, glaucophane and pargasite, and Welch and Lennie (unpublished data) for synthetic end-member potassic-richterite. The scatter for the Comodi et al. (1991) data reflects the uncertainties in the relative compression, whereas the potassic-richterite data (Rietveld refinements of synchrotron XRD data) have standard uncertainties comparable to the size of the symbols. The most precise lattice parameters for equation-of-state determination are obtained when using a diffractometer with a long crystal-to-detector distance, such as a Huber (Angel 2000), which provides high angular (2θ) resolution at the expense of reduced peak intensity. It should be recognized here that Comodi et al. (1991) used a Phillips PW1100 diffractometer, which has a relatively short crystal-to-detector distance, as these workers were also interested in refining crystal structures of the amphiboles, a task for which the Phillips PW1100 is well-suited.

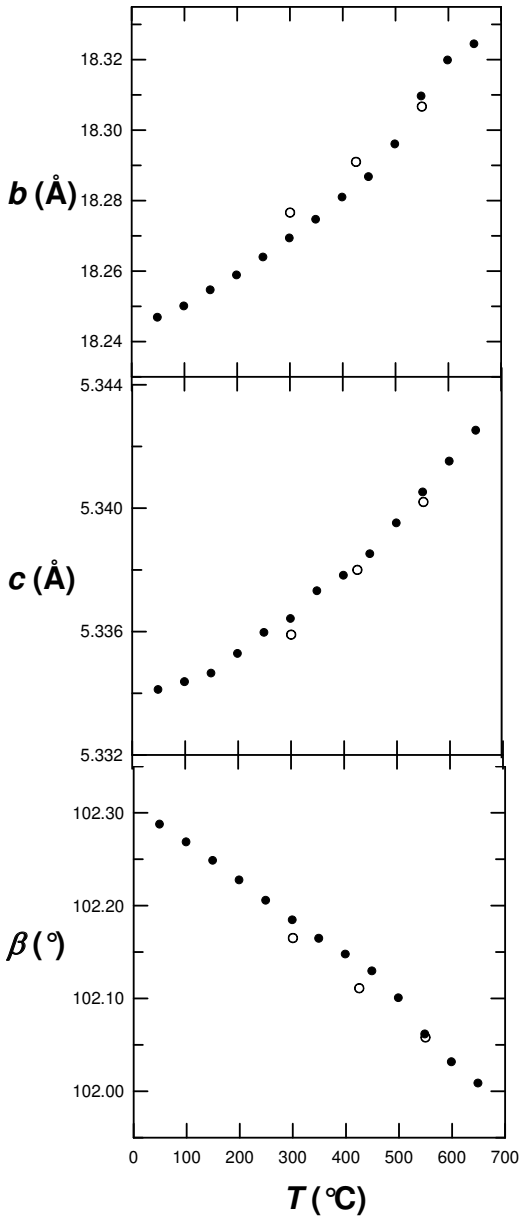


Figure 31. Variation with T of b , c and β lattice parameters for the mangno-manganocummingtonite determined by *in situ* neutron powder diffraction. Filled circles are data points collected on heating, open circles on cooling. Experimental errors are smaller than symbols. [Used by permission of Springer, modified from Reece et al. (2002), *Physics and Chemistry of Minerals*, 29, Fig. 1, p. 564.]

Table 2 summarizes elastic moduli for cummingtonite, grunerite, tremolite, glaucophane, pargasite and potassic-richterite. The values for tremolite, glaucophane and pargasite are redetermined from the data of Comodi et al. (1991) by fitting to a second-order Birch-Murnaghan equation of state, allowing a more meaningful comparison with the results for cummingtonite, grunerite and potassic-richterite. Consistent trends in the compressibilities are evident: in all cases $K_c > K_b \gg K_a$. The differences between K_a and $K_{a\sin\beta}$ (Table 1) reflect the fact that compression along [100] also has a component from compression along [001]. It is, therefore, more appropriate to consider $K_{a\sin\beta}$ rather than K_a . These three orthogonal vectors ($a\sin\beta$, b and c) are parallel to the three directions defining the topological anisotropy of the amphibole structure, and so equation-of-state studies provide key insight into the structural response of amphibole to compression. The trends of compressibilities observed in amphibole contrast with what observed in pyroxene, where $K_c \sim K_{a\sin\beta} \gg K_b$. Again, this different behavior must be related to the low compressibility of the double-chain along the b axis.

Despite the scatter of the data for the compression of tremolite, glaucophane and pargasite in Figure 35a (especially for b/b_0) and the data reported in Table 2, some significant compositional trends are evident, as seen more clearly in the polynomial fits (used as eye-guides) to the compression curves in Figure 35b:

(a) The compression data for $a\sin\beta$ indicate that a full A-site (pargasite, potassic-richterite) stiffens the structure in this direction (by about 15% relative to tremolite). There may also be a secondary stiffening due to high ^{6}Al (glaucophane).

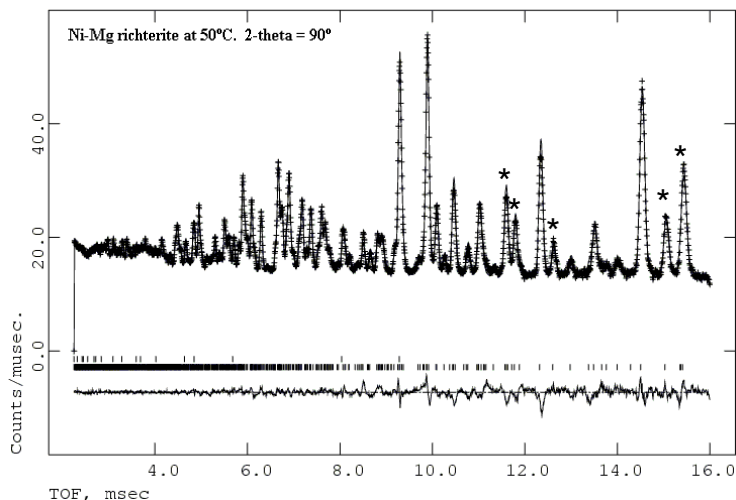


Figure 32. Rietveld refinement (50 °C) of a synthetic potassic-richterite of composition ${}^A\text{K}^B(\text{NaCa})^C(\text{Ni}_{2.5}\text{Mg}_{2.5})^T\text{Si}_8\text{O}_{22}^W(\text{OH})_2$ used in the *in situ* high- T neutron powder diffraction study of Welch et al. (2007). Reflections particularly sensitive to the Ni-Mg distribution are starred. [Used by permission of the Mineralogical Society of Great Britain and Ireland. From Welch et al. *Mineralogical Magazine*, (2007).]

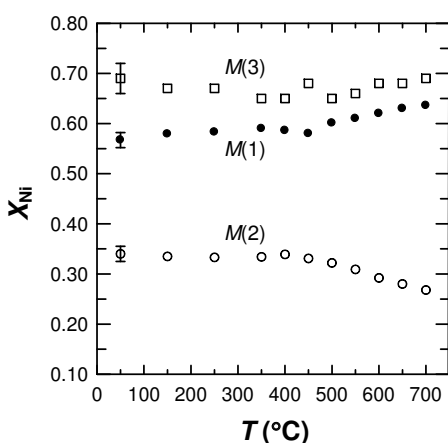


Figure 33. Variations in Ni contents of the $M(1)$, $M(2)$ and $M(3)$ sites in synthetic ${}^A\text{K}^B(\text{NaCa})^C(\text{Ni}_{2.5}\text{Mg}_{2.5})^T\text{Si}_8\text{O}_{22}^W(\text{OH})_2$ determined by *in situ* high- T neutron powder diffraction. Experimental errors are smaller than symbols. [Used by permission of the Mineralogical Society of Great Britain and Ireland. From Welch et al. (2007), *Mineralogical Magazine*.]

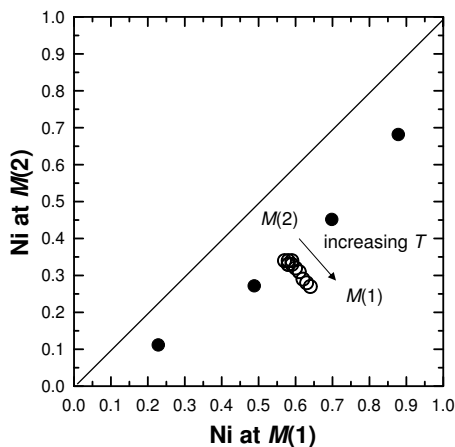


Figure 34. T -induced order of Ni from $M(2)$ to $M(1)$ is shown by the open circles. The original sample was synthesized at 750 °C, 0.1 GPa, 5 days. On heating, Ni begins to order onto $M(1)$ to attain a state of order that is nearer that appropriate for the temperature. Each data point corresponds to a 3–4 h data collection. The solid symbols are taken from Della Ventura et al. (1993) for several ${}^A\text{K}^B(\text{NaCa})^C\text{Mg}_5^T\text{Si}_8\text{O}_{22}^W(\text{OH})_2$ - ${}^A\text{K}^B(\text{NaCa})^C\text{Ni}_5^T\text{Si}_8\text{O}_{22}^W(\text{OH})_2$ solid-solutions synthesized at 750 °C. These data define a 750 °C isotherm upon which the initial values for the ${}^A\text{K}^B(\text{NaCa})^C(\text{Ni}_{2.5}\text{Mg}_{2.5})^T\text{Si}_8\text{O}_{22}^W(\text{OH})_2$ amphibole lie. [Used by permission of the Mineralogical Society of Great Britain and Ireland. From Welch et al. (2007), *Mineralogical Magazine*.]

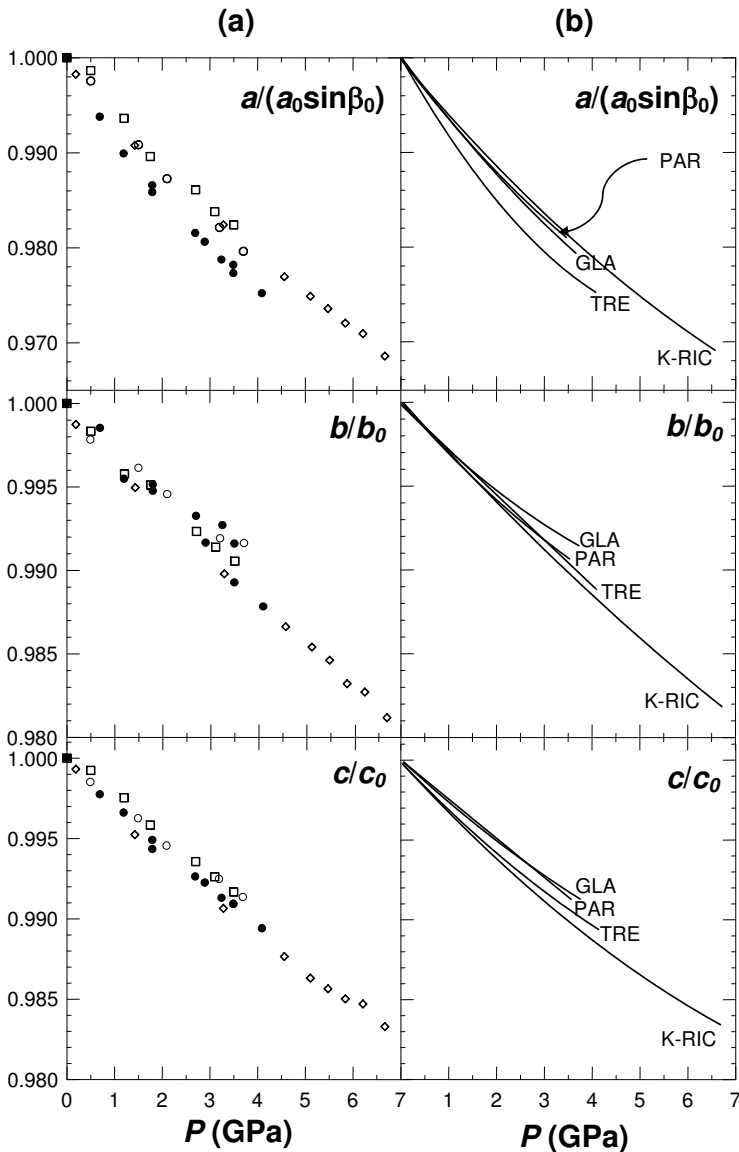


Figure 35. (a) Compression data for tremolite (solid circles), pargasite (squares), glaucophane (open circles) and synthetic potassic-richerite (diamonds). The tremolite, pargasite and glaucophane data are from Comodi et al. (1991) and those for synthetic potassic-richerite are from Welch and Lennie (unpublished data). (b) Trends of the data shown in (a): TRE = tremolite, PAR = pargasite, GLA = glaucophane, K-RIC = synthetic potassic-richerite.

Table 2. Elastic moduli of natural and synthetic amphiboles (in GPa).

	K_a	K_{asinb}	K_b	K_c	K_0	Ref.
tremolite	52(3)	47(2)	106(10)	122(23)	76(3)	1
glaucofane	57(3)	52(1)	130(7)	125(6)	88(6)	1
pargasite	62(3)	58(3)	122(4)	134(10)	91(6)	1
potassic-richterite	76(2)	60(2)	105(3)	121(4)	89(3)	2
cummingtonite- $P2_1/m$	57.9(5)*	47(3)	79(1)	69(1)	62.4(5)	3
cummingtonite- $C2/m$	51(1)	42(3)	85(4)	101(3)	66(2)	3
grunerite	46.6(5)	37(2)	97(2)	107.4(9)	65.4(2)	3

References: 1: Comodi et al. (1991); 2: Welch and Lennie (unpublished data); 3: Boffa Ballaran et al. (2000)

* From fit to a 3rd-order BM EoS for which $K_0' = 6.5$ (1)

- (b) The b parameter behavior reflects the occupancies of $M(4)$ and $M(2)$. Although poorly defined for tremolite, glaucofane and pargasite, the b lattice parameter behavior may indicate that high CAl (e.g., glaucofane) stiffens the structure in this direction.
- (c) Significant CAl contents (glaucofane, pargasite) stiffen the structure along b and c relative to $^C(Mg/Fe^{2+})$ -rich compositions.
- (d) The cummingtonite-grunerite compression data indicate that a small cation (Mg/Fe^{2+}) dominant at $M(4)$ allows considerable deformation of this polyhedron and results in a much higher bulk compressibility.

It is evident that CAl has a significant stiffening effect upon the amphibole structure: this is most clearly seen in the compressional behavior of glaucofane. The role of the $M(4)$ site is more clearly seen when a comparison is made with the cummingtonite-grunerite compression data (Fig. 16): dominant occupancy of this site by small cations (Mg, Fe^{2+}) allows considerable deformation of this polyhedron compared with calcic and sodic-calcic amphiboles. This deformation is enhanced by the $HT-C2/m \leftrightarrow P2_1/m$ transition as a result of the freedom of rotation of the tetrahedra.

In their study of tremolite, glaucofane and pargasite to 4 GPa, Comodi et al. (1991) observed that the most incompressible polyhedral component of the structure is the ribbon of edge-sharing $M(1,2,3)$ octahedra. As described above, deformation of the chains of tetrahedra mainly involves rigid rotations that allow matching of the chains with the changes in the dimensions of the ribbon. The sequences of isothermal polyhedral bulk moduli determined by Comodi et al. (1991) are $K_{M(2)} > K_{M(1)} > K_{M(3)} > K_{M(4)}$ for glaucofane and $K_{M(3)} > K_{M(1)} > K_{M(4)} > K_{M(2)}$ for tremolite and pargasite. It was suggested that the very different compressibilities of the $M(2)$ octahedron in glaucofane and the calcic amphiboles is due to full occupancy of the $M(2)$ site by Al^{3+} in glaucofane compared with dominance of Mg in tremolite and pargasite. In general, the $M(4)$ polyhedron becomes more regular on compression by significant shortening of $M(4)-O(5)$ and $M(4)-O(6)$ bonds (to the two adjacent I-beams). Deformation of the $M(3)$ octahedron is qualitatively similar in the three amphiboles, involving shortening of $M(1)-O(1)$ bonds; $M(3)-O(3)$ does not change length to 4 GPa, probably due to the higher compressibility of the O-H bond which is evinced by the blue shift in the HP -FTIR studies. The $M(1)$ octahedron undergoes slight compression to 4 GPa, with small (< 1%) contractions of $M(1)-O(2)$ and $M(1)-O(3)$. The major structural change observed by Comodi et al. (1991) was flattening of the I-beam along $asinb$ relative to that in the ambient structures in which the chains of tetrahedra are distinctly bowed.

There is clearly much more to be done on the compositional systematics of amphibole compressibilities. Most urgently, high-quality EoS data to 10 GPa are needed for a detailed understanding of topological responses and to allow determination of K_0' (currently constrained

to second-order as equal to 4 because of data quality). Determination of K_0' is highly relevant to predicting the compressional behavior of amphibole at subduction-zone conditions.

THERMAL EXPANSIVITIES

There is a dearth of thermal expansivity data for amphiboles and, consequently, a need for a concerted effort to evaluate the compositional systematics of expansivities. The extremely limited dataset (six compositions) is summarized in Table 3.

Table 3. Mean thermal expansion coefficients of the C2/m structure ($^{\circ}\text{C}^{-1}, \times 10^{-5}$) available in literature.

Reference	Composition*	T-range ($^{\circ}\text{C}$)	αa	αb	αc	αV
1	$\text{A}\square^{\text{B}}(\text{Ca})^{\text{W}}(\text{OH})_2$	24-700	1.20(4)	1.17(8)	0.59(5)	3.13(20)
2	$\text{A}^{\text{K}}\text{B}^{\text{B}}(\text{CaNa})^{\text{W}}\text{F}_2$	24-800	1.27(6)	1.34(4)	0.61(1)	3.39(12)
2	$\text{A}^{\text{Na}}\text{B}^{\text{B}}(\text{CaNa})^{\text{W}}\text{F}_2$	24-900	1.08(6)	1.27(2)	0.62(2)	3.11(9)
3	$\text{A}^{\text{Na}}\text{B}^{\text{B}}(\text{LiMg})^{\text{W}}(\text{OH})_2$	350-560	1.54(2)	0.95(2)	0.92(3)	3.58(5)
4	$\text{A}^{\text{Na}}\text{B}^{\text{B}}(\text{NaMg})^{\text{W}}(\text{OH})_2$	270-420	1.41(9)	1.10(14)	0.68(11)	3.41(20)
5	$\text{A}^{\text{Na}}\text{B}^{\text{B}}(\text{NaMg})^{\text{W}}\text{F}_2$	144-671	1.43(1)	1.28(2)	0.609(3)	3.51(3)
6	$\text{A}\square^{\text{B}}(\text{Na})^{\text{W}}(\text{OH})_2$	24-500	0.87(3)	0.63(3)	0.32(3)	1.90(6)
			$\alpha M(1)$	$\alpha M(2)$	$\alpha M(3)$	$\alpha M(4)$
1	$\text{A}\square^{\text{B}}(\text{Ca})^{\text{W}}(\text{OH})_2$	24-700	4.31	4.86	3.62	4.5
2	$\text{A}^{\text{K}}\text{B}^{\text{B}}(\text{CaNa})^{\text{W}}\text{F}_2$	24-800	4.07	4.25	3.94	4.9
2	$\text{A}^{\text{Na}}\text{B}^{\text{B}}(\text{CaNa})^{\text{W}}\text{F}_2$	24-900	3.54	3.5	3.91	4.34
3	$\text{A}^{\text{Na}}\text{B}^{\text{B}}(\text{LiMg})^{\text{W}}(\text{OH})_2$	350-560	§	§	§	§
4	$\text{A}^{\text{Na}}\text{B}^{\text{B}}(\text{NaMg})^{\text{W}}(\text{OH})_2$	270-420	†	†	†	†
5	$\text{A}^{\text{Na}}\text{B}^{\text{B}}(\text{NaMg})^{\text{W}}\text{F}_2$	144-671	4.09	3.68	2.5	4.26
6	$\text{A}\square^{\text{B}}(\text{Na})^{\text{W}}(\text{OH})_2$	24-500	§	§	§	§

Notes: *Only the A and B cations and W anions are reported, as the C and T cations are fixed to $\text{C}^{\text{Mg}_5\text{T}^{\text{Si}_8}}$, but for the last column glaucophane being $\text{C}^{\text{Mg}_3\text{Al}_2\text{T}^{\text{Si}_8}}$; † Not calculated because only two data points are available; § powder diffraction data, no polyhedral volume reported.

References: 1 Sueno et al. (1978), 2 Cameron et al. (1983), 3 Iezzi et al. (2005), 4 Cámara et al. (2003), 5 Cámara et al. (2007), 6 Jenkins and Corona (2006)

IDEAS FOR FUTURE STUDIES AND DIRECTIONS

Most of the detailed *in situ* studies of amphiboles have focused on a few significant or tractable compositions that provide tantalizing insight into the range of high-PT behavior of amphibole. No simultaneous *in situ* high P-T studies have been made, despite their obvious relevance to natural systems. The details of the HT-C2/m ↔ P2₁/m transition are now well understood. However, while interesting, this transition occurs in a very restricted range of natural amphibole compositions (predominantly cummingtonite-grunerite solid solutions). No *in situ* non-ambient studies of orthorhombic amphiboles have been made. Below, we suggest a few potentially very fruitful topics for future amphibole research on *in situ* behavior and the determination of fundamental physical properties relevant to the calculation of high P-T stabilities of amphiboles in Nature.

- 1) Determination of the structure of the proposed HP-C2/m polymorph and *in situ* spectroscopic mapping of a possible high P-T boundary between HT-C2/m and HP-C2/m polymorphs. Does such a boundary have a positive or negative Clapeyron slope ?

- 2) *In situ* studies of the effect of pressure upon cation ordering, e.g., extension of the high-*T* neutron diffraction study of Ni-Mg potassic-richterite to high *P*.
- 3) Improved and systematic determination of thermal expansivities and isothermal compressibilities. Extending compressibility measurements to higher *P* (10 GPa) is needed in order to improve K_0 and allow meaningful fitting of K_0' .
- 4) Linked to (3) is the determination of the importance of *P*-induced non-ideality in major binary solid solutions, focusing on synthetic samples, e.g., tremolite–pargasite; tremolite–richterite.
- 5) Non-ambient *in situ* studies of orthorhombic amphiboles, including the acquisition of compressibility and expansivity data.

REFERENCES

- Angel RJ, Chopelas A, Ross NL (1992) Stability of high-density clinoenstatite at upper-mantle pressures. *Nature* 358:322-324
- Angel RJ (2000) High pressure structural phase transitions. *Rev Mineral Geochem* 39:35-61
- Arlt T, Angel RJ, Miletich R, Armbruster T, Peters T (1998) High-pressure $P2_1/c \leftrightarrow C2/c$ phase transitions clinopyroxenes: influence of cation size and electronic structure. *Am Mineral* 83:1176-1181
- Arlt T, Kunz M, Stoltz J, Armbruster T, Angel RJ (2000) *P-T-X* data on $P2_1/c$ clinopyroxenes and their displacive phase transitions. *Contrib Mineral Petrol* 138:35-45
- Arlt T, Angel RJ (2000) Displacive phase transition in C-centered clinopyroxenes: spodumene, $\text{LiScSi}_2\text{O}_6$ and ZnSiO_3 . *Phys Chem Mineral* 27:719-731
- Boffa Ballaran T, Angel RJ, Carpenter MA (2000) High-pressure transformation behaviour of the cummingtonite-grunerite solid solution. *Eur J Mineral* 12:1195-1213
- Boffa Ballaran T, Carpenter MA, Domeneghetti MC (2001) Phase transition and thermodynamic mixing behaviour of the cummingtonite-grunerite solid solution. *Phys Chem Mineral* 28:87-101
- Boffa Ballaran T, McCammon CA, Carpenter MA (2002) Order-parameter behavior at the structural phase transition in cummingtonite from Mössbauer spectroscopy. *Am Mineral* 87:1490-1493
- Boffa Ballaran T, Carpenter MA, Domeneghetti MC (2004) Order-parameter variation through the $P2_1/m \leftrightarrow C2/m$ phase transition in cummingtonite. *Am Mineral* 89:1717-1727
- Bruce AD, Cowley RA (1981) *Structural Phase Transitions*. Taylor and Francis, London
- Cámara F, Carpenter MA, Domeneghetti MC, Tazzoli V (2002) Non-convergent ordering and displacive phase transition in pigeonite: *in-situ* HT XRD study. *Phys Chem Mineral* 29:331-340
- Cámara F, Oberti R, Iezzi G, Della Ventura G (2003) The $P2_1/m \leftrightarrow C2/m$ phase transition in synthetic amphibole $\text{Na}(\text{NaMg})\text{Mg}_5\text{Si}_8\text{O}_{22}(\text{OH})_2$: thermodynamic and crystal-chemical evaluation. *Phys Chem Mineral* 30:570-581
- Cámara F, Oberti R, Della Ventura G, Welch MD, Maresch WV (2004) The crystal-structure of synthetic $\text{NaNa}_2\text{Mg}_5\text{Si}_8\text{O}_{21}(\text{OH})_3$, a triclinic $C\bar{1}$ amphibole with a triple-cell and excess hydrogen. *Am Mineral* 89:1464-1473
- Cámara F, Oberti R, Casati N (2007) The $P2_1/m \leftrightarrow C2/m$ phase transition in amphiboles: new data on synthetic $\text{Na}(\text{NaMg})\text{Mg}_5\text{Si}_8\text{O}_{22}\text{F}_2$ and the role of differential polyhedral expansion. *Z Krist* (in press)
- Cameron M, Sueno S, Papike JJ, Prewitt CT (1983) High temperature crystal chemistry of K and Na fluor-richterites. *Am Mineral* 68:924-943
- Carpenter MA, Salje EKH (1998) Elastic anomalies in minerals due to structural phase transitions. *Eur J Mineral* 10:693-812
- Carpenter MA, Salje EKH, Graeme-Barber A (1998) Spontaneous strain as a determinant of thermodynamic properties for phase transition in minerals. *Eur J Mineral* 10:621-691
- Comodi P, Mellini M, Ungaretti L, Zanazzi PF (1991) Compressibility and high pressure structure refinement of tremolite, pargasite and glaucophane. *Eur J Mineral* 3:485-499
- Della Ventura G, Robert J-L, Raudsepp M, Hawthorne FC (1993) Site occupancies in monoclinic amphiboles: Rietveld structure refinement of synthetic nickel-magnesium-cobalt-potassium-richterite. *Am Mineral* 78:633-640
- Dove MT (1997) Theory of displacive phase transitions in minerals. *Am Mineral* 82:213-244
- Evans BW, Yang H (1998) Fe-Mg order-disorder in tremolite-actinolite-ferro-actinolite at ambient and high temperature. *Am Mineral* 83:458-475
- Gatta GD, Boffa Ballaran T, Iezzi G (2005) High-pressure X-ray and Raman study of a ferrian magnesian spodumene. *Phys Chem Mineral* 32:132-139

- Hawthorne FC, Welch MD, Della Ventura G, Liu S, Robert J-L, Jenkins DM (2000) Short-range order in synthetic aluminous tremolites: an infrared and triple-quantum MAS NMR study. *Am Mineral* 85:1716-1724
- Hawthorne FC, Oberti R (2007) Amphiboles: crystal chemistry. *Rev Mineral Geochem* 67:1-54
- Hawthorne FC, Della Ventura G (2007) Short-range order in amphiboles. *Rev Mineral Geochem* 67:173-222
- Hirschmann M, Evans BW, Yang H (1994) Composition and temperature dependence of Fe-Mg ordering in cummingtonite-grunerite as determined by X-ray diffraction. *Am Mineral* 79:862-877
- Hugh-Jones DA, Woodland AB, Angel RJ (1994) The structure of high-pressure $C2/c$ clinoferrosilite and crystal chemistry of high-pressure $C2/c$ pyroxenes. *Am Mineral* 79:1032-1041
- Iezzi G, Tribaudino M, Della Ventura G, Nestola F, Bellatreccia F (2005) High- T phase transition of synthetic ${}^A\text{Na}^B(\text{LiMg})^C\text{Mg}_5\text{Si}_8\text{O}_{22}(\text{OH})_2$ amphibole: an X-ray synchrotron powder diffraction and FTIR spectroscopic study. *Phys Chem Mineral* 32:515-523
- Iezzi G, Liu Z, Della Ventura G (2006) Synchrotron infrared spectroscopy of synthetic $\text{Na}(\text{NaMg})\text{Mg}_5\text{Si}_8\text{O}_{22}(\text{OH})_2$ up to 30 GPa: Insight on a new high-pressure amphibole polymorph. *Am Mineral* 91:479-482
- Iezzi G, Liu Z, Della Ventura G (2007) The role of B-site on the compressional behaviour of synthetic $P2_1/m$ amphiboles in the system ${}^A\text{Na}^B(\text{Na}_x\text{Li}_{1-x}\text{Mg}_1)^C\text{Mg}_5\text{Si}_8\text{O}_{22}(\text{OH})_2$ (with $x = 1, 0.6, 0.2$ and 0): an high pressure synchrotron infrared study. *Contrib Mineral Petrol* (submitted)
- Kudoh Y, Takeda H, Ohashi H (1989) A high-pressure single crystal X-ray study of ZnSiO_3 pyroxene: possible phase transition at 19 kbar and 51 kbar. *Mineral J Jpn* 14:383-387
- Jenkins DM, Corona JC (2006) Molar volume and thermal expansion of glaucophane. *Phys Chem Mineral* 33:356-362
- Le Godec Y, Dove MT, Francis DJ, Kohn SC, Marshall WG, Pawley AR, Price GD, Redfern SAT, Rhodes N, Ross NL, Schofield PF, Schooneveld E, Syfosse G, Tucker MG, Welch MD (2001) Neutron diffraction at simultaneous high temperatures and pressures, with measurement of temperature by neutron radiography. *Mineral Mag* 65:737-748
- Liu S, Welch MD, Klinowski J, Maresch WV (1996) A MAS NMR study of a monoclinic/triclinic phase transition in an amphibole with excess OH: $\text{Na}_3\text{Mg}_5\text{Si}_8\text{O}_{21}(\text{OH})_3$. *Eur J Mineral* 8:223-229
- Maresch WV, Miede G, Czank M, Fuess H, Schreyer W (1991) Triclinic amphibole. *Eur J Mineral* 3:899-903
- Newnham RE (1974) Domains in minerals. *Am Mineral* 59:906-918
- Pommier CJS, Downs RT, Stimpfl M, Redhammer GJ, Denton MB (2005) Raman and X-ray investigations of $\text{LiFeSi}_2\text{O}_6$ pyroxene under pressure. *J Raman Spec* 36:864-871
- Prewitt CT, Papike JJ, Ross M (1970) Cummingtonite: a reversible, non quenchable transition from $P2_1/m$ to $C2/m$ symmetry. *Earth Planet Sci Lett* 8:448-450
- Prewitt CT, Brown GE, Papike JJ (1971) Apollo 12 clinopyroxenes. High-temperature X-ray diffraction studies. *Geochim Cosmochim Acta* 1(Suppl 2):59-68
- Redhammer GJ, Roth G (2002) Structural variations in the aegirine solid-solution series $(\text{Na,Li})\text{FeSi}_2\text{O}_6$ at 298 K and 80 K. *Z Kristallogr* 217:63-72
- Redhammer GJ, Roth G (2004) Structural changes upon the temperature dependent $C2/c \leftrightarrow P2_1/c$ phase transition in $\text{LiMe}^{3+}\text{Si}_2\text{O}_6$ clinopyroxenes, $\text{Me} = \text{Cr, Ga, Fe, V, Sc}$ and In . *Z Kristallogr* 219:585-605
- Reece JJ, Redfern SAT, Welch MD, Henderson CMB (2000) Mn-Mg disordering in cummingtonite: a high temperature neutron powder diffraction study. *Mineral Mag* 64:255-266
- Reece JJ, Redfern SAT, Welch MD, Henderson CMB, McCammon CA (2002) Temperature-dependent Fe^{2+} - Mn^{2+} order-disorder behaviour in amphiboles. *Phys Chem Mineral* 29:562-570.
- Salje EKH (1993) Phase Transitions in Ferroelastic and Co-Elastic Crystals (student edition). Cambridge University Press, Cambridge
- Schlenker JL, Gibbs GV, Boisen Jr MB (1978) Strain-tensor components expressed in terms of lattice parameters. *Acta Crystallogr* A34:52-54
- Smyth JR (1974) The high-temperature crystal chemistry of clinohypersthene. *Am Mineral* 59:1061-1082.
- Sueno S, Papike JJ, Prewitt CT, Brown GE (1972) Crystal chemistry of high cummingtonite. *J Geophys Res* 77:5767-5777
- Sueno S, Cameron M, Papike JJ, Prewitt CT (1978) High temperature crystal chemistry of tremolite. *Am Mineral* 58:649-664
- Tribaudino M, Nestola F, Cámara F, Domeneghetti MC (2002) The high-temperature $P2_1/c$ - $C2/c$ phase transition in Fe-free pyroxenes: structural and thermodynamic behavior. *Am Mineral* 87:648-657
- Tribaudino M, Nestola F, Meneghini C, Bromiley GD (2003) The high-temperature $P2_1/c \leftrightarrow C2/c$ phase transition in Fe-free Ca-rich $P2_1/c$ clinopyroxenes. *Phys Chem Mineral* 30:527-535
- Welch MD, Liu S, Klinowski J (1998) ${}^{29}\text{Si}$ MAS NMR systematics of calcic and sodic-calcic amphiboles. *Am Mineral* 83:85-96
- Welch MD, Reece JJ, Redfern SAT (2007) *In situ* high-temperature study of Ni-Mg site partitioning in synthetic potassic-rich richterite. *Mineral Mag* (submitted)
- Yang H, Hirschmann M (1995) Crystal structure of $P2_1/m$ ferromagnesian amphibole and the role of cation ordering and composition in the $P2_1/m$ - $C2/m$ transition in cummingtonite. *Am Mineral* 80:916-922

- Yang H, Smyth JR (1996) Crystal structure of $P2_1/m$ ferromagnesian cummingtonite at 140 K. *Am Mineral* 81:363-368
- Yang H, Hazen RM, Prewitt CT, Finger LW, Lu R, Hemley RJ (1998) High-pressure single-crystal X-ray diffraction and infrared spectroscopic studies of the $C2/m \rightarrow P2_1/m$ phase transition in cummingtonite. *Am Mineral* 83:288-299
- Zhang L, Ahsbahs H, Kutoglu A, Hafner SS (1992) Compressibility of grunerite. *Am Mineral* 77:480-483

The Synthesis and Stability of Some End-Member Amphiboles

Bernard W. Evans

*Department of Earth and Space Sciences
University of Washington Seattle
Seattle, Washington, 98195-1310, U.S.A.
bwevans@u.washington.edu*

INTRODUCTION

Reliable characterization of the properties of amphibole end-members is a prerequisite for many important things in mineralogy and petrology, especially for the calculation of phase equilibria that involve amphiboles. Laboratory measurements of the thermochemical and thermophysical properties of amphibole end-members, as well as the experimental reversal of critical reactions, require the availability of adequate amounts of appropriately pure samples. More often than not, nature fails to provide material that fulfills the chemical and physical requirements of phase purity. Synthesis of chosen compositions at high pressure and temperature might seem to be the obvious answer to the problem, but it is now well known that amphiboles are difficult customers in this respect (Hawthorne 1983a, 1995; Graham et al. 1989; Raudsepp et al. 1991; Maresch et al. 1994).

In the early days of experimental petrology, in the 1960s and 1970s, phase characterization of products involved optical microscopic measurements and powder XRD, a minimal combination that we now realize was inadequate. Experience has shown that the synthesis of an end-member amphibole commonly yields distinctly less than 100% amphibole, with the result that its composition likely departs significantly from the desired one, often in a reproducible way. In addition, the amphibole may contain unacceptably high concentrations of defects of one sort or another, and, whether or not these drive it off composition, their presence can be energetically detrimental. These deficiencies can be minimized, but not necessarily eliminated, by increasing the pressure, temperature, or duration of synthesis. Heroic efforts have been rewarded in a few cases. For example, by repeated grinding of experimental products, and the use of high pressure and judicious amounts of H₂O, Jenkins and Corona (2006) were able to obtain glaucophane very close to its end-member composition, something that numerous previous workers had failed to achieve. A further problem with many syntheses arises from their extremely fine grain-size; when crystal dimensions are on the order of 0.1 μm or less, a surface energy contribution to the free energy of the substance can compromise the applicability of the measurements and phase-equilibrium experiments conducted on them. Some workers have successfully used saline fluxes to increase the grain-size and optimize the composition of synthetic amphibole (e.g., Zimmermann et al. 1996, 1997a; Gottschalk et al. 1998, 1999). Fractional loss of components to the fluid at high experimental T and P can in some cases drive the solids off composition, and for this reason it has been found prudent in some cases to add small amounts of quartz to the starting material. Few mineralogists will disagree that a fundamental requirement of mineral syntheses nowadays is that they be subjected to characterization by scanning and transmission electron microscopy and modern spectroscopic examination, in addition to the more traditional microprobe, optical, and XRD techniques. It is also important to reconcile the composition and percent yield of product amphibole with that of the starting or "nominal" composition.

A significant mass-imbalance can be indicative of the loss of components, in which case the estimate of percent yield (based on the condensed phases) will be too high.

High synthesis temperatures are usually needed to accelerate growth rates and optimize the quality of the final product. Unfortunately, this can be counterproductive because the end-member composition may be intrinsically unstable at the more extreme conditions of synthesis, as discussed below. It is important for the experimentalist to know in this respect if he or she is simply fighting an unwinnable battle in the synthesis attempt. I will show in this chapter that a review of natural and theoretical metamorphic phase equilibria can in some cases reveal when high *P* and *T* synthesis of pure end-members is doomed to failure, or when the objective is in fact attainable assuming that kinetic barriers can be overcome through hard work, imagination, and some luck. For iron-bearing amphiboles, it is also necessary of course to choose optimal redox conditions, but the experimentalist does not always know at the outset what these are.

What follows is not a comprehensive review of attempts that have been made to synthesize all the end-member amphiboles. It focuses on common rock-forming amphiboles in the system $\text{Na}_2\text{O}-\text{CaO}-\text{MgO}-\text{FeO}_x-\text{Al}_2\text{O}_3-\text{SiO}_2-\text{H}_2\text{O}$ (NCMFASH) for which consideration of metamorphic phase relationships provides some enlightenment regarding the possible attainment or otherwise of end-member compositions.

TREMOLITE □ $\text{Ca}_2\text{Mg}_5\text{Si}_8\text{O}_{22}(\text{OH})_2$

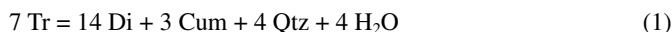
This basic amphibole end-member has received more attention from experimentalists than virtually any other. Bozhilov et al. (2004) provide a complete set of references for reports on the synthesis and stability of tremolite (Tr). Most workers have used synthesis temperatures in the range 750–900 °C, combined with pressures up to 20 kbar. Yields of amphibole in charges on the ideal composition have typically been around 90%, the remainder being diopside and quartz, with the result that synthetic tremolite appears to contain as much as 10% of the cummingtonite (Cum) component. When imaged by high resolution TEM, chain-width defects (or chain-multiplicity faults, CMFs) are generally found to be present in synthetic tremolite (Ahn et al. 1991). Their density decreases with increased temperature of synthesis. Maresch et al. (1994) suggested that the presence of triple-chain defects could account entirely for the off-composition nature (apparent low Ca/Mg ratio) of synthetic tremolite. Hydrothermal time-series synthesis experiments at 850 °C and 6.1 kbar on the bulk composition $\text{Tr}_{90}\text{Cum}_{10}$ by Bozhilov et al. (2004) showed that CMFs decrease with increasing synthesis time and that they account for about 3% of apparent cummingtonite solid solution. Triple-chain defects predominate over others after two days of treatment. The remaining 7% of cummingtonite was attributed to solid solution of cummingtonite in the tremolite. Longer run-times, with intermediate grinding, removed crystals with Mg-rich compositions clearly inside the Cum-Tr solvus.

The uptake of extra Mg that is found in high-temperature synthetic tremolite (Mg on (M4)) persists into compositions along a number of joins extending out from tremolite. Along the join tremolite to tschermakite, Cum substitution is reported in the range 4 to 11 mol% (Cao et al. 1986; Ellis and Thompson, 1986; Jenkins 1988, 1994; Cho and Ernst 1991; Smelik et al. 1994; Hoschek 1995; Jenkins et al. 1997). A similar enrichment in Mg and deficiency in Ca is found along the tremolite-pargasite join (Oba 1980; Sharma 1996; Sharma and Jenkins 1999). Jenkins et al. (2003) found that Cum enrichment declined towards the pargasite end-member, where it became more an artifact of the presence of CMFs. Whereas synthetic end-member richterite was on composition, solid solutions along the join to tremolite were found to contain cummingtonite in the proportion $\text{Tr}_{92}\text{Cum}_8$ (Pawley et al. 1993). Similarly, intermediate synthesis products along the potassic-richterite to tremolite join (Hawthorne et al. 1997) showed Ca-deficiency and Na-enrichment, corresponding to the presence of diopside and enstatite. A smaller amount of Cum solid solution ($\text{Ca/Mg} = 0.38$ or $\text{Tr}_{95}\text{Cum}_5$) was found

in fluor-tremolite synthesized (with trace quartz) by Jenkins and Hawthorne (1995) at 998 °C and 2.96 kbar. In synthetic (CaSr)-tremolite, Gottschalk et al. (1998) reported 1 to 7% Cum in tremolite, whereas the Sr end-member was on composition.

Zimmermann et al. (1996) used an aqueous CaCl₂ fluid to catalyze the growth of coarse-grained CMF-free tremolite at 800 °C and 2 kbar in charges of end-member composition (+excess SiO₂). The larger crystal size greatly facilitated microprobe analysis. The average amphibole composition was 5.8 ± 5.0 (2σ) mol% Cum. The large standard deviation was believed to reflect fractional crystallization during the experiment. A similar effort by Gottschalk et al. (1999) using diverse brines (CaBr₂, NaCl, KCl, NaOH, KOH) produced equally coarse tremolite with the same sort of chemical variation according to the microprobe analyses. However, they argued that the compositional spread in part reflected analytical uncertainty, pointing out the sensitivity of mol% Cum estimates to small differences in analytical Mg and Ca. Instead, they found that lattice parameters were a better fit to composition (mol% Cum) when the latter was based on the integral absorbance of the OH stretching vibration bands in IR spectra rather than on microprobe analysis. This alternative method enhanced precision to the point where it was possible to show that the mol% Cum in synthetic tremolite (accompanied by diopside and quartz) declines inside the range 5 to 1% from 800 down to 670 °C. Now we are left wondering, of course, if we were simply to try harder, would we eventually be able to synthesize pure end-member tremolite at the higher temperatures (e.g., 800-900 °C), or is low temperature essential?

A response to this question is provided by theoretical phase petrology, which demonstrates the likely instability of pure tremolite at high temperature. Tremolite can achieve stabilization via an increase in its configurational entropy (Hawthorne 1995) through the uptake of the Cum component, which on tremolite bulk composition is coupled with the precipitation of diopside (Di) and quartz (Qtz) and release of H₂O. In this process, a composition is soon reached where the system's Gibbs free energy is minimal, at a point on the Tr_{ss}-Di_{ss}-Qtz-H₂O curve, which is the locus of the isobaric univariant equilibrium:



Is this compositional shift trivial (e.g., < 1% Cum), or is it comparable to what the latest synthesis experiments indicate? With reference to the isobaric T - $X_{\text{Ca/Mg}}$ section that is commonly employed for the system (e.g., Jenkins 1987; Graham et al. 1989; Hawthorne 1995; Evans et al. 2000; Ghiorso and Evans 2002), the stable portion of the Tr_{ss}-Di_{ss}-Qtz-H₂O curve terminates at 910 °C for 5 kbar (Fig. 1), at which point tremolite possesses its terminal composition and enstatite joins the products of reaction.

Reaction (1) necessarily inclines to the left (towards lower values of Ca/Mg) on the T - X diagram because it releases H₂O vapor. Its asymptotic convergence at low temperature on the composition of ideal tremolite (Ca/(Ca+Mg) = 2/7) is simply a reflection of the reasonable crystal chemical assumption that Ca is not allowed on the A-site of tremolite (notwithstanding the existence of exceptional synthetic hyper-calcic amphiboles (e.g., Oberti et al. 1995b) and of natural cannilloite, a highly aluminous fluoro amphibole with excess Ca, Hawthorne et al. 1996). Reaction (1) would in principle allow for tremolite to have Ca ≥ 2 apfu at low temperature. In the case of ferro-actinolite (see below, Fig. 2), the leftward inclination in the corresponding reaction curve (producing hedenbergite, quartz, and H₂O) is sufficiently pronounced that it intersects the two-amphibole solvus and creates an isobaric invariant point terminating the stability field of ferro-actinolite altogether. Thermodynamic reasoning indicates that the dT/dX slope of the curve decreases up-temperature, as shown in Graham et al. (1989), Gottschalk et al. (1999), Evans et al. (2000) and Ghiorso and Evans (2002), and it also allows for pure end-member tremolite to be stable at temperatures less than about 650 °C. The syntheses of Zimmermann et al. (1996) and Gottschalk et al. (1999) may well be close to a stable tremolite composition, and further improvements in experimental reaction kinetics will probably not change things much. Their compositions are slightly higher than the calculated 3% Cum solid

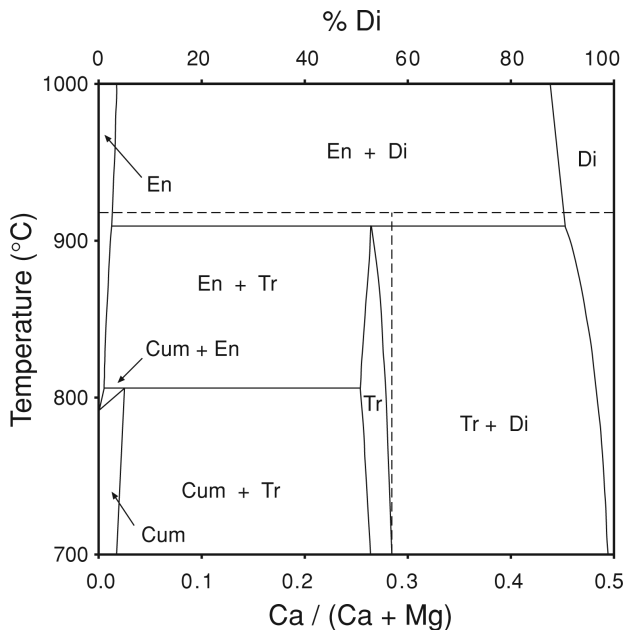


Figure 1. Calculated T - X phase relations at 5 kbar for equilibrium among tremolite, diopside, enstatite, cummingtonite, with Qtz and H₂O-fluid in the system CaO-MgO-SiO₂-H₂O. Dashed lines refer to phase boundaries for standard-state compositions. Below 770 °C, cummingtonite is metastable with respect to talc. [From Evans et al. (2000), *American Mineralogist*, Vol. 85, Fig. 3, p.469.]

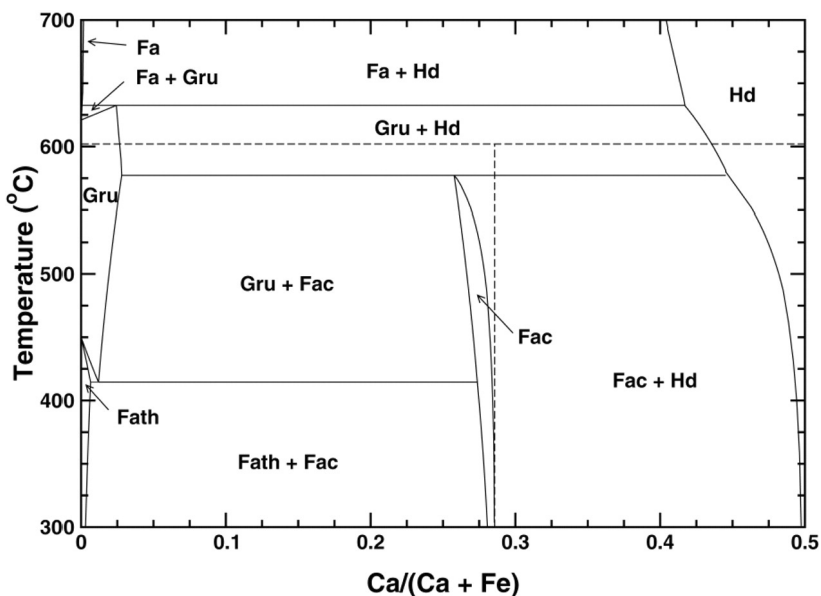
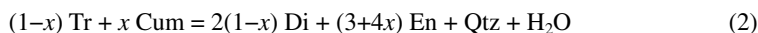


Figure 2. Calculated T - X phase relations at 5 kbar for amphiboles, pyroxenes and fayalite, with Qtz and H₂O-fluid in the system CaO-FeO-SiO₂-H₂O. Dashed lines refer to standard-state ferro-actinolite. [From Ghiorso and Evans (2002), *American Mineralogist*, Vol. 87, Fig. 8, p.93.]

solution for 800 °C and 5 kbar given by Ghiorso and Evans (2002). Some of this difference may stem from the thermodynamic model employed in the calculations of Ghiorso and Evans, for example the assumption of a symmetrical solvus in the quadrilateral. This assumption appears to be reasonable for natural actinolite-cummingtonite pairs of intermediate Fe/Mg ratio, but it may be less so for the Mg-end, and this could increase the inferred cummingtonite content of the tremolite end-member.

It is worth noting that the thermal stability limit of tremolite_{ss} is lower than that of (metastable) pure tremolite (cf. Yang and Evans 1996; Gottschalk et al. 1999), despite the addition of Cum component which, in and of itself, should stabilize the amphibole (Fig. 1; also Ghiorso and Evans 2002, Fig. 7). This result derives from satisfying the energetics of the terminal reaction, where x is the mole fraction of cummingtonite in tremolite:



It is of course consistent with the much lower thermal stability of end-member cummingtonite. It is somewhat academic whether the temperature-dependent increase in Cum component of tremolite in the presence of Di and Qtz is actually driven by amphibole dehydration or by the increase in configurational entropy of the amphibole. More important is that it renders virtually impossible the synthesis of tremolite of ideal composition at high temperature.

Jenkins (1987) noted that most natural tremolite seemed to be characterized by Ca/ΣM less than the ideal 0.40 (or Ca apfu = 2.0). Graham et al. (1989), however, cited two examples of natural tremolite within error limits on end-member composition. Apparently overlooked at this time were 30 electron-probe analyses of prismatic, massive, and asbestiform tremolite by Dorling and Zussman (1987), which showed that more than a third of them have Ca ≥ 1.98 apfu. Zimmermann et al. (1996) questioned whether the real end-member tremolite composition actually exists. Although it is not always the case, the near end-member composition is in fact found in metadolomites recrystallized under amphibolite facies conditions (e.g., Moore and Kerrick 1976; Jansen et al. 1978; Evans et al. 2000) and in low-temperature chrysotile-bearing serpentinites. The tremolite that occurs in metaperidotites together with cummingtonite, antigorite, talc or enstatite contains more cummingtonite in solid solution (Evans 1982). The selection of tremolite samples by Dorling and Zussman (1987) probably favored those of very low temperature origin.

Skippen and McKinstry (1985) provided an illustration of the problem of tremolite synthesis with a phase equilibrium experiment that compared natural tremolite with synthetic tremolite. Synthetic tremolite was prepared at 780 °C and 2 kbar over 28-42 days. Their natural tremolite (Gotthard) at that time was thought to contain 2.12 apfu Ca, but later analysis (Evans et al. 2000) showed that it is very close to ideal end-member tremolite. Powder XRD analysis of run products bracketing the reaction of tremolite + forsterite to diopside + enstatite + H₂O at 1 kbar showed that the synthetic tremolite charge dehydrated at a *minimum* of 80 °C lower than the natural tremolite charge. The XRD pattern of the synthetic tremolite showed broad peaks and reduced intensities in comparison to the natural tremolite, and the authors reasonably concluded that crystal defects were present. From the work of Bozhilov et al. (2004), we can suggest an alternative (or additional) explanation for the equilibrium shift, namely the presence in the synthetic tremolite of crystals with a range of unstable, intra-solvus compositions (e.g., Ca/Mg = 0.10 to 0.30), rather than the appropriate near-endmember composition. After four days of treatment at 850 °C and 6.1 kbar, conditions kinetically more favorable than those used by Skippen and McKinstry (1985), Bozhilov et al. (2004) found that still about 12% of Mg-enriched tremolite crystals were present.

A similar comparative study was conducted by Jenkins and Clare (1990). They found a temperature difference of 40 °C in the equilibrium of tremolite, diopside, enstatite, quartz, and H₂O, between natural tremolite (higher T) and tremolite synthesized at 2 kbar in two steps:

8 days at 740 °C and 9 days at 806 °C with intermediate grinding. It is not really clear why, but it seems likely that their synthesis of tremolite was more successful than the earlier one of Skippen and McKinstry. They argued that, rather than attributing the equilibrium shift to the presence of CMFs or other defects in the synthetic tremolite, it is much more likely in this case that differences in the chemical compositions of the synthetic vs. natural tremolite ($^{\square}\text{Na}$, Al, F and low-Si in the natural, and higher $^{\text{B}}\text{Mg}$ in the synthetic) were responsible. We might note here, parenthetically, that the experimental reversal (bracketing) of a phase boundary in the *PT*-plane assumes the existence of a univariant equilibrium curve. When reactants and products fail to mass-balance (extra components such as Al are present in the amphibole), the reaction is rendered divariant (or greater) and the detection of reversal made ambiguous.

Kinetic problems are certainly real in the synthesis of tremolite, but we have found that longer treatment times, higher pressures, and use of saline solutions, can minimize inhomogeneities, largely eliminate CMFs, grow larger crystals, and approach a likely stable composition. A recent paper by Bozhilov et al. (2007) emphasizes the determining role in kinetics played by precursor phases such as talc and diopside. However, the ideal end-member composition remains unattained not for reasons of kinetics, but more fundamentally from its instability at high temperatures, though it is probably naive simply to recommend going down to 500-600 °C instead!

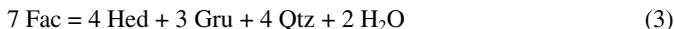
FERRO-ACTINOLITE $\square\text{Ca}_2\text{Fe}_5\text{Si}_8\text{O}_{22}(\text{OH})_2$

This amphibole end-member has also proven to be difficult to synthesize on composition, and there is little reason to believe that further attempts, beyond the few that have so far been made (Ernst 1966; Jenkins and Bozhilov 2003), are likely to be much more successful. Ungaretti et al. (1987) and Oberti et al. (2007, Fig. 35) have advocated the use of geometric constraints (cell dimensions) to evaluate the likely stability or otherwise of amphiboles. Unlike tremolite, ferro-actinolite (Fac) appears marginal in this context, although this may in part reflect the overwhelmingly Mg-rich nature of the sample population. The thermodynamic stability of a compound necessarily relates to that of a compositional alternative; in the present case, an analogous diagram for the clinopyroxenes would be interesting.

Although the ferro-actinolite synthesized by Ernst (1966) appeared to have end-member cell dimensions, it represented an incomplete yield, and Burns and Grieves (1971) found that its Mössbauer spectrum was consistent with Fe on the M(4) site, that is, the presence of a grunerite (Gru) component. The investigation by Jenkins and Bozhilov (2003) brought to bear on the subject all of the procedures in the experimentalist's arsenal that could possibly overcome the kinetic problems hindering amphibole yield and attainment of desired composition. Starting material for their equilibrium bracketing study was prepared by subjecting it to as many as three grindings between five high-*PT* treatments and total synthesis times of as long as 170 days. The best yield obtained amounted to 70% amphibole, the remaining products being routinely hedenbergite and quartz, in many instances with one or more of fayalite, magnetite, and grunerite in addition. Syntheses were attempted over the temperature range from 418 to 605 °C, and the best yield was obtained at 420 °C and 2 kbar.

Acicular amphibole was produced with grain-widths of 0.05 to 0.10 μm . Analytical TEM showed that individual crystals varied considerably in amount of Gru solid solution, as represented by Ca apfu (Fig. 6 of Jenkins and Bozhilov 2003). This is similar to the results on tremolite, where individual "tremolite" crystals extended into the cummingtonite compositional range (Bozhilov et al. 2004). Bulk amphibole compositions of ferro-actinolite (Fac) were estimated from XRD measurements of cell volume, Rietveld refinement (X-ray scattering), and by mass balance based on Rietveld measurement of the modal proportions of product minerals. The overall average Ca content was 1.67 apfu Ca (± 0.25 1σ), a value apparently independent of the bulk composition (Ca/Fe ratio) of the charge.

As we saw for tremolite, the maximum yield of amphibole, and its closeness to end-member composition, are governed in an equilibrium model by an isobaric $T-X_{Ca/Fe}$ curve (Fig. 2), in this case for a reaction producing hedenbergite (Hed) and quartz:



Reaction (3) also represents the terminal breakdown reaction of ferro-actinolite, where the activities of Fac and Gru are those of the amphibole solvus. Both Ernst (1962) and Jenkins and Bozhilov (2003) found that it was impossible to reverse breakdown reaction (3), but that it was possible instead to bracket the metastable reaction:



Bozhilov and Jenkins (2003) calculated a PT -curve for the stable breakdown reaction (3) by combining their data for (4) with the conditions of the reaction of grunerite to fayalite + quartz + H_2O (see below). This gave an estimated breakdown temperature of ferro-actinolite (reaction 3) of 460 °C at 5 kbar (their Fig. 13). This compares with 575 °C at 5 kbar according to Ghiorso and Evans (2002) as shown in Fig. 2. Ghiorso and Evans (2002) derived the enthalpy of formation of ferro-actinolite from the properties of the three other quadrilateral end-members, experimental cation-ordering data, and tie-line orientations and solvus widths from the field.

The 1.67 average Ca apfu of ferro-actinolite in experiments at 420 °C and 2 kbar was used by Jenkins and Bozhilov (2003, Fig. 11) as a critical composition to extract a possible mixing energy ($W = 14.3 \text{ kJ}$) for the grunerite-ferro-actinolite solid solution (Fig. 3). This figure translates into a ferro-actinolite composition of 1.55 Ca apfu (22.5% grunerite in solid solution) at 482 °C, their estimated 2 kbar breakdown temperature of ferro-actinolite. By this model, ferro-actinolite synthesized at 480 °C should be no richer in Ca than about 1.57 apfu, since, according to reaction (3), a more calcic ferro-actinolite is less stable than the compositionally equivalent hedenbergite + quartz + H_2O . About 19 wt% hedenbergite and 2% quartz would be in the run product here. The uncertainty bracket in Figure 3 shows that their estimate of solvus width is very uncertain, and in fact the right-hand limit coincides with the much wider solvus at 420 °C according to Figure 2 after Ghiorso and Evans (2002). What is clear is that the inclination of the ferro-actinolite field in the $T-X_{Ca/Fe}$ diagram (Fig. 2) provides an explanation for why the best amphibole yield was obtained not at the highest possible temperature but at 420 °C.

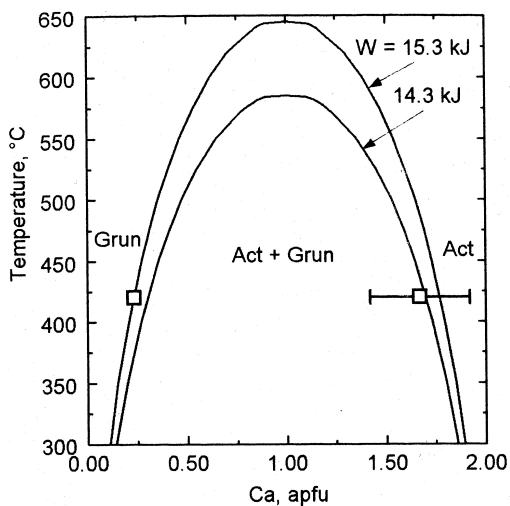


Figure 3. Calculated miscibility gap between grunerite and ferro-actinolite using regular solution theory for the mixing of Ca and Fe on the M4 sites. Squares show the compositions of coexisting grunerite and actinolite from the synthesis experiments at 2 kbar and 420 °C. The solid curves were calculated for Margules parameters (W) of 14.3 and 15.3 kJ. [Used by permission of the American Journal of Science, from Jenkins and Bozhilov (2003), *American Journal of Science*, Vol. 303, Fig. 11, p.744]

Jenkins and Bozhilov (2003) showed by HRTEM that their synthetic ferro-actinolite was very nearly free of CMFs (their Fig. 8), so this issue is not a contributory factor to the problem of ferro-actinolite synthesis in aqueous fluid. They found that aqueous CaCl_2 and FeBr_2 were not useful in the synthesis of ferro-actinolite.

Is there any single explanation for the difference in the two studies in estimates of both solvus width and ferro-actinolite breakdown temperature?

As their time-series study of tremolite synthesis showed (Bozhilov et al. 2004), the attainment of a maximum high-Ca composition required lengthy run-times. It is not unreasonable to suppose that the synthesis of ferro-actinolite at temperatures some 400 °C lower than used for tremolite might encounter even more serious kinetic barriers. A homogeneous ferro-actinolite product was never obtained; and additional phases (beyond hedenbergite and quartz) remained at the end of almost all experiments. It is interesting to note that, in some cases, for example in experiment FETR 3-35-5 (their Fig. 6), compositions measured by analytical TEM are very close to end-member composition. The tremolite experiments of Bozhilov et al. (2004) suggest that experiments of impossibly long duration (plus additional kinetic inducements) might ultimately have yielded a population of ferro-actinolite compositions closer to the Ca end-member (perhaps close to the right-hand uncertainty limit shown in Fig. 3).

In support of the wider solvus, we cite compositional data for coexisting ferro-actinolite and grunerite in sample B-23 (courtesy of B.R. Frost) from the Hedenbergite Zone of the aureole in Biwabik Iron Formation around the Duluth Gabbro, Minnesota. This sample contains hedenbergite, quartz, and calcite, as well as the two amphiboles. The $\text{Mg}/(\text{Mg}+\text{Fe})$ ratios of ferro-actinolite, grunerite and hedenbergite are: 2.4%, 1.8%, and 1.0% respectively. Ca apfu in ferro-actinolite and grunerite are 1.88 ± 0.07 and $0.20 \pm 0.04 (1\sigma)$ respectively. Grunerite and ferro-actinolite are irregularly intergrown in a manner suggestive of replacement of grunerite by ferro-actinolite. According to thermodynamic data in Ghiorsio and Evans (2002, Table 7), this isobaric invariant assemblage occurs at 517 °C and $X_{\text{CO}_2} = 0.62$ at 2 kbar. The sample is a partially retrograded hornfels that was possibly affected by modest fluid infiltration. The hedenbergite could be imagined to be a relic of higher temperature metamorphism. The temperature estimate would be much lower if we were to allow for this and if we adopt the thermodynamic data for grunerite and ferro-actinolite suggested by Jenkins and Bozhilov (2003). Nevertheless, the sample has an amphibolite-facies assemblage, for which 400 °C is perhaps a reasonable lower temperature limit. At lower temperature the carbonate would likely have been ankerite or siderite.

It is therefore the writer's view that the iron end-member amphibole solvus at 420 °C may not be as narrow as the one adopted by Jenkins and Bozhilov (2003). If this is the case, it then raises the possibility that much of the synthetic ferro-actinolite reactant in their experimental reversal of reaction (4) was unstable by virtue of its large content of grunerite. The composition (Ca apfu) of synthetic ferro-actinolite is potentially limited during synthesis by the spinode, but this would not be a restraint if, as suggested by Bozhilov et al. (2004), synthetic Ca-amphibole grows from early-formed pyroxene, amphibole, and wide-chain silicate by a process of solution, nucleation and growth, and simply long treatment times are required to gradually eliminate the low-Ca (intrasolvus) crystals in the reactant material would be capable of yielding to breakdown products hedenbergite + fayalite at temperatures below the stable breakdown curve (for the higher-Ca actinolite). The reverse reaction would proceed at a lower temperature, thus ensuring "reversal." Although the Clapeyron slope of reaction (4) in Jenkins and Bozhilov is more correct than that of Ernst, the general similarity in equilibrium temperatures in the two studies may well reflect reliance in both on synthetic starting materials. The problem is potentially resolvable if it were possible to separate and use a natural, near end-member ferro-actinolite such as that in sample B-23.

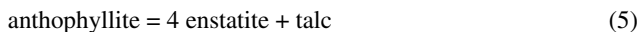
ANTHOPHYLLITE $\square\text{Mg}_2\text{Mg}_5\text{Si}_8\text{O}_{22}(\text{OH})_2$

Very small amounts of an optically orthorhombic amphibole were produced by Bowen and Tuttle (1949) in their pioneering hydrothermal investigation of the MSH system. Greenwood (1963) used seeds of anthophyllite to overcome its reluctance to nucleate and grow, given the competition from early growth of talc, but run products in addition contained one or more of enstatite, forsterite, and quartz, introducing ambiguity into the assessment of reaction direction. Nevertheless, he and later experimentalists (Chernosky and Autio 1979; Chernosky et al. 1985) were able to produce a dataset of internally consistent high *PT*-brackets in the MSH system (Day et al. 1985; Berman et al. 1986) for reaction boundaries among anthophyllite, talc, quartz, enstatite, and forsterite, based on changing peak intensities in X-ray powder diffractograms, even though 100% anthophyllite was never attained. Consistent with the optimized thermodynamic data for anthophyllite were the results of experiments on a natural anthophyllite (Fyfe 1962), MgO-SiO₂ reactions in H₂O-CO₂ fluid (Johannes 1969), and SiO₂ solubility measurements (Hemley et al. 1977). This outcome suggests that the possible effects of crystal defects (see below) on the Gibbs free energy of synthetic anthophyllite are small; if their influence on free energy had been large, there would have been poor agreement with the experiment using natural anthophyllite (notwithstanding its impure composition).

The synthetic Mg end-member of the ferromagnesian amphibole series is reported to be anthophyllite, the orthorhombic form; this may well be correct, but we should note that chain arrangement faults (CAFs: namely, twinning and stacking faults) are abundantly present in synthetic ferromagnesian amphiboles (Maresch and Czank 1988), and they can obscure the presence of the monoclinic form. A calculation of the transition from anthophyllite to the higher temperature, monoclinic cummingtonite, for example, at 800 °C at 5 kbar (Evans et al. 2001), very nearly coincides with the breakdown temperature of anthophyllite to enstatite, quartz and H₂O (Day et al. 1985; Berman et al. 1986). This suggests that end-member cummingtonite might be synthesized, if at all, only where it is metastable with respect to enstatite and quartz.

The simple MSH composition of anthophyllite excludes the possibility of entropy stabilization via miscibility in amphibole of another composition, as is the case for most of the end-members discussed in this chapter. The same limitation applies to cummingtonite and grunerite. Because they cannot deviate from the end-member composition in this particular manner, perhaps the simple amphiboles acquire a gain in entropy in some other way such as by developing disorder in the form of structure “defects”, as proposed by Hawthorne (1995)? Structural disorder caused by random intergrowths of various silicate chain structures will *decrease* the molar free energy of the sample (cf. Ahn et al. 1991, p. 1822), but it is very likely that a concomitant enthalpy increase will counter that effect. Synthetic MgFeMn-amphiboles have been shown consistently to contain significant (5 to 50%) concentrations of CMFs (Veblen et al. 1977; Chernosky and Autio 1979; Veblen 1981; Gilbert et al. 1982; Maresch and Czank 1983, 1988), apparently more than found in most other synthetic amphiboles. CMFs remain in the products of synthesis experiments because of the sluggish kinetics involved in the drive to eliminate those polysome compositions marginally less stable than the desired anthophyllite. What grows is a result of varying rates along different reaction pathways, and temperature, pressure, and bulk composition all seem to be controlling variables. Entropic changes may be involved in the overall evolution and elimination of CMFs, but they lack the predictability of those related to the configuration of atoms on sites in a solid solution.

No experiments have been done on synthetic vs. pure natural anthophyllite analogous to those on tremolite by Skippen and McKinstry (1985) and Jenkins and Clare (1990) to test the energetic consequence of the presence of CMFs. Near end-member natural anthophyllite does occur (Klein 1968; Deer et al. 1997), and so such experiments could in principle be done, preferably with acicular rather than asbestiform anthophyllite (Veblen 1980, 1981) and for best results on the low-entropy reaction:



Calculation of the energetic differences among the commonly found polysomes in the MSH system between enstatite and talc that are “substitutes” for anthophyllite (Abbott and Burnham 1991) indicate a possible stability field for the triple-chain silicate jimthompsonite under certain *PT*-conditions, whereas chesterite, the 2:3 chain silicate, appears to be less stable than anthophyllite + talc. The energetic differences calculated by Abbott and Burnham (1991, Fig. 2) are very large, for example, -3 kJ/mol of oxygen for the H_2O -conserved reaction anthophyllite to orthopyroxene + jimthompsonite. This is equivalent to -72 kJ/mol of anthophyllite. The only independent test of their calculations is provided by reaction (5), for which they calculate an energy difference of 5.5 kJ/mol oxygen or 132 kJ/mol anthophyllite. (These numbers are for the internal energy.) At 298K and 1 bar, this reaction has a $\Delta G/\text{mol}$ of -7.8 , -9.9 , and -5.2 kJ according respectively to Berman (1988), Robie and Hemingway (1995), and Holland and Powell (1998). The tabulated thermodynamic properties of anthophyllite, enstatite, and talc are based on a large amount of internally consistent calorimetric and experimental data. It is hard to account for this enormous disagreement of 140 kJ; as a solid-solid reaction the *PV* and *TS* terms are comparatively small.

Field evidence supports one item in the results of the Abbott and Burnham energy calculations, however. Jimthompsonite has been found to occur in metamorphic ultrabasic rocks as crystals several hundred μm in size (V. Trommsdorff, personal communication 1970s, Veblen and Burnham 1978; Droop 1994), with measurable optical properties, including cleavage intersections at 38° (cf. amphibole at 56°). Retrograde alteration (hydration) and pseudomorphism of anthophyllite has been the favored explanation for most wide-chain MSH pyriboles in nature (Veblen and Buseck 1981). In syntheses the trend of polysome evolution on the other hand is from talc towards anthophyllite (Maresch and Czank 1988). However, Droop (1994) attributed overgrowths of idiomorphic crystals of jimthompsonite and clinojimthompsonite on anthophyllite, cummingtonite and actinolite in Lewisian ultramafic rocks, Scotland, to crystallization during prograde metamorphism. Droop found that, when free from substrate control, the orthorhombic form predominates, and, in an extension of this logic, he suggested that jimthompsonite formed in his samples under conditions where it was more stable than anthophyllite.

Grobéty (1997) examined chain-width distributions of biopyriboles in anthophyllite crystals from the Lepontine Alps, Switzerland, and applied a simple kinetic model based on the rules for chain transformations to show that jimthompsonite likely formed in these rocks by a fluid-conserved reaction involving a quadruple polysome and the double-chain anthophyllite. This mechanism involves chain-width reduction as well as chain-width expansion, and so differs from the progressive hydration reaction that converts anthophyllite two double-chains at a time directly into talc (Grobéty 1997, p. 246). His findings also lend support for a possible stability field for jimthompsonite.

In my opinion, the jury is still out as to whether any of the multiple-chain (3 and 3:2) MSH silicates could have a stability field under certain metamorphic *PT*-conditions: if any, it is likely to be jimthompsonite. One is confronted with the overwhelming field evidence of the widespread occurrence of Mg-rich anthophyllite in middle- to high-grade metamorphic rocks, which emphatically suggests that it is the principal stable MSH polysome lying between the compositions of enstatite and talc.

The target in synthesis experiments is (generally) the growth of the most stable crystal structure that has the composition selected for the charge. As pointed out by Veblen and Buseck (1979), the existence of 2:3 and 3-chain pyriboles in the MSH system unfortunately provides alternative targets with free-energy minima in *T-X* space in close compositional proximity to that of amphibole (the atomic ratios Mg/Si for ideal anthophyllite, chesterite, and jimthompsonite are respectively 0.875, 0.850, and 0.833). Just as free-energy minimization routines in

thermodynamic calculations sometimes close on the wrong minimum, it is not unreasonable to anticipate the same behavior in powder and gel charges whose spatial homogeneity on the finest scale cannot be guaranteed. Reactive gels encourage the growth of anthophyllite (Maresch and Czank 1988), but a drawback may be that they can contain micro-crystalline pyroxene produced during high-temperature sintering or drying (Graham et al. 1989), thus contributing to spatial inhomogeneities in the charge. Furthermore, the seemingly inevitable growth of talc in the early stages of treatment also moves composition off that of amphibole.

GRUNERITE $\square\text{Fe}_2\text{Fe}_5\text{Si}_8\text{O}_{22}(\text{OH})_2$

Grunerite is less prominent than anthophyllite on the petrologist's radar screen, and so there has been less phase-equilibrium work done on it, and its synthesis (see Deer et al. 1997) has not been scrutinized by modern characterization methods. Its upper stability limit was studied by Forbes (1977) and Melnik and Radchuk (1979), but rigorous reversals were not obtained and, in light of later work, their breakdown temperatures (to fayalite + quartz + H₂O) are judged to be too high. Compositions determined by Fonarev et al. (1979) along the grunerite + olivine + quartz $T\text{-}X_{\text{Fe/Mg}}$ phase loop in the system FMSH extrapolate to lower temperatures for the Fe-end-member reaction, consistent with the experimental results (e.g., 560 ± 10 °C at 2 kbar) of Lattard and Evans (1992). At 10 kbar and 650 °C the breakdown curve for grunerite crosses the reaction: fayalite + quartz = 2 ferrosilite, and the resulting change in sign of the Clapeyron slope produces a T -maximum for grunerite. An even lower breakdown temperature for grunerite (540 °C at 2 kbar) was found by Jenkins and Bozhilov (2003). Based on an extrapolation of Fe/Mg partitioning between the monoclinic and orthorhombic ferromagnesian amphiboles, Evans et al. (2001) suggested an extremum (T minimum) in their mutual relations near to the Fe-end (at about 400 °C), reversing the decline in temperature for the occurrence of orthorhombic FeMg-amphibole *vis-à-vis* the monoclinic form. Lending support to this suggestion, Bozhilov and Evans (2001) found that near end-member grunerite from Rockport, Massachusetts, contains a small percentage of *Pnma* ferro-anthophyllite. They also found by HRTEM that the grunerite is free of CMFs.

GLAUCOPHANE $\square\text{Na}_2(\text{Mg}_3\text{Al}_2)\text{Si}_8\text{O}_{22}(\text{OH})_2$

Glaucophane lends its name and distinctive color to one of the dozen or so widely recognized metamorphic facies, specifically one that is indicative of high pressure. It is not surprising, therefore, that many workers have attempted to synthesize glaucophane and experimentally bracket its PT -stability field. Not until very recently though (Jenkins and Corona 2006), have any of these attempts been particularly successful. Especially frustrating has been the growth during synthesis of an apparently metastable NaMgAl-sheet-silicate (commonly called smectite or vermiculite) that interferes with the desired crystallization of glaucophane. Another problem is that glaucophane tends to grow consistently slightly off composition, as recognized by Maresch (2007). These issues, and the previous literature, are reviewed in detail in Corona and Jenkins (2007).

Here I will address the second of these problems. Fundamentally, the problem stems from the fact that glaucophane contains five oxide components (NMASH). A starting composition with mass proportions exactly those of ideal glaucophane (Gln) is theoretically capable of producing during synthesis a lengthy list of possible mineral and mineral-component products, depending on the P and T of synthesis, namely: jadeite, quartz, coesite, albite, enstatite, talc, phlogopite, chlorite, glaucophane, cummingtonite, gedrite, sodic-gedrite, nyböite (Nyb, $\text{NaNa}_2(\text{Mg}_3\text{Al}_2)\text{Si}_7\text{AlO}_{22}(\text{OH})_2$), ^BMg-equivalent of magnesiokataphorite (MgKat, $\text{Na}(\text{NaMg})\text{Mg}_4\text{AlSi}_7\text{AlO}_{22}(\text{OH})_2$), ^BMg-equivalent of magnesiotaramite, and ^BMg-equivalent of richterite. Experimental work in the system NMASH by Carman and Gilbert (1983), Pawley (1992),

Welch and Graham (1992), Tropper et al. (2000), and Jenkins and Corona (2006) has shown that synthetic sodic amphibole close to glaucophane in composition is consistently enriched in ^ANa , ^BMg , and ^TAl , and depleted in ^CAl and ^TSi . How to describe these substitutions in terms of specific amphibole components is somewhat arbitrary, because many of them, after projecting from SiO_2 and H_2O , participate in a colinearity, for example (without coefficients): $\text{Gln} = \text{Nyb} + \text{MgKat}$, $\text{Gln} = \text{Nyb} + \text{Cum}$, $\text{MgKat} = \text{Nyb} + \text{Cum}$, and $\text{MgKat} = \text{Gln} + \text{Cum}$. ^BMg -aluminowinchite, which is the same as “NaAl-cumingtonite” (Tropper et al. 2000), would also be part of the same colinearity.

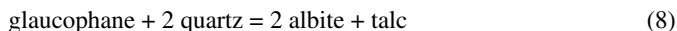
Compositions of synthetic and natural glaucophane tend to fall along the line Nyb-Cum in the projected system, or slightly inside the triangle nyböite – cumingtonite – sodicgedrite. These relations suggest a potential governing mass and energy balance:



Alternatively, we could write this as:

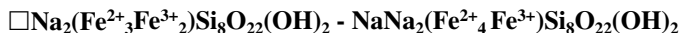


In both cases we have a dehydration reaction liberating SiO_2 . Tropper et al. (2000) showed that increase in T and P had inverse effects on the departure of glaucophane from its ideal composition. In other words, reactions (6) and (7) possess positive Clapeyron slopes, a reasonable conclusion. These considerations suggest that the best yields of on-composition glaucophane are likely to come from experiments at the highest pressures and lowest temperatures. With careful control of water contents in the capsule, and multiple intermediate grindings, Jenkins and Corona (2006) were able to produce glaucophane within analytical error limits possessing end-member composition at 25 kbar and 750 °C. However, their sought-after reversal of the reaction:



at 11.0-12.5 kbar and 600 °C, 14.5-16.0 kbar at 700 °C and 16.5-17.0 kbar at 750 °C (Corona and Jenkins 2007), involved glaucophane with detectable (and probably inevitable) substitution of the nyböite and cumingtonite components (plus minor Na and Al in talc).

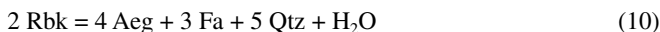
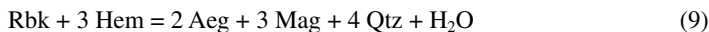
RIEBECKITE – ARFVEDSONITE



We arrive at riebeckite (Rbk) by replacing the Al and Mg in glaucophane with Fe^{3+} and Fe^{2+} . These two end-members are at opposite corners of the rectangular plot (known to petrologists as the Miyashiro diagram) that portrays the full ternary reciprocal system, with vectors FeAl_1 and FeMg_{-1} as x and y axes, and includes ferroglaucophane and magnesioriebeckite (the latter will be discussed below). A large proportion of natural sodic amphiboles, especially from blueschist-facies rocks, have little Na on the A-site, and fit this diagram very well. Arfvedsonite is derived from riebeckite via the coupled substitution: $^A\text{NaFe}^{2+}$ for $\square\text{Fe}^{3+}$. This step increases the ratio of ferrous to ferric iron from 3:2 to 4:1, which of course has consequences for its redox stability.

The only published study on the synthesis and stability relations of riebeckite is that of Ernst (1962). He reported yields of 70-90% amphibole using synthesis temperatures of 408 to 700 °C and pressures up to 2 kbar. Ernst recognized that the product amphibole became more arfvedsonitic as the attendant oxygen fugacity declined from that defined by the hematite-magnetite (HM) oxygen buffer. We can now see why this was the case.

In the system $\text{Na}_2\text{O}-\text{FeO}_x-\text{SiO}_2-\text{H}_2\text{O}$ (NFSHO) we can write two important oxygen-conserving reactions, both producing aegirine (Aeg), which potentially serve to limit the thermal stability of end-member riebeckite, one coinciding with the HM buffer and one on and below the fayalite-magnetite-quartz buffer (FMQ):



The reaction assemblage of (9) occurs at an invariant point on the HM buffer curve in the isobaric plot of $\log f_{\text{O}_2}$ vs. T . Between the HM and FMQ buffers is an isobarically univariant reaction terminal to riebeckite which consumes oxygen:



The difference between reactions (9) and (10) (eliminating Rbk and Aeg) corresponds to the oxygen-conserving reaction:



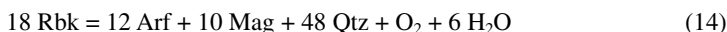
The large negative free energy of reaction (12) (e.g., -26.9 kJ at 800 K, 16.1 kJ at 298 K, Robie and Hemingway 1995) implies a major temperature difference (about 300°C) between reactions (9) and (10) at any given pressure. As a result, reaction (11) has a positive slope in an isobaric $\log f_{\text{O}_2} - T$ diagram (cf. Ernst 1962, Fig. 11).

Oxygen-conserved reactions for end-member arfvedsonite (Arf) corresponding to those given above for riebeckite on the HM, FMQ, and IM buffers are all metastable (with respect to aegirine, fayalite, and magnetite). As for riebeckite, the temperature differences among the arfvedsonite breakdown reactions are controlled by coupling reactions such as (12) or:

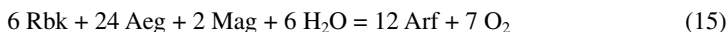


High PT experiments with oxygen buffer control, further discussed below, have shown that end-member riebeckite breaks down on the HM buffer (Ernst 1962) according to reaction (9) (Owen 1985, 1988; Miyano and Klein 1993). Under f_{O_2} conditions below the HM buffer, the stability of riebeckite extends to higher temperatures by incorporating progressively greater amounts of the Arf component (Ernst 1962; Owen 1988). As a result, end-member riebeckite does not have a stable breakdown reaction on FMQ, and reactions (10) and (11) are metastable with respect to reactions involving riebeckite-arfvedsonite solid solution. At lower temperatures the sodic amphibole contains some grunerite component as well (Owen 1988).

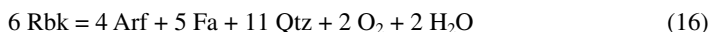
The increasing Arf content of riebeckitic amphibole with temperature rise is driven primarily by a devolatilization reaction that is distinctly oblique to the familiar oxygen buffer curves on the isobaric $\log f_{\text{O}_2} - T$ diagram (Fig. 4ab):



An additional limiting Arf-forming redox reaction between the HM and FMQ buffers involves aegirine:



At f_{O_2} below the FMQ buffer curve another reaction involves fayalite rather than magnetite and aegirine:



Reactions (15) and (16) are sub-parallel to oxygen-buffer curves, and, unlike reaction (14), are probably not important in driving the Rbk-to-Arf reaction. With their markedly different fluid stoichiometric coefficients, reactions (14), (15), and (16) together constrain the stability field of riebeckite-arfvedsonite solid solution compositions inside a narrow envelope on the $\log f_{\text{O}_2} - T$ diagram (Fig. 4). For simplicity, and to aid reference to the well-known oxygen buffer curves FMQ and QFI, I have not introduced grunerite into this phase equilibrium discussion; the presence of grunerite will further constrain the stability of riebeckite. In the field of grunerite, corresponding to (15) is the reaction:

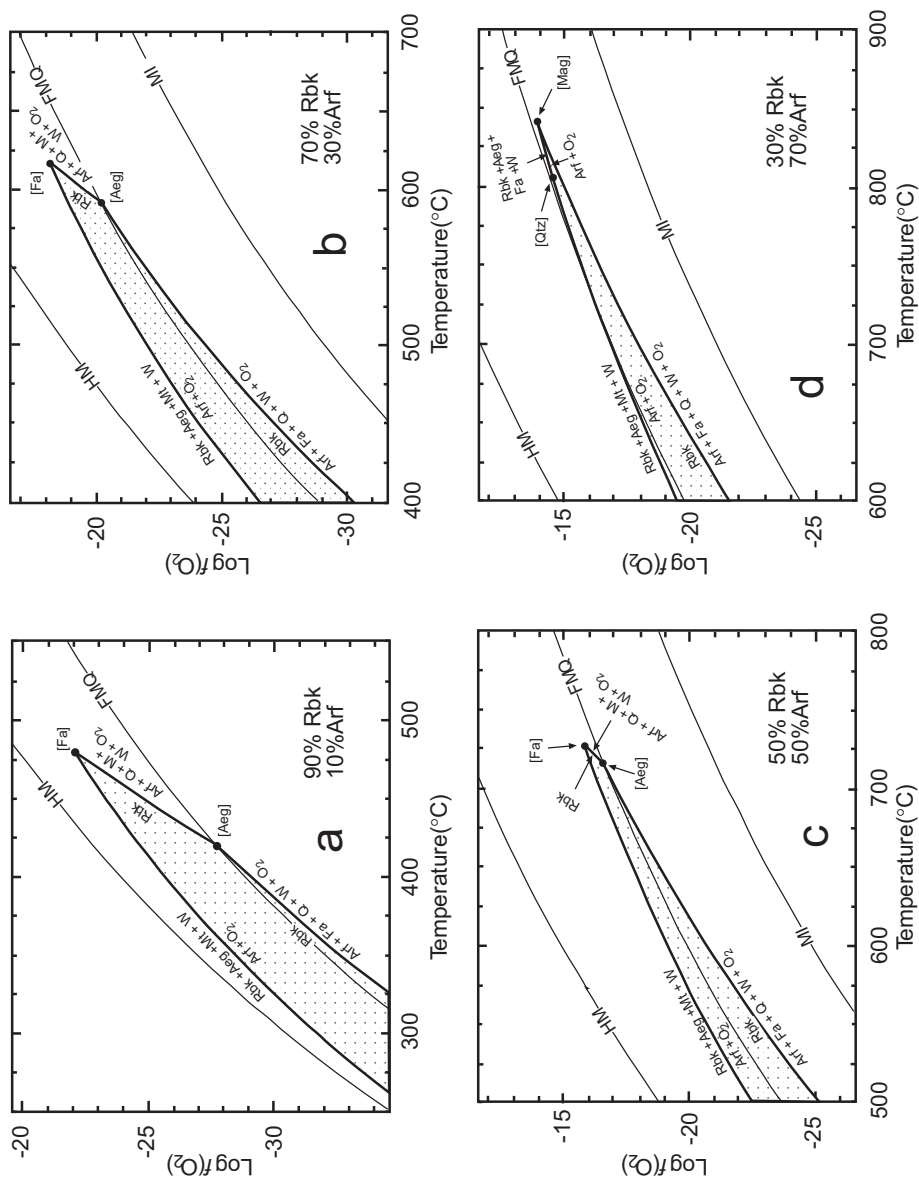
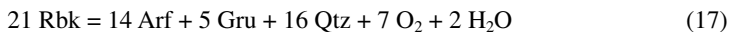


Figure 4. Calculated $\log f(\text{O}_2)$ vs. T diagram for the field of stability (dotted) of four compositions (mol%) of riebeckite-artvedsonite solid solution in the system NaFeSiHO at 2 kbar. Isobaric invariant points are designated in square brackets by the missing phases. See text for caveats.



In experiments up to 30 days duration with excess H₂O on the HM buffer, Ernst (1962) reported a riebeckite breakdown reaction at 515 °C and 2 kbar. To circumvent the problem of synthesizing riebeckite, and to have basically 100% amphibole starting material less ambiguous in its makeup, Owen (1985; 1988) performed 20 to 100 day experiments at the University of British Columbia on a natural crocidolite (Croc) from Western Australia with the composition: Na_{1.90}Ca_{0.05}Mg_{0.48}Mn_{0.01}Fe²⁺_{2.76}Fe³⁺_{1.85}(Fe³⁺_{0.03}Al_{0.01}Si_{7.96})O₂₂(OH)₂. This is equivalent to an amphibole with 5% ferro-richterite, 5% grunerite, and 90% total riebeckite; the ratio Fe²⁺/(Fe²⁺ + Mg) is 0.85. Grain widths of this crocidolite were typically 0.1 μm, and we assume that CMFs (vector towards Na ferriannite?) were probably present close to the grain boundaries (Ahn and Buseck 1991). Owen observed the growth of aegirine from Croc + Hem + Mag + Qtz starting material, that is, reaction (9), in four experiments at 2 and 4 kbar, including one as low as 359 ± 8 °C for 81 days at 2 kbar on the HM buffer. Aegirine grew as pseudomorphs after crocidolite. Owen was unable to reverse the reaction at lower temperatures.

A possible explanation for the ≥ 155 °C difference between Owen's study and that of Ernst (1962, Table 2) is that Ernst interpreted the presence of Aeg + Qtz in all the condensed run products below his designated equilibrium curve to be metastable (inherited from the starting material). Alternatively, one could reinterpret his table of run products as indicative of breakdown as low as 411 °C at 2 kbar. Hematite was not consistently present in the starting material, as required by reaction (9). This meant that, rather than examining the devolatilization reaction as done by Owen (1988), Ernst (1962) was approaching equilibrium with an additional reaction step, namely oxidation of riebeckite to Aeg + iron oxide (reaction 11).

The results of Owen (1988) are more consistent with the large temperature difference that must exist between riebeckite breakdown reactions on the HM and FMQ buffers, and the occurrence of Mag + Qtz + Aeg (up to 90% Aeg component) in epidote-blueschist facies ironstones (Onuki and Ernst, 1969; Brown 1986). It is also consistent with the conclusion of Okay (1980) that end-member riebeckite is not stable with hematite in blueschist-facies rocks. Microprobe analyses by Owen (1988; Fig. 6 here) of sodic amphibole in 24 samples of meta-ironstones from the 330 to 400 °C Shuksan blueschist, Washington (Brown and O'Neil 1982), show that, in hematite-bearing rocks, riebeckite does not reach the Mg-free composition (limit of about 66% Rbk), whereas with magnetite (lower *f*_{O₂}) it does. Owen (1988) recognized that the isothermal-isobaric univariant line on the Miyashiro diagram (Fig. 6) for HM equilibrium in the system NMF₂SHO has no unique location (cf. Okay 1980), but that it varies according to the mineral assemblage, e.g., presence of aegirine, epidote, albite, quartz, etc. In very low-grade (150 to 300 °C) crocidolite- and riebeckite-bearing banded iron-formation (BIF), hematite is commonly present but it is not clear even here whether *end-member* Rbk is stable with hematite (Klein 1974; Klein and Gole 1981; Miyano and Klein 1983). Thus, the stability of end-member riebeckite at any temperature on the HM buffer is uncertain. A low-temperature stable coexistence of pure riebeckite and hematite was calculated by Miyano and Klein (1983) using thermodynamic properties based on Ernst (1962). In the diagrams presented here (Figs. 4 and 5), it was provisionally assumed that reaction (9) occurs at 2 kbar and 150 °C, which is consistent with calculated Arf-Rbk stability up to 739 °C discussed below. Riebeckite is more thermally stable at lower values of *f*_{O₂} such as on FMQ.

On the FMQ buffer Ernst (1962) reversed the breakdown of synthetic Rbk-Arf solid solution to Fa + Aeg + Qtz + H₂O (reaction 10) at 656 °C and 2 kbar, and corresponding temperatures at other pressures. Judging from the cell volume of the sodic amphibole produced (mostly 914-915 Å³; cf. end-member riebeckite at 912.5 Å, Ernst 1960; Deer et al. 1997 Table 30), it contained 15-20% of the Arf component.

Owen (1988) found that starting material of natural, blue crocidolite taken in six experiments on the FMQ buffer to temperatures from 626 to 739 °C at 2 kbar produced blue-green amphibole

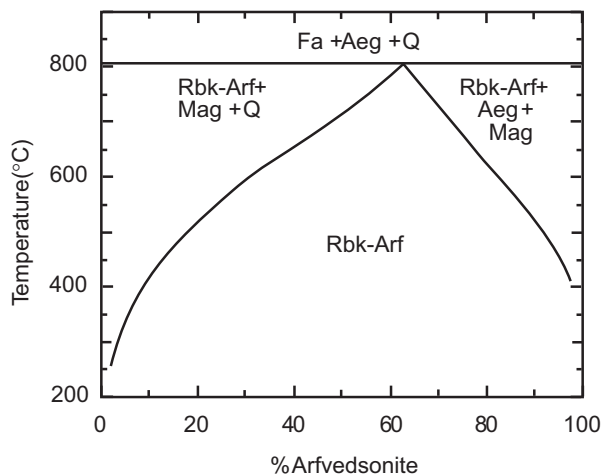


Figure 5. Calculated T_{Arf} - X diagram at 2 kbar for the stability limit of riebeckite-arfvedsonite solid solution at the f_{O_2} of the FMQ oxygen buffer.

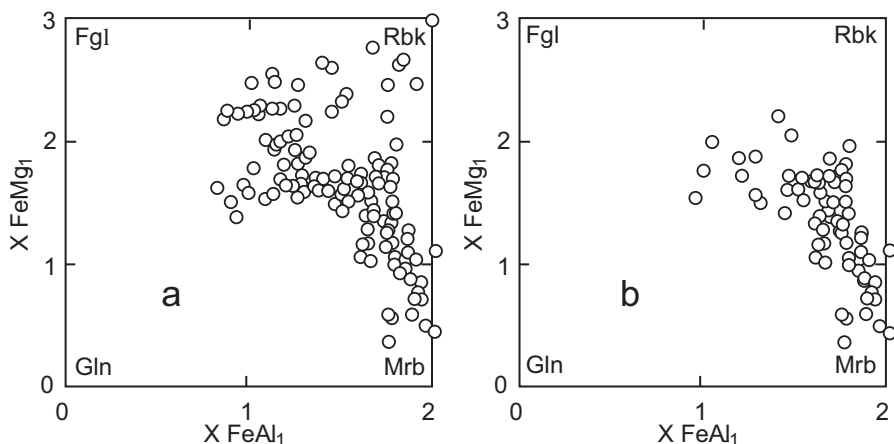


Figure 6. Microprobe analyses of sodic amphibole in Shuksan ironstones in the presence of quartz and magnetite (a) and hematite (b) plotted on the Miyashiro diagram for sodic amphiboles, from Owen (1988, Fig. 6.5).

containing increasing amounts of Na. Additional reaction products were magnetite, quartz, and fayalite. No aegirine was produced. This continuous reaction was reversed by taking blue-green amphibole (plus Mag and Qtz) grown at 690 °C and holding it at 554 °C for 22 days, producing blue amphibole with a lower Na content. Similarly, a synthetic blue-green amphibole grown at 607 °C and 2 kbar reacted in the presence of Mag and Qtz to form a bluer, more riebeckitic amphibole at 530 °C and 2 kbar. The apparently enhanced stability of sodic amphibole (to more than 739 °C at 2 kbar), compared to the results of Ernst (1962), could be due to the presence of Mg in Owen's natural crocidolite. However, that this is not the entire explanation is shown by nine experiments with synthetic aegirine, fayalite, and quartz starting material from 602 to 739 °C at 2 kbar, which produced in every case blue-green amphibole. Na in these amphiboles was higher than in riebeckite; Na increased with temperature, and was highest (2.55 Na apfu) in the experiment at 739 °C. One experiment on the FMQ buffer at 750 °C and 1 kbar was successful in causing complete breakdown of blue-green amphibole to aegirine, magnetite, and quartz, consistent with Figure 5, which is drawn for 2 kbar.

It is not clear why the results of Owen (1988) differ from those of Ernst (1962) with respect to the breakdown of Rbk-Arf on the FMQ buffer. One possibility is that Ernst reversed the metastable breakdown to aegirine, fayalite, quartz and H₂O of a riebeckite with a non-equilibrium (insufficient) content of Arf. Our provisional thermodynamic data for end-member riebeckite produces a metastable breakdown temperature for end-member riebeckite of 650 °C at 2 kbar.

The experimental results of Owen (1988) are incorporated in the diagrams of Figures 4 and 5, based on Evans and Owen (2002). These diagrams should be considered as semi-quantitative approximations of the likely phase relations of the riebeckite-arfvedsonite solid solution series, inasmuch as sizeable uncertainties are attached to their standard-state enthalpies, the solution has been treated as ideal, and the curves are for constant-activities. The log f_{O_2} – T field of any *specific* Rbk-Arf solid solution at 2 kbar (Fig. 4) is a narrow wedge with a high-temperature termination that rises from < 500 °C up to > 900 °C with increasing Arf content. It is scarcely 2 log units of f_{O_2} wide over much of the range. The composition change from Figure 4c to 4d results in the elimination of the curve for reaction (14) and the replacement of isobaric invariant points [Fa] and [Aeg] by [Qtz] and [Mag] on the opposite side of the FMQ curve.

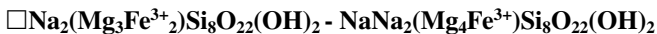
Application of Figures 4 and 5 to rocks in the field is limited by the absence of Mg, although many natural riebeckites and arfvedsonites are quite low in this constituent (Deer et al. 1997). Prograde metamorphism of riebeckite-bearing rocks will result in progress of reaction (14), which increases the Arf/Rbk ratio (Fig. 4a → Fig. 4b → Fig. 4c), and may produce aegirine (reaction 15) when the relative f_{O_2} is high. At redox conditions close to FMQ, little olivine is likely to form until the temperature exceeds 700 °C (Fig. 5). The diagrams are consistent with the occurrence of sodic amphibole in the riebeckite composition range (up to 50% Arf) in metamorphosed BIF and ophiolite-related ferruginous quartzite (metachert) and ironstone, rare marbles, as well as sodic granite, granite pegmatite, quartz-syenite, comendite, and their metamorphosed equivalents (Deer et al. 1997). In many igneous rocks, riebeckite is described as being of late crystallization (for example, in miarolitic cavities, as reaction rims around fayalite, aegirine, and iron oxides, in hydrothermally altered granite). In BIF riebeckite is acicular or alternatively present as cross-fiber or slip-fiber veins of asbestos (crocidolite). Compositions in the arfvedsonite range are found in sodic granite, microgranite, syenite, comendite, pantellerite, and their metamorphosed equivalents, low and very-low grade metasediments, and along shear zones (Deer et al. 1997).

Our calculations indicate that end-member riebeckite can only be synthesized stably at less than 450 °C at 2 kbar, provided f_{O_2} is controlled to midway between HM and FMQ. Syntheses on riebeckite composition attempted at higher temperatures or lower redox states will inevitably yield a riebeckite-arfvedsonite solid solution. Use of higher pressure would raise the temperature limit. The synthesis of arfvedsonite faces a much less stringent temperature maximum, but f_{O_2} must be lower, between FMQ and MI.

Consistent with the above, Iezzi et al. (2003) found that riebeckite synthesized at 500 °C and 4 kbar over 14 days (f_{O_2} internally controlled) has some Na on the A-site (arfvedsonite solution) according to its infrared spectrum, and Fe on M(4) (about 10% grunerite component) according to its Mössbauer spectrum. Its cell volume (916 Å) is larger than that of end-member riebeckite (Ernst 1963; Deer et al. 1997), another feature suggesting the presence of A-site Na. Figure 4 suggests that the f_{O_2} must have been about QFM+1. They noted the presence of quartz in the run products. This is consistent with modest passage from purer Rbk to the right in reaction (14), as well as the presence of some grunerite component.

The envelope of stability of riebeckite-arfvedsonite in our isobaric log f_{O_2} – T diagram resembles that for synthetic hastingsite, NaCa₂Fe²⁺₄Fe³⁺Al₂Si₆O₂₂(OH)₂ (Thomas 1982), another sodic amphibole with both ferrous and ferric iron.

MAGNESIORIEBECKITE – MAGNESIO-ARFVEDSONITE



The coupled substitution represented by this series is analogous to that in Rbk-Arf, except that Fe^{3+} is replaced by Mg^{2+} instead of by Fe^{2+} . As a result, the possible reactions linking the two end-members are somewhat different (see below). Because all iron is ferric, we can expect the stability of this series to extend to higher values of $\log f_{\text{O}_2}$ than was the case for the riebeckite-arfvedsonite series. This was in fact observed by Ernst (1960) in another of his pioneering experimental studies on the amphiboles. He found that “magnesioriebeckite” is apparently stable to above 900 °C at 1 to 2 kbar on the HM buffer, a great contrast to riebeckite. However, the cell volume of magnesioriebeckite (901 Å³) synthesized on the HM buffer by Ernst (1963) corresponds not to pure Mg-riebeckite (Mrb) but to a solid solution with considerable arfvedsonite, according to Figure 2 in Della Ventura et al. (2005), reproduced here as Figure 7. Thus, the breakdown temperature found by Ernst (1960) is probably too high for ideal Mrb. As indicated by Ernst (1960, Fig. 4), the stability limit of Mrb probably does continue to climb in temperature with increase in f_{O_2} above the HM buffer, where its composition will become even less arfvedsonitic.

Figure 7 depicts a ternary reciprocal system, with coordinate vectors $^{\text{A}}\text{Na}\square_{-1}$ and FeMg_1 (Fig. 7) and corner labels Mrb, Rbk, Mg-Arf, and Arf. Della Ventura et al. (2005) synthesized four sodic amphiboles from a starting composition of end-member Mrb. Of the four syntheses, the amphibole closest to Mrb contained 45% of MgFe-arfvedsonite according to Figure 7. This was obtained at 700 °C at NNO+2.3, the highest oxygen fugacity employed. Extrapolation would suggest that a buffer at NNO+5 or 6 would be a good choice for 100% synthesis of Mrb. Ernst (1960) found that “magnesioriebeckite” synthesized on the FMQ, MW, and WI buffers had α refractive indices 0.12 to 0.022 lower than on the HM buffer. For riebeckite (Ernst 1962, Fig. 5) the same trend was found to correlate with increasing amounts of the arfvedsonite

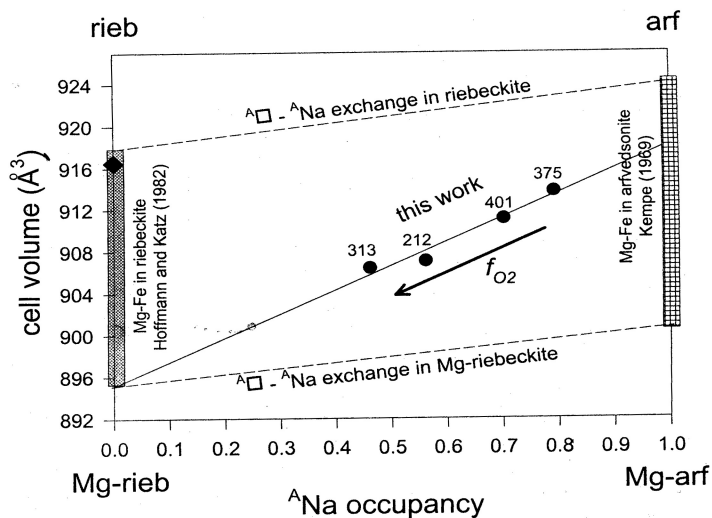


Figure 7. Relation between the cell-volume and the A-site occupancy of amphiboles synthesized in charges with the bulk composition of Mg-riebeckite. A regression line is drawn through the data points. The stippled areas along the ordinate represent the range of cell volume for MgFe^{2+} -riebeckite and MgFe^{2+} -arfvedsonite respectively. Filled diamond is the synthetic riebeckite of Iezzi et al. (2003). The broken lines represent the cell-volume variations for the ideal $\square\text{A}-^{\text{A}}\text{Na}$ solid solution. Note that the riebeckite line should extend down to about 912 Å. [From Della Ventura et al. (2005), *American Mineralogist*, Vol. 90, Fig. 2, p.1377]

component. The growth of arfvedsonitic amphibole from Mrb starting material is driven by the demands of phase equilibrium, and, like reactions (14) and (16) above, necessarily produces much quartz (Della Ventura et al. 2005, Table 1) along with H₂O, and possibly other minerals such as pyroxene and/or magnesioferrite (depending on what constituents are lost to the fluid), for example:



The high-*TP* breakdown of pure Mrb above the HM buffer is hard to predict; whether it is a strong function of f_{O_2} depends on the location of Na among the product phases: aegirine, liquid, or other Na-bearing phases.

The problem of synthesis of magnesioriebeckite is similar to that of riebeckite. Optimal results require selection of an appropriate f_{O_2} , and the lowest temperature possible. The choice of oxygen buffer is less critical for iron-bearing amphiboles whose terminal reaction is oxygen conserved, as for example, ferro-actinolite (reaction 4). I believe that now, with the advantage of hindsight, it should be possible to conduct some useful heterogeneous phase-equilibrium experiments (e.g., Scaillet and MacDonald 2003) on amphibole compositions inside the field of Figure 7.

Up to this point I have made no mention of the synthesis requirement for cation order-disorder to reflect the target, standard-state structure. Of course, this issue does not arise in the case of the simple end-members Tr, Fac, Ath, and Gru, where cations are fully ordered on the *M* and *T* sites. In natural sodic amphiboles (Gln, Rbk, Mrb, Arf, Mg-Arf), the mean bond length $\langle M(2)\text{-O} \rangle$ is short, signifying preferential occupancy of the *M*(2)-site by Al and Fe³⁺ (Hawthorne 1983b). Mössbauer spectra support this assignment (e.g., Van Alboom and De Grave 1996). In synthetic members of the Mrb-MgArf (Della Ventura et al. 2005) and Rbk-Arf series (Iezzi et al. 2003), Mössbauer spectra indicate complete ordering of Fe³⁺ on the *M*(2) site. No comparable data are available yet for synthetic glaucophane. Thus, as far as we know at this time, natural and synthetic sodic amphiboles are similar in having M³⁺ cations ordered onto *M*(2).

RICHTERITE Na(CaNa)Mg₅Si₈O₂₂(OH)₂

There have been numerous syntheses of richterite and yields have been excellent: 98-100% (Charles 1975). Nevertheless, its infrared spectrum indicates significant vacancy at the A-site (Rowbotham and Farmer 1973; Robert et al. 1989; Hawthorne 1995). Assuming that this is compensated by extra Ca and/or Mg (Welch et al. 1998) at the M(4) site (tremolite, cummingtonite), the near-perfect yield suggests that Na dissolved in the fluid during synthesis, otherwise we have not conserved mass. The infrared spectrum of synthetic potassic-richterite indicates the same behavior, although to a less pronounced degree (Hawthorne 1995; Hawthorne et al. 1997). Zimmermann et al. (1997a) synthesized a wide range of KNa-richterites in (KNa)Cl-solutions and found that the product amphiboles (99%, with traces of clinopyroxene and quartz) were large and free of CMFs, and contained on average 96% NaK-occupancy of the A-site, 0.06 apfu Mg on M(4) and 0.96 apfu Ca on M(4), in other words close to ideal. By contrast, the same group (Zimmermann et al. 1997b) observed that KNa cation-exchange experiments (requiring larger free-energy changes) induced disequilibrium richterite compositions with as much as 10 to 35% Cum and Tr in solution. Richterite synthesized by Della Ventura et al. (1999) was reported to be free of CMFs and about 98% pure, but syntheses were less successful for solid solutions along the pargasite-richterite join.

With regard to ferrichterite, the greater yield at low temperature as compared to high temperature (500-530 cf. 600-700 °C, Charles 1974) suggests heterogeneous equilibrium involving the clinopyroxene, olivine and liquid that were reported as additional run-products,

rather like the calcic amphiboles discussed earlier. This behavior may be related to the lower thermal stability of ferro-richterite as compared to its Mg analogue. The Mössbauer spectrum of Charles' (1974) ferro-richterite showed the presence of about 10% Fe³⁺ (Virgo 1972).

PARGASITE $\text{NaCa}_2(\text{Mg}_4\text{Al})\text{Si}_6\text{Al}_2\text{O}_{22}(\text{OH})_2$

The issues of intrinsic stability and kinetics at high synthesis temperatures are not problematic in the case of pargasite (Raudsepp et al. 1987). Westrich and Holloway (1981) reported yields of pargasite greater than 96%. Lykins and Jenkins (1992) confirmed the results of earlier work on the *P-T* stability of pargasite (e.g., breakdown at 960 °C and 500 bars), and showed that the presence of enstatite reduces the stability field of pargasite by 200 °C at 1 kbar. Welch et al. (1994) found no evidence of CMFs or CAFs in pargasite synthesized at 1 kbar and 930 °C for 70 hours, but 2% cummingtonite was present, as well as a small amount (< 2%) of diopside. Pargasite synthesized at 3 kbar and 900 °C by Della Ventura et al. (1999) was free of CMFs and about 98% pure. Jenkins et al. (2003) examined by microprobe, TEM, and FTIR spectroscopy a series of tremolite-pargasite solid solutions containing an initial 2.5 to 11% cummingtonite. The charge closest to pargasite (97.5% Pg) produced an excess of Mg in the product amphibole that they interpreted to be the result of the presence of triple-chain defects.

Spectroscopic and neutron-diffraction work on synthetic pargasite (Hawthorne 1995; Welch and Knight 1999) and XRD refinement of low-Fe natural pargasite (Oberti et al. 1995a) both show that, unlike sodic amphiboles, octahedral Al occurs in significant amounts on the *M*(2) and *M*(3) sites. However, it is also observed that the substitution of Fe²⁺ and Co²⁺ for Mg in pargasite reduces the amount of ⁶Al disorder. With this in mind, Hawthorne (1995) proposed pargasite as a type-example for the idea of entropy-driven disorder as a factor in the stabilization of end-member amphibole compositions. It might not be an easy experiment, but perhaps this idea could be tested by determining the ΔG of the pargasite breakdown reaction (to clinopyroxene, olivine, etc.) as a function of Fe/Mg ratio at constant temperature and pressure?

TSCHERMAKITE $\square\text{Ca}_2(\text{Mg}_3\text{Al}_2)\text{Si}_6\text{Al}_2\text{O}_{22}(\text{OH})_2$

Synthesis on composition is not possible (Raudsepp et al. 1991; Jenkins 1994). This is entirely consistent with the absence of pure tschermakite in nature. In virtually all metamorphic lithologies, actinolitic amphiboles give way with prograde metamorphism, in some cases across a solvus, to hornblendes that combine the tschermaks ($\text{AlAlMg}_{-1}\text{Si}_{-1}$) and edenite ($\text{NaAl}\square_{-1}\text{Si}_{-1}$) components roughly in the proportions that occur in pargasite (Schumacher 2007). Stable aluminous calcic amphiboles occupy a free energy trough lying between edenite and tschermakite in composition space. The tschermakite composition is disfavored by the absence of Na or K on the A-site which leads to local underbonding (low bond-valence) of the oxygen atom at the O(7) site (Hawthorne 1997). Tschermakite has cell dimension that place it outside the range of common calcic amphiboles (Oberti et al. 2007, Fig. 35).

The solution of Ts in Tr is thus limited to about 50-60% Ts (Cho and Ernst 1991; Jenkins 1994; Hosccek 1995), which is a composition close to the IMA designated end-member magnesiohornblende $\square\text{Ca}_2(\text{Mg}_4\text{Al})\text{Si}_7\text{AlO}_{22}(\text{OH})_2$. This behavior contrasts with the evidence for complete miscibility along the tremolite-pargasite join at 840 °C and 1 bar (Sharma 1996). The igneous Al-in-hornblende barometer takes advantage of the substantial influence of pressure on the Al-content of calcic amphiboles in multiphase rocks of broadly granite-granodiorite composition (Martin 2007). However, it is important to note that the Al-content of calcic amphibole is very sensitive to silica activity and that it may increase or decrease with pressure depending on the attendant mineral assemblage (Hosccek 1995).

Like many other amphibole end-members, the standard-state thermodynamic properties of tschermakite cannot be directly obtained by calorimetric investigation of a pure sample, whether synthetic or natural. One might then expect that its Gibbs free energy of formation at P and T would be considerably more uncertain than in the case of well-researched amphibole end-members such as tremolite, anthophyllite, grunerite and glaucophane (Robie and Hemingway 1995; Kahl and Maresch 2001). However, as shown by Holland and Powell (1998), it is possible to extract the thermodynamic properties of tschermakite with excellent precision using those of its compositional neighbor tremolite and laboratory equilibrium data for assemblages with Tr-Ts solid solutions (Jenkins 1994; Hoschek 1995) and an optimized non-ideal solution model. Metamorphic net-transfer and exchange phase-equilibria from nature and complex-system experiments can in many instances provide excellent constraints on the thermodynamic properties of minerals (not only amphiboles) that are never found with end-member compositions.

GENERAL CONCLUSIONS

It is not meant to imply from what has been said above that the stability limit of an amphibole necessarily constrains the conditions under which it can form. Many hydrate minerals show growth in experiments from oxide, gel or mineral starting mixtures at temperatures above their stable limit. Metastable anthophyllite can be grown from talc in the field of enstatite, quartz, and H_2O (Greenwood 1963). Similarly, Maresch and Czank (1988) found that Mn-anthophyllite can be grown in the stability field of pyroxene + quartz. On the other hand, the synthesis of a pure end-member composition that is metastable with respect to a compositionally equivalent amphibole solid solution plus pyroxene and quartz seems to be much more difficult – although it is in principle possible, starting from high free-energy oxides or gels. The growth mechanism of tremolite (Bozhilov et al. 2004) perhaps offers an explanation. At an intermediate stage, amphibole crystals are variable Tr-Cum solid solutions (with diminishing amounts of CMFs) and they include some that are close to ideal tremolite. Dissolution of diopside allows the bulk of the amphibole to shift toward more Tr-rich compositions. Beyond a certain point, however, the growth of end-member tremolite will become impossible because it would require a net *increase* in free energy (Fig. 1).

Syntheses of Ca and Na amphibole end-members almost all have a tendency to incorporate a cummingtonite or grunerite component (B-site substitution of Mg and Fe) and produce small quantities of pyroxene and quartz. The sodic amphiboles show a tendency to establish Na on the A site, as well as Mg and Fe on B. Mass-balances show that these trends reflect a measure of dehydration with respect to the target end-member composition. For some compositions (ferro-actinolite, riebeckite), the onset of dehydration is at relatively low temperature. Basically, these tendencies for modest departure from the ideal composition reflect the near-attainment of equilibrium. The presence of *large* amounts of Cum or Gru in the early stages of CaNa-amphibole synthesis indicate a fundamental instability. Time-series experiments have shown that these compositions tend to get eliminated with time. The general behavior and synthesis problems of Fe-bearing amphiboles relate to the additional role played by redox equilibria. It might be better in some cases not to impose an external control of f_{O_2} during synthesis (as opposed to phase equilibrium study). An inappropriate f_{O_2} constraint can drive redox reactions leading to undesired compositional changes and partial loss of amphibole. To the extent that internal buffering of the redox state can be experimentally maintained, the charge's composition can extend the temperature range of the target amphibole.

The initial growth of sheet or wide-chain silicates during amphibole synthesis (anthophyllite, tremolite, glaucophane, and others) is another problem that the experimentalist has to circumvent, with all the ingenuity he or she can muster.

ACKNOWLEDGMENTS

I would like to thank Claudia Owen for all her contributions to the riebeckite story, and David Jenkins, Roberta Oberti, Frank Hawthorne, and Walter Maresch for critical reviews.

REFERENCES

- Abbott RN, Burnham CW (1991) Energy calculations bearing on biopyriboles. *Am Mineral* 76:728-732
- Ahn JH, Buseck PR (1991) Microstructures and fiber-formation mechanisms of crocidolite asbestos. *Am Mineral* 76:1467-1478
- Ahn JH, Cho M, Jenkins DM, Buseck PR (1991) Structural defects in synthetic tremolitic amphiboles. *Am Mineral* 76:1811-1823
- Berman RG (1988) An internally consistent thermodynamic data for stoichiometric minerals in the system $\text{Na}_2\text{O}-\text{K}_2\text{O}-\text{CaO}-\text{MgO}-\text{FeO}-\text{Al}_2\text{O}_3-\text{SiO}_2-\text{TiO}_2-\text{H}_2\text{O}-\text{CO}_2$. *J Petrol* 29:445-522
- Berman RG, Engi M, Greenwood HJ, Brown TH (1986) Derivation of internally consistent thermodynamic data by the technique of mathematical programming: a review with application to the system $\text{MgO}-\text{SiO}_2-\text{H}_2\text{O}$. *J Petrol* 27:1331-1364
- Bowen NL, Tuttle OF (1949) The system $\text{MgO}-\text{SiO}_2-\text{H}_2\text{O}$. *Bull Geol Soc Am* 60:439-460
- Bozhilov KN, Evans BW (2001) Ferro-anthophyllite in Rockport grunerite: A transmission electron microscopy study. *Am Mineral* 86:1252-1260
- Bozhilov KN, Jenkins DM, Veblen DR (2004) Pyribole evolution during tremolite synthesis from oxides. *Am Mineral* 89:4-84
- Bozhilov KN, Brownstein D, Jenkins DM (2007) Biopyribole evolution during tremolite synthesis from dolomite and quartz in $\text{CO}_2-\text{H}_2\text{O}$ fluid. *Am Mineral* 92:898-908.
- Brown EH (1986) Geology of the Shuksan Suite, North Cascades, Washington, U.S.A. *In: Blueschists and Related Eclogites*. Evans BW, Brown EH (eds), *Geol Soc Am Mem* 164:143-154
- Brown EH, O'Neil JR (1982) Oxygen isotope geothermometry and stability of lawsonite and pumpellyite in the Shuksan Suite, North Cascades, Washington. *Contrib Mineral Petrol* 80:240-246
- Burns RG, Greaves CJ (1971) Correlations of infrared and Mössbauer site population measurements of actinolites. *Am Mineral* 56:2010-2033
- Cao R, Ross C, Ernst WG (1986) Experimental studies to 10 kb of the bulk composition tremolite₅₀-tschermakite₅₀ + excess H_2O . *Contrib Mineral Petrol* 93:160-167
- Carman JH, Gilbert MC (1983) Experimental studies on glaucophane stability. *Am J Sci* 283A:414-437
- Charles RW (1974) The physical properties of the Mg-Fe richterites. *Am Mineral* 60:518-528
- Charles RW (1975) The phase equilibria of richterite and ferrichterite. *Am Mineral* 60:367-374
- Chernosky JV, Autio LK (1979) The stability of anthophyllite in the presence of quartz. *Am Mineral* 64:294-303
- Chernosky JV, Day HW, Caruso LJ (1985) Equilibria in the system $\text{MgO}-\text{SiO}_2-\text{H}_2\text{O}$: Experimental determination of the stability of Mg-anthophyllite. *Am Mineral* 70:223-236
- Cho M, Ernst WG (1991) An experimental determination of calcic amphibole solid solution along the join tremolite-tschermakite. *Am Mineral* 76:985-1001
- Corona JC, Jenkins DM (2007) An experimental investigation of the reaction: Glaucophane + 2 Quartz = 2 Albite + Talc. *Eur J Mineral* 19:147-158
- Day HW, Halbach H (1979) The stability field of anthophyllite: the effect of experimental uncertainty on permissible phase diagram topologies. *Am Mineral* 64:809-823
- Day HW, Chernosky JK, Kumin HJ (1985) Equilibria in the $\text{MgO}-\text{SiO}_2-\text{H}_2\text{O}$: a thermodynamic analysis. *Am Mineral* 70:237-248
- Deer WA, Howie RA, Zussman J (1997) Double-chain silicates, Second Edition, Vol. 2B, The Geological Society, London
- Della Ventura G (1992) Recent developments in the synthesis and characterization of amphiboles. Synthesis and crystal chemistry of richterites. *Trends in Mineralogy* 1:153-191
- Della Ventura G, Hawthorne FC, Robert J-C, Delbove F, Welch MD, Raudsepp M. (1999) Short-range order of cations in synthetic amphiboles along the richterite-pargasite join. *Eur J Mineral* 11:79-94
- Della Ventura G, Iezzi G, Redhammer GJ, Hawthorne FC, Scaillet B, Novembre D (2005) Synthesis and crystal-chemistry of alkali amphiboles in the system $\text{Na}_2\text{O}-\text{MgO}-\text{FeO}-\text{Fe}_2\text{O}_3-\text{SiO}_2-\text{H}_2\text{O}$ as a function of $f\text{O}_2$. *Am Mineral* 90:1375-1383
- Dorling M, Zussman J (1987) Characteristics of asbestiform and non-asbestiform calcic amphiboles. *Lithos* 20:469-489
- Droop GTR (1994) Triple chain pyriboles in Lewisian ultramafic rocks. *Mineral Mag* 58:1-20

- Ellis DJ, Thompson AB (1986) Subsolidus and partial melting relations in the quartz-excess CaO + MgO + Al₂O₃ + SiO₂ + H₂O system under water-excess and water-deficient conditions to 10 kb: Some implications for the origin of peraluminous melts from mafic rocks. *J Petrol* 27:91-121
- Ernst WG (1960) The stability relations of magnesioriebeckite. *Geochim Cosmochim Acta* 19:10-40
- Ernst WG (1962) Synthesis, stability relations, and occurrence of riebeckite and riebeckite-arfvedsonite solid solutions. *J Geol* 70:689-736
- Ernst WG (1963) Polymorphism in alkali amphiboles. *Am Mineral* 48:241-260
- Ernst WG (1966) Synthesis and stability of ferrotremolite. *Am J Sci* 264: 36-65
- Evans BW (1982) Ultramafic amphiboles. *Rev Mineral* 9B:98-113
- Evans BW, Owen C (2002) Phase relations of riebeckite-arfvedsonite solid solutions. *Geol Soc Am, Abstracts with Program*, p. 502
- Evans BW, Ghiorsio MS, Kuehner SK (2000) Thermodynamic properties of tremolite: A correction and some comments. *Am Mineral* 85:466-472
- Evans BW, Ghiorsio MS, Yang H, Medenbach O (2001) Thermodynamics of the amphiboles: Anthophyllite-ferroanthophyllite and the ortho-clino phase loop. *Am Mineral* 86:640-651
- Fonarev VI, Korolkov GY, Dokina TN (1979) Laboratory data on the stability field of the cummingtonite + olivine + quartz association. *Geochem Int* 16:21-32
- Forbes WC (1977) Stability relations of grunerite, Fe₇Si₈O₂₂(OH)₂. *Am J Sci* 277:735-749
- Fyfe WS (1962) On the relative stability of talc, anthophyllite and enstatite. *Am J Sci* 260:460-462
- Ghiorsio MS, Evans BW (2002) Thermodynamics of the amphiboles: Ca-Mg-Fe²⁺ quadrilateral. *Am Mineral* 87:79-98
- Gilbert MC, Helz RT, Popp RK, Spear FS (1982) Experimental studies of amphibole stability. *Rev Mineral* 9B:229-353
- Gottschalk M, Najorka J, Andrut M (1998) Structural and compositional characterization of synthetic (CaSr)-tremolite and (CaSr)-diopside solid solutions. *Phys Chem Mineral* 25:415-428
- Gottschalk M, Andrut M, Melzer S (1999) The determination of the cummingtonite content of synthetic tremolite. *Eur J Mineral* 11:967-982
- Graham CM, Maresch WV, Welch MD, Pawley AR (1989) Experimental studies on amphiboles: a review with thermodynamic perspectives. *Eur J Mineral* 1:535-555
- Greenwood HJ (1963) The synthesis and stability of anthophyllite. *J Petrol* 4:317-351
- Grobéty BH (1997) The replacement of anthophyllite by jimthompsonite: a model for hydration reactions in biopyriboles. *Contrib Mineral Petrol* 127:237-247
- Hawthorne FC (1983a) Characterisation of the average structure of natural and synthetic amphiboles. *Period Mineral Roma* 52:543-581
- Hawthorne FC (1983b) The crystal chemistry of the amphiboles. *Can Mineral* 21:173-480
- Hawthorne FC (1995) Entropy driven disorder in end-member amphiboles. *Can Mineral* 33:1189-1204
- Hawthorne FC (1997) Short-range order in amphiboles: A bond-valence approach. *Can Mineral* 35:203-216
- Hawthorne FC, Oberti R, Ungaretti L, Grice JD (1996) A new hyper-calcic amphibole with Ca at the A-site: fluor-cannilloite from Pargas, Finland. *Am Mineral* 81:995-1002
- Hawthorne FC, Della Ventura C, Robert, J-L, Welch MD, Raudsepp M, Jenkins DM (1997) A Rietveld and infrared study of synthetic amphiboles along the potassium-richterite-tremolite join. *Am Mineral* 82:708-716
- Hawthorne FC, Welch MD, Della Ventura G, Liu S, Robert J-L, Jenkins DM (2000) Short-range order in synthetic aluminous tremolites: An infrared and triple-quantum MAS NMR study. *Am Mineral* 85:1716-1724
- Hawthorne FC, Oberti R (2007) Amphiboles: crystal chemistry. *Rev Mineral Geochem* 67:1-54
- Hemley JJ, Shaw DR, Luce RW (1977) Mineral equilibria in the system MgO-SiO₂-H₂O system: II Talc-antigorite-forsterite-anthophyllite-enstatite stability relations and some geological implications in the system. *Am J Sci* 277:353-383
- Holland TJB, Powell R (1998) An internally consistent thermodynamic data set for phases of petrological interest. *J Metam Geol* 16:309-343
- Holloway JR (1973) The system pargasite-H₂O-CO₂: a model for melting of a hydrous mineral with a mixed volatile fluid. I. Experimental results to 8 kbar. *Geochim Cosmochim Acta* 37:12-18
- Hoschek G (1995) Stability relations and Al content of tremolite and talc in CMASH assemblages with kyanite + zoisite + quartz + H₂O. *Eur J Mineral* 7:353-362
- Hutchison JL, Irusteta MC, Whittaker EJW (1975) High resolution electron microscopy and diffraction studies of fibrous amphiboles. *Acta Crystallogr A* 31:794-801
- Iezzi G, Della Ventura G, Cámara F, Pedrazzi G, Robert J-L. (2003) ^BNa-^BLi solid solution in A-site vacant amphiboles: synthesis and cation ordering along the ferri-clinoholmquistite-riebeckite join. *Am Mineral* 88:955-961
- Jansen JBH, de Kraats AH, van der Rijst H, Schuiling RD (1978) Metamorphism of siliceous dolomites of Naxos, Greece. *Contrib Mineral Petrol* 67:79-288

- Jenkins DM (1987) Synthesis and characterization of tremolite in the system $\text{H}_2\text{O}-\text{CaO}-\text{MgO}-\text{SiO}_2$. *Am Mineral* 72:707-715
- Jenkins DM (1988) Experimental study of the join tremolite-tschermakite: a reinvestigation. *Contrib Mineral Petrol* 99:392-400
- Jenkins DM (1994) Experimental reversal of the aluminum content in tremolitic amphiboles in the system $\text{H}_2\text{O}-\text{CaO}-\text{MgO}-\text{Al}_2\text{O}_3-\text{SiO}_2$. *Am J Sci* 33:13-24
- Jenkins DM, Clare AK (1990) Comparison of the high-temperature and high-pressure stability limits of synthetic and natural tremolite. *Am Mineral* 75:358-366
- Jenkins DM, Hawthorne FC (1995) Synthesis and Rietveld refinement of amphibole along the join $\text{Ca}_2\text{Mg}_5\text{Si}_8\text{O}_{22}\text{F}_2 - \text{NaCa}_2\text{Mg}_4\text{Ga}_3\text{Si}_6\text{O}_{22}\text{F}_2$. *Can Mineral* 33:13-24
- Jenkins DM, Sherriff BL, Cramer J, Xu Z (1977) Al, Si and Mg occupancies in tetrahedrally and octahedrally coordinated sites in synthetic aluminous tremolite. *Am Mineral* 82:280-290
- Jenkins DM, Bozhilov KN (2003) Stability and thermodynamic properties of ferro-actinolite: A re-investigation. *Am J Sc* 303:723-752
- Jenkins DM, Bozhilov KN, Ishida K (2003) Infrared and TEM characterization of amphiboles synthesized near the tremolite-pargasite join in the ternary system tremolite-pargasite-cummingtonite. *Am Mineral* 88:1104-1114
- Jenkins DM, Corona JC (2006) The role of water in the synthesis of glaucophane. *Am Mineral* 90:1062-1068
- Johannes W (1969) An experimental investigation of the system $\text{MgO}-\text{SiO}_2-\text{H}_2\text{O}-\text{CO}_2$. *Am J Sci* 267:1083-1104
- Kahl W-A, Maresch WV (2001) Enthalpies of formation of tremolite and talc by high-temperature solution calorimetry – a consistent picture. *Am Mineral* 86:1345-1357.
- Klein C (1968) Coexisting amphiboles. *J Petrol* 9:281-330
- Klein C (1974) Greenalite, stilpnomelane, minnesotaite, crocidolite and carbonates in a very low grade metamorphic Precambrian iron-formation. *Can Mineral* 12:475-498
- Klein C, Gole MJ (1981) Mineralogy and petrology of parts of the Marra Mamba Iron Formation, Hamersley Basin, Western Australia. *Am Mineral* 66:507-525
- Lattard D, Evans BW (1992) New experiments on the stability of grunerite. *Eur J Mineral* 4:219-238
- Leake BE et al. (1997) Nomenclature of amphiboles: Report of the Subcommittee on Amphiboles of the International Mineralogical Commission on New Minerals and Mineral Names. *Mineral Mag* 61:295-321
- Lykins RW, Jenkins DM (1992) Experimental determination of pargasite stability relations in the presence of orthopyroxene. *Contrib Mineral Petrol* 112:405-413
- Lyons PC (1972) Significance of riebeckite and ferrohastingsite in micropertite granites. *Am Mineral* 57:1404-1412
- Maresch WV (1977) Experimental studies on glaucophane: an analysis of present knowledge. *Tectonophysics* 43:109-125
- Maresch W, Czank M (1983) Phase characterization of synthetic amphibole on the join $\text{Mn}^{2+}_x\text{Mg}_{7-x}\text{Si}_8\text{O}_{22}(\text{OH})_2$. *Am Mineral* 68:744-753
- Maresch W, Czank M (1983) Problems of compositional and structural uncertainty in synthetic hydroxyl amphiboles. *Periodico di Mineralogia, Roma*. 52:463-542
- Maresch W, Czank M (1988) Crystal chemistry, growth kinetics and phase relationships of structurally disordered (Mn^{2+} , Mg) amphiboles. *Fort Mineral* 66:69-121
- Maresch W, Czank M, Schreyer W (1994) Growth mechanisms, structural defects and composition of synthetic tremolite: what are the effects on macroscopic properties? *Contrib Mineral Petrol* 118:297-313
- Martin RF (2007) Amphiboles in the igneous environment. *Rev Mineral Geochem* 67:323-358
- Melnik YP, Radchuk VV (1977) The stability of grunerite $\text{Fe}_7\text{Si}_8\text{O}_{22}(\text{OH})_2$. *Geokhimiya* 15:693-704
- Miyano T, Klein C (1981) Conditions of riebeckite formation in the iron-formation of the Dales Gorge Member, Hamersley Group, Western Australia. *Am Mineral* 68:517-529
- Miyano T, Klein C (1993) Evaluation of the stability relations of amphibole asbestos in metamorphosed iron-formation. *Mining Geology* 33(4):213-222
- Moore JN, Kerrick DM (1976) Equilibria in siliceous dolomites of the Alta aureole, Utah. *Am J Sci* 276:502-524
- Oba T (1980) Phase relations in the tremolite-pargasite join. *Contrib Mineral Petrol* 71:247-256
- Oberti R, Hawthorne FC, Ungaretti L, Cannillo E (1995a) ^{16}O Al disorder in amphiboles from mantle peridotites. *Can Mineral* 33:867-878
- Oberti R, Sardone N, Hawthorne FC, Raudsepp M, Turnock AC (1995b) Synthesis and crystal-structure refinement of fluor pargasite. *Can Mineral* 33:25-31.
- Oberti R, Della Ventura G, Cámara F (2007) New amphibole compositions: natural and synthetic. *Rev Mineral Geochem* 67:89-123
- Okay AI (1980) Sodite amphiboles as oxygen fugacity indicators in metamorphism. *J Geol* 88:225-232

- Onuki H, Ernst WG (1969) Coexisting sodic amphiboles and sodic pyroxenes from blueschist facies metamorphic rocks. *In: Pyroxenes and Amphiboles: Crystal Chemistry and Phase Relations*. Mineral Soc Am Spec Pub No. 2, p 241-249
- Owen C (1985) Constraints on the stability of riebeckite. *EOS Transactions of the Am Geophys Union* 66:1230
- Owen C (1988) The petrogenesis of blueschist facies ironstones in the Shuksan and Easton Schists, North Cascades, Washington. Ph.D. dissertation, University of Washington Seattle, 290p.
- Pavlovich MS, Jenkins DM (2003) Assessment of cation substitutions along the gallium and fluorine analogue of the tremolite-glaucophane join. *Am Mineral* 88:1486-1495
- Pawley AR (1992) Experimental study of the compositions and stabilities of synthetic nyböite and nyböite-glaucophane amphiboles. *Eur J Mineral* 4:171-192
- Pawley AR, Graham CM, Navrotsky A (1993) Tremolite-richterite amphiboles: synthesis, compositional and structural characterization and thermochemistry. *Am Mineral* 78:23-35
- Raudsepp M, Turnock AC, Hawthorne FC, Sheriff B, Hartman JS (1987) Characterization of pargasitic amphiboles ($\text{NaCa}_2\text{Mg}_4\text{M}^{3+}\text{Si}_6\text{Al}_2(\text{OH},\text{F})_2$; $\text{M}^{3+} = \text{Al, Cr, Ga, Fe}^{3+}, \text{Sc, In}$) by infrared spectroscopy, Rietveld structure refinement and ^{27}Al and ^{28}Si MAS NMR spectroscopy. *Am Mineral* 72:580-592
- Raudsepp M, Turnock AC, Hawthorne FC (1991) Amphibole synthesis at low pressure: what grows and what doesn't. *Eur J Mineral* 3:983-1004
- Robert J-L, Della Ventura G, Thauvin J-L (1989) The infrared OH-stretching region of synthetic richterites in the system $\text{Na}_2\text{O-CaO-MgO-SiO}_2\text{-H}_2\text{O-HF}$. *Eur J Mineral* 1:203-211
- Robie RA, Hemingway BS (1995) Thermodynamic properties of minerals and related substances at 298.15 K and 1 bar (10^5 Pascals) pressure and at higher temperatures. U.S. Geol Surv Bull 2131, 461p.
- Rowbotham G, Farmer VC (1973) The effect of "A" site occupancy on the hydroxyl frequency in clinoamphiboles. *Contrib Mineral Petrol* 38:147-149
- Scaillet B, MacDonald K (2003) Experimental constraints on the relationships between peralkaline rhyolites of the Kenya Rift Valley. *J Petrol* 44:1867-1894.
- Schumacher JC (2007) Metamorphic amphiboles: composition and coexistence. *Rev Mineral Geochem* 67:359-416
- Sharma A (1996) Experimentally derived thermochemical data for pargasite and re-investigation of its stability with quartz in the system $\text{Na}_2\text{O-CaO-MgO-Al}_2\text{O}_3\text{-H}_2\text{O}$. *Contrib Petrol* 125:263-277
- Sharma A, Jenkins DM (1999) Hydrothermal synthesis of amphibole along the tremolite-pargasite join and the ternary system tremolite-pargasite-cummingtonite. *Am Mineral* 84:1304-1318
- Skippen G, McKinstry BW (1985) Synthetic and natural tremolite in equilibrium with forsterite, enstatite, diopside and fluid. *Contrib Mineral Petrol* 89:256-262
- Smelik EA, Jenkins DM, Navrotsky A (1994) A calorimetric study of synthetic amphiboles along the tremolite-tschermakite join and heats of formation of magnesiohornblende and tschermakite. *Am Mineral* 79:1110-1122
- Stull RL (1973) Calcic and alkali amphiboles from the Golden Horn batholith, North Cascades, Washington. *Am Mineral* 58:873-878
- Thomas WM (1982) Stability relations of the amphibole hastingsite. *Am J Sci* 282:136-164
- Tropper P, Manning CE, Essene EJ, Kao LS (2000) The compositional variation of synthetic sodic amphiboles at high and ultra-high pressures. *Contrib Mineral Petrol* 139:146-162
- Ungaretti L, Oberti R, Cannillo E (1987) Crystal-chemical studies at different P, T, X conditions: principles and perspectives in earth science. *Atti Ticinensi di Scienze della Terra* 31:142-155
- Van Alboom A, De Grave E (1996) Temperature dependence of the ^{57}Fe Mössbauer parameters in riebeckite. *Phys Chem Mineral* 23:377-386
- Veblen DR (1980) Anthophyllite asbestos: microstructures, intergrown sheet silicates, and mechanisms of fiber formation. *Am Mineral* 65:1075-1086.
- Veblen DR (1992) Electron microscopy applied to non-stoichiometry, polysomatism and replacement reactions in minerals. *Rev Mineral* 27:181-223
- Veblen DR, Burnham CW (1978) New biopyriboles from Chester, Vermont: Descriptive mineralogy. *Am Mineral* 63:1000-1009
- Veblen DR, Buseck PR, Burnham CW (1997) Asbestiform chain silicates: New minerals and structural groups. *Science* 198:359-365
- Veblen DR, Buseck PR (1979) Chain-width order and disorder in biopyriboles. *Am Mineral* 64:687-700
- Veblen DR, Buseck PR (1981) Hydrous pyriboles and sheet silicates in pyroxenes and uralites: intergrowth microstructures and reaction mechanisms. *Am Mineral* 66:1107-1134
- Virgo D (1972) Preliminary fitting of ^{57}Fe Mössbauer spectra of synthetic Mg-Fe richterites. *Carnegie Inst Wash year Book* 71: 513-516
- Welch MD, Graham CM (1992) An experimental study of glaucophanitic amphiboles in the system $\text{Na}_2\text{O-MgO-Al}_2\text{O}_3\text{-SiO}_2\text{-SiF}_4$ (NMAF): some implications for glaucophane stability in natural and synthetic systems at high temperatures and pressures. *Contrib Mineral Petrol* 111:248-259

- Welch MD, Knight KS (1999) A neutron powder diffraction study of cation ordering in high-temperature synthetic amphiboles. *Eur J Mineral* 11:321-331
- Welch MD, Kolodziejski W, Klinowski J (1994) A multinuclear NMR study of synthetic pargasite. *Am Mineral* 79:261-268
- Welch MD, Shuangxi L, Klinowski J (1998) ^{29}Si , MAS NMR systematics of calcic and sodic-calcic amphiboles. *Am Mineral* 83:85-96
- Westrich HR, Holloway JR (1981) Experimental dehydration of pargasite and calculation of its entropy and Gibbs energy. *Am J Sci* 281:922-934
- Whittaker EJW (1979) Mineralogy, chemistry and crystallography of amphibole asbestos. *Mineral Assoc Can, Short Course Handbook* 4:1-34
- Yang H, Evans BW (1996) X-ray structural refinements of tremolite at 140 and 295K: Crystal chemistry and petrologic implications. *Am Mineral* 81:1117-1125
- Zimmermann R, Heinrich W, Franz G (1996) Tremolite synthesis from CaCl_2 -bearing aqueous solutions. *Eur J Mineral* 8:767-776
- Zimmermann R, Gottschalk M, Heinrich W, Franz G (1997a) Experimental Na-K distribution between amphiboles and aqueous chloride solutions, and a mixing model along the richterite - K-richterite join. *Contrib Mineral Petrol* 1126:252-264
- Zimmermann R, Knop E, Heinrich W, Pehlke J, Franz G (1997b) Disequilibrium in cation-exchange experiments between Na-K-Ca amphiboles and aqueous Na-K-Ca chloride solution: effects of fractional crystallization. *Eur J Mineral* 9:97-114

The Significance of the Reaction Path in Synthesizing Single-Phase Amphibole of Defined Composition

Walter V. Maresch

*Institute of Geology, Mineralogy and Geophysics
Ruhr-University Bochum
D 44780 Bochum, Germany
walter.maresch@rub.de*

Michael Czank

*Institute of Geosciences
Christian-Albrechts-University Kiel
D 24098 Kiel, Germany
czank@min.uni-kiel.de*

INTRODUCTION

Amphiboles are common and very complex rock-forming minerals. Knowledge of their physical, chemical and thermodynamic properties allows us to understand rock-forming and geodynamic processes. Amphiboles also possess distinctive physical properties that make them potentially attractive in applied fields. Certainly, millions of dollars, rubles, etc. were spent 30-40 years ago to optimize techniques of amphibole synthesis, and, ironically, comparable sums have been or are still being spent to remediate asbestos danger.

In short, for whatever purpose, be it basic research or applied mineralogy, the task of synthesizing amphiboles of defined composition and crystal-chemical nature has been a challenge for a very long time. However, even a cursory review of the literature on amphiboles converges on one, often recognized and much discussed dilemma (e.g., Hawthorne 1983b, 1995; Maresch and Czank 1983b; Graham et al. 1989; Raudsepp et al. 1991). Compositions of amphibole products most often depart from the nominal experimental target. Is it then possible to synthesize single-phase amphibole products, and, if not, why not?

Ideally, synthesizing single-phase hydroxyl-amphibole from a given bulk composition would be the most accurate way to proceed to a well characterized amphibole product. Simply in terms of chemical composition, a bulk starting material can be prepared with greater accuracy than a multi-grain product can be characterized analytically. What goes in must come out! However, reality is more sobering. Various states of disorder are possible at constant bulk composition (e.g., Oberti et al. 2007; Hawthorne and Della Ventura 2007). Above all, the necessity to introduce H₂O as a fluid, both as an intrinsic component of the structure and as a means of transmitting pressure in the experiment, introduces new and difficult to control degrees of freedom. Changes in valence states become possible. The target stoichiometry of the amphibole may be changed by incongruent dissolution, i.e., fractionation of certain elements between solid and coexisting aqueous fluid. Above all, the need to achieve reasonable reaction rates at laboratory time scales generally requires the use of highly reactive, in other words highly metastable starting materials such as gels or oxide/hydroxide/carbonate mixes. These lead to very rapid reaction in the first few minutes of experiments, in which recalcitrant metastable assemblages and structural states can be imposed that fail to equilibrate during the remaining run duration. In other words, the reaction path of the synthesis experiment can be critical.

In nature, disequilibrium states can often be recognized by zoned crystals. Most experimental amphibole products are very fine-grained, however, so that zoning may be difficult to recognize. Relatively large analytical error with standard techniques such as the electron microprobe on these small crystals typically can also mask intergrain compositional inhomogeneity in an amphibole population. Even spectroscopic techniques may not always yield an unequivocal interpretation. As a result, the appearance of phases in addition to amphibole, i.e., an amphibole yield of less than 100%, is usually a clear harbinger that a desired composition equivalent to the starting material has not been achieved.

The question then arises as to whether the desired amphibole composition is not really stable at all at the given conditions of the experiment, or whether the reaction path of the synthesis run has been delayed in a metastable state due to some kinetic barrier. In fact, both explanations may hold at the same time. We need to differentiate between thermodynamic equilibrium and kinetics. An aphorism attributed to the late experimental petrologist Frank Schairer of the Carnegie Institute in Washington illustrates this neatly. Schairer said "*If you don't know where you're going, you can't get lost.*" We could rephrase this to read "*If you don't know where you're going, it doesn't matter how, or how fast you get there.*"

In a companion chapter in this volume, Evans (2007) addresses the question of intrinsic stability of some common amphibole end-members. In other words, "*where are we going*" when we try to synthesize a specific amphibole composition. In the present chapter, we propose to review some important recent published results on the experimental reaction paths, i.e., "*how do we get there?*"

In the last 20-25 years or so, inspection by high-resolution electron microscopy (HRTEM) of amphibole products has become routine. With these studies has come the realization that in many, if not most cases the reaction paths appear to involve intermediate phases and amphibole defect structures that are best viewed in terms of the concept of polysomatism and polysomatic series (Thompson 1970, 1978, 1981). Such reaction paths commonly leave their mark as clearly recognizable defect structures representing stranded intermediate reaction steps. In most studies only the end-product is characterized, so that reaction paths for given chemical systems can only be inferred and compared. However, time studies have also allowed insight into the progress of such reactions by monitoring changing defect structures (Maresch and Czank 1988; Bozhilov 2004, 2007). More recently, Bozhilov et al. (2004, 2007) have also routinely brought analytical transmission electron microscopy to bear on such time series, allowing changing compositions of individual amphibole crystals and pyriboles to be monitored in great detail. In the following we propose to review some of the most important conclusions from these studies.

Other working groups have noted that the above polysomatic reaction paths can be decidedly influenced by introducing part of the condensed starting material as soluble compounds in halide form, thus directly involving the aqueous fluid phase as a component donor. Some chemical systems, especially those involving alkalis, do not exhibit significant evidence for polysomatic reactions during synthesis. Thus these reaction paths have not been studied in great detail. On the other hand, these systems often show clear evidence of inhomogeneous fractionation of the starting material into the fluid phase. A number of studies have therefore treated the aqueous fluid phase as part of the reacting system, and have manipulated the composition of this phase to counteract incongruent dissolution, improve reaction kinetics and to increase the yield of crystals large enough for accurate electron microprobe analysis. We summarize progress on this aspect in a second section.

Experimental work and the resulting literature on amphiboles have become as complex as the proverbially complex crystal chemistry of this important rock-forming mineral group. We apologize to any colleagues who perceive that their work might be underrepresented in the following overview.

INHERENT PROBLEMS ASSOCIATED WITH THE EXPERIMENTAL METHOD

The accurate characterization of all crystal-chemical aspects of the amphiboles is the main theme of this volume and requires no further comment here. Since the early eighties a number of studies and reviews have also acknowledged the singular problems posed by *synthetic* amphiboles (e.g., Hawthorne 1983b; Maresch and Czank 1983b; Graham et al. 1989; Raudsepp et al. 1991; Hawthorne 1995), for instance,

- compositions of the amphibole products frequently deviate from the nominal run composition;
- the spectrum of crystal sizes is large, and there is some evidence that there may be a systematic correlation between crystal chemistry and/or defect structure with crystal size (e.g., Hawthorne et al. 1997; Maresch and Czank 1983a,b; Ahn et al. 1991; Maresch et al. 1994; Gottschalk and Klein 1994), thus introducing bias when, for example, comparing electron microprobe results (large crystals) with HRTEM studies (small crystals);
- as in other mineral groups, ordering patterns of synthetic analogs may be difficult to engineer in such a way that they reflect natural amphiboles (cf. Oberti et al 2007; Hawthorne and Della Ventura 2007).

However, when turning to kinetic aspects of amphibole synthesis, it is also necessary to consider the “hardware”. Most synthesis studies have been carried out with some variation on three basic types of apparatus: 1) standard cold-seal pressure vessels, 2) piston-cylinder apparatus, and 3) internally heated gas pressure vessels. Common to all these apparatus is that they require a certain amount of time to heat up and reach thermal equilibrium. In typical cold-seal apparatus this may take as long as 30-45 minutes (e.g., Maresch and Czank 1988). The other two types of apparatus reach run conditions more rapidly, although this information is rarely given in relevant publications. A minimum interval of 10-15 minutes can usually be assumed as realistic. In the time series on tremolite studied by Bozhilov et al (2004, 2007), the run-up time in the internally heated gas apparatus used is 8 minutes (Bozhilov pers. comm. 2007).

Although these time intervals may seem short in comparison to the tens to hundreds of hours of run duration of most experiments, it should be noted that the highly reactive starting material usually used crystallizes rapidly within the first minutes of the experiment. Maresch and Czank (1988) found complete reaction of starting gel to talc- and in part amphibole-bearing assemblages at the end of the 30-45 minute run-up path to 675-750 °C. Bozhilov et al. (2004) found complete crystallization to dominant diopside, with amphibole, enstatite and quartz, for tremolite syntheses after 8 minutes run time at 850 °C and 0.6 GPa. In such runs, obviously, non-amphibole phases will represent precursor phases to any further amphibole that forms. The run-up path is therefore a poorly constrained beginning to any amphibole synthesis experiment and may well vary significantly from laboratory to laboratory.

POLYSOMATIC REACTION PATHS

Defect structures as a proxy for the reaction path

The concepts of polysomatism and polysomatic series (Thompson 1970, 1978, 1981) provide a basis for understanding the reaction paths leading to amphibole synthesis. The biopyriboles (Johannsen 1911; Thompson 1978), i.e., pyroxenes, amphiboles and 2:1 sheet silicates, are probably the best-known group of such polysomatic minerals. The powerful concept of a polysomatic series allows structures ranging from single-chain pyroxene and 2:1 sheet silicates such as mica (or talc) to be viewed simply in terms of aggregates of pyroxene-

like and mica-like modules (Fig. 1). Reactions in which one polysome replaces another can be viewed as sequences of polysomatic slabs replacing one another. Structural disorder becomes amenable to analysis and stoichiometries can be calculated even in polysomatically disordered regions of a crystal. Veblen (1991) reviews the concept and its applications in detail.

Considerable information on natural bioypriboles, their ordered and disorder structures and the polysomatic reactions linking them has evolved from HRTEM studies (e.g., Veblen and Buseck 1979, 1980; Veblen 1981, 1991). For the purposes of this presentation, amphibole represents the target phase, and all deviations from the ideal amphibole double-chain structure, outlined in detail elsewhere in this volume, can be considered to be "errors" in this structure. In addition, HRTEM studies of synthetic amphiboles are critically influenced by the elongated tabular habit typical of these crystals (Fig. 2). Because of the small size of the synthetic crystals, most investigations have been carried out on grain mounts. Despite quite variable aspect ratios, these crystals will tend settle mainly on the (100) or (210)/(110) (orthorhombic/monoclinic,

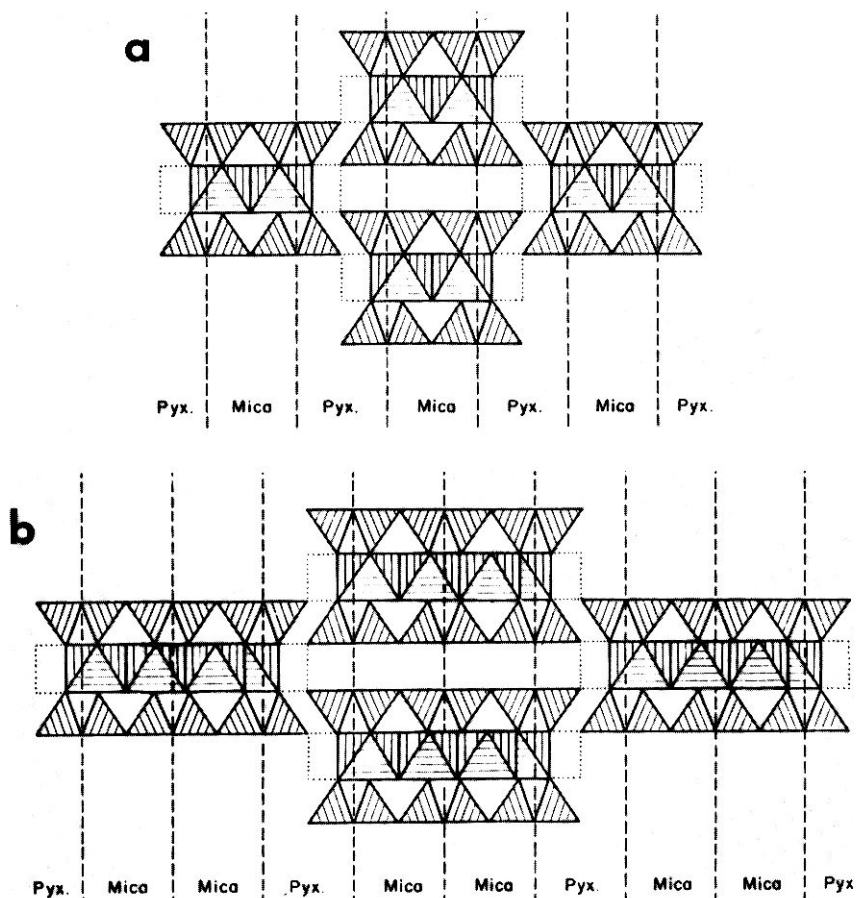


Figure 1. In the polysomatic model of Thompson (1970, 1978, 1981), amphibole can be viewed as consisting of building blocks of mica and pyroxene in a 1:1 ratio (a). By changing this ratio in a regular way, ordered polysomes between pyroxene and mica can be constructed. Panel (b) shows the triple-chain clinojimthompsonite structure built from mica and pyroxene modules in a 2:1 ratio. Allowing disordered sequences of mica and pyroxene building blocks can result in many different possible structure types. View parallel to the silicate chains. From Veblen (1981).

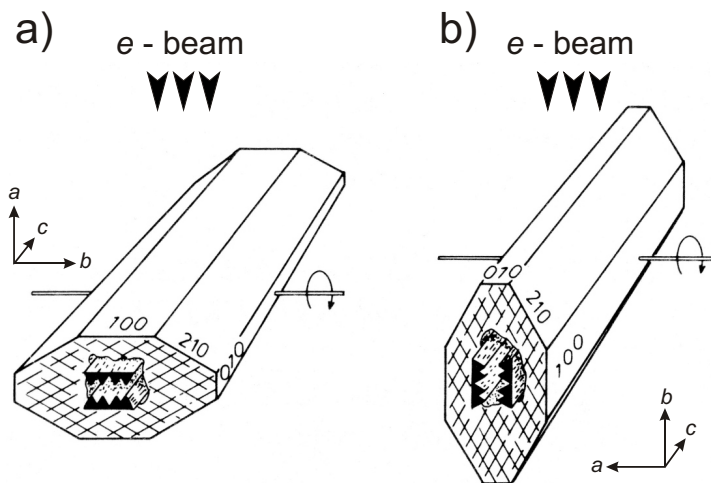


Figure 2. Typical lath-like habit of synthetic amphibole crystals. a) Preferred orientation in grain mounts. Chain multiplicity faults (CMFs) can be imaged by HRTEM. b) Much rarer orientation in grain mounts. Chain arrangement faults (CAFs, i.e., stacking faults in this case) can be imaged by HRTEM. Taken from Maresch and Czank (1988).

respectively) prism faces, and less commonly on or near (010). Thus HRTEM images obtained parallel or close to [100], i.e., perpendicular to b , which yield information on the widths of the chains, are easily obtained. Those parallel or close to [010], i.e., perpendicular to a^* , showing the stacking of the I-beams are rare, and images parallel or close to [001], i.e., “down-chain”, are almost impossible. The general lack of information from the [001] orientation is a serious drawback for interpreting reaction mechanisms. As discussed at length by Veblen and Buseck (1980) and Veblen (1981, 1991), the most convincing mechanism for reactions between biopyriboles is the “zipper” model (Fig. 3), a mechanism that cannot be demonstrated unequivocally without images parallel to [001].

For describing the above “errors” in the amphibole structure, we follow the nomenclature of Liebau (1980, 1985), who defined m as the multiplicity of the fundamental chain of tetrahedra of a chain silicate. The multiplicity m represents the number of subchains that are linked to form a multiple chain. For ideal amphibole $m = 2$. Figure 4 shows a view parallel [100] of the amphibole structure. An ordered sequence of double chains is interrupted by a chain with the “wrong” m , in this case a triple chain. Hutchison et al. (1975) and Veblen and Buseck (1979)

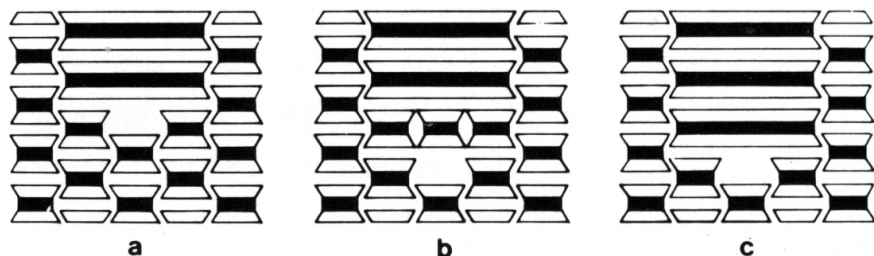


Figure 3. The “zipper model” of Veblen and Buseck (1980) viewed in [001] projection showing the reaction front between a slab with $m = 6$ (above) and three double chains (below). The misfit leads to a “diffusion pipe” in the chain direction. From Veblen and Buseck (1980).

analysis, but also tend to be more defective (Maresch and Czank 1983a,b; Hawthorne et al. 1997). Thus care must be taken to avoid bias.

A very important corollary of the polysomatic model is that different polysomes will have different stoichiometries and compositions (Thompson 1981; Veblen 1981). Thus an amphibole crystal containing CMFs of whatever m not equal to 2 will no longer have the bulk composition of an ideal amphibole (Fig. 6). Because the ratios of the larger, distorted octahedral sites connecting the I-beams to the smaller more regular inner octahedra will also decrease as m increases (Veblen and Burnham 1978b; Cameron and Papike 1980; Thompson 1981; Veblen 1981; Hawthorne 1983a), fractionation effects within the cation populations will also result (Veblen and Buseck 1979; Veblen 1981; Maresch and Czank 1983a,b, 1988). In summary, any chain multiplicity faults incorporated into the amphibole will shift the bulk composition of the crystal aggregate of the experimental runs away from the starting bulk composition. Recalculation schemes for the compositional effects of CMFs are given, for example, in Veblen (1981), Maresch et al. (1994), Jenkins et al. (2003) and Bozhilov et al. (2007). Thus the appearance of additional phases in a run may be due either to lack of stability of the target composition (Evans 2007), the presence of CMFs, or both.

Another general class of planar defects called the *chain arrangement fault* by Czank and Liebau (1980) may be present in amphiboles as stacking faults and twin boundaries (Fig. 7). These can be imaged with the electron beam perpendicular to a^* , an orientation which, as discussed above, is much more rarely encountered. Thus much less information is available on such faults in synthetic amphiboles. No shift in bulk composition is to be expected, but due to the “microtwinning” that may occur close to the unit-cell scale, amphiboles that are monoclinic may appear orthorhombic under the microscope or in X-ray powder diffraction studies (Fig. 8; see also discussion in Maresch and Czank 1988). In reviewing the question of inherent stability of end-member amphiboles, Hawthorne (1995) has suggested that such stacking disorder may be an important contribution to configurational entropy for end-member or near-end-member compositions. For lack of data, this question will not be explored further here.

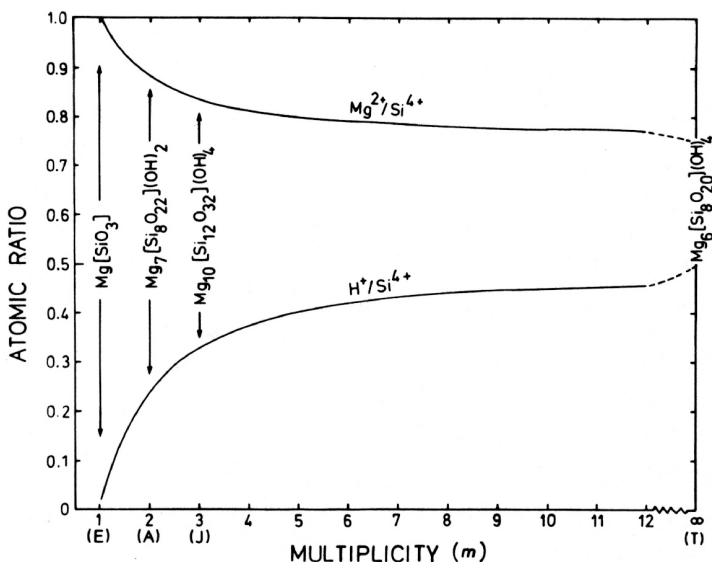


Figure 6. Variation of cation ratios as a function of multiplicity m in pure Mg-biopyrroboles. E = enstatite, A = anthophyllite, J = jimthompsonite, T = talc. From Maresch and Czank (1988).

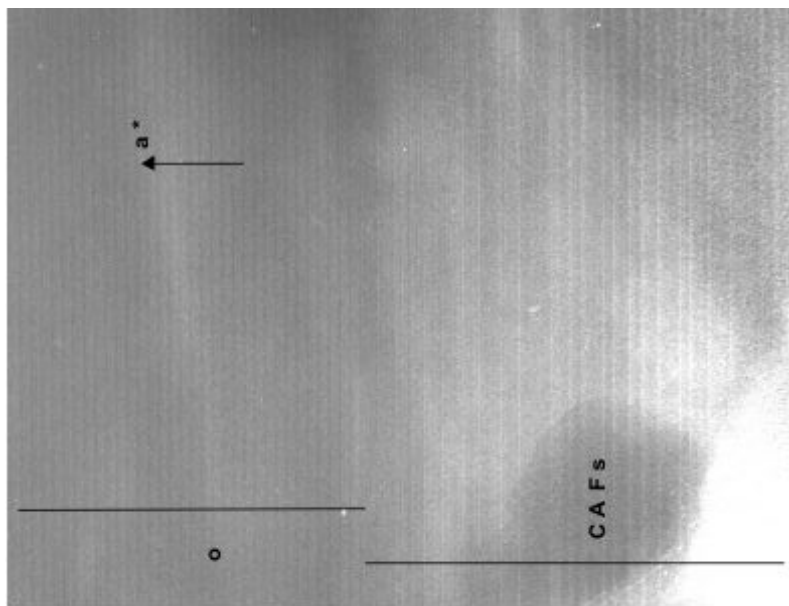


Figure 8. Stacking disorder in synthetic (Mn^{2+} , Mg)-amphibole. The upper part of the image is orthorhombic. (100) lattice fringes correspond to ~ 18 Å. The lower part is monoclinic, but appears macroscopically orthorhombic due to many chain arrangement faults, i.e., "microtwinning."

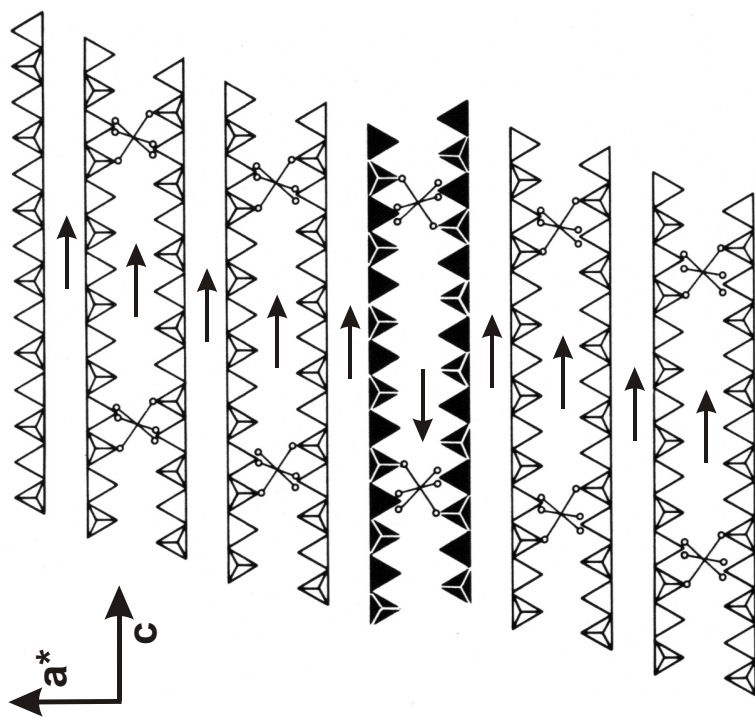


Figure 7. Schematic [010] projection of a stacking fault in a $C2/m$ amphibole. The arrows indicate the direction of $c/3$ stagger. Adapted from Maresch and Czank (1988).

In the following sections, an attempt is made to arrive at some valid generalizations from many detailed observations made on a multitude of experimental studies that may differ in experimental apparatus, run conditions (pressure, temperature, duration), starting material (usually gel or oxide mix, sometimes seeded with small amounts of natural amphibole), deliberate shifts from end-member bulk composition (e.g., excess SiO₂ or Mg vs. Ca enrichment), multiple rerunning with intermittent regrinding to improve yield, etc. It is not realistically possible to separate the individual influence of all these parameters on the results reported, and therefore our conclusions will of necessity have an admitted bias.

End-member synthetic tremolite

Tremolite, Ca₂ Mg₅ Si₈ O₂₂ (OH)₂, is an important anchor phase in amphibole crystal chemistry and amphibole thermodynamics. Beguilingly simple in terms of chemistry, tremolite has been a prime object for experimental petrologists. Evans (2007) and Bozhilov et al. (2004) provide an exhaustive overview of experimental work on this end-member composition, ever since the first studies of Boyd (1959).

As Evans (2007) summarizes, the general result in many experiments between 750 and 900 °C on end-member tremolite composition was 90% amphibole plus diopside and quartz, suggesting that the synthetic amphibole had a 10% solid solution component of cummingtonite. After the early HRTEM descriptions of Maresch and Czank (1988), Maresch et al. (1990) and Ahn et al. (1991), pointing to the common occurrence of wide-chain CMFs in such synthetic tremolites, a lively debate ensued on how much of the solid solution towards cummingtonite could actually be explained by compositional shifts due to these CMFs. Evans (2007) summarizes this discussion and comes to the conclusion that thermodynamic modeling as well as experimental results point to a true solid solution of 3 to 7% at 800 °C, decreasing with decreasing temperature, when buffered by diopside + quartz.

Although satisfactory convergence on this question appears now to have been achieved, this discussion also spurred a number of detailed experimental and HRTEM studies that allow useful insight into the reaction mechanisms leading to amphibole growth.

Jenkins (1987) provided a first systematic study of tremolite synthesis, varying parameters such as bulk composition, as well as pressure and temperature of synthesis over a wide range. Ahn et al. (1991) were the first to provide a systematic overview of CMFs in synthetic end-member or close-to-endmember tremolite. The experimental products were obtained at pressures of 0.2 and 0.6 GPa, both within and beyond the stability field of talc (Fig. 9). Indeed, talc is reported only from the run at 700 °C. The main observations on CMFs reported by Ahn et al. (1991) are summarized in Figure 10. Triple chain CMFs predominate and their abundance is inversely proportional to the abundance of double-chain amphibole structures. A'(1) values, i.e., the proportion of single-chains, show a similar trend, with the exception of the run at 750 °C/0.2 GPa, which however was seeded with natural tremolite. A'(2) values vary from 0.80 (±0.19) to 0.95 (±0.04). Higher synthesis temperatures suggest higher A'(2) values, but the effect is not entirely clear-cut. Ahn et al. (1991) conclude that the excellent correlation between A'(2) and A'(3) can be taken as an indication that the growth mechanism of the synthetic amphibole should not vary significantly as a function of *P*, *T*, and composition. Thick packets of single chains are reported within some amphibole crystals and interpreted as relict pyroxene precursors reacting to produce amphibole. No analogous talc precursors were found, and Ahn et al. (1991) conclude that the talc-to-anthophyllite reaction is a bulk dissolution-reprecipitation mechanism.

Maresch et al. (1994) studied synthetic tremolite products obtained at pressures up to 2.2 GPa and temperatures of 600 to 875 °C. Their results are summarized in terms of three broad *P-T* regions (Fig. 9), where different growth mechanisms are inferred for amphibole. *P-T* region I encompasses relatively low pressures within or very close to the stability field of talc.

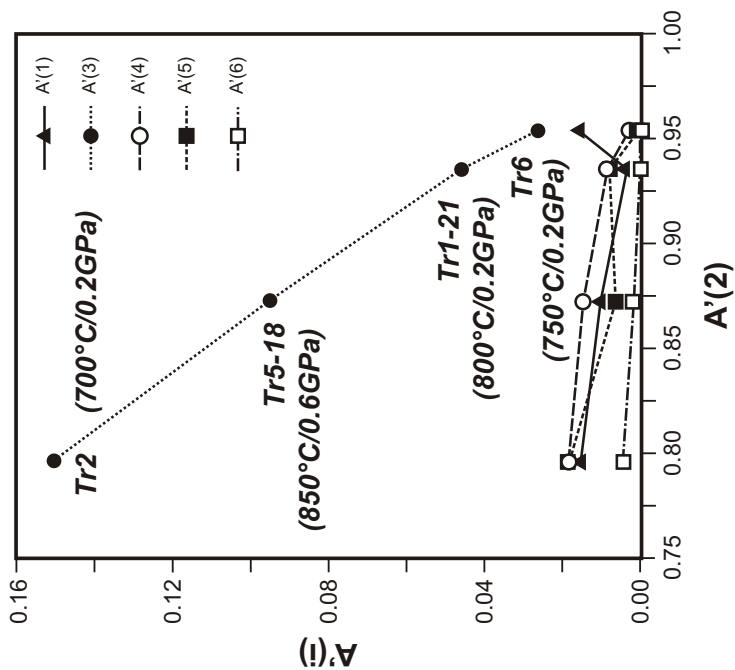


Figure 10. Relative CMF abundances in the synthetic products studied by Ahn et al. (1991). Modified after Ahn et al. (1991).

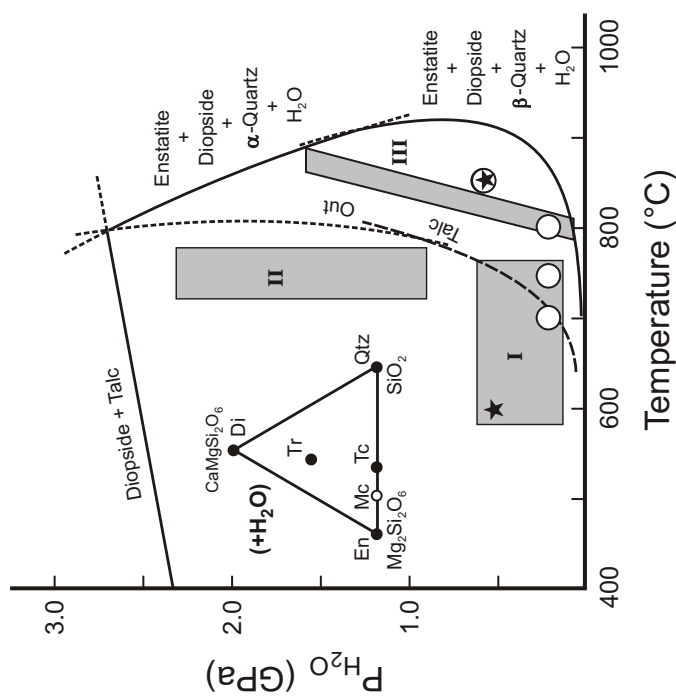


Figure 9. Stability fields of talc and tremolite, as summarized by Maresch et al. (1994) from Jenkins et al. (1991), Chernosky et al. (1985), Day et al. (1985). *P-T* regions I to III: experiments of Maresch et al. 1994; open circles; experiments of Ahn et al. (1991); stars: experiments of Bozhilov et al. (2004, 2007).

The product assemblages are amphibole + diopside + talc \pm quartz. Diopside occurs as discrete crystals. Talc and amphibole were commonly observed to be topotactically intergrown, and reaction fronts were observed between the two phases as documented extensively by Maresch and Czank (1983b, 1988) for (Mn²⁺,Mg)-amphiboles. Product amphiboles contain abundant triple-chain CMFs (Fig. 11). The low $A'(2)$ value of 0.81 ± 0.07 reported by Maresch et al. (1994) corresponds to the result of Ahn et al. (1991) at similar P - T conditions. Although the P - T conditions of region II (Fig. 9) are also within the stability field of talc, and the product assemblages of amphibole + diopside + talc \pm quartz are analogous, HRTEM analysis yields a different picture. CMFs > 2 are rare. Stacking faults (CAFs) are also rare in comparison to tremolites in P - T region I. Typically talc occurs as discrete crystals without coherent amphibole intergrowths, whereas amphibole and diopside tend to form coarse lamellar intergrowths with few intralamellar defects. These lamellae are topotactically oriented as well as extensive and very regular in the crystallographic c -direction. However, cooperative terminations between double-chain and single-chain lamellae are found and interpreted by Maresch et al (1994) as reaction fronts (Fig. 12). In large amphibole crystals diopside lamellae are restricted to the cores, and amphiboles without diopside cores are rare. At crystal terminations differential dissolution of pyroxene is observed (Fig. 13). A similar situation is reported for P - T region III, where talc is no longer stable. Cooperative chain terminations between coherent single-chain diopside and double-chain amphibole lamellae as well as diopside cores in amphibole are common. Maresch et al. (1994) interpret these features to indicate that in P - T regions II and III amphibole growth from diopside occurred, both by topotactic as well as bulk solution/reprecipitation processes. Bimodal size distributions are common, with the larger, more equant crystals virtually defect-free, whereas the more predominant, smaller, acicular ones are intimate topotactic amphibole/diopside intergrowths. Maresch et al (1994) found no conclusive evidence for a strong influence of run time or bulk water content. However, seeding with structurally well-ordered amphibole material led to more defect-free amphibole products.

Whereas the observations and interpretation of Maresch et al. (1994) were made on “final” products of comparable run durations, Bozhilov et al. (1993, 2004, 2007) provide important insight into the development of the tremolite-bearing product in detailed XRD (including Rietveld refinement) and HRTEM (including ATEM) investigations on experimental products obtained in time series. Bozhilov et al. (1993, 2004) studied the reaction path of an oxide mix at

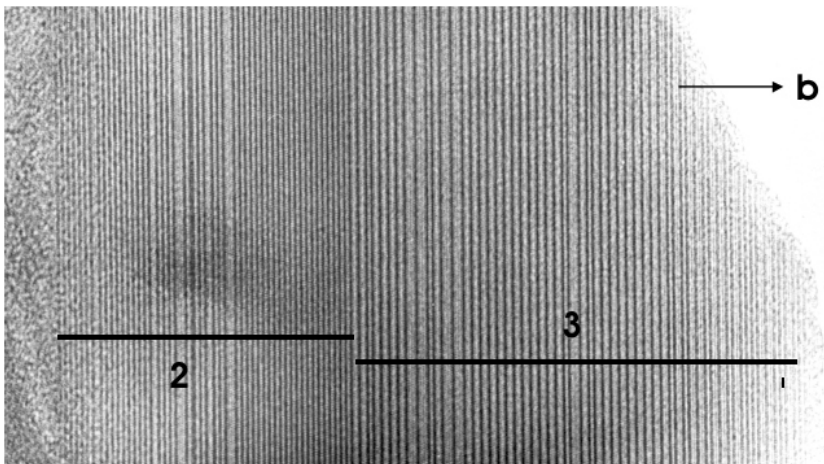


Figure 11. Intergrown double- and triple-chain sequences with CMFs in synthetic tremolitic amphibole of P - T region I (see Fig. 9). Lattice fringes correspond to ~ 9 Å and ~ 13.5 Å, respectively.

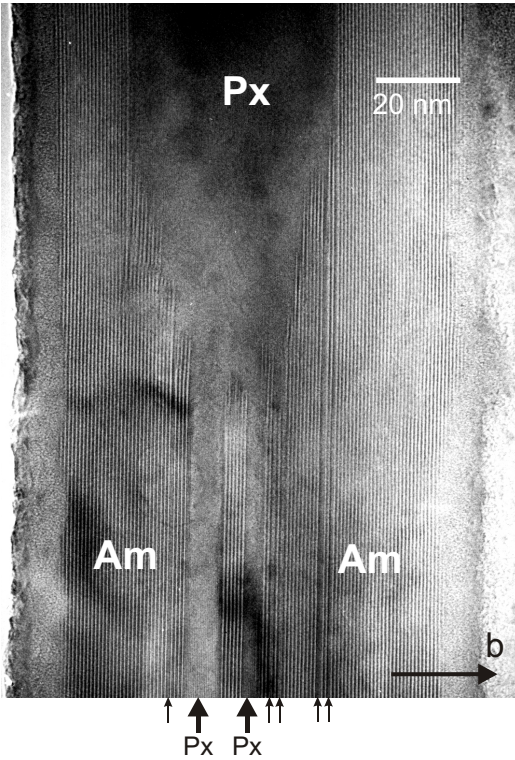


Figure 12. Intergrown amphibole and pyroxene lamellae of *P-T* region II (see Fig. 9) with terminations of amphibole in pyroxene, interpreted by Maresch et al. (1994) as reaction fronts. Small arrows indicate CMFs in amphibole. Lattice fringes correspond to $\sim 9 \text{ \AA}$ in amphibole and $\sim 4.5 \text{ \AA}$ in pyroxene.

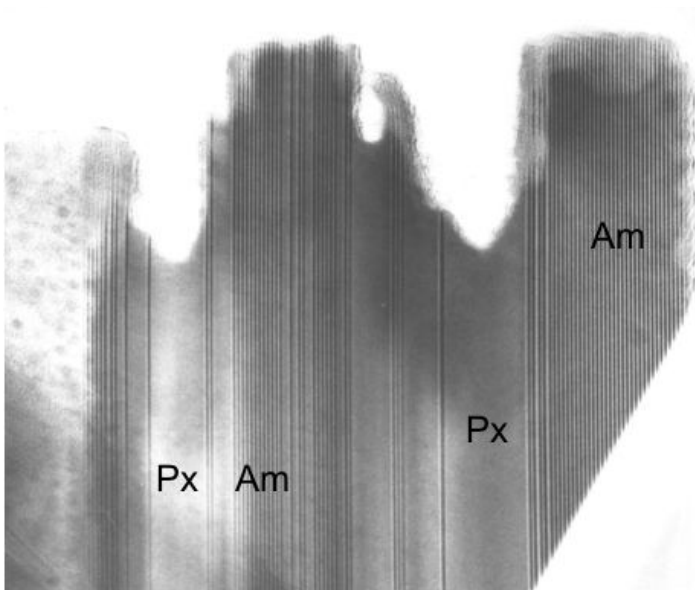


Figure 13. Intergrown amphibole and pyroxene lamellae of *P-T* region II (see Fig. 9). Note preferential dissolution of pyroxene at crystal terminations. Lattice fringes in amphibole correspond to $\sim 9 \text{ \AA}$.

850 °C and 0.6 GPa at run durations of 8 minutes up to 97.3 hours. These conditions essentially correspond to Maresch et al.'s (1994) *P-T* region III (Fig. 9). Bozhilov et al. (2007) report an analogous study, but with dolomite + quartz as starting material, at 600 °C/0.5 GPa in a CO₂-H₂O fluid and run durations of 91 to 582 hours (i.e., *P-T* region I of Maresch et al. 1994).

The results of Bozhilov et al. (2004) provide sobering insight into the complexities of the amphibole-forming process. Early in the experimental run diopside grows rapidly and coexists with amphibole, enstatite and quartz. Enstatite disappears after 20 hours, and the proportion of amphibole increases rapidly to more than 80 wt% after 12.2 hours. After 97.3 hours, the charge consists of 98 wt% amphibole and 2 wt% diopside. However, XRD and HRTEM characterization of the amphibole shows high variability and marked compositional heterogeneity in the amphibole crystals produced. Figure 14 shows that initial Ca/Mg ratios of amphibole crystals are low and highly variable. The scatter decreases and the Ca/Mg ratio increases with time. The value of 0.4 of ideal tremolite is not reached. Three groups of compositionally different amphibole can be identified on the basis of Ca/Mg ratio, one group

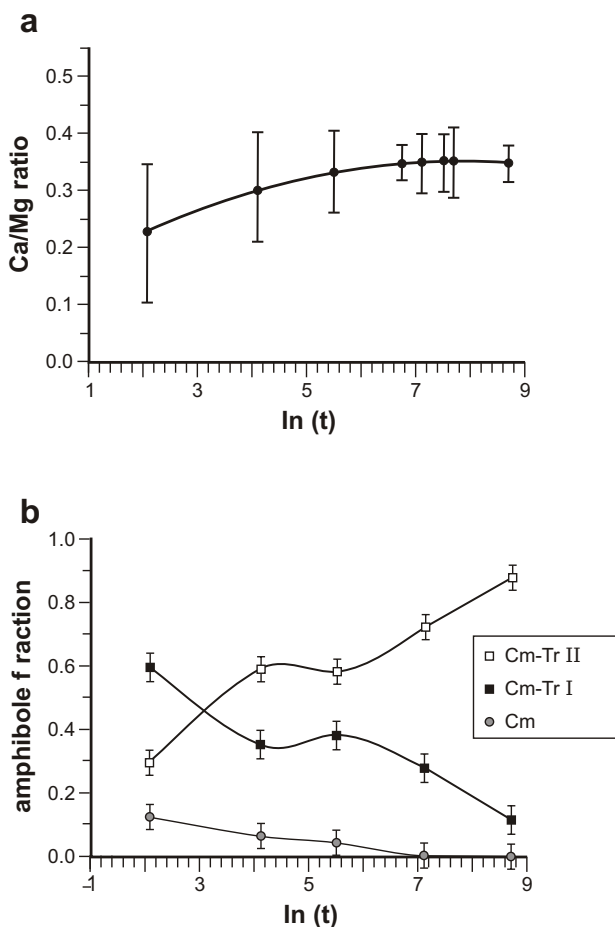


Figure 14. Compositional evolution with time of synthetic amphiboles in the study of Bozhilov et al. (2004) at 850 °C/0.61 GPa. a) Ca/Mg ratio. b) Changing proportions of the three types of amphibole recognized. Error bars represent the standard deviation. Adapted from Bozhilov et al. (2004).

with Ca/Mg below 0.1 (Cm in Fig. 14), a second with intermediate Ca/Mg ratios between 0.15 and 0.3 (Cm-TrI in Fig. 14), and a third with high Ca/Mg ratios between 0.3 and 0.4 (Cm-TrII). All compositions are on the synthetic tremolite–cummingtonite join. Of considerable interest is the fact that the typical *C*-centered amphibole structure is indicated for all three compositional types, but that primitive structure types are also observed for Cm and Cm-TrI types. Imaging by HRTEM shows that *C*-centered and primitive domains are intimately and coherently intergrown and different degrees of structural ordering are evident.

The study of Bozhilov et al. (2007) was undertaken to mimic a reaction of tremolite from starting material relevant to nature. As in the study of Bozhilov et al. (2004), rapid reaction to a metastable assemblage consisting of talc and calcite was observed. Without retreatment of the run products further reaction to tremolite is very sluggish. After 582 hours an uninterrupted run yielded ~ 5 wt% tremolite, whereas at the same conditions and with the same run times, 5-fold intermittent regrinding led to a yield of ~ 65 wt%. CMFs are mainly triple-chain defects. Interestingly, these occur as isolated lamellae in short-duration runs that evolve into groups of lamellae in longer-duration experiments. Bozhilov et al. (2004, 2007) emphasize the evolving habit of both product and reacting crystals with time. Diopside evolves from acicular crystals to prismatic and equant crystals. Amphibole is typically acicular, with aspect ratios of 20 after 259 hours of reaction. In the latter stages of synthesis reactions, amphibole develops bimodal size distributions with aspect ratios of 5 or less and an average width of < 0.2 μm on the one hand and aspect ratios of ≥ 10 with an average width of ~ 1.0 μm on the other. This bimodal distribution is explained by dissolution and regrowth, producing grain coarsening in the amphibole population.

Recasting $A'(2)$ values into Mg-enrichment trends, Bozhilov et al. (2004) conclude that product tremolites after close to 100 hours of run time at 850 °C/0.6 GPa possess on average true cummingtonite solid solution components of 6.3 to 7 mol%. Only 3% are attributed to the effects of CMFs. The experiments of Bozhilov et al. (2007) are somewhat more complex due to a different starting material and variable interruptions of the product during the run. At these lower temperatures Bozhilov et al. (2007) suggest that the equilibrium extent of cummingtonite, corrected for CMFs, is 3.5%. One sample corrects to only 0.6% cummingtonite via a very high CMF density (analogous to the observations of Maresch et al. 1994), and another almost free of CMFs but with 10% cummingtonite component are considered to represent metastable states.

The observations summarized above allow some insight to be gained into the reaction path followed during synthesis of tremolite, even though there are differences in observational basis and interpretation. Bozhilov et al. (2004, 2007) stress the lack of terminations of CMFs within single crystals in their observations, i.e., those interpreted as reaction fronts by Maresch and Czank (1988) and Maresch et al. (1994). For the runs at 800 °C/0.6 GPa, these authors also point out that although the amphibole/diopside volume ratio increases with time, the amphibole are generally much smaller than the diopside crystals. Direct diopside-to-amphibole conversion is considered by them to be unlikely.

One common theme to the above studies is that direct precipitation of amphibole from a saturated solution is not the dominant mechanism for amphibole growth. Only during the first minutes of a synthesis run should this process be operative. A similar conclusion based on experiments in the MnO–MgO–SiO₂–H₂O system was reached by Maresch and Czank (1988). Instead, depending on starting material and *P-T* conditions, other members of the biopyriboles such as diopside and talc nucleate and grow rapidly, from which amphibole must then be produced. Bozhilov et al. (2004, 2007) contend that the ensuing formation of amphibole is dominantly a multi-stage dissolution and regrowth process. Outside of the stability field of talc, Bozhilov et al. (2004) suggest a detailed scenario involving 1) formation of diopside-rich pyroxene, 2) hydration and partial dissolution of diopside, and 3) nucleation and growth of amphibole with continued dissolution of diopside. Pyroxene crystals are assumed to trap

hydroxyl groups during their formation that later can provide suitable environments for amphibole nucleation. Further reaction leads to increased amphibole nucleation and pyroxene dissolution to increase the proportion of amphibole in the composites of pyroxene plus hydrated-chains [sic]. When amphibole crystals have become sufficiently large, amphibole may precipitate directly from solution. Bozhilov et al. (2004) discuss and discount an alternative: Hydrated [sic], wide-chain, mica-like modules could form in pyroxene and later break down to double-chain modules. However, the expected “zipper” terminations (Veblen and Buseck 1980; Veblen 1991) resulting from this conversion have not been documented. Such “zippers” could be expected during the formation of amphibole from talc-rich precursor material in the experiments of Bozhilov et al. (2007), where triple-chain CMFs are very common, but this question is not pursued there.

Although the above scenario explains many of the features observed in the studies of Bozhilov et al. (2004, 2007), the observations of Maresch et al. (1994) cannot be ignored. The latter observed many crystals with double-chain lamellae grading into single-chain pyroxene lamellae or double-chain lamellae passing into talc-like lamellae or regions with abundant CMFs with $m \geq 3$. In the synthesis studies of Maresch et al. (1994), topotactic reactions between biopyriboles must also have played a role. We use the term topotactic in the sense of Veblen (1991) for a solid-state reaction with oriented replacement. The actual reaction front must on the atomic scale provide pathways for rapid exchange of material, such as in the “zipper” model (Veblen and Buseck 1980; Veblen 1991). In this regard, it is not entirely clear how the pyroxene-hydration mechanism of Bozhilov et al. (2004) that leads to coherent pyroxene-amphibole intergrowths should function on the atomic scale. If amphibole nuclei form within pyroxene then their propagation must involve some form of solid-state topotactic reaction and calls for amphibole/pyroxene terminations within pyroxene crystals. As indicated above, it is unfortunate that “zipper” terminations (Veblen and Buseck 1980; Veblen 1991), which could provide the most unequivocal evidence for topotactic polysomatic reactions, cannot be routinely imaged in synthetic grain mounts, and no information on them is available so far in synthetic amphiboles.

Although runs at 750 °C/0.2 GPa should be outside the talc stability field (Fig. 9), talc commonly forms during the run-up and represents a metastable precursor during experiments at these conditions. It is interesting to note here that Baumgarte (1996) attempted to coerce direct tremolite synthesis from highly metastable gel by almost instantaneously achieving experimental temperatures of 750 °C at 0.2 GPa, i.e., by rapidly passing through and beyond the talc stability field. Baumgarte (1996) constructed a double-tipping cold-seal autoclave patterned after Wellmann (1970), which allowed both rapid quenching as well as heating. Run temperatures within the gold capsule were achieved within 3-4 seconds. However, even after 100 hours run time, the product remained a felty intergrowth of unidentifiable crystals less than 20-30 nm in size. Rerunning this product with tremolite seeds for up to one thousand hours failed to achieve tremolite growth. Rapid-heating runs with the same apparatus within the talc stability field yielded products indistinguishable from those of Maresch et al. (1994) within P - T region I.

From the above it is clear that the reaction path to synthetic end-member or close-to-endmember tremolite has probably been studied in greater detail than for any other important synthetic member of the amphibole group. The reaction path is highly complex and a number of unanswered questions remain. From a practical viewpoint, a recipe for the best yields of defect-poor, close to endmember tremolite when using classical synthesis methods can be formulated as follows:

- The lower the temperature, the closer the tremolite product should be to end-member composition (Evans 2007). However, temperatures in the stability field of talc will be counterproductive, because talc as a precursor phase will favor extensive defect structures. A promising suggestion could be to go to pressures ≥ 1.0 GPa in the talc stability field (P - T region II in Fig. 9), where coarsely lamellar pyroxene-amphibole

intergrowths rather than intricate disordered CMF sequences form as intermediate reaction products. However, the effect of pressure on the extent of the buffered cummingtonite solid solution component is not known as yet.

- Seeding with well-ordered, e.g., natural material tends to reduce CMFs in comparison to unseeded runs at the same experimental conditions (e.g., Ahn et al. 1991; Maresch et al. 1994).
- Longer run times with multiple interruption of the run with repeated careful grinding should increase yield and decrease intergrown pyriboles.
- Incongruent dissolution of tremolite starting material (e.g., Jenkins 1987), as discussed below, should be compensated by saturating the coexisting fluid.

Amphibole solid solutions radiating from synthetic end-member tremolite

If amphibole defect structures are accepted as a proxy for complex reaction paths with the potential to lead to stranded metastable product states, then routine CMF imaging can be of use, even if detailed studies such as those of Bozhilov et al. (2004, 2007) and Maresch et al. (1994) are not available.

The good news is that, in general, the incorporation of other solid solution components into tremolite appears to reduce the observed defect density, even if some of the HRTEM characterization in the following studies may have been more cursory than in the studies cited above:

- (1) In their study on synthetic tremolite, Ahn et al. (1991) also imaged products of magnesiohornblende bulk composition $(\text{Ca}_2(\text{Mg}_4\text{Al})(\text{AlSi}_7)\text{O}_{22}(\text{OH})_2)$, i.e., related to tremolite by the Mg-tschermak substitution $^{[6]}\text{Al} + ^{[4]}\text{Al}$ for $^{[6]}\text{Mg} + ^{[4]}\text{Si}$. Synthesis conditions were 751 °C and 1.0 GPa. $A'(2)$ values are 0.90 ± 0.4 , significantly higher than in the unseeded runs also studied by Ahn et al. (1991).
- (2) Skogby and Ferrow (1989) synthesized amphiboles from the following bulk oxide compositions corresponding to actinolite solid solutions: $\text{Ca}_{2-00}(\text{Fe}_{0-33}\text{Mg}_{4-65})\text{Si}_{8-00}\text{O}_{22}(\text{OH})_2$, $\text{Ca}_{1.92}(\text{FeO}_{.32}\text{Mg}_{4.73})\text{Si}_{8-00}\text{O}_{22}(\text{OH})_2$ and $\text{Ca}_{1.75}(\text{Fe}_{0-65}\text{Mg}_{4-60})\text{Si}_{8-00}\text{O}_{22}(\text{OH})_2$ at 500 to 700 °C and 0.2 GPa for a total 2-6 months with intermittent regrinding of the charge. 6% seed of natural actinolite was added. Initially, the charge was kept at 850 °C/0.1 GPa to avoid the formation of metastable talc. Nevertheless, talc was usually a common additional product in the early stages of synthesis. The reported results of 50 structure images indicate few CMFs. The “disordered volume” is estimated to be significantly less than a few percent. The occurrence of intergrown talc-like slabs ($m = 11$) is reported.
- (3) Jenkins and Bozhilov (2003) characterized synthetic ferro-actinolite obtained at 0.2-1 GPa and 420-600 °C at various oxygen fugacity buffers and with starting materials composed of SiO_2 , $\text{Ca}(\text{OH})_2$ and metallic Fe. Despite run durations up to 6 months, with intermittent grinding, the highest yields attained were less than 70 wt%. Hedenbergite and grunerite appear to be the most important precursor phases. An average composition of $\text{Ca}_{1.67}\text{Fe}_{5.33}^{2+}\text{Si}_8\text{O}_{22}(\text{OH})_2$ is reported, although in detail amphibole compositions are quite variable, and grunerite commonly coexists. As in the study on synthetic tremolite by Bozhilov et al. (2004), Ca contents are variable. EDS analyses by TEM indicate Ca contents ranging from 0.50 to 2.0 apfu. Jenkins and Bozhilov (2003) report very few CMFs from samples of 7 to 10 crystals from three runs, with $A'(2)$ exceeding 0.98. Jenkins and Bozhilov (2003) also report that thorough grinding in the early stages of the experiment increases yields markedly, which they suggest could be the result of destroying some form of early grain-boundary armoring.
- (4) Smelik et al. (1994) synthesized amphiboles along the join tremolite towards magnesiohornblende, incorporating a constant 10% cummingtonite solid solution

- component (i.e., a solid-solution series between $\text{Ca}_{1.8} \text{Mg}_{5.2} \text{Si}_8 \text{O}_{22} (\text{OH})_2$ and $\text{Ca}_{1.8} (\text{Mg}_{4.2} \text{Al}) (\text{AlSi}_7) \text{O}_{22} (\text{OH})_2$). Starting materials were oxide mixes. Synthesis conditions ranged from 823 to 875 °C and 0.5 to 1.3 GPa. Single-chain and triple-chain CMFs are observed, and the estimated volume percent of defective material is given as generally less than 5%. However, tremolite compositions have a higher frequency and abundance of defects than more Al-rich samples, with defective material up to 10% in abundance. If all CMFs are assumed to be triple-chain, a *minimum* $A'(2)$ of ~0.86 is indicated, suggesting fewer CMFs than found by Ahn et al. (1991).
- (5) Hoschek (1994) studied the Al content of tremolite in assemblages with kyanite + zoisite + quartz + H_2O . Al contents are in the range 0.5-1.1 pfu. HRTEM imaging of several tremolite products equilibrated at 1-2 GPa and 700-750 °C indicates almost no CMFs.
 - (6) Pawley et al. (1993) synthesized amphiboles between tremolite and richterite, $\text{Na}(\text{NaCa}) \text{Mg}_5 \text{Si}_8 \text{O}_{22} (\text{OH})_2$, with bulk compositions composed of gels constrained to lie between tremolite₉₂cummingtonite₈ and ideal richterite. Synthesis conditions varied between 0.2 and 0.7 GPa at 850 °C. Pawley et al. (1993) report very few CMFs, even for tremolite-rich compositions. The richterite-rich amphiboles are essentially free of CMFs.
 - (7) Hawthorne et al. (1997) present a detailed study on the join tremolite–potassic-richterite ($\text{K}(\text{CaNa}) \text{Mg}_5 \text{Si}_8 \text{O}_{22} (\text{OH})_2$) at 750 °C and 0.1 GPa. With only one exception at 20% potassic-richterite, almost no CMFs or other types of defects are found.
 - (8) Jenkins et al. (2003) studied synthetic ternary amphiboles in the system tremolite–pargasite($\text{NaCa}_2(\text{Mg}_4\text{Al})(\text{Al}_2\text{Si}_6)\text{O}_{22}(\text{OH})_2$)–cummingtonite ($\text{Mg}_7 \text{Si}_8 \text{O}_{22} (\text{OH})_2$), originally synthesized by Sharma and Jenkins (1999). Sharma and Jenkins (1999) discussed at length the problems of obtaining good amphibole yields and optimum reaction rates in this chemically complex system, including the problem of incongruent dissolution of starting material into the fluid (see further below). Oxide mixes were treated at various temperatures ranging mainly from 800 to 950 °C and pressures mainly between 0.3 and 6.0 GPa. $A'(2)$ values cluster at 0.95 and vary very little between tremolite-rich and pargasite-rich compositions. CMFs are reported to be mainly triple chains.

The above summary can only serve as a very perfunctory introduction, because many variable experimental factors combine to make generalizations difficult. In keeping with the “common wisdom” discussed above, single-phase products are only rarely indicated. Although details on the reaction mechanisms are not known, it does appear that the introduction of alkali to the reacting system changes the reaction path so that fewer CMFs are observed in the final products. On the other hand, most of the studies cited in the above list were also carried out at relatively high temperatures well beyond the stability field of talc. As noted by Ahn et al. (1991), higher synthesis temperatures seem to favor lower CMF concentrations. Nevertheless, several studies still indicate a much lower incidence of defects for tremolite-rich compositions than reported by Ahn et al. (1991). The reasons for this are unclear. As noted by Skogby and Ferrow (1989) and Jenkins and Bozhilov (2003), the judicious interruption of the synthesis runs with intermittent grinding can improve amphibole yield. This effect could be due to the higher reactivity of small grains, or, perhaps more likely, to the destruction of overgrowth fabrics (Jenkins and Bozhilov 2003). However, no further systematic details have been reported on this aspect.

Synthetic amphiboles in the system $\text{MgO-FeO-MnO-SiO}_2\text{-H}_2\text{O}$

Synthetic anthophyllite/cummingtonite–ferro-anthophyllite/grunerite. Gilbert et al. (1982) have summarized the early classical work on this chemically simple but experimentally very recalcitrant system. In fact, Greenwood’s (1963) paper on the synthesis and stability of

anthophyllite, $\text{Mg}_7\text{Si}_8\text{O}_{22}(\text{OH})_2$, is a seminal account of how the synthesis reaction path can be engineered to coerce amphibole growth in an extremely sluggish system. Greenwood (1963) reacted oxide mixes in the stability field of talc (650 °C/0.1 GPa, 24 hours) and then tempered this product at 830 °C/0.1 GPa for about 20 hours. Although enstatite + quartz is actually the stable assemblage at 830 °C, and both talc and anthophyllite react to form enstatite + quartz, the metastable intermediate reaction of talc to anthophyllite is so rapid that anthophyllite is the most abundant phase for a transient period of time between 800 to 1500 minutes. Thus having produced about 20% amphibole seeds in the product, further tempering within the anthophyllite stability field can then lead to very amphibole-rich products. Greenwood (1963) speculated that the reaction of talc to anthophyllite proceeded by breaking Si-O bonds in the sheets of tetrahedral to produce strips of double chains.

Greenwood's (1963) recipe became a favorite for many experimental petrologists in the seventies. However, it was also a common observation that the synthetic anthophyllite produced in this way was "poorly crystalline", because the X-ray diffractograms were of poor quality with few and usually broadened reflections. With the advent of high-resolution electron microscopy, it became clear that amphiboles in the solid solution series $(\text{Fe}^{2+},\text{Mg})_7\text{Si}_8\text{O}_{22}(\text{OH})_2$ and $(\text{Mn}^{2+},\text{Mg})_7\text{Si}_8\text{O}_{22}(\text{OH})_2$ are structurally strongly disordered, and that the "real structure" (or "realbau" of Maresch and Czank 1983a) is characterized by abundant CMFs and CAFs. The role of CAFs in this system is especially important, because both orthorhombic and monoclinic amphiboles occur. CAFs lead to "microtwinning," so that thin slabs of monoclinic amphibole can appear orthorhombic in routine optical or X-ray work characterization. CAFs have complicated efforts to define the symmetry relations of synthetic amphiboles in this system (e.g., Popp et al. 1976; Maresch and Czank 1983a,b, 1988).

Synthetic amphiboles of the $(\text{Fe}^{2+},\text{Mg})_7\text{Si}_8\text{O}_{22}(\text{OH})_2$ series have been imaged by Veblen (Veblen et al. 1977; Veblen 1981; Veblen pers. communication to Chernosky and Autio 1979, as well as to Gilbert et al. 1982). To our knowledge, the details of these very important seminal HRTEM studies do not appear to have been published. However, the authors cited above report the general conclusion that the Mg-rich compositions contain significant multiple-chain material. The number of CMFs decreases with increasing Fe content. On the other hand, the number of CAFs is reported to increase with Fe content, leading to macroscopically orthorhombic crystals (Popp et al. 1976; Gilbert et al. 1982), where monoclinic amphiboles should be expected from natural occurrences. Thus, the very important relationships between monoclinic and orthorhombic amphibole types are difficult to study in these synthetic products. From the experimental details reported by Popp et al. (1976) and Chernosky and Autio (1979) it seems clear that at least the Mg-rich members of this series must have grown from talc-bearing assemblages.

Lattard and Evans (1992) report seeded synthesis experiments of grunerite at 1.2-2.0 GPa and 490-620 °C with yields exceeding 90%. Amphibole compositions are estimated to contain between 87 and 98% grunerite end-member. The synthetic crystals are 5-10 μm long and 0.5-1 μm across. In keeping with the observations reported above, HRTEM characterization showed almost no CMFs, but indicated the presence of numerous CAFs. The CAFs are described as polysynthetic micro-twinning. Very small lamellae of true orthoamphibole are also reported.

Synthetic anthophyllite/cummingtonite-manganocummingtonite. Amphiboles from the solid-solution series $(\text{Mn}^{2+}_x\text{Mg}_{7-x})\text{Si}_8\text{O}_{22}(\text{OH})_2$ have been studied in considerable detail by Maresch and Czank (1983a,b, 1988). An extensive detailed catalogue of HRTEM observations on defect structures is given in Maresch and Czank (1983b). In the study of Maresch and Czank (1988), amphibole composition and *realbau*, as well as the pertinent phase assemblage were monitored as a function of bulk composition, *P-T* conditions and run duration to allow some insight into the reaction path during amphibole synthesis. In contrast to the wide pressure-temperature field of stability available for tremolite, that for $(\text{Mn}^{2+},\text{Mg})$ -amphiboles

is much more restricted. Maresch and Czank (1988) studied synthesis reactions mainly at 675-750 °C and 0.2 GPa, on the basis of stability fields reviewed for the analogous synthetic (Fe²⁺,Mg)-amphiboles by Gilbert et al. (1982). Nevertheless, during the studies of Maresch and Czank (1988), reversal runs showed that actual stability is even more restricted for synthetic (Mn²⁺,Mg)-amphiboles (Fig. 15), and many of the successful amphibole syntheses carried out are actually metastable with respect to pyroxene + quartz at conditions within or close to the stability field of talc on its own composition. In keeping with the techniques available at the time, changes in amphibole composition and in the modal amounts of the reactant/product assemblage were based on semiquantitative powder diffraction techniques. The most important conclusions of Maresch and Czank (1988) are summarized here.

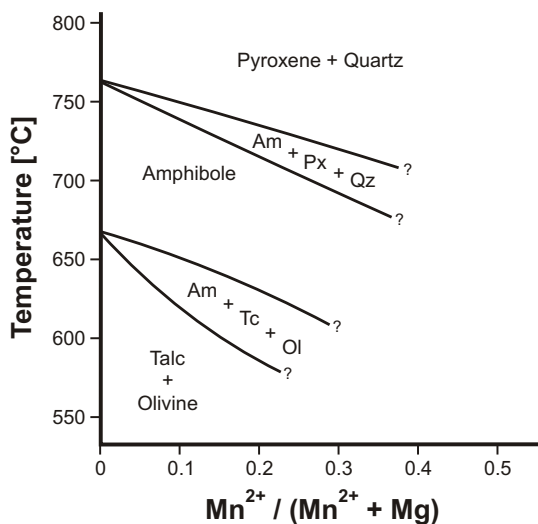


Figure 15. Stability relations of synthetic anthophyllite/cummingtonite-manganocummingtonite amphiboles, as summarized by Maresch and Czank (1988).

Within 15 minutes of reaching run conditions the gel starting material recrystallizes completely to a mixture of talc, Mn²⁺-rich olivine and minor amphibole. Maresch and Czank (1988) monitored phase proportions and compositions (via calibration of lattice parameters) as shown in Figures 16 and 17. The first-formed amphiboles are much more Mn²⁺-rich than the target bulk composition, which, for Mn²⁺-rich compositions, is then rapidly approached as the modal amount of amphibole increases at the expense of talc and olivine (Fig. 18). Depending upon the concomitant rate of olivine consumption, a transient “overshooting” of the target composition can be possible (Fig. 17). The time studies documented in Figures 16 and 17 were not extended beyond 500 hours, but at 750 °C/0.2 GPa target compositions were generally reached between 700 and 2000 hours for Mn_{1.8}- and Mn_{0.9}-compositions, respectively.

The starting material used in these studies was a gel prepared according to the method of Hamilton and Henderson (1968). The method requires organic solvents to be burned off after gelation has been accomplished. This final procedure requires extreme care. If the burn-off procedure is too intense, large quantities of Mg-rich pyroxene can form, metastable talc production is inhibited and amphibole fails to nucleate and grow at all. Partial recrystallization allows some talc to form and consequently amphibole nucleation and growth is observed. However, the product assemblages always contain significant pyroxene and quartz. These observations are in complete accord with the results of Greenwood (1963) on the key role played by talc in the nucleation and growth of amphibole in the Mn²⁺-free system. It is also of interest that the presence of significant proportions of pyroxene and quartz during the synthesis run leads to amphibole products with distinctly fewer CMFs (see below) than amphibole growing from assemblages dominated by talc.

Maresch and Czank (1988) documented the extent of the defect structure in terms of A' values. The most important systematic observations are summarized in Figures 19-21. As a rule of thumb, they found that $A'(2) \approx A + (1.0-A)/2$, where A'(2) is used in the extended sense

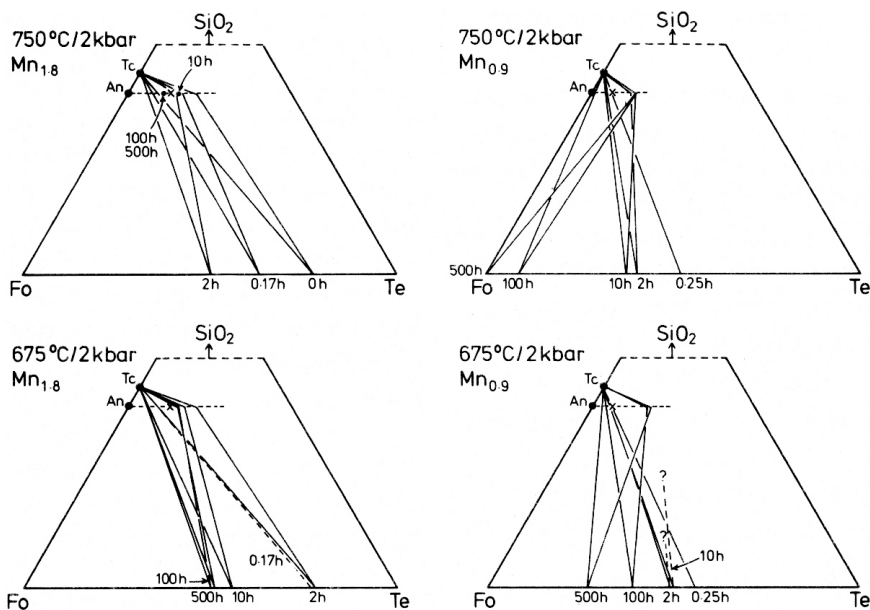


Figure 16. Topological shift of the three-phase field amphibole-olivine-talc as a function of temperature, run time, and bulk composition Mn^{2+}_x (referred to $Mn^{2+}_x Mg_{7-x} Si_8 O_{23}$). An: anthophyllite; Tc: talc; Fo: forsterite; Te: tephroite. From Maresch and Czank (1988).

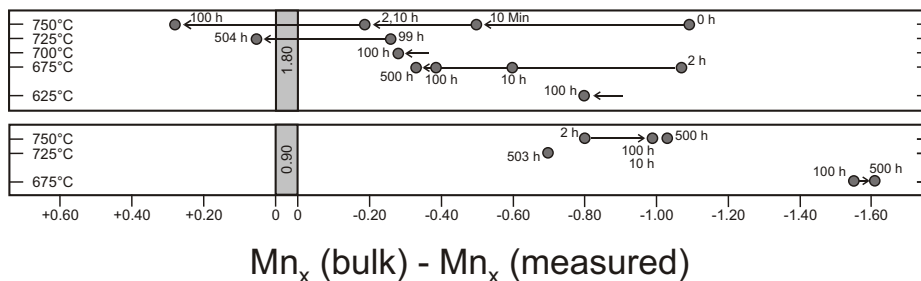


Figure 17. Evolution of amphibole composition with time in the topologies shown in Figure 16. Modified from Maresch and Czank (1988).

of Ahn et al. (1991). This relationship can be used to gauge the absolute proportion of double chains in the disordered amphibole products from these figures.

The large standard deviations of the A-values in Figures 19–21 are a clear indication of the heterogeneity observed in the defect structure of individual amphibole crystals. Nevertheless, Figure 19 clearly shows that higher bulk Mn^{2+} -contents of the starting material lead to higher average A-values. This is in accord with the observations of Veblen noted above in the analogous synthetic (Fe^{2+}, Mg) -amphibole series, that the proportion of CMFs decreases with higher bulk Fe contents. Similarly, Maresch and Czank (1988) also noted that the incidence of CAFs can be quite high, even if the content of CMFs is low. As noted above, the presence of pyroxene + quartz always leads to higher A-values at comparable run conditions. Some experiments were also run with high quartz excess in the bulk composition. These also returned products with markedly fewer CMFs.

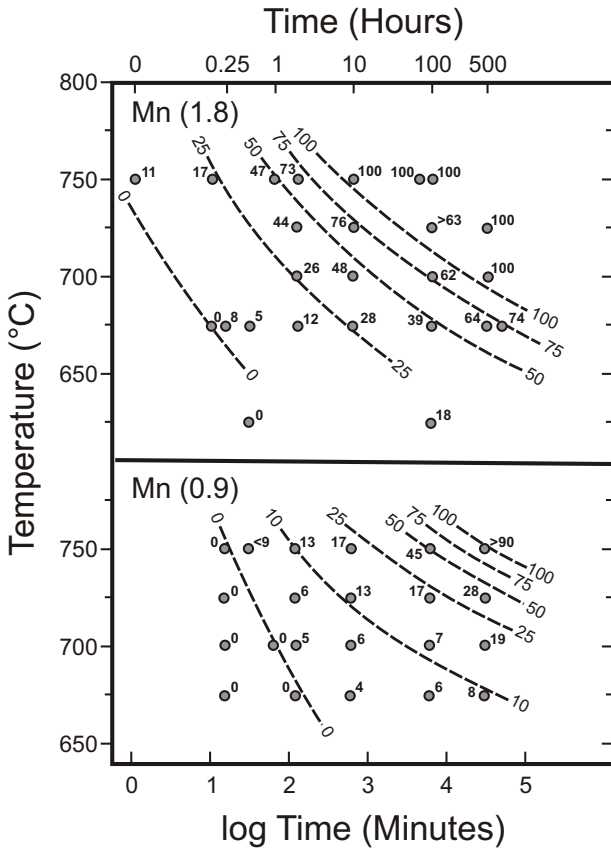


Figure 18. The reaction progress from talc to amphibole, expressed as % of talc consumed, as a function of temperature and run duration for the bulk compositions $Mn_{0.9}$ and $Mn_{1.8}$ (referred to $(Mn^{2+}_x Mg_{7-x}) Si_8 O_{23}$). Modified from Maresch and Czank (1988).

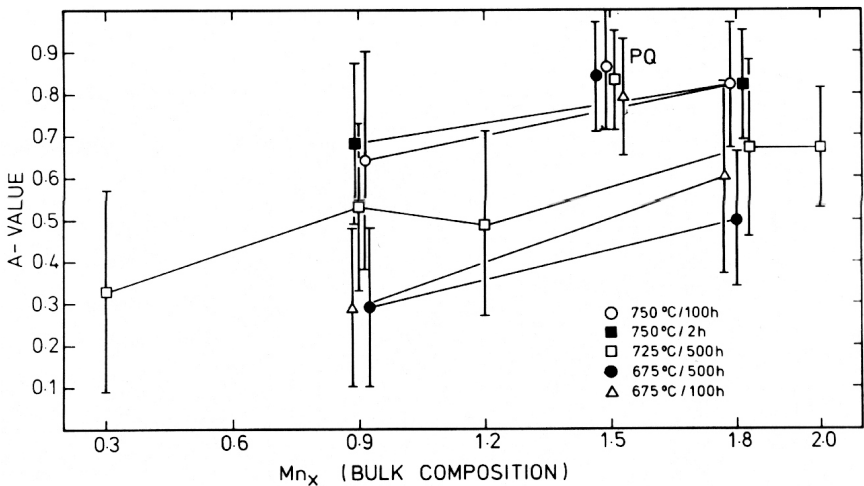


Figure 19. Dependence of A-value on the bulk composition of the starting material. Mn_x stands for $(Mn^{2+}_x Mg_{7-x}) Si_8 O_{23}$. PQ: pyroxene and quartz in the coexisting assemblage at $Mn_{1.5}$. Error bars represent the standard deviation. From Maresch and Czank (1988).

A marked dependence of the defect structure on synthesis temperature is already evident in Figure 19, and is shown more clearly in Figures 20 and 21. The effect is more prominent for Mg-rich compositions. No robust data exist on the influence of synthesis pressure, but comparisons between runs at 0.1 and 0.2 GPa show no discernible differences. Maresch and Czank (1988) found no correlation between A-values and run duration. In fact, regrinding and extended tempering failed to increase A-values. It was possible to identify crystals broken during regrinding whose intricate CMF patterns were still identical after 1000 hours of tempering.

Noting that olivine constitutes less than 9 wt% of the reacting talc + amphibole + olivine assemblage, Maresch and Czank (1988) monitored reaction progress by estimating talc/amphibole ratios from X-ray diffractograms and found a systematic pattern in the time-temperature-transformation curves (Fig. 18). Following the seminal approach of Greenwood

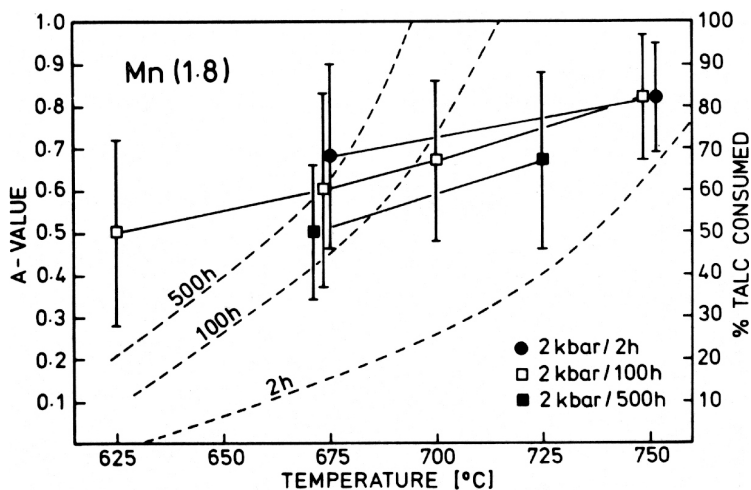


Figure 20. Dependence of A-value on the temperature of the experimental run for bulk composition $(\text{Mn}^{2+}_{1.8}\text{Mg}_{5.2})\text{Si}_8\text{O}_{23}$. Dashed lines show rate of talc consumption from Figure 18 for comparison. Error bars represent the standard deviation. From Maresch and Czank (1988).

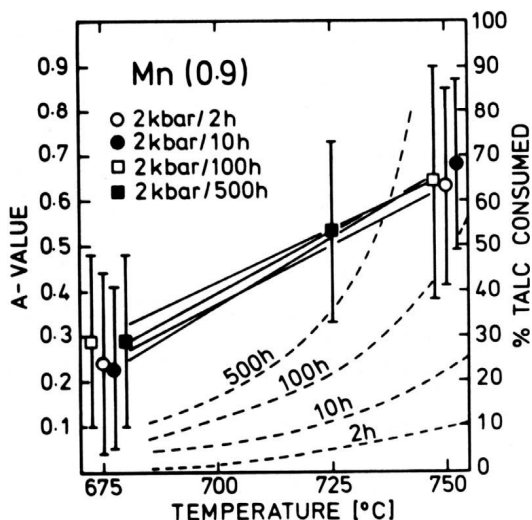


Figure 21. Dependence of A-value on the temperature of the experimental run for bulk composition $(\text{Mn}^{2+}_{0.9}\text{Mg}_{6.1})\text{Si}_8\text{O}_{23}$. Dashed lines show rate of talc consumption from Figure 18 for comparison. Error bars represent the standard deviation. From Maresch and Czank (1988).

(1963), the data of Figure 18 were fit to a first-order rate law and the activation energies of the talc-to-amphibole reaction estimated assuming an Arrhenius-type relationship (Fig. 22). Despite the large uncertainties that must be acknowledged in this approach, two very important conclusions can be drawn from the result. There appears to be a distinct difference between the reaction mechanism in the early stages of the reaction as compared to the results obtained for runs longer than about 200 minutes, where the activation energies are distinctly higher. Bozhilov et al. (2004) came to a similar conclusion in their detailed study of the tremolite synthesis reaction and concluded that in the early stages of the reaction amphibole may precipitate directly from the aqueous fluid. The activation energies (slopes in Fig. 22) for breakdown of talc and growth of amphibole after 200 minutes run duration are ~ 436 kJ/mole for Mg-rich compositions and therefore slightly lower than the ~ 471 kJ/mol obtained for Mn^{2+} -rich compositions. However, the Y-intercepts in Figure 22 are higher for Mn^{2+} -rich compositions, leading to higher frequency factors (activation entropies), explaining why the talc breakdown for Mn^{2+} -rich compositions should be faster.

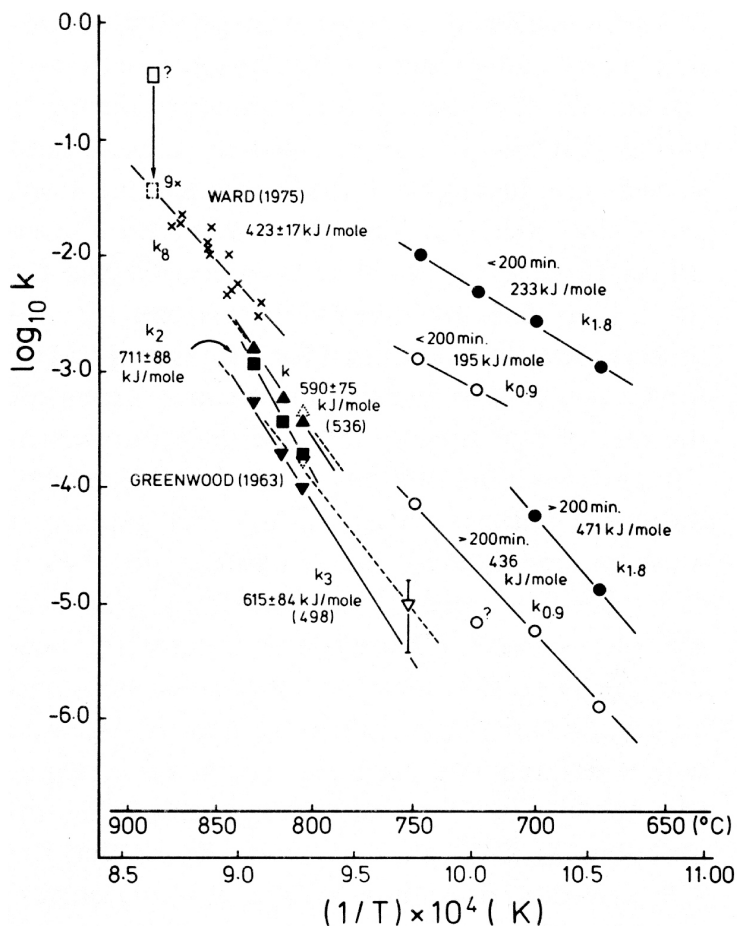


Figure 22. Arrhenius plot of rate constants derived from Figure 18 assuming a first-order rate law (see Greenwood 1963, Maresch and Czank 1988 for further details). The dashed symbols and activation energies in brackets represent corrections of arithmetic errors in the cited literature. From Maresch and Czank (1988).

The activation energies obtained in this way compare well with the literature data of Greenwood (1963) and Ward (1975) for depolymerization of talc, even if the experimental procedures are not entirely comparable. Greenwood (1963) studied the breakdown of talc to both anthophyllite and enstatite well above the thermal stability field of talc, and Ward (1975) investigated the kinetics of the breakdown of talc to enstatite and quartz at 1 bar pressure in an Ar-stream. Nevertheless, the activation energies obtained in these studies also appear to lie between 400 and 600 kJ/mole. Bozhilov et al.'s (2004) study of amphibole growth from pyroxene was carried out at only one temperature; however, if a simple first-order rate law is adopted as in the above studies, then the resultant rate constant at 850 °C fits the data of Greenwood (1963) and Ward (1975) well ($\log_{10}k \approx -2.7$).

Without wishing to overextend the significance of the absolute values derived for the activation energies, one can conclude that they are at least similar in the above studies, and that they are high, more in agreement with a process of structural rearrangement than with growth by nucleation and diffusion in a fluid. Any explanation of such a structural mechanism of the amphibole-forming reaction must take into account the following observations:

- (1) As documented by Maresch and Czank (1983b, 1988), the topotactic relationship between amphibole and talc is a striking feature found in all stages of the reaction runs. Many of the microstructures found in natural examples and attributed to polysomatic reactions (e.g., Veblen and Buseck 1979, 1980, 1981; Grob ty 1997) have also been found in the synthetic products described here. In the very early stages, when talc is also recrystallizing, presumably in an Ostwald ripening process, amphibole may act as a substrate for recrystallizing talc (Fig. 23), and penetrate more than one talc crystal. However, as the reaction proceeds, talc is consumed by internal topotactic growth of amphibole and disordered chain silicates. Cooperative chain terminations between talc and disordered chain silicates along the *c*-axis are common and are most easily explained as reaction fronts (see extensive HRTEM documentation of Maresch and Czank 1983b).
- (2) A number of studies have attempted to analyze the systematics of the relative stabilities of ordered and disordered biopyriboles (Veblen and Buseck 1979, 1980, 1981; Price and Yeomans 1986; Abbott and Burnham 1991; Grob ty 1997). Veblen and Buseck (1979) describe a statistical test for determining whether locally ordered structures are simply random combinations of CMFs or perhaps represent local free energy minima. These tests consider only single "runs" of CMF patterns. We have attempted to extend this approach by also taking into account how *often* an identical pattern may occur in a crystal. However,

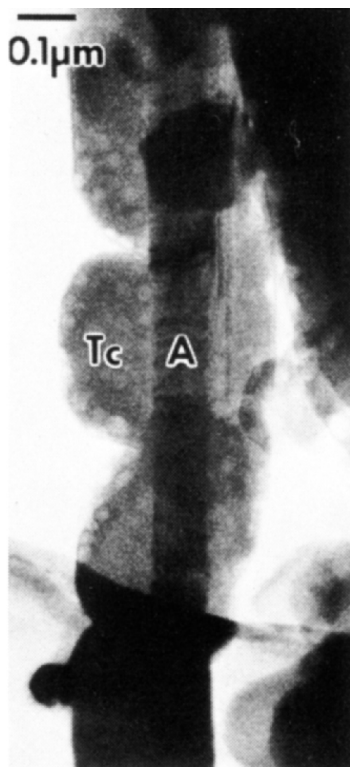


Figure 23. Low magnification TEM image showing long thin amphibole crystal penetrating subhedral talc platelets during the early stages of a synthesis reaction of $(\text{Mn}^{2+}_x\text{Mg}_{7-x})\text{Si}_8\text{O}_{22}(\text{OH})_2$ amphibole. From Maresch and Czank (1988).

every crystal is a world unto itself, and the finite width of these very small amphibole crystals makes statistical analyses very difficult. As an illustration, Figure 24 shows an intriguing pattern of “defectiveness” across single crystals obtained at different run conditions. The patterns were obtained by sliding a “window”, in this case 14 single chains wide, across the crystal and obtaining the proportion of chains in ideal double-chain configuration. A value of “0” indicates that only ideal double chains are encountered in the window. Figure 24 indicates that there is a distinct periodicity of regions approaching ideal amphibole as compared to regions with high CMF concentrations. In broad terms, the periodicity at 675 °C is ~ 160-180 Å, while that at 750 °C is ~ 220 Å. We find it difficult to explain these patterns as due only to random intergrowth of amphibole and talc (cf. Bozhilov et al. 2004, 2007), unless there are strong next-nearest-neighbor interactions between polysomes during intergrowth (Price and Yeomans 1986). We prefer a tentative model in which the defect-poor regions are those where amphibole first nucleates in talc. We speculate that the “periodicities” in Figure 24 could represent a form of amphibole nucleation density. The intervening regions would be those where smaller and smaller “restitute” talc lamellae would lead to CMF interference due to the necessity of cooperative chain arrangements.

- (3) The talc-to-amphibole reaction is rapid (Figs. 16-18), and requires a mechanism of fast exchange of Mn^{2+} and Mg, as well as diffusion of Si and H (Veblen and Buseck 1979, 1980; Veblen 1991).

Veblen and Buseck (1979, 1980) and Veblen (1991) have shown that the topotactic structural relationships of polysomatic reactions, as well as the “fast” diffusion required, are well and logically explained by the “zipper” model (Fig. 3). In the [001] projection of this figure it is evident that slabs of structure are being dissolved and rebuilt, leading to propagation of polysomes in the a^* direction with a minimum of distortion, when the rule that the number of chains above and below the reaction front is the same are obeyed. The misfit at the reaction front is a convenient “tunnel” or “pipe” allowing rapid mass diffusion to and from the reaction site. Maresch and Czank (1988) were not able to image amphiboles in the [001] direction. However, on the basis of their observations they concluded that the primary direction of amphibole growth should be in the c -direction (Fig. 25). Veblen (1991) has pointed out a possible solution to this dilemma. Although the “zipper” propagates in the a^* -direction as implied in Figure 3, the reaction mechanism actually proceeds in the c -direction via one or even a series of “jogs” in the line defect defining the lamellar termination (Fig. 26). If the line defect is

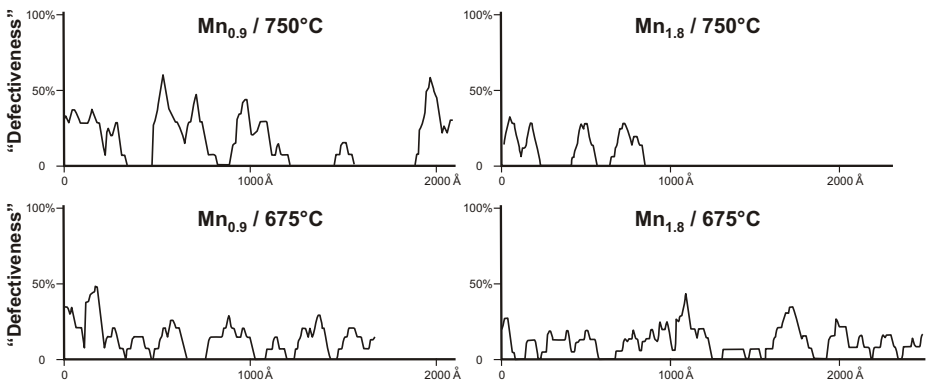


Figure 24. Periodicity in “defectiveness” across four amphibole crystals with given composition (Mn_x stands for $(\text{Mn}^{2+}_x\text{Mg}_{7-x})\text{Si}_8\text{O}_{22}(\text{OH})_2$) and synthesis temperature. See text for explanation.

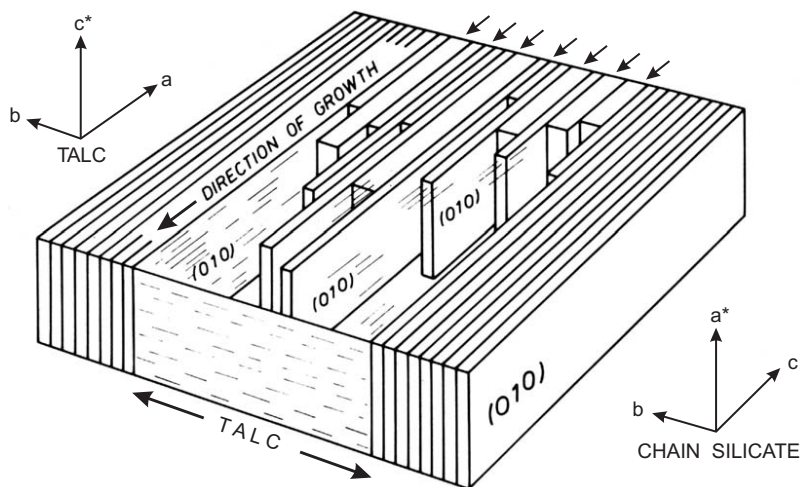


Figure 25. Interpretation of the polysomatic topotactic reaction mechanism based on HRTEM observations of Maresch and Czank (1983a, 1983b, 1988). Adapted from Maresch and Czank (1988).

steep, i.e., subparallel to a^* , then terminations between biopyribole lamellae could appear relatively sharp in HRTEM images perpendicular to b (e.g., Fig. 12).

Is there a recipe?

The above description of attempts to synthesize amphiboles in the MgO-FeO-MnO-SiO₂-H₂O system via the classical “oxide/gel + H₂O” method appears to signal a no-win situation, at least for relatively Mg-rich compositions. The stability fields of these synthetic amphiboles are clearly much more restricted than, for example, in the case of synthetic tremolite. Nucleation and growth to very amphibole-rich assemblages without talc as a precursor has not been achieved. On the other hand, the growth of amphibole from talc, presumably due to predominant topotactic polysomatic reactions leads not only to pronounced chain-multiplicity disorder, but also to numerous CAFs, i.e., stacking faults. The latter obscure the very important and necessary distinction between the various monoclinic and orthorhombic members of this amphibole group. Synthesis above the stability of talc in the field of amphibole + pyroxene + quartz seems to suppress CMFs, but in this case single-phase amphiboles are not possible. There appears to be a positive influence of excess quartz in the bulk composition, as this also increases $A'(2)$ -values in the products, but again, no single-phase amphiboles will result.

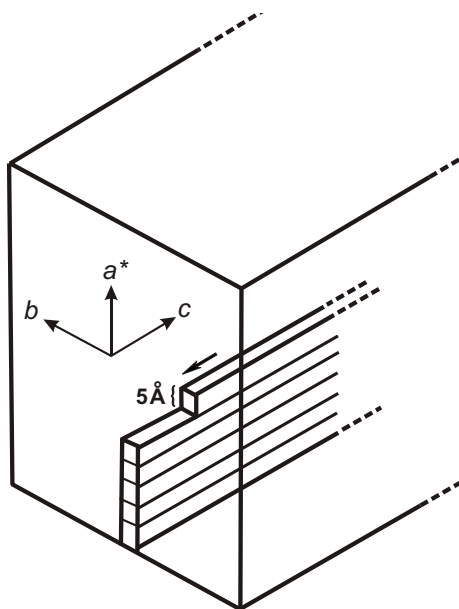


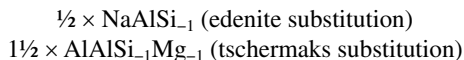
Figure 26. The model of Veblen (1991) for the geometry of polysomatic replacement reactions. The “zipper” of Figure 3 grows in the a^* -direction by rapid advancement in the c -direction of a jog or ledge. Modified from Veblen (1991).

AMPHIBOLE SOLID SOLUTIONS RADIATING FROM SYNTHETIC AMPHIBOLES IN THE SYSTEM MgO-FeO-MnO-SiO₂-H₂O

A few pilot studies have been carried out that change synthetic amphibole compositions out of the system MgO-FeO-MnO-SiO₂-H₂O. It is instructive to summarize HRTEM observations on these products.

Maresch and Czank (1983b) noted that amphiboles synthesized in the system MgO-Li₂O-SiO₂-H₂O (Maresch and Langer 1976) contain almost no defects. We have therefore studied a series of bulk compositions at 675 °C/0.2 GPa/500 hours leading from the (Mn²⁺,Mg)-amphiboles described in the previous sections via the substitutions Li(OH)Mn²⁺₋₁O₋₁ and Li₂Mn²⁺₋₁ towards the compositions reported by Maresch and Langer (1976). Almost no Li could be substituted in this way, as complicated Li-bearing pyroxenoids appeared almost immediately along the substitution vector. However, the effect on the *distribution* of the CMFs is distinct. Compared to the Li-free system, triple and quadruple chains are more abundant, and the triple chains form almost defect-free lamellae exceeding 0.2 μm.

Seifert (personal communication 1989) synthesized amphiboles along the join anthophyllite/cummingtonite-sodicgedrite, Fe²⁺₂ Mg₅ Si₈ O₂₂ (OH)₂ - Na_{0.5} Fe²⁺₂ (Mg_{3.5}Al_{1.5}) (Al₂Si₆)O₂₂ (OH)₂, to model Na- and Al-bearing orthoamphiboles in nature. Synthesis conditions were 700 °C/0.5 GPa/168 hours, and amphibole yields exceeded 90%. Champness (pers. communication to Seifert 1975) indicated that these products contained very many of the lamellar defects first recognized in amphiboles at that time, so that these synthetic amphiboles were not employed in further petrological studies. Figure 27 summarizes the unusual distribution of A'(2)-values that we have obtained for this solid solution series. All compositions have A'(2)-values > 0.85 with the exception of anthophyllite/cummingtonite₉₀-sodicgedrite₁₀, for which A'(2) = 0.5. The large standard deviation indicates considerable heterogeneity for this composition. It should be kept in mind that this solid solution series involves three different sites via the following two coupled substitutions



The data at hand do not allow the individual effects of the two substitutions to be specified. However, the results on an amphibole of the anthophyllite-gedrite series (below), suggest that certainly the tschermaks substitution should lead to fewer defects.

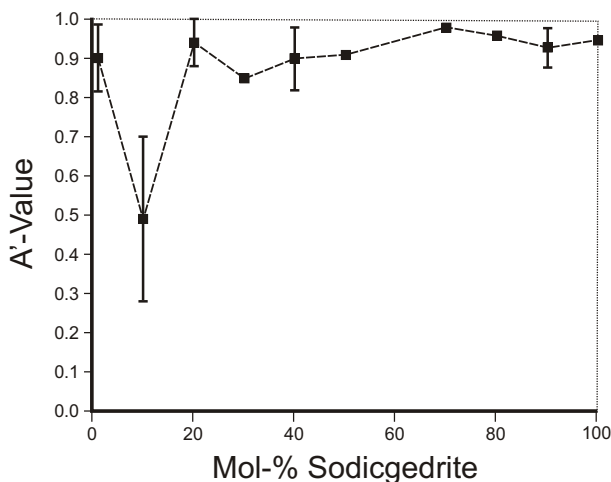


Figure 27. A'(2) values of solid solutions along the join synthetic anthophyllite/cummingtonite-sodicgedrite. Error bars represent standard deviations.

Fischer et al. (1999) synthesized and characterized an amphibole on the join anthophyllite–gedrite with an intermediate composition very close to $(\text{Mg}_6\text{Al})(\text{AlSi}_7)\text{O}_{22}(\text{OH})_2$. The synthesis conditions were 800–900 °C at 1–2 GPa. No significant CMF concentrations were found in this amphibole.

Attempts were made to study the substitution $\text{LiAlMg}_{-1}\text{Mg}_{-1}$ into synthetic anthophyllite, leading to synthetic holmquistite, at temperatures of 600–800 °C and pressures up to 0.7 GPa. Significant amphibole yields were obtained only for a composition deduced to be close to $(\text{Li}_{1.5}\text{Mg}_{0.5})(\text{Mg}_{3.5}\text{Al}_{1.5})\text{Si}_8\text{O}_{22}(\text{OH})_2$. Almost no CMFs were detected and $A'(2)$ values are therefore ~ 1.0 .

THE FLUID PHASE AND THE REACTION PATH

Synthesis with dissolved chlorides in the coexisting fluid

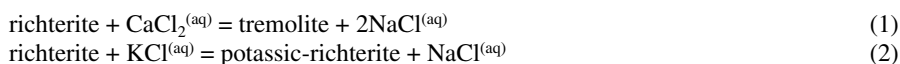
About fifteen years ago, amphibole aficionados working in Tübingen and Potsdam (Germany) tried new techniques in an effort to synthesize amphiboles large enough for routine electron microprobe analysis and also to circumvent reaction paths leading to products with high proportions of CMFs. The technique originally evolved from studies on exchange equilibria between synthetic amphiboles on the join synthetic richterite–potassic-richterite and $(\text{Na},\text{K})\text{Cl}$ -solutions (Knop et al. 1993). These techniques are generally characterized by relatively large fluid/solid ratios as high as 9:1 in the starting material. Size distributions in the products are generally heterogeneous, but the largest crystals can reach 2000 μm by 30–50 μm , and indeed many crystals are large enough for electron microprobe analysis. However, the caveat still holds that the composition and structural order of large and small crystals may differ (Hawthorne et al. 1997; Maresch and Czank 1983a,b; Ahn et al. 1991; Maresch et al. 1994; Gottschalk and Klein 1994).

Gottschalk (1994a,b, 1995) and Gottschalk and Klein (1994) introduced a technique in which the Ca and Mg components of the bulk composition are inserted as CaBr_2 and MgBr_2 to the fluid in order to control the availability of Ca vs. Mg in the solution during the early, critical stages of the synthesis reaction. These authors studied the synthetic tremolite–tschermakite–pargasite system at temperatures of 650–700 °C and 0.1–0.5 GPa. The most important results are that crystals up to 500 $\mu\text{m} \times 50 \mu\text{m} \times 50 \mu\text{m}$ could be synthesized. Except for some pargasitic compositions, the number of CMFs is reported to be low. A key observation is that growth kinetics appear to control the defect structure in the products and the amount of cummingtonite component in the synthetic tremolitic amphiboles (see discussion by Evans 2007). These kinetics can be influenced by varying the ratio of $\text{CaBr}_2/\text{MgBr}_2$ in the starting material. High CaBr_2 contents lead to well-ordered, Ca-rich amphiboles, whereas high MgBr_2 contents lead to amphiboles with high concentrations of CMFs and higher cummingtonite contents. These observations match well with the studies on synthetic tremolite of Bozhilov et al. (2004) discussed above, who found early-formed amphiboles to be very cummingtonite-rich. Obviously, reducing the availability of Mg and increasing that of Ca in the early stages of the reaction will favor the production of Ca-rich amphiboles. Nevertheless, the “bromide method” has been inexplicably inconsistent, and others have not been as successful (e.g., Jenkins and Bozhilov 2003; Sondermann 1996), suggesting that some key experimental parameter must still be controlled. Gottschalk (pers. communication 2007) suggests that the use of CO_2 as pressure medium has a very favorable effect.

Zimmermann et al. (1996) have provided key input into the tremolite discussion (see Evans 2007) by synthesizing near-end-member tremolite (+ diopside + quartz) with crystal sizes up to 900 $\mu\text{m} \times 40 \mu\text{m} \times 15 \mu\text{m}$, allowing electron microprobe analysis. No chain multiplicity faults or stacking faults are reported, despite the fact that talc was identified as a precursor phase in some runs. The experiments were carried out at 800 °C/0.2 GPa from oxide

mixtures in the presence of excess CaCl_2 -bearing aqueous solution and with run durations from 340 to 960 hours. The proportion of fluid varied from 49% to 88%. Yields exceeding 95% tremolite are reported. Zimmermann et al. (1996) suggest that the formation of chloride complexes could be responsible for enhancing both the cation concentrations as well as the transport properties of the fluid.

Zimmermann et al. (1996) evaluated the analytical scatter in their microprobe data, which exceeds analytical uncertainty, and concluded that some form of fractional crystallization must be involved during the dissolution of the starting material and the precipitation of tremolite + diopside + quartz. The corollary of this observation is that, once crystallized, synthetic amphiboles will not re-equilibrate easily to a common composition at 800 °C and run durations of many hundreds of hours. The extent of this problem is underlined in the study of Zimmermann et al. (1997a). These authors studied the cation exchange equilibrium between the following synthetic amphiboles at 700 °C/0.2 GPa:



The experimental recipe essentially followed the approach of Zimmermann et al. (1996). Amphiboles were presynthesized with excess NaOH and KOH in the fluid. Natural tremolite was also used for the exchange experiments, which were carried out with the solid/fluid cation ratios between 0.2 and 0.8. Both presynthesized and product amphiboles rich in richterite component are generally free of CMFs, whereas amphibole reaction products rich in tremolite component are structurally disordered with abundant CMFs. The product amphiboles deviate from the binary joins studied and represent ternary or quaternary solid solutions with tremolite and/or cummingtonite as additional components. Amphibole starting material disappears completely in runs corresponding to reaction (1), whereas some persists in runs of reaction (2). Nevertheless, the latter have obviously recrystallized. Zimmermann et al. (1997a) interpret their results in terms of a fractional crystallization model, in which local equilibrium is maintained at the crystallization surface of the growing amphibole as a function of the effective bulk composition of the fluid at any given time, but diffusional equilibration of the crystal interiors does not occur. Because of limited solubility of the solid reactants only a small fraction of the reactant amphibole is in solution at any given time, and the fluid composition is variable during the experiment. These exchange experiments produce disequilibrium assemblages.

On the basis of these results, Zimmermann et al. (1997b) devised an alternative procedure for the exchange reaction (2). They called this method “exchange synthesis” (Fig. 28). The starting material used was a mixture of oxides for Ca, Mg, and Si, with (Na,K)OH added in solution. An excess of (Na,K)Cl was also added to the solution. During the entire synthesis run the amphiboles grow in equilibrium with a chloridic Na-K-solution of essentially constant concentration and composition. In a conventional exchange reaction or rotating tie-line experiment (Fig. 28, upper panel), the fluid will be saturated with amphibole after a very small amount has been dissolved, and the first product amphibole will, according to the far-from-equilibrium tie-line 1 in Figure 28 have a $K/(K+Na)$ of ~ 0.6 . As potassium-rich amphibole compositions are sequestered from the solution and more Na-rich amphibole dissolves, the effective bulk composition will shift and induce successive equilibrium tie-lines from 1 to 5. The result will be a large range of amphibole product compositions. In the “exchange synthesis” (Fig. 28, lower panel), the first amphibole to grow will be offered a $K/(K+Na)$ as in the fluid. The shift to the final equilibrium composition is small. The ratio of solid to fluid in the reacting assemblage can be adjusted to minimize this shift. Zimmermann et al. (1997b) used this technique and reported products with more than 99% richterite–potassic-richterite solid solution. The amphiboles are up to 1 mm long and up to 40 μm thick. They are chemically homogeneous and contain few CMFs. Subsequent more detailed characterization by Gottschalk and Andrut (1998) indicates that these synthetic amphiboles do in fact generally contain up

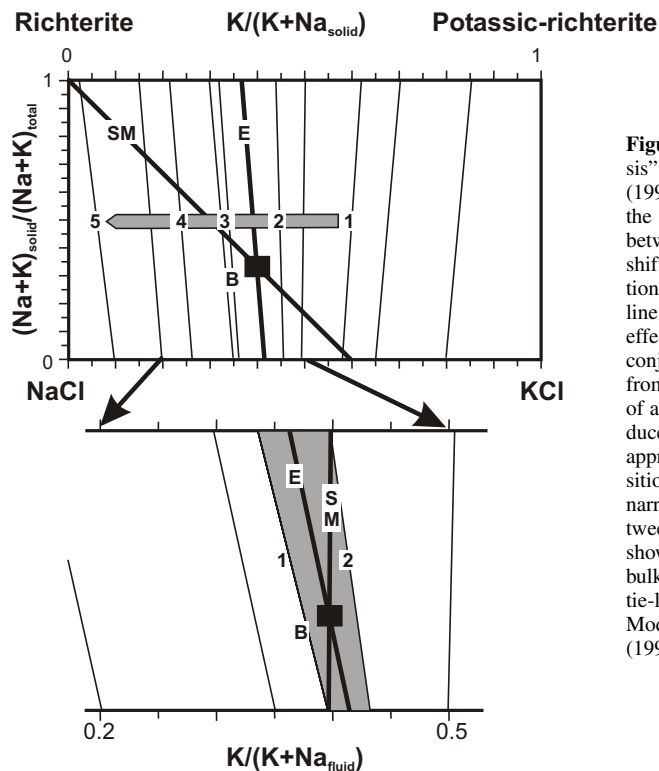


Figure 28. The “exchange synthesis” method of Zimmermann et al. (1997b). As outlined in the text, the lack of pervasive equilibration between solids and fluid leads to shifting effective bulk compositions in the standard rotating tie-line approach (upper panel). As the effective bulk composition and the conjugate equilibrium tie-line shift from position 1 to 5, a spectrum of amphibole compositions is produced. In the “exchange synthesis” approach (lower panel) the compositions of fluid and amphibole are narrowly constrained to lie between the two equilibrium tie-lines shown. SM: starting materials; B: bulk composition; E: equilibrium tie-line of an ideal run product. Modified from Zimmermann et al. (1997b).

to ~9% tremolite + cummingtonite component. The “synthesis exchange” technique has also been successfully used in the studies of Melzer et al. (1998) and Najorka et al. (1999, 2002).

The above methods of amphibole synthesis formed the basis for further studies to synthesize various amphibole compositions with large product crystals. Gottschalk et al. (1998) synthesized and characterized amphiboles on the join $(\text{Ca}_x\text{Sr}_{1-x})_2\text{Mg}_5\text{Si}_8\text{O}_{22}(\text{OH})_2$ in the presence of $(\text{Ca},\text{Sr})\text{Cl}_2$ aqueous solutions at 750°/0.2 GPa. Crystals up to 2000 $\mu\text{m} \times 30 \mu\text{m}$ were obtained with few CMFs. Melzer et al. (2000) studied synthetic solid solutions in the system potassic-richterite–richterite–tremolite at 800 °C/0.2 GPa and 800 °C/1.8 GPa in the presence of chloridic solutions. Crystals are up to 1000 $\mu\text{m} \times 50 \mu\text{m}$ in size, chemically homogeneous and structurally well-ordered. Complete solid solution was observed in the ternary plane with minor cummingtonite components, but compositions close to richterite or potassic-richterite could not be synthesized. Najorka and Gottschalk (2003) synthesized and characterized solid solutions close to the join tremolite–tschermakite at 700–850 °C/0.2–2.0 GPa using oxide-hydroxide mixes with additional CaBr_2 in solution. Crystals up to 300 $\mu\text{m} \times 20 \mu\text{m}$ were obtained. CMFs are reported to be minor ($\leq 5\%$). A “worst case” image shown yields $A'(2) = 0.82$. The compositions of the product amphiboles were found to be tremolite–tschermakite–cummingtonite solid solutions.

In summary, the above results show that synthesis experiments with high fluid/solid ratios and the judicious manipulation of the effective bulk composition of the fluid can produce amphiboles essentially free of structural disorder and very close to a given desired target composition. It is important that the system be kept as close to chemical equilibrium as possible for the desired amphibole composition at all times during the experiment. Conventional

exchange experiments with presynthesized amphiboles compositionally far from the final target composition fail to reach equilibrium even at high temperatures in reasonable run times. It is interesting to note that, paradoxically, the structurally highly disordered synthetic (Mn²⁺,Mg)-amphiboles described by Maresch and Czank (1988) appear much more reactive (Fig. 17), perhaps due to the “fast-diffusion” pipes induced by the polysomatic reaction of talc to amphibole (Veblen 1991).

Synthesis with a saturated aqueous fluid

The above-cited studies were generally carried out with high fluid/solid ratios, which appear to favor amphibole growth. However, this approach raises the problem of incongruent dissolution of the starting material, driving the condensed bulk composition off the desired composition, a fact of life that has plagued hydrothermal experimentation for many years. The presence of H₂O is necessary as a pressure-transmitting medium, as a buffering agent and as a reactive medium via solution-precipitation reactions. The problem has been noted for amphiboles by Maresch and Czank (1983b) in a general way, and in considerable detail by Jenkins (1987) and later Jenkins et al. (1991) and Maresch et al. (1994) for synthetic tremolite. Jenkins (1987) pointed out that the incongruent dissolution of tremolite is primarily controlled by silica solubility in the coexisting fluid. Mainly based on this study, most investigators have since then added excess SiO₂ to their charges to compensate the loss to the fluid phase. Because robust solubility data for SiO₂ at high pressures and temperatures were unavailable in the past, this procedure has generally been rather arbitrary, with additional amounts ranging up to 10 wt%. Whereas for example Bozhilov et al. (2004) added a “slight excess,” Smelik et al. (1994) added 1wt%, Pawley et al. (1993) up to 2 wt%, Ahn et al. (1991) ~ 4 wt%, and Zimmermann et al (1996) 5 wt%. On the other hand, Najorka and Gottschalk (2003) added 3-8 wt% on the basis of the *P-T*-dependent SiO₂ solubility data of Manning (1994), providing a more quantitative justification for their choice.

Sharma and Jenkins (1999) have also invoked the role of Na-leaching into the fluid to interpret their experimental results on synthetic tremolite–pargasite–cummingtonite amphiboles, thus underlining that the problem is not only one of preferential SiO₂ loss. If single-phase amphibole products are the goal, then buffering via additional solid phases is not a good option, and it would be of great interest to saturate the fluid, i.e., to find the specific two-phase tie-line connecting the desired amphibole composition with the composition of the coexisting high-pressure/high-temperature ambient fluid. In their work on synthetic glaucophane, Jenkins and Corona (2006) have approached the problem by extrapolating low-pressure data on aqueous species to high pressures using the well-known linear correlation between the equilibrium constants of dissociation reactions and the density of water (see Manning 1994, 1998; Fockenberg et al. 2006).

At present, progress is being made in understanding the composition and structure of high-pressure aqueous silicate fluids, such that the above goal of precisely saturating the aqueous fluid coexisting with a given amphibole composition may be within reach. If, in addition, the starting material can be conditioned (see section above) such that all components for the amphibole are stoichiometrically available during the experiment, then experiments with high fluid/solid ratios should become feasible.

As an example and a first step in this direction (e.g., Fockenberg et al. 2007), we offer a calculation for aqueous fluid coexisting at 700 °C with tremolite, i.e., in the system CaO-MgO-SiO₂-H₂O. In this approach, water is treated in terms of a statistical thermodynamic model (Gerya et al. 2004, 2005) that allows experimental data to be fitted to a realistic formalism with fit parameters representing conventional thermodynamic parameters. Experimental data for wollastonite (Fockenberg et al. 2006), quartz (Manning 1994; Gerya et al. 2005) and spinel (Zakharchuk 2006) are used. Figure 29 shows the calculated incongruent loss of material from tremolite to the aqueous fluid and other solid phases at pressures between 1.0 and 2.0 GPa. The

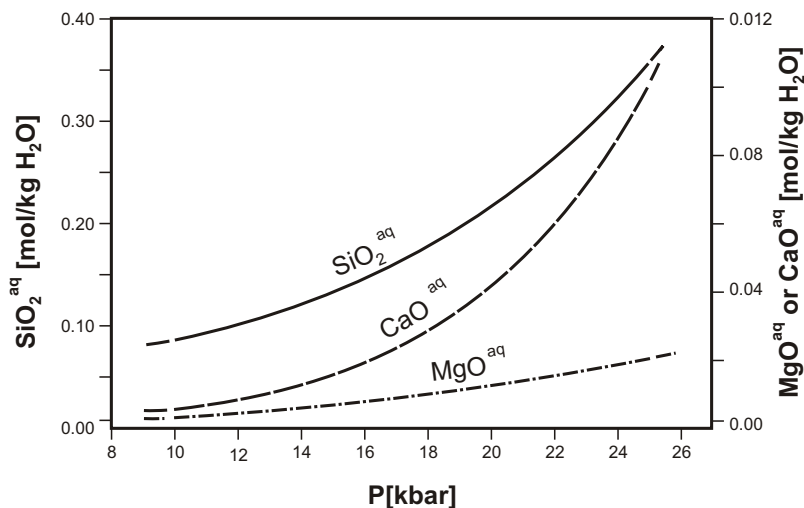


Figure 29. Calculated incongruent loss of tremolite starting material in an ambient aqueous fluid at 700 °C and variable pressures. See text for discussion.

bulk composition is one mol tremolite + 20 wt% H₂O. As noted by Jenkins (1987), SiO₂ would be the primary component lost. However, as pressure increases, CaO loss rapidly increases and there is also a clear fractionation of Ca/Mg. Figure 30 has been obtained by constraining the composition of the fluid such that the activities of the possible solid phases talc, quartz, enstatite and diopside are constrained to be < 1.0, i.e., these phases should not crystallize. It is interesting to note that the content of SiO₂ remains relatively constant at ~ 1.5 wt%. With data like this at hand, it should be possible in the future to predict fluid saturation for a given amphibole of interest.

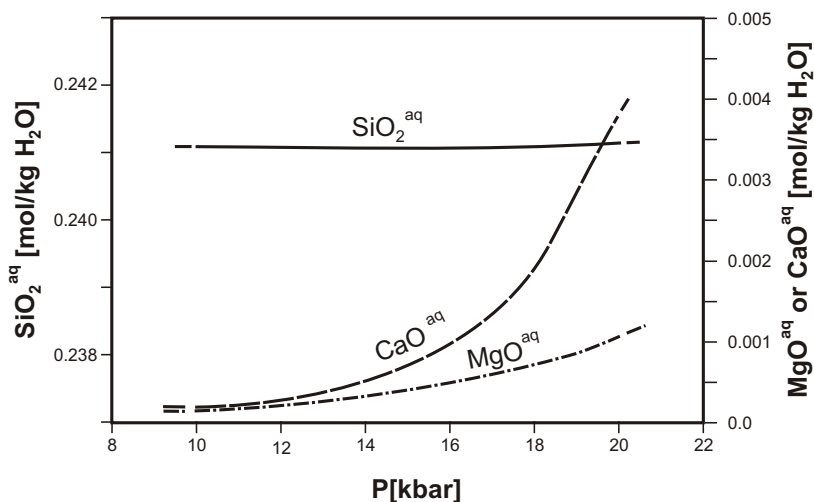


Figure 30. Composition of an aqueous fluid coexisting with tremolite at 700 °C and variable pressure with the constraint that no other solid phases are allowed to form. See text for discussion.

CONCLUSIONS

The summary presented here is a tale of many complications that can beset the experimentalist in his quest to synthesize single-phase amphiboles of desired composition. The problems that arise can be very specific to the actual chemical system in which the synthesis reactions are proceeding. In some cases, such as for synthetic calcic and sodic-calcic amphiboles, very promising results have been achieved. In other cases, such as for members of the synthetic $(\text{Mg}, \text{Fe}^{2+}, \text{Mn}^{2+})_7 \text{Si}_8 \text{O}_{22} (\text{OH})_2$ series, much work still needs to be done to develop viable reaction paths that lead to acceptable products that can serve as analogs of natural examples. In every case, ingenuity has been and will be called for to overcome the specific problems involved.

ACKNOWLEDGMENTS

Michael Burchard patiently went through the calculations on fluid compositions for us. Frau Renate Lehmann was instrumental in getting the figures into a presentable shape. Roberta Oberti's keen eye caught a number of formal errors. All did so under great deadline pressure. Our thanks go to all of them.

REFERENCES

- Abbott RN Jr., Burnham CW (1991) Energy calculations bearing on biopyriboles. *Am Mineral* 76:728-732
- Ahn JH, Cho M, Jenkins DM, Buseck PR (1991) Structural defects in synthetic tremolitic amphiboles. *Am Mineral* 76:1811-1823
- Baumgarte CIR (1994) Eine neue Doppelkipp-Hydrothermalapparat: Optimierung, Kalibrierung und Testversuche zur Synthese von $(\text{Ca}, \text{Mg}, \text{Mn})_2 \text{Mg}_5 [\text{Si}_8 \text{O}_{22} / (\text{OH})_2]$ -Amphibolen. Diploma Thesis, Univ. Münster, Germany, 101 pp.
- Boyd FR (1959) Hydrothermal investigations of amphiboles. *In: Researches in Geochemistry, Volume 1*. Abelson PH (ed) John Wiley & Sons, Inc, p 377-396
- Bozhilov KN, Brownstein D, Jenkins DM (2007) Biopyribole evolution during tremolite synthesis from dolomite and quartz in CO_2 - H_2O fluid. *Am Mineral* 92:898-908
- Bozhilov KN, Jenkins DM, Veblen DR (1993) TEM/AEM observations of chain silicate evolution during synthesis of tremolite. *EOS Trans, Am Geophys Union* 74:166
- Bozhilov KN, Jenkins DM, Veblen, DR (2004) Pyribole evolution during tremolite synthesis from oxides. *Am Mineral* 89:74-84
- Cameron M, Papike JJ (1980) Crystal chemistry of silicate pyroxenes. *Rev Mineral* 7:5-92
- Chernosky JV Jr, Autio LK (1979) The stability of anthophyllite in the presence of quartz. *Am Mineral* 64:294-303
- Chernosky JV Jr, Day HW, Caruso LJ (1985) Equilibria in the system $\text{MgO-SiO}_2\text{-H}_2\text{O}$: experimental determination of the stability of Mg-anthophyllite. *Am Mineral* 70:23-236
- Czank M, Liebau F (1980) Periodicity faults in chain silicates: A new type of planar lattice fault observed with high-resolution electron microscopy. *Phys Chem Mineral* 6:85-93
- Day HW, Chernosky JV, Kumin HJ (1985) Equilibria in the system $\text{MgO-SiO}_2\text{-H}_2\text{O}$: a thermodynamic analysis. *Am Mineral* 70:237-248
- Evans BW (2007) The synthesis and stability of some end-member amphiboles. *Rev Mineral Geochem* 67:261-286
- Fischer W, Schreyer W, Maresch WV (1999) Magnesioedrite: a stable phase in the system $\text{MgO-Al}_2\text{O}_3\text{-SiO}_2\text{-H}_2\text{O}$ (MASH) at 800°C and 10 kbar water pressure, and the influence of FeNaCa impurities. *Contrib Mineral Petrol* 136:184-191
- Fockenberg T, Burchard M, Maresch WV (2006) Experimental determination of the solubility of natural wollastonite in pure water up to pressures of 5 GPa and at temperatures of 400 - 800 °C. *Geochim Cosmochim Acta* 70:1796-1806
- Fockenberg T, Burchard M, Maresch WV (2007) Modeling silicate-rich fluids at high pressures. *Goldschmidt Conference Abstracts 2007, Cologne, A288*
- Gerya TV, Maresch WV, Burchard M, Zakhartchouk V, Doltsinis NL, Fockenberg T (2005) Thermodynamic modeling of solubility and speciation of silica in $\text{H}_2\text{O-SiO}_2$ fluid up to 1300 °C and 20 kbar based on the chain reaction formalism. *Eur J Mineral* 17:269-283

- Gerya V, Podlesskii KK, Perchuk LL, Maresch WV (2004) Semi-empirical Gibbs free-energy formulations for minerals and fluids for use in thermodynamic databases of petrological interest. *Phys Chem Mineral* 31:429-455
- Gilbert MC, Helz RT, Popp RK, Spear FL (1982) Experimental studies of amphibole stability. *Rev Mineral* 9B:229-353
- Gottschalk M (1994a) Das System Tremolit-Tschemmakit: Synthese von Mischkristallen und deren maximaler Aluminiumgehalt. *Ber Deutsche Min Ges* 6:76
- Gottschalk M (1994b) How to synthesise large amphiboles: Method and first results. Abstracts, 16th Gen Meeting Int'l Min Soc, Pisa: 153
- Gottschalk M (1995) The composition of amphiboles in the system CaO-MgO-Al₂O₃-SiO₂-H₂O-CO₂ as a function of *P*, *T*, and bulk composition. *Terra Abstr* 7:320
- Gottschalk M, Andrut A (1998) Structural and chemical characterization of synthetic (Na,K)-richterite solid solutions by EMP, HRTEM, XRD and FTIR spectroscopy. *Phys Chem Mineral* 25:101-111
- Gottschalk M, Klein U (1994) Synthese von Ca-Amphibolen: Einfluß der Ausgangsphasen auf Kettenfehlordnungs-Konzentrationen. *Ber Deutsche Min Ges* 6:7
- Gottschalk M, Najorka J, Andrut M (1998) Structural and compositional characterization of synthetic (Ca,Sr)-tremolite and (Ca,Sr) diopside solid solutions. *Phys Chem Mineral* 25:415-428
- Graham CM, Maresch WV, Welch MD, Pawley AR (1989) Experimental studies on amphiboles: a review with thermodynamic perspectives. *Eur J Mineral* 1:535-555
- Greenwood HJ (1963) The synthesis and stability of anthophyllite. *J Petrol* 4:317-351
- Grobóty BH (1997) The replacement of anthophyllite by jimthompsonite: a model for hydration reactions in biopyroxenes. *Contrib Mineral Petrol* 127:237-247
- Hamilton DL, Henderson CMB (1968) The preparation of silicate compositions by a gelling method. *Mineral Mag* 36:832-838
- Hawthorne FC (1981) Crystal chemistry of the amphiboles. *Rev Mineral* 9A:1-102
- Hawthorne FC (1983a) The crystal chemistry of the amphiboles. *Can Mineral* 21:173-480
- Hawthorne FC (1983b) Characterization of the average structure of natural and synthetic amphiboles. *Per Mineral* 52:543-581
- Hawthorne FC (1995) Entropy driven disorder in end-member amphiboles. *Can Mineral* 33:1189-1204
- Hawthorne FC, Della Ventura G (2007) Short-range order in amphiboles. *Rev Mineral Geochem* 67:173-222
- Hawthorne FC, Della Ventura G, Robert JL, Welch MD, Raudsepp M, Jenkins DM (1997) A Rietveld and infrared study of synthetic amphiboles along the potassium-richterite-tremolite join. *Am Mineral* 82:708-716
- Hutchison J, Irusteta MC, Whittaker EJW (1975) High resolution electron microscopy and diffraction studies of fibrous amphiboles. *Acta Crystallogr* A31:794-801
- Jenkins DM (1987) Synthesis and characterization of tremolite in the system H₂O-CaO-MgO-SiO₂. *Am Mineral* 72:707-715
- Jenkins DM, Bozhilov KN (2003) Stability and thermodynamic properties of ferro-actinolite: A re-investigation. *Am J Sci* 303:723-752
- Jenkins DM, Bozhilov KN, Ishida K (2003) Infrared and TEM characterization of amphiboles synthesized near the tremolite-pargasite join in the ternary system tremolite-pargasite-cummingtonite. *Am Mineral* 88:1104-1114
- Jenkins DM, Corona JC (2006) The role of water in the synthesis of glaucophane. *Am Mineral* 90:1062-1068
- Jenkins DM, Holland TJB, Clare AK (1991) Experimental determination of the pressure-temperature stability field and thermochemical properties of synthetic tremolite. *Am Mineral* 76:458-469
- Johannsen A (1911) Petrographic terms for field use. *J Geol* 19:317-322
- Knop E, Zimmermann R, Heinrich W, Pehlke I, Franz G (1993) Austauschgleichgewichte zwischen Al-freien Amphibolen und chloridischen Lösungen. *Ber Deutsche Min Ges* 5:87
- Lattard D, Evans BW (1992) New experiments on the stability of grunerite. *Eur J Mineral* 4:219-238
- Liebau F (1980) Classification of silicates. *Rev Mineral* 5:1-24
- Liebau F (1985) *Structural Chemistry of Silicates*. Springer, Berlin Heidelberg New York
- Manning CE (1994) The solubility of quartz in H₂O in the lower crust and upper mantle. *Geochim Cosmochim Acta* 58:4831-4839
- Manning CE (1998) Fluid composition at the blueschist-eclogite transition in the model system Na₂O-MgO-Al₂O₃-SiO₂-H₂O-HCl. *Schweiz Min Petrogr Mitt* 78:225-242
- Maresch W, Czank M (1983b) Problems of compositional and structural uncertainty in synthetic hydroxyl amphiboles. *Per Mineral* 52:463-542
- Maresch W, Czank M (1998) Crystal chemistry, growth kinetics and phase relationships of structurally disordered (Mn²⁺,Mg)-amphiboles. *Fortschr Mineral* 66:69-121

- Maresch WV, Czank M (1983a) Phase characterization of synthetic amphiboles on the join $Mn^{2+}, Mg_{7-8}[Si_3O_{22}](OH)_2$. *Am Mineral* 68:744-753
- Maresch WV, Czank M, Schreyer W (1994) Growth mechanisms, structural defects and composition of synthetic tremolite: what are the effects on macroscopic properties? *Contrib Mineral Petrol* 118:297-313
- Maresch WV, Langer K (1976) Synthesis, lattice constants and OH-valence vibrations of an orthorhombic amphibole with excess OH in the system $Li_2O-MgO-SiO_2-H_2O$. *Contrib Mineral Petrol* 56:27-34
- Melzer S, Gottschalk M, Heinrich W (1998) Experimentally determined partitioning of Rb between richterites and aqueous (Na,K)-chloride solutions. *Contrib Mineral Petrol* 133:315-328
- Najorka J, Gottschalk M (2003) Crystal chemistry of tremolite-tschermakite solid solutions. *Phys Chem Mineral* 30:8-124
- Najorka J, Gottschalk M, Franz G, Heinrich W (1999) Experimental determination of the Sr-Ca distribution between amphibole, clinopyroxene and chloridic aqueous solution. *Am Mineral* 84:596-606
- Najorka J, Gottschalk M, Heinrich W (2002) Composition of synthetic tremolite-tschermakite solid solutions in amphibole+anorthite- and amphibole+zoisite-bearing assemblages. *Am Mineral* 87:462-477
- Oberti R, Hawthorne FC, Cannillo E, Cámara F (2007) Long-range order in amphiboles. *Rev Mineral Geochem* 67:124-171
- Pawley AR, Graham CM, Navrotsky A (1993) Tremolite-richterite amphiboles: synthesis, compositional and structural characterization and thermochemistry. *Am Mineral* 78:23-35
- Popp RK, Gilbert MC, Craig JR (1976) Synthesis and X-ray properties of Fe-Mg orthoamphiboles. *Am Mineral* 61:1267-1279
- Price GD, Yeomans J (1986) A model for polysomatism. *Mineral Mag* 50:149-156
- Raudsepp M, Turnock AC, Hawthorne FC (1991) Amphibole synthesis at low pressure: what grows and what doesn't. *Eur J Mineral* 3:983-1004
- Sharma A, Jenkins DM (1999) Hydrothermal synthesis of amphibole along the tremolite-pargasite join and the ternary tremolite-pargasite-cummingtonite. *Am Mineral* 84:1303-1318
- Skogby H, Ferrow E (1989) Iron distribution and structural order in synthetic calcic amphiboles studied by Mössbauer spectroscopy and HRTEM. *Am Mineral* 74:360-366
- Smelik EA, Jenkins DM, Navrotsky A (1994) A calorimetric study of synthetic amphiboles along the tremolite-tschermakite join and heats of formation of magnesiohornblende and tschermakite. *Am Mineral* 79:1110-1122
- Sondermann I (1996) Untersuchungen von natürlichem und synthetischem Tremolit. Diploma Thesis, Univ. Münster, Germany, 79 pp.
- Thompson JB Jr. (1970) Geometrical possibilities for amphibole structures: Model biopyriboles. *Am Mineral* 55:292-293
- Thompson JB Jr. (1978) Biopyriboles and polysomatic series. *Am Mineral* 63:239-249
- Thompson JB Jr. (1981) An introduction to the mineralogy and petrology of the biopyriboles. *Rev Mineral* 9A:141-189
- Veblen DR (1981) Non-classical pyriboles and polysomatic reactions in biopyriboles. *Rev Mineral* 9A:189-236
- Veblen DR (1991) Polysomatism and polysomatic series: A review and applications. *Am Mineral* 76:801-826
- Veblen DR, Burnham CW (1978) New biopyriboles from Chester, Vermont II. The crystal chemistry of jimthompsonite, clino-jimthompsonite, and chesterite, and the amphibole-mica reaction. *Am Mineral* 63:1053-1073
- Veblen DR, Buseck PR (1979) Chain-width order and disorder in biopyriboles. *Am Mineral* 64:687-700.
- Veblen DR, Buseck PR (1980) Microstructures and reaction mechanisms in biopyriboles. *Am Mineral* 65:599-623
- Veblen DR, Buseck PR (1981) Hydrous pyriboles and sheet silicates in pyroxenes and uralites: intergrowth microstructures and reaction mechanisms. *Am Mineral* 66:1107-1134
- Veblen DR, Buseck PR, Burnham CW (1977) Asbestiform chain silicates: New minerals and structural groups. *Science* 198:359-365
- Ward JR (1975) Kinetics of talc dehydroxylation. *Thermochim Acta* 13:7-14
- Wellman TR (1970) The stability of sodalite in a synthetic syenite plus aqueous chloride fluid system. *J Petrol* 11:49-71
- Zakharchuk V (2006) Löslichkeit von Spinell und Korund in reinem H_2O und in $KOH-H_2O$ -Lösung. Ph.D. Dissertation, Ruhr-Universität Bochum, Germany
- Zimmermann R, Gottschalk M, Heinrich W, Franz G (1997b) Experimental Na-K distribution between amphiboles and aqueous chloride solutions and a mixing model along the richterite - K-richterite join. *Contrib Mineral Petrol* 126:252-264
- Zimmermann R, Heinrich W, Franz G (1996) Tremolite synthesis from $CaCl_2$ -bearing aqueous solutions. *Eur J Mineral* 8:767-776

Zimmermann R, Knop E, Heinrich W, Pehlke I, Franz G (1997a) Disequilibrium in cation exchange experiments between Na-K-Ca amphiboles and aqueous Na-K-Ca chloride solutions: effects of fractional crystallization. *Eur J Mineral* 9:97-114

Amphiboles in the Igneous Environment

Robert F. Martin

*Department of Earth and Planetary Sciences
McGill University
3450 University Street
Montreal, Quebec H3A 2A7, Canada
bobm@eps.mcgill.ca*

INTRODUCTION

The time is ripe for a fresh inventory of occurrences of amphibole-group minerals in igneous rocks. Here, I build on the available resources, for example on the review of Wones and Gilbert (1982) in volume 9B of the *RiMG* series. They entitled their chapter "Amphiboles in the Igneous Environment." I adopt the same title, but intend to make the scope of my review somewhat broader by including non-igneous rocks formed in the igneous environments. Much has been written about occurrences of amphibole-group minerals over the last quarter of a century, much of it ably summarized by Deer et al. (1997), and it is quite impossible to do more here than to summarize representative findings concerning the textural development and broad compositional features of minerals of the amphibole group that are important in igneous contexts. Amphibole-group minerals are widespread in igneous rocks produced in zones undergoing extension, as well as in rocks associated with subduction systems. Each setting may be associated with specific late-stage metasomatic phenomena in which amphibole-group minerals play a key role. Metasomatic overprints involving an amphibole also are widespread in the mantle, and act as an essential step in the fertilization of sterile mantle if it is to produce alkali basaltic magmas by partial melting. Finally, selected findings are summarized here on amphibole-group minerals in igneous environments in other parts of the solar system.

Amphibole-group minerals have generally been underutilized in petrological studies. Reasons are not hard to find. The full characterization of an amphibole presents serious challenges, so much so that most investigators have been constrained to examine only those major elements that can be assessed in routine electron-microprobe analyses. As Hawthorne and Oberti (2006) pointed out in their essay on the future of schemes of classification, it has become abundantly clear that progress is within reach, but it will require the application of sophisticated tools to achieve the full characterization of an amphibole. For example, 1) lithium is a much more common constituent than has hitherto been realized, 2) the amount of hydrogen present in an amphibole can no longer be assumed; it is a variable that needs to be established in order to distinguish the amount of hydrogen present in the primary amphibole from that adjusted owing to late-stage oxidation of Fe and Mn, especially prevalent in epizonal and volcanic complexes, 3) the valence state of Fe and Mn must be evaluated in light of findings about 1) and 2) if any assessment of the fugacity of oxygen at the source is to be made. The challenges are amplified if one deals with zoned crystals, fine-grained crystals in an igneous groundmass, and complex telescoped mixtures of primary species and secondary amphiboles that arise by the retrograde reaction of a primary amphibole with an orthomagmatic fluid. Progress in decoding the petrogenetic messages will require major investments in time and effort to properly characterize the amphibole produced by the crystallization of a magma.

AMPHIBOLES IN IGNEOUS ROCKS ASSOCIATED WITH EXTENSION IN THE CRUST

Pargasite - hawaiitic magma as a pseudo-unary system?

Of all the rock-forming minerals, an amphibole has the unique property that it may well approach closely the composition of certain magmas. Consider, for example, the composition of a very coarse homogeneous crystal of titaniferous pargasite in a camptonitic dike-rock (Table 1). The amphibole crystals in such camptonitic dike-rocks, which amount to 15 vol% of the rock, attain 10 cm across, are homogeneous, except for a very narrow rim of kaersutite (Fig. 1). The megacrysts are considered phenocrysts rather than xenocrysts because they seem to have grown around vesicles. If growth occurred once the hawaiitic magma had begun to vesiculate, how is it possible to achieve such an extraordinarily coarse grain-size as illustrated in Figure 1? The fine-grained matrix consists of plagioclase, kaersutite, clinopyroxene, fluorapatite, analcime and calcite (the latter two being secondary). A comparison of the crystals and groundmass reveals a striking similarity (Table 1). The matrix and the phenocrysts contain quite comparable amounts of Si, Al, Ti, Ca, and K. The matrix contains more Fe^{3+} and less Fe^{2+} than the phenocrysts, presumably owing to oxidation accompanying cooling, but the total iron is only slightly higher in the matrix (representative of the melt), whereas the coexisting phenocrysts are more magnesian, as one would expect (Roeder and Emslie 1970). The matrix is enriched in Na by a factor of two, but some of this Na is lodged in analcime, attributed a deuteric origin. The conclusion seems inescapable that the parental magma crystallized *in situ* to a pargasitic amphibole. In crossing

Table 1. Composition of pargasite and kaersutite in camptonitic dike-rocks and megacrysts in basanite.

	1	2	3	4	5	6	7	8
SiO ₂ wt%	39.31	39.86	39.42	43.96	41.5	43.3	39.9	44.54
TiO ₂	1.89	1.96	3.68	2.72	3.4	1.8	5.7	0.38
Al ₂ O ₃	16.70	16.28	14.48	11.67	13.2	15.4	14.6	13.42
Cr ₂ O ₃			0.03		0.25	1.13	0.0	2.85
Fe ₂ O ₃	3.91	6.67	5.09	3.74				
FeO	6.55	5.82	4.97	8.33	8.5	4.7	12.6	4.13
MnO	0.09	0.25	0.10	0.19			0.1	0.11
MgO	14.61	7.32	14.04	12.96	15.0	17.3	11.2	17.68
CaO	11.99	10.86	12.00	10.97	10.9	10.8	10.0	9.79
Na ₂ O	2.26	3.26	2.02	3.31	2.8	3.5	3.1	3.83
K ₂ O	2.06	1.81	2.15	1.26	1.3	0.02	2.2	1.31
P ₂ O ₅	0.07	1.01		0.91				
H ₂ O ⁺	0.41	3.15	1.37				0.30	
CO ₂	0.33	1.08						
F			0.12				0.11	
Cl			0.02				0.00	
Total	100.18	99.33	99.49	100.02	96.8	97.9	99.8	98.04
δ ¹⁸ O ‰		5.63					4.85	

Columns: 1: vesicular pargasite phenocryst and 2: coexisting matrix, GSFC No. 29 of Schnetzler and Philpotts (1968, Table 1), LaFarge quarry, east-end Montreal, Quebec, Canada. 3: Vesicular pargasite phenocryst, same locality (Alarie et al., in prep.). 4: Inferred parental magma of the undersaturated series, Mount Royal, Quebec (Eby 1987, Table 1). 5: Ba-2-1, pargasite vein in sample of fertilized lherzolite in basanite, Dish Hill, California (Wilshire et al. 1980, Table 3). 6: Ba-2-1, interstitial pargasite in lherzolite. 7: H-92: oxidized kaersutite megacryst, Mount Emu basanite, Sturgeon Province, Queensland, Australia (Boettcher and O'Neil 1980, Table 2). 8: 10013, interstitial chromian amphibole in spinel lherzolite xenolith, Nunivak Island, Alaska (Francis 1976b, Table 2).

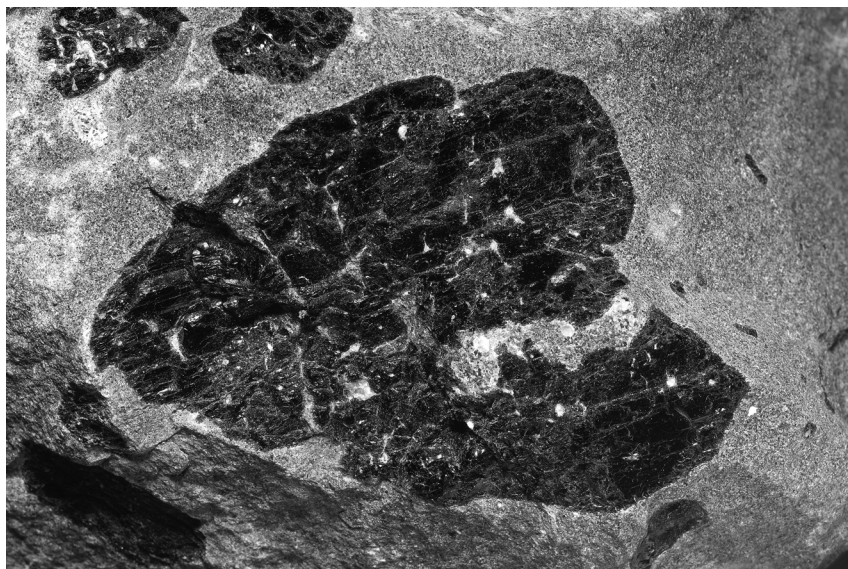


Figure 1. Pargasite megacrysts in camptonite dike, LaFarge quarry, east-end Montreal, Quebec, Canada. The largest megacryst measures 10 cm across. The crystals, considered to be phenocrysts, are homogeneous except for a very thin rind of kaersutite, similar to that found in the surrounding matrix. Note that the phenocrysts are amygdaloidal. Their composition resembles closely that of the matrix (Table 1).

a phase boundary at constant P and T , in this case the solidus, the system can be visualized as being “pseudo-unary,” with the freezing of the melt as amphibole crystals following the same pattern of behavior as blocky crystals of ice nucleating and growing in water. With little or no boundary layer developed, the crystals can attain an impressive size, even though in the case illustrated in Figure 1, they grew relatively rapidly owing to a shallow depth of emplacement of the dike rock. A similar scenario can account for the megacrysts of vesicular kaersutite in the Boulder Dam camptonite, Arizona, inferred by Campbell and Schenk (1950) to have grown in a few hours. It seems a distinct possibility that because the system is close to being unary, a melt of alkali basaltic or hawaiitic composition can crystallize metastably as an amphibole, instead of the equilibrium assemblage of clinopyroxene + plagioclase. This hypothesis could probably be tested experimentally in seeded runs.

Manifestations of camptonite and related lamprophyric dikes abound in the Montegian alkaline complexes, in the Province of Quebec, and in the White Mountain belt of anorogenic igneous activity in New Hampshire and contiguous areas (Bédard 1988). The recurrence of such pargasite-dominant dikes, associated with numerous differentiated intrusive complexes in these belts, motivated Philpotts (1974) and Eby (1987) to propose that they represent the mantle-derived alkaline basic melt that was parental to each complex. These batches of parental magma crystallized in an environment of relatively rapid loss of heat following emplacement in fractures and joints. Several generations of camptonitic dikes may criss-cross each other. The setting is conducive to the metastable crystallization of the incoming magma to give well-developed, homogeneous phenocrysts of pargasite. These are eminently suitable as analytical standards in view of their striking homogeneity.

The importance of pargasite in the fertilization of the upper mantle

A voluminous literature exists on the phenomenon of metasomatic rejuvenation of the depleted mantle in areas undergoing extension, which results from mantle degassing ahead of

a rising mass (plume?) of asthenospheric mantle. Descriptions of metasomatized upper mantle and lower crust brought up as nodules in alkali basalt and related alkaline rock-types include examples of porphyroclastic lherzolite and harzburgite fertilized and cut by undeformed veins of pargasitic amphibole \pm plagioclase (e.g., Wilshire et al. 1980; Menzies et al. 1987; Mukasa and Wilshire 1997, and references therein). At the Dish Hill locality, California, the compositions vary continuously from titanian pargasite in the veins (Table 1, column 4) to less titanian pargasite in the adjacent harzburgite (Table 1, column 5), into which the metasomatizing fluid has infiltrated along hairline fractures and has become progressively depleted in Ti, Fe, and K as it migrated up to 8 cm from the main fracture (Wilshire et al. 1980). The fluid seems to have reacted with the minerals of the harzburgite that it infiltrated, to account for the buildup in Mg, Al and Cr in the interstitial distal pargasite. A continuum exists between pargasite and kaersutite, the IMA-imposed cutoff value being taken as 0.50 atoms of Ti per formula unit (*apfu*). Note, however, that many authors use the label *kaersutite* indiscriminately. True kaersutite seems rarer than its incidence in the literature would indicate. The high-Ti calcic amphibole is more typical of veins and megacrysts (Menzies et al. 1987, Fig. 1b), and is geochemically more evolved than pargasite.

It seems likely that metasomatism proceeding along hairline cracks involved a fluid phase, but what about the wider veins of massive pargasitic or kaersutitic amphibole found crossing porphyroclastic peridotite? Figure 2 shows a close-up of a vein cutting a domain of lherzolite in a pyroxenite xenolith from Nunivak, Alaska. A thin border of orthopyroxene separates the 1.5-mm-wide amphibole vein from the olivine in the lherzolite. Francis (1976a) proposed that the amphibole developed in both the lherzolite and the pyroxenite by deposition from an interstitial aqueous fluid that was not critically undersaturated in SiO_2 . But in view of its low viscosity, a basaltic melt of appropriate alkaline composition could also have been the infiltrating fluid medium (see also Best 1974; 1975).

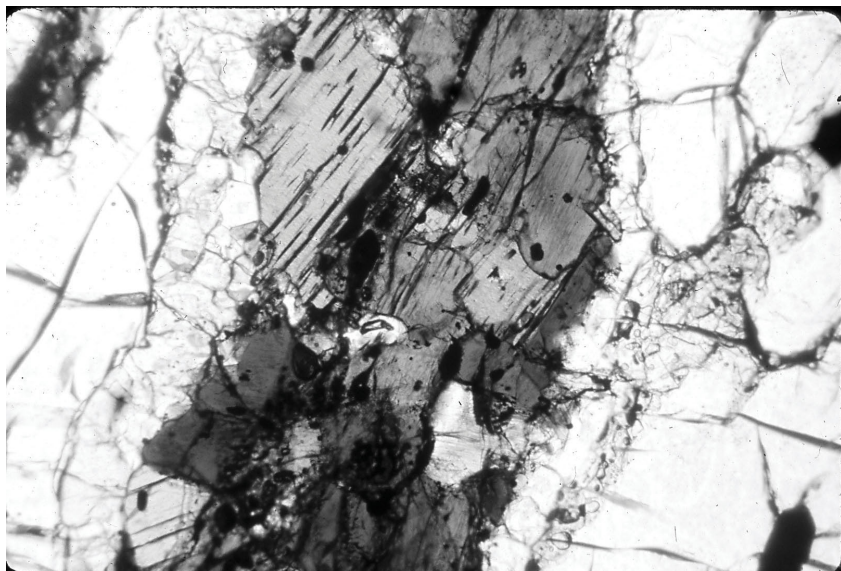


Figure 2. Close-up of vein of pargasitic amphibole cutting a fragment of lherzolite in a xenolith of pyroxenite, Nunivak suite, Alaska. A reaction rim of orthopyroxene has developed between the amphibole and the olivine grains of the spinel lherzolite (see Francis 1976a, Fig. 2). Width of field of view: 3 mm. The photo is contributed by D.M. Francis.

At its type locality, in Østerfjeld, Qaersut, Disko Island, western Greenland, kaersutite is found in meter-wide amphibole-dominant essexitic dikes cutting a sill of peridotite 50 m thick (Heim 1910). In these layers, 5-cm-long crystals more-or-less perpendicular to the wall give way to a jumble of prisms of random orientation, some of them hollow, toward the center of the layer. In view of the possibility of crystallizing the alkaline basaltic magma as a calcic amphibole, as explored above, it seems possible that the Qaersut occurrence of kaersutite and the cross-cutting veins of similar amphibole seen in peridotite nodules result from the crystallization of a low-viscosity magma on the walls of a conduit while in transit. The megacrysts of kaersutite and pargasite found in alkali basalts and related rocks worldwide likely originate by the accidental disruption of such dikes and veins by batches of unrelated magma passing through. In general, minor-element and isotopic studies, as reviewed by Stuckless and Irving (1976) and Boettcher and O'Neil (1980), point to a lack of a connection between the megacrysts and the host basalt. The megacrysts of augite, pargasite and kaersutite, phlogopite, alkali feldspar, corundum and zircon commonly encountered in alkali basalts and related rock-types are considered to represent disaggregated pegmatitic segregations (Irving 1974). Like the associated nodules of variably metasomatized peridotite, these by and large do not bear any genetic relationship with the carrier basalt.

In exceptional cases, however, there is a close isotopic correspondence between pargasite and basaltic host. For example, Menzies and Rama Murthy (1980) showed that pargasite crystals separated from lherzolite nodules and a megacryst of kaersutite from Nunivak Island, Alaska, are indistinguishable from their host alkali basalt in terms of $^{87}\text{Sr}/^{86}\text{Sr}$ value, in the range 0.7027 to 0.7034 for the amphibole and 0.7025 to 0.7032 for the host basalts. The same relationship applies in the case of foliated peridotite nodules from Kirsh volcano, Ataq, South Yemen, although both the lavas and the pargasite from the metasomatized nodules are more enriched in radiogenic Sr than the Alaskan case. This identity in an isotopic indicator is an important finding, as it shows that a pargasitic amphibole may well be the main reactant in the generation of an alkaline basaltic partial melt in the mantle (see below).

Amphibole-bearing pyroxenite and veins of calcic amphibole are commonly encountered in peridotite massifs. Occurrences in the well-known peridotite massifs of the eastern Pyrénées of France led Conquére (1971) to appeal to a local enrichment of H_2O by the fractional crystallization in the mantle of alkaline magmas formed by very-small-degree partial melting at the expense of the lherzolite. Fabriès et al. (2001) attributed the amphibole veins to segregations from a basaltic magma. Recent discoveries in peridotite massifs of the western Pyrénées of dikes of magmatic albitite of pegmatitic texture, some corundum-bearing and all highly enriched in incompatible elements, including the light rare-earths, U and Th, led Monchoux et al. (2006) and Pin et al. (2006) to conclude that these rocks have been subjected to a wave of $\text{H}_2\text{O}-\text{CO}_2$ metasomatism of carbonatitic tendencies in the mantle, and consequent melting just prior to their emplacement 103 Ma ago. By implication, it would seem that the presence of interstitial pargasite and kaersutite in lherzolite at Lherz and the forty or so other massifs emplaced in this environment of transtension in a collisional belt must reflect an episode of mantle metasomatism involving an asthenospheric source.

The importance of pargasite in the generation of alkaline basic magma in the mantle

If it is accepted that in most cases, the megacrysts of amphibole are indeed accidental xenocrysts, what might then be the role of pargasite and kaersutite in the origin of the host mafic alkaline lavas? The evidence is mounting that such calcic amphiboles must be present in a lherzolithic precursor undergoing melting. Thus the development of metasomatic veins of neoformed pargasite and kaersutite must be a very widespread phenomenon in segments of the upper mantle subjected to infiltration of a combined hydrothermal-carbothermal fluid phase and associated melts from a bulging, rising asthenospheric source below. The mantle is highly heterogeneous isotopically, and so conceptually, it should not be too difficult to envision a batch

of isotopically primitive alkaline basic melt formed by the incongruent melting of pargasite at one depth incorporating xenocrysts of more radiogenic pargasite from disrupted veins on its way up, or a deeper more radiogenic melt incorporating less radiogenic megacrysts on its way up, with the door left open to cases like Nunivak Island, in Alaska, where both the amphibole megacrysts and the carrier magma seem truly cogenetic and isotopically congruent.

Of the roughly 2000 nodules of lherzolite examined from the maars on the island of Nunivak, 50% contain relics of chromian pargasite enclosed in fine-grained zones of euhedral diopside, olivine and spinel set in a porous Al-rich mafic glass (Francis 1976b). Compared to the other compositions of pargasite shown in Table 1, the one from Nunivak (column 8) is definitely more strongly chromian and magnesian, less strongly titaniferous and ferroan, and more alkali-rich. The level of both Al and Cr increases, and that of Mg and Si decreases, away from the spinel-pargasite contact. Such compositions of amphibole belie a close relationship between the spinel in the refractory precursor and the neofomed pargasite: one seems to have formed at the expense of the other. Veinlets of pargasite cutting the ultramafic xenoliths in some cases also preserve signs of melting of the amphibole at Nunivak (Fig. 3). The anhedral grains of pargasite are surrounded by vesicular-glass-bearing domains replacing the amphibole. The glass contains euhedral microlites of clinopyroxene and olivine.

That the participation of such an amphibole, whether of hydrothermal or truly magmatic origin, is crucial in the generation of alkaline basic magmas has been carefully tested geochemically and isotopically with Recent volcanic rocks in the Canadian Cordillera by Francis and Ludden (1995) and by Abraham et al. (2005). The juxtaposition of terranes in this tectonically complex area and the development of a continuous array of Late Tertiary to Recent mafic magma-types ranging from olivine nephelinite to orthopyroxene-normative olivine basalt have led to tests of the role of a pargasitic amphibole at the source in these amphibole-free volcanic rocks. Briefly, the systematics of the large-ion lithophile elements and of the

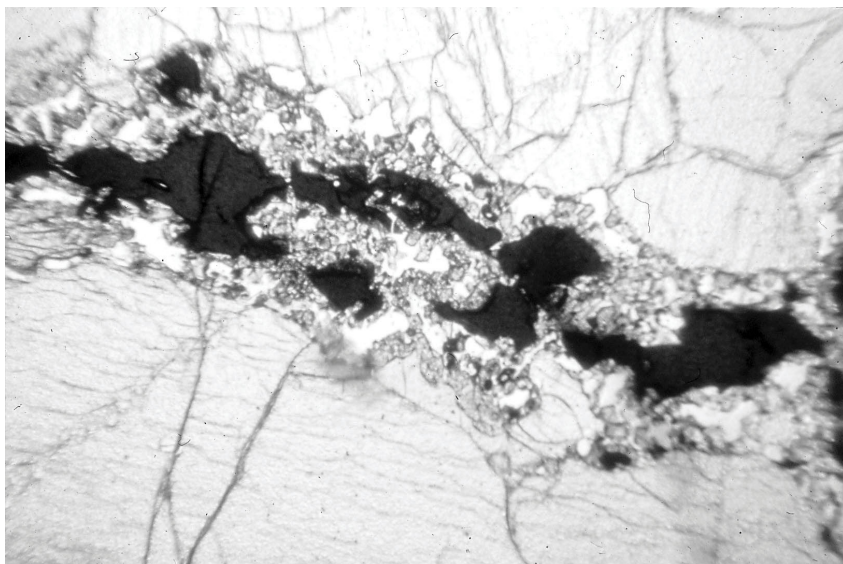


Figure 3. Veinlet of pargasitic amphibole cutting lherzolite in which melting has partially consumed the amphibole. The glass phase that surrounds the relics of amphibole contains microlites of clinopyroxene and olivine, and vesicles (see also Francis 1976b, Plate 1). Width of field of view: 6 mm. The photo is contributed by D.M. Francis.

high field-strength elements in the olivine nephelinite lavas, and the relatively sodic nature of these rocks, indicate that a residual amphibole at the source controlled the partition of these elements in the lithosphere, in particular in a partially molten lithosphere, at a depth where an amphibole would still be a stable phase (roughly, above 100 km). The olivine nephelinite lavas are highly enriched in the high field-strength elements, but have relatively low concentrations of the large-ion lithophile elements, in such a way that an amphibole retained at the source must have controlled the composition of the melt. In contrast, the orthopyroxene-normative basalts are less strongly enriched in most incompatible elements, and are considered to arise by the melting of a lherzolite assemblage following the exhaustion of amphibole at the source.

Francis and Ludden (1995) found clear evidence for the involvement of an amphibole in the residue in the generation of other intraplate alkaline suites also, such as those of the Hawaiian Islands. They inferred that the melting of any amphibole-bearing assemblage likely is a two-step process, regardless of whether the amphibole is segregated as veins or distributed interstitially. Stage I is controlled by the breakdown of such an amphibole, which is not in isotopic equilibrium with its host in most cases. It will produce a basaltic melt that may be SiO₂-oversaturated or SiO₂-undersaturated depending on pressure, less than or greater than 12 kbar, respectively, with only minor contributions from other minerals present. At stage II, following the exhaustion of the amphibole, the bulk composition changes rapidly to reflect equilibrium with the mineral assemblage of the lherzolitic source now devoid of the pargasitic amphibole, but its incompatible trace-element characteristics bear the imprint of the former presence of such an amphibole. It seems clear that a pargasitic amphibole plays a key role in the generation of sodic mafic alkaline lavas of the Earth in general. The very commonly made assumption that an alkaline olivine basalt invariably reflects a very limited extent of partial melting in the mantle thus probably is incorrect.

The oxidation state of iron in mantle-derived amphiboles in nodules and megacrysts

As amphibole megacrysts provide a window on the state of oxidation of the upper mantle, much attention has been given to a characterization of the Fe²⁺/Fe³⁺ value of the amphibole species carried up into the crust by basaltic magma. Dyar et al. (1993) pointed out that the detailed resolution of a Mössbauer spectrum is fraught with difficulties owing to variable OH-for-O substitution at the O(3) site, the importance of patterns of short-range order, and the likelihood that Fe²⁺ and Fe³⁺ are variably distributed over the *M*(1), *M*(2) and *M*(3) sites. The kinetics of hydrogen loss during entrainment and ascent being relatively sluggish, Dyar and coworkers concluded that their sampling of kaersutite crystals likely reveals primary values of the ratio 100Fe³⁺/ΣFe. The very significant spread of values noted, in the range 100 to 21 (Table 2), suggested to the authors that the oxidation state of the metasomatizing fluid is highly variable on a small scale during the process of fertilization of lithospheric mantle. In Table 2, the samples shown in columns 1 and 2 are from the same locality, and reveal values of 100Fe³⁺/ΣFe of 86 and 94. One may infer that these megacrysts, possibly picked up at two different depths of the California lithosphere, indicate a much more oxidized mantle than the pair of samples shown in columns 3 and 4, from a section through the Saudi Arabian lithosphere (100Fe³⁺/ΣFe of 24 and 33). Dehydrogenation during ascent and an attendant increase in 100Fe³⁺/ΣFe most likely were negligible in both cases, because the megacrysts selected for study are devoid of a visibly oxidized rim or pleochroic irregularities. In general, dehydrogenation likely occurs at the surface or en route to the surface where *f*(H₂) is low, cooling is slow, or grain attributes favor the rapid diffusion of H (King et al. 1999). The debate about what is primary and what reflects syn- or post-emplacement dehydrogenation is likely to continue, however, considering the scarcity of experimental studies of the rate of hydrogen diffusion as a function of *f*(O₂) in coarse crystals. Popp et al. (2006) have calibrated the dehydrogenation-oxidation reaction in Ti-bearing calcic amphiboles, and have applied their results to the estimation of *a*(H₂O) at the site of amphibole growth in the mantle.

Table 2. Composition of mantle-derived megacrysts of kaersutite and pargasite, with a focus on the ratio $100\text{Fe}^{3+}/\Sigma\text{Fe}$.

	1	2	3	4	5	6	7	8
SiO ₂ wt%	39.61	39.01	38.91	39.76	39.71	39.69	40.11	39.88
TiO ₂	5.19	4.52	4.84	4.34	5.82	6.21	5.56	5.87
Al ₂ O ₃	14.77	14.26	14.64	14.04	15.16	15.43	15.39	15.37
Cr ₂ O ₃	0.00	0.02	0.03	0.00				
FeO	0.72	0.14	7.92	9.97	11.14	10.81	10.99	10.94
Fe ₂ O ₃	12.34	13.27	4.43	3.37				
MgO	12.41	12.31	12.16	11.29	11.91	11.90	12.25	11.60
MnO	0.12	0.15	0.17	0.15	0.06	0.03	0.00	0.08
CaO	10.43	10.71	11.02	10.24	11.39	11.14	11.18	11.57
Na ₂ O	2.82	2.61	2.61	2.90	2.53	2.58	2.62	2.92
K ₂ O	1.44	1.64	1.66	1.52	1.16	1.12	0.98	1.14
P ₂ O ₅					0.02	0.00	0.05	0.00
F	0.16	0.20	0.14	0.15	0.15	0.15	0.12	0.14
Cl	0.00	0.02	0.01	0.00	0.00	0.00	0.02	0.00
H ₂ O ⁺	0.13	0.16	1.05	1.18	0.22	0.33	0.83	1.10
Total	100.14	99.02	99.59	98.91	99.27	99.39	100.09	100.61
$100\text{Fe}^{3+}/\Sigma\text{Fe}$	93.8	86.2	33.1	23.8	65.5	57.5	33.1	17.0

Columns: 1. Sample DL-5, kaersutite, Deadman Lake, California, Hill 2237 (Dyar et al. 1993, Table 5). 2. Sample DL-9, kaersutite, Deadman Lake, California, Hill 2284 (Dyar et al. 1993, Table 5). 3. Sample H366-92, kaersutite, Harrat Hutaymah, Saudi Arabia (Dyar et al. 1993, Table 5). 4. Sample H366A, titanian pargasite, Harrat Hutaymah, Saudi Arabia (Dyar et al. 1993, Table 5). 5. Sample LC3, kaersutite, Lunar Craters, Nevada (King et al. 1999, Table 1); the proportion of Fe²⁺ and Fe³⁺ is calculated from charge-balance considerations. 6. Sample LC1, same locality. 7. Sample LC2, same locality. 8. Sample LC6, same locality. The amount of H was measured in both studies, and the proportion of Fe²⁺ and Fe³⁺ was measured in the study of Dyar et al. (1993).

The sum Ti + ⁶Al + Cr + Fe³⁺ (in *apfu*) is very strongly correlated (negatively) with the amount of OH at the O(3) site, such that if OH is measured, the ratio $100\text{Fe}^{3+}/\Sigma\text{Fe}$ can be inferred (King et al. 1999, Fig. 7). In their suite of amphiboles, the Ti contents are the highest, attaining 0.75 *apfu*, in kaersutite megacrysts from flows and scoria cones from the Lunar Craters, Nevada; at this high level, the amount of OH varies over the range 0.1 to 1.1 per formula unit. In other words, high levels of Ti are not indicative of a hydrogen-poor amphibole, as it is the sum of Al, Cr, Fe³⁺ and Ti that will correlate negatively with the extent of OH-for-O substitution. This finding has a bearing on those SNC meteorites that contain a high-Ti amphibole (King et al. 1999).

Columns 5 to 8 of Table 2 contain information on four megacrysts found in scoria cones and lava flows at Lunar Craters, Nevada. One could expect these homogeneous and compositionally almost identical samples to have more or less the same value of the ratio $100\text{Fe}^{3+}/\Sigma\text{Fe}$, but in fact they range widely, from 66 to 17. Were these crystals picked from amphibole veins at different levels in the lithospheric mantle, each having its distinctive value of *f*(O₂)? This interpretation seems more plausible than the alternative, that the ratio $100\text{Fe}^{3+}/\Sigma\text{Fe}$ was variably (among crystals) and homogeneously reset (within a crystal) once the crystals had arrived in the upper crust.

Amphibole minerals in derivatives of alkaline basic magmas

In view of the above comments, a pargasitic or kaersutitic amphibole clearly was of critical importance in determining the composition of the partial melt at the source. In this section, it will become clear that amphiboles continue to play an important role as products of the

fractionation of those melts as they underplate the crust and locally rise through it in zones undergoing extension. Associated with an alkaline basaltic magma are batches of hawaiitic, mugearitic, benmoreitic, trachytic and either phonolitic or quartz trachytic and rhyolitic magmas. As a typical example, consider the Trans-Pecos magmatic province of western Texas. Barker (1987) found the fractionation of olivine, Ti-rich augite, kaersutite and plagioclase to cause the derivative magma ultimately to reach the stage of a benmoreitic composition. At this stage, the more evolved magma can go one of two ways: it may be marginally SiO₂-undersaturated and become more strongly undersaturated by fractionation of an alkali feldspar, or it may be SiO₂-oversaturated. Some complexes even contain both in juxtaposition, as will be made clear below. In his review of compositional variations in amphibole-group minerals of alkaline plutonic complexes, Mitchell (1990) has surveyed the compositional spread in many examples of both SiO₂-undersaturated or SiO₂-oversaturated suites in terms of an "amphibole prism" in which data on ^BCa, *mg* and Si (*apfu*) are plotted. His summary plots (Mitchell 1990, Figs. 14, 15) are reproduced here in Figures 4 and 5.

In SiO₂-undersaturated suites, the phenocryst assemblage typically is 1) anorthoclase, 2) a clinopyroxene that follows a trend from sodian augite toward hedenbergite, then to aegirine, 3) manganian fayalite, 4) an amphibole-group mineral spanning the range from the calcic amphibole edenite to the sodic amphibole arfvedsonite, and 5) aenigmatite. What Mitchell (1990) has called the primary magmatic trend features a decreasing *mg* number at relatively constant Si, Al and Ca (Fig. 4). It is a feature of both alkaline and subalkaline (miaskitic) complexes. Early members fractionating from the more strongly alkaline suites like Ilímaussaq are Al-rich ferropargasitic amphiboles. These compositions are Si-poor and Al-rich relative to amphiboles of similar *mg* number and ^BCa in the oversaturated suites. With advancing fractional crystallization, the amphibole evolves through katophorite to ferrichterite. Interestingly, as the host rocks become increasingly SiO₂-undersaturated and approach the "nepheline syenite minimum" in petrogeny's residua, the amphiboles become increasingly Si-rich and ^BCa-poor, and attain an "arfvedsonite" composition. "Arfvedsonite" here is shown in quotation marks because the extent of departure of the arfvedsonite in the evolved members of such complexes toward a ferroleakeite or fluoro-ferroleakeite component remains largely uncharted territory (see below). The discovery of lithium as an essential constituent of alkali amphiboles (Hawthorne et al. 1993, 1996a), ordered at the *M*(3) site, greatly complicates the picture, and has yet to be assessed realistically in the evolved members of these associations. Without accurate data on the level of Li and on the oxidation state of iron in these epizonal complexes, the full crystal-chemical response of an alkali amphibole to the complex and overlapping processes of fractional crystallization, immiscibility, "back reaction" with more primitive rocks, and degassing cannot be determined.

It is instructive at this point to examine the Ilímaussaq intrusive complex, part of the Gardar magmatic province in west Greenland, to see the process of closed-system fractional crystallization pushed to an extreme in a shallow plutonic setting. Larsen and Sørensen (1987) and Sørensen et al. (2006) have described how the earliest apgaitic rocks crystallized successively downward from the roof. First to crystallize was slightly SiO₂-undersaturated augite syenite, apparently amphibole-free. A second phase involved a small pulse of peralkaline granitic magma. The third (and dominant) intrusive phase was emplaced upon subsidence of the central block, and the invading magma was peralkaline, Fe-rich, Mg-depleted, and volatile-enriched. The accumulation of low-melting components ahead of the downward-advancing front eventually suppressed the crystallization of the roof rocks. The high-temperature mafic minerals "reacted out" and were replaced by an alkaline hydrous assemblage of alkali amphibole in the range katophorite–arfvedsonite, aegirine, aenigmatite and eudialyte. Gravitational layering also took place on the floor of the reservoir, resulting in a sequence of 29 cyclically repeated density-graded layered units of kakortokite, each seven meters thick on average. Each unit consists of a lower black layer rich in arfvedsonite, a red layer rich in a eudialyte-group mineral, and a thicker upper white layer rich in alkali feldspar and nepheline. It is beyond the scope of this

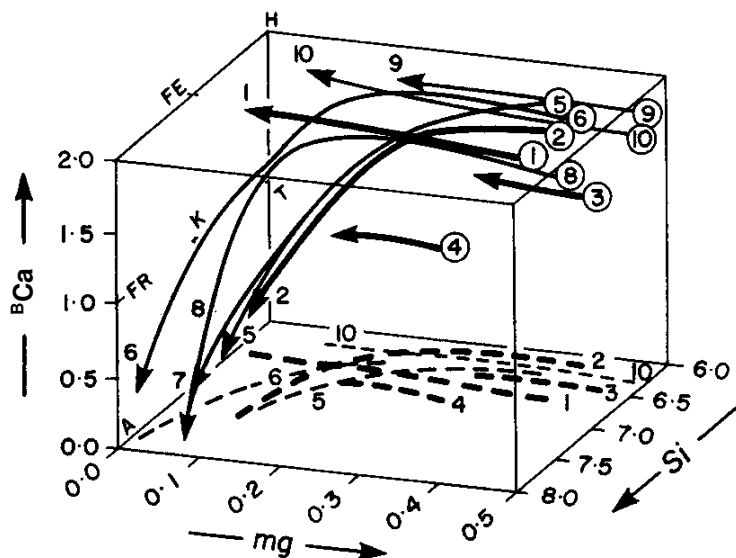


Figure 4. Summary of compositional trends of amphibole-group minerals in undersaturated anorogenic plutonic complexes. Dashed lines are projections of trends onto the base of the prism. Suites shown: 1: Chikala, 2: Mongolwe, 3: Chaone, 4: Chinduzi, all from the Chilwa province, Malawi; 5: North Qorôq, 6: Ilímaussaq, 7: Igdlarfígssalik, 8: Motzfeldt, all from the Gardar province, Greenland; 9: Mont Saint-Hilaire, Quebec, Canada, and 10: Center II, Coldwell complex, Ontario, Canada. Symbols: A: arfvedsonite, FE: ferro-edenite, FR: ferrichterite, H: hastingsite, K: katophorite, T: taramite. [Adapted from Mitchell (1990) and reproduced with permission, Elsevier Science Publishers.]

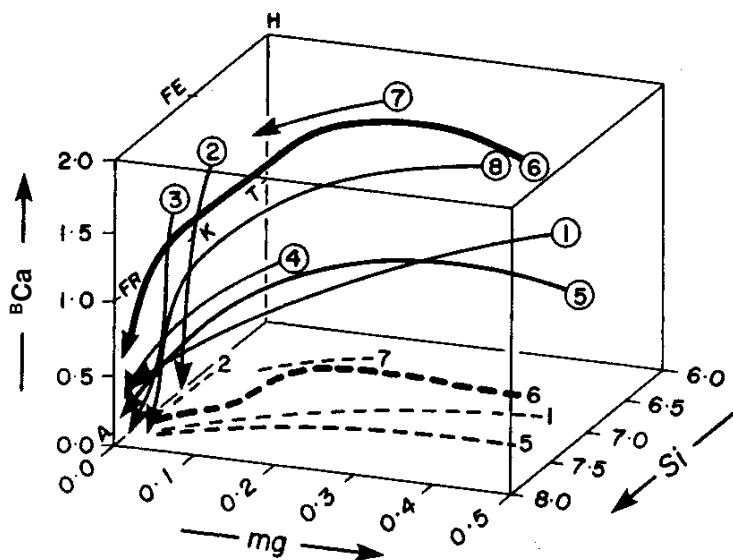


Figure 5. Summary of compositional trends of amphibole-group minerals in oversaturated anorogenic plutonic complexes. Dashed lines are projections of trends onto the base of the prism. Suites shown: 1: Rallier-du-Baty, Kerguelen, 2: Cauro-Bastelica, Corsica, 3: Ras Ed Dom, Sudan, 4: Topsails - St. Lawrence, Newfoundland, Canada, 5: Mulanje, Malawi, 6: Marangudzi, Zimbabwe, and 7: Mahé, Seychelles. Symbols as in Figure 4. [Adapted from Mitchell (1990) and reproduced with permission, Elsevier Science Publishers.]

review to explore the mechanisms called upon to explain the 29 cyclic units; what is important to note is the presence of arfvedsonite as a liquidus phase in the evolved magma.

The final stage of crystallization involved a transition to an even more evolved magma. First to appear on top of the arfvedsonite-bearing kakortokite sequence was a green, aegirine-rich lujavrite, a subsolvus rock containing primary K-feldspar + primary albite (indicative of a temperature of crystallization below the alkali feldspar solvus), aegirine and arfvedsonite, giving way upward into a black, arfvedsonite-dominant lujavrite. Note that the pattern of crystallization has switched in this latest part of the sequence, from the familiar sequence of mafic mineral first, felsic mineral later to felsic mineral first, mafic mineral later. In other words, the arfvedsonite is on the solidus, not the liquidus, and forms an oikocrystic texture in which it envelops the euhedral alkali feldspar phenocrysts. I agree with Mitchell (1990) that this is a magmatic texture, and not a subsolidus product, as some authors have claimed. In such a situation, the progressive fractional crystallization will give rise to an increasingly mafic (or, more correctly, femic) magma approaching arfvedsonite in bulk composition.

Markl (2001) has proposed that the solidus of the lujavritic differentiates is as low as 450 °C owing to extreme enrichment in a host of incompatible elements, including lithium. Near the end of its crystallization history, the melt is considered to undergo an immiscibility phenomenon. The dark (femic) melt at Ilímaussaq is highly enriched in Nb (up to 1.2 wt% Nb₂O₅) and rare-earth elements (up to 6.6 wt% REE₂O₃), and ultimately crystallizes to a mixture of arfvedsonite (dominant), K-feldspar, steenstrupine and a wide variety of mineralogical exotica. Research on his branch of igneous petrology is in its infancy, but it seems clear that the most evolved conjugate melts may well have crystallized ferroleakeite and fluoro-ferroleakeite, which express the buildup in essential Li to offset the buildup in ferric iron, with solid solution toward the Mn-dominant kornite and “fluorokornite” at the border of grains. Representative compositions of late amphibole-group minerals are presented in Table 3. An illustration of the reversal in the order of crystallization, with feldspar on the liquidus and an alkali amphibole at the solidus, is provided in Figure 6, showing a sample of agpaite nepheline syenite from intrusive center III of the Coldwell Complex, western Ontario, sampled on the shore of Lake Superior near Port Coldwell (Mitchell and Platt 1994, Fig. 13). The rock shown in Figure 6 contains coarse euhedra of alkali feldspar and nepheline in a felted matrix of slender zoned crystals of F-bearing hastingsite, a calcic amphibole. Such an amphibole is considered to approach the composition of the femic residual magma, in which the buildup in incompatible elements attains a high level.

Similarly, in a recent compilation of data on the Khibiny complex, no less than 24 species of amphibole are itemized and described, spanning the interval from Si-poor, Ca-rich species like pargasite and kaersutite to Si-rich, Ca-poor species like arfvedsonite (Yakovenchuk et al. 2005). In large alkaline complexes like Coldwell (Ontario), Ilímaussaq, and Khibiny, in the Kola Peninsula of Russia, the primary amphibole-group minerals exhibit an exceptional breadth of compositional space, running from calcic amphiboles through sodic-calcic to alkali amphiboles, such that a careful documentation of the major- and minor-element composition of an amphibole will pinpoint the stage of magmatic evolution attained by the parental mantle-derived magma as it fractionates once in the crust (Mitchell 1990).

A serious complication arises in complexes that become hyperagpaite at the end stages of crystallization (Khomyakov 1995). The melt in this case grades down-temperature to a “hyper-alkaline soup” increasingly enriched in the alkalis and the high-field-strength elements, but also containing elements picked up by the destabilization of higher-temperature (more primitive) rock types or from the wallrock; it seems clear that the caustic low-viscosity “soup” interacts aggressively with its surroundings. This is the phenomenon that explains the appearance, late in the evolution of these large complexes, of such exotic amphiboles as potassic-arfvedsonite, potassic-fluorrichterite and “potassic-richterite” (Table 3). Unlike the well-documented decrease

Table 3. Composition of K-rich amphiboles in evolved and contaminated differentiates in the Ilímaussaq, Khibiny and Lovozero intrusive complexes.

	1	2	3	4	5	6	7	8
SiO ₂ wt%	50.10	51.13	50.13	47.44	56.15	54.57	53.70	50.98
TiO ₂	0.00	0.00	0.11	0.33	0.20	0.86	0.29	1.23
Al ₂ O ₃	0.00	0.00	16.11	3.34	0.20	0.24	1.85	2.69
Fe ₂ O ₃							15.27	4.71
FeO	33.72	29.75	6.21	21.31	10.07	20.43	3.56	10.29
MnO	1.54	2.66	0.92	2.58	0.47	3.17	1.05	0.75
MgO	0.00	0.00	0.05	0.16	16.65	8.04	9.50	13.26
CaO	0.00	0.00	0.3	0.5	5.65	0.33	0.21	4.91
Na ₂ O	6.77	6.39	9.21	5.01	5.30	7.47	19.40	5.78
K ₂ O	2.98	3.93	3.61	4.69	4.50	5.25	1.34	3.14
P ₂ O ₅			0.01	0.02				
Li ₂ O (est.)	0.90	1.70					0.24	
F	0.36	0.33					2.11	1.47
Cl	0.03	0.00					0.00	
Total	96.41	95.90	86.66	85.38	99.19	100.36	100.07	100.34

Columns: 1, 2. "arfvedsonitic" amphibole GM1212–168 and GM1212–171 from highly evolved femic magma, Ilímaussaq complex, west Greenland (Markl 2001, Table 1). 3. Light melt fraction, GM1212, Ilímaussaq complex, west Greenland (Markl 2001, Table 3). 4. Dark melt fraction, GM1212, Ilímaussaq complex, west Greenland (Markl 2001, Table 3). 5. "Potassic-richterite" from nepheline – pyroxene– microcline vein in urtite, Mount Kukisvumschorr, Khibiny complex, Russia (Yakovenchuk et al. 2005, p. 170). 6. Potassic magnesio-arfvedsonite from aegirine – microcline vein, Mount Rasvumschorr, Khibiny complex, Russia (Yakovenchuk et al. 2005, p. 169). 7. Magnesio-arfvedsonite, albite-rich pegmatite, Lovozero complex, Kola Peninsula, Russia (Deer et al. 1997, Table 33). 8. Richterite in lujavrite pegmatite, sample 22–15, Khibiny complex, Russia (Mazdab 2003, Table 2). The total includes 0.21% V₂O₅.

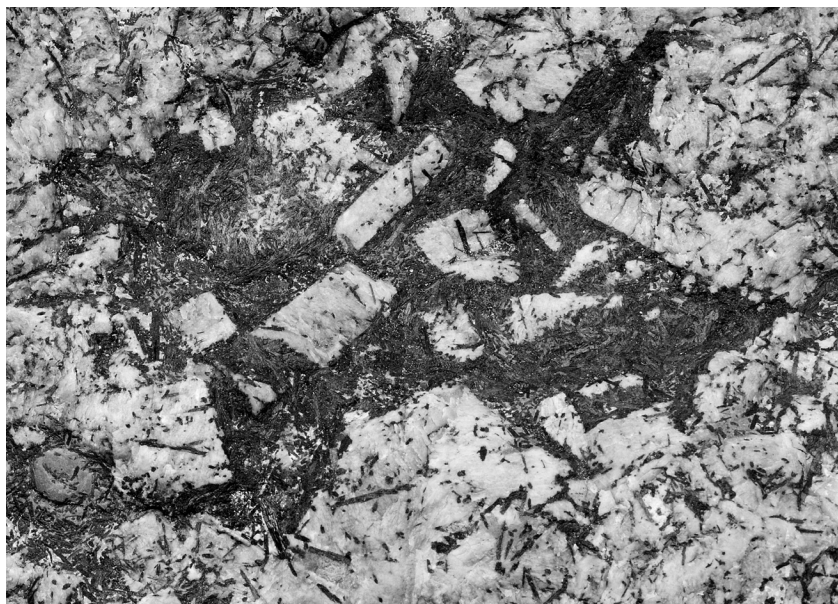


Figure 6. Sample of agpaitic nepheline syenite from intrusive center III of the Coldwell Complex, north shore of Lake Superior, in Ontario, Canada. Coarse euhedra of alkali feldspar and nepheline enclose an early amphibole and are set in a swarm of euhedral crystals of a near-solidus hastingsitic amphibole.

in Ca and Mg and buildup in Si documented along the primary magmatic trend of Mitchell (1990), the aggressive hydrothermal "soup" crystallizes amphiboles with otherwise difficult-to-explain combinations of elements. For example, the K-rich amphiboles in Table 3, columns 5–8, have high *mg* values and levels of Ca that belie the "reprocessing" of more primitive products of magmatic crystallization, or else Archean wallrock in an open-system dissolution-and-precipitation mode of origin. These complexes also display prominent aureoles of fenitized (alkali-metasomatized) country-rocks, the amphibole mineralogy of which may well involve high levels of the alkalis and high levels of recycled elements like Mg and Ca.

Amphiboles in juxtaposed SiO₂-undersaturated and SiO₂-oversaturated derivatives

Where saturation in SiO₂ has been achieved, an amphibole-group mineral is considered by some to play a key role in ensuring the transition. For this to happen, the calcic amphibole, which is relatively poor in SiO₂, must be efficiently removed from the parental melt, presumably to form cumulates at depth. Giret et al. (1980), among others, have shown how the thermal divide separating undersaturated and oversaturated magmas can be crossed by the efficient fractionation of low-Si, high-Ca amphibole from marginally SiO₂-undersaturated magmas. Furthermore, an extraction of early Ca- and ⁴¹Al-rich amphiboles from such a melt can ensure a transition from a metaluminous melt to a peralkaline derivative, as is found in many examples of the association. In the Red Hill complex, New Hampshire, for example, the presence of SiO₂-oversaturated syenite juxtaposed with nepheline syenite is explained by such a fractionation of plagioclase, magnetite, and calcic amphibole, for which petrographic signs are adduced (Dorais and MacRae 1994). Unfortunately, xenoliths of the telltale cumulates typically are not available for study.

However, a more common explanation of the association in the White Mountain magmatic province and elsewhere involves contamination of a Ne-normative felsic magma by quartz-bearing wallrocks (Foland et al. 1993). It seems that each case of the juxtaposed Ne- and Qtz-normative felsic melts will have to be evaluated on its own merits. In the absence of obvious amphibole-dominant cumulates, an evaluation of competing hypotheses must rely on isotopic tests of the openness of the fractionally crystallizing system. An evaluation of the δ¹⁸O values of the minerals produced by the derivative magmas, including the alkali amphibole, offers the opportunity to test not only magmatic lineages, but any adjustments that might have occurred upon cooling, involving, for example, an oxygenated aqueous fluid of local derivation.

Amphiboles in SiO₂-oversaturated anorogenic suites

The primary magmatic trend defined by amphibole compositions in the case of Qtz-normative evolved melts broadly follows that in the Ne-normative suites, except that the spectrum of compositions is not quite as extensive in terms of the amphibole prism (Fig. 5). Each oversaturated suite is characterized by a particular suite of primary amphiboles, the principal differences being in their Si and Ca contents and *mg* number (Mitchell 1990). The level of Ca and the *mg* value in the most primitive members of a Qtz-normative suite are not as high, and the Si content is not as low, as in the compositional spectrum of fractionated Ne-normative suites (Fig. 4). Where a large spectrum of amphibole compositions is recorded, for example in parts of the Coldwell complex, the amphiboles range from hastingsite through katophorite to ferrichterite and arfvedsonite. In other cases, the spectrum of compositions is rather limited, with variations mostly in Fe-rich amphiboles that range from Ca-rich to Na-rich compositions. The sequence of crystallization can be deduced in each case by tracking the composition of the primary amphibole.

The contrast in the spectrum of compositions of primary amphiboles in Ne-normative and Qtz-normative suites (Figs. 4, 5) is easy to explain. With few exceptions, nepheline-normative felsic rocks result from the fractional crystallization of mantle-derived mafic melts, whereas the quartz-normative felsic rocks found in extension-related suites may be the result of 1)

fractional crystallization of a mafic parent, with or without assimilation of crust (AFC), or 2) anatexis of a suitably metasomatized crust, or 3) hybridization of felsic magmas that arose from processes 1 and 2. Martin (2006) has shown how A-type granites commonly involve a granulite-facies source-rock in the lower crust that has been metasomatized (fenitized) from below by the same fluids that have caused metasomatism in the upper mantle. Zones in the crust undergoing extension are known to be sites of focused degassing of the mantle, and one could expect the same type of local veining and fertilization in the lower crust as described above in connection with upper-mantle species of amphibole. As in the mantle, therefore, a Na-Ca amphibole of metasomatic origin could well play a key role in the formation of a geochemically rather "evolved" melt in the deep crust by anatexis, thus accounting for the shorter vectors in $^{87}\text{Sr}/^{86}\text{Sr}$ - $\text{Si} - \text{mg}$ space (Fig. 5). Is the activity of Si in the melt the main control in determining the compositional spectrum of amphibole minerals shown in Figures 4 and 5 (cf. Giret et al. 1980)? The prominent development of arfvedsonitic amphiboles in Ne-normative suites does not seem consistent with this view.

A typical A-type association of gabbro and granite of Late Devonian age has been described by Pe-Piper (2007) in the Cobequid shear zone in Nova Scotia. A "primary magmatic trend" has been documented in the primary amphiboles in gabbro (magnesiohornblende and edenite) and in the related granites, which range from metaluminous bulk-compositions containing a calcic amphibole (ferrohornblende and ferro-edenite) to mildly peralkaline bulk-compositions containing a variety of primary amphiboles. The earlier of the more evolved granites tends to contain arfvedsonite as the principal primary phase, with minor development of the primary sodic-calcic amphiboles ferrichterite, ferrowinchite and katophorite. Arfvedsonite is less prominent in the later granites, inferred by Pe-Piper (2007) to have formed by the remelting of the earlier ones and hybridization with a more mafic magma, presumably the one responsible for remelting. These later granites also include primary ferrichterite and katophorite. The F content is highest in the primary amphiboles, and falls to less than 1% in late-stage (deuteric) amphiboles formed as a result of oxidation reactions, dominantly riebeckite and ferrowinchite. The controls on the appearance of primary sodic or calcic amphiboles are difficult to pinpoint, but must reflect the changes in bulk composition of this complexly evolving system, from a situation of normal fractional crystallization, with buildup in Fe, F, and Li (up to 62 ppm), to a late case involving the mingling of small batches of fractionating melts of mafic and felsic compositions, presumably with superimposed periodic losses of the orthomagmatic fluid and consequent oxidation near the solidus.

The amphibole mineralogy of the Strange Lake peralkaline A-type granite (Quebec - Labrador) is here described as a representative example of a highly evolved suite (Hawthorne et al. 2001). The pluton contains an early hypersolvus granite intruded by even more evolved subsolvus granites and dikes of peralkaline pegmatite + aplite. The amphiboles span the range lithian arfvedsonite and lithian manganian arfvedsonite, characterized by an anomalous scattering at the $M(3)$ site owing to a significant buildup of Li in the suite, up to 0.40 *apfu* Li. The Li is incorporated in the amphibole according to the substitution $\text{Li} + \text{Fe}^{3+} \leftrightarrow 2\text{Fe}^{2+}$. Ion-microprobe analysis shows evidence of limited dehydrogenation that correlates with the amount of Ti at the $M(1)$ site, up to 0.2 *apfu*. The suite illustrates the progressive buildup in Mn, Zn, K and Li (up to 0.40 *apfu*) as $^{87}\text{Sr}/^{86}\text{Sr}$ decreases owing to fractionation.

To judge from the nature of the alkali amphibole, an even more advanced case of magmatic evolution is evident in the resurgent Canada Pinabete pluton, Questa caldera, New Mexico (Czamanske and Dillet 1988; Hawthorne et al. 1996a). The A-type hypersolvus granite is metaluminous and epizonal. Fluoro-ferroleakeite occurs in the groundmass of porphyritic biotite granites, presumably forming as a result of progressive degassing of the magma and the attendant increase in its intrinsic fugacity of oxygen. The holotype fluoro-ferroleakeite contains (in *apfu*) 0.61 Li, 1.93 Fe^{3+} , 0.59 Mn^{2+} and 1.39 F. As stated above in connection with

the most evolved members of the silica-undersaturated suites, solid solution toward the fluoro-ferroleakeite end-member is likely to be an important though still poorly documented trend in all peralkaline granites and related pegmatites of the world.

In miarolitic granitic pegmatites of NYF type, commonly associated with A-type granites, crystallization from an evolved magma gives way to crystallization from a supercritical rare-element-enriched aqueous orthomagmatic fluid at the miarolitic stage. In one case study, lithian fluoro-arfvedsonite rather close to fluoro-ferroleakeite is prominent near the walls of a miarolitic cavity at Hurricane Mountain, near North Conway, New Hampshire (Foord et al. 1996; Hawthorne et al. 1996b). These coarse crystals become progressively depleted in Li and F inward into the cavity. The final amphibole to crystallize in the cavity is a fibrous Li-, F- and K-poor riebeckite that is in fact richer in Nb and Zr than the earlier, more strongly alkaline amphiboles. An interesting question arises here concerning cause and effect: is the lower proportion of ferric iron at a late stage due to an “environmental” control, for example, influx of a more reducing aqueous fluid from the country rocks as the system cooled and cracked, or is there a crystal-chemical control on apparent $f(\text{O}_2)$ governed by the unavailability of lithium in the amphibole as a charge-compensating device?

I will return to the tendency of Li to escape into the exocontact in the section on granitic pegmatites in orogenic suites.

THE AMPHIBOLE MINERALOGY OF OTHER MANTLE-DERIVED ROCKS

Amphiboles in kimberlites and lamproites

The kimberlites of the world invariably contain phlogopite as a clear sign of a metasomatized source in the mantle, but amphibole-group minerals are not prominent. Perhaps the metasomatic overprint of the source largely took place beyond the field of stability of amphibole-group minerals. In fact, Dawson and Smith (1977) have favored a late crystallization of richterite in the so-called MARID assemblage [mica – amphibole – rutile – ilmenite – diopside] found in some xenoliths, perhaps even during the ascent of the kimberlite. The amphibole species they encountered are potassian richterite and “potassic-richterite” (Table 4). Representative compositions have high *mg* values (0.87–0.91), as expected from the provenance of the nodules, and high values of the ratio $\text{K}/(\text{K} + \text{Na})$, in the range 0.47–0.58, as expected from the importance of K in the metasomatizing fluid at the source. The amphiboles are also characterized by a relatively higher Ti and lower Al, Cr and Ca contents than the amphibole typical of mantle xenoliths. What is unexpected is the high Si content of the amphibole in the MARID suite (Table 4). The reason for this characteristic is perhaps to be found in the composition of the coexisting minerals, two of which are devoid of silica completely, but a more likely explanation is that the silica content is dictated by the high proportion of Na and K, and the extreme paucity in Al. Note that the coexisting diopside also is poor in Al, and some of the compositions of phlogopite are deficient in ^{141}Al (Dawson and Smith 1977).

Potassian richterite and “potassic richterite” are the dominant amphiboles documented in the groundmass of the OPRK facies of the Aries micaceous kimberlite, in the central Kimberley Basin, Western Australia (Downes et al. 2006). Their compositions (Table 4, columns 5–7) thus resemble the MARID amphibole, but the level of Ti is significantly greater, up to 0.9 *apfu*, a reflection of the “lamproitic” tendencies of this group-2 kimberlite. The crystals of groundmass amphibole coarsen locally into “segregations” of a more strongly alkaline amphibole like magnesio-arfvedsonite (Table 4, column 8). In the opinion of Downes et al. (2006), the kimberlitic magma at Aries fractionally crystallized once it arrived in the crust, as recorded in patterns of growth zoning in macrocrystals of phlogopite, and it incorporated xenoliths of country-rock sandstone, which would certainly be yet another factor in explaining the formation of Si-rich amphiboles in a mantle-derived rock.

Table 4. Composition of K-rich amphiboles in the matrix of kimberlitic rocks.

	1	2	3	4	5	6	7	8
SiO ₂ wt%	54.2	54.5	54.1	53.4	54.47	53.46	54.03	52.82
TiO ₂	0.64	0.45	0.60	1.03	1.09	1.09	0.48	0.66
Al ₂ O ₃	1.05	0.72	1.41	1.71	1.78	2.15	0.36	0.05
Fe ₂ O ₃								
FeO	5.50	4.14	4.09	3.95	7.52	8.36	13.64	15.82
MnO	0.03	0.01	0.05	0.03	0.19	0.25	0.47	0.76
MgO	18.5	22.0	21.4	21.4	18.82	17.93	14.54	12.41
NiO	n.d.	n.d.	0.03	0.07				
CaO	6.76	5.00	6.84	7.18	6.23	6.24	3.78	2.23
Na ₂ O	3.24	4.68	3.72	2.83	5.84	5.74	5.51	6.58
K ₂ O	5.25	4.28	4.92	5.88	1.75	1.73	3.65	3.38
Cr ₂ O ₃	0.11	0.47	0.22	0.26	0.16	0.08	0.11	0.10
Nb ₂ O ₅					0.04	0.24	0.06	0.31
F					1.48	1.09	0.48	0.25
Total	95.3	96.3	97.4	97.7	99.35	98.37	97.10	95.37

Columns 1–4: Representative compositions of potassian richterite and “potassic-richterite” in the MARID suite of xenoliths (Dawson and Smith 1977, Table 3). 1: “Potassic-richterite,” sample BD1159, Bultfontein kimberlite. 2: Potassian richterite, sample BD1160, Bultfontein kimberlite. 3: Potassian richterite, sample BD1671, Bultfontein kimberlite. 4: “Potassic-richterite,” sample BD1778, Newlands kimberlite. Columns 5–8: K-rich amphiboles reported in the groundmass and segregations in the OPRK facies of the Aries type-2 micaceous kimberlite, central Kimberley Basin, western Australia (Downes et al. 2006, Table 2). 5: Potassian richterite, sample AN65–54.3 m, groundmass. 6: Potassian richterite, same sample, groundmass. 7: “Potassic-richterite,” same sample, segregation. 8: Magnesio-arfvedsonite, same sample, segregation. The name “potassic-richterite” is written with quotation marks because it has not yet been submitted to the CNMNC for ratification.

Lamproites, also high-*mg* mantle-derived rocks, are peralkaline, ultrapotassic, unusually enriched in incompatible elements, and typically amphibole-bearing. The reader should consult Mitchell and Bergman (1991) for details of the compositional spectrum of amphiboles found in rocks of the lamproitic clan. Considered here as an example are dike rocks exposed at Napoleon Bay, Baffin Island, Canada (Hogarth 1997). Coexisting with phlogopite, which may account for 40% of the rock volume and in which close to 10% of the *T* site may be occupied by Fe³⁺, are sparse phenocrysts of late, strikingly zoned K-rich arfvedsonitic amphibole (Fig. 7). Compositions are comparable in level of K to those from the MARID suite listed in Table 4, but the amphibole is much richer in Fe and Ti (attaining 8.2 wt% TiO₂) and much poorer in Mg and Ca. Figure 7 shows an amazing display of the evolving morphology of the phenocrysts, which reflects the rapidly changing composition of the interstitial melt with fractionation. Hogarth (1997) encountered apparent departures in stoichiometry in these amphiboles, and chose to account for these by proposing vacancies at the octahedral positions.

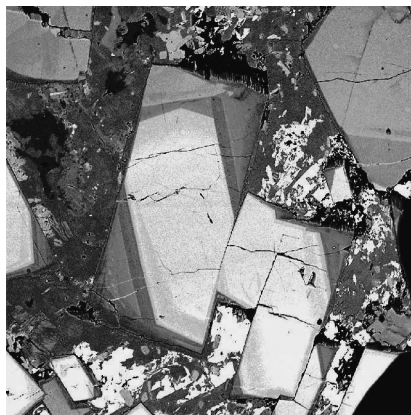


Figure 7. Strikingly zoned late arfvedsonitic amphibole, Napoleon Bay lamproite, Baffin Island, Canada. Width of field of view: 0.6 mm. Photo taken by Lang Shi and contributed by D.D. Hogarth.

I suspect that the shortfall in the octahedral positions may be due to Li, which may thus also have been involved in the episodes of metasomatism that preceded melting in the mantle. A laser-ablation ICP-MS study of such phenocrysts should be undertaken to fully document these unusual occurrences.

Amphiboles in carbonatites and associated metasomatic rocks

Amphibole-group minerals occur throughout the entire span of crystallization of carbonatite complexes, but are rare or absent in effusive carbonatites (Kapustin 1980; Hogarth 1989). The compositional spectrum is sparsely represented in the earliest manifestations of calcite-clinopyroxene carbonatite, reaches a maximum as the iron-enrichment trend develops, and persists in the post-carbonatite calcite-vein stage. The following generalizations are those of Samoylov (1977), and bring out the trends shown in the compositions listed in Table 5: 1) The early amphibole, commonly a calcic amphibole, either magnesiohastingsite or pargasite, is Al- and Ti-rich. 2) The middle-stage amphibole is poor in Al and richer in Na, in the range richterite – magnesio-arfvedsonite. With an increase in Fe content, there is evidence of $^{[4]}Fe^{3+}$, presumably owing to the paucity of Al at this stage, to the buildup in alkalis in the melt by fractionation of the early minerals, and to magmatic degassing. 3) At the end stage of crystallization, there is a shift to amphiboles in veins and dikes, trending toward the series riebeckite – magnesioriebeckite. Dolomite-bearing veins cutting fenitized metasedimentary rocks near Cantley, in southwestern Quebec, contain the new species fluoro-potassic-magnesio-arfvedsonite (Hogarth 2006).

A mantle-derived carbonatitic magma may assimilate and become contaminated as it ascends through crust. Such a situation occurs in the mineralogically complex calcite – amphibole – clinopyroxene rocks found as veins and schlieren in the Afrikanda complex, Kola Peninsula, Russia. Chakhmouradian and Zaitsev (2002) have documented the contamination of a parental

Table 5. Representative compositions of amphiboles in carbonatites.

	1	2	3	4	5	6	7	8
SiO ₂ wt%	37.81	48.38	52.14	55.86	54.52	53.69	54.37	54.08
TiO ₂	1.72	1.48	0.74	0.07	0.10	0.08	0.09	0.77
Al ₂ O ₃	17.33	6.39	4.03	0.10	0.43	0.76	0.81	0.26
Fe ₂ O ₃	4.52	5.56	6.71	7.12	5.13	9.05	12.63	18.24
FeO	4.04	9.82	6.40	0.00	0.55	5.26	1.42	6.00
MnO	0.11	0.16	0.33	0.07	0.07	0.06	0.13	0.13
MgO	16.36	13.07	15.52	20.42	21.16	15.72	16.64	10.01
CaO	12.90	6.55	4.49	3.32	5.07	1.64	0.52	0.35
Na ₂ O	3.47	6.74	7.31	5.88	6.17	8.60	8.96	6.44
K ₂ O	0.73	0.82	0.76	4.27	2.84	1.62	1.67	0.66
BaO	n.a.	n.a.	0.00	0.00	0.00	n.a.	0.05	n.a.
SrO	n.a.	n.a.	0.03	0.06	0.01	n.a.	0.00	n.a.
Cr ₂ O ₃	n.a.	n.a.	n.a.	n.a.	n.a.	0.03	0.00	n.a.
F	n.a.	0.41	0.41	2.05	1.70	n.a.	3.22	n.a.
Cl	n.a.	n.a.	n.a.	0.00	0.01	n.a.	0.00	n.a.
H ₂ O ⁺	n.a.	1.38	1.60	1.15	1.29	n.a.	0.57	n.a.
Total	100.23	100.70	100.03	99.51	98.33	96.51	99.72	100.20

The compositions are taken from the compilation of Hogarth (1989, Table 6.8). Columns 1–2: Stage-I crystallization. 1: Magnesio-hastingsite, Turii Peninsula, Russia. 2: Magnesioiktophorite, Turii Peninsula, Russia. Columns 3–5: Stage-II crystallization. 3: Richterite, Iron Hill carbonatite, Colorado. 4–5: “Potassic-richterite,” core and rim of crystal, Gatineau, Quebec. Columns 6–7: Stage-III crystallization. 6: Magnesio-arfvedsonite, Argor carbonatite, Ontario. 7: Fluoro-magnesio-arfvedsonite, Gatineau, Quebec. 8: Post-carbonatite stage, Magnesioriebeckite, Turii Peninsula, Russia.

carbonatite in silica and alkalis. Magnesiohastingsite enriched in K (ca. 0.20 *apfu*) and Ti (ca. 0.15 *apfu*) is among the earliest minerals to form from the resulting "silicocarbonatite." The occurrence of sodic-calcic amphiboles like richterite and magnesiokatophorite, possibly containing $^{44}\text{Fe}^{3+}$ along the rim and cleavages of the magnesiohastingsite, suggests an autometasomatic reaction with a trapped Na-enriched fluid. Separation of the fluid phase and extensive fracturing of the rock were attributed to decompression of the ascending carbonatitic mush.

Associated with carbonatites are fenites, which typically represent modified wallrocks in the exocontact that have equilibrated mineralogically with the alkali-rich fluid given off by the intrusive carbonatite body. However, the intrusion of a carbonatitic magma commonly is associated with intrusion of a coeval silicate magma, which also may give off an alkaline orthomagmatic fluid out of equilibrium with its surroundings. But the juxtaposition of the solid products of an immiscible pair of magmas forced to equilibrate at the deuteric stage with a common aggressive fluid leads to the development of fenitized assemblages in the silicate assemblage, by what could be called "auto-fenitization." To complicate matters, the fenites so produced can become rheomorphic, i.e., the new assemblage can remelt, which erases traces of its complex antecedence. Fenites are difficult rocks to study, and thus remain poorly studied. They likely are of primordial importance in the middle and lower crust in areas of active extension (Martin 2006). In theory at least, amphibole-group minerals would seem well placed to record the complex interplay between igneous and metasomatic processes.

In this sense, the amphibole mineralogy of classical fenites has been investigated, e.g., by Sutherland (1969), but those compositions are based on partial analytical results only. Morogan and Woolley (1988) found amphiboles to be prominent in almost all exposures of fenitized granitic gneiss around the Neoproterozoic Alnö carbonatite complex, in Sweden, but especially adjacent to the ijolitic rocks. The amphiboles run from richterite \pm eckermannite to magnesioarfvedsonite (or to the F-dominant analogs?), like in an igneous series, but curiously shifted in the direction of excess Si + Na + K in the more silicic amphiboles, with up to 8.2 *apfu*, beyond the maximum of 8.0 *apfu* allowed (Morogan and Woolley 1988, Fig. 2; cf. Sutherland 1969). The same phenomenon occurs in magnesio-arfvedsonite in the low- and medium-grade fenitized granitic gneiss surrounding the Fen carbonatite, in southern Norway (Kresten and Morogan 1986). In view of efforts to choose well-matched standards in their electron-microprobe work, Morogan and Woolley (1988) raised the possibility of chain-width disorder in such metasomatic magnesio-arfvedsonite, but a more likely cause would seem to be the involvement of Li in the metasomatic processes. The grade of fenitization (i.e., position in a thermal gradient) is not correlated with Ca content or *mg* value of the amphibole; rather, the composition of the precursor presumably is here the most important variable governing amphibole mineralogy.

The carbonatite at Alnö is closely associated with a slightly older ijolite - nepheline syenite suite. Skelton et al. (2007) concluded, on the basis of mass-balance relationships and stable isotope values, that most silicate phases now found in the carbonatite result from assimilation of alkali-metasomatized ijolite. In other words, the amphibole mineralogy of carbonatites may well be pseudo-igneous, with the amphibole overprinted by a potent fluid phase prior to incorporation in the very fluid carbonate melt. Much remains to be done to unravel these cases of complex superposition of igneous and metasomatic phenomena, and the attributes of the amphibole so developed would seem to be fertile ground for detailed studies.

On a related theme, but in a thermal gradient that is presumably not as steep as at Alnö, and where the magma is benmoreitic rather than carbonatitic, Gianfagna and Oberti (2001) have documented the development of fluoro-edenite in prismatic and fibrous habits at Monte Calvario, Biancavilla, on the southwestern flank of Mount Etna, in Italy. The metasomatic amphibole fills fractures and cavities in brecciated and altered benmoreitic lavas that crystallized from batches of derivative magma intruded in the flanks of the volcano, which dominantly erupts hawaiitic magma. The crystal-chemical formula of the holotype prismatic fluoro-edenite, $\text{A}(\text{Na}_{0.56}\text{K}_{0.15})$

${}^B(\text{Ca}_{1.62}\text{Na}_{0.30}\text{Mg}_{0.03}\text{Mn}_{0.05})$ ${}^C(\text{Mg}_{4.68}\text{Fe}^{2+}_{0.19}\text{Fe}^{3+}_{0.10}\text{Ti}_{0.03})$ ${}^T(\text{Si}_{7.42}\text{Al}_{0.58})$ O_{22} $\text{O}^{(3)}(\text{F}_{1.98}\text{Cl}_{0.02})_2$, illustrates well the elements that emanate from the subjacent benmoreitic melt, moving in fluids migrating along conduits in the flank area. There is no doubt that H_2O also was present in the slightly alkaline orthomagmatic fluid, but it is fluoro-edenite, being less soluble than edenite, that precipitates directly from the fluid as it cools. The porous rock has been widely used in the construction industry in the area; unfortunately, the fibrous fluoro-edenite, which is slightly poorer in ${}^A\text{Na}$, slightly richer in both Fe^{2+} and Fe^{3+} , and bearing ${}^{16}\text{Al}$ compared to the prismatic variety (cf. the formula shown above; Gianfagna et al. 2007), is carcinogenic, and responsible for an anomalously high incidence of mesothelioma in the area. Mazzotti-Tagliani (2007) has described the apparent incipient replacement of augite in the brecciated benmoreite by fluoro-edenite, and the presence of bulk compositions that are apparently intermediate between fluoro-edenite and augite, which here also opens the door to the possibility of intercalations of pyroxene modules. The propensity of the metasomatic amphiboles to form fibers instead of cleavage fragments may in fact result from the presence of such chain-width discontinuities, a hypothesis that must be tested in future TEM studies.

The amphibole mineralogy of “anatectic pseudocarbonatites”

Mitchell (2005) has made a plea to restrict the term *carbonatite* to products of mantle-derived carbonate-dominant magmas that intruded the crust. But how does one deal with igneous rocks found in the crust that arose by the anatexis of marble and associated evaporitic sequences? Mitchell favors term *pseudocarbonatite*, which is not entirely satisfactory, because such instances of anatectic marble seem to accompany episodes of mantle-related alkali metasomatism in deep granulite-facies rocks in areas of crustal extension. Thus they could well be associated with *bona fide* carbonatites. The pseudocarbonatites are exposed as dike rocks in areas where deep crust has been exhumed, e.g., in the Bancroft terrane of southwestern Ontario, Canada. Perhaps owing to assimilation of the surrounding crust, as encountered at Alnö (see above), these pseudocarbonatites have formed from “silicocarbonatitic” melts that crystallize or otherwise incorporate strikingly euhedral and coarse amphibole-group minerals, among other silicates. The crystals generally are homogeneous, and constitute phenocrysts that are flow-aligned in the carbonate matrix (Fig. 8). Dissolution of the calcite matrix has in some places produced loose accumulations of elongate prismatic crystals of fluorrichterite (Fig. 9), much to collectors’ delight. As the crystals grew in the carbonate melt, they pushed aside (and incorporated, to some extent) other minerals like apatite prisms and flakes of fluorophlogopite also growing in the carbonate melt. The resulting microtopography of the surface may at first glance suggest selective resorption, but the context is one of relatively rapid growth, possibly as a result of loss of a fluid phase rather than a thermal quench; the depth of emplacement of such dikes was probably 25 km or so, as inferred on the basis of geobarometric assessments in the area.

At the Bear Lake diggings, Hawthorne et al. (2006) have characterized structurally three blocky crystals exceeding 5 cm across: richterite (*mg* 0.95) and potassian fluoromagnesiokatophorite (*mg* 0.69, 0.71). On the basis of this preliminary sampling, it seems likely that the crystals, which grew in close proximity in the same melt, are not in equilibrium, perhaps because the pseudocarbonatitic melt itself was highly heterogeneous, perhaps because it cooled quickly. A sign of rapid growth is the incorporation in the amphibole phenocrysts of small crystals of every other phase (e.g., sodian augite, phlogopite, alkali feldspar, titanite, apatite) that was forming in the carbonate melt at that time. The rocks formed in the closing, distensive stage of the Grenville collision-related orogeny, between 1040 and 1070 million years ago, and no post-crystallization modifications took place that could have induced recrystallization in these assemblages. Similar dikes of amphibole-carrying pseudocarbonatites are encountered in southern Madagascar and formerly contiguous areas of East Africa, India and Sri Lanka, where they mark the distensive waning stages of the Pan-African orogenic cycle. These anatectic rocks are in fact a newly recognized category of igneous rock, which obviously requires further documentation.



Figure 8. Flow-aligned prisms of fluororichterite in a calcite matrix, “pseudocarbonatite”, Greenmantle locality, Wilberforce, Ontario, Canada [www.mineraltours.net]. Snow-covered maple leaves at top provide an idea of scale.

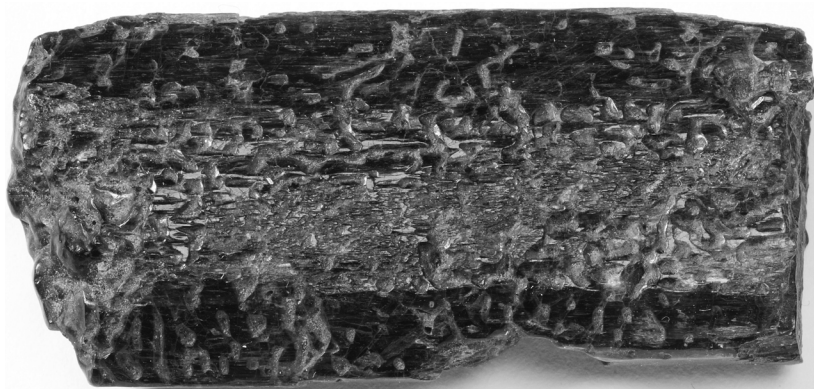


Figure 9. Surface topography of a prism of fluororichterite, naturally liberated from its “pseudocarbonatitic” matrix, Greenmantle locality, Wilberforce, Ontario, Canada [www.mineraltours.net]. The crystals seem corroded, but are interpreted to have pushed aside (and partly incorporated) other minerals that had nucleated in the carbonate melt.

AMPHIBOLES IN IGNEOUS ROCKS ASSOCIATED WITH COMPRESSION IN THE CRUST

Mantle-derived magmas that are regionally associated with the subduction of hydrated oceanic crust are typically calc-alkaline. Although basaltic magmas do occur, the dominant rock-type is intermediate in silica content, quartz-normative, and relatively calcic and aluminous. Calcic amphiboles are considered to play a crucial role in the magmatic evolution of these suites, but commonly are absent in the volcanic products, not because the magmas are poor in dissolved H_2O , but rather because of the shape the field of stability of the primary amphibole.

It will only form from the melt beyond the depth of intersection of the positively sloping curve marking the upper stability of the amphibole in P-T space and the negatively sloping solidus of the H₂O-bearing intermediate magma. The Na content of the system exerts a first-order control on the upper stability of the calcic amphibole (Cawthorn 1976), pargasite being inherently more stable than magnesiohornblende of equivalent *mg* value. In view of the high viscosity of these intermediate magmas, and thus their slow ascent through the crust, it is not unusual to find andesites that contain pyroxene-group minerals as the only primary mafic phases, or at most, vestiges of a primary amphibole that became destabilized after it left its field of stability upon decompression. It seems clear that such a destabilization reaction may well contribute directly to the explosivity of an eruption.

As the relevant magmas form in the mantle wedge above the subduction zone, and in the superjacent crust, an important attribute is their relatively high content of dissolved H₂O and their relatively high fugacity of oxygen. For this reason, a calcic amphibole and magnetite are among the primary minerals that will cocrystallize and fractionate from the magma at depth, in the mantle wedge, or on the way toward the surface. Both minerals accommodate both ferrous and ferric iron, and effectively prevent the development of an iron-enrichment trend. Anderson (1980) has stressed the importance of another factor in this matter, the likelihood of an olivine-melt reaction relationship to produce a calcic amphibole in a rising mafic magma. Such a reaction will temper the tendency of Fe to build up over Mg. As a result of these two phenomena, the trend of a typical calc-alkaline suite of derivative magmas is oriented approximately perpendicular to the Fe-Mg sideline in an AFM diagram.

As a corollary of the importance of H₂O in the system, the calc-alkaline magmas typically show the effects of degassing, which influences the pattern of compositional zoning in the resulting amphibole. This aspect will be reviewed below. Also, the rocks can be expected to undergo a deuteric overprint that yields secondary amphiboles at the subsolidus stage. To sort out which amphibole is primary and which is of deuteric origin in an assemblage is usually straightforward on petrographic grounds, but to distinguish high-temperature subsolidus amphiboles from primary amphiboles likely will be more challenging.

The amphibole mineralogy of arc-related rocks

Calcic amphiboles play a key role in the petrogenesis of calc-alkaline suites. Table 6 shows compositions of calcic amphibole from relatively primitive members of arc-related igneous suites (columns 1 and 2). The amphibole commonly is found trapped in plagioclase, and spans the compositional range from edenite to pargasite to magnesiohornblende and ferrohornblende. The latter are found to crystallize with unusually calcic plagioclase from high-Al "basaltic" magmas containing above 51% SiO₂ and 2–4% dissolved H₂O, probably in the temperature interval 1080°–960 °C (Anderson 1980). Owing to the well-established K-*h* relationship developed perpendicular to the trend of an arc, especially a continental arc, primitive calc-alkaline magmas may vary in K content from 0.2 to more than 2 wt% K₂O, and this certainly will be reflected in the level of K in the primary amphibole (cf. Table 6).

The plutonic rocks that form from such calc-alkaline magmas commonly contain strongly zoned crystals of clin amphibole in which the growth zoning, from a magnesiohornblende core to an actinolite rim, is interpreted to mark the progressive oxidation of the magmatic environment. Kawakatsu and Yamaguchi (1987) documented five distinct zones in the crystals of such amphibole: 1) a brownish core of magnesiohornblende, magnesiohastingsite or edenite, 2) a greenish zone of magnesiohornblende, 3) a green oscillatory zone of magnesiohornblende to actinolite, 4) a uniform zone of actinolite, and 5) a dark green rim of magnesiohornblende to actinolite. The outward zoning is rather patchy and not concentric. Compositions of the core, oscillatory zone and rim are shown in columns 3–5 of Table 6. Overall, the authors found that the *mg* value increases outward. Such a trend, the reverse of that expected in a scenario of closed-system fractional crystallization, probably arises because the magma vesiculates, the H₂O in

Table 6. Composition of calcic amphiboles in calc-alkaline plutonic rocks.

	1	2	3	4	5	6	7	8
SiO ₂ wt%	46.87	42.23	44.78	51.79	49.17	50.36	48.32	48.92
TiO ₂	1.93	2.49	1.74	0.32	0.03	0.72	1.43	1.21
Al ₂ O ₃	7.16	12.23	8.91	3.22	4.68	5.45	6.43	5.88
Fe ₂ O ₃			2.79	2.06	2.45	2.71	5.45	6.50
FeO	6.51	7.60	12.69	10.43	16.21	9.96	7.90	7.79
MnO	0.17	0.08	0.51	0.49	0.44	0.36	0.13	0.17
MgO	18.42	16.44	12.00	15.61	11.13	15.03	14.82	14.32
CaO	11.09	11.78	11.73	12.53	12.34	12.36	11.99	11.37
Na ₂ O	2.69	3.12	1.42	0.52	0.61	0.69	0.99	1.20
K ₂ O	1.18	1.22	0.58	0.21	0.25	0.44	0.67	0.71
F			0.12	0.09	0.17			0.27
Total	96.02	97.25	97.27	97.27	97.48	100.17	99.80	99.78

Columns 1 and 2: edenite intergrown with augite in calc-alkaline basalt RCDS-197, Mt. Hood area, Oregon, and relict pargasite in absarokite DS90-47, Mt. St. Helens area, Washington (Conrey et al. 1997, Table 6), respectively. Columns 3, 4 and 5: magnesiohornblende core, green oscillatory zone and actinolite rim of zoned crystal, quartz diorite, Daito-Yokota area, San-in belt, southwestern Japan (Kawakatsu and Yamaguchi 1987, Table 1). Column 6: Magnesiohornblende, tonalite, Aregos region, central Portugal. 7 and 8: Magnesiohornblende, apinitite suite, Glen Tilt, Perthshire, Scotland, U.K. Compositions in columns 6-8 are taken from Deer et al. (1997, Table 11).

the bubbles dissociates, the H₂ leaves the system preferentially, and magnetite is precipitated, leaving the magma to coprecipitate a silicate assemblage relatively (and increasingly) depleted in Fe. The actinolite rim is considered an overgrowth and a product of a “back-reaction” between the magmatic amphibole and the fluid released by vesiculation. There results a patchy development of actinolite in the original crystal. The case study documented by Kawakatsu and Yamaguchi (1987) shows the close inter-relationship between magmatic and deuteric products of crystallization in relatively shallow calc-alkaline plutons of dioritic bulk-composition.

In the dacite erupted in 1991–1995 from the Unzen volcano, Shibamara Peninsula, Kyushu, southwestern Japan, zoning characteristics of both plagioclase and magnesiohornblende phenocrysts show evidence of the mixing of magmas. The magnesiohornblende phenocrysts typically are resorbed (Sato et al. 1999), and the groundmass contains instead 1–2 vol% of prismatic pargasite of higher *mg* value, higher contents of Na and Al, and lower content of Cl. Degassing of the magma at a depth greater than 3 km is inferred to have preceded and to have caused the crystallization of the pargasite at about 880 °C.

The much more restricted range of primary compositions of amphiboles in calc-alkaline suites, even those having shoshonitic tendencies (compared to those crystallizing from magmas accompanying crustal extension) has allowed a more complete assessment of the conditions of crystallization of calcic amphiboles using geothermometry and geobarometry. For example, Féménias et al. (2006) have focused on the amphibole mineralogy of the Motru dike swarm in the South Carpathian Mountains of Romania. All amphiboles are calcic, even though the rock types range from basaltic andesite to rhyolite. Core compositions of amphibole phenocrysts from basaltic andesites, andesites, and trachyandesites contain low Si and relatively high Na + K values, and correspond to magnesiohastingsite, pargasite and kaersutite, with minor edenite. Core compositions of amphibole phenocrysts in rhyolites and dacites are richer in Si and poorer in Na + K, as are rim compositions in andesites, and correspond to magnesiohornblende. Actinolite is assigned a deuteric origin. The growth zoning displayed by these crystals is of two types, firstly, concentric and regular, and secondly, cross-cutting and associated with resorption and cracks, some penetrating to the core of a crystal. All crystals display a complex interplay of both types.

The pressure of crystallization is directly related to the Al content of the calcic amphibole; many calibrations have been published, but it is important to remember the limitations of the method, especially in terms of the activity of SiO_2 . The nature of the coexisting minerals also must enter into the evaluation. The phenomenon of increasing incorporation of Al ultimately reflects, in larger part, the progressive destabilization of plagioclase as the mantle is approached. The temperature of amphibole growth has been assessed using the Ti content of the calcic amphibole. Estimates of the two parameters for the suite are presented in Figure 5 of Féménias et al. (2006), here reproduced as Figure 10. In all rock types found in the Motru dike swarm, calcic amphibole phenocrysts are shown to have equilibrated at a nearly constant pressure, about 0.6 ± 0.1 GPa, at a temperature of crystallization ranging from 1000–900 °C for the basaltic andesites to 700–600 °C for the dacites. The amphibole in the rhyolites reflect a continuous range of P - T conditions from 700 °C, 6 GPa to 600 °C, 0.1 GPa. In the rhyolites, therefore, there is evidence preserved in the strikingly zoned amphibole phenocrysts for growth at a mid-crust level followed by further growth developed during magma ascent. The approach used by Féménias et al. (2006) is a promising one, especially if combined with refined estimates of $f(\text{O}_2)$ and isotopic indicators of contamination in the rising magma.

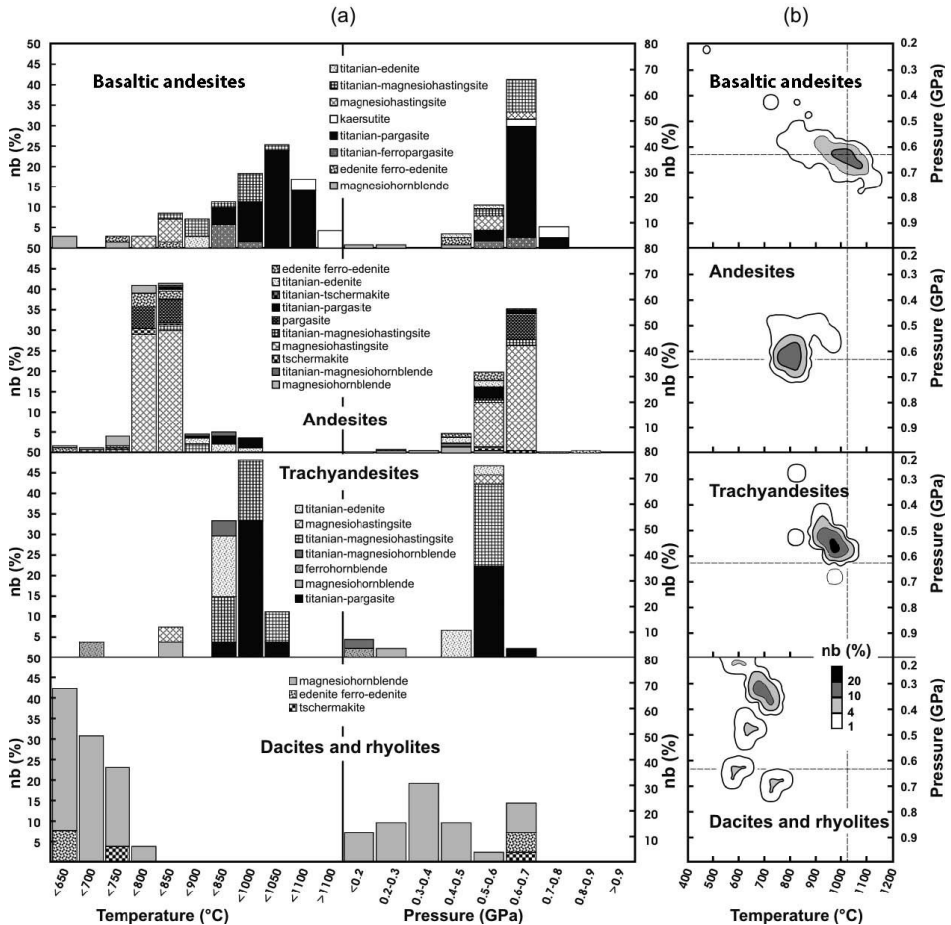


Figure 10. Inferred temperature and pressure of crystallization of the calcic amphibole in the range of magmas employed in the Motru dike swarm, southern Carpathians, Romania (Féménias et al. 2006, Fig. 5).

Although there are many calibrations of the Al-in-amphibole geobarometer, how does the inferred pressure of crystallization compare with carefully executed geobarometry based on metamorphic assemblages in the contact aureole? The calcic amphibole of the Nelson calc-alkaline batholith, in British Columbia, indicates a P of crystallization of 4.8–6.4 kbar using the Johnston and Rutherford (1989) calibration, but 3.3–5.5 kbar using the Anderson and Smith (1995) calibration. Many samples yield pressures considerably above those monitored in the aureole pressure (3–4 kbar: Pattison and Vogl 2005, Fig. 13), and rather sharp differences in P are evident in closely spaced samples of the igneous suite. Pattison and Vogl (2005) documented evidence of tilting of the 40-km-wide batholith on the basis on east–west geobarometric comparisons in the contact-metamorphic assemblages, but no evidence of such tilting is picked up in the amphibole mineralogy of the batholith itself. The message seems clear that caution is required to properly interpret the pressure estimates indicated by the magmatic amphibole in calc-alkaline suites; growth of the amphibole presumably occurred as the magmas were in transit.

Amphibole-rich clots in calc-alkaline granitic rocks

As Castro and Stephens (1992) have pointed out, melanocratic aggregates of amphibole are remarkably common in calc-alkaline granitic rocks. Do these represent clots of restite minerals, fragments of an amphibole-rich cumulate, mafic remnants of mingled magmas, disaggregated enclaves or pseudomorphs of precursor crystals of primary pyroxene? These authors have examined textural and compositional evidence. The interior of such clots consists of a polymineralic granoblastic aggregate of zoned grains. Each grain consists of an actinolitic core surrounded by a rim of more aluminous calcic amphibole (magnesiohornblende) associated with plagioclase and biotite, the magnesiohornblende being similar in composition to that of idiomorphic amphibole in the granodioritic rocks away from the clots (Fig. 11). Representative compositions of the juxtaposed amphiboles in clots from the middle Silurian Strontian I-type pluton, in the Caledonian of Scotland, are listed in Table 7; in columns 1–3 are compositions of the granoblastic actinolite in the core of the clots, in columns 4–6, compositions of the magnesiohornblende typical of the rim of the clots, and in columns 7 and 8, compositions of the idiomorphic magnesiohornblende away from the clots.

The presence of a more silica-rich, less aluminous calcic amphibole like actinolite in the core, giving way to a less silica-rich, more aluminous calcic amphibole like magnesiohornblende in the rim, is the reverse of what is expected as a magma crystallizes, according to experimental results and common experience. Castro and Stephens (1992) concluded that the core amphibole is in fact a pseudomorph after a primary pyroxene, which is expected to be relatively poor in Al. It is not unreasonable to expect that before the magma had achieved much of a buildup in H_2O , a pyroxene-group mineral was on the liquidus. Once saturation in H_2O had been achieved, it is likely that the dissociation of the H_2O , combined with the extraordinary mobility of H_2 , induced the destabilization of this primary pyroxene to give a pseudomorph actinolite. The reaction may have occurred once the pyroxene was armored by the magnesiohornblende-dominant outer assemblage, which is entirely consistent with crystallization from the magma. The reaction may also have occurred as a result of a direct discontinuous reaction of the pyroxene with the ambient melt to give actinolitic amphibole, although I consider that hypothesis less likely than the first. The ultimate origin of the pyroxene precursor (primocryst, restite after melting at the source, fragment of cumulate, or debris from mingling) is left open, and presumably needs to be assessed case by case.

Stephens (2001) has taken the investigation of clots in the Strontian pluton one step further by examining rare-earth-element (REE) distributions in the juxtaposed amphiboles. As in the earlier study, the idiomorphic magnesiohornblende is closely consistent in REE profile with that expected to have crystallized from the melt, but the actinolite in the clot interiors is not. The clot interiors contain a significantly lower level of the REE than the idiomorphic magnesiohornblende, and are better modeled in terms of a restitic assemblage that contains

Figure 11. Sketch of a typical clot in the Strontian calc-alkaline pluton, one of the Caledonian Newer Granites, northern Scotland. The grains of amphibole have been schematically shaded to highlight the compositional difference between clot interiors and clot exteriors. There are compositional variations within single grains in the clot interior. The clot exterior consists of amphibole + minor plagioclase and biotite that are identical to those of the host granite. In contrast, the clot interior contains only amphibole in a polycrystalline aggregate of granoblastic grains. The rim has an aluminous composition identical to what is found in the clot exterior (host rock), whereas the core zone consists of an actinolitic amphibole considered formed at the expense of a clinopyroxene precursor. [Reprinted by permission of the Geological Society of Australia from Stephens (2001).]

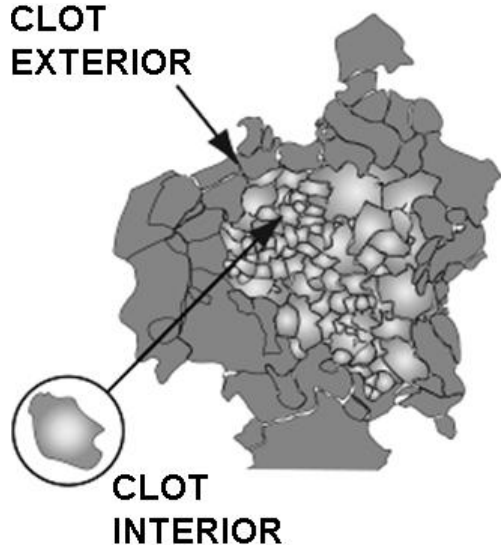


Table 7. Composition of calcic amphiboles representative of the ubiquitous clots in calc-alkaline batholiths.

	1	2	3	4	5	6	7	8
SiO ₂ wt%	52.99	55.02	55.38	48.49	50.94	51.84	48.00	47.78
TiO ₂	0.22	0.10	0.10	0.75	0.46	0.50	1.06	1.04
Al ₂ O ₃	2.72	1.38	1.32	5.89	4.42	3.73	6.66	6.62
Cr ₂ O ₃	—	—	0.03	0.05	0.10	0.07	0.06	0.01
Fe ₂ O ₃	4.61	3.80	3.03	4.92	4.73	3.32	4.42	5.08
FeO	6.88	6.49	6.18	9.19	8.01	7.79	10.70	9.54
MnO	0.35	0.38	0.20	0.36	0.28	0.32	0.40	0.29
MgO	16.64	17.69	18.68	14.27	15.50	16.64	13.31	13.60
NiO	—	0.14	0.09	0.02	0.07	0.08	0.04	—
CaO	11.73	11.85	12.44	11.67	11.76	12.24	11.71	11.16
Na ₂ O	0.56	0.35	0.32	1.21	0.82	0.74	1.19	1.44
K ₂ O	0.22	0.09	0.09	0.58	0.31	0.34	0.68	0.76
Total	96.92	97.28	97.84	97.39	97.39	97.62	98.22	97.31

Columns 1–2: actinolite, core of clot in an enclave, SR6. Column 3: actinolite, core of clot in a hybrid rock, SR5. Column 4–5: magnesiohornblende, rim of clot in an enclave, SR6. Column 6: magnesiohornblende, rim of clot in a hybrid rock, SR5. Column 7: idiomorphic magnesiohornblende in tonalite, SR4. Column 8: idiomorphic magnesiohornblende in enclave, SR2. These compositions are taken from Table 2 of Castro and Stephens (1992), and pertain to the Strontian pluton, in the Caledonides of Scotland.

various proportions of clinopyroxene, plagioclase and calcic amphibole. Stephens (2001, Fig. 8) has illustrated and summarized the four stages of clot formation; his cartoon of stage 4 is reproduced here as Figure 11. Sial et al. (1998) have documented the same juxtaposition of amphiboles in clots in Neoproterozoic calc-alkaline plutons in the Borborema Province, northeastern Brazil, and arrived at the same conclusion about the presence of the non-magmatic actinolite in the core of the clots. Isotopic evidence is adduced to support the view that the actinolite-rich core in the clots represents fragments of the altered basaltic source of the I-type magma (now recrystallized to amphibolite) or vestiges of restite left after the melting process.

The question of appinites

There is a voluminous literature on appinite complexes, well studied in the Caledonian plutons of Scotland. At their type locality, 30 km west of the Strontian pluton mentioned above, the intrusive pipes consist of an explosion breccia associated with porphyritic diorite and appinite, a heterogeneous rock containing an abundance (up to 60–70 vol%) of large phenocrysts of magnesiohornblende (Table 6, columns 7, 8), locally with rhythmic overgrowths of both tremolite and actinolite deposited from the gas phase. The explosive activity is attributed to exsolution of a gas phase that rose ahead of the volatile-rich shoshonitic magma, and accumulated below a structural trap, such as offered by an anticline of massive quartzite (Bowes et al. 1964; Bowes and Wright 1967). The primary crystals of magnesiohornblende have become visibly rounded due to dissolution in the gas phase prior to deposition of the rhythmic overgrowths. The Scottish examples are considered subvolcanic, but the main stage of crystallization was not a pyroxene-dominant assemblage, as would be expected from the location of the solidus of this H₂O-rich magma were crystallization shallow, but clearly to a hornblende-rich assemblage. Crystallization thus is attributed to a mid-crustal depth, with the last stage of emplacement in an environment of fluidization.

Parallels have been established with the durbachite suite exposed in the Bohemian Massif of the Central European Hercynides, in the Czech Republic, another well-studied area of shoshonitic magmatism. “Hornblendite” is a prominent rock-type in these igneous complexes; in the Milevsko complex, durbachite, a melanocratic K-rich syenite, contains magnesiohornblende with a *mg* value equal to 0.75 (Bowes and Košler 1993). Magmas of shoshonitic affinity here, as in Scotland, are a result of the interaction of an asthenospheric-mantle-derived basic magma with the crust, to judge from the presence of measurable amounts of Ni and Cr in the primary amphibole. Detailed studies of the amphibole in these suites likely hold the key to understanding the role of alkali metasomatism at the source in the mantle, upon the ultimate destabilization of phlogopite deep in the subduction system, and of contamination, once the highly potassic magmas had entered the crust.

Amphibole-dominant pegmatites in Alaskan-Uralian-type complexes

Remarkable “hornblende”-anorthite pegmatites are exposed in the Alaskan-Uralian-type complexes of the world. This remains a poorly known and characterized subset of calc-alkaline magmatic suites that commonly are emplaced as concentrically zoned plutons containing everything from ultramafic members to rather evolved syenites. Because of their potential for platinum-group mineralization, these complexes are prospective targets in mineral-exploration programs; on the other hand, knowledge about their silicate mineralogy lags far behind. Irvine (1974) has described the classic association at Duke Island, in southeastern Alaska; dunite and wehrlite at the core are followed by olivine clinopyroxenite and “hornblende”-magnetite clinopyroxenite toward the periphery. The pegmatitic “hornblendites” are developed along the contact between the complex and the envelope of gabbroic rocks. The two compositions of amphibole from pegmatites reported by Irvine (1974, Table 12) consist of pargasite of *mg* value equal to 0.70 and 0.61, respectively. The coarse crystals of pargasite, some longer than one m, are typically oriented normal to the strike of the pegmatite bodies and tend to widen away from the contact. The pegmatites formed at the expense of an ankaramitic rest-liquid (Irvine 1974, Table 19) squeezed out of interstices of an olivine clinopyroxenite cumulate.

In Table 8, I have transcribed the two compositions of pargasite published by Irvine (1974) and two more from the Duke Island suite provided by Joyashish Thakurta (pers. commun., 2007), and compare these with the composition of an ankaramitic rock from the Takla volcanic suite, Aiken Lake, British Columbia, with which Irvine chose to illustrate the type of melt extracted from the interstices of the cumulates. In this context too, therefore, the amphibole crudely resembles a magma composition. This fact undoubtedly favored the formation of gigantic crystals. The coexisting plagioclase in one such dike has a very calcic composition,

Table 8. Composition of calcic amphibole in the “hornblendite” pegmatites at Duke Island, Alaska, and two Russian localities, compared to the ankaramitic melt filter-pressed out of the clinopyroxenite cumulate series.

	1	2	3	4	5	6	7	8
SiO ₂ wt%	41.20	42.28	48.1	40.94	40.88	39.28	38.18	40.2
TiO ₂	1.42	1.38	0.6	1.64	1.72	3.15	2.94	2.01
Al ₂ O ₃	16.16	14.56	11.4	14.96	14.98	11.74	11.87	13.84
Fe ₂ O ₃	4.12	3.92	2.7			4.67		5.13
FeO	7.04	9.51	7.2	12.60	12.41	10.48	15.66	7.87
MnO	0.04	0.33	0.2	0.12	0.22	0.23	0.48	0.1
MgO	13.96	11.63	15.3	13.21	12.78	12.35	10.81	14.61
CaO	12.63	12.26	10.5	11.83	11.85	11.28	11.67	12.22
Na ₂ O	2.27	2.53	2.2	1.98	2.18	2.45	2.92	0.84
K ₂ O	0.62	0.41	1.5	0.88	0.70	1.39	1.43	0.76
P ₂ O ₅	0.03	tr.	0.2					
F				0.00	0.06			
Total	99.49	98.81	100.0	98.16	97.78	97.02	95.96	97.58

Column 1: pargasite from pegmatitic hornblendite (field term), north shore of Kelp Island, Duke Island area. 2: pargasite from hornblende-anorthite pegmatite (field term) in the Judd Harbor ultramafic complex. 3: porphyritic olivine-augite basalt (ankaramite), Takla volcanic suite, Aiken Lake, British Columbia. The data in columns 1–3 are taken from Irvine (1974, Tables 12, 19). 4: pargasite from pegmatitic hornblendite (field term), sample DK05-3-22 Hall Cove, Duke Island. 5: pargasite from hornblende-anorthite pegmatite (field term), sample DK05-JH-7, Judd Harbor ultramafic complex. The data in columns 4 and 5 were contributed by Joyashish Thakurta, Ph.D. candidate, Indiana University (pers. commun., 2007). Both compositions were recalculated on the basis of 23 oxygen atoms. Columns 5 and 6: pargasite in pyroxenite dikes, Konder alkaline-ultrabasic complex, Aldan Shield, Russia (Nekrasov et al. 1994). 8: pargasite in hornblendite (field term), Svetloborskiy Uralian-type complex, Urals, Russia (Ivanov 1997).

An_{92.5}, usually interpreted to indicate an unusually “wet” calc-alkaline mafic melt. On the basis of $\delta^{18}\text{O}$ values for the clinopyroxene, between 5 and 6‰, there is no evidence for the assimilation of crustal rocks at Duke Island (Thakurta et al. 2006). Also reported in Table 8 are compositions of pargasite from pyroxenite dikes of the Konder alkaline-ultrabasic complex, Aldan Shield, Russia, which has affinities to an Alaskan-Uralian-type complex, and from hornblendite (field term) in the Svetloborskiy Uralian-type complex, Urals, Russia. Much remains to be done to characterize the conditions of crystallization of calcic amphibole in such H₂O-rich mafic to ultramafic melts.

Note that patches of coarse-grained “hornblendite” are encountered in the inner parts of hornblende gabbro bodies in the Sanabria appinite-migmatite complex, in Spain (Castro et al. 2003). Their origin may have points of similarity with the pegmatites of the Alaskan-Uralian-type complexes. In the Spanish rocks, the proportion of magnesiohornblende crystals may exceed 90 vol%. Such rocks also are encountered as dismembered blocks in massive diorite and monzodiorite.

The occurrence of two-amphibole pairs

So far in this review, the igneous amphiboles mentioned have largely been single species of primary amphiboles, and they have all been monoclinic amphiboles. What about two-amphibole pairs related by a solvus in orogenic igneous rocks (Table 9)? Yamaguchi (1985) has described intergrown homogeneous ferroan magnesiohornblende or ferro-actinolite and cummingtonite in the quartz dioritic upper portion of the Koyama pluton, in southwestern Japan. The two monoclinic amphiboles crystallized interstitially “in place of pyroxene from residual liquid trapped interstitially in the later stages of solidification of the rock.” The earlier-formed pyroxenes generally appear “corroded” in contact with the amphiboles, but the

Table 9. Composition of coexisting calcic and Mg–Fe–Mn amphibole in mafic cumulates, calc-alkaline suites in Japan and Sweden.

	1	2	3	4	5	6	7	8
SiO ₂ wt%	49.55	52.51	41.14	45.02	43.33	41.41	41.86	42.20
TiO ₂	0.35	0.11	0.03	0.72	0.00	0.04	0.02	0.05
Al ₂ O ₃	4.98	1.94	15.52	13.75	15.07	18.49	18.30	18.13
Fe ₂ O ₃	3.21							
FeO	15.16	23.99	9.73	9.40	10.12	12.45	12.64	12.17
MnO	0.37	0.76	0.16	0.19	0.25	0.26	0.23	0.30
MgO	12.27	14.41	16.14	16.31	16.11	20.83	21.23	20.60
CaO	10.64	3.43	11.10	10.64	10.60	0.98	0.88	1.16
Na ₂ O	0.74	0.28	2.73	2.27	2.59	2.78	2.69	2.66
K ₂ O	0.34	0.08	0.18	0.15	0.22	0.02	0.04	0.02
F			0.05			0.00	0.11	
Cl			0.11			0.02	0.04	
Total	97.61	97.51	96.90	98.45	98.29	97.28	98.04	97.29

Column 1: greenish iron-rich magnesiohornblende, coexisting with cummingtonite (column 2), quartz diorite of the zoned shallow Koyama calc-alkaline pluton, Susa, southwestern Japan (Yamaguchi 1985, Table 1). Column 3: oikocrystic magnesiohastingsite, amp8d. Columns 4–5: oikocrystic ferrotschermakite, amp36 and amp34, respectively. Columns 6–8: sodicgedrite, ged3d, ged2d and ged33, respectively. The compositions listed in columns 3–6 are all from thin section 96115, cut from the mesozonal Proterozoic Eriksberg gabbro, southern Sweden (Claeson and Meurer 2002, Table 1).

plagioclase crystals are euhedral. The *M*(4) site of the actinolite contains 0.1–0.2 *apfu* (Mg + Fe²⁺ + Mn), whereas in the coexisting cummingtonite, *M*(4) contains approximately 1.5 *apfu* (Mg + Fe²⁺ + Mn). The textural development of the two amphiboles (Yamaguchi 1985, Figs. 1A, B) indicates co-crystallization and development of composite grains in contact along a common (100) face. It thus seems clear that the solvus between a calcic and a Mg–Fe–Mn amphibole was an important feature in this instance. If the maximum pressure of freezing of the magma was indeed 1.5 kbar, it seems possible to invoke a solvus relationship developed in a pair of metastable amphiboles (i.e., the melt should have crystallized as a pyroxene – plagioclase assemblage).

What about the possibility of orthoamphibole – clinoamphibole pairs in igneous rocks? The very detailed description of a single thin section of a sodicgedrite-bearing troctolitic cumulate in the Eriksberg gabbro, in southern Sweden, by Claeson and Meurer (2002), raises an interesting question. Is the intercumulus sodicgedrite found there (three grains!) an incredibly rare example of a phenomenon, or is it rather widespread in such cumulate assemblages, but missed previously by others in cursory examinations? It is fair to claim that very little work has been done on cumulates formed from “wet” mafic magmas typical of calc-alkaline assemblages. The sample contains 46% plagioclase, 28% olivine, both surrounded by 20% intercumulus (oikocrystic) calcic amphibole, 4% orthopyroxene and 2% clinopyroxene (Fig. 12), and traces of accessory phases, including the sodicgedrite. In their petrographic dissection, Meurer and Claeson (2002) have shown that the oikocrystic clinoamphibole is highly variable in its trace-element content as a result of *in situ* fractional crystallization, compaction in the cumulus pile, and channelized flow of the last aliquot of melt.

Concerning the two coexisting amphiboles, no exsolution lamellae are found, such that both did crystallize from the melt, and then evidently “froze.” The clinoamphibole crystallized soon after the formation of the intercumulus augite, and was stabilized as the amount of dissolved H₂O rose in the melt. Meurer and Claeson (2002) attributed the appearance of the calcic amphibole to a reaction relationship involving hydrous mafic residual melt and the early-formed cumulus olivine and cumulus plagioclase, which both show a lobate morphology in contact with the

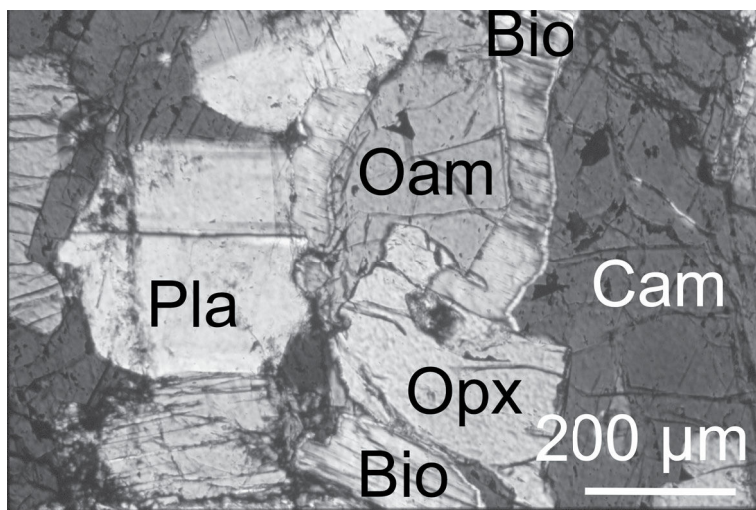


Figure 12. Textural relations involving gedrite, clinoclinoamphibole, plagioclase, and phlogopite, described by Claeson and Meurer (2002). All minerals but plagioclase and phlogopite are in textural equilibrium. Cross-polarized light. Photo contributed by D.T. Claeson.

interstitial amphibole. The clinoclinoamphibole has a *mg* value of 75. The sodicgedrite crystallized later, at a more advanced stage of evolution of the intercumulus melt, and it too has a *mg* value of 75. The sodicgedrite did not appear as a result of a reaction relationship; it coexisted stably with the cumulus plagioclase, which is very calcic (An_{85-92}), as expected in a “wet” gabbroic system. In Table 9, I list representative compositions of the two amphiboles. As in the Japanese case, they are most distinct in the occupancy of the $M(4)$ site; $Mg + Fe^{2+} + Mn$ is 0.2 *apfu* in the calcic amphibole and 1.8 *apfu* in the orthoamphibole. The lack of exsolution lamellae suggests rapid uplift of the assemblage from a mid-crust depth. Note that the Cl in the interstitial melt is incorporated in the intercumulus apatite (X_{Cl} attaining 0.85) rather than in either amphibole, presumably because of their high *mg* value; in more fractionated portions of the cumulates, the amphibole will presumably be richer in both Fe and Cl.

Claeson and Meurer (2002) interpreted the lobate texture to indicate resorption of the very calcic plagioclase and olivine (Fo_{77}) by the interstitial melt at a temperature close to 900 °C. In view of a theme developed earlier in this review, it seems to me a reasonable possibility that the growth of olivine and calcic plagioclase drove the residual melt to a composition rather close to the interstitial monoclinic amphibole, as in other contexts discussed earlier, which would raise a question about the realistic extent of a reaction relationship with a magma at that relatively low a temperature, especially if there is to be rapid uplift during cooling. Could the lobate shape of olivine and plagioclase have another significance than resorption, for example, interrupted growth owing to degassing of the melt upon decompression, perhaps?

Metasomatic phenomena

Plutons located in subduction settings typically show evidence of enrichment in elements that are build up during the metamorphism of seafloor rocks and that are released as these hydrous rocks are subducted. Lithium, boron and sodium are considered to be mobilized early in the subduction trajectory, and a carrier fluid will metasomatize the peridotite in the mantle wedge above the subduction zone and the crust above it. It is thus not unusual to find a Li and B anomaly in the plutons characteristic of orogenic suites. Where the magma has had a protracted history of crystallization, the igneous suite may well include pegmatitic manifestations

enriched in these rare elements, which had been systematically partitioned into the granitic melt and largely rejected by the rock-forming minerals that came before in the fractionating sequence. These granitic pegmatites are coded LCT to emphasize their enrichment in lithium, cesium and tantalum. London (2005) has reviewed the literature on the pervasive metasomatic alteration that is possible around large bodies of such LCT granitic pegmatites. In the present context, it is the mobility of lithium that is of particular interest, because of the development of a pseudomorphic holmquistite-type amphibole at the expense of precursor assemblages. Morgan and London (1987) have documented a halo of holmquistite-bearing amphibolitic host-rocks developed above the part of the Tanco (Manitoba) LCT-type granitic pegmatite that hosts the main mass of (spodumene + quartz)-bearing pegmatite. Such metasomatism takes place over the interval range 250–450 °C in the presence of a fluid that emanates from the most fractionated (internal) parts of the pegmatite body.

On a more regional basis, after the termination of a major collisional event, the inception of an episode of rifting attending the gravitational collapse of an orogen leads to a renewed heating of the already hot, thickened crust, and a hydrothermal mobilization of easily dislodged monovalent ions like Na, Li and F from the “recently” metasomatized block of crust (Martin and De Vito 2005). It is in this environment of granulite-grade metamorphism in the lower crust that orogenic granitic rocks may interact with a corrosive fluid phase that has the ability to dissolve quartz completely. The resulting metasomatic rock is called an episyenite; it is in the episyenites of the Sierra de Guadarrama, of the eastern La Pedriza pluton in the Central Spanish System batholith (Caballero et al. 1996), that newly described Group-5 amphiboles have been discovered, partly in cavities formerly occupied by quartz grains. The metasomatism occurred on a regional scale in the Lower Permian, at the onset of the episode of rifting developed throughout western Europe. The host rocks also underwent Na-metasomatism, which increases the porosity of the rocks. Together, the removal of quartz and the shrinkage of the network of feldspar grains owing to Na-for-K ion exchange allow a thorough soaking of the plutonic rock, even though the reactions (650–350 °C: Villaseca and Pérez-Soba 1989; Caballero et al. 1996) are inferred to have proceeded over a brief interval. The formation of the Li-bearing amphiboles like sodic-ferripedrizite (Oberti et al. 2000), sodic-ferri-ferropedrizite and clino-ferri-ferroholmquistite (Oberti et al. 2003), ferri-ottoliniite and ferriwhittakerite (Oberti et al. 2004) in the episyenites followed the episode of Na-for-K exchange and the dissolution of quartz.

A related manifestation of late Li-metasomatism occurred in the Paleoproterozoic Greenbushes granitic pegmatite, in southwestern Australia, one of the world’s major producers of Sn, Ta and Li. The addition of Li to the LCT pegmatite and to the amphibolitic host-rocks is demonstrably late (cf. Martin and De Vito 2005, Fig. 3, and references therein), and largely subsolidus, occurring once the pegmatite had been metasomatized, weakened by ion exchange and deformed. Such is the context of formation in the Greenbushes pegmatite of ferroholmquistite, a recent addition to the list of lithium amphiboles (Cámara and Oberti 2005).

Such diversity in the assemblages of metasomatic amphiboles in the metasomatized La Pedriza pluton and in the Greenbushes pegmatite result from important local differences in the activity of Na and Li, and in the fugacity of oxygen. Differences among these metasomatic amphiboles are subtle and are sure to challenge the analyst. Proper characterization will be important to define paths of metasomatism keyed to trajectories in temperature – $f(O_2)$ space, which may be of critical importance to understand the associated Ta and Sn mineralization.

AMPHIBOLE IN METEORITES

Amphibole-group minerals are only rarely encountered in meteorites. In most cases, they consist of micrometric inclusions of calcic amphibole in anhydrous mafic minerals. Kaersutite, fluorrichterite and magnesiohornblende are the species found; Floss et al. (2007) listed the

seven relevant references. The subject of their attention, however, is a description of the first find of fluoro-edenite in a meteorite. The Hammadah al Hamra 193 winonaite exhibits assemblages of minerals and bulk composition typical of chondrites, but without the chondritic texture. Such rare meteorites are considered to have experienced “extensive metamorphism and partial melting,” which presumably destroyed the texture of the precursor assemblage. The sample contains roughly 50 vol% orthopyroxene (En₉₅), 19% opaque phases (in part Fe–Ni alloy), 14% olivine (Fo₉₅), 11% sodic plagioclase (An₂₁), 4% fluoro-edenite (proportions: average of two thin sections), 1.6% clinopyroxene and 0.2% fluorapatite. The amphibole forms oikocrystic clusters up to 2 mm across disseminated in the enstatite-dominant rock, and engulfs all other minerals except the enstatite. Its bulk composition in one section is $K_{0.09}Na_{1.11}Ca_{1.68}Mg_{4.85}Fe_{0.15}[Al_{0.97}Si_{6.97}]F_{2.01}$. There is no sign of hydroxyl, and the total Al content is 5.88% Al₂O₃. Floss et al. (2007) raised the possibility that the amphibole originated by a replacement reaction at the expense of diopside, forsterite and oligoclase in response to an influx of a fluorine-rich hydrothermal fluid. Or perhaps it deposited directly from the external fluorine-bearing fluid, like at Biancavilla, Italy, the type locality of fluoro-edenite (see above). As another possibility, not considered by the authors, the bulk composition was heated above the beginning of melting, and the oikocrystic amphibole represents an odd partial melt developed here and there in the rock (Floss et al. 2007, Fig. 1), likely coexisting with a metallic melt, in view of the impressive network of hairline-width metallic veinlets cross-cutting everything.

CONCLUDING STATEMENT

When I undertook to write this review, I naively believed that I could restrict my attention to very well-described case studies in which some of the usual unknowns had been well determined by direct measurements. I quickly came to the realization that cases in which the proportions of Fe²⁺ and Fe³⁺ are well documented by spectroscopic measurements, and in which the amounts of hydrogen and lithium are established by direct measurements, are still very rare in the literature, as one can gather from the nine tables of compositions presented here. Yet these are the challenging measurements that must be done to move forward. Also, I have been struck by the possibility that a basic or hawaiitic melt can crystallize directly to an amphibole, even metastably at shallow depths in the crust. I hope to have pointed the way to interesting avenues of future research.

ACKNOWLEDGMENTS

I thank E. Alarie, A.Y. Barkov, D.T. Claeson, D.M. Francis, G. Garuti, D.D. Hogarth, Lang Shi, V. Loschiavo, F. McCubbin, W.P. Meurer, M. Sokolov, J. Thakurta, N. Tolstykh and F. Zaccarini for contributions to this paper. My research activities are covered by a Discovery Grant from the Natural Sciences and Engineering Research Council of Canada.

REFERENCES

- Abraham A-C, Francis D, Polvé M (2005) Origin of Recent alkaline lavas by lithospheric thinning beneath the northern Canadian Cordillera. *Can J Earth Sci* 42:1073-1095
- Anderson AT Jr (1980) Significance of hornblende and calc-alkaline andesites and basalts. *Am Mineral* 65:837-851
- Anderson JL, Smith DR (1995) The effects of temperature and *f*O₂ on the Al-in-hornblende barometer. *Am Mineral* 80:549-559
- Barker DS (1987) Tertiary alkaline magmatism in Trans-Pecos Texas. *In: Alkaline Igneous Rocks*. Fitton JG, Upton BGJ (eds) *Geol Society Spec Publ* 30:415-431
- Bédard JH (1988) Comparative amphibole chemistry of the Monteregian and White Mountain alkaline suites, and the origin of amphibole megacrysts in alkali basalts and lamprophyres. *Mineral Mag* 52:91-103

- Best MG (1974) Mantle-derived amphibole within inclusions in alkali-basaltic lavas. *J Geophys Res* 79:2107-2113
- Best MG (1975) Amphibole-bearing cumulate inclusions, Grand Canyon, Arizona and their bearing on silica-undersaturated hydrous magmas in the upper mantle. *J Petrol* 16:212-236
- Boettcher AL, O'Neil JR (1980) Stable isotope, chemical, and petrographic studies of high-pressure amphiboles and micas: evidence for metasomatism in the mantle source regions of alkali basalts and kimberlites. *Am J Sci* 280-A:594-621
- Bowes DR, Kinloch ED, Wright AE (1964) Rhythmic amphibole overgrowths in appinites associated with explosion-breccias in Argyll. *Mineral Mag* 33:963-973
- Bowes DR, Košler J (1993) Geochemical comparison of the subvolcanic appinite suite of the British Caledonides and the durbachite suite of the Central European Hercynides: evidence for associated shoshonitic and granitic magmatism. *Mineral Petrol* 48:47-63
- Bowes DR, Wright AE (1967) The explosion-breccia pipes near Kentallen, Scotland, and their geological setting. *Trans R Soc Edinb* 67:109-143
- Caballero JM, Gonzalez Casado JM, Casquet C, Galindo C, Tornos F (1996) Episenitas de la Sierra de Guadarrama: un proceso hidrotermal regional de edad Pérmico Inferior ligado al inicio de la extensión alpina. *Cuaderno de Geología Ibérica* 20:183-201
- Cámara F, Oberti R (2005) The crystal-chemistry of holmquistites: ferroholmquistite from Greenbushes (Western Australia) and hints for compositional constraints in ^BLi amphiboles. *Am Mineral* 90:1167-1176
- Campbell I, Schenk ET (1950) Camptonite dikes near Boulder Dam, Arizona. *Am Mineral* 35:671-692
- Castro A, Corretgé LG, de la Rosa JD, Fernández C, López S, García-Moreno O, Chacón H (2003) The appinite-migmatite complex of Sanabria, NW Iberian massif, Spain. *J Petrol* 44:1309-1344
- Castro A, Stephens WE (1992) Amphibole-rich polycrystalline clots in calc-alkaline granitic rocks and their enclaves. *Can Mineral* 30:1093-1112
- Cawthorn RG (1976) Some controls on igneous amphibole composition. *Geochim Cosmochim Acta* 40:1319-1328
- Chakhmouradian AR, Zaitsev AN (2002) Calcite – amphibole – clinopyroxene rock from the Afrikanda complex, Kola Peninsula, Russia: mineralogy and a possible link to carbonatites. III. Silicate minerals. *Can Mineral* 40:1347-1374
- Claeson DT, Meurer WP (2002) An occurrence of igneous orthorhombic amphibole, Eriksberg gabbro, southern Sweden. *Am Mineral* 87:699-708
- Conqué F (1971) Les pyroxénolites à amphibole et les amphibololites (sic) associées aux lherzolites du gisement de Lherz (Ariège, France) un exemple du rôle de l'eau au cours de la cristallisation fractionnée des liquides issus de la fusion partielle des lherzolites. *Contrib Mineral Petrol* 33:32-61
- Conrey RM, Sherrod DR, Hooper PR, Swanson DA (1997) Diverse primitive magmas in the Cascade Arc, northern Oregon and southern Washington. *Can Mineral* 35:367-396
- Czamanske GK, Dillet B (1988) Alkali amphibole, tetrasilicic mica, and sodic pyroxene in peralkaline siliceous rocks, Questa caldera, New Mexico. *Am J Sci* 288-A:358-392
- Dawson JB, Smith JV (1977) The MARID (mica – amphibole – rutile – ilmenite – diopside) suite of xenoliths in kimberlite. *Geochim Cosmochim Acta* 41:309-323
- Deer WA, Howie RA, Zussman J (1997) *Rock-Forming Minerals. 2B. Double-Chain Silicates* The Geological Society, London, UK
- Dorais MJ, MacRae ND (1994) Amphibole zoning in the Garland Peak syenite, Red Hill complex, New Hampshire: camptonitic parental magmas and differentiation to silica-oversaturated syenites. *Contrib Mineral Petrol* 117:76-86
- Downes PJ, Wartho J-A, Griffin BJ (2006) Magmatic evolution and ascent history of the Aries micaceous kimberlite, central Kimberley Basin, Western Australia: evidence from zoned phlogopite phenocrysts, and UV laser ⁴⁰Ar/³⁹Ar analysis of phlogopite-biotite. *J Petrol* 47: 1751-1783
- Dyar MD, Mackwell SJ, McGuire AV, Cross AR, Robertson JD (1993) Crystal chemistry of Fe³⁺ and H⁺ in mantle kaersutite: implications for mantle metasomatism. *Am Mineral* 78:968-979
- Eby GN (1987) The Monteregian Hills and White Mountain alkaline igneous provinces, eastern North America. *In: Alkaline Igneous Rocks*. Fitton JG, Upton BGG (eds) *Geol Soc, Spec Publ* 30:433-447
- Fabriès J, Lorand J-P, Guiraud M (2001) Petrogenesis of the amphibole-rich veins from the Lherz orogenic lherzolite massif (eastern Pyrenees, France): a case study for the origin of orthopyroxene-bearing amphibole pyroxenites in the lithospheric mantle. *Contrib Mineral Petrol* 140:383-403
- Féménias O, Mercier J-CC, Nkono C, Diot H, Berza T, Tatu M, Demaiffe D (2006) Calcic amphibole growth in calc-alkaline magmas: evidence from the Motru dike swarm (southern Carpathians, Romania). *Am Mineral* 91:73-81
- Floss C, Jolliff BL, Benedix GK, Stadermann FJ, Reid J (2007) Hammadah al Hamra: the first amphibole-bearing winonaite. *Am Mineral* 92:460-467
- Foland KA, Landoll JD, Henderson CMB, Chen J (1993) Formation of cogenetic quartz and nepheline syenite. *Geochim Cosmochim Acta* 57:697-704

- Foord EE, Erd RC, Robie SB, Lichte FE, King VT (1996) Li- and F-bearing alkali amphibole from granitic pegmatite at Hurricane Mountain, Carroll County, New Hampshire. *Can Mineral* 34:1011-1014
- Francis DM (1976a) Amphibole pyroxenite xenoliths: cumulate or replacement phenomena from the upper mantle, Nunivak Island, Alaska. *Contrib Mineral Petrol* 58:51-61
- Francis DM (1976b) The origin of amphibole in Iherzolite xenoliths from Nunivak Island, Alaska. *J Petrol* 17:357-378
- Francis D, Ludden J (1995) The signature of amphibole in mafic alkaline lavas, a study in the northern Canadian Cordillera. *J Petrol* 36:1171-1191
- Gianfagna A, Andreozzi GB, Ballirano P, Mazziotti-Tagliani S (2007) Structural and chemical contrasts between prismatic and fibrous fluoro-edenite from Biancavilla, Sicily, Italy. *Can Mineral* 45:249-262
- Gianfagna A, Oberti R (2001) Fluoro-edenite from Biancavilla (Catania, Sicily, Italy): crystal chemistry of a new amphibole end-member. *Am Mineral* 86:1489-1493
- Giret A, Bonin B, Léger J-M (1980) Amphibole compositional trends in oversaturated and undersaturated alkaline plutonic ring-complexes. *Can Mineral* 18:481-495
- Hawthorne FC, Oberti R (2006) On the classification of amphiboles. *Can Mineral* 44:1-21
- Hawthorne FC, Oberti R, Cannillo E, Ottolini L, Roelofsen JN, Martin RF (2001) Li-bearing arfvedsonitic amphiboles from the Strange Lake peralkaline granite, Quebec. *Can Mineral* 39:1161-1170
- Hawthorne FC, Oberti R, Martin RF (2006) Short-range order in amphiboles from the Bear Lake diggings, Ontario. *Can Mineral* 44: 1171-1179
- Hawthorne FC, Oberti R, Ottolini L, Foord EE (1996b) Lithium-bearing fluor-arfvedsonite from Hurricane Mountain, New Hampshire: a crystal-chemical study. *Can Mineral* 34:1015-1019
- Hawthorne FC, Oberti R, Ungaretti L, Ottolini L, Grice JD, Czamanske GK (1996a) Fluor-ferro-leakeite, $\text{Na}_2(\text{Fe}^{2+}_2\text{Fe}^{3+}_2\text{Li})\text{Si}_8\text{O}_{22}\text{F}_2$, a new alkali amphibole from the Canada Pinabete pluton, Questa, New Mexico, USA. *Am Mineral* 81:226-228
- Hawthorne FC, Ungaretti L, Oberti R, Bottazzi P, Czamanske GK (1993) Li: an important component in igneous alkali amphiboles. *Am Mineral* 78:733-745
- Heim A (1910) Über die Petrographie und Geologie der Umgebungen von Karsuarsuk, Nordseite der Halbinseln Nugsuak. *Meddelelser on Grønland* 47:173-228
- Hogarth DD (1989) Pyrochlore, apatite and amphibole: distinctive minerals in carbonatite. *In: Carbonatites: Genesis and Evolution*. Bell K (ed) Unwin Hyman, London, p 105-148
- Hogarth DD (1997) Mineralogy of leucite-bearing dykes from Napoleon Bay, Baffin Island: multistage Proterozoic lamproites. *Can Mineral* 35:53-78
- Hogarth DD (2006) Fluoro-potassic-magnesian-arfvedsonite, $\text{KNaMg}_5\text{Si}_8\text{O}_{22}\text{F}_2$, from the Outaouais region, Quebec, Canada. *Can Mineral* 44:289
- Irvine TN (1974) Petrology of the Duke Island ultramafic complex, southeastern Alaska. *Geol Soc Am Mem* 138
- Irvine AJ (1974) Megacrysts from the Newer Basalts and other basaltic rocks of southeastern Australia. *Geol Soc Am Bull* 85:1503-1514
- Ivanov OK (1997) Zoned Ultramafic Complexes of the Urals: Mineralogy, Petrology, Genesis. Uralsky University Publishing House, Ekaterinburg, Russia
- Johnson MC, Rutherford MJ (1989) Experimental calibration of the aluminum-in-hornblende geobarometer with application to Long Valley caldera (California) volcanic rocks. *Geology* 17:837-841
- Kapustin YuL (1980) Mineralogy of Carbonatites. Amerind Publishing Co, New Delhi, India
- Kawakatsu K, Yamaguchi Y (1987) Successive zoning in amphiboles during progressive oxidation in the Daito-Yokota granitic complex, San-in belt, southwest Japan. *Geochim Cosmochim Acta* 51:535-540
- Khomyakov AP (1995) Mineralogy of Hyperagpaitic Alkaline Rocks. Clarendon Press, Oxford
- King PL, Hergig RL, Holloway JR, Venneman TW, Righter K (1999) Oxy-substitution and dehydrogenation in mantle-derived amphibole megacrysts. *Geochim Cosmochim Acta* 63:3635-3651
- Kresten P, Morogan V (1986) Fentization at the Fen complex, southern Norway. *Lithos* 19:27-42
- Larsen LM, Sorensen H (1987) The Ilimaussaq intrusion - progressive crystallization and formation of layering in an agpaitic magma. *In: Alkaline Igneous Rocks*. Fitton JG, Upton BGJ (eds). *Geol Society Spec Publ* 30:473-488
- London, D (2005) Geochemistry of alkali and alkaline earth elements in ore-forming granites, pegmatites, and rhyolites. *In: Rare-Element Geochemistry and Mineral Deposits*. Linnen RL, Samson IM (eds). *Geol Assoc Can Short Course Notes* 17:17-43
- Markl G (2001) A new type of silicate liquid immiscibility in peralkaline nepheline syenites (lujarvites) of the Ilimaussaq complex, South Greenland. *Contrib Mineral Petrol* 141:458-472
- Martin RF (2006) A-type granites of crustal origin ultimately result from open-system fentization-type reactions in an extensional environment. *Lithos* 91:125-136
- Martin RF, De Vito C (2005) The patterns of enrichment in felsic pegmatites ultimately depend on tectonic setting. *Can Mineral* 43:2027-2048

- Mazdab FK (2003) The diversity and occurrence of potassium-dominant amphiboles. *Can Mineral* 41:1329-1344
- Mazziotti-Tagliani S (2007) Caratteri mineralogici, genetici e ambientali relativi agli anfiboli di fluoro presenti nell'area vulcanica di Biancavilla (CT, Italia). Dottorato di Ricerca in Scienze della Terra, Università degli Studi di Roma "La Sapienza," Rome, Italy
- Menzies M, Rogers N, Tindle A, Hawkesworth C (1987) Metasomatic and enrichment processes in lithospheric peridotites, an effect of asthenosphere – lithosphere interaction. *In: Mantle Metasomatism*. Menzies MA, Hawkesworth CJ (eds). Academic Press, London
- Menzies M, Rama Murthy V (1980) Mantle metasomatism as a precursor to the genesis of alkaline magmas – isotopic evidence. *Am J Sci* 280-A:622-638
- Meurer WP, Claeson DT (2002) Evolution of crystallizing interstitial liquid in an arc-related cumulate determined by LA ICP–MS mapping of a large amphibole oikocryst. *J Petrol* 43:607-629
- Mitchell RH (1990) A review of the compositional variation of amphiboles in alkaline plutonic complexes. *Lithos* 26:135-156
- Mitchell RH (2005) Carbonatites and carbonatites and carbonatites. *Can Mineral* 43:2049-2068
- Mitchell RH, Bergman SC (1991) *Petrology of Lamproites*. Plenum Press, New York
- Mitchell RH, Platt RG (1994) Aspects of the geology of the Coldwell alkaline complex. *Geol Assoc Can – Mineral Assoc Can, Field Trip A2: Guidebook*
- Monchoux P, Fontan F, de Parseval P, Martin RF, Wang R-C (2006) Peraluminous, mantle-derived felsic dikes in orogenic Iherzolites, western Pyrénées, France: a possible source for corundum and alkali feldspar xenocrysts in basaltic terranes I Mineralogical associations. *Can Mineral* 44:817-842
- Morgan GB VI, London D (1987) Alteration of amphibolitic wallrocks around the Tanco rare-element pegmatite, Bernic Lake, Manitoba. *Am Mineral* 72:1097-1121
- Morogan V, Woolley AR (1988) Fensitization at the Alnö carbonatite complex, Sweden: distribution, mineralogy and genesis. *Contrib Mineral Petrol* 100:169-182
- Mukasa SB, Wilshire HG (1997) Isotopic and trace element compositions of upper mantle and lower crustal xenoliths, Cima volcanic field, California: implications for evolution of the subcontinental lithospheric mantle. *J Geophys Res* 102:20133-20148
- Oberti R, Caballero JM, Ottolini L, López-Andrés S, Herreros V (2000) Sodic-ferripedrizite, a new monoclinic amphibole bridging the magnesium – iron – manganese – lithium and the sodium – calcium groups. *Am Mineral* 85:578-585
- Oberti R, Cámara F, Caballero JM (2004) Ferri-ottoliniite and ferriwhittakerite, two new end-members of the new Group 5 for monoclinic amphiboles. *Am Mineral* 89:888-893
- Oberti R, Cámara F, Caballero JM, Ottolini L (2003) Sodic-ferri-ferropedrizite and ferri-clinoferroholmquistite: mineral data and degree of order of the A-site cations in Li-rich amphiboles. *Can Mineral* 41:1345-1354
- Pattison DRM, Vogl JJ (2005) Contrasting sequences of metapelitic mineral-assemblages in the aureole of the tilted Nelson batholith, British Columbia: implications for phase equilibria and pressure determination in andalusite–sillimanite-type settings. *Can Mineral* 43:51-88
- Pe-Piper G (2007) Relationship of amphibole composition to host-rock geochemistry: the A-type gabbro–granite Wentworth pluton, Cobequid shear zone, eastern Canada. *Eur J Mineral* 19:29-38
- Philpotts AR (1974) The Monteregian Hills. *In: The Alkaline Rocks*. Sørensen H (ed) John Wiley Sons, London, p 293-310
- Pin C, Monchoux P, Paquette J-L, Azambre B, Wang R-C, Martin RF (2006) Peraluminous, mantle-derived felsic pegmatite dikes in orogenic Iherzolites, western Pyrénées, France: a possible source for corundum and alkali feldspar xenocrysts in basaltic terranes II Geochemical and isotopic considerations. *Can Mineral* 44:843-856
- Popp RK, Hibbert HA, Lamb WM (2006) Oxy-amphibole equilibria in Ti-bearing calcic amphiboles: experimental investigation and petrologic implications for mantle-derived amphiboles. *Am Mineral* 91:54-66 [correction: 91:716]
- Roeder PL, Emslie RF (1970) Olivine–liquid equilibrium. *Contrib Mineral Petrol* 29:275-289
- Samoylov VS (1977) Carbonatites: Facies and Conditions of Formation. Nauka, Moscow, Russia (in Russ)
- Sato H, Nakada S, Fujii T, Nakamura M, Suzuki-Kamata K (1999) Groundmass pargasite in the 1991–1995 dacite of Unzen volcano: phase stability experiments and volcanological implications. *J Volcanol Geotherm Res* 89:197-212
- Schnetzler CC, Philpotts JA (1968) Partition coefficients of rare-earth elements and barium between igneous matrix material and rock-forming-mineral phenocrysts. *In: Origin and Distribution of the Elements* Ahrens LH (ed) Pergamon Press, Oxford
- Sial AN, Ferreira VP, Fallick AE, Cruz MJM (1998) Amphibole-rich clots in calc-alkalic granitoids in the Borborema province, northeastern Brazil. *J S Am Earth Sci* 11:457-471
- Skelton A, Hode Vuorinen J, Arghe F, Fallick A (2007) Fluid–rock interaction at a carbonatite–gneiss contact, Alnö, Sweden. *Contrib Mineral Petrol* 154:75-90; doi: 10.1007/s00410-007-0180-1

- Sørensen H, Bohse H, Bailey JC (2006) The origin and mode of emplacement of lujavrites in the Ilímaussaq alkaline complex, South Greenland. *Lithos* 91:286-300
- Stephens WE (2001) Polycrystalline amphibole aggregates (clots) in granites as potential I-type restite: an ion microprobe study of rare-earth distributions. *Aust J Earth Sci* 48:591-601
- Stuckless JS, Irving AJ (1976) Strontium isotope geochemistry of megacrysts and host basalts from southeastern Australia. *Geochim Cosmochim Acta* 40: 209-213
- Sutherland DS (1969) Sodic amphiboles and pyroxenes from fenites in East Africa. *Contrib Mineral Petrol* 24:114-135
- Thakurta J, Ripley EM, Li C (2006) Isotopic and geochemical studies of host rock pyroxenites associated with Cu-Ni-PGE mineralization in the Duke Island complex, Alaska. *Geol Soc Am, Abstr Programs* 37(7):451
- Villaseca C, Pérez-Soba C (1989) Fenómenos de alcalinización en granitoides hercínicos de la Sierra de Guadarrama (Sistema Central). *Cuad Lab Xeol Laxe* 14:201-212
- Wilshire HG, Nielson Pike JE, Meyer CE, Schwarzman EC (1980) Amphibole-rich veins in lherzolite xenoliths, Dish Hill and Deadman Lake, California. *Am J Sci* 280-A: 576-593
- Wones DR, Gilbert MC (1982) Amphiboles in the igneous environment. *Rev Mineral* 9B:355-390
- Yakovenchuk VN, Ivanyuk G, Pakhomovsky Ya, Men'shikov Yu (2005) Khibiny. *Laplandia Minerals, Khibiny, Russia*
- Yamaguchi Y (1985) Hornblende-cummingtonite and hornblende-actinolite intergrowths from the Koyama calc-alkaline intrusion, Susa, southwest Japan. *Am Mineral* 70:980-986

Metamorphic Amphiboles: Composition and Coexistence

John C. Schumacher

*Dept. of Earth Sciences
University of Bristol
Bristol, BS8 1RJ, United Kingdom
j.c.schumacher@bristol.ac.uk*

INTRODUCTION

Amphiboles have long been key players in metamorphic petrology. The concept of facies was developed for rocks of basaltic composition (Eskola 1920, 1939; Fyfe et al. 1958), and within this concept, amphiboles had a leading role. The first appearance of amphiboles, the presence of amphiboles of certain compositions or last appearance of amphiboles that are replaced by pyroxene-bearing assemblages, mark a number of major facies boundaries. The transition from greenschist to amphibolite facies is marked, in part, by hornblende replacing actinolite, and the granulite facies is defined by the breakdown of hornblende to orthopyroxene-bearing assemblages. The blueschist facies is defined by the appearance of glaucophane, while the transition from blueschist-facies to eclogite-facies conditions is indicated by the breakdown of glaucophane to omphacitic pyroxene-bearing assemblages. References to amphibole names (actinolite, glaucophane) or rocks characterized by certain amphiboles (amphibolite/hornblende) figure prominently in six facies names (Turner 1981; Liou et al. 1985; Oh et al. 1988; Evans 1990; Peacock 1993). A large part of the literature that is devoted to metamorphic petrology of amphiboles concerns reactions which produce amphiboles from more hydrated mafic igneous rocks or lead to the destruction of amphiboles as they break down to form anhydrous or nearly anhydrous mineral assemblages. Consequently, amphiboles can be thought of as occupying the wide intermediate portion of P - T - X_{fluid} space in which metamorphic rocks are found.

The number of citations of the published amphibole nomenclature serves as a yardstick (meterstick?) of the interest in amphiboles and a minimum estimate of the amount of literature devoted to this mineral. Two versions of the nomenclature of amphiboles have appeared: 1978 and 1997 (Leake 1978; Leake et al. 1997), and they have been cited a over 2300 times in the past 28 years. This works out to a minimum of more than 80 citations per year for this mineral group.

Amphiboles can have contents of all the major elements and a few minor elements that are measurable in weight percent. Before the widespread use of the electron microprobe provided for better characterization of amphibole compositions, the early recognition of its compositional range and diversity from gravimetric analysis led to amphiboles being regarded as sponges (Engel and Engel 1962) and waste baskets and garbage cans (Ernst 1966) or even as mineralogic sharks in a sea of unsuspecting elements (Robinson et al. 1982) that indiscriminately absorbed, received or consumed elements. These characterizations are perhaps inspired by the derivation of the name *amphibole*, which means *ambiguous* in Greek ($\alpha\mu\phi\iota\beta\omicron\gamma\omicron\varsigma$). Despite their complexity, amphiboles through their macroscopic, optical and chemical properties as well as their textures yield information about their development, their conditions of formation and the bulk composition of the rocks in which they are found that is useful to field geologists, petrologists and geochemists.

In the earlier amphibole volumes, *Reviews in Mineralogy, Volumes 9A and 9B*, the section on metamorphic amphiboles (Robinson et al. 1982) comprised 223 pages that were compiled by seven coauthors. In this volume, the same material in that extensive work will be covered in separate and smaller chapters. Clearly, this chapter on metamorphic amphiboles cannot cover all of the topics in Volume 9B in the same depth. So readers are referred to the excellent and in depth reviews found there.

The amphibole data used in Volume 9B (Robinson et al. 1982) to explore amphibole composition were based on compilations of gravimetric analysis of amphiboles done before 1980. The reinvestigation of metamorphic amphibole compositions that is undertaken in the following pages is based on metamorphic amphibole analysis from literature published after 1980 (mostly) and from the B. E. Leake's catalog of analyzed calciferous and sub-calciferous amphiboles (Leake 1968). The result was more than 3000 amphibole analyses compiled by University of Bristol students David Williams (mostly) and Jane Leiss, as well as by John Schumacher.

CHEMICAL SUBSTITUTION IN METAMORPHIC AMPHIBOLES

The amphibole formula

Metamorphic petrologists and everyone else needing to formulate amphibole analyses for comparisons and plots require a sensible structural formula. The general structural formula given in the latest version of the amphibole nomenclature (Leake et al. 1997) is: $A_{0-1}B_2C_5T_8O_{22}W_2$. The general structural formula amphibole nomenclature (Leake et al. 1997) can be expressed using the crystallographic site designations as: $A_{0-1}M(4)_2M(1,2,3)_5T(1)_4T(2)_4O_{22}W_2$. However, the C group in this formulation has long been recognized to consist of two groups of dissimilar sites with two of the five having a marked preference for trivalent cations. Hawthorne and Oberti (2006) have called these the *tschermakite arrangement* and denoted the structural formula as: ${}^A_0{}^B_2{}^C(2_3\ 3_2) {}^T(4_6\ 3_2) O_{22} W_{1-2}$. Thompson (1970, 1978, 1981) elaborated on the polysomatic or modular nature pyroxenes, amphiboles and sheet silicates (biopyriboles) and on the observation that both structurally and chemically amphiboles can be broken into alternating pyroxene and mica layers. The pyroxene $M(2)$ sites are analogous to the amphibole $M(4)$ sites, and the pyroxene $M(1)$ sites are analogous to the amphibole $M(2)$ sites. The structural analogy extends to the tetrahedral sites as well with four $T(1)$ sites being more comparable to micas, and the four $T(2)$ sites being more similar to pyroxenes (see Hawthorne 1983). A generalized amphibole formula $A_{0-1}B_2C_5T_8O_{22}(OH)_2$ can be rearranged to this:



This general relationship is a boon to budding mineralogists because it is the basis of simple mnemonic that will yield amphibole formulae from real or theoretical pyroxene and mica end-member formulae, 1 mica + 2 pyroxene = 1 amphibole. The simplest amphibole *tremolite* = 2 diopside + talc, *glaucofane* = 2 jadeite + talc, *edenite* = 2 diopside + Na-phlogopite. While the chemical analogy can be extended to other amphibole end-members, *tschermakite* = 2 Ca-tschemmacks component + talc, *pargasite* = 1 diopside + 1 Ca-tschemmacks component + Na-phlogopite, the site-occupancy analogy breaks down. Crystallographic studies (Hawthorne 1981, 1983) demonstrate that tetrahedral Al is strongly ordered at the amphibole $T(1)$ (mica-like) sites in tschermakitic amphiboles, rather than at the amphibole $T(2)$ (CaTs-pyroxene-like) sites. This observation led (Robinson et al. 1982) to speculate that this difference in the behavior

of Al at the tetrahedral sites may be a contributing factor favoring the stability of amphiboles over of pyroxene + mica assemblages in some rocks.

Formula basis and estimates of Fe³⁺

The amphibole compositional data collected for this review required that the electron microprobe analysis be recast to a common set of criteria. A detailed discussion of the amphibole formula and the cation site assignments that were applied here is given in Chapter 1 of this volume (Hawthorn and Oberti 2007). Hawthorn and Oberti (2007) also cover the issue of Fe³⁺ estimations in amphiboles based on stoichiometric assumptions, which is also critical if Fe³⁺ cannot be determined independently. Readers are also referred to Appendix I of this chapter, which contains a review of Fe³⁺ estimates that are based on stoichiometry for metamorphic amphiboles with emphasis on the data used in chapter.

Amphibole composition space used here

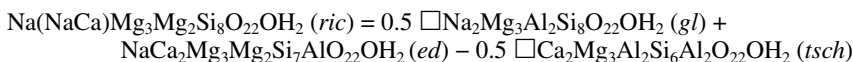
Compositional plots and classification plots. Many formal and informal classification schemes and coordinate systems for plotting amphibole compositions have been used over the past several decades (e.g., Robinson and Jaffe 1969; Leake 1978; Robinson et al. 1982; Leake 1997; Hawthorne and Oberti 2006 and references therein). The amphiboles have been divided into various chemically-defined groups both for classification purposes and as reference points for discussion (e.g., Leake 1997). The important groups for metamorphic amphiboles are the calcic (^BCa ≥ 1.5), sodic-calcic (^BCa + ^BNa ≥ 1.0, 0.5 < ^BNa < 1.5), sodic-calcic (^BNa ≥ 1.5) and (Mg, Fe, Mn) amphiboles (^B(Fe²⁺ + Mn²⁺ + Mg) > 1.0). Plots of A-site occupancy versus tetrahedrally coordinated Al of calcic and (Mg, Fe, Mn) amphibole compositions (e.g., Robinson and Jaffe 1969) show systematic variation in Na and Al contents due to the edenite-like (^ANa^BNa^A□₋₁^BCa₋₁) and tschermakite-like (^CAl^TAl^CMg₋₁^TSi₋₁) coupled substitutions; where quantified along with variations in Fe²⁺ and Mg, most of the compositional variation in amphiboles from these two groups can be represented in this system. The classification schemes presented by Leake (1978) and Leake et al. (1997) use plots that emphasize variations of Si (equivalent to ^[4]Al) versus X_{Mg} to portray the nomenclature of amphiboles for all the chemical groups. The variations—in some cases, ill-conceived ones—on these diagrams have been used by many authors to show amphibole compositions. In this chapter, amphibole compositions will be compared on diagrams that use substitution vectors as axes. These plots involve A-site occupancy versus ^[4]Al and Si versus X_{Mg}, but they are presented in a different fashion, which, I hope, gives a better overview of compositional variations. The relevant end-members from (Leake et al. 1997) are shown on these diagrams, which serve as an alternative coordinate system with many advantages over that currently used for the amphibole nomenclature¹.

Coupled and homovalent substitutions. There are five principal coupled-substitution vectors for amphiboles, but only four of these (tschermakite, glaucophane, edenite and richterite vectors) are common. The fifth vector, which could be called the kaersutite vector, is a coupled substitution that involves Ti and O, is not known to be important for metamorphic amphiboles. As a consequence, this presentation concentrates on variations along the four common vectors. The glaucophane and tschermakite vectors are analogous to the pyroxene-like substitution of jadeite and tschermak's components in diopside. The amphibole edenite vector is analogous to the mica-like substitution of K or Na + Al in the talc structure. The richterite vector is unique to amphiboles and involves substitution of Na at both the mica-like A and pyroxene-like M(4) sites for a vacancy and an R²⁺ cation. These four vectors can be expressed as follows: [^CAl^TAl^CMg₋₁^TSi₋₁] = tschermakite vector, [^BNa^CAl^BCa₋₁^CMg₋₁] = glaucophane vector, [^ANa^TAl^A□₋₁^TSi₋₁] = edenite vector and [^ANa^BNa^A□₋₁^BCa₋₁] = richterite vector, and, where

1 Being involved in some of these efforts has taught that producing a classification scheme is a task suitable only for those with masochistic strains running through their personalities.

combined with tremolite ($\square\text{Ca}_2\text{Mg}_3\text{Mg}_2\text{Si}_8\text{O}_{22}\text{OH}_2$) as a starting composition, can generate all 14 named, root compositions in the system $\text{Na}_2\text{O}-\text{CaO}-\text{MgO}-\text{Al}_2\text{O}_3-\text{SiO}_2-\text{H}_2\text{O}$. Most of the remaining compositional variation in amphiboles can be represented by homovalent exchange vectors like ${}^{\text{B,C}}\text{Mg} = \text{R}^{2+}$, where $\text{R}^{2+} = \text{Ca}^{2+}, \text{Fe}^{2+}, \text{Mn}^{2+}, \text{Ni}^{2+}, \text{Co}^{2+}, \text{Zn}^{2+}$, and ${}^{\text{C}}\text{Al}^{3+} = \text{R}^{3+}$, where $\text{R}^{3+} = \text{Fe}^{3+}, \text{Cr}^{3+}, \text{V}^{3+}, \text{Mn}^{3+}$ and Ti^{4+} (which can be treated as composite R^{3+} cation made up of Fe^{2+} and Ti^{4+} [$\text{Fe}_{0.5}\text{Ti}_{0.5}$] $^{3+}$). The treatment of Ti^{4+} as [$\text{Fe}_{0.5}\text{Ti}_{0.5}$] $^{3+}$ emphasizes its equivalent behavior with other octahedrally coordinated R^{3+} cations ($\text{Al}, \text{Fe}^{3+}$) as seen in the isostructural oxides, corundum, hematite and ilmenite. However, as mentioned above, Ti^{4+} may also substitute in the amphibole structure by the fifth coupled substitution, the kaersutite vector: ${}^{\text{C}}\text{Ti}^{\text{W}}\text{O}^{\text{W}}\text{C}^{\text{Mg}}\text{Mg}_{-1}^{\text{W}}(\text{OH})_{-1}^{\text{W}}(\text{OH})_{-1}$, but at present, amphiboles with these compositions generally are of igneous origin.

In their most simplified form the *tschermakite*, *glaucophane*, *edenite* and *richterite* vectors describe four equations that involve substitution of Na and Al into the basic tremolite formula—each element could enter two different sites in tremolite. Amphibole stoichiometry is an additional constraint, and as a result, the four equations for the *tschermakite* (*tsch*), *glaucophane* (*gl*), *edenite* (*ed*) and *richterite* (*ric*) vectors are not linearly independent. This can be seen easily, as the end-member composition of richterite can be expressed in terms of glaucophane, edenite and tschermakite:



While any three of the substitution vectors can define the amphibole composition space, *tsch*, *gl* and *ed* vectors are used, because richterite is uncommon and substitutions along these three vectors reflect observed compositional variations in most metamorphic amphiboles. Within the $\text{Na}_2\text{O}-\text{CaO}-\text{MgO}-\text{Al}_2\text{O}_3-\text{SiO}_2-\text{H}_2\text{O}$ system, the magnitudes of these vectors are calculated as follows:

$$\text{tsch} = {}^{\text{T}}\text{Al} - {}^{\text{A}}\text{Na}; \text{gl} = {}^{\text{B}}\text{Na}; \text{ed} = {}^{\text{A}}\text{Na}$$

These vectors can be generalized to

$$\text{tsch} = {}^{\text{T}}\text{Al} - {}^{\text{A}}\text{Na} - {}^{\text{A}}\text{K} - 2 {}^{\text{A}}\text{Ca}; \text{gl} = {}^{\text{B}}\text{Na} + {}^{[6]}\text{Li}; \text{ed} = {}^{\text{A}}\text{Na} + {}^{\text{A}}\text{K} + {}^{\text{A}}\text{Ca}$$

which allows all amphibole compositions to be plotted in terms of these vectors. Figure 1 shows the position of 15 Li-Na-Ca-Mg-Al-Si end-members. Three end-members, richterite, eckermannite and pedrizite have a richterite component; on Figure 1, this is represented as negative values of the *tsch* component, because the richterite substitution has the coordinates, *ric* = +1 *gl*, +1 *ed*, -1 *tsch*, within this coordinate system. From these 15 end-members, all other compositional variations can be represented via either homovalent exchange reactions with or substitution along the *kaersutite* vector from the end-members in Figure 1a. The three principal coupled-substitution vectors in Figure 1 and the compositional exchange vectors, FeMg_{-1} , MnMg_{-1} , CaMg_{-1} , $\text{Fe}^{3+}\text{Al}_{-1}$ and $(\text{Fe}_{0.5}\text{Ti}_{0.5})\text{Al}_{-1}$, almost completely describe the observed compositional variation in metamorphic amphiboles. Of these exchange vectors, FeMg_{-1} and $\text{Fe}^{3+}\text{Al}_{-1}$ are the most extensive. Another feature of Figure 1 is that the *gl* and *tsch* vectors of the diagram are extensible. The scalar values along the *ed* (and *ric*) vectors have a limit of 1; however, the scalar values along the *gl* and *tsch* vectors are not limited to the values shown in Figure 1a, although, where plotted, the compositions of the vast majority of amphiboles will not exceed these values. In particular, amphiboles rich in tschermakitic Ti (i.e., not present due to the *kaersutite* substitution) may have ${}^{[4]}\text{Al} > 3.0$.

The locations of planes of constant Si, ${}^{\text{C}}\text{R}^{3+}$ and ${}^{\text{C}}\text{R}^{2+}$ within the amphibole composition space used here (Fig. 1a) are shown in Figure 1b. Si content is one of the major classification parameters used in the amphibole nomenclature of Leake (1978) and Leake et al. (1997); Si and the *tschermakite* vector are related, but not equivalent, parameters.

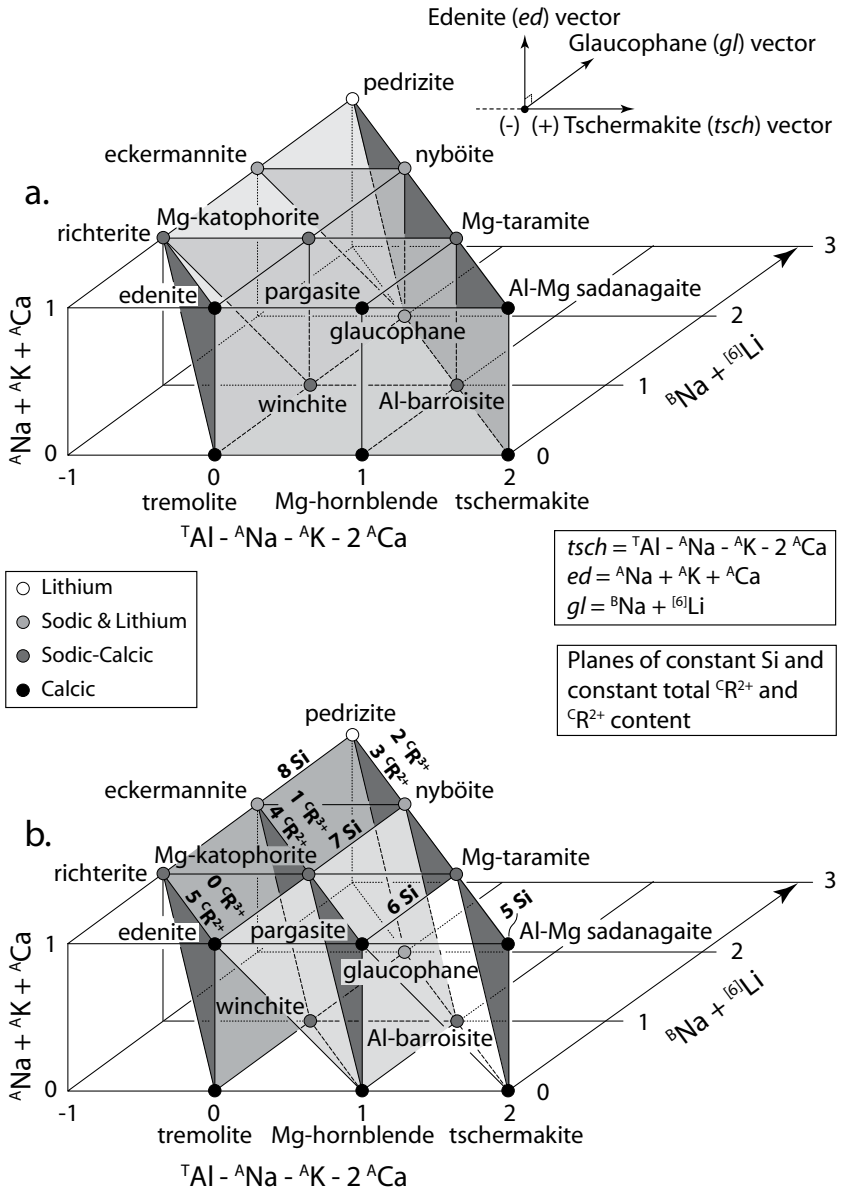


Figure 1. An amphibole composition space based on generalized *tschermakite*, *edenite* and *glaucophane* substitution vectors. (a) The planes edenite–richterite–pedrizite–glaucophane and tremolite–richterite–edenite are limits of amphibole composition. The planes tremolite–edenite–Al-Mg-sadanagaite–tschermakite, winchite–richterite–Mg-taramite–Al-barroisite and glaucophane–eckermannite–nyböite mark the calcic, sodic-calcic and sodic amphibole groups. The glaucophane–pedrizite–Al-Mg-sadanagaite–tschermakite is not a fixed limit of amphibole composition space; for example, the presence of R^{2+} cations at $M(2)$ would permit values along the *tschermakite* vector that extend beyond this plane. (b) The dark gray planes show constant Si content and the lighter gray planes show constant ${}^C\text{R}^{2+}$ and ${}^C\text{R}^{3+}$ in this amphibole composition space.

COMPOSITIONS OF METAMORPHIC AMPHIBOLES

Amphibole data

The data used in RiM Volume 9B was compiled primarily from collections of superior gravimetric analyses (Robinson et al. 1982, p. 12-13), and some of this data, notably Leake (1968) were included in the current study. New data, principally electron microprobe analyses from journal articles, that were published mostly since 1980 make up the bulk of this data; the resulting database has over 3000 entries. One point readers should keep in mind is that diagrams that portray statistical information (e.g., histograms) are not necessarily a true representation on the relative abundance of various amphibole groups (e.g., calcic, sodic-calcic and sodic amphiboles, (Mg, Fe, Mn) amphiboles). Because this data is taken from the literature that mostly spans the past 25 years, the data will reflect the interests and directions of research involving amphiboles over that period. For example, due to the efforts of several authors, a great deal of works was done on Ca-poor amphiboles in the 1970's and early 1980's, and that effort was covered extensively in Robinson et al. (1982). In the course of compiling these data, I noticed that proportionally fewer studies of Ca-poor amphiboles have been published in the intervening time. Another observation is that ultramafic rocks remain popular objects of research, and, as a consequence, tremolite-actinolite are probably over-represented among the calcic amphiboles.

All the analyses used here were recalculated for Fe^{3+} using the *average* of the minimum and maximum estimates (see Appendix 1 and Hawthorne and Oberti (2007), chapter 1). The resulting structural formulae were tested against these criteria: (1) the *T* group consist of 8 Si or Si+Al; (2) the sum of $^{[6]}\text{R}^{3+}$ and $^{[6]}\text{R}^{4+}$ are ≤ 2 ; (3) Ca occurs only at the *M*(4) site²; (4) K occurs only at the *A* site; (5) $15 \leq \text{total cations} \leq 16$; (6) no vacancies are present other than at the *A*-site. Just over one-quarter of these analyses failed to meet these criteria (Fig. 2), which left almost 2400 usable analyses. Of the usable analyses, almost three-quarters are calcic amphiboles with sodic-calcic, sodic and (Mg, Fe, Mn)g amphiboles occurring in roughly equal amounts (Fig. 2).

Among the usable analyses, the minimum Fe^{3+} estimate was the *All ferrous* formula in at least 45% of the examples (Fig. 3) in (Mg, Fe, Mn), calcic, sodic-calcic and sodic amphibole groups. In the sodic-calcic group the all Fe^{2+} formula was the minimum Fe^{3+} estimate for about 80% of the examples. In the sodic and sodic-calcic groups the 8 Si recalculation was the minimum Fe^{3+} estimate for the bulk of the remaining analyses (Fig. 3), and this is probably due to the close compositional correspondence of the natural examples to the ideal end-members, many of which have 8 Si apfu (i.e., the scalar values of the *tsch* vector are near 0). For the (Mg, Fe, Mn) and calcic groups, the 15 *eNK* recalculation gave the minimum Fe^{3+} estimate for most of the rest of the analyses (Fig. 3), and this is likely due to significant ferri-*tsch* component in most of these examples.

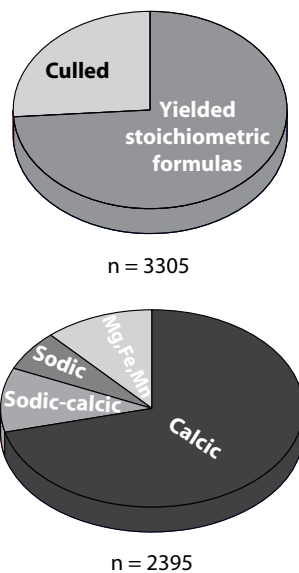


Figure 2. Pie charts showing the total number of analyses used in this study, the number that failed to yield stoichiometric formulas (Culled) based on the conditions discussed in the text, and the proportions of calcic, sodic-calcic, sodic and Fe-Mg amphiboles used in the discussion.

² A known exception to this general rule exists. At the time of this writing, a rare amphibole, cannilloite with Ca at both the *A* and *M*(4)-sites, was reported by Hawthorne et al. (1996) from Pargas, Finland.

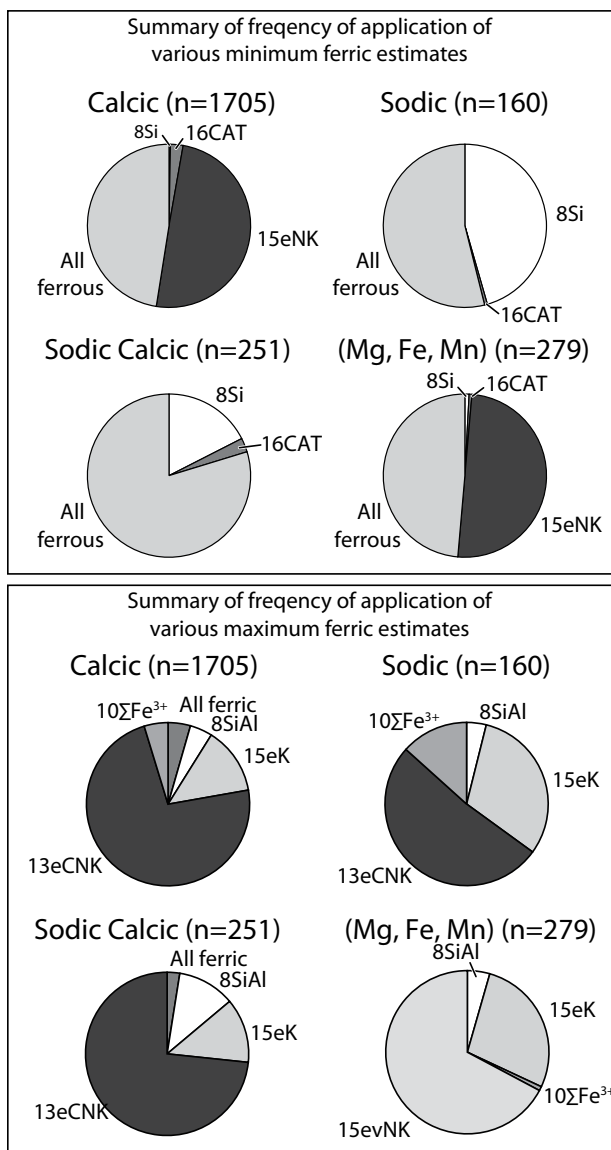


Figure 3. Pie charts showing the kinds and proportions of maximum and minimum ferric iron estimates that were appropriate for the amphiboles collected in this database. See Figure A1 of Appendix I and the associated discussion for an explanation of the correction types (e.g., 15eNK).

The maximum Fe^{3+} estimate among usable analyses also varied among groups (Fig. 3). The 13 *eCNK* recalculation was the maximum Fe^{3+} estimate for more than 50-75% of the amphiboles from the calcic, sodic-calcic and sodic groups, due to the near-complete filling of the *B* site by Ca and Na from these groups. For the calcic group, the 15 *eK* estimates account for about half the remaining examples, which is probably due to low total Fe and variability in Na at the *A* site. For the sodic-calcic group, the 8 *SiAl* and 15 *eK* estimations apply in the majority of the remaining examples, which is probably due to low total $^{[6]}R^{3+}$ cations in end-members

richterite and winchite, and the nearly empty *A* site in barroisite (Fig. 3). For the sodic group, the $10 \Sigma Fe^{3+}$ and $15 eK$ estimates are the most common maximum Fe^{3+} estimates for the rest of the analyses. This is probably due to the competing constraints of ideal $^{6}R^{3+}$ being 2 and ideal *A* occupancy being 0 in the glaucophane-riebeckite series (Fig. 3). In contrast, the Fe-Mg is not constrained by *B* group Ca and Na, so the $13 eCNK$ recalculation does not come into play; instead, $10 \Sigma Fe^{3+}$, $15 eK$ and $15 evNK$ are the most common. The $15 eK$ and $8 SiAl$ estimates are most common for low-Na, (Mg, Fe, Mn) amphiboles like cummingtonite, grunerite and anthophyllite, while $15 evNK$ is more common in orthoamphiboles with intermediate and higher Na and Al contents.

Edenite, tschermakite and glaucophane component vectors, and X_{Mg} and X_{Ca} in calcic, sodic-calcic and sodic amphiboles

Edenite, tschermakite and glaucophane compositions. Compositional variations along the generalized *edenite*, *tschermakite* and *glaucophane* vectors track changes in *A*-site occupancy, Na at the *M*(4) site (and Li at *M*(1,2,3,4)) and ^{4}Al , which are due to coupled substitutions, and Figure 4 shows this distribution for calcic, sodic-calcic and sodic amphiboles. The analyses cluster into two groups. The larger group is comprised of most of the calcic amphiboles and some of the sodic-calcic amphiboles with glaucophane-vector values < 1.0 and tschermakite-vector values > 0 and centered at about 0.5 tschermakite. The second smaller cluster is near the glaucophane composition. Most of these analyses fall in the general fields (Mg-Al root names) for tremolite, Al-hornblende, tschermakite, pargasite and edenite or glaucophane. These compositions can also be viewed along the edenite vector on the plane containing the tschermakite and glaucophane vectors (Fig. 5). The two clusters from Figure 4 are prominent in

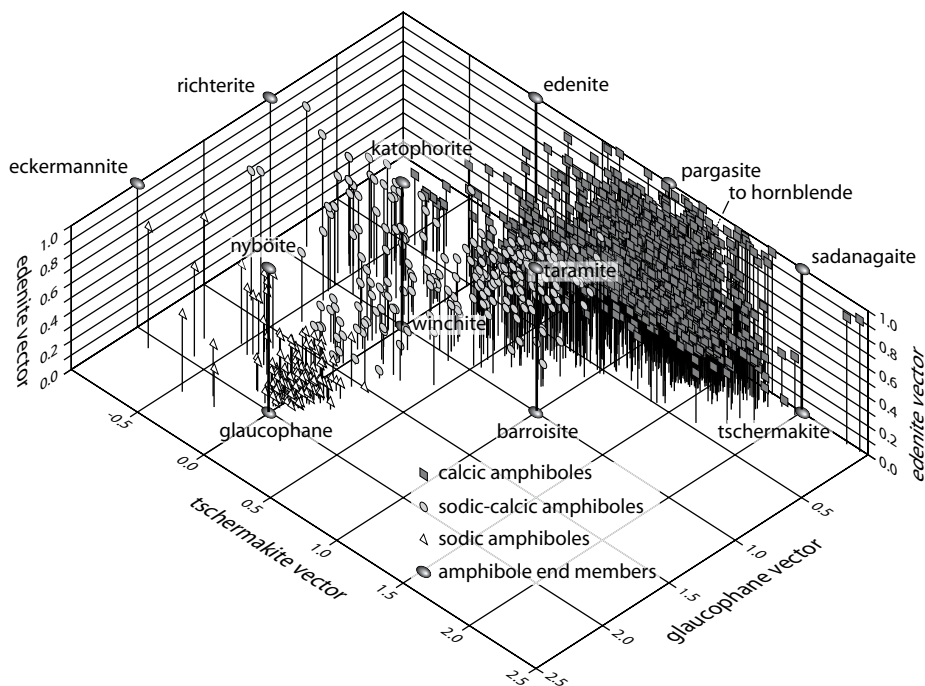


Figure 4. Three dimensional plot of the generalized *tschermakite*, *edenite* and *glaucophane* components of all calcic, sodic-calcic and sodic amphiboles (average ferric estimate) assembled from literature sources for this study.

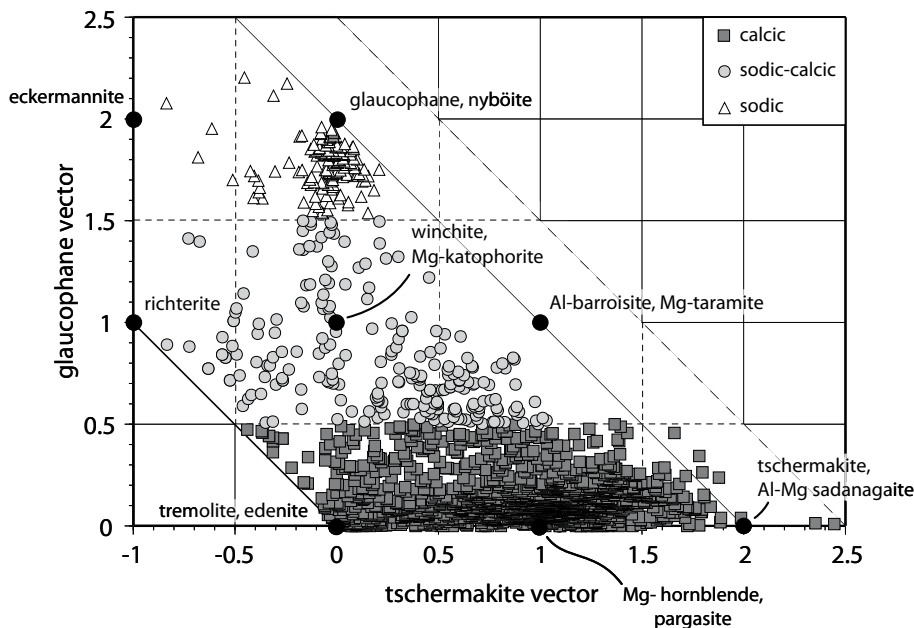


Figure 5. Plot of the generalized *glaucophane* vs. *tschermakite* components for all calcic, sodic-calcic and sodic amphiboles (average ferric estimate) assembled from literature sources for this study. The data points are projected along the *edenite* vector (see Figs. 1 and 4) where *edenite* vector values = 0. The amphibole composition space is bounded by the end members shown in Figure 1a. The long dashed line extends the amphibole composition space higher the *tschermakite* vector values that result from the presence of significant amounts of $^{c}\text{Ti}^{4+}$ in some *sadanagaite* analyses. The short dashed lines separate the composition fields that are assigned to the end members.

Figure 5, which also shows that the *tschermakite* and *glaucophane* components lie mostly within a rhombohedral region defined by the *tremolite-edenite*, *tschermakite-sadanagaite*, *glaucophane-nyböite* and *richterite* points. The concentration of analyses near the *tschermakite-pargasite*, compositions that have long been associated with the term “common hornblende,” is also evident (Fig. 5). Table 1 gives the composition of the average of “common hornblende” based on 1252 analyses with $0.500 < \text{tschermakite component} \leq 1.500$ and any value of *edenite* component.

A more detailed look at the compositions of these amphiboles is possible in sections showing compositions along the [tsch] and [ed] vectors for specified ranges of the scalar values along the [gl] vector. These [gl] vector ranges for three [tsch] versus [ed] vectors are 0.0-0.5, 0.5-1.5 and 1.5-2.5, and are the same as those chosen by Leake et al. (1997) to define the calcic, sodic-calcic and sodic amphibole groups. Within each of these groups, the two most important homovalent substitutions in metamorphic amphiboles are the exchange of Fe^{2+} for Mg and the exchange of Fe^{3+} for ^{6}Al . The dominance of these cations at their respective sites in the amphibole structure are the basis for the common amphibole end-member names (Leake et al. 1997).

Calcic amphiboles. Variation along the *tsch* versus *ed* vectors within the calcic-amphibole group is shown in Figure 6. There are two striking features of this. The first is the general correlation of increasing *tschermakite* and *edenite* components noted by Robinson and Jaffe (1969) and Robinson et al. (1982); the correlation is evident between *tremolite* and values about midway between the *pargasite* and *magnesiohornblende* families are reached—ideally about

Table 1. Average “hornblende” based on 1252 analyses. Individual analyses that were included are calcic amphiboles with $0.500 < \text{tschermakite component} \leq 1.500$, but no restriction on edenite component. Structural formulas for the minimum, average and maximum Fe^{3+} estimates and the site occupancies for the *T*, *M*(2), *M*(1)+*M*(3), *M*(4) and *A* sites are given. At the bottom of each estimate: the wt% H_2O , is calculated based on the presence of 2 (OH); new values of wt% Fe_2O_3 and FeO are based on the estimated proportions of Fe^{2+} and Fe^{3+} ; the Full Total is the adjusted analytical total.

Oxides	wt% oxides	Sites	Cations	Min Ferric Form $\Sigma \text{All Fe}^{2+}$	Ave Ferric Form	Max Ferric Form 13eCNK
SiO_2	44.08	<i>T</i>	Si	6.562	6.510	6.459
TiO_2	1.12		Al	1.438	1.490	1.541
Al_2O_3	11.65					
Cr_2O_3	0.01	<i>M</i> (2)	Al	0.605	0.538	0.471
FeO	15.66		Ti	0.125	0.124	0.123
MnO	0.27		Cr	0.002	0.002	0.002
MgO	11.23		Fe^{3+}	0.000	0.359	0.718
CaO	11.16		Mg	1.268	0.977	0.686
Na_2O	1.69					
K_2O	0.65	<i>M</i> (1,3)	Mg	1.223	1.495	1.766
Cl	0.00		Fe^{2+}	1.777	1.505	1.200
F	0.00		Mn	0	0	0.034
<i>Total</i>	97.51					
		<i>M</i> (4)	Fe^{2+}	0.172	0.069	0
			Mn	0.034	0.034	0
			Ca	1.779	1.765	1.751
			Na	0.015	0.132	0.249
		<i>A</i>	Na	0.473	0.353	0.232
			K	0.123	0.122	0.121
		<i>Total</i>		15.596	15.475	15.353
			wt% H_2O	2.01	2.03	2.05
			wt% Fe_2O_3	0.00	3.23	6.52
			wt% FeO	15.66	12.75	9.79
		<i>Full Total</i>		99.53	99.87	100.21

$\text{Na}_{0.5}\text{Ca}_2(\text{Fe}^{2+}, \text{Mg})_4\text{Al}_1\text{Si}_{6.5}\text{Al}_{1.5}\text{O}_{22}(\text{OH})_2$, which is close to the “average hornblende” composition given in Table 1. The second feature is the broadening of the analysis points into elongate cloud at higher tschermakite values. The line between pargasite and tschermakite roughly marks the highest ^{6}Al content in the majority of calcic amphiboles and the highest tschermakite values are around 1.75 apfu. Two analyses of sadanagaite are unusual because they have ^{4}Al content that exceed 3.0 (Fig. 6), which is the defined maximum value for the sadanagaite. The higher ^{4}Al in these sadanagaites (Shimazaki et al. 1984) are the result of high Ti-tschermakite component ($\text{Ti} = 0.520$ and 0.503), which is balanced by twice this amount of ^{4}Al .

The relative values of X_{Mg} and X_{Ca} are keyed to four different types of symbols. Of the 20 names that are based on these variations, only the ferri-ferrotschermakite composition is not

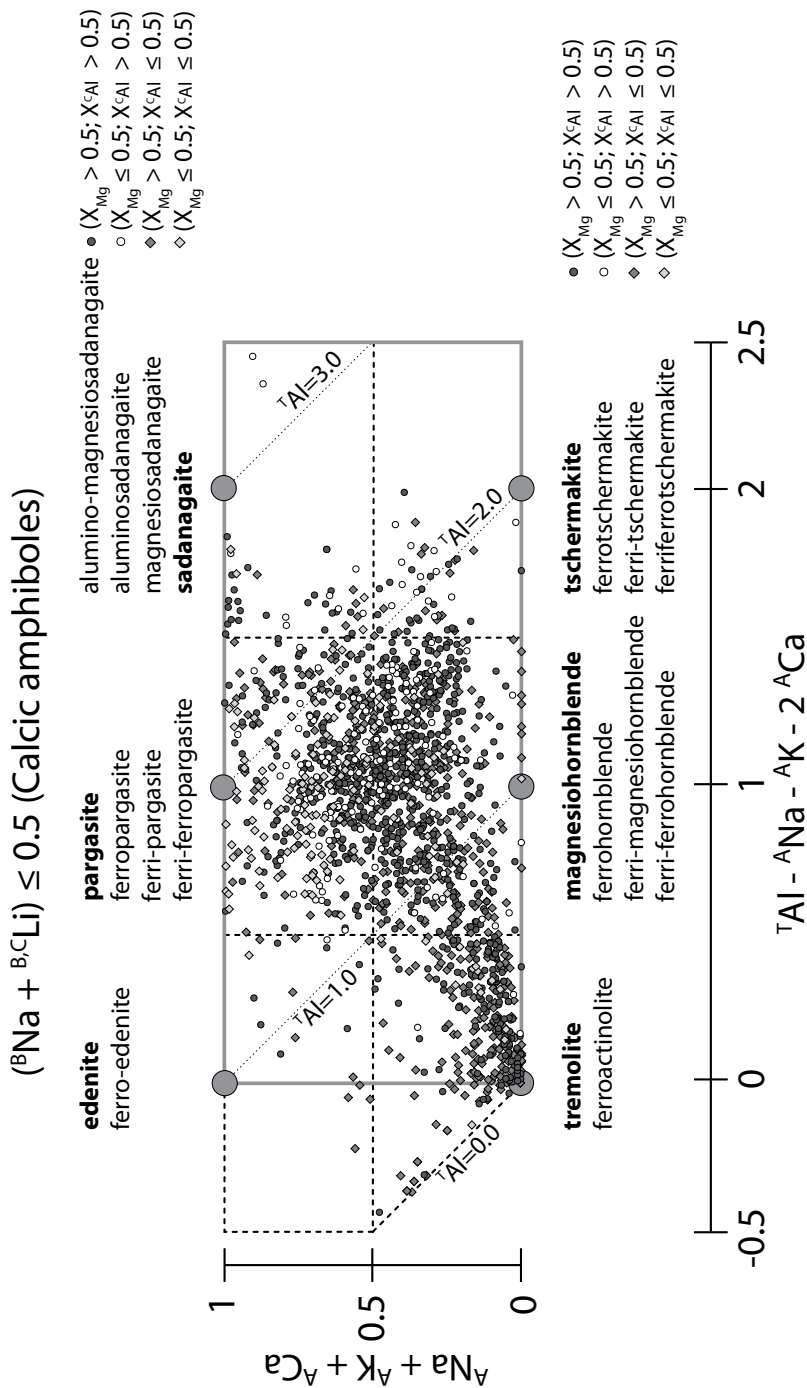


Figure 6. Plot of the generalized *tschermakite* vs. *edenite* components for all calcic amphiboles (average ferric estimate) assembled from literature sources for this study. The data points are projected along the *glaucofane* vector (see Figs. 1 and 4). The *heavy gray rectangle* marks the real amphibole composition space where *glaucofane* vector values = 0. The *dashed lines* separate the composition fields that are assigned to the end members and show the plotting limits for amphiboles with *glaucofane* components ≤ 0.5 . The *dotted lines* show isopleths of constant values of ^{39}Al . $X_{Mg} = Mg/(Mg+Fe^{2+})$ and $X_{CAI} = ^CAl/(^CAI+Fe^{3+})$.

found in these data. The data also show that calcic amphiboles with lower values of X_{Mg} tend to have the highest contents of tschermakite or edenite components (Fig. 6).

Sodic-calcic amphiboles. Variation along the *tsch* versus *ed* vectors within the sodic-calcic amphibole group is shown in Figure 7. Two correlations are evident: (1) A general increase of tschermakite and edenite components away from winchite toward taramite, an approximate one to one increase of these components; (2) a negative correlation of tschermakite and edenite components (i.e., a richterite vector) away from winchite toward richterite at $^{[4]}Al$ values of ~ 0 . Eighteen potential end-member names appear on Figure 7, and the data set includes examples of all except aluminoferrobarroisite, ferrobarroisite and ferritarimite.

Sodic amphiboles. Most of the data clusters near the glaucophane family of compositions, but variation along the *tsch* versus *ed* vectors is present (Fig. 8). The strongest correlation is away from glaucophane toward eckermannite, i.e., the *ric* vector. From the twelve end-members possible, eight are represented: ferro-eckermannite, magnesio-arfvedsonite, ferronyböite and ferric-nyböite are not present among the data for metamorphic amphiboles. Most of the analyses belong to the glaucophane-riebeckite series.

Edenite, tschermakite and glaucophane component vectors, and X_{Mg} and X_{Ca} in (Mg, Fe, Mn) amphiboles

According to the amphibole nomenclature (Leake et al. 1997), (Mg, Fe, Mn) amphiboles have less than 1.00 (Na + Ca) at the $M(4)$ site; natural examples have far less. Within the data set used here, all (Mg, Fe, Mn) amphiboles that give stoichiometric formulae have less than 0.4 Ca pfu (Fig. 9a).

As noted previously, the amphibole $M(4)$ and $M(2)$ sites are comparable to the pyroxene $M(2)$ and $M(1)$ positions. Naturally occurring (Mg, Fe, Mn) amphiboles from the cummingtonite-grunerite series and anthophyllite-gedrite series crystallize have monoclinic ($C2/m$, $P2_1/m$) and orthorhombic ($Pnma$) symmetry, respectively, and are analogous to pigeonite ($C2/c$, $P2_1/c$) and orthopyroxene ($Pcba$) (Robinson et al. 1982). To some extent, the compositional variations in the monoclinic and orthorhombic (Mg, Fe, Mn) amphiboles are analogous to those in orthopyroxene and pigeonite. The ^{B}Ca of the cummingtonite-grunerite and anthophyllite-gedrite series overlap at values less than about 0.15 apfu, but the cummingtonite-grunerite series tends to have higher ^{B}Ca , much like the values of $^{M(2)}Ca$ in pigeonite compared to orthopyroxene. However, the mica-like edenite substitution, which can be extensive in the anthophyllite-gedrite, but minor in cummingtonite-grunerite, strongly distinguishes the two series (Fig. 9a). For rocks in which anthophyllite-gedrite and cummingtonite-grunerite amphiboles coexist, ^{B}Ca and edenite components should be useful as a means to distinguish electron microprobe analyses of orthorhombic (Mg, Fe, Mn) amphiboles from cummingtonite even for cases where anthophyllite from cummingtonite are very similar.

The tschermakite-component values for the cummingtonite-grunerite series are less than 0.3 for near all analyses from these data (Fig. 9b). Comparison of the relative amounts of tschermakite component between anthophyllite-gedrite and cummingtonite-grunerite series shows extensive overlap in X_{Mg} and edenite component at tschermakite-component below about 0.3. The majority of orthoamphibole analyses have tschermakite-component values greater than 0.3. Interestingly, at tschermakite-component values from about 0.4 to 1.3, compositions that span the miscibility gap between anthophyllite and gedrite, most of the orthoamphibole data cluster around X_{Mg} values of about 0.6. At higher tschermakite-component values (greater than about 1.3), increasing tschermakite substitution correlates with an approximate 1:1 increase in edenite component, and gedrite displays almost the full range of X_{Mg} values (Fig. 9b, Fig. 10).

Variation along the *tsch* versus *ed* vectors within (Mg, Fe, Mn) amphibole group is shown in Figure 10. The data display two roughly linear trends: in the first, as the tschermakite-

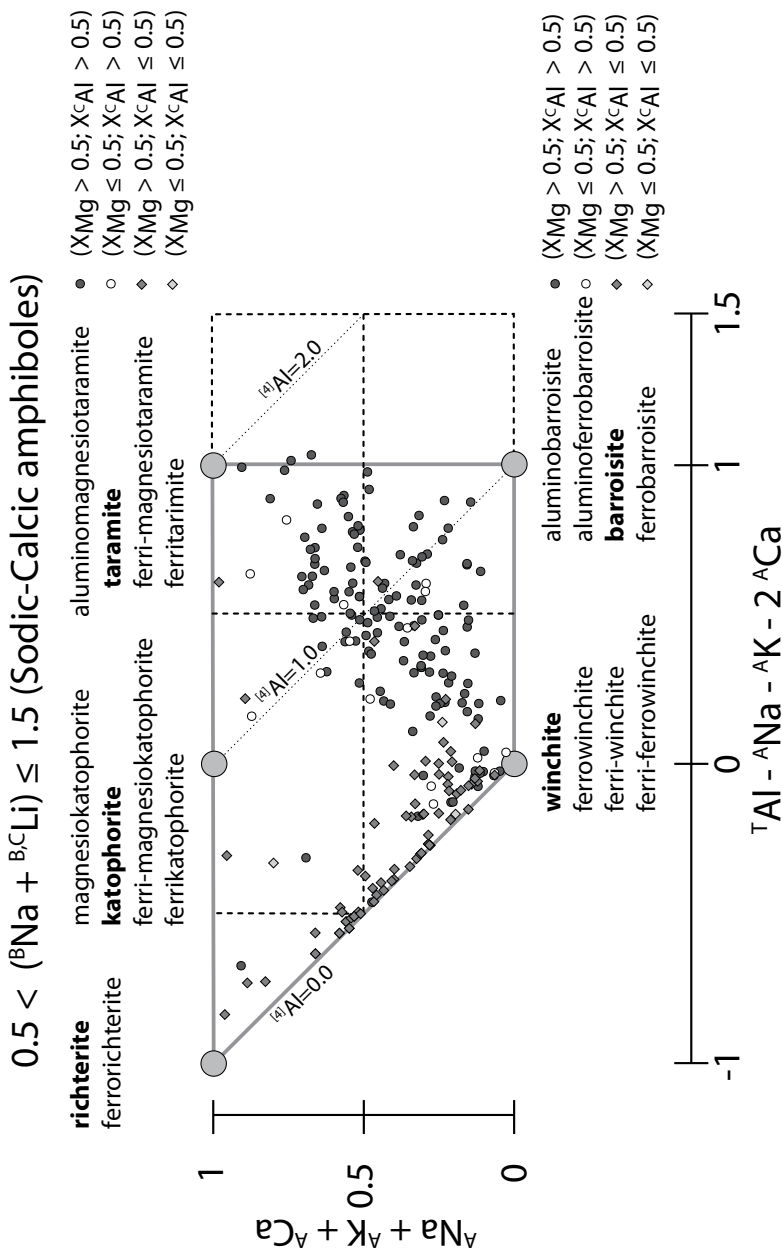


Figure 7. Plot of the generalized *tschermakite* vs. *edenite* components for all sodic-calcic amphiboles (average ferric estimate) assembled from literature sources for this study. The data points are projected along the *glaucofane* vector (see Figs. 1 and 4). The heavy gray rectangle marks the real amphibole composition space where *glaucofane* vector values = 1.0. The dashed lines separate the composition fields that are assigned to the end members and show the plotting limits for amphiboles with *glaucofane* components >0.5 and ≤ 1.5. The dotted lines show isopleths of constant values of ¹⁰Al. X_{Mg} = Mg/(Mg+Fe²⁺) and X_{Ca} = ^{Ca}Al/(^{Ca}Al+Fe³⁺).

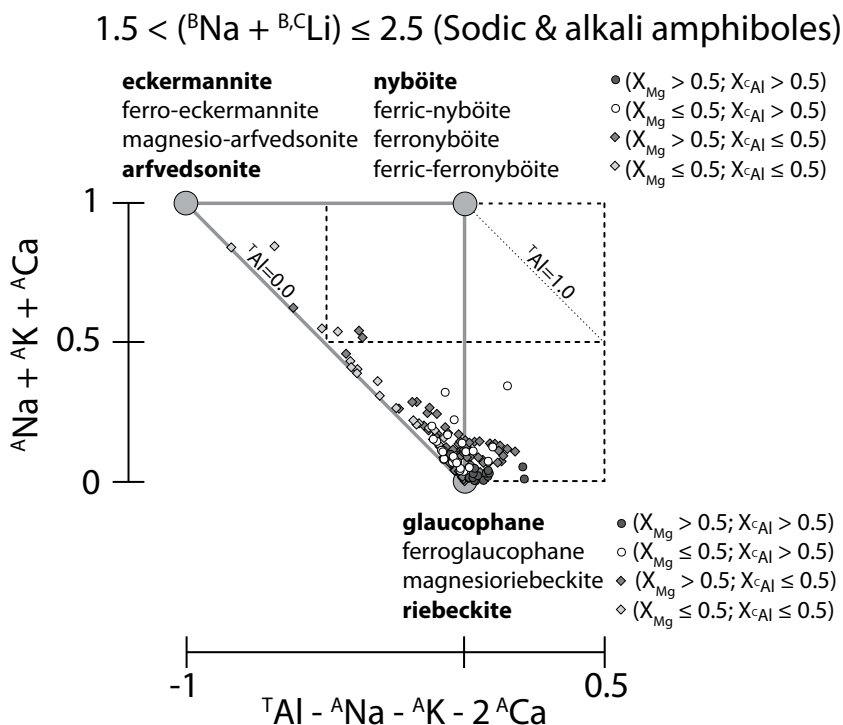


Figure 8. Plot of the generalized *tschermakite* vs. *edenite* components for all sodic amphiboles (average ferric estimate) assembled from literature sources for this study. The data points are projected along the *glaucophane* vector (see Figs. 1 and 4). The heavy gray rectangle marks the real amphibole composition space where *glaucophane* vector values = 2.0. The dashed lines separate the composition fields that are assigned to the end members and show the plotting limits for amphiboles with *glaucophane* components >1.5 and ≤ 2.5 . The dotted lines show isopleths of constant values of ${}^{14}\text{Al}$. $X_{\text{Mg}} = \text{Mg}/(\text{Mg}+\text{Fe}^{2+})$ and $X_{\text{cAl}} = {}^{\text{c}}\text{Al}/({}^{\text{c}}\text{Al}+\text{Fe}^{3+})$.

component increases to about 1.0-1.3, the edenite component rises to about 0.3; in the second, as the *tschermakite*-component increases from about 1.0-1.3 to about 1.9, the edenite component climbs from 0.30 to about 0.95 (Fig. 10). This variation in trends suggests that higher Al content promotes the edenite substitution.

Comparing Figure 10 with the corresponding figures for calcic, sodic-calcic and sodic amphiboles (Figs. 6-8) shows clearly that the end-member positions and boundaries separating the end-members (heavy gray lines) for the (Mg, Fe, Mn) amphibole group (Leake et al. 1997) were chosen on very different criteria from that of the other amphiboles. While the appropriateness of these boundaries may be open to debate, it is important to acknowledge that, at the time, these fields were set as a compromise that preserves historic naming conventions based on the long-recognized existence of a solvus in the orthoamphibole composition series, which is richly cited in the literature as the *anthophyllite-gedrite solvus*.

On Figure 10, the relative values of X_{Mg} and X_{cAl} are keyed to four different symbol types. Unlike the calcic, sodic-calcic and sodic amphiboles, there are no end-member names for (Mg, Fe, Mn) amphiboles with $X_{\text{cAl}} \leq 0.5$. All 10 end-members from (Leake et al. 1997) occur among the data used here, and very few examples have $X_{\text{cAl}} \leq 0.5$ (Fig. 10).

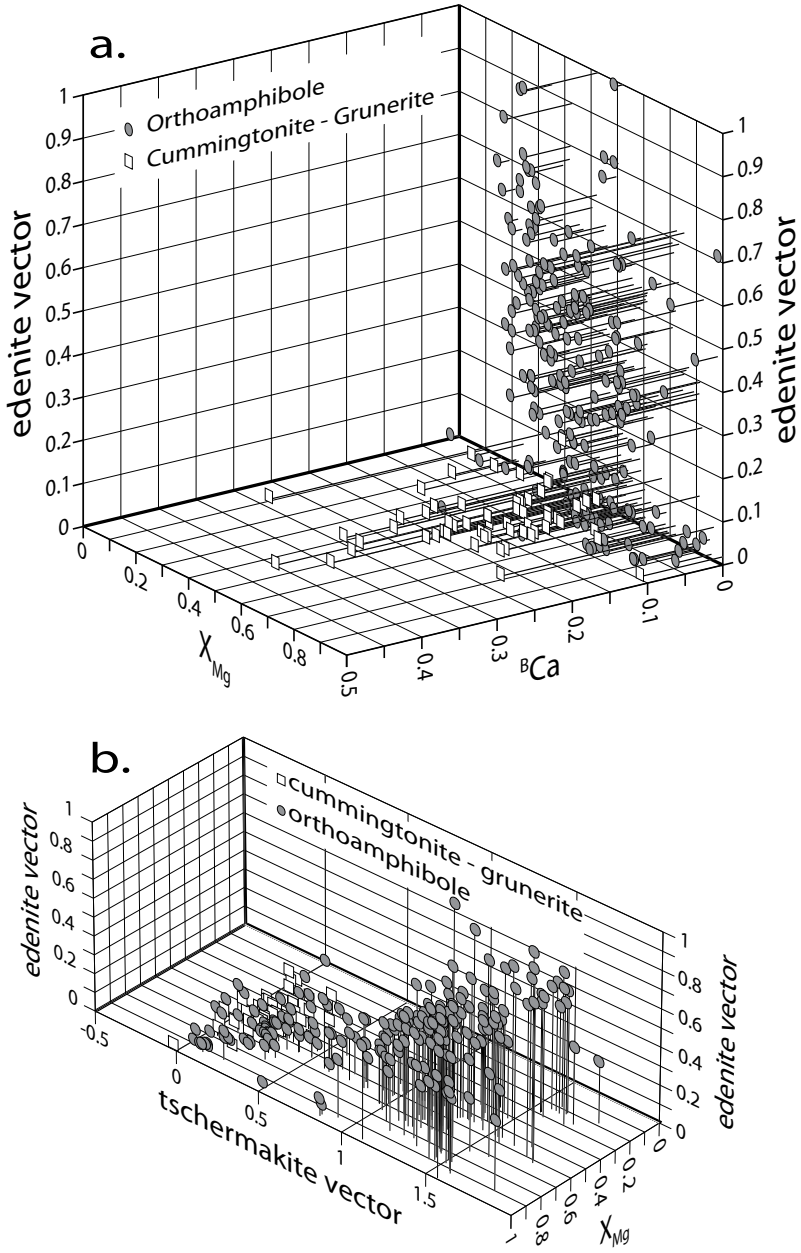


Figure 9. Plots of compositional variations (Mg, Fe, Mn) amphiboles (average ferric estimate) assembled from literature sources for this study. (a) Plot of X_{Mg} -edenite content- B_{Ca} . (b) Plot of *tschermakite* component-edenite components- X_{Mg} , where $X_{Mg} = Mg/(Mg+Fe^{2+})$.

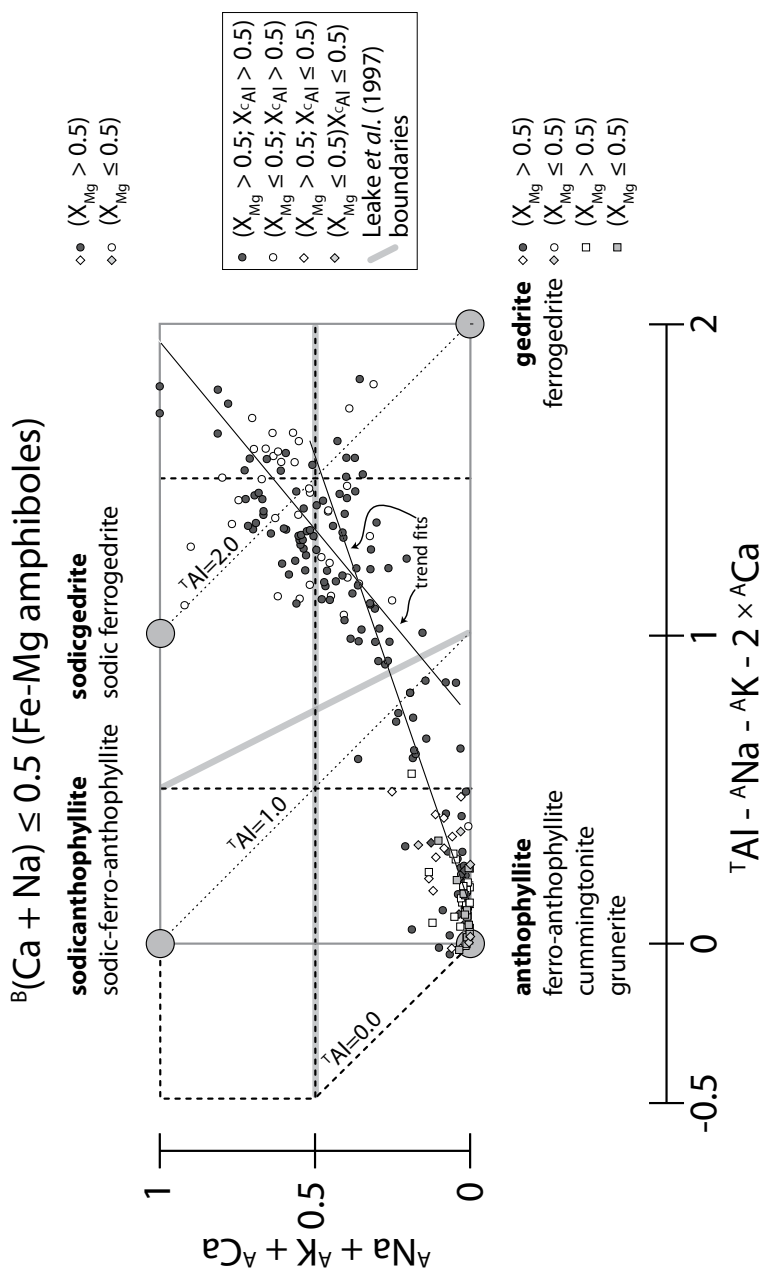


Figure 10. Plot of the generalized *tschermakite* vs. *edenite* components for all (Mg, Fe, Mn) amphiboles (average ferric estimate) assembled from literature sources for this study. The data points are projected along the *glaucophane* vector (see Figs. 1 and 4). The *heavy gray rectangle* marks the real amphibole composition space where *glaucophane* vector values = 0.0. The *dashed lines* separate the composition fields of the end members as in Figures 7-9 and show the plotting limits for amphiboles with *glaucophane* components ≤ 0.5 . The *heavy gray lines* show the four composition fields that are assigned (Mg, Fe, Mn) amphiboles by the amphibole nomenclature of Leake et al. (1997). The *trend lines* are linear regressions using the reduced major axis model for the analyses with *tschermakite* component values below and above 1.0. $X_{Mg} = Mg/(Mg+Fe^{2+})$ and $X_{Ca} = Ca/(Ca+Fe^{3+})$.

Variations in $Mg/(Mg + Fe^{2+})$

Figure 11 is a histogram of $Mg/(Mg + Fe^{2+})$ (X_{Mg}) for calcic, sodic-calcic, sodic and (Mg, Fe, Mn) amphiboles. A striking feature is that all the amphibole groups have broad peaks that lie at X_{Mg} values of about 0.6. The calcic, sodic-calcic and sodic amphiboles show nearly the full spectrum of X_{Mg} values. Few sodic amphiboles lie outside the range 0.35-0.80; few sodic-calcic amphiboles lie below values of 0.4 and the calcic amphiboles are skewed to the high side of the peak (Fig. 11a). The histogram of X_{Mg} for orthoamphiboles (Fig. 11b) is skewed remarkably similarly to that of the calcic amphiboles. The similarity between these histograms may mean that both Mg- and tschermakite-rich (“hornblende” and “gedrite”) and tschermakite-poor (“tremolite” and “anthophyllite”) calcic and orthorhombic amphiboles are abundant in nature. The histogram of X_{Mg} for monoclinic (Mg, Fe, Mn) amphiboles are similar to that of orthoamphibole, but with a less skewed distribution around the centroid.

The tendency of all the amphibole analyses to cluster around X_{Mg} values of about 0.6 suggests that the (Fe,Mg) partitioned at $M(1)$ and $M(3)$ is probably the strongest control on the bulk X_{Mg} of the amphibole. This is implied by the observation that sodic amphiboles with effectively no Mg, Fe^{2+} or Mn^{2+} at $M(2)$ or $M(4)$ show the same peak as do the other amphibole groups. In calcic, sodic-calcic and orthorhombic amphiboles, preference for Mg at $M(2)$ manifests itself as a skew to higher X_{Mg} values, prominent in the calcic and orthorhombic (Mg, Fe, Mn) amphiboles, but more subtle in the sodic-calcic amphiboles, which have by definition at least 0.5 and as many as 1.5 R^{3+} or R^{4+} apfu at $M(2)$.

Compositional variations in Mg, Fe^{2+} , Mn^{2+} and total R^{2+}

Total R^{2+} . The divalent cations Mg, Fe^{2+} and Mn^{2+} are all B and C group cations that occur at $M(4)$ and $M(1,2,3)$ sites in amphiboles. End-members of the calcic, sodic-calcic and sodic amphiboles ideally have 3 to 5 of the $M(1,2,3)$ sites available for the R^{2+} -cations, Mg, Fe^{2+} and Mn^{2+} ; in the (Mg, Fe, Mn) amphiboles all the $M(1,2,3,4)$ sites are available for R^{2+} -cations, which vary ideally from 7 to 5 cations. In the metamorphic amphibole data used here, most of the R^{2+} -cation variation is the result of the variable extent of tschermakite-like or glaucophane-like substitutions, which replace R^{2+} -cations at the $M(2)$ site. The exchange

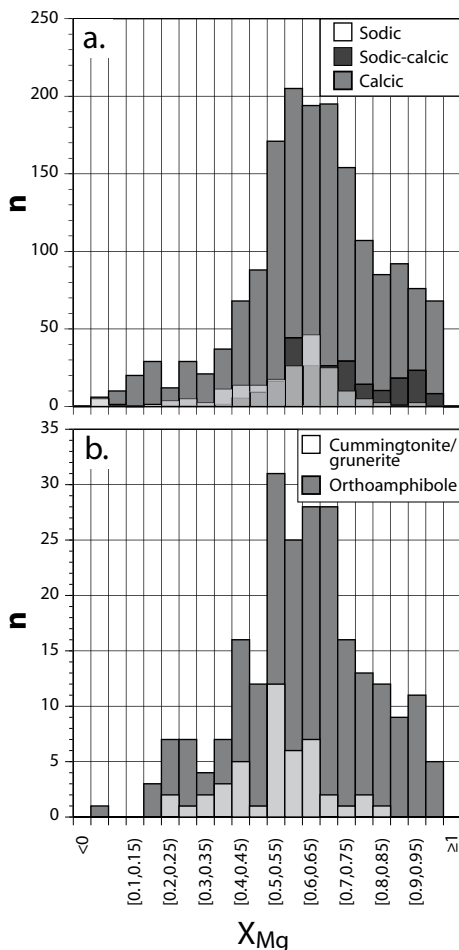


Figure 11. Histograms of X_{Mg} , where $X_{Mg} = Mg/(Mg+Fe^{2+})$ for all amphiboles (average ferric estimate) assembled from literature sources for this study. (a) Calcic, sodic-calcic and sodic amphiboles and (b) (Mg, Fe, Mn) amphiboles. n = number of analyses.

of Mg, Fe²⁺ and Mn²⁺ for Ca at the *M*(4) site is of minor importance in all except in the cummingtonite-grunerite series and calcic, sodic-calcic and sodic amphiboles that coexist with (Mg, Fe, Mn) amphiboles. The total R²⁺-cations in calcic, sodic-calcic and sodic amphiboles lie at about 4.15, 3.85, 3.25 apfu on the histograms (Fig. 12). Three maxima for total R²⁺-cations in (Mg, Fe, Mn) amphiboles (Fig. 12) are present; orthoamphiboles have two maxima at about 5.6 and 6.75 R²⁺-cations.

R²⁺ cations, Na and Ca at the *M*(4) site. Based on site assignments, natural calcic, sodic-calcic and sodic amphiboles commonly have B-group (Na + Ca) slightly less than 2 apfu, so small amounts of R²⁺-cations are will be present. Histograms of total R²⁺-cations at *M*(4) (Fig. 13a,b) for calcic, sodic-calcic and sodic amphiboles show that R²⁺ cations peak at between 0.05 and 0.10 apfu and that most of these amphiboles will have less than 0.20 R²⁺ cations at *M*(4) (i.e., Ca and Na are likely to fill 90% or more of the available *M*(4) sites).

Natural orthorhombic and monoclinic Fe-Mg amphiboles commonly have small amounts of (Na + Ca) at *M*(4). Histograms of the total R²⁺ cations at *M*(4) (Fig. 13c) for orthorhombic and monoclinic (Mg, Fe, Mn) amphiboles show that R²⁺ cations peak at between 1.85 and 1.90 apfu. Most (Mg, Fe, Mn) amphiboles have greater than 1.80 R²⁺ cations pfu at *M*(4) (i.e., Ca and Na may fill up to 10% of the available *M*(4) sites in most examples). For the majority of amphiboles from this dataset, R²⁺ contents at *M*(4) lie either very close to zero apfu (calcic, sodic-calcic and sodic amphiboles) or very close to 2 apfu ((Mg, Fe, Mn) amphiboles).

The Na and Ca contents at *M*(4) of calcic, sodic-calcic and sodic amphiboles are summarized in Figure 13d. The Ca cation contents of calcic amphiboles peak at about 1.9-1.85 apfu, and the histogram is strongly skewed to high Ca values. The ^M(4)Na histogram for calcic amphiboles is effectively the mirror image, strongly skewed to low Na values with a peak at

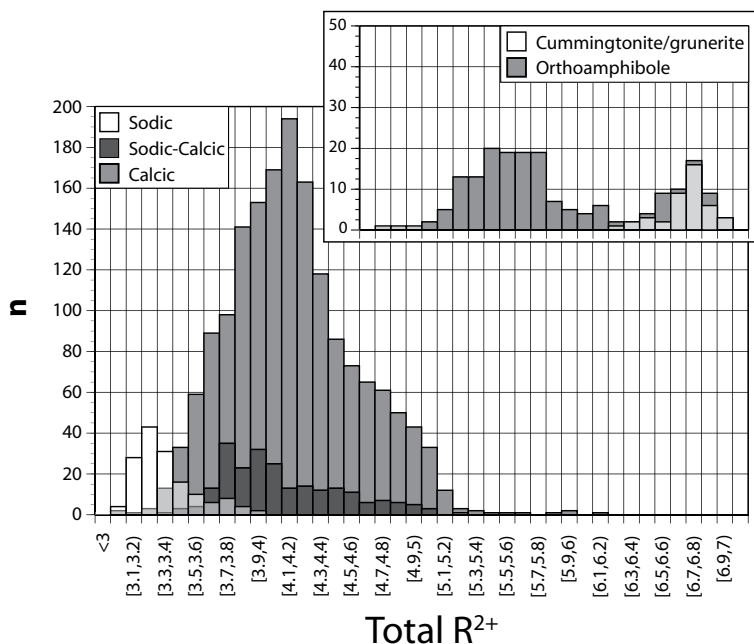


Figure 12. Histograms of total R²⁺ content, where R²⁺ = Mg+Fe²⁺+Mn²⁺ for calcic, sodic-calcic, sodic and (Mg, Fe, Mn) amphiboles (average ferric estimate) assembled from literature sources for this study. n = number of analyses.

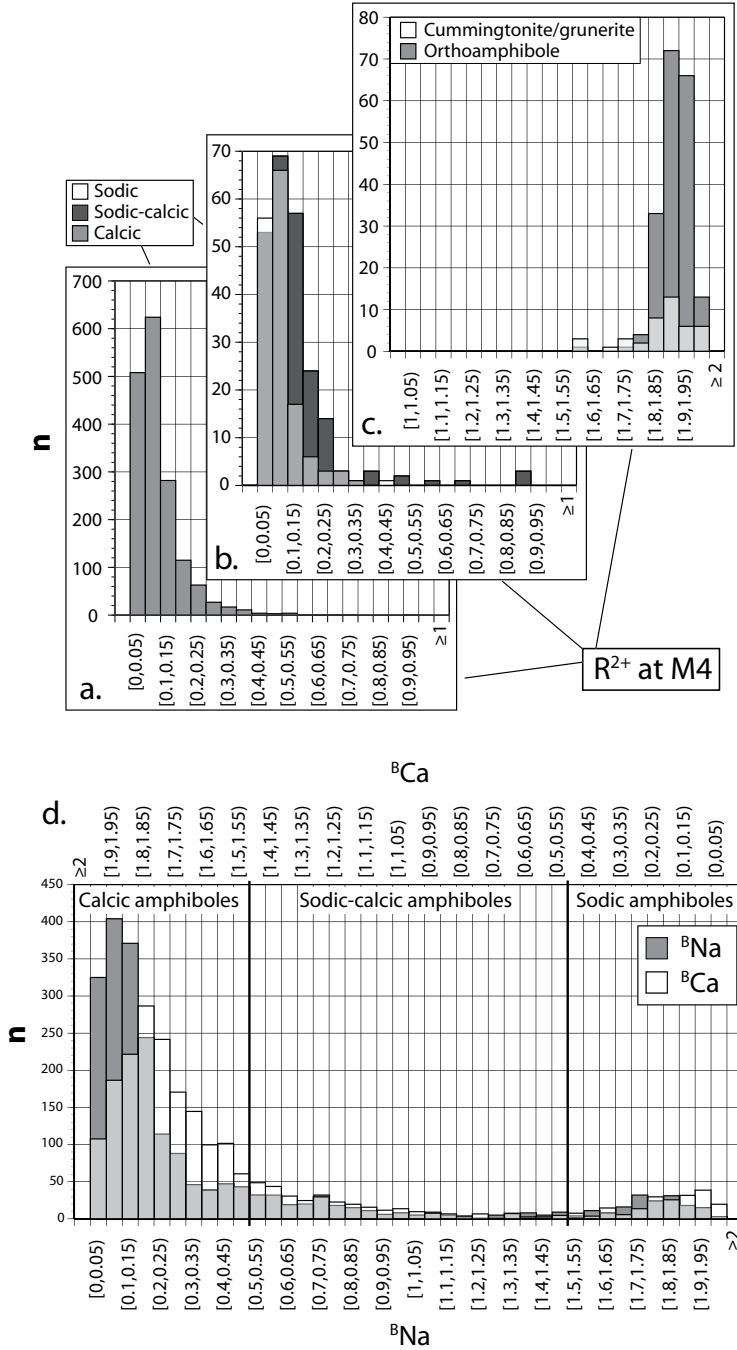


Figure 13. (a, b, c) Histograms of R^{2+} content assigned to the $M(4)$ site, where $R^{2+} = \text{Mg} + \text{Fe}^{2+} + \text{Mn}^{2+}$ for calcic, sodic-calcic, sodic and (Mg, Fe, Mn) amphiboles (average ferric estimate) assembled from literature sources for this study. (d) Histograms of ${}^B\text{Na}$ and ${}^B\text{Ca}$ for calcic, sodic-calcic and sodic and amphiboles (average Fe^{3+} estimate) assembled from literature sources for this study. n = number of analyses.

0.15-0.20 apfu (Fig. 13d). Most sodic-calcic amphiboles have Ca values > 1.0 apfu and ${}^B\text{Na} < 1.0$ apfu (Fig. 13d). For the sodic amphiboles, the ${}^B\text{Na}$ values peak between 1.75a and 1.85 apfu, and the Ca values peak at about 0.1 apfu (Fig. 13d).

Lack of complete mixing of (Ca+Na) relative to $(\text{Mg}+\text{Fe}^{2+}+\text{Mn}^{2+})$ at the $M(4)$ site is basis for the miscibility gap between calcic, sodic-calcic and sodic amphiboles collectively and (Mg, Fe, Mn) amphiboles, and this feature is most commonly observed in coexisting calcic and (Mg, Fe, Mn) amphiboles (Robinson and Jaffe 1969; Robinson et al. 1982). Lack of complete mixing of Ca and Na at the $M(4)$ site under some metamorphic condition and appropriate bulk compositions is the basis for the miscibility gap between coexisting Na-richer versus Ca-richer amphiboles. The histogram in Figure 13d illustrates this miscibility gap in the form of double overlapping peaks for Ca and Na at the $M(4)$ site.

R^{2+} cations at the $M(2)$ site. For all amphiboles, the R^{2+} contents assigned to the $M(2)$ site (2 of the 5 C-group sites) is much more variable. The calcic and orthorhombic amphiboles show the complete range of R^{2+} contents from about 0 to 2 apfu (Fig. 14). This variation is due principally to variable extents of tschermakite-like component. The calcic amphiboles have a peak R^{2+} content of about 1.05 apfu, but the distribution is skewed slightly toward higher values owing to the common occurrence of tremolitic amphiboles (Fig. 14a). The orthoamphiboles show two peaks of R^{2+} -cation contents (Fig. 14b), one at about 0.7 apfu and the other at about 1.75 apfu, which correspond roughly to the range of compositions at the limbs of the anthophyllite-gedrite solvus (Robinson et al. 1982; Spear 1982). The monoclinic (Mg, Fe, Mn) amphiboles (cumingtonite-grunerite) have peak R^{2+} -cation contents of about 1.85 apfu and their distribution mimics the anthophyllite peak in the orthoamphiboles.

In the sodic-calcic amphiboles the R^{2+} contents assigned to the $M(2)$ site range from 0 (richterite) to 2 apfu (barroisite and taramite), but the actual range shown by these samples is 0.3 to 2 apfu with a peak value of 0.75 apfu (Fig. 14a). Amphiboles classed as sodic ideally would have 0 (glaucophane and nyböite) to 1 apfu (eckermannite) have R^{2+} contents at the $M(2)$ site, but natural compositions classed as eckermannite could have up to 1.5 R^{2+} apfu at $M(2)$. The actual peak lies at about 0.15 apfu (Fig. 14a). The range of these samples is 0 to 1.1 apfu, the histogram is asymmetric about the peak and tails off to higher values.

Total Mg, Fe^{2+} and Mn^{2+} contents. In calcic, sodic-calcic and sodic amphiboles,

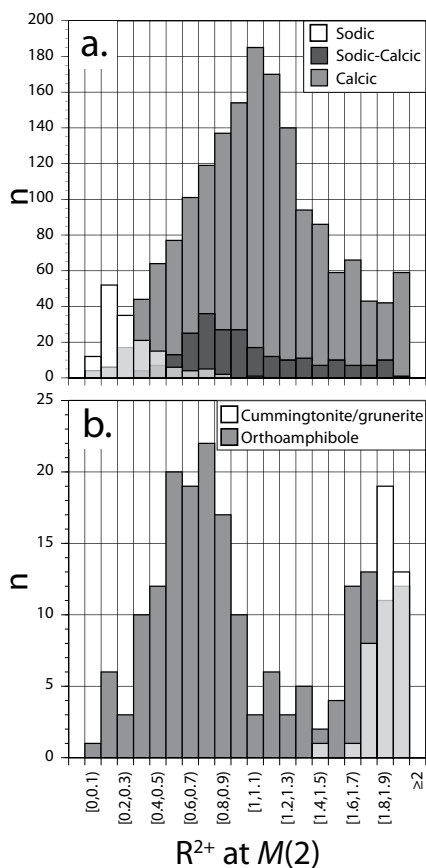


Figure 14. Histograms of Mg, Fe^{2+} and Mn^{2+} content assigned to the $M(2)$ sites, where $R^{2+} = \text{Mg} + \text{Fe}^{2+} + \text{Mn}^{2+}$ for calcic, sodic-calcic, sodic and (Mg, Fe, Mn) amphiboles (average ferric estimate) assembled from literature sources for this study. n = number of analyses.

total Mg peaks at about 2.5, 2.3 and 2.0 apfu respectively (Fig. 15). The Mg values for calcic amphiboles approximate a normal distribution with a slightly positive skew, while the sodic-calcic amphiboles show a positive skew and possible a small secondary peak at about 4.4 apfu. The Mg values for sodic amphiboles also show a positive skew. The orthorhombic and monoclinic Fe-Mg amphiboles give multi-peaked histograms, the highest Mg values for these amphiboles respectively are at 3.7 and about 3.2-3.6 apfu (Fig. 16). The Mg values for both the orthorhombic and monoclinic Fe-Mg amphiboles hint at positive skewness, but more data is required to confirm this.

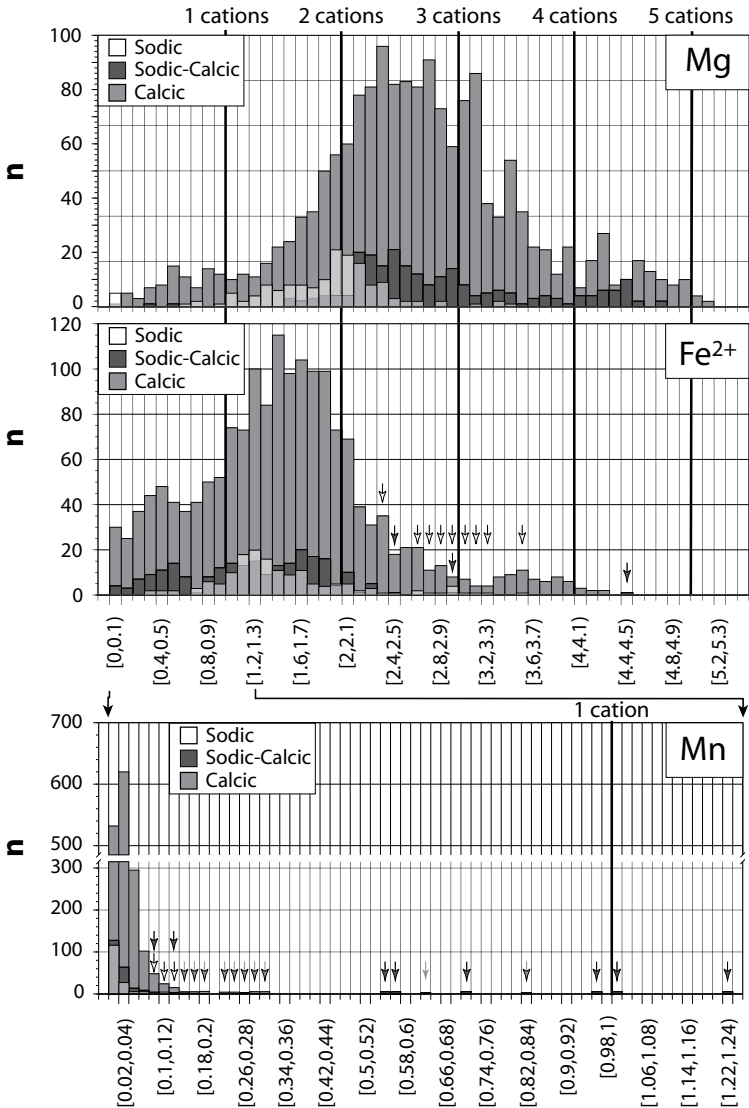


Figure 15. Histograms of for Mg, Fe²⁺ and Mn²⁺ contents of calcic, sodic-calcic and sodic amphiboles (average Fe³⁺ estimate) assembled from literature sources for this study. n = number of analyses.

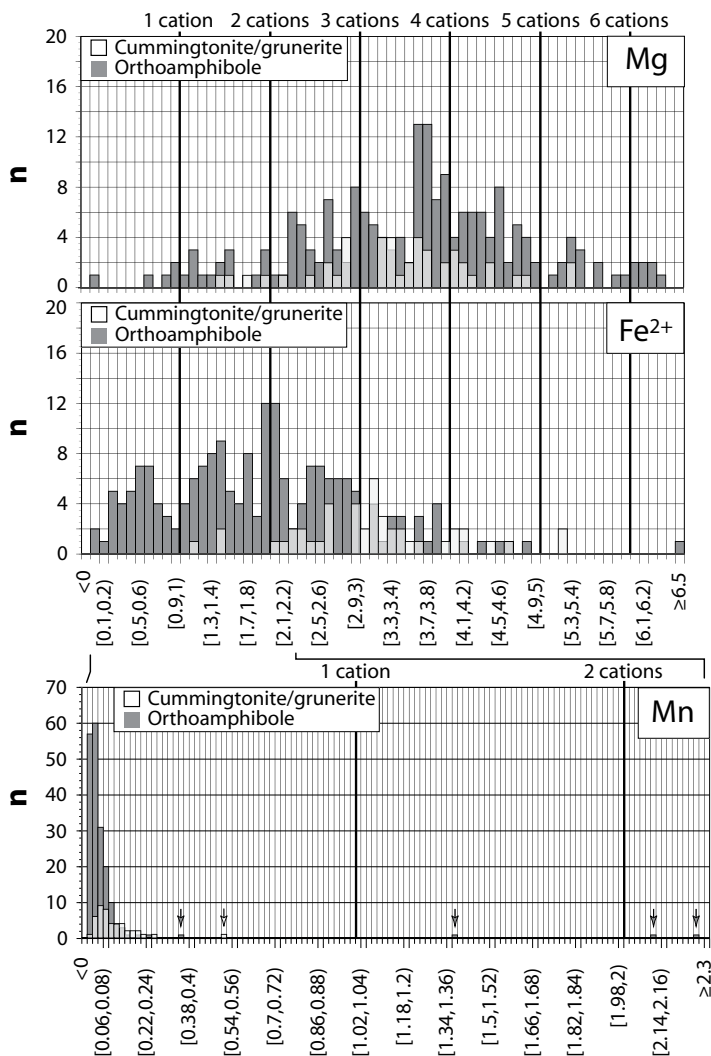


Figure 16. Histograms of for Mg, Fe²⁺ and Mn²⁺ contents of (Mg, Fe, Mn) amphiboles (average Fe³⁺ estimate) assembled from literature sources for this study. n = number of analyses.

The peaks for Fe²⁺ for calcic and sodic amphiboles are about 1.6 and 1.2 apfu, respectively, while the sodic-calcic do not show a distinct peak for Fe²⁺ and are spread more evenly between at values less than 2 apfu. The calcic and sodic amphiboles show negative skews that complement their Mg histograms (Fig. 15). The histograms for Mg and Fe²⁺ for the sodic-calcic amphiboles shows a break at about 2 apfu with most sodic-calcic amphiboles having more than 2 apfu of Mg, but less than 2 apfu of Fe²⁺. The Fe²⁺ contents of the orthoamphiboles lie mostly below 3 apfu with the highest peak of a multi-peaked histogram at 2 apfu (Fig. 16). Most of the monoclinic (Mg, Fe, Mn) amphiboles have values around 3 apfu.

These data show that for calcic, sodic-calcic and sodic amphiboles, occupancy of Mn²⁺ is very minor, and the histograms for this element are strongly negatively skewed. Peaks are at

about 0.03, 0.01 and 0.01 apfu, respectively for the calcic, sodic-calcic and sodic amphiboles. The vast majority of the calcic, sodic-calcic and sodic amphiboles have less than 0.100 Mn²⁺ apfu (Fig. 15), and only 15 have values above 0.14 apfu, but can range as high as 1.24 apfu. Like the calcic, sodic-calcic and sodic amphiboles, orthorhombic and monoclinic (Mg, Fe, Mn) amphiboles have Mn²⁺ histograms that show a strong negative skew. The orthoamphiboles have peak values like those of the calcic amphiboles at 0.03 Mn apfu, but the monoclinic (Mg, Fe, Mn) amphiboles have higher peaks at about 0.05 Mn apfu (Fig. 16). Most of the Mn contents of the orthorhombic and monoclinic (Mg, Fe, Mn) amphiboles lie below 0.21 Mn apfu, but 2 samples from these data have over 2 Mn apfu (Fig. 16).

These histograms show amphiboles tend to be among the minerals most enriched in Mg. Amphiboles from these data show only rare examples enriched in Mn, but amphiboles from all but the sodic amphibole group show a few individuals with higher than average Mn contents, which suggests that amphiboles have the capacity for high Mn content, but that the low Mn contents of common amphiboles reflect low Mn in their protoliths. The orthorhombic and monoclinic (Mg, Fe, Mn) amphiboles have higher Mn contents where compared calcic, sodic-calcic and sodic amphiboles, indicating that Mn competes with Na and Ca at *M*(4) and that *M*(4) is the preferred site for Mn.

Compositional variations in ^CAl, ^CFe³⁺ and ^CTi⁴⁺. In calcic and sodic-calcic amphiboles, ^CAl or ^CFe³⁺ contents in excess of about 1.2 apfu are uncommon (Fig. 17). For the calcic amphiboles, the histogram of ^CAl has a broad peak from 0.00-0.55 apfu and tapers off to higher values, while the ^CFe³⁺ histogram has a distinct, negatively skewed peak at about 0.225 apfu. In the sodic amphiboles, which at a minimum have 0.5 ^CR³⁺ apfu, show the whole range of ^CAl or ^CFe³⁺ from 0.0-2.0 apfu with ^CAl peaks at about 1.65 apfu and lower ^CFe³⁺ peaks at about 0.125 apfu (Fig. 17).

The monoclinic (Mg, Fe, Mn) amphiboles have low ^CAl and ^CFe³⁺ contents mostly less than about 0.200 apfu (Fig. 18). The orthoamphiboles display a whole range of ^CAl contents, from 0.0 to nearly 2.0 apfu, while ^CFe³⁺ contents are less than 1.0 apfu. Histograms for both ^CAl and ^CFe³⁺ for the orthoamphiboles display two peaks that show the existence of the anthophyllite-gedrite solvus; the peak flank at about 0.0-0.15 apfu and the peak at 0.85 apfu for ^CAl and the peak flank at about 0.0-0.15 apfu and the peak at 0.60 apfu for ^CFe³⁺ reflect the anthophyllite and gedrite limbs of the orthoamphibole solvus (Fig. 18).

The ^CTi⁴⁺ content in these data show the calcic amphiboles have less than 0.65 Ti⁴⁺ apfu and all other amphiboles have less than 0.20 apfu. All the histograms show the same half peaks that tail away from their maximum values at the lowest Ti contents (Figs. 17, 18).

The relative values of ^CAl, ^CFe³⁺ and ^CTi⁴⁺ in the calcic, sodic-calcic and sodic amphiboles (ternary diagram, Fig. 17) show that only in the calcic amphiboles does Ti play an important role in coupled substitutions that involve ⁶R³⁺ cations (glaucophane or tschermakite substitution vectors). It is not possible to associate Ti *a priori* with either the tschermakite-like or glaucophane-like substitutions. Nevertheless, the calcic amphiboles, by definition, have lowest glaucophane components, and only in these amphiboles does Ti constitute a major part of the total ⁶R³⁺; whereas, in the sodic-calcic and sodic amphiboles, which have lower average tschermakite components and higher glaucophane components, ⁶Ti is of minimal importance. This observation suggests that Ti probably substitutes via a tschermakite-type substitution. Higher Ti content has also been positively correlated with higher temperature in assemblages with a saturating Ti-phase such as rutile, ilmenite or sphene (Raase 1974; Robinson et al. 1982; Schumacher et al. 1990), and Ernst and Liu (1998) show a calibration of this relation.

Compositional variations at the A-site

Although recent work (Hawthorne et al. 1996) has shown Ca can be the dominant cation at the A-site, this is a rule exception for metamorphic amphiboles. Hawthorne et al. (1996) showed

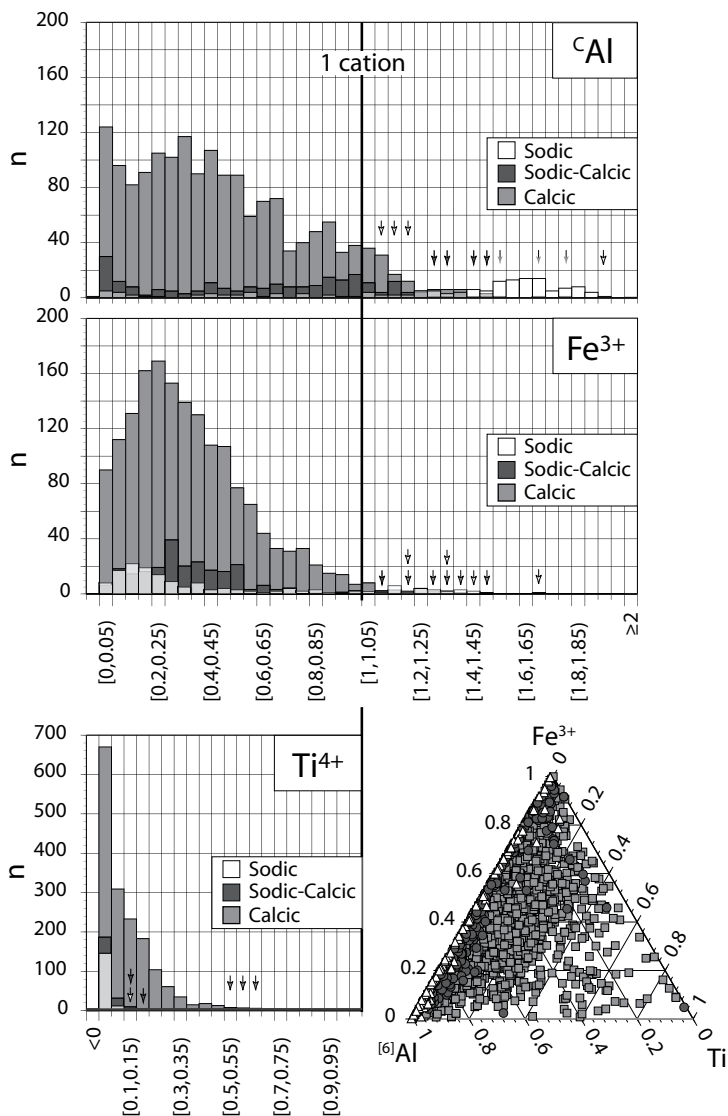


Figure 17. Histograms of for ${}^c\text{Al}$, Fe^{3+} and ${}^c\text{Ti}^{4+}$ contents and a ternary diagram showing the proportions of ${}^c\text{Al}$, Fe^{3+} and ${}^c\text{Ti}^{4+}$ for calcic, sodic-calcic and sodic amphiboles (average Fe^{3+} estimate) assembled from literature sources for this study. n = number of analyses.

that pargasites from Pargas, Finland, had small amounts of Ca (< 0.20 apfu) at the A-site. For all the amphiboles included here, stoichiometric formulae have A sites with only Na or K. In histograms of total A-site occupancy, both calcic amphiboles and sodic-calcic amphiboles show broad peaks centered around $0.4^{\text{A}}(\text{Na} + \text{K})$ apfu, and both sodic amphiboles and cummingtonite-grunerite have peak ${}^{\text{A}}(\text{Na} + \text{K})$ at contents < 0.1 apfu (Fig. 19). The histograms of total A-site occupancy for orthoamphibole show two peaks at < 0.1 apfu and at $0.3\text{--}0.4^{\text{A}}(\text{Na} + \text{K})$ apfu, reflecting the two limbs of the gedrite - anthophyllite solvus (Fig. 19a).

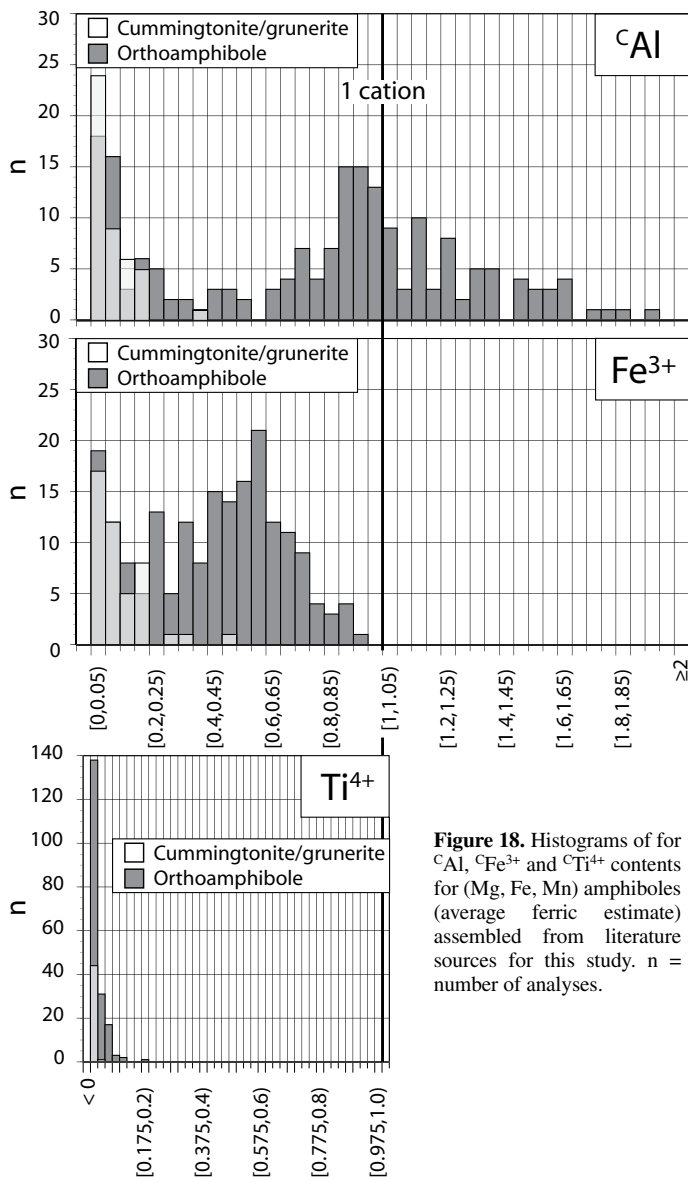


Figure 18. Histograms of for ${}^c\text{Al}$, ${}^c\text{Fe}^{3+}$ and ${}^c\text{Ti}^{4+}$ contents for (Mg, Fe, Mn) amphiboles (average ferric estimate) assembled from literature sources for this study. n = number of analyses.

Sodium is the dominant cation at the A-site. Calcic amphiboles have the highest ${}^A\text{K}$ in general, but in the overwhelming majority of analyses ${}^A\text{Na} > {}^A\text{K}$ (Fig. 20). Most of the sodic-calcic amphiboles have ${}^A\text{Na}/({}^A\text{Na} + {}^A\text{K})$ ratios > 0.80 , and most sodic amphiboles have ${}^A\text{Na}/({}^A\text{Na} + {}^A\text{K})$ ratios > 0.90 . The (Mg, Fe, Mn) amphiboles generally have ${}^A\text{K}$ less than 0.02 apfu. The monoclinic (Mg, Fe, Mn) amphiboles in general have low A-site occupancy, but the orthorhombic (Mg, Fe, Mn) amphiboles, despite the fact that A-site occupancy can reach 1.0 apfu (Fig. 20), also have uniformly low ${}^A\text{K}$, which is due to the smaller A-cavity in the orthorhombic structure that successfully excludes K.

COEXISTING METAMORPHIC AMPHIBOLES

Assemblages with multiple amphiboles

The recognition and characterization of petrographically and chemically different assemblages of two or more coexisting amphiboles in amphibolite-facies rocks constituted research that culminated at about the time of the previous RiM Volume 9B (Robinson et al. 1982), and over 50 pages of that volume is devoted to this topic. In particular, work begun by Robinson and Jaffe (1969) and Klein (1968) led to the description of numerous examples of three- and even four-amphibole assemblages (e.g., Spear 1982) consisting of combinations of the amphiboles hornblende, cummingtonite, anthophyllite and gedrite. Coexisting calcic amphiboles and sodic amphiboles or sodic-calcic amphiboles are also known (Himmelberg and Papike 1969; Klein 1969), and there was a minor controversy concerning the existence of a solvus in the actinolite-hornblende series (Brady 1974; Grapes and Graham 1978; Klein 1969). Reports and descriptions of coexisting amphiboles from additional localities continue to appear, but more of the more recent work on coexisting amphiboles has involved HRTEM,

TEM and AEM studies (e.g., Smelik and Veblen 1989, 1991, 1992a,b, 1993, 1994; Smelik et al. 1991; Klein et al. 1993, 1997; Shau et al. 1993).

Evaluating equilibrium coexistence

One of the most interesting and useful aspects of metamorphic rocks is their ability to record and preserve multiple stages of their *P-T* histories due to incomplete reequilibration of phases and local assemblages as temperature and pressure decrease. This very useful property of metamorphic rocks in some cases can be a hindrance in interpreting textural evidence for equilibrium coexistence of two or more amphiboles. The simple presence of chemically or optically distinct amphiboles in a rock or a thin section is not, in itself, conclusive proof of equilibrium coexistence across either a solvus or a miscibility gap. The competing alternative explanation is metastable persistence of an earlier formed amphibole at conditions under which a new and different amphibole is formed. Depending on the reaction, the new conditions and the rate of cooling, a diverse set of textures could be produced. In the most extreme case of metamorphic fractional crystallization, an early amphibole might persist completely independently of the reactions and phases involved in the production of the second (or even third) generation amphibole. More realistically, an earlier metastable amphibole composition may participate to various extents in the reactions forming the

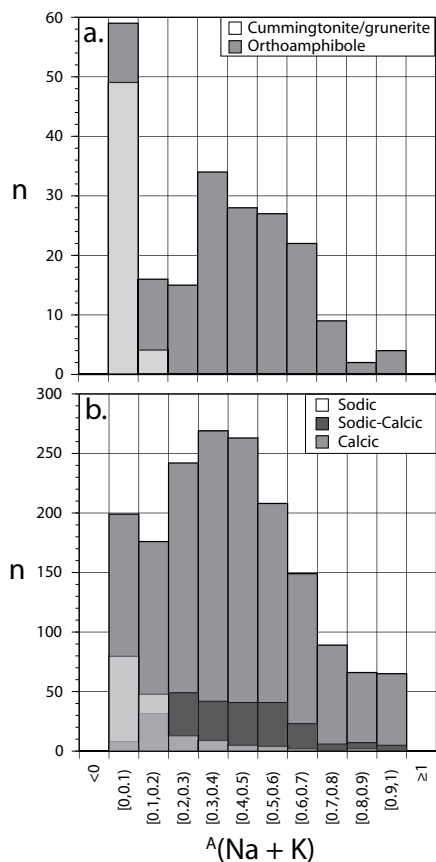


Figure 19. Histograms of A_{Na} and A_K . (a) (Mg, Fe, Mn) amphiboles and (b) calcic, sodic-calcic and sodic amphiboles (average Fe^{3+} estimate) assembled from literature sources for this study. n = number of analyses.

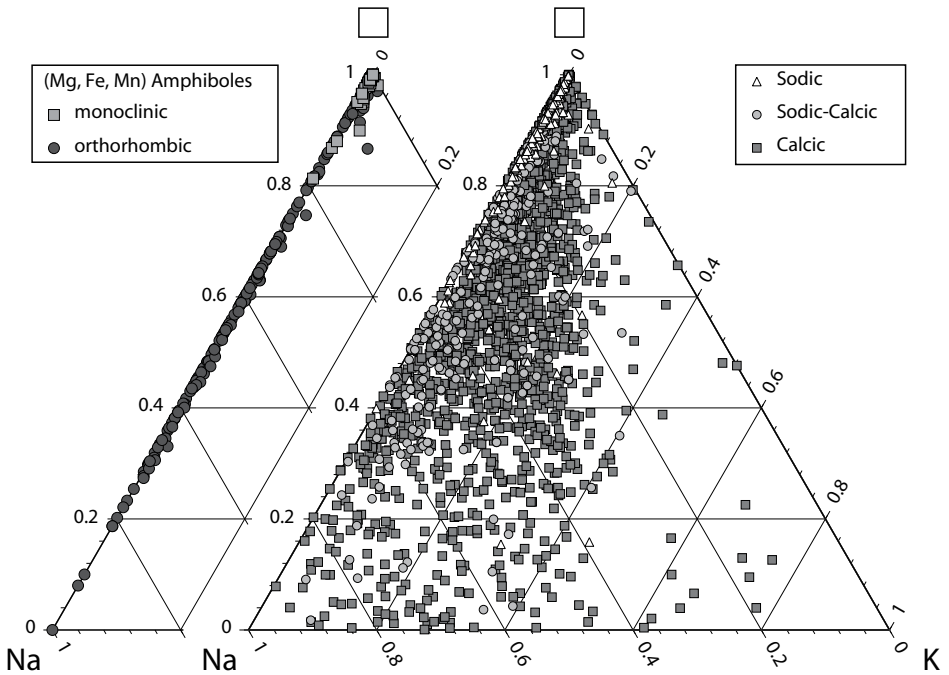


Figure 20. Ternary diagram showing the proportions of ^ANa , ^AK and vacancy (large open square) for (Mg, Fe, Mn) amphiboles and calcic, sodic-calcic and sodic amphiboles (average Fe^{3+} estimate) assembled from literature sources for this study.

new amphibole generation. An earlier metastable amphibole would likely serve as a substrate for the nucleation of later amphibole, which would yield partial or complete overgrowths. At temperatures high enough to promote significant intracrystalline diffusion, but low enough to prevent homogenization, the overgrowths could manifest as continuous chemical and optical zones of variable width. Below some critical temperature, a chemical discontinuity would be preserved between the overgrowth and the metastable amphibole; the extent of the discontinuity and zoning away from the interface of the discontinuity would be a function of the reaction, the temperature of reaction and the cooling rate. As a consequence, chemical discontinuities are equivocal evidence of miscibility gaps.

The problem that remains is to determine textural and chemical criteria to distinguish true equilibrium from disequilibrium textures. The most clear cut evidence that support the equilibrium coexistence is observable exsolution in each member of a multiple amphibole assemblage, which would suggest that the amphiboles coexisted at higher T as homogeneous phases of compositions defined by the limbs of solvi or the limits of miscibility gaps. Petrographic evidence of host and guest phases (Fig. 21) is the easiest way to demonstrate equilibrium. For example, hornblende and cummingtonite may be intergrown or show rimming relationships, but equilibrium defined by a solvus is shown by mutual exsolution (e.g., hornblende lamellae in cummingtonite and cummingtonite lamellae in hornblende (Figs. 21 and 22). Another rarer example of this type of mutual exsolution between cummingtonite and magnesio-arfvedsonite (now ferri-winchite according to Leake et al. (1997)) is given by Robinson et al. (1971a). There is a miscibility gap between orthoamphibole and hornblende, and exsolution of cummingtonite in hornblende will indicate that homogeneous hornblende coexisted with orthoamphibole at compositions defined by the miscibility gap at higher

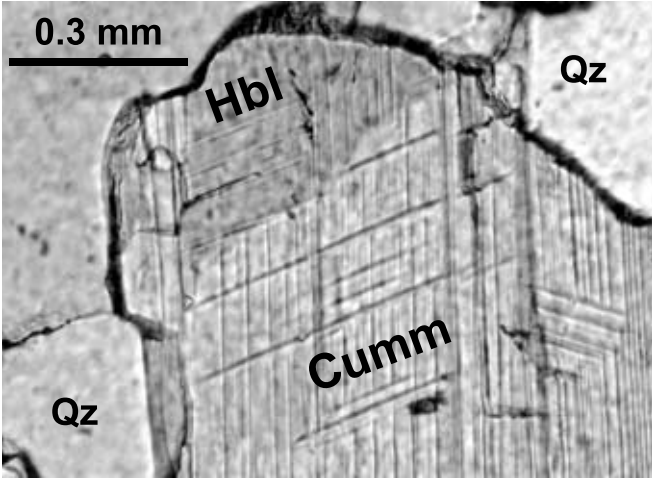


Figure 21. Photomicrograph of intergrown and mutually exsolved “hornblende” and cummingtonite from the locality 7A7 at “Amphibole Hill,” southwestern New Hampshire, USA (see Kahl and Schumacher 2000; Robinson and Jaffe 1969). Hosts are labeled *Hbl* and *Cumm*; fine lamellas in two orientations run approximately north to south and east-northeast to west-southwest.

Exsolution observed in the petrographic microscopic

two monoclinic amphiboles

two orthorhombic amphiboles

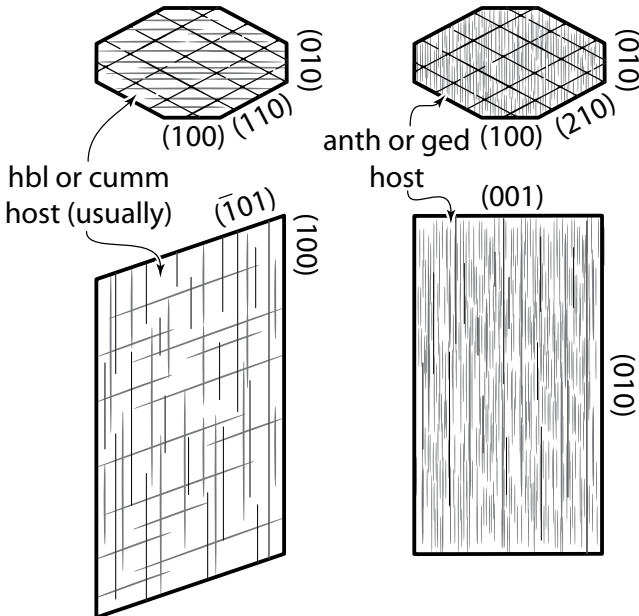


Figure 22. Sketch of the most commonly observed exsolution orientations found in cummingtonite and “hornblende” and in orthoamphibole that can be observed with a petrographic microscope.

temperature. Equilibrium coexistence of two orthoamphiboles can also be demonstrated by mutual exsolution (Fig. 22). Coexisting orthoamphiboles are also commonly intergrown and show rimming relations; however, the color contrast between anthophyllite and gedrite can be subtle, and more difficult to recognize. Mutual exsolution in coexisting orthoamphiboles is best viewed on (001) sections and is apparent as small (010) lamellae in most cases.

The next set of criteria that suggest equilibrium is close proximity, mutual grain boundaries or topotaxial overgrowth/intergrowth of optically or chemically distinct amphiboles. While equilibrium can explain these observations, metamorphic overprinting of a partially preserved or incompletely re-equilibrated relict assemblage provides a competing explanation. In no case were these two interpretations more at loggerheads than in the debate over the existence of an actinolite-hornblende solvus (Grapes and Graham 1978). Two-amphibole assemblages of a calcic amphibole plus either sodic-calcic amphibole or sodic amphibole occur in numerous low-temperature, medium- to high-pressure terrains (e.g., (Klein 1968, 1969; Immega and Klein 1976; Marschall et al. 2004) see also references in Robinson et al. (1982), and many of these examples clearly represent equilibrium. However, extensive compositional zoning seems to be the rule rather than the exception in sodic amphiboles and sodic-calcic amphiboles from these metamorphic conditions. So, the exact compositional limits of coexisting calcic amphibole plus either sodic-calcic amphibole or sodic amphibole are difficult to determine precisely, and even though a miscibility gap exists, partial re-equilibration during overprinting cannot be excluded in all cases.

Electron microscopy by Smelik and Veblen, and their coauthors (Smelik and Veblen 1989, 1991, 1992a,b, 1993, 1994; Smelik et al. 1991) has contributed greatly to our understanding of solvi and miscibility gaps in amphiboles. Their observations of exsolution lamellae in various amphiboles confirm the gaps between sodic amphiboles and cummingtonite-grunerite, sodic amphibole and calcic amphibole, actinolite and hornblende, calcic amphibole and cummingtonite-grunerite and calcic amphibole and orthoamphibole.

The basic crystal chemistry of equilibrium coexistence

The ability of amphiboles to coexist in equilibrium results from differences in their crystal structures that are great enough to support different chemical compositions. The most obvious difference is the monoclinic versus orthorhombic structures. Other, less obvious differences, include various space groups or ordering in the monoclinic amphiboles, and even the configuration of a specific site or set of sites seems to be capable segregating larger versus smaller cations at a site or sites. Table 2 is a general comparison of the crystallographic and chemical properties of pairs of coexisting amphiboles. It is worth noting again that in calcic and (Mg, Fe, Mn) amphiboles, there is a strong positive correlation between the extents of the tschermakite- and edenite-like substitutions. In the context of miscibility gaps, the variation of all the elements involved in these two coupled substitutions may be essential to the existence of a miscibility gap or solvus. An alternative view is that one or the other of these substitutions dominates the definition of the miscibility gap or solvus, and that the extent of the remaining substitution is largely a byproduct of an additional set of chemical and crystallographic controls that produce the covariance.

Two of the best defined and well-documented miscibility gaps are between calcic amphiboles and (Mg, Fe, Mn) amphiboles. The gap between orthoamphiboles and calcic amphiboles is seen in the composition at the $M(4)$ site, which has a different geometry in the $C2/m$ and $Pbca$ structures and is dominantly Ca (not surprisingly) in the calcic amphiboles and $Fe^{2+} + Mg$ in the orthoamphiboles. The gap between the calcic amphiboles and cummingtonite-grunerite is also expressed in the $M(4)$ site compositions (dominantly Ca versus Fe^{2+} , Mg or Mn^{2+}), but these amphiboles are both monoclinic ($C2/m$ at temperatures of geological interest). The $C2/m$ structure clearly can accommodate large amounts of Fe^{2+} , Mg or Mn^{2+} at $M(4)$ but their presence inhibits significant tschermakite substitution.

Table 2. Comparison of structural and compositional parameters that appear to control immiscibility among amphiboles. These include crystal system, space group and the cation occupancies of the A, M(4), M(2) and T sites. M = monoclinic, O = orthorhombic; Hbl = hornblende, Oam = orthoamphibole, Cummm = cummingtonite, Ged = gedrite, Anth = anthophyllite, Ca-amph = calcic amphibole, Na-amph = sodic amphibole, Act = actinolite.

Pairs	Crystal System	Space Group	A-site	M(4)-sites	M(2)-sites	T-sites
Hbl-Oam	M-O	$C2/m-Pbca$	$N_{\text{Hbl}} \sim N_{\text{Oam}}$	$Ca_{\text{Hbl}} \gg Ca_{\text{Oam}}$	$Al_{\text{Hbl}} > to \sim Al_{\text{Oam}}$	$Al_{\text{Hbl}} > to \sim Al_{\text{Oam}}$
Cumm-Oam	M-O	$C2/m (P2_1/m)-Pbca$	$N_{\text{Cumm}} < N_{\text{Oam}}$	$Ca_{\text{Cumm}} > Ca_{\text{Oam}}$	$Al_{\text{Cumm}} < to \ll Al_{\text{Oam}}$	$Al_{\text{Cumm}} < to \ll Al_{\text{Oam}}$
Hbl-Cumm	M	$C2/m-C2/m (P2_1/m)$	$N_{\text{Hbl}} \gg N_{\text{Cumm}}$	$Ca_{\text{Hbl}} \gg Ca_{\text{Cumm}}$	$Al_{\text{Hbl}} \gg Al_{\text{Cumm}}$ $Al_{\text{Act}} \equiv Al_{\text{Cumm}}$	$Al_{\text{Hbl}} \gg Al_{\text{Cumm}}$
Ged-Anth	O	$Pbca$	$N_{\text{Ged}} > N_{\text{Anth}}$	equivalent	$Al_{\text{Ged}} \gg Al_{\text{Anth}}$	$Al_{\text{Ged}} \gg Al_{\text{Anth}}$
Ca-amph-Na-amph	M	$C2/m$	$N_{\text{Ca-amph}} \geq N_{\text{Na-amph}}$	$Ca_{\text{Ca-amph}} \gg Ca_{\text{Na-amph}}$	$Al_{\text{Ca-amph}} \ll Al_{\text{Na-amph}}$	$Al_{\text{Ca-amph}} \sim \text{or} > Al_{\text{Na-amph}}$
Hbl-Act	M	$C2/m$	$N_{\text{Hbl}} > N_{\text{Act}}$	equivalent	$Al_{\text{Hbl}} \gg Al_{\text{Act}}$	$Al_{\text{Hbl}} \gg Al_{\text{Act}}$

A gap also exists between orthoamphiboles and cummingtonite (used inclusively in this section to include grunerite compositions) and their compositional contrast is derived from their *Pbca* and *C2/m* structures (Table 2). Compositionally, orthoamphiboles and cummingtonite can be either very similar or very different, but their principal difference is again the extent of the tschermakite- and edenite-like substitutions (coupled *M(2)-T* and *A-T* substitutions) in cummingtonite versus that of orthoamphibole. Even in examples where coexisting cummingtonite and anthophyllite have very similar compositions, the compositional controls imposed by the *Pbca* and *C2/m* structures are still evident; the anthophyllite will show slightly higher ^{total}Al and ^ANa, while the cummingtonite will have higher ^{M(4)}Ca. Due to the crystal-chemical similarities of pyroxenes and amphiboles, the miscibility and compositional variations of all three of these amphiboles (calcic amphiboles, orthoamphiboles and cummingtonite) are analogous to the compositional variation and phase relations observed among the augite, orthopyroxene and pigeonite.

Another well defined and documented miscibility gap in natural samples is between calcic amphiboles-sodic amphibole compositions, but solution from both the calcic and sodic sides is extensive enough to reach compositions classified as sodic-calcic amphiboles. All these amphiboles have the *C2/m* structure, and the principal chemical difference defining this miscibility gap is the extent of the generalized glaucophane component (coupled *M(4)-M(2)* substitution).

Two miscibility gaps, the gedrite-anthophyllite solvus and the proposed actinolite-hornblende solvus are analogous in many ways. The coexisting amphibole pairs each have the same structure, gedrite - anthophyllite are both *Pbca* and actinolite-hornblende are both *C2/m*. In both cases, the major compositional gap involves the magnitudes of the tschermakite and edenite components (*M(2)-T* and the *A-T* sites). While the existence of the gedrite-anthophyllite solvus is well established and accepted, the existence of an actinolite-hornblende solvus has been disputed, notably by Grapes and Graham (1978). Later TEM work by (Smelik et al. 1992b) reports pervasive exsolution in calcic amphibole to “actinolite” and “hornblende” strongly suggesting the existence of an actinolite-hornblende solvus.

Cummingtonite-hornblende

Cummingtonite is commonly the most Al-poor phase in assemblages with other (Fe, Mg) silicates (e.g., orthoamphibole, chlorite, hornblende and garnet). In assemblages with coexisting cummingtonite and calcic amphibole, calcic amphiboles commonly have significantly higher edenite and tschermakite components, but can vary from a low Na-Al “actinolite” to Na-Al “hornblende” (Fig. 23a). As a result, the Na-Al content of a calcic amphibole that coexists with cummingtonite can vary extensively and independently from (Fe, Mg) content (Fig. 23b). As a result, in the assemblage, cummingtonite will likely be the silicate phase with the lowest Al content.

A comparison of Fe/Mg ratios versus the ^B(Ca + Na) content of coexisting calcic amphiboles and cummingtonite (Fig. 24) shows that the solvus remains open over the entire range of Fe/Mg ratios, which is in contrast to the behavior of analogous pyroxenes (augite-pigeonite) in the pyroxene quadrilateral. At lower temperature and the compositions that are nearer the hedenbergite-ferrosilite join, the gap between augite and pigeonite narrows and can close. Jaffe et al. (1968) noted that exsolution lamellae in Fe-rich cummingtonite-calcic amphibole pairs tend to be coarser than those in Mg-richer counterparts. The only report of near Ca-Fe-Mg amphibole compositions that may have been nearly hypersolvus prior to extensive exsolution are cummingtonite-actinolite from the Ruby Mountains, Montana (Ross et al. 1969). The data suggest that only where both co-existing amphiboles are low in Na and Al, e.g., cummingtonite and actinolite, will the solvus narrow in the Fe-rich regions of the “amphibole” quadrilateral, analogous to the pyroxene quadrilateral; however, the data collected here does not indicate any narrowing of the solvus in Fe-rich amphiboles (Fig. 25). Elevated tschermakite and edenite contents in the calcic amphibole seems to inhibit solid solution at *M(4)*.

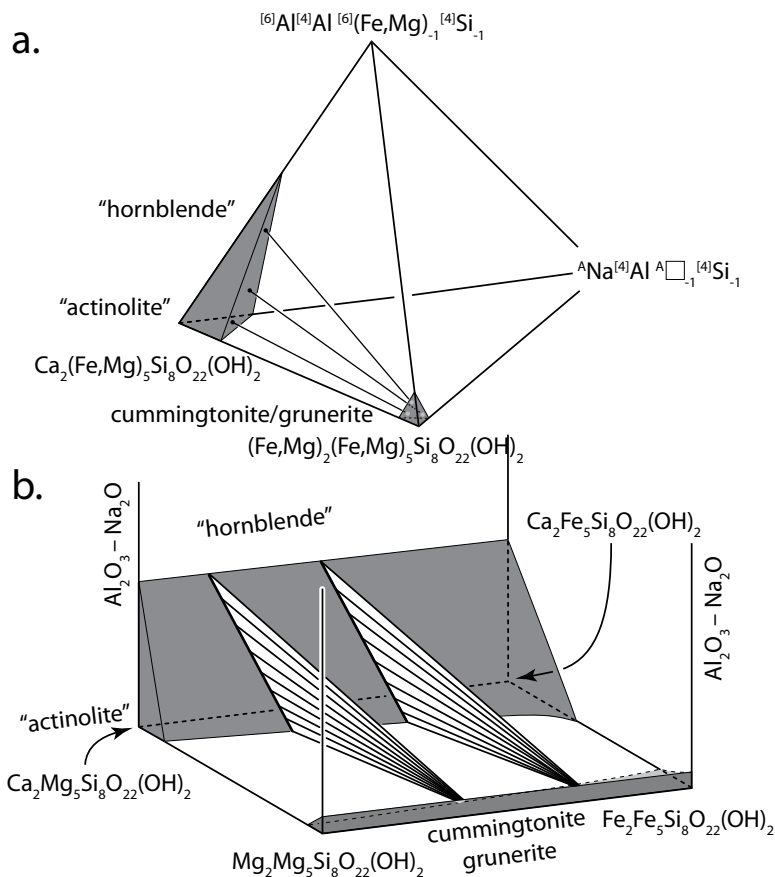


Figure 23. Schematic illustration of the complexity of compositional variations in coexisting “hornblende” and cummingtonite. Part (a) shows that cummingtonite of similar composition may coexist which “hornblende” with a much wider variability of *edenite* and *tschermakite* contents. Part (b) shows that cummingtonite of similar Fe/Mg ratios and Al contents may coexist which “hornblende” with a wide range of *tschermakite* contents.

Several generations of exsolution lamellae can be present in coexisting cummingtonite and calcic amphibole. Optimal-phase boundary theory (Bollman and Nissen 1968) predicts that for these two monoclinic amphibole structures, two strain-free orientations of exsolution will exist at constant temperature and composition of the host and guest phases. In hornblende and cummingtonite these orientations are nearly parallel to (100) and $(\bar{1}01)$. The lattice parameters of the amphiboles change as a function of both temperature and composition, but if the temperature dependence of the lattice parameters are known for a set of compositions, the orientations of the exsolution lamellae relative to a crystallographic reference direction in the host will correlate with the temperature of exsolution.

In a HRTEM study, Klein et al. (1996) applied optimal-phase boundary theory to multiple generations of exsolution in two sets of coexisting cummingtonite-hornblende pairs, one from central Massachusetts and one from southwestern New Hampshire. Klein et al. (1996) observed up to 8 distinct populations of exsolution lamellae based width and lamellar orientation relative to the lattice orientation of the host amphibole. The width of these lamellae

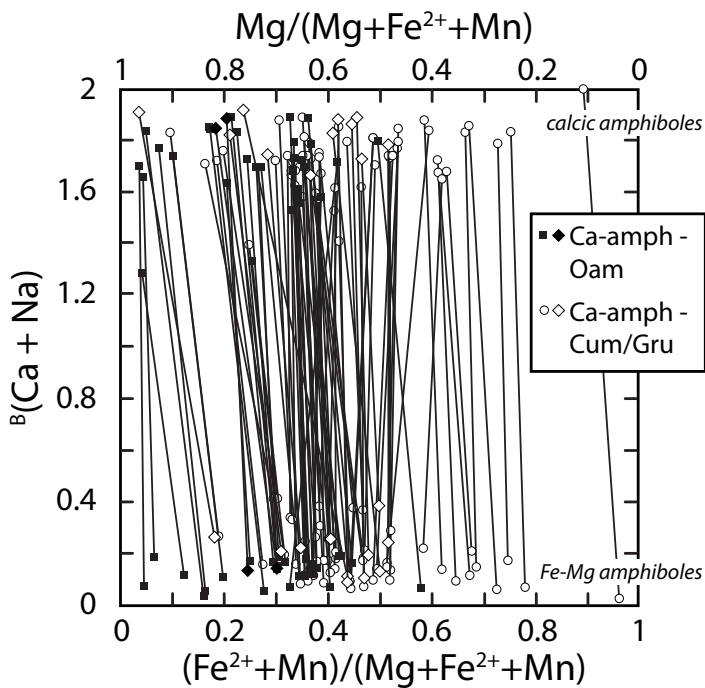


Figure 24. Plot of X_{Mg} vs. $B(Ca + Na)$ for coexisting pairs of calcic amphiboles and (Mg, Fe, Mn) amphiboles modified from Robinson et al. (1982, Fig. 27B). *Open symbols* are cummingtonite/grunerite – calcic amphibole and *filled symbols* are orthoamphibole-calcic amphibole pairs. *Open circles* are taken from Robinson et al. (1982, Fig. 22B); *open diamonds* are data from Hollocher (1991), Mottana et al. (1994) and Kahl and Schumacher (2000). *Filled squares* are taken from Robinson et al. (1982, Fig. 27B); *filled diamonds* are data from Schumacher and Robinson (1987).

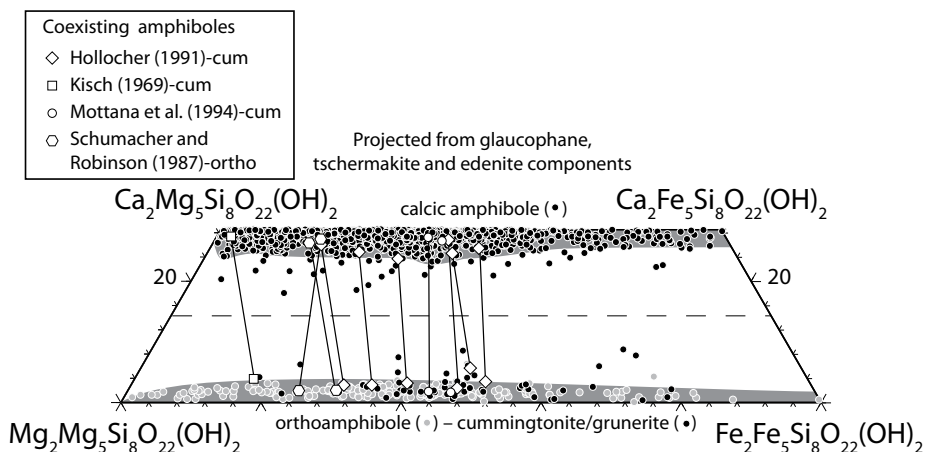


Figure 25. Plot of the proportions of $B(Ca-B)Mg-B(Fe^{2+}+Mn)$ for calcic and (Mg, Fe, Mn) amphiboles (“amphibole quadrilateral”). The X_{Mg} = total Mg/(Mg + $Fe^{2+}+Mn$).

ranged from 2.4 to 0.005 μm . In their study, Klein et al. (1996) determined the T -dependence of the lattice parameters of cummingtonite and hornblende in two samples from 25–600 $^{\circ}\text{C}$. This data and relative orientations of exsolution lamellae were then used to calculate temperatures of exsolution based on optimal-phase boundary theory (Bollman and Nissen 1968) analogous to the successful application of this method to multiple orientations of exsolution lamellae in augite, pigeonite and inverted pigeonite (Robinson et al. 1971a, 1977; Jaffe et al. 1972, 1975; Robinson 1980). Exsolution occurred between about 675 and 300 $^{\circ}\text{C}$. In both of the amphibole samples studied, more distinct generations of exsolution were found in the cummingtonite host than in the hornblende host, which suggests that the coherent solvus is asymmetric and that the cummingtonite limb is slightly flatter. The lowest temperature exsolution of hornblende in cummingtonite (Q-603) were nano-scale and lenticular rather than lamellar exsolution features (Klein et al. 1997). Analytical TEM on these lenticular features gave compositions intermediate between cummingtonite and the coarser hornblende lamellas. This observation, along with compositional zoning in homogeneous cummingtonite between linear zones that are rich in nano-scale lenticular exsolution and parallel the coarser lamellar exsolution, suggest that lenticular exsolution is an example of arrested Ostwald ripening (Gibbs-Thompson effect) that, given sufficient time at the temperature that exsolution commenced, would have coalesced to form another set of exsolution lamellae.

The effect of temperature versus $M(4)$ -site composition and tschermakite content, which are the two largest compositional discriminants between cummingtonite and hornblende, are shown in Figure 26a. The position of the solvus limbs are estimated on the T - $B(\text{Na} + \text{Ca})$ diagram (Fig. 26a), and these data (with the exception of one set of exsolved cummingtonite-hornblende that were re-integrated from electron microprobe analyses) reasonably constrain the solvus limbs between about 500 and 700 $^{\circ}\text{C}$. Interestingly, the tschermakite component for the same samples also does nearly as good a job of defining the positions of the solvus limbs where plotted against temperature (Fig. 26b). Three cummingtonite-hornblende pairs do not fit well, and these are the same re-integrated pair noted above in Figure 26a, and not surprisingly, the three examples with higher tremolite component. One of these pairs is cummingtonite-actinolite from a cotecule (fine-grained garnet quartzite) in southwestern New Hampshire (Kahl and Schumacher 2000), one is a cummingtonite-actinolite-hornblende assemblage from New Hampshire (Spear 1982) and the third cummingtonite coexists with an Al-poor hornblende from a rock (with only a few vol% hornblende and cummingtonite) that is made up almost entirely of orthopyroxene and plagioclase (Hollocher 1991). These observations, taken together with the report of a “nearly hypersolvus” cummingtonite - actinolite from the Ruby Mountains, Montana (Ross et al. 1969) that was mentioned above, suggest that in natural bulk compositions that approach an ideal $\text{CaO-MnO-FeO-MgO-SiO}_2\text{-H}_2\text{O}$ system (e.g., iron formations) the calcic amphibole-cummingtonite solvus is effectively controlled by the $M(4)$ site composition. The solvus relations are closely analogous to those of the pyroxene quadrilateral, and the solvus in the amphibole quadrilateral may also narrow or even close near the Ca-Fe^{2+} join. In calcic amphibole-cummingtonite assemblages where hornblende approaches Al saturation (e.g., in intermediate to mafic volcanic protoliths), both the $M(4)$ site composition and tschermakite content of the hornblende bracket the solvus, and the solvus maintains nearly a constant width over the entire range of (Fe, Mg) compositions (Figs. 24, 25). Consequently, the cummingtonite-“actinolite” pairs and the cummingtonite-“hornblende” pairs could give two different placements of the solvus boundaries on amphibole quadrilateral.

The transition from the amphibolite facies to the granulite facies and the phase relations of the cummingtonite-hornblende solvus will be closely associated in many common rock compositions. The breakdown of both amphiboles to pyroxenes in rocks with basaltic protoliths causes metastability of the crest at the cummingtonite-hornblende solvus, shown schematically in Figure 27. It is interesting to note that although the granulite facies is commonly defined as the first appearance of orthopyroxene due to the breakdown of hornblende, it is quite likely that

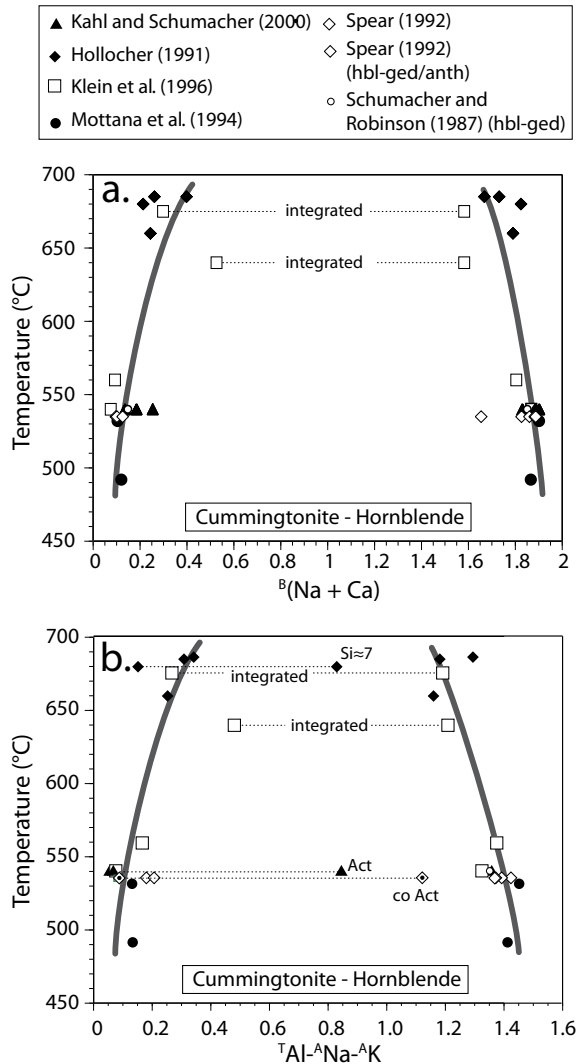


Figure 26. Plot of composition vs. temperature (T) for coexisting “hornblende” and cummingtonite. Part (a) is a $T-B(\text{Na} + \text{Ca})$ diagram and part (b) is a $T-(\text{Al}^{\text{VI}}\text{Na}^{\text{VI}}\text{K})$ diagram. Heavy lines show the estimated location of the solvus limbs. Compositions of “hornblende” - cummingtonite pairs of marked *integrated* are estimated homogeneous amphibole compositions based on averages of multiple electron microprobe analyses of extensively exsolved grains.

in many rocks orthopyroxene first appears due to the breakdown of cummingtonite (Fig. 27). For example, Hollocher (1991) reports these and other reactions in the transitional amphibolite-granulite-facies terrain in central Massachusetts, USA.

Orthoamphibole-hornblende

The miscibility gap between orthoamphibole and calcic amphiboles, like the cummingtonite-calcic-amphibole solvus, is expressed principally in the $B(\text{Ca} + \text{Na})$ content. However, the $Pbca$ structure of orthoamphibole favors smaller cations like Al and Mg where

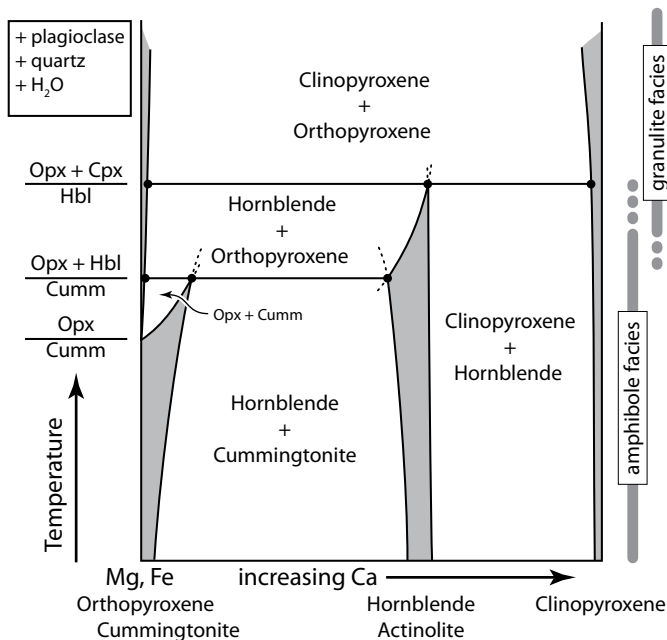


Figure 27. A schematic T - $Ca/(Ca+Mg+Fe^{2+})$ section that shows the relative Ca content of phases and the complex relationships among amphiboles, pyroxenes and various miscibility gaps. These phase relations ignore the variations in X_{Mg} among the silicates and are best thought of as projected onto a T - $Ca/(Ca+Mg+Fe^{2+})$ plane of intermediate and fixed X_{Mg} .

compared with cummingtonite; hence, orthoamphiboles will generally be richer in Mg and have higher tschermakite content. The (Fe, Mg) content of pairs of hornblende-orthoamphibole and cummingtonite-hornblende data are compared in Figure 24. With one exception, orthoamphibole coexisting with calcic amphibole has X_{Mg} values greater than 0.5, while cummingtonite X_{Mg} values are mostly less than 0.7. These data show what many studies have observed (see references in Robinson et al. (1982)), at a given P - T - X , if the only significant composition variable is Fe/Mg ratio, the Mg-richer bulk compositions will contain orthoamphibole-hornblende and the Fe-richer bulk compositions will contain cummingtonite-hornblende (Fig. 24). The overlap and concentration of data for orthoamphibole and cummingtonite paired with hornblende at X_{Mg} values of about 0.4 probably relates to a continuous Fe and Mg reaction among orthoamphibole, cummingtonite and hornblende, such as cummingtonite + plagioclase + water = orthoamphibole + hornblende + quartz, that occurs commonly over a range of temperature.

The ${}^B(Ca + Na)$ content of orthoamphiboles that coexist with hornblende are comparable to those of cummingtonite (Figs. 24, 28). A few examples of orthoamphibole - hornblende pairs are included on Figure 26. There are not enough samples to characterize the T versus composition relations, but T - ${}^B(Na + Ca)$ for orthoamphibole-hornblende are almost indistinguishable from that of cummingtonite-hornblende (Fig. 26a). Since the tschermakite contents are variable in both orthoamphibole and calcic amphibole, the T versus tschermakite relation will not be as useful (Fig. 26b); however, in a few examples with Al-saturating assemblages, the tschermakite content of hornblende coexisting with orthoamphibole is comparable to the tschermakite content of hornblende coexisting with cummingtonite. Where the orthoamphibole coexisting with "hornblende" is gedrite, the calcic amphiboles are generally richer in tschermakite component (Fig. 28) (also see Robinson et al. 1982, their Fig. 28a).

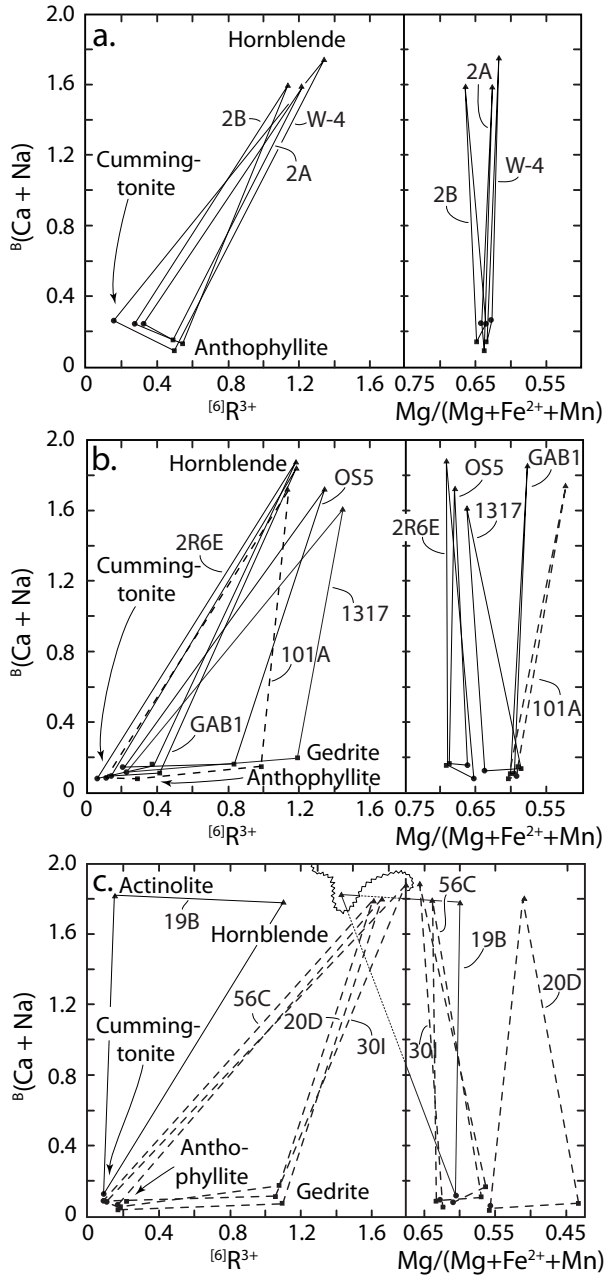


Figure 28. Plots of $\text{Mg}/(\text{Mg} + \text{Fe}^{2+} + \text{Mn})$ and ${}^6\text{R}^{3+}$ vs. $\text{Ca} + \text{Na}$ at $M(4)$ for assemblages with three or four coexisting calcic amphiboles and Fe-Mg amphiboles. The figure is redrawn from Robinson et al. (1982, Fig. 34). (a) Assemblages from high in the sillimanite zone reported by Robinson et al. (1969, 2A, 2B) and James (1978; W-4). (b) Assemblages from low in the sillimanite zone reported by Stout (1972; GAB1, 101A), Hawthorne et al. (1980; 1317), and John C. Schumacher (unpublished data, 2R6E, OS5). (c) Assemblages from the kyanite-stauroilite zone reported by Spear (1980, 1982; 56C, 20D, 30I, 19B). Two parts of figure overlap along jagged line.

In hornblende from orthoamphibole-calcic amphibole pairs, the only visible microscopic exsolution is cummingtonite lamellae along optimal phase boundaries near the (100) and 101 crystallographic directions. In orthoamphibole the most common visible microscopic exsolution is related Na and Al content which defines the anthophyllite-gedrite solvus, and these lamellae are most commonly parallel (010), but Spear (1982) reported rare lamellae approximately parallel (120) in gedrite. These were confirmed by Smelik and Veblen (1993) in a TEM study. They suggest that high Ca and Na content and the Fe/Mg ratio promote the formation of exsolution lamellae in the (120) orientation. Very fine (80 nm) lamellae of calcic amphibole in orthoamphibole parallel to (100) have also been reported by Smelik and Veblen (1992b), but orthoamphibole lamellae in calcic amphibole are not yet confirmed, which contrasts with the analogy to pyroxenes where (100) lamellae of orthopyroxene in augite are known.

Orthoamphibole-cummingtonite

The miscibility gap between orthoamphibole and cummingtonite can range from almost indistinguishable to wide depending on whether the orthoamphibole is anthophyllite or gedrite. The chemical compositions of coexisting cummingtonite and anthophyllite can be almost indistinguishable. The compilation of cummingtonite-orthoamphibole data in Robinson et al. (1982, see also their Fig. 28) indicates that cummingtonite will be richer in Fe^{2+} and Ca, and poorer in Al, Fe^{3+} and Na than orthoamphibole, which is a result of the different configurations of the $M(4)$ and $M(2)$ sites in these two amphibole structures (Fig. 28). Although these compositional variations may be slight in the case of cummingtonite coexisting with anthophyllite, they are still recognizable from electron-microprobe analyses.

Bulk compositions that yield assemblages with cummingtonite and orthoamphibole as the only amphiboles are rare, but in such assemblages exsolution features are commonly absent. Intimate homoaxial intergrowth of two (Mg, Fe, Mn) amphiboles is common, and cummingtonite commonly shows polysynthetic twinning along (100), a feature commonly absent in cummingtonite coexisting with calcic amphiboles.

Coexisting orthoamphiboles

The orthoamphibole solvus is one of the early and well documented of the amphibole miscibility gaps (e.g., Robinson and Jaffe 1969; Robinson et al. 1971a; Ross et al. 1969; Spear 1980; Stout, 1970, 1971, 1972). These authors found both optically visible exsolution and evidence of submicroscopic exsolution by X-ray crystallography in supersolvus orthoamphiboles, and examples of coexisting, subsolvus orthoamphiboles.

The principal compositional differences across the solvus are Na and Al content, which are controlled by the extent of the tschermakite and edenite components in the orthoamphibole. Data collected and presented in Robinson et al. (1982, see also their Fig. 29) show a regular partitioning of Fe and Mg between coexisting anthophyllite and gedrite, with anthophyllite consistently richer in Mg than gedrite. This can be tied directly to the more extensive tschermakite-like substitution in gedrite. This substitution proceeds as a ${}^{\text{C}}\text{Mg}^{\text{T}}\text{Si} = {}^{\text{C}}\text{Al}^{\text{T}}\text{Al}$ substitution rather than a ${}^{\text{C}}\text{Fe}^{2+\text{T}}\text{Si} = {}^{\text{C}}\text{Al}^{\text{T}}\text{Al}$ substitution, which has been pointed out by Papike and Ross (1970), Robinson et al. (1971b) and other authors.

The crest of the orthoamphibole solvus is estimated to be near 600 °C by (Spear 1980), who used metamorphic temperatures from well-documented examples of supersolvus and subsolvus orthoamphibole to plot the solvus limits on T versus ${}^{[4]}\text{Al}$, ${}^{[6]}\text{Al}$ and ${}^{\text{A}}\text{Na}$ plots (Robinson et al. 1982, their Fig. 30). All three of these compositional parameters, ${}^{[4]}\text{Al}$, ${}^{[6]}\text{Al}$ and ${}^{\text{A}}\text{Na}$, which are all reflected in the tschermakite component (${}^{\text{T}}\text{Al} - {}^{\text{A}}\text{Na} - {}^{\text{A}}\text{K}$). On a plot of T versus tschermakite component (Fig. 29) the solvus is slightly asymmetric and skewed towards anthophyllite.

The first evidence of orthoamphibole exsolution comes from iridescent orthoamphibole. Robinson et al. (1982) relate the story that K. L. Giesecke, who was on an open boat trip in

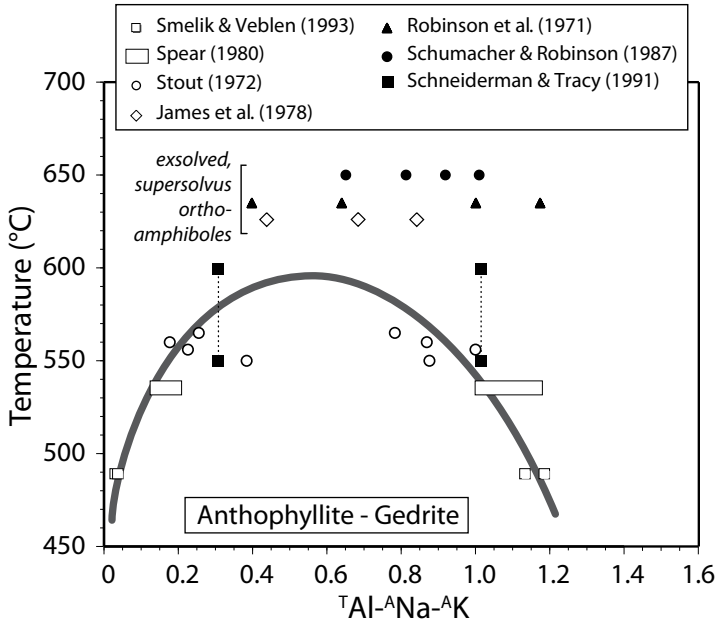


Figure 29. Diagram of T -($T_{Al-A-Na-AK}$) for both supersolvus and subsolvus anthophyllite and gedrite. Heavy line show the estimated location of the solvus.

western Greenland, stopped at Avisisarfik and collected what he described *labradoriserende hornblende*—this was actually gedrite that was mistakenly identified as hornblende. His description indicates the similarity between the iridescence shown in this amphibole and the iridescence of labradorite plagioclase which is commonly as described as *labradorescence*. These amphibole samples were later included in a study by Bøggild of iridescence in plagioclase. As with plagioclase, the iridescence in orthoamphibole is caused by the regular spacing of exsolution lamellae (parallel 010 for orthoamphibole) at widths that correspond to the wavelengths of the visible spectrum. Iridescent orthoamphibole has been recognized at a number of localities and is now traded as a semiprecious gemstone called *nuumite*.

Exsolution is most commonly parallel to (010), but, from an electron microscope study, Gittos et al. (1976) reported (120) orientations in orthoamphibole. The most commonly observed lamellae have the (010) orientation, but visible (120) were reported by Spear (1980) and Hawthorne (1982). Visible exsolution in orthoamphibole is always finer where compared with coarse exsolution seen in cummingtonite and hornblende. In some orthoamphibole samples, this fine exsolution is so pervasive that in plane-polarized light at low power under the petrographic microscope, the grains can appear brownish due to the intense refraction of the transmitted light by lamellae.

In a TEM and analytical electron microscope (AEM) study, Smelik and Veblen (1993) showed that the (010) versus (120) orientation is influenced by misfit of the a and b axes of the exsolving gedrite and anthophyllite pairs. If the Δb is the dominant misfit, then the exsolution will be parallel (010), but, if Δa misfit increases and Δb misfit decreases, the exsolution phase boundary will be parallel to (120). In their AEM investigation, they found that increased Ca was an important cause of the increase in Δa relative to Δb , but that difference in the lattice parameters are also sensitive to Na content and Fe/Mg ratio.

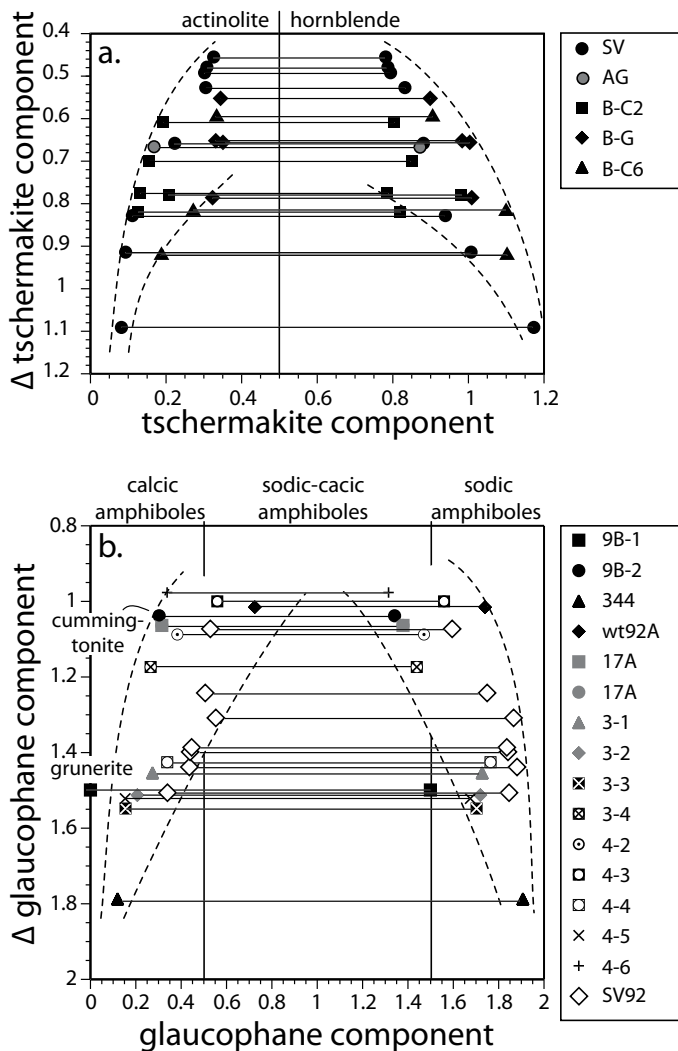


Figure 30. Part (a) Coexisting Al-richer (“hornblende” = hbl) and Al-poorer (“actinolite” = act) calcic amphibole shown on a *tschermakite* content vs. Δ *tschermakite* content diagram; Δ *tschermakite* = $(\text{Al}^{\text{VI}}\text{Na}^{\text{VI}}\text{K})^{\text{hbl}} - (\text{Al}^{\text{VI}}\text{Na}^{\text{VI}}\text{K})^{\text{act}}$. Data: Allen and Goldie (1978; AG), Brady (1974; B-C2, B-G, B-C6), Smelik and Veblen (1991; SV). Part (b) Coexisting Na-richer and Na-poorer calcic, sodic-calcic and sodic amphiboles shown on a *glaucophane* content vs. Δ *glaucophane* content diagram; Δ *glaucophane* = ${}^{\text{B}}\text{Na}^{\text{Ca-poorer}} - {}^{\text{B}}\text{Na}^{\text{Ca-richer}}$. Data: Black (1973, 9B-1), Immege and Klein (1970; 17A), Klein (1966, 1968; 9B-2), Klein (1969; 3-1, 3-2, 3-3, 3-4, 4-2, 4-3, 4-4, 4-5, 4-6), Marschall et al. (2004; 344, wt92A), Smelik and Veblen (1992a; SV92).

Coexisting calcic amphiboles

The actinolite-hornblende miscibility gap is the most contentiously debated case of equilibrium coexistence (or not) amphiboles. The existence of this miscibility gap was initially accepted based on early reports by Shido and Miyashiro (1959). The gap manifests as a discontinuity in the extents of the edenite and tschermakite components between the coexisting

calcic amphiboles. This is the same chemical discontinuity shown by the orthoamphiboles, in fact, these observations led J. B. Thompson in 1968 to predict the existence of the anthophyllite-gedrite solvus before it was documented, based on the analogy with the then accepted existence of the actinolite-hornblende miscibility gap (Robinson et al. 1982).

Most studies pertaining to the actinolite-hornblende gap are summarized either in Robinson et al. (1982, p. 70) or in Zingg (1996). These data are reported mostly from low- and intermediate-pressure metamorphic conditions. As mentioned above, abundant compositional zoning in associated actinolite-hornblende occurrences and some examples of gradational prograde compositional variation have led some workers to question the existence of an actinolite-hornblende miscibility gap, notably Grapes and Graham (1978).

This miscibility gap was investigated experimentally by Oba (1980) and Oba and Yagi (1987) along the tremolite-pargasite and actinolite joins. Along the tremolite-pargasite join, there is miscibility at about 825 °C (1 kbar) and complete miscibility above 800 °C at 5 kbar. In later work, Oba and Yagi (1987) did a similar study in an Fe-bearing system, $\text{Ca}_2\text{Mg}_4\text{Fe}^{2+}\text{Si}_8\text{O}_{22}(\text{OH})_2$ (called actinolite)- $\text{NaCa}_2\text{Mg}_{3.2}\text{Fe}_{0.8}\text{AlSi}_6\text{Al}_2\text{O}_{22}(\text{OH})_2$ (pargasite). At 1 kbar, there is a gap defined by the compositions $\text{Act}_{185}\text{Parg}_{15}$ and $\text{Act}_{55}\text{Parg}_{45}$ at 680 °C and complete miscibility occurred at 720 °C. Jenkins (1988) also experimentally studied the tremolite-tschemmakite join (12 and 3 kbar at 850 °C). At 12 kbar, his experiments showed complete solid-solution between the compositions $\text{Tsch}_0\text{Tr}_{100}$ and $\text{Tsch}_{50}\text{Tr}_{50}$, and at 3 kbar his experiments showed complete solid solution within a more restricted range of $\text{Tsch}_0\text{Tr}_{100}$ and $\text{Tsch}_{10}\text{Tr}_{90}$. Smelik et al. (1994) studied the tremolite-tschemmakite join between the compositions $\text{Tsch}_0\text{Tr}_{100}$ and $\text{Tsch}_{50}\text{Tr}_{50}$ over the temperature range 723-875 °C and pressures from 5.2 to 13 kbar, and these experiments showed complete solid solution between the compositions $\text{Tsch}_0\text{Tr}_{100}$ and $\text{Tsch}_{50}\text{Tr}_{50}$ (see also the summary of amphibole synthesis by Evans 2007).

Perhaps the strongest support for the existence of an actinolite-hornblende miscibility gap from rocks was reported by Smelik et al. (1991), who found pervasive fine-scale exsolution giving a "tweed" texture. These lamellae are nearly parallel to the $(13\bar{2})$ and $(1\bar{3}2)$ directions. Peak metamorphic temperature for this sample are estimated at 475-500 °C at pressures of about 3 kbar, which suggests that this sample was supersolvus at these conditions.

Zingg (1996) re-examined the actinolite-hornblende solvus by analyzing much of the available data reduced to various substitution vectors. He notes there are few examples where a temperature of formation is well known and suggests that, although there is spread in the data, (1) a gap exists, (2) even small amounts of Fe^{2+} significantly reduce the temperatures at which the gap is found, (3) the width of the solvus increases in Mg-rich compositions, (4) tentatively, there may be more than one compositional gap within a compositional space defined by the Fe/Mg ratio and a pargasite compositional vector.

Figure 30a shows some of the data for coexisting actinolite-hornblende taken from Allen and Goldie (1978), Brady (1974) and Smelik et al. (1991). Since the major compositional difference between the actinolite limb and the hornblende limb involve are $^{[4]}\text{Al}$, $^{[6]}\text{Al}$ and $^{\text{A}}\text{Na}$, all three of these compositional parameters are shown in the tschemmakite component ($^{\text{T}}\text{Al} - ^{\text{A}}\text{Na} - ^{\text{A}}\text{K}$), which is used as a measure of the compositional variation of the coexisting amphiboles. Temperature estimates among sources for the pairs are difficult assess, so Figure 30a uses the difference in tschemmakite content (Δ *tschemmakite component*) of the coexisting amphiboles as a proxy for any factor that would cause the solvus to narrow. Temperature would likely be a major factor, and a decrease in the Δ *tschemmakite component* should result from an increase in temperature. However, compositional dependencies could also affect the width of the miscibility gap, so the vertical axis in Figure 30a is not strictly a temperature proxy. The data on Figure 30a show a distinct gap, and inasmuch as disequilibrium should result in pairs with random values of tschemmakite component, the diagram suggests the limits of a valid miscibility gap. On the other hand, the pairs do not yield a well-defined solvus curve, but

rather compositional ranges into which actinolite-hornblende are likely to fall. The explanation is for this observation is speculative. It may be that lattice parameters and site configurations of monoclinic structure are less sensitive to changes in temperature and the variations and dependencies among the principal substitutions (edenite-like, tschermakite-like and Fe-Mg exchange) than are the lattice parameters of orthorhombic structure.

Coexistence involving sodic and sodic-calcic amphiboles

The coexistence of sodic-calcic and sodic amphiboles with calcic amphiboles, other sodic-calcic amphiboles and (Mg, Fe, Mn) amphiboles are among the earliest recognition of amphibole coexistence (Klein 1966, 1968, 1969; Himmelberg and Papike 1969). Differences in the content of the generalized *glauco-phane component* is the basis of this miscibility gap, and recent TEM studies report observations of lamellae of both calcic amphibole and (Mg, Fe, Mn) amphibole in sodic amphibole. In a TEM study of glaucophane that coexists with calcic amphibole, Smelik and Veblen (1992a) found fine (ca. 20 nm width), curved exsolution lamellae of calcic amphibole approximately parallel to (100) and $(\bar{2}01)$ in samples from Vermont and Ward Creek, California. Due to the small width of the lamellae, the exsolved, calcic amphibole could not be analyzed (even by AEM) without a contribution from the host, and this Ca-bearing amphibole could range in composition from winchite to actinolite. Smelik and Veblen (1994) also report complex exsolution in Ca-bearing glaucophane in a sample from Tillotson Peak, Vermont. This sample is interpreted to have exsolved metastable cummingtonite, which concentrated Ca along the an unusual set of planes, $(28\bar{1})$ and $(2\bar{8}\bar{1})$, of the host glaucophane. These unusually Ca-rich cummingtonite lamellae later exsolved actinolite along nearly parallel to 100 direction of the cummingtonite.

Unlike the other amphibole miscibility gaps which are strongly temperature dependent, the width of the miscibility gap between more sodic amphibole and less sodic amphiboles will be strongly affected by both temperature and pressure. An experimental study by Forneris and Holloway (2004) has shown the basic pressure and temperature dependence of both Na-Ca content (*glauco-phane component*) and ^{6}Al - ^{4}Al (*tschermakite component*). High pressure promotes widening while increasing temperature narrows the miscibility gap. Figure 31 compares the compositions of pairs of more sodic amphiboles and less sodic amphiboles to the glaucophane and tschermakite components contents of the entire amphibole database. The more sodic member of the pair can range in composition from sodic-calcic to sodic-amphibole compositions, clustering around a generalized glaucophane composition, while the less sodic member of the pair ranges from calcic (tremolite) to sodic-calcic amphibole compositions (Fig. 31). Figure 31 also shows that “supersolvus” compositions exist, but the miscibility gap is clearly delineated by the more sparsely populated region between the clusters of calcic and sodic amphiboles.

Figure 30b uses the difference in *glauco-phane content* (Δ *glauco-phane component*) of the coexisting amphiboles as a proxy for temperature, pressure and any compositional parameter that would cause the solvus to narrow or widen. On Figure 30b temperature will promote narrowing of the gap, but pressure would cause it to widen. In addition to Fe-Mg exchange, the sodic amphiboles also have a significant ^{6}Al - $^{6}\text{Fe}^{3+}$ exchange capacity, which can stabilize sodic amphiboles to very low temperature. Despite all these influences, plotting the *glauco-phane component* versus the Δ *glauco-phane component* of the pairs shows the existence and rough chemical limits of a miscibility gap, since disequilibrium ought to result in pairs with random values of *glauco-phane component*. This diagram may help access the limits of a valid miscibility gap.

Coexistence of three or more amphiboles

The coexistence of three amphiboles, orthoamphibole, cummingtonite (*sensu lato*) and hornblende was anticipated based on their close structural and compositional similarities with orthopyroxene, pigeonite and clinopyroxene. Robinson (1963) found rocks with orthoamphi-

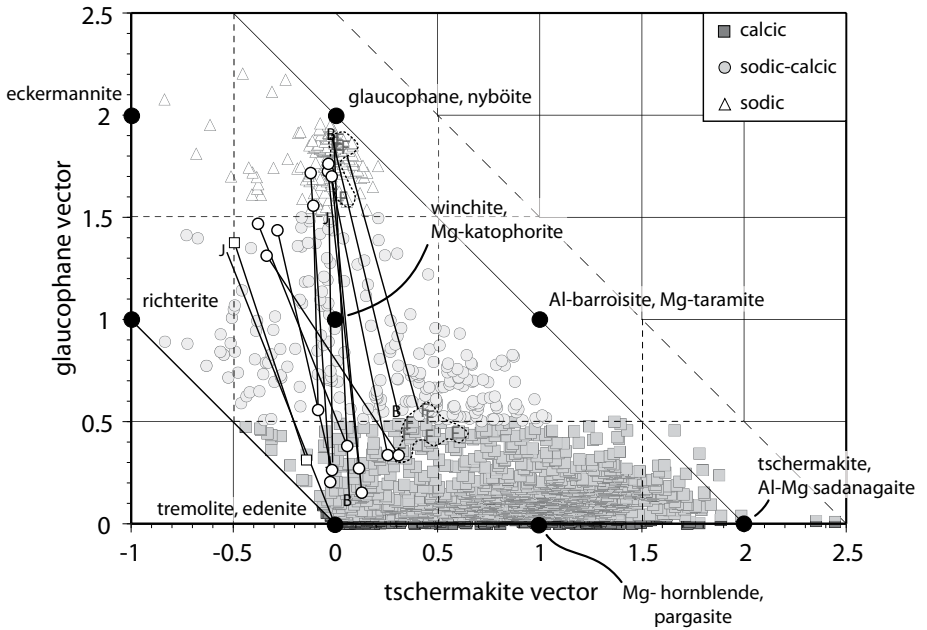


Figure 31. Plot of the generalized *glaucophane* vs. *tschermakite* components comparing coexisting sodic and sodic-calcic amphibole with amphiboles poorer in Ca with all the amphiboles from Figure 6 (see caption). Data: Black (1973), Immege and Klein (1970), Klein (1966, 1968), Klein (1969), Marschall et al. (2004), Smelik and Veblen (1992a).

bole, cummingtonite and hornblende in central Massachusetts, USA, but he not believe that the textures indicated equilibrium among all three amphiboles. Later, Robinson et al. (1969) found a mafic rock with coexisting orthoamphibole, cummingtonite and hornblende in rocks from the sillimanite-orthoclase zone of pelitic schists (upper amphibolite facies) in central Massachusetts, USA. The compositions of these three-amphibole assemblages are shown in Figure 28a along with a three-amphibole assemblage report from similar metamorphic conditions by James et al. (1978).

Just after three-amphibole assemblages were reported, Stout (1970, 1971) found similar multiple amphibole assemblages in rocks formed at lower metamorphic temperature in southern Norway. These assembles, unlike the three-amphibole assemblages of Robinson et al. (1969), formed at temperatures below the crest of the orthoamphibole solvus, and Stout (1971) reported four coexisting amphiboles (hornblende, cummingtonite, anthophyllite and gedrite). Figure 28b shows the effects of the opening of the orthoamphibole solvus in examples of three- and four-amphibole assemblages from lower in the sillimanite zone of metamorphism for pelitic rocks (middle to upper amphibolite facies). Although cummingtonite and anthophyllite have very similar compositions, anthophyllite is consistently richer in Mg than the coexisting cummingtonite.

Spear (1980, 1982) reported the lowest grade multiple-amphibole assemblages from the kyanite-staurolite zone of metamorphism for pelitic rocks (lower amphibolite facies) in Vermont, USA. In these rocks, four-amphibole assemblages are common, and examples are given in Figure 28c.

A comparison of all three parts of Figure 28 shows that the tschermakite component of the anthophyllite in the multiple amphibole assemblages decreases at lower temperature.

Figures 28b,c also illustrate the general widening of the anthophyllite-gedrite solvus at lower temperature. Anthophyllite is generally richer in Mg than coexisting cummingtonite, but gedrite is poorer in Mg than cummingtonite (20D in Fig. 28c). In the highest temperature assemblages (Fig. 28a) cummingtonite shows a distinct preference for Ca and Na at the *M*(4) site (a “hornblende” component) over the coexisting orthoamphibole, but this preference disappears at middle to lower amphibolite-facies conditions.

Spear (1982) also reported a hornblende-actinolite-cummingtonite assemblage (Fig. 28c) that seems consistent with the metamorphic conditions. This suggests hornblende-actinolite-cummingtonite-anthophyllite as a potential stable four-amphibole assemblage. In two studies, Smelik and Veblen (1989, 1994) suggested 5-amphibole assemblages that evolved in an exsolved glaucophane with a complex metamorphic cooling history from Tillotson Peak, north-central Vermont, USA. Although these amphiboles are may not equilibrated, the association glaucophane-winchite-actinolite-cummingtonite-hornblende and glaucophane-winchite-actinolite-cummingtonite (2 compositions) suggest other potential 4-amphibole assemblages, e.g. glaucophane, winchite, actinolite, cummingtonite which might occur in low-temperature, intermediate-pressure mafic rocks. These observations also confirm immiscibility among amphiboles of these compositions.

FINAL REMARKS

This chapter has concentrated on themes; (1) examining compositions and ranges of compositions of several thousand analyses of amphiboles collected by many authors since old RiM Volume 9B was published, and (2) reviewing coexisting amphiboles particularly in the light of TEM done on amphiboles over the past 15 years. Our search for data sources concentrated on material obtained via the internet, and I apologize to anyone with data that that was left out. I hope that a way will be found in the future to make these data generally available and to allow members of the community to add to this database.

The data are revealing on several levels. They provide a means to examine the extent to which the composition space of the most recent amphibole nomenclature (Leake et al. 1997) is populated and which end member names are utilized. For example, of the 50 end member names of calcic, sodic-calcic and sodic amphiboles possible in the system $\text{Na}_2\text{O}-\text{CaO}-\text{FeO}-\text{MgO}-\text{Fe}_2\text{O}_3-\text{Al}_2\text{O}_3-\text{SiO}_2-\text{H}_2\text{O}$, 42 have been reported. On the other hand, many of these 42 ‘pigeon holes’ are sparsely populated.

Amphiboles can be found at almost any metamorphic grade below the granulite- and eclogite-facies, and in just about any common protolith except pelites—although at blueschist-facies conditions even pelitic protoliths may contain some sodic amphibole. The close ties of amphiboles to the facies concept attests to their usefulness as general petrologic indicators. After RiM Volume 9B was published, the development of more sophisticated amphibole solution models coupled with the continued refinement of the thermodynamic database of Holland and Powell (1998), allowed modeling of phase equilibria of amphibole-bearing assemblages. These “thermodynamic tools” are employed in applications like Perplex (Connolly 1990, 2005) and THERMOCALC (Powell et al. 1998) that can model both net-transfer and continuous reactions that involve amphiboles. Although understanding of amphibole phase equilibria has advanced considerably, it is still not possible model all the compositional variability displayed by the amphibole data presented in this chapter.

The data summarized here also show that across the broad spectrum of amphibole types, (calcic, sodic-calcic, sodic and (Mg, Fe, Mn) amphiboles), Fe^{3+} is a significant component of many examples from many settings. Unfortunately, we lack a clear picture of the factors controlling the evolution and distribution of Fe^{3+} in amphibole-bearing assemblages, and the effects of Fe^{3+} in many examples of amphibole phase equilibria (e.g., reactions involving

“hornblende” with variable Fe^{3+}) remain poorly understood. Development of a routine microanalytical method of determining $\text{Fe}^{3+}/\text{Fe}^{2+}$ ratios in amphiboles and other minerals that would allow more reliable characterization of Fe^{3+} components in minerals would permit analysis of the redistribution of Fe^{3+} over changing metamorphic conditions. Ultimately, this type of information could allow the full characterization of the bulk compositional, pressure and temperature controls of amphibole composition allowing amphiboles to become even more precise and useful monitors of metamorphic conditions than they were in their roles as index minerals in many of the facies of Eskola.

ACKNOWLEDGMENTS

I would like to thank LaVerne Friberg (Akron) for sparking my early interest in amphiboles, and for his pointing me toward the University of Massachusetts, Amherst, MA, for Ph.D. work. At Amherst, I experienced the unbelievably supportive petrologic and geologic community that formed under the umbrella of the Five Colleges. I am indebted to Howard Jaffe and especially Peter Robinson who furthered my education in “amphibology.” In particular, the summer of 1981, when I participated in the writing and compilation of the RiM 9B project, led by Peter Robinson, I became fully committed to amphiboles. I would also like to thank Frank Spear, who in 1981 was also wallowing in the ‘brownschists’ of northern New England and was (and still is) a valued source of opinions and insight into the petrology of amphibole-bearing rocks. I would also like to thank two former students, Ulrich Klein and Wolf-Achim Kahl, who worked on amphibole-related projects with me during my years in Germany, and the *Deutsche Forschungsgemeinschaft* who supported the work of Ulrich Klein. I wish also to acknowledge the many students and colleagues (too numerous to mention individually) to whom I have corresponded or talked concerning amphibole petrology and crystal chemistry; I learned something almost every time I discussed these topics with you all. Finally, I wish to again thank University of Bristol students David Williams and Jane Leiss, who did a large part of the work necessary to digitize these amphibole data. I would also like to thank FC Hawthorne, whose comments were greatly appreciated, and George Helffrich, who commented on parts of text.

Time flies like an arrow. Fruit flies like a banana. - Groucho Marx

REFERENCES

- Allen JM, Goldie R (1978) Coexisting amphiboles from Noranda Area, Quebec - extension of actinolite-hornblende miscibility gap to iron-rich bulk compositions. *Am Mineral* 63:205-209
- Brady JB (1974) Coexisting actinolite and hornblende from west-central New-Hampshire. *Am Mineral* 59:529-535
- Bollman W, Nissen H-U (1968) A study of optimal phase boundaries: The case of exsolved feldspars. *Acta Crystallogr A* 24:546-557
- Cámara F, Oberti R, Della Ventura G, Welch MD, Maresch WV (2004) The crystal-structure of synthetic $\text{NaNa}_2\text{Mg}_5\text{Si}_6\text{O}_{21}(\text{OH})_3$, a triclinic C amphibole with a triple-cell and excess hydrogen. *Am Mineral* 89:1464-1473
- Cameron M, Papike JJ (1979) Amphibole crystal chemistry: a review. *Fortschritte der Mineralogie* 57:28-67
- Droop GTR (1987) A general equation for estimating Fe^{3+} concentrations in ferromagnesian silicates and oxides from microprobe analyses using stoichiometric criteria. *Mineral Mag* 51:431-435
- Enders M, Speer D, Maresch WV, McCammon CA (2000) Ferric/ferrous iron ratios in sodic amphiboles: Mössbauer analysis, stoichiometry-based model calculations and the high-resolution microanalytical flank method. *Contrib Mineral Petrol* 140:135-147
- Engel AEJ, Engel CG (1962) Hornblendes formed during progressive metamorphism of amphibolites, northwest Adirondack Mountains. *Geol Soc Am Bull* 73:1499-1514
- Eskola P (1920) The mineral facies of rocks. *Norsk Geologisk Tidsskrift* 6:143-194
- Eskola P (1939) Die metamorphen Gesteine. *In: Die Entstehung der Gesteine*. Barth TFW, Correns CW, Eskola P (eds) Springer, Berlin, p 263-407

- Forneris JF, Holloway JR (2004) Evolution of mineral compositions during eclogitization of subducting basaltic crust. *Am Mineral* 89:1516-1524
- Ernst WG, Liu J (1998) Experimental phase-equilibrium study of Al- and Ti-contents of calcic amphibole in MORB—A semiquantitative thermobarometer. *Am Mineral* 83:952-969
- Evans BW (2007) The synthesis and stability of some end-member amphiboles. *Rev Mineral Geochem* 67:261-286
- Fyfe WS, Turner FJ, Verhoogen J (1958) Metamorphic reactions and metamorphic facies. *Geol Soc Am Memoir* 73, 259 p
- Gittos MF, Lorimer GW, Champness PE (1976) The phase distribution in some exsolved amphiboles. *In: Electron Microscopy in Mineralogy*. Wenk HR (ed) Springer: Berlin, p 238-247
- Grapes RH, Graham CM (1978) Actinolite-hornblende series in metabasites and so-called miscibility gap - review. *Lithos* 11:85-97
- Hawthorne FC (1981) Crystal chemistry of the amphiboles. *Rev Mineral* 9A:1-102
- Hawthorne FC (1983) The crystal-chemistry of the amphiboles. *Can Mineral* 21:173-480
- Hawthorne FC, Oberti R (2006) On the classification of amphiboles. *Can Mineral* 44:1-21
- Hawthorne FC, Oberti R (2007) Amphiboles: crystal chemistry. *Rev Mineral Geochem* 67:1-54
- Himmelberg G, Papike JJ (1969) Coexisting amphiboles from blueschist facies metamorphic rocks. *J Petrol* 10:102-114
- Höfer HE, Brey GP, Oberhansli R (1996) The determination of the oxidation state of iron in synthetic garnets by X-ray spectroscopy with the electron microprobe. *Phys Chem Mineral* 23:241-241
- Höfer HE, Brey GP, Schulzobrick B, Oberhansli R (1994) The Determination of the Oxidation-State of Iron by the Electron-Microprobe. *Eur J Mineral* 6:407-418
- Höfer HE, Weinbruch S, McCammon CA, Brey GP (2000) Comparison of two electron probe microanalysis techniques to determine ferric iron in synthetic wustite samples. *Eur J Mineral* 12:63-71
- Holland T, Blundy J (1994) Non-ideal interactions in calcic amphiboles and their bearing on amphibole-plagioclase thermometry. *Contrib Mineral Petrol* 116:433-447
- Hollocher KT (1991) Prograde amphibole dehydration reactions during high-grade regional metamorphism, central Massachusetts, U.S.A. *Am Mineral* 76:956-970
- Immea I, Klein C (1976) Mineralogy and petrology of some metamorphic Precambrian iron formations in southwestern Montana. *Am Mineral* 61:1117-1144
- Jacobson CE (1989) Estimation of Fe³⁺ microprobe analyses: observations on calcic amphibole and chlorite. *J Metamorph Geol* 7:507-513
- Jaffe HW, Robinson P, Klein C Jr. (1968) Exsolution lamellae and optic orientation of clinoamphiboles. *Science* 160:776-778
- Jaffe HW, Robinson P, Tracy RJ, Ross M (1972) Correlation of angles of pigeonite exsolution lamellae, composition, and calculated optimal phase boundaries in metamorphic augites. *Geol Soc Am Abstracts Programs* 552
- Jaffe HW, Robinson P, Tracy RJ, Ross M (1975). Orientation of pigeonite exsolution lamellae in metamorphic augites: correlation with composition and calculated optimal phase boundaries. *Am Mineral* 60:9-28
- James RS, Grieve RAF, Pauk L (1978) The petrology of cordierite-anthophyllite gneisses and associated mafic and pelitic gneisses at Manitouwadge, Ontario. *Am J Sci* 278:41-63
- Kahl WA, Schumacher JC (2000) Multiple pyroxene and amphibole assemblages in the amphibolite facies: Bulk compositional controls. *Am Mineral* 85:1606-1616
- Klein C (1966) Mineralogy and petrology of the metamorphosed. Wabush Iron Formation, southwestern Labrador. *J Petrol* 7:246-305
- Klein C Jr. (1968) Coexisting amphiboles. *J Petrol* 9:281-330
- Klein C (1969) 2-Amphibole assemblages in system actinolite-hornblende-glaucophane. *Am Mineral* 54:212-237
- Klein U, Schumacher JC, Czank, M (1993) Mutual exsolution in hornblende and cummingtonite: compositions, lamella orientation, and temperature effects. *Terra Abstracts* 5:354
- Klein U, Schumacher JC, Czank M (1996) Mutual exsolution in hornblende and cummingtonite: compositions, lamellar orientations, and exsolution temperatures. *Am Mineral* 81:928-939
- Klein U, Sharp TG, Schumacher JC (1997) Analytical electron microscopy of nanometer-scale hornblende lamellae: low-temperature exsolution in cummingtonite. *Am Mineral* 82:11-12
- Leake BE (1968) A catalog of analyzed calciferous and sub-calciferous amphiboles together with their nomenclature and associated minerals. *Geol Soc Am Special Paper* 68:210
- Leake BE (1978) Compiler for Subcommittee on Amphiboles, I.M.A. Nomenclature of amphiboles. *Am Mineral* 63:1023-1052
- Leake BE, Woolley AR, Arps CES, Birch WD, Gilbert MC, et al. (1997). Nomenclature of amphiboles: Report of the Subcommittee on Amphiboles of the International Mineralogical Association, Commission on New Minerals and Mineral Names. *Am Mineral* 82:1019-1037

- Loewenstein W (1954) The distribution of aluminum in the tetrahedra of silicates and aluminates. *Am Mineral* 39:92-96
- Marschall HR, Altherr R, Gmeling K, Kasztovszky Z (2004) Trace element systematics of high-pressure metamorphic rocks from Syros (Greece). *Geochim Cosmochim Acta Supp* 68:A42
- Oba T (1980) Phase relations in the tremolite-pargasite join. *Contrib Mineral Petrol* 71:247-256
- Oba T, Yagi K (1987) Phase relations on the actinolite-pargasite join. *J Petrol* 28:23-36
- Papike JJ, Ross M (1970) Gedrites: crystal structures and intercrystalline cation distributions. *Am Mineral* 55:1945-1972
- Raase P (1974) Al and Ti contents of hornblende, indicators of pressure and temperature of regional metamorphism. *Contrib Mineral Petrol* 45:231-236
- Robinson P (1963) Gneiss domes of the Orange area, west-central Massachusetts and New Hampshire. Ph.D. Dissertation. Department of Geology, p. 253. Harvard University, Cambridge
- Robinson P (1980) The composition space of terrestrial pyroxenes - internal and external limits. *Rev Mineral* 8:419-494
- Robinson P, Jaffe HW (1969) Chemographic exploration of amphibole assemblages from central Massachusetts and southwestern New Hampshire. *Mineralogical Society of America Special Paper* 2:251-274
- Robinson P, Jaffe HW, Ross M, Klein C (1971a) Orientations of exsolution lamellae in clinopyroxenes and clinopyroxenes: consideration of optimal phase boundaries. *Am Mineral* 56:909-939
- Robinson P, Ross M, Jaffe HW (1971b) Composition of anthophyllite-gedrite series, comparisons of gedrite and anthophyllite-gedrite solvus. *Am Mineral* 56:1005-1041
- Robinson P, Ross M, Nord GL Jr, Smyth JS, Jaffe HW (1977) Exsolution lamellae in augite and pigeonite: fossil indicators of lattice parameters at high temperatures and pressure. *Am Mineral* 62:857-873
- Robinson P, Spear FS, Schumacher JC, Laird J, Klein C, Evans BW, Doolan BL (1982) Phase relations of metamorphic amphiboles: Natural occurrence and theory. *Rev Mineral* 9B:1-227
- Ross M, Papike JJ, Shaw KW (1969) Exsolution textures in amphiboles as indicators of subsolidus thermal histories. *In: Pyroxenes and Amphiboles: Crystal Chemistry and Phase Petrology*. Papike JJ (ed) Mineralogical Society of America Special Paper 2:275-299
- Schumacher JC (1991) Empirical ferric iron corrections of electron microprobe mineral analyses: necessity, assumptions, and effects on some geothermometers and geobarometers. *Mineral Mag* 55:3-18
- Schumacher JC (1997) The estimation of ferric iron in electron analysis of amphiboles. *Eur J Mineral* 9:643-651
- Schumacher JC, Hollocher KT, Robinson P, Tracy RJ (1990) Progressive reactions and melting in the Acadian metamorphic high of central Massachusetts and southwestern New Hampshire, USA. *In: High temperature metamorphism and crustal anatexis*. Brown M, Ashworth JR (eds) Univ. Birmingham, Sch. Earth Sci, Birmingham, United Kingdom, p 198-234
- Shannon RD, Prewitt CT (1969) Effective ionic radii in oxides and fluorides. *Acta Crystallogr* B25:925-946
- Shau YH, Peacor DR, Ghose S, Phakey PP (1993) Submicroscopic exsolution in mn-bearing alkali amphiboles from Tirodi, Maharashtra, India. *Am Mineral* 78:96-106
- Shido F, Miyashiro A (1959) Hornblende of basic metamorphic rock. *J Fac Sci Univ Tokyo Sect II* 12:85-102
- Smelik EA, Jenkins DM, Navrotsky A (1994) A calorimetric study of synthetic amphiboles along the tremolite-tschermakite join and the heats of formation of magnesiohornblende and tschermakite. *Am Mineral* 79(11-12):1110-1122
- Smelik EA, Nyman MW, Veblen DR (1991) Pervasive exsolution within the calcic amphibole series: TEM evidence for a miscibility gap between actinolite and hornblende in natural samples. *Am Mineral* 76:1184-204
- Smelik EA, Veblen DR (1989) A five-amphibole assemblage from blueschists in northern Vermont. *Am Mineral* 74:960-4
- Smelik EA, Veblen DR (1991) Exsolution of cummingtonite from glaucophane: A new orientation for exsolution lamellae in clinopyroxenes. *Am Mineral* 76:971-984
- Smelik EA, Veblen DR (1992a) Exsolution of calcium-amphibole from glaucophane and the miscibility gap between sodic and calcic amphiboles. *Contrib Mineral Petrol* 112:178-95
- Smelik EA, Veblen DR (1992b) Exsolution of hornblende and the solubility limits of calcium in orthoamphibole. *Science* 257:1669-72
- Smelik EA, Veblen DR (1993) A transmission and analytical electron microscope study of exsolution microstructures and mechanisms in the orthoamphiboles anthophyllite and gedrite. *Am Mineral* 78:511-32
- Smelik EA, Veblen DR (1994) Complex exsolution in glaucophane from Tillotson Peak, north-central Vermont. *Can Mineral* 32:233-55
- Spear FS (1980) The gedrite-anthophyllite solvus and the composition limits of orthoamphibole from the Post Pond Volcanics, Vermont. *Am Mineral* 65:1103-1118
- Spear FS (1982) Phase equilibria of amphibolites from the Post Pond Volcanics, Mt. Cube Quadrangle, Vermont. *J Petrol* 23:383-427

- Stout JH (1970) Three-amphibole assemblages and their bearing on the anthophyllite-gedrite miscibility gap. *Am Mineral* 55:312-313
- Stout JH (1971) Four coexisting amphiboles from Telemark, Norway. *Am Mineral* 56:212-224
- Stout JH (1972) Phase petrology and mineral chemistry of coexisting amphiboles from Telemark, Norway. *J Petrol* 13:99-146
- Thompson JB Jr. (1970) Geometrical possibilities for amphibole structures: model pyriboles. *Am Mineral* 55:292-293
- Thompson JB Jr. (1978) Biopyriboles and polysomatic series. *Am Mineral* 63:239-249
- Thompson JB Jr. (1981) An introduction to the mineralogy and petrology of the biopyriboles. *Rev Mineral* 9A:141-188
- Zingg AJ (1996) Immiscibility in Ca-amphiboles. *J Petrol* 37:471-496

SOURCES OF AMPHIBOLE ANALYSES

- Ahn JH, Cho M, Jenkins DM, Buseck PR (1991) Structural defects in synthetic tremolitic amphiboles. *Am Mineral* 76:1811-1823
- Allen JM, Goldie R (1978) Coexisting amphiboles from Noranda Area, Quebec - extension of actinolite-hornblende miscibility gap to iron-rich bulk compositions. *Am Mineral* 63:205-209
- Altherr R, Topuz G, Marschall H, Zack T, Ludwig T (2004) Evolution of a tourmaline-bearing lawsonite eclogite from the Elekdag area (Central Pontides, N Turkey): evidence for infiltration of slab-derived B-rich fluids during exhumation. *Contrib Mineral Petrol* 148(4):409-425
- Arnold J, Sandiford M, Wetherley S (1995) Metamorphic events in the Eastern Arunta-Inlier. 1. Metamorphic petrology. *Precambrian Res* 71:183-205
- Ashley PM, Lottermoser BG, Westaway JM (1998) Iron-formations and epigenetic ironstones in the Palaeoproterozoic Willyama Supergroup, Olary Domain, South Australia. *Mineral Petrol* 64:187-218
- Ashworth JR, Reverdatto VV, Kolobov VY, Lepetyukha VV, Sheplev VS, Bryxina NA (1998) Textures of diffusion-controlled reaction in contact-metamorphosed Mg-rich granulite, Kokchetav area, Kazakhstan. *Mineral Mag* 62:213-224
- Ballaran TB, Carpenter MA, Domeneghetti MC. (2001) Phase transition and mixing behaviour of the cummingtonite-grunerite solid solution. *Phys Chem Mineral* 28:87-101
- Ballèvre M, Möller A, Hensen BJ (2000) Exhumation of the lower crust during crustal shortening: an Alice Springs (380 Ma) age for a prograde amphibolite facies shear zone in the Strangways Metamorphic Complex (central Australia). *J Metamorph Geol* 18:737-747
- Bandli BR, Gunter ME, Twamley, B, Foit FF, Cornelius SB (2003) Optical, compositional, morphological, and X-ray data on eleven particles of amphibole from Libby, Montana, USA. *Can Mineral* 41:1241-1253
- Banno Y (2000) Intermediate high-pressure exhumation of the northern segment of the Sanbagawa belt, Sarutagawa area, central Shikoku, Japan. *Lithos* 50:289-303
- Banno Y, Miyawaki R, Matsubara S, Makino K, Bunno M, Yamada S, Kamiya T (2004) Magnesiosadanagaite, a new member of the amphibole group from Kasuga-mura, Gifu Prefecture, central Japan. *Eur J Mineral* 16:177-183
- Begin NJ, Carmichael DM (1992) Textural and compositional relationships of Ca-amphiboles in metabasites of the Cape Smith Belt, Northern Quebec - implications for a miscibility gap at medium pressure. *J Petrol* 33:1317-1343
- Berg JH (1985) Chemical variations in sodium gedrite from Labrador. *Am Mineral* 70:1205-1210
- Bhowmik SK, Spiering B (2004) Constraining the prograde and retrograde P-T paths of granulites using decomposition of initially zoned garnets: an example from the Central Indian Tectonic Zone. *Contrib Mineral Petrol* 147:581-603
- Binns RA (1967) Barroisite-bearing eclogite from Naustdal Sogn Og Fjordane Norway. *J Petrol* 8:349-371
- Black PM (1970) Coexisting glaucophane and riebeckite-arfvedsonite from New-Caledonia. *Am Mineral* 55:1061-1064
- Black PM (1973) Mineralogy of New Caledonian metamorphic rocks II. Amphiboles from the Ouégoa District. *Contrib Mineral Petrol* 39:53-64
- Blanckenburg VF, Villa IM, Baur H, Morteani G, Steiger RH (1989) Time calibration of a PT-path from the western Tauern Window, Eastern Alps: the problem of closure temperatures. *Contrib Mineral Petrol* 101:1-11
- Bogoch R, Shirav M (2004) Carbonate nodules of probable stromatolitic origin in amphibolite from the Neoproterozoic terrain of southern Israel. *Mineral Mag* 68:579-589
- Bozhilov KN, Evans BW (2001) Ferroanthophyllite in Rockport grunerite: A transmission electron microscopy study. *Am Mineral* 86:1252-1260
- Bucher K, Fazis Y, De Capitani C, Grapes R (2005) Blueschists, eclogites, and decompression assemblages of the Zermatt-Saas ophiolite: High-pressure metamorphism of subducted Tethys lithosphere. *Am Mineral* 90:821-835

- Bucher K, Frost BR (2006) Fluid transfer in high-grade metamorphic terrains intruded by anorogenic granites: The Thor Range, Antarctica. *J Petrol* 47:567-593
- Castelli D, Rolfo F, Compagnoni R, Xu ST (1998) Metamorphic veins with kyanite, zoisite and quartz in the Zhu-Jia-Chong eclogite, Dabie Shan, China. *Island Arc* 7:159-173
- Champness PE, Rodgers KA (2000) The origin of iridescence in anthophyllite-gedrite from Simiuttat, Nuuk district, southern West Greenland. *Mineral Mag* 64:885-889
- Cho MS, Ernst WG (1991) An experimental-determination of calcic amphibole solid-solution along the join tremolite-tschermakite. *Am Mineral* 76:985-1001
- Cosca, MA, Essene EJ, Kunk MJ, Sutter JF (1992) Differential unroofing within the central metasedimentary belt of the Grenville Orogen - constraints from Ar-40 Ar-39 thermochronology. *Contrib Mineral Petrol* 110:211-225
- Currie KL, Knutson J, Temby PA (1992) The Mud Tank Carbonatite Complex, Central Australia - an example of metasomatism at midcrustal levels. *Contrib Mineral Petrol* 109:326-339
- Dachs E, Proyer A (2001) Relics of high-pressure metamorphism from the Grossglockner region, Hohe Tauern, Austria: Paragenetic evolution and PT-paths of retrogressed eclogites. *Eur J Mineral* 13:67-86
- Dale J, Holland TJB (2003) Geothermobarometry, P-T paths and metamorphic field gradients of high-pressure rocks from the Adula Nappe, Central Alps. *J Metamorph Geol* 21:813-829
- Dasgupta S, Sengupta P, Ehl J, Raith M (1999) Petrology of gedrite-bearing rocks in mid-crustal ductile shear zones from the Eastern Ghats Belt, India. *J Metamorph Geol* 17:765-778
- Dilek Y, Whitney DL (1997) Counterclockwise P-T-t trajectory from the metamorphic sole of a Neo-Tethyan ophiolite (Turkey). *Tectonophysics* 280:295-310
- Driscoll J, Jenkins DM, Dyar MD, Bozhilov KN (2005) Cation ordering in synthetic low-calcium actinolite. *Am Mineral* 90:900-911
- Dziggel A, Stevens G, Poujol M, Anhaeusser CR, Armstrong RA (2002) Metamorphism of the granite-greenstone terrane south of the Barberton greenstone belt, South Africa: an insight into the tectono-thermal evolution of the 'lower' portions of the Onverwacht Group. *Precambrian Res* 114:221-247
- Earley D, Stout JH (1991) Cordierite cummingtonite facies rocks from the Gold Brick District, Colorado. *J Petrol* 32:1169-1201
- El-Shazly AK, Sisson VB (1999) Retrograde evolution of eclogite facies rocks from NE Oman: evidence from fluid inclusions and petrological data. *Chem Geol* 154:193-223
- Elliott BA (2001) Crystallization conditions of the Wiborg rapakivi batholith, SE Finland: an evaluation of amphibole and biotite mineral chemistry. *Mineral Petrol* 72:305-324
- Elliott-Meadows SR, Froese E, Appleyard EC (2000) Cordierite-anthophyllite - cummingtonite rocks from the Lar deposit, Laurie Lake, Manitoba. *Can Mineral* 38:545-550
- Enders M, Speer D, Maresch WV, McCammon CA (2000) Ferric/ferrous iron ratios in sodic amphiboles: Mossbauer analysis, stoichiometry-based model calculations and the high-resolution microanalytical flank method. *Contrib Mineral Petrol* 140:135-147
- Engvik AK, Andersen TB (2000) Evolution of Caledonian deformation fabrics under eclogite and amphibolite facies at Vardalsneset, Western Gneiss Region, Norway. *J Metamorph Geol* 18:241-257
- Engvik AK, Austrheim H, Erambert M (2001) Interaction between fluid flow, fracturing and mineral growth during eclogitization, an example from the Sunnfjord area, Western Gneiss Region, Norway. *Lithos* 57:111-141
- Ernst WG, Liu J (1998) Experimental phase-equilibrium study of Al- and Ti-contents of calcic amphibole in MORB - A semiquantitative thermobarometer. *Am Mineral* 83:952-969
- Evans BW, Giorso MS, Kuehner SM (2000) Thermodynamic properties of tremolite: A correction and some comments. *Am Mineral* 85(3-4):466-472
- Faryad SW, Melcher F, Hoinkes G, Puhl J, Meisel T, Frank W (2002) Relics of eclogite facies metamorphism in the Austroalpine basement, Hochgrosven (Speik complex), Austria. *Mineral Petrol* 74:49-73
- Ferrow EA, Ripa M (1990) Al-poor and Al-rich orthoamphiboles - a Mossbauer-spectroscopy and TEM study. *Mineral Mag* 54:547-552
- Franceschelli M, Carcangiu G, Caredda AM, Cruciani G, Memmi I, Zucca M (2002) Transformation of cumulate mafic rocks to granulite and re-equilibration in amphibolite and greenschist facies in NE Sardinia, Italy. *Lithos* 63:1-18
- Franceschelli M, Eltrudis A, Memmi I, Palmeri R, Carcangiu G (1998) Multi-stage metamorphic re-equilibration in eclogitic rocks from the Hercynian basement of NE Sardinia (Italy). *Mineral Petrol* 62:167-193
- Friend CRL, Janardhan AS, Swamy NS (1993) A retrogressive sapphirine-cordierite-talc paragenesis in a spinel-orthopyroxenite from southern Karnataka, India. *Mineral Mag* 57:273-288
- Frimmel HE (1996) Witwatersrand iron-formations and their significance for gold genesis and the composition limits of orthoamphibole. *Mineral Petrol* 56:273-295
- Frimmel HE, Hartnady CJH (1992) Blue Amphiboles and their significance for the metamorphic history of the Pan-African Gariep Belt, Namibia. *J Metamorph Geol* 10:651-669

- Gao J, Klemd R (2001) Primary fluids entrapped at blueschist to eclogite transition: evidence from the Tianshan meta-subduction complex in northwestern China. *Contrib Mineral Petrol* 142:1-14
- Gao J, Klemd R, Zhang L, Wang Z, Xiao X (1999) P-T path of high-pressure/low-temperature rocks and tectonic implications in the western Tianshan Mountains, NW China. *J Metamorph Geol* 17:621-636
- Gazzola D, Gosso G, Pulcrano E, Spalla I (2000) Eo-Alpine HP metamorphism in the Permian intrusives from the steep belt of the central Alps (Languard-Campo nappe and Tonale Series). *Geodinamica Acta* 13:149-167
- Gittos MF, Lorimer GW, Champnes P (1974) Electron-microscopic study of precipitation (exsolution) in an amphibole (hornblende-grunerite system). *J Mater Sci* 9:184-192
- Godard G, Kienast JR, Lasnier B (1981) Retrogressive development of glaucophane in some eclogites from Massif Armoricain (East of Nantes, France). *Contrib Mineral Petrol* 78:126-135
- Gomez-Pugnaire MT, Karsten L, Sanchez-Vizcaino VL (1997) Phase relationships and P-T conditions of coexisting eclogite-blueschists and their transformation to greenschist-facies rocks in the Nerka Complex (Northern Urals). *Tectonophysics* 276:195-216
- Goscombe B, Hand M (2000) Contrasting P-T paths in the Eastern Himalaya, Nepal: Inverted isograds in a paired metamorphic mountain belt. *J Petrol* 41:1673-1719
- Grew ES, Pertsev NN, Vrana S, Yates MG, Shearer CK, Wiedenbeck M (1998) Korerupine parageneses in whiteschists and other magnesian rocks: is korerupine plus talc a high-pressure assemblage equivalent to tourmaline plus orthoamphibole? *Contrib Mineral Petrol* 131:22-38
- Grobety BH (1997) The replacement of anthophyllite by jimthompsonite: A model for hydration reactions in biopyriboles. *Contrib Mineral Petrol* 127:237-247
- Gunter ME, Dyar MD, Twamley B, Foit FF, Cornelius S (2003) Composition, Fe³⁺/Sigma Fe, and crystal structure of non-asbestiform and asbestiform amphiboles from Libby, Montana, USA. *Am Mineral* 88:1970-1978
- Harlov DE, Forster HJ (2002) High-grade fluid metasomatism on both a local and a regional scale: The Seward Peninsula, Alaska, and the Val Strona di Omegna, Ivrea-Verbano zone, northern Italy. Part I: Petrography and silicate mineral chemistry. *J Petrol* 43(5):769-799
- Hefferan KP, Admou H, Hilal R, Karson JA, Saquaque A, Juteau T, Bohn MM, Samson SD, Kornprobst JM (2002) Proterozoic blueschist-bearing melange in the Anti-Atlas Mountains, Morocco. *Precambrian Res* 118(3-4):179-194
- Helms TS, McSween HY, Labotka TC, Jarosewich E (1987) Petrology of a Georgia Blue Ridge amphibolite unit with hornblende+gedrite+kyanite+ staurolite. *Am Mineral* 72:1086-1096
- Himmelberg G, Papike JJ (1969) Coexisting amphiboles from blueschist facies metamorphic rocks. *J Petrol* 10:102-114
- Hirschmann M, Evans BW, Yang HX (1994) Composition and temperature-dependence of Fe-Mg ordering in cummingtonite-grunerite as determined by X-ray-diffraction. *Am Mineral* 79:862-877
- Hisada K, Miyano T (1996) Petrology and microthermometry of aluminous rocks in the Botswana Limpopo Central Zone: Evidence for isothermal decompression and isobaric cooling. *J Metamorph Geol* 14:183-197
- Hoffmann C (1970) Glaucophane-rocks, their chemical equivalents and related rocks in northern Calabria (Southern Italy). *Contrib Mineral Petrol* 27:283-320
- Hollocher KT (1991) Prograde amphibole dehydration reactions during high-grade regional metamorphism, Central Massachusetts, USA. *Am Mineral* 76:956-970
- Humphreys HC (1993) Metamorphic evolution of amphibole-bearing aluminous gneisses from the eastern-Namaqua Province, South-Africa. *Am Mineral* 78:1041-1055
- Ibarguchi JIG, Girones EO (1985) Petrology, structure and geotectonic implications of glaucophane-bearing eclogites and related rocks from the Malpica Tuy (Mt) Unit, Galicia, northwest Spain. *Chemical Geology* 50:145-162
- Ibarguchi JIG, Mendia M, Girardeau J (1991) Mg-rich and Cr-rich staurolite and Cr-rich kyanite in high-pressure ultrabasic rocks (Cabo Ortegal, Northwestern Spain). *Am Mineral* 76:501-511
- Jacobson CE (1997) Metamorphic convergence of the upper and lower plates of the Vincent thrust, San Gabriel Mountains, southern California, USA. *J Metamorph Geol* 15:155-165
- Jappy TG, Leake BE, Fallick AE (2001) Relationships between hornblende K-Ar ages, chemical composition and hydrogen isotopes, Connemara, western Ireland: evidence for a massive extinct hydrothermal system. *J Geol Soc* 158:843-854
- Kahl WA, Maresch WV (2001) Enthalpies of formation of tremolite and talc by high-temperature solution calorimetry - a consistent picture. *Am Mineral* 86:1345-1357
- Kahl WA, Schumacher JC (2000) Multiple pyroxene and amphibole assemblages in the amphibolite facies: Bulk compositional controls. *Am Mineral* 85(11-12):1606-1616
- Kartagas C (1974) Alkali amphiboles intermediate in composition between actinolite and riebeckite. *Contrib Mineral Petrol* 46:257-264
- Kent AJR, Ashley PM, Fanning CM (2000) Metasomatic alteration associated with regional metamorphism: an example from the Willyama Supergroup, South Australia. *Lithos* 54:33-62

- Kihle J, Bucher-Nurminen K (1992) Ortho-pyroxene sillimanite sapphirine granulites from the Bamble Granulite Terrane, southern Norway. *J Metamorph Geol* 10:671-683
- Kisch HJ, Warnaars FW (1969) Distribution of Mg and Fe in cummingtonite-hornblende and cummingtonite-actinolite pairs from metamorphic assemblages. *Contrib Mineral Petrol* 24:245-267
- Klein C (1968) Coexisting amphiboles. *J Petrol* 9:281-330
- Klein C (1969) 2-Amphibole assemblages in system actinolite-hornblende-glaucophane. *Am Mineral* 54(1-2):212-237
- Klein U, Schumacher JC, Czank M (1996) Mutual exsolution in hornblende and cummingtonite: Compositions, lamellar orientations, and exsolution temperatures. *Am Mineral* 81:928-939
- Klein U, Sharp TG, Schumacher JC (1997) Analytical electron microscopy of nanometer-scale hornblende lamellae: Low-temperature exsolution in cummingtonite. *Am Mineral* 82:1079-1090
- Konishi H, Dodony I, Buseck PR (2002) Protoanthophyllite from three metamorphosed serpentinites. *Am Mineral* 87:1096-1103
- Kotopoulos CN, Pepiper G, Katagas CG (1991) The metamorphism and migmatization of the Xanthe-Echinos Metamorphic Complex, Central Rhodope, Greece. *Lithos* 27:79-93
- Kriegsman LM, Schumacher JC (1999) Petrology of sapphirine-bearing and associated granulites from central Sri Lanka. *J Petrol* 40:1211-1239
- Krupka KM, Hemingway BS, Robie RA, Kerrick DM (1985) high-temperature heat-capacities and derived thermodynamic properties of anthophyllite, diopside, dolomite, enstatite, bronzite, talc, tremolite, and wollastonite. *Am Mineral* 70:261-271
- Labotka TC (1987) The garnet + hornblende isograd in calcic schists from an andalusite-type regional metamorphic terrain, Panamint Mountains, California. *J Petrol* 28:323-354
- Labotka TC, Papike JJ (1991) Non-quadrilateral components in amphiboles - an example from metamorphosed iron-formation from the Ruby Mountains, Montana. *Am J Sci* 291:800-823
- Leake BE (1968) A catalog of analyzed calciferous and sub-calciferous amphiboles together with their nomenclature and associated minerals. *Geol Soc Am Special Paper* 68:210
- Leger A, Ferry JM (1991) Highly aluminous hornblende from low-pressure metacarbonates and a preliminary thermodynamic model for the Al content of calcic amphibole. *Am Mineral* 76:1002-1017
- Linthout K, Lustenhouwer WJ (1996) Subsilicic sodium gedrite in lepite of quartz keratophyric origin, Nordmark (Sweden). *Mineral Mag* 60:379-387
- Liogys VA, Jenkins DM (2000) Hornblende geothermometry of amphibolite layers of the Popple Hill gneiss, north-west Adirondack Lowlands, New York, USA. *J Metamorph Geol* 18:513-530
- Lombardo B, Rolfo F (2000) Two contrasting eclogite types in the Himalayas: implications for the Himalayan orogeny. *J Geodynamics* 30:37-60
- Makanjuola A, Howie RA (1972) Mineralogy of glaucophane schists and associated rocks from Ile De Groix, Brittany, France. *Contrib Mineral Petrol* 35:83-118
- Mancini F, Marshall B, Papunen H (1996) Petrography and metamorphism of the Saaksjarvi ultramafic body, southwest Finland. *Mineral Petrol* 56:185-208
- Mange MA, Dewey JF, Floyd JD (2005) The origin, evolution and provenance of the northern belt (Ordovician) of the Southern Uplands Terrane, Scotland: a heavy mineral perspective. *Proc Geol Assoc* 116:251-280
- Maresch WV, Medenbach O, Rudolph A (1982) Winchite and the actinolite glaucophane miscibility gap. *Nature* 296:731-732
- Marschall HR, Ertl A, Hughes JM, McCammon C (2004) Metamorphic Na- and OH-rich disordered dravite with tetrahedral boron, associated with omphacite, from Syros, Greece: chemistry and structure. *Eur J Mineral* 16:817-823
- Marshall D, Kirschner D, Bussy F (1997) A Variscan pressure-temperature-time path for the N-E Mont Blanc massif. *Contrib Mineral Petrol* 126:416-428
- Matthes S, Okrusch M, Rohr C, Schussler U, Richter P, Vongehlen K (1995) Talc-chlorite-amphibole felses of the Ktb Pilot Hole, Oberpfalz, Bavaria - protolith characteristics and phase-relationships. *Mineral Petrol* 52:25-59
- Mattinson CG, Zhang RY, Tsujimori T, Liou JG (2004) Epidote-rich talc-kyanite-phengite eclogites, Sulu terrane, eastern China: P-T-f(O₂) estimates and the significance of the epidote-talc assemblage in eclogite. *Am Mineral* 89:1772-1783
- Meeker GP, Bern AM, Brownfield IK, Lowers HA, Sutley, SJ, Hoefen TM, Vance JS (2003) The composition and morphology of amphiboles from the Rainy Creek complex, near Libby, Montana. *Am Mineral* 88:1955-1969
- Messiga B, Tribuzio R, Caucia F (1991) Amphibole evolution in Variscan eclogite-amphibolites from the Savona Crystalline Massif (Western Ligurian Alps, Italy) - controls on the decompressional P-T Path. *Lithos* 27(4):215-230
- Miyano T, Beukes NJ (1997) Mineralogy and petrology of the contact metamorphosed amphibole asbestos-bearing Penge iron formation, eastern Transvaal, South Africa. *J Petrol* 38:651-676

- Mogessie A, Purtscheller F, Tessadri R (1986) High alumina calcic amphiboles (alumino pargasite-magnesio sadanagaite) from metabasites and metacarbonates of Central Oetztal, Eastern Alps (Northern Tyrol, Austria). *N Jahr Mineral Ab* 154:21-39
- Molina JF, Austrheim H, Glodny J, Rusin, A (2002) The eclogites of the Marun-Keu complex, Polar Urals (Russia): fluid control on reaction kinetics and metasomatism during high P metamorphism. *Lithos* 61:55-78
- Mori Y, Nishiyama T, Yanagi T (2003) Mass transfer and reaction paths in alteration zones around carbonate veins in the Nishisonogi Metamorphic Rocks, southwest Japan. *Am Mineral* 88:611-623
- Mottana A, Bocchio R, Crespi R, Decapitani L, Liborio G, Dellavventura G (1994) Cummingtonite in the amphibolites of the south-alpine basement-complex (Upper Lake-Como Region, Italy) - its relationships with hornblende. *Mineral Petrol* 51:67-84
- Mucke A, Annor A (1993) Examples and genetic significance of the formation of iron-oxides in the Nigerian banded iron-formations. *Mineral Dep* 28:136-145
- Muller WF, Schmadicke E, Okrusch M, Schussler U (2003) Intergrowths between anthophyllite, gedrite, calcic amphibole, cummingtonite, talc and chlorite in a metamorphosed ultramafic rock of the KTB pilot hole, Bavaria. *Eur J Mineral* 15:295-307
- Nam TN, Hyodo H, Itaya T, Matsuda T (2002) Ar-40/Ar-39 single grain dating and mineral chemistry of hornblendes south of the Red River shear zone (Vietnam): new evidence for early Proterozoic tectonothermal event. *Gondwana Res* 5:801-811
- Norlander BH, Whitney DL, Teysier C, Vanderhaeghe O (2002) Partial melting and decompression of the Thor-Odin dome, Shuswap metamorphic core complex, Canadian Cordillera. *Lithos* 61:103-125
- Oh CW, Liou JG, Maruyama, S (1991) Low-temperature eclogites and eclogitic schists in Mn-rich metabasites in Ward Creek, California - Mn and Fe effects on the transition between blueschist and eclogite. *J Petrol* 32:275-302
- Okamoto A, Toriumi M (2001) Application of differential thermodynamics (Gibbs' method) to amphibole zonings in the metabasic system. *Contrib Mineral Petrol* 141:268-286
- Okamoto A, Toriumi M (2004) Optimal mixing properties of calcic and subcalcic amphiboles: application of Gibbs' method to the Sanbagawa schists, SW Japan. *Contrib Mineral Petrol* 146:529-545
- Okamoto A, Toriumi M (2005) Progress of actinolite-forming reactions in mafic schists during retrograde metamorphism: an example from the Sanbagawa metamorphic belt in central Shikoku, Japan. *J Metamorph Geol* 23:335-356
- Okay AI (1980) Mineralogy, petrology, and phase-relations of glaucophane-lawsonite zone blue schists from the Tavsanli Region, northwest Turkey. *Contrib Mineral Petrol* 72:243-255
- Okay AI, Kelley SP (1994) Tectonic setting, petrology and geochronology of jadeite plus glaucophane and chloritoid plus glaucophane schists from north-west Turkey. *J Metamorph Geol* 12:455-466
- Okay AI, Monie P (1997) Early Mesozoic subduction in the eastern Mediterranean: evidence from Triassic eclogite in northwest Turkey. *Geology* 25(7):595-598
- Okay AI, Monod O, Monie P (2002) Triassic blueschists and eclogites from northwest Turkey: vestiges of the Paleo-Tethyan subduction. *Lithos* 64(3-4):155-178
- Operta M, Pamic J, Balen D, Tropper P (2003) Corundum-bearing amphibolites from the metamorphic basement of the Krivaja-Konjuh ultramafic massif (Dinaride Ophiolite Zone, Bosnia). *Mineral Petrol* 77:287-295
- Osanai Y, Hamamoto T, Maishima O, Kagami H (1998) Sapphirine-bearing granulites and related high-temperature metamorphic rocks from the Higo metamorphic terrane, west-central Kyushu, Japan. *J Metamorph Geol* 16:53-66
- Ota T, Terabayashi M, Katayama I (2004) Thermobaric structure and metamorphic evolution of the Iratsu eclogite body in the Sanbagawa belt, central Shikoku, Japan. *Lithos* 73:95-126
- Ota T, Terabayashi M, Parkinson CD, Masago H (2000) Thermobaric structure of the Kokchetav ultrahigh-pressure-high-pressure massif deduced from a north-south transect in the Kulet and Saldat-Kol regions, northern Kazakhstan. *Island Arc* 9:328-357
- Ouzegane K, Djemai S, Guiraud M (1996) Gedrite-garnet-sillimanite-bearing granulites from Amessmessa area, south In Ouzal, Hoggar, Algeria. *J Metamorph Geol* 14:739-753
- Pamic J, Balen D, Tibljas D (2002) Petrology and geochemistry of orthoamphibolites from the Variscan metamorphic sequences of the South Tisia in Croatia - an overview with geodynamic implications. *Int J Earth Sci* 91(5):787-798
- Perchuk AL, Philippot P (2000) Nascent subduction: A record in the Yukon eclogites. *Petrology* 8:1-18
- Poli S (1991) Reaction spaces and P-T paths - from amphibole eclogite to greenschist facies in the Austroalpine Domain (Oetztal Complex). *Contrib Mineral Petrol* 106:399-416
- Puga E, Nieto JM, De Federico AD (2000) Contrasting P-T paths in eclogites of the Betic Ophiolitic Association, Mulhacen Complex, southeastern Spain. *Can Mineral* 38:1137-1161
- Ripa M (1994) The mineral chemistry of hydrothermally altered and metamorphosed wall-rocks at the Stollberg Fe-Pb-Zn-Mn(-Ag) Deposit, Bergslagen, Sweden. *Mineral Dep* 29:180-188

- Sakakibara M, Isono Y (1996) Middle Miocene thermal metamorphism due to the infiltration of high-temperature fluid in the Sanbagawa metamorphic belt, southwest Japan. *Contrib Mineral Petrol* 125:341-358
- Sakakibara M, Ofuka H, Kimura G, Ishizuka H, Miyashita S, Okamura M, Melnikov OA (1997) Metamorphic evolution of the Susunai metabasites in southern Sakhalin, Russian Republic. *J Metamorph Geol* 15:565-580
- Satoh H, Yamaguchi Y, Makino K (2004) Ti-substitution mechanism in plutonic oxy-kaersutite from the Larvik alkaline complex, Oslo rift, Norway. *Mineral Mag* 68:687-697
- Scherth HP, Schreyer W, Chopin C (1991) The pyrope-coesite rocks and their country rocks at Parigi, Dora Maira Massif, Western Alps - detailed petrography, mineral chemistry and Pt-path. *Contrib Mineral Petrol* 108:1-21
- Schneiderman JS, Tracy RJ (1991) Petrology of orthoamphibole-cordierite gneisses from the Orijarvi Area, Southwest Finland. *Am Mineral* 76:942-955
- Schreurs J, Westra L (1985) Cordierite-orthopyroxene rocks: the granulite facies equivalents of the Orij irvi cordierite-anthophyllite rocks in West Uusimaa, southwest Finland. *Lithos* 18:215-228
- Schulz B, Bombach K, Pawlig S, Bratz H (2004) Neoproterozoic to Early-Palaeozoic magmatic evolution in the Gondwana-derived Austroalpine basement to the south of the Tauern Window (Eastern Alps). *Int J Earth Sci* 93:824-843
- Schulz B, Triboulet C, Audren C (1995) Microstructures and mineral chemistry in amphibolites from the western Tauern window (Eastern Alps), and P-T deformation paths of the Alpine greenschist-amphibolite facies metamorphism. *Mineral Mag* 59:641-659
- Schulz B, Triboulet C, Audren C, Pfeifer HR, Gilg A (2001) Two-stage prograde and retrograde Variscan metamorphism of glaucophane-eclogites, blueschists and greenschists from Ile de Groix (Brittany, France). *Int J Earth Sci* 90:871-889
- Schumacher JC, Robinson P (1987) Mineral chemistry and metasomatic growth of aluminous enclaves in gedrite cordierite-gneiss from southwestern New-Hampshire, USA. *J Petrol* 28:1033-1073
- Schumacher R (1991) Compositions and phase-relations of calcic amphiboles in epidote-bearing and clinopyroxene-bearing rocks of the amphibolite and lower granulite facies, Central Massachusetts, USA. *Contrib Mineral Petrol* 108:196-211
- Sengupta P, Raith M, Levitsky VI (2004) Compositional characteristics and paragenetic relations of magnesiohobomite in aluminous amphibolites from the Belomorian complex, Baltic Shield, Russia. *Am Mineral* 89:819-831
- Sharma RS, Macrae ND (1981) Paragenetic relations in gedrite-cordierite-staurolite-biotite-sillimanite-kyanite gneisses at Ajitpura, Rajasthan, India. *Contrib Mineral Petrol* 78:48-60
- Shau YH, Peacor DR, Ghose S, Phakey PP (1993) Submicroscopic exsolution in Mn-bearing alkali amphiboles from Tirodi, Maharashtra, India. *Am Mineral* 78:96-106
- Shi GH, Cui WY, Tropper P, Wang CQ, Shu, GM, Yu HX (2003) The petrology of a complex sodic and sodic-calcic amphibole association and its implications for the metasomatic processes in the jadeite area in northwestern Myanmar, formerly Burma. *Contrib Mineral Petrol* 145(3):355-376
- Shimazaki H, Bunno M, Ozawa T (1984) Sadanagaite and magnesio-sadanagaite, new silica-poor members of calcic amphibole from Japan. *Am Mineral* 69:465-471
- Simon G, Chopin C (2001) Enstatite-sapphirine crack-related assemblages in ultrahigh-pressure pyrope megablasts, Dora-Maira massif, western Alps. *Contrib Mineral Petrol* 140:422-440
- Smelik EA, Nyman MW, Veblen DR (1991) Pervasive exsolution within the calcic amphibole series - TEM evidence for a miscibility gap between actinolite and hornblende in natural samples. *Am Mineral* 76:1184-1204
- Smelik EA, Veblen DR (1991) Exsolution of cummingtonite from glaucophane - a new orientation for exsolution lamellae in clinoamphiboles. *Am Mineral* 76:971-984
- Smelik EA, Veblen DR (1992a) Exsolution of Ca-amphibole from glaucophane and the miscibility gap between sodic and calcic amphiboles. *Contrib Mineral Petrol* 112:178-195
- Smith CA, Sisson VB, Lallemand HGA, Copeland P (1999) Two contrasting pressure-temperature-time paths in the Villa de Cura blueschist belt, Venezuela: Possible evidence for Late Cretaceous initiation of subduction in the Caribbean. *Geol Soc Am Bull* 111:831-848
- Smith CB, Sims K, Chimuka L, Duffin A, Beard AD, Townend R (2004) Kimberlite metasomatism at Murowa and Sese pipes, Zimbabwe. *Lithos* 76:219-232
- Smith CG, Phillips ER (2002) Cummingtonite in the Dalradian of NE Scotland. *Mineral Mag* 66:337-352
- Smulikowski W (1995) Evidence of glaucophane-schist facies metamorphism in the East Karkonosze complex, West Sudetes, Poland. *Geologische Rundschau* 84:720-737
- Sokolova EV, Hawthorne FC, Gorbatova V, McCammon C, Schneider J (2001) Ferrian winchite from the Ilmen Mountains, southern Urals, Russia, and some problems with the current scheme for amphibole nomenclature. *Can Mineral* 39:171-177
- Spear FS (1980) The Gedrite-Anthophyllite Solvus and the Composition Limits of Orthoamphibole from the Post Pond Volcanics, Vermont. *Am Mineral* 65:1103-1118

- Spear FS (1982) Phase equilibria of amphibolites from the Post Pond Volcanics, Mt. Cube Quadrangle, Vermont. *J Petrol* 23:383-427
- Stephenson D (1993) Amphiboles from Dalradian metasedimentary rocks of NE Scotland - environmental inferences and distinction from amphiboles of meta-igneous amphibolites. *Mineral Petrol* 49:45-62
- StOnge MR, Ijewliw OJ (1996) Mineral corona formation during high-P retrogression of granulitic rocks, Ungava Orogen, Canada. *J Petrol* 37:553-582
- Stout JH (1972) Phase petrology and mineral chemistry of coexisting amphiboles from Telemark, Norway. *J Petrol* 13:99-146
- Stunitz H (1998) Syndeformational recrystallization - dynamic or compositionally induced? *Contrib Mineral Petrol* 131:219-236
- Subbanna GN, Kutty TRN, Iyer GVA (1986) Structural intergrowth of brucite in anthophyllite. *Am Mineral* 71:1198-1200
- Sueno S, Matsuura S, Gibbs GV, Boisen MB (1998) A crystal chemical study of protoanthophyllite: orthoamphiboles with the protoamphibole structure. *Phys Chem Mineral* 25:366-377
- Takeuchi M (1994) Changes in garnet chemistry show a progressive denudation of the source areas for Permian-Jurassic sandstones, Southern Kitakami Terrane, Japan. *Sedimentary Geology* 93:85-105
- Terabayashi M (1993) Compositional Evolution in Ca-Amphibole in the Karmutsen Metabasites, Vancouver Island, British-Columbia, Canada. *J Metamorph Geol* 11:677-690
- Todd CS, Evans BW (1994) Properties of CO₂-induced dehydration of amphibolite. *J Petrol* 35:1213-1239
- Triboulet C (1974) Glaucofane schists and associated rocks in Ile-De-Groix (Morbihan, France) - mineralogical and petrogenetic study. *Contrib Mineral Petrol* 45:65-90
- Tribuzio R, Giacomini F (2002) Blueschist facies metamorphism of peralkaline rhyolites from the Tenda crystalline massif (northern Corsica): evidence for involvement in the Alpine subduction event? *J Metamorph Geol* 20:513-526
- Tropper P, Manning CE, Essene EJ, Kao LS (2000) The compositional variation of synthetic sodic amphiboles at high and ultra-high pressures. *Contrib Mineral Petrol* 139:146-162
- Tuisku P (1992) Contact zone interaction of metabasites with metapelites - amphibolite facies mineral assemblages, chemical profiles and their origin, the Puolankajarvi Formation, Finland. *Lithos* 27:279-300
- Vanko DA, Laverne C (1998) Hydrothermal anorthitization of plagioclase within the magmatic/hydrothermal transition at mid-ocean ridges: examples from deep sheeted dikes (Hole 504B, Costa Rica Rift) and a sheeted dike root zone (Oman ophiolite). *Earth Planet Sci Lett* 162:27-43
- Verkouteren JR, Wylie AG (2000) The tremolite-actinolite-ferro-actinolite series: Systematic relationships among cell parameters, composition, optical properties, and habit, and evidence of discontinuities. *Am Mineral* 85:1239-1254
- Visser D (1993) Fluorine-bearing hydrogarnets from Blengsvatn, Bamble Sector, South Norway. *Mineral Petrol* 47:209-218
- Visser D, Thijssen PHM, Schumacher JC (1992) Hogbomite in sapphirine-bearing Rocks from the Bamble Sector, South Norway. *Mineral Mag* 56:343-351
- Woodland AB, Seitz HM, Altherr R, Marschall H, Olker B, Ludwig T (2002) Li abundances in eclogite minerals: a clue to a crustal or mantle origin? *Contrib Mineral Petrol* 143:587-601
- Wylie AG, Verkouteren JR (2000) Amphibole asbestos from Libby, Montana: aspects of nomenclature. *Am Mineral* 85:1540-1542
- Yagi K, Takeshita T (2002) Regional variation in exhumation and strain rate of the high-pressure Sambagawa metamorphic rocks in central Shikoku, south-west Japan. *J Metamorph Geol* 20:633-647
- Yamaguchi Y (1985) Hornblende cummingtonite and hornblende actinolite intergrowths from the Koyama Calc-Alkaline Intrusion, Susa, Southwest Japan. *Am Mineral* 70:980-986
- Yang HX, Evans BW (1996) X-ray structure refinements of tremolite at 140 and 295 K: Crystal chemistry and petrologic implications. *Am Mineral* 81:1117-1125
- Ye K, Hirajima T (1996) High-pressure marble at Yangguantun, Rongcheng county, Shandong province, eastern China. *Mineral Petrol* 57:151-165
- Zeh A, Gerdes A, Will TM, Millar IL (2005) Provenance and magmatic-metamorphic evolution of a Variscan Island-arc complex: Constraints from U-Pb dating, petrology, and geospeedometry of the Kyffhuder Crystalline Complex, Central Germany. *J Petrol* 46:1393-1420
- Zenk M, Schulz B (2004) Zoned Ca-amphiboles and related P-T evolution in metabasites from the classical Barrovian metamorphic zones in Scotland. *Mineral Mag* 68:769-786
- Zhao GC, Cawood PA, Wilde SA, Min S, Lu LZ (2000) Metamorphism of basement rocks in the Central Zone of the North China Craton: implications for Paleoproterozoic tectonic evolution. *Precambrian Res* 103:55-88
- Zhu C, Hu HF, Ilton ES, Veblen DR, Henry DJ, Tivey MK, Thompson G (1994) TEM-AEM observations of Cl-rich amphibole and biotite and possible petrologic implications. *Am Mineral* 79:909-920

APPENDIX I

Recalculating amphibole formulae from electron microprobe analyses

Electron microprobe analysis. The electron microprobe is essential to understand systematic variations in the chemistry of minerals. However, the electron microprobe cannot measure water (i.e., O vs. OH) or easily differentiate among different valence states of the same element, notably Fe and Mn, and these values affect the total numbers of cations in mineral formulae that are calculated from these analyses. An amphibole mineral formula based on 23 oxygens will have too few cations if some OH is actually replaced by O but unrecognized; an amphibole mineral formula calculated to any oxygen basis will have too many cations if a multivalent element like iron is treated as all Fe²⁺, but in fact is partly Fe³⁺. The convention for metamorphic amphiboles is to use the 23 oxygen anhydrous-formula basis, because few documented cases of O for OH substitution are known in metamorphic amphiboles. However, multivalent cations, in particular for Fe, are a problem that has been approached both empirically and analytically.

Petrographic inspection is enough to demonstrate qualitatively the presence of both Fe²⁺ and Fe³⁺ in amphiboles. In thin section, the various hues of blue and green pleochroic colors displayed sodic, sodic-calcic and calcic amphiboles, and the clove to gray colors of the orthoamphiboles are indications of the presence of some Fe³⁺ in addition to Fe²⁺. For this reason, the routine determination of Fe³⁺ in amphiboles is an analytical holy grail. The flank method developed by (Höfer et al. 1994, see also, Höfer et al. 1996, 2000) and correlations of the flank method with other techniques (Enders et al. 2000) show promise under certain circumstances. Nevertheless, at present these methods are not easy to implement and as a result not routinely used. Amphibole compositional zoning at the limits of electron microprobe resolution further is a challenge to the application of these methods. At present, recalculation methods based on stoichiometric or chemical limits on Fe³⁺ content remain the best, albeit imperfect, method of estimating Fe³⁺ for the large numbers of analyses generated by the electron microprobe.

Empirical estimates of Fe³⁺. Empirical Fe³⁺ estimates in amphiboles based on stoichiometric limits have been discussed in works by Stout (1972), Robinson et al. (1982, p. 3-12), Droop (1987), Jacobson (1989), Schumacher (1991, 1997) and Holland and Blundy (1994). Empirical estimates of Fe³⁺ for amphiboles are based on two assumptions: (1) the anhydrous oxygen content is known (here, 23 oxygen) and (2) certain cations are restricted to the various amphibole sites.

Empirical estimates of Fe³⁺ are themselves constrained by the *chemical limits*. Treating the iron either as all Fe²⁺ or all Fe³⁺ define the *chemical limits*. Observations suggest that usually most of the iron in amphiboles (and most Fe-Mg silicates) is Fe²⁺. For many amphibole analyses, the *all-ferrous* chemical limit will yield the structural formula with minimum estimate of Fe³⁺ (Fe³⁺ = 0). Cases where the *all-ferric* chemical limit gives a structural formula that is the maximum estimate of Fe³⁺ will be rarer; for example, the *all-ferric* chemical limit may come into play in oxidized rocks, like some iron formations, where the amphibole solid solution compositions approach magnesioriebeckite.

The *stoichiometric limits* are based on observations that prescribe assumed behavior of certain critical cations. The most important of these are: (1) Si occurs only at the *T* sites; (2) Al occurs at *T* and *M*(2) sites; (3) the sum of ⁶R³⁺ and ⁶R⁴⁺ are ≤ 2; (4) Ca occurs only at the *M*(4) site; (5) Na occurs only at the *M*(4) and *A* sites; (6) K occurs only at the *A* site; (7) Total cations cannot exceed 16, but the sum of all cations exclusive of K is ≥ 15; and (8) no vacancies are present other than at the *A*-site. Note that these simplifying assumptions already exclude those rare examples of amphiboles where ⁴Ti and *A*-site Ca are reported but are the basis of the 7 stoichiometric limits shown in Figure A1 that can be used to estimate Fe³⁺ in most metamorphic amphiboles.

Summary of site assignments, stoichiometric limits and calculation schemes for minimum and maximum Fe ³⁺ estimates based on these limits					
Element Groups	Cation*	Stoichiometric Limit	Type and Name of Estimation		Calculation scheme
			Minimum	Maximum	
T-group	Si	Si ≤ 8	8Si	8SiAl	Σcations = FCT×8/Si
	Al	ΣAl ≥ 8			Σcations = FCT×8/(Si + Al)
	Ti ⁴⁺				
	Cr ³⁺				
	V ³⁺				
C-group	Fe ³⁺				
	Mn ³⁺	ΣR ³⁺ ≤ 10	10R ³⁺	Σcations = (FCT×36)/[46-Σ(R ⁴⁺ +R ³⁺)]	
	Ni ²⁺				
	Mg				
	Zr ⁴⁺				
Zn ²⁺					
B-group	Co ²⁺				
	Li				
	Fe ²⁺				
	Mn ²⁺	ΣMn ≥ 13	13eCNK	Σcations = FCT×13/ΣMn	
	Ca ^{**}	ΣCa ≤ 15	15eNK (15evNK)	Σcations = FCT×15/ΣCa	
A-group	Na	ΣNa ≥ 15	15eK	Σcations = FCT×15/ΣNa	
	K	ΣK ≤ 16	16CAT	Σcations = 16	
	□				

* cations arranged according to increasing ionic radius (smallest, Si to largest, K); values are from Shannon and Prewitt (1969). For C-site cations, ionic radii for octahedral coordination were used.

** Ca assumed to be excluded from the A-site—only known exception is a rare amphibole: cannilloite

Σ = Σ of subtotal of cations (e.g. ΣMn = sum of all cations from Si through Mn in the list)

□ = vacancy at the A-site

FCT = ferrous cation total

Σcations = the formula cation basis for the amphibole ferric estimate. The actual normalization factor = cations/FCT

15evNK: for Fe-Mg-Mn amphiboles, the 15eNK estimation can give both the minimum and maximum estimate. Robinson *et al.* (1982) modified the 15eNK to give a maximum estimate by setting ⁰Na to 0.08. For this 15eNK method with variable ⁰Na, 15evNK, Σcations = FCT×14.92/ΣCa.

Figure A1. Summary of ideal site assignments, limits of various cation subtotals and the type of correction (minimum or maximum) that can be obtained by calculating the formulas to these stoichiometric limits (after Robinson *et al.* 1982, p. 6-12 and Schumacher 1991). Abbreviations of normalizations: **8Si** = normalized to total Si = 8; **8SiAl** = normalized to total Si + Al = 8; **10R³⁺** = normalized so that the sum of the R⁴⁺ and R³⁺ cations = 10; **13eCNK** = normalized so that the sum of the cations Si through Mn (i.e., all cations exclusive of Ca, Na, K) = 13; **15eNK** = normalized such so that the sum of the cations Si through Ca (i.e., all cations exclusive of Na, K) = 15; **16CAT** = normalized so that total the sum of all cations = 16.

In the *all-ferrous* structural formulae of Fe³⁺-bearing minerals, all of the cations are too high—the extra cations and their oxygen make up for the oxygen that is missing from the iron by assuming it is divalent (for discussion see Schumacher 1991 and refs. therein). In amphiboles, these extra cations may or may not cause the resulting *all-ferrous* formula to exceed one of the limits in Figure A1, i.e., Si ≤ 8, ΣCa ≤ 15 or ΣK ≤ 16. If the resulting amphibole formula has no stoichiometric violations, then the *all-ferrous* formula (a chemical limit) is the minimum estimate of Fe³⁺ for that particular analysis (Fe³⁺ = 0). If one of the three limits is exceeded, then the *all-ferrous* formula is not stoichiometric. The formula for the cation values normalized by one of the methods 8Si, 15eNK and 16CAT (Fig. A1) will give minimum estimate of Fe³⁺ (Fe³⁺ > 0) needed to yield a stoichiometric formula. If neither the *all-ferrous* formula or any of the formulae from the 8Si, 15eNK and 16CAT normalization are stoichiometric based on the limits above, then an analytical problem may exist or the chosen limits are too restrictive.

Any analysis that yields a stoichiometric formula for the minimum estimate will also give a maximum estimate of Fe³⁺. Based on the assumptions used here, five possible limits on maximum Fe³⁺ exist. The chemical limit, all Fe³⁺, and four stoichiometric limits, ΣAl = 8, ΣR³⁺ = 10, ΣMn = 13 and ΣNa = 15. The formula for the cation values normalized by one of the methods 8SiAl, 10R³⁺, 13eCNK or 15eK, will give a stoichiometric formula (Fig. A1) for most amphiboles. Be aware that the 15eK does not give a good estimate of the maximum Fe³⁺ for (Mg, Fe, Mn) amphiboles with appreciable ^ANa (e.g., some anthophyllite and gedrite). For sodic orthoamphiboles the 15eK estimate will commonly give the “maximum” Fe³⁺ estimate, but its application to these orthoamphiboles will cause too much Na to enter the M(4) site. Two alternatives to the 15eK exist: (1) use the 15eNK (minimum) Fe³⁺ estimate—the minimum and maximum estimates are the same or (2) set an a limit on the amount of Na that can enter the M(4)-site. For case (2), the limit on M(4)-site Na is somewhat arbitrary, but (Robinson et al. 1982) suggested a value of 0.08 Na as a reasonable maximum based on mineral formulae from gravimetric analyses of orthoamphiboles (this estimate is abbreviated 15evNK—15 cations exclusive variable amounts of Na and K). If neither the *all-ferric* formula or any of the formulae from the 8SiAl, 10R³⁺, 13eCNK or 15eK (15evNK) normalization are stoichiometric based on the limits above, then an analytical problem may exist or the chosen limits are too restrictive.

These calculation procedures with examples are given in Leake et al. (1997). The procedure to obtain the minimum Fe³⁺ estimate is: (1) calculate an all-Fe²⁺ amphibole formula based on 23 oxygen; (2) calculate the Σcation values for each of the stoichiometric minimum estimates (8Si, 15eNK and 16CAT); (3) compare the all-Fe²⁺ cation sum and Σcation values—the lowest value (*min*Σcation) identifies the calculation scheme that gives the minimum Fe³⁺ (Fig. A1); (4) recalculate the analysis on the cation basis using the *min*Σcation; (5) sum the oxygen (ΣO) that is assigned to each of the recalculated cation values (if it is not ≤ 23, an error was made); (6) if the sum of the oxygen is < 23, convert enough Fe²⁺ to Fe³⁺ to achieve 23 oxygen [Fe³⁺ = (23–ΣO)×2] and Fe²⁺ = recalculated Fe²⁺–Fe³⁺].

The procedure to obtain the maximum Fe³⁺ estimate is analogous: (1) calculate an all-Fe²⁺ amphibole formula based on 23 oxygen; (2) calculate the Σcation values for each of the stoichiometric maximum estimates (8SiAl, 10R³⁺, 13eCNK and 15eK); (3) compare the all-Fe³⁺ cation sum and Σcation values—the highest value (*max*Σcation) identifies the calculation scheme that gives the maximum Fe³⁺ (Fig. A1); (4) recalculate the analysis on the cation basis using the *max*Σcation; steps (5) and (6) are as above. The average estimate of Fe³⁺ can be calculated by adding *min*Σcation and *max*Σcation values then and dividing by 2 ((*min*Σcation + *max*Σcation)/2 = *ave*Σcation). An amphibole formula based on *ave*Σcation and 23 oxygens gives the average Fe³⁺ for the analysis; calculation is analogous those described above, except *ave*Σcation is used in place of either *min*Σcation or *max*Σcation. The Σcation values allow an initial evaluation of the quality of the analyses. If the boolean *min*Σcation > *max*Σcation is not true, then something is wrong with either the analysis, calculation or stoichiometric assumptions.

Mn²⁺ and Mn³⁺. Like Fe, Mn has multiple valance states (2+, 3+, 4+ are common), and the difference between Mn³⁺ and Mn²⁺ manganese is not evident in electron microprobe analysis of amphiboles. Fortunately, encounters with amphiboles containing manganese in multiple valance states will be rare. These would potentially only be found in highly oxidized, Mn-rich protoliths, like some chemical sediments associated with seafloor-hydrothermal activity. The MnO-Mn₂O₃ oxygen buffer lies at higher oxygen fugacity values than the FeO-Fe₂O₃ buffer, so, in rocks and minerals bearing Mn³⁺, all iron should be trivalent, providing the assemblages are equilibrated. All the (Mg, Fe) silicates in such rocks would be essentially magnesium end-members, which should be obvious from their optical and chemical properties. Estimating Mn³⁺ would use the same criteria and stoichiometric limits as the procedure for Fe³⁺ described above. The chief difference is the all the iron would need to be treated as Fe³⁺.

Trace-Element Partitioning Between Amphibole and Silicate Melt

Massimo Tiepolo, Roberta Oberti and Alberto Zanetti

*Istituto di Geoscienze e Georisorse, Consiglio Nazionale delle Ricerche
I-27100 Pavia, Italy*

tiepolo@crystal.unipv.it, oberti@crystal.unipv.it, zanetti@crystal.unipv.it

Riccardo Vannucci

*Dipartimento di Scienze della Terra, Università di Pavia, and
Istituto di Geoscienze e Georisorse*

Consiglio Nazionale delle Ricerche, Pavia, Italy

vannucci@crystal.unipv.it

Stephen F. Foley

*Institut für Geowissenschaften
Universität Mainz, Mainz, Germany*

foley@uni-mainz.de

INTRODUCTION

Knowledge of the partitioning behavior of trace elements between solid and liquid is a prerequisite for modern igneous and mantle petrology. Most of the mathematical models simulating melt generation, migration and evolution within the mantle and/or the crust require the availability of reliable solid/liquid partition coefficients for the mineral phases involved in the process.

Calcic amphiboles are extremely important for the understanding of lithospheric processes because of both their common occurrence in a variety of igneous and metamorphic rocks types and their capability of hosting a large number of geochemically important trace elements. A series of studies on the partitioning behavior of trace elements between calcic amphibole and silicate melt have therefore been carried out at different pressures, temperatures and system compositions during the last 15 years. However, due to the complex crystal chemistry of amphiboles, only few studies focused on the role of crystal structure and composition on amphibole-liquid partition coefficients ($D^{\text{Amph/LD}}$). In this chapter, present knowledge of the solid/liquid trace element partitioning between calcic amphiboles and silicate melt is summarized and the role played by the crystal structure and melt composition on $D^{\text{Amph/LD}}$ variations is highlighted in addition to the effects of pressure and temperature. The dataset used in this chapter includes only the results of experimental studies performed under well constrained *P-T* conditions for which trace element determinations were carried out with highly sensitive *in situ* microanalytical techniques.

The available dataset considered in this work are listed in Table 1. Although far less common than the calcic amphiboles, potassic-richterites are potentially important in the generation of potassic magmatic rocks and in re-enrichment processes occurring in the subcontinental mantle lithosphere sampled as xenoliths in kimberlites. A comprehensive experimental study of trace element partitioning between synthetic potassic richterites and silicate melts has been carried

Table 1. Dataset of the partitioning experiments considered in this work.
The code number of reference (#) has to be used for tables 2 to 7

# Ref.	Sample	P (GPa)	T (°C)	SiO ₂	X _{mf} /X	#	Ref.	Sample	P (GPa)	T (°C)	SiO ₂	X _{mf} /X
1 [1]	A-N-melt*	1.4	1015	46.3	0.55	42	[6]	1452	0.5	1000	45.8	0.58
2 [1]	A-N-melt	1.4	1015	52.3	0.62	43	[6]	1518	2.0	1000	41.6	0.53
3 [1]	A-N-synth	1.4	1015	44.9	0.54	44	[6]	1549	2.0	1000	43.3	0.56
4 [1]	A-K-1.00	1.4	1015	50.4	0.59	45	[7]	900°		900	61.0	0.67
5 [1]	A-K-0.81	1.4	1015	52.4	0.61	46	[7]	850°C doped		850	64.0	0.68
6 [1]	A-K-0.71	1.4	1015	53.0	0.62	47	[7]	850°C undoped		850	64.0	0.68
7 [1]	A-M-0.45	1.4	950	51.9	0.63	48	[7]	800°C		800	68.0	0.73
8 [1]	B-N-melt	1.4	1015	52.2	0.65	49	[8]	3048T-1	1.5	1092	44.6	0.56
9 [1]	B-T-0.89	1.4	975	54.6	0.66	50	[9]	1442	2.0	1050	39.9	0.53
10 [1]	B-T-0.89	1.4	1015	48.2	0.65	51	[9]	1446	1.5	1050	44.3	0.55
11 [1]	B-T-0.89	1.4	1035	47.0	0.63	52	[9]	1447	1.0	1000	46.0	0.58
12 [1]	B-T-0.89	1.4	1055	45.7	0.61	53	[9]	1452	0.5	1050	45.8	0.58
13 [1]	B-T-0.94	1.4	1015	48.6	0.59	54	[10]	27	1.5	1100	37.1	0.44
14 [1]	B-T-0.94	1.4	1035	54.6	0.68	55	[10]	34	2.5	1050	34.1	0.43
15 [1]	B-T-0.94	1.4	1055	50.4	0.62	56	[10]	12	1.5	1100	36.6	0.42
16 [1]	B-T-0.94	1.4	1075	41.5	0.50	57	[10]	41	2.5	1075	34.2	0.41
17 [1]	B-T-0.97	1.4	975	53.2	0.65	58	[10]	43	1.5	1050	38.0	0.43
18 [1]	B-T-0.97	1.4	1015	50.5	0.62	59	[10]	2	1.5	1040	35.9	0.49
19 [1]	B-M-0.45	1.4	1045	48.1	0.59	60	[10]	23	1.5	1000	45.3	0.52
20 [1]	B-M-0.75	1.4	1050	48.5	0.59	61	[10]	25	2.2	1000	47.1	0.56
21 [1]	B-M-0.90	1.4	1050	48.4	0.62	62	[11]	T85LLH+NST+YZG	5	940	60.2	0.71

22 [1]	B-M-1.00	1.4	1070	46.6	0.59	63 [11]	ABALLH+NST+YZG	5	940	59.3	0.68
23 [1]	B-K-1.00	1.4	1070	49.7	0.58	64 [11]	478LLH+NST+YZG	5	940	60.0	0.69
24 [1]	B-K-0.50	1.4	1030	48.5	0.58	65 [11]	AT4LLH+NST+YZG	5	940	61.2	0.71
25 [1]	B-K-0.81	1.4	1030	43.3	0.55	66 [11]	557LLH+NST+YZG	5	940	63.7	0.72
26 [2]	BBeLi5	1.5	1000	51.3	0.64	67 [11]	T85LLH+NST+YZG	2	945	61.2	0.72
27 [2]	BBeLi50	1.5	1000	51.3	0.64	68 [11]	T85LLH+NST+YZG	2	940	56.0	0.69
28 [3]	1388	2.0	1050	46.1	0.62	69 [11]	ABALLH	2	940	59.1	0.71
29 [3]	1389	2.0	1050	47.0	0.57	70 [11]	478LLH+NST+YZG	2	940	61.1	0.70
30 [3]	1393	2.0	1000	50.1	0.63	71 [11]	557LLH+NST+YZG	2	940	59.9	0.69
31 [3]	1395	2.0	1025	52.8	0.65	72 [11]	478LLH+NST+YZG	2	900	65.4	0.74
32 [3]	1409	1.0	1000	51.9	0.64	73 [11]	557LLH+NST+YZG	2	900	65.4	0.76
33 [4]	Avg.	0.2	1050	50.9	0.60	74 [11]	AT4NST+YZG	2	940	59.82	0.70
34 [5]	81T116	0.2	1050	55.8	0.60	75 [11]	4095	10	970	63.3	0.68
35 [5]	AYII-V	0.2	1050	62.9	0.69	76 [11]	4498	10	900	64.5	0.67
36 [5]	CL-1	0.2	1050	67.2	0.75	77 [11]	4500	10	900	67.4	0.70
37 [5]	DM-A	0.2	1050	77.7	0.86	78 [11]	4502	10	900	66.6	0.70
38 [5]	DM-B	0.2	1050	76.8	0.85	79 [11]	4505	10	900	64.2	0.68
39 [6]	1442	2.0	1000	39.9	0.53	80 [11]	4749	10	1020	51.9	0.54
40 [6]	1446	1.5	1000	44.3	0.55	81 [11]	4754	10	1020	51	0.53
41 [6]	1447	1.0	1000	46.0	0.58	82 [11]	4755	10	1020	50.9	0.53
						83 [11]	4756	10	1020	51.2	0.53

[1]: Tiepolo et al. 1999; Tiepolo et al. 2000a; Tiepolo et al. 2000b; [2] Brennan et al. 1998; [3] Adam et al. 1993; [4] Brennan et al. 1995; [5] Sisson 1994; [6] Adam and Green 1994; [7] Klein et al. 1997; [8] LaTourrette et al. 1995; [9] Adam and Green 1993; [10] Dalpé and Baker 2000; [11] Hilyard et al. 2000; [12] Nicholls and Harris 1980.

out by Tiepolo et al. (2003), to which the reader is referred for the whole dataset. In the last section of this chapter, the differing partitioning behavior observed in calcic amphiboles and potassic-rich rhyolites is compared and contrasted in terms of the effect of relative dimensions of the relevant structural sites.

PARTITION COEFFICIENTS

Within the Henry's law field the distribution of an element between two phases in chemical equilibrium is independent on the element concentration. The equilibrium ratio between the concentrations (C) of the element in the two phases is defined as the Nernst partition coefficient (D) and in the case that the two phases are a solid and a melt it is defined as:

$${}^{S/L}D_i = \frac{{}^S C_i}{{}^L C_i} \quad (1)$$

where S and L are the solid and the liquid phases, respectively, and i is a generic trace element. This notation is preferred to the usage of K_D for a single element partition coefficient, as K_D should refer to an exchange coefficient of two elements between two phases (Takahashi and Irvine 1983; Beattie et al. 1993). Equation (1) allows estimation of element concentrations in equilibrium melts starting from the solid/liquid partition coefficient and the trace element composition of the mineral phase of interest. This is crucial when no direct record of the melt composition is available (e.g., in cumulus rocks), so that information can be gathered about the geochemical signatures of the full petrogenetic processes.

Solid/liquid partition coefficients (${}^{S/L}D$) are not constant but depend on a number of factors among which pressure, temperature, melt composition and crystal structure are the most important. Given the great variability of extensive and intensive parameters observed in petrogenetic processes, significant variation of the solid/liquid partitioning behavior of trace elements is expected. Therefore, the accuracy of petrogenetic models or computed parental liquids is strongly dependent on the correct choice of the adopted ${}^{S/L}D$. This emphasizes that thorough knowledge of the changes in the solid/liquid partition coefficients as a function of the chemical composition of the system and its intensive parameters is a crucial prerequisite.

In the latest fifteen years, advances in microbeam trace-element analysis have led to the production of a large amount of reliable partitioning datasets for a wide range of P , T and X conditions involving either phenocryst and glassy matrix pairs coexisting in natural samples or quenched run products from experimentally produced analogues. The number of experiments designed to obtain the best ${}^{S/L}D$ s for a given process as a function of the composition of the melt (mainly silica content) and/or the physical conditions (P , T and f_{O_2}) has increased rapidly in recent years. Moreover, the development since the 1990s of predictive models of partitioning based on lattice-strain models which relate ${}^{S/L}D$ values to the physical characteristics of perfectly ionic structural sites allowed better constraints of the control exerted on trace-element incorporation by mineral structure and the available crystal-chemical mechanisms to satisfy local bond-strength requirements. The former "carrier" concept, namely the inference of mechanisms of trace-element incorporation based on the behavior of a chemically analogous major element has been abandoned. However, in very few cases, the determination of major- and trace-element composition in mineral-glass pairs by *in-situ* techniques (such as Electron-MicroProbe, EMP, Laser Ablation (LA)-ICPMS, Secondary Ion Mass Spectrometry (SIMS), and Proton-Induced X-ray Emission, PIXE) has been combined with the characterization of crystal-chemical details by Single-crystal structure REFinement (SREF), thus providing an independent piece of information on both the site populations and the bonding character.

FACTORS AFFECTING SOLID/LIQUID PARTITION COEFFICIENTS

At constant pressure and temperature, trace element solid/liquid partition coefficients depend on both melt and crystal structure. In both cases, bond-strength requirements and ionic radii rule the incorporation of a trace element substituting for a major constituent in a given polyhedron, and thus determine the value of the partition coefficient.

The effect of melt composition is basically related to its degree of polymerization (e.g., Ryerson et al. 1978); the higher the structural organization of the melt, the lower the possibility of hosting those cations that do not fit tetrahedral coordination because of their ionic radius and charge. These cations are defined as network modifiers (Nielsen 1985), and an increase of their concentration in the solid phase (and thus of S/LD) is expected with the increase of melt polymerization. In contrast, those cations which are suitable for tetrahedral coordination or which have a strong affinity with Na and K (which balance the presence of tetrahedral Al in highly polymerized melts) are defined as network formers, and their S/LD decrease with the increase of melt polymerization. The structural organization of a melt is commonly expressed with the NBO/T notation, where T are the cations in tetrahedral coordination and NBOs are the non-bridging oxygen atoms associated with network-modifier cations such as Ca and Mg (and possibly Fe^{2+}), as well as the fraction of Na and K that is not coupled with tetrahedral Al^{3+} . Knowledge of the H_2O content and the Fe^{2+}/Fe^{3+} ratio of the melt is required for correct calculation of the NBO/T value. In order to make all the available data comparable, we decided to use a simpler definition of the structural organization of the melt, namely the X_{nf}/X value. It is defined as the sum of the molar fractions of network-forming cations (X_{nf} , i.e. Si and the fraction of Al balanced by alkalis) normalized to the sum of all cations on a molar basis (X ; Tiepolo et al. 2000a).

The effect of the mineral structure on S/LD can be rationalized in terms of the availability of (1) polyhedra of size and coordination suitable for cation incorporation, and (2) crystal-chemical mechanisms allowing local charge balance (coupled heterovalent substitutions) and satisfaction of bond-strength requirements. In principle, Goldschmidt's rules (Goldschmidt 1937) which consider the difference in valence and ionic radius between the major-element cation and the trace element(s) substituting for it, also describe trace-element incorporation well. These rules can be summarized as follows (Mason 1966, p. 132): (1) if two ions have the same radius and the same charge, they will enter a given crystal structure with equal facility; (2) if two ions have similar radii and the same charge, the smaller ion will enter a given crystal lattice more readily; (3) if two ions have similar radii and different charge, the ion with the higher charge will enter a given crystal lattice more readily. These rules provide the basis for unraveling crystal-chemical control on trace-element incorporation in minerals and thus on trace-element partitioning between solid and melt, a goal first pursued by lattice-site elastic-strain models (Nagasawa 1966; Brice 1975). In these models, trace elements are regarded as impurities introduced in a perfectly elastic and isotropic crystal lattice that minimizes its perturbation by relaxing the adjacent sites and distributing the surplus elastic or electrostatic energy through the lattice (Nagasawa 1966; Brice 1975). Thus, elastic-strain models imply a purely ionic perspective of the mineral structure.

The relationships among partition coefficients, ionic radii and ionic charges have been established qualitatively since the work of Onuma et al. (1968). These authors showed that for a specific site the logarithms of the partition coefficients vary in a quasi-parabolic way with the radius of the cations, thus providing evidence that the elastic-strain energy is roughly symmetrical about an optimum ionic size. More recently, two nearly simultaneous papers (Beattie 1994; Blundy and Wood 1994) provided a physical basis to explain these relations. Both approaches use lattice-site elastic-strain theory to model the energetics of solid solutions. The two mathematical treatments were later shown to give nearly equivalent (within 10%)

results for most cations (Purton et al. 1997), and the Blundy and Wood model was preferred by the scientific community due to its simpler formalism:

$$D_i(P, T, X) = D_0(P, T, X) \exp \left(4\pi E N_A \left(\frac{r_0}{2} (r_i - r_0)^2 + \frac{1}{3} (r_i - r_0)^3 \right) / (RT) \right) \quad (2)$$

where the power's numerator is the equation of Brice (1975), which relates the substitution of a cation i with radius r_i after a cation with radius r_0 (the one ideal for the relevant structural site) to the resulting strain energy stored in the crystal lattice, N_A is Avogadro's number, E is the Young's modulus of the site, D_0 is the strain-compensated partition coefficient of the element with ionic radius r_0 , R is the gas constant, and T is the absolute temperature (K).

Equation (2) allows calculation of the partition coefficient (D_i) of any element with ionic radius r_i starting from that (D_0) of an element with ionic radius r_0 that is ideal for the structural site of interest. When at least three partition coefficients of homovalent ($1+$, $2+$, ... $n+$) cations entering the same structural site are known, the lattice-site parameters (r_0 , D_0 , and E) can be calculated, and the D values for other homovalent substituents at the same P , T , X conditions can be predicted. Moreover, equation (2) allows prediction of D_i under different P , T , X conditions for all the possible substituents, which is particularly important when these conditions cannot be attained experimentally.

AMPH/LD FOR THE LIGHT LITHOPHILE ELEMENTS (LLE)

Source of data

$D_{\text{Amph/LD}}$ for the light lithophile elements (LLE) Li, Be and B are relatively scarce in the literature. The available data were experimentally determined on calcic amphiboles synthesized from basanitic and alkali basaltic compositions at pressures ranging between 0.5 and 2.0 GPa and temperatures between 975 and 1095 °C by LaTourrette et al. (1995), Brenan et al. (1998), Tiepolo (1999), and Adam and Green (2003). The overall dataset is reported in Table 2.

Overall values

The $D_{\text{Amph/LD}}$ values for Li and Be in the various available sets of values are very similar both in terms of absolute values and inter-element fractionation (Table 2 and Fig. 1). The same is not true for boron. Li and Be are highly to moderately incompatible with $D_{\text{Amph/LD}_{\text{Li}}}$ ranging from 0.05 to 0.19 and $D_{\text{Amph/LD}_{\text{Be}}}$ from 0.07 to 0.3. The $D_{\text{Amph/LD}_{\text{Li}}}/D_{\text{Amph/LD}_{\text{Be}}}$ ratio ranges from 0.40 and 1.07, with a mean value of 0.63. With the exception of the partition coefficient measured by Adam and Green (2003),

Table 2. $D_{\text{Amph/LD}}$ for light lithophile elements (LLE).

#	Li	1 σ	Be	1 σ	B	1 σ
2	0.125	0.002	0.226	0.010	0.017	0.009
9	0.115	0.005	0.186	0.014	0.012	0.005
10	0.104	0.008	0.197	0.017	0.014	0.002
11	0.069	0.003	0.065		0.018	
13	0.104	0.009	0.176	0.006	0.012	0.009
14	0.121	0.001	0.221	0.002	0.006	0.003
15	0.112	0.008	0.181	0.022	0.009	
16	0.090	0.002	0.107	0.003	0.016	0.001
17	0.116	0.004	0.145	0.003	0.004	
18	0.107	0.007	0.157	0.015	0.010	0.002
19	0.098	0.002	0.164	0.008	0.010	0.001
20	0.076	0.007	0.161	0.032	0.006	0.003
21	0.080	0.024	0.139	0.036	0.009	
22	0.051	0.024	0.123	0.028	0.018	0.009
23	0.075	0.001	0.126	0.004	0.006	
24	0.073	0.004	0.142	0.011	0.006	0.003
25	0.064	0.008	0.143	0.004	0.010	0.002
26	0.190	0.020	0.260	0.020	0.022	0.003
27	0.130	0.010	0.210	0.010	0.015	0.001
49	0.124	0.008	0.150	0.020		
50	0.110	0.020	0.160	0.100	0.150	0.030
51	0.130	0.050	0.200	0.500	0.080	0.070
52	0.120	0.010	0.300	0.600	0.090	0.060
53	0.090	0.030	0.130	0.290	0.110	0.050

B is highly incompatible in calcic amphiboles, with values (0.004-0.02) about one order of magnitude lower than those of Li and Be. The $D_{Be}^{Amph/L} / D_B^{Amph/L}$ ratios are between 3.6 and 36 with a mean value of 17. $D_B^{Amph/L}$ values from Adam and Green (2003) are significantly higher and comparable to those of Be (0.08-0.15). The $D_{Be}^{Amph/L} / D_B^{Amph/L}$ ratios range between 1.1 and 3.3.

Site preference

Inferences on the site preference of Li, Be and B into the amphibole structure may come from synthetic and natural amphiboles in which these elements occur as major or detectable constituents. The incorporation of Li in amphiboles has been the object of many recent crystal-chemical studies on natural and synthetic (chemically simplified) samples (see Oberti et al.

2007a for more detail). Li can be a major B and C cation. In both cases, its occurrence is restricted to ${}^B\text{Na}$ or ${}^B\text{Li}$ amphiboles (and their solid solutions). ${}^C\text{Li}$ orders at the $M(3)$ sites, and is locally balanced *via* the coupled exchange ${}^{M(3)}\text{Li}_1 {}^{M(2)}\text{Fe}^{3+}_1 {}^{M(2),M(3)}(\text{Mg,Fe})^{2+}_{-2}$. Of relevance to the present work is the observation that ${}^{M(3)}\text{Li}$ is always associated with at least an equal amount of A-site occupancy, which helps to satisfy bond-strength requirements.

Be in amphiboles has been found so far as a major constituent only in joesmithite, ideally $\text{Pb Ca}_2 (\text{Mg}_3\text{Fe}^{3+}_2) (\text{Si}_6\text{Be}_2) \text{O}_{22} (\text{OH})_2$ (Moore et al. 1993). In this very peculiar amphibole, which crystallizes in the $P2_1/a$ space group, Be is completely ordered at the $T(1)B$ site, where it is locally associated with Pb^{2+} ordered at the A site, thus satisfying bond-strength requirements.

In the case of one synthetic sample of fluoro-edenite, B was incorporated as a major T cation (Kohn and Komeforo 1955), and crystal-chemical reasoning suggests that it orders at the $T(1)$ site.

Factors affecting $D_{LLE}^{Amph/L}$

No clear relation can be detected between $D_{Li}^{Amph/L}$ and compositional factors, including the amount of the cations involved in the relevant exchanges in sodic amphiboles, namely ${}^{M(4)}\text{Na}$, ${}^A\text{Na}$ and ${}^C\text{Fe}^{3+}$. A rough and slightly scattered linear correlation is observed between $D_{Li}^{Amph/L}$ and the degree of melt polymerization (Fig. 2) expressed as X_{nf}/X . This evidence suggests that the effect of melt composition on $D_{Li}^{Amph/L}$ is probably dominant over that of the crystal structure in calcic amphiboles. Remarkably, the linearity of the correlation between $D_{Li}^{Amph/L}$ and X_{nf}/X suggests that Li acts as a network modifier. No information on the effect of pressure and temperature on $D_{Li}^{Amph/L}$ is present in the literature. If we consider only amphiboles in equilibrium with melts with similar X_{nf}/X ratios, and compare the $D_{Li}^{Amph/L}$ determined at different P and T , we note that they vary only within error. Thus, the effects of the intensive parameters on $D_{Li}^{Amph/L}$ are apparently negligible within the investigated P , T range.

$D_{Be}^{Amph/L}$ do not show any clear relation with the amount of the major cations, and are only poorly correlated with the X_{nf}/X parameter of the melt. However, a good linear correlation is observed between $D_{Be}^{Amph/L}$ and the $D_{Pb}^{Amph/L}$ (Fig. 3), thus confirming that the crystal-

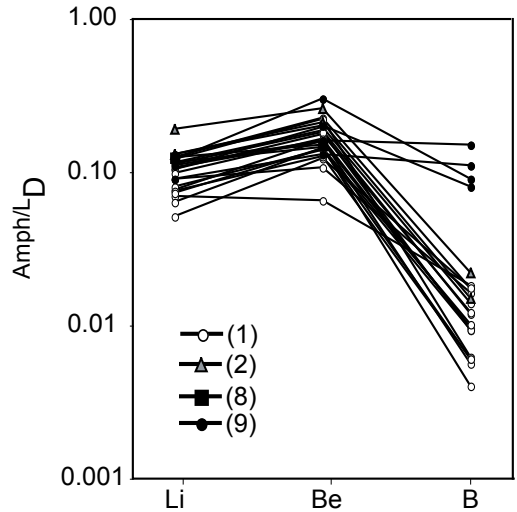


Figure 1. Light Lithophile Element (LLE) partitioning between calcic amphibole and silicate melt. See Table 1 for code numbers.

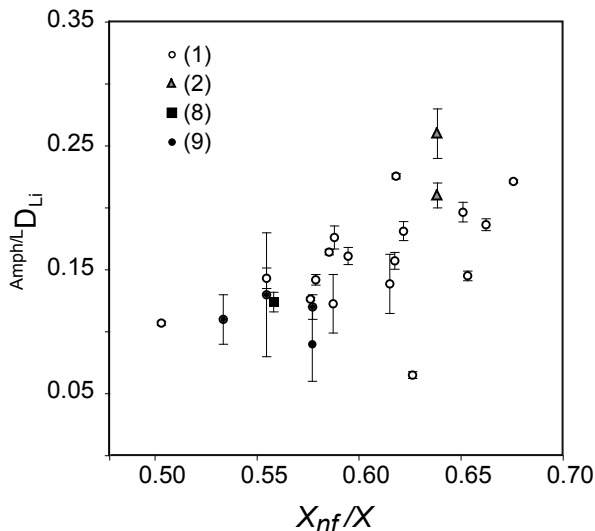
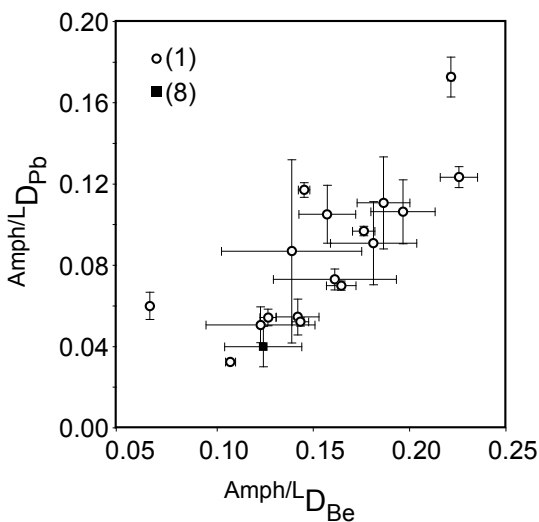


Figure 2. Variation of the $Amph/L D_{Li}$ as a function of melt composition expressed as (X_{nf}/X) . See Table 1 for code numbers. Error bars are 2σ .

Figure 3. Variation of the $Amph/L D_{Be}$ as a function of $Amph/L D_{Pb}$. See Table 1 for code numbers. Error bars are 2σ .



chemical mechanism ruling Be incorporation is the same as in joesmithite. The available dataset however does not allow identification of a first order dependence of the $Amph/L D_{Be}$. The weak linear correlation between $Amph/L D_{Be}$ and the X_{nf}/X parameter may suggest an effect of the melt composition, which cannot, however, be distinguished from a possible influence of the amphibole structure. No evidence of an effect of pressure and temperature was observed.

Similarly to Li and Be, no significant relation with amphibole composition was found for $Amph/L D_B$. In contrast to the other LLE, no significant relation with melt polymerization is observed, which might be expected given that B generally has tetrahedral coordination. More accurate conclusions on the control exerted by the crystal and melt structure on $Amph/L D_B$ are hampered by the relatively large error associated with the available data. Also in the case of $Amph/L D_B$, no evident effect of pressure and temperature was observed.

AMPH/L D FOR ALKALINE AND ALKALINE-EARTH LARGE ION LITHOPHILE ELEMENTS (LILE)

Source of data

$D_{\text{Amph/L}}$ for LIL elements have been reported for compositions ranging from basanite to alkali basalts by Adam et al. (1993), Brenan et al. (1995), Adam and Green (1994, 2003), LaTourrette et al. 1995, Tiepolo (1999) and Dalpé and Baker (2000). These experimental studies were carried out over a pressure range between 0.5 and 2.5 GPa and amphiboles were crystallized at temperatures ranging from 975 and 1075 °C. More evolved systems were considered in the experiments of Sisson (1994) and Klein et al. (1997). The latter, however, determined only the $D_{\text{Amph/L}}$ for Sr. The overall dataset is reported in Table 3.

Overall values

The LIL elements are usually moderately to highly incompatible in calcic amphibole (Fig. 4). Only rarely do they reach a slight compatibility. Cs is the most incompatible element with $D_{\text{Cs}}^{\text{Amph/L}}$ ranging between 0.001 and 0.29. Rb usually has a strong incompatible behavior in calcic amphibole but Dalpé and Baker (2000) found that it might be also slightly compatible ($D_{\text{Rb}}^{\text{Amph/L}} = 1.04$). $D_{\text{Ba}}^{\text{Amph/L}}$ is highly to slightly incompatible and varies between 0.08 and 0.72. Sr is commonly slightly incompatible ($D_{\text{Sr}}^{\text{Amph/L}}$ between 0.3 and 0.9), but it may have $D_{\text{Sr}}^{\text{Amph/L}}$ well above unity (up to 1.65). The $D_{\text{Ba}}^{\text{Amph/L}}/D_{\text{Sr}}^{\text{Amph/L}}$ is extremely variable with values ranging between 0.14 and 2.31. A similar large variation is also observed for the $D_{\text{Rb}}^{\text{Amph/L}}/D_{\text{Sr}}^{\text{Amph/L}}$ ratio (0.06-2.23).

Site preference

According to their relatively large ionic radius, Ba ($r_{\text{Ba}}^{(12)} = 1.61 \text{ \AA}$), Cs ($r_{\text{Cs}}^{(12)} = 1.88 \text{ \AA}$) and Rb ($r_{\text{Rb}}^{(12)} = 1.72 \text{ \AA}$) are preferentially incorporated at the A site, where they can occur in variable coordination depending on local ordering. For Cs¹⁺ and Rb¹⁺, no coupled exchange is required in A-filled amphiboles such as pargasites and kaersutites; in contrast, a coupled heterovalent substitution has to be identified in the case of Ba²⁺. No information is available on this point from experimental studies on synthetic materials, although incorporation of Al into the tetrahedra is the most likely mechanism to satisfy bond-strength requirements. Ordering of Rb, Ba and Cs at the A site is also confirmed by the very low contents of these elements in clinopyroxene, a mineral phase analogous to the amphiboles but for the availability of a highly coordinated site suitable for alkalis (as well as for the absence of OH⁻ anion). The smaller ionic radius of Sr ($r_{\text{Sr}}^{(12)} = 1.44 \text{ \AA}$ and $r_{\text{Sr}}^{(8)} = 1.26 \text{ \AA}$; Shannon et al. 1976) allows for incorporation at both the A and M(4) sites. Experimental studies have shown that Sr orders at the M(4) site in richterites (see Oberti et al. 2007a for more detail); accordingly, relatively high $D_{\text{Sr}}^{\text{S/L}}$ for Sr are measured also in clinopyroxene (Adam and Green 2003). Nevertheless, $D_{\text{Sr}}^{\text{Amph/L}}$ for high-temperature calcic amphiboles are significantly higher than in the associated clinopyroxene (Adam and Green 2003), thus supporting the hypothesis that in calcic amphiboles with high ^TAl contents (1.8-2.0 apfu) disordered between the T(1) and T(2) sites (Adam et al. 2007), Sr can be both an A and B cation. This evidence confirms the importance of local charge-balance and bond-strength requirements on the incorporation of divalent cations at the A site.

Factors affecting $D_{\text{LILE}}^{\text{Amph/L}}$

Understanding whether melt or crystal composition prevails in ruling the variation of the $D_{\text{Amph/L}}$ for LIL elements in calcic amphiboles is not straightforward. None of the $D_{\text{Amph/L}}$ of the elements discussed above show a clear dependence on amphibole composition, and a relatively well-defined inverse dependence on the X_{Hf}/X parameter (Fig. 5) can be detected only for $D_{\text{Rb}}^{\text{Amph/L}}$:

$$D_{\text{Rb}}^{\text{Amph/L}} = 27.509e^{-9.4126(X_{\text{Hf}}/X)} \quad R^2 = 0.79$$

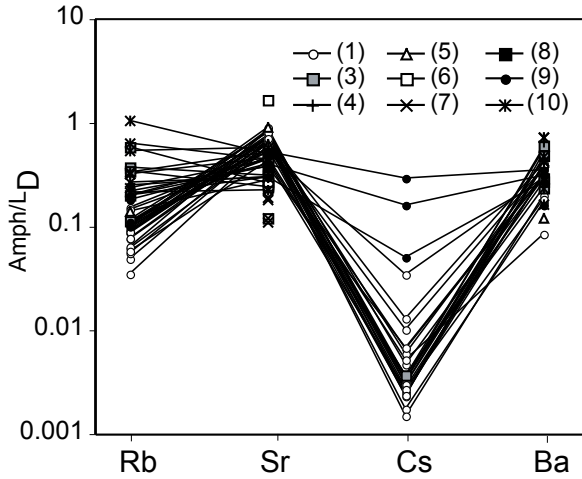
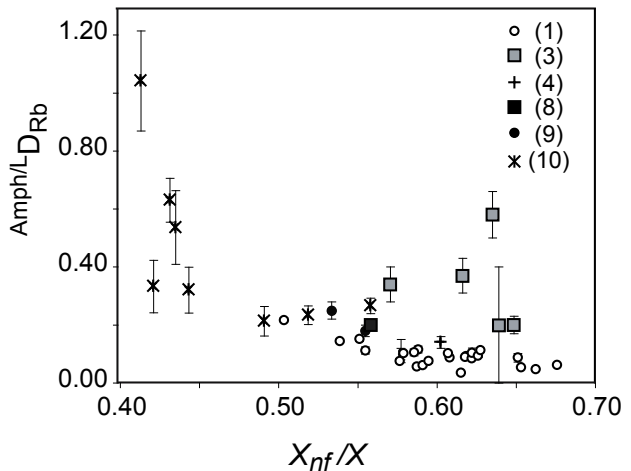


Figure 4. Large Ion Lithophile Element (LILE) partitioning between calcic amphibole and silicate melt. See Table 1 for code numbers.

Figure 5. Variation of the $^{Amph/L}D_{Rb}$ as a function of melt composition expressed as (X_{nf}/X) . See Table 1 for code numbers. Error bars are 2σ .



Here, the $^{Amph/L}D_{Rb}$ values reported by Adam et al. (1993) have been excluded because of the bias induced by Rb volatilization under the proton microprobe. This behavior of Rb is in agreement with its network-forming character of the monovalent cations, similar to Na and K.

$^{Amph/L}D$ for Sr, Cs and Ba do not correlate with melt composition, thus showing that the effect of the crystal structure and the melt cannot be distinguished based on the available data. In the case of Cs, the relatively large error related to its low concentration in amphibole is a likely explanation for the scattering of the data.

The role of pressure on the $^{Amph/L}D$ of the LIL elements was specifically investigated by Adam and Green (1994) and Dalpé and Baker (2000). An inverse linear relation between pressure and $^{Amph/L}D_{Sr}$ was found by Adam and Green (1994), who observed $^{Amph/L}D_{Sr}$ ranging between 0.43 and 0.11 in the P range 0.5-2.0 GPa. Dalpé and Baker (2000) noted that $^{Amph/L}D$ for the elements with ionic radii farther from the r_0 of the A site are much more strongly affected by pressure than those with ionic radius closer to the r_0 . In fact, the dependence of $^{Amph/L}D$ for Rb on pressure is much stronger than that of Na or K (Dalpé and Baker 2000).

AMPH/LD FOR RARE EARTH ELEMENTS (REE) AND Y

Source of data

$A_{\text{Amph/LD}}$ for the REE in calcic amphiboles are relatively abundant in the literature. Experimentally determined $A_{\text{Amph/LD}}^{\text{REE}}$ have been reported by Nicholls and Harris (1980), Adam and Green (1994, 2003), Brenan et al. (1995), LaTourrette et al. (1995), Bottazzi et al. (1999), Tiepolo et al. (2000a) and Dalpé and Baker (2000). All these studies were done in basanitic and alkali basaltic systems at pressures in the range 0.5-2.0 GPa and at temperatures in the range 975-1090 °C. Systems further enriched in silica (basaltic andesite to rhyolitic systems) were considered by Nicholls and Harris (1980), Sisson (1994), Klein et al. (1997) and Hilyard et al. (2000). Experiments were done at pressure ranging between 0.2 and 1.0 GPa and temperature ranging between 800 and 1050 °C. The overall dataset is reported in Table 4.

Overall values

The variability of $A_{\text{Amph/LD}}^{\text{REE}}$ documented by literature data is quite large, and exceeds one order of magnitude (Fig. 6). When plotted against the ionic radius, the $A_{\text{Amph/LD}}^{\text{REE}}$ for calcic amphiboles form near-parabolic moderately-fractionated curves with maxima falling in the M-HREE region and minima at La.

La is moderately to highly incompatible in calcic amphiboles with values ranging between 0.03 and 0.86. An important exception is represented by the amphiboles crystallized from rhyolitic melts, for which Sisson (1994) reported $A_{\text{Amph/LD}}^{\text{La}}$ up to 1.92. MREE and HREE are moderately incompatible to compatible. $A_{\text{Amph/LD}}$ for Gd and Yb are in the range 0.32-4.00 and 0.24-5.5, respectively.

The LREE/MREE fractionation varies by a factor of up to four, with $A_{\text{Amph/LD}}^{\text{La}}/A_{\text{Amph/LD}}^{\text{Sm}}$ ratios between 0.09 and 0.34. A similar range is observed for LREE/HREE fractionation ($A_{\text{Amph/LD}}^{\text{La}}/A_{\text{Amph/LD}}^{\text{Yb}} = 0.08-0.35$). As expected from both ionic radius and valence, the behavior of $A_{\text{Amph/LD}}^{\text{Y}}$ is analogous to that of the HREE.

Site preference

The ionic radii of REE steadily decrease with the increase in atomic number (the so-called lanthanide contraction). The lightest REE in their trivalent state have larger ionic radii than Ca ($^{88}\text{Ca} = 1.12$, $^{138}\text{La} = 1.16$ Å, $^{140}\text{Ce} = 1.143$ Å), whereas the heaviest REE have much smaller ionic radii ($^{175}\text{Lu} = 0.86$ Å, $^{173}\text{Yb} = 0.87$ Å). It is well-known that the B cations in amphibole occupy distinct sites depending on their ionic radius, the smaller (Li, Mg and Fe^{2+}) occurring

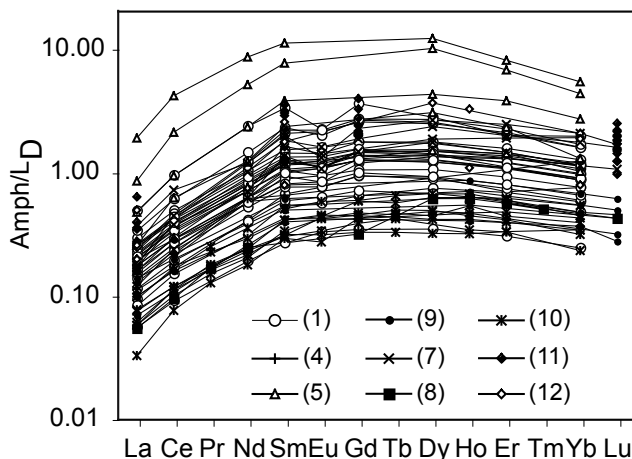


Figure 6. Rare Earth Element (REE) partitioning between calcic amphibole and silicate melt. See Table 1 for code numbers.

Table 4. A_{Ampl}/D for the Rare Earth Elements.

#	La	Ce	Pr	Nd	Sm	Eu	Gd	Tb	Dy	Ho	Er	Yb	Lu	Y	$I\sigma$			
1	0.10	0.02	0.18	0.03	0.68	0.08	0.78	0.06	0.96	0.05	0.94	0.02	0.71	0.07	0.77	0.09	0.90	0.08
2	0.21	0.03	0.36	0.04	1.20	0.07	1.26	0.04	1.49	0.05	1.52	0.06	1.40	0.07	1.15	0.05	1.46	0.06
3	0.09	0.02	0.15	0.03	0.32	0.05	0.55	0.11	0.58	0.10	0.66	0.08	0.70	0.08	0.59	0.07	0.75	0.09
4	0.15	0.02	0.25	0.02	0.58	0.02	0.95	0.02	0.85	0.01	1.22	0.05	1.32	0.05	1.18	0.02	1.38	0.03
5	0.18	0.01	0.30	0.01	0.64	0.00	1.06	0.01	0.96	0.01	1.32	0.03	1.42	0.01	1.16	0.01	1.39	0.05
6	0.23	0.02	0.38	0.04	0.82	0.08	1.27	0.06	1.12	0.02	1.55	0.09	1.57	0.05	1.22	0.03	1.55	0.03
7	0.26	0.04	0.43	0.06	0.90	0.09	1.31	0.11	1.12	0.06	1.51	0.10	1.53	0.06	1.09	0.04	1.45	0.06
8	0.50		0.97		2.43	3.42	2.28	3.70	2.87	2.04	2.01		2.04	2.01			2.85	
9	0.24	0.02	0.45	0.05	1.23	0.14	2.12	0.28	2.19	0.29	2.63	0.35	2.55	0.38	1.63	0.20	2.29	0.31
10	0.30	0.06	0.50	0.07	1.06	0.10	1.56	0.20	1.64	0.19	1.81	0.30	1.77	0.33	1.17	0.21	1.56	0.24
11	0.22	0.02	0.37	0.03	0.82	0.09	1.23	0.15	1.15	0.12	1.40	0.17	1.30	0.16	0.88	0.09	1.22	0.14
12	0.23	0.03	0.39	0.03	0.87	0.06	1.27	0.08	1.31	0.05	1.49	0.06	1.43	0.06	0.92	0.13	1.34	0.04
13	0.26	0.03	0.41	0.04	0.84	0.09	1.18	0.11	1.21	0.10	1.42	0.13	1.39	0.12	1.01	0.07	1.34	0.11
14	0.35	0.02	0.62	0.07	1.49	0.09	2.36	0.02	2.04	0.04	2.72	0.12	2.61	0.15	1.63	0.09	2.36	0.17
15	0.19	0.04	0.33	0.06	0.73	0.10	1.09	0.14	1.14	0.12	1.27	0.11	1.24	0.12	0.89	0.13	1.17	0.13
16	0.06	0.00	0.09	0.00	0.20	0.01	0.27	0.01	0.34	0.00	0.35	0.01	0.36	0.00	0.25	0.01	0.31	0.01
17	0.25	0.01	0.47	0.03	1.26	0.09	2.25	0.23	2.26	0.24	2.77	0.24	2.75	0.29	1.73	0.14	2.45	0.24
18	0.27	0.08	0.45	0.10	0.97	0.14	1.47	0.12	1.46	0.09	1.81	0.11	1.81	0.08	1.30	0.04	1.71	0.07
19	0.21	0.00	0.35	0.01	0.73	0.04	1.05	0.10	1.11	0.10	1.29	0.14	1.24	0.12	0.89	0.05	1.19	0.09
20	0.18	0.01	0.30	0.01	0.64	0.04	0.91	0.07	0.97	0.09	1.07	0.10	1.08	0.11	0.77	0.10	1.01	0.13
21	0.18	0.02	0.40	0.14	0.94	0.22	1.36	0.28	1.37	0.26	1.58	0.36	1.45	0.28	0.99	0.28	1.31	0.24
22	0.14	0.02	0.24	0.03	0.54	0.06	0.78	0.08	0.78	0.09	0.96	0.09	0.91	0.10	0.61	0.05	0.81	0.09
23	0.16	0.00	0.28	0.02	0.64	0.10	1.01	0.21	1.11	0.24	1.30	0.30	1.29	0.29	0.91	0.20	1.17	0.27
24	0.17	0.00	0.27	0.00	0.59	0.06	0.83	0.11	0.86	0.12	1.02	0.18	0.94	0.14	0.67	0.07	0.87	0.11
25	0.12	0.01	0.20	0.02	0.41	0.02	0.60	0.03	0.65	0.02	0.73	0.04	0.69	0.03	0.49	0.01	0.64	0.02
28																	0.37	0.06

Table 4 continued on facing page.

#	La	Ce	Pr	Nd	Sm	Eu	Gd	Tb	Dy	Ho	Er	Yb	Lu	Y	I σ	
29														0.75	0.19	
30														0.41	0.24	
31														1.00	0.30	
32														0.55	0.10	
33		0.22	0.04	0.62	0.09	0.66	0.12					1.25	0.18			
34	0.16	0.01	0.30	0.02	0.77	0.04	1.18	0.05	1.52	0.11	1.44	0.09	1.03	0.07	1.47	0.11
35	0.48	0.05	0.95	0.07	2.36	0.18	3.85	0.41	4.35	0.40	3.85	0.38	2.73	0.18	7.40	0.60
36	0.26	0.04	0.63	0.05	1.24	0.08	2.38	0.13	3.08	0.40	2.34	0.15	1.31	0.10	2.46	0.15
37	1.92	0.58	4.23	0.55	8.70	1.20	11.3	2.40	12.30	1.60	8.20	1.50	5.50	0.90	11.00	1.00
38	0.86	0.32	2.13	0.28	5.19	0.31	7.76	0.31	10.20	0.40	6.86	0.56	4.41	0.40	8.28	0.37
39	0.09	0.07			0.37	0.02					0.44	0.06			0.34	0.06
40	0.12	0.03			0.46	0.06					0.51	0.08			0.40	0.05
41	0.11	0.05			0.64	0.14					0.63	0.05			0.42	0.05
42	0.14	0.05			0.70	0.11					0.73	0.07			0.48	0.05
43	0.17	0.06			0.50	0.05					0.55	0.07			0.43	0.04
44	0.07	0.05			0.40	0.06					0.47	0.12			0.32	0.07
45	0.12	0.03	0.24	0.03	0.63	0.12	1.37	0.11	1.77	0.15	1.47	0.09	1.15	0.05	1.07	0.05
46	0.18	0.05	0.45	0.07	1.02	0.12	1.83	0.22	2.37	0.16	2.01	0.10	1.77	0.15	1.61	0.16
47	0.19	0.03	0.38	0.06	0.71	0.07	1.65	0.23	1.88	0.35	1.92	0.17	1.93	0.13		
48	0.37	0.09	0.73	0.10	1.20	0.13	2.01	0.25	2.68	0.30	2.47	0.26	2.10	0.15	1.70	0.40
49	0.06	0.01	0.10	0.01	0.17	0.01	0.25	0.03	0.62		0.62	0.06	0.57	0.07	0.43	0.05
50	0.10	0.01	0.16	0.02	0.43	0.01					0.41	0.03	0.37	0.05	0.28	0.02
51	0.14	0.00	0.20	0.03	0.54	0.03					0.64	0.04	0.48	0.09	0.46	0.04
52	0.13	0.04	0.22	0.04	0.62	0.12					0.71	0.09	0.55	0.23	0.50	0.05
53	0.20	0.04	0.20	0.04	0.08	0.12					0.87	0.09	0.68	0.23	0.62	0.05
54	0.06	0.01	0.10	0.02	0.15	0.02	0.15	0.02	0.50	0.17	0.42	0.15	0.32	1.02	0.41	0.03
55	0.03	0.00	0.08	0.01	0.13	0.01	0.18	0.02	0.45	0.05	0.54	0.09	0.40	0.12	0.44	0.02

Table 4 continued on facing page.

closer to the strip of octahedra in a position named $M(4')$. The amount of Mg and Fe^{2+} occurring at the $M(4')$ site (defined as cummingtonite component) may become significant (up to 0.30 apfu) in calcic amphiboles crystallized at high-temperature conditions. Analysis of amphiboles with variable cummingtonite component [and thus with variable percentages of smaller $M(4')$ polyhedra detected by SREF] showed that LREE preferentially order at $M(4)$, whereas HREE preferentially order at $M(4')$. The occurrence within the same crystal of two distinct $M(4)$ polyhedra implies that the fit of $^{Amph/L}D_{REE}$ to a single curve in the frame of the Blundy and Wood (1994) elastic-strain model is an oversimplification that may underestimate the predicted $^{Amph/L}D_{HREE}$ in amphiboles with a large cummingtonite component (Fig. 7; Bottazzi et al. 1999; Tiepolo et al. 2000a).

Although the fit to a single curve may appear correct in some cases, the values obtained for r_0 , are biased towards those of the dominant site, and hence the Young's modulus is also underestimated.

Factors affecting $^{Amph/L}D_{REE}$

Magmatic calcic amphiboles in equilibrium with basaltic melts under mantle conditions show modest variation in the $M(4)$ site population, and thus melt polymerization is the main parameter controlling the absolute values of the $^{Amph/L}D_{REE}$. The partitioning of La, Dy, Yb and Y is a well-defined function of the X_{Hf}/X ratio of the melt (Figs. 8 and 9), as expected based on the significant role played by REE as network-modifiers. At X_{Hf}/X between 0.41 and 0.52, roughly corresponding to SiO_2 contents between 34.0 and 45.0 wt%, $^{Amph/L}D_{REE}$ show no appreciable variations. At X_{Hf}/X ranging between 0.52 and 0.7 (about 45.0-60.0 wt% of SiO_2), the relation between $^{Amph/L}D_{REE}$ and melt composition is approximately linear (Tiepolo et al. 2000a). In this range of melt composition, the increase in the REE partition coefficients

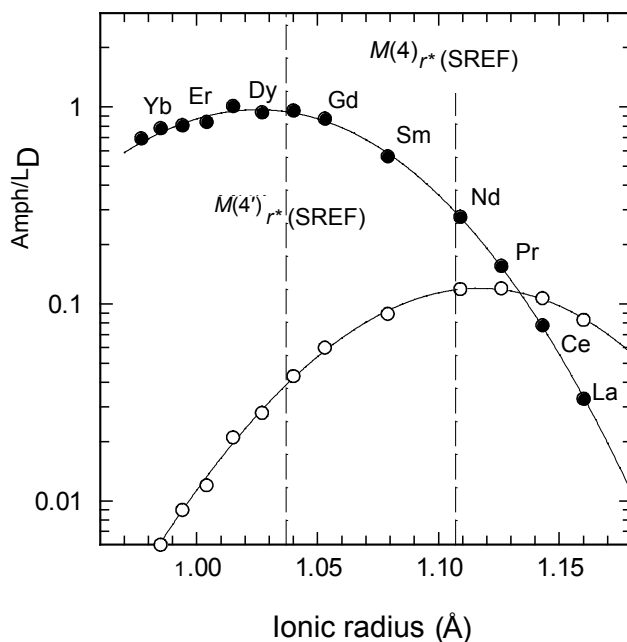


Figure 7. REE partition coefficients versus cation radius for the two distinct sites within the $M(4)$ cavity in calcic amphibole (see text for detail). The curves represent Blundy and Wood's (1984) equation for each site. Dashed lines represent the observed site dimension from SREF. Data are from Bottazzi et al. (1999).

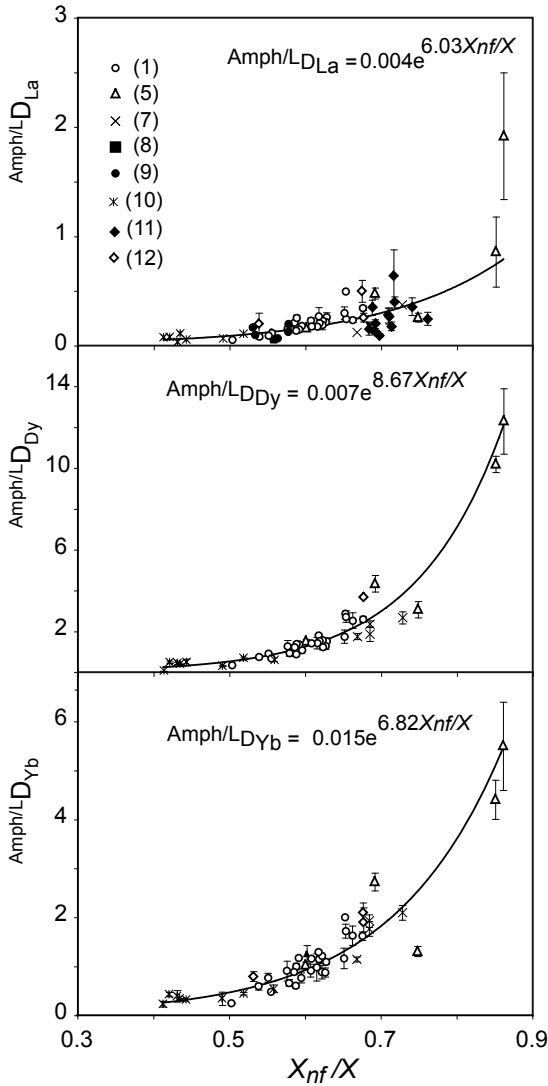


Figure 8. Variation of the $\text{Amph}/L_{D_{La}}$, $\text{Amph}/L_{D_{Dy}}$, $\text{Amph}/L_{D_{Yb}}$ as a function of melt composition expressed as (X_{nf}/X) . See Table 1 for code numbers. Error bars are 2σ

is about a factor of four. Few data are available for higher X_{nf}/X values, but they suggest a strong increase in the $\text{Amph}/L_{D_{REE}}$ for small variations in melt composition (Sisson 1994). In the whole range of X_{nf}/X spanned in the literature, we found that an exponential function can best represent the relation between $\text{Amph}/L_{D_{REE}}$ and melt composition. Examples are:

$$\text{Amph}/L_{D_{La}} = 0.004e^{6.03(X_{nf}/X)} \quad R^2 = 0.65$$

$$\text{Amph}/L_{D_{Dy}} = 0.007e^{8.67(X_{nf}/X)} \quad R^2 = 0.86$$

$$\text{Amph}/L_{D_{Yb}} = 0.015e^{6.82(X_{nf}/X)} \quad R^2 = 0.85$$

$$\text{Amph}/L_{D_Y} = 0.013e^{7.42(X_{nf}/X)} \quad R^2 = 0.83$$

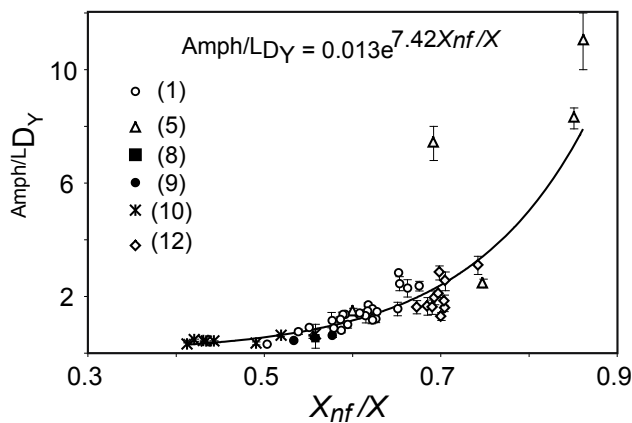


Figure 9. Variation of the $^{Amph/L}D_Y$ as a function of melt composition expressed as (X_{nf}/X) . See Table 1 for code numbers. Error bars are 2σ .

Deviations from the trends described above are observed in F-rich systems (Adam et al. 1993). Fluorine combines preferentially with metal cations (including the REE) in silicate melts (Foley et al. 1986), leading to a decrease in both their activity and $^{Amph/L}D$. These effects are evident when comparing the partitioning results from the experiments of Adam et al. (1993) with those obtained at similar P , T and X_{nf}/X in F-free systems. Suitable data are available only for Y, and show that in F-rich systems $^{Amph/L}D$ are up to four times lower than those measured in F-free experiments.

The relatively large variation (approximately $4\times$) of the fractionation between LREE and M-HREE (i.e., the $^{Amph/L}D_{La}/^{Amph/L}D_{Yb}$ and $^{Amph/L}D_{La}/^{Amph/L}D_{Sm}$ ratios) might be related to a structural modification of either the melt or of the solid phase. La, Sm and Yb have slightly different Z/r ratios, which could imply a change in their behavior with respect to melt polymerization. No apparent relation between the $^{Amph/L}D_{La}/^{Amph/L}D_{Yb}$ fractionation and X_{nf}/X is observed, however, when considering the whole dataset. Tiepolo et al. (2000a) showed that when $^{Amph/L}D_{La}$ and $^{Amph/L}D_{Yb}$ are linearly correlated with the X_{nf}/X of the melt, the slope of variation observed for La and Yb are equal within error. According to the elastic-strain theory of Blundy and Wood (1994), the ratio between the partition coefficients of elements with the same charge but different ionic radii entering the same site is a function of the site dimension (r_0 parameter) and of the Young's modulus (E parameter) of the site. In calcic amphiboles, the $M(4)$ polyhedra occupied either by (Mg, Fe) or Na have significantly different size and coordination. The possible correlation between the $^{Amph/L}D_{La}/^{Amph/L}D_{Yb}$ value and the aggregate $\langle M(4)-O \rangle$ distance is hindered by the lack of information on the local coordination of HREE, which is probably 6-fold (Tiepolo et al. 2000a).

If the observed variation in $^{Amph/L}D_{La}/^{Amph/L}D_{Yb}$ were induced by changes in the Young's modulus, a relation with pressure should be apparent. However, no significant variation in the $^{Amph/L}D_{La}/^{Amph/L}D_{Yb}$ ratio is observed in amphiboles crystallized at 0.5 GPa compared to those formed at 2.0 GPa in the experiments of Adam and Green (1994, 2003). Also, in the experiments of Dalpé and Baker (2000) there is no correlation between the Young's Modulus of the $M(4)$ site and pressure. Thus, understanding the most important factors affecting LREE/HREE fractionation is not straightforward. Because bias can be induced by the simultaneous change in more than one parameter, this goal might be reached with new specific experiments in which as many parameters as possible are kept constant.

The effect of pressure on the overall variation of the $^{Amph/L}D_{REE}$ was investigated by Adam and Green (1994). These authors showed that $^{Amph/L}D$ for Lu, Sm and Ho decrease by up to a factor of about two with increasing pressure from 0.5 to 2.0 GPa. Adam and Green (2003)

showed that the negative correlation observed between D_{REE} and pressure is not predicted by the thermodynamic model of Wood and Blundy (1997), and concluded that variations in $^{\text{Amph/L}}D_{\text{REE}}$ mostly depend on the volume-reducing substitutions occurring at the octahedra and the tetrahedra, which increase the activities of +3 and +4 ions, and decrease those of +1 ions, in sites with 8-fold co-ordination as pressure increases. The incorporation of trivalent REE in the amphibole structure is balanced by the coupled exchange $^{\text{BREE}^{3+}}_1 \text{ } ^{\text{TAI}^{3+}}_1 \text{ } ^{\text{BR}^{2+}}_{-1} \text{ } ^{\text{TSi}^{4+}}_{-1}$, a mechanism well known in clinopyroxenes (Wood and Blundy, 2001), which implies a strong positive correlation between the mole fraction of the CaTs component and the $^{\text{Cpx/L}}D_{\text{REE}}$ values (Gaetani and Grove 1995). In contrast, as pressure increases, volume-decreasing substitutions require that Al is replaced by Si in the tetrahedra and is incorporated in the $M(2)$ octahedron. As a consequence, Na^+ must substitute for Ca^{2+} at the $M(4)$ site. This mechanism determines an increase of the electrostatic energy necessary to accommodate REE^{3+} , thus providing a further drawback to their incorporation in the amphibole structure. All these crystal-chemical changes are observed in the amphibole synthesized by Adam and Green (2003) with the increase of P , thus accounting for the concomitant variation of the $^{\text{Amph/L}}D_{\text{REE}}$.

AMPH/L D FOR HIGH FIELD STRENGTH ELEMENTS (HFSE)

Source of data

Due to their great petrogenetic relevance, the partitioning behavior of HFSE between calcic amphiboles and melt has been extensively studied. $^{\text{Amph/L}}D_{\text{HFSE}}$ were experimentally determined by Adam et al. (1993), Adam and Green (1994, 2003), Brenan et al. (1995), LaTourrette et al. (1995), Bottazzi et al. (1999), Tiepolo et al. (2000b, 2001) and Dalpé and Baker (2000) in basaltic and alkali basaltic systems at pressures in the range 0.5-2.0 GPa and temperatures in the range 975-1090 °C. More evolved systems, ranging in composition between basaltic andesites and rhyolites, were considered by Sisson (1994), Klein et al. (1997) and Hilyard et al. (2000). These studies were done at pressures in the range 0.2-1.0 GPa and a temperature ranging from 800-1050 °C. The overall dataset is reported in Table 5.

Overall values

Ti is moderately incompatible to highly compatible in calcic amphiboles. $^{\text{Amph/L}}D_{\text{Ti}}$ shows a relatively large range of variation (0.37-18.0). In most synthetic amphiboles reported in the literature, Ti has a compatible behavior (Fig. 10). $^{\text{Amph/L}}D_{\text{Ti}}$ lower than unity were observed only in a few experiments from Dalpé and Baker (2000), Tiepolo et al. (2000b) and Adam and Green (2003). Admittedly, Ti is a major element in calcic amphiboles from mantle environments, and its presence is mainly related to the oxo component ($\text{O}^{3}\text{O}^{2-}$), namely to the chemical re-

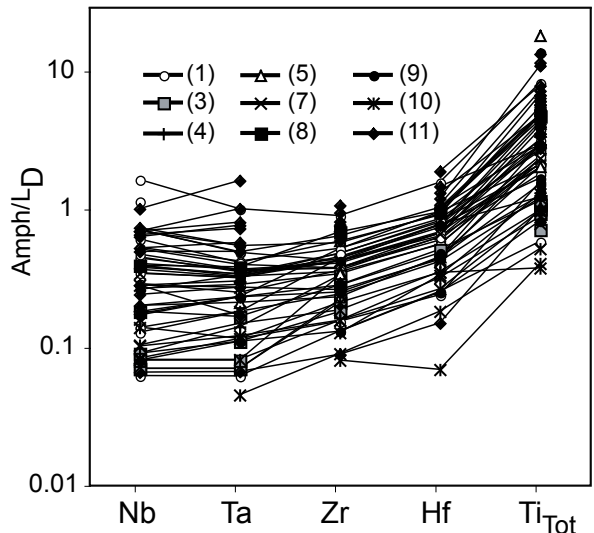


Figure 10. High Field Strength Element (HFSE) partitioning between calcic amphibole and silicate melt. See Table 1 for code numbers.

Table 5. $\text{Amph}^{\text{b}}/\text{D}$ for the High Field Strength Elements (HFSE)

#	Nb	Ta	Zr	Hf	Ti	#	Nb	Ta	Zr	Hf	Ti	Ti(tot)	I σ	I σ	I σ	I σ	I σ	I σ	I σ	Ti(tot)	I σ		
1	0.14	0.00	0.19	0.01	0.00	2.08	0.05	0.23	0.05	0.28	0.07	0.48	0.10	1.24	0.05								
2	0.51	0.05	0.39	0.03	0.37	0.00	0.67	0.00	2.86	0.10	52	0.18	0.01	0.23	0.04	0.25	0.08	0.44	0.08	1.50	0.10		
3	0.14	0.02	0.12	0.02	0.15	0.00	0.24	0.06	1.57	0.16	53	0.26	0.04	0.33	0.02	0.42	0.06	0.77	0.16	1.67	0.08		
4	0.36	0.03	0.32	0.02	0.48	0.11	0.80	0.26	2.72	0.02	54	0.08	0.01	0.08	0.03	0.16	0.02	0.32	0.06	0.87	0.05		
5	0.34	0.04	0.32	0.02	0.45	0.00	0.76	0.03	2.90	0.25	55			0.05	0.01	0.09	0.01	0.18	0.02	0.51	0.06		
6	0.45	0.02	0.35	0.01	0.42	0.02	0.64	0.03	3.76	0.12	56	0.10	0.02	0.15	0.02	0.19	0.02	0.35	0.06	0.98	0.07		
7	0.71	0.07	0.48	0.07	0.42	0.02	0.68	0.01	4.06	0.14	57				0.08	0.01	0.07	0.00	0.40	0.05			
8	1.14						0.55	0.15															
9	0.70	0.13	0.49	0.08	0.64	0.20	1.03	0.35	2.86	0.39	58	0.08	0.03	0.12	0.03	0.21	0.01	0.35	0.02	0.37	0.03		
10	0.52	0.09	0.42	0.10	0.52	0.07	0.84	0.19	2.61	0.14	59	0.14	0.01	0.18	0.02	0.24	0.04	0.42	0.08	1.20	0.12		
11	0.39	0.03	0.34	0.02	0.44	0.07	0.73	0.18	1.99	0.16	60	0.10	0.01	0.12	0.02	0.16	0.02	0.26	0.05	0.96	0.07		
12	0.40	0.01	0.36	0.02	0.40	0.02	0.67	0.04	2.11	0.10	61	0.07	0.02	0.07	0.02	0.09	0.01	0.15	0.02	1.01	0.08		
13	0.44	0.02	0.36	0.03	0.37	0.03	0.59	0.01	2.29	0.19	62							1.19	0.11	10.84	2.46		
14	0.60	0.02	0.41	0.01	0.58	0.05	0.90	0.06	3.16	0.05	63							0.90	0.23	6.68	1.39		
15	0.39	0.08	0.33	0.08	0.35	0.05	0.55	0.05	2.30	0.01	64							0.76	0.18	4.73	1.23		
16	0.06	0.00	0.06	0.00	0.13	0.01	0.25	0.00	0.58	0.00	65							1.07	0.11	7.14	1.66		
17	1.63	0.13	1.00	0.11	0.89	0.06	1.56	0.21	8.15	0.25	66							1.02	0.21	4.85	1.46		
18	0.69	0.05	0.54	0.05	0.57	0.03	0.92	0.10	5.45	0.37	67							1.87	0.20	7.77	1.61		
19	0.47	0.08	0.36	0.03	0.37	0.05	0.62	0.17	2.41	0.05	68							1.00	0.22	4.38	0.98		
20	0.27	0.02	0.28	0.03	0.34	0.01	0.56	0.01	2.15	0.13	69							0.77	0.22	4.25	0.67		
21	0.17	0.03	0.23	0.04	0.51	0.00	0.95	0.00	2.07	0.16	70							0.45	0.09	2.90	0.37		
22	0.13	0.02	0.18	0.03	0.44	0.13	0.77	0.13	1.21	0.20	71							1.45	0.16	2.89	0.66		
23	0.38	0.08	0.34	0.01	0.47	0.13	0.82	0.27	1.92	0.05	72							1.31	0.18	4.73	0.75		
											73								0.98	0.15	4.80	0.80	

24	0.29	0.02	0.25	0.00	0.36	0.09	0.62	0.23	1.78	0.13	74	0.69	0.18	1.00	0.07	13.19	2.29
25	0.18	0.01	0.17	0.01	0.28	0.00	0.51	0.02	1.15	0.04	75	0.20	0.03	0.23	0.06	5.42	0.95
28	0.07	0.01	0.07	0.01	0.21	0.02			0.71	0.05	76	0.52	0.16	0.57	0.14	5.61	1.28
29	0.07	0.01	0.07	0.01	0.22	0.04			0.93	0.14	77	0.24	0.04	0.27	0.09	5.23	1.59
30	0.08		0.08	0.01	0.33	0.01			1.00	0.05	78	0.28	0.09	0.30	0.12	4.40	0.46
31	0.09	0.01	0.11	0.01	0.18	0.04			1.08	0.12	79	1.00	0.19	1.60	0.24	6.04	1.38
32	0.09	0.01	0.14	0.02	0.33	0.07			1.03	0.07	80	0.73	0.17	0.54	0.11	4.13	1.47
33	0.20	0.08	0.21	0.03	0.23	0.06	0.45	0.08	2.02	0.11	81	0.28	0.06	0.17	0.07	2.81	0.65
34					0.35	0.07			3.06	0.05	82	0.49	0.12	0.49	0.11	5.67	1.53
35					0.76	0.07			4.16	0.08	83	0.69	0.18	0.80	0.18	5.12	0.82
36					0.34	0.03			3.66	0.26	84	0.65	0.15	0.72	0.09	3.92	0.76
37					0.59	0.04			18.00	1.60	85	0.63	0.12	0.76	0.17	5.27	0.87
38					0.27	0.04			13.60	0.80	86					6.62	2.70
39									0.87	0.06	87					6.00	2.63
40									1.24	0.05	88					6.33	1.96
41									1.42	0.11	89					5.16	1.23
42									1.77	0.10	90					11.44	1.96
43									1.34	0.05	91					5.67	1.75
44									0.78	0.06	92					4.73	0.34
45	0.28	0.03	0.27	0.03	0.26	0.03	0.43	0.04	2.32	0.22	93					3.36	0.68
46	0.34	0.05	0.32	0.04	0.42	0.04	0.66	0.07	3.20	0.40	94					3.52	0.89
47									2.70	0.50	95					3.94	0.78
48	0.39	0.06	0.38	0.09	0.68	0.24	0.95	0.17	4.70	0.70	96					2.75	0.41
49	0.16	0.01			0.13	0.01	0.33	0.18	1.29	0.30							
50	0.08	0.01	0.11	0.01	0.13	0.01	0.25	0.02	0.82	0.03							

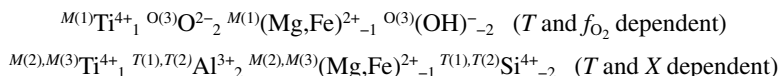
quirements for crystallization at high T conditions. In the whole dataset taken from the literature, Zr in always incompatible ($^{Amph/L}D_{Zr}$ range between 0.08 and 0.89) except for a single experiment (Hilyard et al. 2000; $^{Amph/L}D_{Zr} = 1.06$). In contrast, a couple of examples of $^{Amph/L}D_{Hf}$ higher than unity (up to 1.56) were reported by Tiepolo et al. (2001) for slightly evolved basanitic and alkali basaltic systems.

The $^{Amph/L}D_{Zr}/^{Amph/L}D_{Hf}$ ratio is relatively constant in amphiboles with values close to 0.6 (0.58 ± 0.06 ; over 41 determinations), with the single exception of one sample from the experimental dataset of Dalpé and Baker (2000), which has a $^{Amph/L}D_{Zr}/^{Amph/L}D_{Hf}$ ratio of 1.72. Nb and Ta are usually highly to moderately incompatible in amphibole. Few examples where these elements are slightly compatible in calcic amphiboles have been reported by Tiepolo et al. (2000b) for slightly evolved basanitic and alkali basaltic systems.

The ranges of variation of $^{Amph/L}D_{Nb}$ and $^{Amph/L}D_{Ta}$ in the whole dataset are 0.06-1.63 and 0.05-1.00, respectively. The $^{Amph/L}D_{Nb}/^{Amph/L}D_{Ta}$ ratio is more variable than that observed for Zr-Hf, with values ranging between 0.64 and 1.63.

Site preference

A crystal-chemical setting to understand the incorporation of HFSE in amphiboles and their different partitioning behavior in calcic amphiboles is provided by systematic studies of the crystal-chemical role of Ti^{4+} in different amphibole compositions (Oberti et al. 1992, 2000; Hawthorne et al. 1993, 1998; Tiepolo et al. 1999). Present knowledge shows that tetravalent Ti can be incorporated into calcic amphiboles according to two distinct crystal-chemical mechanisms (see Oberti et al. 2007b for more details):



When present at the $M(1)$ site, Ti occupies a different position, shifted along b towards the $O(3)$ - $O(3)$ edge, named $M(1')$. Thus its local coordination is different (namely, smaller and more distorted) than that of the dominant cations (Mg, Fe^{2+}). The occurrence of $M(3)Ti$ is rare, and is restricted to Fe-depleted systems at high T , where Al has a strong preference for tetrahedral coordination (Tiepolo et al. 1999).

Therefore, in calcic amphiboles HFSE may distribute over the $M(1)$ and $M(2)$ sites, the first location occurring only in the presence of significant oxo component. However, the behavior within the HFSE group is not homogeneous: a decoupling of the behavior of Zr-Hf and Nb-Ta is clearly observed in pargasites and especially in kaersutites.

Inspection of experimental data on calcic amphiboles with significant and variable oxo component shows that HFSE $^{5+}$ are preferentially ordered at the $M(1)$ site, and thus their role is to satisfy electroneutrality and bond-strength requirements deriving from the oxo component. This conclusion is strongly supported by the good correlation observed between the $\langle M(1)-O \rangle$ distance and the $^{Amph/L}D_{Nb}/^{Amph/L}D_{Ta}$ ratio by Tiepolo et al. (2000b). Based on this evidence, these authors inferred that the ionic radius of Nb is larger than that of Ta (possibly by 0.01-0.02 Å). Actually, Blundy and Wood (2003) were able to reproduce (within 2σ) all the available experimental Nb/Ta values using a constant $M(1)E^{5+}$ of 3500 GPa and a Nb $^{5+}$ ionic radius of 0.66 Å inferred from the ionic radius of 0.64 Å tabulated for Ta by Shannon (1976).

Zr and Hf are larger than Ti, Nb and Ta (0.72 Å and 0.71 Å, respectively; Shannon 1976), and thus are not suitable to occur at the $M(1')$ site. They are thus preferentially incorporated into the $M(2)$ site, and their role is to balance the TAl content (Oberti et al. 2000; Tiepolo et al. 2001). Further support for this site preference is given by single-crystal structure refinement of Zr-bearing amphiboles (Hawthorne et al. 2001, and CNR-IGG unpublished).

Factors affecting $\text{Amph/L}D_{\text{HFSE}}$

Similar to what observed for REE, the experimental values of $\text{Amph/L}D_{\text{Ti}}$ are exponentially correlated with melt composition (Fig. 11). Almost no influence on the $\text{Amph/L}D_{\text{Ti}}$ is observed at low X_{nf}/X (0.40-0.55). At higher X_{nf}/X values (> 0.6) the variation of $\text{Amph/L}D_{\text{Ti}}$ with melt composition is stronger, and two separate trends can be distinguished. The first trend is similar to that observed for REE (Dy and Yb), and can be described by the following equation:

$$\text{Amph/L}D_{\text{Ti}} = 0.0273e^{6.9531(X_{\text{nf}}/X)} \quad R^2 = 0.74$$

The second trend is defined by two samples from Tiepolo et al. (2000b) and at least three samples from Hilyard et al. (2000), and shows more than a threefold increase of $\text{Amph/L}D_{\text{Ti}}$ in a narrow X_{nf}/X range (0.60-0.70). In these experiments, amphiboles have similar Ti contents, but melts show relatively low and variable amounts of TiO_2 (< 1.5 wt%). As stated before, Ti is a fundamental constituent of pargasites and kaersutites, and its occurrence at $M(1)$ satisfies the bond-strength requirements deriving from the oxo component. Therefore, at constant $f_{\text{H}_2\text{O}}$ and f_{O_2} conditions, when TiO_2 in the system is low, a larger proportion of Ti is incorporated into the amphibole and $\text{Amph/L}D_{\text{Ti}}$ increases strongly. It can be concluded that in the samples defining the second trend, the structural control on $\text{Amph/L}D_{\text{Ti}}$ for Ti^{4+} prevails over that of the melt. A further factor affecting Ti incorporation in amphiboles is $f_{\text{H}_2\text{O}}$, which determines the amount of the oxo component.

The variation of $\text{Amph/L}D_{\text{Zr}}$ and $\text{Amph/L}D_{\text{Hf}}$ as a function of the melt composition is even more scattered than that of Ti, especially at high X_{nf}/X values. Again, this evidence suggests a strong control exerted by the crystal structure on $\text{Amph/L}D_{\text{Zr,Hf}}$. Because the ionic radii of Zr and Hf are significantly larger than those of the common constituents at the $M(2)$ site, even small changes in the dimensions or elasticity of the $M(2)$ octahedron may imply large changes in the $\text{Amph/L}D_{\text{Zr,Hf}}$. This effect has been quantified by Dalpé and Baker (2000). These authors observed that $\text{Amph/L}D_{\text{Zr}}$ is a function of the $M(2)$ (Ti/Al) ratio measured in different amphibole run products with increasing pressure. Hence, they proposed an empirical equation which

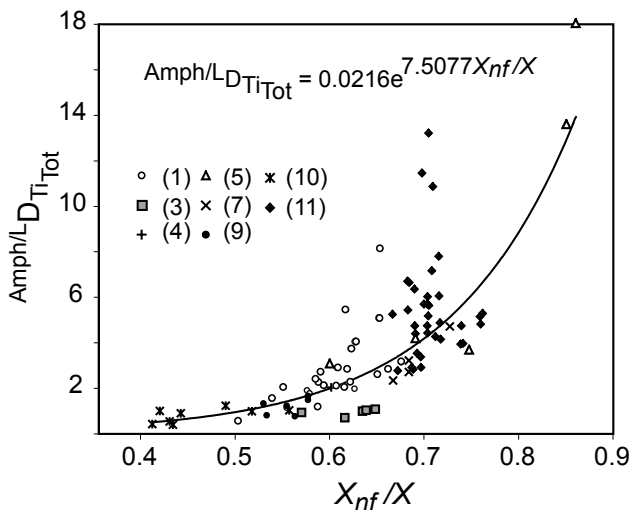


Figure 11. Variation of the $\text{Amph/L}D_{\text{Ti(tot)}}$ as a function of melt composition expressed as (X_{nf}/X) . See Table 1 for code numbers. Error bars are 2σ .

accounts for P -dependent changes in amphibole composition in basaltic systems at upper mantle conditions:

$$\log^{Amph/L}D_{Zr} = 0.4888 \log^{M(2)}(Ti/Al) - 1.6486$$

The variation in $^{Amph/L}D_{Nb}$ and $^{Amph/L}D_{Ta}$ was shown to be strongly related to the $^{Amph/L}D_{Ti}$ values, and in particular to the fraction of Ti incorporated at the $M(1)$ site (Tiepolo et al. 2000b). Tiepolo et al. (2000b) also argued that the increased compatibility of Nb and Ta in a TiO_2 -poor system results from the need for highly charged cations locally associated with the oxo component, similarly to the case previously argued for $^{Amph/L}D_{Ti}$.

Because $^{Amph/L}D_{Nb}/^{Amph/L}D_{Ta}$ is related to the $\langle M(1)-O \rangle$ distance in titanian pargasites and kaersutites (Fig. 12), Tiepolo et al. (2000b) provided a simplified model to predict Nb/Ta fractionation in amphiboles based on major-element composition as determined by the electron probe; therefore, measurement of the $\langle M(1)-O \rangle$ distance is no longer required. The model is based on some simplifying assumptions, namely: (1) the mg# at $M(1)$ can be reasonably approximated to a constant proportion of the bulk mg#, because the $M(1)$ and $M(3)$ sites do not fractionate Mg and Fe^{2+} at high temperatures (> 900 °C); (2) the amount of Ti at the $M(1)$ site can be considered a nearly constant fraction (~ 70 -80%) of the total Ti; (3) Fe^{3+} at the $M(1)$ site is rare in amphiboles where the oxo component is present since crystallization and the F content is low. These assumptions allowed relation of the $\langle M(1)-O \rangle$ distance to mg# and total Ti (Tiepolo et al. 2000b), thus deriving a regression equation that allows prediction of $^{Amph/L}D_{Nb}/^{Amph/L}D_{Ta}$ values:

$$^{Amph/L}D_{Nb}/^{Amph/L}D_{Ta} = 2.10 - 0.023 \text{ mg\#} - 0.014 \text{ Ti}_{Tot} \quad R^2 = 0.83$$

The average error of the predicted values for the experimental data set of Tiepolo et al. (2000b) is 7%, with a maximum error of 20%. Of course, the application of this equation to amphiboles is restricted to titanian pargasites and kaersutites with a significant oxo-component and crystallized at similar temperature and pressure. In fact, significant changes in Ta content or in the oxo component may invalidate the assumptions of the equation.

A specific study on the influence of pressure on the $^{Amph/L}D_{HFSE}$ was carried out by Adam and Green (1994), who documented a decrease of the $^{Amph/L}D_{Ti}$ by a factor 2 with increasing pressure from 0.5 to 2.0 GPa. Unfortunately, this correlation is strongly biased by the concomitant decrease of the H_2O content added to the starting material at increasing P . Comparison of the available data (Adam et al. 2007) shows that the main factor affecting the oxo component, and consequently $^{Amph/L}D_{Ti}$, is actually f_{H_2O} .

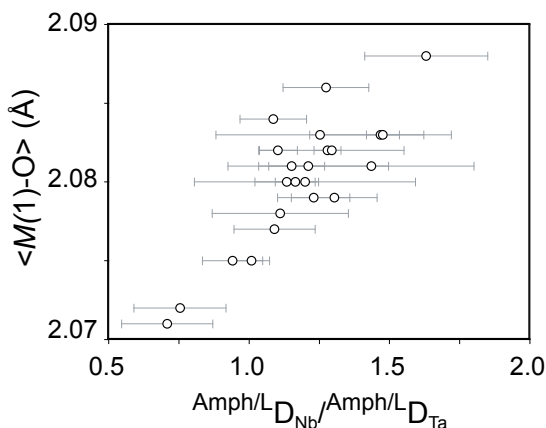


Figure 12. Variation of the $^{Amph/L}D_{Nb}/^{Amph/L}D_{Ta}$ as a function of the size of the $M(1)$ octahedron [$\langle M(1)-O \rangle$]. Data are from Tiepolo et al. (2000b). Error bars are 2σ .

Dalpe and Baker (2000) showed that the $A_{\text{Amph/L}}D$ s for Ti and other tetravalent HFSE (Zr and Hf) ordered at the $M(2)$ site slightly decrease or stay within one standard deviation when pressure increases from 1.5 to 2.5 GPa. As in the case of LILE, Adam et al. (1993) found that the F content of the melt may strongly influence the partitioning of HFSE between calcic amphibole and melt. However, these effects are strong only for F concentrations > 2 wt% and when the melts contain low amounts of Al_2O_3 , FeO, MgO and CaO. Owing to the paucity of F-rich felsic magmas in nature, Adam et al. (1993) concluded that F control on the partitioning of HFSE is unlikely.

From all the above arguments, we should conclude that $A_{\text{Amph/L}}D_{\text{HFSE}}$ cannot be treated as a whole in modeling trace-element behavior according to equation (2). Because HFSE (particularly Ti, Nb and Ta) are involved in two distinct crystal-chemical mechanisms and consequently are incorporated into two distinct M sites, the two fractions must be treated separately. Unfortunately, this conclusion implies that the oxo component must be accurately estimated in amphiboles from mantle environments (cf. Oberti et al. 2007b for more detail on this matter).

AMPH/L-D FOR ACTINIDES AND Pb

Source of data

$A_{\text{Amph/L}}D$ for U, Th and Pb are relatively scarce in the literature and limited to the experimental datasets of Brenan et al. (1995), LaTourrette et al. (1995), Tiepolo et al. (2000a) and Adam and Green (2003). All these experiments were carried out in basaltic and alkali basaltic systems at pressure ranging between 0.5 and 2.5 GPa. The overall dataset is reported in Table 6.

Overall values

Pb in calcic amphibole is highly to moderately incompatible, with $A_{\text{Amph/L}}D_{\text{Pb}}$ ranging between 0.03 and 0.17 (Fig. 13). The whole range of variation is covered by the experiments of Tiepolo et al. (2000a). The $A_{\text{Amph/L}}D_{\text{Pb}}$ values reported by LaTourrette et al. (1995) and Brenan et al. (1995) are close to the lower and upper limits of this range, respectively. U and Th are highly incompatible in calcic amphibole. $A_{\text{Amph/L}}D$ for U and Th vary more than one order of magnitude, and range from 0.004 to 0.21 and from 0.003 to 0.05, respectively. $A_{\text{Amph/L}}D$ for U and Th are relatively consistent among the different datasets. An exception is the experimental run 1446 from

Table 6. $A_{\text{Amph/L}}D$ for Pb, Th and U

#	Pb	1 σ	Th	1 σ	U	1 σ
2	0.12	0.01	0.02	0.01	0.01	0.00
3	0.06	0.01	0.01	0.00	0.01	0.00
4	0.09	0.00	0.02	0.01	0.02	0.01
5	0.12	0.01	0.03	0.00	0.03	0.01
6	0.13	0.01	0.02	0.00	0.02	0.00
7	0.13	0.01	0.03	0.01	0.02	0.01
9	0.11	0.02	0.02	0.00	0.02	0.01
10	0.11	0.02	0.02	0.01	0.01	0.00
11	0.06	0.01	0.02	0.00	0.01	0.00
12	0.07	0.01	0.02	0.00	0.01	0.00
13	0.10	0.00	0.02	0.01	0.02	0.00
14	0.17	0.01	0.03	0.01	0.03	0.00
15	0.09	0.02	0.01	0.00	0.01	0.00
16	0.03	0.00	0.00	0.00	0.00	0.00
17	0.12	0.00	0.02	0.00	0.02	0.00
18	0.11	0.01	0.03	0.01	0.02	0.01
19	0.07	0.00	0.01	0.00	0.01	0.00
20	0.07	0.01	0.02	0.00	0.01	0.00
21	0.09	0.05	0.03	0.02	0.03	0.02
22	0.05	0.01	0.02	0.00	0.01	0.00
23	0.05	0.00	0.01	0.00	0.01	0.00
24	0.05	0.01	0.01	0.00	0.01	0.00
25	0.05	0.00	0.01	0.00	0.01	0.00
33	0.12	0.04	0.02	0.01	0.01	0.00
49	0.04	0.01	0.00	0.00	0.00	0.00
50			0.02	0.01	0.04	0.02
51			0.03	0.04	0.21	0.39
52			0.02	0.01	0.00	0.02
53			0.05	0.01	0.03	0.02

Adam and Green (2003), which is characterized by an exceptionally high $^{Amph/L}D_U$ (0.21 ± 0.39); however, the large error affecting this value challenges its validity. The reported values of the $^{Amph/L}D_{Th}/^{Amph/L}D_U$ ratio are highly variable and, analogously to $^{Amph/L}D_{Nb}/^{Amph/L}D_{Ta}$, can be both lower and higher than unity (0.14-3.75).

Site preference

At wt% concentration level, Pb^{2+} enters the A site, as already noted in the section devoted to LILE. The presence of a stereoactive lone-pair of electrons and local bond-strength requirements (undersaturation of the basal oxygen atoms of the tetrahedron occupied by Be^{2+}) results in the ordering of Pb^{2+} at a strongly off-centered position with highly distorted 6-fold coordination, which is the main reason for a lowering in symmetry of the structure from $C2/m$ to $P2/a$ (Moore et al. 1993). At trace level, the reported correlation between the Pb and Be contents support the same site assignment and crystal-chemical mechanism. This hypothesis is further supported by the strong preference of Pb (about one order of magnitude) for amphibole relative to clinopyroxenes, which do not contain a site with 12-coordination.

In magmatic environments, U and Th are expected to occur mostly as 4+ cations, although U may occur as 5+ and 6+ under strongly oxidizing conditions. Wood et al. (1999) and Blundy and Wood (2003) derived the ionic radii for 8- and 6-fold coordinated Th^{4+} (1.041 and 0.919 Å, respectively) and U^{4+} (0.983 and 0.875 Å, respectively) from their oxides (UO_2 and ThO_2); these ionic radii are slightly smaller than those reported by Shannon (1976), which were derived from fluorides. Based on ionic radii, it could be inferred that Th^{4+} is a B cation and may assume both $^{[8]}M(4)$ - and $^{[6+2]}M(4')$ -type coordination, with a possible preference for the latter as observed for MREE by Bottazzi et al. (1999). A clear confirmation based on the elastic-strain models cannot be obtained due to the large uncertainty in the partition coefficients, which in turn are due to low concentration of the actinides in the amphibole. Analogously to HREE, incorporation of Th and U into the $M(2)$ octahedron in pargasite and kaersutite is to be discarded, because this site is dominated by small highly charged cations.

Factors affecting $^{Amph/L}D_{U,Th,Pb}$

Studies on Pb partitioning between calcic amphibole and melt showed that the $^{Amph/L}D_{Pb}$ is mainly controlled by the melt composition. Tiepolo et al. (2000a) noted a linear correlation between $^{Amph/L}D_{Pb}$ and melt polymerization in the X_{mf}/X range 0.5-0.68. If all the data available in the literature are considered (Fig. 14a), an exponential function better describes the $^{Amph/L}D_{Pb}$ variation with melt composition:

$$^{Amph/L}D_{Pb} = 0.0004e^{8.95(X_{mf}/X)} \quad R^2 = 0.68$$

Tiepolo et al. (2000a) also found that the polymerization of the melt has a strong control on $^{Amph/L}D_{Th}$ and $^{Amph/L}D_U$ (when U^{4+} is considered the dominant species), but did not observe any correlation between $^{Amph/L}D_U$, $^{Amph/L}D_{Th}$ and even $^{Amph/L}D_U/^{Amph/L}D_{Th}$ and the crystal composition. The $^{Amph/L}D_U$ and $^{Amph/L}D_{Th}$ given by Brenan et al. (1995) and LaTourrette et

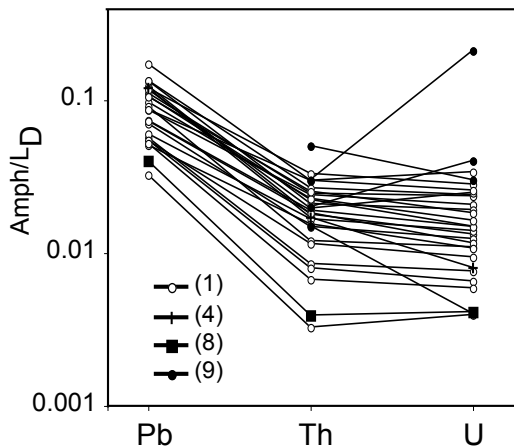
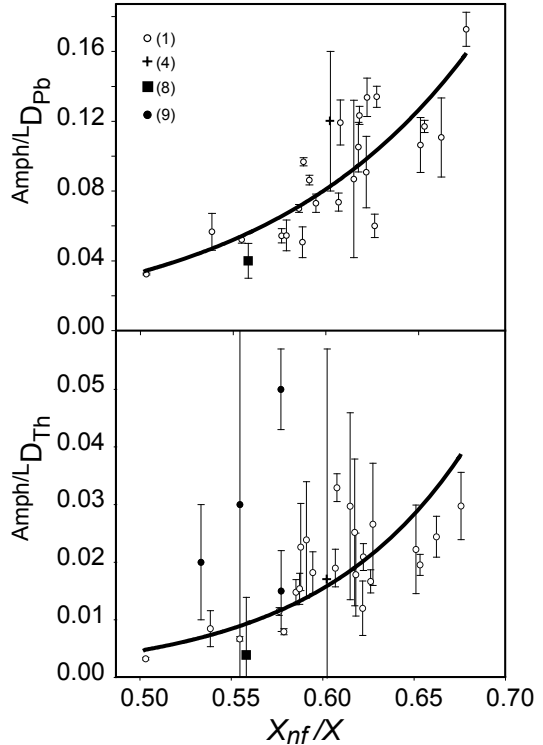


Figure 13. Partitioning of Pb, U and Th between calcic amphibole and silicate melt. See Table 1 for code numbers.

Figure 14. Variation of the ${}^{\text{Amph/L}}D_{\text{Pb}}$ and ${}^{\text{Amph/L}}D_{\text{Th}}$ as a function of melt composition expressed as (X_{nf}/X) . See Table 1 for code numbers. Error bars are 2σ .



al. (1995) lie on the same trend observed by Tiepolo et al. (2000a). Those from Adam and Green (2003) are apparently higher at similar X_{nf}/X ratios, but with the exception of one determination they are within error from the other values reported in literature (Fig. 14b). However, the equations describing the variation of the ${}^{\text{Amph/L}}D_{\text{Th}}$ and ${}^{\text{Amph/L}}D_{\text{U}}$ were calculated excluding the data from Adam and Green (2003), yielding the following results:

$${}^{\text{Amph/L}}D_{\text{U}} = 9E-06e^{12.15(X_{\text{nf}}/X)} \quad R^2 = 0.66$$

$${}^{\text{Amph/L}}D_{\text{Th}} = 1E-05e^{12.24(X_{\text{nf}}/X)} \quad R^2 = 0.62$$

The reason(s) for the observed variation in the ${}^{\text{Amph/L}}D_{\text{U}}/{}^{\text{Amph/L}}D_{\text{Th}}$ cannot be identified on the basis of the dataset presently available in the literature, because no correlation was observed with polyhedra dimension or amphibole composition. An explanation similar to that inferred for Nb/Ta by Tiepolo et al. (2000a) is unlikely. The observed variation may also be related to the oxidation state of U and, thus, may be controlled by oxygen fugacity. In fact, the presence of U^{5+} or U^{6+} would make local electroneutrality difficult to maintain, and thus the apparent ${}^{\text{Amph/L}}D_{\text{U}}$ should decrease with increasing fraction of U^{6+} in the system.

AMPH/LD FOR TRANSITION METALS (Cr, V AND Sc)

Source of data

Reliable values for ${}^{\text{Amph/L}}D$ for Cr, V and Sc are extremely scarce. Sisson (1994) carried out partitioning experiments at low pressure (0.2 GPa), and crystallized amphiboles from

basaltic andesite to rhyolitic systems. Basaltic and alkali basaltic systems were investigated by Tiepolo (1999) at a pressure of 1.4 GPa. The overall dataset is reported in Table 7.

Overall values

Cr, V and Sc are moderately to highly compatible in amphibole. $D_{Cr}^{Amph/L}$ varies between 3.56 and 53. $D_{Cr, V}^{Amph/L}$ for Sc and V are in the range of 1.62-35 and 1.49-22, respectively (Fig. 15).

Site preference

As discussed in detail by Oberti et al. (2007b), Cr, V and Sc are incorporated into the $M(2)$ octahedron in amphiboles, and Cr and Sc may be disordered over the $M(2)$ and $M(3)$ sites in synthetic OH-dominant pargasites (Raudsepp et al. 1987).

Factors affecting $D_{Cr, V, Sc}^{Amph/L}$

The partitioning behavior of V^{3+} and Cr^{3+} is affected by crystal-field stabilization energy (CFSE) which in turn depends on their configurations of d -electrons. The sign of this energy contribution (QCFSE) depends on the relative size and the electronegativity of the individual transition metal. At similar electronegativity values, QCFSE is negative when the metal cation is larger than the dominant cation and positive in the other case. The entrance of Cr^{3+} and V^{3+} in Mg-dominated sites implies $QCFSE > 1$ and a stronger preference of these cations for the solid phase, and thus an increase in $D_{Cr, V}^{Amph/L}$. The opposite is true when the $M(2)$ site is dominantly occupied by the smaller Al.

The solid/liquid partitioning of Cr and V is further complicated by the possible presence of variable amounts of Cr^{2+} and V^{4+} , which should increase and decrease, respectively, the total $D_{Cr, V}^{Solid/L}$.

Based on the above considerations, it is not surprising that among the examined transition metals only $D_{Sc}^{Amph/L}$ shows a well-defined correlation with melt composition (Fig. 16). As for $D_{REE}^{Amph/L}$, the relation with melt composition is exponential, and can be defined by the following equation:

$$D_{Sc}^{Amph/L} = 0.0169e^{9.3277(X_{nf}/X)} \quad R^2 = 0.76$$

The relation between $D_{Cr, V}^{Amph/L}$ for Cr and V and melt composition is even less defined. The partitioning data for Cr and V from Sisson (1994) show a relatively well-defined trend at high X_{nf}/X , which is similar to that observed for Sc. In contrast, at low values of X_{nf}/X the data from Tiepolo (1999) are relatively scattered, especially for V.

Table 7. $D_{Cr, V}^{Amph/L}$ for Sc, V and Cr.

#	Sc	1 σ	V	1 σ	Cr	1 σ
1	3.47	0.17	5.24	0.92	4.05	0.34
2	5.45	0.09	6.54	0.26	6.03	2.36
3	2.99	0.04	7.52	0.47	10.90	0.82
4	4.40	0.65	2.74	0.44	6.50	0.09
5	5.13	0.32	5.08	0.60	6.08	0.71
6	5.91	0.95	6.24	3.85	6.60	0.41
7	7.65	1.19	14.54	9.67	12.98	5.99
9	9.50	3.63	5.57	1.53	6.64	1.59
10	6.34	0.81	6.19	0.49	8.01	1.61
11	4.21	1.49	4.03	2.61	5.53	1.94
12	4.27	0.30	5.04	0.49	3.76	0.12
13	4.56	0.34	6.62	0.27	5.63	1.58
14	7.48	1.25	5.88	0.43	9.27	2.46
15	4.31	0.65	4.98	1.18	4.07	2.49
16	1.62	0.02	5.02	0.12	8.06	0.08
17	8.39	2.26	3.91	1.98	6.86	0.17
18	6.20	0.75	6.31	2.24	5.15	0.24
19	4.95	0.27	6.08	0.86	5.77	1.32
20	3.19	0.18	3.32	0.25	6.13	1.28
21	4.77	0.00	3.29	0.00	4.04	0.00
22	3.31	1.08	3.63	1.68	3.56	1.27
23	4.22	0.07	3.99	1.33	4.55	2.24
24	4.94	0.31	6.91	1.84	10.40	7.38
25	3.02	0.07	3.28	0.66	6.21	1.42
34	4.20	0.20	1.49	0.13	4.20	0.40
35	5.10	0.30	7.50	0.60	5.10	0.30
36	35.00	14.00	4.92	0.27	21.00	5.00
37			22.00	1.70	53.00	19.00
38			17.00	1.00	43.00	21.00

Figure 15. Partitioning of Sc, V and Cr between calcic amphibole and silicate melt. See Table 1 for code numbers.

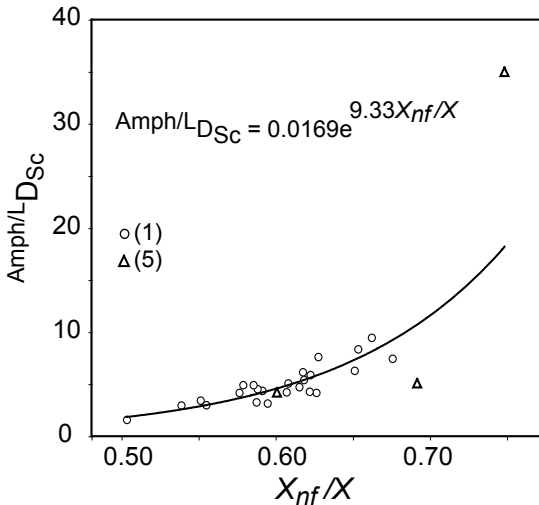
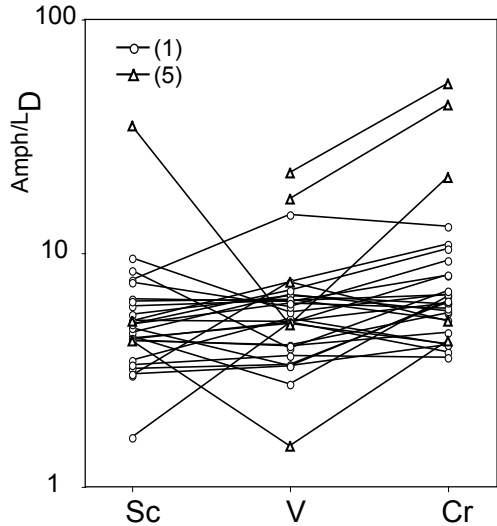


Figure 16. Variation of the $Amph/LD_{Sc}$ as a function of melt composition expressed as (X_{nf}/X) . See Table 1 for code numbers. Error bars are 2σ .

DIFFERENCES TO THE PARTITIONING BEHAVIOR OBSERVED IN POTASSIC-RICHTERITES

As noted in the introduction, the occurrence of potassic-richterite in ultrapotassic magmatic rocks and kimberlite-borne mantle xenoliths suggests that this amphibole may play an important role in specific mantle and magmatic processes. When assessing the role of potassic-richterite in its principal modes of occurrence, namely in lamproites, in peralkaline ultramafic veins in the lithospheric mantle, and in the deeper parts of subduction zones, it must be taken into account that its partitioning behavior is significantly different from that of calcic amphiboles. This issue was investigated by Tiepolo et al. (2003), who synthesized potassic-richterites at upper mantle conditions ($P = 1.4$ GPa and $T = 850$ - 1050 °C) from Si-rich lamproites, and determined their partitioning patterns by means of the SIMS technique. The results of Tiepolo et al. (2003) are summarized below and discussed by groups of elements with reference to calcic amphiboles.

Potassic-richterites have opposite Rb/Ba fractionation and significantly lower $^{Amph/L}D_{Rb}/^{Amph/L}D_{Sr}$ values when compared to calcic amphiboles. The $^{Amph/L}D_{Rb}/^{Amph/L}D_{Ba}$ values (always > 1) and the higher compatibility of Sr in potassic-richterites can be explained by considering both the exchange vectors and the dimensional constraints ruling the incorporation of these elements. Rb^+ ($^{18}i.r. = 1.61 \text{ \AA}$) and Ba^{2+} ($^{18}i.r. = 1.42 \text{ \AA}$) order at the *A* site. In contrast, Sr^{2+} ($^{18}i.r. = 1.26 \text{ \AA}$) orders at the *M*(4) site and acts as a homovalent substituent of Ca (Della Ventura and Robert 1990); its higher compatibility in richterites than in calcic amphiboles is coherent with half of the *M*(4) polyhedra being occupied by Na, and thus larger. Thus the more relaxed structure of richterite makes the incorporation of larger cations easier; in contrast, the lack of tetrahedral trivalent cations in richterite makes the incorporation of divalent A cations more difficult.

Compared to calcic amphiboles, potassic-richterites show significantly lower $^{Amph/L}D_{REE}$, with positive anomalies in the $^{Amph/L}D$ value for Eu. If the $^{Amph/L}D$ values are normalized to $^{Amph/L}D_{Gd}$ to emphasize differences in REE fractionation (Fig. 17), potassic-richterites do not show LREE depletion and have a U-shaped pattern of HREE and Y. Potassic-richterites have $^{Amph/L}D_{La}/^{Amph/L}D_{Sm}$ values close to unity (0.6-1.14), whereas pargasites and kaersutites have values at least 3 times smaller (0.11-0.21). $^{Amph/L}D_{Gd}/^{Amph/L}D_{Yb}$ values are in the range 0.18-1 in potassic-richterites and in the range 1.03-1.83 in pargasites and kaersutites.

We observed before that REE site-preference in pargasites and kaersutites is mainly a function of the nature of the dominant B cation, Na and Ca occurring at *M*(4) and Mg and Fe^{2+} occurring at *M*(4') and being more abundant (0.20-0.50 apfu) at high-*T* conditions. Here we found that other factors should be taken into account. In pargasite and kaersutites, where the presence of highly charged cations makes the *M*(2) octahedron small, LREE preferentially have a $^{18}M(4)$ -type coordination, whereas HREE have a $^{6+2}M(4')$ -type coordination. In potassic-richterite, the dimensional relations between the available structural sites are different; in particular, *M*(2) is the largest octahedron in a particularly relaxed strip of octahedra. Therefore, HREE distribute over the $^{6+2}M(4')$ and the $^{6}M(2)$ site (Fig. 18; Bottazzi et al. 1999). The partitioning of REE between two distinct sites according to two distinct crystal-chemical mechanisms gives rise to the U-shaped patterns of Figure 17.

The different LREE fractionation observed in calcic and in sodic-calcic amphiboles is also related to the major-element *M*(4)-site population. The presence of *M*(4) sites occupied by Na in a Na:Ca ratio around or slightly higher than 1:1 makes the incorporation of LREE and Eu^{2+} easier ($^{18}Eu^{2+} = 1.25$, $^{18}Na = 1.18$, $^{18}Ca = 1.12 \text{ \AA}$; Shannon 1976). Accordingly, a

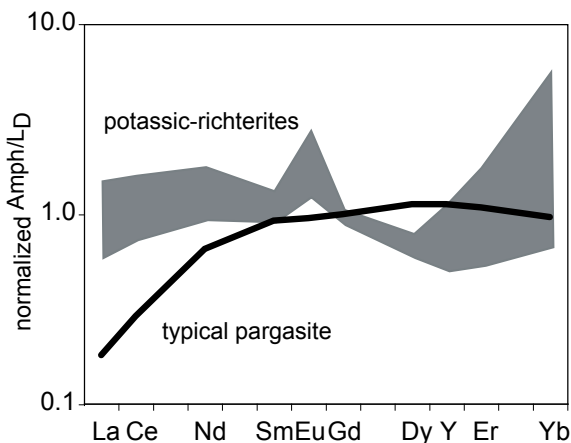
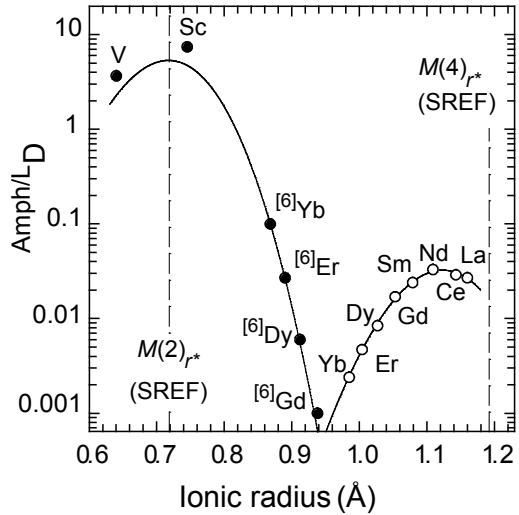


Figure 17. Comparison of the $^{Amph/L}D_{REE}$ between potassic richterite (grey field) and a typical pargasite. In order to highlight the different partitioning behavior, values have been normalized to $^{Amph/L}D_{Gd}$.

Figure 18. REE partition coefficients versus cation radius for the $M(2)$ and $M(4)$ sites in potassic richterites. The curves represent Blundy and Wood's (1994) equation for each site. Dashed lines represent the observed site dimension from SREF. Data are from Bottazzi et al. (1999).



positive Eu anomaly is observed in nearly all the REE patterns of potassic-richterites, whereas a negative Eu anomaly is observed in calcic amphiboles.

$A_{\text{Amph/L}}D_{\text{Ti}}$ for potassic-richterites synthesized from Si-rich lamproites vary in a much narrower range (from 0.52 to 1.2) than in calcic amphiboles. All the other HFSE have a strongly incompatible behavior; the observed ranges being $A_{\text{Amph/L}}D_{\text{Zr}}$ 0.026-0.087, $A_{\text{Amph/L}}D_{\text{Hf}}$ 0.041-0.144, $A_{\text{Amph/L}}D_{\text{Nb}}$ 0.017-0.072, and $A_{\text{Amph/L}}D_{\text{Ta}}$ 0.015-0.07. These results support a different behavior for tetravalent and pentavalent HFSE in calcic and sodic-calcic amphiboles. It is worthy of note here that Ti is about one order of magnitude more compatible than the other HFSE in both pargasites/kaersutites and potassic-richterites; moreover, the $A_{\text{Amph/L}}D_{\text{Ti}}$ values are very similar in potassic-richterites and in pargasites crystallized from melts with similar SiO_2 contents, i.e. at the upper limit of the pargasite field (Tiepolo et al. 2003).

With reference to the partitioning behavior of Ti, it must be remembered that Ti can be incorporated also at the $T(2)$ site in potassic-richterite, according to the T and P dependent exchange ${}^{T(2)}\text{Ti}_1 {}^{T(2)}\text{Si}_{-1}$. As explained in more detail in Oberti et al. (2007a,b), this is another example of the effects of the bulk composition of the system and of the amphibole phase on cation ordering. Richterite is an amphibole end-member with small compositional variations, where deviations from the ideal charge arrangement are always very limited. This feature and the lack of Al in lamproitic melts favor the incorporation of Ti at the (distorted) $T(2)$ site, and restrict the incorporation of Ti at the M sites to the occurrence of the oxo component. Incorporation of the larger (${}^{4}\text{Si} = 0.26$, ${}^{4}\text{Ti} = 0.42$ Å) tetrahedral Ti in potassic-richterite is always significant (${}^{T(2)}\text{Ti}/{}^{\text{tot}}\text{Ti} = 0.2-1$) at high- T and low-to-medium P conditions, but is hindered at high P (Konzett 1997). In contrast, the incorporation of $M(1)\text{Ti}$ is mainly a function of $f_{\text{H}_2\text{O}}$ conditions, and thus $M(1)\text{Ti}/{}^{\text{tot}}\text{Ti}$ may reach 0.55 at the most extreme conditions tested (Tiepolo et al. 2003). The dominance of the ${}^{T(2)}\text{Ti}_1 {}^{T(2)}\text{Si}_{-1}$ exchange vector may explain the nearly constant $A_{\text{Amph/L}}D_{\text{Ti}}$ observed in potassic-richterites. In richterites, even more than in calcic amphiboles, the measured $A_{\text{Amph/L}}D_{\text{Ti}}$ should be better considered as the sum of distinct "split" partition coefficients (i.e., $M(1)D_{\text{Ti}}$, $M(2)D_{\text{Ti}}$, $T(2)D_{\text{Ti}}$; Oberti et al. 2000) to be used separately in modeling trace-element behavior.

In pargasites and especially in kaersutites, HFSE⁵⁺ enter the $M(1)$ site and balance the ${}^{\text{O}(3)}\text{O}^{2-}$ component, whereas HFSE⁴⁺ enter the $M(2)$ site and balance the ${}^{\text{I}}\text{Al}$ content. In contrast,

both HFSE⁴⁺ and HFSE⁵⁺ are likely ordered at the *M*(1) site in synthetic potassic-richterites, as suggested by the positive correlation observed between their $D_{\text{Amph/LD}}$ and the $M(1)\text{Ti}$ content (Tiepolo et al. 2003). In agreement with the relevant ionic radii, $D_{\text{Amph/LD}_{\text{Nb/Ta}}}$ values generally approach unity (they can be either higher or lower than 1), whereas $D_{\text{Amph/LD}_{\text{Zr/Hf}}}$ are always < 1 (Vannucci et al. 2004). This feature is consistent with the observation that *M*(1) is the smallest octahedron in richterites, and that the measured $\langle M(1)\text{-O} \rangle$ distances are similar to the $\langle M(2)\text{-O} \rangle$ distances measured in titanian pargasites and kaersutites (Oberti et al. 2000). Therefore, the relative sizes of the independent octahedra are the key to understand HFSE partitioning in the various amphibole compositions.

$D_{\text{Amph/LD}_{\text{Pb}}}$ in potassic-richterites does not exceed 0.044, a value at the lower end of the range observed in calcic amphiboles; moreover, $D_{\text{Amph/LD}_{\text{Pb}}}$ is closely similar with the $D_{\text{Amph/LD}}$ value for the homovalent Ba (Tiepolo et al. 2003). These results confirm that the incorporation and ordering of Pb and Ba is ruled by the same mechanism, namely their incorporation in the larger *A* site with tetrahedral Al acting as the most likely charge compensating species for the R^{2+}_{-1} (Na,K)¹⁺ substitution. Thus the low ^TAl content of potassic-richterites accounts well for their very low $D_{\text{Amph/LD}_{\text{Pb}}}$ values.

The crystal chemical considerations reported above also indicate that, due to the different mechanisms ruling their incorporation, Sr²⁺ cannot be assumed as a proxy for Pb²⁺ to infer its amphibole/melt partitioning behavior. Site decoupling between these elements is confirmed by the large variability of the $D_{\text{Amph/LD}_{\text{Pb}}}/D_{\text{Amph/LD}_{\text{Sr}}}$ ratios (0.13-0.55) observed in the few experiments where both $D_{\text{Amph/LD}_{\text{Pb}}}$ and $D_{\text{Amph/LD}_{\text{Sr}}}$ have been measured (Brenan et al. 1995; La Tourrette et al. 1995).

Similarly to calcic amphiboles, potassic-richterites show $D_{\text{Amph/LD}_{\text{U}}}/D_{\text{Amph/LD}_{\text{Th}}}$ approaching unity, although with much lower *D* values (down to < 0.0001) and plays no role in fractionation of U from Th in magmas or in the mantle. Based on their ionic radii, incorporation of Th and U in potassic-richterite might occur both at the *M*(2) and the *M*(4) sites. However, the lower compatibility for U and Th relative to calcic amphiboles suggests their incorporation at the *M*(4) site, where Ca abundance is half than in pargasites.

ON THE CORRECT CHOICE OF $D_{\text{AMPH/LD}}$

Literature data show that $D_{\text{Amph/LD}}$ for calcic amphiboles vary significantly. Speculatively, this means that large mistakes can be introduced in petrological models by the choice of inappropriate partition coefficients.

Pressure, temperature, crystal structure and melt composition are all expected to affect the $D_{\text{Amph/LD}}$. However, none of the experimental works in the literature has been yet able to identify the influence of temperature on amphibole/melt trace element partitioning. This is likely due to the relatively small thermal stability field of the amphibole and/or the relation between temperature and melt polymerization.

The effects of pressure, melt and mineral structure are more apparent and can be used to constrain the choice of the $D_{\text{Amph/LD}}$. The effect of melt composition is apparently dominant over that of the crystal structure for a large number of elements such as REE, actinides, Pb and Li. For these elements, $D_{\text{Amph/LD}}$ varies more than one order of magnitude from basaltic to rhyolitic systems. Because the relation of $D_{\text{Amph/LD}}$ with melt composition is exponential, the error introduced into the modeling due to the uncertainty of the real SiO₂ content of the melt exponentially increases moving towards more acidic systems. The SiO₂ content of the parent melt can be inferred based on the major element mineral chemistry and/or the mineral assemblage. These petrologic features allow an easy discrimination between basaltic and rhyolitic systems, but cannot discriminate between melts with 45 or 55 wt% of SiO₂. In this compositional range, approximately 2-3-fold variation of the partition coefficients for most of the above mentioned

trace element is expected, and this error must be taken into account when discussing the results of petrological modeling.

In the case of Ti, Nb and Ta, the effect of the amphibole composition on $D_{\text{Amph/L}}^{\text{Amph/L}}D$ may be even stronger than that of the melt, at least in calcic amphiboles, and thus it must be taken into account when choosing partition coefficients. For instance, a strong increase in the $D_{\text{Amph/L}}^{\text{Amph/L}}D$ for these elements has been observed in dehydrogenated amphiboles crystallized from Ti-poor systems. Unfortunately, detection and quantification of the oxo component in amphiboles can only be obtained by either SIMS analysis of the hydrogen content and/or structure refinements (see Oberti et al. 2007b for more details). In contrast, the effect of amphibole composition on the $D_{\text{Nb}}^{\text{Amph/L}}/D_{\text{Ta}}^{\text{Amph/L}}$ ratio can be rather straightforwardly quantified based on chemical analysis of the major elements.

The effect of pressure is even more difficult to determine, because it is subordinated to that of the melt and even to that of the crystal structure. In many cases, changes in partitioning behavior observed at different pressures are within error (Dalpé and Baker 2000; Adam and Green 2003). According to the experiments of Adam and Green (1994), in the case of Sr, Sm, Ho, and Lu the error that is introduced into the model when neglecting the effect of pressure on $D_{\text{Amph/L}}^{\text{Amph/L}}D$ may reach a factor of two.

ACKNOWLEDGMENTS

Funding from CNR through projects TAP01.004.002 and TAP01.005.002 is acknowledged. This is Geocycles publication number 102.

REFERENCES

- Adam J, Green TH (1994) The effect of pressure and temperature on the partitioning of Ti, Sr and REE between amphibole, clinopyroxene and basaltic melts. *Chem Geol* 117:219-233
- Adam J, Green TH (2003) The influence of pressure, mineral composition and water on trace element partitioning between clinopyroxene, amphibole and basaltic melts. *Eur J Mineral* 15:831-841
- Adam J, Green TH, Sie SH (1993) Proton microprobe determined partitioning of Rb, Sr, Ba, Y, Zr, Nb and Ta between experimentally produced amphibole and silicate melts with variable F content. *Chem Geol* 109:29-49
- Adam J, Oberti R, Cámara F, Green T (2007) An electron microprobe, LAM-ICP-MS and single-crystal X-ray structure refinement study of the effects of pressure, melt-H₂O concentration and f_{O_2} on experimentally produced basaltic amphiboles. *Eur J Mineral* (in press)
- Beattie P (1994) Systematics and energetics of trace-element partitioning between olivine and silicate melts: implications for the nature of mineral/melt partitioning. *Chem Geol* 117:57-71
- Beattie P, Drake M, Jones J, Leeman W, Longhi J, McKay G, Nielsen R, Palme H, Shaw D, Takahashi E, Watson B (1993) Terminology for trace-element partitioning. *Geochim Cosmochim Acta* 57:1605-1606
- Blundy JD, Wood BJ (1994) Prediction of crystal-melt partition coefficients from elastic moduli. *Nature* 372:452-454
- Blundy JD, Wood BJ (2003) Mineral-melt partitioning of uranium, thorium and their daughters. *Rev Mineral Geochem* 52:59-118
- Bottazzi P, Tiepolo M, Vannucci R, Zanetti A, Foley S, Brumm R, Oberti R (1999) Fine-scale structural control of heavy and light rare-earth element ordering in amphibole. *Contrib Mineral Petrol* 137:36-45
- Brenan JM, Neroda E, Lundstrom CC, Shaw HF, Ryerson FJ, Phinney DL (1998) Behaviour of boron, beryllium, and lithium during melting and crystallization: constraints from mineral-melt partitioning experiments. *Geochim Cosmochim Acta* 62:2129-2141
- Brenan JM, Shaw HF, Ryerson FJ, Phinney DL (1995) Experimental determination of trace-element partitioning between pargasite and a synthetic hydrous andesitic melt. *Earth Planet Sci Lett* 135:1-12
- Brice JC (1975) Some thermodynamic aspects of the growth of strained crystals. *J Cryst Growth* 28:249-253
- Dalpé C, Baker DR (1994) Partition coefficients for rare-earth elements between calcic amphibole and Ti-rich basaltic glass at 1.5 GPa, 1100 °C. *Mineral Mag* 58A:207-208

- Dalpe C, Baker DR (2000) Experimental investigation of large-ion-lithophile-element, high-field-strength-element- and rare-earth-element-partitioning between calcic amphibole and basaltic melt: the effects of pressure and oxygen fugacity. *Contrib Mineral Petrol* 140:233-250
- Della Ventura G, Robert JL (1990) Synthesis, XRD and FT-IR studies of strontium richterites. *Eur J Mineral* 2:171-175
- Foley SF, Taylor WR, Green DH (1986) The effect of fluorine on phase relationships in the system $KAlSi_3O_8$ - Mg_2SiO_4 - SiO_2 at 28 kbar and the solution mechanism of fluorine in silicate melts. *Contrib Mineral Petrol* 93:46-55
- Gaetani GA, Grove TL (1995) Partitioning of rare - earth elements between clinopyroxene and silicate melt: crystal-chemical controls. *Geochim Cosmochim Acta* 59:1951-1962
- Goldschmidt VM (1937) The principles of the distribution of chemical elements in minerals and rocks. *J Chem Soc London* 140:655-673
- Hawthorne FC, Oberti R, Cannillo E, Ottolini L, Roelofsen JN, Martin RM (2001) Li-bearing arfvedsonitic amphiboles from the Strange Lake peralkaline granite, Quebec. *Can Mineral* 39:1161-1170
- Hawthorne FC, Oberti R, Zanetti A, Czamanske GK (1998) The role of Ti in hydrogen- deficient amphiboles: sodic-calcic and sodic amphiboles from Coyote Peak, California. *Can Mineral* 36:1253-1265
- Hawthorne FC, Ungaretti L, Oberti R, Bottazzi P, Czamanske GK (1993) Li: an important component in igneous alkali amphiboles. *Am Mineral* 78:733-745
- Hilyard M, Nielsen RL, Beard JS, Patino-Douce A, Blencoe J (2000) Experimental determination of the partitioning behavior of rare earth and high field strength elements between pargasitic amphibole and natural silicate melts. *Geochim Cosmochim Acta* 64:1103-1120
- Klein M, Stosch HG, Seck HA (1997) Partitioning of high field-strength and rare-earth elements between amphibole and quartz-dioritic to tonalitic melts: an experimental study. *Chem Geol* 138:257-271
- Kohn JA, Komeforo JE (1955) Synthetic asbestos investigations, II: X-ray and other data on synthetic fluorichterite, -edenite, and -boron edenite. *Am Mineral* 40:410-421
- Konzett J (1997) Phase relations and chemistry of Ti-rich K-richterite-bearing mantle assemblages: an experimental study to 8 GPa in a Ti-KNCMASH system. *Contrib Mineral Petrol* 128:385-404
- LaTourrette TZ, Hervig RL, Holloway JR (1995) Trace element partitioning between amphibole, phlogopite, and basanite melt. *Earth Planet Sci Lett* 135:13-30
- Mason B (1966) *Principles of Geochemistry* (3rd Ed.). Wiley, New York.
- Moore PB, Davis AM, Van Derveer DG, Sen Gupta, PK (1993) Joesmithite, a plumbous amphibole revisited and comments on bond valences. *Mineral Petrol* 48:97-113
- Nagasawa H (1966) Trace element partition coefficients in ionic crystals. *Science* 152:767-769
- Nicholls IA, Harris KL (1980). Experimental rare Earth element partition coefficients for garnet, clinopyroxene and amphibole coexisting with andesitic and basaltic liquids. *Geochim Cosmochim Acta* 44:287-308
- Nielsen RL (1985) A method for the elimination of the compositional dependence of trace element distribution coefficients. *Geochim Cosmochim Acta* 49:1775-1779
- Oberti R, Della Ventura G, Cámara F (2007a) New amphibole compositions: natural and synthetic. *Rev Mineral Geochem* 67:89-123
- Oberti R, Hawthorne FC, Cannillo E, Cámara F (2007b) Long-range order in amphiboles. *Rev Mineral Geochem* 67:124-171
- Oberti R, Ungaretti L, Cannillo E, Hawthorne FC (1992) The behaviour of Ti in amphiboles: $^{47}Ti^{4+}$ in richterite. *Eur J Mineral* 4:425-439
- Oberti R, Vannucci R, Zanetti A, Tiepolo M, Brumm R (2000) A crystal-chemical re-evaluation of amphibole/melt and amphibole/clinopyroxene D_{Ti} in petrogenetic studies. *Am Mineral* 85:401-419
- Onuma N, Higuchi H, Wakita H, Nagasawa H (1968) Trace element partition between two pyroxenes and the host lava. *Earth Planet Sci Lett* 5:47-51
- Purton JA, Allan NL, Blundy JD (1997) Calculated solution energies of heterovalent cations in forsterite and diopside: implications for trace element partitioning. *Geochim Cosmochim Acta* 61:3927-3936
- Raudsepp M, Turnock A, Hawthorne FC, Sheriff B, Hartman JS (1987a) Characterization of synthetic pargasitic amphiboles $NaCa_2Mg_4M^{3+}Si_6Al_2O_{22}(OH,F)_2$; $M^{3+} = Al, Cr, Ga, Sc, In$ by infrared spectroscopy, Rietveld structure refinement and ^{27}Al , ^{29}Si , and ^{19}F MAS-NMR spectroscopy. *Am Mineral* 72:580-593
- Ryerson FJ, Hess PC (1978) Implications of liquid-liquid distribution coefficients to mineral-liquid partitioning. *Geochim Cosmochim Acta* 42:921-932
- Shannon RD (1976) Revised effective ionic radii and systematic studies of interatomic distances in halides and chalcogenides, *Acta Crystallogr* 32:751-767
- Sisson TW (1994) Hornblende-melt trace element partitioning measured by ion microprobe. *Chem Geol* 117:331-344
- Takahashi E, Irvine TN (1981) Stoichiometric control of crystal/liquid single-component partition coefficients. *Geochim Cosmochim Acta* 45:1181-1185
- Tiepolo M (1999) Determinazione sperimentale dei coefficienti di distribuzione solido/liquido in anfiboli di mantello: ruolo del controllo cristallochimico. Ph. D. Thesis, Università di Pavia, 314 pp.

-
- Tiepolo M, Bottazzi P, Foley S, Oberti R, Vannucci R, Zanetti A (2001) Fractionation of Nb and Ta from Zr and Hf at mantle depths: the role of titanian pargasite and kaersutite. *J Petrol* 42:221-231
- Tiepolo M, Vannucci R, Bottazzi P, Oberti R, Zanetti A, Foley SF (2000a) Partitioning of REE, Y, Th, U and Pb between pargasite, kaersutite and basaltic to trachitic melts: implications for percolated and veined mantle. *Geochem Geophys Geosyst* 1:2000GC000064.
- Tiepolo M, Vannucci R, Oberti R, Foley S, Bottazzi P, Zanetti A (2000b) Nb and Ta incorporation and fractionation in titanian pargasite and kaersutite: crystal-chemistry constraints and implications for natural systems. *Earth Planet Sci Lett* 176:185-201
- Tiepolo M, Zanetti A, Oberti R (1999) Detection, crystal-chemical mechanisms and petrological implications of $^{67}\text{Ti}^{4+}$ partitioning in pargasite and kaersutite. *Eur J Mineral* 11:345-354.
- Tiepolo M, Zanetti A, Oberti R, Brumm R, Foley S, Vannucci R (2003) Trace-element partitioning between synthetic potassic-rich pargasites and silicate melts, and contrasts with the partitioning behaviour of pargasites and kaersutites. *Eur J Mineral* 15:329-340
- Vannucci R, Oberti R, Tiepolo M, Zanetti A (2004) Ruling the incorporation of high field strength elements in mantle minerals. *Geochimica 2000, Accademia Nazionale dei Lincei* 165-186
- Wood BJ, Blundy JD (1997) A predictive model for rare earth elements partitioning between clinopyroxene and anhydrous silicate melt. *Contrib Mineral Petrol* 129:166-181
- Wood BJ, Blundy JD (2001) The effect of cation charge on crystal-melt partitioning of trace elements *Earth Planet Sci Lett* 188:59-71

Amphiboles: Environmental and Health Concerns

Mickey E. Gunter

*Department of Geological Sciences, University of Idaho
Moscow, Idaho, 83844-3022, U.S.A.
mgunter@uidaho.edu*

Elena Belluso

*Dipartimento di Scienze Mineralogiche e Petrologiche
CNR – Istituto di Geoscienze e Georisorse, sez. di Torino
Via Valperga Caluso 35, I-10100 Torino, Italy
elena.belluso@unito.it*

Annibale Mottana

*Università degli Studi Roma Tre, Dipartimento di Scienze Geologiche
Largo S. Leonardo Murialdo 1, I-00146 Roma RM, Italy
mottana@uniroma3.it*

INTRODUCTION

In this chapter, we turn our attention to an issue that is often not based on rational science, but about fear—the issue of asbestos. As the geological community is well aware, all asbestos are minerals, and thus naturally formed; yet in the public arena, many people believe asbestos is something manufactured by humans and that one fiber is enough to kill you if inhaled. It is the intent of this chapter to provide background information for members of differing communities, be they mineralogists, geologists, medical researchers, regulatory workers, or legal professionals to better understand amphibole-related health and environmental issues. This chapter contains an introduction and overview of the health effects associated with the inhalation of amphibole minerals. Also, the chapter will discuss some of the current issues and research trends surrounding asbestos exposure, especially in the natural environment.

At the outset, anyone with knowledge of this field probably wonders why the word asbestos does not appear in the title of this article. As we will see as we progress through this article, there is a debate between the various scientific and regulatory disciplines on the definition of the word asbestos. What is well known and accepted by all is that the occupational exposure to asbestiform amphibole leads to a significant increase in asbestos-related diseases, especially mesothelioma. What is not clear is how the morphology of amphiboles affects the etiology of the disease. However, because the morphology of amphiboles is at least partially gradational from the high aspect-ratio (which is the length divided by the width of a particle) fibrous particles to the low aspect-ratio, nonfibrous particles, we might also assume that the etiology of the diseases might vary.

In this chapter, we will define terminology used by the different fields of study. It is important for those working in any field dealing with asbestos to understand that terms vary significantly among the different fields. Often, attempts by one group to simplify the nomenclature have resulted in more confusion in the scientific literature as well as for the public. For instance, recently the term “naturally occurring asbestos” has become widely used by regulatory groups in the USA to distinguish it from occupational exposure to asbestos. The issue becomes even

more complicated in that the majority of the minerals of concern in the natural environment are amphiboles, and the distinction between fibers and fragments of amphiboles remains a central issue. Clearly we are exposed to amphiboles and different types of asbestos on a daily basis. Many of these exposures are natural (i.e., nonoccupational or nonanthropogenic) while others result from widespread use of asbestos-containing products over the past 70-80 years. However, because approximately 95% of asbestos used in commercial products was chrysotile (which is a sheet silicate), the majority of occupational exposure was to chrysotile, not amphibole asbestos. In the natural environment amphibole exposure is much greater than chrysotile; this is due mainly to the fact that amphiboles are much more widespread than chrysotile. So we are again left to distinguish between amphibole and amphibole asbestos. Regardless, most of us who reach the age of 60 and 70 have not thousands but millions of particles of amphibole in our lungs due to these natural exposures (Churg 1983). Thus, it seems to defy common sense that one fiber of asbestos will lead to death.

The phrase “naturally occurring asbestos” was mentioned above. Exposure relating to it is now at the forefront of health concerns of asbestos exposure, at least in the USA. Because of the general fear of the word “asbestos,” the mere thought of exposure can cause panic in the general public, often driven by the popular media. Again, one of the goals in this chapter is to alleviate some of that fear. However, the media, especially in reports of Libby, Montana, USA, have continued to instill fear into the public by overstating the issues. In the USA, fear of asbestos exposure was heightened based on issues surrounding Libby that made it to the national media in 1999. These concerns were also heightened by the possible widespread asbestos exposure in the September 11, 2001, collapse of the World Trade Center. These two events combined to cause heightened concern to asbestos exposure in the natural setting of El Dorado County, California. While there was an increase in asbestos-related diseases from the miners at Libby (McDonald et al. 2004), those who worked in the processing outside of Libby (Lockey et al. 1984), and health concerns for the local citizens (ATSDR 2000, 2001), there are no confirmed deaths for nonoccupationally exposed citizens living in El Dorado County. Even so, a statistical model shows possible correlations of mesothelioma with proximity to ultramafic rocks (Pan et al. 2005) in El Dorado County. Turning our attention to Italy, there have been increased deaths from mesothelioma on a country-wide basis and even more concern on the island of Sicily in the village of Biancavilla on the side of the Mt Etna where exposure came from the first known occurrence of asbestiform amphiboles in volcanic rock (Burrigato et al. 2006).

NOMENCLATURE AND BACKGROUND INFORMATION

Before we can hope to grasp the issues dealing with amphiboles and health, we need to have a working knowledge of the terms used in this field. The nomenclature used in this field is daunting, challenging, confusing, and bewildering. This is the case because several different disciplines (e.g., geology, mineralogy, industry, the medical fields, regulatory groups, and the legal system) have developed their own nomenclature somewhat independently of each other. Worse yet, they have modified nomenclatures from other disciplines so that now the same word may have different meanings and different words the same meanings.

Mineralogical

Morphology. Geology and mineralogy were two of the first disciplines to discuss asbestos, and to those groups the term generally meant that the material is fibrous. When they started working with this material, they usually did so at a large scale (i.e., hand-sample scale) where it is fairly easy to tell if any amphibole has the asbestos habit or not. Figure 1A shows three large amphibole samples all recently obtained from the Smithsonian Museum; the large dark one is a euhedral (which literally means “with good faces” or well formed) tremolite grain while the other two are asbestos—the lighter colored sample is tremolite and the darker colored

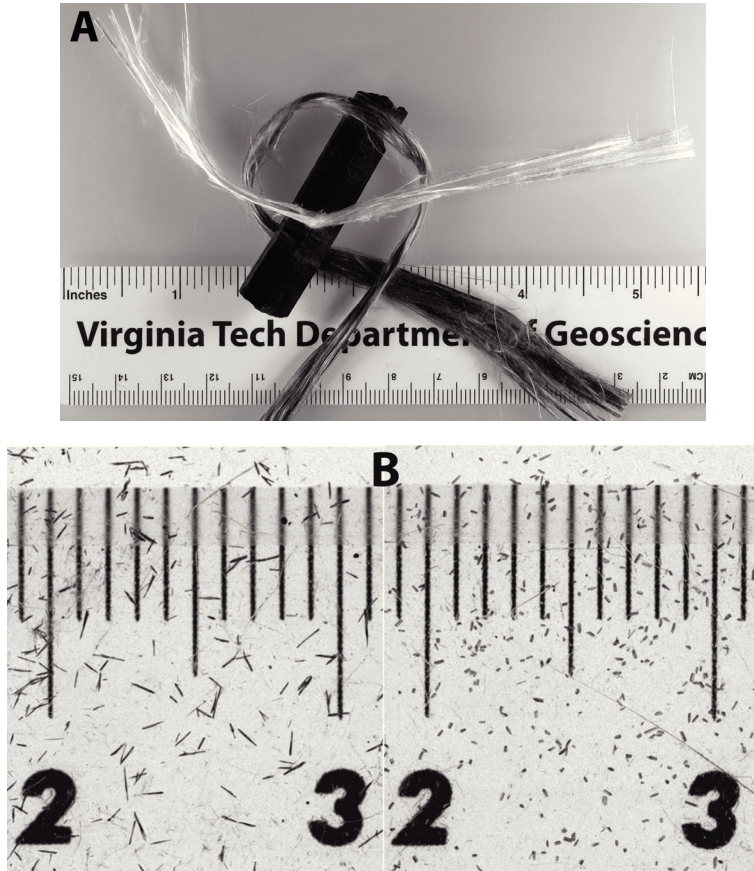


Figure 1. Photographs showing various morphologies of amphiboles at different scales. A) This photograph shows three amphiboles from the Smithsonian Institution collection: two are considered asbestos and the third is a euhedral sample with {110} faces. The light-colored fibrous mineral is tremolite asbestos and the darker one crocidolite. The darker euhedral sample is a single crystal of tremolite. (The euhedral tremolite is from Wilberforce, Ontario, Canada (#117611), tremolite asbestos from Hartford County, Maryland, USA (#118117), and crocidolite from Wittenoom, Australia (#117343)). B) Two different morphologies of an amphibole separated from the same hand sample collected near Libby, Montana, USA (obtained from the Harvard Museum (#100839)). The particles on the left exhibit asbestiform habit (i.e., separable lengthwise), while the particles on the right are near-perfect euhedral single crystals (scale bar is in mm).

one is crocidolite (which is the asbestos variety of the amphibole mineral riebeckite). As the size of the particles become smaller, it becomes harder to determine particle morphology. Figure 1B shows two differing morphologies from the same hand sample. The particles on the left show the asbestiform habit, while the sample on the right is composed of euhedral, very minute single crystals. The term “asbestiform” refers to a type of morphology where a mineral has longitudinal (i.e., lengthwise) parting, and thus can be split into individual fibers. To the mineralogical community the term “fiber” is a textural term meaning that the material looks, and more importantly, behaves as a fiber; thus, it can curve and bend under force. In the industrial world, the fibrous property of these minerals resulted in a high tensile strength in much the same way that a rope’s strength increases because it is made of many interwoven smaller “ropes.” In the regulatory community the term “fiber” has been given certain size and shape characteristics commonly referred to as the aspect ratio (the length of the particle

divided by its width), and depending upon the analytical method used, a particle is considered a fiber if it has a greater than 3:1 (by light microscopy) or 5:1 (by electron microscopy) aspect ratio. These aspect-ratio criteria were never meant to define a fiber but were developed as counting criteria used to determine the amount of asbestos in a material in an industrial setting where it was known that the source of the material is a commercial asbestos product. The regulatory community has been forced to develop guidelines to determine if a particle is or is not a fiber to meet certain health-based concerns. In turn, the legal system has adopted many of the regulatory terminologies instead of the more descriptive mineralogical terminologies, even to the point of using the word “fiber” for any particle found in the human lung. For instance a blocky piece of quartz found in the lung might be called a “nonasbestos” fiber.

Often, especially in regulatory usage, if an amphibole particle does not meet the definition of a fiber (based on aspect ratio), it is termed a “cleavage fragment.” Again, to a mineralogist, the term “cleavage-fragment” has a clear meaning—it is a piece of a mineral bounded by cleavage faces. As with a fiber, some action must be taken to see if a mineral has cleavage—namely it must be broken. Often, amphiboles may display growth faces which may appear as a cleavage face.

Many, especially in the popular media, use the term “asbestos” very loosely. Its use should be restricted to a commercial product, such as for the two samples shown in Figure 1A. The term “particle” should be used for any small piece of amphibole, and the terms “fiber” and “cleavage-fragment” should only be used where the particles clearly meet the mineralogical definitions as stated above. The majority of the time, what are called “cleavage-fragments” should be called “fragments.” Also, many particles are called fibers (based on regulatory guidelines) where they are single crystals. The term “asbestiform” should be applied to noncommercial amphiboles (such as that shown on left side of Fig. 1B) that can split lengthwise into fibers. The term “nonasbestiform” should be used for those that cannot split lengthwise, such as those shown on the right side in Figure 1B. Generally, fibers result from the breaking apart of asbestiform amphiboles whereas fragments result from the breaking apart of nonasbestiform amphiboles.

Chemical composition. Amphiboles are a chemically diverse group of silicate minerals based on double chains of (Si,Al) tetrahedra, and all share this common building block. Also, most amphiboles are elongated parallel to these chains (Fig. 1). Cations are needed to charge balance these double chains as well as hold them together. The individual amphibole species names are based on these cations. Hawthorne and Oberti (2007 - Chapter 2, this volume) present a discussion of amphibole nomenclature and the criteria set forth by Leake et al. (1997). Although several other amphibole species can occur as asbestos (e.g., winchite (Wylie and Huggins 1980) and fluoro-edenite (Gianfagna and Oberti 2001)), currently there are only 5 (of more the 80) species of amphiboles that are regulated: anthophyllite, tremolite, actinolite, riebeckite, and grunerite. The term “crocidolite” is used for the asbestos variety of riebeckite, and amosite to that of the asbestos variety of grunerite. These two variety names originated because crocidolite and amosite are the most commonly used amphibole asbestos. And while anthophyllite was mined and used in small amounts, tremolite and actinolite are regulated because they can occur as accessory minerals in other economically important mineral deposits. As we will see later in this chapter, there are three nonregulated amphiboles species (fluoro-edenite, richterite, and winchite) that have been associated with asbestos-related diseases and should probably be added to the regulated list, as should all asbestiform amphiboles.

Accurate chemical characterization is required to correctly determine the species name of an amphibole, and these names are important for us in the geological community. Figure 2 is an example of what is required to name amphiboles and was taken from a thorough study of the mineral chemistry of amphiboles collected from the Libby vermiculite deposit (Meeker et al. 2003). In this figure, site occupancy is plotted and different regions are assigned names. However, all mineralogists realize that the lines dividing the fields in this graph are somewhat

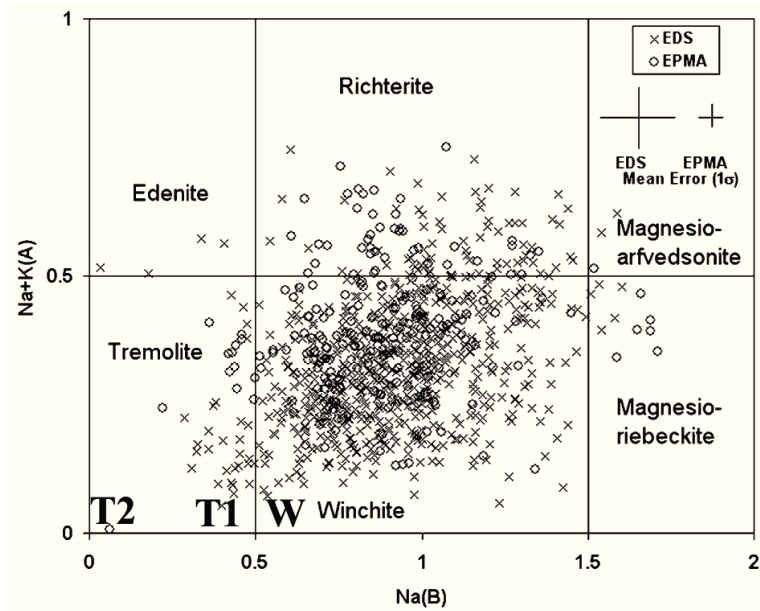


Figure 2. A plot of site occupancies required to determine the species of amphiboles obtained from the former vermiculite mine near Libby, Montana USA (Meeker et al. 2003); the circles are from EPMA-WDS data while the crosses are from EDS data. The plot shows that the amphiboles in that deposit are (at least) six different species, the majority being winchite and richterite.

arbitrary and not defined by Nature. We also know that tremolite plotting at T1 is more similar to winchite (W) than to tremolite plotting at T2. Thus minerals with different names can be more similar than minerals with the same name. This is a consequence of drawing boundaries in continuous compositional fields, and mineralogists understand these consequences of naming minerals in a solid-solution series. However, in the medical, legal, and regulatory fields, the names take on great importance, often more so than the actual compositions. Thus, chemical composition and nomenclature are areas that require different disciplines to try and understand each others needs.

Medical

To understand the issues surrounding asbestos, one needs to know the end points (i.e., the diseases) and what the etiology (i.e., causes) of these diseases might be. There are basically three asbestos-related diseases: asbestosis, mesothelioma, and lung cancer. Table 1 lists deaths and causes in the USA for these three diseases, as well as several others for comparison (modified from Gunter 1994). By far the largest number of deaths results from lung cancer (caused mainly by smoking cigarettes); numbers of deaths resulting from the other two asbestos-related are far fewer.

Table 1. Annual death statistics in the United States (population approximately 300 million). Total deaths for 2003 = 2,448,288. All data from the 2003 (most recent) U.S. Vital Statistics, www.cdc.gov/nchs/deaths.htm.

heart disease	685,089
cancer	556,902
strokes	157,689
lung cancer	126,382
accidents	109,277
asbestosis	583
pleura mesothelioma	181
silicosis	102
bee stings	66
lightning	47
spider bites	8
snake bites	2

We need to have some idea how the human body attempts to rid itself of the dust that we inhale. In the medical literature, the term “clearance” is used to refer to this process. Briefly, clearance first starts when particles enter the nose and are trapped there. Next, they enter the upper airways where the mucociliary escalator moves the particles back up the airway. Here they are either swallowed or spit out. It is notable that CO in cigarette smoke greatly reduces the efficiency of this clearance method. If a particle reaches the alveoli, it may be removed by a specialized white blood cell called an alveolar macrophage, and it is the last line of defense. Our respiratory system is very efficient and is believed to clear 99% of inhaled particles (see Plumlee et al. 2006 for a more complete discussion).

Size is very important in health issues surrounding the inhalation of dust, and we often refer to a particle as being “respirable.” Separate from asbestos, the United States Environmental Protection Agency (EPA) has set limits to respirable particles as function of their size in the natural environment. For instance, PM10 refers to particle matter less than 10 microns in diameter, and PM2.5 refers to particles less than 2.5 microns. Ongoing research shows that smaller particles (i.e., PM2.5) may be more harmful. We are concerned with the size range of respirable particles that cause chronic lung problems, and minerals in the natural environment often do not fall within this size range (Norton and Gunter 1999). Asbestiform minerals in the occupational setting, however, often do because they can separate into very fine fibers as a function of their morphology as they are mined and milled.

Few geologists have seen sections of normal or diseased lungs; however, the medical community uses methods similar to looking at rock thin sections to look at tissue sections. Figure 3 shows three tissue sections that have been cut and mounted on glass slides much like geologists do with minerals and rocks. Also, the samples are stained to aid in identifying cells, much like a petrologist uses different stains to differentiate carbonate or feldspar minerals. Figure 3A is a section through a normal lung showing

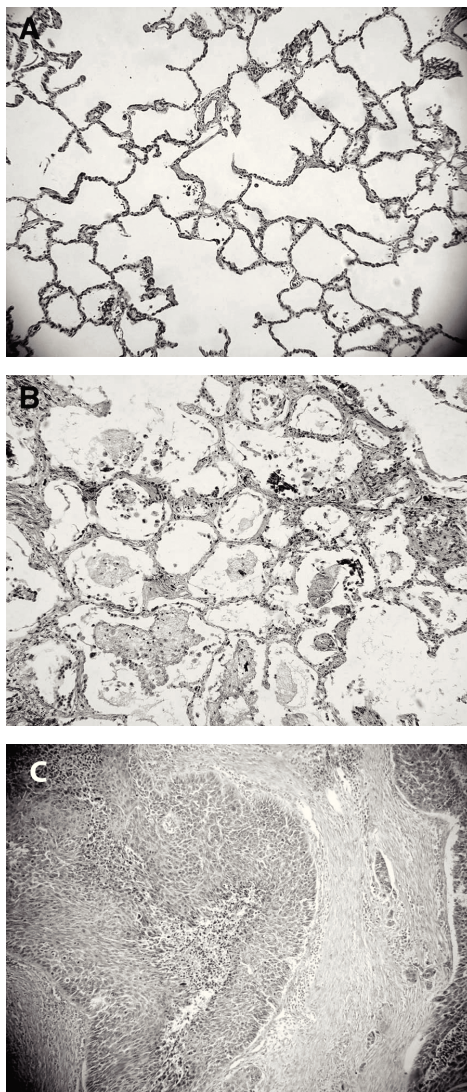


Figure 3. Three photomicrographs of human lung tissue (FOV approximately 1.5 mm). A) A normal lung section; the alveoli are the open areas surrounded by cell walls formed by capillaries. B) A lung section from an individual who suffered from asbestosis. Note that the open air spaces in the alveoli are filled and the alveoli walls thickened. Both of these would restrict $O_2 - CO_2$ exchange in the lung. C) A tumor (which destroys the lungs function).

the alveoli and the thin walls that separate them. The blood that circulates in these walls is responsible for the CO₂-O₂ exchange. In Figure 3B, the individual suffered from asbestosis. One can see that there is material within the alveoli and a thickening of the alveoli walls; both of these features inhibit the lungs' ability to perform CO₂-O₂ exchange. Figure 3C shows a tumor in the lung. When the tumor forms, it not only destroys that particular lung portion's ability to exchange air, but carcinogenic cells from the tumor spread and, unless treated early, the individual succumbs to cancer. Mesothelioma is a specific type of cancer affecting the external lining of the lung. It is not shown well on a glass slide. Most of the deaths from this disease can be correlated to asbestos exposure, especially the amphibole variety. In fact, there are some who would argue that chrysotile does not cause mesothelioma. This is the most dreaded form of all the asbestos-related diseases in that it has a latency period of 30-40 years. Mesothelioma death-rates in amphibole miner cohorts are in the range of 3-5% (McDonald et al. 2004).

Pleural plaques are masses of collagen that form in the lung. Sometimes these plaques are said to be "calcified," which means the plaques contain deposits of calcium phosphates similar in composition to hydroxylapatite. While they are found in the general population, they are found at higher rates among those exposed to asbestos. Pleural plaques can be seen on lung X-rays and can serve as a biomarker for asbestos exposure (Peipens et al. 2003). Pleural plaques do not appear to lead to other asbestos-related diseases, and there is even some debate on whether they are a disease themselves (ATSDR 2006). Regardless, they are a useful asbestos biomarker.

Probably the single most important aspect of asbestos-related disease is the dose. The large doses of asbestos fibers inhaled in the pre-regulated workplace resulted in worker mortality for asbestosis and mesothelioma. To determine dose, three criteria are needed: (1) the amount of air an individual breathes (which is about 10 m³/day, Gunter 1994), (2) the amount of respirable particles in that air, (3) and clearance. Dose is typically measured in f/ml (= f/cc), and thus not a mass measurement because it involves the number of fibers and not their weight or volume, or probably more importantly - surface area. Table 2 gives a list of doses for regulatory purposes, as well as some other examples that will be used in this chapter. So a miner working in a very dusty environment could breathe 1,000,000,000 fibers in an 8-hour workday if there were 100 f/cc. Also, it is worth noting that in outside air (0.00039 f/cc), an individual would breath 12,000 fibers in 24 h.

Table 2. Fibers/cm³ of asbestos (>5 μm with 3:1 aspect ratio). The first series indicates numbers in the workplace and the changing OSHA regulations from 1972 to 1992 (Gunter 1994). The second set indicates average values found in outdoor air, indoor air, schools, and public buildings with ACM (asbestos containing material) in different states of repair (Mossman et al. 1990).

> 100	preregulated workplace
5	OSHA (1972)
2	OSHA (1976)
0.5	OSHA (1983)
0.2	OSHA (1986)
0.1	OSHA (1992)
0.00039	outdoor air
0.00024	schools
0.00099	indoor air, no ACM
0.00054	indoor air, nondamaged ACM
0.00073	indoor air, damaged ACM

The RIM volume 28 (Guthrie and Mossman 1993) entitled "Health effects of mineral dusts" contains a thorough appendix of geological, mineralogical, and medical terms used in health based issues. An electronic version of that information can be found at <http://www.webpages.uidaho.edu/~mgunter/NAGT/manuscripts/glossary.pdf>.

ANALYTICAL METHODS

One of the most important aspects of dealing with minerals is their identification and characterization. This simple statement takes on certain challenges for those involved in the positive identification of asbestiform amphiboles because: (1) there can be discrepancies in defining morphology, and (2) not all species of amphiboles are regulated. Thus, under the current regulatory status, one must precisely establish the chemical composition of the amphibole to determine its species. Regardless of regulatory concerns and from a mineralogical perspective, precise chemical analyses are useful in not only identifying and naming the mineral, but also in thoroughly characterizing the mineral, which is important in understanding the minerals' health impacts. Thus, for mineral use in health-based studies, it is worthwhile to apply several analytical methods for both identification and thorough characterization. The quantity of asbestos in an asbestos-containing material is important to the regulatory community because special precautions must be taken when a material contains greater than a certain amount of asbestos. While there are debates about the specific amount, 1% is typically chosen. What will follow are three broad areas for characterizing these materials: (1) shape and morphology as determined by various microscopic methods (these methods are also used to determine the amount of asbestos in a material), (2) structure studies accomplished by various diffraction methods, and (3) chemical analysis of both single particles and bulk samples. For a more complete review of analytical methods used in characterizing minerals in health-based studies, see Guthrie (1993); for a review of regulatory methods see Millette (2006).

Microscopic methods

Because by definition asbestos deals with the morphology of the material, we will first discuss various types of microscopy methods used to determine morphology. Two of these methods involve very precise regulatory guidelines used in the identification and quantification of asbestos material in the commercial setting. In a research setting, all of these instruments can be used depending mainly on the scale of observation. The instruments are arranged below in order of increasing magnification.

Polarized-Light Microscope (PLM). The first widely used instrument in geology and the asbestos regulatory field was the PLM, and it is still in wide use today (Millette 2006). With correct use it can determine a material's morphology and often its identity. The PLM is useful for observing particles from a few mm down to about 1 μm . Not only can the PLM show sufficiently magnified images to ascertain the morphology of the material, it can also aid in identification based on the correct interpretation of the way the light interacts with the particles. For example, in cross-polarized light, it is simple to distinguish isotropic (e.g., glass) and anisotropic materials (e.g., amphiboles). Whereas there are many fibrous materials in Nature and in the commercial arena, a quick observation in the PLM can distinguish fiberglass from amphibole. The refractive indices of materials can be determined with relatively little difficulty and, in general, the different types of commercial amphibole-asbestos can be distinguished from one another, as well as from chrysotile; however, there is some overlap in refractive indices (Millette and Bandli 2005). There are also PLM techniques used to help aid in distinguishing fibers from fragments (Wylie 1979; Zoltai 1979; Langer et al. 1991; Brown and Gunter 2003).

Geologists use thin sections (30 μm thick slices of rock glued to glass slides and polished) to help identify and characterize minerals in rocks, and to describe the texture of a rock or mineral. Thus, thin sections are useful to study the morphology of amphibole grains. Figure 4 shows four separate amphiboles that exhibit blocky (4A), acicular (4B), and asbestiform (4C) habits, while (4D) contains all three morphologies. The first column in the figure shows approximately 50 mm wide samples of each cut to make thin sections; the second column shows the associated thin sections cut from the rocks viewed in cross-polarized light. In these

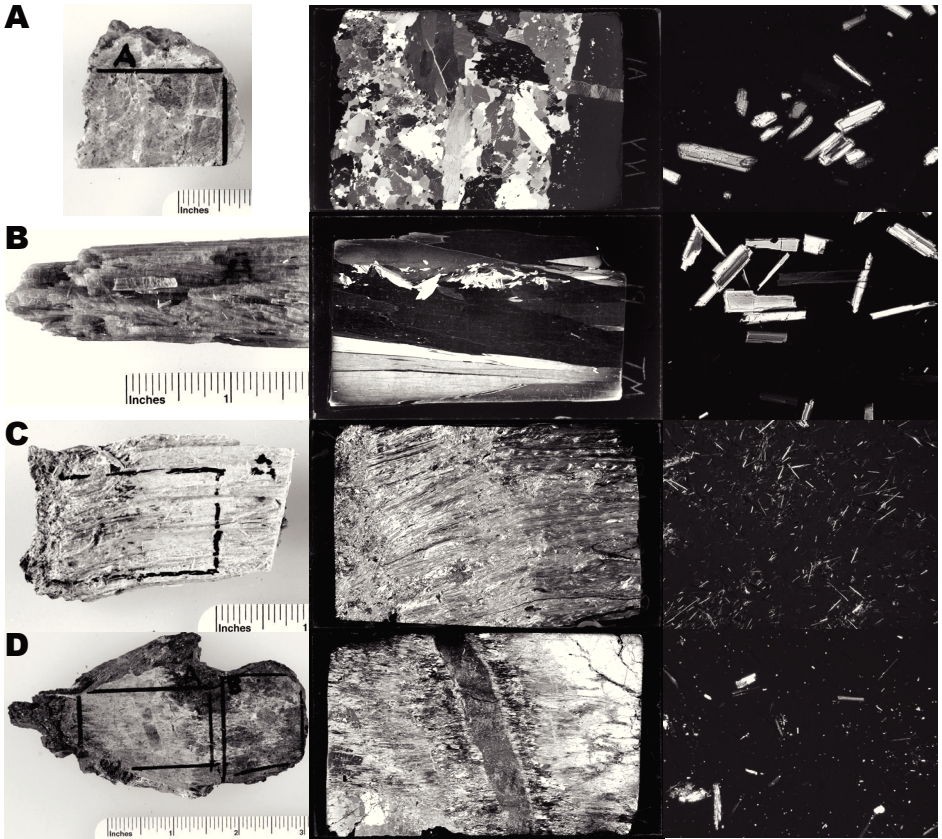


Figure 4. A series of photographs and PLM photomicrographs used to observe and characterize amphibole morphology. The left column shows a rock sample before cutting and polishing into a thin section (glass slide size = 27 x 46 mm). The center column shows sample in cross-polarized light. The right column shows individual particles obtained from the rock sample, placed in an immersion liquid and viewed in cross-polarized light (FOV = 1.2 mm). A) A blocky tremolite sample from New York, B) An acicular tremolite sample from near Bozeman, Montana, C) An asbestiform tremolite from Montgomery County, Maryland, and D) A mixed-morphology sample from Libby, Montana, (the same sample as in Figure 1B).

images, the blocky, acicular, and asbestiform habits are seen. The last column shows immersion mounts of amphiboles from each of the rocks, which are useful in characterizing the shape of the grains liberated from the rocks. Note how the particles become longer and skinnier going from blocky to acicular to asbestiform, and how the last sample shows mixed morphologies.

To further characterize individual particles, the spindle stage can be used. Brown and Gunter (2003) discussed this method at length and used it to explore the relations between extinction angles and morphology for a suite of amphibole particles of differing morphology. The upper row of photos in Figure 5 shows three different morphologies of amphibole particles from Libby, ranging from euhedral to asbestiform. The optimal range in particle size for the spindle stage is 100-300 μm , and characterizing particles at this size range can help understand them at smaller sizes. While extinction angles are often used to aid in identification, precautions in their use should be taken (Su and Bloss 1984; Verkouteren and Wylie 2002; Brown and Gunter 2003).

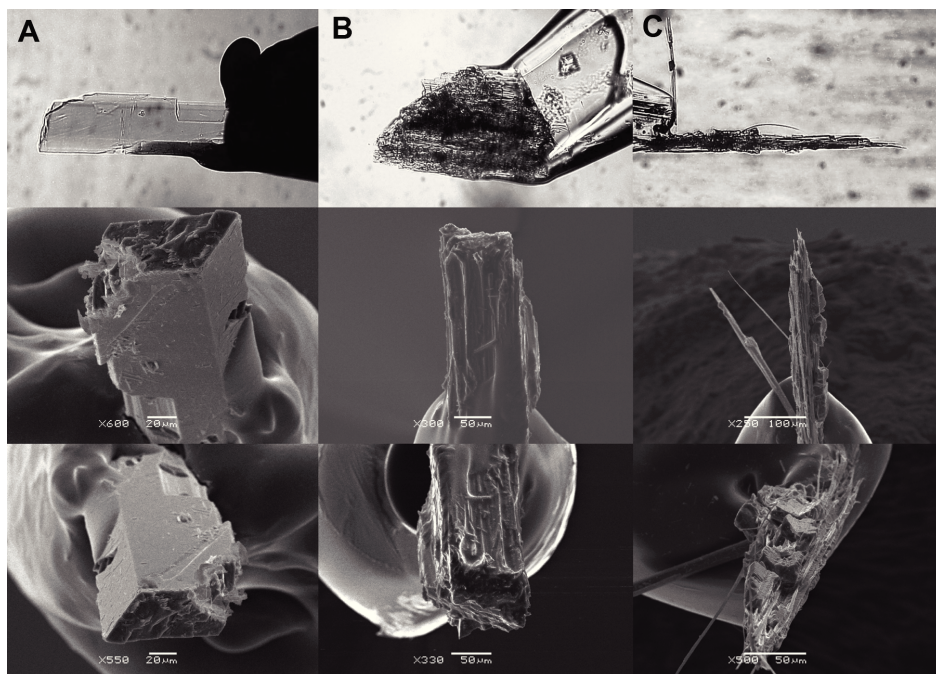


Figure 5. Three different amphibole morphologies from the Libby vermiculite deposit: A) blocky, B) intermediate morphology, and C) asbestiform. The upper row shows single crystals viewed in the PLM and mounted on a glass fiber that can be rotated to different orientations (FOV = 500, 600, and 700 μm respectively for A, B, and C). The lower two rows are the same samples except they have been placed in an SEM and rotated to different orientations to better characterize their morphology. (Sanchez et al. 2006, with SEM photos courtesy of the RJ Lee Group Inc., Monroeville, Pennsylvania, USA.)

Scanning Electron Microscope (SEM). It is surprising that the SEM has found very little use in studying asbestos, at least in the regulatory area, but it is now becoming more widely used in the study of amphiboles in their natural setting (e.g., RJ Lee 2005; Meeker et al. 2006). The regulatory discipline typically goes from the PLM to the TEM (discussed next) to work with smaller particles such as those found in air samples. However, the SEM is useful in extending particle resolution down to approximately 0.1 μm (i.e., one order of magnitude smaller than the PLM) and showing surface morphology. Also, the SEM has an increased depth in field relative to the PLM.

Another unique advantage of the SEM is that a sample can be rotated to observe it in different orientations. Bandli and Gunter (2001) showed how this method is useful in imaging particles of amphibole to better characterize morphology. The lower two rows of Figure 5 (Sanchez 2007) are the same particles as in the upper row. However, in the lower two rows, the particles were placed inside an SEM and rotated to different orientations so as to better observe their morphology. The spindle stage (placed on a PLM) is used in a similar manner, except that the spindle stage does not have as many degrees of freedom of rotation. Combined PLM and SEM studies are useful for the determination of morphology of amphibole materials.

Transmission Electron Microscope (TEM). With routine operation the TEM can resolve 10 nm particles; samples are imaged by electron transmission and thus the samples must be very thin. The TEM has become one of the most used instruments for asbestos characterization in the regulatory field (Millette 2006). The left column in Figure 6 shows three separate TEM

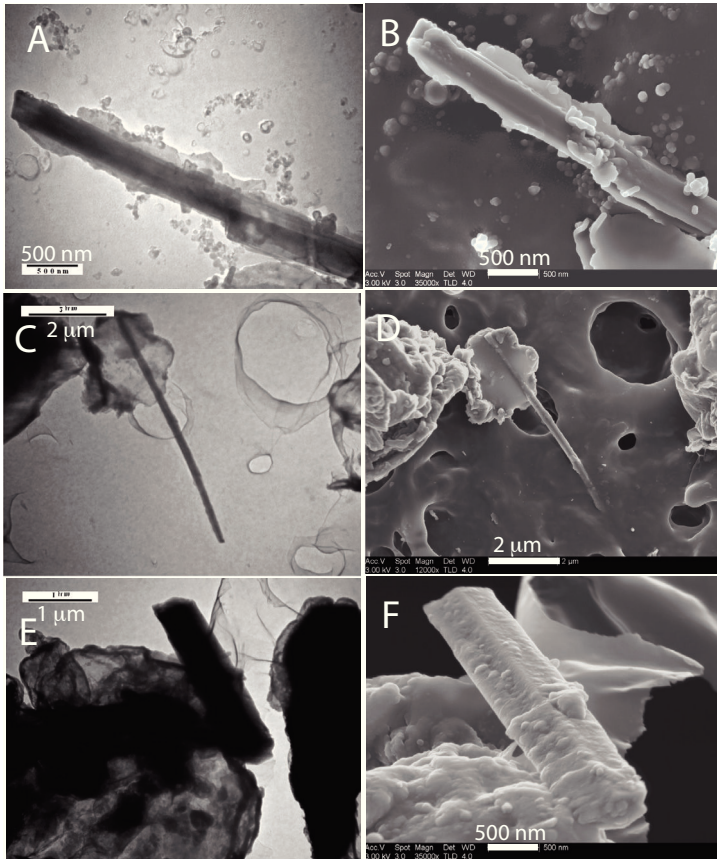


Figure 6. Three amphibole particles collected in air samples from Libby, Montana, imaged in the TEM (left column) and the FESEM (right column). The newer generation FESEMs can obtain magnifications similar to those of a TEM. A & B show an amphibole particle with what appears as wings on its sides. C & D show an amphibole particle with a sheet silicate at one end. In the TEM image, it is unclear if the particle rests on or grows into the sheet silicate; however, the FESEM image shows that the amphibole is grown into the sheet. E & F show a single crystal of amphibole. It is difficult to determine the morphology of the particle in the TEM image, but the FESEM shows a perfect euhedral amphibole with {110} growth faces. (Gunter et al. 2006, images courtesy of the RJ Lee Group Inc., Monroeville, Pennsylvania, USA.)

images obtained on amphibole particles from air samples collected in Libby, Montana. In Figure 6A and 6C, notice that portions of the particles are transparent (i.e., the electrons are going completely through the sample). The TEM is very useful for studying small particles that have been deposited on air filters, and thus determining asbestos content of the in-flowing air.

Field Emission Scanning Electron Microscope (FESEM). The FESEM is a relatively new instrument with some refined design features of the SEM that allow higher resolution than an SEM or TEM. The FESEM can also operate at lower accelerating voltages than older SEMs. Resolution of the FESEM is on the order of 1 nm, at least one order of magnitude greater than the TEM. To date, the FESEM is not routinely used by the regulatory community for analyzing asbestos-containing materials. However, it is starting to find use in the research community for high-resolution imaging of very small particles. The right column of Figure 6 shows the same three particles as the left column, except imaged in an FESEM. The backscattered images in the FESEM allow better characterization of amphibole morphology.

DIFFRACTION METHODS

Positive identification of minerals require more than observing them at higher and higher magnification. Diffraction, either by electrons or X-rays, helps determine the structure of the mineral and aids in identification.

Selected Area Electron Diffraction (SAED). One of the main advantages of using a TEM as in asbestos work is that one can acquire an SAED on the very small particles often found in air samples. Figure 7 shows two particles imaged in a TEM. Below the image (in white squares with dots) are two separate SAED patterns of the two particles. These two patterns look different, suggesting that the two materials are different; interpretation of these patterns show that particle A is an amphibole and particle B is a sheet silicate.

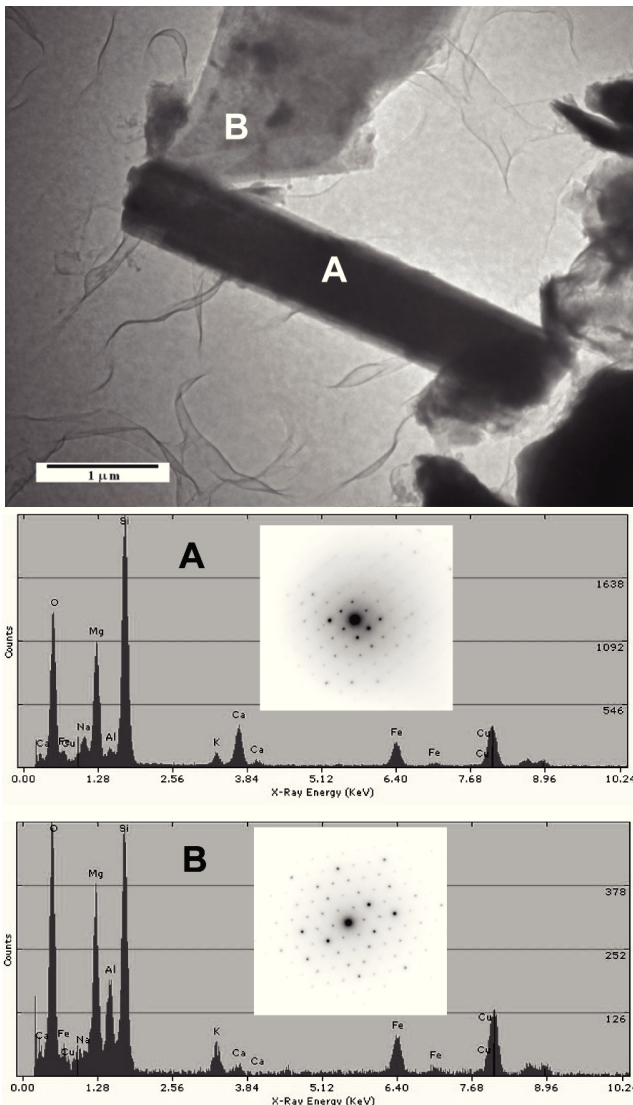


Figure 7. Along with imaging, TEMs can provide chemical and structural information needed to identify a particle. Shown here is a TEM image of two particles, with corresponding EDS plots and SAED patterns. Based on interpretation of compositional and diffraction data, particle A is an amphibole and particle B is a sheet silicate. (Gunter et al. 2006, images courtesy of the RJ Lee Group Inc., Monroeville, Pennsylvania, USA.)

Single Crystal X-ray Diffraction. This method is not used in routine analysis of asbestos particles, probably because in single crystal X-ray diffraction one strives to select perfect single crystals to obtain diffraction data. These samples are usually in the order of 20–200 μm in size, and are thus larger than respirable asbestos fibers. However, single crystal X-ray diffraction photographs can show which samples are monocrystalline or polycrystalline. For instance, Figure 8 shows single-crystal X-ray diffraction patterns of both monocrystalline and polycrystalline samples of elongated amphibole particles. Figure 8A is of a monocrystalline particle of a similar morphology as that in Figure 5B, and thus nonasbestiform, whereas Figure 8B is of a polycrystalline sample (indicating it is composed of several particles and thus would be asbestiform) such as that shown in Figure 5C. This method could find use in larger samples by distinguishing if particles are single crystals or aggregates of crystals.

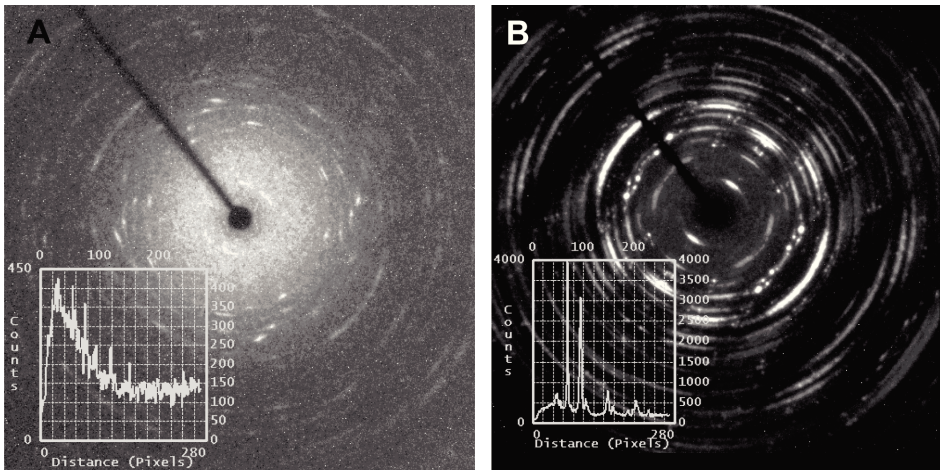


Figure 8. Two rotation X-ray diffraction photographs from Bandli et al. (2003) showing different crystallinities of amphibole particles from Libby, Montana. A) What Bandli et al. termed “monocrystalline” and B) “polycrystalline” based on the resultant diffraction pattern (i.e., the diffraction spots are more spread out in the polycrystalline material). The pattern would be rings if the particle was a powder.

Powder X-ray Diffraction (XRD). XRD methods have also found very little use in dealing with asbestos characterization, even though over 15 years ago, Addison and Davies (1990) showed how it could be used to quantify trace amounts of amphibole in chrysotile and vermiculite ores. One reason it has found little use is the typical concern of the regulatory community is in dealing with very small samples and even individual particles. However given sample sizes of 100 mg and up, XRD can be a valuable method to not only identify the minerals present, but also to quantify the amounts of individual minerals. Currently, the amounts of different minerals are often found by point counting with the PLM or TEM. With newer X-ray diffractometers and better software, it is now possible to measure trace amounts of amphiboles in bulk materials (Sanchez and Gunter 2006). Figure 9 shows three separate XRD scans; both Figures 9A and 9B are chrysotile ores. The lower diffraction scan in each has a count time of 9 s showing the major chrysotile peak. The three scans above (the longer 20 scans) were done at much longer count times (180 s). The areas of major talc and amphibole peaks are outlined on the figures, and it appears that two of the three scans shown might contain small amounts of amphibole (Fig. 9A), whereas in Figure 9B, it appears there is more amphibole in the chrysotile ore. It should be pointed out that this method says nothing about the morphology of the materials. However, the morphology can be determined by one of the

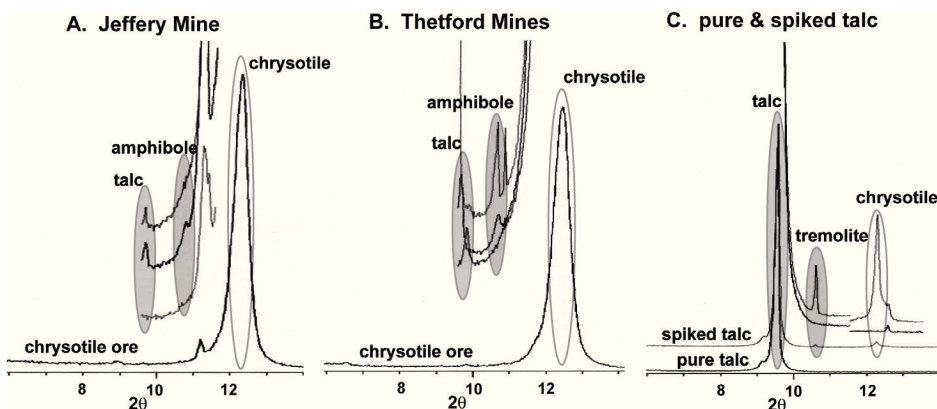


Figure 9. A set of powder X-ray diffraction scans for two chrysotile ores (A and B) and a pure- and tremolite/chrysotile-spiked talc sample. The peak regions for talc, amphibole, and chrysotile are highlighted with vertical ellipses. A) The longer 2θ lower scan shows a chrysotile ore from the Jeffery Mine (count time = 9 s) with its associated shorter 2θ scan (count time = 180 s) directly above it. The other two scans are from other ores from the same mine. One of the scans shows no amphiboles, while the other two show trace amounts. B) The longer 2θ lower scan is a chrysotile ore from the Thetford area (count time = 9 s) with its associated shorter 2θ , longer count time scans with two of three containing amphiboles. C) Long 2θ scan of a pure and 1% tremolite / 1% chrysotile spiked sample (count time = 9 s). The corresponding short 2θ scans for the pure and spiked samples show that the pure samples contain no tremolite or chrysotile, while the spiked sample shows significant peaks at the 1% level.

microscopic methods already discussed. Figure 9C shows a talc sample in both its pure and spiked states. In the spiked state, 1% chrysotile and 1% tremolite have been added. Notice how these peaks are observable on the 9 s scans and are clearly visible on the 180 s scans. This method easily detects minerals present at the 1% or lower level.

Figure 10 shows a recent study (Gunter et al. 2007) using XRD to characterize a suite of samples from a now-closed asbestos mine in Canada. Figure 10A shows diffraction scans for these samples. As expected, these samples all contain chrysotile as the major component, and also brucite. Figure 10B shows a series of scans collected at longer count times than in Figure 10A. The Figure 10B scans were used to ascertain if any of the samples contain trace levels of amphibole. Observation of these scans shows that #10b2 contains a small amount of amphibole. To quantify that amount, a pure chrysotile ore was spiked with different amounts of tremolite; the resultant diffraction patterns are shown in Figure 10C. Notice that the detection limit is on the order of 500-1000 ppm, and sample #10b2 seems to contain approximately 1000 ppm of amphibole. Thus the maximum amount of amphibole asbestos could be 1000 ppm. However, if the amphibole was of mixed morphology (e.g., 50% nonasbestiform and 50% asbestiform), then the sample would only contain 500 ppm amphibole asbestos.

Chemical determination

Going hand in hand with diffraction data on particles, chemical data is needed for positive mineral identification as well as for mineral characterization. The methods presented below are very similar in scope to the diffraction methods presented above in that some work for individual particles while others require bulk samples.

Wavelength Dispersive Spectrometry (WDS). WDS is the most precise way to determine the chemical composition of minerals. WDS is also synonymous with the use of EPMA (electron probe micro analyzer). The sample preparation for this method is very important and requires flat, well-polished mineral samples; unfortunately asbestos particles are often too

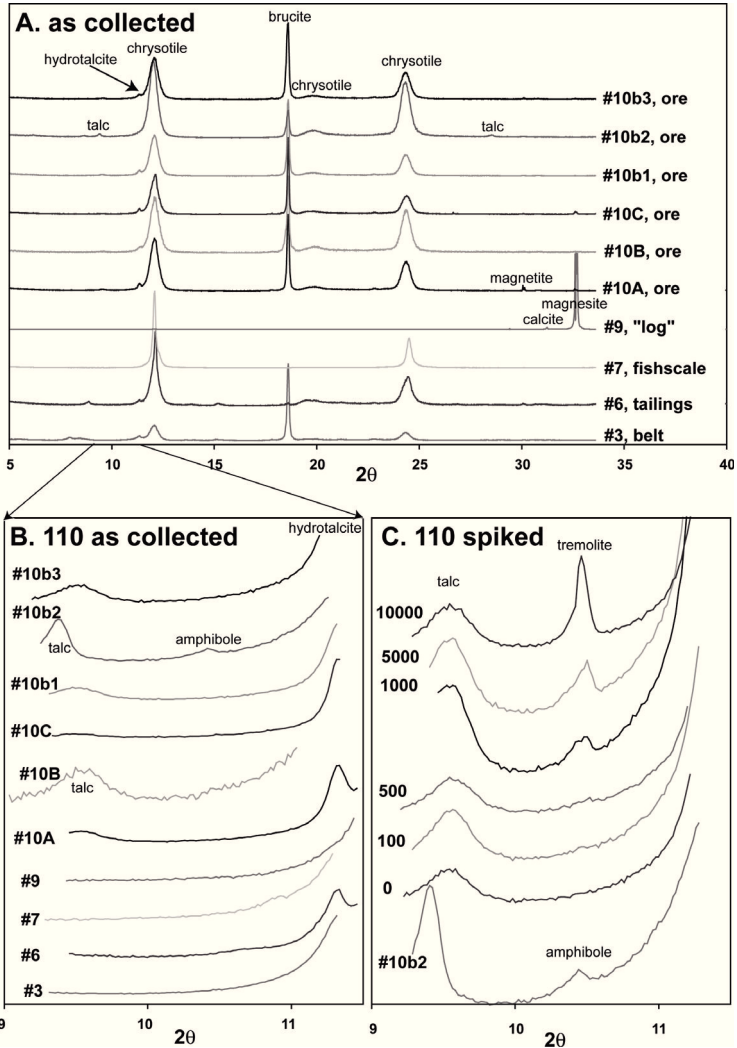


Figure 10. A series of powder X-ray diffraction scans obtained from a suite of samples collected at the former Carey Canadian chrysotile mine. A) The ten samples collected from the mine with brief names (count times = 9 s). B) The same set of samples as in A, except over the 2θ region corresponding to the 110 peak in amphibole with count times of 180 s; all the samples appear amphibole free except #10b2. C) Sample #10b2 is overlain by a series of tremolite-spiked samples made from sample #10b3. The scans over the 110 region show amphibole detection at the 500 ppm level (count times = 180 s; modified from Gunter et al. 2007).

small for this type of sample preparation. This is the best method for determining the chemical composition of an amphibole to determine its species. Figure 2 shows a series of chemical analyses determined by WDS on an EPMA for different amphiboles from Libby, Montana (Meeker et al. 2003). WDS is rarely used in the regulatory community but are widely used in the geological community for the precise and accurate chemical determination of minerals. Even though these instruments are costly and often require a dedicated technician, they are required for precise and accurate chemical analysis of minerals.

Energy Dispersive Spectrometry (EDS). EDS is by far the most routine method for chemical analysis related to asbestos work. EDS systems are commonly on both SEMs and TEMs. Thus one can obtain an EDS spectrum and a semi-quantitative chemical composition of micron-sized areas in the SEM and submicron-sized areas in the TEM. However, EDS data are not as precise or accurate as WDS data. An example showing the differences of precision is shown in Figure 2. The circles on the plot represent WDS data obtained with the EPMA, and the crosses represent EDS data on the same samples. Notice also that the error bars (in the upper right hand corner of the plot) are bigger for EDS than for WDS. However, even though EDS is less precise and accurate than WDS, WDS cannot commonly be used on the smaller particles often encountered in air samples because the samples are not large enough to prepare as polished mounts. Moreover, the accuracy of the EDS data can often be enhanced by using standards (see Gunter et al. 2007). Lastly, along with SEMs and TEMs, FESEMs can also be equipped with an EDS. On FESEMs, light-element EDS spectra can be obtained at voltages as low as 3 kV, which greatly reduces the excitation volume, allowing for chemical determination of particles down 200-300 nm (Gunter et al. 2006).

Figure 7 shows an EDS spectrum from the two particles shown in the accompanying TEM photograph. In this case, with the use of the TEM, one can observe the morphology of the particle, obtain the structural information on the particle by obtaining an SAED pattern, and determine the composition of the particle by obtaining an EDS (also shown in the figure), all on particle sizes down to a micron. This trilogy of data makes the TEM a useful instrument for studying small particles.

X-Ray fluorescence (XRF), Inductively Coupled Plasma (ICP) and Atomic Absorption (AA). XRF, ICP, and AA are all bulk methods that typically require at least a gram of material. These methods are often used in geology to determine the composition of a rock by first crushing and then homogenizing it. In Geology, these methods are often referred to as "whole-rock analysis." Williams-Jones et al. (2001) suggested this method might be used to determine the tremolite content in chrysotile ores. This suggestion was based upon measuring the Ca content of the ore and assuming the only source for Ca is tremolite. Gunter et al. (2007) adopted this method and used the Ca content as a proxy for the tremolite content in the ten samples shown in Figure 10. For each of these ten samples, they measured the Ca content by AA. Figure 11 shows an ideal content of Ca ppm and tremolite concentration in a chrysotile ore (squares). By powder X-ray diffraction, Gunter et al. (2007) determined a small fraction of magnesite occurred in the sample, and the magnesite contained a small amount of Ca as shown by SEM EDS. Thus they acid-treated the samples to remove the magnesite. As Figure 11 shows, this method seems to work for the unique case of tremolite in chrysotile. There might be other mineral relations whereby one can use whole-rock analysis to gain a semi-quantitative estimate for trace minerals.

Laser Ablation Mass Spectroscopy (LAMMS). This is a fairly new method in geology and requires little sample preparation while providing precise and accurate analysis of many trace elements and their isotopes. To our knowledge, no one has yet published any of this type of data on asbestos minerals. An issue still confronting mineralogists is the formation of asbestos minerals. We know part of the answer relates to the material forming into a nonhydrostatic stress field; however, possible chemical differences may have an effect. For instance, we know that trace-element compositions can cause different habits of calcite. Currently, some preliminary work (Sanchez 2007) shows different trace-element compositions in fibers and fragments of the same amphibole sample (Fig. 4C).

Mössbauer spectroscopy. To fully characterize amphiboles, one needs to measure $\text{Fe}^{3+}/\Sigma\text{Fe}$ content; while several methods exist to do this, Mössbauer spectroscopy has been the only one used to our knowledge on asbestiform samples. In the health effects field, it has often been

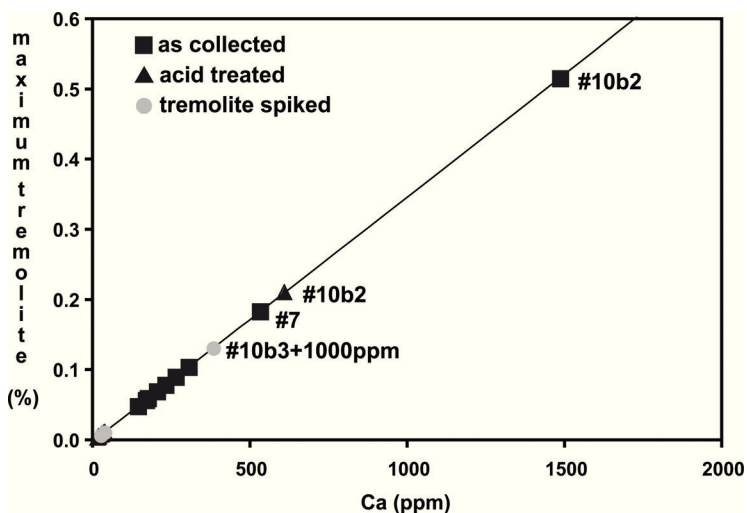


Figure 11. A plot of calculated maximum tremolite content of the ten natural samples of chrysotile ore (squares), the same ten samples after microwave acid treatment used to remove the carbonates (triangles), and three tremolite-spiked samples (circles) as a function of measured Ca content. The line represents the ideal relation between observed Ca and maximum tremolite content. This type of relation could be used to help predict tremolite content in a chrysotile ore in near real-time as in an actual mining operation (Gunter et al. 2007).

hypothesized that the Fenton reaction may play a major role in lung disease, and this reaction would be largely controlled by Fe^{2+} . Thus the oxidation state of Fe is not only important to fully characterize the amphibole, but may play a role in disease. Interestingly, Gianfagna et al. (2007) found differences in the $\text{Fe}^{3+}/\Sigma\text{Fe}$ values for asbestiform and nonasbestiform morphologies of fluoro-edenites from Biancavilla.

MORPHOLOGY MATTERS

It might seem that too much emphasis is being placed on morphology in this chapter, but morphology is at the heart of the issues involving the health effects of exposure to amphiboles. There have been many papers on this single issue over the years, along with several different methods proposed on how to distinguish between fibers and fragments (e.g., Wylie 1979; Nolan et al. 1991; Brown and Gunter 2003). And some of the recommendations for nomenclature to be used to discuss morphology now date back almost 30 years (e.g., Zoltai and Wylie 1979). First, there is the problem that methods developed for commercial asbestos issues are now being applied to all amphiboles, even those found in the natural setting. When this is done, particles that clearly are not asbestos, or even asbestiform, can often meet the definition of asbestos, such as all the particles shown in the grain mounts in Figure 4 and the single crystal shown in Figure 5A. This has led to ongoing issues (discussed later) with amphiboles located in El Dorado Hills, California, where the EPA and its subcontractors (Ecology and Environment 2005) termed many particles as asbestos while another group found almost none (RJ Lee 2005), looking at the same material. As another example, by applying standard fiber-counting methods, Brown and Gunter (2003) found that 48% of the particles in the sample shown in Figure 4B meet the definition of a fiber, whereas none of them have the morphology of a fiber. What is currently needed are clear definitions of what is and what is not a fiber, especially when applied to amphiboles found in a natural setting.

Figure 12 shows an approximately 1-mm long particle of amphibole from Libby in plane- (A) and cross-polarized (B) light. From the left side, there is no argument that the particle is asbestiform; however, from the right side, the particle appears nonasbestiform. Thus a single particle can have different morphologies at either end. Scale also becomes an issue in trying to determine morphology. Figure 13 shows a series of FESEM images at low (left column) and high (right column) magnification. The NIST (The US National Institute of Standards and Technology) crocidolite (Figs. 13A, B) is clearly a fibrous habit in Figure 13A but somewhat less so in Figure 13B. This is a sample similar to that in Figure 1A where there is no doubt that the material is fibrous. Thus as the scale decreases, as is common for single particles found in air sampling, it becomes more difficult to tell fibers from fragments. The particles shown in Figures 13C and 13D are of the NIST tremolite-asbestos standard; this material appears even less fibrous at this scale. Brown and Gunter (2003) found this material to be 100% fibers based on 3:1 aspect ratio counting rules and 92% fibers based on morphology. The last sample in Figures 13E and 13F is an amphibole from Libby, Montana. This sample appears intermediate in morphology from the other two. In a PLM study of this sample, Brown and Gunter (2003) found the samples to be 95% fibers by counting rules, while they found it to be 36% fibers and 33% fragments based on morphology. Notice that these numbers do not sum to 100; they judged they could not determine between fibers or fragments for 31% of the particles.

Going hand-in-hand with trying to determine the morphology of amphiboles are explanations for the formation of asbestos and asbestiform amphiboles (Zoltai 1981). There seems to be a general agreement that stress fields are required to form asbestos. In fact, there are two types of asbestos fibers: cross-fibers that grow to fill joints in rocks (i.e., the growth direction is across the vein) and slip fibers that form along the face of a fault plane in the rock (i.e., the growth occurs between the layers of the slipping surface). Ross and Nolan (2003) give a thorough discussion of asbestos formation in ophiolite complexes, along with associated health concerns.

Others have noticed that asbestiform amphiboles seem to have low (<0.15) apfu values for Al (Dorling and Zussman 1987; Verkouteren and Wylie 2000). In these works, the authors examined amphiboles of differing morphologies from various locations and found no asbesti-

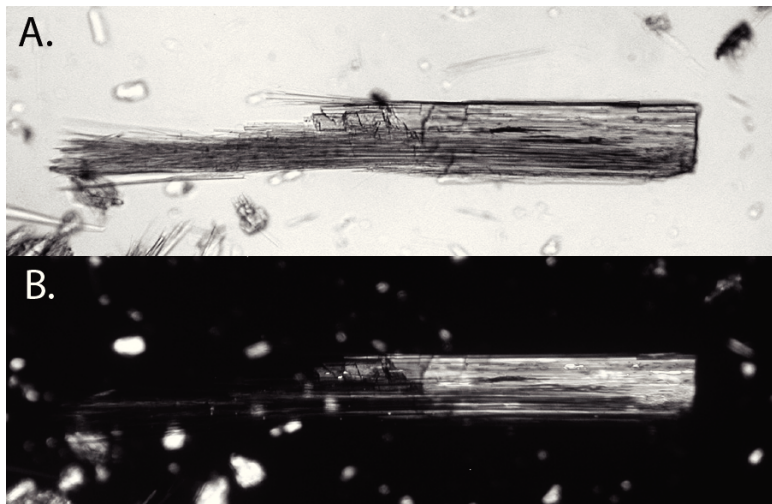


Figure 12. PLM photographs of an amphibole particle from Libby, Montana, in plane-polarized light (A) and crossed-polarized light (B). Notice how the right side of the particle is nonasbestiform, while the left side appears asbestiform (FOV = 1.2 mm).

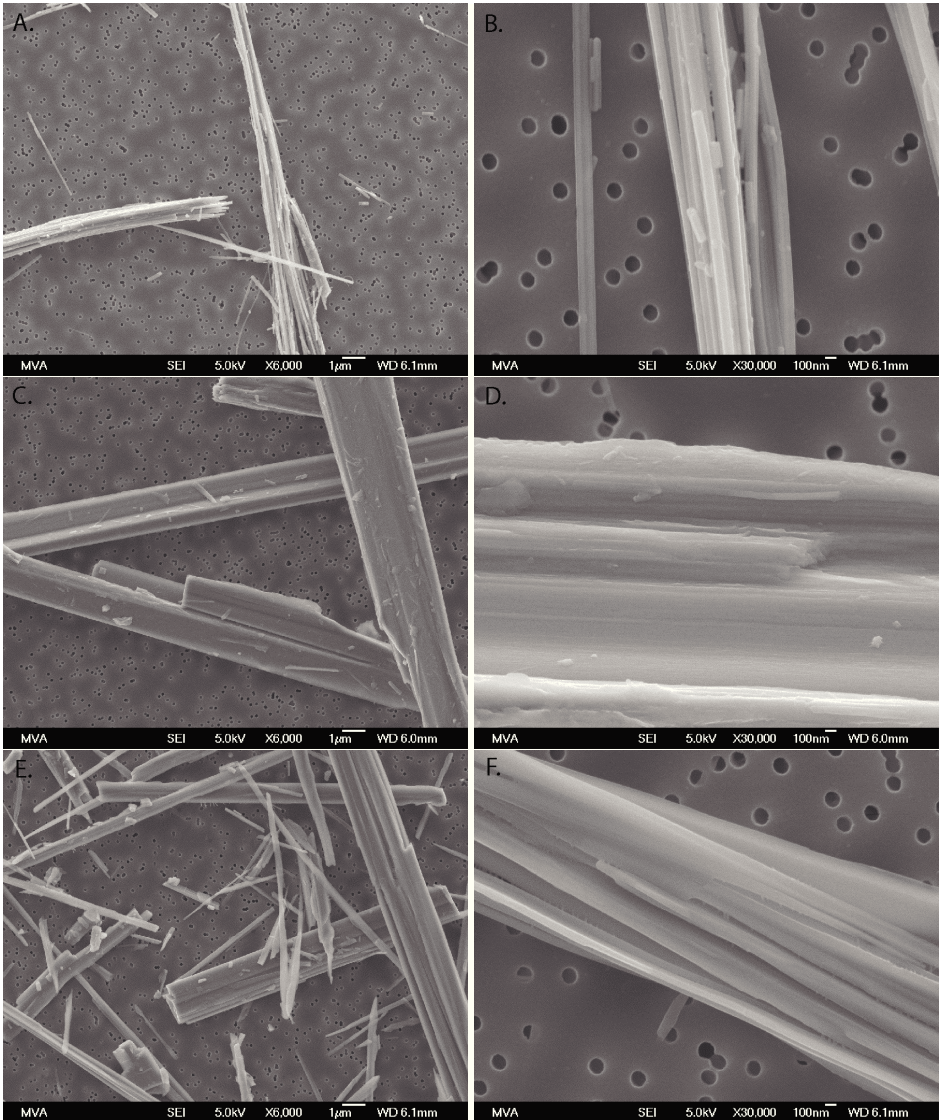


Figure 13. A series of FESEM images at low (left column) and high (right column) magnification of three separate amphiboles. A and B show NIST fibrous riebeckite (i.e., crocidolite), C and D show the NIST tremolite asbestos standard, and E and F show amphiboles from Libby. At the higher magnifications, note that both the riebeckite and Libby sample appear separable into particles on the range of 100 nm, while the NIST tremolite does not appear to have the closely spaced partings. (Photos courtesy of Bryan Bandli, MVA Scientific Consultants, Duluth, Georgia, USA.)

form varieties with Al above 0.15 apfu. The asbestiform fluoro-edenite recently found in Sicily (Gianfagna and Oberti 2001) has an Al content of 0.5 apfu, and violates this trend. There are two possible reasons why Al content could affect morphology: (1) it inhibits the formation of fibers or (2) it relates to the fact the Al is rare in the mafic rocks where most asbestiform amphiboles occur. (The asbestiform fluoro-edenite is associated with more Si- (and in turn) Al-rich rocks.)

Returning to the issue of mixed morphology shown in Figure 12; Figure 14A shows a thin-section photograph of the asbestiform tremolite in Figure 4C. The fibers are obvious, but so are single crystals of tremolite in the center of the image. Also, note how the single crystals appear to be rotated with respect to the fabric formed by the fibers; this rotation indicates a nonhydrostatic stress field, supporting the idea that these asbestiform samples form in rocks that have undergone stress. However, what is also interesting in this photo is that single crystals of amphibole are directly associated with fibers. Figure 14B, a thin section of the rock shown in Figure 4D, is even more intriguing. Here, what appears as a perfect euhedral single crystal of amphibole is in contact with fibrous amphiboles of the same composition (Sanchez 2007). In this case, there are no stress indicators apparent (and for those with a keen eye for optics, note the right side of the crystal exhibits isochromes showing how the sample is dipping into the slide). This single crystal also exhibits perfect {110} growth (*not* cleavage) faces. We know this because the crystal was not broken. This also reinforces the above comments concerning amphiboles as fibers and fragments. Lastly, it is worth pointing out here that the amphiboles at Libby formed from low-temperature alteration of pyroxenes, which differs from amphibole formation in metamorphic rocks.

While regulatory definitions are important, health concerns of exposed individuals are more so. The ongoing debate in this arena is this: are particles derived from non-asbestos sources just as harmful as those derived from asbestos sources? Health studies (e.g., Davis et al. 1991) presented to the US Occupational Safety and Health Administration (OSHA 1992) suggest regulating only the asbestiform varieties of the regulated amphibole minerals because the nonasbestiform amphiboles seems to pose less of a health risk to humans. This would mean that anthophyllite, actinolite, and tremolite would only be regulated if they occurred with asbestiform habit (by definition, crocidolite and amosite always have this habit). Currently, there is debate over the health effects of respirable amphibole particles, regardless of whether they derive from an asbestiform or nonasbestiform source.

REGULATORY AND LEGAL ISSUES

The regulatory and legal communities are more foreign to most geologists than the medical community. Yet as geologists, we must: (1) interact with these communities to help establish

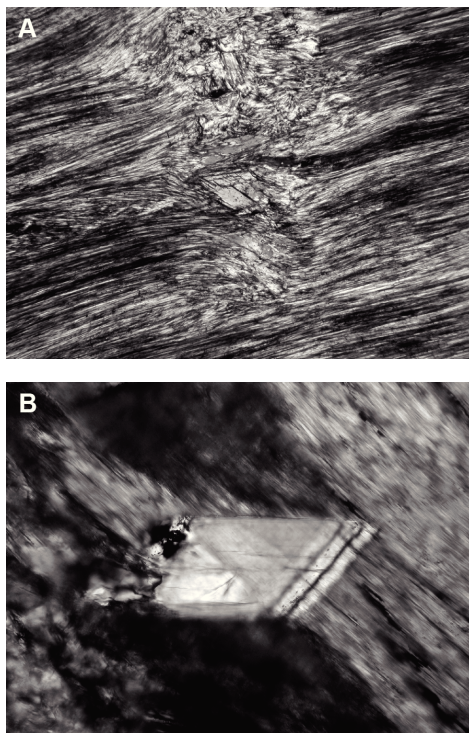


Figure 14. Photomicrographs of two thin sections of asbestiform amphiboles containing euhedral amphiboles. A) Asbestiform material encapsulating a single crystal of tremolite with what appears to be a gradational contact with the fibrous material (FOV = 4 mm, this is the same sample shown in Fig. 4C). B) This is the same sample shown in Figure 4D except at higher magnification; the euhedral crystal has a sharp contact with the fibers (FOV = 1 mm).

regulations that protect worker health while not hamstringing industry, and (2) assist in establishing laws that promote this end. Over the years, there has been some success in setting exposure limits in the industrial setting. Currently, the issues at hand deal more with natural (i.e., the nonanthropogenic) exposure. Thus it is even more critical for geologists to assist in this realm because now we have moved the exposure from the factories to the geological environment.

Regulated mineral species

Currently, the OSHA classifies asbestos as: chrysotile, amosite, crocidolite, tremolite asbestos, anthophyllite asbestos, and actinolite asbestos (OSHA 29 CFR 1910.1001 subpart Z (b)). Asbestos has been added to the name of the last three amphiboles to distinguish them from their massive forms. There are no specific names for the asbestiform varieties of anthophyllite, tremolite, or actinolite, probably because these species have never occurred in commercial asbestos bodies (except for anthophyllite). As reported by the U.S. Senate Committee on the Judiciary (April 19, 2005), there is currently a bill proposing the term asbestos to include: chrysotile, amosite, crocidolite; tremolite asbestos; winchite asbestos; richterite asbestos; anthophyllite asbestos; actinolite asbestos; any of the listed minerals "that has been chemically treated or altered and any asbestiform variety, type or component thereof; asbestos-containing material, such as asbestos-containing products, automotive or industrial parts or components, equipment, improvement to real property, and any other material that contains asbestos in any physical or chemical form." This redefinition may or may not pass, but it is the result of the majority of the amphibole species being nonregulated and issues surrounding the discovery that winchite and richterite are the most abundant amphibole species in the vermiculite deposit near Libby, Montana.

In the European Union (EU), Directive 2003/18/EC of the European Parliament and of the European Council of 27 March 2003 has modified Directive 83/477/EEC, so that the six minerals classified as asbestos are: actinolite of asbestos (n. 77536-66-4 of the Chemical Abstract Service); grunerite of asbestos (or amosite) n. 12172-73-5 of the CAS); anthophyllite of asbestos (n. 77536-67-5 of the CAS); chrysotile (n. 12001-29-5 of the CAS); crocidolite (n. 12001-28-4 of the CAS); tremolite of asbestos (n. 77536-68-6 of the CAS). Member states belonging to the EU, as recipients of the above-mentioned directive, are therefore obliged to implement it in their own legislation and to conform to it by passing the necessary regulations and adopting the new nomenclature by April 15, 2006, when the Directive came into force. The asbestiform amphibole fluoro-edenite, to date found only in Sicily, Italy, and linked to the onset of mesothelioma, has not been included by the Directive as belonging to asbestos.

There are restrictions for the disposal of asbestos in Italy. Asbestos in general (mostly chrysotile, which makes up 95% of asbestos, but also actinolite, anthophyllite, amosite, crocidolite, and tremolite). These are the five amphiboles classified as asbestos (amianto in Italian) according to Italian law DPR 915/82. Fluoro-edenite is currently not one of them, although a site remediation has been carried out in the Biancavilla area based upon health concerns there for the local citizens. Asbestos-containing materials are classified as such when they release fibers in an amount greater than 100 mg/Kg (i.e., 0.01%). They should be disposed of in special sites, depending on their *index of release (I.R.) = wt% asbestos/relative density* (Table 3), and special procedures are imposed to protect workers during the entire clearing, disposal, and beneficiation work. The preferred special types of disposal sites are mostly sites just for asbestos because: (1) it creates fewer problems than the disposal of multiple types of waste; (2) they have higher levels of environmental security than multiple disposal sites; and (3) there is no requirement about closing the system to underground waters because fibers are dangerous only when airborne. Asbestos waste can, however, be mixed with drilling muds and with gypsum produced in the fume-desulfuration process because these two wastes help bind the asbestos and minimize possible re-exposure. In general, disposal is done after packing asbestos-containing materials in sealed polyethylene bags of 0.15 mm thickness, which then

Table 3. Disposal sites for different types of asbestos-containing waste.

Asbestos-containing waste	Dust viz. free fibers (mg kg ⁻¹ : min÷max)	Dump Type
Asbestos-cement cover board (new)	35÷105	2 A
Asbestos-cement cover board (damaged)	75÷150	2 B
Asbestos-cement cover board (strongly damaged)	90÷200	2 B
Asbestos-cement pipe (new)	35÷70	2 A
Asbestos-cement pipe (damaged)	60÷120	2 B
Asbestos-cement wallboard (new)	90÷150	2 B
Asbestos-cement wallboard (damaged)	90÷400	2 B
Asbestos board: gypsum viz. carbonate binder	0.1×10 ⁶ ÷0.2×10 ⁶	2 C
Asbestos board: quartz binder	0.1×10 ⁶ ÷0.2×10 ⁶	2 B+
Asbestos-bearing particle board	0.1×10 ⁶ ÷0.2×10 ⁶	by case
Asbestos-vinyl tiles (new)	0÷10	2 A
Asbestos-vinyl tiles (cut, pierced, damaged)	5÷40	2 B
Asbestos-reinforced polymeric components	not determined	by case
Asbestos felts and bulk insulations	0.1×10 ³ ÷0.7×10 ³	2 C
Asbestos-based powder viz. flake fillers	indeterminable	2 C
Asbestos paper and cardboard	0.1×10 ⁶ ÷0.2×10 ⁶	2 C
Asbestos sprayed (encapsulated)	0.1×10 ⁶ ÷0.2×10 ⁶	2 C
Asbestos sprayed (not encapsulated)	0.1×10 ⁶ ÷0.2×10 ⁶	2 C
Asbestos tissues, textiles, ropes	0.1×10 ⁶ ÷0.2×10 ⁶	2 C
Friction materials (new)	50÷500	2 B
Friction materials (used)	200÷3000	2 B+
Friction material dust	indeterminable	2 C
Other materials from asbestos-bearing wastes that have been modified in some manner		Case by case

Dump types:

2A – for compact asbestos waste derived from demolitions, buildings and diggings;

2B – for waste containing loose asbestos fibers and/or fine dust < 100 mg Kg-1;

2B+ – the same, but with > 100 < 10000 mg Kg-1 (0.01-1 wt% total asbestos);

2C – insulated dumps appropriate for waste with > 10000 mg Kg-1 loose fibers (>1 wt%)

are packed into large metallic cans for further safety. If the asbestos material is friable, the plastic bags must be doubled and thermo-sealed; they should not exceed 1 m³ in size before being disposed. Most disposal cost is shouldered by the private person compelled to clear asbestos from their dwelling, with a small contribution by local authorities. A widespread illegal trade of asbestos-containing waste is known but is difficult to control.

It might seem strange to a mineralogist to read the phrase “How asbestos is defined is a legal question...” yet this quote is taken directly from the ruling of a U.S. federal judge dealing with the federal case of W.R. Grace (Molloy 2006). What prompted the judge to make this ruling were issues surrounding the species names of the amphiboles in the former vermiculite mine of Libby, Montana. The majority of the amphiboles from the deposit are winchite or richterite (Fig. 2). Neither winchite asbestos nor richterite asbestos are listed as regulated asbestos minerals. Thus even though this mineral might meet the definition of asbestos from a mineralogical perspective, it does not from a legal one. The judge’s argument does not even need to refer to morphology because these particular amphibole species were not listed as regulated materials. Clearly the issues surrounding these nonregulated amphibole species are of concern to the regulatory, legal, and mineralogical communities. The mineralogical community must first characterize these materials, then the legal and regulatory communities must establish laws and regulations to protect the public’s health. When these nonregulated

amphiboles were first discovered at the former mine, many in the geological community wanted to change the regulatory rules to include all amphiboles that met the morphological definition of asbestos. The problem with making that change is that determination of mineral species is very objective while determination of morphology can be very subjective.

The major issue with morphology as discussed in other sections of this chapter is that the methods used by the regulatory community were established to deal with asbestos in the industrial setting (i.e., the regulated and widely used asbestos minerals). When these same methods are applied to amphiboles in nonasbestos deposits, which are the great majority of amphiboles on the Earth, several issues arise which need to be resolved.

GEOLOGICAL OCCURRENCE

To those in the geological community, it seems redundant to make the statement that asbestos occurs in rocks naturally; however, as previously stated, many people believe that it is manufactured. Clearly asbestos is mined and it is associated with certain geological features. Amphiboles often form during mountain building events, and as such correlate to current or past tectonically active regions (e.g., Ross 1981; Ross and Nolan 2003). Figure 15 by Van Gosen (2006a) shows the geological distribution of asbestos occurrences in the eastern USA. Notice the correlation between the asbestos locations and the trend of the Appalachian Mountains. Van Gosen (2006b) produced a similar map for the central USA, and as one might expect, there are very few asbestos occurrences there. He is currently compiling a map for the western USA (Van Gosen personal communication). A similar map is currently being compiled for all Italian occurrences (F. de Grisogono personal communication); it will complement and update the sketch maps published years ago only for the Piemontese Alps (Belluso et al. 1994, 1997).

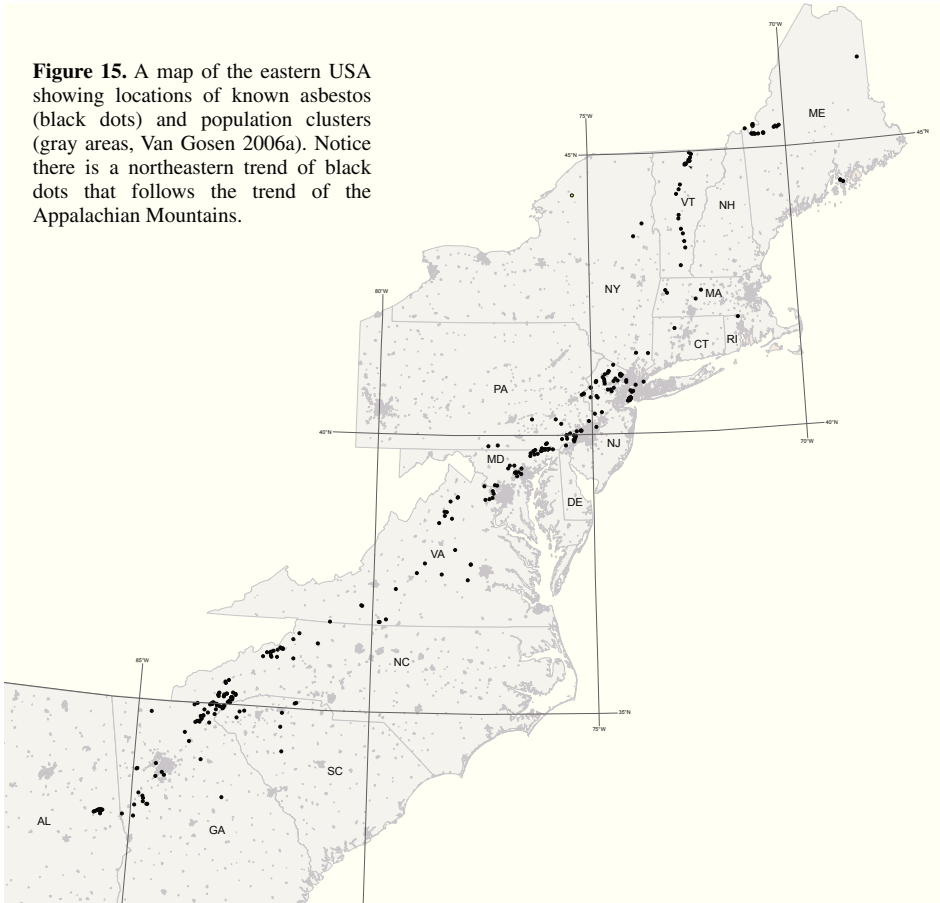
In this section, we provide an overview of the formation of different types of amphibole in general and amphibole asbestos in particular, because (as we are aware in the geological community) there are orders-of-magnitude more amphibole than amphibole asbestos in the geologic environment. From the environmental-exposure concern, the weathered products from geological formations are presently more of an issue than the geological formations themselves. Thus we will spend some time discussing amphiboles in soils and other unconsolidated materials. The geological conditions that conspire to form amphibole asbestos and asbestiform amphiboles (i.e., some type of regional stress environment) will also form other types of fibrous minerals. Thus we also include a section discussing the occurrences of these amphiboles with other fibrous minerals.

Association with rock type

In a general sense, we must consider the major rock types containing amphiboles. Martin (2007, this volume) discusses the occurrence of amphiboles in igneous rocks and Schumacher (2007, this volume) discusses the occurrence of amphiboles in metamorphic rocks, so readers are referred to those chapters for more general discussions on amphibole occurrence. In this chapter we will limit our discussion to the formation of commercial amphibole-asbestos and to areas where asbestiform amphiboles may occur.

Recall that there are two major commercial amphibole asbestos minerals: crocidolite (asbestiform riebeckite), and amosite (asbestiform grunerite). Both occur in banded ironstones. The name “amosite” derives from the Asbestos Mines of South Africa Company, reminding us where it occurs and was mined. On the other hand, crocidolite has been mined in three areas: South Africa, Bolivia, and Australia. Figure 1a shows a photograph of Bolivian crocidolite which appears as a bundle of blue fibers over six inches long; there is no question that the material is fibrous, looking more like human hair than a mineral.

Figure 15. A map of the eastern USA showing locations of known asbestos (black dots) and population clusters (gray areas, Van Gosen 2006a). Notice there is a northeastern trend of black dots that follows the trend of the Appalachian Mountains.



Other amphiboles, most notably anthophyllite, tremolite, and actinolite, will sometimes occur in an asbestiform habit. For these amphiboles to form in this habit, a nonhydrostatic stress field is necessary. Ophiolite complexes favor the formation of asbestos minerals, especially Mg-rich ones, based on the original composition of the parent rock, *P* and *T* conditions, and stress fields. It is in these ophiolite complexes where much of this chrysotile asbestos also occurs. Thus, actinolite, tremolite, and anthophyllite can occur as accessory minerals in association with chrysotile asbestos. For an in-depth discussion of chrysotile deposits and associated amphiboles, see Ross and Nolan (2003) and Ross (1981, 1984), also Veblen and Wylie (1993) provide overviews of the formation of amphiboles.

Amphiboles can also form as low-temperature alteration products of pyroxenes, as at the now closed vermiculite mine in Libby, Montana. The amphiboles in this deposit occur in different morphologies (Figs. 1B, 4D, 5, 6, 12, 14). While some of the amphiboles in the deposit are pyroxene alteration products, amphiboles also occur between the layers of sheet silicates from the deposit. The latter was noted on a macroscale by Clark et al. (2003) and recently on a microscale by Gunter et al. (2006). One interesting aspect of the amphiboles between the sheet-silicate layers is the amphibole dimensions and aspect ratios are similar to those of asbestiform asbestos, but they do not meet the definition of asbestiform morphology (i.e., they were not formed by length-wise separation of amphiboles into fibers). Figure 6

shows examples of amphibole particles occurring as small single crystals between the sheets; this mode of formation is discussed in a following section dealing with Libby.

Association with other fibrous minerals

Amphibole fibers can occur both with mineral fibers of the same species and, as often occurs, with different species to form: (1) bundles of tightly packaged fibers, with fiber axes lying parallel or sub-parallel to the length of the bundle, and (2) aggregates of randomly oriented fibers. The former type of intergrowths have been known for a long time (e.g., the oriented association of tremolite fibers with talc fibers and anthophyllite fibers with talc fibers, Stemple and Brindley 1960; Virta 1985). In this kind of association, the fibers are usually crystallographically rotated with respect to each other and not correlated by twinning operations.

An investigation whose purpose was to determine which types of amphibole occur in vermiculite showed that fibrous bundles are made up of tremolite and actinolite with variable quantities of asbestiform anthophyllite, winchite, and richterite, fibers of diopside, hornblende and talc, vermiculite, calcite, and quartz with an apparently fibrous habit (Atkinson et al. 1982; Wylie and Verkourter 2000). Tremolite fibers are present as accessory minerals in many talc deposits, and in some, tremolite is associated with asbestiform winchite and richterite (Van Gosen et al. 2004).

In the serpentinitic rocks of the Piedmont Zone of the Western Alps, fibers of asbestos occur in association with fibrous antigorite (Belluso et al. 1994). Talc lamellae develop from the grain boundaries, as with anthophyllite (Fig. 16). It is not uncommon to see asbestos fibers associated with crystals of the same (but not asbestiform) species, such as fibrils of anthophyllite surrounding coarse-grained anthophyllite crystals (Veblen 1980). This feature is shown in Figure 14 where fibrous amphibole occurs surrounding single crystals of amphibole.

In some samples, the boundaries between anthophyllite fibers are partially filled with talc, antigorite, chrysotile, and chlorite. These minerals replace amphibole during a retrograde metamorphic hydration reaction (Veblen 1980). These species develop along the entire length of the amphibole fibers, so they too are fibrous; however, they are only identifiable at the

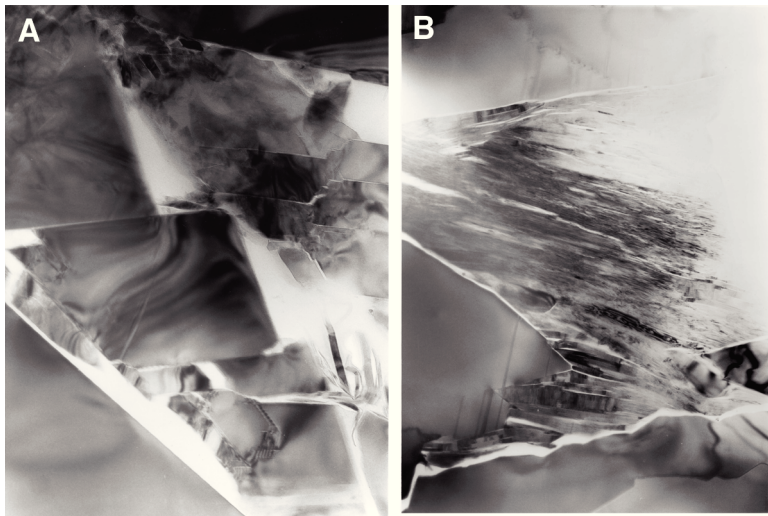


Figure 16. HRTEM image of tremolite fibers as seen along the fiber bundle elongation (c-axis): A) fibrils of different sizes showing typical 120° interfacial angles and transformation into talc (on the right); B) laths of talc replacing fibers of tremolite.

HRTEM scale owing to their small extension in the perpendicular plane. In these associations, chrysotile, which forms from amphibole, gives rise to fascinating textures (as seen in the plane normal to fiber axis). Partially or totally rolled or S-shaped wavy serpentine “moustaches” form along boundaries with the anthophyllite fiber. Figures of eight are also present, made of two intergrown rolls of chrysotile (Veblen et al. 1977). Talc fibers have been found in intimate association with ferromagnesian pyriboles through replacement by sheet silicates. Some fibers, where replacement is not complete, are composed of both pyriboles and talc (Veblen and Buseck 1980). Fibers of crocidolite have been found only in association with mica at grain boundaries between amphibole fibers and have a fibrous morphology (Ahn and Buseck 1991).

Asbestos fiber may also occur in association with other fibrous minerals because of chain width disordering. Chain-width faults may occur in amphibole and develop along the *b* axis. These faults can prevent the classification of fibers into a particular silicate subclass (i.e., sheet vs. double or single chain). In some cases, the fiber should, strictly speaking, be classified as several different species. Indeed, sometimes the chain-width faults become ordered and extend for wide domains, producing pyribole portions with triple-silicate chains or with alternating double and triple chains; these pyriboles are respectively known as jimthompsonite and chesterite. When fibers are almost entirely composed of these kinds of pyriboles, they could be classified as one of two species since these minerals are also fibrous (Veblen et al. 1977). Because of the possibility of such ambiguities, Veblen et al. (1977) suggested using the term pyribole asbestos for all amphibole asbestos, as this term enables all possibilities to be included without preventing them from being distinguished from chrysotile.

Amphiboles in soils and unconsolidated material

In many areas of the world, soils contain mineral fibers that are mostly amphibole. Soils derived from rocks containing asbestiform amphiboles also contain fibers that may potentially become airborne. Some of these rocks are very susceptible to weathering and also very rich in magnesium (e.g., those containing asbestos) and hamper the development of vegetation, inhibiting soil formation. Chrysotile is more soluble in the presence of H₂O and at low pH, and acid leaching removes magnesium from the fibers fairly rapidly, leading to their disintegration. Amphiboles are more resistant, and amphibole fibers are more frequently found in soils (Trescases 1997; Hillerdal 2003). Moreover, soils can become enriched in amphiboles as other minerals in the soil weather away.

Investigation on the presence of asbestos fibers in soils began after the identification of asbestos-related pathologies in human populations not occupationally exposed to asbestos. These soils may expose local populations because they contain amphibole fibers that were easily dispersed in air due to dry climate. The respirable dimensions of amphibole fibers have been related to the formation of calcified pleural plaques in humans and in animals (Abrahams 2002) and some mesothelioma cases (Browne and Wagner 2001). Soils containing less than 1% asbestos fibers can release large quantities of fibers into the air and may constitute health risks (CDPHE 2006). The fibers contained in soils become airborne when the soils are disturbed either by natural processes (mainly wind) or by human activities (such as agriculture, planting trees or bushes) or a combination of the two.

The above scenario occurs in rural areas of southwestern China where the soil is covered by scattered, clay-like, bluish patches (termed “blue clay”) that contain short, rigid crocidolite fibers (Luo et al. 2003). On dry and windy days, the mineral particles are airborne and later settle, covering the villages with bluish dust. The blue-clay was used locally to make building blocks, stoves, plaster, and paint for house interiors. The inhabitants are therefore subject to both natural and anthropogenic exposure. Situations like this have been observed in areas of Cyprus, Greece, Turkey, and New Caledonia where tremolite is present in soils. In these cases, the better-developed soils tend to release fewer tremolite fibers into the air than the Chinese case; nevertheless, the exposures of the inhabitants is high because the local rock was widely

used as whitewash, stucco, or plaster for houses (Browne and Wagner 2001). Tremolite-asbestos fibers were also detected in the soils of an area in Basilicata (southern Italy), and they derive from the natural weathering and erosion of serpentinite (Burrigato et al. 2006). Asbestiform tremolite occurs in the soils of some Balkan areas; various activities cause them to split into fibers, which then subdivide into respirable fibers (Wagner 1980).

Abundant quantities of asbestiform amphiboles, including fluoro-edenite, are present in portions of brecciated lavas in a local quarry in Biancavilla, Sicily. Detrital fine-grained accumulation occurs in this area because of the incoherence and friability of the volcanic rock. Even though the quarry has been closed as a consequence of the identification of airborne fiber-related pathologies, the fibers continue to spread easily in the air and settle on agricultural soil because of the dry, windy climate and the fact the quarry has not been revegetated (Mazziotti Tagliani 2006).

Some soils are originally asbestos-free and then are subsequently contaminated by commercial amphibole-asbestos (and also by chrysotile) owing to human activities. An example of this is the demolition of buildings in which there are various materials containing asbestos. This necessarily causes dispersion of the fibers into the air, many of which fall to the ground, thus becoming constituents of the soil. Further instances are the land-based disposal of waste asbestos materials (e.g., Mangano et al. 2006) and the disposal or abandonment of asbestos that is not properly stored and contains debris that undergoes degradation. Over time, these asbestos fibers penetrate both the soil surface and the subsurface (CDPHE 2006). Fortunately, while disposal of asbestos waste to landfills was a common practice in the past, current regulations restrict this practice.

In Nature, many soils contain asbestos (mainly amphibole) either because (1) they derive from rock material containing asbestos or (2) through proximity to natural or anthropogenic sources of easily airborne asbestos contaminants. In the case of cultivated soils, farmers working these soils may be exposed to high doses of fibers. For example, asbestiform amphibole fibers occur in the soils of Libby, Montana. These fibers are released into the air during routine residential activities (USEPA 2001a); however, to date no one has determined the quantity of fibers that are anthropogenic vs. those that are nonanthropogenic. There are few detailed studies on the chemical and mineralogical composition of soils and the asbestos fibers contained in them. Even so, we know that amphiboles occur in many unconsolidated materials in the western USA associated with various mountain terrains (Gunter and Lee 2006).

In populated areas where soils are heavily contaminated with amphibole fibers, risk assessment is particularly useful and, if necessary, provisions should be adopted to contain air dispersion or to remediate the ground in question. The Colorado Department of Public Health and Environment (CDPHE 2006) has recently published a detailed guideline of modalities for the characterization of asbestos contaminated sites (ACS) and for the management of ACS related to partial or total remediation (involving the excavation, removal and burial of the soil to a suitable depth).

OCCUPATIONAL VS. NONOCCUPATIONAL EXPOSURE

Occupational exposure to asbestos has been covered in past RIM volumes. Ross (1981) did an excellent job discussing mortalities based on different populations in chrysotile and amphibole asbestos exposures. His early work clearly showed that amphibole asbestos exposure induced more disease than chrysotile exposure. In the early 1980's, the nonoccupational exposures often involved the wives of miners, and their exposure roots was from husbands' clothing. In 2007, we focus on nonoccupational exposure to asbestiform amphiboles in their natural setting. The distinction here should also be made that, in general, the term asbestos should be reserved for the commercial product (refer to Fig. 1A for the inch-length fibers of

tremolite and chrysotile). The term asbestiform should be reserved for amphiboles that split lengthwise (as shown in Fig. 1B). These particles, while being separable fibers on a very small scale, would tend to not be used as commercial asbestos because they are too short. Thus we would propose to use the expression nonanthropogenic exposure to asbestiform amphibole to replace the commonly used expression of exposure to “naturally occurring asbestos.”

Asbestosis, silicosis, and lung carcinoma are widely agreed to be related mostly, if not exclusively, to exposure to dusts and fibers that are other than amphibole, namely chrysotile, quartz and various other minerals. By contrast, pleural mesothelioma has almost invariably been related to exposure to amphibole fibers, with erionite, a zeolite, being the only other mineral of possible cause (Metintas et al. 1999). Attention to mesothelioma is particularly acute in Italy after the general public was made aware of the Biancavilla, Sicily, cluster of disease (Comba et al. 2003, 2005; Fano et al. 2005). A much worse case occurred at Casale Monferrato, Piedmont, where nearly 200 mesothelioma cases were diagnosed between 1983 and 2002, and in the year 2003 alone there were 32 new findings of the disease. Indeed, both pleural and peritoneal mesotheliomas are such interesting exposure-related diseases that they have attracted world-wide attention (e.g., Roggli et al. 2002; Dodson et al. 2005).

As for Italy, Table 4 shows the overall mortality rate (defined as mortality rate = number of deaths / total population \times 100,000) due to pleural mesothelioma from 1995 to 2002 (the last year for which full statistical information is available). Also, Table 5 gives mesothelioma death-rates for different regions of Italy. Based on these data, Montanaro et al. (2004) and Marinaccio et al. (2005) made a reasonable estimation of future development of the disease (Fig. 17). They related it to the total consumption of asbestos and found that the peak for mortality should occur in 2015, lagging behind the peak of the 1976 date for the peak of asbestos consumption. However, their statistics may be misleading because they note total consumption and not consumption of only amphiboles, which by consensus is the inferred cause of mesothelioma. Therefore, the statistics may be strongly biased by the fact that most asbestos-containing materials used in Italy until 1989, after which it was forbidden, were chrysotile.

Mesothelioma mortality can best be studied by comparing the data from four provinces of Italy having asbestos quarries with two where no quarries are present and where other sources of exposure can be assessed. Balangero is a village located in the province of Turin and contains the largest asbestos mine in Italy (1918-1979). The now-closed mine is still surrounded by over 65 million m³ of waste hosting an estimated 800,000 m³ of fibers. Most of it is short-fiber chrysotile, but there is an estimated 10% tremolite in the tailings. Figure 18A shows that with steadily decreasing population in Turin province, the mortality rate fluctuated but substantially increased after 20 years of Balangero closure, implying that nonoccupational exposure is a major problem. However, this statistic may be biased by several joint-causes

Table 4. Mortality rate in Italy for pleura mesothelioma

Year	Average Population	Total Deaths	Rate cause specific
1995	56,844,408	925	1.6272
1996	56,844,197	1014	1.7838
1997	56,876,364	972	1.7090
1998	56,904,379	978	1.7187
1999	56,909,109	1096	1.9259
2000	56,923,524	1141	2.0044
2001	56,960,692	1193	2.0944
2002	56,993,742	1203	2.1108

Table 5. Pleura mesothelioma deaths for different regions of Italy.

Region	Men		Women		Total	
	Cases	Rate st.	Cases	Rate st.	Cases	Rate st.
Piemonte	800	3.42	510	2.00	1310	2.68
Valle d’Aosta	6	1.00	7	1.11	13	1,05
Liguria	831	7.81	251	2.07	1082	4.77
Lombardia	1034	2.59	753	1.64	1787	2.07
Trentino-Alto Adige	57	1.45	45	0.99	102	1.20
Veneto	426	2.10	240	1.05	666	1.54
Friuli-Venezia Giulia	274	4.18	74	0.97	348	2.44
Emilia Romagna	403	1.74	207	0.83	610	1.28
Marche	132	1.60	70	0.83	202	1.22
Toscana	397	1.90	197	0.87	594	1.38
Umbria	50	1.03	27	0.56	77	0.80
Lazio	206	0.88	124	0.51	330	0.69
Campania	344	1.65	185	0.84	529	1.24
Abruzzo	67	0.99	41	0.62	108	0.81
Molise	10	0.52	5	0.26	15	0.39
Basilicata	19	0.63	29	0.75	39	0.69
Puglia	321	1.93	125	0.78	446	1.36
Calabria	79	0.87	53	0.60	132	0.75
Sicilia	367	1.63	170	0.78	537	1.22
Sardegna	119	1.69	48	0.71	167	1.21
Italy	5942	2.17	3152	1.09	9094	1.61

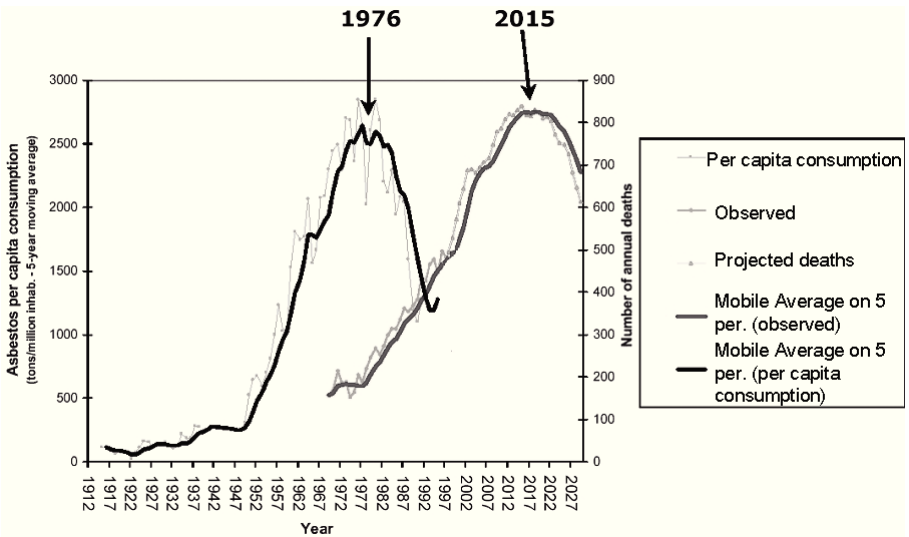


Figure 17. A plot showing the usage of asbestos (left curve) and yearly death rates from mesothelioma (right curve; actual deaths to 1997, then projected deaths to 2032). Note the graph shows offset from the usage to the onset of disease.

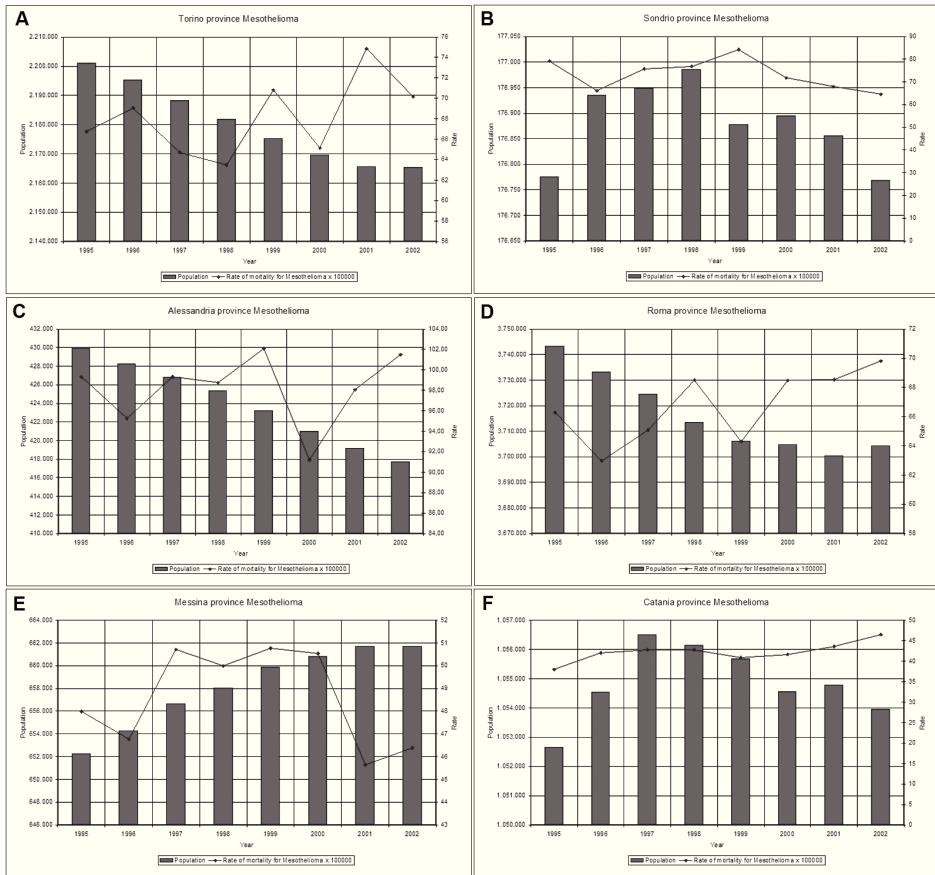


Figure 18. Death rates for mesothelioma in the different regions of Italy from 1995 to 2002. Bars represent the populations (shown on the left axis) and dots connected by lines represent deaths from mesothelioma (shown on right axis).

because Turin is a large city with major factories where asbestos was used (and still is, although exposures will be much lower because of safety regulations). The overall mortality rate may be the sum of occupational and nonoccupational exposure.

The province of Sondrio (Fig. 18B) stretches over a valley in the Alps removed from asbestos plants of any kind, where greenstones have been handcrafted from the time of Pliny, and the first mining license for asbestos (long-fiber chrysotile) in Italy was granted in 1866. The mortality rate can be related to occupational activity, as chrysotile occurs as long fibers coating cracks in serpentinites, together with white, almost visibility indistinguishable tremolite. The provincial population and mortality rate are constant, and the latter is higher than in Turin (Fig. 18A); in fact, it is the highest in Italy.

The province of Alessandria (Fig. 18C), on the lower right corner of Piemonte (i.e., the same region where Turin), has no significant outcrops of asbestos-bearing rocks, but it hosts the largest asbestos-treating manufacturing plant of Italy (now closed) at Casale Monferrato, in the middle of the Po plain. Despite decreasing in total population, Alessandria maintains a high and increasing mesothelioma rate, obviously related to occupational reasons. However, in Rome

(Fig. 18D), a city where there are no asbestos occurrences, but where there was widespread use of all types of asbestos for building, industrial and home applications, show mortality rates that are especially high and are increasing, even though the number of inhabitants is steadily decreasing.

The mortality rate is higher in Messina (Fig. 18E) than Catania (Fig. 18F). Messina is a neighboring Sicilian province to Catania where there are no known occurrences of fluoro-edenite or greenstones, but where both shipyard and railroad industries existed (i.e., industries where asbestos was widely used in the past). Thus, occupational exposure was high in Messina. Catania is the province in Sicily where Biancavilla is located. Mortality rates are not especially high, as most geological occurrences are asbestos-free (sediments and the Etna volcano); however, the rate is increasing, possibly because of the nonoccupational exposure of the inhabitants in the areas contaminated by fibrous fluoro-edenite.

In summary, there are no definitive statistical indicators suggesting that low-level exposure to amphiboles in the natural setting are a direct cause of mesothelioma, as widely believed in the medical circles, but exposure to amphibole fibers may be a contributing factor. What is certain is that mortality due to mesothelioma has not yet reached its peak in Italy.

CURRENT EXAMPLES OF AMPHIBOLE EXPOSURE

A retired colleague recently commented, "asbestos has been a backwater of concern in America until Libby, Montana, made the national news." Libby re-awoke not only interest in, but also the fear of asbestos exposure. Following closely on the heels of Libby was the issue of dust generated from the collapse of the World Trade Center Towers in 2001. Some of the same individuals who worked on the issues surrounding Libby, Montana, also became involved with the issues surrounding the dust from the World Trade Centers. Fortunately, the dust from the World Trade Centers was more-or-less asbestos-free and of such size as to not be respired into the lung. However, there are other respiratory diseases associated with that dust; they are beyond the scope of issues surrounding asbestos and will not be discussed herein. Contemporaneous with Libby and the World Trade Center were issues surrounding asbestos in El Dorado Hills, California. In this area asbestos was never mined; in fact, much of the current debate is whether the amphiboles in El Dorado Hills are actually fibers or fragments. Regardless, issues surrounding El Dorado Hills cause us to focus our concern on nonoccupational exposure to amphiboles. While the exposure might lead to a health risk, the fear of risk might also be detrimental to human health. In Italy, the village of Biancavilla on the flanks of Mount Etna has gained international attention because of higher incidence of mesothelioma and geological occurrences of both fibrous and nonfibrous fluoro-edenite.

Libby, Montana, USA

Issues surrounding the now-closed vermiculite mine near the small town of Libby, Montana, (Fig. 19) brought concerns over asbestos exposure back to public attention, beginning with a series of newspaper articles in the fall of 1999. The ore deposit, the articles reported, contained small amounts of amphiboles, some of which had asbestiform habit. Within days of these articles, the EPA arrived in Libby and is still there today, dealing with asbestos-contamination issues. Even though most of the world had never heard of Libby (or the vermiculite mine) until that fall, health studies had already been performed on the workers (McDonald et al. 1986a,b, 1988; Amandus and Wheeler 1987; Amandus et al. 1987a,b), showing that rates of lung cancer, asbestosis, and mesothelioma are about 2.5 times higher in the miners than expected. Ross et al. (1993) discussed several issues surrounding the amphibole content of the vermiculite ores. A follow-up study by McDonald et al. (2004) showed that out of 406 men who had worked at the mine for at least one year before January 1, 1963, 285 died by January 1999. Out of that group, 107 of the deaths had been from respiratory diseases: 51 deaths from asbestosis, 44

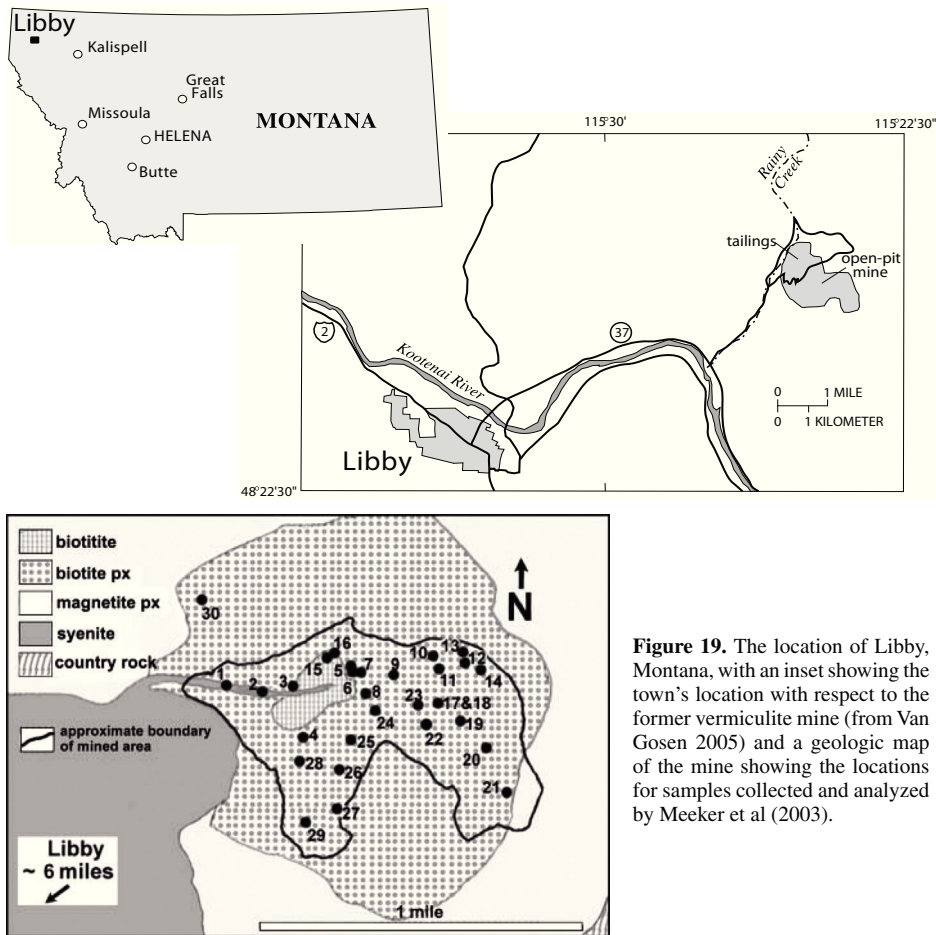


Figure 19. The location of Libby, Montana, with an inset showing the town’s location with respect to the former vermiculite mine (from Van Gosen 2005) and a geologic map of the mine showing the locations for samples collected and analyzed by Meeker et al (2003).

from lung cancer, and 12 from mesothelioma. This study again confirmed that death rates are about 2.5 times the expected rates.

Concern spread from the miners to the general population in Libby and the surrounding area, about 8,000 past and current residents. Peipins et al. (2003) found higher rates of pleural plaques in the residents of Libby, which indicates that the residents were exposed to asbestos. However, their study was disputed (see Environmental Health Perspectives, Feb. 2004, Correspondence section) based upon the claims that Piepens et al. did not follow appropriate experimental procedures for reading the lung X-ray films (i.e., the readers were told which films were from Libby residents). Moreover, the study did not correctly adjust for obesity. Regardless, the popular media has used this study to state that the local population suffers from asbestos-related diseases.

One of the main uses of the vermiculite ore mined at Libby was for attic insulation. A product called Zonolite was produced from “popping” the mined vermiculite: the vermiculite was heated for a few seconds at approximately 1000 °C. Zonolite ore was then shipped nationwide and used as attic insulation; thus, there could be a much larger cohort of individuals exposed to amphibole-contaminated vermiculite than just those in Libby. The popular press

has estimated that from 15-35 million homes in the USA contain this material. These sorts of numbers seem unreasonable given the population of the USA and the fact that there are only 65 million homes in America. Gunter et al. (2005) reviewed these estimates, and along with help from EPA personnel, estimated that there are close to 1,000,000 homes in the USA that may contain this product. The issue now is two-fold: (1) what is the asbestiform amphibole content of this material and (2) what are the risks homeowners face? A legal opinion recently issued by Fitzgerald (2006) stated that there was no reliable evidence indicating that Zonolite attic insulation poses an unreasonable risk of harm. Although some scientists may disagree with this legal view, yet again this points out the interconnectedness of science and legal issues involved in issues surrounding amphiboles.

Figure 19 shows a geological map of the former mine, and the location of samples collected by USGS, discussed by Meeker et al. (2003), and plotted in Figure 2. These data, along with those of Bandli et al. (2003), Gunter et al. (2003), and Sanchez (2007), show that the majority of the amphiboles at the mine are winchite and richterite, which as discussed above, are nonregulated. Also, Brown and Gunter (2003) pointed out that approximately 1/3 of the amphiboles occur in the asbestiform habit. These mineralogical characterizations have been important in legal decisions and play a major role as the issues are debated on what amphiboles should be regulated based on composition and morphology.

Figure 20 shows a series of photographs taken at the mine in the fall of 1999. Briefly, the deposit was an ultramafic intrusion composed mainly of biotite and pyroxene which later underwent partial alteration of pyroxene to amphibole and biotite to vermiculite (Boettcher 1967). Figure 21A shows an intergrown amphibole/pyroxene particle in a near refractive index-matching fluid for the amphibole. Figure 21B shows another recently found occurrence of the amphiboles (Gunter et al. 2006; Harris et al. 2007), where the amphiboles are growing on and into a sheet silicate. The images of air samples collected in Libby (Fig. 6) show these particles after they have been liberated from the sheets.

Sanchez and Gunter (2006) developed a powder XRD method to determine the amount of amphiboles in bulk Zonolite samples. Figure 22A shows a series of standards they made and shows a detection limit of approximately 1000 ppm. In Figure 22B, a series of Zonolite attic samples are plotted with a 1% spiked sample. From this figure, it appears that the amphibole content of these attic samples is below 1% total amphibole. Moreover, because around 1/3 of the amphiboles from Libby appear to be asbestiform (Brown and Gunter 2003), the amphibole-fiber content of this product would be less than 1/3 of the total amphibole content. In a related study, Gunter et al. (2005) showed that the trace elements of Libby vermiculite can be used to differentiate it from other commercial vermiculite products (Fig. 23).

From a risk and worker safety perspective, it is important to understand the dose received by the mine workers. Bandli and Gunter (2006) reviewed the exposure data for 1960 doses ranging from 10.7 to 168.4 f/cc, with the highest value occurring in miners that worked in the dry mill. Doses decrease to less than 1 f/cc in 1980. To date no one has determined a safe level of exposure to amphibole-asbestos; detailed studies of the miners, townspeople, and occupants of Zonolite insulated houses may help answer this question. Regardless, issues surrounding Libby will continue for years.

Last, it is interesting to note that Ross (1981) stated "Epidemiological evidence does not exist to assess the health effects of tremolite." Ten years later, a series of papers by Case (1991), Nolan et al. (1991), and Weill et al. (1990) all concluded that tremolite-asbestos is the most harmful type of asbestos. At the time, much of the evidence to support this came from studies on the Libby miners. Ironically, we now know that several different species of amphiboles occur in that deposit, with tremolite being less than 10% of the total amphibole population (Meeker et al. 2003, Gunter et al. 2005).

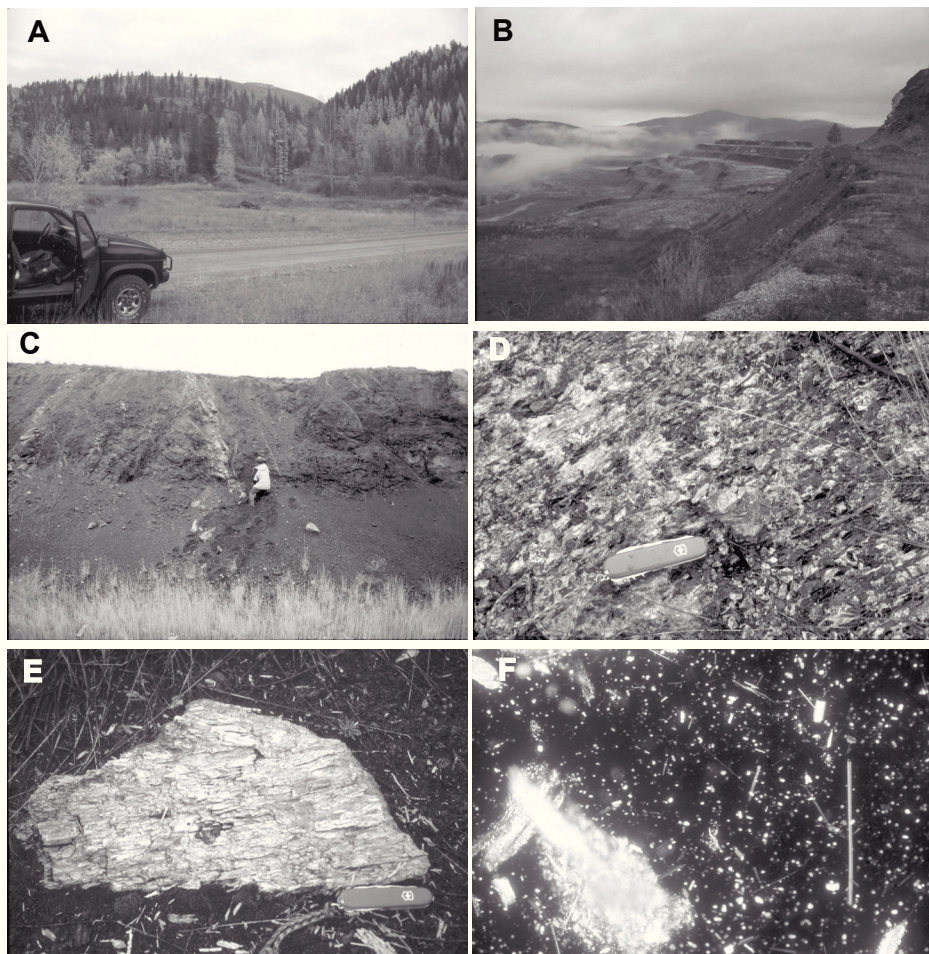


Figure 20. A series of photographs from large to small scale of the former mining operation near Libby, Montana. A) A photograph taken on Rainy Creek road, looking directly east to the top of what is termed locally as Vermiculite Mountain, the location of the former mine. B) A photograph looking west from the eastern side of the mine, showing the mined portion of the mountain top with the individual mined benches. C) A photograph of an individual bench with veins cross-cutting it. D) A close-up photograph of the bedrock at the mine. The lighter color minerals are amphibole, the dark minerals vermiculite or biotite, and the intermediate colors pyroxenes. E) A boulder-sized piece of amphibole on the surface. F) A photomicrograph of amphiboles collected from the mine. The blob in the lower left is a fibrous mass, while the vertical particle on the right is a single crystal of amphibole (modified from Bandli and Gunter 2006).

El Dorado Hills, California, USA

Housing developments in El Dorado Hills have grown over the past few years. The area serves as a bedroom community for Sacramento (Fig. 24). During the development of this area, amphiboles were discovered in the soils near a local school. Early remediation efforts at the school led the EPA (Ecology and Environment 2005) to conduct activity-based sampling to ascertain what exposure the students might be subjected, and the highest level was 0.0019 f/cc. This study was called into question by the National Stone Association (NSA), and a subsequent study funded by them was carried out by the RJ Lee Group (RJ Lee 2005), which examined

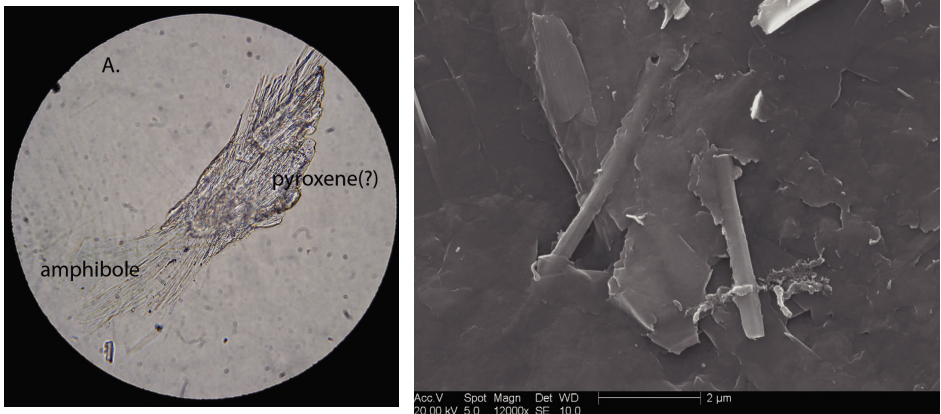


Figure 21. A) PLM photograph of an intergrown pyroxene/amphibole particle in a near refractive index-matching fluid for amphibole. The lower left portion of the particle matches the refractive index of the liquid, while the upper right exceeds it (FOV = 360 μm). B) An FESEM image from the Libby vermiculite deposit, showing amphiboles intergrown with layers of a sheet silicate. (Gunter et al. 2006, image courtesy of the RJ Lee Group Inc., Monroeville, Pennsylvania, USA).

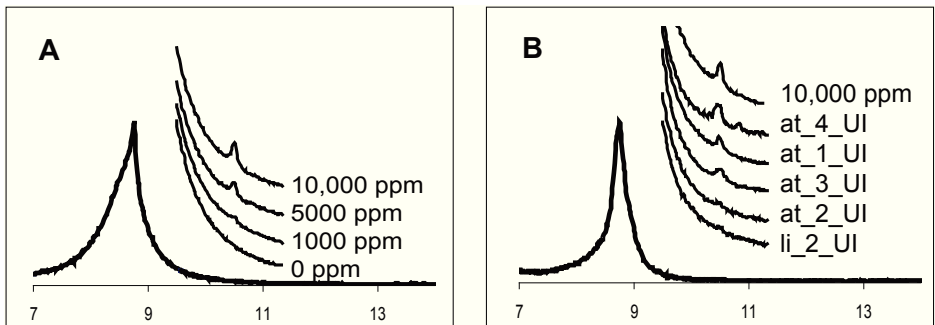


Figure 22. Powder X-ray diffraction scans of K-exchanged vermiculite samples. The long 2θ scan ($7\text{--}14^\circ$) was collected at 0.02° step size and count times of 9 s. The shorter 2θ regions ($8.5\text{--}11.5^\circ$) were collected at 0.02° step size and 180 s count times. A) This set of scans shows an amphibole-free sample and three amphibole-spiked samples. Notice the correlation in the size of the 110 peak for amphibole and the amount of added amphibole. B) This set of scans is vermiculite attic samples with a known Libby source with the 10,000 ppm spiked sample added; by observation, all samples have less than 1% amphibole (modified from Sanchez and Gunter 2006).

the same material as did the EPA. A third study (Meeker et al. 2006, (funded by the EPA) addressed some issues from the earlier studies. At the heart of the El Dorado Hills controversy is: (1) how do we deal with amphiboles that might pose a risk to humans in their natural setting and (2) what methods are appropriate to characterize amphiboles that are not associated with commercial asbestos products (i.e., can the standard methods developed to deal with asbestos in the workplace be used to deal with amphiboles in their natural settings?).

Figure 25A is a series of SEM photographs taken by the RJ Lee Group (2005) showing amphibole particles collected during the EPA-supported study (Ecology and Environment 2005). Even though these particles meet counting rules (i.e., the correct aspect-ratio) to be considered as fiber, they do not have the morphological character of asbestos. While the EPA-

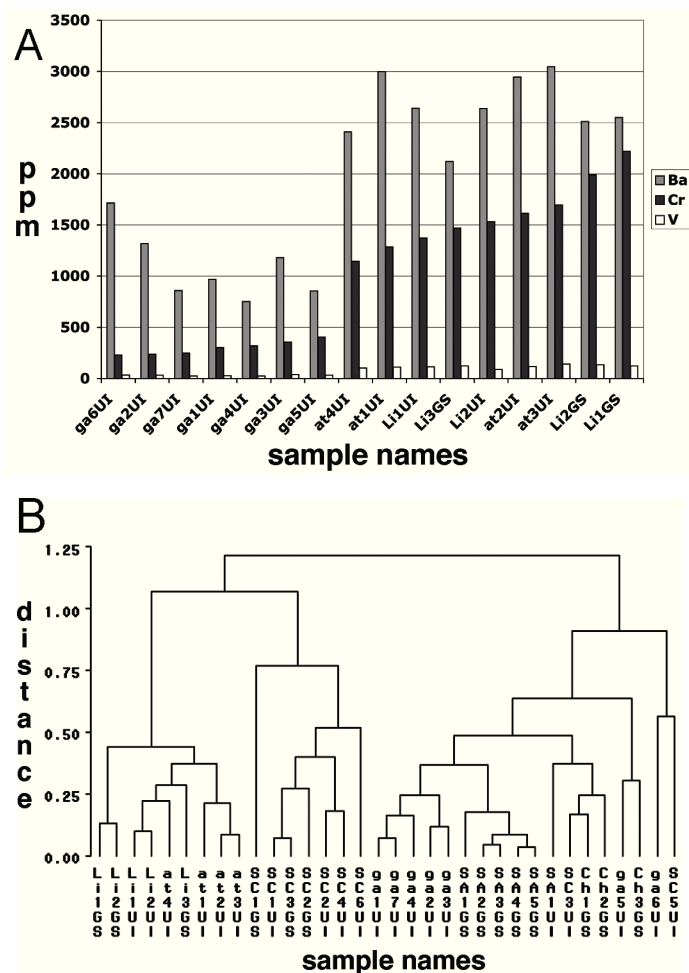


Figure 23. Chemical analysis of vermiculite ores can be used to determine their source. A) The trace element contents are plotted for 14 vermiculite samples. Those starting with “ga” are from commercial garden samples, “at” were obtained from attics, and “Li” are samples from Libby. Note how the “at” samples group with the Libby ones. B) Here, 34 samples are shown and 18 major, minor, and trace elements are used to group the samples. For these samples, “SC” refers to South Carolina and “SA” to South Africa. Note how the “ga” samples group with the “SA” samples (for more details see Gunter et al. 2005).

funded study found amphiboles they considered as asbestos, the RJ Lee Group (2005) found significantly less what they considered asbestos. Figure 25B is a series of photos from Meeker et al. (2006) that seem to show an asbestiform habit for another set of samples collected in the El Dorado Hills area. It is important to note that regardless of whether there are asbestiform amphiboles in the area, dosage is the most important thing to consider when dealing with mineral exposure. In the EPA’s activity-based sampling, the highest value they obtained was 0.0019 f/cc, which is one order of magnitude above ambient air levels (Table 2).

The USGS (United States Geologic Survey) has taken on the challenge first in Libby, then the World Trade Center, and now in the El Dorado Hills to aid in characterization of minerals in their natural setting. During the last 5-6 years, they have assisted local communities and

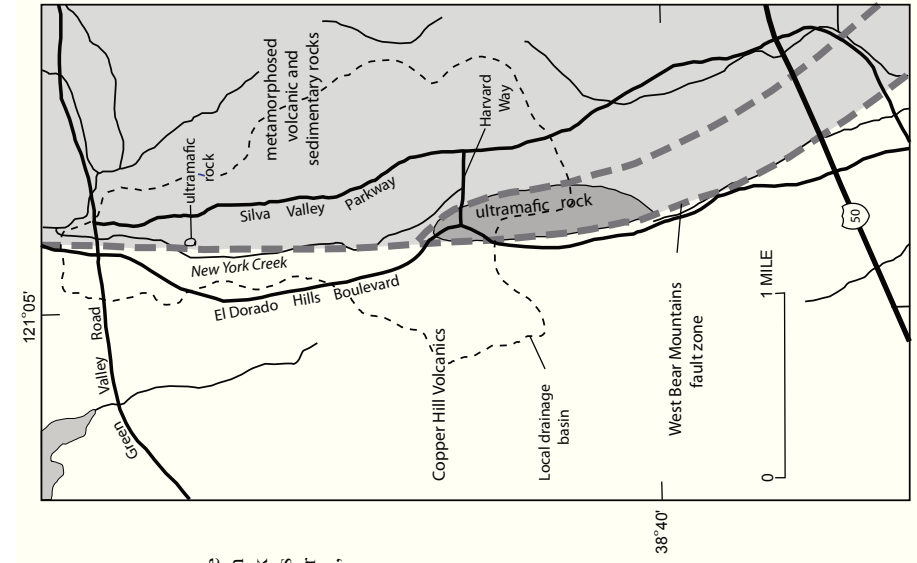
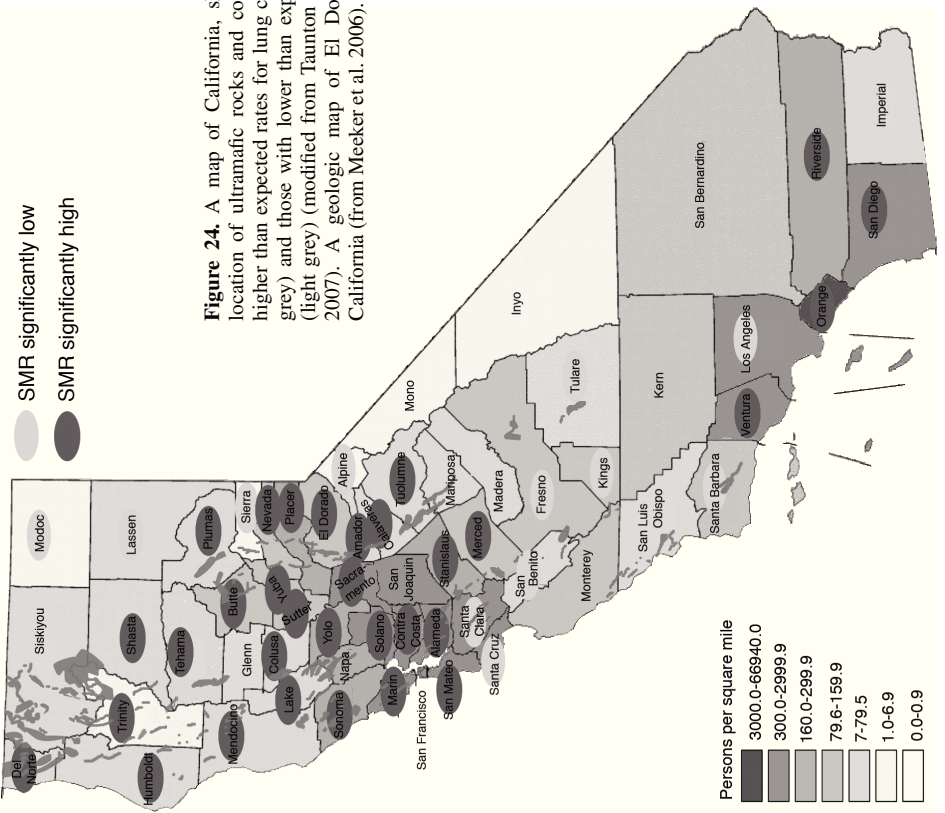


Figure 24. A map of California, showing the location of ultramafic rocks and counties with higher than expected rates for lung cancer (dark grey) and those with lower than expected rates (light grey) (modified from Taunton and Gunter 2007). A geologic map of El Dorado Hills, California (from Meecker et al. 2006).



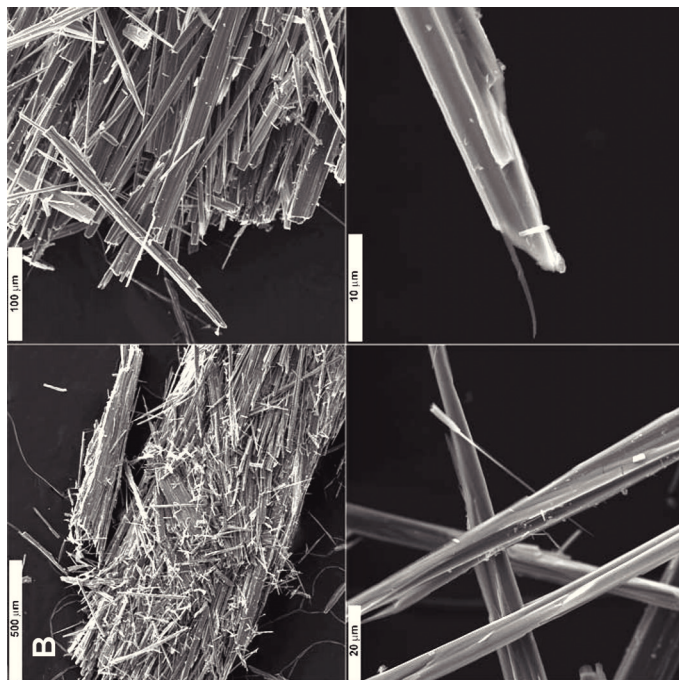
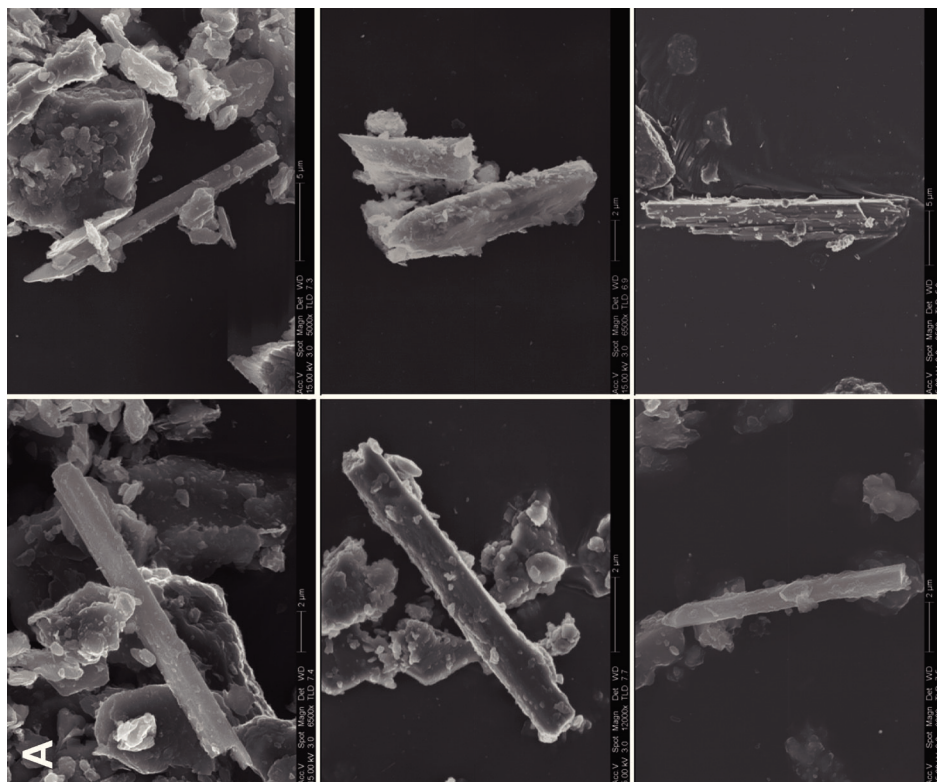


Figure 25. Example SEM photos of amphiboles collected in the El Dorado Hills area. A) Taken from RJ Lee (2005). B) Taken from Meeker et al. (2006).



regulatory agencies in dealing with the issues surrounding these natural exposures. They have brought to bear everything from their analytical experience, as shown in Figure 2, for the characterization of the Libby samples to remote sensing to help locate areas that might contain amphibole-bearing rocks (such as the spectroscopic analysis from a low-flying airplane, Fig. 26).

Unfortunately, some of the asbestos issues become polarized as they are played out in the public media, and no doubt the so-called “naturally occurring asbestos” is one of these issues. It is creating considerable fear not only in this area of California, but in much of the state. And it is not really all that new. Ross (1994) was already speaking of it, yet 13 years later, little has been resolved. What seems to be happening is the fear of nonoccupational exposure is spreading from El Dorado Hills to the rest of the USA (e.g., Dusek et al. 2002 in Virginia) and

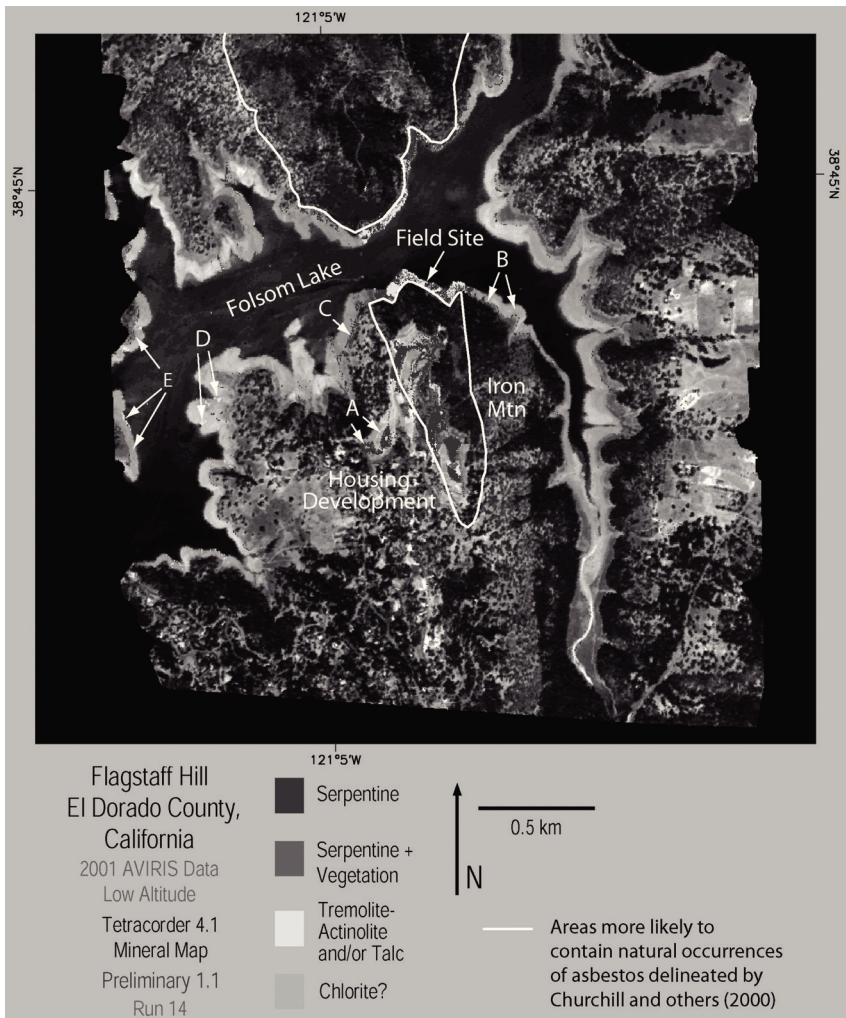


Figure 26. An aerial photograph of the area in and around El Dorado County, California. The different shadings on the map represent different rock types as determined by spectroscopic data obtained from an aircraft (Swayze et al. 2004). (Please see color version of this map at pubs.usgs.gov/of/2004/1304/.)

it will be our role as mineralogists and geologists to try to assist industry, State and Federal agencies, and citizens as they grapple with this issue.

Biancavilla, Sicily, Italy

The small community of Biancavilla on the southern slope of Etna volcano in Sicily (Fig. 27) fell into the international spotlight (much like Libby, Montana) due to a positive anomaly for pleural mesothelioma detected in sanitary maps (Paoletti et al. 2000; Burrigato et al. 2005). Biancavilla is now well-known as the first example of amphibole-fiber occurrence in a volcanic

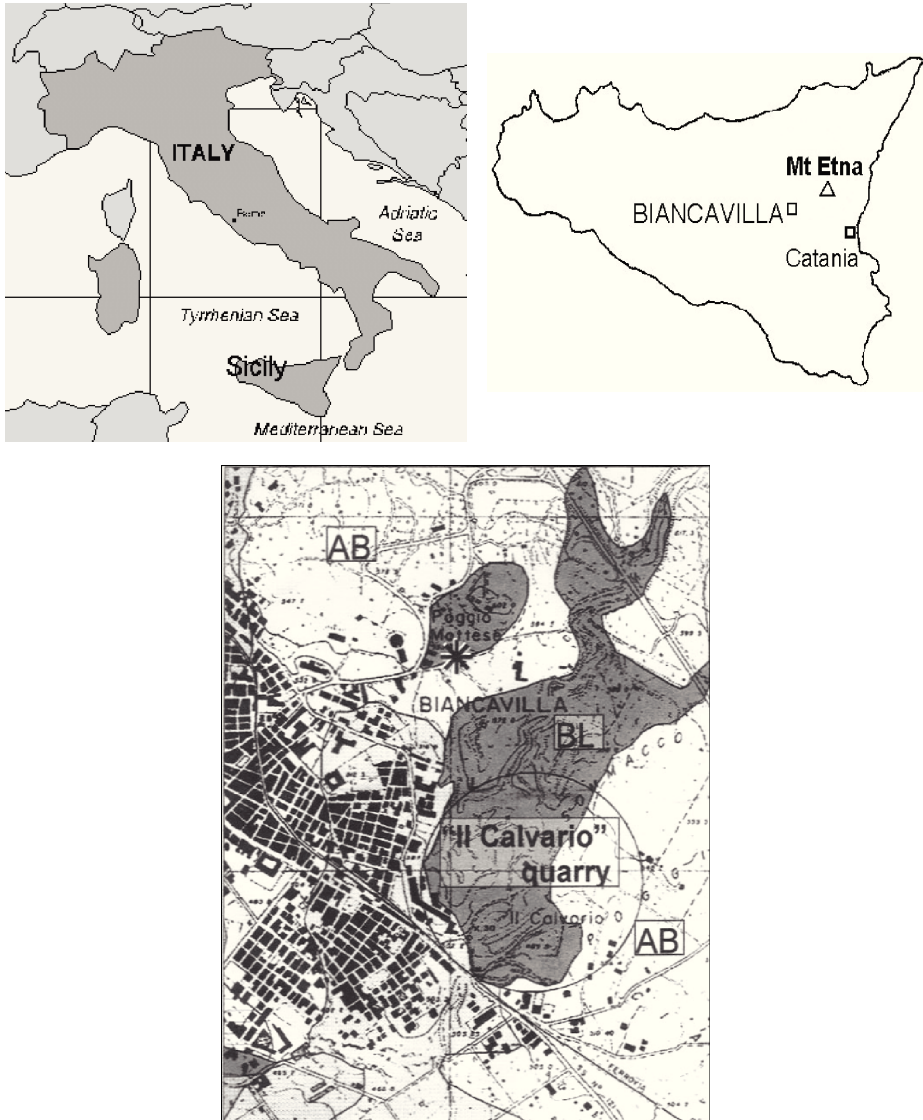


Figure 27. A location and geologic map of the Mt. Etna Biancavilla region. Biancavilla is at the very southern end of the map and the quarry containing fluoro-edenite is located northeast of the village. AB = alkali basalts and BL = benmoreitic lavas. (From Gianfagna et al. 2007.)

context. These fibers have an uncommon composition and are classified as the amphibole species fluoro-edenite (Gianfagna and Oberti 2001). Moreover, they seem to be oncogenic (cancer-causing) minerals. The latter finding of fibers with similar characteristics in human- and sheep-lung parenchyma is strong evidence that environmental exposure produces mesothelioma, especially when associated with exposure to building materials such as those produced from the Biancavilla Il Calvario quarries (Pasetto et al. 2004a; Burrigato et al. 2005).

The stratigraphic succession exposed in the Biancavilla area comprises (from top to bottom):

Recent and present-day lava debris;

Lava flows of the Recent Mongibello (i.e., present Etna) activity stage (alkali-basalts, hawaiites and mafic mugearites);

Massive and stratified ash and scoria flow-deposits of the Biancavilla-Montalto ignimbrite (De Rita et al. 1991), which is benmoreitic in composition. This major explosive event, which deposited a tephra marker layer (Y-1) to be found elsewhere around the Mediterranean Sea at distances as great as 1000 km, is dated radiometrically at $14,500 \pm 5,000$ (Gillot et al. 1994), thus constraining the age of the underlying Biancavilla lava complex;

Lava flows, domes, dikes, and autoclastic breccias of the Ellittico center (Ancient Mongibello stage), mainly hawaiites, mugearites, and benmoreites; they include the autoclastic benmoreite lava body, reported as "lava autobrecciata" in the geological map of Mt. Etna, which hosts the fluoro-edenite fibers; the contact with the overlying ignimbrite deposits is well-exposed along the gorge Vallone di S. Filippo, and it is marked by a 10-cm thick reddish-brown palaeosoil;

Lava flows erupted from early alkaline eruptive centers: mainly alkali-basalts, hawaiites and mafic mugearites;

Tholeiite basalt lava flows of the earliest sub-alkaline period of Palaeo-Etna activity;

Clayish marls with interbedded sandstones of the pre-Etna sedimentary basement (Pliocene to Quaternary).

The severe and widespread environmental contamination of the entire Biancavilla community area by fluoro-edenite fibers is related to the volcanic materials present in the local quarries at the Il Calvario hill (Comba et al. 2003; Gianfagna et al. 2003). Fluoro-edenite occurrences are scattered in and around Il Calvario quarries throughout an area of about 2 km². The outcrops where fluoro-edenite occurs are in a benmoreitic lava dome and dike complex with the associated autoclastic breccias; all are metasomatized in places. The fluoro-edenite crystals occur within a friable material in the altered lava, in fractures, and in the breccias. However, fluoro-edenite is not the only amphibole present; a mixture of fibrous minerals containing a different asbestiform amphibole (described below) was found in a stone quarry to the north of Il Calvario hill that had been used extensively for local building activities under the name "azolo." These loose products contain fibrous amphiboles which were first identified as tremolite or actinolite, but which turned out to be partly fluoro-edenite.

Fluoro-edenite typically occurs either as prismatic or acicular millimeter-scale crystals or as fibers with asbestiform morphology (Fig. 28) in the cavities of the altered gray reddish benmoreitic lavas. Fluoro-edenite is generally associated with feldspars, quartz, clino-, and orthopyroxene, F-Cl-apatite, ilmenite and hematite, and probably crystallized from high-temperature volcanic fluids. The other type of fibrous amphibole in Biancavilla is yellowish and whitish in color and shows a strongly asymmetric morphology. This amphibole fills the pores of the altered volcanic rock (metasomatic benmoreitic lavas and pyroclastic rocks). Rietveld analysis shows it as a mixture of 24% amphibole-asbestos, 73% feldspar, and 3%

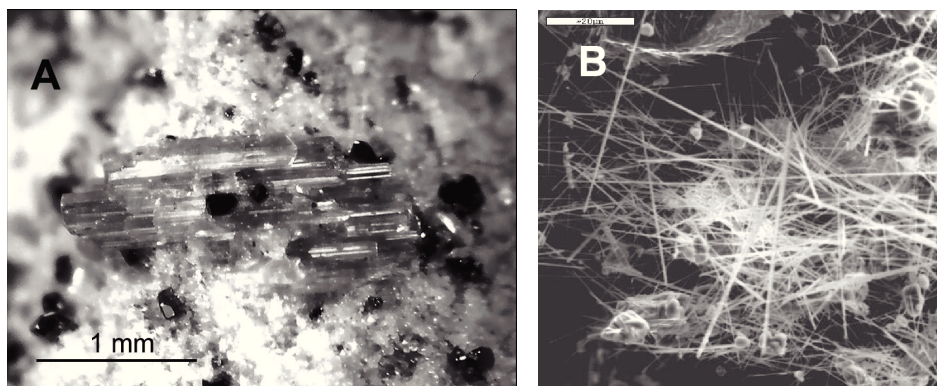


Figure 28. Photographs of fluoro-edenite from Biancavilla. A) Fluoro-edenite crystal exhibiting a blocky texture. B) Fluoro-edenite exhibiting a fibrous texture at a much finer scale. (From Gianfagna et al. 2007.)

hematite. Crystal size and morphology of these amphibole fibers do not allow quantitative EPMA analysis, but they are generally low in Ca and Mg, although both morphologies seem to have the same high fluorine content (Gianfagna et al. 2003). The high F content of all volatile-bearing minerals in the Biancavilla rocks is worth noting, not only in fluoro-edenite but also in fluorophlogopite (A. Gianfagna, personal communication). Also, as shown in Figure 29, Gianfagna et al. (2007) found different $\text{Fe}^{3+}/\Sigma\text{Fe}$ values for prismatic and fibrous fluoro-edenite in this deposit. To our knowledge, this is the first chemical difference ever determined between fibers and fragments of amphiboles.

AMPHIBOLES IN BIOLOGICAL MATERIALS AND ASSOCIATED BIO-MARKERS

In 1914, (otherwise undefined) crystals were observed in lung tissue during the autopsy of an asbestos worker who had died of pleuro-pneumonia. For many years, the recognition of minerals in the lungs of asbestos workers occurred essentially through correlation between the cause of death and the subject's occupation. It was only with the use of electron microscopy in

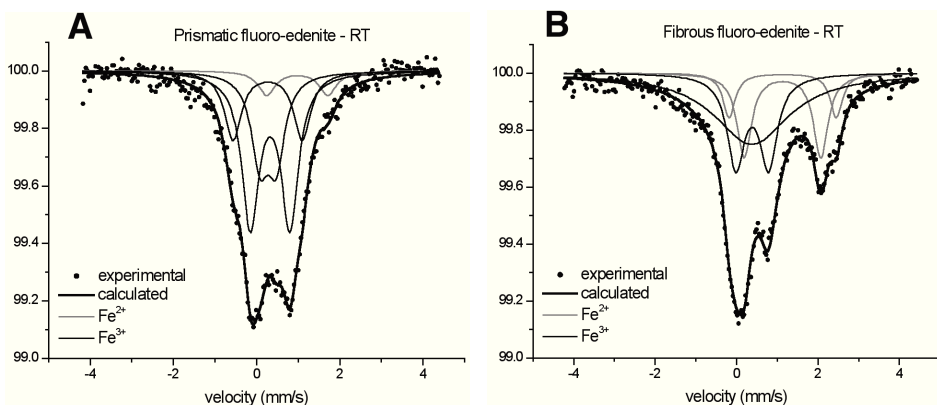


Figure 29. Mössbauer spectrum of fluoro-edenite (A) and fibrous fluoro-edenite (B); note the differing amounts of $\text{Fe}^{3+}/\Sigma\text{Fe}$. (From Gianfagna et al. 2007.)

the 1970s that it became possible to unequivocally identify asbestos amphiboles (in the lungs), to determine their burden in the lung tissue, and to understand that other inorganic fibrous species can enter the body (Roggli and Sharma 2004). Because fibers are inhaled, the lungs and the surrounding tissues were the first biological materials to be examined, and amphibole asbestos was commonly found in them.

At present it seems certain that the main repository of asbestos fibers in the human body is the lung parenchyma. However, fibers of amphibole asbestos have been found at high levels (both in the presence and absence of pathologies) in various other organs and tissues: in the visceral and parietal pleura (Tossavainen et al. 1994), in the larynx (Griffits and Malony 2003), in ovarian and intratesticular mesothelium (Attanos and Gibbs 2000), in omentum and mesentery (Dodson et al. 2000a), in lymph nodes (Dodson et al. 2000b), in the urothelium and the bladder wall (Pollice et al. 1995), in the intestinal mucosa (Storeygard et al. 1977), in the kidneys (Holt 1981), in the placenta (Haque et al. 1998), and in the liver and muscles of stillborn (Haque et al. 1998). Amphibole asbestos has been found also in biological fluids: in sputum (e.g., Putzu et al. 2006) and in bronchoalveolar lavage fluid – *BALF* (e.g., Sartorelli et al. 2001). To the authors' knowledge, there do not seem to have been any studies on amphibole asbestos (and chrysotile) in the blood. However, it is reasonable to think that the finest fibrils may pass into the blood circulation system after being inhaled. Indeed, the experiment by Nemmar et al. (2002) has shown that ^{99m}Tc -labeled ultrafine (5 to 10 nm in diameter) carbon particles inhaled by volunteers pass into the blood in one minute. Also, an experiment with hamsters has shown that a substantial fraction of intratracheally instilled particles with a diameter < 100 nm diffuse rapidly from the lung into the circulation system (Nemmar et al. 2001). Amphibole asbestos, as well as other fibrous minerals and synthetic inorganic fibers, have also been found in urine (e.g., Battaglia et al. 2005).

Amphibole in human lungs

There is a large body of scientific literature on the presence of amphibole asbestos and chrysotile in the human lungs (e.g., Chrug 1993; Roggli 2004). Many of the studies were done to correlate the cause of death with the subject's occupation (cases of occupational and paraoccupational exposure). Recently, investigations have been aimed at assessing the possible correlation between pathologies of the respiratory system and anthropogenic or natural environmental exposure, and to ascertain whether it is possible to determine the threshold value below which there is no risk of disease.

Asbestos fibers found in the lungs must have been respired. Thus an excellent way of assessing lifelong exposure to airborne and respirable fibers is to investigate fibers contained in the lungs. After fiber inhalation, a portion of the fiber burden is eliminated (by clearance) from the lungs. Both the clearance-persistence ratio and the difference in clearance mechanisms among individuals are unknown, so the dose-response relation between exposure and fiber burden in the lung is unclear. Nevertheless, this type of study is useful for classifying exposure, especially when information about the subject's activities is lacking. This type of study is also useful for assessing the type and relative quantities of asbestos fibers to which individuals were exposed with respect to respirable sizes and biopersistence characteristics (Roggli and Sharma 2004). If the examination of the fiber burden is done on biologic material, the data obtained provide useful information for assessing the risk of subsequent disease (Roggli 1990).

The finding of amphiboles in human lungs, like other minerals and toxicants in general, can be attributed to three kinds of exposure: occupational (and paraoccupational), anthropogenic in the environment, and natural environmental. Nevertheless, it is not rare for exposure to be of mixed origin and variable quantities. The finding of amphibole asbestos in the lungs proves that the subject has been exposed in some way to these minerals. The respired amphiboles can be airborne from an anthropogenic and/or natural source. We know that only crocidolite and amosite have been used in large quantities and in thousands of products by industry. The use of

anthophyllite has been undoubtedly far less and not widespread worldwide, essentially because of the scarcity of the economically exploitable deposits. Tremolite and actinolite have not been industrially exploited because their technological properties are not particularly useful, and as for anthophyllite, economically exploitable deposits are lacking.

While the distribution of crocidolite and amosite is high in the anthropogenic environment because of their widespread use, tremolite and actinolite are commonly only found in the natural environment. Indeed, these two calcic amphiboles are ubiquitous in ophiolite complexes and greenstones in many areas of the world (e.g., Ross and Nolan 2003). In areas where there are outcropping rocks bearing only tremolite and actinolite as amphibole asbestos, their presence in the air can be reasonably related to a natural source. If in the same air environment, crocidolite fibers are also present, the source must necessarily be anthropogenic, such as an asbestos-cement roofing (Fornero 2005). For example, if tremolite and actinolite fibers are the only types found in the lungs of a subject, it is possible to exclude professional exposure to commercial amphibole asbestos (i.e., crocidolite and amosite). The presence of different kinds of asbestos fibers in the air depends on their presence in different matrices. Obviously, asbestos inhalation is possible only if the minerals are airborne. In distinguishing occupational, anthropogenic, or natural fiber sources, the situation may become more complicated because: (1) there are no physical barriers limiting fiber distribution, (2) asbestos fibers are spread worldwide due to occupational, anthropogenic, and natural occurrences, (3) for reasons of work, residence and lifestyle, human beings are exposed to very different environments, and (4) humans respire fibers regardless of the sources.

In order to have a general view of the various situations leading to amphibole asbestos in the lungs, some case studies regarding different types of exposure are briefly illustrated below. In some cases, the fiber concentrations found in humans are reported in Table 6, together with information about the presence or absence of asbestos-related pathologies in the subjects. The fiber concentration is indicated as the number of fibers $\times 10^6$ per gram of dried tissue (ff $\times 10^6$ /gdt), as most commonly indicated in the literature.

The determination of the fiber burden in the lungs and in other biological materials requires the fibers' identification and quantification by SEM-EDS and/or TEM-EDS; however, there is a possibility to use powder XRD. The means of acquiring, treating, and investigating biological samples by SEM and/or TEM with EDS and the type and quantification of the inorganic fibers are discussed by Roggli (2004), Roggli and Sharma (2004), and Belluso et al. (2006a). However, it is necessary to bear in mind that an internationally adopted protocol for studying fiber burden in biological samples does not exist, and various laboratories use slightly different techniques (Tossavainen et al. 2001). Therefore, the data reported in Table 6 have to be viewed with some caution. To be able to make an interlaboratory comparison, it is international practice to indicate the fiber concentration (i.e., mineralogical burden) as fibers per gram of dry tissue (ff/gdt).

High quantities of crocidolite and amosite amphiboles in the lungs are common not only in miners of the material but also in subjects professionally exposed to asbestos. Different species of amphibole have been found in the lungs of workers exposed to various kinds of fibers. This is the case for workers from a factory producing insulation boards predominantly using amosite (occupational exposure). In the workers' lungs, high quantities of amosite fibers and lesser amounts of crocidolite, chrysotile, mullite, and anthophyllite were detected (Gibbs et al. 1994). Also, the same kinds of fibers as used in an asbestos-cement factory were found in the lungs of inhabitants who lived near the factory (i.e., anthropogenic environmental exposure). In addition to crocidolite, amosite, and anthophyllite (the fibers present at the asbestos-cement factory), a small quantity of tremolite was also present in the neighbors' lungs (e.g., Magnani et al. 1998; Table 6). Similarly, for people who lived in the proximity of amosite or crocidolite mines and subjected to anthropogenic environmental exposure, amphiboles deposited and accumulated in their lungs (e.g., Roggli et al. 2002).

Table 6. Amphibole asbestos fiber burden ($ff \times 10^6/gdt$) found in human lungs.

	Tremolite	Actinolite	Anthophyllite	Amosite	Crocidolite
general population (not professionally exposed - no pathologies asbestos correlated)					
Vancouver (Churg 1993) ²	0.4	0	0	0.002	0.001*
East Texas (Dodson et al. 2000a) ²	0.002	0.002	0.002	0.002	0.002
hSV north-western Italy (Belluso et al. 2006b,c; Fornero 2005) ¹	0.327	0.030	0	0	0
ISV north-western Italy (Belluso et al. 2006b,c; Fornero 2005) ¹	0.053	0.007	0	0.006	0.002
LV north-western Italy (Belluso et al. 2006b,c; Fornero 2005) ¹	0.026	0.005	0	0	0
professional exposition, talc mine workers (with pathologies asbestos correlated)					
New York talc mine (Hull et al. 2002) no mesothelioma	0.1*		22.4	0	0
New York talc mine (Hull et al. 2002) with mesothelioma	556*		2.5	0	0
professional exposition, chrysotile mine workers (no pathologies asbestos correlated)					
South African mine (Rees et al. 2001)	0.33	0	0	0.14	0.13
professional exposition, chrysotile mine workers (no pathologies asbestos correlated)					
Churg 1983	50.0	0	0	0	0
professional exposition, vermiculite plant workers (no pathologies asbestos correlated)					
Libby (Wright et al. 2002)	5.94	1.78	0.05	0	0
professional exposition, asbestos-cement workers (unselected cases)					
Casale Monferrato, Italy (Magnani et al. 1998)	0.045	0	0.281*		0.706
anthropic environmental exposition near asbestos-cement factory (unselected cases)					
Casale Monferrato, Italy (Magnani et al. 1998)	0.006	0	0.004*		0.010
environmental exposition (with pathologies asbestos correlated)					
Corsica (Rey et al. 1993) ¹	21.0	0	0	0	0
Cyprus (Mc Connochie et al. 1987, 1989) ³	220.0	0	0	0	0

¹ natural environmental exposition to rocks bearing tremolite; ² general population; ³ anthropic-domestic environmental exposition; *not elsewhere specified
hSV = high Susa Valley - Piedmont, north-western Italy, cow lungs; ISV = low Susa Valley - Piedmont, north-western Italy, cow lungs; LV = Lanzo Valley - Piedmont, north-western Italy, cow lungs; AT = control group, Asti - Piedmont, north-western Italy, cow lungs; gdt = gram of dried tissue

Amphiboles used industrially are also present in the lungs of the general population (i.e., not professionally exposed), because the materials that contain and release asbestos are extremely widespread where humans live (e.g., Churg 1993; Dodson et al. 2000a; Table 6). Nevertheless, their fiber burden is generally much lower than the quantities found in the lungs of those professionally exposed. Also, in the general population, small quantities of other types of asbestos can be present. Crocidolite fibers in significant quantities have been found in the lungs of subjects professionally exposed to it in an almost unique way - crocidolite was used in the manufacture of cigarette filters (Dodson et al. 2002).

Tremolite and actinolite are commonly found in human lungs because they are widespread in the geological environment. The quantities are usually low, except in cases of indirect professional exposure, such as in people working in talc mines (together with anthophyllite asbestos: Hull et al. 2002; Table 6), chrysotile mines (e.g., Churg 1983; Table 6), and dolomite mines (with acicular wollastonite: Selden et al. 2001), where calcic amphiboles are naturally present at trace levels in the deposit. But there are also cases in which the contamination in the ore body is very low, so the same kind of professional activity (chrysotile mine workers) produces a far lower presence of tremolite asbestos in the lungs (e.g., Rees et al. 2001; Table 6). Even so, the amphiboles are very biopersistent, and with continuing exposure, amphiboles accumulate and remain unaltered in the lung. This behavior is different from that of chrysotile fibers; the chrysotile fibers are fragmented at their ends, and to a large extent they start to dissolve much more rapidly than amphiboles (e.g., Gibbons 1998; Bernstein 2005).

The quantity of amphibole present in human lungs through anthropogenic environmental exposure is generally low. However, in particular cases of exposure defined as domestic (i.e., in a household environment), the burden can be very high and comparable to occupational exposure. Tremolite fibers (usually with actinolite in smaller quantities) have been discovered in high quantities in the lungs of residents in Cyprus (McConnochie et al. 1987, 1989; Table 6), Greece (Constantopoulos et al. 1987), Turkey (Yazicioglu et al. 1980), New Caledonia (Luce et al. 1994, 2000; Browne and Wagner 2001), and Afghanistan (Voisin et al. 1994). The presence of abundant quantities of these types of asbestos in lungs has been attributed to anthropogenic environmental exposure (mainly of the domestic kind). These people lived in villages where houses were whitewashed and plastered using materials from local rock deposits that contained tremolite, and where streets were covered with materials containing amphibole asbestos. Interestingly, exposures in Turkey also include the use of baby-powder containing tremolite. Considerable quantities of amphibole asbestos have been seen in the lungs of the inhabitants of some areas in Corsica, France because they live in areas with outcropping rocks bearing a very high quantity of asbestiform tremolite (Magee et al. 1986; Rey et al. 1993; Table 1). However, in the lungs of inhabitants of Basilicata (southern Italy) with similar exposure routes to those in Corsica, lower quantities of these minerals have been found (Pasetto et al. 2004b).

It is common to find amphiboles in the lungs of the general population when they live near asbestos-bearing rock outcrops (e.g., in Piedmont, Belluso et al. 2006b,c; Fornero 2005; Table 6). Table 6 lists the lung burdens of subjects who lived in three different areas of Piedmont with actinolite- and tremolite-bearing rock outcrops and various levels of industrialization: the upper part (hSV) of the Susa Valley, which is industrialized to a limited extent; the lower part (lSV) of the Susa Valley, which is highly developed; and the Lanzo Valley (LV), which is moderately developed. On the basis of the geologic characteristics of these three areas, the presence of two calcic amphiboles is correctly attributable to release from a natural source.

Asbestos fibers of anthophyllite are not frequently found in the lungs because its deposits are not very widespread, occurring in only a few places in the world where it was produced economically. Nevertheless, in Finland, this asbestos has commonly been used (with chrysotile) in the manufacture of insulation materials. Anthophyllite fibers have been detected

in construction workers' lungs in variable quantities with crocidolite and lesser quantities of tremolite and amosite (Anttila et al. 1993). Abundant quantities of anthophyllite fibers have been detected in the lungs of talc-mine workers, because anthophyllite is naturally associated with talc (Hull et al. 2002). High and almost equal quantities of anthophyllite and tremolite have been seen in the lungs of workers of an asbestos plant using rocks from chrysotile mines as raw material (Tossavainen et al. 2001). Much higher quantities have been found in an unusual case of mixed-dust exposure of a worker in an iron pipe foundry (Dodson and Levin 2001).

In recent years, in addition to regulated amphibole asbestos species, three other species of amphiboles have been found in human lungs and related to pathologies analogous to those that have traditionally been linked to commercial asbestos exposure. Fibers of an amphibole species recently discovered in Sicily, fluoro-edenite, have been found in the lungs of a subject nonoccupationally exposed to fibrous minerals who lived in an environment contaminated by this kind of fibers (anthropogenic and domestic environmental exposure). This is similar to what happened in Greece with regard to tremolite and actinolite (Paoletti et al. 2000). Winchite and richterite fibers, historically identified as tremolite and occurring in the former vermiculite mine near Libby, Montana (Bandli et al. 2003; Gunter et al. 2003; Meeker et al. 2003), have been detected in high quantities in workers at an expansion plant using vermiculite from this deposit (Wright et al. 2002).

Biomarkers

There exists the possibility of using asbestos biomarkers to determine possible asbestos exposure to an individual human or a human population. (See ATSDR (2006) for a review of the use of asbestos biomarkers.) These can be, for example, agents or their metabolites that in particular conditions are present and detectable in the body. To have an indication of the level of exposure to a contaminant, selective markers of exposure are based on the direct measurement of the chemical substance or its metabolites. Amphibole asbestos particles are altered to only a small extent on inhalation, thus they are suitable for use as biomarkers to evaluate exposure. One kind of exposure assessment is based on counting peculiar biomarkers that are golden brown elongated objects, beaded or segmented, and clearly visible with the light microscope. In 1929, these formations were recognized as structures that had formed around asbestos fibers, and they were named "asbestos bodies" (ABs). Their identification was related to the pathology causing death and attributed to professional exposure to asbestos. Afterward, however, *in vivo* animal experiments observed similar structures forming around inorganic dusts of nonelongated habit (such as cosmetic talc intratracheally instilled into the lungs; Roggli 2004) as well as asbestos, so a new term was used to describe them: pseudoasbestos body (Churg et al. 1979; Roggli 2004). It has now been verified that these bodies form around inorganic fibrous material of any chemical nature whatsoever (e.g., fibers of TiO_2 ; Bologna et al. 2005) and refractory ceramic fibers (Dumortier et al. 2001), the generic term "ferruginous bodies" (FB) is preferred when the precise nature of the core is not known (Roggli 2004).

The formation of these structures seems related to the dimensions of the inorganic particle inhaled and deposited in the lung parenchyma. The smallest particles are phagocytized by the macrophages. Fibers with a significantly greater length than the size of the macrophages (whose diameter is about 15-20 μm) are instead covered, partially or totally, by iron-protein-mucopolysaccharide material (Roggli 2004). It seems that this coating can reduce the cytotoxicity of fibers. On the basis of the considerable scientific literature on this subject, it is possible to state that the majority of ferruginous bodies isolated from human lungs and morphologically identifiable as ABs possess an amphibole core (Fig. 30), suggesting a preferential protective mechanism toward these mineralogical species. The amphibole species covered are not limited to the regulated amphiboles, and this would seem logical. Indeed, the study by Paoletti et al. (2000) reports the post-mortem finding of FB with a fluoro-edenite amphibole core in the lung of a subject who lived in Biancavilla.

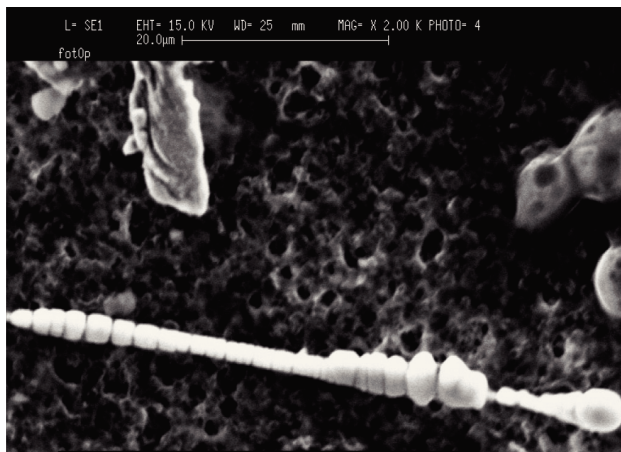


Figure 30. A secondary-electron image of an asbestos body with a tremolite fiber core, extracted from autopsy lung tissue.

FBs are used as biomarkers of internal dose, and specifically as selective biomarkers of exposure, because their presence in the various biological samples in any case indicates exposure to respirable inorganic fibers. If the core is identified as asbestos (and therefore they are true ABs), it follows that the subject has been exposed to asbestos. AB counting in BALF or in lung tissue may be used as a valid biomarker, on condition that the core is undeniably identified as asbestos. The AB quantities internationally established by the International Expert Meeting on Asbestos, Asbestosis and Cancer of Helsinki (Tossavainen 1997) and made official by the European Respiratory Society guidelines exposition (De Vuyst et al. 1998) to indicate high probabilities of professional exposure to asbestos are:

ABs burden in lung tissue more than 1×10^3 / gdt (gram of dried tissue);

ABs burden in lung tissue more than 1×10^2 / gwt (gram of wet tissue);

ABs concentration in the BALF more than 1 / ml.

The AB concentrations in the BALF and in the lungs are correlated (De Vuyst et al. 1998). Knowledge of the AB burden is also useful when the exact type of asbestos exposure is not available. Similarly to the ABs, the concentration of fibers is used as an exposure biomarker. Indeed, their presence in biological material is indicative of exposure. The evaluation of the fiber presence in BALF (e.g., De Vuyst et al. 1997) and in sputum (e.g., McDonald et al. 1992) is more suitable as a qualitative biomarker, while the detection and fiber counts in autopsied or surgically resected lung tissue samples supply more representative data (e.g., Dodson et al. 1999). To determine the effective kind of exposure, it is also possible to use fibers detectable in urine as a biomarker, but this marker does not reflect the quantity accumulated and it is not predictive of health effects.

Generally speaking, high quantities of fibers indicate exposure in an occupational setting. The quantities internationally established by the International Expert Meeting on Asbestos, Asbestosis, and Cancer of Helsinki (Tossavainen 1997) and made official by the European Respiratory Society guidelines exposition (De Vuyst et al. 1998) as indicative of significant asbestos exposure are:

amphibole fiber burden with a length of $> 5 \mu\text{m}$ more than 1×10^5 / gdt,

amphibole fiber burden with a length of $> 1 \mu\text{m}$ more than 1×10^6 / gdt.

Some studies have concluded that AB concentrations over 250 ABs/gdt and chrysotile or tremolite fiber concentrations greater than 1×10^5 / gdt are “robust indicators of mining-area residence” (Case 1994). For an accurate assessment of past asbestos exposure, it is considered that an analysis of the concentration of ABs or asbestos fibers in lung tissue samples may be better than the analysis of BALF or sputum. However, investigations of fiber burden and relation to asbestos exposure are not without difficulties and present both advantages and disadvantages owing to the presence of many variables (ATSDR 2006).

The concentration of retained amphibole asbestos in lung-tissue samples has also been used to try to determine potential dose-response relation for asbestos-induced pathologies and to attribute risk to specific fiber-types and dimension classes. The medical risks are higher in relation to the dimensions of the fibers (the most dangerous fibers are very thin with a high length-width ratio), surface structure and interactions (ion exchange, acid-base catalysis, oxidation-reduction), duration of exposure, quantity of fibers breathed, fiber biodurability, and fiber Fe-content, with the latter being the least important factor (Van Oss et al. 1999; Committee on Asbestos 2006). On the basis of these factors, the pathogenicity of amphibole asbestos seems to be: crocidolite, tremolite asbestos, and amosite (Van Oss et al. 1999).

When discussing biomarkers for asbestos in general, the term “biomarker” means some pathological formation indicating the presence of asbestos-related pathologies, such as the ferruginous bodies described above or pleural plaques as markers of asbestos exposure (e.g., Churg 1983). However more recently, biological alterations, such as differences in modulation in DNA-adduct formation between people exposed to asbestos and those without exposure (Committee on Asbestos 2006), are being used as biomarkers. Even so, to date there is not an ideal biomarker for asbestos (ATSDR 2006).

Amphiboles in animal lungs

After the discovery of the pathogenicity of asbestos in humans, *in vivo* experiments began and continue today on various kinds of animals in an attempt to understand the mechanisms that lead to disease (i.e., where the fibers are deposited in the lung, the fate of the inhaled fibers, biopersistence and clearance, toxicity mechanisms provoked by fibers, comparison between responses to various types of asbestos and other kinds of fibers, etc.). These experiments have also shown the high biopersistence and biodurability of amphibole asbestos in the lungs (e.g., Bernstein et al. 2005) and that chrysotile is much less so (e.g., Hume and Rimstidt 1992). While these experiments provide valuable information for high-dose exposure, comparable to occupational levels, they do not address the question that is more recently become of greater concern - the health effects from long-term, low-dose exposure that occurs in the natural environment. Investigations into this kind of exposure have been done on animal populations, defined as the “animal sentinel system” (ASS), which are exposed to various airborne and potentially toxic pollutants, among which is asbestos, to evaluate their possible health effects. The concept of using animals as sentinel markers is not new: canaries were used for a long time in mines to detect the presence of carbon monoxide (van der Schalie 1999). However, it was much easier to see when the canary died (because it was very susceptible to oxygen level in the mine) than to relate the lung contents of an animal to the health risk of a human.

Regardless, ASS shows some promise because: (1) the reactions of animal bodies to various kinds of exposure are comparable to that of humans; (2) in animals the latency period for the development of some diseases is shorter; and, (3) animals do not have confounders such as possible occupational or paraoccupational exposure or lifestyle (e.g., smoking cigarettes). One limit of ASS is that the anatomy of the respiratory system and the clearance mechanisms are different from humans, and there are anatomical and physiological differences among the various animal species. Therefore, fiber deposition in the lungs does not occur in the same way (Backer et al. 2001). Nevertheless, the advantages of the ASS may be extremely useful for the purposes of the indirect evaluation of the kind and quantity of airborne fibers of breathable

dimensions in the environment. For instance, animals in isolated parts of the world could be used to obtain ambient, nonanthropogenic levels of minerals. The animals in question would act as a biological sampler and could be used to map natural environmental risk of asbestos exposure (Belluso et al. 2006b). Pets, especially dogs, are particularly useful in predicting the health risk of their owners. For example, this is the case for dogs who have died of mesothelioma; the dog's pathology permitted the recognition of domestic environmental pollution of high doses of amphibole asbestos (Glickman et al. 1983).

At present, there are very few studies on natural environmental evaluation based on ASS. Moreover, each study has too few animals to obtain a statistically reliable assessment of environmental risk. Tremolite fibers have been detected in the parietal pleura of one dog and two goats that lived in some areas of Corsica where there are outcropping serpentinitic rocks bearing this material (Rey et al. 1993). Comparable results have been obtained from goats that lived in areas contiguous to those described above (Dumortier et al. 2005). The concentrations are lower than those detected in occupationally exposed humans. A recent study reports a high burden of tremolite and actinolite fibers in the lungs of cats and dogs from El Dorado Hills, California (Abraham et al. 2005). Fluoro-edenite fibers have been detected in the lungs of sheep near Biancavilla in Sicily, where this asbestiform amphibole was discovered after the detection of a mesothelioma cluster (De Nardo et al. 2004).

Table 7 shows the tremolite fiber burden in 11 animal groups at three different locations (California, Corsica, Piedmont). Nine groups had environmental exposure to amphibole. The remaining two groups were used as controls because they live in areas where amphiboles do not occur. Fibers of tremolite and actinolite were detected in the lungs of all exposed animals, whereas none were observed in the control groups. The concentrations are low in Italian animals, and from low to high, depending on the zone, in Corsican and Californian animals. Commercial asbestos fibers (amosite and crocidolite) have been detected in the lungs of two groups of

Table 7. Amphibole asbestos fiber burden ($\text{ff} \times 10^6/\text{gdt}$) in animal lungs.

Location/Group	Tremolite	Actinolite	Anthophyllite	Amosite	Crocidolite
hSV	0.007	0.006	0	0	0
ISV	0.050	0.011	0	0.003	0.002
LV	0.034	0.008	0	0.001	0
SVVC	0.002	0	0	0	0
ATcg	0	0	0	0	0
COa	0.405	0	0	0	0
COb	3.350	0	0	0	0
COc	0.141	0	0	0	0
CAa	0.121		0	0	0
CAb	2.976		0	0	0
CACg	0		0	0	0

hSV = High Susa Valley - Piedmont, north-western Italy, cow lungs (Belluso et al. 2006b,c)

ISV = Low Susa Valley - Piedmont, north-western Italy, cow lungs (Belluso et al. 2006b,c)

LV = Lanzo Valley - Piedmont, north-western Italy, cow lungs (Belluso et al. 2006b,c)

SVVC = Sesia Valley Vercelli - Piedmont, north-western Italy, cow lungs (Battaglia 2006)

ATcg = control group, Asti - Piedmont, north-western Italy, cow lungs (Belluso et al. 2006b,c)

COa = north-eastern Corsica, dog parietal pleural (Rey et al. 1993)

COb = north-eastern Corsica, goats parietal pleural (Rey et al. 1993)

COc = north-eastern Corsica, goat lungs (Dumortier et al. 2005)

CAa = El Dorado, California, cat lung (Abraham et al. 2005)

CAb = El Dorado, California, dog lung (Abraham et al. 2005)

CACg = control group, California, cat lung (Abraham et al. 2005)

gdt = gram of dried tissue

animals from Italy (Piedmont Region). Their presence is compatible with the considerable industrialization of the area and the use of asbestos containing materials.

Amphiboles in human urine

Once the possibility of detecting amphibole asbestos fibers in the urine (Cook and Olson 1979) was verified, the few studies done since then have shown that the quantity of fibers expelled with urine is not related to the concentration of fibers present in the air or in the ingested drinking water (Boatman et al. 1983; Finn and Hallenbeck 1985). Nevertheless, it is evident that the presence and concentrations of asbestos in urine can be used as biomarkers of exposure both for individuals occupationally exposed and the general public. Indeed, high concentrations are indicative of exposure to high doses, while low quantities are indicative of normal environmental exposure, like those found in the general population. However, the presence of asbestos fibers in urine is only an indicator of recent exposure, from a few days to a few months before the sample was taken (Cook and Olson 1979; ATSDR 2006). This is because the fibers enter the digestive system as they are rapidly cleared from the respiratory system, and the residence time in the digestive system is short. The detection of fibers in urine is therefore not suitable for biomonitoring of chronic exposure to asbestos, but it is particularly useful for monitoring, almost "in real time," the presence of respirable fibers. These data enable evaluation of both environmental background of fibers and those from anthropogenic sources. Also for these investigations, the distinction between natural and anthropogenic source for the detected fibers may be made when knowledge is available about the minerals of the local geological environment.

Table 8 shows the types and quantities of amphibole fibers detected in the urine of people living in five areas of the Piedmont Region of northwestern Italy. Four of the areas have rock outcrops bearing tremolite and actinolite, and have various levels of industrialization. The areas have been divided into the upper part (HSV, not very industrialized), the lower part (ISV, very highly industrialized), the Lanzo Valley (LV, moderate industrialization), and the Sesia Valley (SVVC), a mountain area with low industrialization and few rocks bearing tremolite and actinolite. The latter is a control group from an area in which tremolite and actinolite are geologically lacking.

The data are shown as the number of fibers per 1 cc (ff/1 cc), the internationally accepted unit system, to indicate the urine-fiber concentration for inter-laboratory comparison. Asbestos fibers classifiable as from the natural source (i.e., tremolite and actinolite) have been detected in two areas, and their quantity is higher than in the control group (ATcg). This result shows that the subjects have been exposed to these fibers, that these fibers were airborne, and that their quantity is higher than in the control area. Changes in exposure can be evaluated only if the tests are repeated for the same area at regular intervals. The fact that other types of fibers have

Table 8. Types and quantities (ff/1 cc) of amphibole fibers detected in the urine of people living in five areas of the Piedmont Region of northwestern Italy.

Location/Group	Tremolite	Actinolite	Anthophyllite	Amosite	Crocidolite
hSV	2.7	0	0	0	0
ISV	1.6	0	0	0	0
LV	0	0	0	0	0
SVVC	0	0	0	0	0
ATcg		1	0	0	0

hSV = High Susa Valley - Piedmont, north-western Italy (Belluso et al. 2006b,c)

ISV = Low Susa Valley - Piedmont, north-western Italy (Belluso et al. 2006b,c)

LV = Lanzo Valley - Piedmont, north-western Italy (Belluso et al. 2006b,c)

SVVC = Sesia Valley Vercelli - Piedmont, north-western Italy (Battaglia 2006)

ATcg = control group, Asti - Piedmont, north-western Italy (Belluso et al. 2006b,c)

not been detected in these samples cannot be interpreted as their absence in the environment. To have more certain data, more sampling tests are needed. Also, it is necessary to consider what minerals might dissolve in the low pH environment of the stomach.

Conclusion for humans and animals

Today, nearly all scientific papers on the identification of pathologies and pathological symptoms (e.g., pleural plaques) attribute their formation to fibrous species to which the subject has been exposed in his or her living or working environment - without any research into mineral identification and quantification of fibers in the tissues involved. This failure may give rise to assessment errors in the medical investigations (and some medical researchers like Governa et al. 2006, have begun to consider it important) and certainly does not supply any information about the quantity of fibers, per individual species, that were inhaled and biopersisted. The quantity of airborne fibers that may be inhaled and respired from the environment of the various areas has not been assessed. Therefore, information about the fibrous respirable fraction constituting the environmental background of various areas of the world is not known, and neither is the amount of fibers that have been placed into the air by human activities.

In the attempt to understand whether it is possible to approximately quantify an accumulation *threshold value* above which clearance is no longer active and cancer pathologies develop for these types of asbestos, it may be useful: (1) to examine the mineralogical burden of human lungs for nonoccupational individuals and the lungs of animals that lived in areas with outcropping rocks bearing crocidolite and amosite asbestos (this investigation would provide the natural background of respirable asbestos fibers, for these areas, as well as the other minerals that occur in the lungs), and (2) to compare the values of the local natural background with the asbestos fiber burden in the lungs of subjects occupationally exposed to this type of asbestos and of those who died of mesothelioma (Belluso et al. 2005).

For a correct evaluation of the amphibole (and also chrysotile) asbestos risk for each area of interest, the following procedures are necessary:

1. Investigation and identification of the mineral fibers that may be present in the outcropping rocks and soils;
2. Environmental-background evaluation, including mineralogical studies of the type, quantity, and dimensions of airborne fibers and the distinction between asbestos from natural and from anthropogenic sources;
3. Assessment of the mineralogical burden in ASS to determine the respirable fraction of amphibole fibers present in the environmental background;
4. Assessment of the mineralogical burden in the lungs of people with asbestos-related pathologies who lived or are living in these areas.

In the areas assessed as being of amphibole asbestos risk by these investigations, periodic investigation of and identification of mineral fibers in urine would enable the environmental situation to be monitored almost in "real time" and, when necessary, it would make it possible to activate suitable measures of medical prevention. In the areas where the mineralogical investigations have shown the presence (in the outcropping rocks) of noncommercial asbestos (e.g., tremolite and actinolite) and the anemometric characteristics exclude transportation of these from other areas, the above-mentioned types of asbestos can be used as biomarkers of natural environmental exposure insofar as it is airborne from a natural source.

STABILITY OF AMPHIBOLES

It comes as no surprise to the geological community that amphiboles can and do alter in the geological environment to other minerals. However, this often comes as a major surprise

to those outside of our community. For example, once when mentioned that an amphibole can convert to a pyroxene by heating, non-geological colleagues commonly insist that it is a mineral and will not change! However, in the fields relating to amphiboles many geologists would think about amphibole stability in terms of varying metamorphic conditions (i.e., that is to say the formation of amphiboles during metamorphic events), while others would think of their stability during formation in igneous rocks and yet others their occurrence in sediments. What we would like to do in this section is to turn our attention to the formation of amphiboles from other minerals or the alteration of amphiboles into other minerals that may occur in the arena of human exposures or the human body itself.

Temperature conversions

It is well known in the geological community that amphibole will convert to pyroxene with increasing temperature. Figure 31 shows two powder X-ray diffraction patterns: one of an unheated sample of amphibole from Libby, Montana, and the other of the same sample heated to 1,000 °C for 10 minutes. Note that the amphibole peaks have disappeared and have been replaced by pyroxene peaks. Thus in any industrial setting where temperatures were above approximately 900 °C, the amphibole could convert to pyroxene if the kinetics of reaction were fast enough. Based on our knowledge of geologic conditions, we can predict when some of these conditions will occur, and then verify them experimentally. These temperature conversions could be significant for the Libby amphiboles in two separate conditions: (1) during the expansion

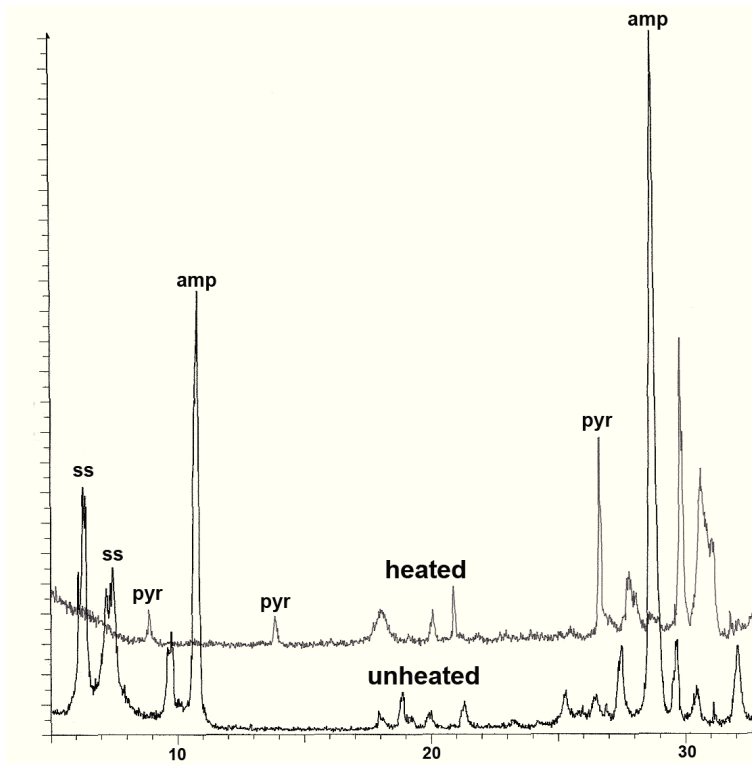


Figure 31. The lower powder diffraction pattern is of an amphibole (amp) sample from Libby that contains some sheet silicates (ss). The upper pattern is of the same sample after heating for 10 minutes at 1,000 °C; note how the amphibole has converted to pyroxene (pyr).

process (popping) of the Libby vermiculite during which the samples are heated to over 1,000 °C for a few seconds; (2) in a woodstove in which temperature can reach upwards of 900 °C. The issue here is that fibers of amphibole have been found in the bark of trees near Libby and burning this wood might disperse the fibers. Even though (to our knowledge) no converted amphiboles have been found in either setting, it is this sort of thought process that the geological community needs to make more widely known to the regulatory and health communities.

In the lung

The conditions in the human lung are somewhat similar to the conditions at the surface of the Earth: 37 °C with pH 7.35, and lung fluid has a known composition. Thus we can use our knowledge of mineral reactions on the surface of the Earth to help understand mineral reactions in the lung. The impetus for this line of research comes from basic observations of the mineral content of chrysotile-asbestos workers on autopsy. It was noted by Wagner et al. (1987) that the chrysotile-miners' lung loads are typically very high in tremolite with only a low content of chrysotile. However, Figures 9 and 10 show that the amphibole content of these ores is very small (i.e., <1%). In Wagner's study, they said that they could find no tremolite in chrysotile ores from Canada unless they put the material into a rat lung and waited for six months. Clearly, something happens to the chrysotile:tremolite ratio in the lung. Based upon the work of several researchers (e.g., Hume and Rimstidt 1992), chrysotile dissolves in the lung at a fairly rapid rate. Thus we are seeing the chemical weathering (i.e., dissolution) of a mineral in the lung in a manner similar to that at the Earth's surface. Figure 32 shows calculations for a mixture of quartz, tremolite, and chrysotile in lung fluid (Wood et al. 2006). The diagram shows that quartz does not dissolve, and that tremolite starts to dissolve (but only after a long period of time), and chrysotile dissolves in less than one year. Interestingly, two other minerals form: dolomite and hydroxylapatite. Dolomite forms as chrysotile dissolves, whereas hydroxylapatite appears to form at the expense of none of the dissolving minerals. This makes sense from a human physiology perspective in that a body is in near equilibrium with hydroxylapatite. As part of our ongoing research, we are attempting to model more mineral reactions in the lungs and to study materials that occur in the lung. Figure 33 shows a large solid particle with the approximate chemical formula of hydroxylapatite observed in autopsied lung tissue. This particle could not have been respired because it is too large; thus, it grew in place in the lung.

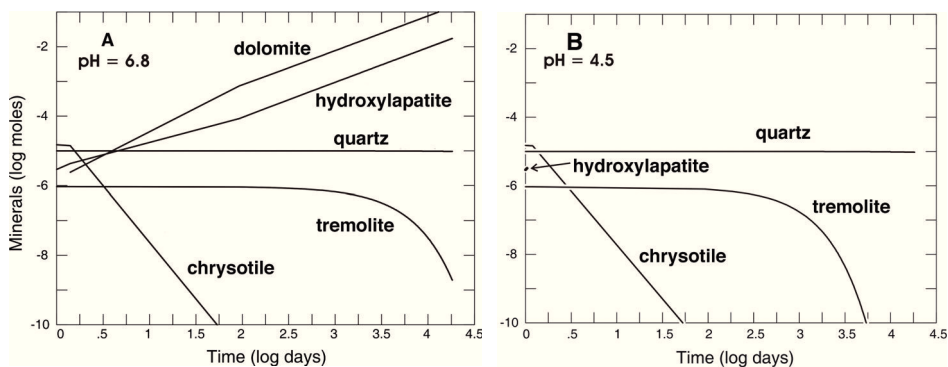


Figure 32. Two calculated reaction paths for a mixture of chrysotile, tremolite, and quartz placed in a simulated lung fluid at 37 °C and pH = 6.8 (A) and pH = 4.5 (B), the former representing lung fluid and the latter representing lysosome fluid in a macrophage. In both cases, chrysotile dissolves in about 60 days, while quartz is stable. Tremolite starts to dissolve in about eight years (A) and six years (B). Also note that hydroxylapatite forms under both pH conditions, but remains only in the higher pH run (modified from Wood et al. 2006).

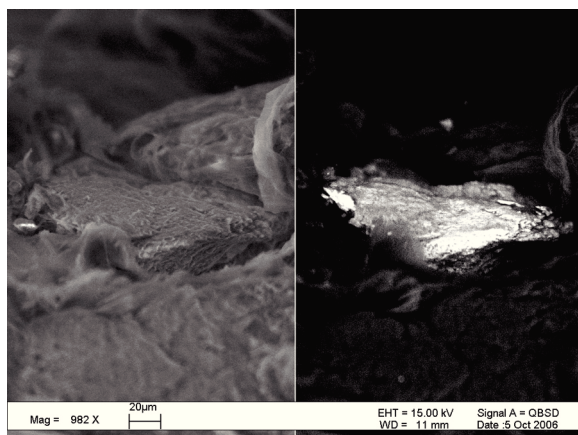


Figure 33. FESEM images of a lung tissue sample of a human pleural plaque, post autopsy. The particle in (A) is almost 100 μm long, too big to be respired; it formed in the lung. B) A backscattered-electron image of the same particle.

Based on previous discussion, we know that minerals may: (1) persist in the lung (i.e., quartz), (2) dissolve (i.e., chrysotile), or (3) form (e.g., hydroxylapatite). A fourth possibility is one mineral could alter to another mineral; this occurs often in the geological environment. Our original idea that sent us down the research path for calculating mineral stabilities in the lung, was the possibility that chrysotile might alter to tremolite; this would help explain the large amounts of tremolite in the lungs of chrysotile miners. Preliminary calculations indicated this transformation might occur (Taunton et al. 2002) whereas later more refined calculations indicate that it will not occur (Wood et al. 2006). However, this does not preclude the possibility of other mineral reactions occurring in the lung. Along with our calculations, we have also placed chrysotile ore in simulated lung fluid. To date, these experiments are only of one-year duration, and we have seen no conversion of chrysotile to tremolite. However, we have seen formation of hydroxylapatite as predicted from the calculations.

FUTURE AREAS OF RESEARCH

What seems like the most important issue for the mineralogical community is to assist the regulatory community in distinguishing between fibers and fragments of amphiboles. However, the single most important area for future research is to determine if there are significant differences between the health effects of fibers and fragments of amphiboles. To do this will require collaborative efforts between mineralogists and the medical community for both *in vivo* and *in vitro* experiments. Probably the largest single role of the mineralogy community will be to provide well-characterized suites of these samples to the medical community [e.g., the preliminary work of Bellamy and Gunter (2006) on the Libby material and more thorough studies of Guthrie (1992, 1997) which reviewed several mineral groups]. Another major contribution for mineralogists and geochemists is to predict how minerals behave in the lung by modeling the lung as a low-temperature aqueous system (see the recent work of Taunton et al. 2002, Plumlee et al. 2006, Wood et al. 2006 for examples).

Other major contributions from the geologic community would be to help determine environmental exposure to minerals based on dust sampling, geological mapping, and integrated epidemiological studies. For example, Norton and Gunter (1999) examined the relation between respiratory disease and quartz content of dust in Idaho. Such studies go in concert with the recommendations made at the end of the section on amphiboles in biological materials. Currently in California, Pan et al. (2005) proposed a relation between mesothelioma and proximity to ultramafic rock bodies. More of these types of studies are needed to confirm

or disprove these types of geological relations. Also, the geologic community can aid in educating the public and teaching students on the risks associated with exposure to minerals in the environment. One example of this was discussed by Gunter (1994) using the general issues of asbestos, another by Gunter (1999) for issues dealing with quartz as a “known human carcinogen.” A classroom exercise is given by Taunton and Gunter (2007) for correlation (or lack thereof) of lung cancer and breast cancer with geologic maps.

There are many areas outside the fields of Mineralogy and Geochemistry that are in need of more research. One of the main areas is in the determination of other causes of mesothelioma. Recently, Dogan et al. (2006) showed that mesothelioma cases caused by erionite in Turkey is also related to genetics. It seems that there is a genetic predisposition for those who succumb to the disease if the parents also had the disease (Dogan et al. 2006). There is still another concern that SV-40 may be a cofactor causing mesothelioma (Baldi et al. 2001). As we have seen in this chapter, the mesothelioma rate in Italy is increasing; can this increase be related solely to amphibole-asbestos exposure?

SUMMARY

Throughout history, humans have been exposed to dust. Yet for all such dust exposure, the case of asbestos has received the most attention, probably because more people have been afflicted with asbestos-related disease than for any other mineral. Why is this? Clearly, the dose is the most important single criteria for contracting a disease. Increased dose resulting from asbestos exposure might relate to the fact that asbestos fibers are very small and, in turn, more respirable than other minerals. Thus the property of asbestos, becoming thinner and thinner as it is mined and processed, will cause it to produce many more respirable particles than any other mineral (i.e., the asbestiform habit lends itself to producing very small particles with only a minimum amount of applied force). The fact that asbestos minerals may be the only minerals in Nature that can easily be reduced to respirable size, coupled with high doses of these minerals for workers and the fact that the asbestos minerals are more biopersistent than other minerals such as calcite, might explain why workers suffer from asbestos-related diseases.

Four concluding points on the discussion of human health, environmental concerns, and amphiboles are: (1) the health impact of inhalation of amphibole asbestos is worse than that of chrysotile asbestos, (2) occupational exposure to amphibole asbestos is much more harmful than nonoccupational exposure to amphibole asbestos, (3) it is not clear whether low-level environmental exposure to amphibole is a significant health risk, and (4) there is still considerable research needed to understand how minerals behave in the lung. Also, in the USA, there needs to be a coming together of the different groups (i.e., mineralogist, geochemist, geologist, medical, legal, regulatory, and industrial communities) to try and educate the public to reduce the fear of exposure to minerals in their natural environment.

ACKNOWLEDGMENTS

MEG would like to thank his past students who have worked with him in this area, as well as Nicole Bellino for her efforts in assisting with the references and formatting of this chapter, and Anne Taunton for reading and editing an earlier draft. EB would like to thank pathologist Donata Bellis, collaborator Silvana Capella, and Professor Giovanni Ferraris for useful medical information, data to build tables, and critical incitement respectively. AM would like to thank his student F. de Grisogono for his assistance in preparing this chapter. Last we would like to thank Frank Hawthorne for a meticulous job of editing this chapter, and Jodi Rosso for the wonderful layout of this chapter and its many figures.

REFERENCES

- Abraham JL, Case BW, Burnett BR, Trent T (2005) Lung-retained fiber in pets confirms environmental exposure to naturally-occurring asbestos in Western El Dorado County, California. *Proc Am Thoracic Soc* 2:A818
- Abrahams PW (2002) Soils: their implications to human health. *Sci Tot Environ* 291:1-32
- Addison J, Davies LST (1990) Analysis of amphibole asbestos in chrysotile and other minerals. *Ann Occup Hygiene* 34:159-175
- Ahn JH, Buseck PR (1991) Microstructures and fiber formation mechanisms of crocidolite asbestos. *Am Mineral* 76:1467-1478
- Amandus HE, Wheeler R (1987) The morbidity and mortality of vermiculite miners and millers exposed to tremolite-actinolite: Part II. Mortality. *Am J Ind Med* 11:15-26
- Amandus HE, Wheeler R, Jankovic J, Tucker J (1987a) The morbidity and mortality of vermiculite miners and millers exposed to tremolite-actinolite: Part I. Exposure estimates. *Am J Ind Med* 11:1-14
- Amandus HE, Althouse R, Morgan WKC, Sargent EN, Jones R (1987b) The morbidity and mortality of vermiculite miners and millers exposed to tremolite-actinolite: Part III. Radiographic findings. *Am J Ind Med* 11:27-37
- Anttila S, Karjalainen A, Taikin-Aho O, Kyyrönen P, Vainio H (1993) Lung cancer in the lower lobe is associated with pulmonary asbestos fiber count and fiber size. *Environ Health Perspect* 101:166-170
- Atkinson GR, Rose D, Thomas K, Jones D, Chatfield E, Going J (1982) Collection, analysis and characterization of vermiculite samples for fiber content and asbestos contamination. Midwest Research Institute Report to EPA, Project 4901-A32, Contract No 68-01-5915, Washington DC
- ATSDR (2000) Health consultation, Libby asbestos site, Libby, Lincoln County, Montana. Mortality from asbestosis in Libby, Montana, 1979-1998, December 12, 2000. Agency for Toxic Substances and Disease Registry, Atlanta, Georgia
- ATSDR (2001) Medical testing of individuals potentially exposed to asbestiform minerals associated with vermiculite in Libby, Montana. A report to the community. Division of Health Studies, US Dep of Health and Human Services, Atlanta, Georgia
- ATSDR (2006) Report on the expert panel on biomarkers of asbestos exposure and disease. ERG contract 2006
- Attanos RL, Gibbs AR (2000) Primary malignant gonadal mesotheliomas and asbestos. *Histopathol* 37:150-159
- Backer LC, Grindem CB, Corbett WT, Cullins L, Unter JL (2001) Pet dogs as sentinels for environmental contamination. *Sci Total Environ* 274:61-169
- Baldi F, Baldi A, Giordano G, Giordano A (2001) p53 and the retinoblastoma gene family in human mesothelioma: the SV40 hypothesis. *In: The Health Effects of Chrysotile Asbestos. Can Mineral Spec Publ* 5:141-144
- Bandli BR, Gunter ME (2001) Identification and characterization of mineral and asbestos particles using the spindle stage and the scanning electron microscope: The Libby, Montana, USA. amphibole-asbestos as an example. *The Microscope* 49:191-199
- Bandli BR, Gunter ME (2006) A review of scientific literature examining the mining history, geology, mineralogy, and amphibole asbestos health effects of the Rainy Creek Igneous Complex, Libby, Montana USA. *Inhal Toxicol* 18:949-962
- Bandli BR, Gunter ME, Twamley B, Foit FF Jr, Cornelius SB (2003) Optical, compositional, morphological, and X-ray data on eleven particles of amphibole from Libby, Montana, USA. *Can Mineral* 41:1241-1253
- Battaglia T (2006) Valutazione indiretta dell'inquinamento ambientale da amianto e fibre asbestiformi nel territorio della Valsesia tramite indagini di campioni biologici animali, Report, Torino University
- Battaglia T, Belluso E, Capella S, Fornero E, Ferraris G, Bellis D, Biagini G, Pugnali A, Panico AM, Cardile V (2005) Monitoring of respirable mineral fibres in the Biancavilla area (Sicily) by SEM-EDS analysis of urine. *In: Proc Int Conf Asbestos Monitoring and Analytical Methods*, p 68-69
- Bellamy JM, Gunter ME (2006) Morphological characterization of amphiboles used in *in vivo* studies. *Geological Society of America Abstracts with Programs*, vol. 38, #7, p 366
- Belluso E, Bellis D, Fornero E, Capella S, Ferraris G, Coverlizza S (2006a) Assessment of inorganic fibres burden in biological samples by SEM-EDS. *Microc Acta* 155:95-100, doi:10.1007/s00604-006-0524-y
- Belluso E, Bellis D, Bruni BM, Capella S, Coverlizza S, Ferraris G, Fornero E, Paoletti E, Rinaudo C (2006b) Studio preliminare sulla valutazione indiretta delle fibre inorganiche respirabili aerodisperse in Valle di Susa (Piemonte - Alpi Occidentali). *Rend Soc Geol Ital* 3:41-45
- Belluso E, Bellis D, Capella S, Fornero E, Battaglia T, Rinaudo C, Coverlizza S, Ferraris G, Pelissero F, Rey C, Benedetto F, Colzani A, Curti PC, Gobetto M, Graziano E (2006c) Indirect assessment of breathable inorganic fibres by sentinel animals of Piedmont areas (N-W Italy). *In: Proc Int Conf Asbestos Monitoring and Analytical Methods*, p 209
- Belluso E, Compagnoni R, Ferraris G (1994) Occurrence of asbestiform minerals in the serpentinites of the Piemonte Zone, Western Alps. *In: Giornata di studio in ricordo del Prof. Stefano Zucchetti*, Politecnico di Torino (ed), p 57-64

- Belluso E, Ferraris G, Alberico A (1997) Amianto, la componente ambientale: dove, quali e come sono gli amianti nelle Alpi Occidentali? *In: L'amianto: dall'ambiente di lavoro all'ambiente di vita. Nuovi indicatori per futuri effetti.* Minoia C, Scansetti G, Piolatto G, Massola A (eds) Fondazione Salvatore Maugeri, IRCCS, Pavia 1997 - I Documenti 12, p 167-174
- Bernstein DM (2005) Understanding chrysotile asbestos: a new perspective based upon current data. *In: Proc IOHA 2005 Pilanesberg*, J3:1-10
- Bernstein DM, Rogers R, Smith P (2005) The biopersistence of Canadian chrysotile asbestos following inhalation. Final results through 1 year after cessation of exposure. *Inhal Toxicol* 17:1-14
- Boatman ES, Merril T, O'Neill A, Polissar L, Millette JR (1983) Use of quantitative analysis of urine to assess exposure to asbestos fibers in drinking water in the Puget sound region. *Environ Health Perspect* 53:131-139
- Boettcher AL (1967) The Rainy Creek alkaline-ultramafic igneous complex near Libby, Montana. I: Ultramafic rocks and fenite, *J Geol* 75:526-553
- Bologna L, Ferri A, Lauria E, Wojtowicz M (2005) The necessity of SEM analysis in outdoor environment monitoring of airborne asbestos fibres. *In: Proc Int Conf Asbestos Monitoring and Analytical Methods*, p 22-23
- Brown BM, Gunter ME (2003) Morphological and optical characterization of amphiboles from Libby, Montana USA, by spindle stage assisted polarized light microscopy. *The Microscope* 51:121-140
- Browne K, Wagner JC (2001) Environmental exposure to amphibole-asbestos and mesothelioma. *In: The health effects of chrysotile asbestos. Contributions of Science to Risk-Management Decisions*, Nolan RP, Langer AM, Ross M, Wicks FJ, Martin RF (eds) *Can Mineral Special Pub* 5:21-28
- Burragato F, Comba P, Baiocchi V, Palladino DM, Simei S, Gianfagna A, Paletti, Pasetto R (2005) Geo-volcanological, mineralogical and environmental aspects of quarry materials related to pleural neoplasm in the area of Biancavilla, Mount Etna (Eastern Sicily, Italy). *Environ Geol* 47:855-868
- Burragato F, Crispino M, Montangano G, Monti A, Monti F, Papacchini L, Rossigni F, Schettino B, Sperduto B (2006) Environmental pollution from airborne asbestiform fibres: development of fibre propagation maps. Abstracts of the European Conference on Asbestos Risks and Management, p 85-90
- Case BW (1991) Health effects of tremolite. *In: The third wave of asbestos disease: Exposure to asbestos in place.* Landrigan PJ, Kazemi H (eds) *Annals of the New York Academy of Sciences* 643:491-504
- Case BW (1994) Biological indicators of chrysotile exposure. *Ann Occup Hyg* 38:503-518
- CDPHE: Colorado Department of Public Health and Environment (2006) Asbestos-contaminated soil. Guidance document. Hazardous Materials and Waste Management Division, Colorado Dept. of Public Health and Environment (303) 692-3300
- Clark RN, Hoefen TM, Sawzye GA, Livo KE, Meeker GP, Sutley S, Wilson S, Brownfield I, Vance JS (2003) Reflectance spectroscopy as a rapid assessment tool for the detection of amphiboles from the Libby, Montana region. *USGS OFR* 03-128.
- Churg A (1983) Asbestos fiber content of the lungs in patients with and without asbestos airways disease. *Am Rev Respir Dis* 127:470-473
- Churg A (1993) Asbestos lung patterns and disease patterns in man. *Rev Mineral* 28:410-426
- Churg A, Warnock ML, Green N (1979) Analysis of the cores of ferruginous (asbestos) bodies from the general population: II. True asbestos bodies and pseudoasbestos bodies. *Lab Invest* 40:31-38
- Comba P, Gianfagna A, Paoletti L (2003) The pleural mesothelioma cases in Biancavilla are related to the new fibrous amphibole fluoro-edenite. *Arch Environ Health* 58:229-232
- Comba P, Merler E, Pasetto R (2005) Asbestos-related diseases in Italy: Epidemiologic evidences and public health issues. *Int J Occup Environ Health* 11:36-44
- Committee on Asbestos (2006) Asbestos: selected cancers. Institute of Medicine, The National Academies Press, Washington, DC
- Constantopoulos SH, Saratzis N, Kontogiannis D, Karantanas A, Goudevenos JA, Katsiotis P (1987) Tremolite whitewashing and pleural calcifications. *Chest* 92:709-712
- Cook PM, Olson GF (1979) Ingested mineral fibers: elimination in human urine. *Science* 294:195-198
- Davis JMG, Addison J, McIntosh C, Miller BG, Niven K (1991) Variations in the carcinogenicity of tremolite dust samples of differing morphology. *In: The third wave of asbestos disease: Exposure to asbestos in place.* Landrigan PJ, Kazemi H (eds) *Annals of the New York Academy of Sciences* 643:473-490
- De Nardo P, Bruni B, Paoletti L, Pasetto R, Sirianni B (2004) Pulmonary fibre burden in sheep living in the Biancavilla area (Sicily): preliminary results. *Science Tot Environ* 325:51-58
- De Rita D, Frazzetta G, Romano R (1991) The Biancavilla-Montalto ignimbrite (Etna, Sicily). *Bull Volcanol* 53:121-131
- De Vuyst P, Dumortier P, Gevenois PA (1997) Analysis of asbestos bodies in BAL from subjects with particular exposures. *Am J Ind Med* 31:699-704
- De Vuyst P, Karjalainen A, Dumortier P, Pairon JC, Monso E, Brochard P, Teschler H, Tossavainen A, Gibs A (1998) Guidelines for mineral fibre analyses in biological samples: report of the ERS Working Group. *Eur Respir J* 11:1416-1426

- Dodson RF, Graef R, Shepherd S, O'Sullivan M, Levin J (2005) Asbestos burden in cases of mesothelioma from individuals from various regions of the United States. *Ultrastructural Pathology* 29:415-433
- Dodson RF, Levin JL (2001) An unusual case of mixed-dust exposure involving a "non commercial" asbestos. *Environ Health Perspect* 109:199-203
- Dodson RF, O'Sullivan M, Huang J, Holiday DB, Hammer SP (2000a) Asbestos in extrapulmonary sites Omentum and mesentery. *Chest* 117:486-493
- Dodson RF, Huang J, Bruce JR (2000b) Asbestos content in the lymph nodes of nonoccupationally exposed individuals. *Am J Ind Med* 37:169-174
- Dodson RF, Williams MG, Huang J, Bruce JR (1999) Tissue burden of asbestos in nonoccupationally exposed individuals from East Texas. *Am J Ind Med* 35:281-286
- Dodson RF, Williams MG, Satterley JD (2002) Asbestos burden in two cases of mesothelioma where the work history included manufacturing of cigarette filters. *J Toxic Environ Health Part A* 65:1109-1120
- Dogan AU, Baris YI, Dogan M, Emri S, Steele I, Elmishad AG, Carbone M (2006) Genetic predisposition to fiber carcinogenesis causes a mesothelioma epidemic in Turkey. *Cancer Res* 66:1-6
- Dorling M, Zussman J (1987) Characteristics of asbestiform and non-asbestiform calcic amphiboles. *Lithos* 20:469-489
- Dumortier P, Göcmen A, Laurent K, Manço A, De Vuyst P (2001) The role of environmental and occupational exposures in Turkish immigrants with fibre-related disease. *Eur Resp J* 17:922-927
- Dumortier P, Rey F, Viallat JR, Broucke I, Boutin C, De Vuyst P (2005) Chrysotile and tremolite asbestos fibres in the lungs and parietal pleura of Corsican goats. *Occup Environ Med* 59:643-646
- Dusek CJ, Yetman JM (2002) Control and prevention of asbestos exposure from construction in naturally occurring asbestos: Fairfax County Health Department, Fairfax, Virginia, 6, <http://www.co.fairfax.va.us/service/hd/docs/TBRDPUBFIN.doc>
- Ecology and Environment (2005) El Dorado Hills naturally occurring asbestos multimedia exposure assessment, El Dorado Hills, California: Preliminary assessment and site inspection report, Interim final, Contract No. 68-W-01-012
- Fano V, Cernigliaro A, Scondotto S, Pollina Addario S, Caruso S, Mira A, Forastiere F, Perucci CA (2005) Stato di salute della popolazione residente nelle aree ad elevato rischio ambientale e nei siti di interesse nazionale della Sicilia. *ESA Regione Sicilia, Dipartimento di Epidemiologia, ASL RME, Palermo* p 118
- Finn MB, Hallenbeck WH (1985) Detection of chrysotile in workers' urine. *Ann Ind Hyg Ass J* 46:162-169
- Fitzgerald JK (2006) WR Grace vs Debtors. *Bankruptcy No. 01-011139 (JKF)*
- Fornero E (2005) Asbestos hazard in Western Alps. Mineral burden investigation in humans and animals to assess the environmental exposure in the Susa and Lanzo Valleys. PhD thesis, Università degli Studi di Torino, Torino
- Gianfagna A, Andreozzi GB, Ballirano P, Mazziotti-Tagliani S, Bruni BM (2007) Structural and chemical contrasts between prismatic and fibrous fluoro-edenite from Biancavilla, Sicily, Italy. *Can Mineral* 45:249-262
- Gianfagna A, Ballirano P, Bellatreccia F, Bruni B, Paoletti L, Oberti R (2003) Characterization of amphibole fibres linked to mesothelioma in the area of Biancavilla, Eastern Sicily, Italy. *Mineral Mag* 67:1221-1229
- Gianfagna A, Oberti R (2001) Fluoro-edenite from Biancavilla (Catania, Sicily, Italy): crystal chemistry of a new amphibole end-member. *Am Mineral* 86:1489-1493
- Gibbons W (1998) The exploitation and environmental legacy of amphibole asbestos: a late 20th century overview. *Environ Geochem Health* 20:213-230
- Gibbs AR, Gardner MJ, Pooley FD, Griffiths DM, Blight B, Wagner JC (1994) Fiber levels and disease in workers from a factory predominantly using amosite. *Environ Health Perspect Suppl* 102:261-263
- Gillot PY, Kieffer G, Romano R (1994) The evolution of Mount Etna in the light of potassium-argon dating. *Acta Vulcanol* 5:81-87
- Glickman LT, Domanski LM, Maguire TG, Dubielzig RR, Churg A (1983) Mesothelioma in pet dogs associated with exposure of their owners to asbestos. *Environ Res* 32:305-313
- Governa M, Amati M, Bellis D, Bichisecchi E, Santarelli L (2006) Diagnosis of asbestos-related pleuropulmonary diseases. *Med Lav* 97:463-474
- Griffith H, Malony NC (2003) Does asbestos cause laryngeal cancer? *Clin Otolaryngol* 28:177-182
- Gunter ME (1994) Asbestos as a metaphor for teaching risk perception. *J Geol Ed* 42:17-24
- Gunter ME (1999) Quartz - the most abundant mineral species in the earth's crust and a human carcinogen? *J Geol Ed* 47:341-349
- Gunter ME, Dyar MD, Twamley B, Foit FF, Cornelius S (2003) Composition, Fe³⁺/ΣFe, and crystal structure of non-asbestiform and asbestiform amphiboles from Libby, Montana, USA. *Am Mineral* 88:1970-1978
- Gunter ME, Lee RJ (2006) And we thought all minerals were naturally occurring: The need for a rational public policy dealing with so-called naturally occurring asbestos. *Geological Society of America Abstracts with Programs*, vol. 38, #7, p 123

- Gunter ME, Singleton E, Bandli BR, Lowers, HA, Meeker GP (2005) Differentiation of commercial vermiculite based on statistical analysis of bulk chemical data: Fingerprinting vermiculite from Libby, Montana USA. *Am Mineral* 90:749-754
- Gunter ME, Williams TJ, Sanchez MS, Harris KE, Bunker KL, Wyss RK, Lee RJ (2006) Amphiboles between the sheets: An interesting occurrence with even more interesting morphologies. *Geological Society of America Abstracts with Programs*, vol. 38, #7, p 114
- Gunter ME, Sanchez MS, Williams TJ (2007) Characterization of chrysotile samples for the presence of amphiboles: the Carey Canadian deposit, southeastern Quebec, Canada. *Can Mineral* 45:263-280
- Guthrie GD Jr (1992) Biological effects of inhaled minerals. *Am Mineral* 77:225-243
- Guthrie GD Jr (1993) Mineralogical characterization in biological studies. *Rev Mineral* 28:251-274
- Guthrie GD Jr (1997) Mineral properties and their contributions to particle toxicity. *Environ Health Perspect* 105:1003-1011
- Guthrie GD Jr, Mossman BT (1993) Health Effects of Mineral Dusts. *Reviews in Mineralogy*, Volume 28. Mineralogical Society of America, Washington DC
- Haque AK, Vrazel DM, Uchida T (1998) Assessment of asbestos burden in the placenta and tissue digests of stillborn in South Texas. *Arch Environ Contam Toxicol* 35:532-538
- Harris KE, Bunker KL, Strohmeier BR, Hoch R, Lee RJ (2007) Discovering the true morphology of amphibole minerals: complementary TEM and FESEM characterization of particles in mixed mineral dust. *In: Modern Research and Educational Topics in Microscopy*, Formatex Microscopy Book Series, No. III. Méndez-Vilas A, Díaz J (eds) Formatex Research Center, Badajoz, Spain, 2007 (accepted)
- Hawthorne FC, Oberti R (2007) Classification of the amphiboles. *Rev Mineral Geochem* 67:55-88
- Hillerdal G (2003) Health problems related to environmental fibrous minerals. *In: Geology and Health: Closing the Gap*. Skinner HCW, Berger AR (eds) Oxford University Press, New York, p 113-118
- Holt PF (1981) Transport of inhaled dust to extrapulmonary sites. *J Pathol* 133:123-129
- Hume LA, Rimstidt JD (1992) The biodegradability of chrysotile asbestos. *Am Mineral* 77:1125-1128
- Hull MJ, Abraham JL, Case BW (2002) Mesothelioma among workers in asbestiform fiber-bearing talc mines in New York State. *Ann Occup Hyg* 46:132-135
- Langer AM, Nolan RP, Addison J (1991) Distinguishing between amphibole asbestos fibers and elongate cleavage fragments of their non-asbestos analogues. *In: Mechanisms in fibre carcinogenesis*, Brown RC, Hoskins J, Johnson N (eds) Plenum Press, New York, p 252-267
- Leake BE, Woolley AR, Arps CES, Birch WD, Gilbert MC, Grice JD, Hawthorne FC, Kato A, Kisch HJ, Krivovichev VG, Linthout K, Laird J, Mandarino JA, Maresch WV, Nickel EH, Rock NMS, Schumacher JC, Smith DC, Stephenson NCN, Ungaretti L, Whittaker EJW, Youzhi G (1997) Nomenclature of the amphiboles: Report of the subcommittee on amphiboles of the International Mineralogical Association, Commission on New Minerals and Mineral Names. *Can Mineral* 35:219-246
- Lockey JE, Brooks SM, Jarabek AM, Khoury PR, McKay RT, Carson A, Morrison JA, Woit JF, Spitz HB (1984) Pulmonary changes after exposure to vermiculite contaminated with fibrous tremolite. *Am Rev Respir Dis* 129:952-958
- Luo S, Liu X, Mu S, Tsai SP, Wen CP (2003) Asbestos related diseases from environmental exposure to crocidolite in Da-yao, China. I. Review of exposure and epidemiological data. *Occup Environ Med* 60:35-42
- Luce D, Brochard P, Quenel P, Salomon-Nekiriai C, Goldberg P, Billon-Galland MA, Goldberg M (1994) Malignant pleural mesothelioma associated with exposure to tremolite. *Lancet* 344:1777
- Luce D, Bugel I, Goldberg P, Goldberg M, Solomon C, Billon-Galland MA, Nicolau J, Quenel P, Fevotte J, Brochard P (2000) Environmental exposure to tremolite and respiratory cancer in New Caledonia. A case-control study. *Am J Epidemiol* 151:259-265
- Magee F, Wright JL, Chan N, Lawson L, Churg A (1986) Malignant mesothelioma caused by childhood exposure to long-fiber low aspect ratio tremolite. *Am J Ind Med* 9:529-533
- Magnani C, Mollo F, Paoletti L, Bellis D, Bernardi P, Betta P, Botta M, Falchi M, Ivaldi C, Pavesi M (1998) Asbestos lung burden and asbestosis after occupational and environmental exposure in an asbestos cement facturing area: a necropsy study. *Occup Environ Med* 55:840-846
- Mangano D, Gualtieri AF, Torri G, Ferraris S, Ricchi A, Foresti E, Lesci G, Roveri N, Mariotti M, Pecchini G, Zapparoli M (2006) Asbestos monitoring in civil and industrial environments of selected Italian sites. The case of a ceramic factory. Abstracts of the European Conference on Asbestos Risks and Management, p 140-145
- Marinaccio A, Montanaro F, Mastrantonio M, Uccelli R, Altavista P, Nesti M, Costantini AS, Gorini G (2005) Predictions of mortality from pleural mesothelioma in Italy: a model based on asbestos consumption figures supports results from age-period-cohort models. *Int J Cancer* 115:142-147
- Martin RF (2007) Amphiboles in the igneous environment. *Rev Mineral Geochem* 67:323-358
- Mazziotti Tagliani S (2006) Mineralogical, genetic and environmental aspects of the fluorine-rich amphiboles from Biancavilla (Mt. Etna, Sicily, Italy). PhD thesis, Università degli Studi La Sapienza, Roma
- McConnochie K, Simonato L, Mavrides P, Christofides P, Pooley FD, Wagner JC (1987) Mesothelioma in Cyprus: the role of tremolite. *Thorax* 42:342-347

- McConnochie K, Simonato L, Mavrides P, Christofides P, Mitha R, Griffiths DM, Wagner JC (1989) Mesothelioma in Cyprus. *In: Non-occupational exposure to mineral fibres.* Bignon J, Peto J, Saracci R (eds) IARC Scientific Publ 90:411-419
- McDonald JC, Harris J, Armstrong B (2004) Mortality in a cohort of vermiculite miners exposed to fibrous amphibole in Libby, Montana. *Occup Environ Med* 61:363-366
- McDonald JC, McDonald AD, Armstrong B, Sebastien P (1986a) Cohort study of the mortality of vermiculite miners exposed to tremolite. *Br J Ind Med* 43:436-444
- McDonald JC, McDonald AD, Armstrong B (1986b) Radiological survey of past and present vermiculite miners exposed to tremolite. *Br J Ind Med* 43: 445-449
- McDonald, JC, McDonald AD, Sebastien P, Moy K (1988) Health of vermiculite miners exposed to trace amounts of fibrous tremolite. *Br J Ind Med* 45:630-634
- McDonald JC, Sebastien P, Case B, McDonald AD, Dufresne A (1992) Ferruginous body counts in sputum as an index of past exposure to mineral fibres. *British Occ Hyg Society* 36:271-282
- Meeker GP, Bern AM, Brownfield IK, Lowers HA, Sutley SJ, Hoefen TM, Vance JS (2003) The composition and morphology of amphiboles from the Rainy Creek Complex, near Libby, Montana. *Am Mineral* 88:1955-1969
- Meeker GP, Lowers HA, Swayze BS, Van Gosen BS, Sutley SJ, Brownfield IK (2006) Mineralogy and morphology of amphiboles observed in soils and rocks in El Dorado Hills, California. USGS OFR 2006-1362
- Metintas M, Hillerdal G, Metintas S (1999) Malignant mesothelioma due to environmental exposure to erionite: follow-up of a Turkish emigrant cohort. *ERS Journal Ltd* 13:523-526
- Millette JR (2006) Asbestos analysis methods. *In: Asbestos Risk Assessment, Epidemiology, and Health Effects.* Dodson RF, Hammer SP (eds) Taylor & Francis, p 9-37
- Millette JR, Bandli BR (2005) Asbestos identification using available standard methods. *Microscope* 53:179-185
- Molly DW (2006) USA vs WR Grace, CR 05-07-M-DWM. US District Court, Missoula MT
- Montanaro F, Marinaccio A, Gorini G, Silvestri S, Altavista P, Mastrantonio M, Uccelli R (2004) Stima dell'andamento della mortalità per mesotelioma pleurico in Italia nel prossimo futuro in relazione alla produzione ed al consumo di amianto grezzo http://www.ti.ch/dss/IstCP/RCT/documenti/GRELL04_mesotelioma.ppt
- Mossman BT, Bignon J, Corn M, Seaton A, Gee JBL (1990) Asbestos: Scientific developments and implications for public policy. *Science* 247:294-301
- Nemmar A, Hoet PHM, Vanquickenborne B, Dinsdale D, Thomer M, Hoylaerts MF, Vanbilloen H, Mortelmans L, Nemery B (2002) Passage of inhaled particles into the blood circulation in humans. *Circulation* 105:411-414
- Nemmar A, Vanbilloen H, Hoylaerts MF, Hoet M, Verbruggen A, Nemery B (2001) Passage of intratracheally instilled ultrafine particles from the lung into the systemic circulation in hamster. *Am J Respir Crit Care Med* 164:1665-1668
- Nolan RP, Langer AM, Oechsle GW, Addison J, Colflesh DE (1991) Association of tremolite habit with biological potential: Preliminary report. *In: Mechanisms in Fibre Carcinogenesis.* Brow RC, Hoskins JA, Johnson NF (eds) Plenum Press, New York, p 231-251
- Norton MR, Gunter ME (1999) Relationships between respiratory diseases and quartz-rich dust in Idaho. *Am Mineral* 84:1009-1019
- OSHA (1992) Occupational exposure to asbestos, tremolite, anthophyllite, and actinolite. *Federal Register* 1992, 57, 24310
- Pan X, Day HW, Wang W, Beckett, LA, Shenker MB (2005) Residential proximity to naturally occurring asbestos and mesothelioma risk in California. *Am J Respir Crit Care Med* 172:1019-1025
- Paoletti L, Batisti D, Bruno C, Di Paola M, Gianfagna A, Mastrantonio M, Nesti M, Comba N (2000) Unusually high incidence of malignant pleural mesothelioma in a town of eastern Sicily: an epidemiological and environmental study. *Arch Environ Health* 55:392-398
- Pasetto R, Bruni B, Bruno C, D'Antona C, De Nardo P, Di Maria G, Di Stefano R, Fiorentini C, Gianfagna A, Marconi A, Paoletti L, Putzu MG, Soffritti M, Comba P (2004a) Problematiche sanitarie della fibra anfibolica di Biancavilla: aspetti epidemiologici, clinici e sperimentali. *Not Ist Super Sanità* 17:8-12
- Pasetto R, Bruni B, Bruno C, Cauzillo G, Cavone D, Convertini L, De Mei B, Marconi A, Montavano G, Musti M, Paoletti L, Comba P (2004b) Mesotelioma pleurico ed esposizione ambientale a fibre minerali: il caso di n'area rurale in Basilicata. *Ann Ist Super Sanità* 40:251-265
- Peipens LA, Lewin M, Campolucci S, Lyparger JA, Miller A, Middleton D, Weis C, Spence M, Black B, Kapil V (2003) Radiographic abnormalities and exposure to asbestos-contaminated vermiculite in the community of Libby, Montana, USA. *Environ Health Perspect* 111:1753-1759
- Pollice L, Ferri GM, Paoletti L, Gentile A, Iacobellis U, Batisti D, Di Tonno P, Caruso G, Molinari R (1995) Concentrazione di fibre di asbesto nei tumori uroteliali e nella parete vescicale esente da neoplasia, *G Ital Med Lav* 17:11-15

- Plumlee GS, Morman SA, Zeigler TL (2006) The toxicological geochemistry of earth materials: An overview of processes and the interdisciplinary methods used to understand them. *Rev Mineral Geochem* 64:5-274
- Putzu MG, Bruno C, Zona A, Massiccio M, Pasetto R, Piolatto PG, Comba P (2006) Fluoro-edenitic fibres in the sputum of subjects from Biancavilla (Sicily): a pilot study. *Environ Health, A Global Access Science Source* 5:20
- Rees D, Phillips JJ, Garton E, Pooley FD (2001) Asbestos lung fibre concentration in South African chrysotile mine workers. *Ann Occup Hyg* 45:473-477
- Rey F, Viallat JR, Boutin C, Fariisse P, Billon-Galland MA, Hereng P, Dumortier P, De Vuysts P (1993) Les mésothéliomes environnementaux an Corse du Nord-Est. *Rev Mal Resp* 10:339-345
- RJ Lee (2005) Evaluation of EPA's analytical data from the El Dorado Hills asbestos evaluations project. RJ Lee Group, Monroeville, Pennsylvania, USA
- Roggli VL (1990) Human disease consequences of fiber exposures: a review of human lung pathology and fiber burden data. *Environ Health Perspect* 88:295-303
- Roggli VL (2004) Asbestos bodies and nonasbestos ferruginous bodies. *In: Pathology of Asbestos-Associated Diseases*. Roggli VL, Oury TD, Sporn TA (eds) Springer-Verlag New York, p 34-70
- Roggli VL, Sharma A (2004) Analysis of tissue mineral fiber content. *In: Pathology of Asbestos-Associated Diseases*. Roggli VL, Oury TD, Sporn TA (eds) Springer, New York, p 309-354
- Roggli VL, Sharma A, Butnor KJ, Sporn T, Vollmer RT (2002) Malignant mesothelioma and occupational exposure to asbestos: a clinicopathological correlation of 1445 cases. *Ultrastruct Pathol* 26:55-65
- Ross M (1981) The geologic occurrences and health hazards of amphibole and serpentine asbestos. *Rev Mineral* 9A:279-323
- Ross M (1984) A survey of asbestos-related disease in trades and mining occupations and factory and mining communities as a means of predicting health risks of nonoccupational exposure to fibrous minerals. *In: Definitions for Asbestos and Other Health-related Silicate*. Levadie B (ed), ASTM STP 834, American Society for Testing Materials, Philadelphia, Pennsylvania, p 51-104
- Ross M (1994) The New Idria serpentinite of California: a toxic rock? *Geological Society of America Abstracts with Programs*, 1994 Annual Meeting, Seattle, Washington, October 24-27, No 7 26:A320
- Ross M, Nolan RP (2003) History of asbestos discovery and use and asbestos-related disease in context with the occurrence of asbestos within ophiolite complexes. *Geol Soc Am Special Paper* 373:447-470
- Ross M, Nolan RP, Langer AM, Cooper WC (1993) Health effects of mineral dusts other than asbestos. *Rev Mineral* 28:361-409
- Sanchez MS (2007) Characterization methods for asbestiform minerals. MS Thesis, University of Idaho, Moscow, Idaho
- Sanchez MS, Gunter ME (2006) Quantification of amphibole content in expanded vermiculite products from Libby, Montana USA. *Am Mineral* 91:1448-1501
- Sanchez MS, Gunter ME, Dyar MD, Badger SR, Hobbs GC, Van Orden DR, Potter MS (2006) Characterization of historical amphibole samples from the former vermiculite mine near Libby, Montana USA. *Geological Society of America Abstracts with Programs*, vol 38, #7, p 293
- Sartorelli P, Scancarello G, Romeo R, Marciànò G, Rotoli P, Arcangeli G, Palmi S (2001) Asbestos exposure assessment by mineralogical analysis of bronchoalveolar lavage fluid. *J Occup Environ Med* 43:872-881
- Schumacher JC (2007) Metamorphic amphiboles: composition and coexistence. *Rev Mineral Geochem* 67:359-416
- Selden AI, Berg NP, Lundgren EAL, Hillerdal G, Wik N-G, Ohlson C-G, Bodin LS (2001) Exposure to tremolite asbestos and respiratory health in Swedish dolomite workers. *Occup Environ Med* 58:670-677
- Stemple IS, Brindley GW (1960) A structural study of talc and talc-tremolite reaction. *J Am Ceram Soc* 43:34-42
- Storeygard AR, Brown AL Jr (1977) Penetration of the small intestinal mucosa by asbestos fibers. *Mayo Clin Proc* 52: 809-812
- Su S, Bloss FD (1984) Extinction angles for monoclinic amphiboles or pyroxenes: a cautionary note. *Am Mineral* 69:399-403
- Swayze GA, Higgins CT, Clinkenbeard JP, Kokaly RF, Clark, RN, Meeker GP, Sutley, SJ (2004) Preliminary report on using imaging spectroscopy to map ultramafic rocks, serpentinites, and tremolite-actinolite-bearing rocks in California. USGS OFR 2004-1304
- Taunton AE, Gunter ME (2007) Introducing medical geology to undergraduates as a critical thinking and risk assessment tool. *J Geol Ed* 55:169-180
- Taunton AE, Wood SA, Gunter ME (2002) The thermodynamics of asbestos mineral dissolution and conversion in the human lung. 12th Annual Goldschmidt Conference, Davos, Switzerland.
- Tossavainen A (1997) Asbestos, asbestosis and cancer: the Helsinki criteria for diagnosis and attribution. *Consensus Report Scand J Work Environ Health* 23:211-216

- Tossavainen A, Dumortier P, Billon-Galland MA, Burdett G, Mitha R, Monso E, Rödelsperger K, Taikin-Aho O, Tuomi T, Vanhala E, Maier EA (2001) The certification of the content of asbestos fibres in lung tissue. European Commission, BCR 665 and BCR 666, reference materials, Directorate-General for Research, EUR 19073 EN
- Tossavainen A, Karjalainen A, Karhuinen PJ (1994) Retention of asbestos fibers in the human body. *Environ Health Perspect* 102:253-255
- Trescases JJ (1997) The lateritic nickel-ore deposits. *In: Soils and Sediments Mineralogy and Geochemistry*. Paquet H, Clauer N (eds) Springer, Berlin, p 125-138
- USEPA (2001a) Weis Memorandum to Paul Peronard: Re "Fibrous amphibole contamination in soil and dust at multiple locations in Libby, Montana." USEPA Region 8, July 2001
- USEPA (2001b) EPA's actions concerning asbestos-contaminated vermiculite in Libby, Montana. EPA 744-R-00-010, United States Environmental Protection Agency, Washington
- Van der Schalie WH, Gardner HS Jr., Bantle JA, De Rosa CT, Finch RA, Reif JS, Reuter RH, Backer LC, Burger J, Leroy CF, Stokes WS (1999) Animals as sentinels of human health hazards of environmental chemicals. *Environ Health Perspect* 107:309-315
- Van Gosen BS, Lowers HA, Sutley SJ, Gent CA (2004) Using the geologic setting of talc deposits as an indicator of amphibole asbestos content. *Environ Geol* 45:920-939
- Van Gosen BS, Lowers HA, Meeker GP, Plumlee GS, Brownfield IK, Sutley SJ (2005) Reconnaissance study of the geology of US vermiculite deposits – are asbestos minerals common constituents. *USGS Bull* 2192
- Van Gosen BS (2006a) Reported historic asbestos miners, historic asbestos prospects, and natural asbestos occurrences in the Eastern United States. *USGS OFR* 2005-1189
- Van Gosen BS (2006b) Reported historic asbestos miners, historic asbestos prospects, and natural asbestos occurrences in the Central United States. *USGS OFR* 2006-1211
- Van Oss CJ, Naim JO, Costanzo PM, Giese RF Jr., Wu W, Sorling AF (1999) Impact of different asbestos species and other mineral particles on pulmonary pathogenesis. *Clays Clay Mineral* 47:697-707
- Veblen DR (1980) Anthophyllite asbestos: microstructures, intergrown sheet silicates and mechanisms of fiber formation. *Am Mineral* 65:1075-1086
- Veblen DR, Buseck PR (1980) Microstructures and reaction mechanisms in biopyriboles. *Am Mineral* 65:599-623
- Veblen DR, Buseck PR, Burnham CW (1977) Asbestiform chain silicates: new minerals and structural groups. *Science* 198:359-365
- Veblen DR, Wylie AG (1993) Mineralogy of amphiboles and 1:1 layer silicates. *Rev Mineral* 28:61-138
- Verkouteren JR, Wylie AG (2000) The tremolite-actinolite-ferro-actinolite series: Systematic relationships among cell parameters, composition, optical properties, and habit, and evidence of discontinuities. *Am Mineral* 85:1239-1254
- Verkouteren JR, Wylie AG (2002) Anomalous optical properties of fibrous, tremolite, actinolite, and ferro-actinolite. *Am Mineral* 87:1090-1095
- Virta RL (1985) The phase relationship of talc and amphiboles in a fibrous talc sample. U.S. Bureau of Mines, Report of Investigations 8923
- Wagner JC (1980) The pneumoconiosis due to mineral dusts. *J Geol Soc London* 137:537-545
- Wagner JC, Griffiths DM, Munday DE (1987) Recent investigations in animals and humans. *In: The Biological Effect of Chrysotile*. Wagner JC (ed) 1:111-120
- Wylie AG (1979) Optical properties of the fibrous amphiboles. *In: Health Hazards of Asbestos Exposure*. Selikoff IJ, Hammond EC (eds) *Annals of the New York Academy of Sciences* 330:611-619
- Wylie AG, Huggins CW (1980) Characteristics of a potassian winchite-asbestos from the Allamoore Talc District Texas. *Can Mineral* 18:101-107
- Wylie AG, Verkouteren JR (2000) Amphibole asbestos from Libby, Montana: aspects of nomenclature. *Am Mineral* 58:1540-1542
- Weill H, Abraham JL, Balmes JR, Case B, Chrug A, Hughes J, Schenker M, Sebastien P (1990) Health effects of tremolite. *Am Rev of Resp Dis* 142:1453-1458
- Williams-Jones AE, Normand C, Clark JR, Vali H, Martin RF, Dufresne A, Nayebzadeh A (2001) Controls of amphibole formation in chrysotile deposits: Evidence from the Jeffrey Mine, Asbestos, Quebec. *In: The Health Effects of Chrysotile Asbestos*. *Can Mineral Spec Publ* 5:89-104
- Wood SA, Taunton AE, Normand C, Gunter ME (2006) Mineral-fluid interaction in the lungs: Insights from reaction-path modeling. *Inhalation Toxicology* 18:975-984
- Wright RS, Abraham JL, Harper P, Burnett BR, Morris P, West P (2002) Fatal asbestosis 50 years after brief high intensity exposure in a vermiculite expansion plant. *Am J Respir Crit Care Med* 165:1145-1149
- Yazicioglu S, İlçayto R, Balci K, Sayli BS (1980) Plural calcification, pleural mesothelioma and bronchial cancers caused by tremolite dusts. *Thorax* 35:564-569
- Zoltai T (1979) Asbestiform and acicular mineral fragments. *In: Health Hazards of Asbestos Exposure*. Selikoff IJ, Hammond EC (eds) *Annals of the New York Academy of Sciences* 330:621-643

Zoltai T (1981) Amphibole asbestos mineralogy. *Rev Mineral* 9A:237-278

Zoltai T, Wylie AG (1979) Definitions of asbestos-related mineralogical terminology. *In: Health Hazards of Asbestos Exposure*. Selikoff IJ, Hammond EC (eds) *Annals of the New York Academy of Sciences* 330:707-709

Amphiboles: Historical Perspective

Curzio Cipriani

*Museo di Storia Naturale, sez. Mineralogia
Università di Firenze, Via La Pira 4
50121 Firenze, Italia
curzio.cipriani@unifi.it*

INTRODUCTION

For centuries, asbestos and jade were the only known representatives of the group of minerals called amphiboles. In the XVIII century, rock minerals with naturalistic descriptions and little more than semiquantitative chemical analyses were also considered, while the XIX century saw an enormous number of goniometric determinations and chemical analyses to try to classify the many species that were gradually being discovered. Chemical analyses that were precise and without preconceptions were developed in the early XX century, but it was mainly X-ray diffraction that helped to clarify the nature of this group of minerals. The present discussion of the evolution of knowledge about the amphiboles stops at the second world war. In the second half of the XX century, there has been great technical progress in mineralogical research, especially in the field of spectroscopy. This has led to detailed crystallochemical knowledge of the amphiboles, which has also allowed their use for the solution of petrological problems.

German miners of the early XVIII century gave the name *Hornblende*, i.e., “dazzling horn,” to a mineral that had a toughness similar to that of horse hooves and did not contain useful metals. A century later, René J. Haüy decided to give it a different name, *Amphibole*, i.e., ambiguous, because it often had a similar appearance but a different composition. Today, we know that amphiboles are a complex group of rock-forming minerals with numerous lattice sites that can host many different constituents; indeed, it has jokingly been defined as a “waste basket.”

It is hoped that this note will give the reader an idea of how hard the road has been for researchers on amphiboles. It started with the simple description of the external appearance of these materials and has led today, at the beginning of the third millennium, to the acquisition of increasingly detailed knowledge as the methods of chemical and physical analyses became ever more refined.

The history of research on amphiboles is marked by several crucial discoveries that were essential to the knowledge of this group of minerals and of the similarities and differences with respect to the pyroxenes. In a 150-year period, from the late XVIII century to the early XX century, there have been at least five such milestones: Torbern Bergman identified silica as an essential component, René J. Haüy coined the name “amphiboles” and identified the “integral molecule,” Heinrich Rose underlined the close similarities with the pyroxenes among the so-called “metasilicates,” Waldemar T. Schaller demonstrated the fundamental role of water in the chemical composition, and Bertram E. Warren determined the crystalline structures. A sixth contribution, albeit less important, can be attributed to Gustav Tschermak, not only in recognition of his great work but also because he helped solve the problem of the variable content of Al.

ANTIQUITY

Nothing is known about the knowledge of common amphiboles as rock minerals in antiquity. However, the conspicuous varieties were obviously known for their physical properties, e.g., the marked fibrosity of asbestos and the gemstone characteristics of jade-nephrite.

The earliest mention of asbestos seems to be by Pliny the Elder (Plinio 1988) in book XIX of *Historia Naturalis* devoted to Botany. After describing the characteristics and uses of flax, he reported in paragraphs 19 and 20 "*Inventum [linum] iam est etiam quod ignibus non absumeretur,*" that is

There has also been discovered, long ago now, a kind of linen which is incombustible ... It is called "live" linen, and I have seen napkins made of this fabric thrown into the fire in the banqueting hall and, after the stains were burnt away, come out whiter and cleaner than they could have been rendered by water. This material has been used to make the funereal cloths of monarchs, to ensure that the ashes of the body can be separated from those of the funeral pyre. This substance grows, amid deadly serpents, in the sun-scorched deserts of India, where rain never falls, and it is adapted to resist the blazing heat ...

Pliny's great work obviously contains no mention of amphiboles as rock minerals, but there are not even any references to jade-nephrite, except perhaps in the passage in book XXXVII, among the gems: [*jaspis*]*smaragdo similem Indi*, that is "jasper similar to the emerald of India."

In the XVI century, Georg Bauer, known by his Latinized surname Agricola (1494-1555), Saxon physician and metallurgist and for many good reasons considered the "father of mineralogy," did not hesitate to transcribe entire pages of the rumours of the ancients. In book V of his *De Natura Fossilium*, (Agricola 1546) however, he added some personal observations concerning the composition, "*asbestos is not composed of calcareous stone or gypsum but is formed from its own juice,*" physical characteristics like the series of colors, from white to ashen-grey, from red to iron grey, the taste, quite unlike that of alum, "*this one is astringent, that one tingles the tongue,*" and, finally, the provenience, adding Noricum to the classic Mediterranean sites.

THE EIGHTEENTH CENTURY

No particular information about the common amphiboles is available for the Renaissance up until the early XVIII century, apart from the old name given by the German miners - *Hornblende*. This name, along with amianthus (or asbestos) and nephrite, minerals that were easily recognizable because of their appearance and their use, are the ones that must be sought in the various treatises in order to trace the evolution of knowledge about the group of minerals later called "amphiboles."

A very important, in many ways fundamental, mineralogical treatise (Fig. 1) was that (1772) of Johann Gottschalk Wallerius (1709-1785), professor at Uppsala, which presented a simple classification based on the external characters of the materials (Wallerius 1778). The III order of the II Class (*Lapides fusibiles*) contained the common rock minerals in genus no. 26 "*Lapides cornei.*" However, of the four listed species (no. 169 to no. 172), only no. 171 seems to refer to minerals, while the rest can be attributed to various types of rocks. Species no. 169 *Corneus nitens*, translated into German as "*Glentzenden Hornfelsstein,*" can be referred to the cornubianites, no. 170 *Corneus fissilis*, translated as "*Derben Hornschiefer,*" can be assigned to the amphibolic schists and no. 172 *Corneus trapezius*, translated as "*Schwachstein,*" likely corresponds to the clay schists, also because of the stated ease of breaking into "*fragmenta cubica vel rhomboidalia.*" There remains only species no. 171 *Corneus spathosus*, which as the name indicates appears well crystallized, indicating the minerals for which the name

D. D.
**SYSTEMA
 MINERALOGICUM,**
 QUO
CORPORA MINERALIA

IN
 CLASSES, ORDINES, GENERA ET SPECIES,
 SUIS CUM VARIETATIBUS DIVISA,
 DESCRIBUNTUR,

ATQVE
 OBSERVATIONIBUS, EXPERIMENTIS
 ET FIGURIS ÆNEIS ILLUSTRANTUR,

A
JOHAN. GOTSCH. WALLERIO
 EQVITE ORDIN. REG. WASÆI,

CHEMIÆ, METALLURG. ET PHARMACEUT. PROFESS.
 REG. ORD. ET EMER. UPS.

ACADEM. IMPER. NAT. CURIOS. NEC NON
 RR. ACAD. STOCKH. ET UPS.

MEMBRO.

TOM. II.

In quo
 MINERÆ & CONCRETA describuntur.

Cum *Indice* quadruplici.

Editio nova & correctæ.

CUM PRIV. SER. ELECT. SAXONIÆ.

VIENNÆ,

EX OFFICINA KRAUSIANA, 1778.

Figure 1. Title page of the 2nd edition (1778) of the Treatise of Mineralogy (*Systema Mineralogicum*) by J.G. Wallerius.

“Hornblende” appears in German translation. Oddly, this species lacks a reference to Linnaeus, which is present in the other three species, containing only that to Cronstedt, with the vague “*Bolus induratus particulis squamosus*,” the only analytical datum provided is an iron content between 13 and 15%, while four color varieties of *Corneus spathosus* are listed: *niger*, *obscurus fuscus*, *griseus*, *viridescens*. Nephrite is included among the jaspers of genus no. 21 (*Jaspis*) of the II Order (*Lapides vitrescentes*) of the same class, with references to Linnaeus. Defined as *Lapis nephriticus* (or *Jaspis unicolor*), its density is given as 2.600, similar to the other jaspers, and it is divided into three varieties: *L. n. albescens* ex China, *L. n. subviridiscens* (*divinus*) ex Orient, *L. n. obscure viridescens* (*amazonicus*) ex America.

The first English treatise in mineralogy appeared in 1784. It was a slender text by the Irish naturalist Richard Kirwan (1733-1812), a skilled chemical analyst and one of the first to recognize the importance of the chemical composition of minerals (Kirwan 1784). Naturally, he presented his own classification, although it was practically the same as Cronstedt’s, based on four classes: Earths and stones, Saline substances, Inflammables, Metallic substances. The minerals that interest us here are in the first class (Earths and stones) divided into five genera according to the prevailing “earth:” Calcareous, Ponderous (i.e., barytic), Muriatic (inexplicably magnesiac), Argillaceous (i.e., alumina), Siliceous. The high magnesium content revealed by the analyses places the amphiboles in the “Muriatic” genus, specified as “where magnesia predominates or where magnesia follows silica.” Asbestos constitutes the III species, characterized by the presence of magnesia, silica, lime, clay and iron; there are two varieties: I) “fibrous asbestos,” greenish, with parallel or interwoven filaments, and II) “coriaceous asbestos” (*Suber montanum*), which floats on water and has a colour varying from whitish to black. Three chemical analyses are reported: one by Bergmann referring to the first variety, the other two without citation (presumably by the author) for the first and second varieties, respectively:

<i>silica</i>	<i>magnesia</i>	<i>lime</i>	<i>clay</i>	<i>iron</i>
53 – 74	12 – 28	7 – 14	2 – 6	1 – 10
62	13.7	12	1.7	10.6
56 – 62	22 – 26	10 – 12	2 – 2.8	3

These substantially similar data identify what we know today as the amphibole actinolite. Apart from an excess of silica, the second analysis is extraordinarily close to that reported by Tilley in 1938 (Deer et al. 1997, p.144, anal. 18) for actinolite, a constituent of the amphibolic schist of southern Devon in England; hence, it cannot be excluded that Tilley was reporting Kirwan’s data. For the IV species, Amianthus, the reported analysis (again by Bergmann) indicates an unlikely presence of barium (ponderous lime), which if attributed to normal lime leads to a tremolite. The V species, *Lapis nephriticus*, “or serpentine or Gabro of the Italians,” can in effect be referred to serpentine on the basis of the analysis by a certain Bayen in which a substantial quantity of water appears.

Eighteenth-century texts contain twenty chemical analyses for amphiboles, repeated several times: ten by Bergmann, two each by Louis-Nicolas Vauquelin (1763-1829), Wiegleb and Kirwan, and one each by Höpfner, Hermann, Patrin and Klaproth. When recalculated in modern terms and compared with the current species, the most frequent errors are for silica (two underestimates and four overestimates) and for calcium, magnesium and aluminum (always overestimated), while the data for iron are acceptable. It is noteworthy that Klaproth (1743-1817), professor at Berlin, had already recorded 6% (H₂O+ CO₂), i.e., a generic volatile component that was considered an impurity until the late XIX century. Very reliable values include those of Wiegleb for serpentine asbestos and of Bergman for actinolite, despite a slight excess of silica, even though they are generally no more than semiquantitative analyses.

After the references to nephrite in antiquity and the first descriptions in the 1700s, research on this mineral only made progress in the last years of the eighteenth century, following the

exploration of the Pacific Ocean and the discovery of deposits in New Zealand and its use in native weapons, which led to the name *Beilstein* (ax stone) given by Emmerling in 1793. Haüy placed this material among the unclassifiable substances, but Breithaupt divided the “genus nephrite” into two species, Common nephrite and Beilstein, on the basis of the hardness, compactness and thermal conductivity (Breithaupt 1815). Damour deserves credit for the correct interpretation of nephrite in 1865; after a new analysis, he considered it a particular tremolite, reviving the preceding subdivision into two varieties, “oriental jade” and “oceanic jade,” which had greater toughness (Hintze 1897).

THE NINETEENTH CENTURY

For mineralogy in general, the XIX century opened with the *Traité de Minéralogie* (1801) by René-Just Haüy (1743-1822), the founder of crystallography, which represented a true turning point in this discipline, particularly for Systematics (Haüy 1801). In fact, it gave the following definition of species, largely similar to the current one, based on the chemical composition and crystalline form:

une collection de corps dont les molécules intégrants sont semblables et composées des mêmes éléments (!) unis en même proportion.

This relegated the external characteristics to the identification of varieties and thus robbed them of taxonomic validity, as previously proposed by Bergman in his “*Sciagraphia*” (Bergman 1783).

The one of Haüy was an essentially chemical classification, defined as natural given that minerals are chemical compounds. Yet, for reasons not sufficiently clear, or at least not very convincing, Haüy moved away from the chemical nomenclature, indeed reversing it, i.e., giving more weight to the “base” than to the “acid,” speaking of carbonated lime and not carbonate of lime, returning to a Linnaeus-like binomial nomenclature, in which lime is the “genus” and then is qualified as carbonated. This is the proposed nomenclature for simple compounds, but it then becomes a mineralogical nomenclature, with a single species name, for more complex compounds. The strictly chemical binomial nomenclature, which in reality contradicted the very definition of species, was subsequently abandoned after the discovery of polymorphism a few years later (1814) by Mitscherlich; this discovery was vigorously opposed by Haüy in the case of the above-mentioned carbonated lime with regard to the identification of aragonite (or rather “arragonite,” as it was called at the time). The apparently contradictory behavior of the French scholar can be explained by his conviction that chemical composition and integral molecule were not independent factors, as the form of the latter should have been determined by the former.

The merits of Haüy in the field of systematic mineralogy do not end at the mere definition of species and at classification but extend to the coining of two names of fundamental rock-forming mineral groups: amphiboles and pyroxenes.

We will not discuss the pyroxenes here; the name comes from the Greek for “extraneous to fire,” so-called because the fully formed crystals were sticking out of a shapeless mass of Vesuvian lava. Instead, let us consider the reason for the name “amphibole,” i.e., “*équivoque ou ambigu*”:

Les minéralogistes...ont réuni pendant long-temps, l'amphibole sous le nom commun de schorl, avec beaucoup d'autres espèces de minéraux... seize espèces. L'histoire naturelle ne présente, peut-être, nulle part un plus grand nombre d'erreurs resserrées dans un plus petit espace.

Further ahead, Haüy states that some substances, namely tourmaline and pyroxene, could be confused with the amphiboles upon superficial examination, and that was why he suggested

the name “amphibole,” to put the observer on the alert, especially since the name *schorl* was used in Germany to designate tourmaline. Moreover, it did not make sense to preserve the name *hornblende* because

Il étoit trop impropre pour être conservé..... ce qui conduisoit à adopter une nouvelle dénomination pour remplacer celle de schorl ... un mot qui avoit occasionnée tant d'erreurs, en le proscrivant de la nomenclature des minéraux.

For Häüy, amphibole (XVIII species of the II class) includes minerals given various names by preceding authors, above all *hornblende* (e.g., by Werner, Emmerling, Brochant) or *schorl opaque rhomboidal* (by Romé de l'Isle). He lists a long series of characters, but without reporting any chemical analysis or mentioning the composition, something that is common in most of the treatises but truly inexplicable given that the author made chemical composition one of the pillars on which rested the identification of species. The “essential” character was the cleavage parallel to the face of a rhomboid prism of $124^{\circ}1/2$ and $55^{\circ}1/2$, followed by the density of 3.25, the hardness (the Mohs scale did not yet exist) given as able to scratch glass, no electricity either by rubbing or heating, the chemical character of fusion under the torch into a black glass, and, as a fundamental geometric trait, the primitive form (coincident with the integral molecule) of an oblique prism with rhombic base whose faces have slopes of $124^{\circ}34'$ and $55^{\circ}26'$ and whose bases have angles of $122^{\circ}56'$ and $57^{\circ}4'$.

After comparing the distinctive characters with those of similar minerals (tourmaline, epidote, grammatite [actually another amphibole, tremolite] and actinote), he listed the five “determinable” varieties, i.e., those that occur as measurable crystals, giving particular names to the combinations of simple forms, *dodécaèdre, equi-différent, ondécimal, sexdécimal, surcomposé* (all illustrated in the atlas of the treatise), as well as four “indeterminable” varieties: *cylindröide, laminaire, lamellaire, aciculaire*.

Therefore, by “amphibole” Häüy meant a species, the original *hornblende* or a loathed *schorl*, since he included other similar species, today part of the amphiboles group.

One of them (XIX species) is *actinote*, defined as *corps rayonné*, a species already known as *schorl vert*, one of the many reviled by Lametherie, later given a better name, *Strahlstein* (radiated stone), by Emmerling and by Werner, then Graecized to *actynolite* by Kirwan and slightly modified by Häüy. The description of all the characters is identical to that of amphibole, except for a slight difference in density (3.33) and another modest dissimilarity, fusion leading to a greyish glass. In effect, Häüy admits that the differences are minimal and largely related to the different colours of the crystals, in this case a more or less light green, suggesting a prevalence of magnesium over iron. The varieties include a well crystalline form (*hexaèdre*), with six faces without bases, and another four, *lamellaire, étalé, aciculaire, fibreux*, the last two very similar to asbestos.

An obvious disadvantage of a chemical classification founded on “bases” becomes clear only after many pages of the treatise. There we find, among the magnesium-containing minerals, the XL species, *grammatite*, a name clarified as *marquée d'une ligne*. For the author, it replaces *tremolite*, discovered by Ermenegildo Pini in the Tremola Valley of the Italian-Swiss Alps, proposed by de Saussure and used by all subsequent scholars from Bergman to Emmerling, from Werner to Daubenton and Brochant. Obviously, the presented characters are not much different from those indicated for the other two species, with only slight differences in the form of the rhomboid cleavage prism (angles of 127° and 53° , specified in the primitive form as $126^{\circ}52'12''$ and $53^{\circ}7'48''$), density varying from 2.93 to 3.2, and fusion leading to a bubbly white glass; the only appreciable difference is in the phosphorescence: percussion causes a reddish glint, which instead is greenish if emitted by powder thrown on glowing coals. Finally, a chemical analysis by Klaproth in 1790 (already mentioned above) showed a composition of calcium silicate and magnesium without aluminum, almost completely lacking iron and

with a significant presence of “water and carbonic acid,” which was ignored by researchers for more than a century. Three of the presented varieties are the “determinable” forms, duly illustrated in the atlas, *ditétraèdre*, *bis-unitaire*, *triunitaire*, while the “indeterminable” forms include *cylindröide*, *comprimée* and *fibreuse*, the last (corresponding to Asbestos Tremolit of the German authors) divided into *fasciculée* and *radiée* according to the arrangement of the fibers. The explanation of the name change comes after the description of the species:

Les prismes de grammatite offrent souvent, dans leur cassure trasversale, un accident assez remarquable

This refers to the appearance, after breaking, of a line that crosses the orthorhombic cleavage base, bisecting the acute angles; this suggests the formation of a “hemitropic” (i.e., a twin) by the overturning of one half on the other. However, the author continues, this can be excluded because this phenomenon does not occur when a very hot crystal is placed in cold water: it appears fractured but with continuous rhombi. The description ends with the observation that the mineral always presents minute granules of dolomite exactly in correspondence to the “line,” which could alter the results of the analysis; perhaps it is this comment that caused the presence of water in the amphiboles to be ignored.

The last species considered is the one known since antiquity and discussed by the eighteenth-century authors: asbestos. For Haüy, it is the XLIII species, *asbeste*, i.e., *inextinguible*, a name almost always given as a synonym of asbestos (as mentioned earlier in this note). The essential character is, obviously, “filamentous,” with fibers that seem to be rhomboid prisms; the density is very variable, for “hard asbestos” it is 2.9958 (with four decimals!), while for the other varieties the data are almost always less than 1. Fusion under the torch produces a blackish glass. The varieties include the four well known to all previous authors; only their names change: *linum montanum* becomes *A. flexible*, *A. maturus* becomes *A. dur*, *Suber montanum* is now called *A. tressé* (i.e., woven), *lignum montanum* is called *A. ligniforme*. The notes include the usual information about the curiosities reported for this material, from the quotation of Pliny the Elder on the incombustible flax adapted for living in the torrid deserts of India to the shrouds seen in the Vatican by “citizen” Dolomieu to the permanent wick of Father Kircher; however, there is also an indirect chemical datum, namely the marked loss to fire observed in experiments by the Royal Society in London.

After more than 20 years, the great French scholar published a second edition of his treatise a few months before his death (Haüy 1822). This was in the middle of the Restoration and not only had the institutions changed but mineralogy had also taken great steps forward, thanks mainly to two scholars, the Swede Jöns Jacob Berzelius (1779-1848) and one of his students, the German Eilhard Mitscherlich (1794-1863). Berzelius made an enormous contribution to chemistry, analyzing a large number of minerals and devising the chemical symbols and relative atomic weights. Mitscherlich discovered two fundamental characteristics of minerals, polymorphism and isomorphism.

Haüy was compelled to take note of these essential novelties, but he did so reluctantly, as the discoveries by Mitscherlich demolished his ideas about the “integral molecule.” The integral molecule had been conceived as a unique whole, which, in addition to the above-mentioned definition of species, meant that a given chemical compound had one and only one “primitive” crystalline form. The discovery of aragonite, with chemical composition equal to that of calcite but with a different form, led to the collapse of Haüy’s theory and consequently also his chemical nomenclature: in the specific case, calcite could not be defined as *chaux carbonatée* (even though it remained so!) because aragonite was also *chaux carbonatée*.

For the minerals referable to amphiboles, there was an important step forward in grouping the three different species listed in the first edition, amphibole, actinote and grammatite, into a single species *amphibole*. A single species justified by the new ideas about the chemistry of

minerals, which admitted broad substitutions in observance of Haüy's basic idea of species, now formulated in a slightly different manner, "equal form and composition of the integral molecule," so as to explain polymorphism. The chemical composition is fairly variable, as shown by the 11 analyses reported, but the form remains identical in all three of the old species, even though tremolite presents a slightly different angle from hornblende and actinote ($126^{\circ}52'$ vs. $124^{\circ}30'$). Again in this edition, Haüy repeats the usual objection to the old name of *schorl* (too generic) and he considers it his duty to explain the uniting in a single species of apparently very different minerals, differing especially in colour (black, green and white, respectively called amphibole, actinote and grammatite by Haüy in the first edition, and *Hornblende*, *Strahlstein* and *Tremolit* by Werner); in reality, however, they can have colours ranging to greenish black, dark olive or greenish, respectively, so that their distinction is sometimes difficult. This is even without considering that crystals have been found with ends that have different colours, i.e., black and green, and the ends can hardly be attributed to different species. The reality, Haüy added (albeit fleetingly), is that "the amphiboles" [the plural makes one think not of the name of a species but of a group] can have different contents of chemical components, for instance iron, which is reflected in some physical properties, such as different electrical attraction.

Many of the 11 reported chemical analyses refer to "grammatite" of S. Gottardo, which is poorly indicative since it was contaminated with dolomite; however, iron is practically absent in all of them. Iron is subordinate to magnesium in the only analysis of actinote, while the three analyses of "amphibole" present a high content of iron and aluminum, with water always present, as well as appreciable percentages of "losses." The 124° cleavage traces are always taken as a distinctive character with respect to similar minerals: tourmaline 120° (as symmetry joints), pyroxenes 92° , epidote 114° ; the distinction of acicular amphibole from asbestos is based instead on the powder, which is soft and pasty to the touch in asbestos, but rough in amphibole. There are 11 determinable forms, i.e., the combinations of simple forms, with 15 figures in the atlas: *ditétraèdre*, *bisunitaire*, *dihexaèdre*, *dodécaèdre* (also in the form *hémitrope*), *ondécimal*, *imitatif*, *triunitaire*, *sexoctional*, *accélééré*, *octoduodécimal*, *trioctional*, some of which are new (Fig. 2). A novelty is the "partly determinable forms," i.e., incomplete forms: *périhexaèdre*, *comprimé*. The indeterminate forms are largely unchanged, with the sole addition of *laminaire*, corresponding to *Karinthin*, a species created by Werner.

Even before Haüy's II edition was published, there appeared a French translation of a work by the great Swedish chemist Berzelius dedicated to mineralogical classification (Berzelius 1819). Berzelius immediately declared his conviction that the only logical criterion of mineralogical classification is the chemical one, also because the chemical composition largely determines the external characteristics of the mineral. The various classifications proposed in the 1700s were mainly based on the external characters, given the inadequate chemical knowledge at the time. Examination of the most important classifications shows that there was an increasing tendency to consider the chemical composition. Therefore, although Linnaeus wanted to apply the classification method that had worked so well in the organic [biological] field to inorganic materials [minerals], Wallerius and Cronstedt had already introduced chemical concepts, and even Haüy and Werner, leaders of the two dominant schools of thought of the era, had recognized the importance of chemistry, albeit in different ways.

For Berzelius, the classification based on external characters was convenient for the collector, who only sought the name of the mineral, but only the application of chemistry could be called scientific and valid for the researcher who wanted to determine the nature of the mineral.

Berzelius felt much closer to Haüy, with whom he agreed upon the definition of species (same chemical composition with the same primitive form), but demanded greater use of the chemical nature of minerals in the classification he was proposing. Much space was dedicated to what perhaps remains his most important scientific contribution: chemical symbols, one or two letters to indicate not only qualitatively the presence of an element but also the proportions

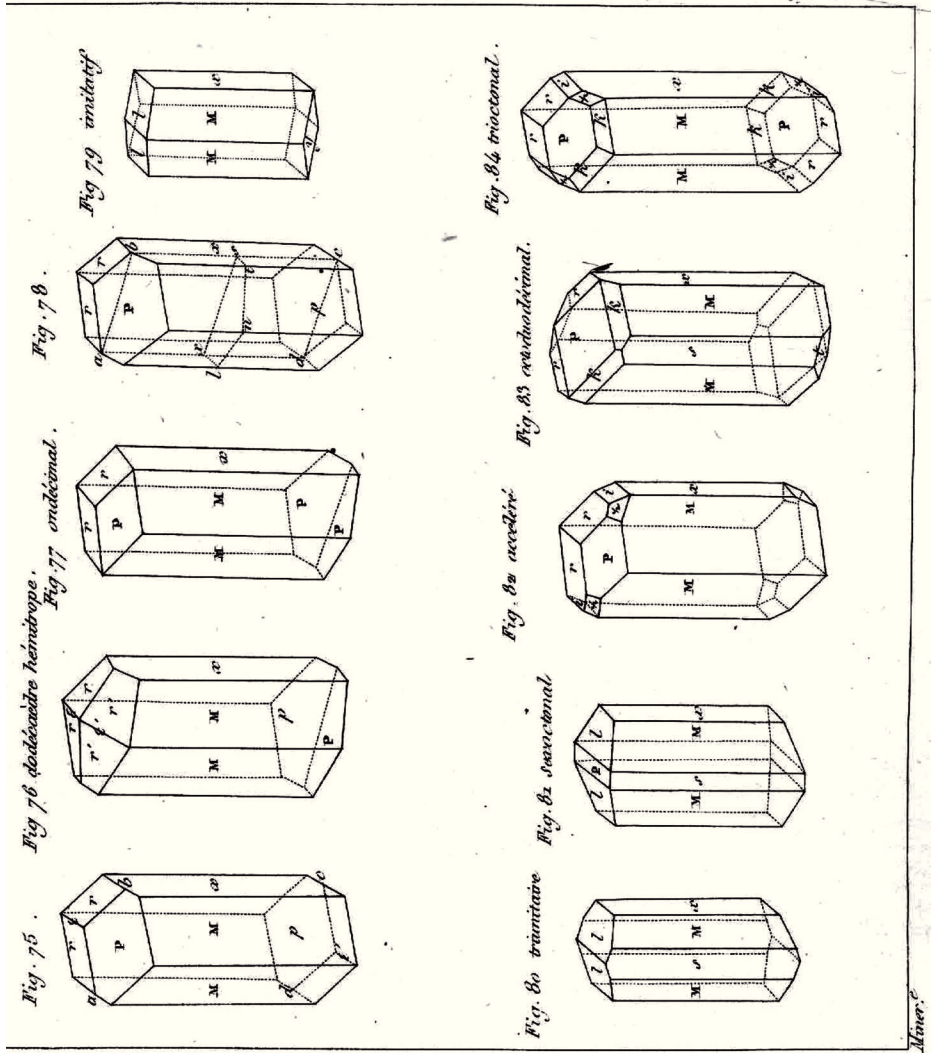


Figure 2. A page of the Atlas of the Haüy's *Traité de Minéralogie* (1822) showing some forms of amphibole crystals.

in which it is included in a compound. These symbols could provide the “chemical formula,” which schematically represents the composition of the compound without reporting the long list of percentages values from the analysis. In truth (as we will see further on), the still imperfect knowledge did not make the quantitative meaning of the symbols immediately clear, since they generally referred to equivalent weights rather than to the actual atomic weights; everything was rendered even more complicated by mistakes in the composition of many oxides (for instance, in silica, the silicon atom would be bound to three oxygen atoms) and by the setting of oxygen as 100 (as a reference value). Although the introduction of chemical symbols was a great contribution by the Swedish scholar, the same cannot be said of the proposal of mineralogical symbols, which apparently were simplifying but in fact were a source of confusion, e.g., “S” stood for sulfur in sulfides but for silicon in silicates, and so on.

The classification scheme follows a logical order related to a fundamental discovery by Berzelius: the electrochemical scale, which he indicated in a note in 1811. It arranges the elements, known or hypothesized at the time, in increasing order of electropositivity on the basis of affinity, starting with oxygen, passing to the “metalloids,” a name he coined (i.e., sulfur, “nitric,” “muriatic radical” up to carbon and hydrogen), and ending with the long series of metals (from arsenic to chromium and finally sodium and potassium).

This series forms the basis of the classification; in fact,

Chacun de ces corps simples [elements] peut constituer une famille minéralogique, qui sera composée en ce cas de ce corps simple et de toutes ses combinaisons avec les corps qui sont électro-négatifs par rapport à lui..... qui le précèdent dans la série....

The families are divided into orders according to the different electronegative elements with which the most electropositive is combined (for instance, sulfides, oxides, carbonates...). Yet, Berzelius’ open-mindedness is revealed by his immediate declaration that nothing forbids one from adopting a reverse classification by using orders for families and vice versa, i.e., basing it on the electronegative “ingredients” rather than on the electropositive ones. Each of the two types of classification has its advantages and its disadvantages; it is necessary to choose the one that is more useful and especially the one that appears more logical, also taking account of the external characteristics: which ones are more similar to each other, the copper minerals (from the native metal to the sulfide to the carbonate) or the sulfides (of copper, of lead, of iron)? Berzelius seems to favor the first solution, which he also lists in detail (albeit schematically); but, he does not deny that the second one may also have its benefits, and he presents a very synthetic scheme of it. Nevertheless, it was the second one that became a common heritage within a few decades.

The amphiboles appear in class I, order III “Electropositive metals,” subdivision II “Metals not reducible with carbon,” family 6 “Calcium” in the genus “Silicates based on calcium and magnesium,” under the mineralogical name “amphibole” having formula $C S^2 + 2MS^2$ with two dots above the C and M (2 oxygens) and three dots above the S (3 oxygens). As mentioned above, these are not the normal chemical symbols but the mineralogical ones, where C stands for CaO_2 , M for MgO_2 and S for SiO_3 ; moreover, we should not be surprised at the formulae of these oxides, since they reflect the knowledge of the time. “Asbestos” is assigned to the same genus, although without a formula. “Anthophyllite,” also without a formula, appears in another genus, “silicates with a triple base.” All the known minerals are mentioned in the tables. Not all have a formula, but about 40 species have annotations, so that about one-third of the volume is filled in this way.

The note that interests us here is the one for amphibole, especially in comparison with pyroxene, a comparison that would last exactly a century starting from the original idea of H. Rose. Berzelius attributed Haüy with the great merit of having grouped all the different species presented by Werner and his school in a single species, amphibole, demonstrating

the importance that geometric analysis rightly played, particularly at a time when chemical analysis was not widespread. He then emphasized that both types of analysis must provide their contributions for an exact systematics, especially in the case of complex materials like the amphiboles and their close relatives the pyroxenes.

The first half of the century did not record other substantial novelties in the knowledge of amphiboles, as demonstrated by various treatises. Another typical sign of the mid-XIX century was the presentation of chemical composition, since the analytical percentage data (presented since the end of the 1700s) were now accompanied, almost timidly, by their interpretation according to Berzelius' chemical formula, i.e., in binary terms. Obviously, this occurred when it was made possible, perhaps directly by the particular analyst-author.

The middle of the century saw the publication of the IV edition of a treatise that would become a classic in systematic mineralogy, the *System of Mineralogy* of the American naturalist, James Dwight Dana (1813-1895), in 2 volumes (Dana 1855). He did not take a position between the two opposing schools but tried to use them both, as appears clear from the obvious principle: "since we often do not have crystalline forms, we must also consider other characters." For classification, he favored Berzelius, particularly underlining the advantages of chemical taxonomy, but choosing the electronegative alternative, with five classes: 1) Native elements, 2) Sulfides, 3) Fluorides and chlorides, 4) Oxygenated compounds, 5) Organic compounds. It is a clear and simple classification, with the single large defect of presenting minuscule classes next to very abundant classes, above all class 4.

Indeed, the amphiboles are in the "Oxygenated compounds" class, within a single species called *Hornblende* in the section "Augite" in the genus "Anhydrous silicates" of the order "Acids of form RO³" in the family "Double binary compounds (Salts)." The following essential data are reported for this species: monoclinic with axial ratios $a:b:c=0.5527:1:1.8825$, perfect prismatic cleavage with angle 124°30', values of angles between the faces, hardness 5-6, density 2.9-3.4, various characteristics. The text character size becomes small for the chemical composition $R^3Si^{9/4}$, R^3Si^2+RSi , followed by an explanation: R can be lime, magnesia, iron protoxide or manganese, while alumina replaces silica in some varieties, the most important being: *tremolite*, *calamite*, *raphilite*, *actinolite*, *anthophyllite*, *asbestos*, *amianthus*, *pargasite*, *hornblende*, *carinthine*, *arfvedsonite*, *aegirine*, in addition to the rocks *amphibolite* and *corneite* as well as *uralite*, a pseudomorph transformation product from pyroxene, and, among the explanations of the analyses, also *cummingtonite*, *gedrite*, *nephrite*. There are 34 chemical analyses divided by variety, some of which are assigned a formula (ignoring the dots):

Tremolite	$CaSi+Mg^3Si^2$
Anthophyllite	$FeSi+Mg^3Si^2$
Arfvedsonite	$NaSi+Fe^3Si^2$
Cummingtonite	$(^{5/8}Fe+^{3/8}Mg)^4Si^3$

These formulae, especially the first three, indicate that there was already a chemical subdivision similar to the current one: magnesium-iron (anthophyllite, cummingtonite), calcium (tremolite), sodium (arfvedsonite).

However, Dana's classification includes three materials considered as a different species, probably because they were considered identical: *wichtyne*, *glaucothane*, *violan*. The first two are given the chemical formulae: $(^{1/2}R^{\cdot 3}+^{1/2}R^{\cdot \cdot 3})Si^{\cdot \cdot 2}$ and $(^{3/5}R^{\cdot 3}+^{2/5}R^{\cdot \cdot 3})Si^{\cdot \cdot 2}$, respectively, but with a ratio $R^{\cdot}/R^{\cdot \cdot}$ up to 1:1, where R^{\cdot} stands for Na, Ca, Mg, Fe" and $R^{\cdot \cdot}$ stands for Fe"".

The inclusion of the amphiboles in the section "Augite" underlines the close similarity attributed to amphiboles and pyroxenes, even though a slight chemical difference in the ratio between bases and silica is reported: 1:2 in the pyroxenes ($R^{\cdot 3}Si^{\cdot \cdot 2}$), 1:2¼ in the amphiboles ($R^{\cdot 4}Si^{\cdot \cdot 3}$), again considering silica as SiO₃. However, the exactness of the chemical determinations achieved in those years is remarkable: today, the bivalent bases/silica ratio is

1:1 for pyroxenes and 7:8 for amphiboles, with ratios between the two silica contents of 1:8/7, i.e., practically identical to 2:2¼.

The V edition of Dana's *System of Mineralogy* was published 13 years later (Dana 1868). In many aspects, it was a great step forward; the treatment is more thorough, with a large number of chemical analyses, i.e., over one hundred for the amphiboles. Yet, in another way, it was a step backward that persisted for a further half century: it announced the close similarity, indeed polymorphism, between amphiboles and pyroxenes, as had been proposed 30 years earlier by Rose and later confirmed by Rammelsberg, even though it noted the constant and prevailing presence of Ca in the pyroxenes alone. It talks of "dimorphism" between these two mineral groups, involving (albeit with great similarity of crystalline form, "*an essential isomorphism*") two different prismatic cleavage angles (87° vs. 124°) leading to a doubled crystallographic ratio *b:c* (i.e., *b:2c*) in the amphiboles, different crystalline habit with long forms common in the amphiboles and rare in the pyroxenes, different optical signs (positive for pyroxenes and negative for amphiboles), density always higher (by ca. one-tenth of the value) in the pyroxenes for corresponding chemical compositions. Finally, it reports the peculiarity of twins, with portions of amphibole close to parts of pyroxene, testifying both to the isomorphism and to the dimorphism of the two "species."

The step backward is shown by the chemical compositions given for all the amphiboles; the small differences between amphiboles and pyroxenes in the bases/silica ratios disappear completely and there is a return to equality of the formulae with those of the pyroxenes: it is perfect polymorphism. In reality, this seems to be a prejudice because, even with hindsight, one can see that the very many chemical analyses (100 for amphiboles and 90 for pyroxenes) reveal a different behavior of water: in amphiboles, it was found in 61 cases with a mean of 0.94% and a median of 0.46%, while it was reported in pyroxenes in 34 cases with a mean of 0.53% and a median of 0.34%. Although these are certainly not large differences, especially since there are no differential values between low water and high water, they perhaps could have been discussed, also in view of the relatively frequent presence of fluorine in the amphiboles, i.e., in 16% of the analyses with a median of 0.90%, but its complete absence in the pyroxenes.

This edition is also interesting because it mentions a "new system of chemistry," essentially consisting in recognition of the true atomic weights instead of the equivalent ones used for the elements with unequal charges since the time of Berzelius, namely since the 1820s. A new system that was probably not very well accepted by the author, as shown by the table of atomic weights identical to the one in the preceding edition, i.e., according to the old system. However, something was moving. Finally, after almost half a century, Avogadro's Law (that equal volumes of different gases under equal conditions of temperature and pressure contain an equal number of molecules [enunciated in 1811 but never applied]) is taken into consideration, leading to a whole series of corrections for the true atomic weights, e.g., giving water the formula H₂O instead of HO and thus oxygen with the atomic weight of 16 instead of 8, and so on. However, despite this correction, the old notation is still occasionally used in the text, even though the author often passes to the new notation, with one important change: finally from Si^{···} to Si[·]. This passage is combined with another important novelty: Dana proposes to abandon the system of binary representation of compounds devised by Berzelius, admitting that oxygen is part of both the "acidic" part (in our case Si) and the "basic" part (i.e., various metals); for instance, the formulae of olivine and pyroxene, respectively Mg^{·2}Si[·] and Mg[·]Si[·], can be written as Si||O₄||Mg₂ and SiO||O₂||Mg, which introduces the subscript exponents of the symbols (as we use today). These representations can be clarified even more by the so-called structural formulae, indicating the charges of the various atoms (represented by bars):



Dana divides the silicates into anhydrous and hydrated. He further divides the former according to the ratio of oxygens between bases and silica, i.e., 1:2 “bisilicates,” 1:1 “unisilicates” and 1:<1 “subsilicates.” The *Amphibole group* figures among the most important bisilicates; it includes “minerals with “anisometric” crystallization with prism angles not at 120° [i.e., not hexagonal and thus orthorhombic, monoclinic or triclinic] divided into three subgroups: Pyroxenes, Spodumene and Amphiboles. The amphiboles are defined by a prism of ~ 123°-125°, while the others are of ~86°-88°, although spodumene is distinct in having Al. For the amphiboles, he begins with the orthorhombic ones, divided into kuppferite with only Mg and anthophyllite with ¼ Fe, and continues with the monoclinic ones, the most important being amphibole (as a species), which can present an entire range of compositions with or without alumina substituting silica, with mainly Ca and Mg but also Fe (sometimes also ferric iron) and in some cases also alkali. In the absence of alumina, there are terms with Ca-Mg (tremolite and nephrite), Ca-Mg-Fe (actinolite), Ca-Mg-Mn (richterite), Fe-Mg (cummingtonite), Fe-Mn (dannemorite) and only Fe (grunerite); finally, as an appendix, he mentions asbestos. Also in the presence of alumina, the various terms are described according to the nature of the base, with Ca-Mg (whitish edenite and grass-green smaragdite), Ca-Mg-Fe (green pargasite and black hornblende). Three other names are mentioned, but they have subsequently disappeared: waldheimite, with a strong Na content, kokscharoffite, with much alumina, and schefferite, with a strong presence of ferric iron. Other species of the group include arfvedsonite, with ferric iron and sodium, and crocidolite with similar composition but fibrous and blue. Finally, the list of amphiboles is completed in an appendix including wichtisite and glaucophane, of similar composition with Na-Al, sordavalite, a hypothetical Mg-Fe-Al phospho-silicate, and tachylite, of uncertain composition; the last two were reported in the 1820s but are very dubious.

Naturally, these treatises provide an overview of the scientific knowledge of the time but they are much more important when their authors give direct contributions, with original research, to certain sectors of mineralogical systematics, especially concerning the amphiboles. This is the case of two authors in the second half of the XIX century: Carl Friedrich Rammelsberg and Gustav Tschermak.

Rammelsberg (1813-1899), professor of chemistry and mineralogy in Berlin, and very devoted to Berzelius, focused on the chemical study of mineralogy, *Mineralchemie*, publishing a series of treatises (and relative appendixes) with this name from 1841 to 1895, a few years before his death. Despite the changes that occurred in chemistry during that half century, particularly in the interpretation of the composition and the chemical notation in formulae, he always remained faithful to the ideas of the great Swede, as is evident from the binary nature of the compounds and superscript exponents in the formulae. A simple example is a phrase contained in his last work, the II supplement to the II edition (Rammelsberg 1895), regarding the nature of the pyroxenes: “*CaSiO₃ and MgSiO₃ are known. Diopside CaMgSi²O⁶ is [therefore] a mixture of both molecules and not a combined molecule (Gesamtmolekül).*” Another example of the persistence of the original interpretation is the perfect reversibility claimed between the concept of isomorphism and the analogy of the crystalline forms; this would have meant that similar crystals, as in the case of pyroxenes and amphiboles, must have a close correspondence of chemical composition, i.e., RSiO³. The symbol R stands for a generic atom, from univalent (Na, Li, K) to bivalent (Ca, Mg, Fe, Mn, Zn) to trivalent (Al, Fe), obviously present in different quantities, one if bivalent, two if of unequal charge, in particular tripling the silicic radical (Si³O⁹) with trivalent cations. In fact, the last case does not occur because the entry of trivalent cations is only partial with the mixture, for instance, of the molecule MgAl²SiO⁶, always indicated so as not to divide the basic molecule Al²O³ which, in turn, would have combined with the other two, MgO and SiO², all exactly with the basic idea of Berzelius from 80 years before. Even more illuminating is the discussion of the role of fluorine in silicates, particularly its relationships with water. After correctly observing that high fluorine contents are generally accompanied by low concentrations of water and vice versa, Rammelsberg wonders about the correctness

of the recently advanced hypothesis that the hydroxyl group OH could be replaced by F. The answer was: *Diese Hypothese ist in hohen Grade unchemisch... weil OH nur eine hypothetische Atomgruppe ist* (this hypothesis is highly unchemical ... since OH is only a hypothetical atomic group), given that HOH (or KOH) has a chemical character completely different from HF (or KF), and equivalence should not be confused with substitutability, e.g., O is equivalent to 2 Cl but they certainly cannot substitute each other, just as 2 Cl cannot substitute S.

This discussion must not, however, diminish the contribution and especially the figure of Rammelsberg. We are indebted to him for a very large quantity of chemical analyses of amphiboles (and pyroxenes), many of which are reported in his treatises along with analyses by many other authors. His effort to draw a purely chemical explanation of the composition of these minerals from this mass of data is evident: the formulae are calculated, and the ratios between the constituents, particularly between “bases” and silica and between the various bases, are evaluated.

There are no substantial differences in the treatment of amphiboles between the 1875 edition (Rammelsberg 1875) and the second supplement twenty years later, (Rammelsberg 1895) although the latter contains a clearer definition of silicates as salts, just like carbonates, sulphates and similar compounds, while admitting that silicic acid, like carbonic acid, is little known. Rammelsberg observes that the ratios between bases and silica are often different but generally referable to whole numbers; by analogy with carbonates, he mentions “normal silicates” with $R':Si=2:1$, that is R'^2SiO^3 , but not occurring with univalent atoms, “basic silicates,” divided into “halves,” “thirds,” “quarters,” respectively with ratios 4:1, 6:1, 8:1, or, in contrast, “acidic silicates” with ratio 2:2, that is $R'^2Si^2O^5$.

The amphiboles constitute the *Hornblendetypus* which, together with the similar augite type, is part of the *Augitgruppe*. They are all “normal” silicates, mainly with bivalent metals, sometimes with bi-, uni- and trivalent bases instead, or with “mixtures” of these two. The parallelism between pyroxenes and amphiboles is almost complete: apart from very few cases (such as wollastonite), for every pyroxene there is a corresponding amphibole.

Since this is a treatise of “*Mineralchemie*,” it only provides the chemical data useful to indicate the chemical composition of each mineral, usually in terms of “mixtures” of binary compounds. The most frequently reported ratios regard the group of bivalent atoms, both in comparison with silica, i.e., R'' (Ca, Mg, Fe):Si, generally very close to unity, and within the group itself, i.e., Ca:(Mg, Fe), correctly representing their different behavior, with values that are rather variable but mainly between 1:2 and 1:3. It mentions the irregular presence of fluorine but does not give particular importance to water, which is often measured, sometimes hypothesized from the lack of closure at 100 of the analysis, and explained both by a beginning of alteration and as hydrogen to be counted between the R' .

For tremolite and *Strahlstein* (actinote), the formula is simple $RSiO^3$ with a possibility of variation: for the former, between $\{CaSiO^3 - 3MgSiO^3\}$ or with simple ratios of 2:5 or 3:8 between the two constituents, since Fe is practically absent; for the latter, a generic $\{mCaSiO^3 - nMgSiO^3 - FeSiO^3\}$ with coefficient values of $m \sim 3$, $n \sim 6$. For richterite, the situation is complicated by the presence of alkali, initially giving a prevalence of potassium over sodium but subsequently with inverted proportions. The proposed formula thus becomes $\{R'^2 SiO^3 - nRSiO^3\}$ with n varying from 6 to 13. The amphiboles that lack Ca, with only Mg-Fe, i.e., anthophyllite and gedrite (distinguished by the absence or presence of Al), are characterized by the formulae $\{4MgSiO^3 - FeSiO^3\}$ and $\{4RSiO^3 - Al^2O^3\}$, respectively, where Al does not figure as a silicate, as will be discussed further ahead. Cummingtonite, as appears from the preceding table, is indicated as corresponding to rhodonite, with a high content of Mn shown by an analysis that is very old and unreliable, as it refers to a pink material. The description of asbestos is clearer, indicated as the fibrous variety of some minerals, either with Ca, like tremolite and hornblende, with a water content no greater than 3%, or lacking Ca, for which the

water content is around 10%, without doubt serpentine. For arfvedsonite and glaucophane, the problem of the trivalent components (Al and Fe) should be addressed, but the following mixed formulae are indicated instead, after the usual tables of ratios between the various components: $\{Na^2SiO^3 - FeSiO^3 - Fe^2Si^3O^9\}$ and $\{pNa^2SiO^3 - qR''SiO^3 - rR'''Si^3O^9\}$, respectively.

Now we can deal with the problem of the trivalent components, Al and Fe, to which Rammelsberg devotes entire pages. As mentioned briefly for gedrite, the question was important not only for the alkali-amphiboles but also for the most important mineral, hornblende. In the 1875 treatise and in the first supplement of 1886, Rammelsberg includes a long discussion of the problem "The nature of the terms containing alumina and ferric oxide." He begins with the original idea of Hisinger in the 1820s that alumina was present in tremolite as a substitute for silica; this idea was later supported by Rammelsberg's discovery in 1858 that the trivalents were usually accompanied by alkali, so he thought of the presence as an isomorphic mixture of the aluminate $R^3Al^4O^9$. Later, however, since the ratios of both the mono- and divalent cations with silica were those of "normal" silicates, i.e., $RSiO^3$, he was convinced that hornblende, like the corresponding augite, contained an isomorphic mixture of the type $\{mRSiO^3 - nR^2O^3\}$.

Numerous editions of the treatise by Gustav Tschermak von Seysenegg (1836-1927), professor at Vienna for almost 40 years and director of the Imperial Museum of Natural History, were published (Fig. 3). The first edition (Tschermak 1882) already contains important



Figure 3. Portrait of G. Tschermak (courtesy of G. Kurat former director of Mineralogical Section of the *Naturhistorisches Museum* of Vienna).

differences with respect to contemporary texts, particularly that of Rammelsberg. Some are trivial, like the chemical formulae written with subscripts, others substantial and related to Tschermak's studies of amphiboles published since 1871 in a journal that he had founded: *Mineralogische-Petrographische Mittheilungen*.

Although the classification does not bring great credit to the author, the rest of the treatise shows a much more modern tone. The three crystallographic notations in use are presented and discussed: the out-of-date one of Weiss; that of Miller, perhaps more difficult for beginners but clearly superior for brevity and simplicity and the one that would be increasingly adopted by the author; that of Naumann, commonly used by German-language authors but that was only able to indicate the form and not the face of the crystal. In the chemistry part, the periodic systems of Meyer and Mendeleev appear for the first time in a mineralogy text, with a table of atomic weights practically equal to the current one, except that it is limited to the 67 elements discovered thus far; all of this was preceded by a clear explanation of the difference between equivalent weights (pure combinational proportions) and atomic weights obtained using Avogadro's Law on gases. But above all, the chemical formulae of "structure" are presented, particularly for the silicates; in the absence for another half century of the determinations of the true crystalline structures, these formulae would constitute an attempt to visualize the sometimes very complex chemical nature of the silicates. Naturally, Tschermak deals with ortho- and metasilicic acid and proposes possible concatenations of it: in this regard, he advances the idea that, just as functional groups in organic chemistry are quickly identified in the laboratory by means of the decomposition products (viewed as fragments of the initial compound), information on the nature of silicates, known only in the solid state, could be obtained from their alteration materials produced over geological time. The reported examples concern the orthoclase-mica-kaolin, tremolite-talc and olivine-serpentine ratios, with the relative structural formulae that could be inferred from the similarities of the various compositions.

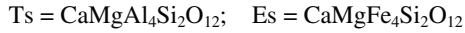
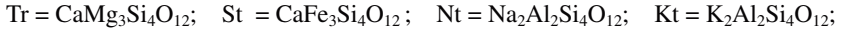
The order "silicids" of the V class "Silicoids" contains the "pyroxenes-amphiboles group," including normal metasilicates and aluminosilicates of Ca, Mg, Fe, Mn. They present a similar crystalline habit and cleavage according to the {110} prism with 4 faces with angles of around 90° or around 60°, identifying two different series, respectively called pyroxenes and amphiboles, with substantially parallel chemical composition. Three different symmetries, orthorhombic, monoclinic and, rarely, triclinic, are presented by both series, which however can be distinguished by the axial relationships: for the monoclinic terms, they are $a:b:c \sim 1.09:1:0.58$ for the pyroxenes but $a:b:c \sim 0.54:1:0.29$ for the amphiboles with a β angle $\sim 74^\circ$ for both. This difference disappears if the symbol {210} is attributed to the prism of the amphiboles, obtaining the ratios $a:b:c \sim 1.06:1:0.59$ and β angle $\sim 89^\circ$ for both. The relationship between the two series suggests that the "polymerism" is expressed as a similar percentage composition but different molecular weight (double for the amphiboles); hence, the pyroxene enstatite can be indicated as $Mg_2Si_2O_6$ (with a doubled formula by analogy with the pyroxene diopside $CaMgSi_2O_6$) but the amphibole anthophyllite as $Mg_4Si_4O_{12}$, thus identifying the two concatenated silicic acids $H_4Si_2O_6$ and $H_8Si_4O_{12}$ starting from the monomer H_2SiO_3 .

For some time, more constant ratios had been obtained for the amphibole tremolite (the analogue of the pyroxene diopside) by comparing Ca with the sum Mg+Fe rather than with other groupings or with single atoms. The most frequent values of Ca: (Mg+Fe) were around 1:2.6-2.7; on the assumption that the sum was 4, this gave the formula $CaMg_3Si_4O_{12}$ for tremolite and $Ca(Mg,Fe)_3Si_4O_{12}$ for actinolite. A great contribution by Tschermak was to provide a solution to the problem of the presence of a large quantity of Al in hornblende, schematized as $CaMg_2Al_2Si_3O_{12}$ (Tschermak 1871). After mentioning the complexity of the problem of the composition of this mineral, which from the chemical analysis appears to consist of twelve elements plus water, he underlines the uncertainty of the results that could derive not only from analytical errors (over- or underestimations) but also from difficulties due

to the possible presence of inclusions or intergrowths. Going on to illustrate his thinking, he advanced a timid premise:

I have accepted for the moment the following compounds to clarify the complication of the composition of hornblende.

He identifies six possible molecules that, in an isomorphic mixture, could contribute to the constitution of this mineral complex



The first three are easily identifiable respectively as tremolite, actinolite (*Strahlstein*) and glaucophane (with Na), while the fourth is its theoretical equivalent with potassium (K). The last two are hypothetical compounds; in particular, the fifth would later be called Tschermak's silicate and the sixth is its analogue with Fe. With this artifice, the author is able to explain the composition of three different hornblendes analyzed by Rammelsberg, a colourless one from Edenville, a grey-green one from Saualpe and a black one from Bogoslawsk, and he attains perfect agreement with the compositions obtained from the percentages of the six above-mentioned terms. There is no difficulty for the composition of the alkaline terms, glaucophane $\text{Na}_2\text{Al}_2\text{Si}_4\text{O}_{12}$ and arfvedsonite $\text{NaFe}''_2\text{Fe}'''\text{Si}_4\text{O}_{12}$. The formula of wollastonite is interesting, even though it is not part of the amphiboles because it is placed among the pyroxenes. It is given correctly as $\text{Ca}_3\text{Si}_3\text{O}_9$ on the basis of the comparison of the axial ratios with enstatite $\text{Mg}_2\text{Si}_2\text{O}_6$: for the former $a:b:c \sim 1.05:1:0.96$ and for the latter $1.03:1:0.59$, where the ratio of the third values is substantially 3:2; morphological crystallography opened the road to structural crystallography, which only after half a century could identify the two different periodicities of the silicate chain according to the vertical axis. Similarly, it is interesting that the amphiboles show halved values for a and for c in their ratios; in other words, their values become similar if $b = 2$, which is what was found with the double chain of silicon-oxygen tetrahedra by means of structural determination, but was anticipated with the angular measures.

A prestigious figure in mineralogy in the late XIX century was Paul Groth (1843-1927), professor first a Strasbourg and then Munich and founder in 1877 of the important journal *Zeitschrift für Kristallographie*, which is still active today albeit in the English language.

Groth's contribution to systematic mineralogy was a series of editions of "Mineralogical tables" containing all the known data for the recognized species, with detailed notes including a high-quality crystallochemical classification. The first edition was in 1874, the fourth in 1898. The first classification faithfully follows that of Dana, with the silicates grouped in the vast V class "Oxygenated salts." However, in the second edition, the classification is modified in a more logical manner corresponding substantially to the currently accepted one, with the silicates (and titanates) in the own IX class.

In the first edition (Groth 1874), the amphiboles are a subgroup of an *Augitgruppe*, like the pyroxenes with which they are closely compared because of the isomorphic relationship as "bisilicates" with composition R_2SiO_3 . This is discussed by considering the possibility of a Si-Al substitution in hornblende and explaining the trimorphism by the prevalence of the various metals: orthorhombic series with Mg, monoclinic with Ca (or Na) and triclinic with Mn. The second edition (Groth 1882) includes a detailed and clear definition of isomorphism and assigns pyroxenes and amphiboles to the order *Metakieselsäuresalze* (Salts of metasilicic acid), with the first three groups of pyroxenes with variable symmetry, the fourth of orthorhombic amphiboles with anthophyllite $(\text{Mg,Fe})\text{SiO}_3$ and the fifth of monoclinic amphiboles; a note specifies that tremolite, thus far considered as diopside, has a ratio $\text{Mg}:\text{Ca}=3:1$ and thus the formula should be doubled, as for actinolite with respect to hedenbergite. In the continuous comparison between the two parallel series, Groth mentions that the amphiboles are less well known than the pyroxenes

and he makes an interesting observation “*ist es nicht unwahrscheinlich*” (it is not unlikely) that the amphiboles contain hydrated silicates since completely fresh varieties yield water when heated. This is an interesting observation because, after the above-mentioned differences of tremolite, the dogma of the perfect chemical correspondence between the two series is beginning to collapse. Another observation concerns criticism of Rammelsberg (even though he is praised for his innumerable analyses) because of his obstinacy in remaining anchored to the chemical formulae, writing them as the result of two different silicic salts with the acids arbitrarily coupled with the bases. A more detailed examination of the composition of silicates appears in the 1898 edition, where reference to the two acids, ortho $\text{Si}(\text{OH})^4$ and meta $\text{SiO}(\text{OH})^2$ with the respective radicals SiO^4 and SiO^3 , is repeated and, in particular, the formulation is fiercely criticized, e.g., for diopside, $\text{SiO}^3(\text{Mg,Ca})$ instead of the correct one $(\text{SiO}^3)^2\text{MgCa}$. Although only indirectly relevant to amphiboles, there is an interesting discussion of the formulation of the Al silicates, with a rough formula SiO^3Al^2 (only andalusite and distene were known then). In other words, should they be considered orthosilicates, and thus the formula should be written $\text{SiO}^4\text{Al}(\text{AlO})$, or metasilicates $\text{SiO}^3(\text{AlO})^2$, or one different from the other? The author favors the last hypothesis, recalling that orthosilicates are generally more easily alterable than metasilicates (see olivine – enstatite), and thus it is probable that andalusite, more easily alterable, is an orthosilicate and distene is a metasilicate, with the relative formulae mentioned above.

The amphiboles are considered salts of a tetrapolymer of the meta acid $\text{SiO}(\text{OH})^2$, with a structural formula that sees the Si atoms at the vertices of a square with four O atoms bridging them and the other eight saturating (e.g., in tremolite) a Ca and three Mg: this lovely symmetry explains why it is still preferred to round off to 3 Mg + 1 Ca despite the fact that the mean of dozens of analyses indicates a ratio Ca:Mg~2.6. This structural formula also nicely explains the close relationship with pyroxene: by alteration, pyroxene passes to amphibole via the linking of two opposite sides of the square, by fusion of amphibole, pyroxene crystallizes by breakage of the square into two symmetrical portions. It also explains the decrease in symmetry passing from orthorhombic (anthophyllite) to monoclinic (tremolite) via the entry of a Ca in place of a Mg, while it remains the same in hornblende because two $(\text{AlO})^2$ groups replace one of the MgO^2Si groups and the CaO^2Si group.

Other worthy observations are: water (no longer considered negligible) is considered present as H^2 , e.g., in the orthorhombic amphiboles we have $(\text{SiO}^3)^4(\text{Mg, Fe, H}^2)^4$; among the amphiboles, there is no analogue of rhodonite with Mn; it is doubtful that aenigmatite belongs to the amphiboles group given the clear difference in parametric ratios. An apparent step backward is that the chemical formulae of the complex terms are always indicated with at least two formulae (three for hornblende) of ideal compounds in an isomorphic mixture, e.g., for glaucophane, there are the two formulae $(\text{SiO}^3)^4\text{Al}^2\text{Na}^2$ and $(\text{SiO}^3)^4(\text{Mg,Fe,Ca})^4$ between curly brackets. Another step cannot be defined as backward, but certainly neither forward: maintenance of the superscript exponents in the formulae instead of subscripts, as used for some time by Tschermak.

In the last years of the century, the famous geochemist Frank W. Clarke (1847-1931) attempted to classify the silicates in a large paper published in the Bulletin of the U.S. Geological Survey and reviewed in the *Zeitschrift* (Clarke 1897). In trying to combine the physical properties (particularly crystalline form and density) and natural history (type of deposit and alteration) with the chemical composition, Clarke proposes a scheme of the main silicates, considering them salts of the five hypothesized acids: ortho-, diortho-, meta-, dimeta- and trisilicic; however, he also mentions that the complexity of the various chemical compositions requires that one think not only of “normal” salts but also of double or even triple and generally multiple ones. Al is considered to play an important role for many silicates, because they can be derived by substitution of the normal orthosilicate $\text{Al}_4(\text{SiO}_4)_3$, e.g., muscovite $\text{Al}_3(\text{SiO}_4)_3\text{KH}_2$, where Al is replaced by the KH_2 group. Contrary to general opinion that viewed amphiboles as metasilicates, Clarke believes that better agreement with the analytical data can be attained

by considering the contemporary presence of variably saturated ortho- and tri-radicals of both bivalent atoms (Ca and Mg) and univalent atoms or radicals (Na, H, AlO, FeO).

The XIX century ended without particular novelties, as demonstrated by the VI edition of Dana's treatise (Dana 1892) now published by Edward Salisbury Dana after the death of his father James Dwight Dana, who had begun the series way back in 1837. Indeed, the possibility of distinguishing the various species of amphiboles on the basis of minimal angular differences of the cleavage solids thanks to the precise measurements of Krantz (1899), a piece of news immediately reported in the first appendix to the treatise, cannot be considered a very important advance (Dana 1899).

THE TWENTIETH CENTURY

The second appendix to Dana's classic treatise (Dana 1909) did not contain any substantial changes. However, an important work was the oddly titled "*Tetramorphism of the compound $MgSiO_3$* " by Allen et al. (1908), which commented on its synthesis via different methods: fusion of the components MgO and SiO₂, heating to 1300 °C, heating of other phases, reaction of fused MgCl₂ with amorphous silica. In all these cases, the prevalent phase is monoclinic pyroxene; slow cooling produces orthorhombic pyroxene but also small quantities of amphibole, orthorhombic for fairly rapid cooling, monoclinic for very rapid cooling. In truth, a later study by Bowen and Posnjak (1931) showed that the supposed amphibole was actually olivine, confirming that the synthesis of amphiboles cannot occur in dry conditions. This finding brought honor to the first true synthesis of amphiboles by Kruscioff (Chruschoff, in German usage) in 1890 in an aqueous environment: all the components were held at 550 °C for 3 months.

Another important work, that of Penfield (Penfield and Stanley 1907), was issued posthumously and dealt in general with the chemical composition of the amphiboles. It includes a summary of the knowledge of these minerals, discussing the views of both Rammelsberg and Tschermak on the role of Al, i.e., present as a sesquioxide or as a virtual molecule, respectively, as well as the essential role of F and water, erroneously considered to be related to alteration processes. Concerning water, Penfield discusses the analytical method that bears his name and was commonly used until a few years ago, mentions that amphiboles are also pegmatitic and pneumatolytic minerals, i.e., of strongly hydrated environments, and underlines the double role (unfortunately indistinguishable in the analysis) that water plays in amphibole. i.e., as OH or as H. The complex composition of amphiboles, compared with the simplicity of olivine, is explained by a "mass effect," a concept still accepted today for isomorphic substitutions, which requires an "amphibolic acid" that is more complex than the common metasilicic acid, e.g., structured as rings with 4 or 8 Si atoms. The two different types of amphiboles, tremolite and hornblende, share the same acid radical but have different compositions: tremolite is simpler, with a ratio RO:SiO₂ approximately equal to 1, with small variations explained by the presence of a $[R''''_2O(OH)_2]$ radical; in hornblende, the ratio is greater than 1 due to the presence of R₂O₃ but the ratio could return to 1 if more or less imaginary radicals, with R' or R''' bound to O, are considered, producing charges of 2 plus.

The new century did not bring any novelties, not even with the eighteenth-century habit of creating new species (or even varieties) and just as many new names, most of which will be later be discredited by the IMA Commission.

An important event was the publication, a decade apart, of two monumental mineralogy treatises, rich of data but without any important novelty. The first was a general, encyclopaedic type treatise in several volumes – the *Handbuch der Mineralogie* by Carl Hintze (1851-1917), professor first at Bonn and then Breslau (Hintze 1897). The second had a mainly chemical approach, the *Handbuch der Mineralchemie*, a substantial work by Cornelius Doelter (1850-1930), born in Puerto Rico but working in Austria (Doelter 1914).

War was raging in Europe, while America seemed a happy island since it was not yet involved in the conflict. The year was 1916 and a slim issue of the Bulletin of the American Geological Service was published by Waldemar Schaller (1882-1967), a young but promising scholar, under the anonymous title: *Mineralogic notes, series 3*, with a subtitle *The chemical composition of tremolite*. In the paper, Schaller maintains, also on the basis of preceding studies, that water is an essential component of tremolite in the form of hydroxyl groups (Schaller 1916).

Although some priority must be attributed to Penfield, we can truly speak of a turning point in understanding the nature of amphiboles, which would later be demonstrated definitely by the structural determinations of Warren in 1929 for tremolite and Warren and Modell in 1930 for anthophyllite.

The XVII edition of Tschermak's classic treatise was issued in war-ravaged Europe, although more than a new edition, it seemed like a simple reprint, at least for the amphiboles (Tschermak 1915).

In the treatises, practically nothing had changed, even in the post-war period, as shown by Paul Niggli (1888-1953) in the second edition of his *Lehrbuch der Mineralogie* (Niggli 1926). This famous Swiss scholar, professor at Zurich, presents a slightly different classification from the classic one, but then follows a completely different criterion in the descriptions of the minerals; he uses the morphological criterion by which, despite the asserted great similarity between pyroxenes and amphiboles, the former are placed among the "tetragonals," with a linear-axial aspect, and the latter are included in the "hexagonals," of columnar type. A step forward is provided by the recognition of a maxi-series of pyroxene-amphibole-mica rock minerals, characterized by formation temperatures that decrease as alkali and volatile components increase, which means a simple anhydrous composition for the first group, a more complex "often" hydrated composition for the second, and a very complex always hydrated composition for the third. Metasilicates (SiO_3) are not mentioned, but all the silicates are divided into three groups according to the radical: α) $[\text{SiO}_4]$, β) $[\text{SiO}_4\cdot\text{SiO}_2]$, γ) $[\text{SiO}_4\cdot\text{SiO}_2\cdot\text{SiO}_2]$, largely corresponding to those of olivine, the pyroxenes and orthoclase. The amphiboles are of type β with the basic molecule augite $[\text{SiO}_4\cdot\text{SiO}_2]\text{R}^{\cdot 2}$, but other molecules may also be present, e.g., $[\text{SiO}_4\cdot\text{SiO}_2]$ Al (Na,K), but also H in place of either the bivalent R or Na, or even F in place of O or OH. He continues in this way to underline the irregular and random presence of water, revealed by the analysis, as a typical oxide of H, a metal interpreted as a substitute of other metals.

The following mixed division of the amphiboles, partly chemical, partly crystallographic, is presented: I) Amphiboles low in alkali and Al, divided into orthorhombic and monoclinic, II) Amphiboles with sesquioxides low in alkali, divided into low and high in Fe, III) Alkaline amphiboles, divided into low in Ca and high in Na.

The 1920s saw the race to determine crystalline structures—a race certainly led by the Manchester school headed by William Lawrence Bragg (1890-1971), winner together with his father William Henry Bragg (1862-1942) of the 1915 Nobel Prize for Physics for the crystallographic applications of X rays. Within a mere five years, from 1925 to 1930, the younger Bragg and his collaborators, such as Brown, Taylor, West, Naray-Szabo and Warren, solved the structures of quartz, olivine, beryl, chrysoberyl, monticellite, phenacite, cyanite, staurolite, the chondrodite series, norbergite, melilite, analcime and andalusite, in addition to pyroxenes and amphiboles.

A young American, Bertram Eugene Warren (1902-1991) had gone to Manchester in those years to learn structural crystallography and had the fortune to solve, together with his mentor, the structure of the pyroxene diopside (Warren and Bragg 1928) and, alone, that of tremolite (Warren 1930). He then returned, as Assistant Professor of Physics, to M.I.T. in Cambridge,

Massachusetts, where he turned to anthophyllite (Warren and Modell 1930), completing the amphiboles with one monoclinic term and one orthorhombic term.

The structure of diopside is taken as the reference for tremolite, given the great similarity of the three-axis rotating crystal photographs made with Mo radiation; the lattice data are virtually identical except for doubling of the constant b in the amphibole. The material is from "New York localities" and "the chemical composition is presumed to be that of the localities." The difference in space group symmetry (" $2Ci - 3$ " or $C 2/m$, with symmetry planes, for tremolite; " $2Ci - 6$ " or $C 2/c$ with glide planes for diopside) suggests that the unit-cell of the amphibole, double that of the pyroxene, incorporates the blocks of the latter and the reflection planes. When the symmetry plane is located, the structure is largely solved, with good qualitative agreement (the R discrepancy factor was not known at that time) between the recorded intensities of the reflections (such as W., M., S. and V.S.) and the calculated structural factors. The previously adopted chemical formula for this mineral, $CaMg_3(SiO_3)_4$, does not conform to the proposed structure because the possible positions for the bivalent cations are 4 for Ca and only 10 (instead of 12) for Mg. Moreover, the role of water has to be fully re-assessed because, although the new formula is given as $H_2Ca_2Mg_5(SiO_3)_8$, OH groups are clearly present since the structure indicates an O bound not to Al but only to 3 Mg and thus, according to Pauling's recently enunciated principle of electrostatic bonds, it must have a negative charge of 1, i.e., an OH. The last formula does not even indicate the substantial difference between tremolite and diopside, namely the double Si-O chain that leads to the Si_4O_{11} radical. The work ends with a figure that would be repeated in all the following treatises, i.e., the explanation of the different values of the angle of the cleavage prisms of the pyroxenes and amphiboles (Fig. 4), and with the statement that all the monoclinic amphiboles present this structural type because the patterns of tremolite, kupfferite, actinolite, hornblende and grünerite are very similar, apart from some intensity differences in the reflections of grünerite due to its high Fe content. The work is dated Manchester, June 1929, and was submitted on July 8, 1929.

Less than a year passed and, on May 28, 1930, the paper on the structure of anthophyllite was sent from Cambridge (Massachusetts), in which Warren announces another just-finished work on the structure of enstatite, which would close the cycle of the pyroxenes and amphiboles (monoclinic and orthorhombic). The technique used is the one learned in England, both for the rotating crystal photographs and for solution of the structure by comparison with enstatite and tremolite. The lattice constants of anthophyllite determined a few months earlier by Johansson are confirmed, i.e., with a doubled with respect to the other amphibole and with b doubled with respect to the pyroxene with one cell, and thus quadrupled with respect to diopside, as also appears from a scheme that visualizes this doubling of parameters from pyroxenes to amphiboles and from monoclinic to orthorhombic counterparts. The chemical composition is clarified as $H_2Mg_7(SiO_3)_8$, although with the same remarks on Pauling's principle the author underlines the presence of OH, also indicating the formula as $(OH)_2Mg_7Si_8O_{22}$, in particular arranged around Mg. Once again, to localize the atoms, he prefers to refer to the structure of the analogous pyroxene (however still unpublished), adding the usual plane of symmetry to spatial group " V_h^{16} ," i.e., $Pbca$, to obtain the double cell of anthophyllite, expressly rejecting the other possibility of referring to the structure of the monoclinic amphibole. The result is the same double chain typical of the amphiboles, just as the simple one is typical of the pyroxenes; these chains develop along the c axis and explain the long habit of the crystals, increasingly marked and reaching the extreme in the amphiboles, probably thanks to a forcing action of the double chain.

The fundamental work by W.L. Bragg (1930) on the structure of the silicates, which appeared in the *Zeitschrift für Kristallographie* (received March 22, 1930), solved a problem that mineralogists had worked on and discussed for more than a century, vainly seeking in the chemical composition what was also, and especially, related to geometric-crystallographic factors. Bragg's paper is based on the crystalline structures of many rock minerals determined largely in his laboratory and/or by his students, with minor contributions from others such as

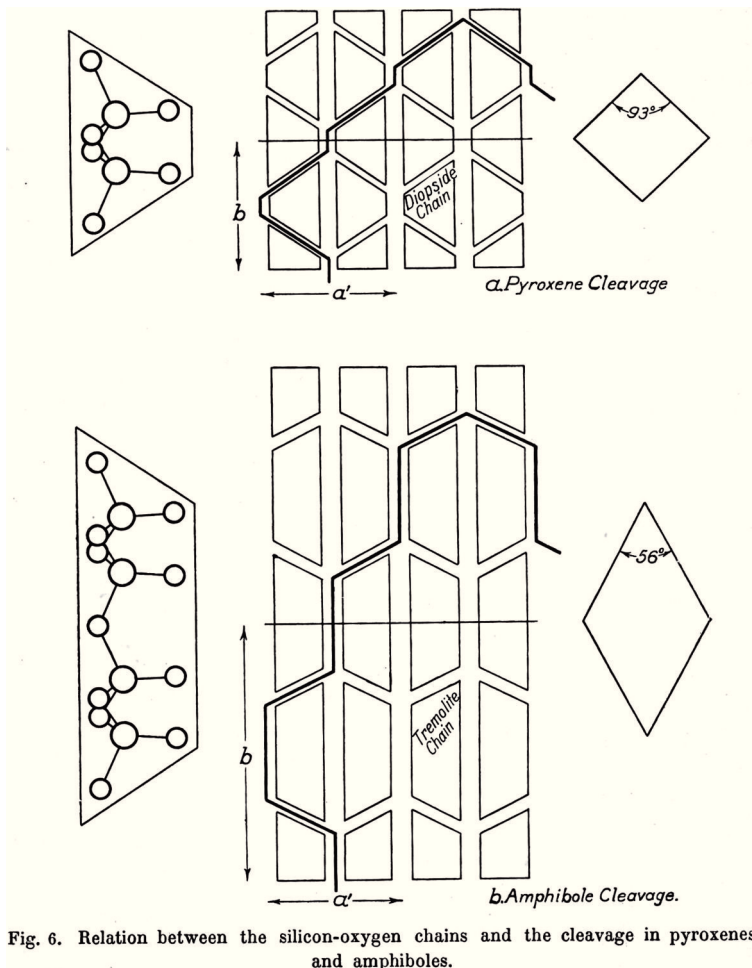


Fig. 6. Relation between the silicon-oxygen chains and the cleavage in pyroxenes and amphiboles.

Figure 4. The Warren's original drawing (1930) of explanation of cleavage in pyroxenes and amphiboles (Z Kristall 72).

Wyckoff in Washington, Menzer in Berlin and Zachariasen in Chicago, as well as the crystal chemical research by Pauling and the intuition of Machatschki. Acknowledging everyone, he formulates a perfect outline of the crystal chemistry of silicates, which has remained substantially unchanged and is so well known that it is superfluous to report it here. However, it should be emphasized that immediately before listing the various Si-O groups, characterized by different forms but also different Si:O ratios, Bragg credits Machatschki for having recently distinguished three different types of silicates on the basis of the already determined structures: "Ortho," with separate SiO_4 groups (olivine), "Meta," with chains of tetrahedra and a SiO_3 radical (diopside), and "With feldspath," with three-dimensionally bound tetrahedra. Bragg modestly declares that, thanks to the new structures, he can also add "self-contained groups" (the current soro- and cyclosilicates), the double chain and the layer. The two last possibilities ideally arise from the simple chain (pyroxenes type) lining up with another in a process that "if continued [indefinitely] would cause the type of concatenation of the next group [the layer]."

For the amphiboles, Bragg reports the results of Warren's study in detail, recognizes that the true chemical composition had already been established by Gossner (1924) and that he has only confirmed the structure; he also mentions the possibility that the position facing the base of the silicate group, which is empty in tremolite, could be occupied by alkaline atoms, bringing the total number of metallic atoms from seven to eight when the Al-Si substitution occurs:

an example of variation of the total number of metallic atoms in the cell. Exceptions, however, that do not destroy the general principle [advanced by the author in 1927] that a silicate must be viewed as a structure having a constant number of oxygen atoms in the cell, with a constant number of positions for metals and silicon that can be occupied by these elements in various proportions consistent with the balance of the valences. An idea widely confirmed by the subsequent work.

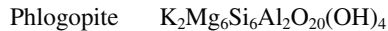
He also reports some considerations advanced by Pauling a few months earlier on the relationships between tremolite and mica (from which the structure that would be confirmed the following year by Jackson and West was hypothesized): first of all, the correspondences between the cell parameters

<i>Tremolite</i>		<i>Mica</i>	
$2a \text{ sen } \beta$	18.9 A.	c	20.0 A.
$b/2$	8.90	b	8.94
c	5.26	a	5.17

But the gradual passage can also be observed in the chemical composition from pyroxene to amphibole to talc with a loss of $(\text{CaO})_2$ replaced by $\text{Mg}(\text{OH})_2$

Diopside	$\text{Ca}_4\text{Mg}_4\text{Si}_8\text{O}_{24}$
Tremolite	$\text{Ca}_2\text{Mg}_5\text{Si}_8\text{O}_{22}(\text{OH})_2$
Talc	$\text{Mg}_6\text{Si}_8\text{O}_{20}(\text{OH})_4$

from which, by a partial but fixed Al-Si substitution and consequent charge deficit, the entrance of alkali is allowed, as in the micas:



The 1920s also saw the development of what might be called the classic view of amphibole crystal chemistry, based on the variably interpreted chemical data alone; in other words the "German school," considering the enormous effort made by these researchers. Most important among the last proponents of this school was undoubtedly B. Gossner, professor at Tubingen, who would also undertake roentgenographic determinations at the end of the decade. In a comprehensive work on the chemistry of pyroxenes and amphiboles, published in two parts but in the same year (Gossner 1924a,b), he attempts to draw information on the nature of these minerals from the analytical data, reproducing the theoretical "modal" components by means of calculations based on the single chemical constituents. Thus, for the pyroxenes, considered to be formed by the union of SiO_3Ca and SiO_3Mg (it is not clear why the symbols are inverted in the French manner!), he calculates the proportions separately starting with the Ca and Mg contents. The problem occurs when Al is present, as is the rule in the monoclinic species. The author rejects Tschermak's idea about the virtual molecule $\text{SiO}_6\text{Al}_2\text{Mg}$, but revives the old theory of Rammelsberg (without acknowledging him) of the real presence of Al_2O_3 which would replace SiO_3Mg ; this is the same as saying that a $\text{SiMg} - 2 \text{Al}$ substitution occurs, but not for the SiCa pair, prefiguring the present crystal chemical views. Therefore, in the calculation, he attributes all the Al_2O_3 content to the magnesium fraction, all the $\text{CaO} + \text{SiO}_2$ content to the calcium fraction, and divides the MgO between the two fractions so as to balance them perfectly, obtaining the formula $\text{SiO}_3\text{Ca}\cdot\text{SiO}_3\text{Mg}$, which in reality becomes $\text{SiO}_3\cdot(\text{Ca,Mg})\cdot[\text{SiO}_3\text{Mg}\cdot\text{Al}_2\text{O}_3]$. From the data presented, the differences in the quantities of

silica with respect to the calculated values (over- or underestimation) are minimal for very many pyroxenes.

For the amphiboles, the problem is more complex, but is tackled with the assumption that the pseudohexagonal symmetry of the crystals reflects a chemical reality, consisting of a base composed of six formula units. Thus, in orthorhombic terms, the formula is $6 \text{SiO}_3\text{Mg}$, and in monoclinic terms, with a loss of symmetry analogous to the calcite-dolomite passage, $[2\text{SiO}_3\text{Ca}\cdot 4\text{SiO}_3\text{Mg}]$, to which must be added, however, the terms related to the presence of Al_2O_3 and also of the hydroxides MgO_2OH and AlO_2OH . Thus, in reality the following formulae must be written for the typical reference species:

anthophyllite $6\text{SiO}_3\text{Mg}\cdot[2\text{SiO}_2\cdot\text{MgO}_2\text{OH}]$
 tremolite $[2\text{SiO}_3\text{Ca}\cdot 4\text{SiO}_3\text{Mg}] [2\text{SiO}_2\cdot\text{MgO}_2\text{OH}]$
 hornblende $[2\text{SiO}_3\text{Ca}\cdot 4\text{SiO}_3\text{Mg}] [\text{SiO}_2\cdot 2\text{AlO}_2\text{OH}]$

and gradually more complex ones for the various terms with binary or also multiple compositions, e.g., quadruple for

anhydrous basaltic hornblende $[2\text{SiO}_3\text{Ca}\cdot 4\text{SiO}_3\text{Mg}] [\text{SiO}_3\text{Mg}\cdot\text{Al}_2\text{O}_3]$
 $[2\text{SiO}_3\text{Ca}\cdot 4\text{SiO}_3\text{Mg}] 2\cdot\text{Al}_2\text{O}_3$

When these formulae, including units that can be called “Gossner molecules,” are recalculated in the modern way, they give the effective composition, re-establishing the ratios $\text{Ca}:\text{Mg}=2:5$ and $(\text{Ca}+\text{Mg}):\text{Si}=7:8$ that clearly result from all the analyses which until then had been poorly interpreted, without taking into account the correct role recognized for OH. Therefore, despite the complexity of the modal calculations, these works marked a step forward, also detailed in a later work (Gossner 1925) on other less common amphiboles.

Another two notes (Gossner 1930a,b) appeared at the end of the decade when Gossner moved to Munich to succeed the illustrious von Groth. In the first, he discusses the results of his roentgenographic studies on different amphiboles (arfvedsonite, barkevikite, kaersutite). He reports cell parameters that are very similar to each other and to those known for tremolite and glaucophane, indicates the probable spatial group as C_{2h}^6 given the extinctions and the centered lattice, and reports the identified reflections with their intensity and the number of molecules per cell (4). At this point, Gossner retracts all the considerations made in the preceding works relative to the number 6, which had led to correct formulae, and returns to the old-fashioned idea of the ratio $\text{Ca}:\text{Mg}=1:3$, for which the composition of tremolite is $3\text{SiO}_3\text{Mg}\cdot\text{SiO}_3\text{Ca}$. If we look at the date of acceptance of the paper in the *Zeitschrift*, July 9, 1929, we see that Warren’s manuscript on the structure of tremolite arrived only the day before, July 8, so that the two papers appeared in the same volume 72. A few months passed and a comment on Warren’s paper was published on November 15, 1929; it is a one-page article entitled “*On the composition of tremolite*” that is a masterpiece of tightrope walking. On the one hand, Gossner confirms the composition “*vor langerer Zeit*” proposed in 1924 but, unable to deny the one exhumed a few months earlier, he clings, as if to a lifeline, to the observation that not all the oxygens form part of the chains since some of them are coordinated by Mg, exactly as he had maintained (in square brackets) in the early versions. He concludes:

Our previous molecular unit is now, in its atomic consistence, identical to the formula that Warren has found on the basis of the structural analysis. But he has also found that, in the lattice, 4 atoms of O are not bound to Si. Also in our aforesaid formula, it appears that 4 O atoms have different bonds; in particular, they are not bound to a Si atom. Therefore, it must be remarked that that two independent methods, structural analysis and statistical treatment of purely chemical data, have led to the same result for part of the molecular unit. The problem of arriving at the representation of the composition of silicates with the so-called constitutional formula is still not solved

..... The method of decomposition of molecular units is still useful to determine the unknown chemical composition.

In those years so rich in publications, two works deserve special mention. In Helsinki, still with the Swedish name of Helsingfors, Walter Wahl (1928) dealt in a fairly traditional manner with pyroxenes and amphiboles as part of a series of notes on the constitution of silicates. He gives much importance to the various structural formulae, particularly for the aluminiferous terms which he considers mixtures between the classic metasilicates and the virtual molecule of Tschermak, exhuming the old name of *syntagmatite* for the term with composition $\text{CaMg}_2\text{Al}_2\text{Si}_3\text{O}_{12}$. Our interest in this work is due to the proposed structural formulae that have 4 bars around the Al and 6 around the Si in the formula of Tschermak's molecule and 6 around both in the formula of syntagmatite, i.e., the real amphibole. This does not represent a return to the dawn of Berzelius but rather different concepts of valence and coordination, which are well specified in the German words: Si remains *viervertig* and Al *dreivertig*, i.e., tetra- and trivalent, but in the structural formulae they figure respectively as *sechszählig* and *vierzählig*, i.e., hexa- and tetracoordinates, in the first structural formula and both as hexacoordinates in the second. Therefore, the Al-Si substitution does not occur with a trivalent to a tetravalent but with the tetracoordination of two atoms, thus predicting a continuous Si-Al-Si-Al-Si chain. A difference between pyroxenes and amphiboles, of lower temperature, would involve a change in the coordination of Al from 4 to 6, in exact accordance with current general concepts of crystal chemistry.

Something similar was also proposed by Machatschki (1928). Although remaining faithful to the old Ca:Mg=1:3 ratios, he somehow overcomes them, passing to a crystal chemical formula $\text{XY}_3(\text{Si},\text{Al})_4(\text{O},\text{OH},\text{F})_{12}$. This goes beyond the classic chemical symbols, reintroducing them as $\text{X} = \text{Ca}, \text{Na}, \text{K}$ and $\text{Y} = \text{Mg}, \text{Fe}, \text{Mn}, \text{Al}$, with the possibility of heterovalent substitutions and a necessary balance of charges, presaging the crystal chemical concept of "site." As determined for diopside by Warren and Bragg, he suggests the existence in amphiboles of Si-O metasilicate chains, albeit with a different link between them because of the different ratio of the number of X:Y cations that pair with the O atoms free from the link in the chains. This is what Bragg gave him credit for, as mentioned above.

PROBLEM OF WATER

Today, we know that the hydroxyl groups of the amphiboles are driven away from the structure only at high temperatures, much higher, for example, than those of the clay minerals.

The dehydration measurements of Posnjak and Bowen (1938) showed that the temperatures range between 900 °C for tremolite and 1000-1100 °C for hornblende. These values are well above the temperatures obtainable with gas in the old laboratories, around 600 °C for Bunsen burners and 700-800 °C for blowtorches.

Therefore, it was impossible in the old laboratories to reach the temperatures necessary to drive out water; in any case, without direct determination methods, with the loss on ignition there was a risk of falsifying the results because of the fixation of O_2 by oxidation of ferrous Fe.

The tables of analytical data in the old treatises demonstrated that:

- (a) the water was often not measured, but the corresponding analyses often had low total values (96-97%),
- (b) when measured, the values for water were ca. 0.5-1% and rarely ca. 2%,

in the latter case, especially if the samples were fresh and clearly unaltered, the water was attributed to H considered together with the alkaline or alkaline-earthly "R," further complicating the calculations of the ratios between the components.

It was only in the early XX century that Penfield and Stanley (1907) proposed a possible bond between F and H₂O (considered as OH and not as H), but they were thought to be present in bivalent radicals like R^{'''}₂OF₂ or R^{'''}₂O(OH)₂ in the wake of, and perhaps also at least partially replacing, what Tschermak had suggested for the trivalents with his virtual molecule.

The problem seems to have interested mainly the many Americans who had begun to conduct research in this field. Allen and Clement (1908), for example, address the subject, albeit with a step backward since they consider the water to be “lost or dissolved” in the mineral and not essential for its constitution, given its inconstant content.

As mentioned above, however, another American, W. Schaller (1916), carried out accurate analyses of three tremolites and established their composition as 8SiO₂·5MgO·2CaO·H₂O, specifying that the presence of OH ions was essential for the constitution of the amphibole.

Definitive confirmation came from the structure determined by Warren. However, we should not forget other Americans, Posnjak and Bowen who, contradicting their past colleagues of the Geophysical Laboratory, determined the precise temperatures of loss of the “constitutional water” after a modest gradual loss of the adsorbed water.

NOMENCLATURE

In the last quarter century, the mineralogy community decided to revise the nomenclature of this fundamental group of minerals and, within a short time, two subcommissions of the *Commission of New Mineral and Mineral Names* of the I.M.A. had made important progress. The first, presided by Horace Winchell, presented its conclusions in a report by Bernard Leake (1978). The orthorhombic-monoclinic crystallographic division was abandoned and the classification is now based on the nature of the B cation in the general formula A₀₋₁ B₂ C₅ T₈ O₂₂ (OH)₂, which occurs in the 8-fold coordinated site M(4), this choice yields four different groups.

The subdivision of the fields of the various species, based on numerous end members, occurs in great detail using as nomenclature both prefixes and adjectives.

Mg,Fe group with	5 names	with	14 end members
Ca " with	8 " "		16 "
Na,Ca " with	5 " "		18 "
Na " with	5 " "		9 "
	---		-----
	23		57

The need to revise the nomenclature that had accumulated in almost two centuries of research led the subcommission to officially discredit 193 old names: only 90 of them are real names given to hypothetical species, while many are only orthographic variants and 18 are related merely to external features of asbestos. Unfortunately, the discredited names include some related to illustrious scientists, e.g., the Irishman Kirwan, the Russian Kokscharow and the Italian Spezia.

Shortly thereafter, two volumes of *Reviews in Mineralogy*, 9A and 9B, of the Mineralogical Society of America, edited by David Veblen, were issued as a compendium of current knowledge (Veblen 1981; Veblen and Ribbe 1982).

These volumes were followed in 1983 by a huge review work by F. Hawthorne, who had made a long and thorough study of amphiboles. Consisting of 300 pages in *Canadian Mineralogist*, it summarizes the knowledge of amphiboles, with new structural studies and the results of various spectroscopic techniques that improve the knowledge of this group of

rock minerals; it also discuss and support the first attempts to use crystal-chemical data can to constrain petrogenetic processes (Hawthorne 1983).

Twenty years passed, albeit years of intense research, and a new subcommission presided directly by Leake presented a new Nomenclature of the Amphiboles (Leake et al. 1997). The differences with respect to the previous nomenclature were not particularly sensational: the attributions to species were merely simplified with much more schematic divisions, still at 50% between the extreme terms.

The borderline between the various groups, again based on the nature of the B cation, was shifted from 1.34 or 0.67 atoms per formula unit to 1.00 or 0.50. Hence, the division between the groups became the following:

- 1) Mg, Fe, Mn, Li amphiboles with $(Ca+Na) < 1.00$
- 2) Ca “ “ $(Ca+Na) \geq 1.00$ and $Na < 0.50$
- 3) Na-Ca “ “ $(Ca+Na) \geq 1.00$ and $0.50 \leq Na < 1.50$
- 4) Na “ “ $(Na) \geq 1.50$

The coining of new root-names was restrained to dominant heterovalent substitutions, while for homovalent substitutions the use prefixes was adopted, modifiers are also suggested to account for minor but significant substitutions. The approved root-names rose to 30 and the species \geq to 75:

- 1) Mg,Fe group with 6 names for 19 end members
- 2) Ca “ with 10 ” “ 21 ” “
- 3) Na,Ca “ with 5 ” “ 18 ” “
- 4) Na “ with 9 ” “ 17 ” “

Some years later (Leake et al. 2003) the Subcommittee advanced some additions and revisions to the 1997 recommendations. It was held the previous scheme based on the nature of B cations, but it was added a fifth group defined “Na-Ca-Mg-Fe-Li” group. The reason was the detection of solid solution terms with B-site composition (NaLi) ottoliniite and whittakerite and a general better knowledge of Li crystal-chemistry after the availability of ion-probe analysis.

In another chapter of this volume (Hawthorne and Oberti 2007) it is discussed another contribution to the classification of the amphiboles first proposed by Hawthorne and Oberti (2006). Based on recent knowledge, in particular on the crystal-chemistry of Li and the role of Ti in dehydrogenated amphiboles (e.g., obertiite and dellaventuraite), these authors suggest a different approach to classification based on the dominant ion in: 1) the W site, 2) the B sites, 3) the C sites. This proposal must obviously be approved by IMA Commission.

Until today 34 mineral names are approved, almost all with prefixes and adjectives, these names can be divided according to the date of their proposals:

- 18th century n. 3
- First half of the 19th century n. 6
- Second half of the 19th century n. 6
- First half of the 20th century n. 6
- Second half of the 20th century n. 10
- 21st century n. 3

In particular, while for hornblende we can speak generally of the early 1700s, actinolite (1794) and tremolite (1796) date to the end of the 18th century; the list ends in the last year of the 20th century (2000) with obertiite and pedrizite and in this millennium with ottoliniite and whittakerite (2004) and dellaventuraite (2005).

The II edition of volume 2B (*double chain silicates*) of the classic treatise by Deer, Howie and Zussman was published in 1997 (Deer et al. 1997) and adopts the nomenclature of

Leake et al. (1997). It summarizes all the knowledge on amphiboles, with an appendix on the biopyriboles, particular minerals with mixed chains, and another on two peculiar minerals that bear the names of two co-authors, with a double chain different from that of the amphiboles.

CONCLUSIONS

Although the first amphibole structures were solved in the laboratory of W.L. Bragg in Manchester, England, Warren was an American from M.I.T. Therefore, we can credit the American school with solving the problem of the amphiboles—starting with Penfield, whose observations were formalized by Dana, and ending with Warren, although with the crucial contribution of Schaller.

However, it is important to underline a parallel with the German school: the polymorphism between pyroxenes and amphiboles proposed by Rose and tenaciously supported by Rammelsberg who, with an enormous number of analyses, confirmed the crude formulae of the various species, and finally Tschermak who brilliantly solved the problem of the role of Al, hypothesizing the presence in solid solution of the theoretical aluminiferous component that bears his name. This school remained a prisoner of the firmly rooted ideas of absolute correspondence between pyroxenes and amphiboles, first by ignoring the often-reported presence of water and then, certainly because of the lack of communication during the first world war, the conclusions of Schaller. Hence, even in the post-war period, illustrious scientists belonging to the German school, such as the Swiss Paul Niggli (1888-1953), in his 1926 treatise, the Austrian Felix Machatschki (1895-1970), in his 1928 article, and Gossner, in his publications from 1924 to 1930 (albeit in an ambiguous and contradictory manner), remained mired in the XIX-century ideas of a close analogy with the pyroxenes.

Therefore, great credit must be given to the American school, to Penfield, to Schaller and to Warren, for definitively clarifying the nature of the amphiboles. Yet, German science was not defeated, because of the clear German origin of Schaller and because it was thanks to X-ray diffraction, i.e., to von Laue, that the crystalline structures were determined, although with the crucial contribution of two Englishmen, Bragg father and Bragg son, who acted as a bridge between old Europe and new America.

REFERENCES

- Agricola G (1546) *De Natura Fossilium*. Froben, Basileae
- Allen ET et al. (1908) Mineralien von der Zusammensetzung $MgSiO_3$: ein Fall von Tetramorphie. (Auszüge) *Z Kristallogr* 44:537-538
- Allen ET, Clement JK (1908) The role of water in tremolite. *Am J Sci* 20:101-109
- Bergman T (1783) *Sciagraphia. Regni Mineralis. Signum Roboris*, Florentia
- Berman H (1937) Constitution and Classification of the Natural Silicates. *Am Mineral* 22:342-408
- Berzelius JJ (1819) *Nouveau Système de Minéralogie*. Mequignon, Paris
- Bragg WL (1930) The structure of silicates. *Z Kristallogr* 74:237-305
- Breithaupt A (1815) *Vollständiges Handbuch der Mineralogie*. Arnold, Dresden
- Chrustschoff K (1894) Über künstliche Hornblende. (Auszüge). *Z Kristallogr* 22:297
- Clarke FW (1897) Die Constitution der Silicate. (Auszüge) *Z Kristallogr* 28:326-333
- Dana ES (1892) *A System of Mineralogy*. VI ed. Wiley, New York
- Dana ES (1899) First Appendix to the VI Edition of Dana's System of Mineralogy. Wiley, New York
- Dana ES (1909) Second Appendix to the VI Edition of Dana's System of Mineralogy. Wiley, New York
- Dana JD (1855) *A System of Mineralogy*. IV ed. Trübner, London
- Dana JD (1868) *A System of Mineralogy*. V ed. Trübner, London
- Deer WA et al. (1997) Rock-forming minerals. Vol 2B Double-chain silicates. The Geological Society, London
- Doelter C (1914) *Handbuch der Mineralchemie*. III/1 Band. Steinkopff, Dresden
- Gossner B (1924a) Die chemische Zusammensetzung von Alkali-amphibole. *Z Kristallogr* 60:302-310

- Gossner B (1924b) Die chemische Konstitution der monoklinen Pyroxene und der Amphibole. *Z Kristallogr* 60:361-378
- Gossner B (1925) Die chemische Zusammensetzung von Crossit, Arfvedsonit, Aenigmatit, Rhoenit und von Babingtonit. *Z Kristallogr* 61:538-545
- Gossner B (1930) Zur Frage der Zusammensetzung des Tremolits. *Z Kristallogr* 73:114-115
- Gossner B, Mussgnung F (1929) Über Enstatit und sein Verhältnis zur Pyroxen- und Amphibolgruppe. *Z Kristallogr* 70:234-248
- Gossner B, Spielberger F (1930) Chemische und röntgenographische Untersuchungen an Silikaten. Ein Beitrag zur Kenntnis der Hornblendegruppe. *Z Kristallogr* 72:111-142
- Groth P (1874) Tabellarische Übersicht der Mineralien. Vieweg, Braunschweig
- Groth P (1882) Tabellarische Übersicht der Mineralien. II Aufl. Vieweg, Braunschweig
- Häüy RJ (1801) *Traité de Minéralogie*. Louis, Paris
- Häüy RJ (1822) *Traité de Minéralogie*. II ed. Bachelier-Huzard, Paris
- Hawthorne FC (1983) The Crystal Chemistry of the Amphiboles. *Can Mineral* 21:173-480
- Hawthorne FC, Oberti R (2007) Classification of the amphiboles. *Rev Mineral Geochem* 67:55-88
- Hintze C (1897) *Handbuch der Mineralogie*. II Band. Von Veit, Leipzig
- Kirwan R (1784) *Elements of Mineralogy*. Elmsly, London
- Leake B (1978) Nomenclature of Amphiboles. *Miner Mag* 42:533-563
- Leake BE, Woolley AR, Arps CES, Birch WD, Gilbert MC, Grice JD, Hawthorne FC, Kato A, Kisch HJ, Krivovichev VG, Linthout K, Laird J, Mandarino JA, Maresch WV, Nickel EH, Rock NMS, Schumacher JC, Smith DC, Stephenson NCN, Ungaretti L, Whittaker EJW, Guo Y (1997) Nomenclature of amphiboles: Report of the subcommittee on amphiboles of the International Mineralogical Association, Commission on New Minerals and Mineral Names. *Can Mineral* 35:219-246
- Leake BE, Woolley AR, Birch WD, Burke EAJ, Ferraris G, Grice JD, Hawthorne FC, Kisch HJ, Krivovichev VG, Schumacher JC, Stephenson NCN, Whittaker EJW (2003) Nomenclature of amphiboles: additions and revisions to the International Mineralogical Association's amphibole nomenclature. *Can Mineral* 41:1355-1370
- Machatschki F (1928) Über die Formel der monoklinen Amphibole und Pyroxene. *Z Kristallogr* 71:219-236
- Niggli P (1924) *Lehrbuch der Mineralogie*. II Aufl. Borntraeger, Berlin
- Penfield SL, Stanley FC (1907) Über die chemische Zusammensetzung des Amphibols. *Z Kristallogr* 43:231-260
- Plinio GS (1988) *Storia Naturale* (trad.ital.) Einaudi, Torino
- Posnjak E, Bowen NL (1931) The role of water in tremolite. *Am J Sci* 22:202-214
- Rammelsberger CF (1841) *Handwörterbuch des chemischen Teils der Mineralogie*. Berlin
- Rammelsberger CF (1875) *Handbuch der Mineralchemie*. II Aufl. Engelmann, Leipzig
- Rammelsberger CF (1886) *Handbuch der Mineralchemie*. Ergänzunghefte. Engelmann, Leipzig
- Rammelsberger CF (1895) *Handbuch der Mineralchemie*. II Supplement II Aufl. Engelmann, Leipzig
- Schaller WT (1916) Mineralogical notes, series 3. The chemical composition of tremolite. *Bull US Geol Survey* 610:136
- Tschermak G (1871) Über Pyroxen und Amphibole. *Miner Petr Mitth* 1:17-46
- Tschermak G (1884) *Lehrbuch der Mineralogie*. I Aufl. Hölder, Wien
- Tschermak G (1915) *Lehrbuch der Mineralogie*. VII Aufl. Hölder, Wien
- Veblen D (ed) (1981) Amphiboles and Other Hydrous Pyriboles-Mineralogy. *Reviews in Mineralogy*, vol. 9A. Mineralogical Society of America
- Veblen D, Ribbe PH (ed) (1982) Amphiboles: Petrology and Experimental Phase Relations. *Reviews in Mineralogy*, vol. 9B. Mineralogical Society of America
- Wahl W (1928) Über der Konstitution der Silikate. Die Additionsverbindungen zwischen Alumosilikaten und anorganische Salzen. *Z Kristallogr* 66:173-190
- Wallerius JG (1778) *Systema Mineralogicum*. Officina Krausiana, Vienna
- Warren BE (1930) The structure of tremolite. *Z Kristallogr* 72:42-57
- Warren BE, Bragg WL (1928) The structure of diopside. *Z Kristallogr* 69:168-193
- Warren BE, Modell DI (1930) The structure of anthophyllite. *Z Kristallogr* 75:161-178

Amphiboles:

Crystal Chemistry, Occurrence, and Health Issues

CONTENTS

- 1-54 **Amphiboles: Crystal Chemistry** *Frank C. Hawthorne, Roberta Oberti*
- 55-88 **Classification of the Amphiboles** *Frank C. Hawthorne, Roberta Oberti*
- 89-123 **New Amphibole Compositions: Natural and Synthetic**
Roberta Oberti, Giancarlo Della Ventura, Fernando Cámara
- 125-171 **Long-Range Order in Amphiboles**
Roberta Oberti, Frank C. Hawthorne, Elio Cannillo, Fernando Cámara
- 173-222 **Short-Range Order in Amphiboles** *Frank C. Hawthorne, Giancarlo Della Ventura*
- 223-260 **Non-Ambient *in situ* Studies of Amphiboles**
Mark D. Welch, Fernando Cámara, Giancarlo Della Ventura, Gianluca Iezzi
- 261-286 **The Synthesis and Stability of Some End-Member Amphiboles**
Bernard W. Evans
- 287-322 **The Significance of the Reaction Path in Synthesizing Single-Phase Amphibole of Defined Composition**
Walter V. Maresch, Michael Czank
- 323-358 **Amphiboles in the Igneous Environment** *Robert F. Martin*
- 359-416 **Metamorphic Amphiboles: Composition and Coexistence** *John C. Schumacher*
- 417-451 **Trace-Element Partitioning Between Amphibole and Silicate Melt**
Massimo Tiepolo, Roberta Oberti, Alberto Zanetti, Riccardo Vannucci, Stephen F. Foley
- 453-516 **Amphiboles: Environmental and Health Concerns**
Mickey E. Gunter, Elena Belluso, Annibale Mottana
- 517-546 **Amphiboles: Historical Perspective** *Curzio Cipriani*

ISBN 978-0-939950-799



9 780939 950799